Hepacivirus / hepatocyte interplay leading to liver metabolic disorders

Angeliki Anna Beka

Université Paris Cité

École doctorale Bio Sorbonne Paris Cité – ED 562

Institut Pasteur

Département de Virologie

Hepacivirus/hepatocyte interplay leading to liver metabolic disorders

Par **Angeliki Anna BEKA**

Thèse de doctorat d'Infectiologie

Dirigée par **Annette MARTIN**

Présentée et soutenue **publiquement**

le 15/12/2023

Devant un jury composé de :

I. **Annette MARTIN**, DR-HDR, Institut Pasteur, Directrice de thèse
II. **Darius MORADPOUR**, Full Professor, Université de Lausanne, Rapporteur
III. **Mirjam ZEISEL**, CR-HDR, Université de Lyon 1, Rapportrice
IV. **Pierre-Emmanuel CECCALDI**, PU-HDR, Université Paris Cité, Examinateur
V. **Edward EMMOTT**, Lecturer, University of Liverpool, Examinateur
VI. **Hervé LERAT**, PhD-HDR, Université Grenoble Alpes, Membre invité

Acknowledgements

As my PhD thesis is coming to its end it is hard not to reflect back to all the people who were instrumental in the completion of this work in one way or another. Therefore, before guiding you through the networks of hepacivirus-driven interferences, I would like to start by presenting the top enriched terms of gratitude in my network of "partners in crime".

AB Scientific, "The supervisor", 1 core node in my network

There is no one who deserves to be in this section more than my guiding light through this endeavor, my thesis supervisor, **Dr Annette Martin**, head of the Hepacivirus-Host Interactions (HEPA) group. Thank you for the privilege of interacting with you in a both scientific and human level, for always making yourself available and ready to provide rigorous feedback and suggestions, and for patiently allowing me to mature as a scientist over the past years. For your confidence in me and the trust you showed me by allowing me to pursue this project and to present our collective results in national and international conferences, while always cheering for me. For your patience and all the life lessons you generously delivered. For fighting to provide the best working conditions possible for our group and for trying your best to ensure that work flowed effortlessly. For being a true mentor, I will always be indebted.

AB Scientific, "PhD Thesis jury", 6 nodes in my network

I want to express my gratitude to the scientists who I admire and who have willingly accepted to evaluate my thesis work. **Dr Mirjam Zeisel** it has been a great pleasure interacting with you during the various HCV-related conferences, only to find out that the great scientist is also a very gracious human being. **Prof Darius Moradpour** it is an honor to have the person, whose publications have guided me since I started my HCV career, assess my labor. Thank you both *in advance* for taking the time to thoroughly examine my manuscript and provide insightful suggestions.

I also want to thank both **Dr Edward Emmott**, who so amiably accepted to help a strange student, and **Prof Pierre-Emmanuel Ceccaldi**, who has been an inspirational figure ever since my Master 2 at Institut Pasteur, for their availability and for kindly agreeing to be part of my PhD jury and the scientific discussions this entails.

A very big thanks is dedicated to the invited member of my jury, **Dr Hervé Lerat**, who has been the kindest collaborator anyone could wish for. Thank you for all the discussions, time and effort put in our project, which without you could not have been possible!

AB Scientific, "Best lab-mates ever", 10 nodes in my network

Whether currently in the lab, or long gone to pursue their dreams this work could not have been accomplished without the collective efforts of all the people mentioned in this set of PPIs (person-person interactions).

I primarily want to thank the person who took the time to train me when I first joined the HEPA lab and whose incredible work has been a basis for a large part of this thesis, the formerly PhD student and now doctor, **Dr Emeline Simon**. I am so grateful for everything you taught me, for your continuous availability, your precious scientific insight and for becoming a great friend who was there for me in times of need.

A heartfelt, gigantic thank you goes out to **Dr Houda Tabbal**, former post-doctoral fellow in the HEPA group, who performed the preliminary purification experiments of HCV NS5A protein complexes and helped me set up the protocol, while carrying out the purifications of HCV Core protein complexes herself. Habibi, I am blessed to have shared this lab experience with you and I will forever be grateful for your unconditional support, understanding and life lessons on empathy and compassion!

It can never be enough, but I hope this paragraph can serve as a token of my never-ending appreciation of the future doctor **Eftychia Filippopoulou**, who did not only prove to be invaluable in the generation of the NS5A chimeras we produced, but was also the voice of reason at times I got desperate. You were my favourite "minion" in the lab in Greece and I am now an extremely proud lab-mama watching you evolve and accomplish amazing things! I hope your thesis turns out as incredible as you made mine with your friendship. You were my biggest cheerleader and gave me so much strength to push forward. Rock on Euti!

I also wish to thank **Brigitte Blumen**, technician in the HEPA group, who was instrumental in constructing and sequencing most of the viruses used in the projects presented in this manuscript. Madame Brigitte, thank you from the bottom of my heart for your help and for always being yourself! -Le haricot vert.

To **Damien Batalie**, the HEPA group pillar with a technician's badge, I owe an enormous thank you for primarily making sure the materials and tools we might need are readily available and second for all the long experiments he had to do in my place while I was writing this manuscript. Thank you, Dam, for slowly, but surely becoming a dear friend during my Parisian days.

I am also so incredibly moved to thank **Noémi Beuscart**, who started as a stagiaire in the HEPA lab, and is now continuing in our group as a technician. Noémi your progress has been amazing and your help in the construction and characterization of the tagged NS5A chimeras has been priceless!

A big thanks is dedicated to **Dr Stephanie Aicher**, former member of the HEPA lab, the one who initiated the Core-related projects and did an excellent job in paving the way to France for all of us Greeks who followed.

My gratitude is also extended to **Dr Matthieu Fritz**, who was the first to pursue HCV-host PPIs in our group, using NS2 as his bait. Without Matthieu's initial work, none of my accomplishments could have been in time for a 3-year PhD.

Lastly, I want to thank the newest member of our group, **Eleanora Stouthamer**, who is now attempting to co-immunoprecipitate selected Core and NS5A host partners and to functionally characterize them. Noor, you've been a delight to work with, a torpedo of energy and joy, you required minimal efforts to be trained and I'm so grateful you chose our lab for your internship!

AB Scientific, "Collaborators", 18 nodes in my network

Following the advice instilled by the favourite African proverb of the person who initiated me to the magical world of viral hepatitis, **Prof Penelope Mavromara**, "If you want to go fast, go alone, if you want to go far, go together", together I went.

I want to acknowledge the key contribution of **Dr Claire Gondeau** in the early stages of these projects, for providing and characterizing the clinical strains and for leading the preliminary experiments on primary hepatocyte cultures.

A thank you is also addressed to **Dr Richard Njouom** and **Dr Gabriela Oprisan** for the clinical viral strains they so kindly provided.

I am particularly thankful to **Thibaut Douche**, **Dr Quentin Giai Gianetto** and **Dr Mariette Matondo** from the Proteomics platform of Institut Pasteur for their collaboration in our proteomics projects and for their availability and patience with my many ideas and questions.

I also thank **Dr Thomas Cokelaer, Juliana Pipoli Da Fonseca,** and **Dr Marc Monot**, members of the Biomics platform of Institut Pasteur for running the RNA-Seq experiments and for the preliminary analysis. Thank you, Thomas, for taking the time to discuss and elaborate on the controls used and what each meant.

The warmest thank you in this respect goes to the person I never thought I'd find, who understood and shared my vision for the transcriptomics analyses from the first moment we discussed about the project, **Dr Emeline Perthame**. Thank you for being a model of professionalism. If every cross-disciplinary collaboration was as flawless and flowing as ours scientific advancements would have proceeded much faster.

I need to also thank **Prof Philippe Roingeard**, the third co-collaborator in our RHV project, which would not have been initiated weren't for him, and has since evolved through our multiple scientific discussions and exchanged together with Hervé and Annette.

For their participation in this project in the side of Hervé in Grenoble, I need to also thank **Marion Ressejac Mercey**, who performed the viral titrations in the first procedure of the RHV project, and **Maryline Cossin,** who assisted in the first intrahepatic inoculations of the virus.

I also thank **Dr Thibault Tubiana** and **Dr Stéphane Bressanelli** for the AlphaFold based reconstructions of hepaciviral proteins in relation to the RHV studies.

Lastly, our collaboration with the group of **Prof Philippe Chouteau**, has allowed us to further our hepacivirus observations in a system better mimicking the liver environment. Thank you, Philippe, for your participation in this project and for all of our interesting discussions. Thank you, **Dr Mathilde Couteaudier**, for the effort and time put into the characterization of our HCV recombinants in your hypo-diff system and for performing the infections towards a transcriptomic analysis in this system.

AB Scientific, "The amazing HCV Community", 8 nodes in my network

There is something unique and invitingly special about **the HCV community**, which I have been a member of for the past seven years. I am thankful to all of those with which I have interacting during meetings and events, for always being polite and encouraging and for openly discussing science in a scientific era of secrecy and animalistic competition.

I am particularly grateful to **Prof John McLauchlan** for the fruitful discussions and sharing of precious antibodies, **Prof Ralf Bartenschlager, Prof Charles Rice, Prof Jens Bukh, Dr Takaji Wakita, Dr Eliane Meurs, Dr Robert Purcell** and **Dr Agata Budkowska,** who have shared essential biological materials with us.

AB Scientific, "CSI", 3 nodes in my network

I would also like to express my appreciation to the members of my *Comité de Suivi Individuel*, **Dr Nicole Pavio** and **Dr Pascal Pineau**, for their insightful input in this work and for their kindness.

I would be remiss in not mentioning my Pasteurian PhD thesis tutor, **Dr Han Li**, who met with me at least once every year to ensure that the conditions of my thesis were optimal. As this was not always the case, I thank you for being there to record that and console me.

AB Scientific, "Financial Aid", 4 nodes in my network

This work would not have been implemented without the 3-year doctoral fellowship attributed to me by the **Université Paris Cité** and the research allowance provided by the **Virology Department of Institut Pasteur**, which allowed me to extend my time in the lab for three more months.

I'd like to also recognize the contribution of **ANRS** in funding the research proposals of our group, allowing us to bring them to life.

Lastly, I'd like to mention the **organizing committee of the HCV-Flavi meeting**, who facilitated my participation in this conference with the travel fellowships they allocated to me.

AB Support Groups, "In the lab", 11 nodes in my network

I'm extremely grateful to **Prof Sylvie van der Werf**, who initially welcomed me in her Unit back in 2019 and has been an idol ever since, thanks to her scientific rigor, her tremendous appreciation of students and her devotion to virology research.

I am also deeply indebted to **Dr Nicolas Escriou** for his numerous scientific and technological advice. Thank you, Nicolas, for bringing an extra brain to help solve these puzzles, but also for your paramount contribution in extinguishing my tiny home invaders, so that I can finish writing my manuscript in serenity.

I am further grateful for meeting and interacting with **Zeineb Choucha** and **Jérémy Brunet** during our common lab events or while having a drink afterwork to steam off.

I wish to expand my gratitude to **Martine Vandaele, Edmond Bellance, Jennifer Chevalier, Mohamed Hicaine**, as well as **Leila Campanaro** and **Tom Benayoun** for continuously providing all of us with the necessary consumable equipment to perform our experiments before and after the move of our lab, respectively.

A special thanks goes to **Dr Julien Fernandes**, research engineer in the Photonic Bioimaging platform at Insitut Pasteur, for training and advising me on the use of the confocal microscope and imaging tools.

AB Support Groups, "StaPa", at least 17 nodes in my network

My time at IP would not have been as enjoyable and rewarding without the Young Researchers' Association of Institut Pasteur, or **StaPa**. I want to thank all the former and current members of the **StaPa Bureau** with whom I shared this sometimes difficult, yet rewarding task of making this association grow and become acknowledged by the state. Thank you to the **StaPa Direction** for your trust in me becoming the Head of Communications and for having the immense pleasure of being one of the first people to welcome new students on campus and initiate them to the addiction StaPa has become!

In particular, I want to thank **Laura Pedro-Cos**, who except for a fellow fighter, she also became one of my closest friends on campus. Thank you, hon, for your understanding, availability and for just being you!

I am also extremely appreciative of **Francesco Andreace**, the Spanish guy trapped in an Italian body, with whom I clicked since the moment we met. Thank you, Frank, for always being a shoulder to cry on or a punching bag to release some of the stress. I hope I have been there for you as much as you were for me!

I would like to extend my sincerest thanks to **Lorenzo Zolfanelli**, who stayed longer at work -on a Sunday of all days- to witness the revelation of the western blot that made me exclaim "Sh*t! I'm going to become a Doctor!". Thank you, Lor, for all of our deep discussions and for always having the right and well-thought thing to say!

I'd like to also recognize the significant efforts and contribution of **Clarisabel Garcia Rodriguez** in conceptualizing many and organizing all of the outreaching StaPa events. Clari, thank you for making it possible for us to take part in these enriching experiences and witness the awe in children's eyes as food coloring dyes are separated under current!

My gratitude is further extended to all the members of this association, without whom StaPa would not have been the same, including but not limited to **Valerio Laghi** and **Franka D'Angelo** (our Mr and Mrs President, who so warningly opened their house to us), **Puck Nasman Norell** (*the best* secretary we could have ever wished for), **Samuel Garcia Huete** (who we shared and bonded over our struggles with the French language in the beginning of our PhDs and is now one of my dearest friends on campus), **Sara Napolitano** (the kindest soul of the group), **Viktoriia Gross** (our amazing photographer), **Agnès Baud** (the friendliest of the French), **Manuel Ares Arroyo** (the craziest, funniest post-doc), **Remy Walocha** (the *très chic* party animal) and the recent PPU additions, who thanks to Eftychia's praise have also been cheering for me the past months, helping me stay strong: **Juan Sienes Bailo, Bruno Tello Rubio,** and **Léa Manke**.

AB Support Groups, "PhirologisDs", at least 8 nodes in my network

I further wish to express my gratitude to the PhD students of the Virology Department of Institut Pasteur who elected me their representative, allowing me to advocate for our needs and rights.

Thank you in particular to **Felix Streicher**, my fellow co-representative, who was always there to support me emotionally and to take over whenever I was too overwhelmed by the thesis. I am so grateful I shared this adventure with you and I am so proud of what we have accomplished!

My thanks are further extended to **all the PhD Reps** of the different IP departments, together with who we have fought for the rights and mental health of the students on campus. We have been many over the years, but each one of us has put a little stone towards a better PhD experience for the rest, so thank you guys!

I would also like to thank the students who actively participated in our monthly meetings, becoming a true support groups for all of us, namely **Elodie Couderc**, **Mauro Castello Sanjuan, Heidy Maria Vera Peralta, Kyle Raymond, Maxim Chazal, Alexander Bergman** and **Martin Groznica** (now Jungbauer-Groznica). To you, Martin, I am especially grateful for your kindness and involvement in the PhD issues, for the trust you put in Felix and me, and for never neglecting to check up on us, the Reps, as well, to make sure we are doing okay.

AB Support Groups, "The IP Greek community", 6 nodes in my network

Studying abroad is accompanied by a strong -at times- saudade of one's original country, language, food, and traditions. My saudade never became too intense thanks to the ever-growing Pasteurian Greek community composed of, well, Eftychia, but also **Stelios Papadopoulos**, **Artemis Matrakis, Thea Chrysostomou, Alexandros Belavilas Trovas** and the always delightful to interact with κυρία **Evi Melanitou**, who made sure I felt at home.

AB Support Groups, "Making plans for the future", 1 node in my network

I am also delighted to add **Marion Guessoum**, career advisor within the MAASC, in my list of acknowledgements. Marion, thank you for guiding me through a crazy, beautiful adventure of getting to know myself, my professional needs and my strengths better than ever before! I am particularly grateful for your encouragement, support and patience with my unconventional ways to twist every exercise you gave me into something creative and aesthetically pleasing.

AB Friends, "SMAD4", 3 nodes in my network

I would also like to articulate my sincerest appreciation of the three people who were beside during my whole scientific career, since the first day at DuTH, **Sofia Gkagkaridou, Michaela Moula** and **Dimitris Palamidas**. You guys have been my guides, advisors, therapists, friends and so much more. I consider myself so lucky to have you in my life and by my side on the big defense date!

AB Friends, "Friends for life", 4 nodes in my network

I want to further thank my friends **Maro Anagnostopoulou, Sofia-Maria Tsakotelli** and **Giorgos Zarpapis**, who have been by my side for almost as long as I can remember and continue to be there for me through good times and bad. After all, Maro, Sofia and I share the same age…

I could not omit my purring companion, who was instrumental to my stress relief every time I got to cat-sit him, **Ilo the cat**.

AB Family, "Relatives", at least 2 nodes in my network

My appreciation is extended to my relatives, who in one way or another helped me reach this point. Notably, my fairy godmother, **Katerina Fountedaki**, or Arina Mpoumpina, who made the trip to be with me in my special day, and her bright son, **Giannis Koutsoumpinas**.

AB Family, "Strangers who became family", 3 nodes in my network

In times of crisis, it is important to have one constant to rely on. I am sanctified to have at least five. The two came in one package from the same womb. **Eirini** and **Christina Kyrgialani** my childhood friends, have always been there for me, especially through the most difficult times, helping me get up and fight, like true sisters. Thank you for all the beautiful moments we have shared and for never giving up on me!

The core of my strength, happiness and peace of mind through this PhD came from no other than my better half, my safe haven, the best man -*human*- walking on earth, **Giannis Koutsoliakos**. You never stop surprising me and making me feel the luckiest girl on this planet. I am beyond words proud of you and I admire you for all that you are and do, so your encouragement and awe of my work mean the world to me! Thank you for your patience and understanding the past three years – we made it!

AB Family, "Μπεκαίοι", 2 nodes in my network

Dedicating everything I have ever accomplished to my father, my hero, **Giannis Bekas**, and my brother, my pillar, **Giorgos Bekas**, can only merely show my gratitude and appreciation of their moral and financial support during my entire life. I thank you for helping me pursue my dreams, never giving up on me and always looking out for me. I've always kept your advice and words of wisdom close to my heart, serving me well during this journey. I hope you can be as proud of me and as I am of both of you!

AB Supernatural, "Guardian angels", ~ nodes in my network

Lastly, I wish to pay my tribute to those who are no longer with us, whose presence and input have nonetheless one way or another been decisive to me becoming who I am and to the successful completion of the present thesis.

To my mother, **Sofia Prifti**, my role model, who nurtured me very wisely and managed to transfer to me her knowledge, her ways (of thinking, of writing, of behaving), her strength, and everything that made her so beloved and unique in our community.

To my partner's mother, **Anita Josepha Cornelia Mocking**, who welcomed me into her home and her life, making me feel as her own, who taught me the importance of diversity and unconditional acceptance.

To my aunt **Maria Beka**, whose early loss underlined the importance of appreciation.

To my grandmothers, **Anna Prifti** and **Angeliki Beka**, who neither deserved the pain that they went through, but taught me that life can be utterly unfair and all we can do is hold on and fight.

To my godfather **Stefanos Koutsoumpinas**, with the deep appreciation and love for the French language and culture, the oil which he used during my christening apparently transferred several of his traits to me.

And to many other family friends and relatives taken too early, who taught me how to live, learn and explore.

To all of the enriched terms in my network,
but primarily to my family and
our guardian angels

Résumé

Etude des interactions entre hepacivirus et hépatocytes conduisant à des perturbations métaboliques du foie

L'hépatite C chronique est une maladie progressive du foie, entraînant la stéatose, une accumulation anormale de lipides, ainsi qu'une cirrhose et un carcinome hépatocellulaire (CHC) à long terme. La prévalence de ces manifestations varie selon le génotype (Gt) viral, le Gt3 étant très fortement associé à la stéatose. Ces pathologies sont le résultat de mécanismes à la fois directs, supposés être principalement médiés par les protéines Core et NS5A du virus de l'hépatite C (VHC), et indirects. La compréhension des mécanismes moléculaires mis en jeu souffre de l'absence d'un modèle d'étude pertinent. Un modèle de substitution prometteur a émergé avec la démonstration en 2018 qu'un nouvel hepacivirus de rongeur (RHV-rn1) établit une infection chronique chez le rat.

Ce travail visait à élucider les bases moléculaires de la dérégulation des voies hépatocytaires menant à la stéatose et au CHC, notamment les effets communs et différentiels des Gts du VHC. Dans le premier projet, les partenaires cellulaires (IPs) des protéines NS5A et Core et les voies de signalisation dérégulées spécifiquement ont été identifiés dans un système d'infection pertinent. Le deuxième projet a permis de disposer d'un modèle animal immunocompétent, celui des rats Sprague Dawley infectés par le RHV-rn1, pour réaliser l'étude des désordres métaboliques *in vivo*.

Nous avons produit un ensemble de virus chimériques dérivés d'une souche adaptée du Gt2a (Jad) codant NS5A ou Core d'isolats de patients de Gt1-4 pour lesquels les données cliniques étaient disponibles, et des recombinants Jad exprimant Core ou NS5A dotées d'un tag twin-strep (ST) à des fins de purification de complexes protéiques à partir de cellules d'hépatome humain Huh-7.5 infectées. Les IPs ont été identifiés par nano-chromatographie liquide couplée à la spectrométrie de masse en tandem. Les IPs forts ont été discriminés par rapport à des contrôles non spécifiques avec un nouvel algorithme que nous avons développé. À l'aide des outils CytoScape et STRING, les voies cellulaires en majorité enrichies parmi les 134 IPs de Core s'avèrent impliquées dans la régulation de l'expression des gènes de l'hôte, tandis que les 527 IPs de NS5A font essentiellement partie des voies impliquées dans les processus métaboliques, du transport, des réponses immunes et du CHC. Nous avons ensuite identifié des IPs de NS5A spécifiques de souche/Gt, les voies de biosynthèse du cholestérol et de gluconéogenèse étant enrichies principalement pour les IPs de NS5A du Gt3. Le séquençage comparé des ARNm des cellules Huh-7.5 infectées par les différents virus intergénotypiques exprimant Core des Gt1-4 a démontré un impact élevé de tous les virus par rapport aux cellules non infectées. Des dérégulations transcriptomiques différentielles selon les souches/Gts ont été observées par analyse d'enrichissement de gènes.

En parallèle, nous avons développé avec succès le modèle animal de substitution du VHC basé sur des rats Sprague Dawley infectés par RHV-rn1, montrant un taux élevé d'infections chroniques et de stéatose hépatique. Des analyses pilotes lipidomiques et métabolomiques comparatives de rats chroniquement infectés par rapport à des rats non infectés ont révélé une gluconéogenèse perturbée, ainsi qu'une augmentation des esters de cholestérol et des diacylglycérides dans les foies infectés.

En conclusion, dans des systèmes d'infection pertinents, nous avons montré que NS5A et Core du VHC peuvent contribuer à la progression des lésions hépatiques d'une manière spécifique selon le génotype viral, respectivement en interagissant directement avec des protéines impliquées dans des voies spécifiques de l'hôte ou en dérégulant le transcriptome. Nous avons également identifié des altérations métaboliques au cours des infections chroniques à hepacivirus dans un modèle animal de substitution, ouvrant la voie à une caractérisation plus approfondie, y compris en présence de facteurs de comorbidité de l'hôte comme le régime alimentaire.

Mots cles : VHC, NS5A, Core, interactomique, transcriptomique, métabolisme du foie, stéatose, carcinome hépatocellulaire, modèle animal, virus recombinants

Abstract

Hepacivirus/hepatocyte interplay leading to liver metabolic disorders

Chronic hepatitis C is a progressive liver disease, resulting in metabolic disorders, such as steatosis, an abnormal lipid accumulation in hepatocytes, and long-term complications of cirrhosis and hepatocellular carcinoma (HCC). The prevalence of clinical manifestations varies according to hepatitis C virus (HCV) genotypes (Gt), with Gt3 being highly associated with steatosis. HCV-induced pathologies can be driven by both indirect mechanisms and virus-driven host deregulations, thought to be essentially mediated by two pleiotropic viral proteins, the capsid protein (Core) and a nonstructural protein, NS5A. A detailed understanding of the molecular mechanisms involved has been hindered by the absence of a fully pertinent study model. A promising surrogate model emerged with the demonstration in 2018 that a new rodent hepacivirus (RHV-rn1) establishes chronic infection in rats.

This work aimed at elucidating the molecular bases for HCV manipulation of host pathways leading to steatosis and HCC, with a focus on the common and distinct effects of HCV Gts. The first project targeted the identification of cellular interacting partners (IPs) of HCV NS5A and Core and specifically deregulated signaling pathways in a relevant infection system. The second project provided an immunocompetent surrogate animal model to focus on the study of metabolic disorders *in vivo*.

We generated a panel of functional recombinant viruses encoding HCV NS5A or Core of Gt1-4 within the backbone of a Gt2a highly cell culture-adapted strain (Jad). NS5A and Core sequences were selected from clinical isolates of patients with known stages of liver damage. In frame twin strep-tag (ST) fusion to NS5A or Core allowed affinity purification of protein complexes from infected human hepatoma Huh-7.5 cells. IPs were identified by liquid nano-chromatography coupled to tandem mass spectrometry. Strong IPs were discriminated with respect to nonbinding V5-tagged controls by a novel scoring algorithm that we developed. Using CytoScape and STRING tools, the highest scored pathways enriched among the 134 IPs of Jad Core were involved in the regulation of host gene expression, while for the 527 Jad NS5A IPs, enrichment highlighted pathways involved in metabolic, transport, immune system and HCC processes. We next unveiled Gt/strain-specific IPs of NS5A, with cholesterol biosynthesis and gluconeogenesis pathways being enriched mainly in the Gt3 NS5A IPs. To further proteomic data obtained on Core, we examined hepatocyte transcriptomic deregulations in response to infection of Huh-7.5 cells with Core intergenotypic recombinant viruses. RNA sequencing analysis demonstrated a high impact of all viruses compared to noninfected cells. Differential regulations by specific strains and/or Gts were observed by gene set enrichment analyses.

In parallel, we successfully developed the HCV surrogate animal model based on Sprague Dawley rats infected with RHV-rn1, showing a high rate of chronic infections and liver steatosis. Pilot comparative lipidomic and metabolomic analyses of chronically infected versus noninfected rats revealed perturbed gluconeogenesis, as well as increased cholesteryl ester and diacylglycerides in infected livers. Moreover, the composition of cholesteryl esters, free fatty acids, diacylglycerides and triacylglycerides was found altered by RHV-rn1 infection, with a preferential accumulation of longer fatty acyl chains in the infected rats.

In conclusion, in relevant infection systems, we found that NS5A and Core may contribute to the progression of HCV-induced liver damage in a genotype-specific manner, by directly interacting with proteins involved in specific host pathways or by deregulating the host transcriptome, respectively. We also identified hepacivirus-induced metabolic alterations during chronic infection in a surrogate hepacivirus animal model, paving the way for further characterization, including in the presence of host comorbidity factors like western diet.

Keywords: HCV, NS5A, Core, interactomics, transcriptomics, liver metabolism, steatosis, hepatocellular carcinoma, animal model, recombinant virus

Résumé substantiel en français

Introduction

Le virus de l'hépatite C (VHC) est un hepacivirus humain, qui infecte globalement 1.5 millions d'individus par an. L'hépatite C chronique est une maladie progressive du foie, entraînant une stéatose, une accumulation anormale de lipides dans les hépatocytes, ainsi que des complications à long terme telles que la fibrose, la cirrhose et le carcinome hépatocellulaire (CHC). La prévalence de ces manifestations cliniques varie selon le génotype viral (8 génotypes et >90 sous-types identifiés à ce jour). L'infection par le génotype 3, très répandue parmi les utilisateurs de drogues par voie intraveineuse (UDVI) en Europe, présente une prévalence accrue de la stéatose de l'ordre de 80% des infections, et l'infection par le sous-type 1b serait associée à un risque accru de développement du CHC, alors que des données cliniques font défaut pour les génotypes 4 à 8.

Les pathologies induites par le VHC peuvent être provoquées par une combinaison complexe de mécanismes à la fois directs et indirects tels que l'inflammation chronique du foie, potentiellement aggravée par un régime alimentaire de type occidental, le diabète ou la consommation d'alcool. Les mécanismes directs semblent principalement médiés par deux protéines virales pléiotropes : la protéine de capside, Core, et une protéine non structurale, NS5A, qui seraient associées à la dérégulation de multiples processus cellulaires de l'hôte, notamment les cascades des réponses immunitaires ainsi que les voies de signalisation métaboliques, qui pourraient être associées au développement de la stéatose, et celles connues pour être impliquées dans le développement du CHC. Cependant, en l'absence de systèmes de culture cellulaire permettant l'étude des souches cliniques du VHC, ces dérégulations spécifiques de génotype et/ou impliquant les protéines du VHC ont été principalement étudiées dans des systèmes *in vitro* de surexpression protéique transitoire et/ou dans des cellules non hépatiques.

De plus, une compréhension détaillée des mécanismes moléculaires impliqués dans la pathologie induite par le VHC est entravée par l'absence de modèles d'étude pleinement pertinents, que ce soit en culture cellulaire ou *in vivo*. Cette connaissance reste pourtant cruciale, même à l'ère des agents antiviraux directs (AAD), qui peuvent actuellement guérir plus de 95% des infections chroniques, car la clairance virale n'élimine pas toujours le risque de progression vers des lésions hépatiques graves induites par le VHC. De plus, le coût élevé des traitements ciblés et la proportion accrue d'individus infectés qui ignorent leur statut sont des facteurs restrictifs importants qui doivent réglés avant de pouvoir envisager la diminution drastique de 80% de l'incidence des nouvelles infections à VHC et de 65% de la mortalité liée au VHC, objectif fixé par l'Organisation Mondiale de la Santé à l'échelle mondiale à l'horizon 2030. Dans ce contexte et en l'absence de vaccin préventif contre le VHC, il reste important de compléter nos connaissances sur le cycle viral, les interactions du VHC avec les composants cellulaires et l'association entre la variabilité génotypique du VHC et la pathogenèse.

Une découverte prometteuse a été faite en 2014 : le séquençage d'un nouvel hepacivirus de rat, le RHV-rn1. Malgré sa forte divergence génétique par rapport au VHC, l'infection par le RHV-rn1 présente chez le rat, son hôte naturel, des caractéristiques très similaires à celles du VHC chez l'homme, incluant un hépatotropisme, une virémie persistante détectable pendant plus d'un an et de nombreux traits de la pathologie hépatique liée au VHC, tels que les micro- et macro- stéatose vésiculaire, agrégation lymphoïde et lésions épithéliales biliaires.

Dans la partie introductive du manuscrit de thèse, ces informations sont développées, et une revue plus générale de l'état de l'art synthétise de très nombreuses études concernant les hepacivirus humain, VHC, et animaux, notamment le RHV, les données moléculaires relatives au cycle infectieux du VHC, la pathogenèse de l'hépatite C chronique, les modèles d'étude disponibles et les interférences connues entre le VHC et l'hépatocyte hôte.

Objectifs des travaux de thèse

Notre groupe vise à élucider les interactions moléculaires entre les hepacivirus et leurs hôtes conduisant à des troubles métaboliques hépatiques. Ma thèse est ainsi composée de deux projets visant à élucider dans des systèmes d'infection pertinents les bases moléculaires de la manipulation par le VHC des voies de signalisation de l'hôte conduisant à la stéatose et au CHC, en mettant l'accent sur les effets communs et distincts de protéines du VHC d'origines génotypiques diverses.

À cette fin, un premier projet a ciblé l'identification (i) des partenaires cellulaires d'interaction (IP) des protéines Core et NS5A de virus prototypiques et de virus de différents génotypes et (ii) des voies de signalisation cellulaires spécifiquement dérégulées. Ce projet comprenait le développement de nouveaux outils viraux capables de se répliquer dans des cellules d'hépatome humain et codant les protéines Core ou NS5A dérivées de souches cliniques de différents génotypes, isolées de patients présentant divers degrés de troubles hépatiques. Ces modèles ont été utilisés pour l'étude des dérégulations transcriptomiques spécifiques de l'origine génotypique de ces protéines. La génération d'un ensemble de virus recombinants parentaux et inter-génotypiques codant les protéines Core et NS5A respectives fusionnées en phase avec un twin strep-tag (ST) a permis la purification par affinité de complexes protéiques impliquant d'une part Core et d'autre part NS5A, et la détermination de l'interactome de ces deux protéines virales.

Dans le second projet, le modèle animal de substitution immunocompétent basé sur des rats Sprague Dawley infectés par le RHV-rn1, initialement établi en 2018 par le laboratoire du Dr Amit Kapoor (Ohio State University, Columbus, Ohio, USA) a été mis en place en France grâce à son don généreux de l'ADNc de longueur génomique du RHV-rn1. Avec ce modèle, nous avons cherché à caractériser les troubles métaboliques hépatiques déclenchés par une infection chronique par le RHV, à l'aide, dans un premier temps, de cohortes de rats de taille limitée, afin d'établir une preuve de concept de l'intérêt de ce modèle de substitution pour poursuivre des études de physiopathologie, alors que d'autres groupes dans le monde l'utilisent pour des études vaccinales.

Ces deux projets font partie d'études collaboratives soutenues par l'agence ANRS | MIE, qui devraient à terme contribuer à une meilleure compréhension des mécanismes moléculaires impliqués dans la stéatose et le CHC induits par le VHC en lien direct avec des facteurs viraux spécifiques et des polymorphismes génotypiques, ainsi que livrer des informations précieuses sur l'incidence de facteurs de co-morbidité et sur la persistance potentielle des perturbations métaboliques après élimination de l'hepacivirus infectant, études qui n'ont quasiment pas pu être abordées chez l'homme.

Matériels et Méthodes

Une partie détaillée de Matériels et Méthodes décrit l'ensemble des matériels disponibles au laboratoire et produits au cours de ma thèse, ainsi que toutes les approches méthodologiques que j'ai suivies au cours de ces travaux ou qui ont été mises en oeuvre sur les plateformes technologiques avec lesquelles nous avons collaboré.

Résultats

Nous avons généré avec succès par génétique inverse une série de virus recombinants fonctionnels dérivés d'une souche du génotype 2a (Jad) hautement adaptée à la culture cellulaire et codant les protéines Core ou NS5A de VHC de génotypes 1 à 4. Les séquences Core et NS5A ont été sélectionnées à partir d'isolats cliniques de patients présentant des stades connus de lésions hépatiques ou de souches prototypiques du VHC. Certains virus recombinants (codant Core) avaient été préalablement développés au laboratoire, tandis que les séquences consensus des protéines NS5A ont été établies et les virus recombinants ont été

produits au cours de ma thèse après substitution de la séquence codante de NS5A au sein de l'ADNc du Jad par ces séquences de génotypes différents, puis transfection de cellules d'hépatome humain avec les ARN synthétiques correspondants produits *in vitro*. Les virus recombinants ont ensuite été caractérisés. Les virus intergénotypiques exprimant les protéines NS5A hétérologues des sous-types 1a, 1b et 2a se sont avérés hautement réplicatifs, alors que ceux exprimant les protéines NS5A des génotypes 3 et 4 ont nécessité des mutations de compensation au sein des séquences codant les protéines non structurales NS3 et NS4B afin d'aboutir à des virus hautement infectieux.

Des virus Jad recombinants exprimant les protéines Core ou NS5A parentales étiquetées par l'insertion en phase d'un "twin strep tag" (ST) ont été produits à des fins de purification des complexes protéiques impliquant ces protéines virales. Les insertions ont été réalisées près de l'extrémité amino-terminale de Core ou à l'une des deux positions identifiées dans le segment carboxy-terminal de NS5A. Pour les recombinants intergénotypiques exprimant les protéines NS5A d'autres génotypes, une seule des deux positions d'insertion était utilisable et a été sélectionnée. Dans tous les cas, l'insertion de l'étiquette a été un succès sans abroger la réplication virale, la morphogenèse ou altérer la localisation subcellulaire des protéines virales.

Les complexes protéiques ont alors été purifiés par affinité à partir de trois ou cinq réplicats biologiques issus de l'infection de cellules d'hépatocarcinome humain Huh-7.5, à l'aide de billes magnétiques recouvertes de résine StrepTactin. Les partenaires d'interaction ont été identifiés par nano-chromatographie liquide couplée à la spectrométrie de masse en tandem (Nano-LC-MS/MS). Les IP forts ont été discriminés par rapport à des contrôles non spécifiques étiquetés avec un tag V5, en ayant recours à un nouvel algorithme de notation que nous avons développé en intégrant les statistiques d'interaction par spectrométrie de masse (MiST) et l'analyse de significativité des scores INTeractome (SAINT) à notre analyse statistique initiale "label free". À l'aide des outils CytoScape et STRING, les voies de signalisation qui se sont avérées les mieux notées après enrichissement à partir des 134 IP de la protéine Core du parent Jad sont celles impliquées dans la régulation de l'expression des gènes de l'hôte. En revanche, pour les 527 IP de la protéine NS5A du parent Jad, l'enrichissement a mis en évidence les voies impliquées dans les processus métaboliques, de transport, du système immunitaire et du CHC. L'analyse comparative des interactomes déterminés pour les différentes isoformes de NS5A a révélé 96 partenaires d'interaction communs à tous les génotypes, ainsi que certains partenaires spécifiques. Nous avons en outre pu identifier certains partenaires cellulaires impliqués dans le métabolisme de la cellules hôte interagissant spécifiquement avec les protéines NS5A de sous-type 3a associées au phénotype stéatogène, ce qui corrobore l'association observée sur le plan clinique du génotype 3 du VHC avec une prévalence plus élevée de stéatose. Les données protéomiques nous ont également permis d'identifier des sites de phosphorylation connus pour le génotype 2a et utilisés différentiellement pour les protéines NS5A des différents génotypes, ainsi que deux sites sites de phosphorylation de NS5A, qui n'ont à notre connaissance encore jamais été décrits et qui mériteraient d'être explorés davantage.

Pour approfondir les données protéomiques obtenues avec Core, nous avons examiné les dérégulations transcriptomiques des cellules Huh-7.5 en réponse à l'infection par des virus recombinants intergénotypiques exprimant des protéines Core de divers génotypes. L'analyse du séquençage à haut débit de l'ARN a démontré un impact élevé de tous les virus par rapport aux cellules non infectées. Des régulations communes et différentielles par des souches et/ou des génotypes spécifiques ont été déterminées par l'analyse d'enrichissement d'ensembles de gènes. Ce travail a révélé que les gènes impliqués dans les processus métaboliques étant régulés négativement par tous les virus recombinants exprimant Core de différents génotypes et que la régulation négative de la majorité de ces gènes était plus forte quand les protéines Core exprimées étaient issues de génotypes autres que le génotype 3.

En parallèle, nous avons réussi à implémenter le modèle animal de substitution du VHC basé sur des rats Sprague Dawley infectés par le RHV-rn1, qui a révélé un taux élevé (> 90%) d'infections chroniques et de stéatose hépatique. Des analyses lipidomiques et métabolomiques pilotes comparées, avec des cohortes de taille limitée de rats chroniquement infectés par rapport à des rats non infectés ont révélé une gluconéogenèse perturbée, ainsi qu'une augmentation des esters de cholestérol et des diacylglycérides dans les foies infectés. De plus, la composition des esters de cholestérol, des acides gras libres, des diacylglycérides et des triacylglycérides s'est avérée altérée par l'infection par le RHV-rn1, avec une accumulation préférentielle de "fatty acyl chains" plus longues dans le foie des rats infectés, en accord avec des mécanismes d'altération métabolique observés pour le VHC.

Conclusion et Perspectives

En conclusion, dans les systèmes d'infection utilisés, nous avons constaté que Core et NS5A sont impliquées dans la progression des lésions hépatiques induites par le VHC de manière spécifique à la souche et/ou au génotype infectant, en dérégulant, respectivement le transcriptome de l'hôte ou en interagissant directement avec des facteurs cellulaires impliqués dans des voies de signalisation spécifiques de l'hôte. Nous avons également identifié des altérations métaboliques du foie induites par un hepacivirus au cours d'une infection chronique dans un modèle animal de substitution, ouvrant la voie à une caractérisation plus approfondie, y compris en présence de facteurs de co-morbidité de l'hôte, comme un régime alimentaire de type occidental riche en sucres et en graisses. Il est important de noter que nos observations réalisées dans le modèle animal de substitution avec un hepacivirus animal sont en accord avec celles conduites dans des cultures de cellules infectées par le VHC, validant ainsi nos résultats et mettant en évidence certaines cibles cellulaires dont nous avons entrepris d'approfondir le rôle. Il s'agit désormais d'avoir recours à des systèmes encore plus physiologiques, comme les cultures de cellules Huh-7.5 différenciées et maintenues sous hypoxie, qui recréent un environnement se rapprochant du foie. Des études transcriptomiques réalisées dans ces modèles cellulaires renforceront les données acquises au cours de ces travaux de thèse et pourraient dévoiler de nouvelles voies de signalisation d'intérêt. Nous nous concentrons également sur la validation d'une sélection de partenaires cellulaires des protéines Core et NS5A et sur la caractérisation fonctionnelle plus approfondie de ces interactions. Enfin, nous attendons des études dans le modèle animal de substitution du VHC qu'elles étayent la compréhension des mécanismes plus généralement impliqués dans le développement de la stéatopathie non alcoolique, en combinaison ou non avec l'infection virale.

Table of Contents

Abbreviations

Numerical

2'5'OAS: 2'-5'-oligoadenylate synthase

A

aa: Amino acid residue(s)
ABHD5: 1-acylglycerol-3-phosphate O-acyltransferase
Abs: antibodies
ACACA: acetyl-CoA carboxylase alpha
ACC1: acetyl-coenzyme A carboxylase 1
ACN: acetonitrile
ACSL3: acyl-CoA synthetase long chain family member 3
ACSL5: acyl-CoA synthetase long chain family member 5
ADRP: adipose differentiation-related protein
ALDH1A1: aldehyde dehydrogenase 1 family, member A1
ALT, GPT2: alanine amino transferase
ANOVA: Analysis of variance
ANXA2: annexin A2
ANXA3: annexin 3
AP: Affinity purification
AP-MS: Affinity purification coucpled to mass spectrometry
AP2M1: clathrin adaptor protein complex 2
APEX: ascorbic acid peroxidase
Apo: apolipoprotein
ARFGAP1: ADP-ribosylation factor GTPase-activating protein 1
ARFI: acoustic radiation force impulse imaging
ARLD: alcohol-related liver disease
AST, GOT1, GOT2: aspartate amino transferase
ATGL: adipose triglyceride lipase
ATP: adenosine triphosphate

B

BIN1: amphiphysin II
BOC: Boceprevir

C

CALX: calnexin
CD81: cluster of differentiation 81
Cdk1: cyclin-dependent kinase 1
CE: Cholesteryl esters
CERT: ceramide transfer protein
CGI-58: Comparative Gene Identification 58
CHC: chronic HCV infection
CHIM(s): Controlled Human Infection Model(s)
CK1a: casein kinase Ia
CKII: casein kinase II

CLIA: chemiluminescence immunoassay
CLND1: claudin1
COH: Free Cholesterol
COPI: cargo sorting in coat protein complex I
CPT1A: carnitine palmitoyltransferase 1A
CsA: cyclosporin A
CypA: Cyclophilin A

D

D: Domain
DAA(s): direct antiviral agent(s)
DAB: 3,3'-diaminobenzidine
DAG: diacylglycerol
DAPI: 4-, 6-diamidino-2-phenylindole
DC(s): dendritic cell(s)
DCV: Daclatasvir
DEG(s): differentially expressed gene(s)
DGAT1: diacylglycerol O-acetyltransferase 1
DHAP: dihydroxyacetone phosphate
DMEM: Dulbecco's Modified Eagle Medium
DMV(s): double membrane vesicle(s)
DPBS: Dulbecco's Phosphate Buffered Saline
dsRNA: double-stranded RNA
DSV: Dasabuvir
DTT: dithiothreitol

E

EASL: European Association for the Study of the Liver
EBR: Elbasvir
ECM: extracellular matrix
EGF: Epidermal Growth Factor
EGFR: epidermal growth factor receptor
ELISA: enzyme linked immunosorbent assay
EMCV: encephalomyocarditis virus
EMT: epithelial mesenchymal transition
EphA2: ephrin type-A receptor
ER: endoplasmic reticulum
ESC: embryonic stem cells
ESYT1: extended synaptotagmin 1
ETC: electron transport chain

F

FA: formic acid
FAD: flavin adenine dinucleotide
FADH2: dihydroflavine-adenine dinucleotide
FAM: 6-carboxyfluorescein
FAs: fatty acids
FAS1: fatty acid synthetase 1

FASN: fatty acid synthase
FBS: fetal calf serum
FDR: false discovery rate
FFA(s): free fatty acid(s)
FOXO1: forkhead box O1

G

G6PD: glucose-6-phosphate dehydrogenase
GA3P: glucose-6-phosphate
GBVB: GB virus B
GEQ: genome equivalent
GLE: Glecarevir
GLRX: glutaredoxin-1
GPC3: glypican-3
GST: glutathione s-transferase
GZR: Grazoprevir

H

H&E: Hematoxylin-eosin
HADH: hydroxyacyl-CoA dehydrogenase
HAV: Hepatitis A Virus
HBV: Hepatitis B Virus
HCC: Hepatocellular carcinoma
HCV: Hepatitis C Virus
HCVcc: hepatitis C virus cell cuclture system
HCVpp: hepatitis C virus pseudo particles system
HDL: High-density-lipoproteins
HEK: human embryonic kidney
HIF-1α: the hypoxia-inducible factor 1α
HIV: Human Immunodeficiency Virus
HMG-CoA: β-Hydroxy β-methylglutaryl-CoA
HMGCR: 3-hydroxy-3-methylglutaryl-CoA reductase
HRP: 3,3'-diaminobenzidine peroxidase
HSCs: Hepatic Stellate Cells
HSPGs: heparan sulfate proteoglycans
HVR(s): Hypervariable region(s)

I

ICC-MS: immuno-competitive capture mass spectrometry
ICTV: International Committee on Taxonomy of Viruses
IFNα: interferon alpha
IL: interleukin
IP: immunoprecipitation
IPs: interacting partners
IPSC: induced pluripotent stem cells
IR: insulin resistance
IRES: internal ribosome entry site
IRS-1: insulin receptor substrate signaling 1

ISDR: Interferon Sensitivity Determining Region
ISG: interferon-stimulated gene
ITGB1: Integrin β1
IVDU: intravenous drug users

J

Jad: JFH1 adapted
JFH1: Japanese fulminant hepatitis strain 1

K

KEGG: Kyoto Encyclopedia of Genes and Genomes
KO: knockout

L

LB: Luria Bertani
LBR: delta(14)-sterol reductase LBR
LC-MS/MS: liquid chromatography–tandem mass spectrometry
LCS: low complexity sequence
LD(s): Lipid droplet(s)
LDL: Low-density-lipoproteins
LDLR: low-density lipoprotein receptor
LDV: Ledipasvir
lncRNAs: long noncoding RNAs
LPC: Lysophosphatidylcholine
LPE: Lysophosphatidylethanolamine
LVP(s): Lipo-viro-particle(s)

M

MAG: monoacylglycerol
MAPK: mitogen-activated protein kinase
MASLD: metabolic dysfunction-associated steatotic liver disease
MAVS: mitochondrial antiviral-signaling protein
MDA5: melanoma differentiation-associated protein 5
MICOS: mitochondrial contact site and cristae organizing system
MMPs: metalloproteinases
MNPs: multi-nucleotide polymorphisms
MR: magnetic resonance
MRI-PDFF: magnetic resonance imaging proton density fat fraction
mRNA: messenger RNA
MS: mass spectrometry
MSigDB: Molecular Signatures Database
MTP: microsomal transfer protein
MTTP: microsomal triglyceride transfer protein
MVB: multi-vesicular bodies

N

NADH: nicotinamide adenine dinucleotide hydride

NANBH: nonA, nonB hepatitis
nano-LC-MS/MS: nano liquid chromatography coupled to mass spectrometry
NAP1L1: Nucleosome Assembly Protein 1 Like 1
NAP1L4: Nucleosome Assembly Protein 1 Like 4
NCCVH: National Committee for the Control of Viral Hepatitis
NDUF: NADH dehydrogenase ubiquinone
neo: neomycin phosphotransferase gene
NF-κB: Nuclear factor kappa-light-chain-enhancer of activated B cells
NFAT5: nuclear factor of activated T cells 5
NH3: ammonia
NK: natural killer (cells)
NMR: Nuclear Magnetic Resonance
NP-40: octylphenoxypolyethoxyethanol
NPC1L1: Niemann-Pick C1-like 1
NPHV: nonprimate hepacivirus
NrHV-1, RHV-rn1: Norway rat hepacivirus 1
NrHV-2, RHV-rn2: Norway rat hepacivirus 2

O

OAA: oxaloacetate
OBV: Ombitasvir
OCLN: occludin
ORF: open reading frame
ORO: Oil-Red-O
OSBP: oxysterol-binding protein
OXPHOS: oxidative phosphorylation

P

PATL1: Protein PAT1 homolog 1
PBS-T: Dulbecco's Phosphate Buffered Saline containing 0.1% Tween-20
PC: Phosphatidylcholine
PCA: protein-fragment complementation assay
PCA: principal component analysis
PCBP1: Poly(rC)-binding protein 1
PCCB: mitochondrial propionyl-CoA carboxylase beta chain
pDC: plasmacytoid dendritic cell
PE: Phosphatidylethanolamine
PEG: polyethylene glycol
PEP: phosphoenol pyruvate
PG: Phosphatidylglycerol
PHH: primary human hepatocytes
PI: Phosphatidylinositol
PI4KIIIα, PI4KA: phosphatidylinositol 4-kinase IIIα
PI4KIIIβ, PI4KB: phosphatidylinositol 4-kinase IIIβ
PI4P: phosphatidylinositol 4-phosphate
PIB: Pibrentasvir
PKA: protein kinase A
PKR: protein kinase R
PLAs: proximity ligation assays

PLIN1: phosphorylates perilipin 1
PLIN2: phosphorylates perilipin 2
PNPLA2: patatin-like phospholipase domain-containing proteins 2
PNPLA3: patatin-like phospholipase domain-containing proteins 3
PPARGC1A: peroxisome proliferator-activated receptor gamma coactivator 1 alpha
PPARα: peroxisome proliferator-activated receptor alpha
PPARγ: peroxisome proliferator-activated receptor gamma
PREB: prolactin regulatory element-binding protein
PRR: pattern recognition receptors
PS: Phosphatidylserine
PTEN: Phosphatase and tensin homolog deleted on chromosome ten
PTT: pyruvate tolerance test
PTV/RTV: Paritaprevir/Ritonavir

R

RAF: RAF proto-oncogene serine/threonine-protein kinase
RBV: ribavirin
RDH11: Retinol dehydrogenase 11
RdRp: RNA-dependent RNA polymerase
RHV: Rodent hepacivirus
RHVcc: Rodent hepacivirus cell culture system
RIBA: recombinant immunoblot assays
RIG-I: retinoic acid-inducible gene I
ROS: reactive oxygen species
RT: reverse transcription
RT-(q)PCR, qRT-PCR: quantitative real-time PCR

S

SARS-CoV-2: severe acute respiratory syndrome coronavirus 2
SCARB1: scavenger receptor class B member 1
SCD: stearoyl-CoA desaturase
SEC14L2: SEC14-like protein 2
siRNA: short interfering RNA
SIV: Simian Immunodeficiency Virus
SM: sphingomyelin
SMV: Simeprevir
SMYD3: Histone-lysine N-methyltransferase SMYD3
SN: supernatants retrieved following binding to Strep-Tactin beads
sncRNAs: small noncoding RNAs
SNPs: single-nucleotide polymorphisms
SOCS3: suppressor of cytokine signaling 3
SOF: Sofosbuvir
SPP: Signal peptide peptidase
SR-B1: Scavenger Receptor class B type 1
SREBF2: sterol regulatory element binding transcription factor 2
SREBP1: sterol regulatory element binding protein 1
SREBP1c: sterol regulatory element binding protein-1c
ST: strep tag
STAT3: signal transducer and activator of transcription 3

SVR: sustained virological response
SWE: dynamic shear wave transient elastography

T

T2DM: type 2 diabetes mellitus
TAG: triacylglycerol
TAMRA: 6-carboxytetramethylrhodamine
TB: tuberculosis
TBK1: tank binding kinase
TCA cycle: tricarboxylic acid cycle
TCEP: tris(2-carboxyethyl)phosphine reducing agent
TCID50: 50% tissue culture infectious dose
TE: transient elastography
TEL: Telaprevir
TEV: tobacco etch virus
TG(s): triglyceride(s)
TGF-β: Transforming Growth Factor beta
TIMP(s): Tissue inhibitor(s) of metalloproteinase
TLR: Toll-like receptor
TM(s): transmembrane segment(s)
TNF-α: Tumor Necrosis Factor alpha
TRAM1: translocating chain-associated membrane protein 1
TRIF: Toll/IL-1 receptor domain-containing adapter inducing IFN-beta

U

UHTS: unbiased high-throughput sequencing
UMP-CMPK1: monophosphate-cytidine monophosphate kinase 1
UPR: unfolded protein response
UTR(s): untranslated region(s)

V

VAP: vesicle-associated membrane protein-associated protein
VAPA: vesicle-associated protein A
VAPB: vesicle-associated protein B
VEGF: Vascular endothelial growth factor
VEL: Velpatasvir
VLDL: Very-low-density-lipoproteins
VLDLR: Very-low-density-lipoprotein receptor
VOX: Voxilaprevir
VST: Variance Stabilizing Transformation

W

WHO: World Health Organization

Y

Y2H: yeast 2 hybrid

List of Figures

List of Tables

List of Supplementary Figures

List of Supplementary Tables

I. Introduction

I.A Hepacivirus genus

I.A.(α) What is a hepacivirus?

Hepacivirus is the genus of lipidated enveloped viruses with spherical virions of about 40-75nm in diameter, which are known to infect the livers of mammals[1]. Hepacivirus have evolved to infect a variety of hosts including humans[2], rodents[3], bats[4], cattle[5], boars[6], small primates[7], possums[8], shrews[9], treeshrews[10], squirrels[11], sloths[12], dogs[13]and horses[14,15]. They can also be found in nonmammalian hosts (reptiles[16], amphibians[17], birds[16,18], sharks and other fish[19,20]), as well as nonvertebrates, such as ticks[21,22] and mosquitos[23]. No geographical restriction is evident, since hepacivirus infections have been documented worldwide[24,13,9,3,16,25]. However, certain of these viruses are endemic in specific regions. In most instances, they cause acute infections accompanied by liver inflammation or hepatitis. However, this is not the same in humans, as it will be described in §I.B.(στ).

The only known human hepacivirus was also the first to be identified in 1989[26]: the hepatitis C virus (HCV). HCV has been studied widely, and our knowledge on the hepacivirus genus comes almost exclusively from studies of this virus. Therefore, the extent and limitations of shared attributes between HCV and the nonhuman hepaciviruses are still not fully uncovered, especially with respect to pathology, possible virus recombination, immune evasion, evolutionary dynamics and rate of infection.

Although HCV was the first hepacivirus to be discovered, it was not the first to emerge and is hypothesized that it has a zoonotic origin of millions of years ago[27,28]. The foundation of this SIV/HIV (Simian Immunodeficiency Virus/Human Immunodeficiency Virus) reminiscing hypothesis lies on the geographical circulation of HCV in areas co-populated by Old World monkeys, humans, and apes. Convincing evidence to this remark is still missing, but the identification of the huge animal reservoir of hepacivirus and the study of the genetic distances and evolution among them may provide a definite answer. For the moment, multiple evidence of hepacivirus crossing over species[25] and even orders[27,12] favour the hypothesis of HCV originating from an animal hepacivirus.

I.A.(β) Classification and genetic variability

Hepacivirus are a member of the group IV in the Baltimore Classification system, with their genome consisting of a single positive-strand RNA molecule of about 10kb that encodes the structural and nonstructural viral proteins in a polyprotein format. Hepacivirus classification and evolution has been studied based on the differences found in their coding sequences, attributing them the following lineage: Riboviria; Orthornavirae; Kitrinoviricota; Flasuviricetes; Amarillovirales; Flaviviridae.

Table 1: Hepacivirus species recognized by ICTV and their natural host range.

Hepacivirus species	Natural host
Hepacivirus bovis	Cattle
Hepacivirus colobi	Non-human primate
Hepacivirus equi	Horse & Dog
Hepacivirus glareoli	Rodent
Hepacivirus hominis	Human
Hepacivirus macronycteridis	Bat
Hepacivirus myodae	Rodent
Hepacivirus norvegici	Rodent
Hepacivirus otomopis	Bat
Hepacivirus peromysci	Rodent
Hepacivirus patyrrhini	Non-human primate
Hepacivirus ratti	Rodent
Hepacivirus rabdomysis	Rodent
Hepacivirus vittatae	Bat

Although hepaciviruses were only discovered in the past thirty-five years, their emergence is suggested to have happened millions of years ago, resulting to their high diversity and variety of species[28,10].

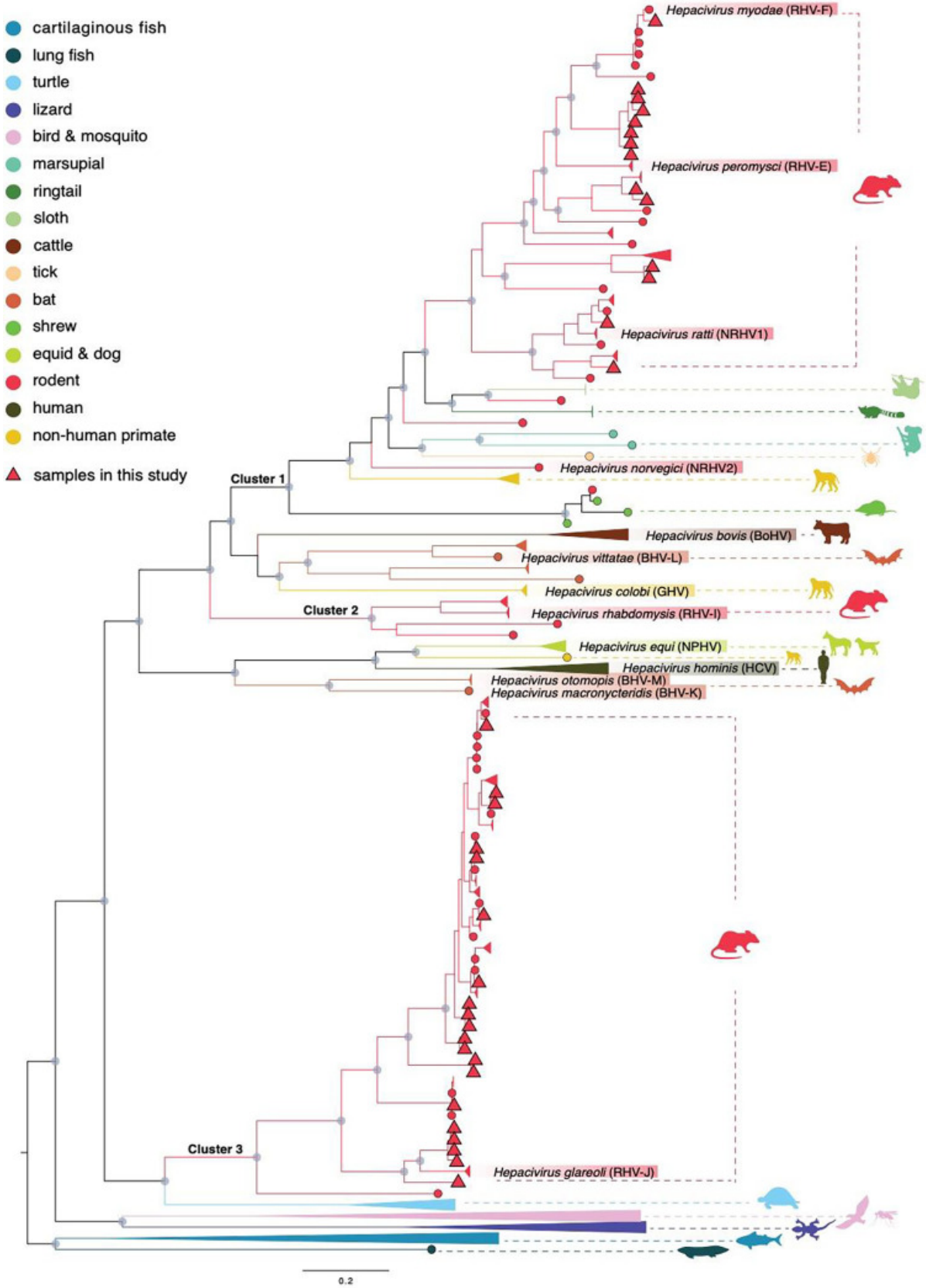

Figure 1: Up-to-date phylogenetic tree of Hepacivirus genus based on complete genomes by Li et al.[29], 2023.

The figure was used according to and is protected by Creative Commons Attribution-NonCommercial-NoDerivatives 4.0 International License (CC BY-NC-ND 4.0).

The species recognised by the International Committee on Taxonomy of Viruses (ICTV) and their respective natural hosts are summarized in Table 1. According to this, a single species is recognized to be infecting cattle, equine, canine, and human hosts, two species nonhuman primates, three species bats and six species rodents, while it becomes evident that a wide variety of hosts described in the previous paragraphs is missing from this list. In fact, there is an ever-growing number of nonclassified hepaciviruses, probably due to the increased discovery rate of the past years, thanks to the scientific advancements and the expanding interest in identifying surrogate animal models for HCV.

The most recent phylogenetic tree of the Hepacivirus genus has been constructed by Li et al.[29], as shown in Figure 1. The authors have respected the most recent ICTV classification, hence the tree branches of identified hepaciviruses without official nomenclature. Some interesting information arising from the clustering and proposed evolution of these viruses include the close proximity of HCV (Hepacivirus hominis) with the species infecting horses and dogs (Hepacivirus equi). Furthermore, in accordance with previous findings[4,25], the uppermost observed genetic heterogeneity across species of bat and rodent hepaciviruses tentatively renders them a highly probable initial source of transmission among mammals[27]. However, this might simply be due to greater search in these small animal populations that are more readily accessible. Lastly, the phylogenetically most distant viruses are the nonclassified hepacivirus infecting the genetically most distant hosts, the poikilotherms, indicating that they have co-evolved with their hosts. The evolution of hepaciviruses thus seems to have followed the evolution of life.

I.B Hepatitis C Virus

I.B.(α) Hepatitis C history

Hepatitis is the medical term describing liver inflammation, often caused by viral infection. The history of human hepatitis goes back to the ancient times, with first references of a similar disease called “epidemic jaundice” being written by Hippocrates. However, the first report of hepatitis being caused by a pathogen was made in 1963, with the identification of the Australia antigen, the envelope of hepatitis B virus (HBV) [30,31]. HBV infection results in chronic hepatitis with severe manifestation in the liver. A decade later, the causative agent of an acute hepatitis, the hepatitis A virus (HAV), was first seen under the microscope[32]. One of the great differences between HAV and HBV is the method of transmission: HAV is transmitted through infected sources of water and food, while HBV is a bloodborne virus, transmitted through infected blood and its byproducts.

Following the discovery of HBV, blood screening begun, in order to eliminate the transmission of the pathogen through transfusion. However, over the following years, a high percentage of blood recipients continued to develop hepatitis. In order to exclude the probability of the blood being infected despite the screening, Dr Harvey J. Alter and his colleagues tested the blood for the presence of the Australia antigen and for cross-reactivity with HBV and HAV antibodies. In 1975, they reported receiving only negative results, giving rise to the nonA, nonB hepatitis (NANBH)[33]. In 1978, Dr Harvey J. Alter further inoculated chimpanzees with plasma or serum from patients with NANBH and observed that they developed hepatitis, concluding that NANBH is caused by a transmissible agent[34].

This agent was isolated and identified in 1989 by Dr Michael Houghton and his colleagues, in a clone of a cDNA library generated from the plasma of chimpanzees presenting NANBH, that cross-reacted with the serum of NANBH positive patients. This new agent was named hepatitis C virus and the NANBH was then called hepatitis C[26]. Towards keeping the blood supply clean from both HBV and HCV and in order to be able to identify HCV carriers, Dr Houghton and his colleagues also developed a diagnostic test against HCV in 1989[35].

Further significant advancements in the HCV research were made in 1997 by Dr Charles M. Rice, who, using molecular biology, achieved to clone a genome-length cDNA and recapitulated the virus life cycle following intrahepatic inoculation of cDNA-derived, synthetic RNAs, that caused chronic infection and similar manifestations in the chimpanzee study model, as those observed in humans[36].

However, despite the attempts to control its transmission, HCV infection remains today one of the main causes of chronic hepatitis worldwide. Chronic hepatitis C is a silent disease, that takes years to manifest its symptoms, allowing the carriers to unknowingly spread the virus. With World Health Organization (WHO) most recent report accounting for 57.8 million infections worldwide attributed to 0.8% of Earth's population, and over 280.000 annual deaths[37], chronic hepatitis C is a major global health problem. Due to this, the discoveries and advancements made by Drs Alter, Houghton and Rice, rightfully earned them the 2020 Nobel in Physiology or Medicine. It is, though, unfortunate that the tremendous contribution of Dr Ralf Bartenschlager in the development of HCV cell culture study systems was not equally recognized, since highly efficient HCV therapy could not have been available today without the efforts of him and his team in Germany.

Selected milestones of the HCV history, as will be presented in the following paragraphs, are illustrated in Figure 25, page - 48 -.

I.B.(β) Transmission and prevention

Like HBV, HCV is mainly transmitted parenterally, meaning through contact with infected blood. Hence, one mode of transmission is through untested blood transfusion, or unsafe medical procedures, occurring mainly in underdeveloped countries. Nowadays, injected drug use if considered to be the most common way of contracting HCV[38]. Although less documented, incidences of infection through sexual intercourse, during cosmetic procedures that may lead to exposed blood (e.g. tattooing, shaving at a barber's shop), after medical personnel's interaction with infected material have also been reported[39]. Transmission from infected mother to infant during labor is also rare, but has been associated to the mother's viral load, while the risk is doubled in mothers co-infected with HCV and HIV[40,41].

Though reduced, compared to the global prevalence of the past years, the HCV burden is not alleviated, with a multitude of individuals either remaining chronically infected, or becoming infected every day. Since 2016, the WHO has adopted an HCV elimination strategy, aiming at reducing HCV incidence by 80% and HCV-induced mortality by 65% by the year 2030. This goal implies the adoption of both national and international policies and collaboration among decision makers, health care providers, scientists, and pharmaceutical companies.

In the absence of an HCV prophylactic vaccine, prevention relies solely on elimination of exposure. This can be achieved by thorough testing of donated blood for HCV and other pathogens, the sterilization of the equipment used in any medical, dental, or cosmetic intervention that could involve blood, and the appropriate training of personnel conducting it, as well as by managing the spread among the groups of intravenous drug users (IVDU). However, harm reduction is not the only way to achieve exposure management. An increase in testing, in order to identify the unaware infected individuals, and access to the available therapy (see § I.B.(ζ)) would help towards reduction of the infected population, hence the pool of the virus[42].

Implementation of the WHO strategy has helped decrease the overall number of global active HCV infections, when compared to before the WHO strategy. However, modelling studies indicate that the reduction rate observed is not sufficient to achieve the WHO goal by 2030, with some western countries not reaching this target before 2050 and several underdeveloped countries possibly never succeeding in this endeavor[43,44].

I.B.(γ) Virus particle organization, genome, and proteins

I.B.γ.(i) HCV virion and structural proteins

HCV particles are comprised of the viral genome, enclosed in a nucleocapsid of no apparent symmetry, formed by the capsid protein, or Core, surrounded by a phospholipid envelope, in which the viral glycoproteins, E1 and E2, neutral lipids (cholesterol esters and triglycerides), and cellular apolipoproteins (ApoB, ApoC, ApoE, ApoM) are embedded[45-47] (Figure 2). HCV virions are spherical, highly heterogenous particles, depending on their association or not with lipoproteins or immunoglobulins[48]. The association of HCV with different cellular lipoproteins of diverse densities, such as low-density-lipoproteins (LDL), very-low-density-lipoproteins (VLDL) has resulted into HCV particles of a wide range of sizes (40-100nm in diameter[49]), buoyant densities and associated components[50]. This heterogenous population of HCV particles has been observed in both infected cell cultures and in patient sera by electron tomography, cryo-electron microscopy, or transmission electron microscopy[51,47,52], and is considered to affect HCV infectivity. Particles related to lipoproteins (lipo-viro-particles, LVPs) are more infectious and constitute the majority of blood-circulating virions[53]. Moreover, LVP immunogenicity is reduced, due to their resemblance to cellular circulating lipoproteins, and due to the decreased accessibility of anti-E2 antibodies.

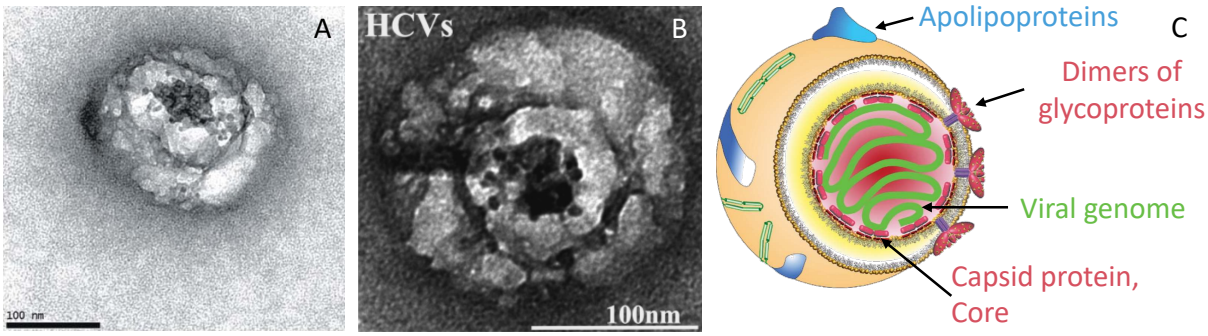

Figure 2: Structural organization of the HCV particle.
(A, B) Representative electron micrographs of particles immunocaptured with anti-E2 monoclonal antibody AR3A from the serum of an HCV-infected patient (A-B). Photos reproduced from Piver et al., 2017[52] with permission from BMJ Publishing Group Ltd (License No 5612391449360). (C) The theoretical model of the lipoviroparticle illustrating the similarities in structure and composition with serum lipoproteins. The surface glycoproteins E1 and E2, the apolipoproteins (ApoB, ApoC, ApoE) and the nucleocapsid composed of Core and viral RNA are shown. Adapted with permission from Lavie et al., 2015[54].

E1 and E2

Each viral envelope glycoprotein E1 and E2 consists of an amino-terminal protruding region, a transmembrane domain and a carboxyl-terminal hydrophobic region, features that in E2 are separated by an amphipathic stem helix, amounting to their computed molecular weight of 31 kDa for E1 and 70 kDa for E2[55]. Both glycoproteins are highly glycosylated, with 4-5 N-glycosylation sites in E1 and 9-11 sites found in E2, depending on the viral genotype and/or strain (for genotypes see §I.B.δ.(ii)). Glycosylation not only protects E1 and E2 from humoral immune recognition and neutralization[56], but also ensures the proper folding of the proteins, together with the disulfide bonds created by the cysteine residues present in their ectodomains[57].

Of note, there are three hypervariable regions (HVR1, HVR2 and IgVR)[58], differing up to 80% among HCV genotypes (see §I.B.δ.(ii)), within the N-terminus of E2 with dual roles[59]. First, as exposed E2 represents an immunogenic target, HVR1, HVR2 and IgVR can function as "decoys" and hide the most conserved regions from the host immune cells, in order to protect

the virus against neutralizing antibodies. Second, HVR1 is essential for recognition and attachment to the host target-cell. Despite the lack of conservation in the exact residue sequence of HVR1, the charge of the residues in certain positions and the overall conformation are maintained[60]. Entry in the host-cell is thought to be the result of coordinated action between E2 recognition and binding to cell receptors and E1-mediated fusion with the endosomal membrane[61], as further described in §I.B.(δ).

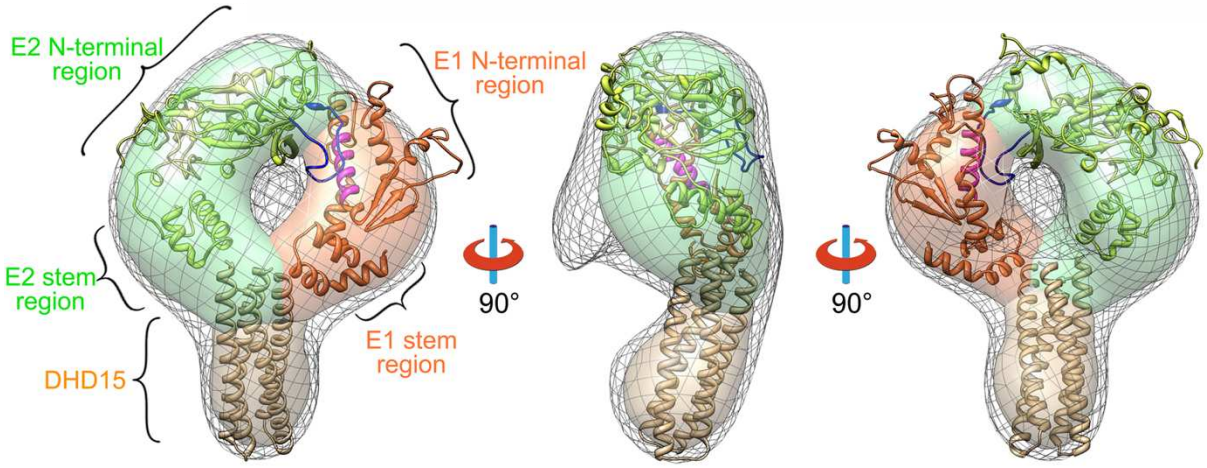

Figure 3: The structural model and 3D electron microscopy (EM) reconstruction of HCV E1E2 heterodimer.
A pair of de novo designed helical hairpins (DHD15, PDB entry: 6DMA) was used to replace the transmembrane domains of E1 and E2 in order to maximize the yield of E1E2 heterodimer. Three views at different angles of the coevolution-based E1E2-DH15 structural model (low-density contour: grey mesh; high-density contour: surface) fitted into the EM reconstruction are shown. The solved structures of E2 (PDB entry: 4MWF, green), E1 (PDB entry: 4UOI, orange), and DHD15 (brown) are plotted against the EM density, revealing that a significant fraction of E1 and E2 are missing in the known crystal structures. In the high-density contour, the densities corresponding to E2, E1, and DHD15 are colored green, orange, and brown, respectively. The structural model depicts E2 hypervariable region 2 (HVR2, blue) and E1 probable fusion peptide (magenta). Figure from Cao et al., 2019[62], with Creative Commons Attribution 4.0 International License (CC BY 4.0).

To shape the viral envelope, E1 and E2 are arranged in heterodimers through their transmembrane domains. A resolved 3D structure of the E1-E2 dimers is only available through computational reconstruction of or in complex with neutralizing antibodies (Figure 3). Furthermore, according to computational prediction modelling, the E1-E2 dimers may form trimers (trimers of dimers)[63], which are stabilized by disulphide bonds, and finally adopt a conformation of twelve pentamers of trimers of dimers[64].

Core

In contrast, the 3D arrangement of Core homo-oligomers is not yet resolved. The only available nuclear magnetic resonance (NMR) data come from a partial region, with Core still in complex with E1, revealing the mechanism of Core maturation through cleavage by the cellular signal peptide peptidase (SPP)[65]. Immature Core protein, localized at the ER, consists of 191 amino acid residues (aa), and requires a cleavage of its carboxyl-terminus in order to produce its mature, active form of 173-179 residues and 21 kDa[66]. Mature Core can be found on the surface of cytosolic lipid droplets (LDs), an association essential for viral replication and HCV particle assembly[45], as illustrated in §I.B.(ε).

Core is composed of two principal (D1, D2) and a provisional (D3) domains (Figure 4) and its amino acid sequence is highly preserved across HCV genotypes[67]. RNA binding and oligomerization capacity of Core lie within its N-terminal D1 domain, a flexible hydrophilic domain, further divided in three arginine-, lysine-, glycine- and proline-rich basic subdomains[68,69]. D1 is also essential for the mediation of Core-host interactions, as described in §I.B.θ.(ii). D2 contains residues 118-177, forms two amphipathic α-helices separated by a highly hydrophobic loop and is responsible for Core association to LDs. More specifically, aa 138-169 are essential for Core localization at LD surface[70]. Lastly, D3 is formed by the 20 C-terminal residues of the protein, which are responsible for its retention to the ER. This region contains a sequence recognized and cleaved by SPP, allowing the maturation of Core[71].

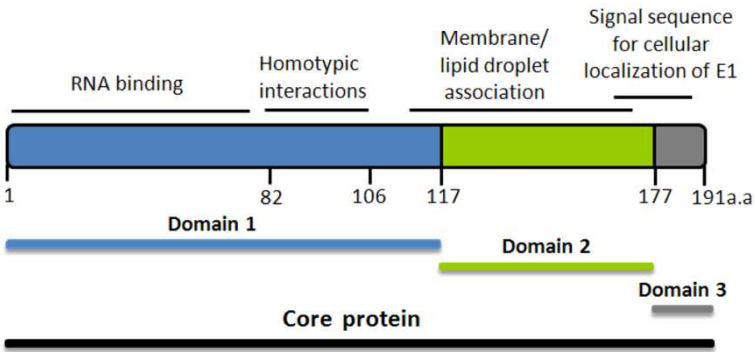

Figure 4: HCV Core protein structural domains.
Figure from Strosberg et al., 2010[72], with Creative Commons Attribution 3.0 Unported License (CC BY 3.0).

I.B.γ.(ii)HCV genome

HCV genome (see Figure 5 & Figure 6), similar to that of the other species of the Hepacivirus genus, consists of a positive single stranded RNA of approximately 9.6kb. The viral genome serves not only as a messenger RNA (mRNA) for the translation of all the viral proteins, but also as a matrix for the production of multiple copies of itself, during viral replication. Furthermore, one copy of the genome is allocated per virus particle, during HCV assembly. Due to its critical roles, the protection of the viral genome is of utmost importance and RNA viruses have developed strategies to protect and mask their genetic material, such as 5'-capping. No such tactic was uncovered for HCV, until the publication of Sherwood et al.[73], this year, demonstrating that in ~75% of HCV RNA the 5'end of the genome consists of a redox-active coenzyme, the flavin adenine dinucleotide (FAD), resulting in 5'-FAD capping! Importantly, the 5'-FAD cap was conserved across genotypes, was also identified *in vivo,* and was shown to inhibit HCV recognition by the innate immunity pathway of the retinoic acid-inducible gene I (RIG-I).

The coding sequences of the genome (open reading frame, ORF) are framed by the 5'- and 3'- untranslated regions (UTRs), which form secondary structures and are essential for virus replication and/or assembly.

The 5'-UTR is a well conserved sequence of ~340 nucleotides forming four stem-loops (I-IV)[45]. HCV genome replication and translation is dependent on regulatory elements found in this region. Parts of stems I and II form a pseudoknot[74], while stems II-IV and the first 30 nucleotides coding the capsid protein shape a type III internal ribosome entry site (IRES)[75]. The IRES allows the docking of the small ribosomal subunit (40S) and is crucial for the initiation of viral RNA translation[76]. Two binding sites of miR-122, a micro-RNA expressed exclusively in the liver[77], have been identified adjoining stem I and below stem II. Whether one of the two annealing positions is more significant than the other is still debated[78-82], however miR-22 binding to both positions is essential for HCV RNA stability, promotion of replication and translation. Additional annealing sites of miR-122 in NS5B and in the 3'-UTR have been reported, although their relevance is still under investigation[83]. Overall, the significance of miR-122 in HCV replication and translation, taken together with the liver specificity of the microRNA, could justify the strict hepatotropism of the virus.

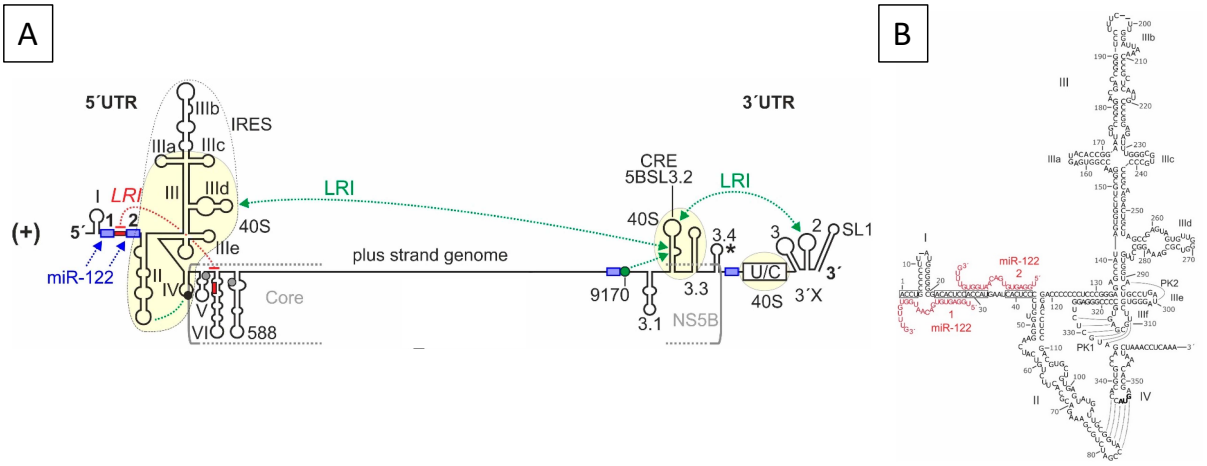

Figure 5: Structure of the HCV UTRs and cis-acting replication elements (CRE) that are involved in the regulation of genome translation and replication.
Regions of the 5'-UTR, 3'-UTR, and CRE that bind to the ribosomal 40S subunit are highlighted in light yellow. Stem-loops (SLs) in the 5'UTR are numbered by roman numerals. The IRES includes SLs II–IV of the 5'UTR but also spans into the Core coding region. The canonical AUG start codon in SL IV of the 5'UTR is illustrated by a black dot. The 3'UTR contains the variable region, a poly(U/C) tract (U/C), and the so-called 3'X region including SLs 1, 2, and 3. The SL 5BSL3.2 in the 3'-region of the NS5B coding region is a CRE, flanked by upstream SL 5BSL3.1 and downstream 5BSL3.3. The polyprotein stop codon is located in the SL 5BSL3.4 indicated by an asterisk. Alternative reading frame start codons are shown in grey dots. Positively and negatively acting long-range RNA–RNA interactions (LRIs) are shown in green or red arrows, respectively. Selected binding sites for miR-122 are shown in blue. Binding of miR-122 within the 5'-UTR is also illustrated together with the sequence and canonical RNA secondary structure of the HCV IRES in (B). The sequence shown is from genotype 2a (J6 isolate). Length variations among HCV isolates are indicated by short horizontal dashes at nucleotide positions within Core and NS5B sequences. Figure adapted from Niepmann et al., 2020[75], protected by Creative Commons Attribution License.

The 3'-UTR is shorter than the 5'-UTR by approximately 100 nucleotides and is composed of three distinct domains. A low-conservation sequence of 40 nucleotides is situated directly downstream of the ORF, followed by a pyrimidine-rich sequence of about 90 nucleotides (poly-U/C) and a highly conserved sequence of 98 nucleotides, forming the 3' X-tail[84]. Similar to the 5'-UTR, the first domains of the 3'-UTR have been found to enhance the IRES-mediated translation[85], while the second of the three stem-loop structures within the 3'X-tail has been found to promote genome replication *in cis* through interaction with the loop 5B-SL3.2 present in the coding sequence of the HCV RNA-dependent RNA polymerase, NS5B[86].

I.B.γ.(iii) HCV nonstructural proteins

Translation of the viral genome through the IRES within the 5'-UTR generates a polyprotein of ~3000 aa residues. The polyprotein is proteolytically cleaved simultaneously with or directly after the translation[87], leading to the formation of three structural (Core, E1, E2) and seven nonstructural (p7, NS2-NS5B) proteins. The structural proteins and the p7 oligopeptide are cleaved by cellular signal peptidases, while the rest of the nonstructural proteins are cleaved by the two virus-encoded proteases, NS2 or NS3/4A, as described in the paragraphs of the virus life cycle (I.B.(δ)). The existence of an alternative ORF, overlapping with the core coding sequence at the frame +1, has been reported following computer-assisted analysis of the HCV genome[88]. This ORF may code for an accessory HCV protein, the alternative reading frame protein (ARFP), frameshift (F) or Core+1[89]. Despite the reports of

anti-Core+1 antibodies present in patient sera[90,91], the expression of the protein itself has yet to be verified in patients or in infected cells, allowing for scientific controversy in the field[92].

The structural proteins, as described in §I.B.γ.(i), constitute the HCV virus particles. Heterodimers of E1 and E2 are embedded into the HCV virion envelope, while the capsid protein, Core, forges the viral capsid, in which the viral genome is insulated.

The nonstructural proteins are responsible for carrying out the various steps of the HCV life cycle. Many of these proteins are involved in multiple viral processes, a multi-functionality that can by favoured by either frequent conformational changes or by alterations in the cellular microenvironment, involving a specific network of interactions with other viral and cellular partners, as described in §I.B.(θ).

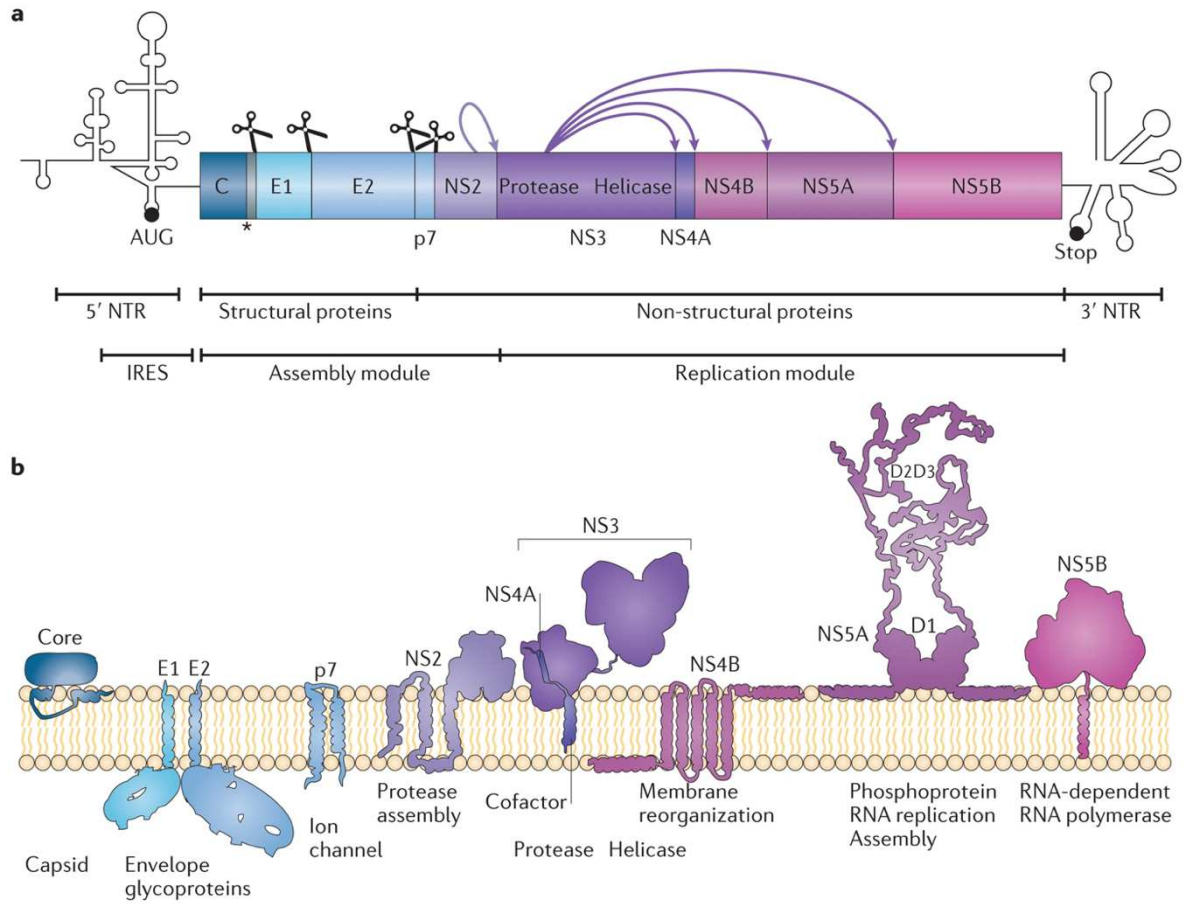

Figure 6: The HCV genome (a) and encoded proteins function and topology with respect to membrane bilayer (b).

(a) The ORF of HCV is illustrated between the predicted secondary structures of 5'- and 3'-UTRs, also called nontranslated regions (NTRs). Start and stop codons of the ORF are indicated by black bullets. Cleavage sites of cellular signal peptidases are indicated by scissors at the corresponding ORF position, while the cleavage removing the carboxy-terminal region of the Core, required for protein maturation, mediated by cellular signal peptide peptidase, is indicated by an asterisk. Arrows illustrate cleavage sites of the viral protease. (b) The key roles and membrane topologies of the HCV polyprotein cleavage products are shown. Each HCV protein is connected to ER membranes by at least one transmembrane segment or, in the case of Core and NS5A, by amphipathic α-helices. NS3 binds to membranes through a short α-helix and through its cofactor, NS4A, which intercalates into the NS3 amino-terminal protease domain. Only NS5A is represented as a dimer, although the vast majority, if not all, of HCV proteins form homo- or heterodimers. Figure reproduced from Bartenschlager et al., 2013[93], with permission from Springer Nature (License No 5633130933991).

Protein p7

P7 is a small polypeptide of 63 aa residues, localized in the endoplasmic reticulum (ER). P7 is a viroporin, consisting of two transmembrane α-helices connected by a cytoplasmic loop. It serves as an ion channel upon oligomerization (hexamer or heptamer) and the regions forming the channel are highly conserved across genotypes)[94]. A graphical representation of models from NMR examination of the ion channel created by p7 of genotypes 1a, 1b and 5 can be found in Figure 7. This protein is essential for the assembly and release of infectious HCV particles[95] and can induce cellular immune responses[96].

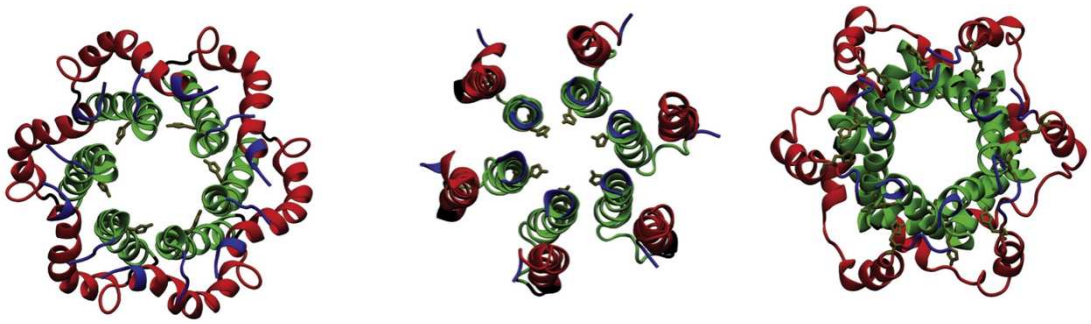

Figure 7: Representation of p7 viroporin models of GT1a, 1b, or 5a (from left to right) from NMR. *Differences in conformation of p7 monomers forming the ion channel based on the genotypic origin of the protein are shown. Reprinted from Kalita et al., 2015[97], with permission from Elsevier (Licence No: 5612020870723).*

NS2

Nonstructural protein 2 (NS2) is a transmembrane protein of 217 aa residues and estimated molecular weight of 23 kDa. NS2 amino-terminus has 3 predicted transmembrane passages and a protruding end within the ER, while the C-terminal catalytic domain (aa 94–217) has cytosolic localization and forms a dimeric cysteine protease with two composite active sites (Figure 8). NS2 3D atomic structure was obtained by X-ray crystallography in 2006[98].

NS2 role during the virus life cycle is to self-cleave from the polyprotein at the NS2/NS3 junction and to promote the assembly of viral particles[99].

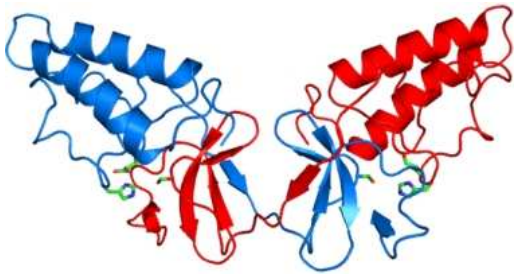

Figure 8: Crystal Structure of the dimeric NS2 Protease Domain.
Monomers are in blue and red, respectively. Side chains of the residues contributing the two protease catalytic triads are shown. Reprint from Lorenz, 2010[100]. Creative Commons Attribution License.

NS3

NS3 is a multifunctional protein of 631 aa residues with a predicted molecular weight of 70 kDa. NS3 has two distinct domains, with two distinct roles: the N-terminal serine protease domain (aa 1–180) and the NTPase/RNA helicase domain in its C-terminal two-thirds (aa 181–631). Those NS3 activities are crucial for the processing of the polyprotein, viral genome replication and HCV assembly[101].

To form the active HCV protease, carrying out the cleavage of the peptide bonds between NS3/NS4A (autoregulation), NS4A/NS4B, NS4B/NS5A and NS5A/NS5B[55], NS3 creates a noncovalent complex with its co-factor, NS4A. The amino-terminal transmembrane segment of NS4A, together with NS3 N-terminal α-helix are responsible for the complex' association to ER membranes, as shown in Figure 9. NS3 protease fold resembles that of chymotrypsin, with with two β-barrel subdomains and a zinc (Zn^{2+}) binding site. The latter is essential for the

stabilization of the structure and for the NS2/NS3 processing by NS2[102]. The protease catalytic triad consists of His 57, Asp 81 and Ser 139 and NS3/4A substrates are composed of an acidic residue at P6 position, a cysteine or threonine at P1 and a small side chain amino acid at the P1´. However, cellular substrates of the protease do not always bear the consensus recognition site of the enzyme, while a plethora of host proteins with the exact consensus cleavage pattern are not cleaved by NS3/4A, indicating that additional parameters are required for determination of NS3/4A substrate specificity. Such substrates include the cellular Toll/IL-1 receptor domain-containing adapter inducing IFN-beta (TRIF) and mitochondrial antiviral-signaling protein (MAVS), which are necessary for natural innate immune responses[101] (see I.B.θ.(i)).

The NS3 helicase contains 3 subdomains and is a member of the DExH/D-box group of the helicase superfamily 2. Its role is to unwind double-stranded or single-stranded RNA regions with extensive secondary structure, while hydrolyzing ATP. The exact function(s) of NS3 helicase remains elusive, yet it is known to be vital for HCV genome replication and assembly[103]. Reverse genetic analysis of NS3 surface residues have correlated alteration of conserved NS3 aa residues with decreased NS5A hyperphosphorylation (see below), genome replication and virion assembly, indicating that NS3 participates in the regulation of the HCV life cycle and its different steps[104,105]. A recent study further showed that the ATP-binding domain of the NS3 helicase is required for NS5A sequential phosphorylation, probably by recruiting casein kinase Ia (CKIa)[106].

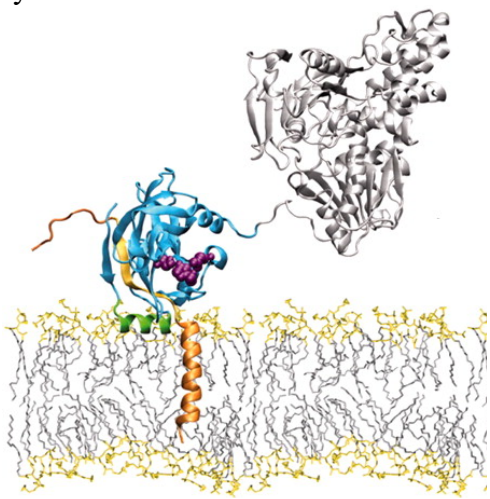

Figure 9: NS3/4A protease structural model and topology.
The cytosolic side of the membrane bilayer is illustrated on the top. Green represents the N-terminal α-helix of NS3 (amino acids 13–23), cyan represents the serine protease domain, while the side-chain atoms of the catalytic triad (His 57, Asp 81, and Ser 139) are highlighted in magenta. Co-factor NS4A is shown in yellow/orange. Adapted from Brass et al.,2008[107] with permission from PNAS. Copyright 2008 National Academy of Sciences, USA.

NS4A

NS4A is a small protein (54 aa), which in spite of its length has multiple functions. As a co-factor of NS3, NS4A central portion (aa 21-32) is necessary for NS3 proper folding, while its N-terminal α-helix (aa 1-21) ensures integral membrane association of the NS3/4A protease. NS4A is also responsible for the regulation of NS5A hyperphosphorylation (see below) and can have an effect on HCV replication and assembly through its carboxyl-terminal portion (aa 40-54)[108,109,101].

NS4B

NS4B is a hydrophobic protein of 27kDa and 261 aa in length. NS4B structure, as shown in Figure 10A, is composed of an N-terminal domain of ~70aa forming two consecutive α-helices (AH1 and AH2), a middle potion of ~120aa with 4 transmembrane segments (TMs), and a C-terminal domain (~70aa) similar to amino-terminus, with two α-helices (H1 and H2)[110].

NS4B has been found to induce the formation of the membranous web[111], the site of HCV RNA replication (see §I.B.ε.(iii)) and to interact with other viral nonstructural proteins and RNA[112], highlighting its role in HCV replicase. The N-terminus of NS4B may adopt two different topologies, either a cytosolic, or an ER luminal. Its orientation has been found to be

affected by the expression of other viral proteins, especially NS5A, proposing a dynamic, protein-protein-interaction-dependent topology of NS4B AH1 and AH2[113]. NS4B has further been reported to oligomerize, alterations of which are inhibiting membranous web formation and viral genome replication[114,115], while it is also important for HCV particle assembly[116].

Apart from the virus life cycle, NS4B may also favor HCV immune evasion by interaction with STING protein, further hindering the interaction of STING with Cardif, therefore suppressing the RIG-I induced IFN-b pathway[117].

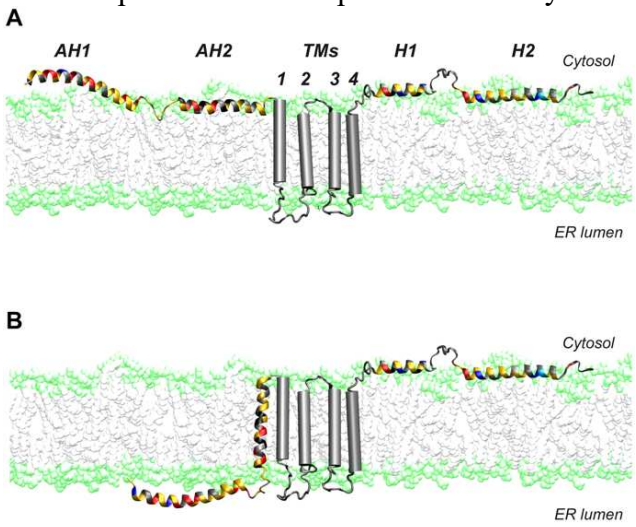

Figure 10: HCV NS4B N-terminus has dual topology. Illustrations of the (A) cytosolic and the (B) ER membrane topology.
The predicted transmembrane segments (TMs) of the protein are shown as grey cylinders. Figure reprinted from Gouttenoire, 2014[110]. Creative Commons Attribution License.

NS5A

NS5A is a membrane-associated protein of ~460 aa residues, with an N-terminal amphipathic α-helix (AH), three domains (DI-DIII), and two intermediate low complexity sequences (LCSI and LCSII) (for review, Ross-Thriepland & Harris, 2015[118]). Via its AH, NS5A is predominantly embedded in the cytosolic leaflet of the ER or ER-derived membranes. NS5A has no known enzymatic activity, but has been found to be involved in several steps of the virus life cycle, rendering it a perfect example of viral genetic economy.

Functional NS5A is a homodimer generated by the interaction of their DI domains, the most conserved region of NS5A across genotypes, whose crystal structure was first resolved in 2005[119]. DI has the ability to bind RNA and, in this original structural model reported, an RNA binding groove was formed at the interface of the DI monomers[120]. However in a NS5A crystal structure solved later, the previously hypothesized RNA binding residues were located within two flat surfaces that were further apart[121]. NS5A RNA binding capacity is actually not restricted *in vitro* to DI and the essentially disordered DII and DIII have also been reported to bind RNA[122]. NS5A DI is involved in virus replication and can induce re-arrangements of the ER membrane to form the HCV replication factories (see I.B.ε.(iii))[123,124]. The reported existence of different NS5A DI dimer conformations is suggestive of distinct NS5A roles during HCV life cycle, an attribute further supported by the proposed mechanisms of action of NS5A-targeted therapeutic small molecules (see I.B.ζ.(ii)).

DII is largely dispensable for HCV replication, although specific residues in its C-terminus are essential for this process[125,126]. NS5A was found to interact with Cyclophilin A (CypA), which catalyses the cis/trans isomerization of peptidyl-prolyl bonds within domain II of NS5A (P319 for subtype 1b and P315 for type 2a), stimulating NS5A binding to the 3'UTR of HCV genome[127]. NMR experiments have revealed that CypA may influence HCV genome replication efficiency by fine-tuning the dynamic ensemble of the disordered DII[128], while also revealing evidence of three α-helices formation near the NS5A carboxyl-terminus, when expressed together with the low complexity sequences[129]. DII also contains a 39-residue region called Interferon Sensitivity Determining Region (ISDR), which is considered to suppress the activation of cellular protein kinase R (PKR), conferring interferon-resistance to HCV[130]. Intriguingly, the most conserved region of DII among the most well-studied HCV subtypes 1b and 2a is also located at its C-terminal part. However, despite the high conservation, mutational analysis of these amino acids revealed different phenotypes for these viruses, possibly

reflecting differential protein–protein interactions of NS5A proteins of this genotypic origin with factors involved in the virus life cycle[131,132].

NS5A LCSII of all genotypes contains a PxxPxR motif, allowing the protein to interact with cellular Src homology 3 (SH3)-domain-containing proteins, such as amphiphysin II (BINI). Amino acid substitutions within this motif abolished PxxPxR/SH3 interactions in a subgenomic replicon system[133], and were found to have no effect on genome replication or virion assembly, while they inhibited the activation of a pro-apoptotic potassium channel (Kv2.1) in response to oxidative stress, highlighting a putative role of NS5A in establishing viral persistence[134].

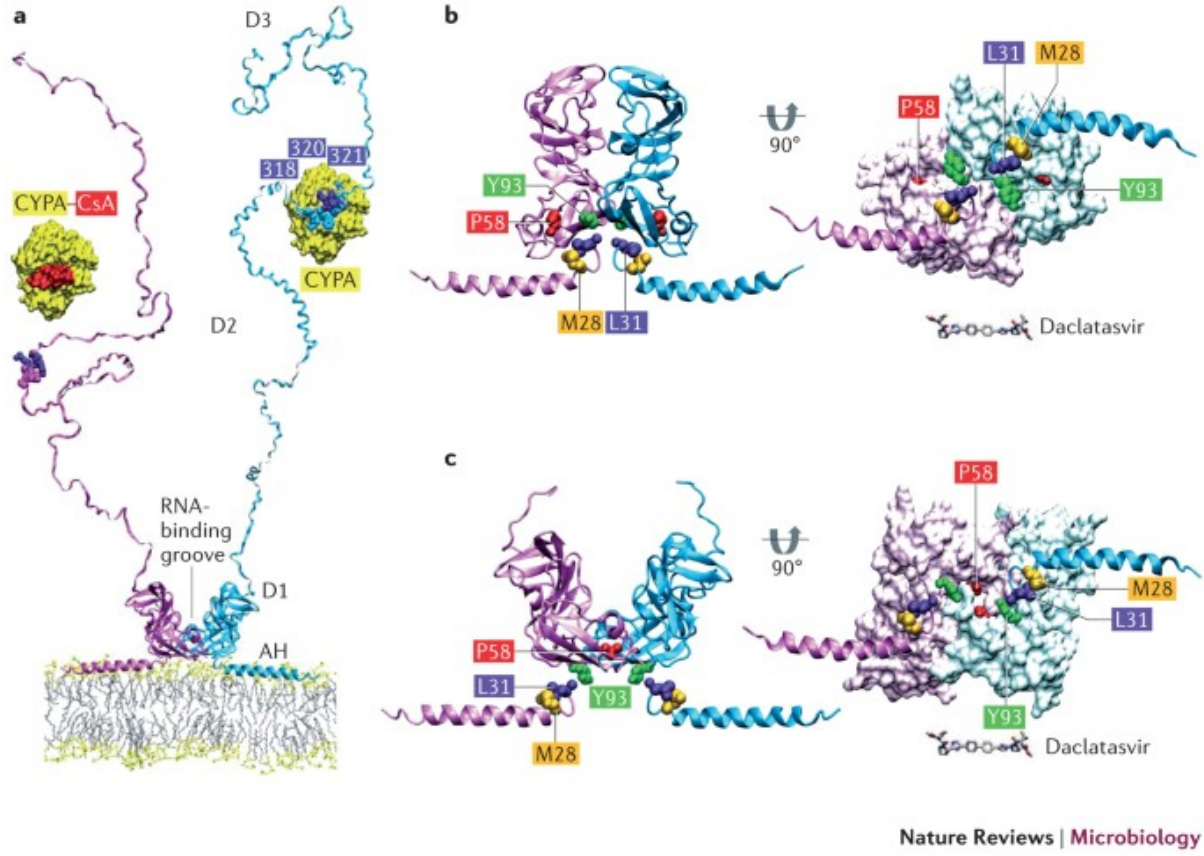

Figure 11: Illustration of the full-length NS5A dimer associated with a phospholipid membrane and a more detailed representation of the NS5A DI dimer structure according to data published in Love et al., 2009[121] (PDB accession 3FQQ) (b) and in Tellinghuisen et al., 2005[120].

Each monomer (lilac or cyan) consists of the N-terminal amphipathic α-helix (AH; Protein Data Bank (PDB) accession 1R7E), the highly structured domain 1 (DI; PDB accession 1ZH1) — which is shown in position relative to a 1-palmitoyl-2-oleoyl-3-sn-glycero-3-phospholcholine membrane bilayer, according to data published in Tellinghuisen et al., 2005 [120]— and the intrinsically unfolded DII and DIII. A surface representation of cyclophilin A (CypA) in complex with cyclosporin A (CsA) is shown on the upper left (PDB accession 1CWA), while a putative structure for CypA and its main binding site in NS5A DII is shown on the upper right. (a) The left images of panels b and c illustrate side views, and the right images show views of the putative membrane-interacting surface of DI homodimers. The respective positions of mutations conferring resistance to NS5A inhibitors are shown. Mutation of Pro58 has been associated with secondary daclatasvir resistance, but does not confer resistance by itself[135]; this residue is shown to distinguish the alternative monomer orientations in the different homodimer structures. The structure of the NS5A targeting antiviral daclatasvir (see I.B.ζ.(ii)), shown by stick representation in scale, is also added. Figure reproduced from Bartenschlager et al., 2013[93], with permission from Springer Nature (License No 5633130933991).

NS5A DIII has no significant role in HCV genome replication, but is indispensable for efficient virus assembly. Mutational analysis revealed that deletion of small region within DIII and mutation of a single serine residue within this region in particular, serine 457, can abrogate HCV virion assembly at early assembly stages[136].

Moreover, NS5A is a phosphoprotein existing in two forms, a basally- and a hyper-phosphorylated one, with corresponding molecular weights of 56kDa and 58kDa, respectively[137]. NS5A basal-phosphorylation determinants cluster mainly in DII and DIII, while hyperphosphorylation is targeting a serine rich cluster within LCSI. This latter highly conserved cluster contains eight serine residues, six of which have been identified by mass spectrometry as phosphorylation sites: S222, S225, S229, S232, S235 and S238 (see Figure 12). Phosphorylation of NS5A is mediated by several cellular kinases, but the two best characterized are CKIa and casein kinase II (CKII). CKIa is primarily responsible for NS5A hyperphosphorylation, while CKII phosphorylates residues within DII and DIII representing the basal phosphorylation of the protein[138]. CKII in particular is known to phosphorylate serine 457 (S457), within NS5A DIII, leading to augmented infectious HCV particle production. S457-phosphorylated NS5A is mainly recruited to low density membrane structures around LDs and has been associated with Core/NS5A interaction[139].

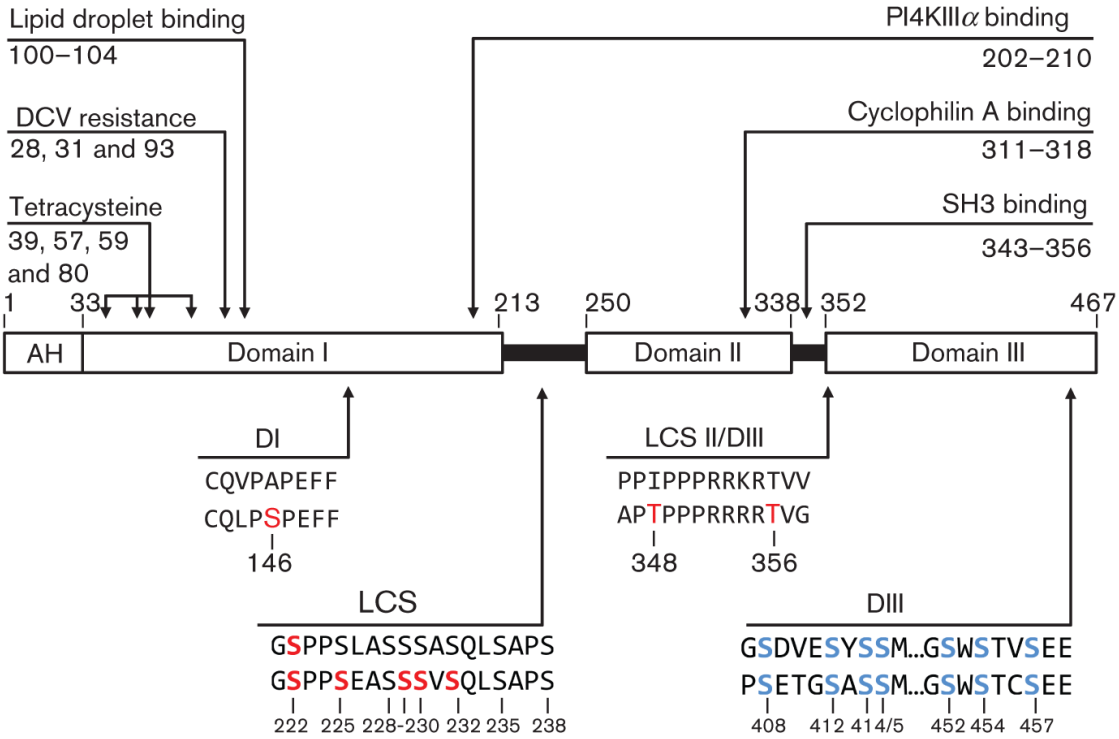

Figure 12: NS5A protein domain organization with a focus on positions of key interactions with cellular protein (top) and phosphorylation sites (bottom).
The protein-protein interaction sites highlighted include the tetracysteine zinc-coordination motif (Tellinghuisen et al., 2005[120]), specific residues implicated in daclatasvir (DCV) resistance (Fridell et al., 2010[135]), the reported lipid droplet-binding motif (Miyanari et al., 2007[140]), PI4KIIIα-binding motif (Reiss et al., 2013[141]), the binding site of Cyclophilin A (Hanoulle et al., 2009[142]) and P2 polyproline SH3-binding motif (Hughes et al., 2009[133]). Previously reported phosphorylation sites that have been determined by mass spectrometry (in red), or predicted phosphorylation sites based on genetic evidence in the absence of any biochemical data (in blue) are also shown for NS5A sequences of genotype 1b (J4 isolate, GenBank accession number AF054250, upper sequence) and genotype 2a (JFH-1 isolate, GenBank accession number AB047639, lower sequence). Figure reproduced from Ross-Thriepland & Harris, 2015[118], permission conveyed by Copyright Clearance Center, Inc (License ID 1403228-1).

Both pulse-chase and mutational studies have shown that basal and hyper-phosphorylation of NS5A occur only after the proteolytic NS4B/NS5A and NS5A/NS5B cleavages are completed, indicating that NS5A phosphorylation in general is dependent on correct cleavage and/or NS5A protein structure[143-145,137]. NS5A hyperphosphorylation is the result of sequential phosphorylation of residues within DI, LCSI and DIII. More specifically, phosphorylation of S457 is considered to be a prerequisite towards the modification of other phospho-acceptors involved in p58 NS5A generation[136], while phosphorylation of S146 in DI is also considered to promote NS5A hyperphosphorylation in genotype 2 HCV strains. Within LCSI, the sequence of phosphorylation by CKIα is hypothesized to commence by NS3-mediated recruitment of the kinase and phosphorylation of S225[106]. Subsequent phosphorylation of S229 triggers the phosphorylation of S232, S235, and S238[146]. A negative feedback loop starts with the phosphorylation of S235, signaling dephosphorylation of S229, putting a pause to the hyperphosphorylation cascade[147]. Mutational analysis of these serine residues in NS5A proteins of genotype 1, 3, 4, and 5 revealed that S>A mutation reduces p58 and enhances HCV genome replication[148], while, surprisingly, the same mutations decreased both hyperphosphorylation and viral replication in genotype 2 strains[149-152,146]. These mutations, however, did not affect NS5A phosphorylation but rather resulted in reduced activation of the lipid kinase phosphatidylinositol 4-kinase IIIα (PI4KIIIα), whose overactivation was shown to be detrimental to viral replication[153]. Recently, S229, S232 and S238 phosphorylation was also found to regulate DI-mediated NS5A dimerization and HCV genome translation[154]. Furthermore, a threonine-rich cluster downstream of LCSI was found to also affect p56/p58 balance[155].

Each of p56 and p58 forms are considered to regulate either HCV genome replication or assembly. Inhibition of basal NS5A phosphorylation in DII and/or DIII had no evident effect on HCV RNA replication[148], but reduced HCV virion production, while mutagenesis in DIII reduced Core/NS5A interaction[139]. These data, together with the findings by Secci et al.[138], indicate that basal NS5A phosphorylation is essential for HCV assembly. On the other hand, the functions of hyperphosphorylated NS5A are a subject of controversy. Phosphorylated S222 (pS222) and p58 in general are considered negative modulators of HCV genome replication[156,157], while other researchers claim that pS235 promotes the formation of HCV replication complex[151] and is essential for HCV RNA replication[158] and Goonawardane et al.[159] report no direct effect of NS5A hyperphosphorylation on virus genome replication.

A collective conclusion could be that p56/p58 balance might function as a regulatory switch between RNA replication and virion assembly, with different effects for strains of various genotypic origins. Because of this intricacy, the experimental characterization of the diverse NS5A functions is extremely challenging. Although the exact mechanisms for this multifunctionality of NS5A remain unknown, recent evidence show that the NS5A phosphovariants interact with distinct host cell components[160].

NS5B

The last protein to be encoded in the HCV polyprotein format is the RNA-dependent RNA polymerase (RdRp), NS5B. NS5B consists of 591aa and has an estimated molecular weight of 66 kDa. The N-terminal 530 aa of the enzyme form its catalytic domain, which is linked by 40 aa with the carboxyl-terminal membrane anchor α-helix of the protein (aa 570-591)[161]. HCV RdRp is responsible for the synthesis of positive HCV RNA strands, as well as of the intermediate negative copies[162].

Similar to the RdRps of the other member of the Flaviviridae family, HCV NS5B comprises a highly conserved GDD motif in its catalytic domain and an overall structure of subdomains resembling a right palm with fingers and a thumb[163] (Figure 13). The enzyme's

active center is represented by the palm, while the thumb and fingers regulate the interaction with the viral RNA substrates[164].

Due to its crucial role in HCV replication, NS5B constitutes the perfect target for anti-viral drugs (see §I.B.(ζ) for more information).

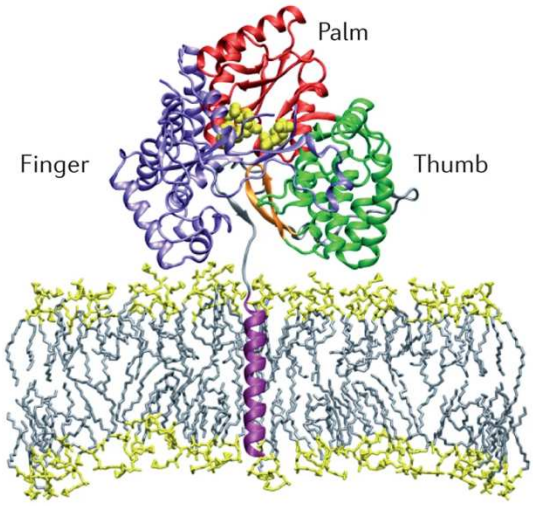

Figure 13: Illustration of the full-length NS5B (Protein Data Bank accession 1GX6) and its topology with respect to a membrane bilayer via its C-terminal transmembrane tail.
The finger, thumb and palm subdomains are indicated, with the β-loop shown in orange. The C-terminal linker sequence (grey) links the enzyme's core to the membrane insertion anchor (magenta). Two priming nucleotides (yellow) highlight the active site. The RNA-binding groove is masked in this predicted closed conformation by the NS5B ectodomain, which stacks to the membrane. Figure reproduced from Bartenschlager et al., 2013[93], with permission from Springer Nature (License No 5633130933991).

I.B.(δ) Heterogeneity and Prevalence

I.B.δ.(i) HCV Global Prevalence

HCV infection constitutes a pandemic spread across all continents. However the burden of hepatitis C is unevenly distributed across and within continents, geographic regions and countries. HCV prevalence is low in the developed countries of Europe and North America, while the higher percentages of highly affected countries are located within Asia and Africa, as shown in Figure 14A. Since 2015, and stably every year, the countries with the highest HCV distribution have been Pakistan, China, and India, with almost 10, over 8 and over 5 million chronic infections recorded, respectively (Figure 14B).

Until 2016, the country following these three in total number of infections was Egypt, which in 2008 had the highest global prevalence of HCV in percentage (15% of Egypt population was HCV seropositive). Now, despite Egypt still being in the top 20 countries in total number of infections, the national HCV prevalence has been decreased to below 0.4%, nominating it one of the few countries that might actually achieve the goals set by WHO for 2030. Egypt's success story relies on important initiatives embraced by the government, such as the establishment of the National Committee for the Control of Viral Hepatitis (NCCVH) in 2006, the launch of the national treatment program with direct antiviral agents (DAAs) in 2014 and the adoption of a national screening program in 2018. These efforts, however, would not have prospered without the significant contribution of pharmaceutical companies developing the highly efficient and extremely expensive DAA drugs against HCV (see §I.B.(ζ) for virus treatment options). In an unprecedented token of humanity, John Martins, the then CEO of Gilead, the big pharma in charge of production and distribution of these new drugs, accepted not only to distribute the pills in almost 1/100th of the initial price to low-income sub-Saharan African countries, but also to waive patent protection of the product in the area, allowing other companies to manufacture and distribute the therapy at the same low price. Overall, the example of Egypt shows that HCV elimination is achievable in a welfare state with the coordinated efforts of all actors responsible and benevolence as a guide (for a review see Waked, 2022[165]).

I.B.δ.(ii) HCV heterogeneity and distribution

Isolation of the virus from around the globe and analysis of its genomic sequence revealed substantial nucleotide sequence variability throughout the viral genome. This evolutionary advantage of RNA viruses usually arises from exerted pressure by the host's immune system and the combination of high replication rates of the viral genome, together with errors made by the RdRp lacking a proofreading capacity[166]. The mutation rate introduced by HCV NS5B per replicative cycle is estimated at $3.5x10^{-5}$[167].

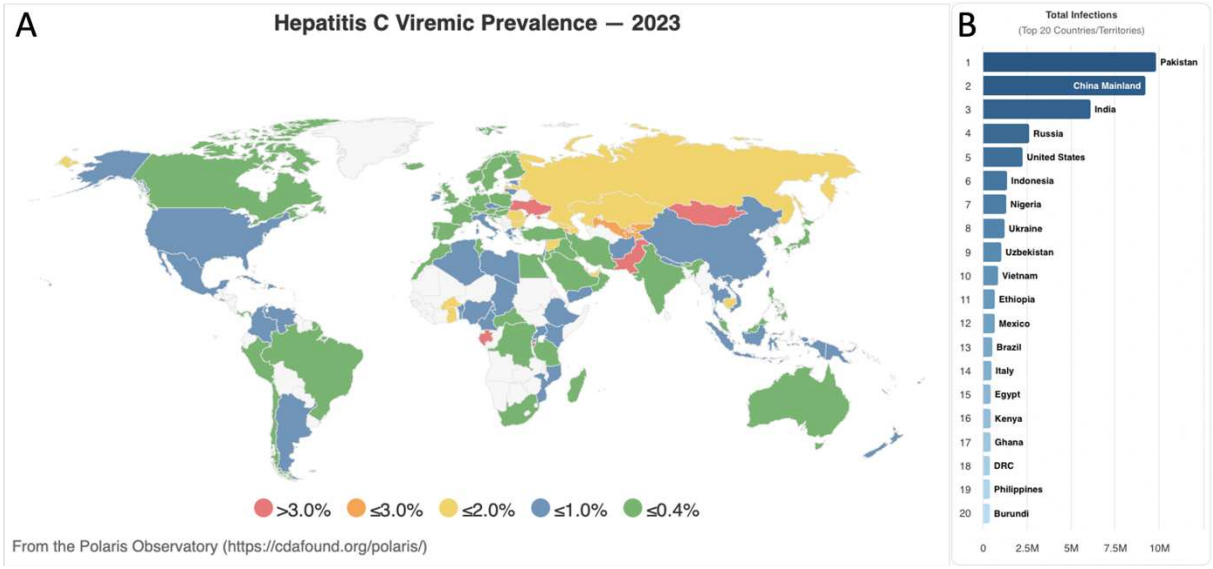

Figure 14: HCV viremic prevalence (A) and top 20 countries/territories with most HCV infections (B) in 2023.
Adapted from CDA Foundation's Polaris Observatory; 2023 [updated Aug 21 2023]. Available from https://cdafound.org/polaris/ (Accessed 24/08/2023).

In the interest of organisation and simplification of future epidemiological and phylogenetic studies of HCV, Simmonds et al. proposed an HCV classification system in 1994. According to this system, variants with analogous sequences were grouped together in "genotypes", while groups of variants with more similar sequences within these genotypes were grouped into individual "subtypes"[168]. The adopted nomenclature followed the chronological order of discovery, staring with the classification of the strain identified by Choo et al., in 1989[26] in genotype 1, subtype a, or subtype 1a. The strains considered for classification of a novel geno- or sub-type have some common characteristics, such as formation of a distinct phylogenetic group, representation by at least three isolates of unrelated epidemiology and absence of recombination (see I.B.δ.(iv)). Today, HCV is classified in 8 genotypes, differing by 30% or more among each other, and 93 recognized subtypes, with a nucleotide sequence divergence below 15% among the members of each subtype[169,170] (Figure 15). The genotypic and subtypic differences among the different HCV strains are defined within the conserved sequences of the 5'-UTR, the 98 nucleotides of 3'-UTR, the Core or the NS5B coding sequences[169].

In contrast to these conserved sequences, the viral genome also comprises some sequences of high variability, such as those encoding the hypervariable region 1 (HVR1) within E2 amino terminus and NS5A[171]. NS5A varies up to 50% at the nucleotide level and by ~20 aa residues in length, notably in DII-III. Interestingly, NS5A AH, DI, DII and LCSI are all indispensable for HCV genotype 1-7 genome replication, while mutations in LCSII and deletions in DII and DIII have been found to cause genotype-specific effects, such as reduced RNA replication and/or viral titers, indicating functional diversity among the NS5A protein of diverse genotypic

origin[172]. HCV heterogeneity affects to a great extent the virus-induced pathology (see I.B.(στ)) and the response to some treatment regiments (see I.B.ζ.(ii)).

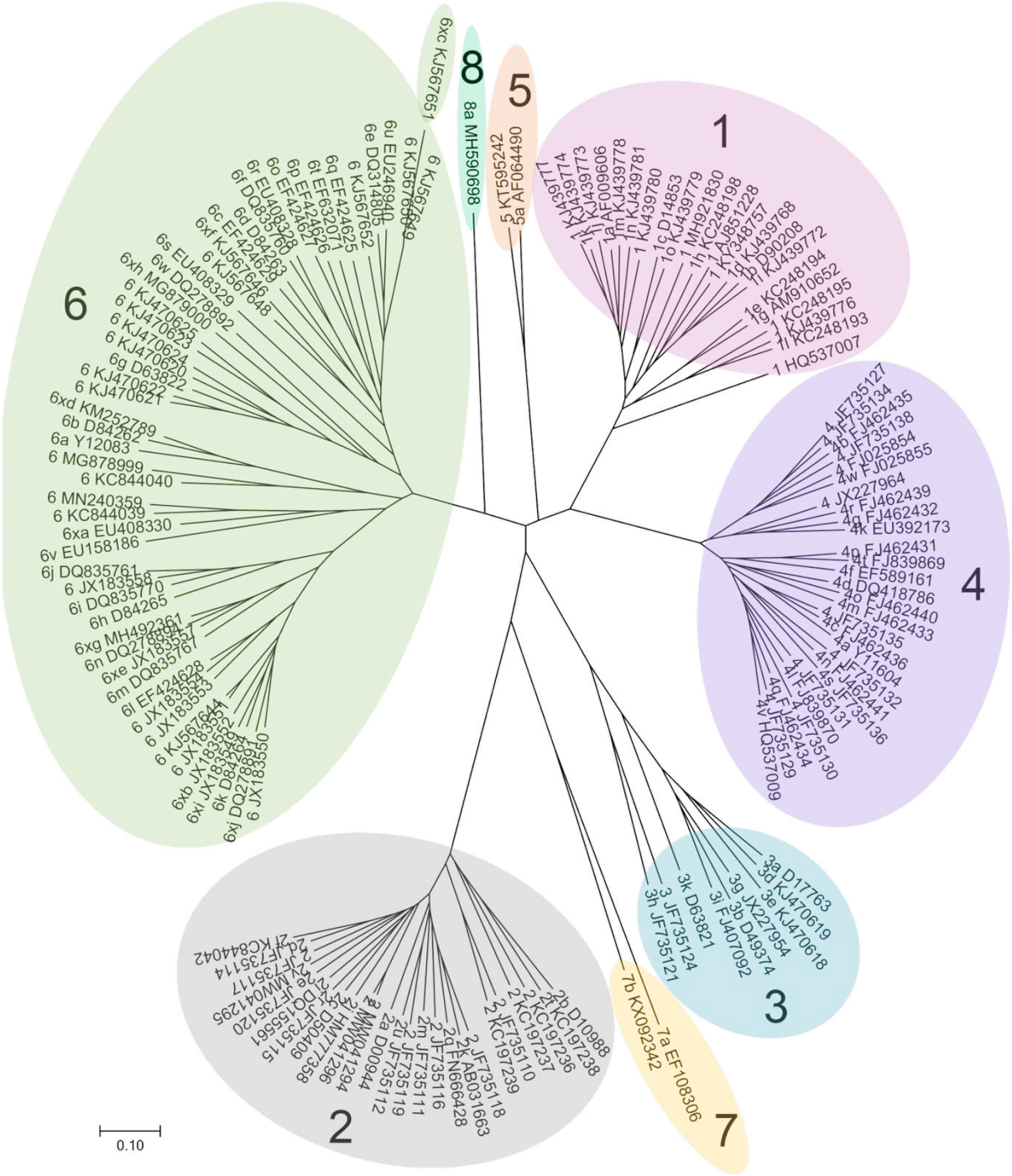

Figure 15: Phylogenetic tree of the 93 identified HCV strains as of March 2022.
Figure from International Committee on Taxonomy of Viruses[169]. CC BY-SA 4.0 license.

Matching the imbalanced distribution of HCV infections across the globe, genotype and subtype distribution also varies, as shown in Figure 16. Genotypes 1-3 circulation is not restricted, while genotypes 4-7 are mostly found in distinct geographical areas of the African and Asian WHO region[173]. Genotype 8 was identified only 5 years ago in the plasma of four patients originated from Punjab, India[174]. Almost half of the global infections occur by strains of genotype 1, while genotype 3 is the second most prevalent[175].

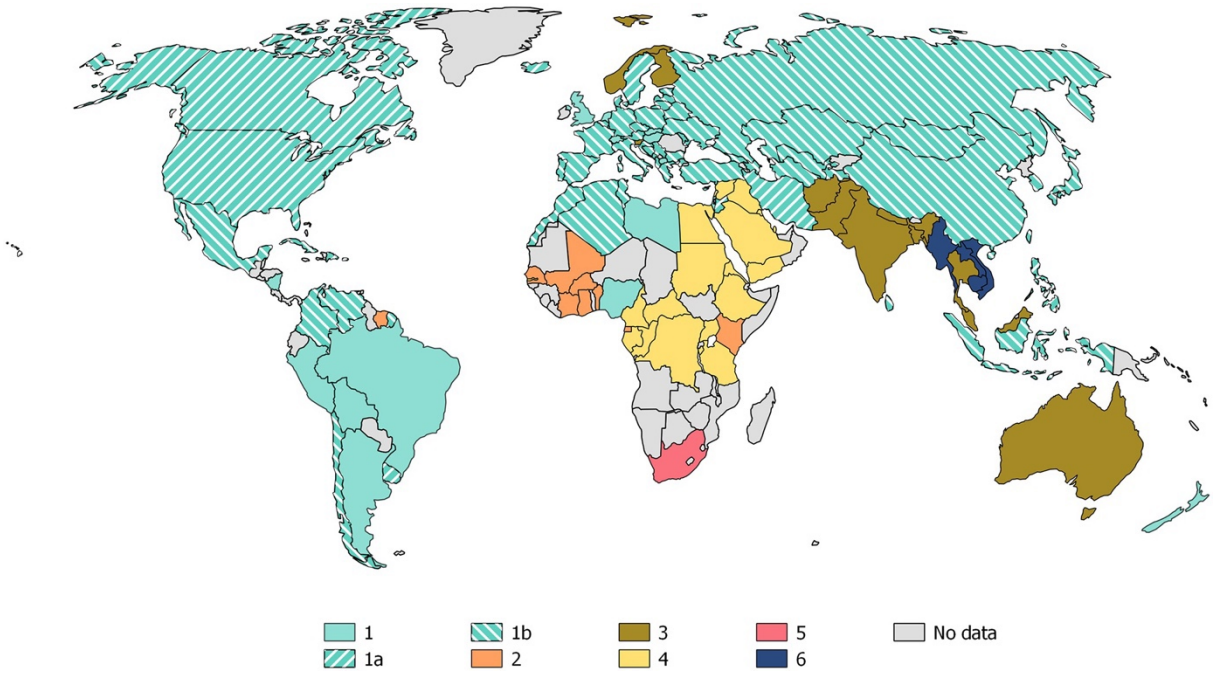

Figure 16: Global distribution of HCV genotypes.
Figure from Cuypers et al, 2016[176], with permission from John Wiley and Sons (License No 5615300718825).

I.B.δ.(iii) HCV quasi-species

The same mechanisms that are responsible for HCV evolution and genotypic divergence, i.e. high replication rates, NS5B introduced mutations and pressure by host immunity, are also liable for the development of a high number of close related, yet distinct HCV RNA sequences within one host, called "quasi-species". This term was first introduced in 1977 in an attempt to mathematically model and predict the evolutionary process of primitive life forms[177]. Since then, it has been found and extensively studied in viruses, which usually differ by no more than 1-3%. The sequences of the different quasi-species found in an organism verge to a consensus sequence, which may, at times, be nothing but a nonexistent, averaged creation of the alignment of the different mutated sequences.

The accumulation of these mutation might have either a detrimental or an evolutionary advantageous effect on the virus. If the mutations occur in genomic sequences of great value for viral functions (e.g. replication, translation, particle production), or if the mutation rate is increased, deficient genomes are produced. Intracellular accumulation of deficient genomes has been shown for other viruses to be attenuating, either due to the inability of the virus to retain genetic information or due to increased probability of the viral genome to be sensed by the immune system (reviewed in Domingo et al., 2005[178] and Bordería et al., 2016[179]). On the other hand, a few mutation in less conserved sequences may increase the adaptation of the virus and provide an escape mechanism from immune sensing[180] and antiviral factors[181]. Furthermore, this attribute of HCV increases the difficulty in vaccine development attempts.

I.B.δ.(iv) Natural HCV recombination

HCV evolution is additionally promoted by viral recombination, i.e. the formation of chimeric viruses comprising genomic sequences of distinct phylogenetic origin. HCV recombination was first reported in 2002. Today, 14 natural HCV recombinants have been reported bearing sequences of either different HCV genotypes (intergenotypic recombination) or of different HCV subtypes (intragenotypic recombination).

A necessary event for recombination to occur is a simultaneous infection of a host-cell with two different viral strains. For some RNA viruses, HCV included, infected cells have been shown to become refractory to subsequent infection of the same or related virus species (superinfection exclusion)[182] severely limiting the possibility of finding two viruses in the same cell. Nonetheless, superinfection has been detected in HCV patients receiving blood donation, undergoing haemodialysis, organ transplantation or using drugs intravenously[183-185]. *In vitro* studies have further demonstrated that HCV co-infection of a cell is possible when it is simultaneous, while a pre-infected cell is resistant to another infection[186]. Additionally, 18% of chronically infected patients have been found to host recombinant viruses[187].

Most of the natural HCV chimeras include sequences of genotype 2 genetic origin, suggesting the putative existence of genotype-specific elements that could stabilize or favor the functionality of recombinant viruses. The process of recombination takes place during the simultaneous replication of two viral genomes, as the RdRp exchanges RNA matrices in frame, leading to the formation of complementary hybrid strands[188]. Usually, the recombination occurs at the NS2/NS3 junction, resulting in a replication-necessary fraction of one strain/genotype and a structural fraction of another[189]. This is also the case for the only actively circulating chimera, encoding the structural genes of a subtype 2k strain and the nonstructural genes of a subtype 1b strain. This virus has been isolated from patients in Austria[190], Georgia[191], the Netherlands[192], Cyprus[193], France[194], Uzbekistan[195] and Ireland[196]. Interestingly, all the circulating 2k/1b chimeras have originated from the same strain, identified in 2002 in St Petersburg[197].

For the time-being, HCV chimeras are being characterized and studied, but not classified, since this would require identification of the exact junction point between the two strains combined in each chimera[171].

I.B.(ε) Virus life cycle

Although significant advancements have been made in the characterization and resolution of crucial steps of the HCV life cycle, certain aspects remain elusive. A simplified view of the main steps of the viral life cycle is illustrated in Figure 17. HCV entry, genome translation, formation of the replication factories, genome replication and particle assembly are described in the following paragraphs with an emphasis on the roles of lipids in these steps.

I.B.ε.(i) HCV entry in hepatocytes

As a hepacivirus, the main target of HCV are the liver cells. Following HCV parenteral transmission, as described in I.B.(β), viral particles circulating in host's blood may cross the endothelium of the hepatic sinusoid cells and end up in the space of Disse. There, HCV particles are exposed to the basolateral pole of hepatocytes and can infect them through the "cell-free" HCV entry process. However, viral persistence is also achieved thanks to cell-to-cell transmission of HCV from an infected hepatocyte to adjacent ones. The cell-free HCV entry will be described below, while highlighting the common and discrete aspects with comparison to cell-to-cell transmission.

HCV entry consists of three key steps: (1) viral attachment to the hepatocyte, (2) cellular receptor-mediated endocytosis of the viral particle, and (3) endosomal fusion for the release of the viral genome (Figure 18).

As described in §I.B.γ.(i), HCV particles circulating in the bloodstream are coupled to lipoproteins, hence the low-density lipoprotein receptor (LDLR)[198], glycosaminoglycans such as heparan sulfate proteoglycans (HSPGs)[199] and Scavenger Receptor class B type 1 (SR-B1)[200] have been found to contribute to viral attachment. Additionally, cholesterol transporter Niemann-Pick C1-like 1 (NPC1L1) has also been found to be involved in HCV entry, although

its exact role remains evasive[201]. These factors are likely contributing to cellular HCV transmission as well[202]. SR-B1 seems to be promoting a modification of the lipid profile of the LVP, allowing the interaction of SR-B1 with the HVR1 of E2, further exposing the domain of E2 interacting with cluster of differentiation 81 (CD81). E2 interaction with CD81 and epidermal growth factor receptor (EGFR) leads to translocation from the hepatocyte basolateral membrane to the tight junctions and association of CD81 to tight junction protein claudin1 (CLDN1)[203], while occludin (OCLN) is also essential for HCV entry[204]. Other host factors, such as protein kinase A (PKA) and ephrin type-A receptor 2 (EphA2), are also known to promote this association, both in cell-free and cell-to-cell related HCV entry[205,206]. However, CD81 presents an example of a factor that is not essential for cell-to-cell transmission[207].

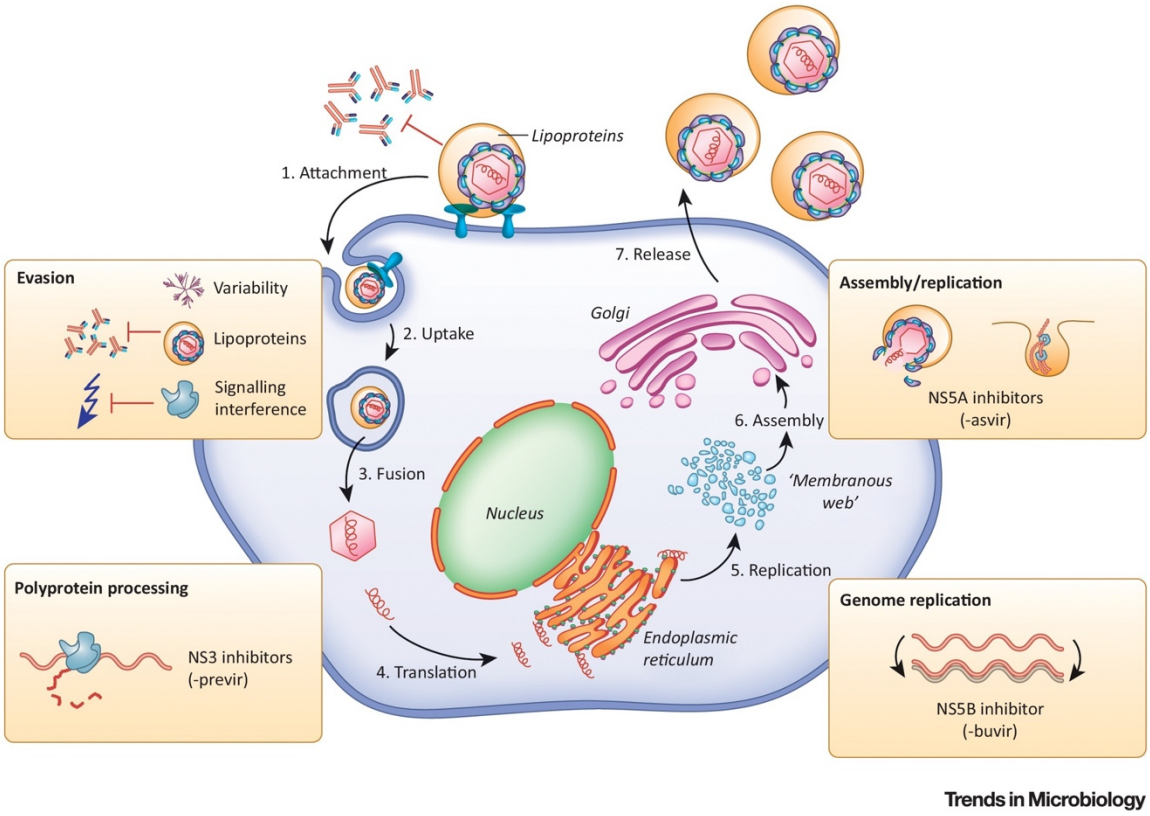

Figure 17: Main steps of HCV life cycle and targets of therapeutic regimes.
Reprinted from Pietschmann & Brown, 2019[208], with permission from Elsevier (License No: 5614301403047).

Viral internalization is dependent on plasma membrane rearrangements, leading to clathrin-mediated HCV endocytosis. Cellular factors, namely phosphatidylinositol 4-kinases type III alpha (PI4KIIIα) and beta (PI4KIIIβ) have been suggested to affect membrane remodelling and HCV trafficking during entry in a genotype-specific manner[209]. Following endocytosis, E2 and E1 heterodimerize promoting fusion between the viral envelope and the endosomal membrane. The viral fusion is promoted by acidification of the endosomal lumen by V-type ATPases, while the endosomes containing the virus are transported into the cell by cellular microtubules. Cellular factors, such as EGFR and EphA2 may also contribute to HCV fusion[205]. Lastly, the virus capsid disassembles, and releases the viral RNA in the cytoplasm, allowing the initiation of translation and replication.

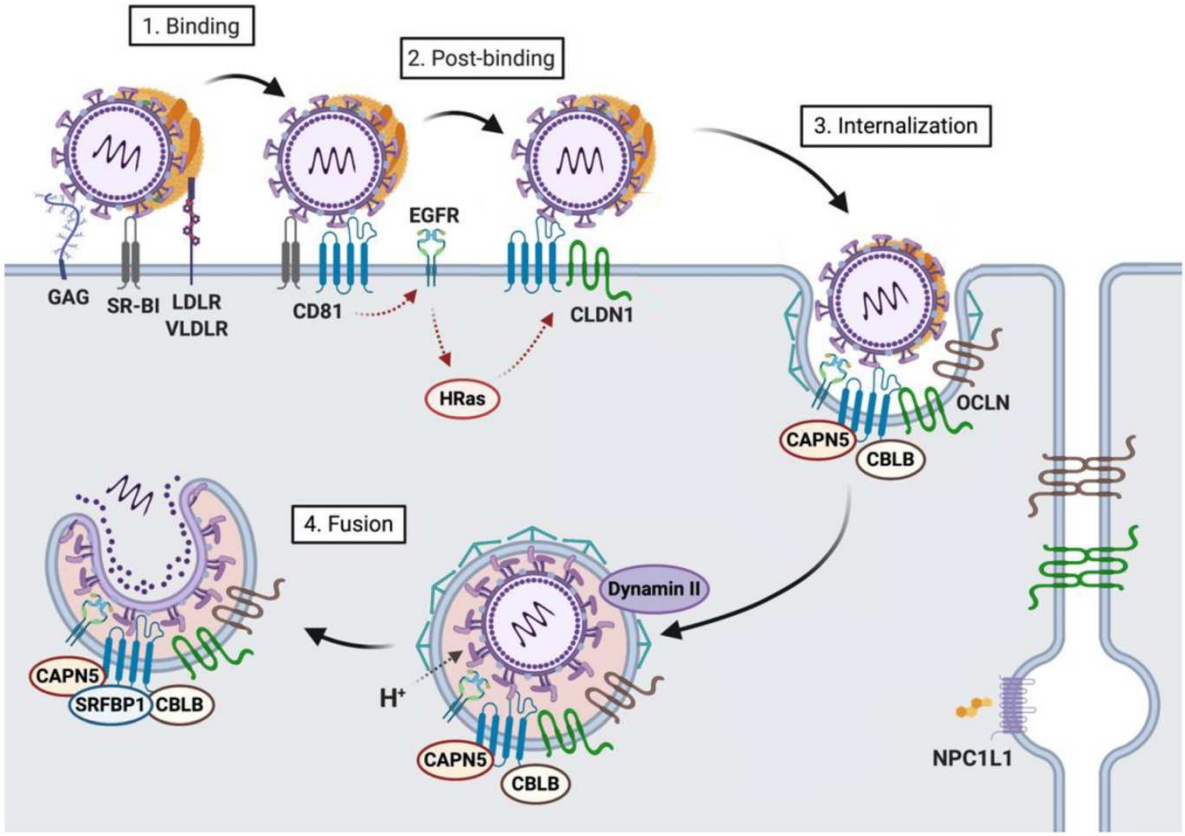

Figure 18: Schematic representation of the HCV LVP "cell-free" entry process from cell attachment to genome cytoplasmic release.
Interaction with cellular glycosaminoglycans (GAG), LDLR and SR-BI, promotes HCV binding to CD81 and EGFR activation (1). HCV/CD81 coupled to EGFR are translocated to the tight junctions, where CD81 interacts with claudin1 (CLDN1). Internalization is completed by clathrin-mediated endocytosis (3-4), while the viral genome is released in the cell via a pH-dependent membrane fusion mechanism, mediated by the viral glycoproteins E1 and E2 (4). Figure adapted from Colpitts et al., 2020[210]. Creative Commons Attribution License.

I.B.ε.(ii) HCV genome translation

Upon release in the cytoplasm, the (+)ssRNA genome of HCV serves directly as an mRNA to produce the viral polyprotein. As described above, the 5'-UTR of HCV forms an IRES, allowing the docking of the 40S subunit of the ribosome[211]. Towards ribosome assembly, the cellular factors eIF2, eIF3 and RNA initiation factors (tRNA) are required[212]. These are successively recruited to the IRES. Binding of miR-122, as previously described, initiates the recruitment of translation initiator factors eIF2 and eIF3. The pre-initiation complex (48S) is formed by eIF3 and eIF2 in complex with the methionine-tRNA and a guanosine triphosphate (GTP) molecule. The 80S functional ribosome is formed by the recruitment of the 60S ribosomal subunit, following the hydrolysis of eIF2-GTP and eIF5B-GTP by eIF5. During this process eIF2 and eIF3 disassociate from HCV IRES[213,214]. Met-tRNA is then placed at the P ribosomal position, signaling the initiation of protein elongation.

The N-terminal part of the viral polyprotein is directed to endoplasmic reticulum (ER) lumen by four signal peptides present within C-E1-E2-p7 coding sequences. There, the polyprotein is subjected in meta-translational modifications, towards release of functional HCV proteins. It is co-translationally cleaved by cellular signal peptidases (SP), catalysing the cleavage at Core/E1, E1/E2, E2/p7, and p7/NS2 junctions. NS2 self-cleaves at the junction with NS3, the release of which initiates its serine protease activity. NS3, while still C-

terminally associated with its cofactor NS4A, cleaves sequentially the NS5A/NS5B, NS4B/NS5A, and NS4A/NS4B junctions. The NS4B/NS5A cleavage site in particular seems to be cleaved in two paces, either rapidly, attested by the early detection of NS4A/NS4B precursors, or more slowly, with a half-life of ~1h, supported by the detection of a stable NS4A/NS4B/NS5A[55,215].

Released mature viral proteins are retained at the ER through a process mediated by geranylgeranyl pyrophosphate, a product of cholesterol biosynthetic pathway whose role in the association of HCV proteins with the membranes is largely dependent on cellular fatty acid contents of the cell[216,217]. HCV ER-integrated envelope proteins are in the ER lumen, the nonstructural proteins are oriented towards the cytosolic face, while Core and NS5A are not solely localised in the ER. Core requires an additional cleavage of its transmembrane segments retaining it at the ER, by cellular SPP, towards protein maturation. Mature Core is mainly found in association with cytosolic LDs[71]. Lipid droplets are lipid storage organelles consisting of a hydrophobic core of neutral lipids and cholesterol esters, surrounded by a monolayer of phospholipids. Core localization at the LD surface is a prerequisite for assembly of virions[218]. NS5A has a peculiar subcellular localization and can either remain anchored at the ER, in order to assist HCV genome replication, or be found in close proximity to LDs, probably to further HCV particle assembly (for review see He et al., 2006[219]).

I.B.ε.(iii) Formation of the HCV replication factories

Viral replication is the next stage of the viral life cycle. HCV transcription and replication take place in a "replication niche", within the membranous web. The membranous web is generated by HCV-induced remodelling of the ER, forming mainly double membrane vesicles (DMVs). These alterations have been described within hepatocytes from either patients or chimpanzees infected with HCV and constitute typical replication sites of (+)RNA viruses[220].

Their formation confers a micro-environment protected from RIG-I and MDA5 (melanoma differentiation-associated protein 5) immune system sensing[221], nucleases, and proteinases[222], in which the local concentration of the factors necessary for HCV genome replication is increased, further boosting RNA replication efficiency. Moreover, this spatial separation of viral proteins and cellular components may aid in the coordination of the different stages of the viral cycle.

The exact mechanisms of the membranous web biogenesis are undetermined, yet kinetics of DMV formation has been correlated with HCV RNA replication during cell infection. The expression of NS3-NS5B subgenomic replicon (see §I.B.η.(i)) has been found sufficient to induce these alterations in ER organization[223]. Experiments of independent expression of each nonstructural protein have shown that NS4B alone can cause the formation of a membrane network resembling that observed in infected cells. However, NS4B was found to provoke the formation of single-membrane vesicles instead of DMVs. On the other hand, although not highly efficient, NS5A alone could lead to the appearance of DMV structures[220], while mutagenesis and/or deletion of NS5A α-helix and possibly DI would abrogate DMVs formation, in the context of NS3-NS5B expression without RNA replication[124]. Importantly, if the cleavage of the polyprotein at the NS4B/NS5A junction is too fast or if the synthesis of the NS4B-NS5A precursor is prevented (e.g. insertion of an IRES), the formation of DMVs is reduced or completely perturbed, respectively, demonstrating the importance of the NS4B/NS5A precursor in the DMV biogenesis[124]. This study by Romero-Brey et al. also highlighted the role of NS3 in this process. Furthermore, the observed compensatory mutations in the NS5A coding sequence, in response to mutations introduced into the sequence of NS4B, suggest a further coordinated role between these two proteins[224,110].

Nevertheless, the effect of viral protein expression in ER rearrangement is bolstered by cellular factors. The most well described roles of host proteins aiding DMV formation are those of the prolactin regulatory element-binding protein (PREB), and a variety of factors involved in lipid metabolic processes, such as sphingomyelin (SM), oxysterol-binding protein (OSBP) and PI4KIIIα.

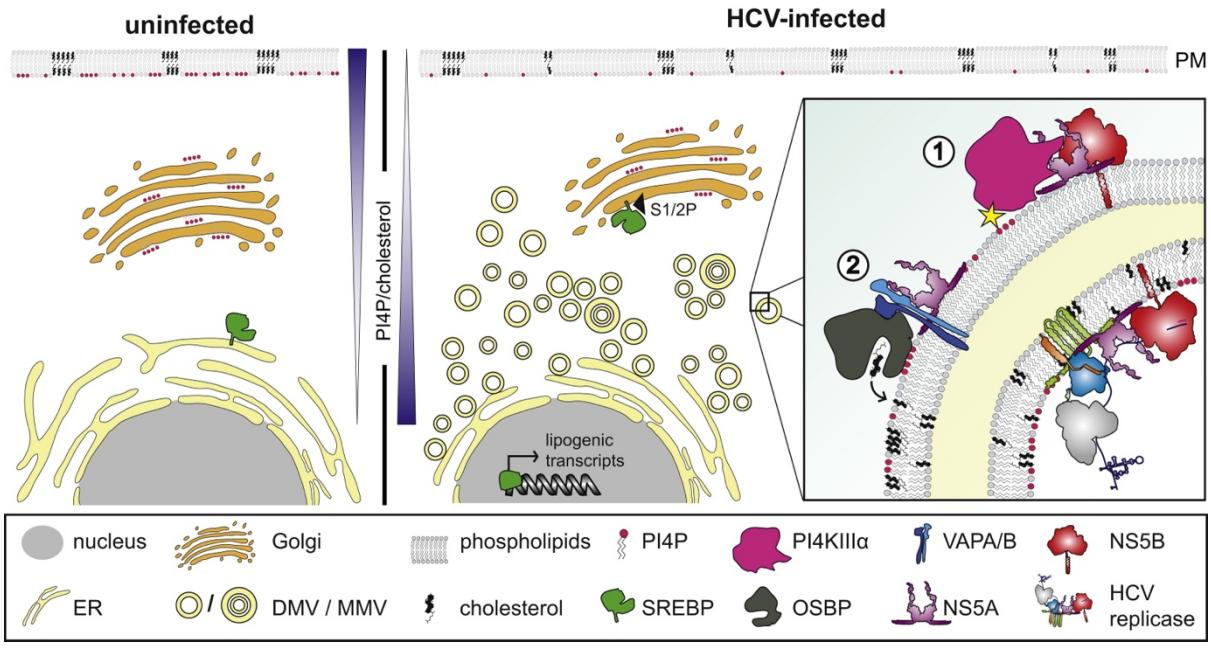

Figure 19: HCV-induced formation of double-membrane vesicles (DMVs) and multimembrane vesicles (MMVs) following subversion of host lipid homeostasis.
In the left panel a representation of an uninfected hepatocyte is shown, with decreased phosphatidylinositol 4-phosphate (PI4P) and cholesterol levels. In the right panel a model of HCV-subverted host cell proteins and lipids is shown with respect to DMV/MMV formation. PI4KIIIα interacts with NS5A and NS5B to induce elevated levels of PI4P (1), which in turn induce the recruitment of oxysterol-binding protein (OSBP). OSBP recruitment, further facilitated by NS5A interaction with VAPA and VAPB (2), also delivers cholesterol to the remodelled membranes. Inside the enlarged DMV on the right, the replication complex of HCV is depicted, consisting of the viral genome and the nonstructural proteins NS3-4A (in grey-blue-orange), NS4B (in green), NS5A (in purple) and NS5B (in red). Illustration reprinted from Paul et al., 2014[225], with permission from Elsevier (License Number 5644900180336).

PREB expression has been reported to be induced by HCV infection *in vitro* and *in vivo*, while the protein had been was found to interact with the central portion of NS4B. Inhibition of this interaction demonstrated the importance PREB in the formation of the membranous web and the maintenance of its structural integrity[226].

The first steps of SM biosynthesis in the ER give rise to ceramide, which is then transferred to the Golgi apparatus by ceramide transfer protein (CERT). There, ceramide is converted to SM. Reduced SM biosynthesis, induced by either inhibitors or by knockout (KO) of CERT, leads to observed low numbers of DMVs and decreased viral genome replication in HCV-replicon transfected human hepatoma cells. SM supplementation or CERT expression reverted the phenotype, only when CERT mutants that were able to associate with the vesicle-associated membrane protein-associated protein (VAP) or phosphatidylinositol 4-phosphate (PI4P) were used. These findings suggest that SM is important for the HCV-induced ER deregulations, while VAP and PI4P are essential for virus replication[227].

The PI4P phospholipid is physiologically transferred from the Golgi apparatus to the ER in a counter-exchange of cholesterol transportation from the ER to the Golgi apparatus by

OSBP. OSBP is hijacked by PI4KIIIα recruitment to DMVs[228], leading to increased PI4P levels at HCV replication sites[229]. This process is regulated by PPIs between the viral NS5A protein, OSPB[230] and PI4KIIIα[231]. As expected, OSBP/PI4KIIIα depletion significantly alters HCV-induced DMV structure, with clusters of smaller diameters being observed. Of note, NS5A interaction with PI4KIIIα has a dual role in HCV replication, since it prevents NS5A hyperphosphorylation by CK-Iα, leading to an abundance of the RNA replication associated p56 form of NS5A[141,149]. In fact, NS5A seems to play a major role in HCV genome replication, not only as a co-factor of the replication complex, as described below, but also as a key regulator of PI4P levels in the DMVs. This is coordinated, not only by the mechanism described above, but also by interaction of NS5A with ADP-ribosylation factor GTPase-activating protein 1 (ARFGAP1), a central player of cargo sorting in coat protein complex I (COPI) transport[232]. COPI is a highly conserved pathway of protein and lipid trafficking between the ER and the Golgi.

Overall, these findings reveal the importance of both viral proteins and host factors in the ER remodelling and DMV formation. Nonetheless, transmission electron microscopy imaging of liver biopsies from patients chronically infected with HCV strains of diverse genotypic origin has not validated the formation of DMVs *in vivo*, despite the presence of virus-induced membrane rearrangements. This discrepancy might either be due to either the lack of interferon in human hepatoma cultures, which highly affects HCV RNA replication, or due to higher virus replication rates in cell culture, resulting in higher levels of expression of viral proteins, which are possibly essential for this phenotype[233].

I.B.ε.(iv) HCV genome replication

Within the "replication niche" of the remodelled ER, the HCV RNA is copied through an intermediate step of negative, complementary ssRNA synthesis. The RNAs of the two polarities constitute a double-stranded RNA intermediate, which is possibly unwinded by the NS3 helicase, although the exact NS3 role has not yet been uncovered[234]. The (-)ssRNA then serves as a matrix for *de novo* production of new (+)ssRNA molecules[235]. The HCV RNA replication is mediated by the viral RdRp, NS5B, in collaboration with other viral and cellular factors, forming the replication complex. Among the mature HCV proteins, only NS3-NS5B are indispensable for RNA replication, as proved by the development of self-replicating subgenomic RNA[236]. Elements present in HCV 5'- and 3'-UTRs are also important for the *cis*-regulation of this process, as described in §I.B.γ.(ii).

NS5B initiates RNA synthesis from the 3' end of the (+)ssRNA in a primer-independent manner[237]. The positive HCV genome starts with an adenosine (A) or guanosine (G) and terminates with a 3′ uridine (U) for all known strains. Propagation of viruses with other nucleotides in their termini results in reversion to the original A/G or U, respectively, suggesting selective pressure for A-priming of the (-)ssRNA and some of the (+)ssRNA, such as JFH1 (see §I.B.η.(iii))[238-240].

This year, the Danish groups of Drs Jens Bukh, Troelsch Scheel and Jeppe Vinther (University of Copenhagen, Copenhagen, Denmark) uncovered that NS5B initiates (-)ssRNA with the cellular metabolite FAD, resulting into 5'-FAD-capping of the reverse HCV genome. The researchers reported a high frequency of 75% FAD-capped 5'-termini in genomes of both polarities in Huh-7.5 hepatoma cells infected with the HCV subtype 2a J6/JFH1 recombinant variant c2. FAD cap was also found in RNA intermediates of strains from genotypes 1-6, in the positive RNA genomes of genotypes 2a, 3a and 6a and was also detected *in vivo*! No effect of the metabolite on HCV RNA stability was documented. This study further constitutes the first report of an immune escape mechanism at the 5' of (-)ssRNA, since FAD was also found to protect the RNA from RIG-I sensing[73].

On the other hand, the well-studied proximal binding of the liver-specific cellular micro RNA miR-122 in 5'-UTR is known to stabilize the viral RNA, to protect it from recognition by the host innate immune system and to increase the number of viral RNA copies *in vitro* and *in vivo*[241-243].

A cellular protein interacting with NS5A and NS5B, CypA, is another well-documented host factor that is critical for HCV genome replication. CypA/NS5B interaction facilitates RdRp proper folding[244,245], while CypA catalyzes the isomerization of certain domains of NS5A towards a functional replication complex[246,245]. VAPA, apart from its role in PI4P level regulation at the DMVs, further promotes HCV RNA replication by facilitating the correct positioning of NS5B within the lipid rafts[247].

I.B.ε.(v) HCV particle assembly

Once copies of the HCV genome and mature viral proteins are in abundance, the formation of new virions commences. Although the HCV particle assembly process is not yet completely understood, certain steps and key factors of both viral and cellular origin have fairly been characterized. Overall, HCV assembly can be subdivided in the sequential processes of encapsidation, envelopment though budding into the ER lumen, virion lipidation towards "mature" LVP production and release in the extracellular environment.

Encapsidation

HCV encapsidation involves the interaction of Core with the RNA genome and the formation of the viral capsid by progressive Core oligomerization. However, there is a spatial issue in this process, since mature Core protein is anchored at the surface of cytosolic LDs[248], while the copies of (+)ssRNA of HCV are produced and localized at the viral factories in the ER-derived DMVs.

Core/LD association is vital for virus morphogenesis, since HCV assembly is abolished in the presence of mutated Core unable to traffic to the LDs. Another element supporting this notion is the high conservation of the Core/LD anchoring motif across HCV genotypes[249,140,250]. Whether the localization of Core at the surface of LDs is important for (i) divergence of the protein from the replication sites to abrogate competition with the replication complex for RNA binding, (ii) interaction of Core with key components of HCV life cycle stored in the LDs (proteins and lipids), (iii) redirection of cellular proteins from other cellular compartments to the LDs in order to inhibit their natural function, (iv) indirect regulation by Core of LD factors/activators/inhibitors thereby brought in proximity, or (v) all of the above remains still unclear[225].

As a matter of fact, in support of notions (ii) and (iv) Core has been found to decrease intracellular triglyceride (TG) degradation (lipolysis) by interfering with the activity of a key enzyme of the first lipolytic steps, the adipose triglyceride lipase (ATGL). Camus et al.[251] showed that Core/LD association is a pre-requisite for Core-induced inhibition of ATGL-mediated lipid mobilization. These researchers further demonstrated that Core increased the interaction of ATGL with its activator, the Comparative Gene Identification 58 (CGI-58), as well as their recruitment to LDs. Furthermore, in support of notion (iii), recent experiments by Boson et al.[252], revealed Core-directed re-localization of Nup98 from annulate lamellae to LD-apposed areas. This nucleoporin was further found to bind viral RNA, while downregulation of Nup98 expression was associated with exclusion of HCV genome from areas containing active translating ribosomes and the Core and NS5A proteins. Increased concentrations of HCV RNA and Nup98 in the vicinity of LDs suggest a favourable role of this host protein in HCV encapsidation. Taken together, these results endorse the multifunctional theory of Core dispatch from ER to LDs.

Nonetheless, Core is eventually required to verge towards the RNA, or vice-versa, in order to commence the encapsidation process. Whether HCV encapsidation occurs at the LD surface or at the ER membranes is still unclear. Additionally, exactly how Core and HCV RNA come together stands ambiguous, yet HCV NS5A has been documented to play an important role in this process. Immunofluorescent observations have revealed NS5A localization in the periphery of LDs, in a concentric distribution external to that of core[253], while yeast two-hybrid and NS5A/Core co-immunoprecipitation experiments[254] are further attesting to NS5A/Core/LD interactions. Inhibition of this synergy by mutations in NS5A DIII has been shown to perturb HCV virion production[125,139]. This interplay may additionally be regulated by cellular and viral factors, such as diacylglycerol O-acetyltransferase 1 (DGAT1), which has been reported to promote the co-localization and interaction of Core and NS5A to LDs[255,256]. In addition, NS3 has been proposed to both interact with and modulate NS5A hyperphosphorylation, hence the switch between NS5A participation in HCV genome replication or assembly[144]. Of note, mutations of conserved residues of NS3 have recently been reported to interfere with early HCV assembly steps, but not with lipidation of nucleocapsids, nor release of infectious particles[105].

The RNA binding capacity and mobility of NS5A across cellular membranes would allow the protein to deliver HCV RNA to Core at the surface of LDs[139,122,257], while on the other scenario, its interaction with Core, could recruit the LDs at the ER for encapsidation, in coordination with NS2 and p7[258]. Despite its instrumental role in HCV encapsidation, the mechanism of p7 action in this process is yet undetermined[259]. Nevertheless, eventual release of Core from the LDs is necessary for HCV infectivity. This is mediated by interaction of Core with the μ subunit of clathrin adaptor protein complex 2 (AP2M1). AP2M1 is physiologically involved in targeting cargo proteins to clathrin vesicles and inhibition of its interaction with Core was shown to confer increased accumulation of Core at the LDs, leading to a defect of HCV assembly[260].

Although it is not clear on which exact step(s), NS5A also plays a decisive role in viral assembly, mainly through its DIII. This is supported by the fact that several mutations and deletions in this region have been found to (i) abolish virus production at an early assembly stage[136], (ii) significantly reduce viral titers[125], (iii) perturb NS5A/Core association[125,257], (iv) reduce NS5A RNA binding capacity and therefore trafficking of viral RNAs to LDs for assembly[257], without in any case affecting genomic replication. It is hypothesized that these results are linked to an alteration or loss of a N-terminal cluster of four positively charged residues within DIII and/or of the CKIIα recognition sequence, leading to impaired NS5A phosphorylation at serine 457[257]. Furthermore, a region that is essential for NS5A association with LDs and subsequently Core has been found within NS5A DI[136].

Budding

Neosynthesized encapsidated virions acquire their envelope glycoproteins through budding in the ER lumen, where non-covalent heterodimers of E1 and E2 remain localized[261,218]. Deletion of E1 and E2 coding sequences was found to decrease the interaction between Core and viral RNA, indicating that encapsidation and envelopment are two related steps of the virus life cycle. Electron microscopy studies revealed that envelopment is taking place at the ER membrane in close proximity LDs[262,263]. Progressive formation of the viral nucleocapsid promotes intussusception of the ER membrane towards the lumen, allowing the envelopment[257].

HCV budding is mainly coordinated by the viral E2, NS2 and p7 proteins. Notably, NS2 is known to interact with E1/E2 and to induce the migration of the heterodimer to the assembly sites[264,265].

Post-envelopment lipidation

HCV virion maturation takes place upon diversion of the VLDL assembly route towards lipidation of the particles. Cholesterol, sphingolipids and some of the main components of LDs are essential for the production of highly infectious viral particles[266] and are made available to HCV by ATGL-dependent lipolysis of the LDs under the control of 1-acylglycerol-3-phosphate O-acyltransferase (ABHD5)[267]. Cholesterol-esters and TG are incorporated to the virions via the action of the microsomal transfer protein (MTP). MTP physiologically acts in VLDL synthesis via interaction with ApoB100 and formation of luminal LDs, incorporating ApoE and ApoCIII at their surface. HCV may also fuse with pre-VLDLs or with luminal LDs to incorporate the necessary lipids. Luminal LD association to HCV virions has been found to be an effect of E2 interaction with ApoE under the control of a regulator of the endo- and exo-cytosis trafficking pathways, the annexin 3 (ANXA3)[268]. Many apolipoproteins can be found at the surface of circulating HCV particles, such as ApoB, ApoAI, and ApoCI-III, though incorporation of ApoE alone would be sufficient to render the particle infectious, in accordance with its role in viral entry (see §I.B.ε.(i))[269,270]. ApoE has also been shown to physically interact with HCV NS5A in yeast two-hybrid and co-immunoprecipitation studies[271,272]. Interestingly, ApoE dependence and association to LVPs has been found to differ across HCV genotypes and cell lines[273].

Release

Egress of infectious particles is dependent on endosomal sorting complex components and *trans*-Golgi network-associating adaptors, supporting viral release by a TGN-endosomal secretion pathway, distinctive of the VLDL secretion route[274,275]. In support of the Golgi-mediated HCV secretion, unlike the heterodimers observed in the ER, E1/E2 dimers on infectious particles are found in covalent complexes by disulphide bridges, N-glycosylated and associated with complex sugars resistant to treatment with endoglycosidase H[276].

Furthermore, viral particles have been found in COP-II vesicles, an anterograde transport of cargo proteins from the ER to the Golgi[277]. In addition, inhibition of the Rab1b GTPase, which is responsible for the regulation of the ER-Golgi trafficking, reduces the rate of LVPs release[278]. Virion maturation is completed while egressing, once their density resembles that of VLDLs. In parallel, p7 oligomerizes to form an ion channel to balance the pH in the transport vesicles of the maturing viral particles, towards protecting them from an acidic environment. A defect in the capacity of p7 to form the channel inhibits HCV release, but can surprisingly be compensated by the expression of viroporin M2 of the influenza virus [279]. Within the trans-Golgi network, LVPs join the endosomal compartment[280], and are secreted via clathrin vesicles[281] or via exosomes budding from multi-vesicular bodies (MVB)[282,283].

Alternatives to this secretory pathway, which do not involve the Golgi apparatus in the final steps of the virus life cycle have also been proposed. In this model the COP-II vesicles may fuse directly with the plasma membrane or with the late endosomes and successively release the cargo in the extracellular matrix[284].

Overall, virus assembly and release are regulated by both viral and cellular factors and the exact mechanisms are still to be uncovered. Recent, studies unravelled the role of Poly(rC)-binding protein 1 (PCBP1) in regulation of HCV assembly and release[285]. PCBP1 is known to interact with the 5'-UTR of the viral genome[286]. Although PCBP1 knock down decreases viral RNA accumulation, it simultaneously increases virion secretion, suggesting that PCBP1 may play a regulatory role in preventing RNA molecules from entering the assembly and release step of the virus life cycle. To further support this, PCBP1 knockdown had no direct impact on viral entry, translation, genome stability or replication. Experiments in Huh-7.5 cells infected with the J6/JFH1 chimeric strain revealed the role of PCBP1 in both virion packaging and release, while the same experiments with a cell culture-adapted JFH1 strain suggest that the

RNA has already been packaged into new infectious viral particles before the assistance of PCBP1 is required[285].

I.B.(στ) Pathogenesis

The HCV incubation period lasts approximately 7 weeks and corresponds to the period during which the virus multiplies in the hepatocytes of its new host. Following this incubation phase, a sudden elevation of the serum levels of two markers of hepatic cell lysis, the alanine amino transferase (ALT) and the aspartate amino transferase (AST), mark the acute phase of HCV infection. In general, this phase is more often asymptomatic, while symptoms such as discomfort, nausea, and jaundice may emerge in 20% of reported cases. About one in four HCV infected individuals may spontaneously clear the virus during the first 12 months post-infection[287,288], while the lack of CD4+ responses during the acute phase is associated with the development of chronic disease[289,290]. During chronic infection, the virus damages the hepatic cells, causing inflammation, the seriousness of which increases over time and its persistence can lead to liver fibrosis and liver cirrhosis development. Ultimately, 1-7% of viral infected patients with established cirrhosis will form hepatocellular carcinoma each year, due to chronic HCV infection (CHC). A large proportion of chronically infected patients have been found to develop an additional liver pathology associated with the accumulation of triglycerides and cholesterol esters in the form of LDs in infected hepatocytes, called steatosis. Steatosis prevalence has been found to be double in patients infected with HCV genotype 3 strains over those infected with non3 genotypes[291]. Rarely, another form of hepatitis may be manifested early in the weeks following the infection. This is called fulminant hepatitis, corresponding to rapid and massive necrosis of hepatic parenchyma, accompanied by a decrease in liver size, that winds up fatal in the majority of cases. The overall evolution of hepatitis C pathology is summarized in Figure 20.

The assessment of liver damage in patients may be performed by both invasive (e.g. liver biopsy) and noninvasive methods. As biopsies are generally limited due to invasiveness, sampling errors (liver sections of biopsy samples usually represent 1/50,000th of the total liver mass, depending on the individual[292]), possible complications and ineptness of regular repetition to monitor progression, noninvasive imaging techniques are generally preferred (for a review on fibrosis see Sebastiani et al., 2014[293], Horowitz et al., 2017[294], for a review on steatosis see Park et al., 2022[295]). These include ultrasound elastography, acoustic radiation force impulse imaging (ARFI), dynamic shear wave transient elastography (SWE), the most validated transient elastography (TE) and the most accurate, especially for the determination of mild fibrotic stages, magnetic resonance (MR) elastography for the assessment of liver fibrosis. Liver steatosis can noninvasively better be assessed by MR spectroscopy and magnetic resonance imaging proton density fat fraction (MRI-PDFF). Direct or indirect markers of hepatic fibrosis can also be found in patients' sera, allowing serological tests to detect respectively either the byproducts of collagen synthesis/degradation, or serum aspartate aminotransferase to platelet ratio index, indicative of altered hepatocyte function. However, serological tests are not able to discriminate among stages of liver damage except for low to high fibrosis, and their results may be influenced by the existence of extrahepatic inflammation in the patient's body.

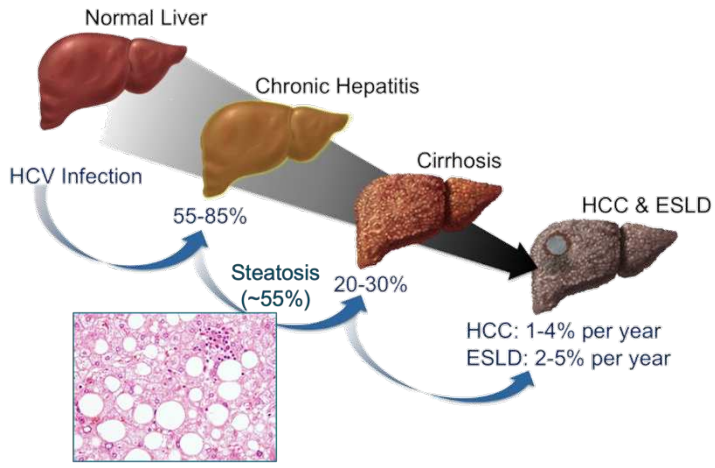

Figure 20: Evolution of HCV-induced pathogenesis.
HCC: Hepatocellular carcinoma, ESLD: End stage liver disease. Images adapted and put together from HCV online (Cartoon liver representations, Creative Commons Attribution Noncommercial License) and from Liang et al., 2014[296] (electron microscopy photo of human steatotic liver, Creative Commons Attribution License) with percentages of occurrence from Lingala et al., 2015[297].

I.B.στ.(i) Steatosis

Steatosis is generally characterized as fatty liver disease, with no early manifestation of symptoms, resulting to its detection most commonly during routine blood tests, by the abnormally increased levels of liver enzymes (e.g. AST, ALT transaminases) or biomarkers, such as albumin and bilirubin. Hepatic steatosis is defined as a hepatic fat content exceeding 5% of liver weight[298], which is in clinical practice diagnosed by the quantification of hepatocytes containing fatty vacuoles, otherwise known as LDs[299]. The severity of liver steatosis is determined histologically by the percentage of lipid-rich hepatocytes. Mild steatosis is defined by a maximum of 33% LD-containing hepatocytes, moderate steatosis by 34-66% and severe steatosis by more than 66%[300].

Two forms of steatosis with distinct hepatocyte alterations may be detected in steatotic patients: macrovesicular steatosis, in which few large vacuoles occupy the cytoplasm of the cell, displacing the nucleus and distorting the cellular architecture, and microvesicular steatosis characterized by numerous, small finely defined LDs in hepatocellular cytoplasm, as a result of mitochondrial damage leading to impaired β-oxidation. Microvesicular steatosis is less common but generally more serious than its counterpart.

Human liver might be protected by controlled accumulation of lipids, but prolonged lipid accumulation may induce inflammation and reduction of liver metabolic competence[301]. This leads to lobular inflammation with mixed infiltration of neutrophils, lymphocytes and macrophages, a condition called steatohepatitis. The exact virological mechanisms inducing this type of liver damage are yet not completely resolved, but HCV is known to deregulate the intrahepatic metabolism of lipids by altering lipid peroxidation, lipid synthesis, insulin resistance, VLDL assembly and secretion, as well as to induce oxidative stress, in order to promote its highly lipid-dependent life cycle [302-304]. A simplified overview of critical pathways of the human metabolism can be found in “Information box 1”. More mechanistically, excessive storage of TGs in LDs could be the result of increased in TG synthesis, combined with LD biogenesis, decreased lipid catabolism and LD lipolysis, altered lipoprotein secretion or a combination of these processes (reviewed in Gluchowski et al., 2017[305]). Physiologically, LD formation is increased in response to excessive accumulation of lipids under hypoxic conditions, which modulate the expression of genes involved in the absorption and synthesis of fatty acids[306]. The excess of free fatty acids (FFAs) as substrates for β-oxidation results in increased synthesis of acetyl-CoA that may uncouple the tricarboxylic acid cycle (TCA cycle) function from mitochondrial respiration in the liver and promote the production of reactive oxygen species (ROS). In addition, it might further shift the normal metabolic process to the synthesis of toxic lipid intermediates, such as ceramides.

Hepatic steatosis was considered to be a benign and reversible pathology, though now, it has become a serious HCV-driven issue, that has been associated with higher fibrosis scores in chronically infected patients[307], and varying response to HCV treatment depending on the viral genotype[308].

I.B.στ.(ii) Fibrosis

Liver fibrosis is developed following the persistent inflammation induced by the expression of HCV proteins in hepatocytes, promoting certain signaling and metabolic pathways and inducing host's immune responses. Hepatic inflammation is a wound-healing process coordinated by a population of liver cells, the activated Hepatic Stellate Cells (HSCs). Upon HCV induced hepatic injury, HSCs are differentiated into their active form, myofibroblasts, which are responsible for the regulation of extracellular matrix (ECM) production and degradation balance, by metalloproteinases (the ECM degradation enzymes, MMPs) and their inhibitors (TIMPs). CHC-induced inflammation disrupts the equilibrium between MMPs and TIMPs production, subsequently resulting in ECM overproduction. A progressive thickening of fibrotic septae and chemical crosslinking of collagen ensues in the liver, namely fibrosis[309]. The formation of fibrous scar tissue in the liver can be induced by HCV either directly, due to oxidative stress induced by HCV replication[310] and activation of HSCs by Core protein[311], or via indirect mechanisms that involve activating immune responses and certain host signaling pathways.

Using the *Metavir* Score, fibrosis is divided into five stages ranked from zero to four (F0-F4), with patients assigned a stage based on their hepatic stiffness and F4 representing mostly cirrhotic stages of liver damage[300].

I.B.στ.(iii) Cirrhosis

Liver cirrhosis follows the stage of fibrosis and is the result of the combined action of several cellular and molecular factors over a course of approximately three decades. The main clinical manifestations of cirrhosis are the gradual loss of liver function, portal hypertension and progress of liver disease to the HCC development stage. Cirrhosis is marked by distortion of the liver parenchyma and vascular architecture, with one of its most prominent features being the formation of degenerative parenchyma nodules surrounded by fibrotic septae. Cirrhosis cases can be divided into compensated or decompensated stages. During the initial stage of compensated cirrhosis the liver is still capable of performing most of its basic functions and no significant symptoms are present, with the rare exceptions of possible fatigue, nausea, anorexia, and weight loss[312]. However, when patients with compensated cirrhosis are left unattended, there is a great risk of progression to an uncompensated phase, which is characterized by the appearance of more serious complications (e.g. variceal bleeding, portal hypertension, ascites, encephalopathy, jaundice, and spontaneous bacterial peritonitis)[313]. The survival of the patient is at risk during decompensated cirrhosis since half of the patients might not survive more than five years after entering this stage[314]. This leaves in many cases liver transplantation as the only option of survival.

I.B.στ.(iv) Hepatocellular carcinoma (HCC)

Hepatocellular carcinoma (HCC) is the most common form of primary liver cancer, the 7th most prevalent and 2nd deadlier type of cancer globally[315]. The main causal factor of HCC formation is chronic infection with hepatitis B and C viruses, as well as pre-existing liver cirrhosis due to these chronic infections. Hepatocarcinogenesis is a complex process that evolves over decades and involves the accumulation of genetic changes that will ultimately lead to the malignant transformation of hepatocytes. Regardless of the causative agent,

malignant transformation of hepatocytes is believed to be the result of the continuous changes that cells undergo due to chronic and recurrent liver injury and regeneration, that lead to an imbalance between controlled cell proliferation and apoptosis[316]. In transgenic animal models expression of independent HCV proteins has been associated with HCC development, data that may also be corroborated by the epidemiology observed in HCV patients. Several signaling pathways that regulate cell proliferation, differentiation, survival, as well as inflammatory and angiogenic responses are affected during HCV-induced hepatocarcinogenesis (for review see Virzi et al., 2018[317], Goto et al., 2020[318] and Farzaneh et al., 2021[319]). Briefly, these pathways are mainly the Transforming Growth Factor beta (TGF-β), Wnt/β-catenin, Hedgehog, Notch, Epidermal Growth Factor (EGF), Vascular endothelial growth factor (VEGF), mitogen-activated protein kinase (MAPK), Stat3, PI3K-Akt-mTor-PTEN, peroxisome proliferator-activated receptor gamma (PPARγ), Nuclear factor kappa-light-chain-enhancer of activated B cells (NF-κB), Tumor Necrosis Factor alpha (TNF-α), p53, and pRB signaling pathways. The interplay between HCV and these pathways will be more extensively described in §I.B.(θ). HCV-induced DNA modifications may also play a role in HCV carcinogenesis, notably alterations in CpG methylation, histone modifications and expression of small noncoding RNAs (sncRNAs) and long noncoding RNAs (lncRNAs).

Information box 1: Simplified overview of human energy metabolism.

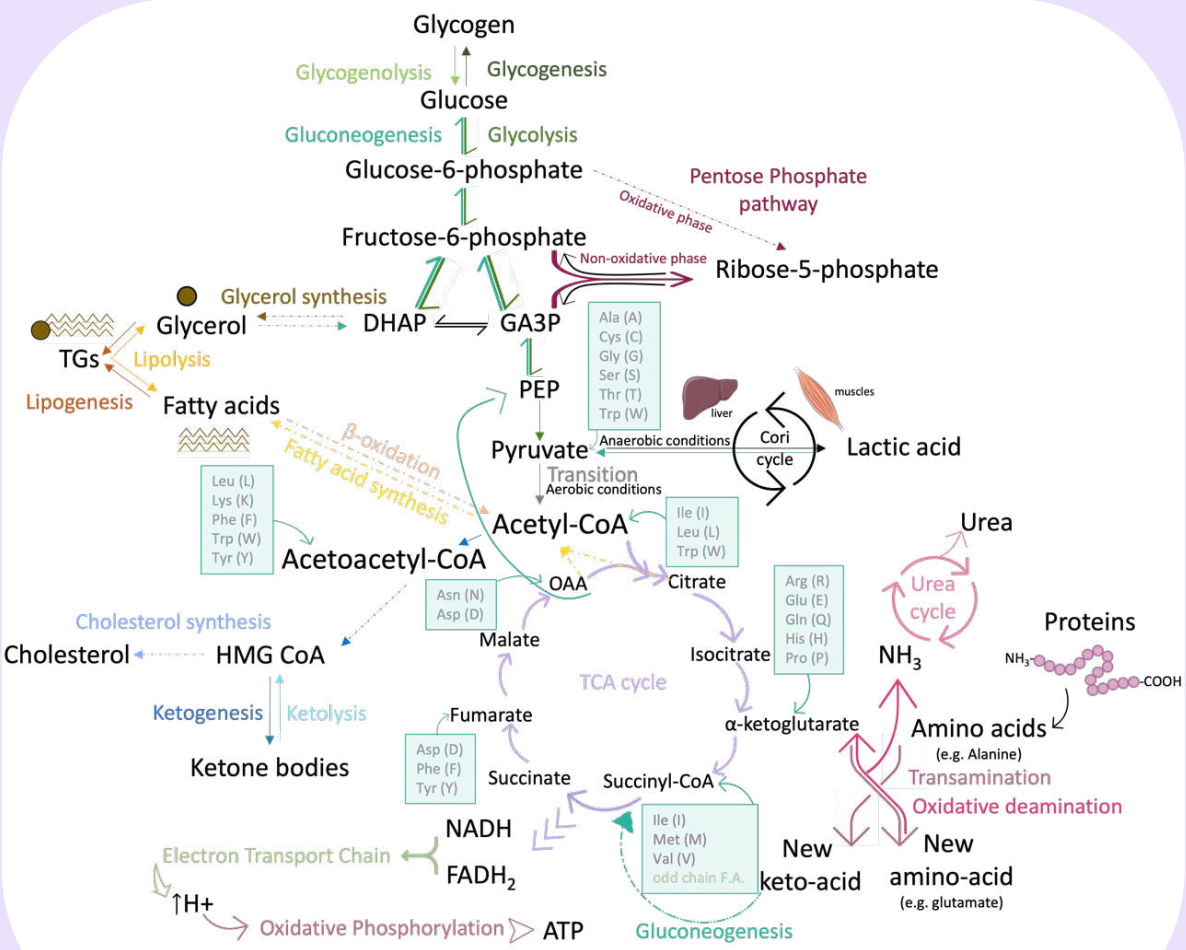

Information box 1: Simplified overview of human energy metabolism. (…continued)

The liver is a major player in human metabolism, regulating the balance among energy production over storage, based on the signals from elements in the bloodstream (e.g. insulin and glucagon). The primary source of energy for the cells is glucose, which can be stored in the form of glycogen through glucogenesis. Conversion of glycogen to glucose is done by a process called glycogenolysis, while through glycolysis glucose is converted to pyruvate. With the exception of a few steps in this process, such as phosphoenol pyruvate (PEP) conversion to pyruvate by the pyruvate kinase, most of the reactions are reversible. Some intermediate steps, such as fructose-6-phosphate conversion to fructose-1,6-biphosphate are not illustrated for conciseness purposes.

In the aerobic conditions of the liver mitochondria, pyruvate goes through a transition phase to acetyl-CoA. Acetyl-CoA has a central role in energy metabolism, linking glycolysis to the tricarboxylic acid cycle, (TCA cycle), also known as Krebs cycle and citric acid cycle, to cholesterol synthesis, to lipid and ketone metabolism. The result of TCA cycles are nicotinamide adenine dinucleotide hydride (NADH) and dihydroflavine-adenine dinucleotide ($FADH_2$) molecules, that enter the electron transport chain (ETC) in the mitochondria. ETC involves iron and cytochrome c, leading to the production and release of protons (H^+) from the mitochondria matrix to the intermembrane space. High H^+ concentration chemiosmotically activates oxidative phosphorylation (OXPHOS) for the production of energy in the form of adenosine triphosphate (ATP).

Acetyl-CoA can also be the result of lipid metabolism, and more specifically of triglycerides (TGs). TGs are produced by a process called lipogenesis, during which a glycerol molecule sequentially incorporates three fatty acid (FA) chains, generating monoacylglycerol (MAG), diacylglycerol (DAG) and triacylglycerol or TGs. The FA used in this process are synthetized during hyperglycemia and/or when ATP levels are increased. In these instances, citrate concentrations are increased, leading to its transfer to the cytoplasm, where it is broken back down to oxaloacetate (OAA) and acetyl-CoA. Part of the acetyl-CoA is then used for the production of the FA "building block", the malonyl-CoA and the other part is directly used together with malonyl-CoA by the fatty acid synthetase 1 (FAS1) for the initiation of FA synthesis, generating a 4-carbon molecule that gets enriched in every round of synthesis by 2 carbons from malonyl-CoA. To produce, for example, a palmitoleic acid (16 carbons), 7 rounds of FA synthesis are required. The inverse process of breaking down FA to acetyl-CoA that could be used for ATP production through the TCA cycle is called β-oxidation. Interestingly, even-chain FA β-oxidation gives rise to 8 acetyl-CoA molecules through 7 rounds, while in odd chain FA, the final 5-carbon chain yields one molecule of acetyl CoA and one molecule of propionyl CoA, which can then be converted to succinyl-CoA and enter the TCA cycle. Peroxisomes are another site of β-oxidation, with the difference that instead of redirection of the byproducts to the ETC, H_2O_2 is generated, further converted by the enzyme catalase to H_2O and oxygen. In any case, the availability of FA is dependent on TG mobilization and lipolysis, a process regulated by protein kinase A (PKA), which phosphorylates perilipin 1 (PLIN1), allowing lipases to break down the TGs.

Information box 1: Simplified overview of human energy metabolism. (...last part)

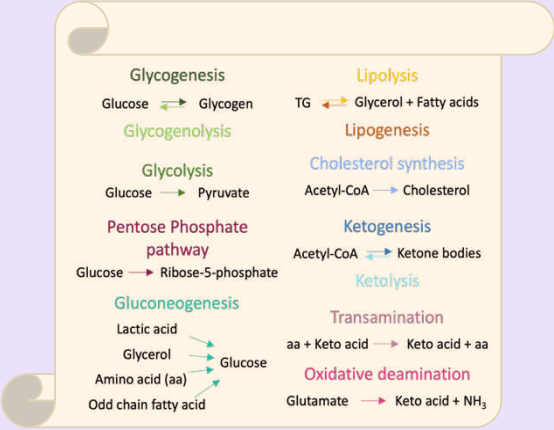

Accumulated acetyl-CoA molecules in hypoglycemic conditions, not allowing the furthering of the TCA cycle, can be combined together in a pathway that will eventually form β-Hydroxy β-methylglutaryl-CoA (HMG-CoA), which serves as a substrate for either cholesterol synthesis or ketone bodies, such as acetoacetate and β-OH-buterate. Ketone bodies travelling to the muscles and brain can be catabolized back to acetyl-CoA, providing ATP to these organs via TCA cycle and ETC coupled to OXPHOS.

On the other hand, the cholesterol formed after several steps in the cholesterol synthesis process is important for membrane preservation, steroid hormone production, lipid emulsification through the production of bile salts and generation of VLDL, LDL and HDL upon transformation to cholesterol-ester.

Proteins can be another source of energy in cases of severe stress or starvation since their amino acids (aa) can participate in the formation of new glucose molecules through gluconeogenesis. The first steps towards this process involve aa transamination in the presence of a keto acid (e.g. α-ketoglutarate), leading to the formation of a new aa and a new keto acid, from the exchange of the amine group and the oxygen between the two molecules. The new aa can undergo oxidative de-amination, reverting this process and generating ammonia (NH_3). To reduce the effects of its toxicity, ammonia is converted to urea, through the urea cycle. Different aa give rise to different keto acids. The green boxes in the figure indicate the aa whose transamination can lead to the direct or indirect production of the indicated products.

Pentose phosphate pathway has an oxidative and a nonoxidative phase, leading to the production of ribose-5-phosphate, using glucose-6-phosphate or fructose-6-phosphate and glucose-6-phosphate (GA3P) as substrates, respectively. Ribose-5-phosphate can further be used for the synthesis of DNA, RNA, ATP, NAD+, FAD, CoA, or be converted back to fructose-6-phosphate and GA3P towards gluconeogenesis.

Pyruvate produced from glucose or from protein transamination in the anaerobic conditions of muscles can be converted to lactic acid. Lactic acid can be released in the bloodstream, uptaken by the liver and be used for gluconeogenesis. The glucose produced can travel through the bloodstream back to the muscles and enter a new glycolysis pathway. This cycle is known as the Cori cycle.

Lastly, gluconeogenesis is the process of producing glucose within the cells, independent of dietary intake. As shown in the box summarizing the substrates and products of each metabolic process, gluconeogenesis can be initiated from 4 pathways, although the contribution of odd chain FA β-oxidation is minimal. The other three involve (i) the Cori cycle and the lactic acid produced in the muscles uptaken by the liver to produce glucose, (ii) dihydroxyacetone phosphate (DHAP) production by glycerol, that can follow the inverted pathway of glucose synthesis, and (iii) aa transamination, leading to the production of keto acids involved in the TCA cycle, of acetyl-CoA or pyruvate that can end up in OAA synthesis, further going back to PEP, and from there to glucose.

HCV induced extrahepatic manifestations

Despite the hepatotropism of the virus, HCV exhibits extrahepatic manifestations, some of which are better supported by epidemiological data than others. By disrupting its host's glucose and lipid homeostasis HCV may extend its burden to a systemic level. Summarized in Figure 21 are metabolic, cardiovascular, autoimmune, neoplastic, neuropsychiatric, and organ-specific manifestations that have been associated with HCV infection (reviewed in Cacoub et al., 2021[320]).

More specifically, metabolic disorders include insulin resistance (IR) and type 2 diabetes mellitus (T2DM). HCV infection may induce IR through downregulation of insulin receptor substrate signaling 1 (IRS-1), by overexpression of suppressor of cytokine signaling 3 (SOCS3) and TNF-α[321]. IR together with the release of proinflammatory cytokines, and other HCV-induced immune-mediated processes may drive T2DM development, which has an increased incidence rate in HCV infected patients versus non infected individuals[322].

These alterations may further cause cardiovascular events, by inducing chronic endothelial lesions and accelerated atherosclerosis in a pro-inflammatory, pro-fibrogenic environment[323]. The most commonly reported cardiovascular events include carotid atherosclerosis, myocarditis, acute coronary syndrome, and dilated or hypertrophic cardiomyopathy[324].

Autoimmune manifestations are referred to cryoglobulinemic vasculitis, an immune-mediated inflammation of blood vessels, and to the rare cases of rheumatoid arthritis. Autoimmunity may be organ directed, leading to thyroid dysfunction, pulmonary fibrosis, dermatological disorders, ocular Sicca or Sjögren's syndromes[325]. Cryoglobulinemic vasculitis is the most common HCV-induced extrahepatic manifestation that may appear after the production of auto- anti-IgG antibodies after chronic antigen stimulation by the virus. This chronic stimuli, together with the action of HCV proteins, may also lead to clonal proliferation of B-cells and lymphoma development. HCV has been also found to cause endothelial and mesangial inflammation, as well as podocyte and tubular damage in the kidneys, in addition to chronic inflammation caused by atherosclerosis and insulin resistance, that could result into chronic nephropathy[326]. Glomeruli may be the epicenter of cryo-precipitable deposits, which are commonly expressed as type I membranoproliferative glomerulonephritis.

Nonetheless, the extent and type of liver damage observed in HCV patients, whether intra- or extra-hepatic, is influenced by both viral and host determinants, as described below.

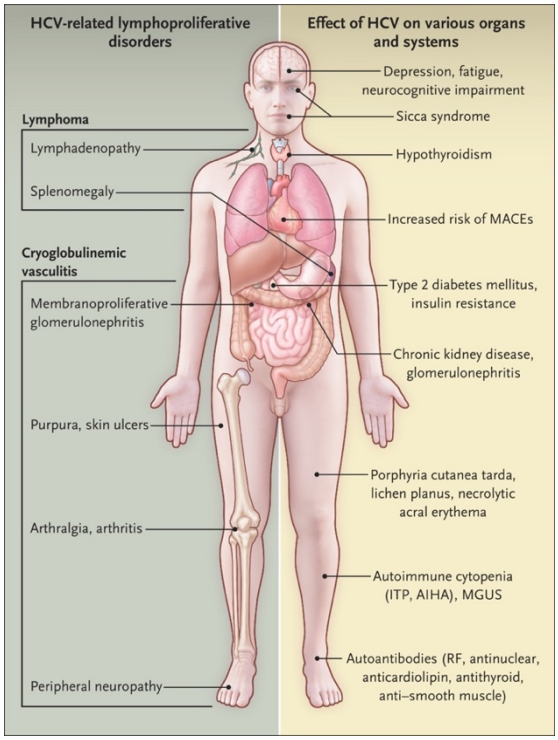

Figure 21: Illustrative summary of extrahepatic manifestations of HCV infection.
HCV-related benign (cryoglobulinaemic vasculitis) or malignant lymphoproliferative disorders are shown at the left, while HCV effects on various organs are shown in the yellow panel at the right. AIHA: autoimmune haemolytic anaemia, ITP: immune thrombocytopenia, MACE: major adverse cardiovascular event, MGUS: monoclonal gammopathy of undetermined significance, RF: rheumatoid factor. Reproduced with permission from Cacoub et al., 2021[320], Copyright Massachusetts Medical Society.

I.B.στ.(v) HCV genotype-related pathologies

Viral determinants refer to the genotypic origin of the HCV strain causing the chronic infection. More specifically, the globally most prevalent genotype 1, and subtype 1b in particular, has been found to be more aggressive and associated with a higher incidence rate of HCC development in CHC patients[327,328]. Certain aa polymorphisms within HCV 1b NS5A DI have also been correlated with HCC incidence, such as S3T, T122M, M133I, and Q181E[329]. On the contrary, HCV genotype 2 is rarely related to HCC incidence. CHC by genotype 3 strains has been linked to a higher prevalence of steatosis and therefore an increased risk of progression to severe hepatic complications of fibrosis, cirrhosis and HCC[330]. In fact, steatosis found in HCV genotype 3 infected patients has been correlated with expression of the HCV proteins and with viral loads. It could be reverted upon elimination of the virus, giving it the title of "viral steatosis", while in the presence of non3 HCV genotypes "metabolic steatosis" is mostly developed in the presence of comorbidity factors described in the next paragraph[331-333]. Genotype 4, although generally less characterized for its clinical manifestations, was highly endemic in Egypt, accounting for over 65% of Egyptian patients with HCC, while the distribution of HCV genotype 4 infection within the country was closely paralleled by the distribution of HCC development. However, solely these epidemiological data do not suffice for a conclusion on HCV genotype 4 association with HCC[334]. Similarly, the clinical characteristics of patients infected with HCV genotypes 5-8 are even less studied, for a conclusion to be made on the association of these genotypes with liver pathology.

Nonetheless, the data on genotypes 1-3 underline the importance of combined clinical studies and fundamental analyses in order to identify signatures specific to certain genotypes, or even directly "at risk" residues within viral sequences.

I.B.στ.(vi) Host comorbidity factors and reversal of liver damage

Liver damage can, of course, be developed independently of HCV infection, influenced by patient factors and characteristics. However these factors in the presence of the virus, whether induced by HCV or not, may drive the development of liver damage either faster, or to greater degrees. In the initial stages of HCV infection, comorbidity factors are relatively less prominent, although the host's age, gender, and genetic factors can influence the progression of liver disease. In general, age at the time of infection has been found to impact the rate of fibrosis progression, with older individuals often experiencing a more rapid deterioration of liver function[335], while male gender has also been associated with increased risk of advanced liver disease.

Liver steatosis is mainly attributed to increased alcohol consumption that can inhibit fat mobilization by altering the redox balance through the recurrent detoxification of ethanol to acetate[336], in the frame of alcohol-related liver disease (ARLD), or to other nonalcohol related risk factors, in the frame of metabolic dysfunction-associated steatotic liver disease (MASLD)[337]. Risk factors of MASLD include obesity, T2DM, IR, thyroid function abnormalities, high blood pressure, high cholesterol, metabolic syndrome (a combination of diabetes, high blood pressure and obesity), increased age and smoking (reviewed in Huang et al., 2021[338]). More specifically, increased intake of omega 6 and fructose stimulate de novo lipogenesis, while excess nutrition in general can lead to desensitization of the liver to insulin secretion. IR promotes the release of free fatty acids from adipose tissue into the blood and their re-absorption by the liver[339]. High glucose and free fatty acid levels, in the presence of increased insulin lead to overstimulation of lipogenesis, and eventual to liver steatosis[340]. Of note, host genetic polymorphisms in the PNPLA3[341] and TM6SF2[342] genes that are involved in a defect in lipoprotein lipidation, are also risk factors for the development of steatosis.

In HCV fibrotic stages, host-dependent factors, including age, sex, coinfection with HIV or HBV, and alcohol intake become increasingly significant. Moreover, obesity and IR can exacerbate liver damage during this stage, as they are linked to increased inflammation and fibrogenesis[343].

In advanced stages of HCV-induced liver disease host-dependent comorbidity factors continue to be crucial, with HCV aetiology of cirrhosis varying according to the geographic region. Alcoholism, chronic HCV infection and MASLD are the main causes in Western countries, while chronic HBV infection is the main cause of cirrhosis in regions of Asia and sub-Saharan Africa[344]. Risk factors for cirrhosis also include increased age, male sex, obesity, T2DM, autoimmune hepatitis, and inherited diseases such as cystic fibrosis, Wilson's disease and hemochromatosis[345]. Risk factors for HCC development include all of the above and the development of liver steatosis[316]. It should be noted however, that liver damage caused by HCV may progress to the severest forms of cirrhosis and HCC even upon SVR, with the progression risk being higher in the presence of alcoholism, older age, infection with HCV genotype 3, and elevated markers of hepatic fibrosis[346].

For the moment, there are no approved treatments of liver damage, although some steatosis targeting therapies are in pre-clinical development or in clinical trials. However, steatosis is a reversible condition, which can disappear by elimination of the cause, e.g. weight loss and a more appropriate diet, in the case of MASLD[347,348], a cessation of alcohol consumption in the case of ARLD and SVR in the case of CHC. However, the more advanced the liver disease, the more limited the effects of elimination of the cause will be. Therefore, at this stage, the only available treatment options would be liver transplantation or tumor removal coupled to elimination of the cause. Maximum life expectancy without liver transplantation for patients with decompensated cirrhosis is 3 years, provided that they remain under close monitoring and heavy medical treatment and 5 years for HCC. Liver transplantation is the second most common organ transplantation after kidney transplantation. However, less than one in ten people requiring liver transplantation can successfully undergo the procedure, due to a limited number of donors[349]. Despite the measures taken to encourage donations and to develop emergency transplant procedures following cardiac arrests, the number of liver transplants remains insufficient in Western and developing countries. The selection of the patients who will receive the valuable organ is based on criteria predicting the benefit of transplantation for each patient[350].

I.B.(ζ) Diagnosis and Treatment options

I.B.ζ.(i) HCV Diagnosis

A timely diagnosis of active HCV infection is not only essential towards prevention of virus spreading, but can also be decisive of an auspicious outcome. Unfortunately, though, most of HCV cases are diagnosed upon turning into a chronic state, due to the absence of symptoms during the onset of infection. Diagnosis of HCV infection typically occurs in three stages with three types of tests: (i) indirect tests examining the presence of antibodies against the virus, (ii) direct tests, detecting viral components, and (iii) genotyping of the infectious strain (reviewed in Roger et al., 2021[351]).

HCV serological tests were developed soon after the identification of HCV, following the cloning of the HCV genome, mainly towards screening of blood donations. Antibodies against specific epitopes of HCV Core and NS3-5 are detected in the plasma of HCV infected patients by immunoassays, such as ELISA (enzyme linked immunosorbent assay) or CLIA (chemiluminescence immunoassay). Third generation ELISA is most commonly used and can detect seroconversion at 8-12 weeks following infection. Fourth generation tests, introduced in 2008, have decreased the waiting period to 4 weeks, allowing both anti-HCV antibodies (Abs)

and HCV antigen (Core, cAg) detection[352,353]. Despite the low incidence of false positive results, mostly associated with patients in haemodialysis or profoundly immunocompromised, the reported sensitivity and specificity of these tests approaches 99%[354]. Determination of false positive tests could be achieved by recombinant immunoblot assays (RIBA), which are no longer in use.

In case of positive HCV-Ab detection, patients are screened for viral components, such as HCV RNA or cAg antigen. This test is important to distinguish patients with active HCV infection from those who have successfully cleared the virus, yet still carry antiviral Abs. HCV RNA genome detection and quantification is performed by quantitative real-time PCR (qRT-PCR). WHO has established an international unit for the evaluation of HCV loads, expressed in IU/mL[355], with the qRT-PCR tests conferring a high sensitivity of 10-50 IU/mL[356]. However, these tests can be expensive and required certain expertise to be conducted. Therefore, ELISA or CLIA tests against the cAg were developed in the early 2000[357], with a limit of detection now at 500-3000 HCV RNA IU/mL[358].

Lastly, identification of the HCV genotype is essential to determine the most appropriate therapeutic approach and duration of treatment, as discussed below. HCV genotyping is based on the sequencing of conserved HCV regions. Sequencing of the 5'-UTR is mostly selected by the laboratories, providing an accuracy rate higher than 97%[356].

I.B.ζ.(ii) HCV treatment

Nonspecific therapies have been widely available not long after the virus was identified. The desired outcome of HCV treatment is the persistent elimination of viral RNA from patient sera, called sustained virological response (SVR). SVR is considered achieved by the end of treatment, in the absence of HCV RNA detection for a minimum of twelve (SVR_{12}) or twenty-four (SVR_{24}) weeks thereafter[359]. However, the high number of infections globally, even in the era of highly efficient treatment options, as it will be discussed below, is indicative of restraints in achieving the goals set by WHO for 2030. Recently, a meta-analytic study, evaluated the reported barriers of CHC treatment and found significant differences among geographic locations for factors such as prioritization of HCV management, comorbidities, patients' psychology and cost of treatment (Figure 22).

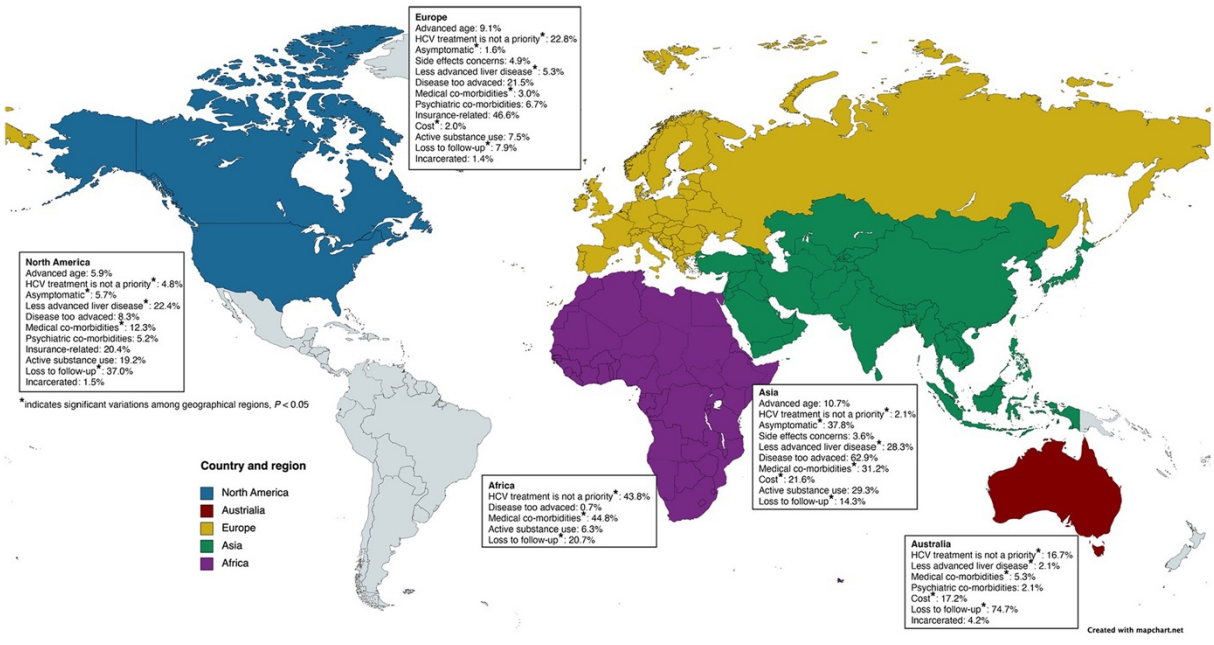

Figure 22: Meta-analysis results of types of barriers of untreated chronic hepatitis C (CHC) patients by continent.
Restriction factors with significant variation among geographic regions include HCV not being a priority, advancement of liver disease, inability to follow-up, lack of knowledge of infection due to the absence of symptoms, medical co-morbidities, and cost of treatment. HCV, hepatitis C virus. Figure from Nguyen et al., 2023[360], reproduced with permission from John Wiley and Sons (License N° 5615950332562).

Interferon against HCV

Similar to the treatment scheme against hepatitis B and other viruses, since 1989 patients with chronic HCV infection received interferon alpha (IFNα) as therapy. IFNα is a key mediator of antiviral innate immune responses, yet its exact mechanism of action against HCV has not yet been identified. IFNα alone exhibited low percentages of successful virus clearance, hence it was complemented in 1998 by ribavirin (RBV), another known antiviral agent, doubling SVR rates from ≤20% to ~40%[361,362]. A further augmentation of SVR was achieved with the replacement of IFNα by a covalent conjugate of it with polyethylene glycol (PEG). Up until 2011, administration of PEG-IFNα/RBV for 24-48 weeks was the standard of care against HCV, with an SVR rate of 90% for acute infections and 55% for chronic ones[363,364]. Response to PEG-IFNα/RBV therapy is highly dependent on both virus and host characteristics. Viral genotypes 2 and 3 are easier to treat, with an SVR rate of 65-80%, while genotypes 1 and 4 are more resistant[365]. Furthermore, patient's gender, age, ethnicity, nutrition habits and certain polymorphisms (e.g. IFNL3 rs12979860 and IFNL4 rs368234815) have been shown to affect both response to treatment and SVR rates[366,367]. Finally, on top of PEG-IFNα/RBV low efficiency, this treatment was also associated with a multitude of side effects, such as anemia, neutropenia, thrombocytopenia, fatigue, depression, autoimmunity, and thyroid dysfunction, driving ~10% of the patients to quit before completion of the treatment cycle.

Direct Antiviral Agents (DAAs)

Over the time following HCV discovery, the accumulated deeper understanding of the virus life cycle and its key components allowed researchers to identify ideal targets for drug development. This led to the introduction of Direct Antiviral Agents or DAAs in 2011, which were designed to inhibit viral polyprotein processing, genome replication and virion assembly (see also Figure 17, page - 21 -). DAAs can be divided into three categories according to their viral target:

1. NS3/4A protease inhibitors: drug name ending in "-previr", such as Grazoprevir (GZR), Paritaprevir/Ritonavir (PTV/RTV), Telaprevir (TEL), Boceprevir (BOC), Simeprevir (SMV), Voxilaprevir (VOX) and Glecarevir (GLE)
2. NS5A inhibitors: drug name ending in "-asvir", such as Daclatasvir (DCV) Elbasvir (EBR), Ledipasvir (LDV), Ombitasvir (OBV), Pibrentasvir (PIB) and Velpatasvir (VEL)
3. NS5B polymerase inhibitors, drug name ending in "-buvir", which are either nucleotide analogues (Sofosbuvir, SOF), which act by competing for binding to the active site of the RdRp or nonnucleoside inhibitors (Dasabuvir, DSV) that bind at allosteric sites

These new drugs presented significant advantages compared to PEG-IFNα/RBV therapy, since they can be administered orally, they present fewer and easily manageable side effects (e.g. fatigue, headaches, nausea), require shorter treatment cycles (8-12 weeks), and exhibit an SVR of above 90%, even in patients with compensated cirrhosis. However, there are some contra-indications for patients with specific co-morbidities. For example, protease inhibitors should not be prescribed to patients with decompensate cirrhosis, due to possible liver toxicity,

while SOF and RBV in combination with any DAA should be avoided in severe renal impairment cases (glomerular filtration rate<30ml/min).

Table 2: Simplified recommendations for HCV therapeutic regimens and duration, depending on HCV genotype, cirrhosis status, prior treatment experience, issued by the European Association for the Study of the Liver (EASL) in 2020[368].

Table adjusted and reproduced with permission from Elsevier (License Nº 5615960490326).

Type of treatment	Genotype	Cirrhosis status	Prior treatment experience	Sofosbuvir/ velpatasvir	Glecaprevir/ pibrentasvir	Sofosbuvir/ velpatasvir/ voxilaprevir	Grazoprevir/ elbasvir
Simplified treatment, no genotype/subtype determination[d]	All genotypes	No cirrhosis	Treatment-naïve	12 weeks	8 weeks	No	No
			Treatment-experienced				
		Compensated (Child-Pugh A) cirrhosis)	Treatment-naïve		12 weeks		
			Treatment-experienced				
Genotype/subtype determination-based treatment	Genotype 1a, 1b, 2, 4, 5 and 6	No cirrhosis	Treatment-naïve	12 weeks	8 weeks	No	12 weeks (genotype 1b only)
			Treatment-experienced				
		Compensated (Child-Pugh A) cirrhosis)	Treatment-naïve		12 weeks		
			Treatment-experienced				
	Genotype 3	No cirrhosis	Treatment-naïve	12 weeks	8 weeks	No	No
			Treatment-experienced		12 weeks		No
		Compensated (Child-Pugh A) cirrhosis)	Treatment-naïve	12 weeks with weight-based ribavirin[a]	8-12 weeks[b]	12 weeks[a]	No
			Treatment-experienced		16 weeks		No
	Subtype 1l, 4r, 3b, 3g, 6u, 6v or any other subtype naturally harbouring one or several NS5A RASs[c]	No cirrhosis	Treatment-naïve	Unknown	Unknown	12 weeks	No
			Treatment-experienced				
		Compensated (Child-Pugh A) cirrhosis)	Treatment-naïve				
			Treatment-experienced				

IFN, interferon; RASs, resistance-associated substitutions.
[a]If resistance testing is performed, only patients with the NS5A Y93H RAS at baseline should be treated with sofosbuvir/velpatasvir plus ribavirin or with sofosbuvir/velpatasvir/voxilaprevir, whereas patients without the Y93H RAS should be treated with sofosbuvir/velpatasvir alone.
[b]In treatment-naïve patients infected with genotype 3 with compensated (Child-Pugh A) cirrhosis, treatment with glecaprevir/pibrentasvir can be shortened to 8 weeks, but more data are needed to consolidate this recommendation.
[c]As determined by sequence analysis of the NS5A region by means of population sequencing or deep sequencing (cutoff 15%).
[d]Whenever HCV genotype and subtype determination is not available, not affordable and/or limits access to care.

Importantly, since 2015[369], clinical trials have shown that two or more inhibitors may be combined, resulting in SVR rates of 95-100%, with potentially pan-genotypic effects! The pan-genotypic combinational regimens currently in use and approved by the European Association for the Study of the Liver (EASL)[368] are the protease/NS5A inhibitors GLE/PIB, under the commercial name *Maviret*® and the NS5A/NS5B inhibitors SOF/VEL, under the commercial name *Epclusa*®. *Maviret*® proposed administration period is 8 weeks, with weeks added depending on previous therapy attempts, infection with HCV genotype 3 strains and liver cirrhosis, while for *Epclusa*® 12 weeks are required. Two more combinational regimes are also in use, with a genotype-specific effect. These are the NS5A/NS5B inhibitors LED/SOF, under the commercial name *Harvoni*® and the protease/NS5A inhibitors GZR/EBR, under the commercial name *Zapatier*®. *Harvoni*® is indicated for patients infected with HCV genotype 1, 4, or 6, independently of liver cirrhosis, for 12 weeks. This period may be decreased to 8 weeks in some very specific cases depending on HCV genotype and liver damage. *Zapatier*® is efficient against genotypes 1 and 4 with a duration of therapy of 12 weeks, independently of liver cirrhosis. Both *Harvoni*® and *Zapatier*® are only rarely used, due to the approval of pan-genotypic regimens, while the high efficiency of these combinational regimes has led to the voluntary discontinuation of some DAAs, such as TEL and BOC, by the owner companies. For the few patients with failed IFN-free, DAA-based therapy, the highly efficient VOX/VEL/SOF against all three HCV targets is proposed for a duration of 12 weeks. These most recent EASL guidelines for HCV therapy are summarized in Table 2, in a simplified version.

The greatest barrier to universal therapy using DAAs is their high cost, which prevents some patients from receiving such treatment and necessitates prioritizing. This year, the first DAA pharmacovigilance study accentuated their safety, while revealing the correlation of certain regimens with higher incidences of side effects, such as the association of

OBV/PTV/RBV with a 4-fold increase in the risk of renal impairment and 9-fold increase of anaemia, when compared to SOF-based regimens[370].

Nevertheless, the need for a protective vaccine remains, since HCV cure does not eliminate the risk of re-infection, nor the progression of HCV-induced liver damage to the severest forms of cirrhosis and HCC, even upon SVR[371]. Several aspects of HCV may hinder vaccine development attempts, i.e. its high genetic diversity, its immune evasion mechanisms, the low immune responses mounted by the host and the lack of an easily manageable, immunocompetent, animal model to evaluate the efficacy of vaccine candidates. However, with the great success of DAAs, some researchers are considering to assess vaccine candidates in humans, in a controlled human infection model[372].

I.B.(η) Study models

HCV research was greatly impacted for almost a decade following the discovery of the virus, due to the absence of cellular or animal study models amenable to reproducing the virus life cycle. Initially, virus-containing serum from HCV infected patients was used in an attempt to infect cultured cells, with extremely low replication efficiency and inefficient viral production, if at all. The construction of the first infectious cDNA clone from a subtype 1a isolate of HCV, H77, allowed the in vitro transcription of HCV genome-length synthetic RNAs, which could be intrahepatically inoculated to chimpanzees, causing productive infection. Nonetheless, such HCV RNAs were not infectious in cell culture[373,36]. Soon after, the first subgenomic replicon systems in cell culture were developed, followed by pseudo-typed particle study systems and the infectious models we are using today in cell culture or in the various animal models described below (reviewed in Ramirez & Bukh, 2018[240], Lohmann, 2019[374] and Burm et al., 2018[375]).

I.B.η.(i) Replicon systems

In 1999, the construction of HCV bicistronic subgenomic RNAs, that self-replicate in vitro in human hepatoma cells was a milestone in HCV research. In their original form, viral RNA replicons were derived from a subtype 1b viral strain (Con1b), in which the coding sequences of the structural proteins and p7-NS2 were replaced by the neomycin phosphotransferase gene (neo), conferring resistance to the antibiotic neomycin (G418). The viral genome was separated in two cistrons, the one downstream of HCV 5'UTR and IRES driving neo synthesis and a second cistron downstream of the heterologous encephalomyocarditis virus (EMCV) IRES driving translation of the HCV non-structural proteins NS3-NS5B followed by HCV 3'UTR of the virus[236,376373] (Figure 23). The constructed replicon was cloned under the transcriptional control of a phage promoter, that would allow the transcription of the full-length viral RNA. Importantly, the neo gene may be replaced by genes coding for luminescent proteins, such as the firefly luciferase, allowing researchers to quantify viral replication through measurement of the intensity of luminescence.

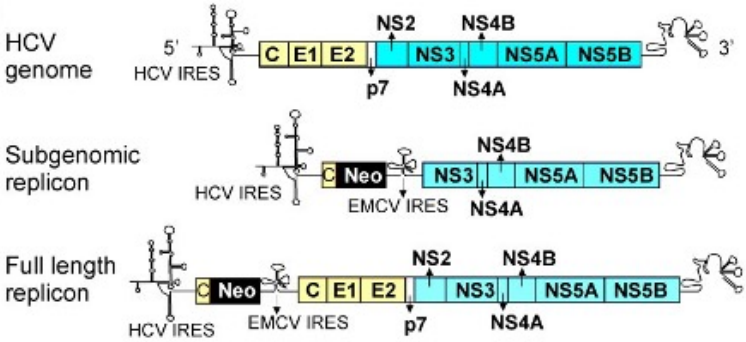

Figure 23: Schematic representation of HCV genomic and replicon RNAs. *ECMV: Encephalomyocarditis Virus, IRES: Internal ribosome entry site, Neo: Neomycin phosphotransferase gene. Figure reproduced from Uprichard et al., 2006[377]. Creative Commons Attribution 2.0 Generic License (CC BY 2.0).*

Transfection of the human hepatoma cell line Huh-7 with the subgenomic RNA and maintenance of the cells under selective pressure of G418 yielded only a small number of neomycin-resistant cell colonies, in which HCV RNA was stably replicating. Of course, in the absence of structural proteins, no infectious particles can be produced in this system. Following the construction of the Con1b subgenomic replicon, the development of other replicon systems followed, in which the sequences of various strains from genotypes 1-6 were used[378-389]. Nonetheless, the replication efficiency of subgenomic replicons was still low unless adaptive mutations providing replication fitness were selected[378,390-393]. The replicons system has further been significantly improved following the identification of SEC14-like protein 2 (SEC14L2) as a critical host factor allowing increased RNA replication of this system without the requirement of adaptive mutations[394].

In parallel to viral adaptive mutations, the cell lines clones harboring stably replicating HCV replicons, such as Huh-7.5[395] and Huh-7-Lunet[86] cells were shown to have evolved to support high HCV replication rates. At least two phenotypes may support an HCV-replication favorable environment: first, host factors essential for this process can be highly expressed (e.g. PI4KIIIα), and second, pathways of innate immunity, such as RIG-I in the case of Huh-7.5, are defective in these cells[396].

Altogether, this subgenomic replicon system has been extremely useful in the study of the molecular details of HCV genome replication, including the characterization of the membranous network involved in this process[45] and in the development of antiviral therapies[397]. Regardless, this system also presents some limitations, the main of which is the inability to undergo the full life cycle of the virus, not allowing the study of crucial steps, such as the entry, particle assembly and release of infectious virions.

I.B.η.(ii) Pseudo-particles

Early stages of the HCV life cycle can be studied using the pseudo-typed system (HCVpp), introduced in 2003, in which defective retroviruses coding for a reporter gene (e.g. luciferase) express the HCV glycoproteins E1 and E2 on their surface[398,399]. For the production of HCVpp a human embryonic kidney cell line (HEK-293T) is co-transfected by three independent vectors encoding (i) the HCV glycoproteins, (ii) the structural proteins gag-pol-env of a retrovirus (usually the human immunodeficiency virus, HIV or the murine leukemia virus, MLV), and (iii) the recombinant retroviral genome including a reporter gene. This approach has been adopted for the generation of HCVpp expressing E1 and E2 of diverse genotypic origin (genotypes 1-6), allowing comparative studies of HCV entry across genotypes[400] and strains isolated derived from HCV patients[401].

This system has been extensively used for the identification of essential HCV entry factors, for the characterization of E1/E2 conformational changes during HCV entry, for *in vitro* studies of HCV neutralization, and for extensive screening of putative HCV entry inhibitors[402,403,61,404]. This models further allows the investigation of conserved protein functions across genotypes and clinical isolates[405]. However, the limitations of this HCVpp model include an observed alteration of E1/E2 glycosylation patterns compared to virions produced in cell culture (HCVcc)[406] and an absence of associated lipoproteins and proper particle lipidation upon production of HCVpp in HEK-293T[407,398,408,409].

I.B.η.(iii) Cell culture infection systems

A major breakthrough in HCV research was accomplished in 2003, with the isolation of a peculiar HCV strain of subtype 2a from a Japanese patient with fulminant hepatitis, the JFH1 strain, and the demonstration that a subgenomic replicon derived from it was able to readily replicate at high levels without requirement for adaptive mutations[410]. Two years later, genome-length JFH1 RNA was found to not only efficiently yield to progeny virus in Huh-7

cells and chimpanzees[411], but cell cultured-grown JFH1-derived virus was able to also infect chimpanzees and humanized mice (see §I.B.η.(iv))[412]. The first HCV infectious model was born.

Nonetheless, the infectivity of this viral clone was low, turning researchers into a quest for virus adaptation. Through serial passaging of the virus in cell culture, recurring mutations in certain region of the viral genome conferred higher viral replication rate. Most commonly, the mutations were clustered in NS5A and E2, while a p7 mutation was also highly associated with increased viral titers of HCVcc. The combination of three adaptive mutations, two in NS5A (V2153A, V2440L) and one in NS5B (V2941), were found to boost viral production to high titers in Huh-7.5 cells[413], giving rise to the JFH-1 adapted (Jad) virus, that we are using in our lab today. Other groups have selected strains with different single or combined adaptive mutations for their studies.

Another mechanism that proved to increase HCV titers in cell culture by up to 2-3 log units was the construction of intragenotypic chimeric viruses, comprised of the 5'-UTR and NS3-3'UTR sequences of JFH1 and Core-NS2 sequences of another subtype 2a strain, the J6[414]. Another widely used chimeric HCV virus, with high propagation in cell culture is the Jc1 strains, which is again a (J6/JFH1) chimera, with the only difference that in which Core to the first transmembrane domain of NS2 haves the J6 sequence, while the rest of the NS2 to the 3'UTRremaining comes from the JFH1 strain. With exchanges like this similar designs, several HCV chimeras intra- or inter-genotypic recombinant viruses have been developed, using Core-NS2, or Core-NS2 and NS5A sequences of J6 and/or sequences from strains of other genotypes within the JFH1 backbone, with additional substitutions of JFH1 sequences in some instances to produce infectious virus. A summary of these attempts is illustrated in Figure 24, reproduced from Ramirez et al., 2018[240].

Over the past few years, a restricted number of strains from the most commonly circulating genotypes have been adapted by serial passage in cell culture, as well as through the introduction of multiple point mutations within several protein coding sequences by genetic engineering. Ultimately, these accumulated coding alterations have enabled a moderately efficient replication of these viruses in cell culture. These strains, however, remain scarce and heavily mutated in comparison to the initial clinical strains.

Despite its multiple advantages, this Huh-7.5 infection cell culture system has limitations. The necessity of adaptive mutations for efficient virus production prevents the use of clincial strains. The blocked IFN signaling pathway precludes host's immune pressure on virus evolution during infection and such a hepatoma cell line does not allow the evaluation of carcinogenesis mechanisms[415].

An alternative to this system, could be the less accessible, yet more liver-resembling option of culturing primary human hepatocytes (PHH), differentiating stem cells or using liver organoids. However, even these models come with significant considerations. PHH, for example, coming from non-cancerogenic liver sections retrieved during a biopsy are difficult to obtain, they vary considerably from one donor to another, they have only a limited life span in culture, where they also eventually lose the biological characteristics of hepatocytes[416]. On the other hand, despite the increased reproducibility conferred by differentiation of embryonic stem cells (ESC) or induced pluripotent stem cells (IPSC) to mature hepatocytes, the latter are not highly permissive to HCV infection and may clear the virus within ~10 days of infection[417,418]. The same issues on permissivity are uncovered through attempts to infect liver organoids, which can be produced from stem cells cultured in extracellular matrices in the presence of spontaneous tissue self-organization growth factors, giving rise to hepatocytes and the three main nonparenchymal cells of the liver (HSCs, Kupffer cells and endothelial cells)[419].

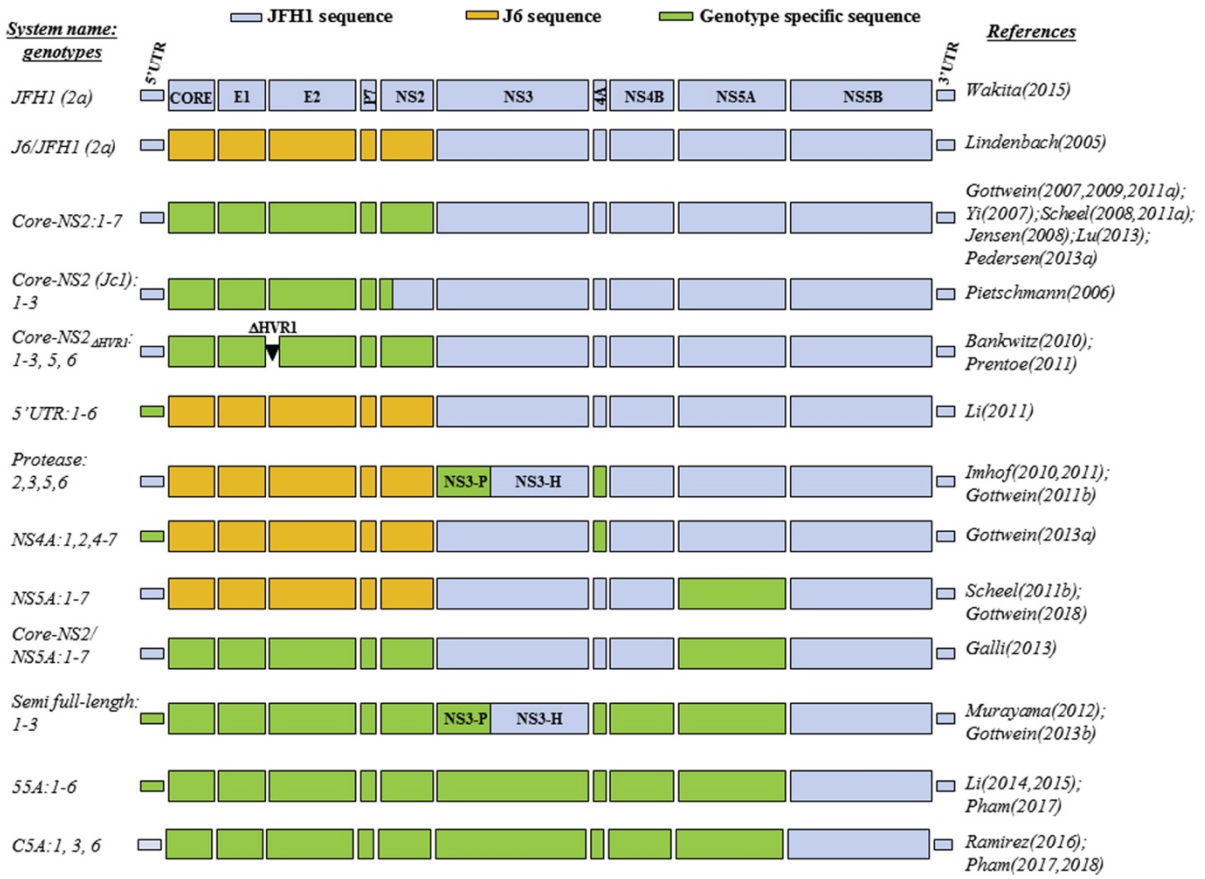

Figure 24: A summary of the HCV chimeric genomes developed within the JFH1 backbone. *Full-length JFH1 and J6/JFH1 genomes are shown on top. Sequences derived from JFH1are displayed in blue, from J6 in orange, and from various other genotypes in green. The names of the various HCV genomic sections encoded proteins are only shown in the JFH1 genome depiction, but are comparable in the schematic representations of the rest remaining genomes schemes. The name of each virus recombinant and the genotypes available for that chimera are displayed on the left side of the illustration indicate the viral sequence exchanged and genotypic origins available, while the corresponding literature references to the literature are presented on the right. NS3-P: NS3 protease domain, NS3-H: NS3 helicase, ΔHVR1: deletion of the hypervariable region 1 in E2.Figure from Ramirez et al., 2018[240], reproduced with permission from Elsevier (License No 5618870536666).*

I.B.η.(iv) Models for *in vivo* studies

Since the discovery of the virus, HCV research has greatly been contingent on animal models, that can support the infection and/or develop similar pathologies as the humans. The *in vivo* models for HCV studies can be divided in five big categories (summarized in Table 3): (i) hosts that can be naturally infected by the virus without the need of viral adaptation and/or host manipulation, (ii) transgenic animals, (iii) genetically humanised mice, (iv) xenotransplant mice, and (v) surrogate animal models (for review see Vercauteren et al., 2015 [420], Catanese et al., 2015[405], Burm et al., 2018[375] and Yong et al., 2019[421]).

Hosts supporting natural infection

Besides humans, chimpanzees are the only animal species to be naturally susceptible to highly productive HCV infection rendering it the only acceptable model for the evaluation of therapeutic and vaccine strategies. However, since 2010, new ethical guidelines have hampered the use of chimpanzees as animal testing models for HCV in the European Union and since 2015 in the United States as well[422].

Almost a decade following the discovery of HCV a small mammal resembling squirrels, the tree shrew, was found to support HCV infection[423], and develop liver fibrosis, cirrhosis, and oxidative stress just as chronic HCV infected patients might do[424,425]. However, the viremia induced was not high and this model is not widely available.

Recently, well-renowned scientists of the hepatitis C field have been contemplating that in the absence of a better animal model, either due to ethical or financial restrictions, and in the presence of highly efficient and effective antiviral treatment, vaccine candidate testing could be redirected to the natural HCV host, the humans[372]. In fact, this is not the first instance in which such a concept is being proposed[426]. Controlled Human Infection Models (CHIMs) entail deliberate exposure of healthy human volunteers to a well-documented pathogen towards in depth investigation of disease processes, treatment, and vaccine assessment, and are already undergoing optimisation and refinement for tuberculosis (TB) and severe acute respiratory syndrome coronavirus 2 (SARS-CoV-2) studies[427,428]. A lot of collective thinking has been put into this model, with specific workshops being held over the past years, led mainly by Drs Jake Liang and Jordan Feld. During these meetings several considerations have been raised and an in-depth proposal addressing them has been recently submitted[429]. Personally, I fail to comprehend how the ethical and financial repercussions of a human animal model are lesser that those of a nonhuman one. Even more so, when the consensus proposal on the human cohort suggested to undergo the controlled infection targets a vulnerable subgroup of people, those addicted to intravenous drug use. No matter the extended knowledge we have acquired over HCV life cycle, we are still not completely aware of the associated pathology inducing mechanisms and we are only recently beginning to fathom the extent to which an HCV infection may still affect the host upon clearance, e.g. through epigenetic alterations and reprogramming of host gene expression[430]. Despite scientists' thirst for knowledge and need to serve the public, it might be beneficial to occasionally ask ourselves "Would I enroll my child in this?".

Transgenic mice

Mice do not express human hepatocyte factors essential for HCV entry (for review, Sandmann and Ploss, 2013[431]) and they do express factors restricting viral multiplication in murine hepatocytes[432], rendering them resistant to HCV infection. Transgenic animal technology, allowing for the germline insertion of exogenous genes, has provided researchers with a model in which HCV coding regions, from selected proteins to the whole polyprotein, are expressed in mice and the effects of this expression can be observed (for review Barth et al., 2008[433]). Transgenic mice are unable to recreate the full life cycle of the virus, but they have been reported to exhibit liver pathology. Steatosis, HCC and oxidative stress have been documented, following the expression of HCV Core protein[434-436], while the expression of the complete viral polyprotein was associated with an increased risk of cancer[437] suggesting that hepatocarcinogenesis is the result of the combined action of several HCV proteins. It should be noted however that the observed pathogenesis has not always been successfully reproduced by independent groups[438,439]. Nonetheless, as this model does not support HCV infection, not all findings are directly relevant to the HCV pathogenesis *in vivo*.

Genetically humanized mice

In order to address this this constraint, mice can be rendered susceptible to infection through transgenic introduction of the human orthologs required for HCV entry[440]. Indeed, expression of the HCV co-receptors CD81, SR-B1, CLDN1 and OLCN permitted HCV entry in mouse hepatocytes *in vivo*[441], while in the context of immunodeficient mice HCV persistent infection could be recapitulated[442].

Although no apparent pathology has been observed in these mice, possibly due to the absence of inflammation in this immunodeficient background, they embody an appropriate model for the study of antivirals and murine vaccine responses[443-445]. They have also largely been used for *in vivo* examination of the virus life cycle[446-448]. Fibrosis development has been reported in this model (Table 3), an observation made by a single group in immunocompetent humanized mice that developed sustained viremia for more than 12 months in parallel with hepatic lesions[449].

Xenotransplanted mice

Another method to overcome the species barrier entails xenotransplantation of PHH or *in vitro* cultured human hepatic organoids towards humanization of the murine liver[450]. However, this process can only be successful in the absence of B-, T- and natural killer (NK) cell responses, meaning that these mice are severely immunocompromised. To improve this model, transplantation of both PHH and human hematopoietic cells has led to the development of immunocompetent chimeric mice, with human liver and immune system. These can prove to be invaluable in the investigation of HCV-induced liver damage and in the pre-clinical validation process of vaccine candidates, once proven to be permissive to HCV infection[451,452].

HCV surrogate animal models

For several years, the only available surrogate animal model for HCV was the distantly related GB-virus B (GBV-B) infection of small New World primates, such as tamarins and marmosets. GBV-B is the exemplar virus of the Hepacivirus platyrrhini species, within the Hepacivirus genus. GBV-B can cause acute hepatitis and rare persistent infections upon experimental administration in small primates, serving as a useful model for the understanding of immune responses and possible restrictions in vaccine development attempts for HCV[453-455].

With the recent advancements in the Hepacivirus field, several new species have been identified and phylogenetically analysed, revealing the increased genetic proximity of the human Hepacivirus hominis to the canine Hepacivirus equi. Otherwise known as nonprimate hepacivirus (NPHV), this virus was first isolated from infected dogs[456]. However, it was later found that its natural host are horses (Equus ferus), in which NPHV can induce persistent infection, with hepatotropism and development of liver inflammation. The chronicity of infection is decreased compared to HCV in humans, but the exerted immune response is highly similar, with delayed seroconversion and inflammation in the liver[457]. Therefore, the immunocompetent horses infected with NPHV would be a great model to study Hepacivirus pathology and responses, had the animal been easier to manage and less costly to sustain.

Lastly, the rodent hepaciviruses identified over a decade ago also constitute a greatly interesting surrogate model for HCV and will be described with in more detail at the dedicated section (see §I.C).

Table 3: In vivo models for the study of HCV, possible surrogate animal models and their applications.
All immunocompetent surrogate animal models are appropriate for the study of therapies and vaccine development against the respective virus, hence not applicable (NA) for HCV. HCC: hepatocellular carcinoma.

Animal model details		Viremia	Liver pathology	Adaptive Immunity	Good for the study of HCV		Availability	Bibliographic references
					Therapies	Vaccines		
Hosts supporting natural infection	Pan troglodyte (Chimpanzee)	Chronic or acute	-	✓	✓	✓	-	Bukh et al., 2001[458]; Lanford et al., 2001[459]
	Tupaia belangeri (Tree shrew)	Intermediate	Fibrosis, Cirrhosis	-	-	-	Low	Feng et al., 2017[460]
Transgenic mice	expressing viral proteins	NA	Steatosis, HCC, Oxidative stress	✓	NA	NA	High	Perlemutter et al., 2002[435]; Liang et al., 2004[436]
	expressing HCV polyprotein	NA	Steatosis, HCC	✓	NA	NA	High	Lerat et al., 2002[437]
Genetically humanized mice	expressing HCV essential entry factors	Persistent	Fibrosis	✓	✓	✓	High	Chen et al., 2014[449]
Xenotransplanted mice	Human liver chimeric mice	Persistent	-	-	✓	-	Low	Meuleman et al., 2008[461]; Bukh et al., 2010[462]; Burchill et al., 2017[463]; Andreo et al., 2017[464]
	Human liver and immune system chimeric mice	Low/only in liver extracts	Inflammation, fibrosis	-	-	✓	Very low	Washburn et al., 2011[465]; Keng et al., 2016[466]; Zeng et al., 2017[467]
Hosts supporting natural infection with viral homologs	Hepacivirus platyrrhini (GB-virus B) infected small primates	Persistent or acute	Acute hepatitis, Steatosis	✓	NA	NA	Low	Martin et al., 2003[453]
	Hepacivirus equi infected Equus ferus (horses)	Persistent or acute	Inflammation	✓	NA	NA	Low	Pacchiarotti et al., 2022[15]
	Hepacivirus ratti (norway rat hepacivirus-1) infected rats	Persistent chronic	Steatosis	✓	NA	NA	High	Trivedi et al., 2018[468]
	Hepacivirus ratti or Hepacivirus norvegici (norway rat hepacivirus-2) infected mice	Depends on animal immunocompetency	Fibrosis	✓	NA	NA	HIgh	Billerbeck et al., 2017[469] Brown et al., 2023[470]

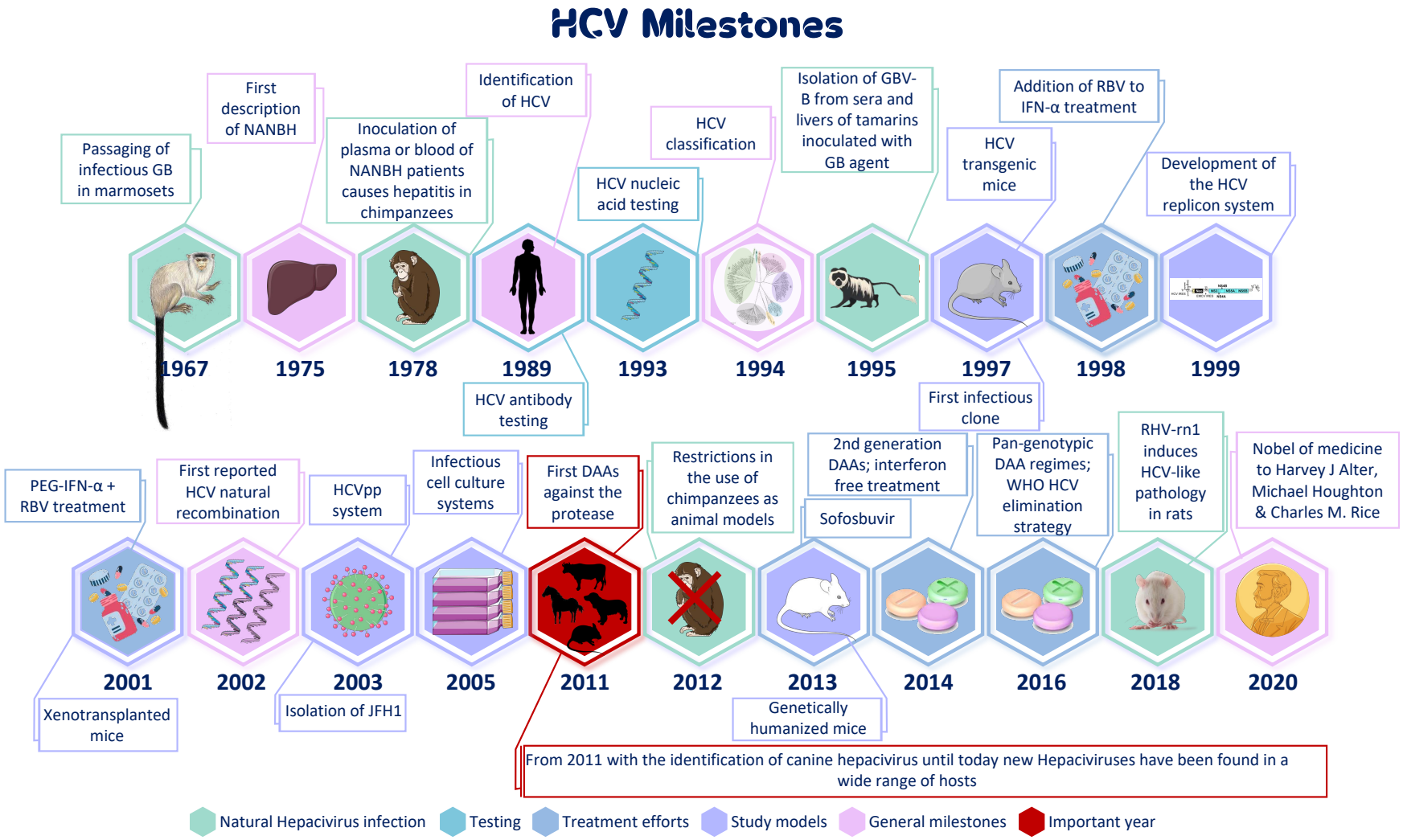

Figure 25: A summary of the HCV milestones described so far in this manuscript.
Bibliographic references can be found within the corresponding section of the manuscript. Figures reproduced with permission from SmartServier (https://smart.servier.com/), Freepik (https://www.freepik.com/), Inotiv (https://www.inotivco.com/), or Uprichard et al., 2006[377] (CC BY 2.0).

I.B.(θ) Virus-host interactions

HCV promotes its life cycle and induces deregulations in the host cells through the actions of virus-encoded proteins, which may cause rewiring of cellular pathways either by direct interaction with cellular proteins implicated in these processes or by modifying the expression of cellular genes. A schematic synopsis of the HCV-induced perturbations of hepatocellular homeostasis essentially leading to HCC is provided in Figure 26, with an emphasis on the implications of the viral proteins modulating each process. These disturbances of host processes may be induced at the protein or at the gene level. Since a detailed overview of all host cell modulations is beyond the scope of this manuscript, the interactions of HCV with the host immunity is briefly presented below, followed by an outline of reported PPIs and regulation of cellular gene expression by HCV proteins, with stress on the roles of Core and NS5A.

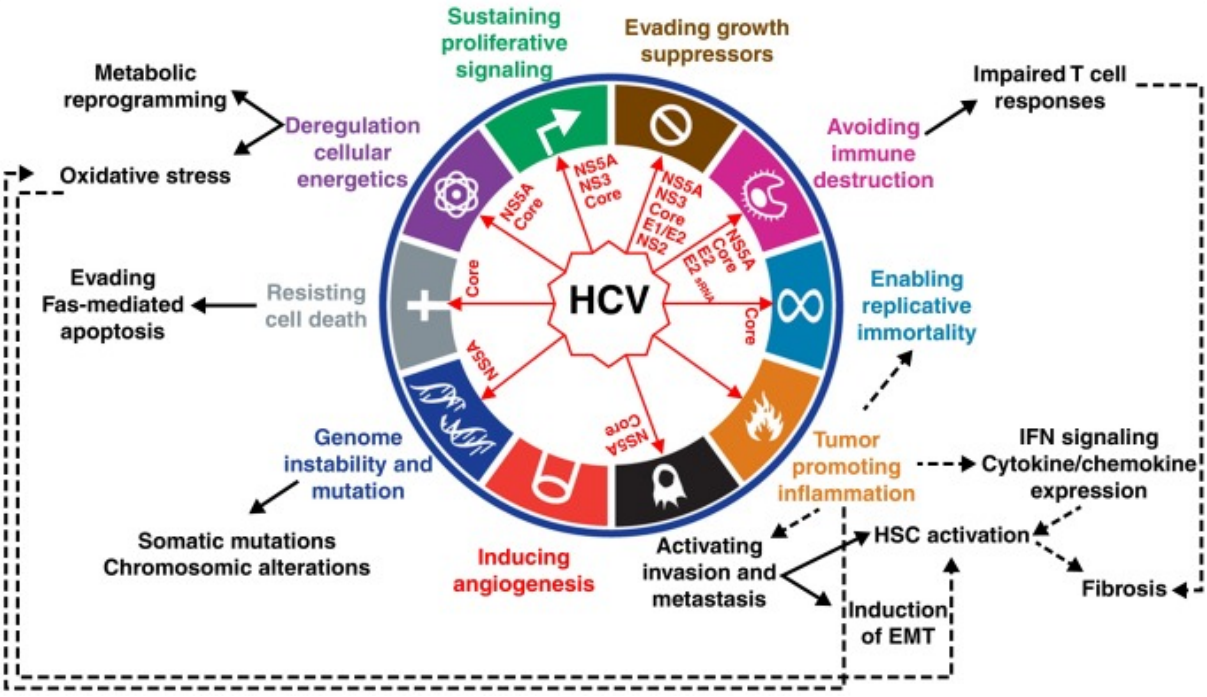

Figure 26: Schematic summary of HCV-induced perturbations of hepatocellular homeostasis. *The main focus is on HCV-host interactions and signaling during viral infection that contribute to cellular transformation and HCC development. Red arrows are indicative of the direct effects of HCV RNA or proteins on specific hallmark processes. HCC mechanisms observed in the clinics and in in vivo models are linked to the hallmarks by the black arrows. Dotted lines represent examples of inflammation-driven carcinogenesis. EMT: epithelial mesenchymal transition, HSC: hepatic stellate cells, IFN: interferon, sRNA: small RNA. Reprinted from Bandiera et al., 2016[471], with permission from Elsevier (License number: 5623560073115) and from original Mesri et al., 2014[472] (License number: 5623561123899).*

I.B.θ.(i) Immune evasion

Infection of hepatocytes with HCV triggers the activation of the immune system in order to clear the virus[473]. To this end, dendritic cells (DC), HSCs, and Kupffer cells express cytokines (MIP-1, IL-12, IL-15, and IL-18) to attract NK cells that will produce IFNγ in the liver[474,475]. The production of type I and III interferons causes sinusoidal endothelial cells to secrete chemokines (CXCL10, MIG), further attracting T lymphocytes toward viral clearance[476].

Nonetheless, HCV can evade the host immune system and cause persistent infection. The virus accomplishes this in a variety of ways, including the disruption of DCs and NK cells. HCV has been demonstrated to increase the levels of indoleamine-2,3,-deoxygenase, disrupting DC maturation and antigen-presenting capabilities[477]. DC disruptions further include altered phagocytic capabilities through induced plasmacytoid dendritic cell (pDC) apoptosis and impaired DC proteasomal subunits[478]. Early in HCV infection, impaired DC activity leads to low levels of NK cell maturation and an immunosuppressive regulatory T-cell phenotype due to poor priming of CD4+ and CD8+ T cells[479,480]. Persistent HCV infection also results in varying expansion and differentiation of NK cells among patients[481], while NK cell function during HCV acute and chronic infection have also been found to permutate[482].

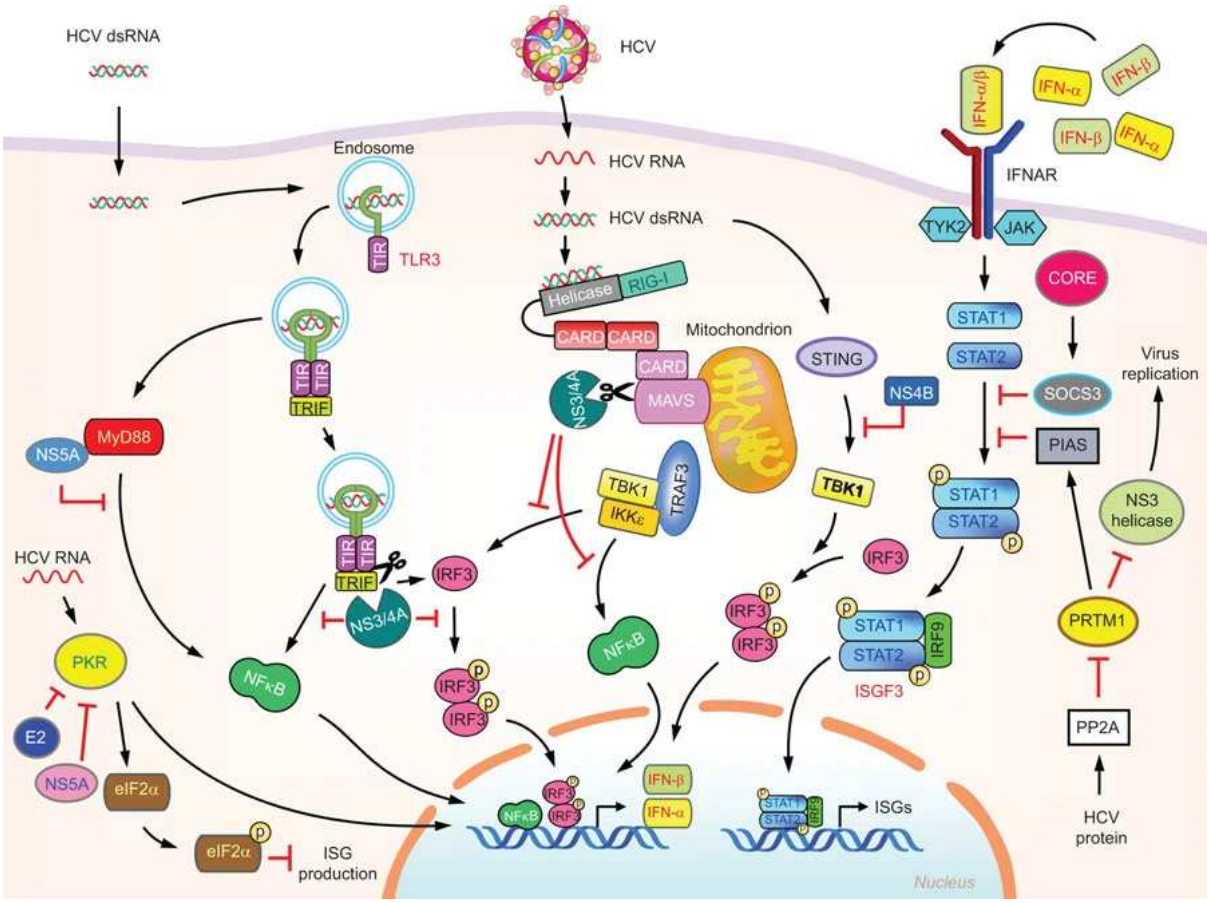

Figure 27: Mechanisms of HCV evasion of innate immunity.
The steps in which viral proteins interfere with physiological host immunity pathways are highlighted by red "stop" signs. eIF2α: eukaryotic initiation factor 2α, HCV: hepatitis C virus, IFN: interferon, IRF: IFN regulatory factor, ISG: IFN-stimulated gene, MAVS: mitochondria antiviral signaling protein, MITA: mediator of IRF3 activation, MyD88: myeloid differentiation pro-inflammatory response 88, PIAS1: protein inhibitor of activated STAT1, PKR: protein kinase R, PRMT1: protein arginine methyltransferase 1, SOCS3: suppressor of cytokine signaling 3, STAT: signal transducer and activator of transcription, STING: stimulator of interferon gene, TLR: Toll-like receptor, TRIF: TIR domain-containing adaptor inducing IFN-β. Figure reproduced from Wong et al., 2016[484] under Creative Commons Attribution-NonCommercial-NoDerivatives 3.0 Unported License (CC BY-NC-ND 3.0).

At the molecular level, host cells possess several recognition and defence mechanisms against viral intrusion (Figure 27). Two important signaling pathways that activate the host innate immunity against viral infection can be subverted by HCV-encoded proteins. One of these pathways utilizes members of Toll-like receptor (TLR) family and the other senses intracellular viral double-stranded RNA (dsRNA) via the RNA helicase RIG-I and is involved

in the activation of transcription factors. Viral detection by these pattern recognition receptors (PRR) is the first step to type I IFN (α and β) and interferon-stimulated gene (ISG) induction, via the activation of IRF3, IRF7 and NF-κB transcription factors by adapter proteins such as TRIF, MYD88 and MAVS. Secreted IFN is detected by interferon receptors of neighbouring cells and induces through the JAK/STAT pathway the transcription of ISGs, such as inflammatory cytokines, pattern recognition receptors and effector proteins[483].

The best characterized mechanism of subversion of HCV immunity is the NS3/4A protease-induced inhibition of the RIG-I and TLR3 signaling pathways through the cleavage of MAVS and TRIF, respectively[485,486]. Additionally, NS3 itself has been found to bind tank binding kinase (TBK1) in order to prevent the engagement of IRF3 and the expression of IFN[487]. TBK1 is also a target of NS4B, which in turn targets the STING-mediated activation of the protein, to suppress the induction of type I IFN[488]. Core also plays an important role by inhibiting the JAK/STAT signaling through direct interaction with STAT1[489] and by inducing the production of suppressor of cytokine signaling proteins (SOCS1 and SOCS3)[490,491]. Core binding to STAT1 was shown to prevent its phosphorylation and thus, its activation[492]. Core, in its monomeric form, can additionally stimulate TLR2 pathway assisting the virus evasion of the innate immune system[493,494]. Moreover, E2 and NS5A are known to inhibit PKR[495,496], while NS5A additionally interacts with 2'-5'-oligoadenylate synthase (2'5'OAS), blocking its antiviral effect and reducing ISG expression levels[497] and with the TLR adaptor MyD88 to inhibit TLR-mediated innate immune evasion[496]. Furthermore, NS5A induces gene transcription of interleukin 8 (IL-8), which has been found to suppress the antiviral actions of IFN-α[498] and to downregulate the expressions of NKG2D, an activating cell surface receptor on NK cells, via TLR4 pathway, impairing the functional ability of these cells[499].

Nonetheless, despite all these subversion mechanisms, activation of the IFN pathway is still detected in HCV infected patients, an attribute that could be explained by the fact that not all hepatocytes are infected or by induction of the signaling before the production of viral proteins[500]. These mechanisms are collectively represented in Figure 27[484].

I.B.0.(ii) Protein-protein interactions

The identification and functional characterization of individual HCV-host PPIs can be of great importance towards better understanding the mechanisms of viral pathogenesis and promotion of the HCV life cycle. On the other hand, a more collective mapping of these PPIs into networks may reveal valuable insights into functional constitution of the viral protein interactomes, through analysis of different aspects of the network, such as its complexity and size.

Several researchers of the HCV field have undertaken to identify HCV-host PPIs by different small-scale or high-throughput experimental approaches, or by computational prediction models. The wet lab techniques more commonly used to identify direct or indirect PPIs include the *in vivo* Yeast 2 Hybrid (Y2H) system, and the *in vitro* glutathione s-transferase (GST) pull-down, affinity chromatography, co-immunoprecipitation, protein-fragment complementation assays (PCA), biotin-based proximity labeling techniques (BioID, APEX)[501], and (tandem) affinity purification of protein complexes coupled to identification of retrieved peptides by mass spectrometry (AP-MS) (for review see Rao et al., 2014[502]).

Whether attempting to produce a comprehensive map of HCV by determining the interactomes of multiple viral proteins, or just focusing on a single viral protein and functionally characterizing few selected partners, the list of publications on HCV PPIs is enormous. For a time, a group of researchers had created and manually curated an HCV-specific PPI publicly available database called HCVpro[503] (http://cbrc.kaust.edu.sa/hcvpro/), which unfortunately has not been maintained during the past few years. Similarly, the VirusMINT database[504] (http://mint.bio.uniroma2.it/virusmint/), containing viral PPIs includes

only limited HCV-related data, that are rarely linked with specific HCV proteins, but rather with the polyprotein.

Hence, exhaustive lists of HCV protein PPIs are currently lacking. Some researchers have employed text-mining approaches attempting to tackle this, such as in the publications of:

(i) Mukhopadhyay & Maulik (2014), who performed mining of HCVpro to uncover HCV-host PPIs, String database to extract cellular PPIs and the Genetic Disease Association Database to collect protein associations to disease phenotypes[505],
(ii) Saik et al. (2016), who developed a mining tool, ANDSystem, and recovered HCV-host PPIs from PubMed abstracts and full text articles[506],
(iii) Farooq & Khan (2019), who extracted HCV PPIs from a selected list of 13 papers with accessible interaction data, out of the 729 studies retrieved by advanced search of PubMed for HCV PPIs[507],

or, in an attempt to complement their own experimental data, the works of:

(i) de Chassey et al. (2008), who complemented the interactome of Con1b derived proteins obtained by Y2H using a fetal brain and spleen cDNA library by text-mining data obtained by BIND database and PubMed[508], and
(ii) Thripathi et al. (2013), who focused solely on HCV NS5A protein, performing a Y2H screen using truncated NS5A (aa1973-2419) of genotype 1b J1 strain and a human liver cDNA library and reported previously described pairwise NS5A-human interactions mined from Medline, supplemented by follow-up manual inspections[509].

Original high-throughput studies addressing the HCV interactome include those of:

(i) Dolan et al. (2013), who carried out large scale Y2H screens using genotype 2a JFH1-derived whole or truncated proteins (Core, E2, NS2, NS3, NS4B, NS5A, NS5B) and a human liver cDNA library to identify HCV-host PPIs[510],
(ii) Germain et al. (2014), who used HEK 293T cells expressing 3xFLAG-tagged Core (JFH1-derived), NS2, NS3/4A, NS4B, NS5A (Con1b-derived), or NS5B viral proteins to perform immunoprecipitation (IP) of viral–host protein complexes coupled to liquid chromatography–tandem mass spectrometry (LC-MS/MS) expreiments[511], and
(iii) Ramage et al. (2015), who implemented affinity purification (AP) coupled to MS (AP-MS) experiments using the lysates of Huh-7 cells independently overexpressing each JFH1 protein and verified the retrieved interaction in a replicon system[512].

High-throughput investigation of the Core interactome has been carried out in the studies of:

(i) Roohvand et al. (2009), who performed protein chip and direct Core-dependent pull-down assays, followed by mass spectrometry, using C-terminally His-tagged Core proteins aa 2–169 (D1 and D2) and aa 2–122 (D1) expressed in Huh-7 cells[513],
(ii) Tripathi et al. (2010), performing a Y2H screen using Core of Con1b strain and a human liver cDNA library[514], and
(iii) Dolan et al. (2015), who investigated the interactomes of two N-terminal computationally predicted molecular recognition features of JFH1-derived Core in a Y2H screen with a human liver cDNA library[515].

For NS5A, while the distinct interactomes of the two phosphorylation forms has been studied by Pan et al.[160], using lysates of genotype 2a J6/JFH1 infected Huh-7.5.1 cells to perform AP-

MS/MS using antibodies specific to either p56 or p58 NS5A, other studies evaluating the NS5A interactome without discriminating NS5A phosphorylation status include those of:

(i) Meistermann et al. (2013), who identified NS5A interactors in Huh-7 cells stably expressing Con1b subgenomic replicon by immuno-competitive capture mass spectrometry (ICC-MS) experiments[516],

(ii) Eberle et al. (2014), who performed a TAP-MS screen using HEK293 cells ectopically expressing genotype 2a Jc1 NS5A[517], and

(iii) Vlaicu et al. (2017), who constructed a full-length functional replicon in the context of a modified JFH1 genome encoding tagged NS5A protein with a compensatory deletion of 40aa (previously described by Moradpour et al.[518], and Gottwein et al.[519]) towards AP-MS experiments using Huh-7 cells[520].

Many of these data, including additional PPIs are reported in the review papers of Kao et al.[521] for Core and Ross-Thriepland & Harris[118] for NS5A (Supplementary Table 1 and Supplementary Table 2). As detailed above, the limitations of the vast majority of these studies lie in the fact that they have rarely been performed in fully relevant infection systems.

Concerning NS5A, its interaction with certain cellular factors has well been documented and functionally characterized. More specifically, the crucial role of CypA and PI4KIIIα for HCV replication has already been presented in §I.B.ε.(iv) and is supported by extensive experimental evidence. Furthermore, interaction of NS5A with Amphiphysin II (BIN1) was shown to down-regulate NS5A phosphorylation, affecting the HCV life cycle[522], although the interaction was found to be dispensable for HCV RNA replication[523]. NS5A interaction through its DIII with annexin A2 (ANXA2) was also extensively studied, while ANXA knockdown or silencing were shown to dramatically affect HCV Jc1 titers in infected cells[524], or to decrease the formation of membranous web-like structures and HCV genotype 1b and 2a RNA replication[525], respectively. NS5A/Heat shock protein 72 PPI was also thoroughly examined, with the interaction being mapped to aa 147-301 of NS5A and aa 231-380 of Hsp72. Overexpression and knockdown experiments in Huh-7.5.1 cells stably carrying HCV subgenomic replicon pSGR-JFH1 showed that Hsp72 acts as a positive regulator of HCV replication possibly by increasing the stability of viral proteins levels within the replicase or by enhanced IRES translational efficiency[526]. Moreover, Hsp72 levels were found increased in the presence of NS5A, an effect that could be linked to increased nuclear factor of activated T cells 5 (NFAT5) activity due to ROS production by NS5A. Hsp72 modulation via NFAT5 might be a potential mechanism implicated in NS5A-directed induced liver pathology[527].

The host factors mentioned above are only a few of the reported NS5A interacting partners, with a more extensive list in Supplementary Table 2.

I.B.θ.(iii) Regulation of gene expression

Microarray studies in liver biopsies from HCV-infected patients in comparison to non-HCV infected controls showed that HCV infection can perturb host gene expression[528,529]. Combined experiments in HCV infected cell culture, chimeric mice with humanized liver and liver tissues from HCV patients revealed HCV-induced perturbations in metabolic, immune response, and HCC-related pathways[530].

The role of HCV Core, in particular, in host gene expression disturbances has been underlined by many studies in cell culture systems and in animal models, focusing on the effects on both the virus life cycle and the viral pathogenesis (for review see Kao et al., 2016[521]). Ectopic expression of the protein alone in transgenic mice has been extensively studied and found to be in link with pathologies observed in HCV infected patients. Notably

activation of retinoid X receptor alpha, alteration of cytokine expression, oxidative stress, steatosis, and HCC are part of the liver phenotypes observed in such mice (for review see Barth et al., 2008[433]). One mechanism of HCV Core-induced development of steatosis may rely on the reported downregulation of peroxisome proliferator-activated receptor alpha (PPARα), an important regulator of fatty acids degradation in the liver[531]. Core has also been found to induce the expression of TGF-β1[532], the levels of which are found significantly elevated in HCV infected patients[533]. An overstimulation of the genes encoding PPARα and TGF-ß by genotype 3a highly cell culture-adapted strains compared to genotype 1a strain was reported by Patra et al., 2019[534]. In support of the role of HCV Core in steatosis development, this viral protein has also been found to upregulate the transcription of the sterol regulatory element binding protein 1 (SREBP1) and of the peroxisome proliferators-activated receptor gamma (PPARγ), which are involved in the regulation of hepatocellular lipid metabolism[535]. HCV Core has further been found to regulate the expression of antioxidant genes[536], proto-oncogenes, as well as hepatic miR-122, which has the intrinsic property to regulate genes involved in suppression of metastasis. Core exhibits both pro- and anti-apoptotic properties, such as its ability to stimulate or inhibit intrinsic or extrinsic pathways mediated by p53 or by TNF-α[537].

Sharing some host signaling pathways with Core, NS5A seems to modulate MAPK, phosphatidylinositol 3-kinase, Wnt/β-catenin, p53 and NF-κB, resulting in the activation of cell proliferation and the inhibition of apoptosis, thus likely contributing to HCV pathology[538,118]. NS5A is also involved in HCV-induced lipid metabolism perturbations, as it has been found to increase the expression levels of sterol regulatory element binding protein-1c (SREBP1c), acetyl-coenzyme A carboxylase 1 (ACC1) and fatty acid synthase (FASN) *in vitro* and by ectopic expression in mice[539].

Despite the apparent huge body of reported data with regard to hepatocyte pathways deregulated by HCV, many works have not been carried out in physiologically relevant infection systems or with a diversity of HCV genotypes or have led to discrepant statements, calling for additional works to consolidate and reconciliate these data.

I.C Rodent Hepacivirus

I.C.(α) History

Following the identification of Hepacivirus equi, many researchers attempted to find HCV-related viruses in a plethora of hosts. One of these groups was the lab of Dr. Ian Lipkin (Center for Infection and Immunity, Columbia University, New York, USA), who captured and examined more than 400 wild rodents from four Rodentia species, for the presence of novel viruses[24]. Brown sewer rats (Rattus norvegicus) from New York city were found to be infected with two novel hepaciviruses among others, the Norway rat hepacivirus 1 (NrHV-1, RHV-rn1 or Hepacivirus ratti) and the Norway rat hepacivirus 2 (NrHV-2, or Hepacivirus norvegicus)[540]. These viruses were identified in rat sera by unbiased high-throughput sequencing (UHTS) using degenerate primer sets targeting conserved domains within the NS3 helicase of known hepaciviruses and the closely related pegiviruses within the Flaviviridae family.

The identification of RHV was followed by the reported presence of such viruses in the sera and organ tissues of South African four-striped mice (Rhabdomys pumilio) and European bank voles (Myodes glareolus), following the screening of 4,770 rodents (Rodentia, 41 species) from Africa, Europe, Mexico, and Thailand. The hepatotropism of these viruses was supported by the presence of viral RNA and low levels of lymphocytic invasion found by histopathological and molecular analyses of liver samples from RHV-infected bank voles. Moreover, these animals seem to be able to control hepacivirus infections, since low

serological co-occurrence of viral RNA and anti-RHV NS3 antibodies was reported in PCR-positive animals (5.3%)[541].

I.C.(β) Genome, proteins, and virus particle organization

As shown in Figure 1 (page - 2 -), phylogenetic analyses of the various RHV species identified up to date have revealed a substantially great molecular divergence from HCV, unlike that observed between HCV and NPHV, indicating an absence of hepaciviral cospeciation[29,24,541,542]. A considerable level of genetic diversity has also been observed among RHV species, rendering the individual RHV species as unrelated to each other as they are to other species among the Hepacivirus genus identified in a plethora of hosts[457].

The overall genome organization of rodent hepaciviruses is highly similar to that of HCV, with 5'- and 3'-UTRs and a long ORF encoding three structural and seven nonstructural proteins, with homologous predicted cleavage sites[24]. However, distinct differences are found in the sequence and structure of the UTRs, with their complete functional characterization remaining unmet to date. More specifically, the number of miR-122 binding sites within the 5'-UTR ranges from one to two among the different species, while two of the RHV lineages obtained from European bank voles contain an IRES resembling that present in the species of the Pegivirus genus[541]. The main difference among RHV species and HCV within the 3'-UTR seems to be the absence of a poly(U) tract in the former, whereas similarities exist within the terminal stem-loop of certain RHV isolates[24,541].

The hepacivirus ratti, or RHV-rn1 that is used in the present study was first sequenced by the group of Dr Amit Kapoor (Ohio State University, Columbus, Ohio, USA). In spite of the high nucleotide divergence with HCV species, hepacivirus ratti harbours a well-structured 5'-UTR containing an IRES and two miR-122 seed sequences, like HCV, an important determinant for efficient replication in liver cells. In contrast, hepacivirus norvegici, or RHV-rn2, was found to harbour only one miR-122 binding sites within its 5'-UTR[469].

As for HCV, little is known about the structure of infectious RHV particles, although recent studies in cell culture (see I.C.(δ)) revealed that cell-culture derived RHV-rn1 particles have biophysical properties characteristic of HCV, such as a very low density, and lack of correlation of increased levels of RHV E2 embedded in the virion envelope with highest infectivity in *vitro*[543].

I.C.(γ) Host information

The order Rodentia constitute the most diverse and over-represented group of mammals (40%). In the absence of a clearly matching phylogenetic clustering of the evolutionary history of RHV and mammals, it is suspected that the unexpected diversity found among RHV species is the result of several cross-species transmissions. Nonetheless, further research is required to determine whether hepaciviruses from other mammalian hosts are capable of crossing species and infecting rodents.

Rodents' ecology and behaviour are incredibly diversified, rendering them viable in practically any terrestrial ecosystem, including man-made habitats. All rodents, however, share numerous physical characteristics, the most representative of which is their pairs of continually developing, razor-sharp, open-rooted incisors. The majority of rodents are herbivorous, meaning they only eat plant material such as seeds, stems, leaves, flowers, and roots, while some are omnivorous, and others are predators.

Rats is the common name for the genus Rattus of muroid rodents. Rats are medium-sized, long-tailed rodent. The main discriminatory factor among rats and mice (Mus) is their size, with rats being significantly bigger. The black rat (Rattus rattus) and the brown rat (Rattus norvegicus) have become the most well-known rat species, with the latter often used as model

organisms for scientific research. Interestingly, despite the high genetic differences among rats and humans, the livers of these mammals present more similarities than differences. The differences include the presence of lobation and the absence of a gallbladder in rats, though in the presence of a highly similar liver microarchitecture[544].

The existing resemblances, taken together with the intrinsic predisposition of certain rat species to develop obesity, DM2 and MASLD, and the fact that large sequences of the genome of Rattus norvegicus are now known, render rats a unique model for liver-disease associated studies[545]. For experimental purposes, entirely new breeds or "lines" of brown rats have been outbred, including the Wistar, the Long–Evans, and the Sprague Dawley rats.

Wistars are albino rats, developed by the Wistar Institute in 1906 for use in biological and medical research as a model organism over the predominantly utilized house mouse (Mus musculus) at the time. The original colony formed by physiologist Henry Herbert Donaldson, scientific administrator Milton J. Greenman, and genetic researcher/embryologist Helen Dean King is the source of more than half of all laboratory rat lines. The Wistar rat, distinguished by its broad head, big ears, and a tail that is usually shorter than its body length, is today one of the most often used laboratory rodents.

Figure 28: Different lines of laboratory rats that have been used for setting up the RHV model[468]. *Wistar Han (A), Long Evans (B), Sprague Dawley (C) and Holtzman (D) rats are not shown in scale. Photos reproduced with permission from Inotiv (https://www.inotivco.com/).*

Wistars were used for the breeding of the Long–Evans, and the Sprague Dawley rats and are usually more energetic than these other breeds. Long and Evans produced the Long-Evans rats in 1915 by crossing Wistar females with wild grey males. Long-Evans rats are white with a darker coloured hood (black or brown). They are commonly used as a versatile model organism in behavioral studies, particularly in alcohol research, as they consume alcohol at a considerably faster rate than other lines, allowing for more time-efficient behavioral investigations.

The Sprague Dawley rats were first produced by the Sprague Dawley farms in Madison, Wisconsin in 1925, by crossbreeding a hooded male hybrid of unknown origin with a Wistar female, and repeating with the female's progeny for 7 generations. Sprague Dawley rats are albino, and typically have an elongated head and a longer tail in proportion to their body length than their parental breed, Wistars. They are extensively used in medical and nutritional research, and they are preferred due to their rapid growth, docility, and ease to handle. Sprague Dawleys have been further used for the outbreeding of other laboratory rat lines, such as the Harlan Sprague-Dawley rats by Harlan Co. (Indianapolis, IN) and the Holtzman Sprague-Dawley rats by Holtzman Co. (Madison, WI).

I.C.(δ) Pathogenesis and surrogate animal model for HCV

As described in §I.B.η.(iv), HCV can robustly infect only humans and chimpanzees, with the restricted use of the latter in biomedical research tremendously limiting *in vivo* modeling of chronic infection and pathogenesis. Hence, in the absence of a more appropriate animal model available, RHV infecting its natural host, rats, seems to be an ideal alternative thanks to the manageability and extended knowledge researchers possess of the animal, the chronicity of

infection reported in immunocompetent animals, the HCV-like pathogenicity observed, and the permissivity for vaccine studies.

More specifically, serum from a wild brown rat infected with one of the rat hepacivirus species isolated from Rattus norvegicus, the RHV-rn1, has been used to infect Sprague Dawley laboratory rats. The viral genome thereof has been cloned and synthetic RNA derived from this cDNA has been intrahepatically inoculated in Sprague-Dawley, Holtzman, Long-Evans, and Wistar Han outbred laboratory rats, resulting in liver infection. This study by the group of Dr Amit Kapoor revealed moderate hepatic inflammation in experimentally infected rats, characterized by a consistent pattern of dense lymphocytic aggregates focused on the portal tracts, and more parenchymal damage with hepatic plate disarray at later times in chronically infected animals. Interestingly, liver steatosis was also observed in these animals. Furthermore, analysis of differentially expressed genes in the liver of a small cohort of infected rats showed activation of interferon signaling pathways that increased in late stages of chronic infection, as in HCV infected patients[468].

Importantly, this RHV strain fails to establish persistent infection in immunocompetent laboratory mice, though immunocompromised mice lacking type I interferon and adaptive immunity (A129, AG129, and NRG) can be chronically infected. Evidence of possible RHV adaptation to the immunocompromised mouse host also surfaced from these attempts[469].

As *in vivo* studies are usually coupled to molecular analyses *in vitro*, the group of Dr Troels Scheel (University of Copenhagen, Copenhagen, Denmark) undertook to establish an *in vitro* model to culture RHV in hepatic cells of rat origin. First, efficient RHV-rn1 selectable subgenomic replicons were developed and then cell clones that could harbour stably replicating RHV-rn1 subgenomic RNAs without the need of adaptive mutations were selected. Interestingly, the efficiency of RHV replication in cells of rat origin may be increased following the introduction of adaptive mutations in NS4B and NS5A, previously identified in transfected hepatoma cell lines of murine origin, implying that adaptive mutations are not species-specific but rather boost RHV genome replication in cell culture more broadly. Miravirsen, a miR-122 antagonist that suppresses HCV replication, was also shown to suppress RHV-rn1 genome replication, demonstrating the ubiquitous relevance of this host factor for hepaciviruses, the importance of the existence of the miR-122 binding sites in RHV 5'-UTR, further highlighting significant commonalities between RHV and HCV[546].

Scheel et al. further described an infectious reverse genetic cell culture system for RHV-rn1 employing the selected highly permissive rat hepatoma cells and RHV-rn1 bearing adaptive mutations in E2, NS4B, and NS5A viral proteins. RHV-rn1 particles produced in cell culture (RHVcc) present similar biophysical properties as HCV and are infectious in rats. In immunocompetent rats, culture adaptive mutations attenuated RHV, and the mutations reversed after extended infection[543].

Overall, RHV-rn1 in rats has a profile very similar to that of HCV in humans, characterized by hepatotropism, persistent viremia detectable for over 1 year and recapitulation of many aspects of liver pathology, such as micro- and macro-vesicular steatosis, lymphoid aggregation, and biliary epithelial damage[468]. These attributes render it an appropriate surrogate model to study viral persistence, the role of various interferon stimulating genes and immune responses in hepacivirus pathogenesis, as well as vaccine candidate efficiency. In fact, the group of Dr Kapoor is now devoted to exploring vaccine strategies, recently showing that single-dose immunization with vaccine candidate composed of a recombinant adenovirus vector expressing RHV nonstructural proteins can induce effective immunity in vaccinated rats. Resolution of RHV infection was found to coincide with a vigorous recall of intrahepatic cellular responses, while this study also provided direct evidence of the importance of co-operation between CD4+ and CD8+ T cells for hepacivirus immunity[547]. Furthermore, viruses containing escape mutations within MHC class I-restricted epitopes reduced the efficacy of

this vaccine candidate upon challenge[548]. Further research into the immune responses that result in protection against various RHV challenges in this model may aid in the development of widely effective HCV vaccines, increasing the appeal of this rat model.

II. Objectives

Chronic HCV infection is a progressive and long-term asymptomatic disease, resulting in metabolic disorders, such as steatosis, an abnormal accumulation of neutral lipids in hepatocytes, and long-term complications of cirrhosis and hepatocellular carcinoma (HCC). The prevalence of clinical manifestations varies according to the hepatitis C virus (HCV) genotype (8 genotypes and >90 subtypes identified so far), with g. Genotype 3 infection, which is highly prevalent among IVDU in Europe presenting an increased association with steatosis, with an incidence rate of 80%, and subtype 1b infections being are associated with increased risk for HCC development, while significant clinical data are lacking for genotypes 4-8

HCV-induced pathologies can be driven by a complex combination of both direct, as well as indirect mechanisms such as chronic liver inflammation. Virus-driven mechanisms are thought to be essentially mediated by two pleiotropic viral proteins, the capsid protein, Core, and the nonstructural protein NS5A. Core and NS5A are reportedly involved in the deregulation of several host pathways (see I.B.(θ)), including metabolic signaling pathways that could be associated with steatosis development, immune system cascades and signaling pathways known to be involved in HCC development. However, in the absence of cell culture systems allowing the study of clinical strains of HCV, these HCV genotype- and/or protein-specific deregulations have mainly been studied in transient protein over-expression systems and/or in non-hepatic cells in vitro.

Moreover, a detailed understanding of the molecular mechanisms involved in HCV-induced pathology is hindered by the absence of a fully pertinent study model. This knowledge remains crucial, even in the era of DAAs, which can currently cure ≥95% chronic infections, since SVR does not always eliminate the risk of developing liver complications. In addition, the high cost of the treatment and the increased proportion of unknowingly infected individuals are restrictive factors of prominent HCV elimination, highlighting the need of a preventive vaccine. A promising surrogate model emerged with the demonstration in 2018 that a new rodent hepacivirus (RHV-rn1) establishes chronic infection in rats, its natural host and can, similar to HCV in humans, cause steatosis.

Our group is aiming at elucidating in relevant infection systems the molecular bases of HCV manipulation of host pathways leading to steatosis and HCC, with a focus on the common and distinct effects of HCV proteins with diverse genotypic origins.

Towards this end, a first project targeted the identification of (i) cellular interacting partners (IPs) of Core and NS5A and (ii) specifically deregulated signaling pathways. This project included the development of new virological models capable of replicating in human hepatoma cells, encoding Core or NS5A from clinical strains of different genotypes isolated from patients with varying degrees of liver disease. These systems were used for the study of transcriptomic deregulations specific to the genotypic origin of the protein. The generation of a panel of HCV Core and NS5A intergenotypic recombinants encoding respective proteins tagged in frame with a twin strep-tag (ST) allowed the affinity purification of protein complexes and the determination of the interactome of these proteins.

In our second project, the immunocompetent surrogate animal model based on Sprague Dawley rats infected with RHV-rn1, initially established by the lab of Dr. Kapoor[468] (Ohio State University, Columbus, Ohio, USA) was set up in France thanks to his generous gift of RHV-rn1 genome-length cDNA. With this model, we aimed at characterizing liver metabolic disorders triggered by chronic RHV infection using small rat cohorts, in order to validate the high potency of this surrogate model to pursue pathobiology studies, while other groups in the world are using it for vaccine-related investigations[547,548].

Both projects are part of collaborative studies supported by the ANRS and are expected to ultimately contribute to a better understanding of the molecular mechanisms involved in HCV-

induced steatosis and HCC in direct link with specific viral factors and genotypic polymorphisms, as well as provide information about the interaction with co-morbidity factors and potential persistence of metabolic perturbations following hepacivirus cure.

III. Materials and Methods

III.A Ethics Statement

This study complied with the ethical guidelines of the Declaration of Helsinki (1975) and has been approved by the following committees and institutes concerning:

(i) animal experimentation
- The Ethics Committee on animal experimentation n°012 (number C3851610006) delivered to our collaborator running the animal facility, Dr. Hervé Lerat (UMS hTAG, Université Grenoble Alpes, Inserm US46, CNRS UAR2019, La Tronche, France).

(ii) clinical virus strains
- The National Consultative Ethics Committee for the Life Sciences and health in France (declaration number DC-2008-531), delivered to our collaborator, Dr. Claire Gondeau (Institut de Médecine Régénératrice et de Biothérapie, Hôpital Saint-Eloi, Montpellier, France)
- The National Ethics Committee of Cameroon (number 199/CNE/SE/2011) and the Ministry of Cameroon Health (number 631-01.12), delivered to our collaborator Dr. Richard Njouom (Centre Pasteur du Cameroun, Yaoundé, Cameroon)
- The *Bioethics Committee of the Cantacuzino National Medical-Military Institute of Research and Development* of Romania (number 16/CEE), delivered to our collaborator Dr. Gabriela Oprisan (Titu Maiorescu University, Faculty of Pharmacy, Bucharest, Romania).

Written informed consent was obtained from all patients or their families. Patient data communicated to the laboratory were restricted to patient gender, age, the reason for the surgical resection and comorbidity factors, when available. HCV RNAs extracted from patients' sera were provided to the laboratory by its collaborators.

III.B Cell culture

Human hepatocarcinoma Huh-7.5 cells, highly permissive to HCV infection[395], were a kind gift from Dr. Charles Rice (The Rockefeller University, New York, USA). Huh-7.5 is a cell clone derived from Huh-7 hepatocarcinoma cells harboring stably autonomously replicating subgenomic HCV RNA, that have been cured from it by interferon treatment.

Huh-7.5 cells were cultured as a monolayer at 37°C in an atmosphere of 5% CO_2 in complete medium, i.e. DMEM medium (Dulbecco's Modified Eagle Medium, Gibco, #11574486) supplemented with decomplemented 10% fetal calf serum (FBS, Gibco, #10270-106), 1mM sodium pyruvate (Gibco, #11360039), 100 U/mL penicillin, 100µg/mL streptomycin (Gibco, #11548876) and non-essential amino acids (Gibco, #11140035). Cells were split every 3–4-days following detachment with trypsin/EDTA solution. Cells were quantified by the *Countess™ II Automated Cell Counter* (Invitrogen™) in Trypan blue solution and were seeded at a range of 0.6-1.2x10^6 cells per 75cm^2-flask, or proportionally adjusted for the sizes of other flasks and multi-well plates.

III.C Recombinant hepatitis C viruses

III.C (α) Clinical isolates and prototypical strains of HCV

Viral RNAs extracted from the serum of chronically infected HCV patients with varying degrees of micro- and macro-steatosis were provided by Dr. Claire Gondeau (Institut of

Research in Biotherapy, Montpellier, France)[549]. The degree of steatosis was determined by semi-quantitative estimation of the percentage of hepatocytes containing fat vacuoles compared to all hepatocytes by optical microscopy of stained liver sections.

The sequence coding Core of subtype 4a isolate (designated 4aR, ENA #ERZ655054) was isolated from an HCV positive blood donor and provided by Dr. Gabriela Oprisan. The Core coding sequence of the subtype 4f isolate (designated 4fC, ENA #ERZ672786) was isolated from a patient with HCC and provided by Dr. Richard Njouom. The 4aR and 4fC Core sequences have been determined and published in a previous study from our laboratory[550]. The Core coding sequence of the prototypical strain H77 subtype 1a was derived from the genome-length cDNA (1aH77, GenBank #AF011751)[373], generously provided by Dr. Robert Purcell (National Institute of Health, Bethesda, United States). Core and NS5A coding sequences of subtype 2a prototypical JFH-1 (GenBank #AB047639) and J6 (GenBank #D00944) strains were derived from full-length cDNAs, pJFH1 and pJc1-2EI3 or pJFH1-(C-NS2)J6-(NS5A)2a-J6 (GenBank #HQ852461), generously provided by Drs. Takaji Wakita (National Institute of Infectious Diseases, Tokyo, Japan)[411] and Ralf Bartenschlager (University of Heidelberg, Heidelberg, Germany)[99] and Jens Bukh (University of Copenhagen, Copenhagen, Denmark)[172], respectively.

The sequences of Core used by Emeline Simon, Brigitte Blumen and Stephanie Aicher to produce the Core intergenotypic recombinant viruses presented in this study are summarized in Table 4.

Table 4: Clinical HCV strains used to retrieve NS5A sequences.
LS: low steatosis, MS: moderate steatosis, HS: High steatosis, nc: not communicated.

Viral Genotype	Patient Code	Patient Birth year	Steatosis	Steatosis Ranking	Remarks
1a	S411	1960	Moderate steatosis	MS	Cirrhosis - No response to IFN/RBV
3a	P98L	1964	Micro-steatosis and macro-steatosis 50%	MS	-
	376	1968	Macro-steatosis 20%	MS	Treatment naïve - Diabetic
	S389	1965	<5%	NS	Treatment naive
	S390	1974	Micro-steatosis and macro-steatosis 60%	HS	Treatment naïve - Obese
	S395	1962	Macro-steatosis 40%	MS	Relapser - Alcohol consumption
	S401	1952	Micro-steatosis and macro-steatosis 5%	LS	Intolerance to IFN/RBV
4	4aR	n.c.	n.c.	n.c.	-
	4fC	n.c.	n.c.	n.c.	-

III.C (β) Sequencing and cloning of NS5A from clinical HCV strains

Clinical strains incorporated in this study were selected based on viral genotype and the level of assessed steatosis severity in patient liver sections. Exclusion criteria were treatment attempts before or during the period of liver damage estimation and the existence of comorbidity factors, as described in §I.B.στ.(vi). This resulted into the selection of the strains summarized in Table 5.

Table 5: Clinical HCV strains used to retrieve NS5A sequences.
LS: low steatosis, MS: moderate steatosis, HS: High steatosis, nc: not communicated.

Viral Genotype	Patient Code	Patient Birth year	Steatosis	Steatosis Ranking	Remarks
1a	S411	1960	Moderate steatosis	MS	Cirrhosis - No response to IFN/RBV
1b	S434	1962	Not communicated	nc	Treatment naive
3a	S401	1952	Micro-steatosis and macro-steatosis 5%	LS	Intolerance to IFN/RBV
	S385	1956	Macro-steatosis 50%	MS	Treatment naive
	S407	1966	Macro-steatosis 80%	HS	Intolerance to IFN/RBV
4	S431	1965	Not communicated	nc	Relapse

The NS5A coding sequences from the clinical strains were obtained after reverse transcription (RT) of the viral RNAs using a non-specific random hexamer primer and the *Transcriptor High Fidelity cDNA Synthesis* kit (Roche), followed by PCR amplification using the *Phusion Hot Start II High-Fidelity DNA Polymerase kit* (Thermo Scientific™). In some instances semi-nested or nested PCR amplification was required, To design specific primer pairs that would hybridize to subtype-specific NS4B and NS5B consensus coding sequences framing NS5A sequence, HCV genome-length or target-protein-specific nucleotide sequences were retrieved from euHCVdb (https://euuhcvdb.lyon.inserm.fr/euHCVdb/) and aligned using CLC Main Workbench 20.0 (QIAGEN). Primer sequences are summarized in Table 6.

The amplified PCR fragments were purified using the *NucleoSpin® Gel and PCR clean-up* kit (Macherey-Nagel) with 50% buffer NTI and were sequenced as bulk products by Sanger (Eurofins), as described in §III.F.(γ). Additional internal primers were designed for sequencing purposes, based on the first sequences retrieved with external primers (see Table 6). Next, the DNA fragments were cloned in a shuttle vector using the *Zero Blunt® TOPO® PCR Cloning kit for Sequencing* (Thermo Fisher Scientific), in order to acquire a clonal sequence to substitute that of Jad NS5A, as well as to appreciate the presence and the frequency of possible quasispecies. For this second step, twelve (12) clones were selected for expansion, plasmid purification with the *NucleoSpin® Plasmid* kit (Macherey-Nagel), and sequencing of NS5A coding sequence by Sanger (see §III.F.(γ)). The predominant consensus sequences encoding NS5A were established from these analyses, and the clones reflecting them at the protein level were selected to construct the intergenotypic recombinant cDNAs.

Table 6: Custom primers designed to amplify and/or sequence NS5A sequences of clinical HCV strains.

The targeted viral genotype (Gt), subtype (St) or sample (S), the polarity of the primer (FW: forward, RV: reverse) and the position with respect to viral proteins (int: NS5A internal) were incorporated in the primer name. To increase the primers' efficiency, degenerate nucleotides were incorporated; H =A/C/T, Y =C/T, R =A/G, K=T/G when required. More external primers are indicated with odd numbers, while more internal ones, used for (semi-)nested PCR reactions are indicated with even numbers in their name.

Target Genotype/Subtype	Primer name	Primer Sequence (5'→ 3')
1a	Gt1a_NS4B_FW-1	CCCGCGTCACTGCCATACT
	Gt1a_NS4B_FW-2	GCACCAGTGGATAAGCTCGGA
	Gt1a_NS5B_RV-3	CTTTGGCAAGCACTGCGTGA
	Gt1a_NS5B_RV-4	AGCAACGAGTTGCTCAGTGC
	S411_NS4B_FWint	CAGGAGATGGGCGGTAATATC
	S411_NS4B_RVint	GATATTACCGCCCATCTCCTG
1b	St1b_NS4B_FW-1	CGCGTGTCACTCAGATCCT
	St1b_NS5B_RV-4	AGCAAAGAGTTGCTCAACGC
	S434_NS5A_FWint-2	GGATTTCCACTACGTGACGG
	S434_NS5A_FWint-3	CAGCTAGCCAGTTGTCTGC
	S434_NS5A_RVint-1	GATCGGTGAGCATGGAAGTG
	S434_NS5A_RVint-2	CCGTCACGTAGTGGAAATCC
	S434_NS5A_RVint-3	GCAGACAACTGGCTAGCTG
3a	Gt3a_NS4B_FW-1	CACCAGTGGATCAATGAAGACTA
	Gt3a_NS4B_FW-2	CAGTGGATCAATGAAGACTACCC
	Gt3a_NS5B_RV-3	GGCAGTTTCTCCTCCTCAGC
	Gt3a_NS5B_RV-4	CTCCTCAGCACTACATGGTG
	Gt3a_NS4B_FWint	CCTCCATCAGAGGCAAGCTC
	Gt3a_NS4B_RVint	GAGCTTGCCTCTGATGGAGG
4	Gt4_NS4B_FW-1	TCATCCCTCACTGTGACHTCCC
	Gt4_NS4B_FW-2	CGCCTCCACAAGTGGATCAAYG
	Gt4_NS5B_RV-3	ARGAGTGARTTGCTCAGGGG
	Gt4_NS5B_RV-4	TTGCTCAGGGGGYTRATKGGC
	S431_NS4B_FWint	GCTGACAGATCCGTCTCAC
	S431_NS4B_RVint	GTGAGACGGATCTGTCAGC

III.C (γ) Plasmids

Plasmid **pJad** contains the genome-length cDNA of a highly cell culture-adapted derivative[413] of HCV subtype 2a JFH1 strain[411], (JFH1-adapt or Jad), cloned downstream of bacteriophage T7 RNA polymerase promoter. Three codon substitutions, two in NS5A (V2153A, V2440L) and one in NS5B (V2941M) coding sequences (see Figure 29) confer high titer growth to Jad.

Plasmids **pJad/GAA** and **pJad/ΔEp7** are derived from pJad, containing codon substitutions in NS5B coding sequence (GDD-->GAA) or an in-frame cDNA deletion of the E1-E2-p7 coding sequence, respectively. Plasmids **pJad/NS5A-(TEV)-ST-418, -ST-449, -V5-418, -V5-449** and **pJad/C17-ST**, **/C17-V5** were constructed and available in the laboratory. They derived from pJad and contain in-frame insertions of heterologous sequences within NS5A coding sequence following codon 418 or 449, as indicated, or Core coding sequence following codon 17, respectively. In addition to the twin-strep tag (ST) or V5 tag

itself, a 7-aa coding sequence was inserted upstream (ENLYFQS), corresponding to the recognition site of tobacco etch virus (TEV) protease for purification purposes. The (TEV)-ST and (TEV)-V5 sequences were framed by Ser-Gly and Ser-Gly-Gly, Ser-Gly-Ser or Gly-Gly flexible hinges at their N- and C-termini, respectively, that were either additionally inserted or present in the authentic NS5A sequence.

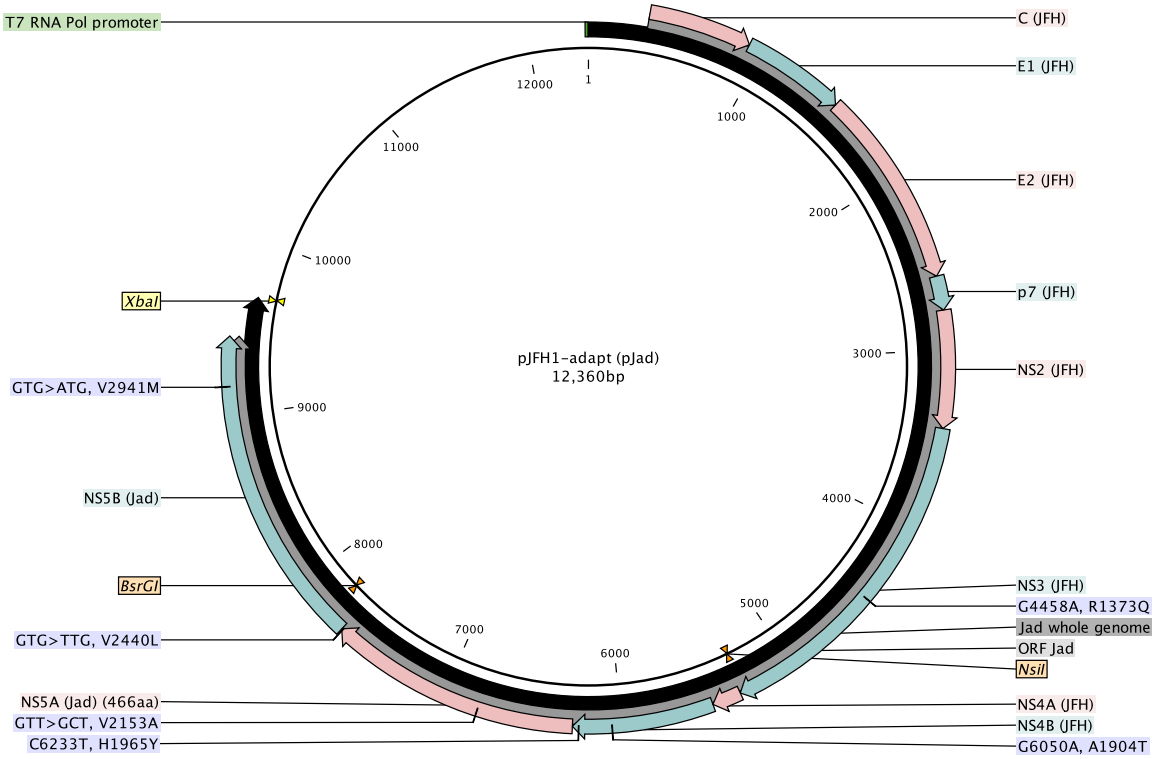

Figure 29: Map of the pJad plasmid.
The genome-length cDNA of the Jad strain (black) was inserted downstream of the T7 RNA polymerase promoter, generating the 12,360-base pair (bp) plasmid pJad. The open reading frame coding the Jad proteins is indicated in grey, while each protein is shown by alternating pink and blue colours. Jad adaptive mutations V2153A, V2440L and V2153M are indicated in purple, together with the positions of the mutations required for the adaptation of the chimeras with the NS5A sequence of the genotype 3 or 4 strains (G4458A, G6050A, C6233T). The unique restriction site (XbaI) used towards DNA linearization prior to in vitro transcription is shown in yellow, while the unique restriction sites (NsiI and BsrGI) used for construction of the intergenotypic recombinant cDNAs are indicated in orange. The map was using the CLCMainWorkbench software.

III.C.γ (i) Construction of chimeric pJad plasmids

The construction of the plasmids containing the chimeric cDNAs is based on an over-lapping PCR strategy designed to exchange only the Jad NS5A coding sequence for those of the predominant NS5A sequences from the clinical strains previously obtained in pTOPO vectors. Briefly, three segments of viral cDNA were amplified as a first step, two segments upstream and downstream of NS5A coding sequences, respectively, using pJad as a template and a middle segment corresponding to the heterologous NS5A coding sequence using pTOPO vectors. For this, primers with extensions complementary to the segments to be fused were used, which in turn allowed the overlapping of the products and the amplification of fusion products with exact junction points (see Table 7) using the 3 PCR products from the first step as templates. Following digestion with appropriate enzymes recognizing restriction sites close to the extremities of the fusion product, the hybrid fragments were lastly cloned in the pJad

vector digested with these same enzymes, yielding the **pJad/NS5A(x)** plasmids indicated in Table 7.

Table 7: Custom primers for overlapping PCR reactions to exchange NS5A sequence of pJad to that of other prototypic virus or clinical strains.
The sample number and the polarity of the primer (+: forward, -: reverse) were incorporated in the primer name. Blue font colour represents the sequence of the corresponding clinical strain or other prototypic virus. Pink font colour represents JFH1 sequences. Black letters correspond to Jad adaptive mutation V2440L within NS5A sequence. Underlined sequences fully hybridized on selected templates for PCR reactions. Highlighted sequences represent primer overlap for overlapping PCR reactions and lowercase characters indicate nucleotide differences between Jad NS5A sequence and the corresponding selected strain.

Plasmid names (Genotype)	**Primer name**	**Primer Sequence (5'→ 3')**
pJad/NS5A-411 (1a)	3.411-NS5B+	GCCCCATCCCATGCTCCGGtTCCTGGCTaaG
	2.411-NS3-	GCCAGGAaCCGGAGCATGGGATGGGGC
	4.411end-411-	GTATGACATGGAGCAGCACAGGacatccTCc
	5.411end-5B+	gatgtCCTGTGCTGCTCCATGTCATACTC
pJad/NS5A-434 (1b)	3.434-NS5B+	GCCCCATCCCATGCTCCGGcTCqTGGC
	2. 434-NS3-	GCCAcGAgCCGGAGCATGGGATGGGGC
	4.434end-434-	GTATGACATGGAGCAGCAaAGGacGtccTCAC
	5.434end-5B+	gaCgtCCTtTGCTGCTCCATGTCATACTCC
pJad/NS5A-J6 (2a)	1.J6end-NS3-	GACATGGAGCAGCACAGGACGGAGTCG
	2.J6end-5B+	CGACTCCGTCCTGTGCTGCTCCATGTC
pJad/NS5A-385 pJad/NS5A-401 pJad/NS5A-407 (3a)	3.385-NS5B+	CTGCCCCATCCCATGCaqCGGtqatTGGC
	2.385-NS3-	CAatcaCCGctGCATGGGATGGGGCAGTCC
	3.401-7-NS5B+	CTGCCCCATCCCATGCaqCGacqatTGGCTqCG
	2.401-7-NS3-	CAatcgtCGctGCATGGGATGGGGCAGTCC
	4.3aend-3a-	GTATGACATGGAGCAGCAqAGcacGcTcTqc
	5.3aend-NS5B+	gAgCgtgcTCTGCTGCTCCATGTCATACTCC
pJad/NS5A-431 (4)	Gt4_NS4B_FW-1	CCCCATCCCATGCgatcGcTCtTGGtTatGqGAq
	Gt4_NS4B_FW-2	AaCCAaGAgCgatcGCATGGGATGGGGCAGTCC
	Gt4_NS5B_RV-3	GACATGGAGCAGCACAGtacatccTCcg
	Gt4_NS5B_RV-4	gGAggatgtaCTGTGCTGCTCCATGTCATACTC

XL1-Blue competent bacteria (Agilent) were transformed with the ligation mixtures (*Rapid DNA ligation* kit, Roche) following a heat-shock and cultured for 16h at 37°C on Luria Bertani (LB) Petri dishes containing 500 µg/mL ampicillin. Plasmid DNA was purified from bacterial colonies using *Nucleospin plasmid* kit (Macherey-Nagel) and screened by restriction reactions with the cloning enzymes (NsiI^{HF} + BsrGI^{HF}) and with enzymes allowing to discriminate the desired NS5A sequence from that of Jad. More specifically, genotype 1 and 3 strains were discriminated by SalI^{HF} digestion, genotype 4 by PstI and the J6 strain by triple digestion with NsiI + BsrGI^{HF} and PstI. All restriction enzymes and respective buffers were from New England Biolabs. The nucleotide sequence of NS5A within selected plasmid DNAs was further verified by Sanger sequencing (see §III.F.(γ)). Large scale DNA preparations of the clones found to have substitutions were performed using *Nucleobond Xtra Midi Plus* kit (Macherey-Nagel).

Custom primers to insert identified adaptive mutations within the NS3 and/or NS4B coding regions were designed to accommodate the overlapping PCR strategy described above (see Table 8). The plasmids pJad and pJad/NS5A(x) were used as templates for the primary

PCR reactions, while pJad digested either with NsiI^{HF} + BsrGI^{HF} or with SpeI^{HF} + BsrGI^{HF} served as vector for the insertion of a single mutation in NS4B sequence (genotype 4 NS5A recombinant) or one mutation in NS3 and one in NS4B (genotype 3 NS5A recombinants), respectively. Since point mutations were introduced, the clones obtained were first validated by restriction with the respective cloning enzymes and then by Sanger sequencing (see §III.F.(γ)). The names of the derived plasmids were: pJad/G4458A/G6050A/NS5A-385, pJad/G4458A/G6050A/NS5A-401, pJad/G4458A/G6050A/NS5A-407, pJad/G4458A/G6233A/NS5A-407 and pJad/G6050A/NS5A-431.

Table 8: Custom primers to insert adaptive mutations in intergenotypic pJad recombinants.
The position and nature of the substitution, as well as the polarity of the primer (FW: forward, RV: reverse) were incorporated in the primer name. Pink font colour represents JFH1 sequences. Black letters correspond to the position of the indicated adaptive mutations within the indicated viral protein sequence.

Mutation	**Viral protein**	**Primer name**	**Primer Sequence (5'→ 3')**
G4458A	NS3	G4458A_FW	GGTCATCTGCGCG**A**CCATTCTGCGCCG
		G4458A_RV	CGGCGCAGAATGG**T**CGCGCAGATGACC
G6050A	NS4B	G6050A_FW	GTAGGCCTCGGGC**A**GGAGGGTGAGATC
		G6050A_RV	GATCTCACCCTCC**T**GCCCGAGGCCTAC
C6233T		C6233T_FW	CTCAGAAGACTC**T**ACAATTGGATAACTG
		C6233T_RV	CAGTTATCCAATTGT**A**GAGTCTTCTGAG

The substitution of Jad core coding sequence by core sequences from other genotypes was previously done according to the same strategy by other members of the group. The Jad Core recombinant viruses did not require adaptive mutations (Aicher et al., 2018 and unpublished data).

III.C.γ (ii) Construction of chimeric pJad plasmids encoding tagged NS5A

Custom primers to insert ST- or V5-tag sequences following a conserved Pro codon equivalent to codon 418 of NS5A in Jad were designed to accommodate the overlapping PCR strategy described above (see Table 9). The plasmid pJad digested either with NsiI^{HF} + BsrGI^{HF} served as vector for the insertion of PCR-amplified fragments introducing the tagged clinical or J6 NS5A sequences produced from the following templates used for the primary PCR reactions: pJad/NS5A(x), pJad-NS5A-(TEV)-418-ST, pJad-NS5A-(TEV)-418-V5 and pJFH1-(C-NS2)J6-(NS5A)2a-J6. The nucleotide sequence of the fragment between the ligation points in the selected clones was verified with triple digestion with NsiI, BsrGI^{HF} and PstI and by Sanger sequencing (see §III.F.(γ)).

Table 9: Custom primers for insertion of twin-strep or V5 tag in NS5A of intergenotypic pJad recombinant at position 418.

The genotype or sample number and the polarity of the primer (+: forward, -: reverse) were incorporated in the primer name. Blue font colour represents the unique sequence of the corresponding clinical strain or other prototypic virus. Pink font colour represents common sequences of JFH1 and the clinical or prototypic strains. Green font colour corresponds to silent nucleotide substitutions inserted by the primer within subtype 3a strains. Orange font colour represents the sequence of flexible linker - Tobacco Etch Virus (TEV) protease recognition site – tag. Underlined sequences fully hybridize on selected templates for PCR reactions. Highlighted sequences represent primer overlap for overlapping PCR reactions.

Sample Genotype	**Primer name**	**Primer Sequence (5'→ 3')**
1a	2.1a-NS3-	CTCTCCGGAGGGGGGCATGGAAGAGCAAG
	3.1a-tag+	TGCTCTTCCATGCCCCCCTCCGGAGAG
	4.1aend-ST-	CTCCCCCTCTAGGCCGCCAGACTTCTC
	5.1aSTend-5B+	GAGAAGTCTGGCGGCCTAGAGGGGGAGCCTGGG
	4.1aend-V5-	CAGGCTCCCCCTCTAGGCCACCCGTAG
	5.1aV5end-5B+	CTACGGGTGGCCTAGAGGGGGAGCCTGGG
1b	2.1b-NS3-	CTCCGGAGGGGGGCATGGAGGAGTACG
	3.1b-ST+	CGTACTCCTCCATGCCCCCCTCCGGAG
	4.1bend-ST-	CCCCCGGCTCCCCCTCAAGGCCGCCAG
	5.1bend-5B+	CTGGCGGCCTTGAGGGGGAGCCGGGGG
2a	2.J6-NS3-	CTCTCCGGAGGGGGGCATGGAAGAGATG
	3.J6-ST+	CATCTCTTCCATGCCCCCCTCCGGAGAG
	3_ST-5A419-	CCCCTCGAGGCCGCCAGACTTCTCAAACTGGGGATGGC
	5.J6STend-5B+	TTTGAGAAGTCTGGCGGCCTCGAGGGGGAGCTTGG
3a	2.3a-385-NS3-	TTCTCTCCGGAAGGAGGCATGGACGAGCACG
	2.3a-401/7-NS3-	TTCTCTCCGGAAGGAGGCATGGACGAGCATG
	3.3a-ST+	CTCGTCCATGCCTCCTTCCGGAGAGAATTTG
	4.3aend-ST-	CCCGGTTCTCCCTCGAGGCCGCCAGAC
	5.3aend-5B+	CTGGCGGCCTCGAGGGAGAACCGGGCG
4	2.4-NS3-	TTCTCTCCGGATGGAGGCATTGACGAGTAAGAC
	3.4-ST+	CTCGTCAATGCCTCCATCCGGAGAGAATTTG
	4.4end-ST-	CCGGGTTCCCCTTCAAGGCCGCCAGACTTC
	5.4end-5B+	CTGGCGGCCTTGAAGGGGAACCCGGCG

III.C (δ) In vitro RNA transcription of genome-length viral cDNAs

Jad-derived plasmids were linearized by XbaI restriction enzyme, generating a protruding 3' end, which was subsequently eliminated by treatment with Mung Bean nuclease (New England Biolabs), and purified by phenol/chloroform (Sigma-Aldrich) extraction and ethanol precipitation. Linearized DNAs (1µg, quantified on 1% agarose gel) served as templates for *in vitro* transcription of the cDNAs using bacteriophage T7 RNA polymerase (*T7 RiboMAX Express Large Scale RNA Production System*, Promega). DNA templates were subsequently removed by treatment with 1U of *RQ1 RNase-free DNase* (Promega). Synthetic RNAs were purified by extraction with phenol/chloroform and precipitated with 1 volume of isopropanol supplemented with 0.3M sodium acetate. The quality and quantity of RNA resuspended in RNAse-free H_2O were evaluated by electrophoresis on 1% agarose gel and by measurement of the absorbance at 260nm using *mySPEC* microvolume spectrophotometer (Ozyme).

III.D Cell transfection

Huh-7.5 cells ($2x10^6$ cells) diluted in opti-MEM Reduced Serum Medium (Gibco, Thermo Fisher) were electroporated with 5µg *in vitro*-transcribed viral RNA using 4mm-width cuvettes in a *Gene pulser XCELL electroporation system* (Bio-Rad) and a pulse at 240V, 900µF. In case more cells were required (e.g for purification of protein complexes), the above-mentioned quantities were adjusted proportionally for the experiments concerning the parental Core and NS5A, or an increase of 30% in RNA over the number of cells was employed for the purification of NS5A complexes with the inter- and intra-genotypic recombinant viruses. Following electroporation, cells were immediately resuspended in complete DMEM.

(i) For transfections performed toward protein expression monitoring through Western blotting, transfected cells ($3x10^5$ cells) were seeded in 1 well of 6-well plates and cultured for 72h post-transfection (p.tf.) Protein extracts were prepared in 200µL *NuPage LDS Sample Buffer* (Lithium Dodecyl Sulfate buffer, Invitrogen™) supplemented with 0.71M ß-mercaptoethanol (Sigma-Aldrich), as indicated in §III.G.

(ii) For transfections performed toward virus passage and amplification, transfected cells ($1.7x10^6$ cells) were seeded in $75cm^2$-flasks and cultured for up to 18 days (d) p.tf., with cell splitting ranging from 1:2-1:8 dilutions every 3-4 days. Supernatants were collected at each cell passage and were clarified by centrifugation at 12,000g, 4°C for 10min. Clarified supernatants were stored at 4°C for a short period of time (<1 month) or stored in aliquots at -80°C. Part of the split cells was kept for intracellular total RNA extraction with *RNAzol® RT* (Sigma-Aldrich).

(iii) For transfections performed toward immuno-labelling and confocal microscopy kinetic experiments, transfected cells ($1x10^4$ cells) were seeded per channel in glass µ-Slide VI 0.5 (Ibidi) and fixed at 48h, 72h or 96h p.tf. (see §III.H).

(iv) For transfections performed toward Core protein complex purification, transfected cells ($4.5x10^6$ cells) were seeded in $175cm^2$-flasks and cultured for 3d p.tf. For purification of protein complexes involving NS5A of diverse genotypic origins, transfected cells ($2.5x10^6$ cells) were seeded in $175cm^2$-flasks and cultured for 5d p.tf. Cell lysates were collected from trypsinised cells, as indicated in §III.J.

In all cases, following transfection, cells were incubated at 37°C under 5% CO_2 for 4h and then the medium was replaced by fresh DMEM to remove the cellular debris from electric shock.

III.E Cell infection

Huh-7.5 cells were seeded 24h prior to infection and were then infected by replacement of the growth medium with the appropriate viral inoculum diluted in complete DMEM as needed.

i) For preparation of viral stocks, $1.3x10^6$ cells were seeded in $75cm^2$-flasks and infected at a multiplicity of infection (MOI) of 0.01 Tissue Culture Infectious Dose 50% (TCID50) /cell. Infected cells were expanded by passaging every 2-3 days up until 10d post-infection (p.i.). Supernatants were collected and clarified at every passage.

ii) For confocal microscopy, $5x10^3$ cells were seeded per channel of glass slides (µ-Slide VI 0.5, Ibidi) and infected with the viral inoculum at the maximum MOI possible for each virus. Infected cells were incubated at 37°C in a 5% CO_2 atmosphere for 96h prior to processing for indirect immunofluorescence, as indicated in §III.G.

iii) For protein purification, $1.8x10^6$ cells were seeded in $175cm^2$-flasks 24h prior to infection were infected with the tagged NS5A parental Jad viruses at MOI of 1. Infection volumes were adjusted with fresh DMEM between pairs of ST/V5 corresponding viruses to be equal, depending on the viral titers of the replicate stocks used. Cells were cultured in 23mL DMEM for 4d p.i. before lysis, as indicated in §III.J.

iv) For total RNA extracts toward transcriptomic studies, $1.5x10^4$ cells were seeded per well in 24-well plates, infected with an MOI of 3 in a total inoculum volume of 300µL. Infected cells were cultured in 1mL fresh DMEM, until lysis at 5d p.i., as indicated in §III.K

In all cases, following infection, cells were incubated at 37°C under 5% CO_2 for 4h and then the inoculum was replaced by fresh DMEM to better support cell growth. When recquired, cells were washed with fresh DMEM at this stage to remove any traces of infectious inoculum towards specific titration of neosynthesized virus.

III.F HCV characterization

III.F.(α) HCV genome quantification

To extract intracellular RNAs, infected Huh-7.5 trypsinised from half 175cm²-flask were thoroughly washed in Dulbecco's Phosphate Buffered Saline (DPBS) and resuspended in 500µL *RNAzol® RT* (Sigma-Aldrich). The lysates were transferred in RNase free Eppendorf tubes and frozen at -20°C. After thawing, total RNA was extracted according to the manufacturer's guidelines. RNA pellets were resuspended in 15-30µL ribonuclease-free H_2O, quantified by optical density using a nano-spectrophotometer (*MySpec*, Ozyme) and stored at -80°C.

For extractions of viral RNAs from 140µL infected cell culture supernatant, the *QiaAmp Viral RNA Mini kit* (Qiagen) was used, according to the manufacturer's guidelines. Viral RNAs were eluted in 60µL ribonuclease-free H_2O and stored at -80°C.

Viral genomes were quantified in 20ng of total intracellular RNA or 5µL of particulate RNA by one-step RT-qPCR using the *TaqMan Fast-virus 1 Step Master Mix* kit (Applied Biosystems), with a pair of primers that target the 5'-UTR of HCV and the 5'-FAM (6-carboxyfluorescein)- 3'-TAMRA (6-carboxytetramethylrhodamine) fluorescent probes. Measurements were acquired by the *7500 Fast Real-Time PCR System* (Applied Biosystems) real-time thermocycler with the following program: RT at 50°C for 5 min, then after denaturation of the RT enzyme at 95°C for 20s, the qPCR steps were carried out over 40 cycles of 15s at 95°C and 1min at 60°C.

Absolute quantification of viral genomes was obtained using a standard curve established from HCV RNA transcribed *in vitro*, for which the concentration in genome equivalents per microliter (copies/µL) was determined by measuring the absorbance at 260nm. Quantities of intracellular RNA were normalized with respect to the amount of ribosomal RNA measured using primers and a VIC fluorescent probe (20-chloro-70phenyl-1,4-dichloro-6-carboxy-fluorescein) specific for the 18S RNA (*Eukaryotic 18S rRNA Endogenous Control*, Applied Biosystems). Values were expressed in copies/mL or in copies/µg of total RNA.

III.F.(β) HCV infectivity titration by endpoint dilutions

Huh-7.5 cells ($1.8\text{-}2.5x10^3$ cells) were seeded in 96-well plates 24h prior to infection. Serial dilutions of virus inocula were prepared in complete DMEM and each dilution was used to infect 8 wells. Dilution factors were chosen such as to start with a virus dilution ensuring infection of all 8 wells and end with a virus dilution unable to infect a single cell in all 8 wells. Cells were infected with 100µL of each viral dilution and cultured for 5 days. Cells were then fixed and permeabilized in methanol.

Staining of infected cell foci was performed by quenching endogenous peroxidase activity with 0.3% hydrogen peroxide, blocking nonspecific antigenic sites with 1.25% normal horse serum in DPBS (blocking solution, *ImmPRESS HRP* kit, Vector Laboratories), and probing infected cells by an overnight incubation with anti-HCV NS3 mouse monoclonal antibody 2E3

(BioFront Technologies) diluted 1:3000 in DPBS containing 0.1% Tween-20 (PBS-T). After washing, cells were incubated with anti-mouse IgG–HRP ImmPress reagent (*ImmPRESS HRP* kit, Vector Laboratories) diluted 1:2 in PBS-T and stained brown with chromogenic substrate 3,3'-diaminobenzidine (DAB), using the *DAB Peroxidase (HRP) Substrate* kit (Vector Laboratories) according to manufacturer's guidelines. Plates were observed under a light microscope to score infected wells containing at least one focus of ≥2 infected cells. Data were introduced into the Reed and Muench TCID50 algorithm[551], in order to obtain TCID50/mL titers.

III.F.(γ) Sequencing of HCV genome(s)

Intracellular (1µg total RNA) or particulate (10µL) viral RNA extracted as described above (§III.F.(α)) was subjected to reverse transcription using 3-6µM pdN(6) hexamer, 2mM dNTP mix, 10mM dithiothreitol (DTT), 20U ribonuclease inhibitor and 22U THFT enzyme in THFT Reaction Buffer (*Transcriptor High Fidelity cDNA Synthesis* kit, Roche). Following denaturation of RNA structures by incubation at 65°C for 10min, then immediate transfer onto ice, RT reactions were assembled and subjected to successive incubations at 25°C for 10min, at 42°C for 50min and at 70°C for 15min.

The cDNAs (1-2µL) were further subjected to PCR amplification using the *Phusion Hot Start II High-Fidelity DNA Polymerase* kit (Thermo Scientific™) according to the manufacturer's guidelines, with 0.5µM of each forward (+) and reverse (-) HCV-JFH1-specific primers (summarized in Table 10). The following cycling program was used: 1 cycle at 98°C for 30s, 30-40 cycles comprising 98°C for 30s, 58°C for 30s, 72°C for 1min/1000 base pairs, 1 cycle at 72°C for 5min. RT-PCR products were checked on 1% agarose gels and were purified using *Nucleospin PCR Clean up* kit (Macherey-Nagel) with 50% Buffer NTI. Following purification, RT-PCR product concentration was determined by electrophoresis on agarose gels and comparison with a DNA molecular weight ladder (*Mass ruler express forward DNA ladder mix*, Thermo Scientific™) containing known quantities of DNA fragments.

Sanger sequencing reactions (in 10µL total volume) were performed in 96-well plates using 15-30ng RT-PCR product, 0.32µM appropriate primer (Table 10) and *Big Dye Terminator v3.1 cycle sequencing* kit (Applied Biosystems™). The cycling program was the following: 1 cycle at 95°C for 1min and 25 cycles comprising 95°C for 45s, 50°C for 30s, 60°C for 4min. Sequencing reactions were then processed by Eurofins and data were analyzed using *CLC Main Workbench* (Qiagen).

Table 10 : List of oligonucleotides complementary to JFH1 sequences, used as primers for PCR and/or Sanger sequencing of virus-genome-containing plasmids, viral cDNAs or RNAs.
The polarity of the primer was incorporated in the primer name and represented in black for forward (+) and pink for reverse (-). Primers used for PCR amplification are indicated by asterisks (*).

Primer Name	HCV genome position (nts)	Viral protein	Primer Sequence (5'→ 3')
**JFH 181+*	181-200	5'UTR	AAGACTGGGTCCTTTCTTGG
JFH 596+	596-616	Core	TATGGGAATGAGGGACTCGGC
**JFH 940+*	940-970	E1	CTACATGGTGACCAATGACTGCTCCAATGAC
JFH 1039+	1039-1057	E1	GAATACGTCACGGTGTTGG
**JFH 1412+*	1412-1422	E1	GGCTTGGCCTACTTCTCTATG
JFH1724+	1724-1743	E2	ATCGAGGCTTTCCGGATAGG
JFH 2180+	2180-2200	E2	CACTACCCTTACAGACTCTGG
**JFH 2556+*	2556-2575	E2	TGTGGATGCTCATCTTGTTG
JFH 2564+	2564-2590	E2	CTCATCTTGTTGGGCCAGGCCGAAGCA

JFH 2699+	2699-2718	p7	GTCCCCTTGACCACCTATTG
JFH 3200+	3200-3220	NS2	TATGACCACCTCACACCTATG
JFH 3699+	3699-3718	NS3	GGACCAAGTCTTTGGAGCCG
**JFH 3945+*	3945-3966	NS3	TTGAGACACTCGACGTTGTTAC
JFH 4698+	4698-4718	NS3	ACTCCGTGATCGACTGCAATG
**JFH 5019+*	5019-5038	NS3	AATTTTGGGAGGCAGTTTTC
JFH 5216+	5216-5236	NS3	ACACCTCTCCTGTACCGTTTG
JFH 5715+	5715-5735	NS4B	CTTCCATGATGGCATTCAGTG
JFH 6197+	6197-6217	NS4B	GGCTCTCTTACTATAACCAGC
JFH 6235+	6235-6256	NS4B	CAATTGGATAACTGAGGACTGC
JFH 6244+	6244-6264	NS4B	AACTGAGGACTGCCCCATCCC
JFH 7693+	7693-7713	NS5B	TCTAATAACTCCCTGTAGCCC
JFH 8021+	8021-8041	NS5B	ATCAAGTCCGTGTGGAAGGAC
**JFH 8528+*	8528-8547	NS5B	AGCATGGGTAACACCATCAC
JFH 9200+	9200-9219	NS5B	ATCTCCCGTGGAGGGAAAGC
JFH 963-	943-963	E1	GAGCAGTCATTGGTCACCATG
**JFH 1672-*	1672-1691	E2	CTGACGAGTTAAAGCGGTTG
JFH 2432-	2432-2451	E2	TGTACGTCCACGATGTTCTG
**JFH 2877-*	2877-2897	NS2	GATAGCACAACCACCACAGAC
JFH 2951-	2933-2951	NS2	GCACCTGCATGGGTGGTAC
**JFH 3463-*	3443-3463	NS3	TCGTGTTTGCTGGGCATAAGC
**JFH 4149-*	4149-4168	NS3	ATGTGCCTTGGATAGGTACG
JFH 4453-	4433-4453	NS3	GAGGCCTACCTCTTCTATATC
JFH 4971-	4952-4971	NS3	CTAAGCCTGACGGTGGTCTC
**JFH 5322-*	5287-5322	NS3	GTCATGACCTCAAGGTCAGCTTGCATGCATGTGGCG
JFH 5469-	5449-5469	NS4A	TCAAAAGCCTCATACAGGACC
JFH 5965-	5945-5965	NS4B	GCCAGACATGATCTTGAATGC
JFH 6469-	6449-6469	NS5A	GACATTGCCAGAGATGTTGGC
**JFH 6496-*	6496-6515	NS5A	TGTTCATGCAGGTTTTAGGC
JFH 7767-	7744-7767	NS5B	TGGTATCGCAACAGCGAGTTACTC
JFH 7753-	7753-7772	NS5B	TGTTATGGTATCGCAACAGC
JFH 7960-	7941-7960	NS5B	TCTTGCAGAATGGGGTGGAG
JFH 8040-	8020-8040	NS5B	TCCTTCCACACGGACTTGATG
JFH 8456-	8436-8456	NS5B	CTCCTACGTAAAGTCTCTCAG
**JFH 9070-*	9070-9089	NS5B	GCATAGAAAAGGCGTCAAGC
**JFH 9461-*	9461-9484	3'UTR	AAAGGAACAGTTAGCTATGGAGTG

III.G Immunoblotting

Protein extracts from transfected or infected Huh-7.5 cells lysed in denaturating Lithium Dodecyl Sulfate buffer (*NuPAGE™ LDS Sample Buffer*, Invitrogen™) complemented with 5% ß -mercaptoethanol (Sigma-Aldrich) were denaturated by a 15min incubation at 95°C and stored at -20°C. Aliquots of these extracts were loaded onto 4-12%, 10% or 12% 10- or 12-well polyacrylamide gels (*NuPAGE Bis-Tris Gels*, Invitrogen™ & *BOLT Bis-Tris Gels*, Invitrogen™). The samples were electrophoresed in *MOPS SDS Running Buffer* (Invitrogen™) at 200V for ~45min. Proteins were transferred onto a nitrocellulose membrane (*Nitrocellulose Premium*, 0.45µm, Amersham) by wet transfer at 40V for 1h45, using *NuPAGE Transfer Buffer* (Invitrogen™), or onto a PVDF membrane by semi-dry transfer, using the *iBlot™ 2 Gel Transfer Device* (Thermo Fisher Scientific) and pre-cast *iBlot™ Transfer Stack* (Thermo Fisher Scientific), according to manufacturer's guidelines. The membrane was saturated by incubation in DPBS containing 5% skimmed milk (blocking solution) for 1h at room temperature under shaking, then overnight at 4°C with the appropriate primary antibody (see

Table 11), diluted in PBS-T containing 1% milk. Following three PBS-T washes, the membrane was incubated for 30min with fluorescent anti-Ig conjugates (see Table 12) diluted 1:20,000 in 1% milk-PBS-T. Following three PBS-T and one DPBS washes, fluorescent signals were acquired by scanning the membrane on the *Odyssey CLx infrared imaging system* (LI-COR) and analysed using the *ImageStudioLite* software (LI-COR).

In case the membrane was re-used to hybridize another primary antibody, antibody stripping was performed using *Antibody Stripping Buffer* (Gene Bio Application) for 15min under shaking. The membrane was then washed extensively with H_2O and western blotting was performed as described above, starting from blocking step.

III.H Indirect Immunofluorescence

Infected cells in Ibidi slides were fixed at 48h, 72h, 96h or 120h p.i. using 4% paraformaldehyde (Electron Microscopy Sciences) and permeabilized in 40µg/mL digitonin (Sigma-Aldrich). Blocking of unspecific antigenic sites was performed by a 15min incubation in DPBS containing 5% animal serum (Sigma-Aldrich). Serum origin was determined by origin of secondary antibodies. If the different antibodies used were generated in both goat and donkey, 2.5% of each serum was used. Cells were successively incubated for 1h with the appropriate primary antibodies (see Table 11), then with the secondary antibodies coupled to fluorochromes Alexa Fluor 488, 555, or 647 (Thermo Fisher Scientific, see Table 12), both diluted in DPBS containing 1% corresponding animal serum. LDs were either labelled metabolically for 15h before fixation using a fluorescently-labeled fatty acid (*BODIPY® 558/568 C12*, Invitrogen™) diluted 1:10,000 in DMEM without serum, or immuno-labelled post-fixation, using an antibody against adipose differentiation-related protein (ADRP) that is found on LD surface, or by a 30min incubation in *HCS LipidTOX™ Red Neutral Lipid Stain, for cellular imaging* (Invitrogen™) at a dilution of 1:1,000 in DPBS. Following immunolabeling, cells were incubated with 4-, 6-diamidino-2-phenylindole (*DAPI*, 1µg/mL, Invitrogen™) for 10 min at room temperature and were conserved at 4°C in non-polymerizing mounting medium (*Ibidi mounting medium*, Ibidi).

Table 11: List of primary antibodies used for immunolabelling.
IF: used for indirect immunofluorescence experiments, WB: used for western blotting, MAb: monoclonal antibody, PAb: polyclonal antibody.

Target protein	Provider	Origin and clonality	Specific clone	Catalog Number	Dilution used
HCV Core	Santa Cruz	mouse MAb	1851	SC-58144	IF/WB : 1:1,000
HCV Core	BioFront TECHNOLOGIES	mouse MAb	4F5	HCV-4F5	IF : 1:1,000
HCV Core	Gift from Dr. Agata Budkowska (Institut Pasteur, Paris, France)	mouse MAb	ACAP27	-	WB : 1:3,000 IF : 1:1,000
HCV NS5A	BioFront TECHNOLOGIES	mouse MAb	7B5	HCV-7B5	WB : 1:2,000
HCV NS5A	abcam	mouse MAb	H26	ab13833	WB : 1:1,000
HCV NS5A	ID Labs	mouse MAb	-	IDVG1127	WB : 1:1,000
HCV NS5A	Sigma-Aldrich	mouse MAb	9E10	MABF2775	WB : 1:1,000 IF : 1:100
HCV NS5A	BioFront TECHNOLOGIES	mouse MAb	2F6	HCV-2F6	IF: 1:4,000

HCV NS5B	BioFront TECHNOLOGIES	mouse MAb	4B8	HCV-4B8	WB : 1:2,000
Human ADRP	Gift from Dr John McLauchlan (MRC, Glasgow, UK)	sheep PAb	-	-	IF : 1:1,000
Human ERp72	Invitrogen	rabbit PAb	-	PA1-007	IF : 1:100
Strep Tag	Qiagen	mouse MAb	-	34850	WB : 1:2,000
Strep Tag	Gift from Dr. Pierre Lafaye (Institut Pasteur, Paris, France)	mouse MAb	-	-	IF : 1:100
V5 tag	Invitrogen	mouse MAb	-	R960-25	IF/WB : 1:1,000

Table 12: List of secondary antibodies used for immunolabelling.

Target Organism IgG (H&L)	Conjugated fluorophore	Origin	Provider	Catalog Number	Dilution used
Mouse	Dylight 680	**Goat**	LI-COR	926-68070	1:10,000
Mouse	Dylight 800	**Goat**	Invitrogen	SA5-35521	1:10,000
Rabbit	Dylight 800	**Goat**	Invitrogen	SA5-35571	1:10,000
Mouse	Alexa Fluor **488**	**Goat**	Invitrogen	A-11029	1:500
Rabbit	Alexa Fluor **555**	**Donkey**	Invitrogen	A-31572	1:500
Rabbit	Alexa Fluor **647**	**Donkey**	Invitrogen	A-31673	1:500
Rabbit	Alexa Fluor **647**	**Goat**	abcam	ab150079	1:500
Sheep	Alexa Fluor **647**	**Donkey**	Invitrogen	A-21448	1:500

III.I Confocal Microscopy

Slides were observed with an LSM 700 inverted confocal microscope (Zeiss). Images were acquired using the 40X or the 63X objective in oil immersion and the ZEN software (Zeiss). The emission filters were configured to detect signals sequentially with a restriction of ≤460nm for DAPI, 490 to 555nm for Alexa Fluor 488, 550 to 620nm for Alexa Fluor 555, and ≥640nm for AlexaFluor 647. Confocal diaphragm was adjusted such as to prevent light outside the focal plane from reaching the detector by placing it in 1 Airy unit and the resolution of acquired images was either 1024x1024 or 2048x2048, in order to obtain a pixel size of 0.05µm x 0.05µm, which is optimal for image deconvolution. Once laser power and voltage (gain) for all channels were fixed for the control sample, snapshots or z-stacks were acquired for all samples of the slide with the same conditions. The vertical interval between stacks was standardly set to 0.15 µm.

III.J Protein complex purification and identification

III.J.(α) Affinity Purification of HCV Protein Complexes

Huh-7.5 cells were infected as described in §III.E with verified stocks of Jad/NS5A-(TEV)-ST-418, -V5-418, -ST-449, -V5-449 viruses, or transfected with genome-length RNAs of Jad/C17-ST, /C17-V5, or Jad/NS5A-(TEV)-1a-411-V5, -1a-411-ST, -1b-434-ST, -2a-J6-ST, -3a-385-ST, -3a-401-ST, -3a-407-ST, -4-431-ST, as indicated in §III.D. Cells were cultured in 175cm^2-flasks (T175) for the indicated period and trypsinised for lysate preparation. Lysis buffer was composed of 25 mM Tris-HCL pH 8 (Sigma-Aldrich), 150mM NaCl (Sigma-Aldrich), 2mM ß-mercaptoethanol (Sigma-Aldrich), 0.5% NP40 (Thermo Scientific),

200µg/mL avidin, anti-protease cocktail (*Complete*, Roche) and, only in the NS5A experiments, anti-phosphatase cocktail (*PhosSTOP*, Roche). Cell lysates were collected at 96h p.i. from 1xT175 per replicate sample for infected cells, at 120d p.tf. from 1xT175 per replicate sample for transfected cells for NS5A-related experiments and at 72d p.tf. from 5xT175 per replicate sample for Core-related experiments. Cell lysis was performed in 1.2mL lysis buffer per T175 for each replicate sample for 20min in ice with regular agitation. Cell debris were removed by a 20min centrifugation at 16,000g at 4°C and supernatants were transferred in a clean Protein LoBind® 5mL tube (Eppendorf). At this step, a lysate aliquot corresponding to approximately 0.04xT175 (i.e. ~ $9x10^4$ cells) was retrieved and mixed with appropriate volume of LDS+ß-mercaptoethanol to be used for immunoblotting.

The remaining lysates were mixed with 300µL prepared *MagStrep "type3" XT* magnetic beads (IBA Lifesciences) for NS5A complex purifications or 75µL *StrepTactin Sepharose High Performance* beads (Cytiva) for Core complex purifications. Bead preparation entails three (3) washes in washing buffer (25 mM Tris-HCL pH 8, 150mM NaCl, 2mM ß-mercaptoethanol, 0.5% NP40, anti-protease cocktail ± anti-phosphatase cocktail). Protein binding was performed on a rotating wheel at 4°C for 1h for NS5A and 1.5h for Core.

Beads were then successively washed three times in wash buffer without NP40 for NS5A, or once with wash buffer and twice with wash buffer without NP40 for Core purification, in order to eliminate unspecifically bound proteins and the detergent itself. During the last wash, aliquots corresponding to approximately $9x10^4$ cells were retrieved to be used for immunoblotting. Washed beads were resuspended in 560µL 50mM ammonium bicarbonate (NH_4HCO_3) buffer containing 20 mM tris(2-carboxyethyl)phosphine reducing agent (TCEP, $C_9H_{15}O_6P$).

Five biological replicates of these samples for each tagged-NS5A and three for tagged-Core viruses were provided to the Proteomics Platform of Institut Pasteur (UTechS MSBio) for the nano liquid chromatography coupled to mass spectrometry (nano-LC-MS/MS) analysis of proteins retrieved..

III.J.(β) Nano-LC-MS/MS

III.J.β.(i) On-beads protein digestion

Digestion of the proteins were performed on-bead using 0.5µg of Sequencing Grade Modified Trypsin (Promega) for 16 hours at 37°C under agitation at 1,000 rpm.

For NS5A interactomic experiments:

First supernatants were retrieved following a short centrifugation step (4,000 rpm, 30 sec, room temperature). Next, a 1 min incubation of the beads with100µL of NH_4HCO_3 50 mM on a magnetic device led to a second supernatant that was pooled with the first one, and formic acid (FA) was added at 1% final concentration.

For Core interactomic experiments:

First supernatants were retrieved following a centrifugation step at 10,000 rpm for 5 min at room temperature. Then, 100 µL of NH_4HCO_3 50 mM were added to the beads and placed in a membrane-containing filter unit (Corning™ Costar™ Spin-X™ Centrifuge Tube Filters, Fisher Scientific), 200µL of the same buffer was then added and the flow-through was retrieved by a centrifugation at 6,000 g for 30 sec at room temperature. This operation was repeted in the same conditions. Pooled supernatants were acidified with FA at 1% final concentration and filtered on a new filter unit.

III.J.β.(ii) Peptide desalting

For Jad NS5A and Core interactomic experiments:

Acidifed peptide solutions were desalted using stage-tip[552] and three C18 Empore discs, and were eluted with 80µL acetonitrile (ACN) 80%, FA 0.1%. All samples were dried in a Speed-Vac and peptides were resuspended in ACN 2%, FA 0.1% prior to LC-MS/MS analysis.

For other NS5A interactomic experiments:

Acidifed peptide solutions were desalted using an automatic workflow with the AssayMAP Bravo (Agilent). Peptides were eluted from the C18 cartridge (Agilent Technologies, 5µL bead volume) with 60µL ACN 80%, FA 0.1% and all samples were speed-vac dried. Peptides were resuspended in ACN 2%, FA 0.1% prior to LC-MS/MS analysis.

III.J.β.(iii) LC-MS/MS: Data Dependent Acquisition

For Jad NS5A and Core interactomic experiments:

A nanochromatographic system (Proxeon EASY-nLC 1200, Thermo Fisher Scientific) was coupled on-line to a Q Exactive HF mass spectrometer (Thermo Fisher Scientific) using an integrated column oven (PRSO-V1, Sonation). For each sample, peptides were loaded on a home-made 39cm capillary column picotip silica emitter tip (75µm inner diameter) with C18 resin (1.9µm particles, 100Å pore size, Reprosil-Pur Basic C18-HD resin, Dr. Maisch) after an equilibration step in 100 % solvent A (H_2O, FA 0.1%). Peptides were eluted with a multi-step gradient using 2-7% solvent B (ACN 80%, FA0.1 %) for 5min, 7- 23% for 70min, 23-45% for 30min and 45-95% for 5min at a flow rate of 250nL/min over 132min. Column temperature was set at 60°C.

Mass spectra were acquired using Xcalibur software and a data-dependent Top 10 method with survey scans (300-1700 m/z) at a resolution of 60,000 and MS/MS scans (fixed first mass 100 m/z) at a resolution of 15,000. The AGC target and maximum injection time for the survey scans and the MS/MS scans were set at 3.0E+06, 50ms and 2.0E+05, 60ms, respectively. The isolation window was set at 1.2m/z and normalized collision energy fixed at 28 for HCD fragmentation. A minimum AGC target of 2.5E+03 for an intensity threshold of 4.2E+04 was used. Unassigned precursor ion charge states, as well as 1, 7, 8 and >8 charged states were rejected and peptide match was disable. "Exclude isotopes" was enabled and selected ions were dynamically excluded for 30 seconds.

For other NS5A interactomic experiments:

A nanochromatographic system (Proxeon EASY-nLC 1200, Thermo Fisher Scientific) was coupled on-line to a Q Exactive Plus mass spectrometer (Thermo Fisher Scientific) using an integrated column oven (PRSO-V1, Sonation). For each sample, peptides were loaded on a home-made 49cm capillary column picotip silica emitter tip (75µm inner diameter) with C18 resin (1.9µm particles, 100Å pore size, Reprosil-Pur Basic C18-HD resin, Dr. Maisch) after an equilibration step in 100% solvent A (H_2O, FA 0.1%). Peptides were eluted with a multi-step gradient using 5- 25% solvent B (ACN 80%, FA 0.1%) for 95min, 25- 40% for 15min and 40-95% for 10min at a flow rate of 250nL/min over 130min. Column temperature was set at 60°C.

Mass spectra were acquired using Xcalibur software using a data-dependent Top 10 method with survey scans (300-1700 m/z) at a resolution of 70,000 and MS/MS scans (fixed first mass 100m/z) at a resolution of 17,500. The AGC target and maximum injection time for the survey scans and the MS/MS scans were set at 3.0E+06, 20ms and 1.0E+06, 60ms, respectively. The isolation window was set at 1.6m/z and normalized collision energy fixed to 28 for HCD fragmentation. We used a minimum AGC target of 1.0E+04 for an intensity threshold of 1.7E+05. Unassigned precursor ion charge states, as well as 1, 7, 8 and >8 charged states were rejected and peptide match was disable. "Exclude isotopes" was enabled and selected ions were dynamically excluded for 45 seconds.

III.J.β.(iv) Data processing for protein identification and quantification

Raw data were analysed using MaxQuant software version 1.6.6.0[553] using the Andromeda search engine[554]. The MS/MS spectra were searched against a UniProt *Homo sapiens* database (downloaded in 18/06/2020, 20,353 entries) and virus databases including ST- and V5- tagged proteins (Jad NS5A: 10 entries, Core: 13 entries, other NS5A: 20 entries). Usual known mass spectrometry contaminants and reversed sequences of all entries were included.

Andromeda searches were performed choosing trypsin as specific enzyme with a maximum number of two missed cleavages. Possible modifications included carbamidomethylation (Cys, fixed), oxidation (Met, variable), N-terminal acetylation (variable) and phosphorylation (Ser, Thr, Tyr, variable). The mass tolerance in MS was set to 20ppm for the first search, then 4.5ppm for the main search and 20ppm for the MS/MS. Maximum peptide charge was set to 7 and 7aa were required as minimum peptide length.

The "match between runs" feature was applied for samples having the same experimental condition with a maximal retention time window of 0.7 min. One unique peptide to the protein group was required for the protein identification. A false discovery rate (FDR) cut-off of 1% was applied at the peptide and protein levels.

III.J.β.(v) Specific case for NS3, NS4B and NS5A proteins

NS5A proteins derived from various genotypes share > 55% aa sequence identity. A number of peptides, notably short peptides retrieved can therefore be common to all NS5A proteins, while some peptides are unique and specific to each of the NS5A proteins. In MaxQuant software, razor peptides[553] are peptides that are found in more than one protein. In "razor" peptide assignment, the peptide and its related intensity is assigned to the protein group with the larger number of identified peptides or, in case of a tie, to the protein group with more highly scoring peptides. In our case, 8 NS5A sequences were gathered in a database and peptides were wrongly assigned by MaxQuant rules to nonmatching NS5A proteins. Because we know which NS5A protein was expressed in a given sample, "razor" peptides were reattributed to the proper NS5A protein, leading to the real intensity of each NS5A in each genotype. Same was applied for NS3 and NS4B with compensatory mutations.

III.K Hepatocellular transcriptome analysis by RNA-Seq

Infected Huh-7.5 (see §III.E) were lysed in 350µL lysis buffer (*RNeasy Plus Mini* kit, Qiagen) supplemented with 0.1 % ß-mercaptoethanol (Sigma-Aldrich), following the manufacturer's instructions, and total RNAs were extracted. Genomic DNA was eliminated by DNase treatment on the column for 15min (*RNase-free DNase Set*, Qiagen). RNA integrity and quality were assessed by *MySpec* nano-spectrophotometer (Ozyme) and the *2100 Bioanalyzer* (Agilent). Following the *MGI's RNA Direction Library prep set user Manual* (MGI Tech, Shenzen Shi, China), poly(A) mRNAs were enriched from 200ng total RNA using *Dynabeads mRNA Purification Kit* (Thermo Fisher Scientific), and were subsequently cleaved into fragments of 150 bp, reverse-transcribed and complemented. MGI adapters were ligated before a 14-cycle DNA fragment amplification step. The quality of the DNA libraries was checked by capillary electrophoresis (*Fragment Analyzer*, Agilent) using the *HS NGS Fragment* Kit (Agilent). The DNA libraries were then assembled and prepared according to the *RNA Directional Library prep set* and *High-throughput (Rapid) Sequencing Set* user manuals of MGI (MGI Tech, Shenzen Shi, China) and sequenced on a high-throughput cell in single 100bp reads (DNBSEQ-G400, MGI Tech, Shenzen Shi, China).

III.L RHV-rn1 virus production

III.L.(α) RHV-rn1 genome-length RNA

RHV-rn1 genome-length cDNA (GenBank accession No KX905133)[468] cloned in pUC57 was kindly provided by Dr Amit Kapoor (Ohio State University, Columbus, Ohio, USA). XL1-Blue competent bacteria (Agilent) were transformed with this vector following a heat-shock and cultured for 16h at 37°C on LB Petri dishes containing 500 µg/mL ampicillin. Plasmid DNA was purified from cultured bacterial colonies using *Nucleospin plasmid* kit (Macherey-Nagel) and screened by restriction reactions spanning both the plasmid and the inserted viral cDNA sequences with the following enzymes:

i) EcoRI
ii) BamHI
iii) SmaI
iv) MluI & BspEI

All restriction enzymes and respective buffers were from New England Biolabs. Large scale DNA preparations of two clones with a correct pattern were performed using *Nucleobond Xtra Midi Plus* kit (Macherey-Nagel) and the nucleotide sequence was further verified by Sanger sequencing (see §III.F.(γ)) using the primers indicated in Table 13.

Table 13 : List of oligonucleotides complementary to RHV-rn1 sequences, used as primers for PCR and/or Sanger sequencing of viral RNAs.
The polarity of the primer was incorporated in the primer name and represented in black for forward (F) and pink for reverse (R). Primers used for PCR amplification are indicated by asterisks (*).

Primer Name	Primer Sequence (5'→ 3')	Primer Name	Primer Sequence (5'→ 3')
*RHV_1_F	ACCATCACACTCCCCAATG	RHV_570_R	CACACAGATTCCACCACAGG
RHV_287_F	TGGCTCTGTGGAGATAAAGC	RHV_1019_R	GAAAATGCCAGCACTAGCC
RHV_842_F	TGATCTCCTGCATCACGTTC	RHV_1826_R	GCAGGCCAAGTTAGTCCATC
RHV_1467_F	GCCATCCAGCTGAATACCAC	RHV_2382_R	AAATGAGGCCAGTGCTCAAG
RHV_2159_F	GGCTGGCTTCAACCTACC	RHV_2966_R	TTGCTGCAAACATACCAAGC
RHV_2703_F	GTGGTTGAGGCTTACGAAGG	*RHV_3570_R	GGGGATAAGTGGCAAAGTCC
**RHV_3246_F*	TACGCAAGATTGGGCAAGAC	RHV_4211_R	AATTCCAAGCACGGTAGTGG
RHV_3834_F	AAGGTTGGAGCCCAGATACC	RHV_4727_R	GTAGTACGTTCCCGGTTTGC
RHV_4573_F	ACTCCGTGTACGACTGTTGC	RHV_4810_R	AAGTATGCCAGGCCAGAATC
RHV_5059_F	TTTCAGGCAAGGCAAAATTC	RHV_5416_R	ATTTTGTCTCCGAGCCACTG
RHV_5637_F	ACAAAGCTAACAACACAGACG	RHV_6024_R	TTTCCAGCCACTTGATGATG
*RHV_6262_F	TAAAATCAACGTGCGAGTGC	*RHV_6612_R	GACACTTCCGCCAATCAGTC
RHV_6828_F	CCGTATGACACCGAGGAAAC	RHV_7229_R	CATGGGAATCTCCAATCGTG
RHV_7474_F	CGCTAAAAATCAAGGGCAAG	RHV_7813_R	ATTTGGTAGCGCAACTCAGG
RHV_8086_F	TTGCTTATCCCCACCTTGAG	RHV_8434_R	CTCCTGTAGCCCACTTCAGC
RHV_8706_F	AACGTCTCCTCTGCCAACAC	RHV_9055_R	TGGCTCACACGCTGTATTTC
RHV_9302_F	TCTAGGCATGGGAATCATAGC	*RHV_9656_R	AGTTGAGGTGGGCGTAACG

RHV-rn1 plasmid was linearized by MluI digestion and purified by phenol/chloroform (Sigma-Aldrich) extraction and ethanol precipitation. Linearized DNAs (1µg, quantified on 1% agarose gel) served as templates for *in vitro* transcription of the viral cDNA using bacteriophage T7 RNA polymerase (*T7 RiboMAX Express Large Scale RNA Production System*, Promega). In preparation of two types of samples for intrahepatic inoculations of Sprague Dawley rats, some reactions underwent DNase treatment (Promega), and purifications as described in §III.C (δ), while others were kept unpurified. Purified products subjected to a second round or purification with ethanol, to eliminate the residual un-incorporated

ribonucleotides, served for the preparation of aliquots with known quantity of RHV-rn1 molecules towards standard curve necessary for RT-qPCR assays. The quality and quantity of RNAs were evaluated by electrophoresis on 1% agarose gel and by measurement of the absorbance at 260nm using *mySPEC* microvolume spectrophotometer (Ozyme), while their sequence was verified following reverse transcription, amplification in overlapping PCR fragments spanning the entire genome (see Table 12), and sequencing by Sanger sequencing as indicated above.

III.L.(β) RHV-rn1 viral stocks generation

Sprague Dawley rat intrahepatic inoculations of purified or nonpurified RHV-rn1 genome-length RNAs were performed by our collaborator, Hervé Lerat (hTAG, La Tronche, France). Briefly, the procedure was performed under general anaesthesia of the rats with isoflurane: anaesthetic induction by inhalation of a mixture of oxygen at a flow rate of 3L/minute and isoflurane at 4% for 2 minutes in an appropriate hermetic cage. The animals were kept asleep by inhaling a mixture of 2.5% isoflurane and oxygen at a rate of 1.5L/minute. This technique is the one with the least reported impact on liver metabolism. The viral RNA solution was injected intra-hepatically at 4 different injection points (in the left lateral and median lobes), according to the following procedure:

- The laparotomy was performed by first making a skin incision of about 2cm along the linea alba, then an incision in the peritoneal wall, 1 cm below the xiphoid process, on shaved, Vetadine treated area.
- Part of the left lobes of the liver was pushed slightly outwards and stabilized with a cotton applicator. Intrahepatic injection was performed using a 30G needle mounted on a 0.3 mL syringe. After removal of the needle, light pressure was applied by a cotton applicator to ensure haemostasis. After each injection, the absence of haemorrhage was verified and, if necessary, a Gelfoam resorbable haemostatic gelatine sponge was be placed at the injection sites.
- The liver was pushed back into the abdomen, making sure that there is no active bleeding.
- Closure was performed in two planes: first of the peritoneo-muscular plane and then of the cutaneous plane with sterile 5/0 silk thread.

Rats that underwent surgery were isolated for a maximum of 1 week, depending on their recovery, and were then grouped with their original congeners to re-establish social links. Free access to drinking water and food pellets was provided to all animals. Blood samples were recovered from the sublingual vein, following general anaesthesia, every 4 days for 12 days to detect and quantify the viremia, by RT-(q)PCR, as described below.

Infectious serum (viral) stocks were generated by intrahepatic inoculation of 3 rats that were exsanguinated post-mortem at day 12 post-inoculation.

III.L.(γ) RHV-rn1 genome quantification

Viremia was quantified by RT-(q)PCR by analysing 5µL of RNA extracted from 70µL rat sera samples using the *QiaAmp Viral RNA Mini* kit (Qiagen), according to the manufacturer's guidelines. One-step RT-(q)PCR reactions were performed using the *TaqMan Fast-virus 1 Step Master Mix* kit (Applied Biosystems), with a pair of primers and 5'-FAM (6-carboxyfluorescein)- 3'-TAMRA (6-carboxytetramethylrhodamine) fluorescent probe, as previously described by Trivedi et al.[468].

Optimal concentrations of primers and probe were worked out as 400/400/100nM, respectively. Measurements were acquired by the *7500 Fast Real-Time PCR System* (Applied Biosystems) real-time thermocycler with the following program: RT at 50°C for 5 min, then

after denaturation of the RT enzyme at 95°C for 20s, the qPCR steps are carried out over 45 cycles of 15s at 95°C and 1min at 60°C.

III.L.(δ) Next Generation Sequencing of viral RNA extracted from rat sera

RHV-rn1 genomic RNA was extracted from 70µL pooled rat sera representing viral stocks, using the *QiaAmp Viral RNA Mini* kit (Qiagen) according to the manufacturer's guidelines, in the absence of carrier RNA.

RNA was reverse transcribed and successful RNA extraction was tested by PCR amplification using RHV-specific primers RHV_1_F and RHV_3570_R, as described in §III.F.(γ) (see Table 13). Resulting cDNA was then used to synthesize a second DNA strand and generate Illumina TruSeq nano libraries following fragmentation into 350bp-long fragments, UDI indexation and 15-cycle amplification (Illumina). Paired-end sequencing was performed on a NextSeq 2000 system with a P1 flowcell and reagents for 151 cycles (Illumina) by the Biomics platform at Institut Pasteur.

Quasispecies were analyzed using the variant calling pipeline from the Sequana project (v0.8.5)[555]. First, the homogeneity of the coverage was checked with Sequana coverage[556]. Next, single-nucleotide polymorphisms (SNPs), insertions and deletions (indels) and multi-nucleotide polymorphisms (MNPs) were detected with Freebayes (v1.3.2) using the default option except for the ploidy option, which was set at 25[557]. Variants were filtered, and only those with a Freebayes score >1, a frequency ≥5%, a minimal depth of 10, and a minimal forward and reverse strand ratio of 0.2 were retained.

Titers of viral stocks were also quantified according to the procedure described in §III.M.

III.M RHV-rn1 experiments in Sprague Dawley rats

Towards **infection**, the rats underwent light general anaesthesia to perform a sublingual harvest and were directly after intravenously injected with 10-100µL of infectious serum, so as to receive $3x10^4$, $3x10^5$ or $3x10^6$ viral genome equivalents.

Towards **treatment evaluation**, the DAA combination called *Maviret (*Glecaprevir & Pibrentasvir) was administered orally according to the dosage described in the studies performed in humanized mice infected with HCV (*Maviret*: Glecaprevir 60mg/kg/day and Pibrentasvir 25 mg/kg/day for 6 weeks)[558].

For **pyruvate tolerance test (PTT)**, the animals were fasted for 5 hours prior to injection of a solution of pyruvate (2 g/kg, IP), and the blood sugar of the animals was monitored by *OneTouch®Ultra®* glucometer for 120 minutes. For this, a blood sample of 5µL was taken from the end of the rat tail at t=0, 15, 30, 45, 60, 90 and 120 minutes after the injection. Intraperitoneal injection and blood sampling are not painful for the animal and do not require any anaesthesia or restraint.

Liver tissues were fixed in formalin solution, neutral buffered at 10% (Sigma-Aldrich) and paraffin-embedded, then four-micrometer sections of tissue were prepared. Hematoxylin-eosin (H&E) staining was used for the histopathological examination. Frozen tissue sections were prepared (8 µm) and stained with Oil-Red-O (ORO) dye (Sigma-Aldrich) to identify neutral lipids. Images were acquired with an AxioCamMR5 camera (ZEISS Industrial Metrology) and the degree of steatosis was estimated by calculating the percentage of the area occupied by oil red O–stained lipid droplets using Image-J software (https://imagej.net/), averaging 3–5 separate, randomly selected fields.

Towards **metabolomics and lipidomics** analyses, upon rat sacrifice, liver tissues were snap-frozen in liquid nitrogen and stored at -80ºC. Whole frozen livers were then pulverized using a mortar. A biphasic extraction was performed on 50mg of each sample. The polar phase was used for metabolomic analysis of 56 different metabolites by NMR, while the nonpolar

phase was used for lipidomic analysis by GC-MS/LC-MS by the GEMELI lipidomics platform (C. Botté, IAB, La Tronche).

III.N Bioinformatic tools and statistical analyses

III.N.(α) Analysis of LC-MS/MS data

III.N.α.(i) Statistical analysis

To identify the proteins more abundant in one condition than in another (ST- Vs V5-tag), the intensity values from Maxquant were compared. Reverse hits, potential contaminants, and proteins "Only identified by site" were removed from the analysis. Then, proteins identified with at least one peptide that is not common to other proteins in the FASTA file used for the identification (at least one "unique" peptide) were kept. Additionally, only proteins with at least four intensity values (NS5A replicates) and 2/3 or 3/3 intensity values (Core replicates) in one of the two compared conditions were kept for further statistics. Proteins absent in a condition and present in another were put aside ("exclusive" partners). These proteins can directly be assumed differentially abundant between the conditions. After this filtering, intensities of the remaining proteins were first log-transformed (log2). Next, intensity values were normalized by median centering within conditions (section 3.5 in Giai Gianetto, 2023[559]). Statistical testing was conducted using a limma t-test thanks to the R package limma[560]. An adaptive Benjamini-Hochberg procedure was applied on the resulting p-values thanks to the function adjust.p of the cp4p R package[561] using the robust method described in Pounds & Cheng, 2006[562] to estimate the proportion of true null hypotheses among the set of statistical tests. The proteins associated to an adjusted p-value inferior to an FDR level of 5% and an absolute $\log_2$(fold-change) superior to 1 have been considered as significantly differentially abundant proteins. Therefore, the proteins of interest are those which emerge from this statistical analysis supplemented by exclusive partners which are be present in one condition and absent in another.

III.N.α.(ii) Scoring of protein-protein interactions and network analysis

In order to score PPIs with ST-tagged bait proteins in infected samples, two dedicated software were used: SAINTexpress[563] and MiST[564]. In both methods, corresponding samples infected with V5-tagged recombinant viruses were used as controls.

For SAINTexpress, posterior probabilities of true interactions (AvgP) superior to 0.5 can be associated to potentially true interactors. For MiST, a score superior to 0.75 can be associated to potentially true interactors.

To enrich the representation of our data from the nano-LC-MS/MS statistical analysis, we generated a "final score" based on the collective results of these statistical analyses, as well as MiST and SAINT scores. The statistical analysis was essential to consider a hit as a putative interactor in all cases (score +1). This score was increased by 1 in case the same hit was also found as a significant potential interactor by MiST (>0.75) or by SAINT(>0.5). For Core, taking into account the dual statistical analysis performed (2/3 or 3/3 intensity values), we increased the final score by 0.5 for partners coming up in both. Exceptionally, taking into consideration our additional aim at putatively identifying partners' domain of interaction with Jad NS5A, we considered as common interactors of NS5A-ST-418 and NS5A-ST-449 those that significantly came up in both statistical analyses, or in the statistical analysis of the one and the MiST score of the other, making the analysis of retrieved 418- or 449-specific partners more stringent. Based on the comparative analysis of scoring tools by Verschueren et al.[565], who found MiST to be the more accurate scoring tool among those tested, we also decided to assign an additional 0.5 in the final score in case a hit was reproducibly coming up in our

statistical analysis and with MiST, but not with SAINT. For the putative interacting partners of NS5A proteins of diverse genotypic origins, we instead assigned an additional 0.5 in the final score for each partner retrieved exclusively with NS5A-ST. For all NS5A analyses the final score was normalized with respect to the number of baits it was significantly identified with.

III.N.(β) Analysis of RNA-Seq data

Statistical analyses were performed to identify host genes for which the expression profiles were significantly different between viruses and genotypes. Differential analyses were performed using the DESeq2 R package. All log_2FC were shrunken with the "ashr" option (see lfcShrink() function). For each comparison of interest, one separate DESeq2 model was fitted to perform the following comparisons:

- Jad_C1a_411_vs_Mock
- Jad_C1a_H77_vs_Mock
- Jad_C2a_J6_vs_Mock
- Jad_C3a_389_vs_Mock
- Jad_C3a_390_vs_Mock
- Jad_C3a_395_vs_Mock
- Jad_C3a_401_vs_Mock
- Jad_C3a_376_vs_Mock
- Jad_C3aP98L_vs_Mock
- Jad_C4aR_vs_Mock
- Jad_C4fC_vs_Mock
- Genotype 1 strains Vs Mock (G1M)
- Genotype 2 strain Vs Mock (G2M)
- Genotype 3 strains Vs Mock (G3M)
- Genotype 4 strains Vs Mock (G4M)
- Non-genotype 3 strains Vs Mock (G124M)

Based on the same contrasts, a functional analysis was performed using CAMERA model from limma R package with default parameters for inter-gene correlations. The model was applied on Kyoto Encyclopedia of Genes and Genomes (KEGG)[566], The Molecular Signatures Database (MSigDB) Hallmark gene set collection[567], reactome[568,569], wikiPathways[570,571].

Batch correction for visualization (PCA, heatmaps) was performed with RemoveBatchEffect() function from limma R package, on log counts with batch factor set as the concatenation of the library preparation and extraction dates and the batch kit. In differential and functional analysis, batch was accounted for by adjusting the statistical model on the biological condition (viruses, genotypes) and on the concatenated batch factor simultaneously.

Principal Component Analysis was performed taking the 500 most variable genes, on scaled Variance Stabilizing Transformation (VST) transformed expression table.

III.N.(γ) Representation of results in figures

Illustrations of results were created by either of the following tools, unless otherwise indicated: Prism 9 (GraphPad, San Diego, United States), Cytoscape 3.9.1[572,573], stringApp 2.0.1[574].

Pathway databases exploited were Gene Ontology[575,576], Kyoto Encyclopedia of Genes and Genomes (KEGG)[566], The Molecular Signatures Database (MSigDB) Hallmark gene set collection[567], reactome[568,569] , wikiPathways[570,571], and DISEASES[577].

Upset graphs

Upset graphs are extensions of Venn diagrams to allow the visualization of the intersections between more than 5 sets of genes. Upset graphs from the UpSetR R package were used to compare lists of differentially expressed genes (DEGs) for some comparisons between genotypes and viruses. The bars on the left indicate the size of each set of genes. The vertical bars indicate the size of the intersection between combinations of comparisons indicated by black dots and connected with black lines.

Heatmap of DEGs

DEGs were represented with heatmaps based on genes expression table standardized with VST transformation or batch correction expression table. To allow comparisons among genes, the gene expression table was scaled by gene. Only genes significant (p-adjusted < 0.05) for at least one comparison are used in the heatmaps.

Heatmap of functional analysis

Pathways and gene sets deregulated between groups were represented by heatmaps based on the CAMERA analysis output (limma R package). We used the enrichment score computed by CAMERA as a proxy of the regulation direction of significant genes sets (p-adjusted < 0.05): for a comparison of group A vs group B, a positive enrichment score (in red) suggests that a given genes set has higher expressions in group A rather in group B. Similarly for negative enrichment score (in blue) and lower expressions.

Bubble plots of enrichment analysis (ORA)

Enrichment of the intersection of significant genes for several comparisons (among all viruses and among all viruses except Jad) was performed using Over-Representation Analysis (ORA) implemented in the enricher() function of clusterProfiler R package. After filtering the significant genes sets (p-adjusted < 0.05), the results are represented by bubble plots showing the averaged log_2FC (from DESeq2 analysis) within each genes set, for all viruses. Colour indicates the amplitude (the darker, the higher) and the direction of the average log2FC (blue for negative value, red for positive values). Size of the bubbles shows the level of significance (*: p-adjusted < 0.05, **: p-adjusted < 0.01, ***: p-adjusted < 0.001

Volcano plots for comparisons between viruses

The differential analysis output involving comparisons between viruses and Mock was visualized with volcano plots. For better visualization, log_2FC higher than 5 in absolute value were set to 5 or -5 depending on their sign. Then we used EnhancedVolcano R package to show distribution of adjusted p-values against log_2FC. The dotted lines correspond to the 5% threshold for p-values and to (-1,1) threshold for log_2FC. Colours of the points are derived from these thresholds.

Volcano plots for comparisons between genotypes

Differential analysis output involving comparisons between genotypes are visualized using complex volcano plots in which comparisons between genotypes are enriched with the results of comparisons with the Mock. Each panel shows the adjusted p-values against the log_2FC of comparisons between genotypes (e.g. G1 vs G4) or combinations of genotypes (e.g. G3 vs G1+G2+G4 without Jad). Colours indicate if a gene is significant only for genotypes (blue), only compared to Mock (green), both (red) or none of the above (grey).

IV. Results

Part 1: HCV-host interplay in infected cell cultures

This first part of my PhD was focused on examining the interplay between HCV proteins of diverse genotypic origins and the host *in vitro*, in a system as physiological as possible. To this end, we have chosen to conduct our experiment in an infection system comprised of cultured human hepatoma Huh-7.5 cells and intra-/inter-genotypic recombinant viruses generated in the backbone of the JFH1-adapted strain, Jad.

The two proteins of interest, Core and NS5A, were selected based on their reported diverse induced hepatocyte deregulations, as described in §I.B.(θ).

Core intra- and inter-genotypic recombinant viruses were previously generated and characterized in the lab, during the respective PhD theses of Stephanie Aicher and Emeline Simon. Core sequences were derived either from HCV prototypic strains, or from clinical strains isolated from patient sera and collected by Dr Claire Gondeau (Institut de Médecine Régénératrice et de Biothérapie, Montpellier, France). Core substitution did not significantly affect viral genome replication or viral assembly, leading to the generation of viruses that exhibited similar growth curves, allowing comparative studies at the same time-points (Aicher et al., 2018[550]; Simon, Aicher, et al., unpublished data, Supplementary Figure 2).

The successful production of NS5A intra- and inter-genotypic recombinant viruses was previously described by Scheel et al.[172], within the backbone of chimeric virus J6/JFH1, consisting of the Core to NS2 sequences of subtype 2a J6 strain and the remaining of subtype 2a JFH1 strain. The sequences of NS5A that were selected in the Scheel study were derived from prototypic HCV isolates: H77C(1a), TN(1a), J4(1b), J6(2a), S52(3a), ED43(4a), SA13(5a), HK6a(6a), or QC69(7a). Most of the recombinant viruses were reported to grow equally well as the parent without the need for adaptive mutations, with the exception of the 1b, 3a and 4a chimeras. Wang et al[578] also described a 2a-1b triple chimera (FL-J6/JFH1-NS5A.J4N) and Okamoto et al.[579] reported other NS5A chimeric viruses within the JFH1 backbone bearing NS5A sequences from strains of genotypes 1a (JFH1-NS5A.H77), 1b (JFH1-NS5A.Con1b), 2a (JFH1-NS5A.J6CF), and 2b (JFH1-NS5A.MA). These findings supported that the development of NS5A intra- and inter-genotypic recombinant viruses within the Jad backbone with NS5A sequences from field strains was feasible, although some adaptive mutations might be required. Our successful generation of these viruses is described in the following §I.B.(θ).

The study of the interplay of HCV proteins with the host cells is divided in two sections: the interactions of Core and NS5A with human hepatocyte proteins (proteomic/interactomic studies) and the HCV protein-driven regulations of host gene expression (transcriptomic studies), which are both described in this chapter.

- For the transcriptomic studies, Core intergenotypic chimeras briefly described above were used.
- For the interactomic studies, parental, as well as intra- and inter-genotypic NS5A recombinant viruses expressing tagged NS5A were developed and characterized during my thesis, as described in the following paragraphs (§IV.C.(α) and §IV.C.(β)). Jad recombinant viruses expressing similarly tagged Core were previously developed and characterized by Stephanie Aicher and Houda Tabbal, a former post-doctoral researcher in the laboratory.

Evidence for tolerance of insertions within Core and/or NS5A sequences has previously been reported in ectopic protein expression[580], subgenomic replicon[518] and infection systems[581,186,582,583], without abolishing HCV RNA replication or virion morphogenesis. Additional specific positions within the Core and NS5A sequences that may tolerate insertions

have also been identified by transposon-based insertional mutagenesis coupled to next-generation sequencing[584].

A schematic summary of the viral tools produced, the experimental processes followed and the analyses performed can be found in Figure 30.

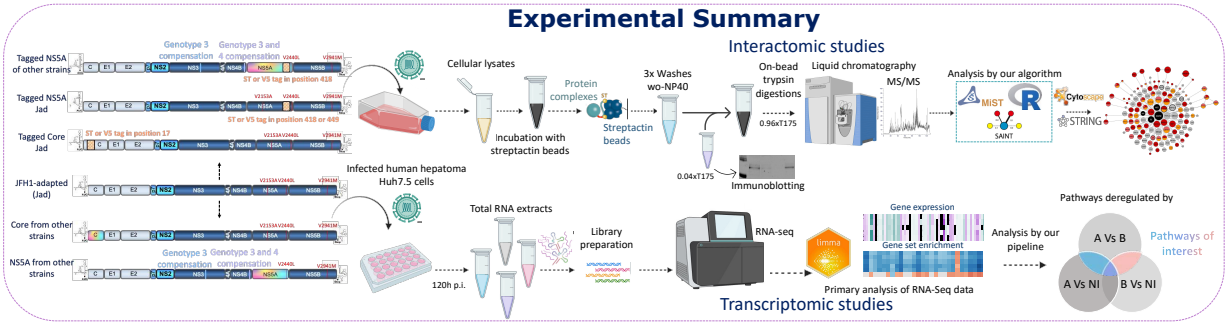

Figure 30: Schematic illustration of the viral tools, experimental processes and analyses in this study. *For certain items BioRender.com was used (https://www.biorender.com/).*

IV.A Characterization of the NS5A sequences derived from clinical isolates

HCV patient sera were kindly provided by C. Gondeau, together with the patient information summarized in Table 5 (see §I.B.στ.(vi), page - 36 -). The clinical isolates to be used in this project were selected based on the level of patient's assessed liver damage and the absence of known co-morbidity factors that could influence a quicker progression to more severe steatosis. RNAs were extracted from the sera, reverse transcribed in two independent reactions, then amplified by PCR with the primers indicated in Table 6 (Materials and Methods, page - 64 -) and sequenced by Sanger sequencing. Consensus aa sequences were compared to each other and to the consensus aa sequences of NS5A from all respective genotypes and/or subtypes in euHCVdb[585]. These alignments first confirmed the genotyping of the selected strains and second revealed the specific features of these strains with respect to the consensus NS5A sequences of each geno-/sub-type of HCV (data not shown). In the case of sample 431 of genotype 4, alignment of this NS5A sequence with those retrieved from the euHCVdb revealed closest phylogenetic distance of our sequence of interest with that of genotype 4d. Blasting of 431-NS5A also returned subtype 4d sequences with the highest percentages of identity, similarity and best e-values. Therefore, we may consider that the 434 NS5A sequence is likely of subtype 4d, although no definite conclusion can be drawn in the absence of sequencing data in any other genomic region.

In a second step, the PCR products were cloned in TOPO vector to select a clone with the desired consensus sequence, to be further cloned in pJad, as described in §III.C (γ). Overall, at least 10 TOPO clones for each strain were sequenced. For 1a-411 18% of the sequenced clones was found with the consensus sequence, for 1b-434 60%, for the three subtype 3a sequences, the percentage of consensus sequence recovered clones was 40-44% and for 431 only 9%. Notably, both NS5A aa Val-2153 and Val-2440 were 100% conserved in a total of 86 clones sequenced for all strains and differ from residues corresponding to the two Jad adaptive mutations at these positions in NS5A. Since we were aiming at developing the intergenotypic recombinants within the Jad backbone and given that the adaptive mutation V2440L was shown by Kaul et al.[413] to be the most important of the three substitutions within the Jad sequence for virus highly cell culture adaptation, we incorporated it in the sequence of all clinical strains.

The alignment of the different NS5A sequences of the clinical isolates bearing the engineered NS5A C-terminal adaptive mutation with the parental sequence and the sequence

of another prototypic strain of subtype 2a (J6) can be found in Figure 31. Figure 32 shows phylogenetic proximity/distance between these strains.

Analyses presented in Figure 31 and Figure 32B reveal low conservation of NS5A protein sequences in general, both in aa identities, with up to 45% divergence among strains, and in protein lengths, with over 35 residues missing in certain strains. Proteins of the same genotypic origin do cluster together in a phylogenetic UPGMA tree constructed using the Jukes-Cantor model to measure protein distance (Figure 32A), however, quantified percentages of identity differ among genotypes. For example, the three subtype 3a strains differ from each other by only 6-7%, while subtype 2a strains differ by ~15% and genotype 1 strains by ~20%. There are no differences in protein length among the subtype 3a strains and among the subtype 2a strains, but there is one additional residue in the C-terminal NS5A sequence (aa468 in alignment) derived from the 1a strain, when compared to the 1b strain.

A few regions of NS5A are conserved among strains of all four genotypes, including the hyper-phosphorylation region within LCSI, which bears only few differences at position 226 and a highly conserved A231 aa residue in all sequences except for Jad. A sequence of ~20 aa within NS5A C-terminal domain III, which includes one of the positions that tolerate insertions, downstream of aa 449, is specific to subtype 2a strains and is absent from all clinical NS5A sequences. In contrast, the other possible insertion position, downstream of aa 418, together with its surrounding region are highly conserved in all strains examined (Figure 31).

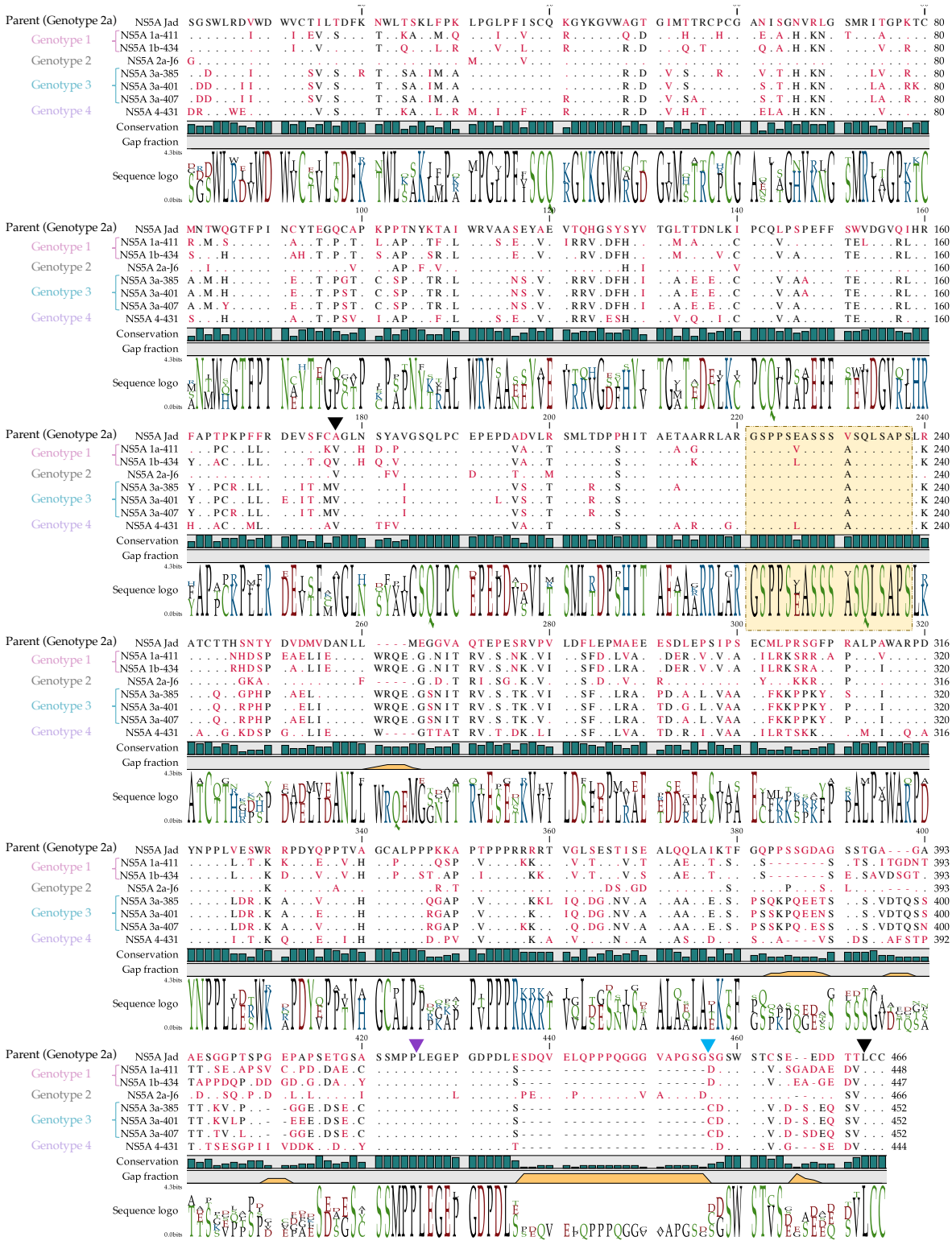

Figure 31: Alignment of NS5A protein sequences derived from clinical or prototypic strains. *Consensus aa sequences from RNA nucleotide sequencing of viruses from patient sera are classified according to the genotype of the infecting strain. Identical residues are depicted by dots and missing residues, by dashes. The most representative aa of each position is in black colour, while different or unique residues are in red. A bar diagram showing the percentage of sequence conservation is included below the alignment, followed by a line diagram depicting the gap fraction within the aligned sequences, and the sequence logo, incorporating all residues present in each position, with the more prevalent in higher font size. The adaptive mutation V2153A of Jad, and V2440L, present in Jad and engineered in all other sequences, are shown by black arrows. A purple and a blue arrow illustrate the*

418 and 449 putative tag insertion positions, respectively. The yellow box spans the NS5A hyper-phosphorylation region within LCSI.

Since there is only one representative strain of HCV subtype 3a associated to each grade of steatosis, it is difficult to conclude on a potential correlation between a particular sequence or aa and the steatosis likelihood. However, it is interesting to note that there seems to be no association between the genetic distance of NS5A and the steatosis severity observed in patients infected with HCV subtype 3a, since the sequences of the strains with no steatosis (401) and high steatosis (407) are clustered closer together, while the NS5A of the strain causing medium steatosis (385) is genetically more distant. In fact, looking at the percentages of sequence identity, the 385 strain is closer genetically to the 401 strain, than the 407.

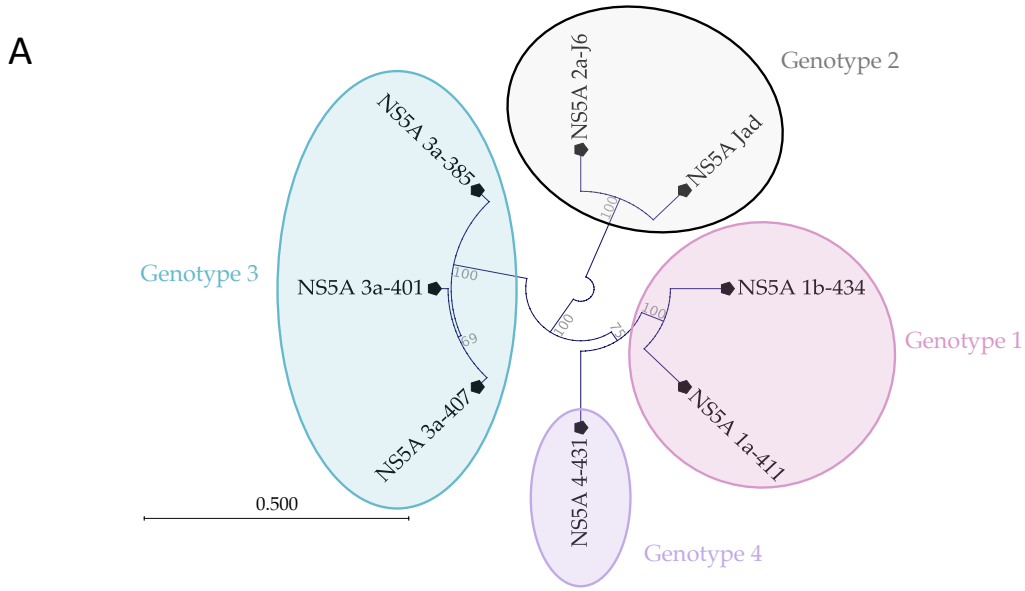

B

		1	2	3	4	5	6	7	8
NS5A Jad	1		56.42	58.74	84.76	55.49	55.49	55.91	57.02
NS5A 1a-411	2	36		80.58	57.47	70.77	70.77	72.09	71.84
NS5A 1b-434	3	37	1		59.16	71.21	70.77	71.21	72.89
NS5A 2a-J6	4	0	36	37		55.70	55.91	56.33	57.87
NS5A 3a-385	5	30	10	11	30		94.03	93.58	65.20
NS5A 3a-401	6	30	10	11	30	0		94.91	66.08
NS5A 3a-407	7	30	10	11	30	0	0		65.86
NS5A 4-431	8	30	10	9	30	12	12	12	

% ID

Gaps

Figure 32: Analysis of the sequence alignment of the NS5A proteins derived from prototypic strains or clinical isolates.
(A) Circular Phylogenetic tree of NS5A sequences of diverse genotypic origins used in this study. The UPGMA tree was constructed using the Jukes-Cantor model to measure protein distance. Resampling from 100 replicates was performed to assess the reliability of clustering. Significant values (>65%) are indicated in light grey. The tree is drawn to scale, the length of the branches being proportional to the average number of aa substitutions per site, as shown by the scale bar. (B) Pair-wise comparisons of NS5A sequences of diverse genotypic origins used in this study, shown by percentage of aa sequence identity (top right comparisons) and by number of gaps between the two compared sequences (bottom left). Low values are shown in shades of blue and high values in shades of red.

IV.B Development of NS5A inter- and intra- genotypic recombinant viruses

IV.B.(α) Virus production and characterization

The strategy of chimeric viruses, rather than transient expression systems, was selected in order to monitor the effects of the proteins in the context of viral infection, to sustain the physiological subcellular localization of NS5A, that might be perturbed in the absence of the other viral proteins, and to avoid triggering irrelevant cellular disturbances by protein overexpression.

The goal of our approach, as described above, was to produce recombinant cDNAs derived from Jad, by substituting the NS5A coding sequence with the sequences corresponding to either other prototypical strains or clinical isolates of other genotypes. Introduction of a heterologous NS5A sequence can have three potential deleterious implications on the viral cycle: (i) a cleavage defect at the intergenotypic hybrid junctions NS4B/NS5A and NS5A/NS5B by the Jad protease NS3/4A, (ii) an impairment of viral RNA genome replication, and/or (iii) an alteration in the synthesis of viral particles. NS5A is indeed part of the HCV replication complex and has to interact with the other viral members of the replicase and with viral RNA, as well as with cellular proteins to be effective in both genome replication and virion morphogenesis. Should these interactions be genotype-specific, they might be disrupted at least to some extent by heterologous NS5A.

Recombinant cDNAs have been constructed and synthetic, genome-length RNAs have been produced, as described in the Materials and Methods section. Following transfection of Huh-7.5 cells with these RNAs, in order to quickly assess whether rescued chimeras would require adaptation, as was the case for some of the recombinant viruses described by Scheel et al.[172], viral protein expression and infectious particle production were first monitored at 72h p.tf.

Infectious particle production was severely impaired in genotype 3 and 4 NS5A recombinant viruses and observably, though not significantly lower, in the subtype 1b NS5A chimera (Figure 33A), while it was at parent-like levels for subtype 1a and 2a chimeras. Jad Core detection, as a common protein to all chimeras, demonstrated decreased levels for genotype 3 and 4 NS5A chimeras and Jad-like levels for genotype 1 and 2a chimeras (Figure 33B). These data are indicative of a probable defect in polyprotein cleavage and/or RNA replication for genotype 3a and 4 recombinant viruses.

Transfected cells from two independent transfections were passaged for 11days and, as shown in Figure 33C, no evolution of viral titers was noted for the genotype 3 and 4 NS5A recombinant viruses, indicating that there was a marked virus replication defect that might be rescued only at later time-points upon genome adaptation. In contrast, the viral titers of the subtype 1a chimera (411) were consistently high over this observation period, as were those of the 1b NS5A chimera (434) in one transfection. In the replicate 434 transfection, titers were initially lower but increased over time, eventually reaching those of 411, suggesting that replication of this virus may be slightly delayed. A validation of this assumption came when the entire ORF of 411 and 434 intracellular RNAs extracted at 14d p.tf. were sequenced and no mutation was found in the genome of both chimeras.

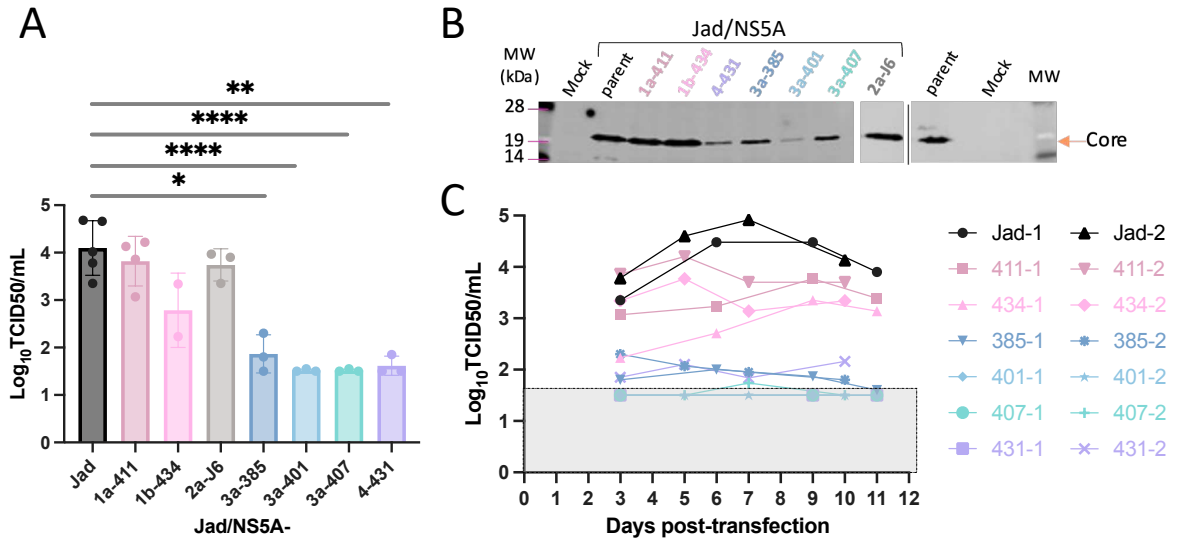

Figure 33: Monitoring of protein expression and infectious titers of intergenotypic NS5A chimeras over the course of transfection.

(A) Mean viral titers (log_{10} TCID50/mL) quantified at 72h p.tf.in transfected cell supernatants from 2-4 independent replicate transfection experiments. Statistical analysis with respect to Jad parent was performed by a t-test with hypothetical value set at the mean of Jad quantified values. Only significantly different data are shown according to: (*)<0.05, (**)<0.01, (****)<0.0001 (B) HCV Core protein expression monitoring at 72h p.tf. using anti-Core monoclonal antibody 1851. Electrophoretic mobilities of proteins with known molecular weights (MW, kDa) is shown at the left. (C) Viral titer evolution (expressed in log_{10}TCID50/mL) in two independent transfection experiments (marked as -1 and -2) over a course of 11 day-observation period. Replicate viruses are represented by the same colour with different symbols to discriminate the two experiments. The grey area covers values below the limit of quantification of the assay, which is indicated by the dotted line.

IV.B.(β) Virus adaptation

Towards adaptation of the NS5A chimeric viruses with significantly reduced infectious virus production, transfected Huh-7.5 cells of the two independent experiments were serially passaged for a period of two months. The viral titer evolution during this period is illustrated in Figure 34. Passaging of subtype 1a and 1b chimeras was stopped when viral titers reached parent-like levels. Passaging of Jad was also interrupted at 14d p.tf. during the first experiment and at 21d p.tf. during the second, since the virus cytopathic effect did not allow us to continue cell splitting at the same pace as chimeras.

We were unsuccessful in adapting the subtype 3a 401 virus, but we did successfully rescue adapted viruses for the other two constructs bearing NS5A sequence of subtype 3a (385 and 407) in one or in both adaptation attempts, as well as for NS5A 434 of genotype 4. As summarized in Table 14, RT-PCR products spanning either the whole ORF or only the NS5A coding region of these viruses, produced from extracted intracellular RNAs as templates were sequenced by Sanger method. In addition, the p7-NS5A coding region was also sequenced using particulate RNAs extracted from corresponding infected cell culture supernatants.

For both genotype 1 NS5A sequences (411 and 434), intracellular RNAs were collected at day 14 p.tf. in the two transfections. No mutation was found over the ORFs, confirming the robust fitness of these 2a/1a and 2a/1b NS5A recombinant viruses.

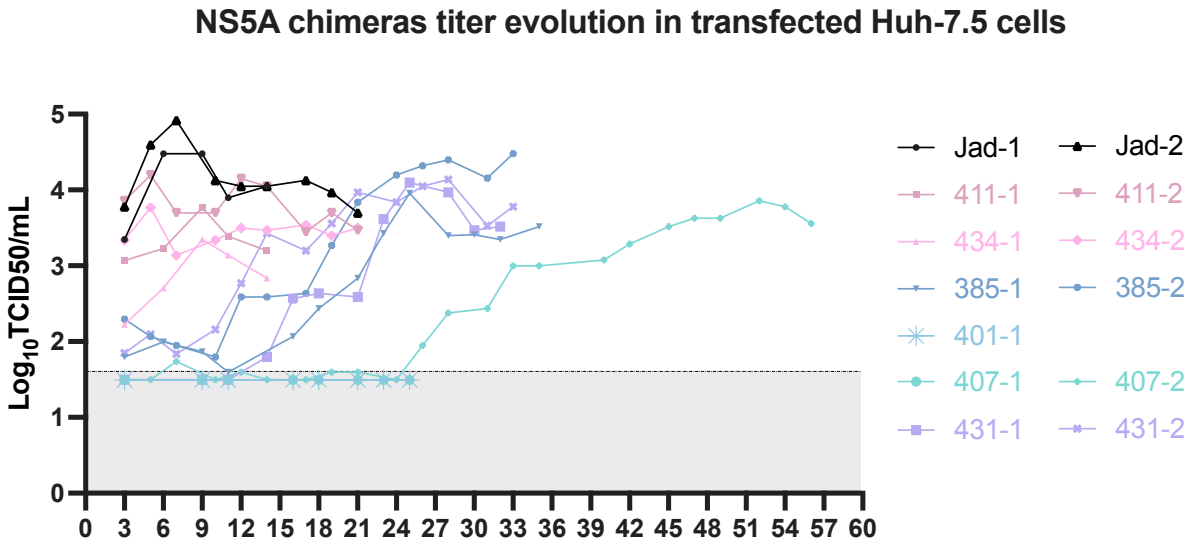

Figure 34: Intergenotypic NS5A chimera adaptation.
Viral titer evolution in two independent transfection experiments (marked as -1 and -2) over a course of 56-day observation period. Titration experiments were performed on fresh cell culture supernatants collected at the indicated times p.tf. Replicate viruses are represented by the same colour and different symbols to discriminate between the two experiments. The grey area covers values below the limit of detection of the assay, which is indicated by the dotted line.

Subtype 3a 385 virus was sequenced at 25d p.tf. in the first transfection and at 19d p.tf. (NS5A) and 33d p.tf. (ORF) in the second transfection. Five fully established or quasi-species, non-synonymous substitutions were identified in attempt 1 and three, in attempt 2. These mutations were found within E2, NS3 and NS4B coding sequences, respectively, in both experiments. One mutation toward a biochemically similar aa (Ile>Leu), but with high occurrence rate was also identified within NS5A of attempt 1. Interestingly, one of the NS3 mutations (G4458A), encoding an arginine to glutamine substitution was present in both adaptation attempts, indicating that this mutation is likely highly significant for the fitness of this virus. Notably, the same mutation was found in the genome of adapted Jad/NS5A-3a-407, which was eventually rescued at a very late time point (56d p.tf.). These findings strongly suggest that the Arg1373Gln substitution within the helicase region of NS3 is likely essential for an optimal crosstalk of Jad NS3 with subtype 3a NS5A to ensure an essential virus life cycle step.

The rescued Jad/NS5A-3a-385 virus also bore a G6050A substitution, encoding an alanine to threonine substitution in NS4B. Similarly, the same NS4B mutation was also found in one of the Jad/NS5A-4-431 rescued virus, with equally high occurrence rate. Furthermore, the presence of another mutation in the same NS4B coding region (G6060A), found in the replicate 385 rescued virus pointed towards the importance of an adaptive mutation within this NS4B region for the efficient adaptation of the genotype 3 and 4 NS5A chimeras.

Subtype 3a 407 virus was rescued after a long delay and only in one attempt. Intriguingly, in addition to the NS3 helicase substitution discussed above and a point substitution in NS4B (C6233T), this virus also harboured a T9120C mutation within NS5B coding sequence. This mutation targeted the Jad NS5B high titer-adaptive mutation. However, instead of reverting the methionine to valine, the original aa found in JFH1, methionine was substituted to threonine.

Lastly, genotype 4 431 virus was sequenced at 16d p.tf. (NS5A) and 32d p.tf. (NS5A & ORF) in attempt 1 and at 19d p.tf. (NS5A & ORF) in attempt 2. Substitutions occurred in NS4B in the two independently rescued viruses, remarkably also including the same G6050A substitution in one virus, as indicated above. One case of each NS5A and E2 quasi-species was also reported.

Table 14: Genome sequence of intergenotypic NS5A chimeric viruses collected at various times p.tf. *The time-points selected were either close to the beginning of viral adaptation or close to the end of passaging when the viral titer was the highest. The coding region sequenced indicated is that from intracellular RNAs. Estimated percentages of mutation occurrence was based on Sanger electropherograms from multiple sequencing reactions. The numbering of nucleotides subjected to mutations corresponds to their position within the genome of each virus. Due to differences in NS5A lengths (see §IV.A), nucleotide positions in NS5A and NS5B coding sequences may vary form one virus to the other. Recurring mutations are in the same font colour (either red or yellow). "-": no mutation found, "NA": not applicable, "Unknown": region not sequenced.*

Virus	Transfection	Days post-transfection	Coding region sequenced	Nucleotide mutation	Amino acid mutation	Targeted protein region	Estimated occurrence in intracellular RNAs	Estimated occurrence in Infectious particles
411	1	14	NS5A	-	-	-	NA	NA
	2	14	ORF	-	-	-	NA	NA
434	1	14	NS5A	-	-	-	NA	NA
	2	14	ORF	-	-	-	NA	NA
385	1	25	NS5A	A6290C	Ile > Leu	NS5A	45%	100%
			ORF	T1572C	Ile > Thr	E2	100%	Unknown
				T3492C	Met > Thr	NS3	100%	70%
				G4458A	Arg > Gln	NS3	100%	100%
				G6060A	Arg > His	NS4B	100%	100%
				A6290C	Ile > Leu	NS5A	45%	100%
	2	19	NS5A	-	-	-	NA	NA
		33	NS5A	-	-	-	NA	NA
			ORF	G1593A	Gly > Asp	E2	45%	Unknown
				G4458A	Arg > Gln	NS3	50%	50%
				G6060A	Ala > Thr	NS4B	80%	80%
407	2	56	NS5A	C7421T	Pro > Ser	NS5A	20%	<10%
			ORF	G4458A	Arg > Gln	NS3	25%	10%
				C5259T	Thr > Ile	NS3	25%	25%
				C6233T	His > Tyr	NS4B	30%	20%
				C7421T	Pro > Ser	NS5A	25%	<10%
				T9120C	Met > Thr	NS5B	35%	-
431	1	16	NS5A	-	-	-	NA	NA
		32	NS5A	G6311A	Val > Ile	NS5A	50%	55%
			ORF	T1581C	Ile > Thr	E2	10%	Unknown
				G6060A	Ala > Thr	NS4B	85%	60%
				G6311A	Val > Ile	NS5A	50%	55%
	2	19	NS5A	-	-	-	NA	NA
			ORF	A6146G	Thr > Ala	NS4B	10%	-
				G6155A	Val > Met	NS4B	10%	30%

Altogether, it was remarkable that mutations were not reliably selected in heterologous NS5A coding sequences, but that rather second-site, recurrent point mutations appeared in Jad NS4B and/or NS3 coding sequences for both genotype 3 and 4 NS5A intergenotypic recombinant viruses. Therefore, one NS4B mutation is likely to confer some level of compensation for the exchange of both genotype 3 and 4 NS5A sequences. In addition, another adaptive mutation in NS3 is likely necessary for genotype 3 NS5A chimeric viruses, and one or more substitutions are possibly needed in E2 for both genotype 3 and 4 NS5A recombinants. In contrast, no adaptive mutation appeared to be required for subtype 1a and 1b NS5A chimeras.

IV.B.(γ) Characterization of adapted viruses obtained by reverse genetic analysis– Genotype 3 and 4 NS5A chimeras

The observed decrease in protein production from genotype 3a and 4 NS5A recombinants suggested impaired replication of these nonadapted intergenotypic chimeras. Some published studies reported compensatory mutations in the NS5A coding sequence in response to mutations introduced into the NS4B sequence, indicating a coordinated role of these two proteins in JFH1 genome replication[224,124]. Therefore, based on these reports and on the well

described role of the NS3 helicase in HCV genome replication, we hypothesised that introduction of the NS3 and NS4B mutations in the genotype 3 recombinant viruses and of the NS4B mutation alone in the genotype 4 chimera would suffice to rescue fully functional viruses. Hence, as a first step, G4458A NS3 codon substitution and G6050A NS4B substitution were introduced in the cDNAs of Jad/NS5A-3a-385, 3a-401, 3a-407, while only G6050A NS4B substitution was introduced in the cDNA of Jad/NS5A-4-431 (summarized in Figure 35). For the 3a-407 chimera, another mutant was generated, in which in addition to the NS3 codon mutation, the C6233T NS4B codon substitution that was uniquely recovered during the adaptation process of this virus was incorporated.

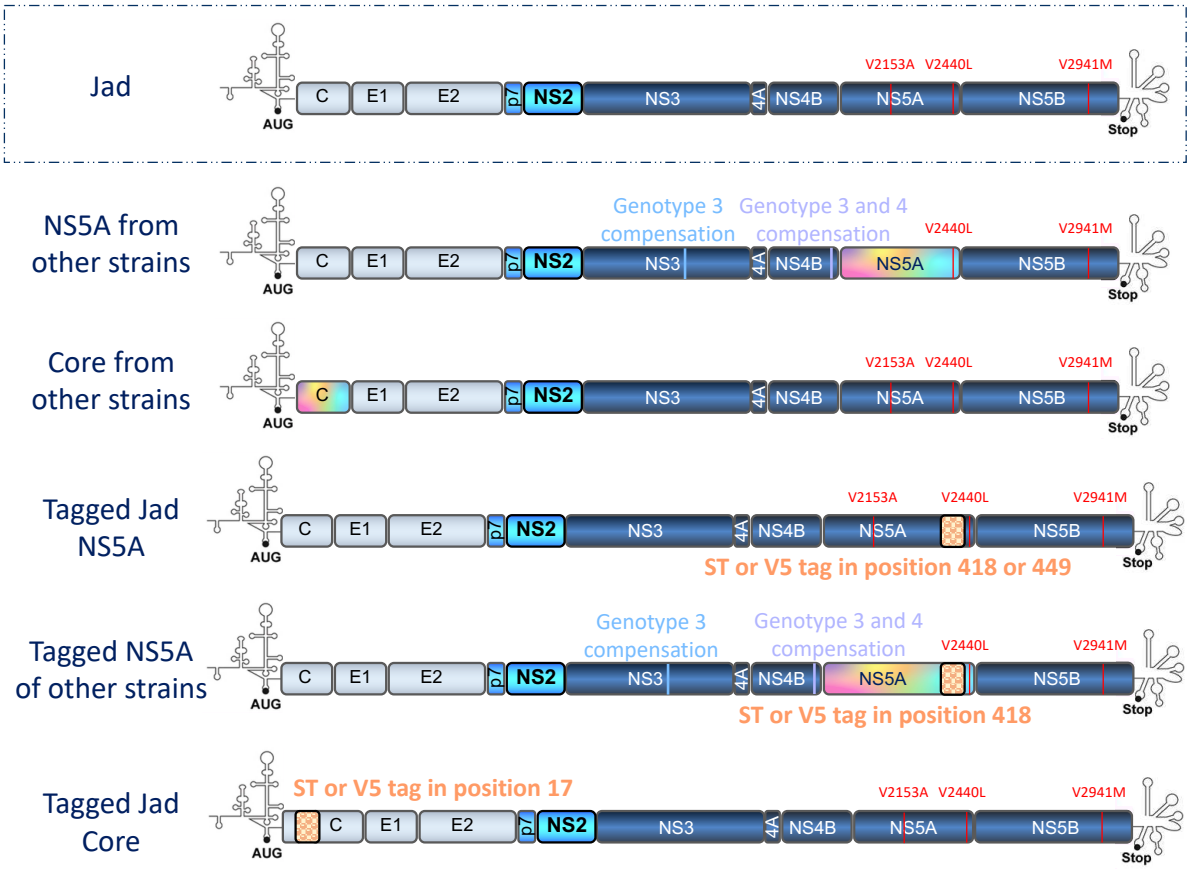

Figure 35: Schematic representation of the NS5A and Core recombinant genomes used in this work. *Core and NS5A sequences of diverse genotypic origins are illustrated in colourful boxes, while Twin-strep (ST) or V5 tags are shown by orange textured rectangles. JFH1 cell culture adaptive mutations are represented by red lines, while compensatory mutations introduced in NS3 and NS4B for the rescue of genotype 3 and 4 NS5A chimeras are represented by blue and purple lines, respectively. The NS4B compensatory mutation finally chosen for adapted virus Jad/NS5A-3a-407 is C6233T, while it is G6050A in the other chimeras (see text).*

Genome replication and infectious virus production were monitored at 96h p.tf. in Huh-7.5 cells electroporated with the genome-length RNA transcripts of the genotype 3 and 4 NS5A recombinants carrying or not engineered putative compensatory mutations in NS3 and NS4B sequences. Three control RNAs were used for comparison purposes: i) Jad parent, ii) Jad/GAA in which the sequence encoding the active site of NS5B polymerase (Gly-Asp-Asp) has been substituted by nonfunctional codons (Gly-Ala-Ala), providing a replication-deficient control, and iii) Jad/ΔEp7 containing an in-frame deletion of E1-E2 envelope glycoprotein and p7 viroporin coding sequences, as an assembly-deficient control.

For RNA replication, intracellular RNAs were extracted and viral RNAs were quantified by RT-(q)PCR, following normalization with respect to quantified ribosomal 18S values (Figure 36A). The quantification of remaining RNA of the input replication-deficient GAA control set the baseline of replication-incompetent RNAs. ΔEp7 quantified log_{10} genome equivalents (GEQ) /µg total RNA were as high as the parent, indicating full genome replication competency. For all four NS5A intergenotypic recombinant viruses in the absence of any compensatory mutation, the quantified viral RNA levels were significantly lower compared to the parent (2.0-2.5 log, one-way ANOVA test; p <0,001), yet reproducibly higher than the replication deficient GAA control, indicating substantially impaired RNA replication. The introduction of the adaptive mutations in NS3 and/or NS4B increased the RNA replication levels to different degrees, with an average of 1.5 log increase in GEQ/µg total RNA that rescued 385, 401 and 431 genome replication to Jad-like levels (one-way ANOVA test; p > 0,05). For both 407 adapted chimeras, the increase in genome replication was more modest (~0.6 log and significantly different from Jad, one-way ANOVA test; p < 0,01), but similar for either NS4B compensatory mutation (one-way ANOVA test; p > 0,05).

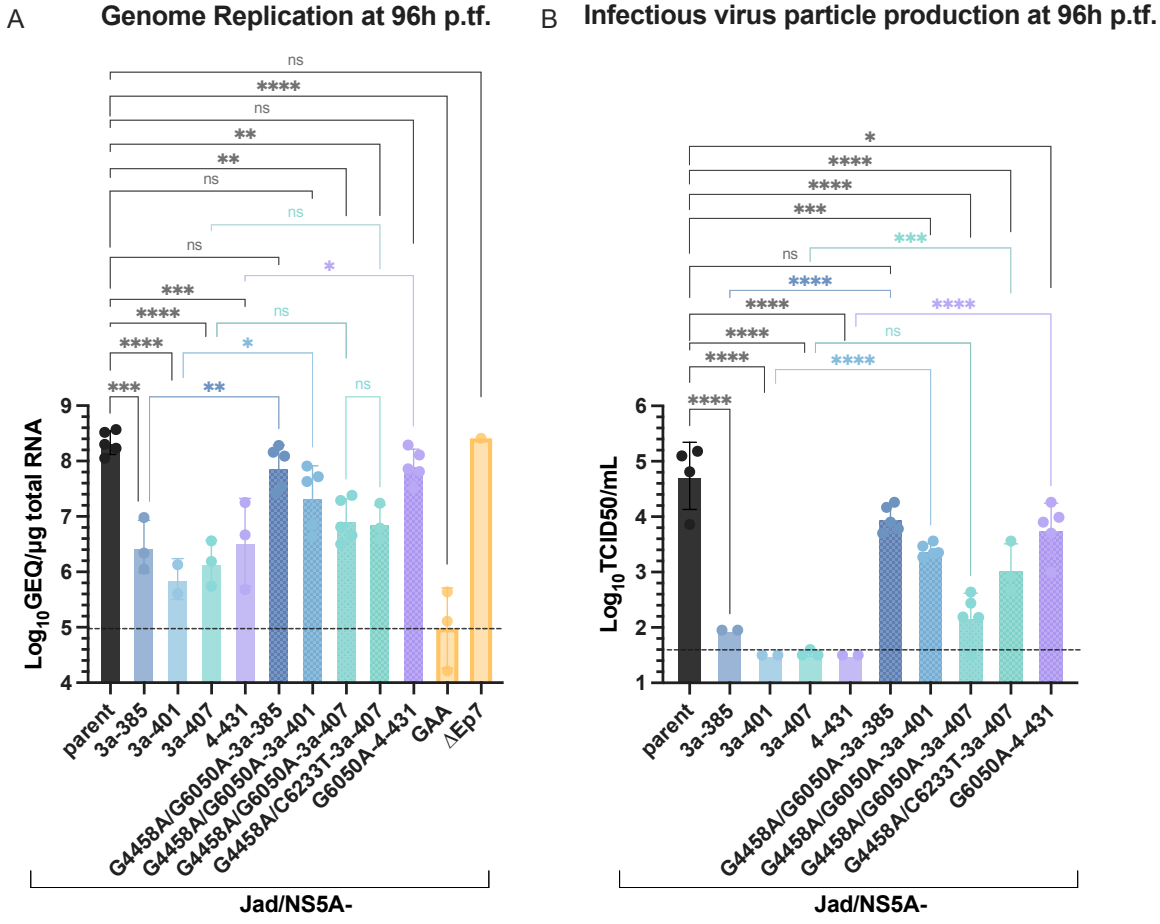

Figure 36: Comparative monitoring of viral genome replication and infectious virion production for NS5A intergenotypic recombinant viruses in the presence and absence of putative compensatory mutations.

Viral RNAs quantified in intracellular RNA extracts from transfected Huh-7.5 at 4d p.tf. are expressed in log_{10} GEQ per µg total RNA (A), while infectious titers are expressed in log_{10}TCID50/mL (B). Cells transfected with genome-length parental RNA, the replication deficient GAA construct, or the assembly deficient ΔEp7 construct served as controls. Asterisks represent p-values obtained following one way ANOVA and correction with the Tukey's multiple comparisons test: p <0,05 (*) ; p <0,01 (**) ; p <0,001 (***) ; p <0,0001 (****) ; p >0,05 (ns : not significant).

We then examined the efficiency of infectious virus production by end-point dilution titration of the respectively collected transfected cell culture supernatants. We found that three out the four genotype 3a and 4 NS5A recombinant viruses produced viral titers below the detection limit of our assay, while the fourth, 385, was significantly impaired in virus production compared to the parent (Figure 36B, one-way ANOVA test; $p < 0{,}001$). Introduction of the compensatory mutations led to the successful rescue of all viruses, with the exception of the 407 intergenotypic recombinant bearing the G6050A mutation. There was a 1 log difference in TCID50/mL viral titers between the Jad/G4458A/G6050A/NS5A-3a-407 and Jad/G4458A/C6233T/NS5A-3a-407 viruses. These data, taken together with their similar RNA replication levels (Figure 35A) support a specific effect of the NS4B C6233T mutation in boosting virion assembly. These findings further point to a role of NS4B in the particle assembly step of the virus life cycle. It should be noted that 385 and 431 were rescued at or close to parent levels, whereas 401 and 407 remain less efficient in virus production. These data indicate that alternative aa changes in NS3, NS4B, and/or in additional genomic regions, as found in selected 407 virus, may be more prone to provide fitness to these 2a/3a chimeras.

IV.B.(δ) Evaluation of recognition of heterologous NS5A proteins from different genotypes by monoclonal antibodies

NS5A expression levels from NS5A intergenotypic recombinants were more tricky to monitor, since most of the commercially available NS5A-pecific antibodies are produced using HCV prototypic strains, such as JFH-1 of subtype 2a or Con1b of subtype 1b, while NS5A sequence is not well conserved across genotypes (see §IV.A).

To find pan-genotypic antibodies, we tested a panel of antibodies against protein lysates collected at 3d.p.tf. from Huh-7.5 cells transfected by the different intra- and intergenotypic chimeras, or by the parent. Detection of the cellular ß-actin served to attest to similar total protein loads, while detection of HCV Core, a shared JFH1 protein showed that all viruses exhibited similar viral protein expression levels (Figure 37).

Anti-NS5A antibodies that did not recognize the majority of the NS5A proteins were all monoclonal antibodies raised in mice against either the JFH1 NS5A, as 7B5 (Biofront Technologies), or against full-length NS5A of unknown genotypic origin, H26 (abcam) and IDVG1127 (kindly gifted by Dr. Eliane Meurs, Institut Pasteur, Paris, France). The only antibody that did recognize the NS5A proteins of all genotypic origins, except for the 2a-J6 strain was the mouse monoclonal 9E10 (IgG2aλ clone) raised in the laboratory of Dr Charles Rice[414] (The Rockefeller University, New York, USA) against a C-terminal epitope of Con1b NS5A protein. This antibody was kindly provided to us by Prof. John McLauchlan (University of Glasgow, Scotland, UK) and also became commercially available by Merck during the second year of my PhD thesis. It should be noted that NS5A of the various virus strains used have different electrophoretic mobilities that are not necessarily in link with the number of aa of the protein.

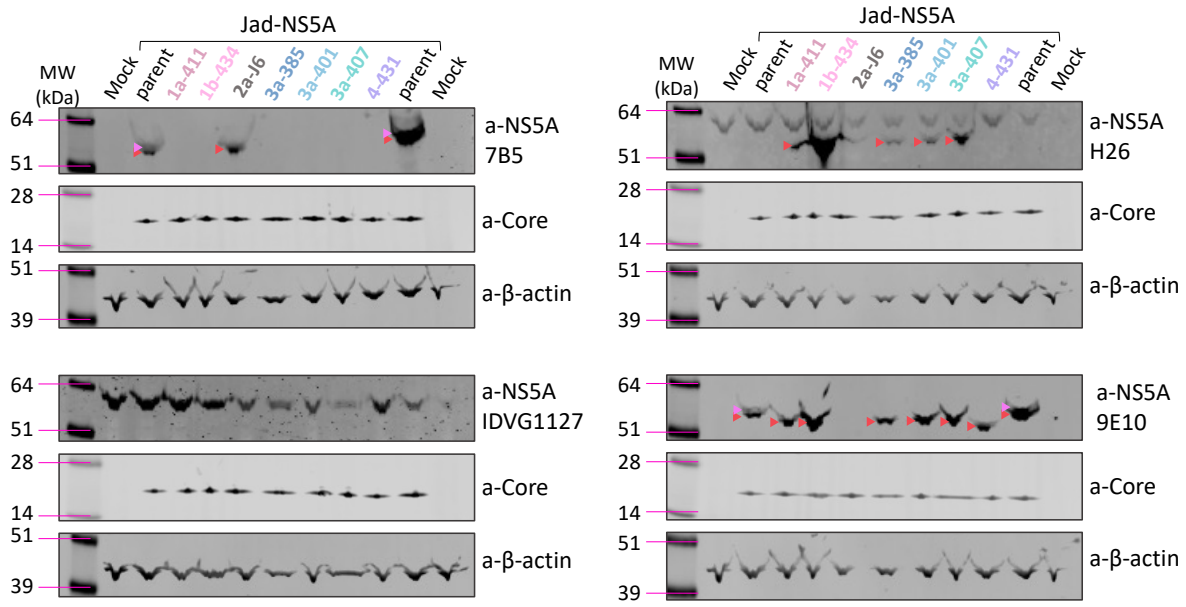

Figure 37: Evaluation of the recognition efficiency of NS5A proteins of diverse genotypic origins by a panel of monoclonal mouse antibodies.

Total proteins extracted at 72h p.i. from Huh-7.5 cells infected with intergenotypic recombinant viruses, the parental strain, or PBS (mock infected) were separated by SDS-PAGE electrophoresis and probed with the antibody indicated at the side of each panel. Genotype 3a and 4 NS5A chimeras used were those bearing compensatory mutations in NS3 and/or NS4B. When detected, NS5A p56 is shown by red arrows and p58 by pink. Detection of viral Core protein and β-actin are shown separately. Markers of molecular masses (kDa) are indicated at the left of the images.

IV.C Development of tagged NS5A recombinant viruses towards protein complex purification

IV.C.(α) Parental Jad protein tagging

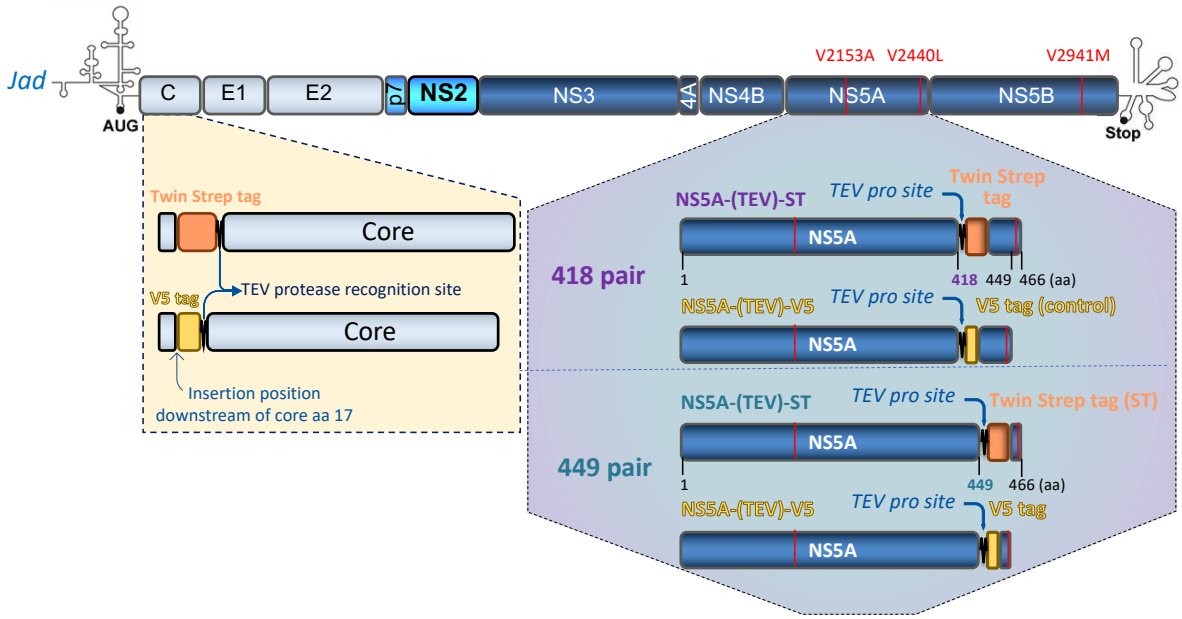

For space economy , Core and NS5A tagged viruses are illustrated below a single backbone.

Figure 38: Schematic representation of Jad encoding tagged Core or NS5A.
The Jad genome with the 3 structural and 7 nonstructural proteins is illustrated at the top. The three Jad adaptive mutations are represented by red bars, twin-strep tag insertions are illustrated in orange boxes and V5 tag, in yellow. Tobacco Etch Virus (TEV) protease recognition peptide inserted C-terminally from the tag in Core and N-terminally from the tag in NS5A chimeras is illustrated by a black broken line.

IV.C.α.(i) Jad NS5A

Towards affinity purification of Jad NS5A protein complexes and identification of NS5A interacting partners in infected cells, a twin strep-tag (ST) or a control V5 tag was fused in frame with the protein downstream of aa 418 or aa 449 within the Jad backbone (Figure 38).

NS5A insertion position 418 has previously been described in the context of a replicon Con1b system[518] and has previously been exploited by our laboratory for the insertion of a fluorescent protein gene (mCherry) within the 2a-Jad genome-length cDNA. This was found to substantially impair infectious viral production (reduction of >2.0 log TCID50/mL titers with respect to Jad parent) and lead to virus genomic instability resulting in large in-frame deletions of the mCherry gene as well as NS5A DIII sequences upon virus passage (Kotanidou et al., unpublished data).

NS5A insertion position 449 appeared as relatively tolerant to insertions from a study monitoring the effect on Jc1 replication and infectivity of random, transposon-driven 15nt-insertions throughout the genome[584]. Our aim was to insert the purification tag at the most C-terminal point within NS5A without preventing NS5A/NS5B cleavage and such as to avoid the disruption of any NS5A/cellular factor interaction, keeping in mind that the important interaction with CypA, for example, involves the C-terminus of NS5A DIII[586]. In that respect, insertion position 449 was downstream of the most C-terminal Pro residue affected by CypA and still reasonably distant from the NS5A/NS5B cleavage site to expect no polyprotein cleavage defect. Of note, previous works from the laboratory have explored the possibility to

insert small tags 2 to 5 aa upstream of the NS5A/ NS5B cleavage site. However, this resulted in drastic impairment of viral RNA infectivity (Aicher et al., unpublished data).

In addition to the ST or V5 tag itself, a 7-aa coding sequence was inserted upstream, corresponding to the recognition site of tobacco etch virus (TEV) protease for intended purification purposes. The (TEV)-ST and (TEV)-V5 sequences were framed by Ser-Gly and Ser-Gly-Gly, Ser-Gly-Ser or Gly-Gly flexible hinges at their N- and C-termini, respectively, that were either additionally inserted or present in the authentic NS5A sequence.

IV.C.α.(ii) Jad Core

Towards affinity purification of Jad Core protein complexes and identification of Core interacting partners in infected cells, a twin strep-tag (ST) or a control V5 tag were fused in frame near the N-terminus of the protein, downstream of aa 17 within the Jad backbone (Figure 38, also see Figure 35, page - 93 -). Additional TEV protease recognition site sequence and flexible linkers were also inserted, as described for Jad NS5A. Different insertion positions were previously examined in our laboratory, based on the random, transposon-driven 15nt-insertion data of Remenyi et al.[584] or previously reported to bear very short tetracystein tag insertion (Coller et al., 2012[583]; Counihan et al., 2011[582]). Namely, positions downstream of codons 2, 3, 8, or 15 have been investigated in the presence or absence of the TEV protease recognition site. However, these attempts were found to affect profoundly (positions 2, 3, 8) or significantly (position 15) HCV infectious particle production and/or distort Core subcellular localization and association with the LDs (unpublished group data).

IV.C.(β) Tagging of intra- and inter-genotypic NS5A chimeras

Alignment of the NS5A protein sequences of the clinical isolates, J6 and Jad revealed high conservation of the residues in and around the Jad 418 position across samples and the absence of the residues in and around the Jad 449 position in non-genotype 2a samples (see Figure 31, page - 87 -). Therefore, towards affinity purification of protein complexed with NS5A of diverse genotypic origins from infected cells, the corresponding Jad position 418 was used for the insertion of the TEV protease recognition site, followed by a ST or control V5 tag, framed by Ser-Gly and Ser-Gly-Gly, Ser-Gly-Ser or Gly-Gly flexible linkers (Figure 35, page - 93 -).

In order to minimize the number of replicate samples required for the AP-MS/MS, only one V5 control was produced in the 1a-411 intergenotypic recombinant Jad backbone and used for further experiments.

IV.D Characterization of recombinant viruses expressing Core or NS5A in fusion or not with ST/V5 tags

IV.D.(α) Jad viruses encoding tagged Core

Both tagged Core Jad and intra-/inter-genotypic Core recombinant viruses were previously developed and characterized in the group by combined efforts of Stephanie Aicher, Brigitte Blumen, Emeline Simon and Houda Tabbal.

Briefly, chimeras expressing Core sequences of diverse genotypic origins were used to infect Huh-7.5 cells at an MOI of 3 TCID50/mL and viral genome replication, particle assembly and infectious virion production were monitored by quantification of intracellular viral RNA and extracellular viral RNA by RT-(q)PCR and infectious viral titers by endpoint dilution assays. Interestingly, all chimeras were found to grow according to similar kinetics, with no requirement for compensatory mutations, allowing their use in comparative transcriptomic studies (Simon, PhD manuscript, Supplementary Figure 2).

Jad/C17-ST and Jad/C17-V5 Core protein expression was monitored at 72h p.tf. in protein extract collected from cells transfected with the respective genome-length RNAs and compared to parental Jad Core expression. Fusion proteins C17-ST and C17-V5 were detected with apparent electrophoretic mobilities consistent with their increasing molecular masses due to inserted sequences, the TEV-V5 and TEV-ST insertions introducing 24 and 39 additional aa in Core, respectively (Figure 39A). Insertion of the tag was found to only minimally decrease infectious virus particle production (by ≤ 0.5 log units), but consistently for both tags (Figure 39B), allowing the use of these tagged viruses in comparative interactomic studies.

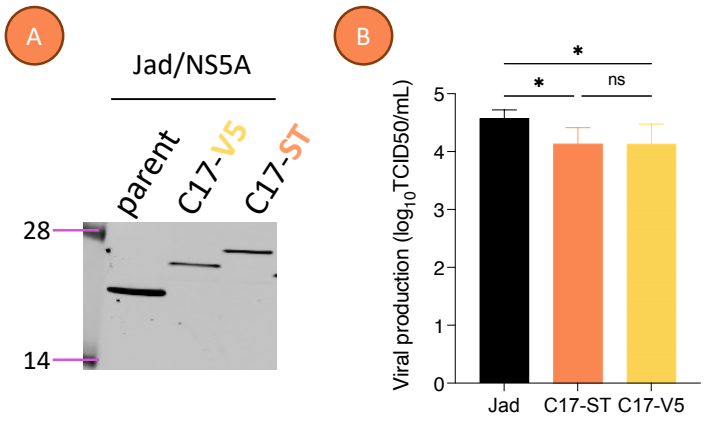

Figure 39: ST/V5-Corefusion protein expression and viral titers monitored in cells transfected with genome-length Jad/C17-V5, /C17-ST or Jad RNAs.
(A) Core protein expression monitored in transfected cell lysates collected at 72h p.tf. using monoclonal anti-Core 1851 antibody (B) Viral production measured in the supernatant of transfected cells at 72h p.tf. Asterisks represent p-values obtained following one way ANOVA and correction with the Tukey's multiple comparisons test: p <0,05 (*); ns : not significant.

IV.D.(β) Fusion of ST/V5 tags to Jad NS5A does not affect virus production or subcellular NS5A localization

NS5A is released from viral polyprotein by NS3/4A protease-mediated cleavage, according to HCV polyprotein maturation scheme. The tag insertion in the C-terminal part of NS5A could potentially alter the folding of the protein, hence its stability and /or interfere with proteolytic cleavage at the NS5A/NS5B junction. To address these questions, expression levels of tagged NS5A and cleavage from polyprotein were monitored for all recombinant RNAs.

Toward this end, Huh-7.5 cells were electroporated with *in vitro* transcribed recombinant Jad/NS5A-tagged RNAs or with H_2O as a negative control (Mock). Protein extracts were prepared from transfected cells at 72h p.tf. and probed for expression of NS5A with mouse anti-NS5A monoclonal antibody 7B5. An example of the images obtained from replicate transfections is shown in Figure 40.

Jad NS5A is detected as a doublet of products, corresponding to basally and hyper-phosphorylated NS5A forms. Similarly, all NS5A-V5, NS5A-ST (with insertions at either 418 or 449 position) were detected under these two phosphorylation forms and with apparent electrophoretic mobilities consistent with their increased molecular masses following insertion lengths (Figure 40A). Consistent results were also obtained when a mixture of anti-ST and anti-V5 monoclonal antibodies was used to probe NS5A-(TEV)-V5 and NS5A-(TEV)-ST tagged proteins (data not shown). Detection of β-actin to roughly similar levels in all samples indicated similar total protein loading across samples.

In order to monitor the genetic stability of Jad/NS5A-(TEV)-ST and NS5A-(TEV)-V5 viruses, transfected cells were serially passaged every 3-4d for 14d p.tf. At each passage, transfected cell supernatants were collected and viral infectivity was monitored by endpoint dilution virus titration. Jad parent was used as a control in parallel. Infectious titers of all NS5A tagged recombinants were consistently high and Jad parent-like over the observation period (Figure 40B). The experiment was stopped at 14d p.tf. due to the high cytopathic effect induced by these viruses.

Viruses were amplified to generate high amounts of viral stocks dedicated to the infection of Huh-7.5 cells toward AP/MS-MS experiments. Titers of viral stocks were not significantly different from those of the parental virus (Figure 40C), and the NS5A-tagged nucleotide sequences were shown to be identical to the engineered sequences.

Since the Jad/NS5A-(TEV)-ST viruses were meant to be used to seek host interacting partners of NS5A in infected cells using a high-throughput mass spectrometry analysis, we also verified that the fusion with ST did not alter subcellular localization of NS5A during Jad life cycle. In addition, we undertook to comparatively investigate subcellular localization of NS5A-ST/V5 and Jad NS5A with respect to ER and LDs. Representative figures from experiments performed with Jad virus bearing ST insertion at position 449, along with the V5-449 virus and Jad parent are shown in Figure 41 (For NS5A-(TEV)-ST-418 related data, please see Figure 44, page - 109 -).

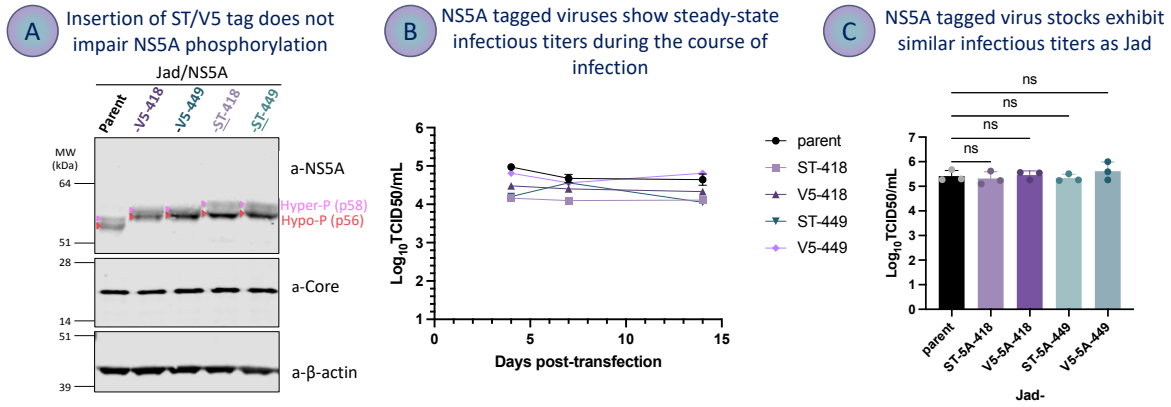

Figure 40: Characterization of Jad/NS5A-tagged recombinant viruses.
(A) Comparative analysis of tagged NS5A expression levels. Protein extracts were prepared from Huh-7.5 cells transfected with the indicated RNAs and probed for HCV NS5A (upper panel), HCV Core (middle panel) and β-actin (lower panel). Protein molecular weight markers (MW) are shown at the left of the images. Red and magenta arrows pinpoint basally and hyper-phosphorylated NS5A, respectively. (B) Evolution of infectious viral titers over time post-transfection. Supernatants were collected from cells transfected with parental RNA Jad or with the indicated recombinant RNAs over the indicated days p.tf., then titrated by endpoint dilution assay. (C) Comparison of viral stock titers obtained for parental virus and tagged-NS5A chimeras.

Huh-7.5 cells seeded in Ibidi slide channels were infected at the highest MOI achievable with respect to viral stock titers, given that our purpose was to analyze single infected cells. Jad was used at an MOI of 0.2 TCID50/cell, while Jad/NS5A-(TEV)-ST-449 and -V5-449 were used at an MOI of 0.07 TCID50/cell. Cells incubated with complete medium served as noninfected controls. Infected cells were fixed at 96h p.i. and processed for indirect immunolabeling using a mixture of three primary antibodies: a mouse anti-JFH1 NS5A monoclonal antibody, rabbit anti-calnexin (CALX) polyclonal antibodies to label ER, and sheep anti-ADRP polyclonal antibodies to label LDs. Following incubation with appropriate anti-species Ig conjugates, then DAPI to label cell nuclei and mounting in a nonpolymerizing medium, cells were observed by confocal microscopy. NS5A labelling was revealed with the 488 channel (green), CALX with the 555 channel (red) and ADRP with the 647 channel (white).

NS5A of the two recombinant viruses, as well as Jad NS5A presented similar patterns, either a cytoplasmic localization in a large peri-nuclear region or a localization in dot- or ring-like structures (green arrows, Figure 41, left images). From these images, it was difficult to conclude whether the first was exclusively reticulate and coincides with ER labelling. Interestingly, the dot- or ring-like pattern of NS5A was found to coincide, at least in part, with

ADRP labelling of LDs (overlapping green arrows and grey arrowheads in merged images). Of note, dot/ring-like labelling of LDs with anti-ADRP was easier to visualize in noninfected cells (Mock and "NI" cells) than in infected cells, a feature that has already been reported by us and others. Altogether, these observations indicate that neither ST nor V5 tag alters Jad NS5A intracellular localization during the viral life cycle.

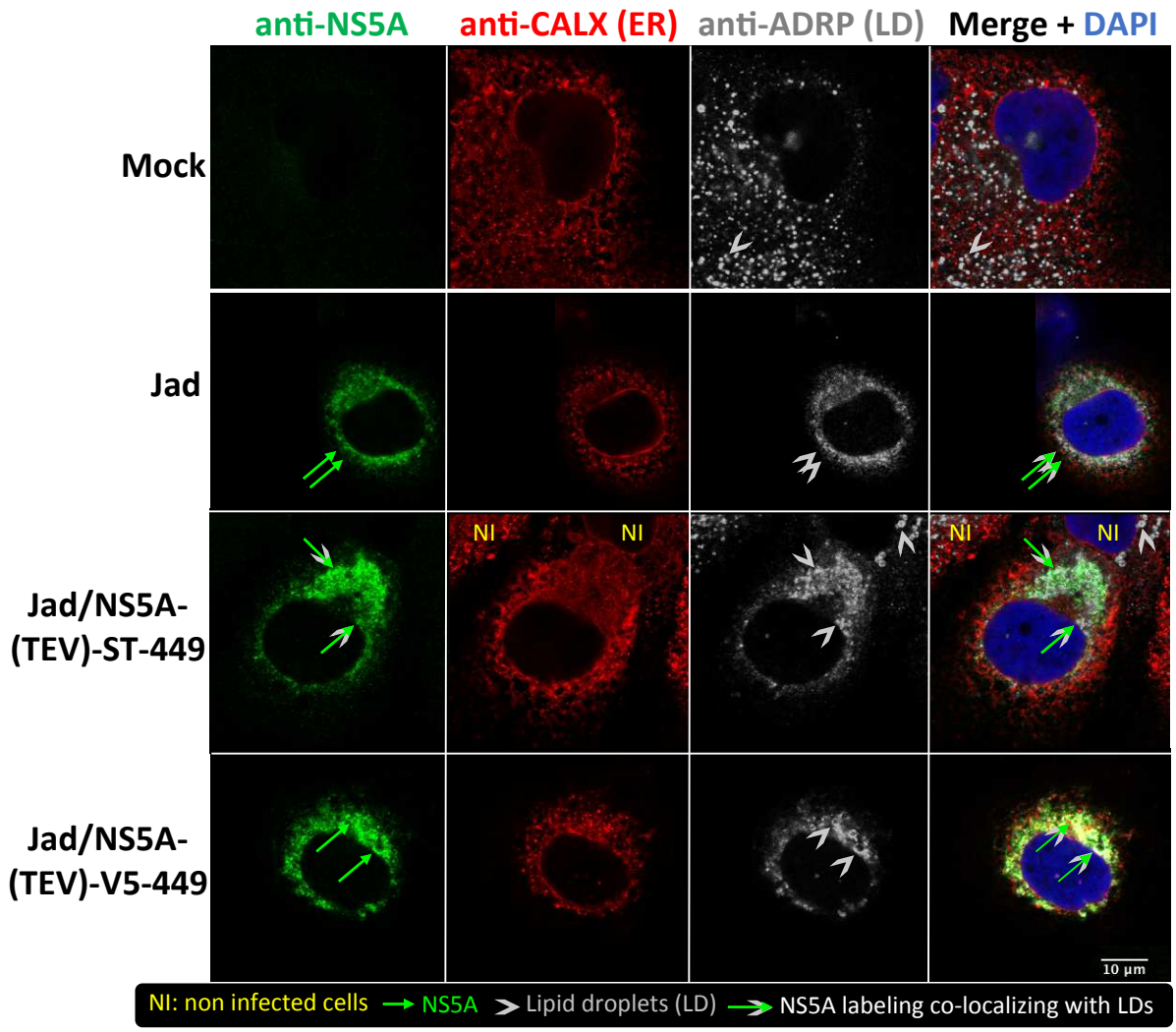

Figure 41: Subcellular localization of NS5A-(TEV)-ST-449, NS5A-(TEV)-V5-449 and parental NS5A with respect to LDs and ER.
Huh-7.5 infected with the indicated viruses and noninfected cells were probed for expression of proteins indicated on top of each column and color-coded according to the channel used. Merged images with additional DAPI staining are shown at the right. Images were acquired on a confocal microscope using a 63X objective. The scale bar indicates 10µm.

IV.D.(γ) Comparative characterization of all chimeric viruses encoding NS5A from different genotypes

IV.D.γ.(i) Monitoring of viral replication and protein expression

Comparative monitoring of virus genome replication and infectious virus production of all NS5A intra-/inter-genotypic recombinant viruses described thus far was performed by quantification of intracellular viral RNAs and infectious titers in supernatants collected at 72h

p. tf. from Huh-7.5 cells transfected with the respective genome-length RNAs. Cells transfected with genome-length parental RNA, the replication deficient GAA construct, or the assembly deficient ΔEp7 construct served as controls.

As illustrated by the solid filled bars in Figure 42, exchange for cognate proteins of genotypes 1 and 2a did not affect viral RNA replication nor infectious virion production compared to the parental virus (one-way ANOVA test; $p > 0,05$). With genotype 3a and 4 NS5A, viral genome replication and infectious virus production was rescued by the insertion of compensatory mutations in NS3 and NS4B proteins, with the exception of the 3a-407 virus carrying G6050A substitution in NS4B, as already described above (IV.B.(γ)).

Interestingly, insertion of ST or V5 tag within the backbone of viruses bearing NS5A of genotypes 1, 2 or 4 did not significantly affect genome replication capacity compared to Jad nor to corresponding chimeras encoding untagged NS5A (Figure 42A). Infectious titers of these tagged NS5A recombinants were also not significantly different from the titers of their respective untagged counterparts (Figure 42B). In genotype 3 NS5A chimeras, insertion of the ST tag significantly affected both RNA replication and infectious virus production only in the case of 385 NS5A ($p < 0.0001$), while assembly of infectious particles was also impacted in the Jad/G4458A/C6233T/NS5A-3a-407 virus ($p = 0.0025$). Presence of the inserted tag sequences were verified in intracellular viral RNAs in all cases.

Altogether, among the eight intra- or inter-genotypic recombinant viruses encoding tagged NS5A, only two viruses (385-ST and 407-ST) were significantly affected in infectious particle production, although most of them were not as efficiently replicating as the Jad parent.

These data were further supported by the monitoring of HCV Core and NS5A expression in infected cell lysates collected at 72h p.tf., as shown in Figure 43. For the labelling of NS5A, two different monoclonal antibodies were used, 9E10 recognizing the majority of NS5A homologues and 7B5, recognizing (at least to some extent) the J6 derived NS5A.

Unfortunately, insertion of the tag disrupted the recognition of NS5A by the 9E10 antibody in all cases, except for NS5A of genotype 1b (data not shown), as the epitope recognized spans aa 414–428[587]. Hence, for the monitoring of tagged protein expression, we relied on anti-ST and anti-V5 antibodies (Figure 43). As a consequence, comparative observations across all viruses can only be made with respect to the expression of Core protein, which is common to all viruses and for which the same antibody was used.

In aggregate, viral protein expression was as high as with the parental Jad in all intra- and inter-genotypic chimeras, with or without a tag insertion, provided that the identified compensatory adaptive mutations were introduced into the backbone of 3a and 4 chimeras.

Furthermore, the hyperphosphorylated form of NS5A was evident as an additional band of higher molecular weight only in the genotype 2a samples, Jad and J6. Of note, 7B5 affinity for J6 NS5A appeared considerably reduced compared to 9E10 affinity for Jad (compare relative Core and NS5A intensities), hence preventing from visualizing p58 band in the 2a-J6 chimera. Over-exposure of the same membrane actually revealed a second product of slightly higher molecular weight in the 2a-J6 lane (data not shown). Hyperphosphorylation of genotype 1 NS5A proteins has previously been reported[148,138], while there is a paucity of information regarding the phosphorylation status of NS5A of genotypic origins other than genotype 2. Hence, the absence of a visible second NS5A-reactive product that may represent the hyper-phosphorylated form of genotype 1, 3a, 4 NS5A could either be attributed to closer electrophoretic mobilities of the two forms of non-genotype 2 NS5A that were not resolved in these gel conditions, to technique limitations or to the actual absence of the hyper-phosphorylated form in some or all instances.

High volume stocks were produced for untagged viruses, which had titers in the range of 4.1-5.3 $\log_{10}$TCID50/mL. The genomic sequence of chimeric viruses thus amplified was found to be as expected over the ORF by Sanger sequencing, supporting their genetic stability.

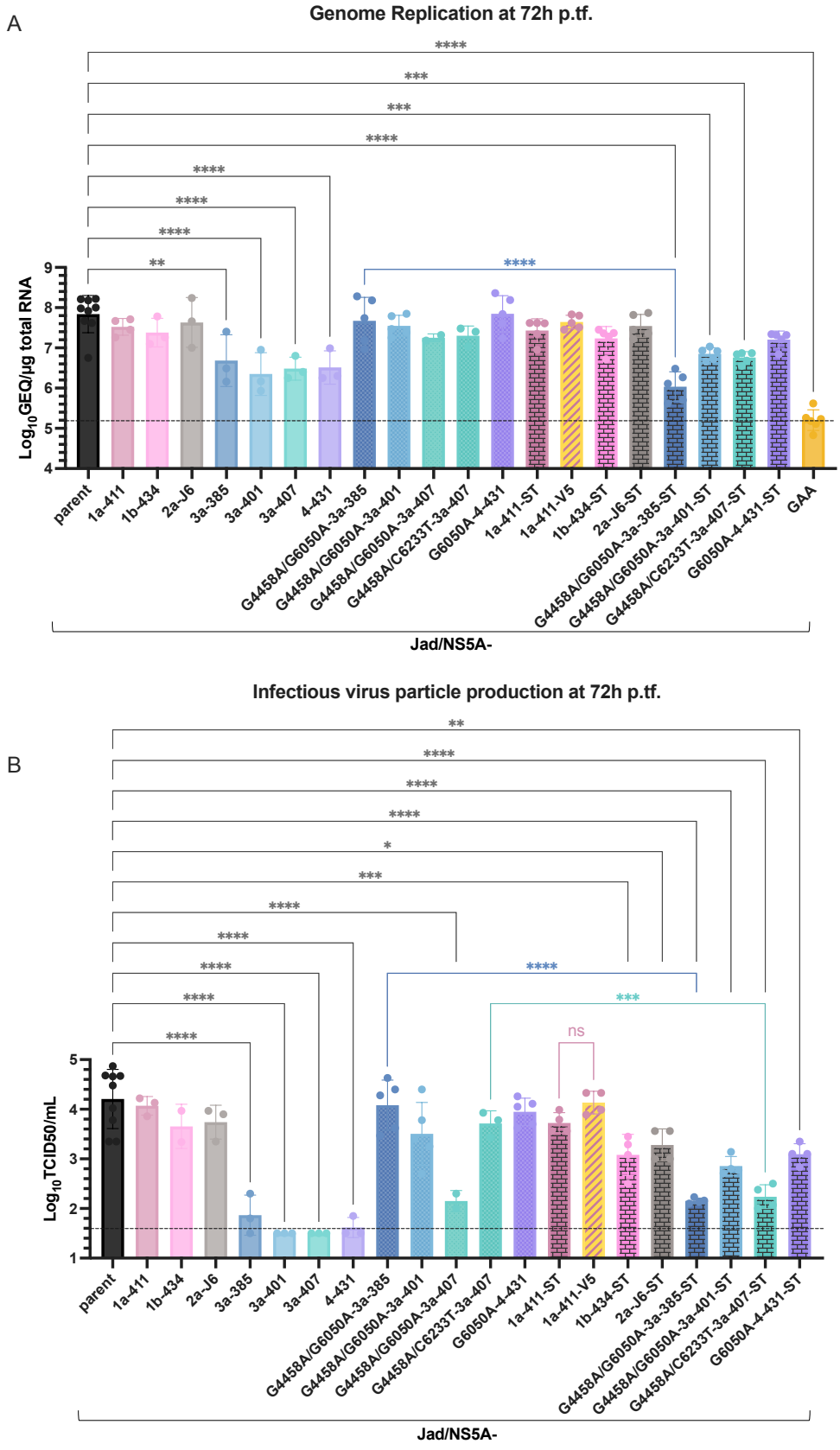

Figure 42: Comparative monitoring of viral genome replication and infectious virion production of all NS5A recombinant viruses developed in this study.

Viral RNAs quantified at 72h p.tf. in intracellular RNA extracts from transfected Huh-7.5 are expressed in log_{10} genome equivalents per µg total RNA (A), while infectious titers measured by virus end-point

dilution assays in the respectively collected culture supernatants are expressed in log_{10}TCID50/mL. Cells transfected with genome-length parental RNA, the replication deficient GAA construct, or the assembly deficient ΔEp7 construct served as controls. Asterisks represent p-values obtained following one way ANOVA and correction with the Tukey's multiple comparisons test: p <0,05 (*); p <0,01 (**); p <0,001 (***); p <0,0001 (****); p >0,05. For space economy nonsignificant (ns) comparisons with the parent or between the non-tagged and the tagged chimeras are not illustrated.

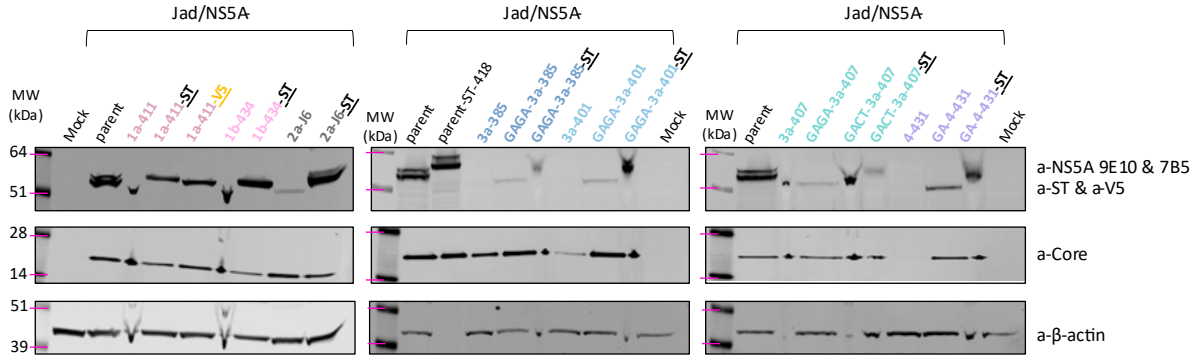

Figure 43: Comparative characterization of protein expression of all NS5A recombinant viruses developed in this study.

A comparative analysis of NS5A expression levels was performed in protein extracts prepared from Huh-7.5 cells transfected with the indicated RNAs and probed with HCV NS5A, ST and V5 (upper panel), HCV Core (middle panel) and β-actin (lower panel) -specific antibodies. The migration of protein molecular weight markers (MW) is indicated on the left of the images. GAGA: G4458A/G6050A mutations, GA: G6050A mutation, GACT: G4458A/C6233T mutations.

I.A.α (i) Monitoring of subcellular NS5A localization

NS5A subcellular localization was studied following infection of Huh-7.5 cells seeded in Ibidi slide channels with intra- and inter-genotypic recombinant viruses at an MOI of 1 TCID50/cell (Figure 44, - 109 -). For tagged NS5A-encoding viruses, cells electroporated with *in vitro* transcribed genome-length RNAs were seeded in Ibidi slides. Cells incubated with complete medium ("Mock-infected") or transfected with H_2O served as noninfected controls. Infected cells were fixed at 120h p.i./p.tf. and processed for indirect immunolabeling using a mixture of two primary antibodies: either the mouse 9E10 anti-NS5A monoclonal antibody or anti-tag mouse monoclonal antibodies, and rabbit anti-CALX polyclonal antibodies to label ER. LDs were labelled metabolically with the use of a fatty acid analogue, the 4,4-difluoro-4-bora-3a,4a-diaza-s-indacene or BODIPY. Following incubation with appropriate anti-species Ig conjugates, then DAPI to label cell nuclei and mounting in a nonpolymerizing medium, cells were observed by confocal microscopy. NS5A labelling was revealed with the 488 channel (green), BODIPY with the 555 channel (red) and CALX with the 647 channel (magenta). J6 NS5A intragenotypic recombinant virus is not shown, since none of the NS5A-specific antibodies available recognized 2a-J6 NS5A in its native conformation, but J6-NS5A-ST is shown with anti-ST labelling.

LD staining with BODIPY was clearer than the anti-ADRP staining described previously, allowing us to identify the LDs in the form of solid and clear spheres. We have previously shown that HCV infection leads to a redistribution and progressive strong clustering of LDs, as attested by the increase in LD observed average size and simultaneous decrease in number. We have identified HCV Core as the driver of this LD association. The LD distance observed at 120h p.i. by confocal microscopy is below the threshold of the microscope's resolution, leading us to believe that Core might even drive fusion of LDs over the course of Jad infection (Simon et al., manuscript in preparation).

Here, we also observed clustered LDs, polarized preferentially around the nuclei in most cells infected at a late stage (denoted by red arrows with a yellow frame, for a few examples), while in cells that are at an earlier stage of infection or that are not infected, LDs are spread evenly over the cytoplasm.

The NS5A proteins of intergenotypic viruses and Jad NS5A exhibited relatively similar intracellular distributions, which are in all cases not homogenous from one cell to another within the infected cell monolayers. Either a reticulate localization throughout the cytoplasm, with variable amounts of intense dots of diverse sizes (blue frames, as examples), or a localization in the form of larger "aggregates" or "clusters" (yellow frames) was observed. The reticulate pattern mainly coincided with the labelling of the ER, while the more clustered pattern overlapped with or was found adjacent to the LD labelling (yellow signal or apposed green/red signals in the merged channel images). However, this is not equally straightforward in all images, due to a potential differential affinity of the 9E10 anti-NS5A antibody for the different NS5A homologues. In addition, technical issues stemmed from different volumes of the cells and single Z-stack acquisitions, leading to potentially different signal intensities for each labelled object (nucleus, ER, LD and viral protein).

Altogether, we can conclude that for all intergenotypic viruses, two distinct NS5A intracellular distribution profiles can be visualized within the same cell monolayer, with proportions possibly varying from one virus to another. The different NS5A patterns may suggest that cells do not host the virus at the same stage of the infectious cycle. With NS5A undergoing translation (reticular distribution) or involved at the stage of genomic replication (punctiform distribution), the cell would present an earlier stage of the viral cycle. NS5A aggregation could reflect the viral particle assembly stage during which viral proteins accumulate in the cytoplasm of the infected cell and NS5A tends to interact with the LDs.

Importantly, NS5A-1b-434-ST protein was efficiently detected by both anti-NS5A 9E10 and anti-ST antibodies. Both reticulate and LD-associated patterns were also observed with the two antibodies in cells infected with Jad/NS5A-1b-434-ST, indicating that the ST labelling can substitute for 9E10 labeling for tagged viruses. This observation also held true for parental Jad-NS5A-(TEV)-ST (data not shown).

For all tagged recombinant viruses, as for their untagged counterparts, both reticulate-like and clustered NS5A was observed, in association with the ER or the LDs, respectively, allowing us to conclude that the insertion of the ST or the V5 tag did not alter NS5A subcellular localization. Therefore, these tools were employed for the investigation of NS5A-host PPIs.

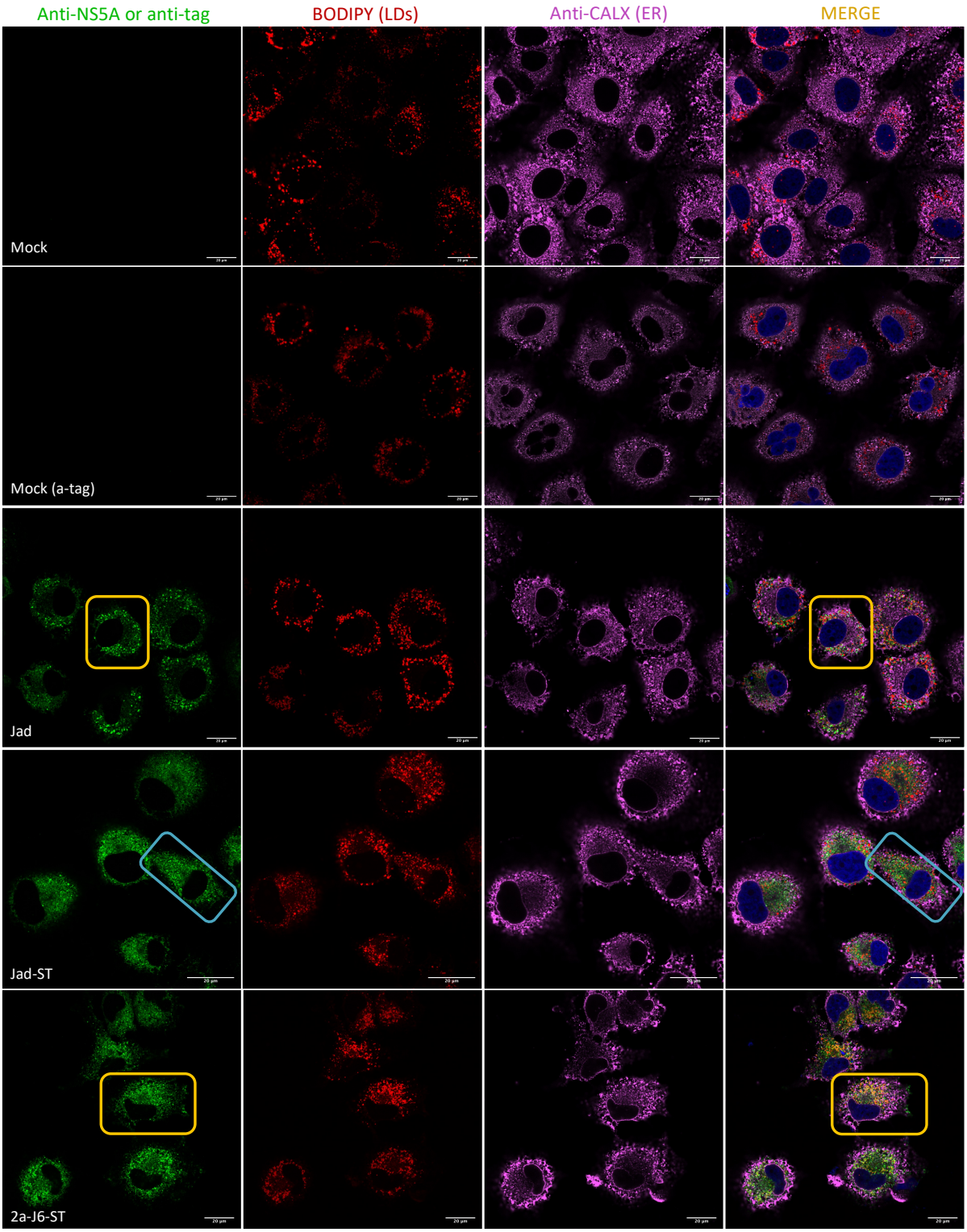
Anti-NS5A or anti-tag
BODIPY (LDs)
Anti-CALX (ER)
MERGE
Mock
Mock (a-tag)
Jad
Jad-ST
2a-J6-ST

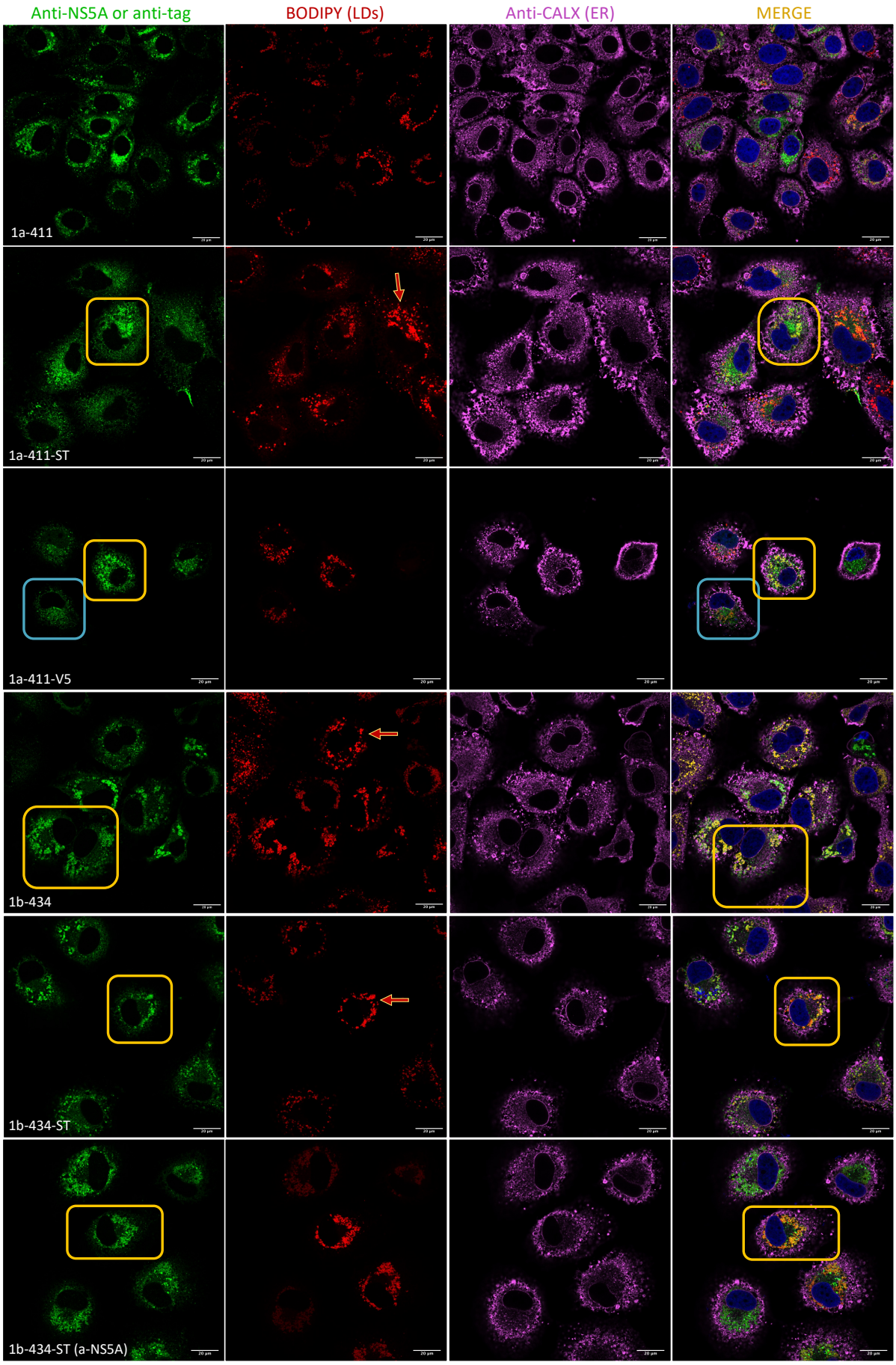
Anti-NS5A or anti-tag
BODIPY (LDs)
Anti-CALX (ER)
MERGE
1a-411
1a-411-ST
1a-411-V5
1b-434
1b-434-ST
1b-434-ST (a-NS5A)

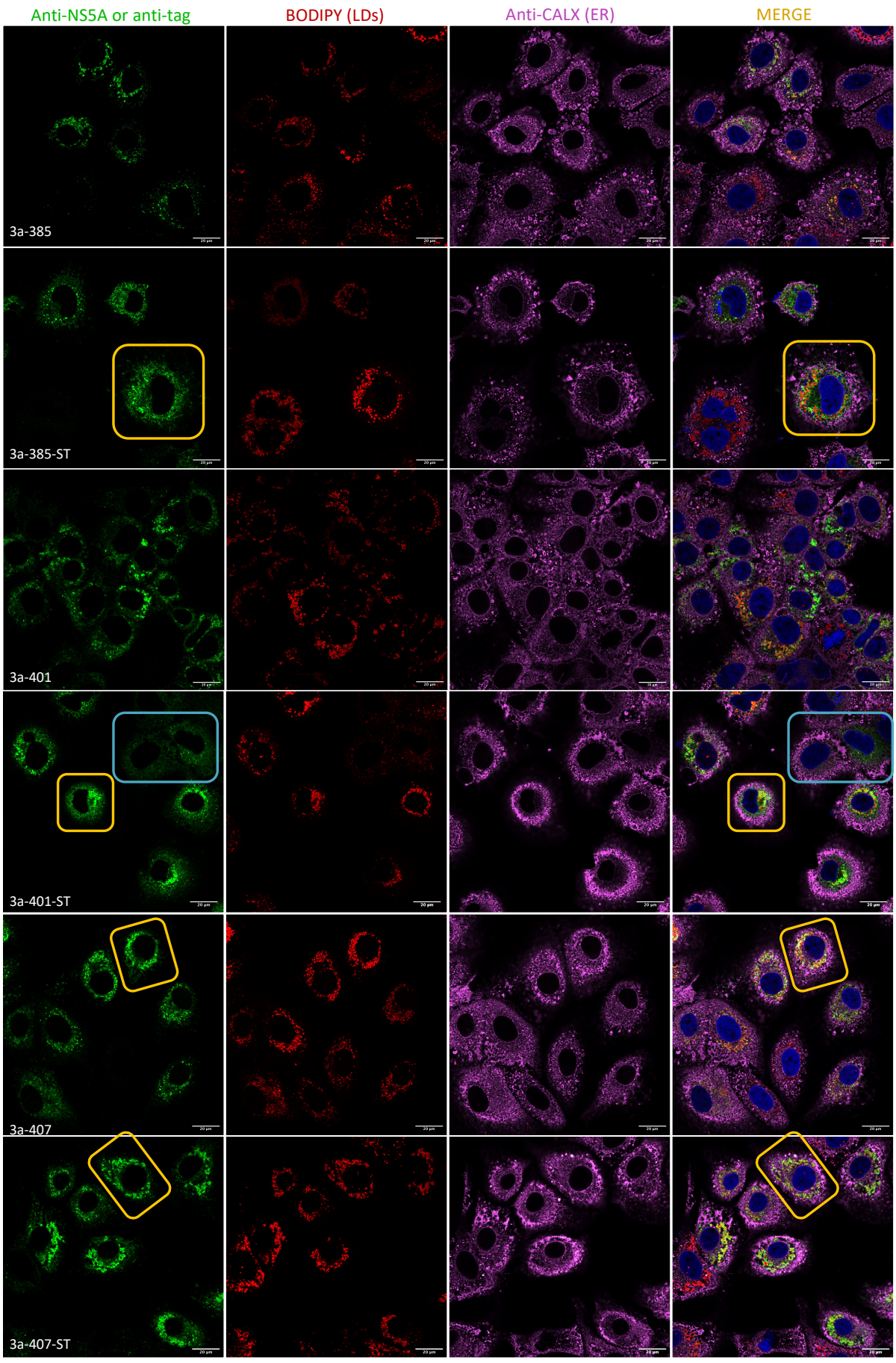
Anti-NS5A or anti-tag
BODIPY (LDs)
Anti-CALX (ER)
MERGE
3a-385
3a-385-ST
3a-401
3a-401-ST
3a-407
3a-407-ST

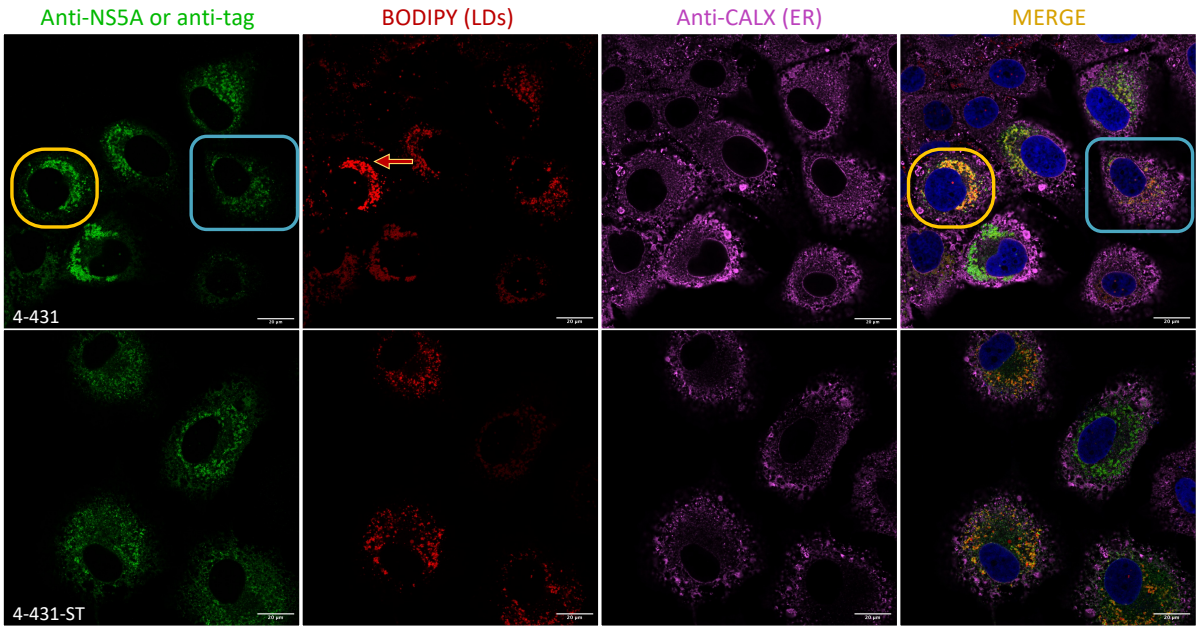

Figure 44: Comparative analysis of the subcellular localization of native or ST/V5-tagged NS5A of various genotypes in infected Huh-7.5 cells

Representative images of Huh-7.5 cells infected with intergenotypic viruses or transfected with tagged intergenotypic RNAs, acquired at 120h p.i./p.tf. NS5A(-ST) proteins are shown in green, LDs are marked in red, ER is revealed in magenta, and nuclei in blue. The "MERGE" images show the superposition of all stainings. Anti-NS5A 9E10 antibody was used to label NS5A in the absence of a tag and anti-ST, or anti-V5 antibodies were used to stain tagged NS5A proteins, unless otherwise indicated. All illustrated pictures were acquired using an inverted confocal microscope and a 40X objective. Scale bars (20µm) are shown at the bottom right of each image. Blue and yellow rectangles depict representative cells with different NS5A subcellular localization patterns and red arrows point to cells in which LD redistribution and clustering are prominent.

IV.E Protein-protein interaction networks of HCV Core and NS5A

In order to identify the Core and NS5A interactomes of the parental Jad virus, the tagged recombinant viruses developed (see Figure 35, page - 93 -) were used to infect human hepatoma Huh-7.5 cells, as described in §III.J.(α). Cell lysates were independently incubated with Strep-Tactin beads to allow the binding of tagged viral proteins and their protein complexes. Following on-bead trypsin digestion and identification of retrieved proteins by nano liquid chromatography coupled to mass spectrometry (nano-LC-MS/MS), hits were scored following our stringent algorithm, incorporating the label-free statistical analysis, the MiST[564] and the SAINT[563] scores. Core and NS5A interactomes were visualized in the form of networks using Cytoscape[572] and StringApp[574]. Further enrichment of the networks revealed interesting pathways for each protein, as described below. An illustration of the experimental processes followed can be found in Figure 30 (page - 85 -).

IV.E.(α) The interactome of Jad NS5A

IV.E.α.(i) Successful affinity purification and identification of NS5A-ST complexes

Five biological replicates of each of the Jad/NS5A-(TEV)-ST-418, -V5-418, -ST-449, -V5-449 infected Huh-7.5 cell lysates collected at 96h p.i. were subjected to an affinity purification protocol relying on the high affinity of the twin-strep tag fused to NS5A with a

Strep-Tactin®XT resin covering magnetic agarose beads (see III.J). To monitor the success of the affinity purification process, aliquots of proportional quantities of infected Huh-7.5 lysates (Lysate), supernatants retrieved following binding to Strep-Tactin beads (SN), pools of post-binding washes of the beads with an appropriate buffer (Wash), and final eluates of bound proteins retrieved upon incubation of beads for 10min at 70°C in LDS+β-mercaptoethanol buffer (Eluate) were analysed by western blotting. Proteins were revealed using the anti-NS5A 7B5 antibody (Figure 45A-B).

NS5A-(TEV)-ST and NS5A-(TEV)-V5 were detected in similar amounts in lysate aliquots from cells infected with the corresponding viruses for both pairs with 418 and 449 insertion positions, indicating equivalent bait protein abundances in the cell lysates. NS5A-ST products were detected in eluates for both ST samples, whereas the absence of signal in both V5 eluates demonstrated specific purification of tagged NS5A and protein complexes. This was further supported by the fact that most NS5A-V5 present in the lysates was retrieved in the post-binding supernatants for both V5 control samples. Of note, the retrieval of a faint NS5A-ST signal in the lanes corresponding to post-binding supernatants of the ST-tagged samples was indicative of probable bead saturation. Moreover, the absence of detectable NS5A signal in the Wash samples suggested that the wash conditions performed did not interfere with NS5A-ST retention on the beads.

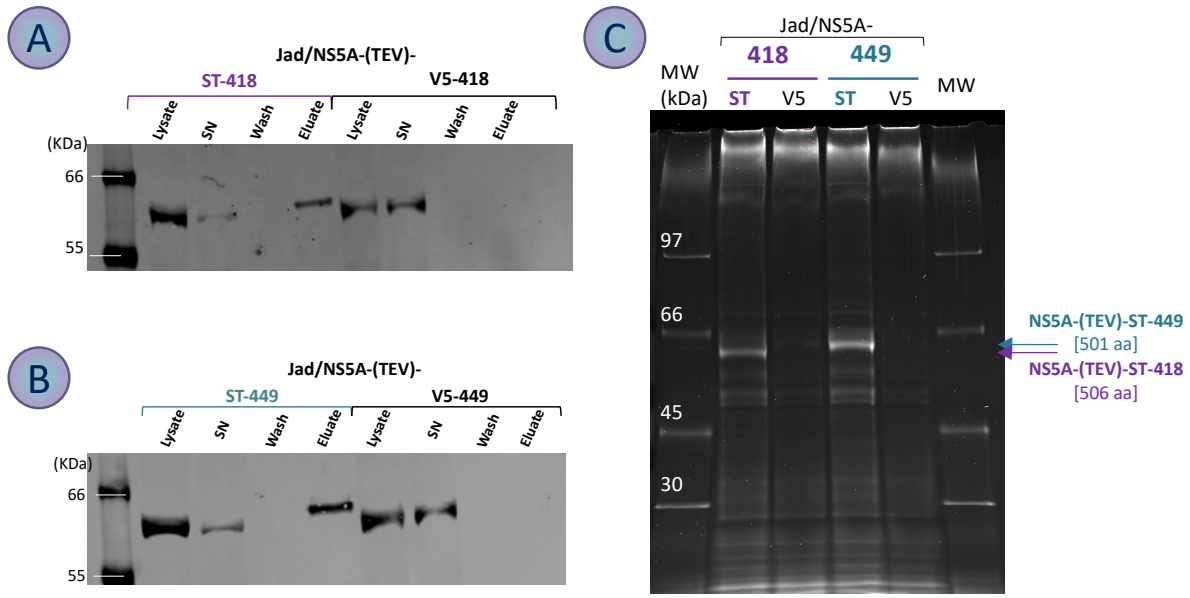

Figure 45: Affinity purification of Jad NS5A-ST protein complexes.
(A, B) Western blotting analysis of the indicated samples for the 418 virus pair (A) or the 449 virus pair (B) aliquoted during the course of the affinity purification of infected Huh-7.5 lysates: Lysate; SN: supernatant retrieved following binding of the lysate onto Strep-Tactin beads; Wash: pool of supernatants retrieved following binding to Strep-Tactin beads and 3 washes each with a buffer that does not contain NP40; Eluate: elution of bound proteins with LDS+β-mercaptoethanol solution. Loaded sample quantities correspond to 0.02xT175 in all cases, except Wash, which is equivalent to 0.01xT175. Immunoblotting was performed with a-NS5A 7B5 antibody. (C) SDS-PAGE gel stained with fluorescent total protein SyproRuby staining solution. Samples loaded correspond to affinity-purified proteins (eluates) from a T175 flask of cells infected with the indicated viruses. MW: Molecular Weight marker (kDa).

A sixth replicate sample was prepared under the same conditions in parallel with the five biological replicates set aside for nano-LC-MS/MS analyses, but all bound proteins were eluted by a 10min incubation of the beads with LDS+β-mercaptoethanol at 70°C. The whole eluate, which was equivalent to the total protein load of one replicate provided to the Proteomics platform, was loaded onto a denaturing polyacrylamide-SDS gel. Protein staining of the gel with SyproRuby also demonstrated specific purification of NS5A-ST and partners only in the presence of the ST, whereas no NS5A-V5 product, expected to migrate with a slightly faster electrophoretic mobility, was visualized in V5 samples (Figure 45C). Other discrete, specific protein products were present only in the ST samples, possibly representing specific NS5A partners.

Following this sixth control and verification of aliquots from all five replicate samples prepared for the MS study, as exemplified in Figure 45A-B, the nano-LC-MS/MS was the next step, carried out in collaboration with the Proteomics platform at Institut Pasteur. Pearson correlation coefficients between ST and V5 replicates were computed using all complete pairs of observations in these samples. These demonstrated that sets of ST and V5 replicates clustered tightly together and segregated in two groups, as expected (Figure 46A, C).

A differential analysis of peptides retrieved by the nano-LC-MS/MS was then performed with the limits of the $\log_2$[Fold-Change(ST/V5)] and the FDR set at 1 and 5%, respectively. Overall, 160 proteins were specifically retrieved from the NS5A-ST-418 replicate samples and 213 proteins were significantly more abundant in the ST-418 versus the V5-418 replicate samples, adding up to 388 proteins reliably interacting with NS5A-ST-418 (Figure 46B). In the NS5A-ST-449 replicate samples,193 proteins were specifically retrieved and 237 proteins were significantly more abundant in the ST-449 than in the V5-449 replicate samples, adding up to 430 proteins reliably interacting with NS5A-ST-449 (Figure 46D). The whole list of retrieved potential NS5A interactors, with their respective scores can be found in Supplementary Table 3.

The fact that we found a higher number of interacting factors with NS5A-ST-449 than with NS5A-ST-418 suggested that more interactions were disrupted by ST insertion at position 418.

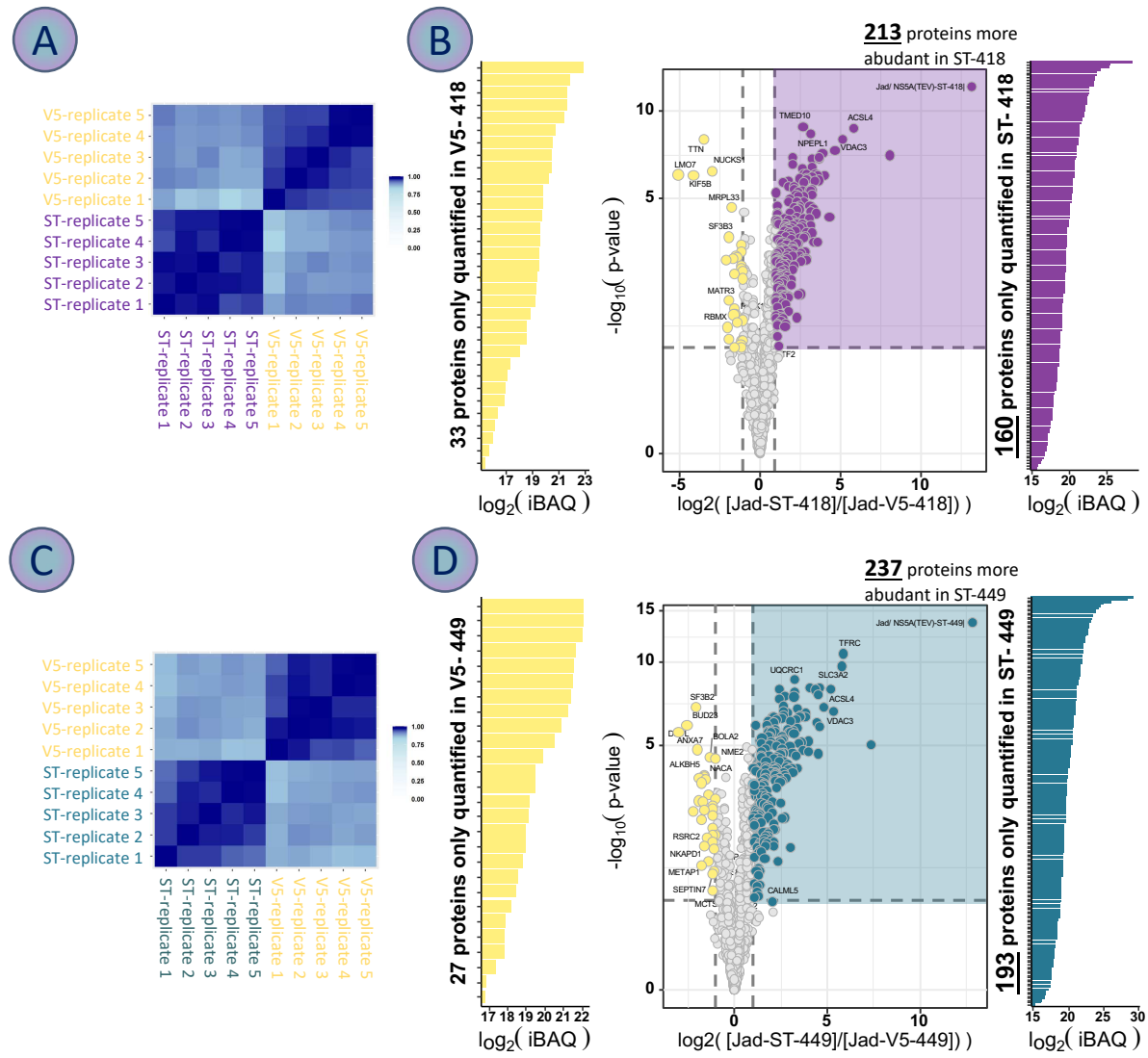

Figure 46: Pearson correlation of tagged NS5A replicate samples and differential analysis of retrieved proteins.

(A, C) Quality control correlation matrix based on Pearson correlation coefficient among ST replicate samples and V5 replicate samples, with the tag insertion downstream of amino acid 418 (A) or 449 (C). (B, D) The volcano plots and framing graphs show proteins identified following the label-free analysis of the liquid chromatography coupled to mass spectrometry data. Proteins retrieved uniquely in the NS5A-ST (preys of interest) or the NS5A-V5 samples (nonspecific preys) are plotted in the graphs as horizontal bars on the right and left of the volcano plots, respectively, according to the logarithmic value in the base of 2 of their iBAQ values. Proteins retrieved in both NS5A-ST and -V5 samples are represented as dots in the Volcano plots according to the logarithmic value in the base of 2 of their respective intensities in the NS5A-ST replicates over the NS5A-V5replicates (X axis) and the negative logarithmic value in the base of 10 of their corresponding adjusted p-values (Y axis). This defines significant preys of interest in the coloured upper right quarters of the Volcano plots.

IV.E.α.(ii) Analysis of NS5A phosphopeptides retrieved

As the different forms of phosphorylated NS5A have been linked to distinct roles of the protein during the various steps of the HCV life cycle (see Figure 12 and the corresponding introductory section on NS5A) and as p56 and p58 have been reported to differentially interact

with specific host factors[160], we examined our retrieved NS5A peptides for post-translational modifications.

We identified phosphorylation of Jad NS5A serine residues at positions 146, 174, 222, 225, 230, 232, 235, and 360, and threonine residues at positions 164, 348 and 356, as well as of serine 12 within the twin-strep tag insertion. Most of these sites have previously been found to be phosphorylated by mass spectrometry in studies using genotype 2a HCV strains, subgenomic replicons or over-expressed NS5A, while fewer studies addressed the NS5A phosphorylation of genotype 1 derived sequences (Appel et al., 20005[148]; Cordek et al., 2014[588]). The overlap of our data and published findings is represented in Table 15, which also includes NS5A residues that might support phosphorylation based on mutational analyses, in the absence of biochemical evidence and MS observations, but that we did not recover in our nano-LC-MS/MS work.

Focusing specifically on the peptide mainly associated with NS5A hyperphosphorylation, G**S**PP**S**EASS**S**V**S**QL**S**APS, the underlined and bolded five serine residues were found to be phosphorylated in our ST replicate samples, while unmodified counterparts of this peptide were also recovered, indicating that phosphorylation of NS5A was not affected by the insertion of the ST tag, and that neither the p56 nor the p58 form were preferentially selected during the affinity purification process. As we were aiming at recovering NS5A interacting partners acting at the different stages of the viral life cycle, these results corroborate that we have reached this goal.

Table 15: Phosphorylated NS5A residues reported in the literature or found in the present study.
Phosphorylated amino acids found by us and not previously reported in the literature are highlighted in dark purple, while those previously reported as detected by mass-spectrometry (MS) are highlighted in light pink. Putative phosphorylated residues supported by genetic data from the literature but not by biochemical or MS evidence, and phosphorylated residues retrieved by MS but not found in our study are highlighted in blue and white, respectively. "-": no detail available

p-amino acid	Protein Domain	Type of evidence	Phenotype	Reference
S146	DI	MS	p-S146 reduces p58 and p-S222 (Ala instead of Ser in subtype 1b)	Ross-Thriepland & Harris, 2014[126]; Goonawardane et al., 2020[159]
T164		Our MS	-	-
S174		Our MS	-	-
S222	LCSI	MS & Mutagenesis	Mild regulator of RNA replication – No effect on viral replication for subtype 2a	Lemay et al., 2013[157]
			p-S222 predominates in the p58 species (subgenomic replicon)	Ross-Thriepland & Harris, 2014[126]
			No apparent phenotype	Appel et al., 2005[148]; Fridell et al., 2013[589]; Masaki et al., 2014[149]; Chong et al., 2016[151]; Eyre et al., 2016[158]
S225		MS	p-S225 essential for both genome replication and assembly	Ross-Thriepland & Harris, 2014[126]
		Mutagenesis	Essential for viral replication - Role in NS5A hyperphosphorylation	Masaki et al., 2014[149]
			p-S225 regulates NS5A interactions with VAPA, BIN1, NAP1L1, & NAP1L4	Goonawardane et al., 2017[152]
S229		MS	Important for RNA replication	Ross-Thriepland & Harris, 2014[126]
		p-S229 specific antibodies	p-S229 found in both p56 and p58 and inverse correlation with p-S235	Chia-Ni Tsai et al., 2019[147]

S230		MS	No phenotype mentioned	Ross-Thriepland & Harris, 2014[126]
S232		MS	Essential for RNA replication	Ross-Thriepland & Harris, 2014[126]
		Mutagenesis	Essential for viral replication - Involved in NS5A **hyperphosphorylation** – Phosphorylated by CKIα	Masaki et al.,2014[149]; Hsu et al., 2018[146]
S235		MS & Mutagenesis	Reduced RNA replication – p-S235 may promote the replication complex formation via increasing NS5A/VAPA interaction – phosphorylated by CKIα– regulated by PI4KIIIα	Chong et al., 2016[151]; Hsu et al., 2018[146], Eyre et al., 2016[158]
S238		MS	Phosphorylated by CKIα	Chong et al., 2016[151]; Hsu et al., 2018[146]
T348	LCSII	MS	No apparent phenotype (Val or Iso instead of Thr in genotype 1)	Eyre et al., 2016[158]; Ross-Thriepland & Harris, 2014[126]
T356	LCSII-DIII	MS	Phosphorylated by PKA – Essential for genome replication	Cordek et al., 2014[588]
S360	DIII	Our MS	-	-
SST12	tag	Our MS	-	-
S452	DIII	Mutagenesis	In p56 - Decreased NS5A-Core interaction, virion production and disturbance of NS5A subcellular localization.	Masaki et al., 2008[139]
S454				
S457				
		Mutagenesis & deletions	Phosphorylated by CKII	Tellinghuisen et al., 2008[136]

IV.E.α.(iii) Analysis of previously reported NS5A interacting partners

As an additional verification step of our AP-MS/MS method, we screened the lists of Jad NS5A interacting partners for previously reported HCV NS5A cellular interactors. In the absence of an up-to-date maintained database of HCV-host PPIs, we relied on the databases and publications described in I.B.θ.(ii) to construct a more complete list of HCV NS5A interacting partners (Supplementary Table 2). To achieve this, we used the data from the HCVpro database[503] and the "HCV Hypo- vs. Hyper-Phosphorylated NS5A Interactome Database"[160], the review paper of Ross-Thriepland & Harris, 2015[118] and the original papers of Saik et al., 2016[506], de Chassey et al., 2008[508], Tripathi et al., 2013[509], Germain et al., 2014[511], Dolan et al., 2013[510], Ramage et al., 2015[512], Meistermann et al., 2014[516], Eberle et al., 2014[517] and Vlaicu et al., 2017[520]. To avoid redundancy, the paper of Mukhopadhyay & Maulik, 2014[505], in which they performed text mining of the HCVpro database, was not incorporated, while due to the absence of available data at the time of the preparation of this list, the paper of Farooq & Khan, 2019[507] and the VirusMINT database[504] were also not used.

Since some of these papers relied on text-mining tools to generate their lists of NS5A interacting partners, we sorted the previously reported NS5A partners in our list by method of identification. Hence, data from papers using both experimental methods and *in silico* mining were separated in two respective columns.

We then compared the combined list of 527 NS5A interacting partners retrieved in this work with ST-418 and ST-449 after removal of redundant proteins interacting with both (see next paragraph) with the list of previously reported NS5A interactors we generated. As shown in the Venn diagram in Figure 47B, we uncovered 408 previously unreported cellular interacting partners of NS5A and 115 partners previously reported in the literature. Of those, the vast majority had been reported in high-throughput original studies using either two-hybrid

screens or different methods of protein complex purification coupled to MS identification of retrieved peptides.

We identified well-known NS5A partners, such as PI4KIIIα, ApoE, VAPA, VAPB and BIN1, whose roles in the HCV life cycle have been well documented and presented throughout this manuscript (I.B.(ε), page- 20 -, I.B.θ.(ii), page - 51 -, Table 15), fully validating our experimental approach. Furthermore, our study unveiled many more, previously unreported NS5A interacting partners. Actually, the overlap between our data and findings from published high-throughput original studies, databases, review publications and text-mining approaches was remarkably low. This could easily be explained by the different experimental approaches followed in most original studies, which, with the exception of those by Vlaicu et al.[520] and Pan et al.[160], were not performed in infection systems, nor in many cases even in hepatic cells lines. In addition, one should mind the pitfalls of text-mining, including unspecific recovery of cellular hits whose gene expression is known or suspected to be regulated in the presence of the viral protein, while no physical interaction with NS5A has been shown.

Finally, the higher overlap of our data with experimentally reported NS5A partners, in contrast to the relatively low overlap with proteins from databases, review studies or text-mining calls for the maintenance of an exhaustive and up-to-date database.

IV.E.α.(iv) Network and enriched pathways of Jad NS5A interactome

Organization of the network representing the Jad NS5A interactome

We performed additional analyses of our MS data on top of the label-free analysis, using the MiST and SAINT scores. Incorporating the three analyses in a final combined score, as described in §III.N.(α) allowed us to discriminate more reliable interactors of NS5A and to increase the stringency for the identification of cellular proteins differentially interacting with NS5A according to the ST insertion position.

Retrieved Jad NS5A interacting partners were organised in a network using the Cytoscape software[572], as shown in Figure 47. The nodes represented correspond to those retrieved with statistical significance based on the label free analysis of the MS data, with increased size if the corresponding protein also passed the MiST and SAINT filters. Proteins found to interact with NS5A-ST-418 are linked with the 418 node with purple lines, while proteins found to interact with NS5A-ST-449 are linked with the 449 node with teal-coloured lines. A protein was considered as a specific interactor of NS5A-ST-418 or NS5A-ST-449 in case it was retrieved only in one of the two screens by all label free, MiST, and SAINT scores, hence it was represented around the corresponding NS5A node in the network.

Proteins found to interact with both NS5A-ST-418 and NS5A-ST-449 and have no known physical interaction with any of the cellular proteins represented in the network, according to String database, were clustered in the central big circle at the top of the network, while proteins entertaining more than three interactions between themselves are clustered in the bottom center. Interactions among cellular proteins are shown by node connections with grey lines.

NS5A interacting partners previously reported in the indicated list of publications and databases are discriminated by a black edge, amounting to 115 cellular proteins already known or proposed to interact with NS5A. The 4 viral proteins found to interact with NS5A, namely E2, NS3, NS4B and NS5B are depicted in black nodes.

This organization of the NS5A interactome network allowed us to discriminate more probable physical NS5A interacting partners (those that do not have other cellular partners, found in circles around the NS5A nodes and in the top central circle) from strong protein partners that may have been pulled down via interaction with third partner cellular intermediates. Nonetheless, such a claim would need to be substantiated by additional protein

complementation assays or co-immunoprecipitation experiments with each cellular protein used as bait.

Furthermore, PPIs that were retrieved with NS5A-ST-418 but not with NS5A-ST-449 or vice-versa provided an indication of the interaction site within NS5A for these specific partners. It is likely that the ST alters NS5A folding at least in the insertion region and/or interrupts a peptide sequence that may be required for the interaction of some partners. The incidence of ST insertion at position 418 may be more detrimental than at position 449, which is more C-terminal to the protein. In agreement with this, a well characterized interactor of NS5A, Nucleosome Assembly Protein 1 Like 1 (NAP1L1), which we found to specifically interact with NS5A-ST-418, was shown to be unable to bind NS5A in the absence of aa 443-457, and was further mapped to a cluster of serine residues in the C-terminal NS5A region[590]. Similarly, another NS5A interactor previously studied in-depth, the protein called SET And MYND Domain Containing 3 (SMYD3), was previously shown to interact with NS5A only in the presence of aa 343-448, pointing to a potential role of sequences around position 418 for this interaction and supporting our specific retrieval of SMYD3 with NS5A-ST-449 and not with NS5A-ST-418[517].

Enriched pathways in the Jad NS5A interactome

String enrichment of the Jad NS5A interactome using the Gene Ontology, KEGG, reactome, WikiPathways and Disease Ontology resources of the StringApp withing the Cytoscape software revealed a plethora of enriched pathways within our network (Supplementary Table 4). With a redundancy cutoff set at 0.5, the top three hits based on each term's FDR were the GO Biological Process "Transport" pathway, with an FDR of 5.89E-35 (253 proteins in our network) and the reactome Pathways "The citric acid (TCA) cycle and respiratory electron transport" (FDR 6.4E-31, 52 proteins in our network) and "Metabolism" (FDR 4.48E-28, 153 proteins in our network). These findings indicate that Jad NS5A is highly involved in these specific cellular processes through direct or indirect interactions with the proteins orchestrating the intracellular transport and metabolism. Due to redundancy among the two highly enriched reactome Pathways, only the proteins included in the more inclusive "Metabolism" term are highlighted in Figure 47.

Notably, the separation of NS5A cellular interacting partners retrieved that are reported in STRING to physically interact with each other and their organization at the bottom part of our network revealed some interesting clustering of protein complexes that may have been co-purified with NS5A in aggregate. These groups are indicated within coloured dashed boxes in Figure 48 and represent proteins involved in or belonging to the mitochondrial contact site and cristae organizing system (MICOS), the cell cycle, immunity, protein production, degradation and modifications (translation, proteasome, N-linked glycosylation, protein folding upon ATP hydrolysis), metabolic processes (Krebs cycle, electron transport chain, oxidative phosphorylation) and proteins known to physically interact with each other by two, three, or four that are involved in intracellular transport. Indeed, a redundancy of enriched pathways can be observed across and within resources highlighting pathways involved in transport and metabolism in general, including more specifically pathways involved in pentose, protein and lipid metabolism, as well as the coupled Krebs cycle, electron transport chain and oxidative phosphorylation (TCA-ETC-OXPHOS). Pathways implicated in host immune responses and HCC development were also found enriched with good FDR values (Figure 49), being indicative of possible NS5A-driven deregulation of all these processes. The illustrated pathways in Figure 49 no longer represent exact terms enriched within the interrogated resources, but manually curated subsets of all the pathways implicated in each cellular process, upon removal of pathways with 100% redundant protein content, for visualization purposes.

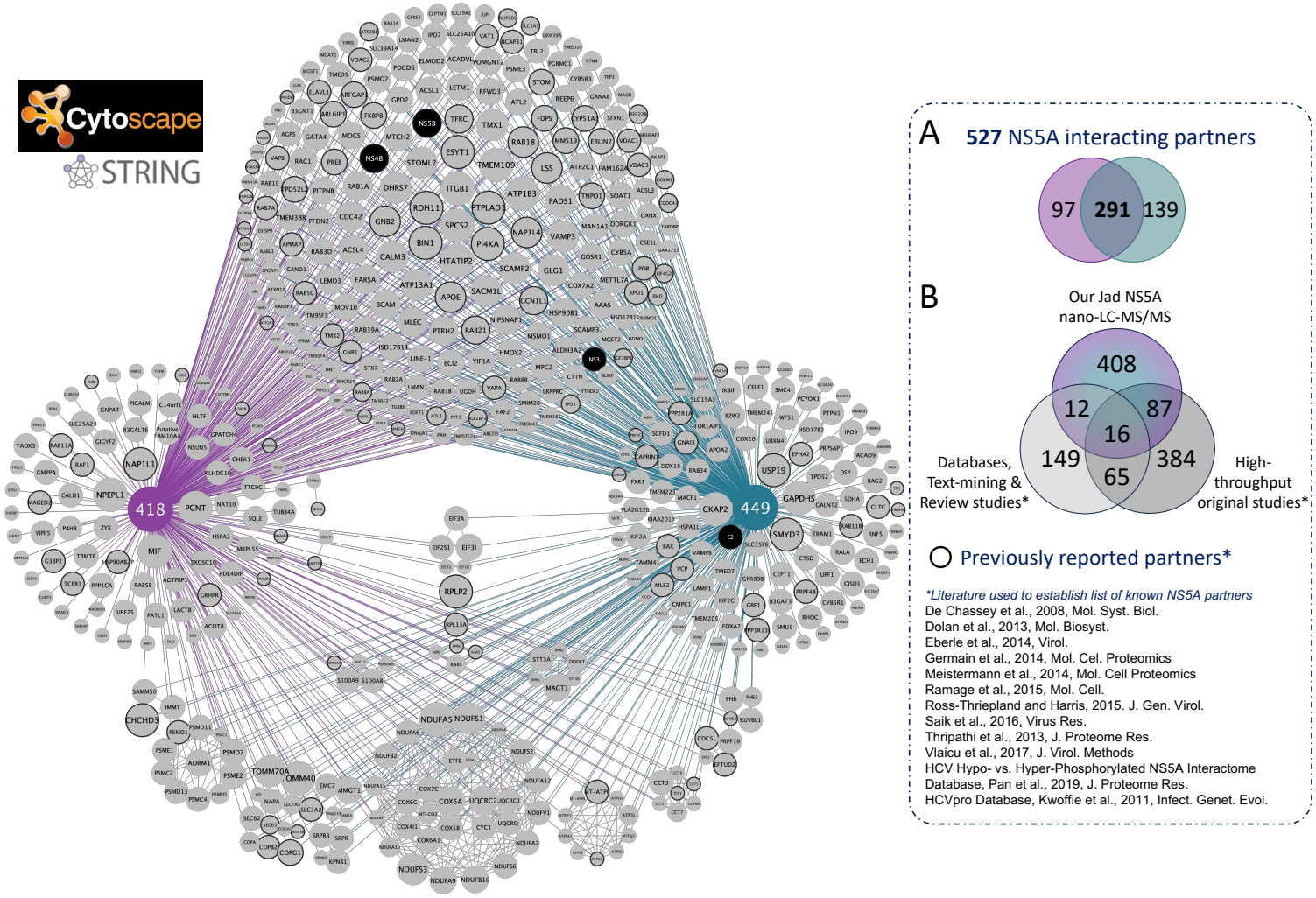

Figure 47: Jad NS5A interactome identified in infected Huh-7.5 cells.
The network was created with the Cytoscape software with the use of StringApp. Protein names are shown in the center of the respective nodes. 418 and 449 correspond to the bait proteins NS5A-ST-418 and NS5A-ST-449, respectively. Node size of the partners corresponds to the final combined score of label-free analysis, MiST and SAINT. (A) Venn diagram of common and distinct PPIs of NS5A-ST-418 (left, purple) and NS5A-ST-449 (right, teal). (B) Venn diagram of common and distinct NS5A PPIs found in our work compared to published literature and databases, as shown in the indicated list of publications.

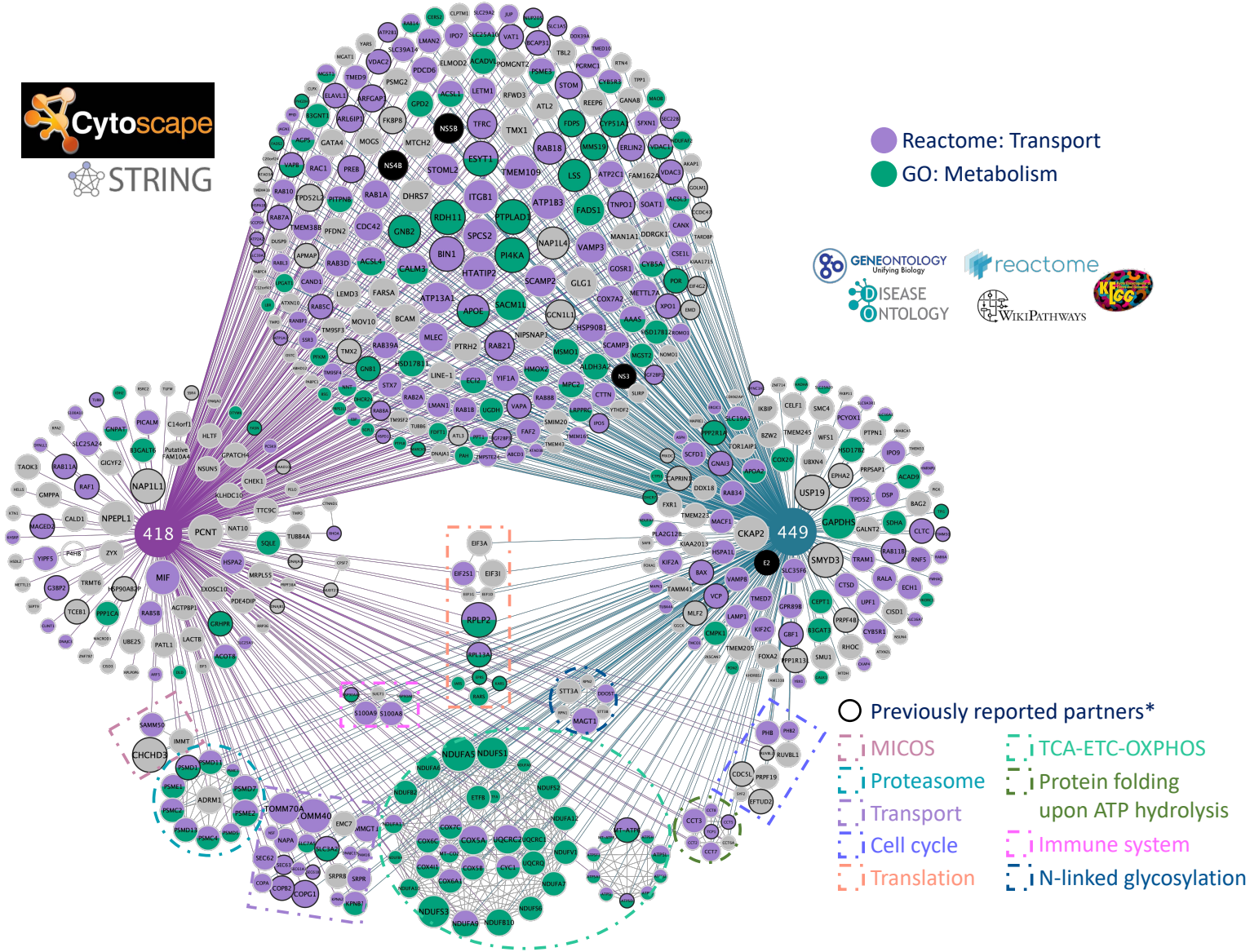

Figure 48: Pathway enrichment of the Jad NS5A interactome identified in infected Huh-7.5 cells.
The network was created in Cytoscape with the use of StringApp. String Enrichment primarily highlighted pathways involved in intracellular transport (purple) and metabolism (green). Clusters of NS5A partners known to physically interact with each other were also found to be part of specific cellular processes, as indicated by dashed rectangles and coloured legend at the bottom right.

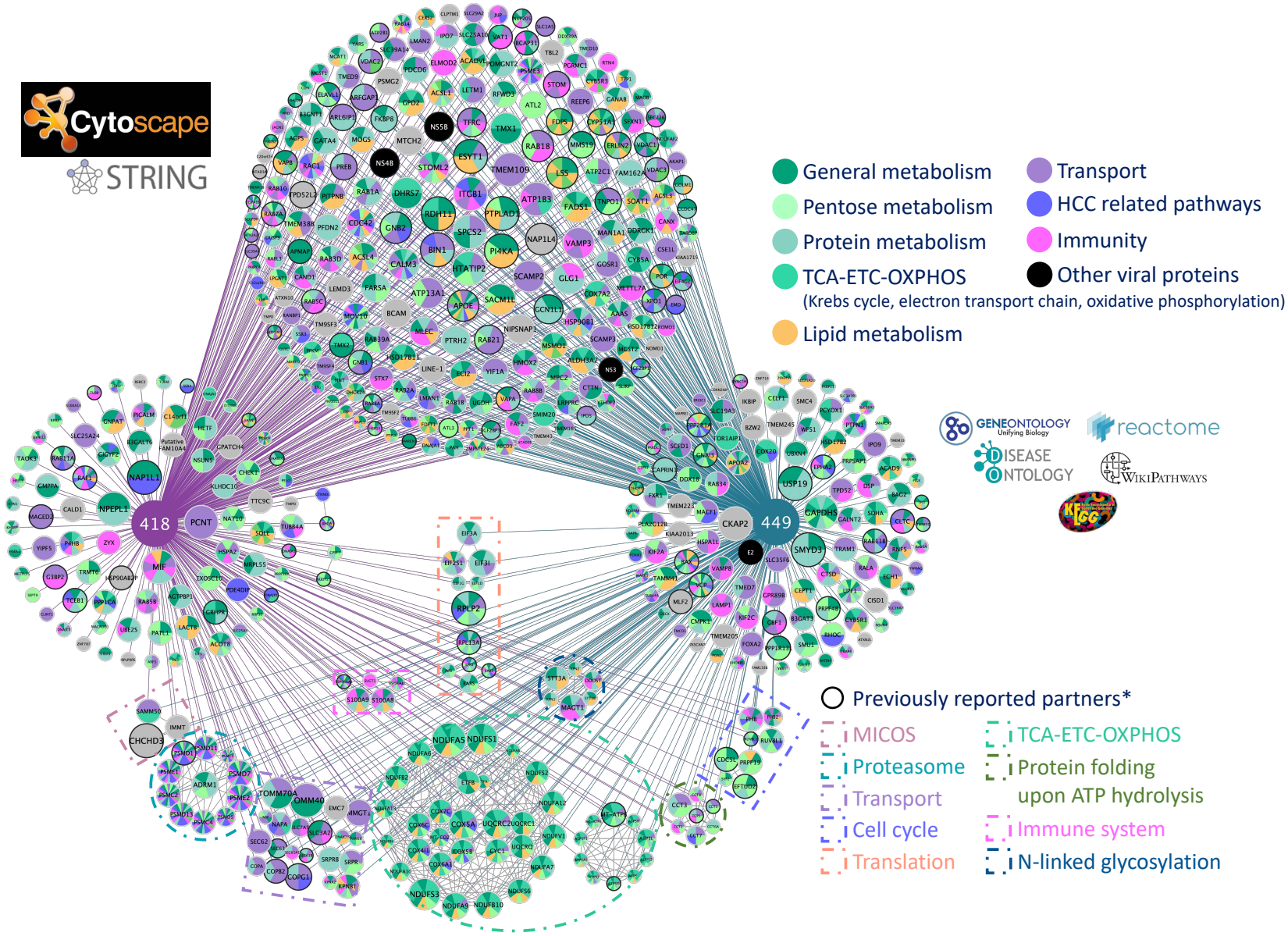

Figure 49: Extensive pathway enrichment of the Jad NS5A interactome identified in infected Huh-7.5 cells.
The network was created in Cytoscape with the use of StringApp. String Enrichment highlighted pathways involved in metabolism (shades of green and yellow), transport (purple), immune responses (pink) and HCC development related pathways (blue).

IV.E.(β) The interactome of Jad Core

IV.E.β.(i) Successful affinity purification and identification of ST-Core complexes

Triplicate samples of ST-Core and V5-Core infected cell lysates collected at 72h p.tf. were subjected to our affinity purification protocol and tagged Core and protein complexes were successfully retrieved only in the ST samples, whereas no unspecific Core product was visualized by western blot with the control V5 tag (Figure 50A). These experiments were standardized and performed by Dr Houda Tabbal during her post-doctoral fellowship in our laboratory. It should be mentioned that due to either the instability or short half-life of the C17-ST protein or to the difficulty in successfully extracting or purifying this protein, a lot more infected cells were required to reach sufficient protein complex quantities for further analyses.

Ward's method with a correlation-based distance among quantified values of replicate ST-tagged and V5-tagged samples revealed high correlation among the ST-Core replicates and among the control samples, as expected (Figure 50B).

A differential analysis of peptides retrieved via nano-LC-MS/MS was then performed with the limits of the $\log_2$[Fold-Change(ST/V5)] and the FDR set at 1 and 5%, respectively. Overall, 78 proteins were specifically retrieved in the ST-Core replicate samples and 56 proteins were significantly more abundant in the ST-Core than in the V5-Core replicate samples, adding up to 134 proteins reliably interacting with ST-Core (Figure 50C). The whole list of retrieved potential Core interactors, with their respective scores can be found in Supplementary Table 5.

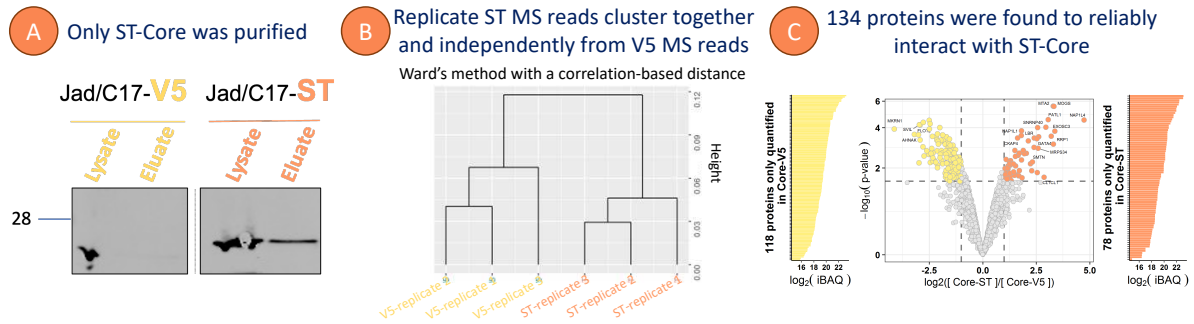

Figure 50: Jad ST-Core protein complex purification.
(A) Western blotting of Huh-7.5 lysates (0.02xT175) and LDS+β-mercaptoethanol eluates (0.4xT175) of bound ST or V5-tagged Jad Core on StrepTactin Sepharose High Performance beads. Immunoblotting was performed with a-core 1851 antibody. (B) Ward's method with a correlation-based distance among replicate ST-tagged and V5-tagged samples. The distance height is plotted on the Y axis. (C) The volcano plot and framing graphs show proteins retrieved following the label-free analysis of the liquid chromatography coupled to mass spectrometry data. Proteins retrieved uniquely in the ST-Core (preys of interest) or the V5-Core samples (nonspecific preys) are plotted (as horizontal bars) on the right and left of the volcano plot, respectively, according to their iBAQ values. Proteins identified in ST- and V5-Core samples are represented as dots in the Volcano plot according to the logarithmic value in the base of 2 of their respective intensities in the ST-Core replicates over the V5-Core replicates (X axis) and the negative logarithmic value in the base of 10 of their corresponding adjusted p-values (Y axis). Significant preys appear in orange.

IV.E.β.(ii) Analysis of previously reported Core interacting partners

As for the NS5A analyses, we screened our lists of Jad Core interacting partners for previously reported HCV Core cellular interactors. For Core, we relied on the data from the HCVpro database[503], the review paper of Kao, 2016[521] and the original papers of Saik et al.,

2016[506], de Chassey et al., 2008[508], Tripathi et al., 2010[514], Germain et al., 2014[511], Dolan et al., 2013[510], Ramage et al., 2015[512], Dolan et al., 2015[515] and Roohvand et al., 2009[513]. Again, the papers of Mukhopadhyay & Maulik, 2014[505] and of Farooq & Khan, 2019[507], as well as the VirusMINT database[504] were not incorporated in this list. Data from the literature were separated in experiment-derived PPIs and text-mining hits (Supplementary Table 1).

For Core we only retrieved seven previously reported interacting partners, while the remaining 131 cellular proteins we identified following the AP-MS/MS experiments were novel hits (see Figure 51).

IV.E.β.(iii) Network and enriched pathways of Jad Core interactome

Strikingly, String enrichment of the Jad Core interactome using the Gene Ontology, KEGG, reactome, WikiPathways and Disease Ontology resources of the StringApp within the Cytoscape software mainly highlighted pathways involved in the regulation of gene expression, such as the illustrated GO Biological Process "Gene expression" (FDR 2.85E-16, 55 proteins in our network), "Regulation of transcription by RNA polymerase II" (FDR 0.015, 30 proteins in our network), and reactome "Gene expression (Transcription)" (FDR 5.25E-7, 33 proteins in our network) pathways, as illustrated in Figure 51. Moreover, an important proportion of enriched pathways within the Core interactome, including the top enriched GO Molecular Function term represent proteins involved in RNA-binding, -metabolism and -transport, underlining the strong association of Core with RNA, RNA-related processes, and their regulation (Supplementary Table 6).

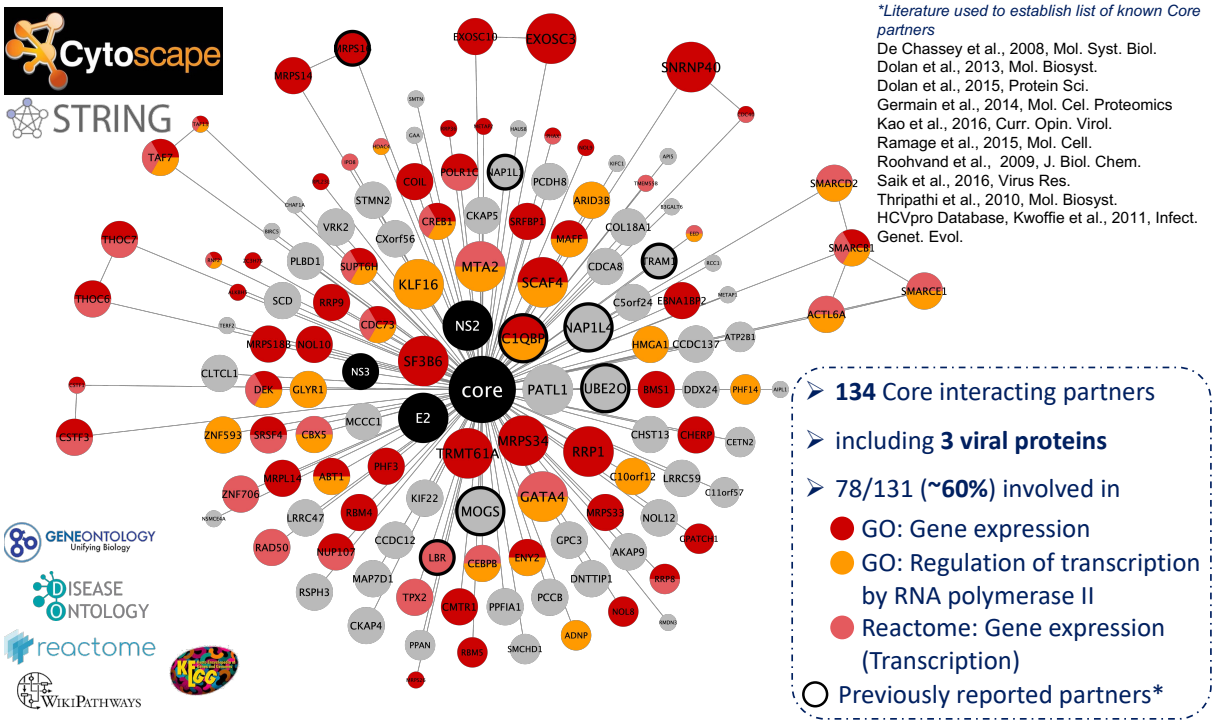

Figure 51: Jad Core interactome identified in infected Huh-7.5 cells and enrichment of host pathways involved in regulation of gene expression.

The network was created with the Cytoscape software with the use of StringApp. Protein names are shown in the center of the respective nodes. Node size of the partners corresponds to the final combined score of label-free analysis, MiST and SAINT. The seven Core PPIs previously published in the selected, indicated literature and database sources are discriminated by a black node border, while the three

viral proteins retrieved are shown in black nodes. Proteins from three selected pathways involved in the regulation of gene expression are highlighted by nodes in shades of orange and red.

IV.E.β.(iv) Common Jad Core and NS5A interacting partners

Once the interactomes of Jad NS5A and Core were analysed, we undertook to identify proteins retrieved by both AP/MS-MS experiments, which would be indicative of common Core and NS5A interacting partners during infection. Though not directly comparable and in no case exhaustive since the Core analysis was performed at 72h p.tf., while the NS5A analysis was performed at 96h p.i., we believe that the cellular proteins that we did retrieve with both Core and NS5A are highly likely to interact with both proteins, since no physical interactions are reported among the cellular hits based on STRING (see network in Figure 52). To support this claim, we do find two proteins, Nucleosome Assembly Protein 1 Like 1 and 4 (NAP1L1 and NAP1L4) that have previously been reported to interact with both Core and NS5A. Interestingly, we also retrieved two proteins previously reported to interact with Core, which were now also included in our interactome of Jad NS5A and would be of interest to further validate: the delta(14)-sterol reductase LBR (LBR) and the translocating chain-associated membrane protein 1 (TRAM1). LBR is physiologically participating in a metabolic pathway leading to cholesterol biosynthesis[591], while TRAM1 has been found to participates in the disposal of misfolded ER membrane proteins as part of the unfolded protein response (UPR) under conditions of ER stress[592].

Overall, we retrieved 14 common Core/NS5A PPIs, including two with the viral proteins E2 and NS3. Among those, three common PPIs were specific to NS5A-ST-449 and five to NS5A-ST-418, while six were retrieved by Core and NS5A ST-tagged in both positions. Enrichment of this network was also performed, with a single pathway coming up with good FDR values across databases, the Gene Ontology Molecular Function "RNA binding pathway", in link with the known capacity of both HCV Core and NS5A in binding viral RNA.

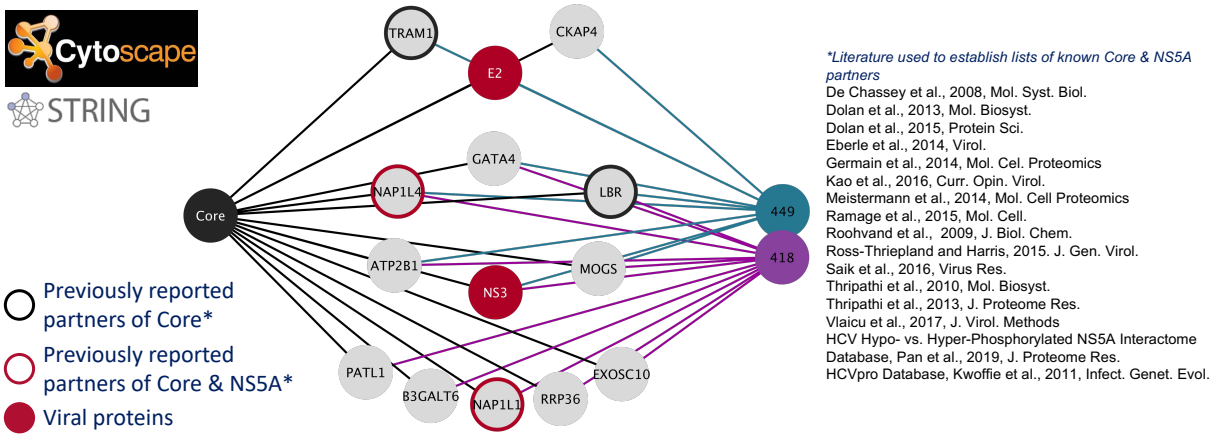

Figure 52: Common Jad Core and NS5A interacting partners identified in infected Huh-7.5 cells. *The network was generated in Cytoscape with the use of StringApp. Protein names are shown in the center of the respective node. Proteins interacting with Core are connected with it with black edges, purple edges are used to connect the PPIs of Jad/NS5-ST-418 and teal ones to connect the PPIs of Jad/NS5-ST-449. The three common Core/NS5A-ST-449 PPIs are clustered in the top, the five common Core/NS5A-ST-418 PPIs are clustered in the bottom and the six proteins retrieved by all three baits are clustered in the center of the network. Core partners previously published in the selected, indicated literature and database sources are discriminated by a black node border, while those previously found for both Core and NS5A by a red node border. Viral proteins found to interact Core and/or NS5A are illustrated in red nodes.*

Despite the unveiling of these few common interactors of Jad Core and NS5A, the overlap between the two networks is quite low. Interestingly, the pathways found significantly enriched in each network vary drastically. The majority of Core interacting partners are associated with RNA and regulation of gene expression, whereas NS5A interacting partners are involved in a wider range of pathways. Based on this observation, we next undertook to explore the common and differential PPIs of NS5A of diverse genotypic origins in similar infection system. In parallel, the regulation of host gene expression in cells infected by recombinant viruses encoding core from different genotypes was explored.

IV.E.(γ) NS5A from clinical and prototypic strains of diverse genotypic origins exhibit common and distinct PPIs

In order to explore the interactomes of NS5A proteins of genotypes 1-4, we relied on the tagged NS5A intra- and intergenotypic recombinant viruses that we produced and characterized, as described in §IV.C and §IV.D. Huh-7.5 cells were transfected with genome-length, synthetic RNAs of the following 7 ST-tagged chimeras and 1 V5-tagged control viruses: Jad/NS5A-1a-411-V5 (nonspecific binding control), Jad/NS5A-1a-411-ST, Jad/NS5A-1b-434-ST, Jad/NS5A-2a-J6-ST, Jad/G4458A/G6050A/NS5A-3a-385-ST, Jad/G4458A/G6050A/NS5A-3a-401-ST, Jad/G4458A/C6233T/NS5A-3a-407-ST and Jad/G6050A/NS5A-4-431-ST. For simplicity, these viruses or the respective NS5A proteins will be referred to in the subsequent paragraphs only with the strain number and tag inserted (e.g. 385-ST instead of Jad/G4458A/G6050A/NS5A-3a-385-ST).

IV.E.γ.(i) Successful affinity purification and identification of the interactomes of ST-tagged NS5A of diverse genotypic origin

A kinetic analysis of protein expression levels at 72h, 96h, 120h p.tf. in cells transfected with the different NS5A-tagged chimeras demonstrated progressive accumulation of NS5A-ST/V5 over time, reaching maximal levels at 120h p.tf. for all viruses, including viruses whose replication appeared weaker at earlier time-points or delayed, such as e.g. 3a-385 (Figure 53). The 120h p.tf. time-point was thus selected for further proteomic studies.

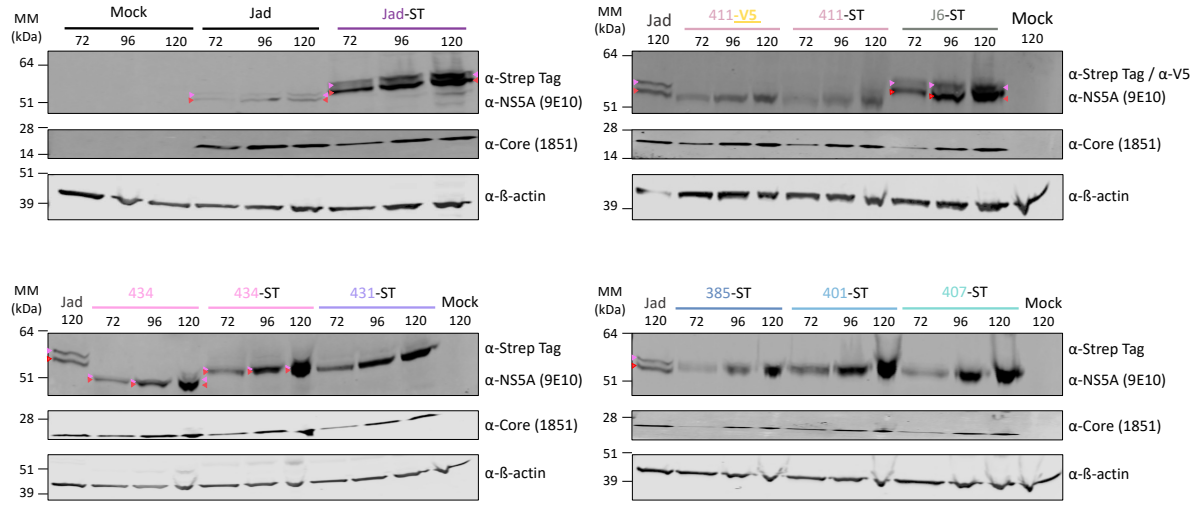

Figure 53: Kinetic analysis of tagged NS5A protein expression over a 120h infection pediod.
A comparative analysis of tagged NS5A expression levels at different time-points p.tf. was performed in protein extracts prepared from Huh-7.5 cells transfected with the indicated RNAs and probed with HCV NS5A, ST and V5 (upper panels), HCV Core (middle panels) and β-actin (lower panels)-specific antibodies. The migration of protein molecular weight markers (MW) is indicated on the left of the

images. Red and pink arrows point to the NS5A p56 and p58 forms, respectively. In bottom left panel nontagged 434 protein expression is also shown.

Transfected cell lysates from five replicate experiments collected at 120h p.tf. underwent the same affinity purification procedures as described for parental Jad NS5A protein complex purification. Tagged-NS5A was specifically retrieved only with the ST-tagged samples and not with the control V5 tag, as shown by the staining of the totality of an eluate loaded onto an SDS-polyacrylamide gel, corresponding to a replicate of the samples analyzed by nano-LC-MS/MS (Figure 54A). This was further confirmed by immunoblotting of a fraction of the eluates (corresponding to 2% of a T175) from a series of samples provided to the platform, revealed with a mixture of anti-ST and anti-V5 primary antibodies (Figure 54B). No control NS5A-411-V5 was visualized in the V5 eluate, whereas all corresponding lysate content was found unbound, in the post-binding supernatant retrieved following incubation with StrepTactin beads. In contrast, all ST samples were readily detected. In addition, in Figure 54C, proportionate aliquots of lysates and eluates of all ST- or V5-tagged samples were loaded on a gel (Figure 54C). This showed that for ST-viruses, NS5A-ST is entirely bound to the StrepTactin beads and retrieved at the end of the purification process, whereas in the case of the control V5 virus, NS5A-V5 is found in the respective post-binding SN as shown in Figure 54B. For comparison purposes, the same amount of StrepTactin beads was used for all purifications, leading to bead saturation for some ST samples, as attested by the detection of low levels of NS5A-ST in the post-binding SNs of 434-ST, J6-ST, 401-ST and 431-ST (Figure 54C), also corresponding to the samples with higher quantities of total NS5A retrieved following purification (Figure 54A). These modest differences in the amounts of NS5A-ST eluted proteins were reflected in the corresponding lysates and are likely due to slightly different viral replication efficiency and/or induced cytopathogenicity of these viruses at 120h p.tf. (also see Figure 42 at 72h p.tf., page - 103 -). Aliquots of all 5 replicates provided to the platform were verified by western blot analysis as in Figure 54B.

Altogether, these data demonstrated that the quantities retrieved across samples and replicates were adequate to identify NS5A partners by nano-LC-MS/MS. As for the previous MS work, Pearson correlation using all complete pairs of observations in these samples confirmed ST and V5 replicate independent clustering, as expected (Supplementary Figure 1).

Differential analysis of peptides retrieved by nano-LC-MS/MS was then performed as previously, with the limits of the $\log_2$[Fold-Change(ST/V5)] and the FDR set at 1 and 5%, respectively. Adjusted p-values were used to set the thresholds of identification of differentially abundant hits between V5-tagged control and ST-tagged samples.

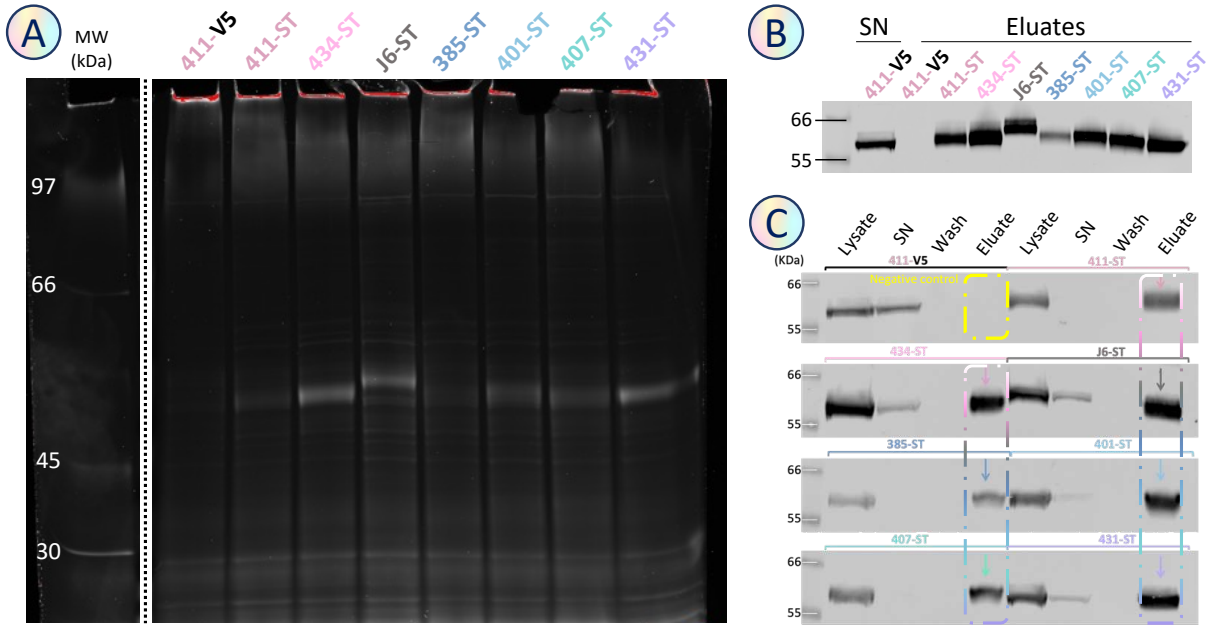

Figure 54: NS5A-ST protein complex purification from Huh-7.5 cells infected with intergenotypic NS5A recombinant viruses.

(A) SDS-polyacrylamide gel stained with fluorescent total protein SyproRuby allowed the probing of the indicated LDS-β-mercaptoethanol protein eluates, purified with MagStrep "type 3" XT magnetic beads from lysates of infected Huh-7.5 cells collected at 120h p.tf. (B) Western blotting of protein eluates shown in (A), in parallel with control V5 post-binding supernatant (SN). (C) Western blotting of infected Huh-7.5 lysates, supernatants retrieved after binding of lysates to StrepTactin beads (SN) followed by 3 washes in the absence of NP40 (Wash), and purified proteins eluted in LDS+β-mercaptoethanol (Eluate). Sample quantities loaded correspond to 1xT175 for total protein staining (A) and 0.02xT175 for all samples except Wash (0.01xT175) for western blots (B-C). Immunoblotting was performed with a mixture of a-ST and a-V5 antibodies. MW: Molecular Weight marker.

Overall, 639 cellular proteins were specifically retrieved in the NS5A-ST replicate samples across genotypes. More specifically for each of the 7 chimeric viruses, 194 cellular proteins were found either exclusively or statistically more abundant in the genotype 1a 411-ST replicates over the control 411-V5, 350 in the genotype 1b 434-ST, 376 in the genotype 2a J6-ST, 252, 395 and 367 in the genotype 3a 385-ST, 401-ST, and 407-ST, respectively, and 314 in the genotype 4 431-ST replicate samples (Figure 55A-G).

A meta-analysis of the retrieved proteins for each NS5A highlighted 96 proteins commonly retrieved with NS5A proteins of all selected clinical strains and J6, as shown in the center of the 7-branch Venn diagram illustrated in Figure H. In this flower-shaped illustration, each number represents the sum of host factors only retrieved together with the NS5A-ST protein(s) of the strain(s) corresponding to the coloured outer line(s) with respect of the center of the plot. For example, within the 434-dedicated petal, there are 32 proteins specifically retrieved with 434-ST and no other NS5A-ST (only enclosed by the pink line), 7 retrieved with 434-ST, 431-ST and no other NS5A-ST (pink and purple line are above number 7), 2 retrieved with 434-ST, 407-ST and no other NS5A-ST (pink and turquoise line are above number 2), 2 retrieved with 434-ST, 431-ST, 407-ST and no other NS5A-ST (pink, purple and turquoise line are above number 2), and so on. The whole list of retrieved potential NS5A interactors, with their respective scores can be found in Supplementary Table 7.

Organization of the network representing the interactomes of NS5A of diverse genotypic origins

We then used MiST and SAINT to further stringently score our list of 639 potential NS5A interactors and we represented the combined results of these analyses in the Cytoscape-derived network illustrated in Figure 56, whose organization is described in the figure legend. In the presence of a single control condition, to consider a cellular protein as a significant interactor of a given NS5A-ST, we relied solely on the label free statistical analysis, then increased the final combined score of interaction by a fixed factor in case PPI was also above the thresholds of the MiST and SAINT analyses.

We further compared our list of retrieved NS5A interacting partners with those previously reported in the selected list of publications and databases mentioned in §IV.E.α.(iii), amounting to 713 cellular proteins already known to interact to some extent with NS5A.

As shown in the Venn diagram in Figure 56, we uncovered 491 previously unreported cellular interacting partners of NS5A and 148 partners previously reported in the literature. Again, we observed a higher overlap of our list of hits with preys derived from high-throughput original studies (112 common hits) than with those found in databases or by literature mining (17 common hits). Once again, the overlap of the three groups is just as low as that observed for Jad NS5A, probably due to the same reasons previously elaborated in §IV.E.α.(iii).

We then examined the overlap between the NS5A interactome of the intergenotypic recombinant viruses with that of Jad NS5A (Figure 56). Although an exact comparison between the two sets of data cannot be made, since one analysis was performed at 96h p.i. and the other at 120h p.t.f., the identification of commonly retrieved hits can testify to the reliability of such PPIs. Overall, 270 cellular proteins of this chimera network have also been retrieved by Jad-ST-418 (36), Jad-ST-449 (30) or both (204). Besides, 218 Jad NS5A partners were also retrieved in this AP-MS with J6-NS5A of the same 2a subtype. Interestingly, out of the 96 common cellular interactors to all genotype NS5A-ST baits used in this analysis, 77 were also retrieved with parental Jad NS5A-ST, whether Jad-ST-418 (7), Jad-ST-449 (9) or both (61), such as the previously described HCV-essential BIN1, VAPA, VAPB, PI4KIIIα. Surprisingly, APOE was only recovered by J6 and 401 NS5A proteins, in addition to the parental.

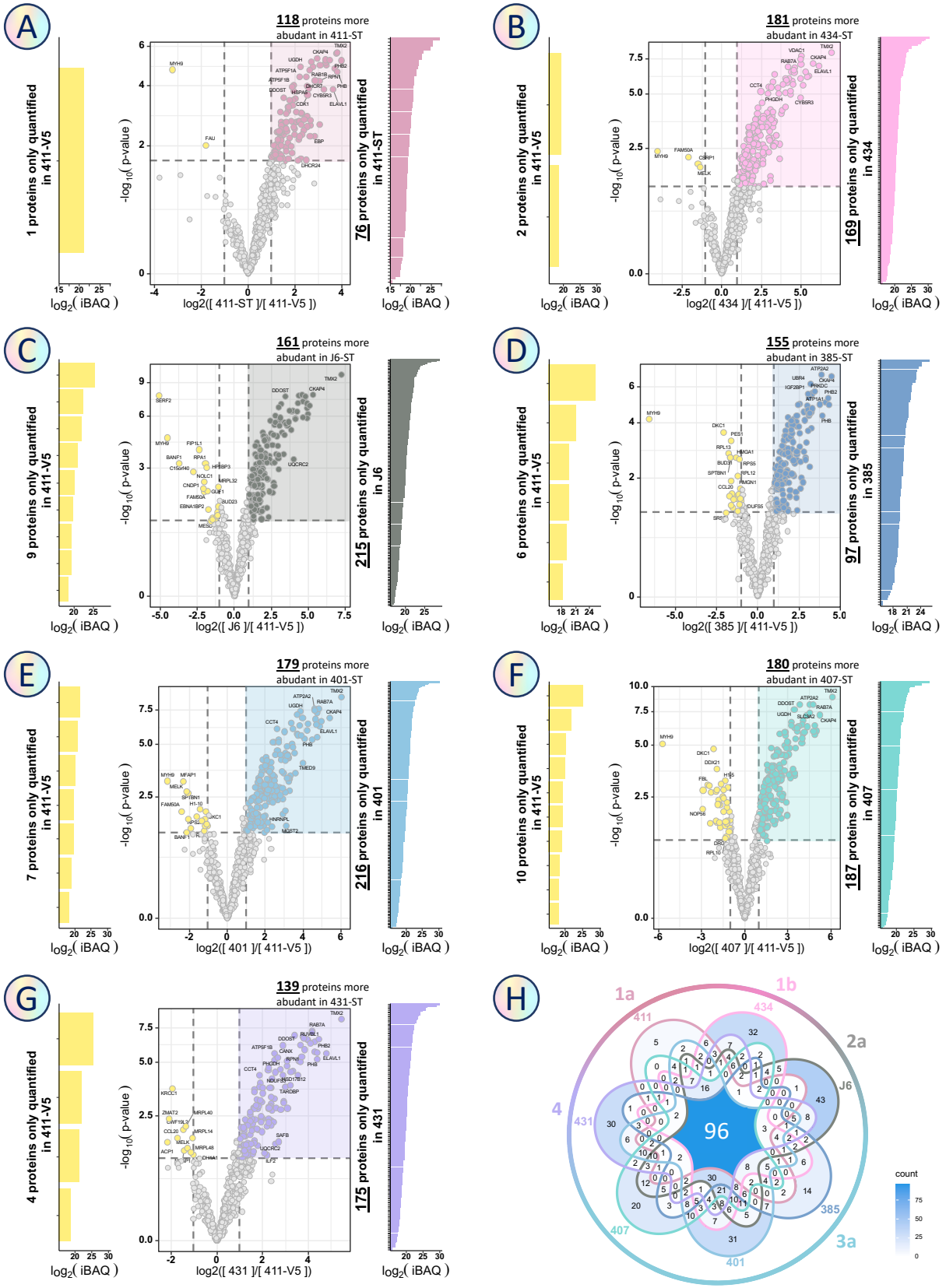

Figure 55: Illustrations of the differential label-free statistical analyses of NS5A interacting partners using NS5A of diverse genotypic origins as baits.

(A-G) Hits retrieved uniquely in the NS5A-ST (preys of interest) or the NS5A-V5 samples are shown in the graphs on the right and left of the volcano plots, respectively, according to the logarithmic value in the base of 2 of their iBAQ values. Proteins retrieved in both NS5A-ST and -V5 samples are represented

by dots in the Volcano plots according to the logarithmic value in the base of 2 of their respective intensities in the NS5A-ST replicates over the NS5A-V5replicates (X axis) and the negative logarithmic value in the base of 10 of their corresponding adjusted p-values (Y axis). Significant preys of interest thus appear in the colored upper right quarters of the Volcano plots. (H) A 7-branch Venn diagram illustrating the distribution among the 7 NS5A-ST species of the 639 interactors found more abundant in at least one the NS5A-ST versus the V5 control.

IV.E.γ.(ii) Enriched pathways of NS5A interactomes

String enrichment of the pan-genotypic (to the limits of this study) NS5A interactomes was performed as described for the Jad NS5A network and revealed a number of identical enriched pathways (Supplementary Table 8).

Interestingly, using the same 0.5 redundancy cutoff of String enriched terms, the top three enriched pathways based on each pathway FDR were GO Molecular Function "RNA binding", with an FDR of 1.42E-75 (203 proteins in our network), the reactome Pathway "Metabolism" (FDR 7.46E-35, 189 proteins in our network) and GO Biological Process "Metabolic Process" term, with an FDR of 1.48E-33 (431 proteins in our network). Included in the full list of enriched terms, we also found terms related to (i) intracellular transport, (ii) metabolism in general, including more specifically pathways involved in pentose, protein and lipid metabolism, as well as the coupled Krebs cycle, electron transport chain and oxidative phosphorylation (TCA-ETC-OXPHOS), (iii) host immune responses, and (iv) HCC development. Interestingly, in addition to shared enriched pathways with parental NS5A, we also uncovered NS5A partners that specifically led to the enrichment of gluconeogenesis and cholesterol metabolism pathways, as well as regulation of gene expression.

More in-depth analysis of the genotype 3-specific partners and the nongenotype 3-specific ones unveiled enrichment of the gluconeogenesis and cholesterol metabolism pathways only in the genotype 3 specific network, in line with metabolic disorders that are more prevalent for genotype 3 HCV strains. On the other hand, the GO Biological Process "gene expression" term only came up in the nongenotype 3 network (data not shown).

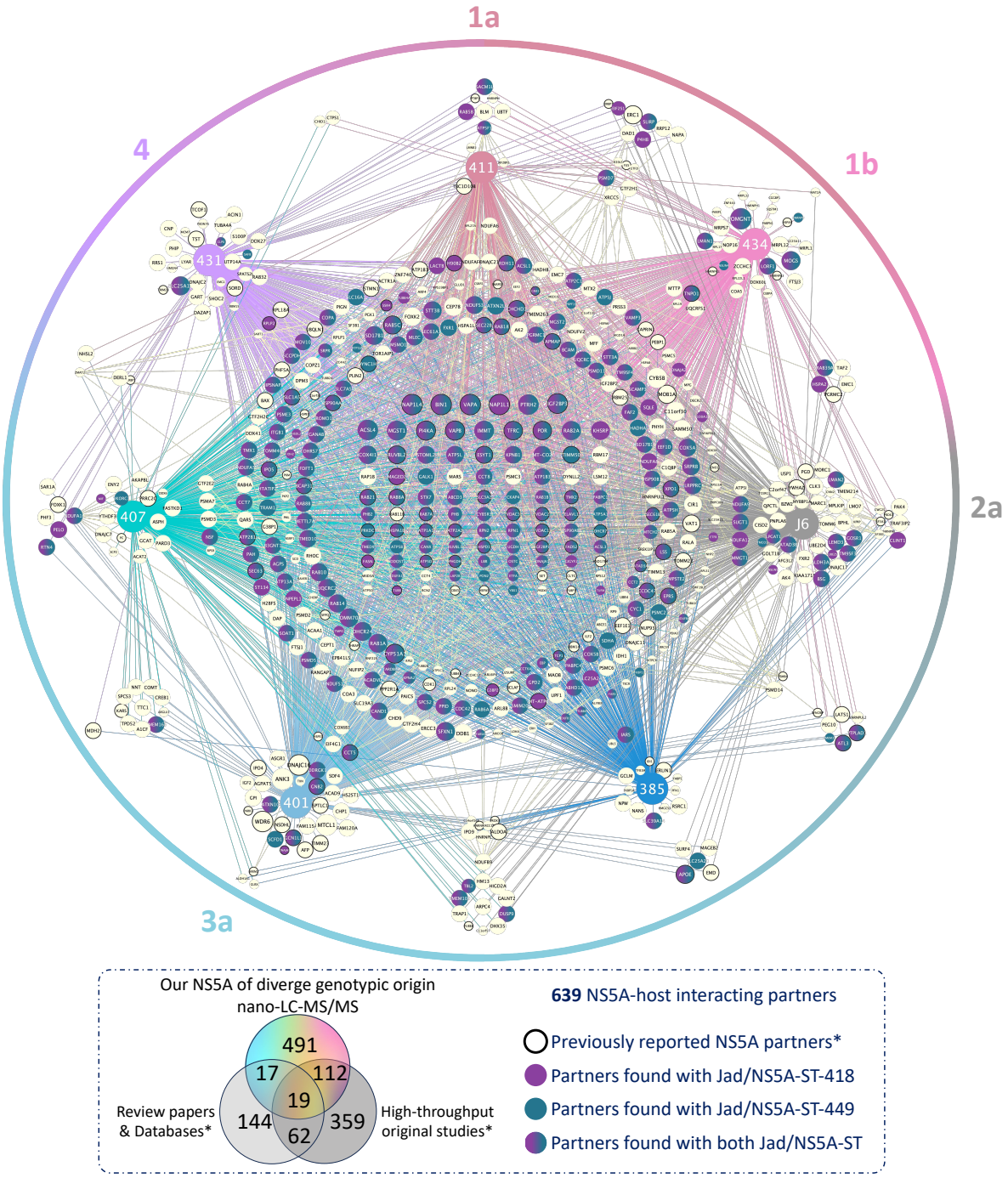

Figure 56: The interactome of HCV NS5A from clinical strains of various genotypes and 2a-J6 identified in infected Huh-7.5 cells.

The network was created in Cytoscape with the use of StringApp. Protein names are shown in the center of each node. Three-digit numbers within the big, coloured nodes correspond to the identification of NS5A-ST bait proteins. Shades of pink represent genotype 1 derived NS5A sequences, grey, genotype 2a, shades of blue, genotype 3a and purple, genotype 4, as also indicated by the external gradient coloured circle. Each cellular protein/NS5A PPI is shown by lines colour-coded according to baits, while cellular PPIs are depicted by yellow lines. Strain-specific hits are clustered around the corresponding bait in the absence of known physical PPIs within the network, or in front of the corresponding bait towards the center in the presence of such PPIs. The 96 PPIs common to all baits are shown in the center of the network, with each concentric circle moving outwards representing PPIs retrieved by 6, 5, 4, or 3 of the baits, respectively. Hits common among two baits are represented in clusters inbetween NS5A nodes. Node size of the partners corresponds to the final combined score of label-free statistical analysis, MiST and SAINT. Previously reported NS5A PPIs (see IV.E.α.(iii)) are

circled in black and the overlap of our network with the published PPIs can be found in the Venn diagram at the bottom. Proteins previously found in the Jad NS5A network are coloured according to the squared legend.

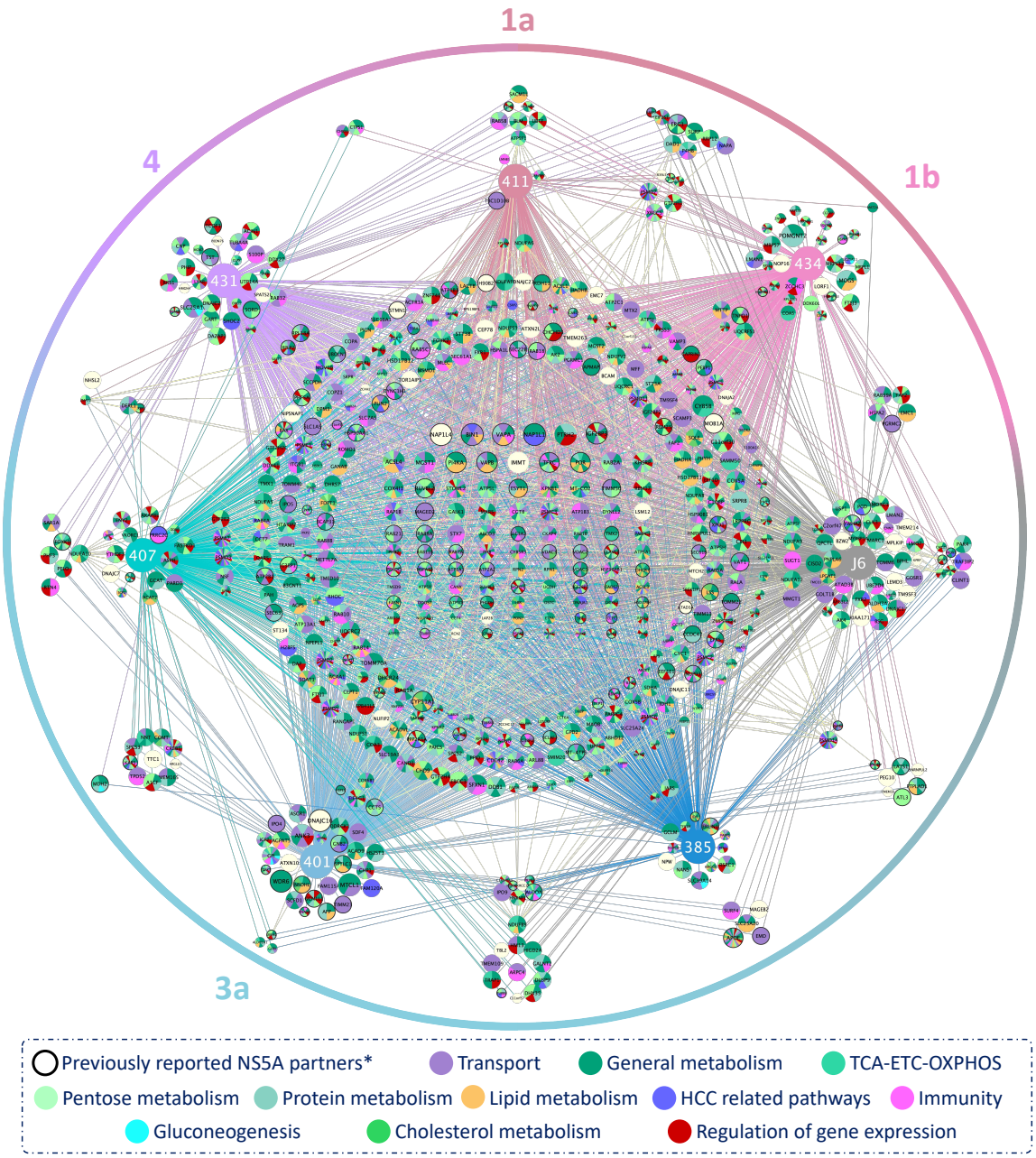

Figure 57: Extensive pathway enrichment of the NS5A interactome identified in infected Huh-7.5 cells.
The network was created as in Figure 56. String Enrichment highlighted pathways involved in metabolism (shades of green and yellow), transport (purple), immune response (pink), HCC development related pathways (dark blue), gluconeogenesis (turquoise) and regulation of gene expression (red).

IV.E.γ.(iii) NS5A intra-viral interactome

We further performed an analysis of retrieved peptides corresponding to HCV proteins, in order to identify the intra-viral NS5A network across genotypes and in comparison to the

parental virus. These results are illustrated in Figure 58. Due to the compensatory mutations introduced into NS3 and NS4B of some of the NS5A intergenotypic recombinants, peptides identified by the MS/MS and derived from these two Jad proteins were not identical in all viruses. For this reason and also to compare with independently-ran parent data, no combined score of statistical analysis, MiST and SAINT was implemented. Hence, the lines illustrate the retrieval of peptides of each viral protein together with the indicated NS5A based solely on the label-free analysis. Interaction of NS3, NS4B and NS5B with all NS5A proteins we tested was evident from these data. Core and NS2 derived peptides were also identified in the majority of the NS5A-ST eluates, except for Jad and 385. For the latter, it might be attributed to the lower NS5A-ST level in infected cell lysates and AP-MS eluates. E2 was specifically retrieved with subtype 1b and 2a derived NS5A baits, for reasons that are unclear without further investigation.

Overall, the identification of both nonstructural and structural HCV proteins in complex with NS5A is indicative of the documented implication of the protein in both genome replication and particle assembly steps of the virus life cycle. Moreover, NS5A/NS3 and NS5A/NS4B PPIs found in this study strongly substantiate the selection of second-site substitutions in these nonstructural proteins to compensate for heterologous NS5A.

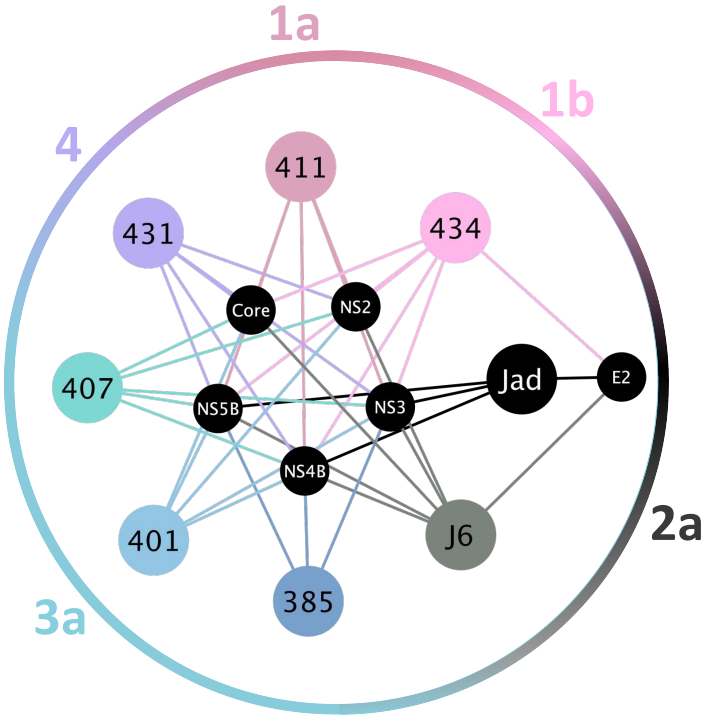

Figure 58:The intraviral network of NS5A proteins of diverse genotypic origins identified in infected Huh-7.5 cells.
NS5A proteins derived from genotype 1 clinical isolates are shown in shades of pink, proteins of prototypic genotype 2a strains are shown in black (parent, Jad) or grey (J6), NS5A derived from genotype 3a clinical isolates are shown in shades of blue and the genotype 4 derived NS5A is illustrated in purple. Color-coded lines connect the proteins retrieved with the respective NS5A-ST as bait.

IV.E.γ.(iv) Analysis of retrieved NS5A phosphopeptides

Exhaustive research about the phosphorylation status of NS5A of diverse genotypic origins is missing. In light of data supporting differential effects of NS5A hyperphosphorylation in HCV life cycle according to the viral genotype, either promoting (genotype 2a) or inhibitory (genotype 1)[148,589,149,153], we next examined the NS5A peptides we retrieved for post-translational modifications, with a specific focus on phosphorylation. A summary of NS5A phosphopeptides and phosphosites identified can be found in Table 16. Six peptides were found to be phosphorylated at aligned sites within the different NS5A isoforms, spread throughout the NS5A DI, LCSI, DII, LCSII, and DIII, with more than one phosphosites identified within each peptide in some instances.

Table 16: Retrieved NS5A phosphopeptides and identification of specific phosphosites.
Peptides found at aligned sequences within the different NS5A isoforms are highlighted in the same colour within the first column. Phosphosites identified are shown in bigger case letters and those recovered with a localization probability above 0.75 are in bold.

Peptide sequence	Leading proteins	Position within protein	Position in alignement	Amino acid	Localization probability
TCSNTWHGTFPINAHTTGPC**T**PSPAPNYSR	NS5A_Jad/NS5A(TEV)-ST-418-434	**99**	**99**	**T**	**0,96**
G**S**PPSEASSSASQLSAPSLK	NS5A_Jad/NS5A(TEV)-ST-418-385; NS5A_Jad/NS5A(TEV)-ST-418-401; NS5A_Jad/NS5A(TEV)-ST-418-407	**222**	**222**	**S**	**1,00**
G**S**PPSLASSSASQLSAPSLK	NS5A_Jad/NS5A(TEV)-ST-418-431	**222**	**222**	**S**	**1,00**
G**S**PPSLASSSASQLSAPSLK	NS5A_Jad/NS5A(TEV)-ST-418-434	**222**	**222**	**S**	**1,00**
G**S**PPSEASSSASQLSAPSLR	NS5A_Jad/NS5A(TEV)-ST-418-J6	**222**	**222**	**S**	**1,00**
G**S**PPSVASSSASQLSAPSLK	NS5A_Jad/NS5A(TEV)-ST-418-411	**222**	**222**	**S**	**1,00**
GSPP**S**LASSSASQLSAPSLK	NS5A_Jad/NS5A(TEV)-ST-418-431	**225**	**225**	**S**	**1,00**
GSPP**S**LASSSASQLSAPSLK	NS5A_Jad/NS5A(TEV)-ST-418-434	**225**	**225**	**S**	**1,00**
GSPP**S**LASSSASQLSAPSLK	NS5A_Jad/NS5A(TEV)-ST-418-401	225	225	S	0,65
GSPP**S**VASSSASQLSAPSLK	NS5A_Jad/NS5A(TEV)-ST-418-411	**225**	**225**	**S**	**0,98**
GSPPSLA**S**SSASQLSAPSLK	NS5A_Jad/NS5A(TEV)-ST-418-434	228	228	S	0,69
GSPPSLAS**S**SASQLSAPSLK	NS5A_Jad/NS5A(TEV)-ST-418-434	**229**	**229**	**S**	**0,76**
GSPPSLASS**S**ASQLSAPSLK	NS5A_Jad/NS5A(TEV)-ST-418-431	**230**	**230**	**S**	**0,92**
GSPPSLASS**S**ASQLSAPSLK	NS5A_Jad/NS5A(TEV)-ST-418-434	**230**	**230**	**S**	**0,92**
GSPPSVASS**S**ASQLSAPSLK	NS5A_Jad/NS5A(TEV)-ST-418-411	**230**	**230**	**S**	**0,99**
GSPPSLASSSASQLSAP**S**LK	NS5A_Jad/NS5A(TEV)-ST-418-431	**235**	**235**	**S**	**0,91**
GSPPSLASSSASQLSAP**S**LK	NS5A_Jad/NS5A(TEV)-ST-418-434	**235**	**235**	**S**	**0,91**
GSPPSEASSSASQLSAP**S**LR	NS5A_Jad/NS5A(TEV)-ST-418-J6	**235**	**235**	**S**	**0,79**
AACTGHKD**S**PGVDLIEANLLWGTTATR	NS5A_Jad/NS5A(TEV)-ST-418-431	**249**	**249**	**S**	**0,78**
HD**S**PDADLIEANLLWR	NS5A_Jad/NS5A(TEV)-ST-418-434	**249**	**249**	**S**	**1,00**
VE**S**ETKVVILDSFEPLRAEPDDAELSVAAECFK	NS5A_Jad/NS5A(TEV)-ST-418-385	**274**	**274**	**S**	**0,96**
VE**S**ETKVVILDSFEPLRAETDDGELSVAAECFK	NS5A_Jad/NS5A(TEV)-ST-418-401	**274**	**274**	**S**	**0,97**
VE**S**ETKVVVLDSFEPLRAETDDAELSVAAECFK	NS5A_Jad/NS5A(TEV)-ST-418-407	**274**	**274**	**S**	**1,00**
VE**S**ENKVVILDSFDPLVAEEDEREVSVPAEILR	NS5A_Jad/NS5A(TEV)-ST-418-411	**274**	**274**	**S**	**1,00**
VESE**T**KVVILDSFEPLRAEPDDAELSVAAECFK	NS5A_Jad/NS5A(TEV)-ST-418-385	276	276	T	0,55
VESE**T**KVVILDSFEPLRAETDDGELSVAAECFK	NS5A_Jad/NS5A(TEV)-ST-418-401	276	276	T	0,55
VESE**T**KVVVLDSFEPLRAETDDAELSVAAECFK	NS5A_Jad/NS5A(TEV)-ST-418-407	276	276	T	0,50
VVILDSFEPLRAE**T**DDGELSVAAECFK	NS5A_Jad/NS5A(TEV)-ST-418-401	**291**	**291**	**T**	**0,79**
KPDYEPPVVHGCPLPPPQ**S**PPVPPPR	NS5A_Jad/NS5A(TEV)-ST-418-411	**349**	**349**	**S**	**1,00**
KTP**T**PPPRR	NS5A_Jad/NS5A(TEV)-ST-418-J6	**348**	**352**	**T**	**1,00**
RR**T**VGLSEDSIGDALQQLAIK	NS5A_Jad/NS5A(TEV)-ST-418-J6	**356**	**360**	**T**	**1,00**
TIQLDGSNVSAALAALAEK	NS5A_Jad/NS5A(TEV)-ST-418-401	**360**	**360**	**T**	**1,00**
KK**T**VVLTESTVSSALAELATK	NS5A_Jad/NS5A(TEV)-ST-418-434	**360**	**360**	**T**	**1,00**
AVVL**S**ESNISAALASLADK	NS5A_Jad/NS5A(TEV)-ST-418-431	**360**	**364**	**S**	**1,00**
TVGL**S**EDSIGDALQQLAIK	NS5A_Jad/NS5A(TEV)-ST-418-J6	**360**	**364**	**S**	**0,99**
TVVL**T**ESTVSTALAELATK	NS5A_Jad/NS5A(TEV)-ST-418-411	364	364	T	0,59
AVVLSE**S**NISAALASLADK	NS5A_Jad/NS5A(TEV)-ST-418-431	**362**	**366**	**S**	**1,00**
TIQLDG**S**NVSAALAALAEK	NS5A_Jad/NS5A(TEV)-ST-418-401	**366**	**366**	**S**	**1,00**
TVQLDG**S**NVSAALAALAEK	NS5A_Jad/NS5A(TEV)-ST-418-407	**366**	**366**	**S**	**1,00**
TVVLTE**S**TVSSALAELATK	NS5A_Jad/NS5A(TEV)-ST-418-434	**366**	**366**	**S**	**1,00**
TVVLTE**S**TVSTALAELATK	NS5A_Jad/NS5A(TEV)-ST-418-411	**366**	**366**	**S**	**1,00**
TVVLTES**T**VSSALAELATK	NS5A_Jad/NS5A(TEV)-ST-418-434	**367**	**367**	**T**	**0,75**
AVVLSESNI**S**AALASLADK	NS5A_Jad/NS5A(TEV)-ST-418-431	**365**	**369**	**S**	**0,87**

Importantly, for all discovered phosphopeptides, the nonphosphorylated counterpart was also detected, indicating that there was no bias regarding phosphorylation status of NS5A during the affinity purification process. These data show for the first time dynamic phosphorylation of NS5A across genotypes.

Interestingly, we identified phosphorylation of two aa residue within DIII, which to our knowledge has not previously been reported. We found them either phosphorylated for the majority of NS5A proteins studied, or naturally occupied by a phospho-mimetic aa residue (D), suggesting that phosphorylation of this particular residue might be of great importance for the virus life cycle. More specifically, aa at position 364 of the alignment shown in Figure 31 (page - 88 -) was found phosphorylated in the form of a serine residue for Jad, J6 and 4-431 NS5A and in the form of threonine for 1a-411 NS5A, while it is an aspartic acid residue in all of the genotype 3a strains we studied. Similarly, aa 366 in the alignment is a serine in all sequences, except for the phospho-mimetic aspartic acid in J6, and was found phosphorylated in all genotype 1, 3 and 4 strains, except for 385.

For J6 NS5A, we also did identify the p-T348 (Val or Ile in the other strains, position 352 in the alignment) and p-T356 (position 360), as we did for Jad, with the latter being reportedly phosphorylated by PKA and essential for genome replication[588]. Surprisingly, although aa 174 is conserved across strains to receive phosphorylation (S or T), we did not recover this modification in any of these NS5A isoforms, unlike Jad NS5A. Moreover, S146 that was found phosphorylated in Jad NS5A and is reported in the literature to be phosphorylated in genotype 2a strains, was not recovered for J6, similarly to T164, nor for 1a-411, while it is an alanine residue in the rest of the NS5A sequences we examined.

Upon further investigation of the peptide mainly associated with NS5A hyperphosphorylation (Table 17), we detected differential phosphorylation of specific aa residues in the different isoforms of NS5A. More specifically, although S222 was found phosphorylated by all studied isoforms, the remaining serine residues of the peptide were found modified only in NS5A proteins of some genotypes or strains. For example, S228 and S229 modification was only evident in the genotype 1b derived NS5A, S232 only in Jad NS5A, S225 and S230 in all but genotype 3a NS5A proteins, with the exception of S225 in J6- and 401-NS5A, while S235 was found modified only in genotype 1b, 2a and 4 NS5A proteins and not in 1a and 3a ones. The unique extent of hyperphosphorylation of this peptide for 434-NS5A-ST, similar to Jad NS5A, is likely to account for the detection of a clearly separated hyperphosphorylated NS5A species by western blot for this strain.

Table 17: Phosphorylated residues identified by mass spectrometry within the different isoforms of the NS5A peptide associated with the p58 form of the protein.
The intensities of each phosphosite identified are coloured from 0 (green) to high intensity (red) with yellow for intermediate values. The total intensities of NS5A (phosphorylated and nonphosphorylated NS5A counterpart) are coloured from the lowest to greatest values in a scale from blue to red.

phosphopeptide	phosphosites							protein
GSPPSEASSS ASQLSAPSLK	222	225	228	229	230	232	235	NS5A
ST-418	1,68E+09	2,80E+07	0,00E+00	0,00E+00	2,27E+07	3,75E+07	2,53E+07	3,53E+11
ST-449	2,13E+09	9,69E+07	0,00E+00	0,00E+00	3,73E+07	1,29E+07	3,55E+07	3,53E+11
411-ST	2,26E+09	9,41E+06	0,00E+00	0,00E+00	2,74E+08	0,00E+00	0,00E+00	3,14E+11
434-ST	2,47E+09	3,94E+08	6,80E+07	3,51E+07	4,84E+08	0,00E+00	1,02E+08	7,37E+11
J6-ST	1,36E+09	0,00E+00	0,00E+00	0,00E+00	0,00E+00	0,00E+00	4,84E+06	3,97E+11
385-ST	4,95E+08	0,00E+00	0,00E+00	0,00E+00	0,00E+00	0,00E+00	0,00E+00	2,46E+11
401-ST	2,76E+09	4,17E+08	0,00E+00	0,00E+00	0,00E+00	0,00E+00	0,00E+00	5,78E+11
407-ST	1,62E+09	0,00E+00	0,00E+00	0,00E+00	0,00E+00	0,00E+00	0,00E+00	4,09E+11
431-ST	4,51E+08	1,16E+08	0,00E+00	0,00E+00	3,75E+08	0,00E+00	1,42E+07	5,16E+11

IV.F Differential modulation of host pathways by Core sequences from various genotypes

With a high percentage of Core interacting partners being involved in the regulation of gene expression, we next undertook to investigate the effect of infection of Huh-7.5 cells with Core intergenotypic recombinant viruses expressing Core proteins derived from clinical isolates of genotypes 1, 3, or 4. Our aim was to further investigate potential differential regulations of gene expression induced by genotype 3 Core with respect to steatosis development. The examination of the abundance of cellular mRNAs was carried out using RNA extracts collected at 120h p.i., a late time point at which an infection rate close to 100% was observed for all viruses (Simon et al., unpublished data, see Supplementary Figure 2). Furthermore, it has been shown that from 96-120h p.i., the hepatocyte transcriptional deregulation profile is established and stable in partially differentiated Huh-7.5 cells infected with the subtype 2a Jc1 recombinant strain[530].

Four biological replicates of noninfected cultures or cultures infected with our panel of intergenotypic viruses or with the parental Jad strain were prepared. These experiments and preliminary analyses to address each of the questions related to independent gene expression were performed by Emeline Simon (former PhD student in our laboratory). The groups of viruses used and their respective Core genotypic origins are summarized in Table 18.

Jad/C1a-H77 Jad/C1a-411	**Genotype 1**
Jad/C2a-J6	**Genotype 2**
Jad *	
Jad/C3a-P98L Jad/C3a-376 Jad/C3a-389 Jad/C3a-390 Jad/C3a-395 Jad/C3a-401	**Genotype 3**
Jad/C4aR Jad/C4fC	**Genotype 4**

Table 18: Grouped list of Core intergenotypic recombinant viruses used for the study of genotype-specific, HCV-induced transcriptomic alterations with respect to steatosis development.
**Parental virus, the data of which were not used in the analyses presented here.*

The preliminary analysis of the data obtained towards the identification of enriched Core-regulated pathways was performed in collaboration with Dr Emeline Perthame from the Biostatistics Hub of Institut Pasteur and is presented in the following pages.

IV.F.(α) Correction of batch effect introduced by RNA extraction

Our data first underwent a correction of the batch effect which was introduced by performing the extraction of total RNAs from infected cells during different rounds, due to technical restrictions. The principal component analysis (PCA) obtained is presented in Figure 59. In panel A, the batch effect was evident since replicate samples unexpectedly segregated in two, well defined groups, a feature that was clearly visible for the control Mock infected and Jad infected samples. Hence, the batch effect was attributed to dimension 1 (Dim1), or principal component 1 (PC1), which accounts for over 83% of the variation observed in the gene expression levels in our data set. Dim2, or PC2 is the second level of variation, introduced by the infection with the different viral strains. Before batch correction it is evident that our observations are highly affected by the batch effect and the virus strain-induced variance is below 7%. In Figure 59B, following the batch correction of the whole dataset, as described in Materials & Methods, the PCA showed that replicate samples clustered closer together, as expected. The groups of Mock control and parent Jad segregated with clearly marked higher variance compared to the rest of the dataset, while the variance retrieved among the RNA reads in cells infected with the different Core intergenotypic recombinant viruses was surprisingly low, though in probable link with relatively conserved Core sequences. This shows that the batch effect was successfully masked and replaced by the viral strain as the first source of variation, then accounting for 56% of the observed differences. In this instance, Dim2 corresponds to the biological variability introduced by the replicate experiments, e.g. cell passage.

In order to focus on expectedly subtle transcriptional differences induced by these various Core sequences, in my PhD manuscript, transcriptomic analyses were performed exclusively with the intra-/inter-genotypic recombinant viruses compared to noninfected cells.

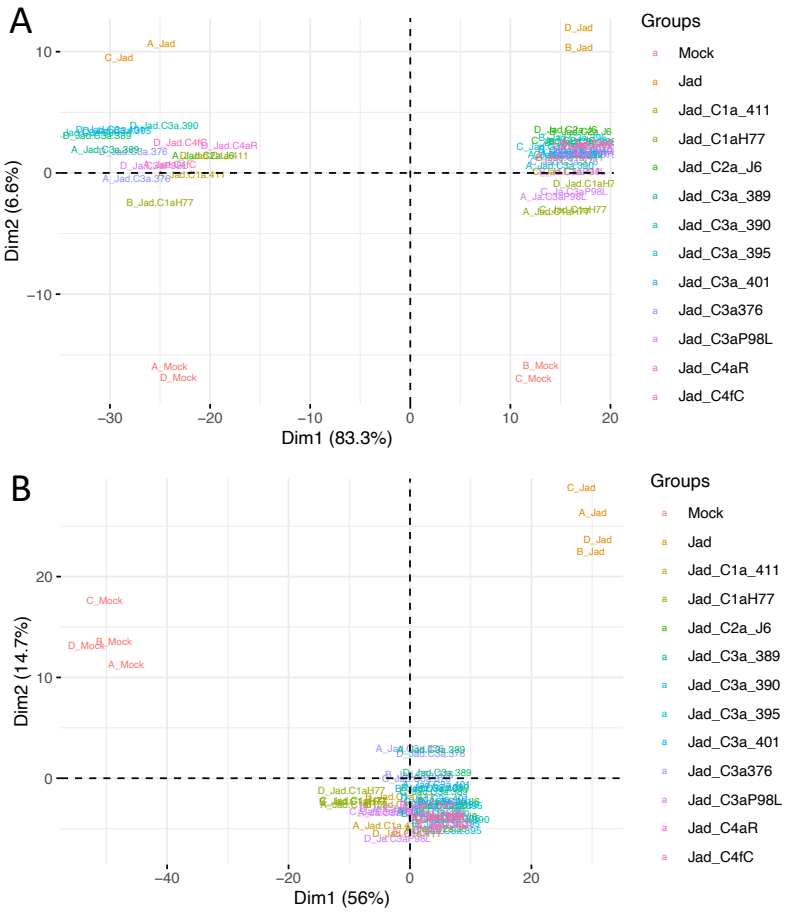

Figure 59: Principal component analysis (PCA) of the replicate samples of Core intergenotypic recombinants, the parental virus and mock infected control cells that underwent RNA-sequencing before (A) and after batch effect correction (B).
PCA dimensions 1 (Dim1) and 2 (Dim2) are illustrated with the respective PCA values in parentheses.

IV.F.(β) HCV induced deregulations irrespective of Core genotype

Comparative analysis of the genes significantly deregulated by infection compared to noninfected cells revealed 864 genes commonly deregulated by all Core recombinant viruses (Figure 60). Gene set enrichment analysis of these commonly deregulated genes using the Hallmark, KEGG, reactome and WikiPathways gene set databases highlighted interesting gene sets deregulated by all Core recombinants.

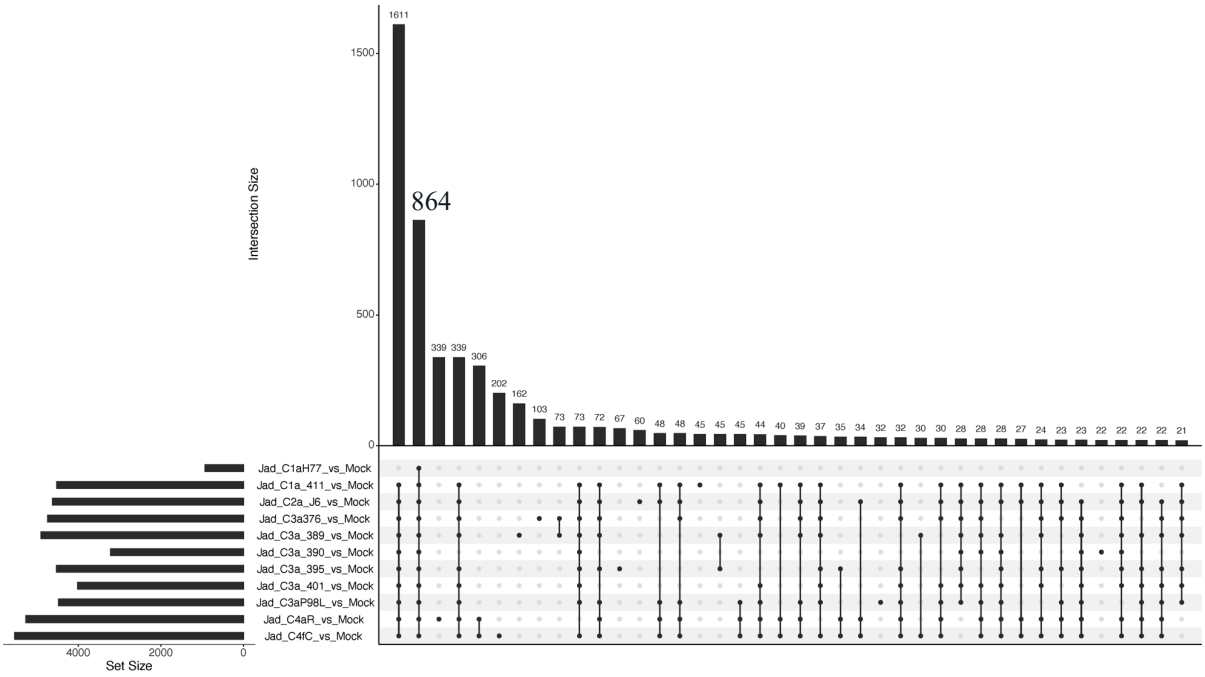

Figure 60: Comparative analysis of significantly deregulated hepatocyte genes identified by sequencing of total intracellular RNAs extracted from cells infected with each Core intergenotypic recombinant virus or noninfected (Mock) cells collected at 120h p.i.
In this up-set graph, black dots refer to the comparisons indicated on the left that apply to each bar. Values above bars indicate the number of significantly commonly deregulated mRNAs by the corresponding group of viruses.

More specifically, gene sets involved in intracellular transport, metabolism, and HCC related pathways (Figure 61) were found to be deregulated by all Core intergenotypic recombinants examined, as they were also found to be enriched in the NS5A PPI networks. Specific gene sets such as reactome glycolysis, amino acid transport across the plasma membrane, regulation of Insulin Like Growth Factor IGF transport and uptake by Insulin Like Growth Factor Binding Proteins IGFBPS, and Hallmark mtorc1 signaling were reproducibly enriched in a similar set of experiments aiming at identifying the Core induced transcriptional alterations in link with genotypes 1 and 4, further validating our data (Tabbal et al., data not shown). Gene sets related to glycolysis and gluconeogenesis were also found enriched in this list of genes commonly deregulated by all strains compared to mock infected cells.

We further identified gene sets, such as hypoxia and epithelial mesenchymal transition (EMT) significantly deregulated across HCV Core recombinant strains. This makes sense, as hypoxic conditions are known to enhance HCV replication[593], while the virus is also known to stabilize the hypoxia-inducible factor 1α (HIF-1α) through oxidative stress[594]. Similarly, EMT has been found to be induced by HCV in primary hepatocytes[595] and is known to be involved in the processes of fibrosis and HCC development.

The expression levels of a list of selected genes were examined based on the fact that their products or their expression levels have been reproducibly found associated with HCV-induced liver damage in cell culture or in the livers of infected patients[596-598,530], together with enzymes

known to be essential in the processes of β-oxidation and gluconeogenesis[599,598]. As shown in Figure 62, the expression of the majority of these selected genes was deregulated by infection to various extents. However, acetyl-CoA carboxylase alpha (ACACA), acyl-CoA synthetase long chain family member 3 and member 5 (ACSL3, ACSL5), FASN, forkhead box O1 (FOXO1), glucose-6-phosphate dehydrogenase (G6PD), 3-hydroxy-3-methylglutaryl-CoA reductase (HMGCR), PPARγ, scavenger receptor class B member 1 (SCARB1), sterol regulatory element binding transcription factor 2 (SREBF2), signal transducer and activator of transcription 3 (STAT3) and the hydroxyacyl-CoA dehydrogenases (HADH, HADHA and HADHB) were surprisingly not significantly regulated.

To the contrary, almost all of the remaining genes were deregulated by all Core proteins derived from the clinical strains to seemingly equal degrees. Notably, the very low-density lipoprotein receptor (VLDLR), the secretion pathway of which is used by HCV for egress was found significantly upregulated by all strains. The expression levels of PPARα αnd PPARγ were found unchanged, yet the PPARγ coactivator 1 alpha (PPARGC1A) gene transcription was found significantly elevated by infection. In accordance with the published literature, the pyruvate carboxylase (PC)[597] and the microsomal triglyceride transfer protein (MTTP)[600] were found downregulated by HCV, while the transcription of gene coding for alanine aminotransferase 2 (GPT2 - ALT) was found significantly elevated. Surprisingly, aspartate aminotransferase 1 and 2 (GOT1, GOT2 - AST) genes were significantly downregulated, and the carnitine palmitoyltransferase 1A (CPT1A) expression was more than doubled in infected versus non infected cells, in contrast to what has previously been reported in HCV infected patients[601,602].

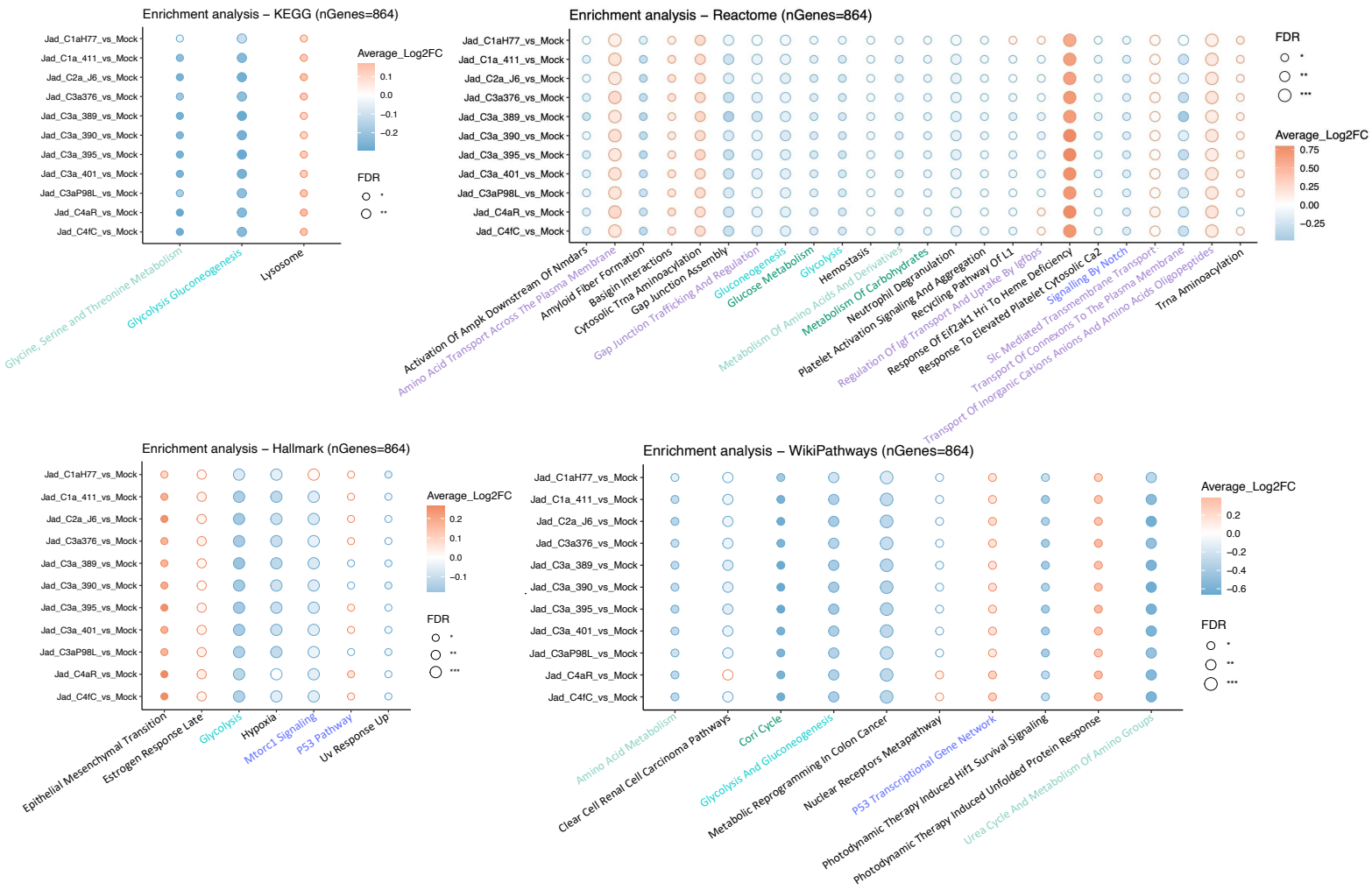

Figure 61: Gene Set Enrichment Analysis of genes commonly deregulated by Core intergenotypic recombinants in the steatosis-targeted studies.
Average Log_2 fold change within each enriched pathway is indicated by the node colour intensity of red for upregulated and blue for downregulated pathways with respect to noninfected cells, while the size of the node indicates the significance according to the false discovery rate (FDR). Pathways involved in the cellular processes highlighted by the enrichment of the NS5A PPI networks are shown in similarly-coloured fonts. IGF: insulin like growth factor, IGFBPT: Insulin Like Growth Factor Binding Proteins, Slc: solute-carrier.

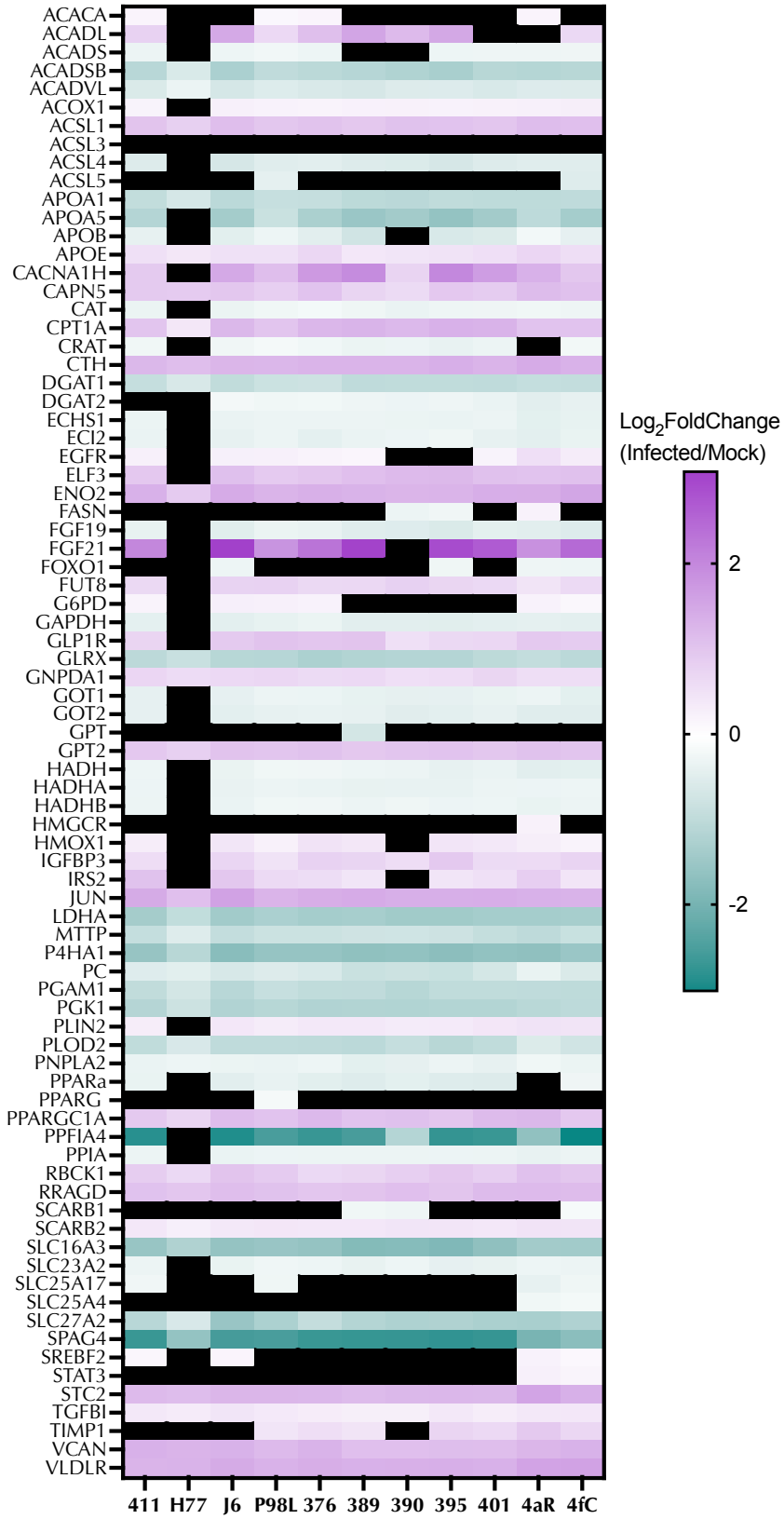

Figure 62: Expression levels of selected genes with respect to Mock infected cells, based on their roles in steatosis development, gluconeogenesis, β-oxidation and oxidative phosphorylation.
Differentially expressed genes (DEGs) are represented with heatmaps based on genes expression Table standardized with variance stabilizing transformation or batch correction expression Table and are listed by alphabetical order. Nonsignificant values (p-adjusted > 5%) are shown in black.

IV.F.(γ) Differential, genotype-specific Core-induced deregulations

Volcano plots of the genes deregulated between viral genotypes or groups of genotypes are shown in Figure 63A-E.

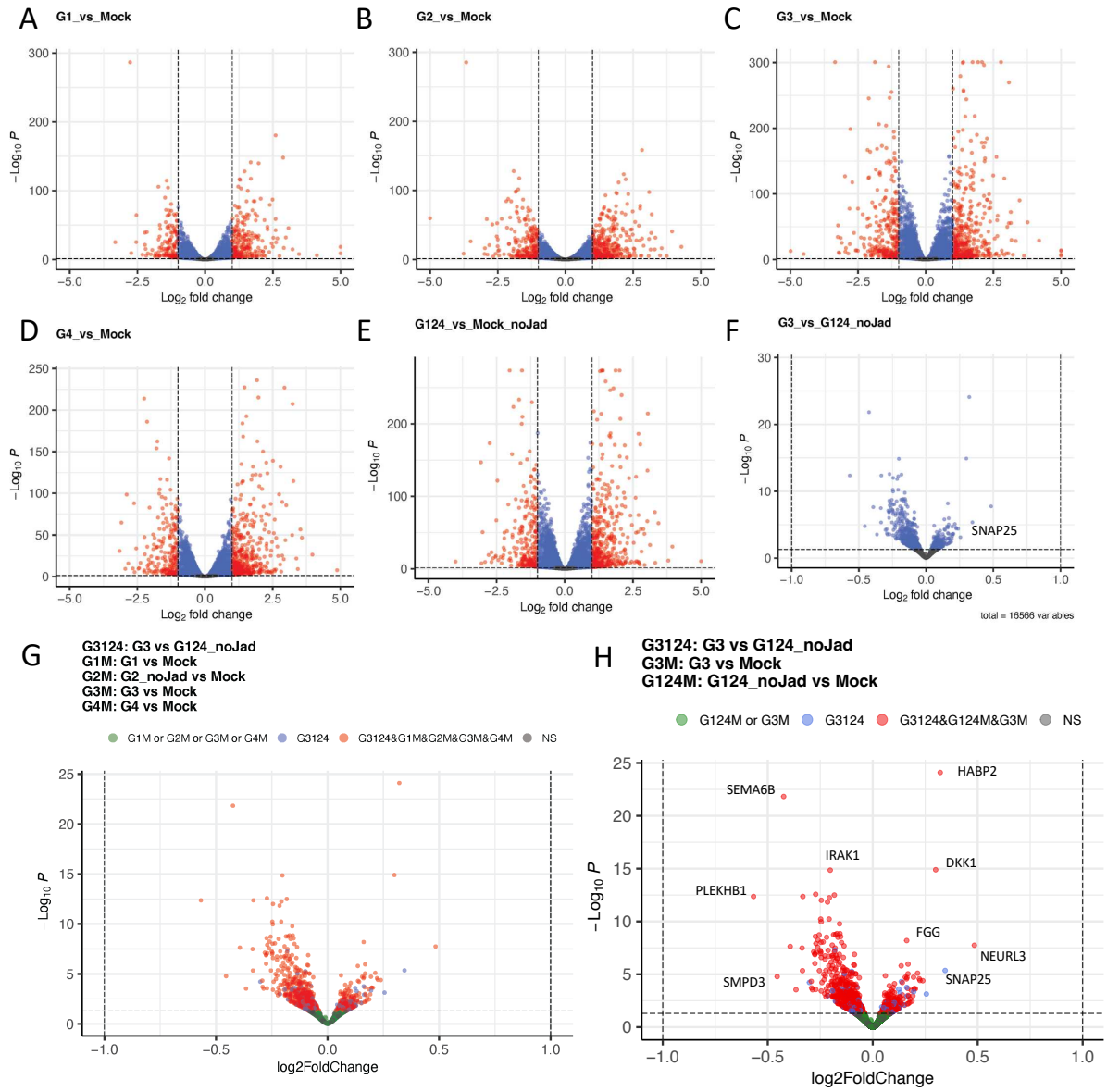

Figure 63: Volcano plots representing genes (dots) deregulated by each viral genotype or group of genotypes versus mock infected cells (A-E) or differentially deregulated genes between genotype 3 (G3) and nongenotype 3 (G124_noJad) strains (F-H).
In A-E, red dots represent genes above the $log_2FC=1$ or below $log_2FC=-1$thresholds. In G-H, green dots represent genes significantly deregulated between each of the compared groups and the mock condition, blue dots represent differentially expressed genes among the two compared conditions but not with respect to the control condition, while this comparison is taken into account in the red dots. Grey dots represent non significantly differentially expressed genes (NS). Some gene codes are assigned to corresponding dots.

To study the differential, genotype-specific Core-induced pathway deregulation, significance was obtained provided that we considered as differentially deregulated the genes and gene sets that were enriched not only in the comparisons among two genotypes or groups of genotypes (e.g. genotype 3 versus nongenotype 3), but also at least in one of the compared conditions versus the control, Mock infected cells. This strategy was undertaken in order to

identify even the slightest differentially deregulated genes or enriched gene sets without being poisoned by artifacts, that would come up as differentially deregulated parameters among two tested conditions, while they are actually not deregulated with respect to noninfected cells. One such example is highlighted when comparing SNAP25 in panels F and H of Figure 63. Interestingly, the more intuitively, biologically solid way to approach the differential deregulations induced by Core sequences of genotype 3 versus nongenotype 3 Core (Figure 63G) was to compare independently each set of strains of each genotype with the Mock, then to compare all of them together. The more sound choice from a statistician's perspective (Figure 63H) was to compare each group of genotypes with the Mock condition, then to compare groups of genotypes between them. No difference could be observed between the two retrieved volcano plots, allowing us to use the latter method in our analysis.

Gene set enrichment analysis performed on the batch-corrected data aimed at identifying Core genotype-specific deregulated pathways using the MSigDB Hallmark, KEGG, reactome, and WikiPathways gene sets. This analysis revealed enriched pathways commonly deregulated by all studied Core genotypes, highlighting global HCV-driven deregulations, as well as pathways differentially regulated among Jad recombinants expressing Core proteins derived from genotype 3a clinical strains in comparison to those expressing non-genotype 3a Core. The totality of enriched networks for Hallmark, KEGG, and WikiPathways is represented in Figure 65, while due to the length of the list, only selected reactome enriched gene sets are illustrated. The full list can be found in Supplementary Figure 3.

Overall, we observed a downregulation in the majority of Huh-7.5 pathways by infection with any recombinant virus, with a few exceptions. Gene sets previously identified to be enriched by all studied strains were also found to be commonly deregulated by all genotypes, with the expression of the respective genes being lower in infected than in noninfected cells. These include a wide range of metabolism related pathways, namely those involved in glucose-related energy metabolism (*Hallmark* glycolysis / *KEGG* glycolysis gluconeogenesis / *reactome* gluconeogenesis, glucose metabolism, glycolysis, glyoxylate metabolism and glycine degradation, pyruvate metabolism and citric acid TCA cycle, pyruvate metabolism / *WikiPathways* aerobic glycolysis, glycolysis and gluconeogenesis, glycolysis in senescence, cori cycle, glycogen synthesis and degradation), lipid metabolism (*Hallmark* peroxisome, bile acid metabolism, fatty acid metabolism / *reactome* β-oxidation of octanoyl CoA to hexanoyl CoA, β-oxidation of hexanoyl CoA to butanoyl CoA), protein metabolism (*KEGG* arginine and proline metabolism, alanine, aspartate and glutamate metabolism, cysteine and methionine metabolism / *reactome* branched chain amino acid catabolism, glutamate and glutamine metabolism / *WikiPathways* urea cycle and metabolism of amino groups, urea cycle and associated pathways, amino acid metabolism, biomarkers for urea cycle disorders), and pentose metabolism (*KEGG* pentose phosphate pathway, pyrimidine metabolism, purine metabolism, fructose and mannose metabolism, galactose metabolism, starch and sucrose metabolism / *WikiPathways* purine metabolism and related disorders).

On the other hand, the upregulated pathways are those involved in immune responses, e.g. *Hallmark* interferon alpha response / *reactome* interleukin 6 signaling / *WikiPathways* cytokines and inflammatory response, or in perturbation of cell cycle in link with HCC, such as *Hallmark* TNF-α signaling via NF-κB, TGF-β signaling / *reactome* MAPK1 Erk2 activation.

Interestingly, these pathways were found commonly down- or up-regulated by all strains, regardless of the Core genotype.

In fact, the direction of deregulation was found common among all genotype chimeras for all deregulated pathways, meaning that differential effects of Core from different genotypes would have to be investigated either in the absence/presence of regulation of certain pathways,

or at the level of induced deregulation. Indeed, the genes set enrichment analysis of the genes found significantly deregulated by infection with HCV expressing Core of genotype 3 versus Core of nongenotype 3 origin (Figure 63H) highlighted a number of differentially deregulated pathways (Figure 65).

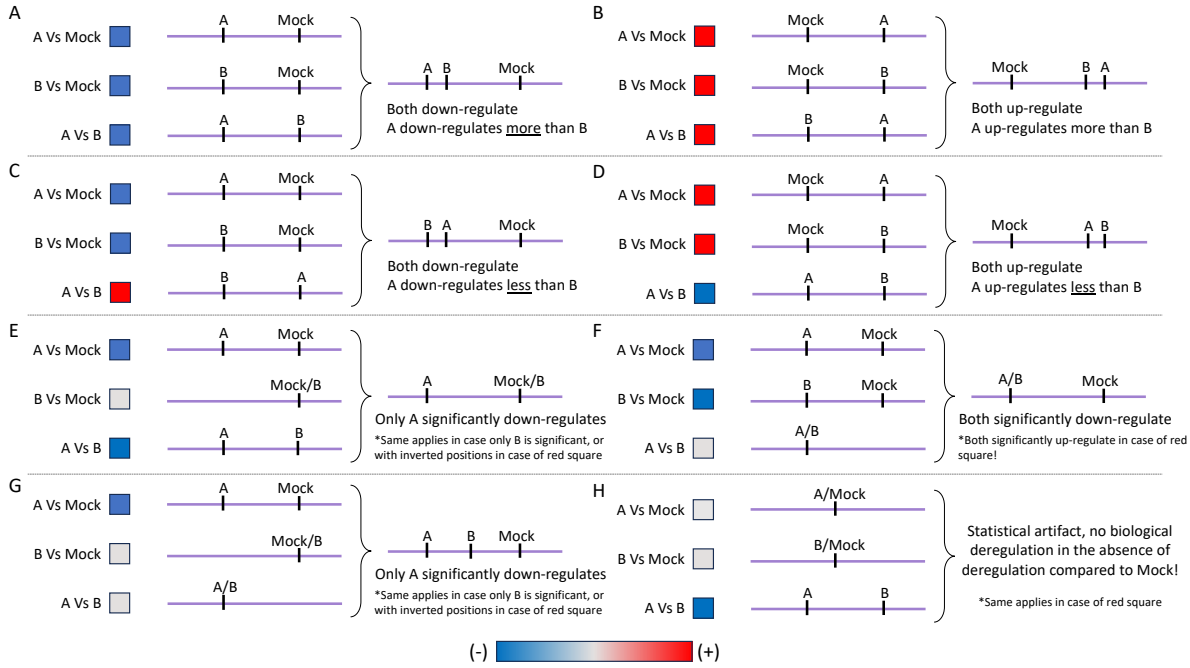

Figure 64: Pipeline to interpret the various scenarios of differential pathway enrichment.
An illustration of a scale used across our analyses is at the bottom of the figure without values. For a comparison of group A vs group B, a negative enrichment score, represented in blue suggests that the given gene set has lower expression in group A rather in group B. Inversely, for positive enrichment score (in red) and higher expression. An illustration of these scenarios is shown immediately at the right of the coloured boxes. The combined, final interpretation of enrichment, taking into account the enrichment score of each group with respect to Mock and the comparison between them is shown at the right of the brackets, accompanied by the respective conclusion.

The direction of deregulation between the genotype 3 versus the nongenotype 3 group is shown in the last column of each enriched gene set database (Figure 65). However, this is not informative to also conclude on the direction of deregulation with respect to Mock infected cells, that needs to be taken into consideration, as elaborated in Figure 64. For example, a negative enrichment score between the genotype 3 versus the nongenotype 3 groups could be any of the scenarios A, D, E or H of Figure 64, coming up with a different conclusion in each case.

Using this pipeline to analyse our data, we mainly came across a positive enrichment score of the G3 Vs G124 comparison (Figure 65), which, taken together with the negative enrichment score compared to Mock in the majority of the cases, indicated that in most instances Core of the non-3 genotypes induce a stronger gene downregulation than Core of genotype 3 (case C in Figure 64). This is particularly true for many HCC-related pathways found differentially enriched, such as the *Hallmark* c-Myc targets V1 and the *reactome* regulation of PTEN stability and activity gene set, with tumor suppressor Phosphatase and tensin homolog deleted on chromosome ten (PTEN) reduced expression associated with HCC in human livers (for review see Peyrou et al.[603]). Surprisingly, some sets of genes involved in metabolic pathways were also found more downregulated by the expression of nongenotype 3 Core over genotype 3 Core, including metabolism of amino acids, such as the highly recurrent oxidative phosphorylation pathway.

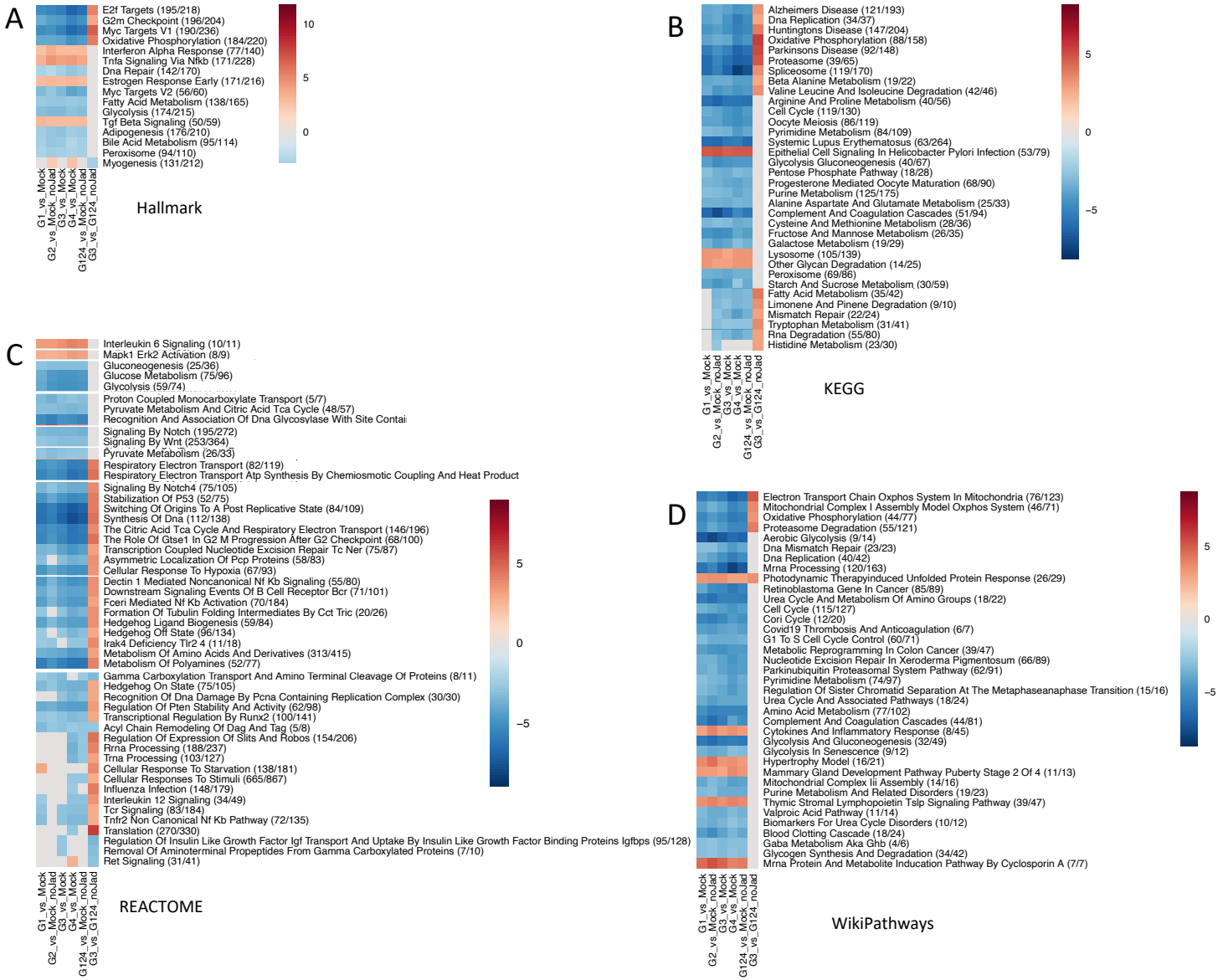

Figure 65: Pathways and gene sets deregulated between groups of genotype 3 Vs vs nongenotype 3 Core intergenotypic chimeras were represented by heatmaps based on the CAMERA analysis output (limma R package).

Enrichment score computed by CAMERA was used as a proxy of the regulation direction of significant genes sets (p-adjusted < 5%) and the scale for each gene set database illustrated are added on the right. Positive enrichment score (in red) suggests higher expression of the respective gene set in group A rather in group B for each A Vs B comparison. Similarly for negative enrichment score (in blue) and lower expression. All enriched gene sets of MSigDB Hallmark (A), KEGG (B) and WikiPathways (D) are represented, while only selected enriched reactome gene sets are shown (C). Comparisons among HCV genotypes (G) and Mock infected cells are shown in the first five columns, while genotype 3 (G3) versus nongenotype 3 (G124_no Jad, excluding the parent Jad) comparisons are shown in the last column.

However, we also did retrieve pathways that were either exclusively deregulated by or more deregulated in the presence of Core from genotype 3. Interestingly, genes involved in the hydrolysis of DAG and TAG fatty acids by patatin-like phospholipase domain-containing proteins 2 and 3, PNPLA2 and PNPLA3 (*reactome* acyl chain remodelling of DAG and TAG) were found more downregulated by genotype 3 Core, suggesting a G3 Core-driven accumulation of DAG and TAG in hepatoma cells. Excess lipid storage in hepatocytes in the form of LDs is the hallmark of hepatic steatosis. In accordance with toxic lipid accumulation in the form of DAG and TAG, the genes involved in UPR were also found more upregulated in genotype 3 Core expressing infected cells. The role of UPR in lipid homeostasis and in relation to hepatic steatosis is very eloquently described in a review by Song et al[604]. Lastly, the significant, differential upregulation of the *reactome* "metallothioneins bind metals" and "response to metal ion" gene sets, in combination with the differential downregulation of the "zinc influx into cells by the slc39 gene family" suggests an increased oxidative stress when Core of genotype 3 is expressed.

Part 2: Surrogate animal model for the study of hepacivirus-driven metabolic disorders

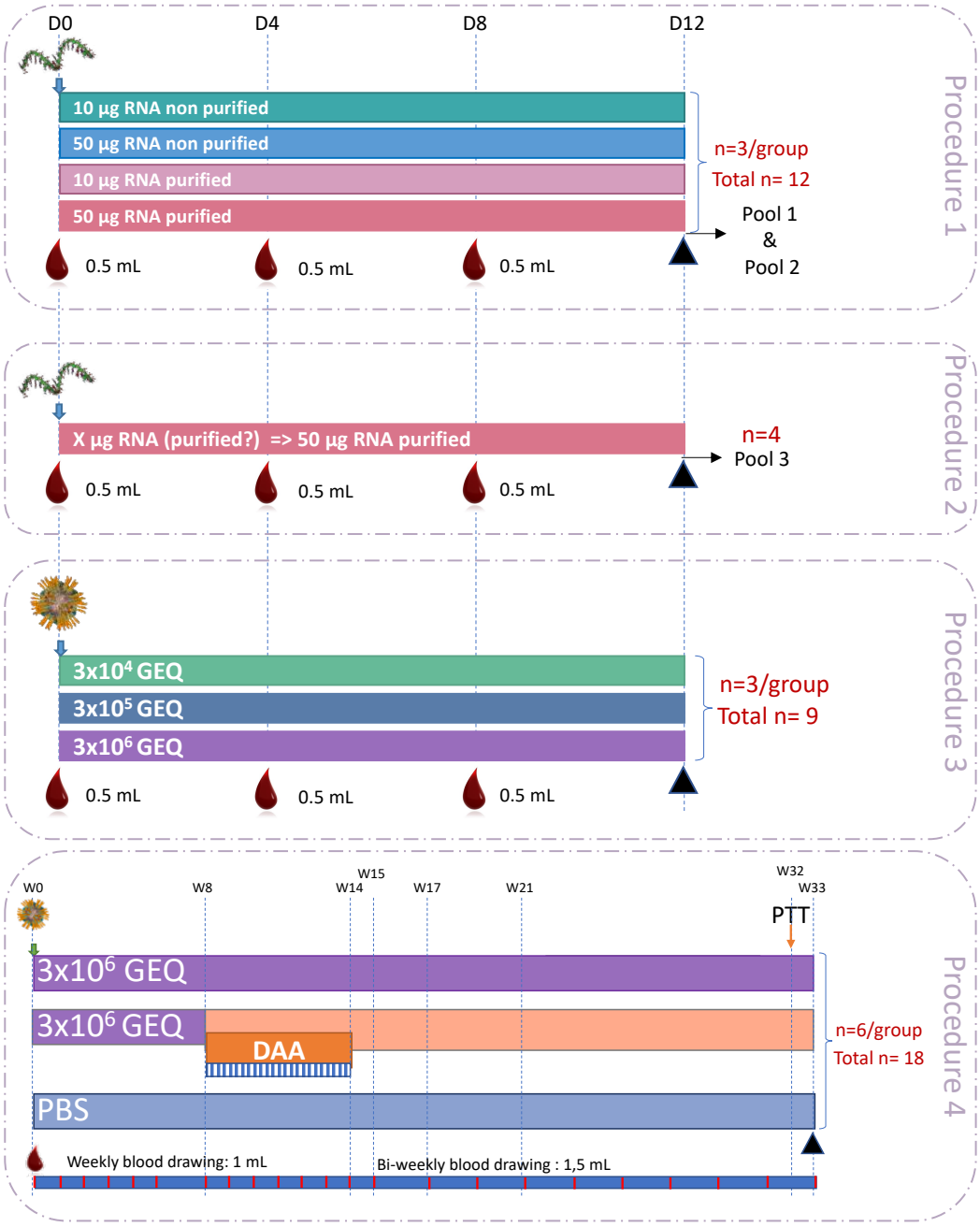

Figure 66: Summary of experimental procedures towards setting up RHV-rn1 Sprague Dawley rat infection model.

Procedure 1 & 2: Intrahepatic inoculation of the indicated quantities and purification status of RHV-rn1 genome-length RNA in Sprague Dawley rats. Each group consisted of 3-4 rats. By the end of this procedure, rat sera titrating around similar GEQ/mL were pooled together, generating virus stocks Pools 1-3. Procedure 3: Intravenous inoculation of the indicated GEQ quantities of Pool1 stock serum in three groups of rats. Each group consisted of 3 rats. Procedure 4: Intravenous inoculation of the indicated GEQ quantities of Pool1 stock serum in two groups of rats or PBS. Each group consisted of 6 rats. One of the two infected groups received HCV-specific antiviral treatment (Maviret) for six weeks. PTT: Pyruvate Tolerance Test; GEQ: genome equivalent; DAA: direct antiviral agent.

In order to tackle the mechanisms of hepacivirus-driven metabolic disorders and putative contribution of co-morbidity factors like western diet, and challenge our finding in HCV-infected cell culture systems, an *in vivo* immunocompetent model of infection was required. Our aim was to set up the surrogate RHV-rn1-based rat model initially described in the US and bring proof of concept that it was amenable to such hepacivirus-linked pathobiology studies. This led us to the experimental work summarized in Figure 66.

IV.G Setting up of RHV-rn1 Sprague Dawley rat infection model

IV.G.(α) Production and characterization of RHV-rn1 viral stocks

Towards production of viral stocks, starting from a fully sequenced RHV-rn1 cDNA, synthetic, genome-length RNAs were produced and intrahepatically inoculated in Sprague Dawley rats, as described in §0 and shown in Figure 66, Procedure 1. The quantity of inoculated RNA and/or the purification status of the inoculum may affect the efficacy of the procedure (A. Martin, personal communication). Therefore, the first step was to establish the best condition by inoculating two different quantities (10µg or 50µg) of purified or nonpurified genome-length *in vitro* transcribed RHV-rn1 RNA in four groups of three rats. One rat that received 10µg of nonpurified RNA passed away the day following the procedure. Viral titers in rat sera were monitored at day 12 post-inoculation by RT-(q)PCR, as described in §III.L.(γ). No consistent effect of RNA quantity or purity was observed on the titers. Hence, sera from three rats with similar titers were pooled together, generating the first two viral stocks, as shown in Table 19.

Table 19: Sprague Dawley rat intrahepatic inoculations with genome length RHV-rn1 RNA towards viral stock production.
10 or 50µg of in vitro transcribed, purified (P) or nonpurified (NP) RNA were inoculated in the respective groups of rats (1-3). Rat 10NP1 did not survive until day 12. GEQ: genome equivalent.

Time post-inoculation	Rat serum Nº	Titer (GEQ/mL)	pool 1	pool 2
12d p.i.	50NP1	1,01E+09		
	50NP2	5,46E+07		
	50NP3	4,43E+08		
	50P1	2,13E+08		
	50P2	1,73E+08		
	50P3	2,63E+08		
	10NP2	1,86E+08		
	10NP3	4,33E+08		
	10P1	3,38E+09		
	10P2	1,14E+09		
	10P3	3,95E+08		

Since the viral titers in rats inoculated with 50µg purified RNA were the most consistent, this condition (same batch of RNA transcripts as in Procedure 1) was chosen for the generation of viral pool 3 (Figure 66, Procedure 2). All three pools were sequenced by next generation sequencing, as described in §III.L.(δ), and re-titrated by RT-(q)PCR. Final viral titers of the three stocks and identified quasi-species identified by NGS are summarized in Table 20. NGS coverage was satisfactory with means of ~360, 290, 55 reads per nt position for pool stocks 1, 2, 3, respectively. One synonymous quasi-species, C384T (Gly>Gly) in Core coding sequence was identified in all three stocks with varying frequency (18-43%), possibly accounting for a spurious error of the T7 RNA polymerase upon synthetic RNA production. An additional

synonymous quasi-species (T8033C, Ile>Ile) was identified in NS5B coding region of pool 3 with low frequency (6.9%), while in pool 2 a low frequency (7.7%) of a non-synonymous quasi-species (T1936C) leading to Val/Ala change was found withing E2 coding sequence. Altogether, no consistent quasi-species or mutation emerged, demonstrating that the RHV genomic sequence of the initial clonal inoculum was stable *in vivo* at this early time post-infection. Thanks to its highest viral titer and lack of significant mutations, pool 1 was used in further experiments.

Table 20: RHV-rn1 stock characteristics. GEQ: genome equivalent.

	RHV-rn1 stock		**Next Generation Sequencing data**					
	Titer (GEQ/mL)	Total Volume (mL)	Genome Position	Nucleotide quasi-species	Quasi-species Frequency	Protein region targeted	Encoded amino acid change	Note
pool 1	5.2 x 10^8	6,3	384	C >T	18.4%	Core	—	Silent
pool 2	1.4 x 10^8	6,4	384	C >T	23.7%	Core	—	Silent
			1936	T > C	7.7%	E2	Val > Ala	Low frequency
pool 3	5.0 x 10^7	9,3	384	C >T	43.3%	Core	—	Silent
			8033	T > C	6.9%	NS5B	—	Silent

Next, we examined conditions of intravenous RHV-rn1 inoculation for successful infection of rats (Figure 66, Procedure 3). To this end, three groups of three rats were infected by the intravenous route with 3x10^6, 3x10^5, or 3x10^4 GEQ of pool 1 RHV-rn1 stock. Viral titers were measured in rat sera at 4, 7 and 11days p.i. by RT-(q)PCR (Table 21). One rat receiving 3x10^5 RHV-rn1 GEQ and one rat receiving 3x10^4 RHV-rn1 GEQ did not survive throughout this follow-up period, limiting the statistical significance of the group size numbers for the two lower doses inoculated.

No consistent virus dose-specific effect was observed in this experiment. The lowest-titrated inoculum led to viremia as high as in the group of rats which received the highest dose, while viral loads varied by up to 7-fold among animals inoculated with the same dose. We decided to use the 3x10^6 GEQ dose in the subsequent experiment.

Table 21: Monitoring of viremia in rats intravenously inoculated with various doses of RHV-rn1. *GEQ: genome equivalent.*

Virus dose	Rats	Serum viral titer (GEQ/mL) at day p.i.		
		4	7	11
3x10^6 GEQ	1	1,3E+07	3,8E+07	1,6E+08
	2	7,7E+06	4,3E+07	1,3E+08
	3	9,7E+06	3,4E+07	7,9E+07
3x10^5 GEQ	4	7,1E+07	5,8E+07	1,4E+08
	5	5E+06	1,1E+07	2,1E+07
3x10^4 GEQ	6	2,5E+08	1,8E+08	3,6E+08
	7	2,4E+07	4,6E+07	1,5E+08

IV.G.(β) RHV-rn1 induces chronic infection.

In order to corroborate in our system the findings of chronic RHV-rn1 infection rate described in Trivedi et al.[468], six Sprague Dawley rats were infected by intravenous inoculation of 3x10^6 RHV-rn1 GEQ from pool 1, while six rats were "mock" infected by intravenous inoculation of PBS (Figure 66, Procedure 4). Rats were bled weekly or bi-weekly and viral titers were monitored for a course of 227 days. As shown in Figure 67 all six rats of the infected

group were successfully infected at 7 d p.i. and serum measurements of all noninfected rats were below the limit of detection for the duration of the experiment. For all animals, viral titers peaked at 10^8-10^9 GEQ/mL from the first time p.i. measured at 4d p.i., then started to progressively slowly decreased. Five out of the six rats (~85%) remained chronically infected throughout the observation period with titers ranging from ~$5x10^6$ to 10^8 GEQ/mL. The sixth rat exhibited suppression of the viremia starting from day 56 and remained under or close to the detection limit from this time-point on until the end of this study. Occasional virus clearance was also reported by Trivedi et al.[468] in HTZ rats infected with RHV-rn1, but had not been described in Sprague Dawley rats yet. High chronic infection rate thus appears to be a common attribute of RHV infection in rats and HCV infection in humans, with similar percentage of occurrence[287,288]. RHV-rn-1 loads were between $4x10^6$ and $4x10^7$ GEQ/mL at the time of sacrifice.

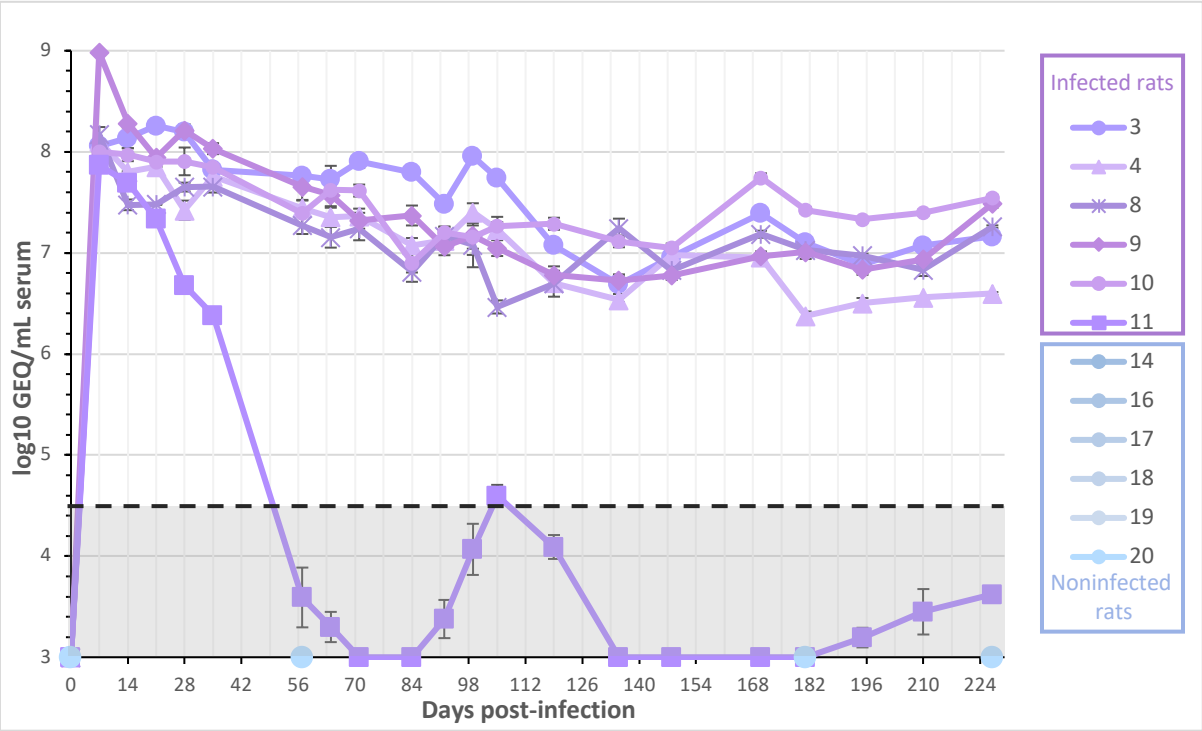

Figure 67: RHV-rn1 RNA titers measured in the serum of infected and noninfected Sprague Dawley rats.
Six rats were infected with $3x10^6$ genome equivalents (GEQ) pool 1 RHV-rn1, shown in shades of purple. In noninfected rats (shades of blue), PBS was intravenously inoculated. Serum was collected at the indicated time-points and viral RNAs were extracted and quantified by RT-(q)PCR. Titers are expressed in GEQ/mL serum.

Infection had no effect on rat weight, as indicated in graph A of Figure 69. Although not significant, infection tended to lead to an increase of rat liver weight, as measured at the time of sacrifice and to liver over body weight, as shown in graphs C and D of Figure 69, respectively. A macroscopic examination showed that the livers of infected rats were pale in

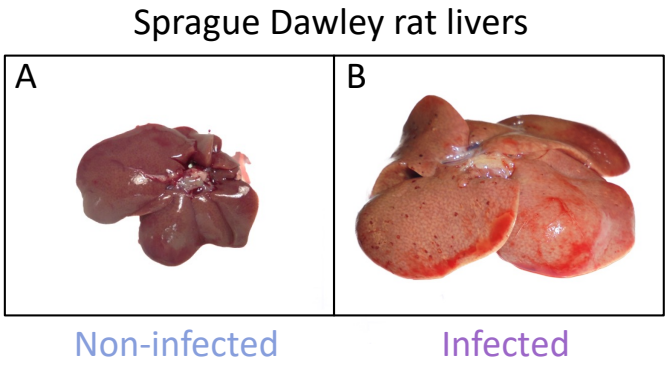

Figure 68: Representative photos of (A) noninfected or (B) RHV-rn1 infected Sprague Dawley rat livers.

colour and enlarged in size, reflecting potential lipid accumulation and hepatomegaly (Figure 68).

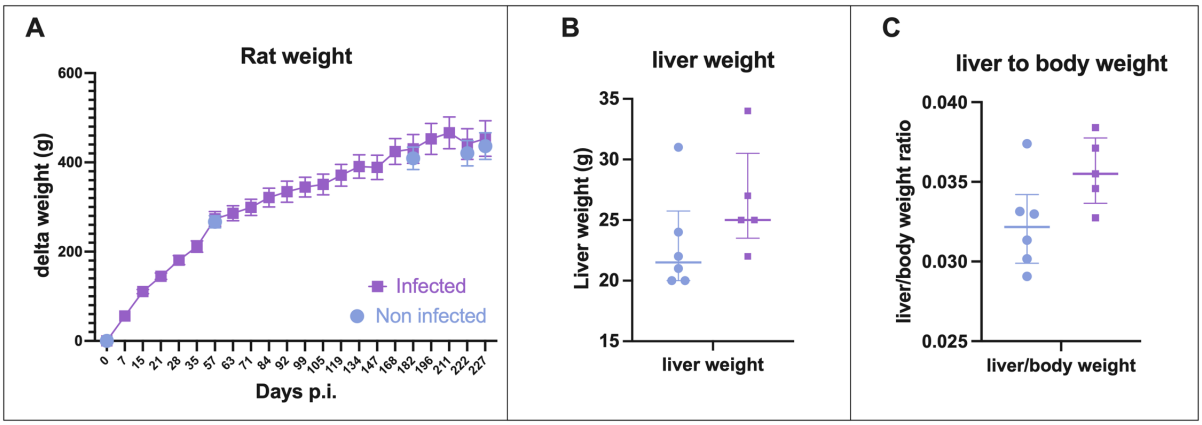

Figure 69: Effect of RHV-rn1 infection on rat body and liver weights.
Weight (grams) gained by rats over the course of the experiment (A). Liver weight (B) and liver to body weight ratio (C), as measured at the time of euthanasia at day 227 post-infection. Infected rat values are shown in purple, while noninfected condition is depicted in light blue.

IV.G.(γ) HCV Maviret therapy is ineffective when administered orally to RHV-rn1 infected Sprague Dawley rats.

In an effort to clear RHV-rn1 infection and evaluate the evolution of various parameters following virus clearance, we also examined whether the readily available, HCV-specific therapeutic regimen *Maviret* could be effective against RHV-rn1. As mentioned in §I.B.ζ.(ii), *Maviret* is the combination of two DAAs, one against HCV NS3 protease, glecaprevir, and one targeting NS5A, pibrentasvir. Dr Stéphane Bressanelli (I2BC Paris Saclay, Paris, France) recently generated a three-dimensional atomic model of RHV-rn1 NS3 protease domain using AlphaFold[605]. These studies revealed that the overall structure was relatively conserved compared to the crystallographic three-dimensional structure of HCV cognate protease. However, marked divergence in the vicinity of the active site of RHV and HCV NS3 proteases suggested that the former may be a poor target for at least some HCV-optimized protease inhibitors like glecaprevir (Tubiana & Bressanelli, data not shown). This is in agreement with the findings of Wolfisberg et al.[546], who reported lack of inhibition of RHV subgenomic RNA replication in rat or mouse hepatoma cells treated with glecaprevir. For the non-enzymatic NS5A with the largely unstructured domains II and III, refined predictive structural models would be required, moreover, the exact mechanism of action of pibrentasvir, hence docking of the compound on HCV NS5A has not been solved.

Maviret was administered in another group of six infected rats at 56d (8 weeks) p.i. and for the course of 6 weeks, as described in §III.M. The viremia pattern in this group of rats was very similar to what was observed in the other group of infected rats described above during the first 4 weeks p.i. (Figure 70).Animals were assigned to the treated and untreated groups based on serum viral titers at 35d p.i., which were in the same range between 10^7 and 10^8 GEQ/mL in all animals except for rat 11, in which RHV load had started to decrease and which was therefore attributed to the untreated group. Of note, rats 1, 2 and 12, assigned to the treated group, actually turned out to have slightly decreased RHV loads at the time of treatment initiation (< 10^7 GEQ/mL). As shown in Figure 70, viral titers remained stable during the treatment window for both treated and nontreated rats, ranging between approximately 10^7 to 10^8 GEQ/mL, except for the 3 rats, which had already a declining viremia before the treatment onset and showed stable lower titers (~1-5x10^6 GEQ/mL) during the treatment period. RHV

titers appeared more variable in the treated group when compared to the nontreated rats, however no statistically significant variation was observed between the two groups, neither during the administration period, nor in the following weeks.This indicates that either the HCV-specific DAAs of this regimen cannot interfere with the function of cognate RHV proteins, or the DAA mode of administration, dose, and/or bioavailability were not appropriate in rats.

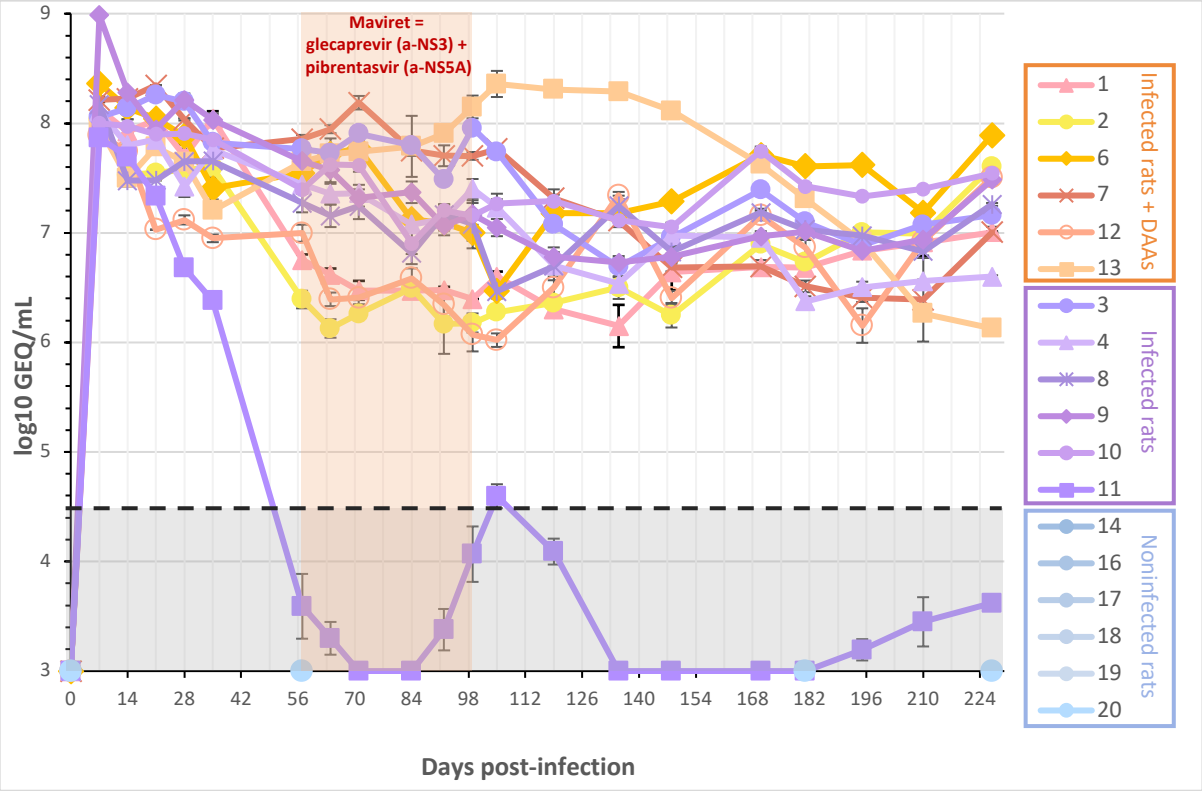

Figure 70: Effect of Maviret treatment on the RHV-rn1 RNA titers measured in the serum of infected treated, infected untreated and noninfected Sprague Dawley rats.
Twelve rats were infected with 3x10^6 GEQ of RHV pool 1 and six rats were inoculated with PBS. Serum was collected at the indicated time-points and RHV loads were quantified by RT-(q)PCR and expressed in genome equivalents per serum mL (GEQ/mL). Six infected rats (illustrated in shades of orange) received Maviret by gavage during a period of six weeks, as depicted by an orange area. Six untreated infected rats are shown in shades of purple, while the six noninfected rats are represented by blue dots.

IV.H Preliminary results support that RHV-rn1 induces similar liver disorders in Sprague Dawley rats as HCV in humans.

IV.H.(α) Steatosis

The livers of 6 noninfected rats and 5 chronically infected rats were examined at 33 weeks p.i., i.e. more than 8 months after virus infection. Hematoxylin and eosin (H&E) staining of livers sections revealed higher steatosis grade and higher inflammation in infected animals, yet without reaching statistical significance with these small cohorts and type of staining (Figure 71A-B). Importantly, neutral lipid quantification following Oil Red O (ORO) staining of liver sections showed significant accumulation of LDs in infected livers as compared to noninfected livers (Figure 71C-D).

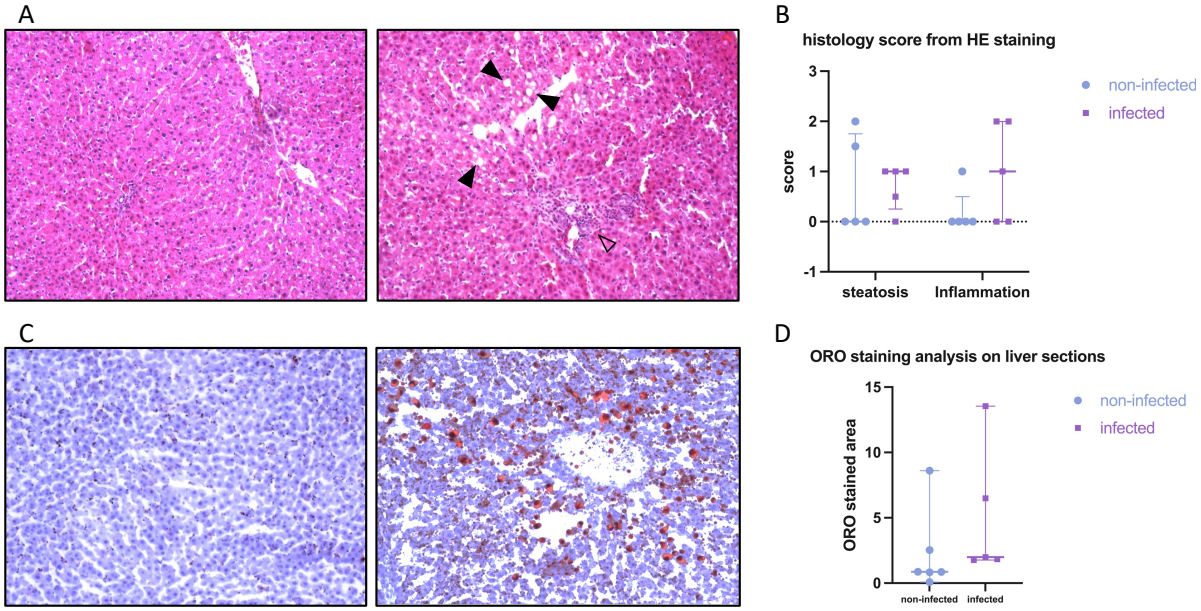

Figure 71: Histopathological analysis of liver sections.
(A, B) Scoring of inflammation and steatosis in RHV infected liver sections stained with H&E. Examples of periportal inflammatory foci (open arrowhead) and steatosis (filled arrowheads) are shown in (A). Steatosis and inflammation were evaluated in 4 liver sections per animal with steatosis score defined as: 0, <5% of hepatocytes in the field; 1, 5-33%; 2, 33-66% and 3, >66%, and inflammation score, as: 0, no inflammation in the field; 1, <2 inflammation foci per field; 2, 2-4 inflammation foci, 3, >4 inflammation foci. Results are plotted in (B) for the n=5 infected animals and n=6 noninfected rats. Field of view: 200X. (C, D) Scoring of lipid droplet accumulation in RHV infected livers. Representative images show ORO staining of LDs in red (C). The extent of ORO-stained areas evaluated from 4-5 liver sections per animal has been quantified (D).

IV.H.(β) Alterations in glucose metabolism

To test estimate gluconeogenesis in the livers of infected and noninfected rats, we performed a pyruvate tolerance test (PTT) at 8 months p.i. (222d p.i.). PTT indirectly measures gluconeogenesis by assessing the levels of glucose following administration of pyruvate and its conversion to glucose. As shown in Figure 72A, we found that glucose production was statistically significantly increased in infected versus noninfected rats during PTT, indicating impaired liver gluconeogenesis in all infected animals. In addition, there was a highly

significant positive correlation between fasted glycemia before and during the test (T0 and T+60min glycemia) and viral titers (Figure 72B).

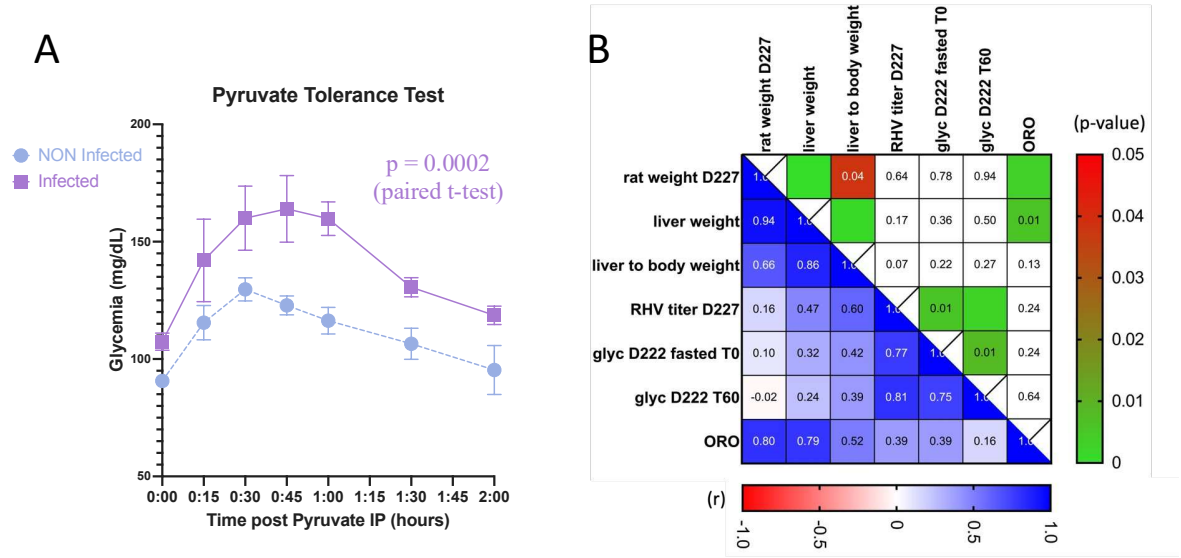

Figure 72: Assessment of gluconeogenesis in RHV infected rats.
(A) Pyruvate Tolerance Test (PTT) results. Mean glycemia measurements in RHV infected rats (purple, n=5) versus noninfected (blue, n=6) over the 2h observation period. (B) Linear correlations by Pearson testing between rat/liver weight characteristics, RHV titers at 227d p.i. (D227) and observed liver damage. Pearson correlation coefficient (r) is illustrated in the bottom left triangle, while respective p-values are illustrated on the remaining top half. Glyc: glycemia measured in mg/dL before (T0) and during PTT (T60); ORO: Oil Red O staining assessment of liver steatosis.

IV.H.(γ) Serum biochemical parameters

HCV infection may induce severe alterations in serum biochemical parameters due to the excessive liver damage. We examined whether RHV infection induced similar alterations of several biochemical parameters, namely urea, creatinine, urea/creatinine ratio, total protein, glucose, cholesterol, total bilirubin, uric acid, alanine aminotransferase, aspartate aminotransferase, alkaline phosphatases, gamma glutamyl aminotransferase, creatinine kinase, amylase, calcium, phosphorus, albumin, globulins and albumin/globulin ratio. We found no statistically significant differences between infected and noninfected groups at 8 months p.i. (227d p.i.) for any of the tested parameters. However, there was a trend for higher values for glucose in infected with respect to noninfected animals, in line with PTT data (Figure 73), as well as for aspartate aminotransferase, alanine aminotransferase and total bilirubin, indicative of liver damage.

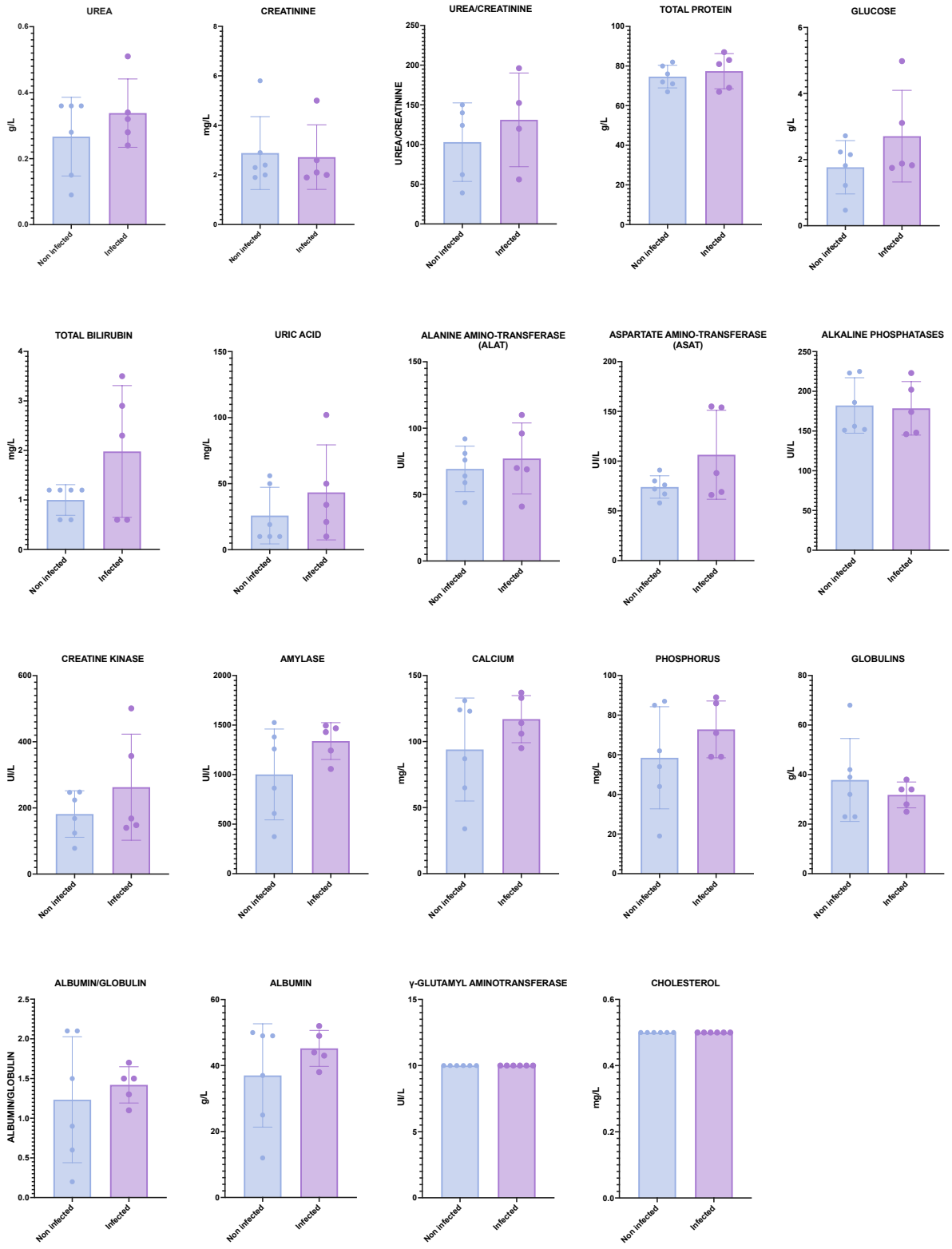

Figure 73: Assessment of serum parameters in infected rats.
Indicated biochemical parameters were measured in blood samples of RHV infected (purple, n=5) and noninfected rats (blue, n=6) collected at day 227 p.i.

IV.H.(δ) Lipid and metabolic alterations in rat livers during infection

A pilot metabolomic/lipidomic analysis of the livers recovered from 5 chronically infected and 6 noninfected rats at 8 months p.i. was then undertaken. The rat who exhibited spontaneous clearance (rat 11) was also independently included as a single representative of a third "group" in this analysis. Frozen liver tissue retrieved upon sacrifice was homogenized and separated in aqueous and nonaqueous phases. Fifty-six metabolites were analysed from the polar phase by NMR, while lipids were analysed from the nonpolar phase by gas chromatography coupled to mass spectrometry (GC/MS) or nano LC-MS/MS. These analyses allowed us to list and quantify most metabolites from the central carbon metabolism (glycolysis, TCA cycle, gluconeogenesis), as well as all lipid metabolites, including FAs, the major building blocks of membrane lipids, phospholipids (structural components of biological membranes), and neutral lipids (DAG, TAG, cholesterol, and cholesteryl-esters).

We found no observable difference in the total lipids quantified among chronically infected and noninfected rats (Figure 74A), but we did observe a notable trend in infected rats displaying higher concentrations of total fatty acid abundance (Figure 74B).

Furthermore, the abundance of different subsets of hepatic lipids were significantly modified by RHV infection. We noted a significant increase in cholesteryl ester (CE) and DAG in chronically infected livers (Figure 74C). Interestingly, for these lipid subsets, corresponding values in the single case of spontaneous clearance were close, if not lower than those of noninfected rats, providing a first hint in support of either absence of alteration of metabolic and lipid homeostasis during acute infection or regression of altered parameters back to normal following virus clearance.

CE fatty acid composition is a typical biomarker of fatty acid intake from the diet, such as polyunsaturated FAs (C18:3, C20:5, C20:4). Interestingly, we found that the composition of CE was profoundly impacted by RHV infection, since most molecular species of CE were significantly deregulated (Figure 75A). Most importantly, the levels of CE 20:4 were significantly decreased in infected livers, whereas levels of CE18:1 were found significantly increased. Typically, this suggests that RHV infection may have a direct impact on immune responses in infected livers concomitantly to a putative boost in membrane biogenesis in these infected individuals. Indeed, C20:4 is the precursor for the synthesis of most pro-inflammatory molecules (prostaglandin, leukotriene) and C18:1 (oleate) is more often used as the main building blocks of membrane lipids and/or lipid storage. This is in line with previous observations made in HCV infected cultured cells, in which the remodelling of ER membranes to produce the membranous web supporting genomic replication was accompanied by an increase in C18:1 content[606]. Thus, our observations could possibly reflect both the modulation of membrane biogenesis, favouring viral propagation, and a putative downregulation of the host immune response, also favouring RHV replication. Such intriguing results could indicate a metabolic reprogramming of the host upon viral infection, which begs for further analyses and experimental confirmation.

Similarly, certain molecular species comprising FFAs, DAG and TAG were affected to different degrees by infection (Figure 75B-D). More specifically, significant deregulations were found for palmitic (16:0), heptadecanoic (17:0), oleic (18:1), and behenic (22:0) free fatty acids. In support to HCV-related data[606], a significant enrichment of short-fatty-acyl-chain DAG and TAG was observed in noninfected rats, while a preferential accumulation of longer fatty acyl chains was observed in the infected rats. In these preliminary data, it seems that the switch of preference from shorter to longer fatty acyl chain triacylglycerides (TAG) starts from 52 carbon atoms.

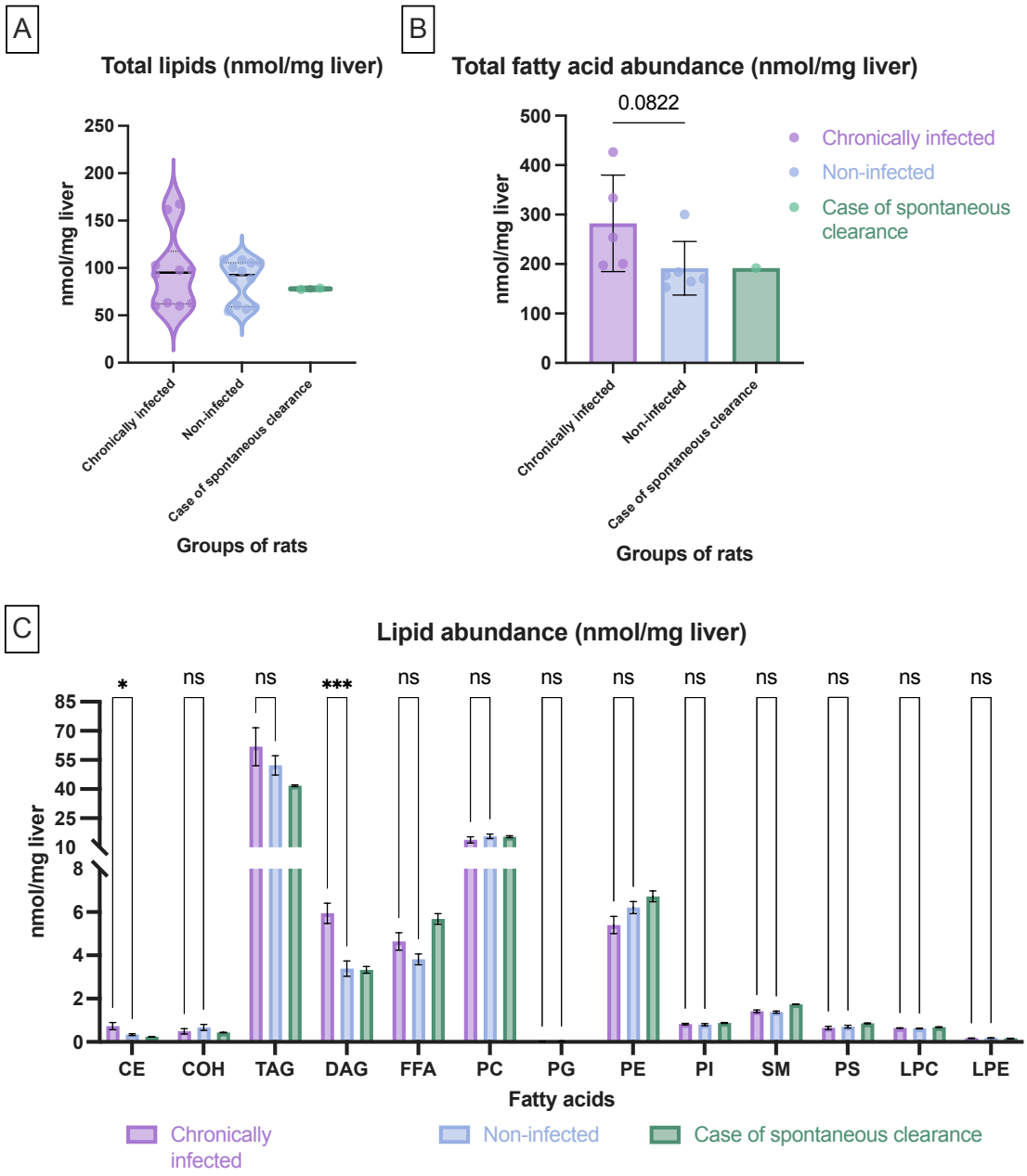

Figure 74: Lipid and fatty acid abundance in the liver of RHV chronically infected (purple), noninfected (blue) or infection-cleared rats.
CE: Cholesteryl esters, COH: Free Cholesterol, TAG: Triacylglycerol, DAG: Diacylglycerol, FFA: free fatty acids, PC: Phosphatidylcholine, PG: Phosphatidylglycerol, PE: Phosphatidylethanolamine, PI: Phosphatidylinositol, SM: Sphingomyelin, PS: Phosphatidylserine, LPC: Lysophosphatidylcholine, LPE: Lysophosphatidylethanolamine.

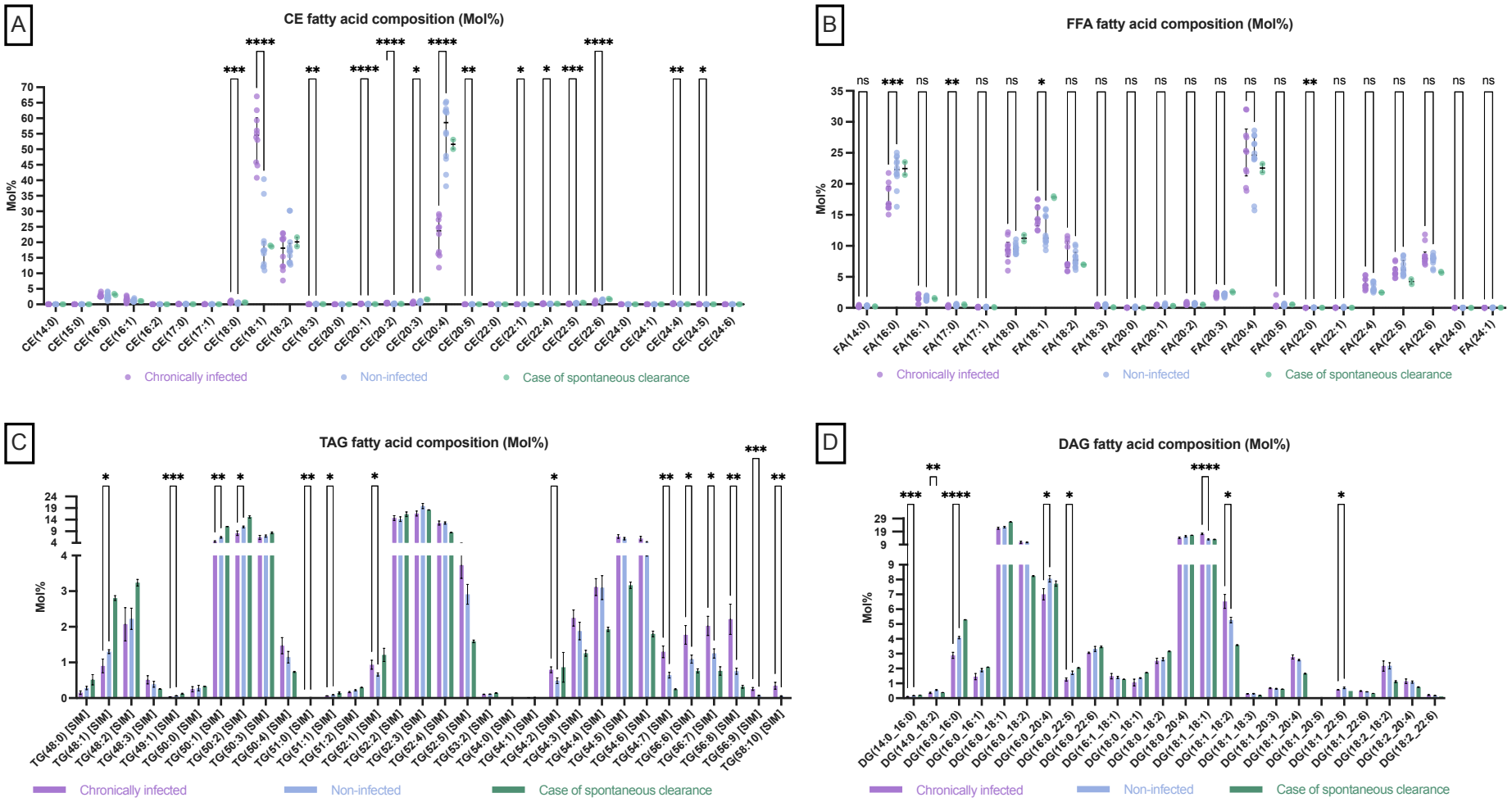

Figure 75: Fatty acid compositions of cholesteryl esters (CE, A), free fatty acids (FFA, B), triacyl glycerides (TAG, C) and diacyl glycerides (DAG, D).

V. Discussion

The availability of highly efficient therapeutic options based on various combinations of direct antiviral agents (DAAs) against HCV does not, unfortunately, despite its undeniable importance, erase the imprinting of virus-driven deregulations, thus does not necessarily prevent progression toward hepatocellular carcinoma (HCC), maybe nor sustain full improvement of metabolic disorders following successful HCV cure[607-609]. The potential mechanisms through which chronically infected patients successfully undergoing HCV cure may still progress toward HCC or persistent increase in fasting glucose are just starting to be unveiled and are still subjected to debates. Therefore, research aimed at deciphering and understanding the molecular and pathophysiological mechanisms linked to HCV infection remains essential to date, yet is hampered by the lack of appropriate culture systems and animal models permissive to infection. In particular, the mechanisms linked to the disturbances induced by the infection with specific HCV genotypes remain poorly understood.

In an attempt to contribute to the understanding of HCV-host interplay, my thesis focused on the identification of HCV NS5A and Core interacting partners and associated deregulated cellular pathways in a relevant infection system. Keeping in mind the clinical and epidemiological meta-data obtained from patient cohorts revealing a prevalence of 80% cases of severe steatosis in chronic infections with genotype 3 strains[330], which was interpreted as the result of a direct “steatogenic” effect of viruses of this genotype[610], we also explored the effects of the expression of Core and NS5A of diverse genotypic origins in the same infection system. Using high-throughput -omic analyses with novel viral tools and infections models, my work documented interesting differential interacting partners and hepatocyte deregulations according to the genotypic origin of HCV NS5A and Core proteins.

In parallel, we relied on the work of the group of Dr Amit Kapoor[468] to establish a highly relevant immunocompetent surrogate animal model in France and to preliminary characterize the effects of hepacivirus infection on host metabolites and lipids. This part of the work allowed us to provide proof of concept that this surrogate *in vivo* model recapitulates the chronic infection rate and the metabolic disorders observed in HCV chronically infected patients, setting the stage for further investigation of this important field.

V.A The production of chimeric viruses expressing heterologous HCV proteins as new tools to evaluate the potential direct link between the genotypic origin of NS5A and induced hepatocyte deregulations revealed essential intra-viral interactions in HCV life cycle

One category of the aforementioned DAAs, the "-asvir", exemplified by Daclatasvir, directly targets NS5A, underlying the importance of this viral protein in HCV life cycle. NS5A is critical for both HCV genomic replication and virion assembly, is implicated in the manipulation of the infected cellular membranous environment and is known to deregulate a wide range of host signaling pathways[538], despite its lack of known enzymatic function and incompletely understood detailed mechanisms of action. This justified the focus of my work on this viral protein.

A central and genotype-specific role in HCV-associated cellular metabolism dysfunctions, including lipogenesis, steatosis and β-oxidation has been attributed to the Core protein (for review, Kao et al., 2016[521]). Conversely, other studies based on histological analyzes of liver biopsies from patients widely diverge on this subject and call into question the preferential association of HCV genotype 3 with hepatic steatosis (for a review, Roingeard, 2013[611]). These

contradictory testimonies reinforced the need to use relevant infection systems for such studies of physio-pathological correlates and led me to complement this work with studies focused on HCV Core.

The JFH-1 strain of HCV genotype 2a is the only natural isolate that spontaneously recapitulates the entire viral cycle leading to the production of HCV particles in the human hepatoma cell line Huh-7.5[411]. The panel of intergenotypic chimeric viruses we successfully developed within the backbone of the Jad strain[413] that express in lieu of the native NS5A or Core the equivalent protein from field strains of genotypes 1, 3 or 4 allowed us to address the role of protein sequences derived from isolates associated with known induced liver damage documented from patient liver biopsies. In this study, field strains were mainly isolated from patients who developed varying degrees of macro- and micro-vesicular steatosis, with variable accumulation of fatty vesicles in the hepatocytes, and in some cases to known developing HCC. Sequences from prototypic strains of genotypes 1 or 2a have also been used for comparison purposes.

Forcing crosstalk of heterologous NS5A proteins of various genotypes with the remaining HCV 2a elements revealed permissive combinations and secondary site rescue for genome replication and viral particle assembly

Chimeric genomes expressing different variants of the NS5A proteins of subtypes 1a, 1b, 2a or 3a, as well as NS5A derived from a genotype 4 strain, the nucleotide sequence of which was found to be phylogenetically closer to subtype 4d strain sequences, were newly produced for this study. The genotype 1 and 2a NS5A chimeras were found to readily result in robust RNA replication and synthesis of infectious viral particles without the requirement for compensatory mutations, supporting efficient cross-talks between intra-genotypic 2a elements, as well as between 1a or 1b and 2a viral sequences. This is in agreement with previous works from Scheel et al.[172] showing that NS5A substitution for 1a, 2a and 7a corresponding prototypic sequences in the context of a chimeric J6/JFH1 virus was amenable to relatively efficient HCV replication without the need for compensatory substitutions.

The intergenotypic viruses encoding the NS5A proteins of genotype 3a and 4 were found to be suboptimal, with reduced viral RNA replication levels. An adaptation following successive passages over a course of 8 weeks of Huh-7.5 cells transfected with the corresponding *in vitro* transcribed RNAs made it possible to generate variants of viruses Jad/NS5A-3a-385, -3a-407 and -4-431 as robust as the parental virus. Examination of the genomic sequence of these variants from replicate experiments revealed reproducible compensatory mutations in NS3 (R1373Q) and NS4B (A1904T or H1965Y) codons for the subtype 3a adapted strains and in NS4B (A1904T) for the genotype 4. Interestingly, no mutations were reliably selected in heterologous NS5A coding sequences. The fact that substitutions in NS3 helicase domain and in NS4B can compensate for heterologous NS5A for efficient genome replication are in line with previously described interactions between these HCV nonstructural proteins and the findings supporting the regulation of the NS3-NS5B replication complex by NS4B[612,613]. The C-terminus of NS4B has further been reported to influence NS5A hyperphosphorylation and motility, with certain mutations in that region being detrimental to viral replication[116]. We found a 1-log difference in TCID50/mL viral titers but similar genomic replication levels between Jad/G4458A/G6050A/NS5A-3a-407 and Jad/G4458A/C6233T/NS5A-3a-407 harboring different compensatory mutations in NS4B. These findings support a specific effect of the NS4B H1965Y mutation in boosting virion assembly and further point to a role of NS4B in the particle assembly step of the virus life cycle. Interestingly, other authors previously reported the selection of NS5A substitutions within DI that partially compensated a defect introduced within the C-terminal domain of JFH1

NS4B, nicely complementing our data and strengthening the critical role of NS4B/NS5A interaction for virus replication[224,110].

The panel of chimeric Jad genomes previously constructed in our group and encoding Core from prototypic or clinical strains of subtypes 1a, 1b, 3a, 4a, 4f and 4p of HCV was found to yield to robust viral progeny, with comparable replication kinetics and protein expression levels without the need for further adaptive mutations (Aicher et al., 2018[550], and Simon, Aicher, et al., unpublished data, see Supplementary Figure 2). These data demonstrated that there was no genotype-specific interactions between Core and other viral proteins and/or viral RNA to ensure efficient particle assembly.

Overall, these joint studies from our group demonstrate for the first time the existence of largely permissive interactions between heterologous Core proteins of subtypes 1a, 1b, 3a, 4a, 4f and 4p or between heterologous NS5A proteins of genotypes 1 and 2a, and native Jad-2a elements, which efficiently lead to genome replication and assembly of infectious viral particles. With the successful rescue of intergenotypic recombinant viruses expressing NS5A of subtypes 3a or 4d with second site compensatory mutations in NS3 and/or NS4B, this work further documented permissive or essential intra-viral interactions that widen the spectrum of known features of HCV infectious life cycle [59,614].

Of note, to date, no natural HCV recombinant with exact substitution of the coding sequence of a single viral protein has been detected in the field. The “hot spots” of natural intergenotypic recombination identified are clustered within the NS2 coding sequence or in the first nucleotides of the NS3 gene, thus encoding hybrid proteins, or at the NS2/NS3 junction, separating the presumed “assembly module” (Core-NS2) from the “replication machinery” (NS3-NS5B) (for a review, see Echeverria et al., 2015[166]). This frequent junction could be indicative of the importance of preserving homologous interactions between the elements specific to each module, in order not to disrupt HCV genomic replication and assembly of viral particles. This is why most of the functional intergenotypic genomes generated by genetic engineering towards the study of pathophysiological properties of other viral genotypes or for testing pan-neutralizing humoral responses carry the coding sequence of heterologous Core-E1-E2-p7-NS2 (for review see Ramirez et al., 2018[240], Figure 24, page - 44 -). Another approach was to successfully adapt strains of various HCV genotypes into hepatocyte lines, such as the H77-S, TN and HCV1 genotype 1a strains[615-617], strains J6 and T9 of genotype 2a[618], strains DH8 and J6 of genotype 2b[619], the clinical strain S83 of genotype 2c[620], and the clinical strains DBN3a, S52, S310 of genotype 3a[621-623]. However, not only do these hyper-adapted strains not reflect the native sequence of clinical strains, since they contain multiple adaptation mutations throughout the genome, but their multiplication remains very variable, which makes their use difficult for comparative transcriptomic studies.

The added value of the new type of intergenotypic viruses we describe in this work lies in the fact that solely the sequence of NS5A or Core is substituted in each chimera, allowing the expression of identical remaining HCV proteins (derived from Jad). Therefore, the phenotypes observed can be promptly associated with each different heterologous NS5A or Core protein with unmodified field sequence.

Identification of permissive insertion positions for affinity purification tags in Core and NS5A allowing the determination of NS5A domains involved in PPIs

Toward proteomic studies, tagged NS5A and Core recombinant viruses encoding proteins fused to an affinity purification twin strep tag or a nonspecific V5 tag were produced, relying on permissive insertion positions previously reported in the literature[518], or investigated according to a published 15-nt transposon-based screen[584] . We found that insertion sites in Core between aa 17 and 18, among several positions tested, and in NS5A between aa 418 and

419 or aa 449 and 450 were well tolerant to 21-40 aa-long exogenous insertions. The viruses generated were highly replication and assembly competent, genetically stable and highly infectious. Insertion of the tags in the parental virus only minorly affected viral replication in the case of Core recombinants, and equally for the ST- and V5-insertions. It is interesting to note that insertion of short exogenous sequences of 12 aa representing a tetracystein tag devoted to protein tracking in live cells was successfully achieved within HCV Jc1 or J6/JFH Core downstream of aa 2 or 3 of the protein, respectively without abrogating virus replication[582,583]. We attempted to insert longer ST/V5 sequences fused to TEV protease recognition site and framed by flexible hinges at both these positions but failed to obtain replication competent viruses, notably with the longer ST tag, pointing to existing constraints on the N-terminus of Core, maybe in link with the involvement of the N-terminal Core codons in IRES-driven translation. Importantly in our work, the insertion of ST/V5 tag in Core or NS5A did not affect the stability of the protein nor the phosphorylation status of NS5A, as observed by immunoblotting. Tagging of the NS5A intra-/intergenotypic recombinant viruses significantly affected, without completely abrogating, the RNA replication of Jad/G4458A/G6050A/NS5A-3a-385, further resulting in decreased viral titers. The titers of Jad/G4458A/C6233T/NS5A-3a-407 were also significantly decreased by the ST insertion, without the corresponding effects in genome replication.

We hypothesize that the insertion of the tag in these latter viruses might impair the association of NS5A with E2 and/or ApoE, thus decreasing viral assembly. This hypothesis is based on data derived both from our experiments and from the published literature. First, we found in the parental virus that both Core and NS5A interact with E2, an interaction that is, however, disrupted by the tag insertion at position 418 of NS5A for the parent. Accordingly, Core, E2, and NS5A have been found to colocalize with ApoE[624], an essential factor for infectious HCV production[270], the silencing of which impairing viral assembly and release[272]. E2 in particular exhibited stronger interaction with ApoE than the other viral proteins, while the triple ApoE-E2-NS5A association has repeatedly been reported[625]. Taken together with the lack of retrieved ApoE in the interactomic networks of 385-ST and 407-ST, it is tempting to speculate that the introduction of the mutation that spontaneously appeared in E2 coding sequence during the cell culture adaptation process of these viruses might enhance infectious viral production.

Notably, HCV E2 was specifically retrieved with Jad/NS5A-ST-449, not with Jad/NS5A-ST-418, but with 2a-J6-ST and 1b-434-ST bearing ST at a position equivalent to 418. This suggested that the E2 interaction could be mapped in a region relatively distant from, but still affected by conformational changes around aa 418. In fact, the dual positions of ST insertion in Jad NS5A allowed us not only to avoid losing the interactions disrupted by insertion of the tag at one of the positions, but also to putatively characterize the domains of interaction of the 418- and 449-specifically retrieved NS5A PPIs. In support of this notion, the interaction between NS5A and the Histone-lysine N-methyltransferase SMYD3 (SMYD3) protein has been characterized by Eberle et al.[517], and was mapped in genotype 2a NS5A DIII to overlap with the recognition site of the 9E10 antibody, which is surrounding the 418 insertion position. Accordingly, insertion of the tag in Jad NS5A disrupted interaction with SMYD3, which was recovered with the highest final score achievable specifically with NS5A-ST-449.

Hence, the lists of 418- and 449-specific PPIs that we identified could be exploited to determine the likely interaction site of previously reported or novel NS5A partners.

All NS5A proteins from genotypes 1-4 exhibit two distinct subcellular localization patterns

In our infectious system, we observed two subcellular localization patterns by confocal microscopy of fixed infected Huh-7.5 cells for all of the NS5A proteins of genotypes 1-4 that

we studied: either scattered throughout the cytoplasm in close proximity to ER, or in dot/ring-like foci. We also found that the dot/ring-like patterns coincided with some NS5A wrapping around the LDs. These observations are in accordance with NS5A localization studies performed with genotype 1 or 2 prototypic strains, which further reported that the NS5A dot-like pattern coincided with LD and Core colocalization[626,627]. Core wrapping around the LDs, reminiscing the NS5A pattern we observed, has previously been well characterized by our group (Simon et al., manuscript in preparation).

Taking this into account, we hypothesize that cells with more scattered, ER-like NS5A distribution were probably more recently infected, representing viral genome translation and replication, while NS5A in close proximity with LDs would mark a switch to virion assembly. This assumption is corroborated by the findings of Eyre et al.[628], who monitored the NS5A dynamics in living, virus-producing hepatoma cells and found that newly synthesized NS5A foci are small and distinct from aged foci. Core-NS5A colocalization was actually found to be transient by in situ proximity ligation assays (PLAs) coupled to confocal microscopy, with only a few copies of NS5A in close proximity to Core (<40nm)[628]. This transient and low-copy interaction would provide a possible explanation to the differential retrieval of NS5A complexed with Core protein by our AP-MS/MS, i.e. Core was not identified in complex with NS5A-3a-385 and Jad-NS5A, and vice-versa Jad NS5A was absent in the Jad Core PPI network.

The subcellular localization of NS5A of diverse genotypic origins in our system could have been affected by the chimeric nature of our viruses, since ectopically expressed genotype 1b-NS5A protein exhibited distinct distribution from the pattern observed when it was co-expressed with the remaining nonstructural proteins from a subgenomic replicon, indicating that NS5A subcellular localization is affected by the co-expression of viral proteins[626]. However, our observations are in line with those made by Galli et al.[587], who studied the subcellular localization of NS5A in Huh-7.5 cells infected with Core–NS2/NS5A HCV chimeric viruses developed in the JFH1 backbone with Core–NS2 and NS5A sequences of genotype 1–7 prototypic strains. During productive infection, the authors found NS5A to adopt a localization similar to that described in subgenomic replicon systems. Furthermore, NS5A colocalization with each homologous Core and LDs was found similar across all studied recombinants in that study.

NS5A proteins of different genotypes exhibit differential phosphorylation patterns

Phosphorylation is a well-established post-translational modification of NS5A, however, the function and emergence of the two phosphorylation forms of NS5A (p58 and p56) have been a matter of scientific controversy (see NS5A paragraph, page - 8 -). In the paucity of data regarding the phosphorylation levels of NS5A of diverse genotypes, especially those derived from clinical isolates, and in light of the high conservation across genotypes of the main peptide associated with NSA hyperphosphorylation, our study of the phosphorylation status of the NS5A peptides retrieved following AP-MS/MS shed some light on the phosphorylation patterns of NS5A proteins from genotypes 1-4.

We identified both common and distinct phosphorylation sites in the different NS5A isoforms, with pS222 found across genotypes and pS228/pS229 identified only in NS5A-1b-434. Interestingly, two novel phosphosites were identified within NS5A DIII, aa 364 and aa 366 in the alignment shown in Figure 30 (page - 85 -). These sites were both highly conserved and found to be either a phosphoreceptive or a phosphomimetic residues. This high conservation might be indicative of the importance of an aa with specific conformation at this position for HCV regardless of the genotype, and is worthy of further characterization, by mutational analysis.

Importantly, for all discovered phosphopeptides, we also identified the nonphosphorylated counterpart peptides, corroborating the postulated role of NS5A phosphorylation in the regulation of the switch from replication to assembly.

V.B HCV NS5A and Core preferred mode of action is revealed by their respective interactomes

This is -to our knowledge- the first report of an HCV Core interactome identified in an infection system and of a comparative study of the interactomes of NS5A from circulating strains identified in Huh-7.5 hepatoma cells infected with different intergenotypic viruses. Our studies were not only performed in a more relevant system, but they also enriched the lists of previously reported Core (>250) and NS5A (>700) cellular interactors (see paragraph I.B.θ.(ii)) by 123 and 675 putative additional cellular interacting partners, respectively (Supplementary Table 1 and Supplementary Table 2). However, given that one protein cannot possibly interact with as many factors at the same time, even in the presence of the postulated intrinsically disordered DII and DIII, a hypothesis can be made on distinct spatial and temporal NS5A PPIs, based on the subcellular localization of the protein, the stage of the virus life cycle and the transience of the interaction. This would allow NS5A to be a main orchestrator of the different steps of the HCV life cycle. In this regard, the regulation of such processes has been proposed to be heavily dependent on the phosphorylation of the protein by cellular kinases, such as the casein kinase 1α (CK1α)[629,149], the casein kinase 2 (CKII)[136,138], the cyclin-dependent kinase 1 (Cdk1)[630] and cAMP-dependent protein kinase A (PKA)[631]. While we cannot discriminate specific interactors of NS5A p56 or p58 in our study, Pan et al.[160] have identified cellular proteins that are significantly more abundant in the p58 interactome over the p56, supporting our abovementioned assumption.

Since HCV is a virus with a relatively compact genome, we would expect that any role of its encoded proteins in disruption or alteration of host cellular functions would be limited to a few targets per pathway/process. However, with the extent of networks recovered here, it was highly tempting to investigate the enrichment of cellular signaling pathways and processes.

Unexpectedly, this enrichment in the case of Jad Core and NS5A revealed a putative preferred mode of action for each protein in promoting the viral life cycle and the subsequent HCV-induced pathology. For Jad Core, a significant enrichment of pathways involved in the regulation of gene expression was found, suggesting that Core might regulate cellular processes by subverting or by activating host transcription factors. On the other hand, Jad NS5A was found to interact with proteins involved in metabolic, intracellular transport, HCC-linked, and immune processes. For the metabolic processes in particular, complexes of more than 40 proteins responsible for the Krebs cycle, the electron transport chain and the oxidative phosphorylation machinery were affinity purified together with Jad NS5A as bait, pointing to a strong interaction of NS5A with mitochondrial proteins. These pathways were further found enriched in the interactomic network of NS5A proteins derived from field isolates, supporting a more unified mode of action. Additionally, enrichment of gene sets involved in the regulation of gene expression, gluconeogenesis and cholesterol metabolism was identified in this network, with the two latter indicating a putative mode of virus-induced host metabolic deregulations, which are more extensively described in §V.E.

Interestingly, preliminary gene set enrichment analyses of the proteins identified only, one the one hand in the genotype 3 NS5A interactomes and, on the other hand only in the nongenotype 3 NS5A interactomes highlighted the gluconeogenesis and cholesterol metabolism pathways exclusively in genotype 3, and the gene expression enrichment only in

the second group (data not shown). This is suggestive of differential HCV NS5A induced regulations in link with the higher prevalence of steatosis in HCV genotype 3 infected individuals due to NS5A-mediated perturbations in cholesterol metabolism and gluconeogenesis. In fact, a key enzyme in energy metabolism, the pyruvate catalase was found to specifically interact with genotype 3a NS5A-407, the one derived from the patient with the highest degree of steatosis, suggesting a possible differential mechanism in link with increased steatosis development.

Similarly, aldehyde dehydrogenase 1 family member A1 (ALDH1A1), an enzyme involved in the major oxidative pathway of ethanol metabolism, and glutaredoxin-1 (GLRX) were found to specifically interact with both NS5A-407 and NS5A-385 (50% steatosis in the infected patient). GLRX in particular is essential to maintain normal hepatic lipid homeostasis and prevent fatty liver disease[632] and GLRX mRNA was found to be downregulated by infection in our Core transcriptomic studies. Therefore, we hypothesize that NS5A interaction with GLRX could possibly have a role as safety valve within a general inhibition strategy of this pathway together with transcriptional shut down, that eventually results in the deregulation of glutathione-protein mixed disulfide bonds and increase of oxidative stress. Even if all the tagged intergenotypic NS5A viruses used in our study do not have identical growth kinetics, it should be noted that NS5A-385 and NS5A-407 are the lowest titrated viruses at 120h p.tf., strengthening that retrieval of interactors with these viruses and not with other chimeras is likely to be meaningful. One should keep in mind, however that absence of PPIs should be considered with caution given putative limitations in the mass spectrometry identification of peptides present in low concentration that could affect the retrieval of certain interactors.

A limitation of our study involves the lysis of the infected cells in the presence of NP-40 detergent, in order to inactivate the virus, which does not ensure a sustained integrity of cellular organelles during lysis. Hence, it might theoretically be possible to recover interactions of our proteins of interest with proteins that might not physiologically be accessible during infection in the living cells. For example, Core is an RNA binding protein, which could potentially bind different RNA molecules upon lysis of the cells and potential permeabilization of the nucleus, leading to the co-purification of indirectly bound RNA-binding proteins. However, such interactions are generally less stable and would not reproducibly withhold the AP procedures thereafter. In support of the specific retrieval of RNA-binding proteins complexed with Core, RNA binding proteins retrieved with Jad NS5A as bait were scarce, despite NS5A known RNA binding capacity.

V.C Focus on HCV NS5A and Core PPI roles in the virus life cycle

The collective identification of HCV Core and NS5A respective interactomic networks allowed us to increase our knowledge of the cellular targets of these proteins, as well as strengthen previously reported data. For example, we reproducibly recovered well characterized NS5A interacting partners, such as PI4KIIIα (or PI4KA), VAPA, VAPB, the roles of which in the formation of the viral replication factories have extensively been presented in §I.B.ε.(iii). This was the case with all of our tagged NS5A proteins, including with the insertion of the tag in both Jad NS5A positions, with great final scores, further validating our screens.

We are beginning to explore the functional characterization of selected partners, the biological function of which could indicate a potential role in HCV life cycle or HCV-induced pathogenesis. To do so, we validate the interaction with additional co-immunoprecipitation experiments and protein complementation assays. In parallel, we are using small interfering RNAs (siRNA) to shut down the expression of these partners and monitor the effect of the silencing on the virus life cycle by infectious titration. The list of partners we are exploring

includes the above-described proteins ALDH1A1, GLRX and PC in link with genotype 3-specific pathogenesis, as well as the proteins described in the next paragraphs.

Extended synaptotagmin 1 (ESYT1), an ER protein involved in the transport of glycerolipids and Ca^{2+} was found to interact with all NS5A proteins we tested. We hypothesize that ESYT1 interaction with NS5A might be involved in the ER membrane rearrangements towards the formation of HCV replication factories[633].

Retinol dehydrogenase 11 (RDH11) was found to interact with NS5A proteins of nongenotype 1 origins. The role of the enzyme is self-explanatory by its name, retinoic acid is regulating intracellular antiviral innate immune responses in hepatocytes[634] and hepatic retinol levels have been found increased in MASLD mice[635]. We therefore are interested in validating the RDH11 interaction (or absence of it) with our different NS5A isoforms and to then monitor the effect in of RDH11 silencing in cell culture.

Similarly, we found Integrin β1 (ITGB1) to interact with NS5A proteins of nongenotype 1 origins. ITGB1 is a well characterized receptor for viruses of different orders, such as Picornavirales[636], Herpesvirales[637,638], Piccovirales[639], and Reovirales[640,641], and has been associated with virus-induced pathogenesis[642]. ITGB1 is also involved in liver regeneration processes, through activation of growth factor signaling[643] and has been found to mediate IFN signaling with implications in HCV replication[644]. While this manuscript was in preparation, a paper was published reporting on an APEX2-based proximity biotinylation screen of NS5A partners, with ITGB1 being in the list of identified biotinylated proteins[645].

Interestingly, another NS5A interactor similarly retrieved with all tagged NS5A proteins and both Jad NS5A-ST with good final scores, had previously been reported to have an effect on HCV assembly. More specifically, the role in cellular processes of long chain acyl-CoA synthetase 3 (ACSL3), an enzyme catalyzing the activation of FA towards their incorporation to various lipids including TAG, CE, and phospholipids such as phosphatidylcholine (PC) and phosphatidylethanolamine (PE) was characterized by Yao and Ye in 2007[646]. These authors found that ACSL3 is specifically required for incorporation of FA into PC, an essential reaction for VLDL assembly. They further showed that targeting of ACSL3 by small interfering RNAs inhibited the secretion of ApoB and the release of HCV from Huh-7.5 cells. Our reproducible retrieval of ACSL3 and ACSL4, the predominant ACSL isoform expressed in Huh-7.5 cells, by all studied NS5A proteins, as well as of ACSL1 by half of them is a strong indication of a putative role of these PPIs in the regulation of HCV assembly by NS5A. Further co-immunoprecipitation experiments would be required to verify this interaction. As a second step, identification of the NS5A domain of interaction and further disruption of the interaction would be necessary in order to functionally characterize its role in the HCV assembly process.

Protein PAT1 homolog 1 (PATL1), an RNA-binding protein involved in mRNAs decapping, leading to the degradation of mRNAs, was reported by Scheller et al.[647] to be essential for HCV translation and replication of genotype 1b and 2a replicons and viruses. We identified PATL1 as a putative interactor of both Jad Core and NS5A-ST-418, PPIs that are being further investigated to verify whether this factor is involved in HCV genome translation and replication.

A cell surface proteoglycan, glypican-3 (GPC3) was affinity purified in complex with Core. GPC3 has been found to negatively regulates the hedgehog signaling pathway and to positively regulate the canonical Wnt signaling pathway by binding to the Wnt receptor Frizzled and stimulating the binding of the Frizzled receptor to Wnt ligands[648], while it also binds CD81, an entry factor of HCV[649] [650]. Thus, further validation and functional characterization of this interaction would be of interest to unravel possible HCV Core-induced deregulations in link with HCV pathology through PPIs.

Lastly, two proteins that could potentially be involved in HCV-induced pathogenesis in link with metabolic disorders, PCCB and SCD, will also be explored. The roles and possible effects of HCV interaction with these proteins will be presented in the following paragraphs.

V.D The liver transcriptome is differentially modulated according to the genotypic origin of Core

Our comparative study of the transcriptomes of hepatoma cells infected with different intergenotypic viruses revealed for the first time in an infection system a differential deregulation of the expression profile of hepatic genes depending on the genotypic origin of Core. Overall, we found the vast majority of deregulated gene sets to be significantly downregulated by HCV infection. Importantly, the majority of deregulated genes were more downregulated by the expression of nongenotype 3 Core than Gt 3. Looking in more details into the nonGt3 group, the most extreme downregulation seemed to be induced by genotype 4 Core recombinants. A previous study from our group focused on the link between natural Core polymorphisms present in genotype 4 strains emerging in Central Africa and the Wnt/ß-catenin signaling pathway which contributes to the development of HCC[550]. The main conclusion of this study reveals that Jad/C4fC induced a significantly greater activation of the Wnt/ß-catenin pathway than Jad/C4aR, which could be linked to a single aa difference in Core sequences.

In tentative link with steatosis development, we did find some gene sets significantly more disturbed by genotype 3 Core, namely the downregulated reactome "acyl chain remodelling of DAG and TAG" that could lead to increased intracellular lipid accumulation, the upregulated WikiPathways "Photodynamic Therapy induced Unfolded Protein Response", a mechanism activated in response to hypoxia, altered protein glycosylation and ER stress due to dysregulated lipid homoeostasis and toxic lipid accumulation. Oxidative stress may activate metallothioneins, which have recently been found to be induced by HCV infection *in vitro*[651]. Hence, increased expression of genes involved in "metallothioneins bind metals", "response to metal ion" and "zinc influx into cells by the slc39 gene family" by genotype 3 Core might be an indirect indication of particularly elevated intracellular accumulation of reactive oxygen species triggered by genotype 3 Core.

Differential modulation of hepatic genes depending on the genotypic origin of Core had previously only been described in expression systems of isolated Core protein of genotype 1b, 2a, 3a or 4d [601,652,653], or in liver biopsies from patients infected with a genotype 1 or 3 strain[654,600,655,656]. The conclusions of these authors relating to a proven effect of genotype 3 on lipid metabolism or on pro-inflammatory pathways diverge according to the study models, which make it difficult to derive a universal statement without additional investigations.

V.E Combined hepacivirus–induced metabolic reprogramming from analyses in cell culture and *in vivo*

We successfully reproduced in France the RHV-rn1 model initially described by Trivedi et al.[468] and we recovered a high chronicity rate in outbred Sprague Dawley rats infected with RHV-rn1 (11/12 infected rats, 92%).

This model allowed us to uncover some very interesting metabolic and lipid alterations induced in the liver of animals chronically infected by this hepacivirus, despite the low number of rats used in this preliminary study. These alterations were either absent or reverted in the single case of an infected rat with spontaneous sustained viral suppression. RHV-rn1 chronically infected rats displayed increased fasted glucose levels compared to non-infected rats, impaired gluconeogenesis, increased levels of CE18:1, signifying RHV-induced modulation of membrane biogenesis, and an increased accumulation of TAG lipids with more than 52 carbon atoms in total, coupled to a decrease in TAG lipids with 51 or less carbon atoms.

Impaired gluconeogenesis may lead to increased reliance on amino acids for glucose production, while high levels of fatty acids and non-polar amino acids contribute to liver dysfunction and insulin resistance, further complicating glucose homeostasis. The virus might benefit from these modifications for balancing energy production and for redirecting lipoproteins production essential for the viral life cycle. In fact, impaired gluconeogenesis, attested by high glucose levels and decreased levels of TCA metabolites, such as malate was also observed in Huh-7.5.1 differentiated cells persistently infected with HCV genotype 2a Jc1[530], bringing closer observations in RHV and HCV models. Our transcriptomic studies also uncovered a significant downregulation of gluconeogenesis in link with HCV infection regardless of the Core genotypic origin, while the significant downregulation of Cori cycle was a further testament to reduced lactate conversion to glucose. Moreover, our NS5A interactomic data showed an enrichment of factors involved in gluconeogenesis in the interactomes of genotype 3 NS5A proteins, also pointing to a deregulation of this process.

In link with decreased TCA metabolites, an HCV-induced Warburg-like effect (for a review, see Gerresheim, et al., 2019[657]) was also characterized by a metabolic switch, with a reduced activity of the TCA cycle and OXPHOS, which was reproducibly statistically enriched in our transcriptomic data. The Warburg effect is a characteristic of cancer cells, and more marked downregulation by nongenotype3 Core expressing chimeras over the genotype 3 Core chimeras could be a testament to higher cancerogenic capacity of these Core proteins. Despite the fact that these observations were made in hepatocarcinoma cells, they were also found significant in comparison to non-infected control cancer cells, while similar assumptions were previously made by Diamond et al.[597], and Lupberger et al.[530]. Furthermore, the highly reproducible identification of the various NADH dehydrogenase ubiquinone complex proteins (NDUF*xx*) of the TCA cycle and the ATP synthase subunits (ATP*xx*) carrying out OXPHOS as potential NS5A interactors, regardless of the HCV genotype of NS5A, attest to HCV-induced perturbation of TCA-OXPHOS at both the gene expression and protein levels.

Studies in animal models and in HCV patients have shown HCV induced IR coupled to elevated blood glucose levels and a (pre-)diabetic state of the patients (reviewed in Chang et al., 2016[658]). Both high glucose[659] and HCV infection have been shown to downregulate the expression of PPARα[601], leading to reduced peroxisomal function. Indeed, in our transcriptomic data, we found both the PPARα gene expression significantly downregulated by almost all Core intergenotypic recombinants, and the peroxisomal pathways impaired in the presence of Core proteins of any HCV genotype. Intracellular accumulation of lipids further signifies impaired mitochondrial and/or peroxisomal β-oxidation. Very long chain fatty acids (VLCFA) are degraded exclusively in peroxisomes[599], pointing rather to a peroxisomal β-oxidation perturbation in RHV-rn1 infected Sprague Dawley rats. A preference of HCV for VLCFA has also been well documented in infected hepatoma cultures[606,530], while elevated FFAs were found in HCV patients pre-SVR, in a multi-omic study performed in blood, feces and liver tissue samples of said patients[660]. The authors further reported downregulation of all enriched metabolic pathways, as in our case, and a significant downregulation of KEGG gene sets in common with our transcriptomic study, e.g. peroxisome, bile acid metabolism and metabolism of aa, such as glycine, serine, threonine, valine, leucine and isoleucine. Furthermore, in accordance with the transcriptomic and proteomic data reported by Lupberger et al.[530] in liver tissues of chronically infected HCV patients and in differentiated Huh-7.5.1 infected with HCV Jc1 strain, we found that regardless of the genotype of Core expressed in the context of productive infection, the hallmark gene sets fatty acid metabolism, bile acid metabolism, peroxisome and KEGG peroxisome are downregulated by HCV infection.

According to our interactomic data, the modulation of cellular lipid metabolism might further be induced through Core and NS5A PPIs. We found that ST-Core pulled down mitochondrial propionyl-CoA carboxylase beta chain (PCCB), an enzyme involved in the

catabolism of odd chain fatty acids, branched-chain amino acids isoleucine, threonine, methionine, and valine and other metabolites[661], whose action might be enhanced or perturbed through interaction with Core. Furthermore, stearoyl-CoA desaturase (SCD), which we also identified as a putative Jad Core interactor, is a key contributor in the biosynthesis of membrane phospholipids, cholesterol esters and triglycerides, utilizing O_2 and electrons from reduced cytochrome b5 to introduce the first double bond into saturated fatty acyl-CoA substrates and giving rise to a mixture of 16:1 and 18:1 unsaturated fatty acids[662]. Notably, the expression levels of the PCCB and SCD respective genes were found unaltered by HCV infection in the presence of any Core genotype (data not shown), suggesting that any regulation of these factors is probably exerted at the protein level. Lastly, delta(14)-sterol reductase LBR (LBR) was one of the few common putative interactors of Core and NS5A, a protein catalyzing the reduction of the C14-unsaturated bond of lanosterol towards cholesterol biosynthesis[591,663], which was also found significantly downregulated by all strains used in our transcriptomic analysis (average $\log_2FC = -0.31$, $p < 0.05$).

Taken together, our combined data from interactomic and transcriptomic studies in cell culture with metabolomic and lipidomic observations in a surrogate animal model allowed us to pinpoint and elaborate on specific steps/processes of host metabolism disturbed by hepacivirus infection, namely increased glucose levels coupled to impaired gluconeogenesis, TCA-OXPHOS, β-oxidation and a preference for longer fatty acyl chains in infected cells. With this work, the contributions of Core and NS5A proteins of various HCV genotypes in these regulations is now well established.

V.F Evolution towards more physiological study systems

Despite the questionable ethics of the act, the retrieval of cervical tumor cells from Henrietta Lacks in 1953 greatly impacted virology studies. With the advent of the easy-to-maintain, immortal HeLa cells and the cell lines that followed, it has been made possible to culture and study many human viruses *in vitro*. However, when studying pathogens, it is important to consider the limitations of the respective model used for each experiment. Immortalized cellular models are not always physiologically close to natural infection and it would be more prudent to perform studies of the pathology drivers of a cancerogenic virus in a non-cancerous cell line, if at all possible.

Preliminary PHH infection attempts using the recombinant viruses constructed in the Jad backbone were carried out in collaboration with C. Gondeau (Institut de Recherche en Bioothérapie, Montpellier, France), but we were unable to show a robust and reproducible infection in PHH cultures from different donors. Our additional analyses suggested that intergenotypic viruses constructed in the native JFH-1 backbone would be more suitable in this model, since Jad adaptation mutations confer a replication attenuation phenotype in these cultures.

A cell culture model that more physiologically reproduced the hepatic environment was recently developed by the laboratory of Dr Philippe Chouteau, who partially differentiated Huh-7.5 cells, which were then maintained under hypoxia[664]. This new, more relevant cellular model emulates the characteristics of primary hepatocytes and the production of highly lipidated HCV LVPs, hence representing a model of choice for the future directions of our projects. Collaborative preliminary experiments performed in this system showed that Jad intergenotypic recombinant viruses described in this work, whether expressing Core or NS5A isoforms were infectious in this system, allowing for a rate of infection amenable to subsequent RNA-Seq analyses. This would allow us to verify and extend the Core transcriptomic data we obtained in plain Huh-7.5, as well as examine the effects of NS5A of different genotypic origins on host gene expression in a more physiological system.

Lastly, the development of the HCV surrogate model may also serve for the validation of certain cell-culture based observations. We aim at using this surrogate animal model to do an in-depth characterization of the RHV-driven metabolic disorders we found during the course of chronic infection, and to evaluate how a combination of chronic hepacivirus infection and high fat/high sugar (western) diet may aggravate these pathologies. This would entail deciphering the lipid metabolism disorders occurring in the liver of chronically infected rats using larger number of rats for increased statistical depth and identification of highly deregulated hepatic pathways in response to RHV infection and/or western diet.

VI. Bibliographic References

1 Hartlage, A. S., Cullen, J. M. & Kapoor, A. The Strange, Expanding World of Animal Hepaciviruses. *Annu Rev Virol* **3**, 53-75 (2016). https://doi.org:10.1146/annurev-virology-100114-055104

2 Robertson, B., Myers, G., Howard, C., Brettin, T., Bukh, J., Gaschen, B., Gojobori, T., Maertens, G., Mizokami, M., Nainan, O., Netesov, S., Nishioka, K., Shin-i, T., Simmonds, P., Smith, D., Stuyver, L. & Weiner, A. Classification, nomenclature, and database development for hepatitis C virus (HCV) and related viruses: proposals for standardization. *Archives of Virology* **143**, 2493-2503 (1998). https://doi.org:10.1007/s007050050479

3 de Souza, W. M., Fumagalli, M. J., Sabino-Santos, G., Jr., Motta Maia, F. G., Modha, S., Teixeira Nunes, M. R., Murcia, P. R. & Moraes Figueiredo, L. T. A Novel Hepacivirus in Wild Rodents from South America. *Viruses* **11** (2019). https://doi.org:10.3390/v11030297

4 Quan, P. L., Firth, C., Conte, J. M., Williams, S. H., Zambrana-Torrelio, C. M., Anthony, S. J., Ellison, J. A., Gilbert, A. T., Kuzmin, I. V., Niezgoda, M., Osinubi, M. O., Recuenco, S., Markotter, W., Breiman, R. F., Kalemba, L., Malekani, J., Lindblade, K. A., Rostal, M. K., Ojeda-Flores, R., Suzan, G., Davis, L. B., Blau, D. M., Ogunkoya, A. B., Alvarez Castillo, D. A., Moran, D., Ngam, S., Akaibe, D., Agwanda, B., Briese, T., Epstein, J. H., Daszak, P., Rupprecht, C. E., Holmes, E. C. & Lipkin, W. I. Bats are a major natural reservoir for hepaciviruses and pegiviruses. *Proceedings of the National Academy of Sciences of the United States of America* **110**, 8194-8199 (2013). https://doi.org:10.1073/pnas.1303037110

5 da Silva, M. S., Junqueira, D. M., Baumbach, L. F., Cibulski, S. P., Mósena, A. C. S., Weber, M. N., Silveira, S., de Moraes, G. M., Maia, R. D., Coimbra, V. C. S. & Canal, C. W. Comprehensive evolutionary and phylogenetic analysis of Hepacivirus N (HNV). *The Journal of general virology* **99**, 890-896 (2018). https://doi.org:10.1099/jgv.0.001082

6 de Martinis, C., Cardillo, L., Esposito, C., Viscardi, M., Barca, L., Cavallo, S., D'Alessio, N., Martella, V. & Fusco, G. First identification of bovine hepacivirus in wild boars. *Sci Rep* **12**, 11678 (2022). https://doi.org:10.1038/s41598-022-15928-7

7 Lauck, M., Sibley, S. D., Lara, J., Purdy, M. A., Khudyakov, Y., Hyeroba, D., Tumukunde, A., Weny, G., Switzer, W. M., Chapman, C. A., Hughes, A. L., Friedrich, T. C., O'Connor, D. H. & Goldberg, T. L. A novel hepacivirus with an unusually long and intrinsically disordered NS5A protein in a wild Old World primate. *J Virol* **87**, 8971-8981 (2013). https://doi.org:10.1128/jvi.00888-13

8 Chang, W. S., Eden, J. S., Hartley, W. J., Shi, M., Rose, K. & Holmes, E. C. Metagenomic discovery and co-infection of diverse wobbly possum disease viruses and a novel hepacivirus in Australian brushtail possums. *One Health Outlook* **1**, 5 (2019). https://doi.org:10.1186/s42522-019-0006-x

9 Guo, H., Cai, C., Wang, B., Zhuo, F., Jiang, R., Wang, N., Li, B., Zhang, W., Zhu, Y., Fan, Y., Chen, W., Chen, W., Yang, X. & Shi, Z. Novel hepacivirus in Asian house shrew, China. *Sci China Life Sci* **62**, 701-704 (2019). https://doi.org:10.1007/s11427-018-9435-7

10 Mifsud, J. C. O., Costa, V. A., Petrone, M. E., Marzinelli, E. M., Holmes, E. C. & Harvey, E. Transcriptome mining extends the host range of the Flaviviridae to non-bilaterians. *Virus Evol* **9**, veac124 (2023). https://doi.org:10.1093/ve/veac124

11 Li, L. L., Liu, M. M., Shen, S., Zhang, Y. J., Xu, Y. L., Deng, H. Y., Deng, F. & Duan, Z. J. Detection and characterization of a novel hepacivirus in long-tailed ground squirrels (Spermophilus undulatus) in China. *Arch Virol* **164**, 2401-2410 (2019). https://doi.org:10.1007/s00705-019-04303-z

12 Moreira-Soto, A., Arroyo-Murillo, F., Sander, A. L., Rasche, A., Corman, V., Tegtmeyer, B., Steinmann, E., Corrales-Aguilar, E., Wieseke, N., Avey-Arroyo, J. & Drexler, J. F. Cross-order host switches of hepatitis C-related viruses illustrated by a novel hepacivirus from sloths. *Virus Evol* **6**, veaa033 (2020). https://doi.org:10.1093/ve/veaa033

13 van der Laan, L. J., de Ruiter, P. E., van Gils, I. M., Fieten, H., Spee, B., Pan, Q., Rothuizen, J. & Penning, L. C. Canine hepacivirus and idiopathic hepatitis in dogs from a Dutch cohort. *J Viral Hepat* **21**, 894-896 (2014). https://doi.org:10.1111/jvh.12268

14 Abbadi, I., Lkhider, M., Kitab, B., Jabboua, K., Zaidane, I., Haddaji, A., Nacer, S., Matsuu, A., Pineau, P., Tsukiyama-Kohara, K., Benjelloun, S. & Ezzikouri, S. Non-primate hepacivirus transmission and prevalence: Novel findings of virus circulation in horses and dogs in Morocco. *Infection, genetics and evolution : journal of molecular epidemiology and evolutionary genetics in infectious diseases* **93**, 104975 (2021). https://doi.org:10.1016/j.meegid.2021.104975

15 Pacchiarotti, G., Nardini, R. & Scicluna, M. T. Equine Hepacivirus: A Systematic Review and a Meta-Analysis of Serological and Biomolecular Prevalence and a Phylogenetic Update. *Animals (Basel)* **12** (2022). https://doi.org:10.3390/ani12192486

16 Porter, A. F., Pettersson, J. H., Chang, W. S., Harvey, E., Rose, K., Shi, M., Eden, J. S., Buchmann, J., Moritz, C. & Holmes, E. C. Novel hepaci- and pegi-like viruses in native Australian wildlife and non-human primates. *Virus Evol* **6**, veaa064 (2020). https://doi.org:10.1093/ve/veaa064

17 Harding, E. F., Russo, A. G., Yan, G. J. H., Mercer, L. K. & White, P. A. Revealing the uncharacterised diversity of amphibian and reptile viruses. *ISME Communications* **2**, 95 (2022). https://doi.org:10.1038/s43705-022-00180-x

18 Zhang, X. L., Yao, X. Y., Zhang, Y. Q., Lv, Z. H., Liu, H., Sun, J. & Shao, J. W. A Highly Divergent Hepacivirus Identified in Domestic Ducks Further Reveals the Genetic Diversity of Hepaciviruses. *Viruses* **14** (2022). https://doi.org:10.3390/v14020371

19 Smith, D. B., Becher, P., Bukh, J., Gould, E. A., Meyers, G., Monath, T., Muerhoff, A. S., Pletnev, A., Rico-Hesse, R., Stapleton, J. T. & Simmonds, P. Proposed update to the taxonomy of the genera Hepacivirus and Pegivirus within the Flaviviridae family. *The Journal of general virology* **97**, 2894-2907 (2016). https://doi.org:10.1099/jgv.0.000612

20 Shi, M., Lin, X. D., Chen, X., Tian, J. H., Chen, L. J., Li, K., Wang, W., Eden, J. S., Shen, J. J., Liu, L., Holmes, E. C. & Zhang, Y. Z. The evolutionary history of vertebrate RNA viruses. *Nature* **556**, 197-202 (2018). https://doi.org:10.1038/s41586-018-0012-7

21 Yuan, S., Yao, X. Y., Lian, C. Y., Kong, S., Shao, J. W. & Zhang, X. L. Molecular detection and genetic characterization of bovine hepacivirus identified in ticks collected from cattle in Harbin, northeastern China. *Front Vet Sci* **10**, 1093898 (2023). https://doi.org:10.3389/fvets.2023.1093898

22 Harvey, E., Rose, K., Eden, J. S., Lo, N., Abeyasuriya, T., Shi, M., Doggett, S. L. & Holmes, E. C. Extensive Diversity of RNA Viruses in Australian Ticks. *J Virol* **93** (2019). https://doi.org:10.1128/jvi.01358-18

23 Williams, S. H., Levy, A., Yates, R. A., Somaweera, N., Neville, P. J., Nicholson, J., Lindsay, M. D. A., Mackenzie, J. S., Jain, K., Imrie, A., Smith, D. W. & Lipkin, W. I. Discovery of Jogalong virus, a novel hepacivirus identified in a Culex annulirostris

(Skuse) mosquito from the Kimberley region of Western Australia. *PloS one* **15**, e0227114 (2020). https://doi.org:10.1371/journal.pone.0227114

24 Kapoor, A., Simmonds, P., Scheel, T. K., Hjelle, B., Cullen, J. M., Burbelo, P. D., Chauhan, L. V., Duraisamy, R., Sanchez Leon, M., Jain, K., Vandegrift, K. J., Calisher, C. H., Rice, C. M. & Lipkin, W. I. Identification of rodent homologs of hepatitis C virus and pegiviruses. *mBio* **4**, e00216-00213 (2013). https://doi.org:10.1128/mBio.00216-13

25 Bletsa, M., Vrancken, B., Gryseels, S., Boonen, I., Fikatas, A., Li, Y., Laudisoit, A., Lequime, S., Bryja, J., Makundi, R., Meheretu, Y., Akaibe, B. D., Mbalitini, S. G., Van de Perre, F., Van Houtte, N., Těšíková, J., Wollants, E., Van Ranst, M., Pybus, O. G., Drexler, J. F., Verheyen, E., Leirs, H., Gouy de Bellocq, J. & Lemey, P. Molecular detection and genomic characterization of diverse hepaciviruses in African rodents. *Virus Evol* **7**, veab036 (2021). https://doi.org:10.1093/ve/veab036

26 Choo, Q. L., Kuo, G., Weiner, A. J., Overby, L. R., Bradley, D. W. & Houghton, M. Isolation of a cDNA clone derived from a blood-borne non-A, non-B viral hepatitis genome. *Science* **244**, 359-362 (1989). https://doi.org:10.1126/science.2523562

27 Pybus, O. G. & Thézé, J. Hepacivirus cross-species transmission and the origins of the hepatitis C virus. *Curr Opin Virol* **16**, 1-7 (2016). https://doi.org:10.1016/j.coviro.2015.10.002

28 Bamford, C. G. G., de Souza, W. M., Parry, R. & Gifford, R. J. Comparative analysis of genome-encoded viral sequences reveals the evolutionary history of flavivirids (family Flaviviridae). *Virus Evol* **8**, veac085 (2022). https://doi.org:10.1093/ve/veac085

29 Li, Y., Ghafari, M., Holbrook, A., Boonen, I., Amor, N., Catalano, S., Webster, J., Li, Y., Li, H., Vergote, V., Maes, P., Chong, Y., Laudisoit, A., Baelo, P., Ngoy, S., Mbalitini, S., Gembu, G., Akawa, P. M., Bellocq, J. G. d., Leirs, H., Verheyen, E., Pybus, O., Katzourakis, A., Alagaili, A., Gryseels, S., Li, Y., Suchard, M., Bletsa, M. & Lemey, P. The evolutionary history of hepaciviruses. *bioRxiv*, 2023.2006.2030.547218 (2023). https://doi.org:10.1101/2023.06.30.547218

30 Blumberg, B. S. POLYMORPHISMS OF THE SERUM PROTEINS AND THE DEVELOPMENT OF ISO-PRECIPITINS IN TRANSFUSED PATIENTS. *Bull N Y Acad Med* **40**, 377-386 (1964).

31 Blumberg, B. S., Alter, H. J. & Visnich, S. A "NEW" ANTIGEN IN LEUKEMIA SERA. *Jama* **191**, 541-546 (1965). https://doi.org:10.1001/jama.1965.03080070025007

32 Feinstone, S. M., Kapikian, A. Z. & Purceli, R. H. Hepatitis A: detection by immune electron microscopy of a viruslike antigen associated with acute illness. *Science* **182**, 1026-1028 (1973). https://doi.org:10.1126/science.182.4116.1026

33 Feinstone, S. M., Kapikian, A. Z., Purcell, R. H., Alter, H. J. & Holland, P. V. Transfusion-associated hepatitis not due to viral hepatitis type A or B. *N Engl J Med* **292**, 767-770 (1975). https://doi.org:10.1056/nejm197504102921502

34 Alter, H. J., Purcell, R. H., Holland, P. V. & Popper, H. Transmissible agent in non-A, non-B hepatitis. *Lancet* **1**, 459-463 (1978). https://doi.org:10.1016/s0140-6736(78)90131-9

35 Kuo, G., Choo, Q. L., Alter, H. J., Gitnick, G. L., Redeker, A. G., Purcell, R. H., Miyamura, T., Dienstag, J. L., Alter, M. J., Stevens, C. E. & et al. An assay for circulating antibodies to a major etiologic virus of human non-A, non-B hepatitis. *Science* **244**, 362-364 (1989). https://doi.org:10.1126/science.2496467

36 Kolykhalov, A. A., Agapov, E. V., Blight, K. J., Mihalik, K., Feinstone, S. M. & Rice, C. M. Transmission of hepatitis C by intrahepatic inoculation with transcribed RNA. *Science* **277**, 570-574 (1997). https://doi.org:10.1126/science.277.5325.570

37 Cui, F., Blach, S., Manzengo Mingiedi, C., Gonzalez, M. A., Sabry Alaama, A., Mozalevskis, A., Séguy, N., Rewari, B. B., Chan, P. L., Le, L. V., Doherty, M., Luhmann, N., Easterbrook, P., Dirac, M., de Martel, C., Nayagam, S., Hallett, T. B., Vickerman, P., Razavi, H., Lesi, O. & Low-Beer, D. Global reporting of progress towards elimination of hepatitis B and hepatitis C. *The lancet. Gastroenterology & hepatology* **8**, 332-342 (2023). https://doi.org:10.1016/s2468-1253(22)00386-7

38 Alter, M. J. HCV routes of transmission: what goes around comes around. *Seminars in liver disease* **31**, 340-346 (2011). https://doi.org:10.1055/s-0031-1297923

39 Roudot-Thoraval, F. Epidemiology of hepatitis C virus infection. *Clinics and research in hepatology and gastroenterology* **45**, 101596 (2021). https://doi.org:10.1016/j.clinre.2020.101596

40 Benova, L., Mohamoud, Y. A., Calvert, C. & Abu-Raddad, L. J. Vertical transmission of hepatitis C virus: systematic review and meta-analysis. *Clin Infect Dis* **59**, 765-773 (2014). https://doi.org:10.1093/cid/ciu447

41 Deng, S., Zhong, W., Chen, W. & Wang, Z. Hepatitis C viral load and mother-to-child transmission: A systematic review and meta-analysis. *J Gastroenterol Hepatol* **38**, 177-186 (2023). https://doi.org:10.1111/jgh.15998

42 Pitcher, A. B., Borquez, A., Skaathun, B. & Martin, N. K. Mathematical modeling of hepatitis c virus (HCV) prevention among people who inject drugs: A review of the literature and insights for elimination strategies. *J Theor Biol* **481**, 194-201 (2019). https://doi.org:10.1016/j.jtbi.2018.11.013

43 Cooke, G. S., Andrieux-Meyer, I., Applegate, T. L., Atun, R., Burry, J. R., Cheinquer, H., Dusheiko, G., Feld, J. J., Gore, C., Griswold, M. G., Hamid, S., Hellard, M. E., Hou, J., Howell, J., Jia, J., Kravchenko, N., Lazarus, J. V., Lemoine, M., Lesi, O. A., Maistat, L., McMahon, B. J., Razavi, H., Roberts, T., Simmons, B., Sonderup, M. W., Spearman, C. W., Taylor, B. E., Thomas, D. L., Waked, I., Ward, J. W. & Wiktor, S. Z. Accelerating the elimination of viral hepatitis: a Lancet Gastroenterology & Hepatology Commission. *The lancet. Gastroenterology & hepatology* **4**, 135-184 (2019). https://doi.org:10.1016/s2468-1253(18)30270-x

44 Global change in hepatitis C virus prevalence and cascade of care between 2015 and 2020: a modelling study. *The lancet. Gastroenterology & hepatology* **7**, 396-415 (2022). https://doi.org:10.1016/s2468-1253(21)00472-6

45 Moradpour, D., Penin, F. & Rice, C. M. Replication of hepatitis C virus. *Nat Rev Microbiol* **5**, 453-463 (2007). https://doi.org:10.1038/nrmicro1645

46 Mazumdar, B., Banerjee, A., Meyer, K. & Ray, R. Hepatitis C virus E1 envelope glycoprotein interacts with apolipoproteins in facilitating entry into hepatocytes. *Hepatol.* **54**, 1149-1156 (2011). https://doi.org:10.1002/hep.24523

47 Catanese, M. T., Uryu, K., Kopp, M., Edwards, T. J., Andrus, L., Rice, W. J., Silvestry, M., Kuhn, R. J. & Rice, C. M. Ultrastructural analysis of hepatitis C virus particles. *Proceedings of the National Academy of Sciences of the United States of America* **110**, 9505-9510 (2013). https://doi.org:10.1073/pnas.1307527110

48 Zeisel, M. B., Fofana, I., Fafi-Kremer, S. & Baumert, T. F. Hepatitis C virus entry into hepatocytes: molecular mechanisms and targets for antiviral therapies. *Journal of hepatology* **54**, 566-576 (2011). https://doi.org:10.1016/j.jhep.2010.10.014

49 Dearborn, A. D. & Marcotrigiano, J. Hepatitis C Virus Structure: Defined by What It Is Not. *Cold Spring Harbor perspectives in medicine* **10** (2020). https://doi.org:10.1101/cshperspect.a036822

50 André, P., Komurian-Pradel, F., Deforges, S., Perret, M., Berland, J. L., Sodoyer, M., Pol, S., Bréchot, C., Paranhos-Baccalà, G. & Lotteau, V. Characterization of low- and

very-low-density hepatitis C virus RNA-containing particles. *J Virol* **76**, 6919-6928 (2002). https://doi.org:10.1128/jvi.76.14.6919-6928.2002

51 Yu, X., Qiao, M., Atanasov, I., Hu, Z., Kato, T., Liang, T. J. & Zhou, Z. H. Cryo-electron microscopy and three-dimensional reconstructions of hepatitis C virus particles. *Virology* **367**, 126-134 (2007). https://doi.org:10.1016/j.virol.2007.05.038

52 Piver, E., Boyer, A., Gaillard, J., Bull, A., Beaumont, E., Roingeard, P. & Meunier, J. C. Ultrastructural organisation of HCV from the bloodstream of infected patients revealed by electron microscopy after specific immunocapture. *Gut* **66**, 1487-1495 (2017). https://doi.org:10.1136/gutjnl-2016-311726

53 Rice, C. M. New insights into HCV replication: potential antiviral targets. *Top Antivir Med* **19**, 117-120 (2011).

54 Lavie, M., Penin, F. & Dubuisson, J. HCV envelope glycoproteins in evirion assembly and entry. *Future Virology* **10**, 297-312 (2015). https://doi.org:10.2217/fvl.14.114

55 Grakoui, A., Wychowski, C., Lin, C., Feinstone, S. M. & Rice, C. M. Expression and identification of hepatitis C virus polyprotein cleavage products. *J Virol* **67**, 1385-1395 (1993). https://doi.org:10.1128/jvi.67.3.1385-1395.1993

56 Helle, F., Duverlie, G. & Dubuisson, J. The hepatitis C virus glycan shield and evasion of the humoral immune response. *Viruses* **3**, 1909-1932 (2011). https://doi.org:10.3390/v3101909

57 Castelli, M., Clementi, N., Pfaff, J., Sautto, G. A., Diotti, R. A., Burioni, R., Doranz, B. J., Dal Peraro, M., Clementi, M. & Mancini, N. A Biologically-validated HCV E1E2 Heterodimer Structural Model. *Sci Rep* **7**, 214 (2017). https://doi.org:10.1038/s41598-017-00320-7

58 Troesch, M., Meunier, I., Lapierre, P., Lapointe, N., Alvarez, F., Boucher, M. & Soudeyns, H. Study of a novel hypervariable region in hepatitis C virus (HCV) E2 envelope glycoprotein. *Virology* **352**, 357-367 (2006). https://doi.org:10.1016/j.virol.2006.05.015

59 Moradpour, D. & Penin, F. Hepatitis C virus proteins: from structure to function. *Current topics in microbiology and immunology* **369**, 113-142 (2013). https://doi.org:10.1007/978-3-642-27340-7_5

60 Penin, F., Combet, C., Germanidis, G., Frainais, P.-O., Deléage, G. & Pawlotsky, J.-M. Conservation of the Conformation and Positive Charges of Hepatitis C Virus E2 Envelope Glycoprotein Hypervariable Region 1 Points to a Role in Cell Attachment. *J Virol* **75**, 5703-5710 (2001). https://doi.org:doi:10.1128/jvi.75.12.5703-5710.2001

61 Zeisel, M. B., Felmlee, D. J. & Baumert, T. F. Hepatitis C virus entry. *Current topics in microbiology and immunology* **369**, 87-112 (2013). https://doi.org:10.1007/978-3-642-27340-7_4

62 Cao, L., Yu, B., Kong, D., Cong, Q., Yu, T., Chen, Z., Hu, Z., Chang, H., Zhong, J., Baker, D. & He, Y. Functional expression and characterization of the envelope glycoprotein E1E2 heterodimer of hepatitis C virus. *PLoS pathogens* **15**, e1007759 (2019). https://doi.org:10.1371/journal.ppat.1007759

63 Falson, P., Bartosch, B., Alsaleh, K., Tews, B. A., Loquet, A., Ciczora, Y., Riva, L., Montigny, C., Montpellier, C., Duverlie, G., Pécheur, E. I., le Maire, M., Cosset, F. L., Dubuisson, J. & Penin, F. Hepatitis C Virus Envelope Glycoprotein E1 Forms Trimers at the Surface of the Virion. *J Virol* **89**, 10333-10346 (2015). https://doi.org:10.1128/jvi.00991-15

64 Freedman, H., Logan, M. R., Hockman, D., Koehler Leman, J., Law, J. L. M. & Houghton, M. Computational Prediction of the Heterodimeric and Higher-Order Structure of gpE1/gpE2 Envelope Glycoproteins Encoded by Hepatitis C Virus. *J Virol* **91** (2017). https://doi.org:10.1128/jvi.02309-16

65 Oehler, V., Filipe, A., Montserret, R., da Costa, D., Brown, G., Penin, F. & McLauchlan, J. Structural analysis of hepatitis C virus core-E1 signal peptide and requirements for cleavage of the genotype 3a signal sequence by signal peptide peptidase. *J Virol* **86**, 7818-7828 (2012). https://doi.org:10.1128/jvi.00457-12

66 McLauchlan, J. Properties of the hepatitis C virus core protein: a structural protein that modulates cellular processes. *J Viral Hepat* **7**, 2-14 (2000). https://doi.org:10.1046/j.1365-2893.2000.00201.x

67 Bukh, J., Purcell, R. H. & Miller, R. H. Sequence analysis of the core gene of 14 hepatitis C virus genotypes. *Proceedings of the National Academy of Sciences of the United States of America* **91**, 8239-8243 (1994). https://doi.org:10.1073/pnas.91.17.8239

68 Matsumoto, M., Hwang, S. B., Jeng, K.-S., Zhu, N. & Lai, M. M. C. Homotypic Interaction and Multimerization of Hepatitis C Virus Core Protein. *Virology* **218**, 43-51 (1996). https://doi.org:https://doi.org/10.1006/viro.1996.0164

69 Cristofari, G., Ivanyi-Nagy, R., Gabus, C., Boulant, S., Lavergne, J. P., Penin, F. & Darlix, J. L. The hepatitis C virus Core protein is a potent nucleic acid chaperone that directs dimerization of the viral (+) strand RNA in vitro. *Nucleic Acids Res* **32**, 2623-2631 (2004). https://doi.org:10.1093/nar/gkh579

70 Boulant, S., Montserret, R., Hope, R. G., Ratinier, M., Targett-Adams, P., Lavergne, J. P., Penin, F. & McLauchlan, J. Structural determinants that target the hepatitis C virus core protein to lipid droplets. *J Biol Chem* **281**, 22236-22247 (2006). https://doi.org:10.1074/jbc.M601031200

71 McLauchlan, J., Lemberg, M. K., Hope, G. & Martoglio, B. Intramembrane proteolysis promotes trafficking of hepatitis C virus core protein to lipid droplets. *The EMBO journal* **21**, 3980-3988 (2002). https://doi.org:10.1093/emboj/cdf414

72 Strosberg, A. D., Kota, S., Takahashi, V., Snyder, J. K. & Mousseau, G. Core as a Novel Viral Target for Hepatitis C Drugs. *Viruses* **2**, 1734-1751 (2010).

73 Sherwood, A. V., Rivera-Rangel, L. R., Ryberg, L. A., Larsen, H. S., Anker, K. M., Costa, R., Vågbø, C. B., Jakljevič, E., Pham, L. V., Fernandez-Antunez, C., Indrisiunaite, G., Podolska-Charlery, A., Grothen, J. E. R., Langvad, N. W., Fossat, N., Offersgaard, A., Al-Chaer, A., Nielsen, L., Kuśnierczyk, A., Sølund, C., Weis, N., Gottwein, J. M., Holmbeck, K., Bottaro, S., Ramirez, S., Bukh, J., Scheel, T. K. H. & Vinther, J. Hepatitis C virus RNA is 5'-capped with flavin adenine dinucleotide. *Nature* **619**, 811-818 (2023). https://doi.org:10.1038/s41586-023-06301-3

74 Wang, C., Le, S. Y., Ali, N. & Siddiqui, A. An RNA pseudoknot is an essential structural element of the internal ribosome entry site located within the hepatitis C virus 5' noncoding region. *Rna* **1**, 526-537 (1995).

75 Niepmann, M. & Gerresheim, G. K. Hepatitis C Virus Translation Regulation. *International journal of molecular sciences* **21** (2020). https://doi.org:10.3390/ijms21072328

76 Friebe, P., Lohmann, V., Krieger, N. & Bartenschlager, R. Sequences in the 5' nontranslated region of hepatitis C virus required for RNA replication. *J Virol* **75**, 12047-12057 (2001). https://doi.org:10.1128/jvi.75.24.12047-12057.2001

77 Chang, J., Nicolas, E., Marks, D., Sander, C., Lerro, A., Buendia, M. A., Xu, C., Mason, W. S., Moloshok, T., Bort, R., Zaret, K. S. & Taylor, J. M. miR-122, a mammalian liver-specific microRNA, is processed from hcr mRNA and may downregulate the high affinity cationic amino acid transporter CAT-1. *RNA Biol* **1**, 106-113 (2004). https://doi.org:10.4161/rna.1.2.1066

78 Jangra, R. K., Yi, M. & Lemon, S. M. Regulation of hepatitis C virus translation and infectious virus production by the microRNA miR-122. *J Virol* **84**, 6615-6625 (2010). https://doi.org:10.1128/jvi.00417-10

79 Pang, P. S., Pham, E. A., Elazar, M., Patel, S. G., Eckart, M. R. & Glenn, J. S. Structural map of a microRNA-122: hepatitis C virus complex. *J Virol* **86**, 1250-1254 (2012). https://doi.org:10.1128/jvi.06367-11

80 Shimakami, T., Yamane, D., Welsch, C., Hensley, L., Jangra, R. K. & Lemon, S. M. Base pairing between hepatitis C virus RNA and microRNA 122 3' of its seed sequence is essential for genome stabilization and production of infectious virus. *J Virol* **86**, 7372-7383 (2012). https://doi.org:10.1128/jvi.00513-12

81 Mortimer, S. A. & Doudna, J. A. Unconventional miR-122 binding stabilizes the HCV genome by forming a trimolecular RNA structure. *Nucleic Acids Res* **41**, 4230-4240 (2013). https://doi.org:10.1093/nar/gkt075

82 Thibault, P. A., Huys, A., Amador-Cañizares, Y., Gailius, J. E., Pinel, D. E. & Wilson, J. A. Regulation of Hepatitis C Virus Genome Replication by Xrn1 and MicroRNA-122 Binding to Individual Sites in the 5' Untranslated Region. *J Virol* **89**, 6294-6311 (2015). https://doi.org:10.1128/jvi.03631-14

83 Panigrahi, M., Palmer, M. A. & Wilson, J. A. MicroRNA-122 Regulation of HCV Infections: Insights from Studies of miR-122-Independent Replication. *Pathogens* **11** (2022). https://doi.org:10.3390/pathogens11091005

84 Tanaka, T., Kato, N., Cho, M. J., Sugiyama, K. & Shimotohno, K. Structure of the 3' terminus of the hepatitis C virus genome. *J Virol* **70**, 3307-3312 (1996). https://doi.org:10.1128/jvi.70.5.3307-3312.1996

85 Song, Y., Friebe, P., Tzima, E., Jünemann, C., Bartenschlager, R. & Niepmann, M. The hepatitis C virus RNA 3'-untranslated region strongly enhances translation directed by the internal ribosome entry site. *J Virol* **80**, 11579-11588 (2006). https://doi.org:10.1128/jvi.00675-06

86 Friebe, P., Boudet, J., Simorre, J. P. & Bartenschlager, R. Kissing-loop interaction in the 3' end of the hepatitis C virus genome essential for RNA replication. *J Virol* **79**, 380-392 (2005). https://doi.org:10.1128/jvi.79.1.380-392.2005

87 Svitkin, Y. V., Pause, A., Lopez-Lastra, M., Perreault, S. & Sonenberg, N. Complete translation of the hepatitis C virus genome in vitro: membranes play a critical role in the maturation of all virus proteins except for NS3. *J Virol* **79**, 6868-6881 (2005). https://doi.org:10.1128/jvi.79.11.6868-6881.2005

88 Ina, Y., Mizokami, M., Ohba, K. & Gojobori, T. Reduction of synonymous substitutions in the core protein gene of hepatitis C virus. *J Mol Evol* **38**, 50-56 (1994). https://doi.org:10.1007/bf00175495

89 Walewski, J. L., Keller, T. R., Stump, D. D. & Branch, A. D. Evidence for a new hepatitis C virus antigen encoded in an overlapping reading frame. *Rna* **7**, 710-721 (2001). https://doi.org:10.1017/s1355838201010111

90 Dalagiorgou, G., Vassilaki, N., Foka, P., Boumlic, A., Kakkanas, A., Kochlios, E., Khalili, S., Aslanoglou, E., Veletza, S., Orfanoudakis, G., Vassilopoulos, D., Hadziyannis, S. J., Koskinas, J. & Mavromara, P. High levels of HCV core+1 antibodies in HCV patients with hepatocellular carcinoma. *The Journal of general virology* **92**, 1343-1351 (2011). https://doi.org:10.1099/vir.0.023010-0

91 Elsheikh, M. E. A., McClure, C. P., Tarr, A. W. & Irving, W. L. Sero-reactivity to three distinct regions within the hepatitis C virus alternative reading frame protein (ARFP/core+1) in patients with chronic HCV genotype-3 infection. *The Journal of general virology* **103** (2022). https://doi.org:10.1099/jgv.0.001727

92 Vassilaki, N. & Mavromara, P. The HCV ARFP/F/core+1 protein: production and functional analysis of an unconventional viral product. *IUBMB life* **61**, 739-752 (2009). https://doi.org:10.1002/iub.201

93 Bartenschlager, R., Lohmann, V. & Penin, F. The molecular and structural basis of advanced antiviral therapy for hepatitis C virus infection. *Nature Reviews Microbiology* **11**, 482-496 (2013). https://doi.org:10.1038/nrmicro3046

94 Griffin, S. D., Beales, L. P., Clarke, D. S., Worsfold, O., Evans, S. D., Jaeger, J., Harris, M. P. & Rowlands, D. J. The p7 protein of hepatitis C virus forms an ion channel that is blocked by the antiviral drug, Amantadine. *FEBS Lett* **535**, 34-38 (2003). https://doi.org:10.1016/s0014-5793(02)03851-6

95 Steinmann, E., Penin, F., Kallis, S., Patel, A. H., Bartenschlager, R. & Pietschmann, T. Hepatitis C virus p7 protein is crucial for assembly and release of infectious virions. *PLoS pathogens* **3**, e103 (2007). https://doi.org:10.1371/journal.ppat.0030103

96 Callendret, B., Bukh, J., Eccleston, H. B., Heksch, R., Hasselschwert, D. L., Purcell, R. H., Hughes, A. L. & Walker, C. M. Transmission of clonal hepatitis C virus genomes reveals the dominant but transitory role of $CD8^+$ T cells in early viral evolution. *J Virol* **85**, 11833-11845 (2011). https://doi.org:10.1128/jvi.02654-10

97 Kalita, M. M., Griffin, S., Chou, J. J. & Fischer, W. B. Genotype-specific differences in structural features of hepatitis C virus (HCV) p7 membrane protein. *Biochim Biophys Acta* **1848**, 1383-1392 (2015). https://doi.org:10.1016/j.bbamem.2015.03.006

98 Lorenz, I. C., Marcotrigiano, J., Dentzer, T. G. & Rice, C. M. Structure of the catalytic domain of the hepatitis C virus NS2-3 protease. *Nature* **442**, 831-835 (2006). https://doi.org:10.1038/nature04975

99 Jirasko, V., Montserret, R., Appel, N., Janvier, A., Eustachi, L., Brohm, C., Steinmann, E., Pietschmann, T., Penin, F. & Bartenschlager, R. Structural and functional characterization of nonstructural protein 2 for its role in hepatitis C virus assembly. *Journal of Biological Chemistry* **283**, 28546-28562 (2008). https://doi.org:10.1074/jbc.M803981200

100 Lorenz, I. C. The Hepatitis C Virus Nonstructural Protein 2 (NS2): An Up-and-Coming Antiviral Drug Target. *Viruses* **2**, 1635-1646 (2010).

101 Morikawa, K., Lange, C. M., Gouttenoire, J., Meylan, E., Brass, V., Penin, F. & Moradpour, D. Nonstructural protein 3-4A: the Swiss army knife of hepatitis C virus. *J Viral Hepat* **18**, 305-315 (2011). https://doi.org:10.1111/j.1365-2893.2011.01451.x

102 Schregel, V., Jacobi, S., Penin, F. & Tautz, N. Hepatitis C virus NS2 is a protease stimulated by cofactor domains in NS3. *Proceedings of the National Academy of Sciences of the United States of America* **106**, 5342-5347 (2009). https://doi.org:10.1073/pnas.0810950106

103 Murray, C. L., Jones, C. T. & Rice, C. M. Architects of assembly: roles of Flaviviridae non-structural proteins in virion morphogenesis. *Nat Rev Microbiol* **6**, 699-708 (2008). https://doi.org:10.1038/nrmicro1928

104 Isken, O., Langerwisch, U., Jirasko, V., Rehders, D., Redecke, L., Ramanathan, H., Lindenbach, B. D., Bartenschlager, R. & Tautz, N. A conserved NS3 surface patch orchestrates NS2 protease stimulation, NS5A hyperphosphorylation and HCV genome replication. *PLoS pathogens* **11**, e1004736 (2015). https://doi.org:10.1371/journal.ppat.1004736

105 Isken, O., Pham, M. T., Schwanke, H., Schlotthauer, F., Bartenschlager, R. & Tautz, N. Characterization of a multipurpose NS3 surface patch coordinating HCV replicase assembly and virion morphogenesis. *PLoS pathogens* **18**, e1010895 (2022). https://doi.org:10.1371/journal.ppat.1010895

106 Yu, C. C., Lin, P. C., Chiang, C. H., Jen, S. T., Lai, Y. L., Hsu, S. C., Lo, L. C., Lin, J. J., Chan, N. L. & Yu, M. J. Sequential Phosphorylation of Hepatitis C Virus NS5A Protein Requires the ATP-Binding Domain of NS3 Helicase. *J Virol* **96**, e0010722 (2022). https://doi.org:10.1128/jvi.00107-22

107 Brass, V., Berke, J. M., Montserret, R., Blum, H. E., Penin, F. & Moradpour, D. Structural determinants for membrane association and dynamic organization of the hepatitis C virus NS3-4A complex. *Proceedings of the National Academy of Sciences of the United States of America* **105**, 14545-14550 (2008). https://doi.org:10.1073/pnas.0807298105

108 Lindenbach, B. D., Prágai, B. M., Montserret, R., Beran, R. K., Pyle, A. M., Penin, F. & Rice, C. M. The C terminus of hepatitis C virus NS4A encodes an electrostatic switch that regulates NS5A hyperphosphorylation and viral replication. *J Virol* **81**, 8905-8918 (2007). https://doi.org:10.1128/jvi.00937-07

109 Phan, T., Kohlway, A., Dimberu, P., Pyle, A. M. & Lindenbach, B. D. The acidic domain of hepatitis C virus NS4A contributes to RNA replication and virus particle assembly. *J Virol* **85**, 1193-1204 (2011). https://doi.org:10.1128/jvi.01889-10

110 Gouttenoire, J., Montserret, R., Paul, D., Castillo, R., Meister, S., Bartenschlager, R., Penin, F. & Moradpour, D. Aminoterminal amphipathic α-helix AH1 of hepatitis C virus nonstructural protein 4B possesses a dual role in RNA replication and virus production. *PLoS pathogens* **10**, e1004501 (2014). https://doi.org:10.1371/journal.ppat.1004501

111 Egger, D., Wölk, B., Gosert, R., Bianchi, L., Blum, H. E., Moradpour, D. & Bienz, K. Expression of hepatitis C virus proteins induces distinct membrane alterations including a candidate viral replication complex. *J Virol* **76**, 5974-5984 (2002). https://doi.org:10.1128/jvi.76.12.5974-5984.2002

112 Einav, S., Sklan, E. H., Moon, H. M., Gehrig, E., Liu, P., Hao, Y., Lowe, A. W. & Glenn, J. S. The nucleotide binding motif of hepatitis C virus NS4B can mediate cellular transformation and tumor formation without Ha-ras co-transfection. *Hepatol.* **47**, 827-835 (2008). https://doi.org:10.1002/hep.22108

113 Gouttenoire, J., Castet, V., Montserret, R., Arora, N., Raussens, V., Ruysschaert, J. M., Diesis, E., Blum, H. E., Penin, F. & Moradpour, D. Identification of a novel determinant for membrane association in hepatitis C virus nonstructural protein 4B. *J Virol* **83**, 6257-6268 (2009). https://doi.org:10.1128/jvi.02663-08

114 Moradpour, D., Gosert, R., Egger, D., Penin, F., Blum, H. E. & Bienz, K. Membrane association of hepatitis C virus nonstructural proteins and identification of the membrane alteration that harbors the viral replication complex. *Antiviral research* **60**, 103-109 (2003). https://doi.org:10.1016/j.antiviral.2003.08.017

115 Gouttenoire, J., Roingeard, P., Penin, F. & Moradpour, D. Amphipathic alpha-helix AH2 is a major determinant for the oligomerization of hepatitis C virus nonstructural protein 4B. *J Virol* **84**, 12529-12537 (2010). https://doi.org:10.1128/jvi.01798-10

116 Jones, D. M., Patel, A. H., Targett-Adams, P. & McLauchlan, J. The hepatitis C virus NS4B protein can trans-complement viral RNA replication and modulates production of infectious virus. *J Virol* **83**, 2163-2177 (2009). https://doi.org:10.1128/jvi.01885-08

117 Nitta, S., Sakamoto, N., Nakagawa, M., Kakinuma, S., Mishima, K., Kusano-Kitazume, A., Kiyohashi, K., Murakawa, M., Nishimura-Sakurai, Y., Azuma, S., Tasaka-Fujita, M., Asahina, Y., Yoneyama, M., Fujita, T. & Watanabe, M. Hepatitis C virus NS4B protein targets STING and abrogates RIG-I-mediated type I interferon-dependent innate immunity. *Hepatol.* **57**, 46-58 (2013). https://doi.org:10.1002/hep.26017

118 Ross-Thriepland, D. & Harris, M. Hepatitis C virus NS5A: enigmatic but still promiscuous 10 years on! *The Journal of general virology* **96**, 727-738 (2015). https://doi.org:10.1099/jgv.0.000009
119 Moradpour, D., Brass, V. & Penin, F. Function follows form: the structure of the N-terminal domain of HCV NS5A. *Hepatol.* **42**, 732-735 (2005). https://doi.org:10.1002/hep.20851
120 Tellinghuisen, T. L., Marcotrigiano, J. & Rice, C. M. Structure of the zinc-binding domain of an essential component of the hepatitis C virus replicase. *Nature* **435**, 374-379 (2005). https://doi.org:10.1038/nature03580
121 Love, R. A., Brodsky, O., Hickey, M. J., Wells, P. A. & Cronin, C. N. Crystal structure of a novel dimeric form of NS5A domain I protein from hepatitis C virus. *J Virol* **83**, 4395-4403 (2009). https://doi.org:10.1128/jvi.02352-08
122 Foster, T. L., Belyaeva, T., Stonehouse, N. J., Pearson, A. R. & Harris, M. All three domains of the hepatitis C virus nonstructural NS5A protein contribute to RNA binding. *J Virol* **84**, 9267-9277 (2010). https://doi.org:10.1128/jvi.00616-10
123 Huang, L., Hwang, J., Sharma, S. D., Hargittai, M. R., Chen, Y., Arnold, J. J., Raney, K. D. & Cameron, C. E. Hepatitis C virus nonstructural protein 5A (NS5A) is an RNA-binding protein. *J Biol Chem* **280**, 36417-36428 (2005). https://doi.org:10.1074/jbc.M508175200
124 Romero-Brey, I., Berger, C., Kallis, S., Kolovou, A., Paul, D., Lohmann, V. & Bartenschlager, R. NS5A Domain 1 and Polyprotein Cleavage Kinetics Are Critical for Induction of Double-Membrane Vesicles Associated with Hepatitis C Virus Replication. *mBio* **6**, e00759 (2015). https://doi.org:10.1128/mBio.00759-15
125 Appel, N., Zayas, M., Miller, S., Krijnse-Locker, J., Schaller, T., Friebe, P., Kallis, S., Engel, U. & Bartenschlager, R. Essential role of domain III of nonstructural protein 5A for hepatitis C virus infectious particle assembly. *PLoS pathogens* **4**, e1000035 (2008). https://doi.org:10.1371/journal.ppat.1000035
126 Ross-Thriepland, D. & Harris, M. Insights into the complexity and functionality of hepatitis C virus NS5A phosphorylation. *J Virol* **88**, 1421-1432 (2014). https://doi.org:10.1128/jvi.03017-13
127 Foster, T. L., Gallay, P., Stonehouse, N. J. & Harris, M. Cyclophilin A interacts with domain II of hepatitis C virus NS5A and stimulates RNA binding in an isomerase-dependent manner. *J Virol* **85**, 7460-7464 (2011). https://doi.org:10.1128/jvi.00393-11
128 Dujardin, M., Madan, V., Gandhi, N. S., Cantrelle, F. X., Launay, H., Huvent, I., Bartenschlager, R., Lippens, G. & Hanoulle, X. Cyclophilin A allows the allosteric regulation of a structural motif in the disordered domain 2 of NS5A and thereby fine-tunes HCV RNA replication. *J Biol Chem* **294**, 13171-13185 (2019). https://doi.org:10.1074/jbc.RA119.009537
129 Feuerstein, S., Solyom, Z., Aladag, A., Favier, A., Schwarten, M., Hoffmann, S., Willbold, D. & Brutscher, B. Transient structure and SH3 interaction sites in an intrinsically disordered fragment of the hepatitis C virus protein NS5A. *J Mol Biol* **420**, 310-323 (2012). https://doi.org:10.1016/j.jmb.2012.04.023
130 Gale, M. J., Jr., Korth, M. J., Tang, N. M., Tan, S. L., Hopkins, D. A., Dever, T. E., Polyak, S. J., Gretch, D. R. & Katze, M. G. Evidence that hepatitis C virus resistance to interferon is mediated through repression of the PKR protein kinase by the nonstructural 5A protein. *Virology* **230**, 217-227 (1997). https://doi.org:10.1006/viro.1997.8493
131 Tellinghuisen, T. L., Foss, K. L., Treadaway, J. C. & Rice, C. M. Identification of residues required for RNA replication in domains II and III of the hepatitis C virus NS5A protein. *J Virol* **82**, 1073-1083 (2008). https://doi.org:10.1128/jvi.00328-07

132 Ross-Thriepland, D., Amako, Y. & Harris, M. The C terminus of NS5A domain II is a key determinant of hepatitis C virus genome replication, but is not required for virion assembly and release. *The Journal of general virology* **94**, 1009-1018 (2013). https://doi.org:10.1099/vir.0.050633-0

133 Hughes, M., Gretton, S., Shelton, H., Brown, D. D., McCormick, C. J., Angus, A. G., Patel, A. H., Griffin, S. & Harris, M. A conserved proline between domains II and III of hepatitis C virus NS5A influences both RNA replication and virus assembly. *J Virol* **83**, 10788-10796 (2009). https://doi.org:10.1128/jvi.02406-08

134 Mankouri, J., Dallas, M. L., Hughes, M. E., Griffin, S. D., Macdonald, A., Peers, C. & Harris, M. Suppression of a pro-apoptotic K+ channel as a mechanism for hepatitis C virus persistence. *Proceedings of the National Academy of Sciences of the United States of America* **106**, 15903-15908 (2009). https://doi.org:10.1073/pnas.0906798106

135 Fridell, R. A., Qiu, D., Wang, C., Valera, L. & Gao, M. Resistance analysis of the hepatitis C virus NS5A inhibitor BMS-790052 in an in vitro replicon system. *Antimicrobial agents and chemotherapy* **54**, 3641-3650 (2010). https://doi.org:10.1128/aac.00556-10

136 Tellinghuisen, T. L., Foss, K. L. & Treadaway, J. Regulation of hepatitis C virion production via phosphorylation of the NS5A protein. *PLoS pathogens* **4**, e1000032 (2008). https://doi.org:10.1371/journal.ppat.1000032

137 Kaneko, T., Tanji, Y., Satoh, S., Hijikata, M., Asabe, S., Kimura, K. & Shimotohno, K. Production of two phosphoproteins from the NS5A region of the hepatitis C viral genome. *Biochemical and biophysical research communications* **205**, 320-326 (1994). https://doi.org:10.1006/bbrc.1994.2667

138 Secci, E., Luchinat, E. & Banci, L. The Casein Kinase 2-Dependent Phosphorylation of NS5A Domain 3 from Hepatitis C Virus Followed by Time-Resolved NMR Spectroscopy. *Chembiochem : a European journal of chemical biology* **17**, 328-333 (2016). https://doi.org:10.1002/cbic.201500551

139 Masaki, T., Suzuki, R., Murakami, K., Aizaki, H., Ishii, K., Murayama, A., Date, T., Matsuura, Y., Miyamura, T., Wakita, T. & Suzuki, T. Interaction of hepatitis C virus nonstructural protein 5A with core protein is critical for the production of infectious virus particles. *J Virol* **82**, 7964-7976 (2008). https://doi.org:10.1128/jvi.00826-08

140 Miyanari, Y., Atsuzawa, K., Usuda, N., Watashi, K., Hishiki, T., Zayas, M., Bartenschlager, R., Wakita, T., Hijikata, M. & Shimotohno, K. The lipid droplet is an important organelle for hepatitis C virus production. *Nat Cell Biol* **9**, 1089-1097 (2007). https://doi.org:10.1038/ncb1631

141 Reiss, S., Harak, C., Romero-Brey, I., Radujkovic, D., Klein, R., Ruggieri, A., Rebhan, I., Bartenschlager, R. & Lohmann, V. The lipid kinase phosphatidylinositol-4 kinase III alpha regulates the phosphorylation status of hepatitis C virus NS5A. *PLoS pathogens* **9**, e1003359 (2013). https://doi.org:10.1371/journal.ppat.1003359

142 Hanoulle, X., Badillo, A., Wieruszeski, J. M., Verdegem, D., Landrieu, I., Bartenschlager, R., Penin, F. & Lippens, G. Hepatitis C virus NS5A protein is a substrate for the peptidyl-prolyl cis/trans isomerase activity of cyclophilins A and B. *J Biol Chem* **284**, 13589-13601 (2009). https://doi.org:10.1074/jbc.M809244200

143 Tanji, Y., Kaneko, T., Satoh, S. & Shimotohno, K. Phosphorylation of hepatitis C virus-encoded nonstructural protein NS5A. *J Virol* **69**, 3980-3986 (1995). https://doi.org:doi:10.1128/jvi.69.7.3980-3986.1995

144 Koch, J. O. & Bartenschlager, R. Modulation of Hepatitis C Virus NS5A Hyperphosphorylation by Nonstructural Proteins NS3, NS4A, and NS4B. *J Virol* **73**, 7138-7146 (1999). https://doi.org:doi:10.1128/jvi.73.9.7138-7146.1999

145 Neddermann, P., Clementi, A. & Francesco, R. D. Hyperphosphorylation of the Hepatitis C Virus NS5A Protein Requires an Active NS3 Protease, NS4A, NS4B, and NS5A Encoded on the Same Polyprotein. *J Virol* **73**, 9984-9991 (1999). https://doi.org:doi:10.1128/jvi.73.12.9984-9991.1999

146 Hsu, S. C., Tsai, C. N., Lee, K. Y., Pan, T. C., Lo, C. W. & Yu, M. J. Sequential S232/S235/S238 Phosphorylation of the Hepatitis C Virus Nonstructural Protein 5A. *J Virol* **92** (2018). https://doi.org:10.1128/jvi.01295-18

147 Tsai, C. N., Pan, T. C., Chiang, C. H., Yu, C. C., Su, S. H. & Yu, M. J. Serine 229 Balances the Hepatitis C Virus Nonstructural Protein NS5A between Hypo- and Hyperphosphorylated States. *J Virol* **93** (2019). https://doi.org:10.1128/jvi.01028-19

148 Appel, N., Pietschmann, T. & Bartenschlager, R. Mutational analysis of hepatitis C virus nonstructural protein 5A: potential role of differential phosphorylation in RNA replication and identification of a genetically flexible domain. *J Virol* **79**, 3187-3194 (2005). https://doi.org:10.1128/jvi.79.5.3187-3194.2005

149 Masaki, T., Matsunaga, S., Takahashi, H., Nakashima, K., Kimura, Y., Ito, M., Matsuda, M., Murayama, A., Kato, T., Hirano, H., Endo, Y., Lemon, S. M., Wakita, T., Sawasaki, T. & Suzuki, T. Involvement of hepatitis C virus NS5A hyperphosphorylation mediated by casein kinase I-α in infectious virus production. *J Virol* **88**, 7541-7555 (2014). https://doi.org:10.1128/jvi.03170-13

150 Ross-Thriepland, D., Mankouri, J. & Harris, M. Serine phosphorylation of the hepatitis C virus NS5A protein controls the establishment of replication complexes. *J Virol* **89**, 3123-3135 (2015). https://doi.org:10.1128/jvi.02995-14

151 Chong, W. M., Hsu, S. C., Kao, W. T., Lo, C. W., Lee, K. Y., Shao, J. S., Chen, Y. H., Chang, J., Chen, S. S. & Yu, M. J. Phosphoproteomics Identified an NS5A Phosphorylation Site Involved in Hepatitis C Virus Replication. *J Biol Chem* **291**, 3918-3931 (2016). https://doi.org:10.1074/jbc.M115.675413

152 Goonawardane, N., Gebhardt, A., Bartlett, C., Pichlmair, A. & Harris, M. Phosphorylation of Serine 225 in Hepatitis C Virus NS5A Regulates Protein-Protein Interactions. *J Virol* **91** (2017). https://doi.org:10.1128/jvi.00805-17

153 Harak, C., Meyrath, M., Romero-Brey, I., Schenk, C., Gondeau, C., Schult, P., Esser-Nobis, K., Saeed, M., Neddermann, P., Schnitzler, P., Gotthardt, D., Perez-Del-Pulgar, S., Neumann-Haefelin, C., Thimme, R., Meuleman, P., Vondran, F. W., De Francesco, R., Rice, C. M., Bartenschlager, R. & Lohmann, V. Tuning a cellular lipid kinase activity adapts hepatitis C virus to replication in cell culture. *Nature microbiology* **2**, 16247 (2016). https://doi.org:10.1038/nmicrobiol.2016.247

154 Kandangwa, M. & Liu, Q. HCV NS5A hyperphosphorylation is involved in viral translation modulation. *Biochemical and biophysical research communications* **520**, 192-197 (2019). https://doi.org:10.1016/j.bbrc.2019.09.105

155 Schenk, C., Meyrath, M., Warnken, U., Schnölzer, M., Mier, W., Harak, C. & Lohmann, V. Characterization of a Threonine-Rich Cluster in Hepatitis C Virus Nonstructural Protein 5A and Its Contribution to Hyperphosphorylation. *J Virol* **92** (2018). https://doi.org:10.1128/jvi.00737-18

156 Neddermann, P., Quintavalle, M., Di Pietro, C., Clementi, A., Cerretani, M., Altamura, S., Bartholomew, L. & De Francesco, R. Reduction of hepatitis C virus NS5A hyperphosphorylation by selective inhibition of cellular kinases activates viral RNA replication in cell culture. *J Virol* **78**, 13306-13314 (2004). https://doi.org:10.1128/jvi.78.23.13306-13314.2004

157 Lemay, K. L., Treadaway, J., Angulo, I. & Tellinghuisen, T. L. A hepatitis C virus NS5A phosphorylation site that regulates RNA replication. *J Virol* **87**, 1255-1260 (2013). https://doi.org:10.1128/jvi.02154-12

158 Eyre, N. S., Hampton-Smith, R. J., Aloia, A. L., Eddes, J. S., Simpson, K. J., Hoffmann, P. & Beard, M. R. Phosphorylation of NS5A Serine-235 is essential to hepatitis C virus RNA replication and normal replication compartment formation. *Virology* **491**, 27-44 (2016). https://doi.org:10.1016/j.virol.2016.01.018

159 Goonawardane, N., Yin, C. & Harris, M. Phenotypic analysis of mutations at residue 146 provides insights into the relationship between NS5A hyperphosphorylation and hepatitis C virus genome replication. *The Journal of general virology* **101**, 252-264 (2020). https://doi.org:10.1099/jgv.0.001366

160 Pan, T. C., Lo, C. W., Chong, W. M., Tsai, C. N., Lee, K. Y., Chen, P. Y., Liao, J. C. & Yu, M. J. Differential Proteomics Reveals Discrete Functions of Proteins Interacting with Hypo- versus Hyper-phosphorylated NS5A of the Hepatitis C Virus. *Journal of proteome research* **18**, 2813-2825 (2019). https://doi.org:10.1021/acs.jproteome.9b00130

161 Schmidt-Mende, J., Bieck, E., Hugle, T., Penin, F., Rice, C. M., Blum, H. E. & Moradpour, D. Determinants for membrane association of the hepatitis C virus RNA-dependent RNA polymerase. *J Biol Chem* **276**, 44052-44063 (2001). https://doi.org:10.1074/jbc.M103358200

162 Behrens, S. E., Tomei, L. & De Francesco, R. Identification and properties of the RNA-dependent RNA polymerase of hepatitis C virus. *The EMBO journal* **15**, 12-22 (1996).

163 Bressanelli, S., Tomei, L., Roussel, A., Incitti, I., Vitale, R. L., Mathieu, M., De Francesco, R. & Rey, F. A. Crystal structure of the RNA-dependent RNA polymerase of hepatitis C virus. *Proceedings of the National Academy of Sciences of the United States of America* **96**, 13034-13039 (1999). https://doi.org:10.1073/pnas.96.23.13034

164 Karam, P., Powdrill, M. H., Liu, H. W., Vasquez, C., Mah, W., Bernatchez, J., Götte, M. & Cosa, G. Dynamics of hepatitis C virus (HCV) RNA-dependent RNA polymerase NS5B in complex with RNA. *J Biol Chem* **289**, 14399-14411 (2014). https://doi.org:10.1074/jbc.M113.529743

165 Waked, I. Case study of hepatitis C virus control in Egypt: impact of access program. *Antivir Ther* **27**, 13596535211067592 (2022). https://doi.org:10.1177/13596535211067592

166 Echeverría, N., Moratorio, G., Cristina, J. & Moreno, P. Hepatitis C virus genetic variability and evolution. *World journal of hepatology* **7**, 831-845 (2015). https://doi.org:10.4254/wjh.v7.i6.831

167 Geller, R., Estada, Ú., Peris, J. B., Andreu, I., Bou, J. V., Garijo, R., Cuevas, J. M., Sabariegos, R., Mas, A. & Sanjuán, R. Highly heterogeneous mutation rates in the hepatitis C virus genome. *Nature microbiology* **1**, 16045 (2016). https://doi.org:10.1038/nmicrobiol.2016.45

168 Simmonds, P., Smith, D. B., McOmish, F., Yap, P. L., Kolberg, J., Urdea, M. S. & Holmes, E. C. Identification of genotypes of hepatitis C virus by sequence comparisons in the core, E1 and NS-5 regions. *The Journal of general virology* **75 (Pt 5)**, 1053-1061 (1994). https://doi.org:10.1099/0022-1317-75-5-1053

169 Smith, D. B., Bukh, J., Kuiken, C., Muerhoff, A. S., Rice, C. M., Stapleton, J. T. & Simmonds, P. *Classification and genotype / subtype assignments of hepatitis C virus*, <https://ictv.global/sg_wiki/flaviviridae/hepacivirus> (2022).

170 Hedskog, C., Parhy, B., Chang, S., Zeuzem, S., Moreno, C., Shafran, S. D., Borgia, S. M., Asselah, T., Alric, L., Abergel, A., Chen, J. J., Collier, J., Kapoor, D., Hyland, R. H., Simmonds, P., Mo, H. & Svarovskaia, E. S. Identification of 19 Novel Hepatitis C Virus Subtypes-Further Expanding HCV Classification. *Open Forum Infect Dis* **6**, ofz076 (2019). https://doi.org:10.1093/ofid/ofz076

171 Simmonds, P., Bukh, J., Combet, C., Deléage, G., Enomoto, N., Feinstone, S., Halfon, P., Inchauspé, G., Kuiken, C., Maertens, G., Mizokami, M., Murphy, D. G., Okamoto, H., Pawlotsky, J. M., Penin, F., Sablon, E., Shin, I. T., Stuyver, L. J., Thiel, H. J., Viazov, S., Weiner, A. J. & Widell, A. Consensus proposals for a unified system of nomenclature of hepatitis C virus genotypes. *Hepatol.* **42**, 962-973 (2005). https://doi.org:10.1002/hep.20819

172 Scheel, T. K., Gottwein, J. M., Mikkelsen, L. S., Jensen, T. B. & Bukh, J. Recombinant HCV variants with NS5A from genotypes 1-7 have different sensitivities to an NS5A inhibitor but not interferon-α. *Gastroenterology* **140**, 1032-1042 (2011). https://doi.org:10.1053/j.gastro.2010.11.036

173 Global prevalence and genotype distribution of hepatitis C virus infection in 2015: a modelling study. *The lancet. Gastroenterology & hepatology* **2**, 161-176 (2017). https://doi.org:10.1016/s2468-1253(16)30181-9

174 Borgia, S. M., Hedskog, C., Parhy, B., Hyland, R. H., Stamm, L. M., Brainard, D. M., Subramanian, M. G., McHutchison, J. G., Mo, H., Svarovskaia, E. & Shafran, S. D. Identification of a Novel Hepatitis C Virus Genotype From Punjab, India: Expanding Classification of Hepatitis C Virus Into 8 Genotypes. *J Infect Dis* **218**, 1722-1729 (2018). https://doi.org:10.1093/infdis/jiy401

175 Guntipalli, P., Pakala, R., Kumari Gara, S., Ahmed, F., Bhatnagar, A., Endaya Coronel, M. K., Razzack, A. A., Solimando, A. G., Thompson, A., Andrews, K., Enebong Nya, G., Ahmad, S., Ranaldo, R., Cozzolongo, R. & Shahini, E. Worldwide prevalence, genotype distribution and management of hepatitis C. *Acta Gastroenterol Belg* **84**, 637-656 (2021). https://doi.org:10.51821/84.4.015

176 Cuypers, L., Ceccherini-Silberstein, F., Van Laethem, K., Li, G., Vandamme, A.-M. & Rockstroh, J. K. Impact of HCV genotype on treatment regimens and drug resistance: a snapshot in time. *Reviews in Medical Virology* **26**, 408-434 (2016). https://doi.org:https://doi.org/10.1002/rmv.1895

177 Eigen, M. & Schuster, P. The hypercycle. A principle of natural self-organization. Part A: Emergence of the hypercycle. *Naturwissenschaften* **64**, 541-565 (1977). https://doi.org:10.1007/bf00450633

178 Domingo, E., Escarmís, C., Lázaro, E. & Manrubia, S. C. Quasispecies dynamics and RNA virus extinction. *Virus research* **107**, 129-139 (2005). https://doi.org:10.1016/j.virusres.2004.11.003

179 Bordería, A. V., Rozen-Gagnon, K. & Vignuzzi, M. Fidelity Variants and RNA Quasispecies. *Current topics in microbiology and immunology* **392**, 303-322 (2016). https://doi.org:10.1007/82_2015_483

180 Ball, J. K., Tarr, A. W. & McKeating, J. A. The past, present and future of neutralizing antibodies for hepatitis C virus. *Antiviral research* **105**, 100-111 (2014). https://doi.org:10.1016/j.antiviral.2014.02.013

181 Pawlotsky, J. M. Hepatitis C Virus Resistance to Direct-Acting Antiviral Drugs in Interferon-Free Regimens. *Gastroenterology* **151**, 70-86 (2016). https://doi.org:10.1053/j.gastro.2016.04.003

182 Tscherne, D. M., Evans, M. J., von Hahn, T., Jones, C. T., Stamataki, Z., McKeating, J. A., Lindenbach, B. D. & Rice, C. M. Superinfection exclusion in cells infected with hepatitis C virus. *J Virol* **81**, 3693-3703 (2007). https://doi.org:10.1128/jvi.01748-06

183 Eyster, M. E., Sherman, K. E., Goedert, J. J., Katsoulidou, A. & Hatzakis, A. Prevalence and changes in hepatitis C virus genotypes among multitransfused persons with hemophilia. The Multicenter Hemophilia Cohort Study. *J Infect Dis* **179**, 1062-1069 (1999). https://doi.org:10.1086/314708

184 Laskus, T., Wang, L. F., Radkowski, M., Vargas, H., Nowicki, M., Wilkinson, J. & Rakela, J. Exposure of hepatitis C virus (HCV) RNA-positive recipients to HCV RNA-positive blood donors results in rapid predominance of a single donor strain and exclusion and/or suppression of the recipient strain. *J Virol* **75**, 2059-2066 (2001). https://doi.org:10.1128/jvi.75.5.2059-2066.2001

185 Herring, B. L., Page-Shafer, K., Tobler, L. H. & Delwart, E. L. Frequent hepatitis C virus superinfection in injection drug users. *J Infect Dis* **190**, 1396-1403 (2004). https://doi.org:10.1086/424491

186 Schaller, T., Appel, N., Koutsoudakis, G., Kallis, S., Lohmann, V., Pietschmann, T. & Bartenschlager, R. Analysis of hepatitis C virus superinfection exclusion by using novel fluorochrome gene-tagged viral genomes. *J Virol* **81**, 4591-4603 (2007). https://doi.org:10.1128/jvi.02144-06

187 Sentandreu, V., Jiménez-Hernández, N., Torres-Puente, M., Bracho, M. A., Valero, A., Gosalbes, M. J., Ortega, E., Moya, A. & González-Candelas, F. Evidence of recombination in intrapatient populations of hepatitis C virus. *PloS one* **3**, e3239 (2008). https://doi.org:10.1371/journal.pone.0003239

188 Simmonds, P. Genetic diversity and evolution of hepatitis C virus--15 years on. *The Journal of general virology* **85**, 3173-3188 (2004). https://doi.org:10.1099/vir.0.80401-0

189 González-Candelas, F., López-Labrador, F. X. & Bracho, M. A. Recombination in hepatitis C virus. *Viruses* **3**, 2006-2024 (2011). https://doi.org:10.3390/v3102006

190 Stelzl, E., Haas, B., Bauer, B., Zhang, S., Fiss, E. H., Hillman, G., Hamilton, A. T., Mehta, R., Heil, M. L., Marins, E. G., Santner, B. I. & Kessler, H. H. First identification of a recombinant form of hepatitis C virus in Austrian patients by full-genome next generation sequencing. *PloS one* **12**, e0181273 (2017). https://doi.org:10.1371/journal.pone.0181273

191 Karchava, M., Waldenström, J., Parker, M., Hallack, R., Sharvadze, L., Gatserelia, L., Chkhartishvili, N., Dvali, N., Dzigua, L., Dolmazashvili, E., Norder, H. & Tsertsvadze, T. High incidence of the hepatitis C virus recombinant 2k/1b in Georgia: Recommendations for testing and treatment. *Hepatol Res* **45**, 1292-1298 (2015). https://doi.org:10.1111/hepr.12505

192 Raghwani, J., Thomas, X. V., Koekkoek, S. M., Schinkel, J., Molenkamp, R., van de Laar, T. J., Takebe, Y., Tanaka, Y., Mizokami, M., Rambaut, A. & Pybus, O. G. Origin and evolution of the unique hepatitis C virus circulating recombinant form 2k/1b. *J Virol* **86**, 2212-2220 (2012). https://doi.org:10.1128/jvi.06184-11

193 Demetriou, V. L., Kyriakou, E. & Kostrikis, L. G. Near-full genome characterisation of two natural intergenotypic 2k/1b recombinant hepatitis C virus isolates. *Adv Virol* **2011**, 710438 (2011). https://doi.org:10.1155/2011/710438

194 Morel, V., Descamps, V., François, C., Fournier, C., Brochot, E., Capron, D., Duverlie, G. & Castelain, S. Emergence of a genomic variant of the recombinant 2k/1b strain during a mixed Hepatitis C infection: a case report. *J Clin Virol* **47**, 382-386 (2010). https://doi.org:10.1016/j.jcv.2010.01.011

195 Kurbanov, F., Tanaka, Y., Avazova, D., Khan, A., Sugauchi, F., Kan, N., Kurbanova-Khudayberganova, D., Khikmatullaeva, A., Musabaev, E. & Mizokami, M. Detection of hepatitis C virus natural recombinant RF1_2k/1b strain among intravenous drug users in Uzbekistan. *Hepatol Res* **38**, 457-464 (2008). https://doi.org:10.1111/j.1872-034X.2007.00293.x

196 Moreau, I., Hegarty, S., Levis, J., Sheehy, P., Crosbie, O., Kenny-Walsh, E. & Fanning, L. J. Serendipitous identification of natural intergenotypic recombinants of hepatitis C in Ireland. *Virology journal* **3**, 95 (2006). https://doi.org:10.1186/1743-422x-3-95

197 Kalinina, O., Norder, H., Mukomolov, S. & Magnius, L. O. A natural intergenotypic recombinant of hepatitis C virus identified in St. Petersburg. *J Virol* **76**, 4034-4043 (2002). https://doi.org:10.1128/jvi.76.8.4034-4043.2002
198 Agnello, V., Abel, G., Elfahal, M., Knight, G. B. & Zhang, Q. X. Hepatitis C virus and other flaviviridae viruses enter cells via low density lipoprotein receptor. *Proceedings of the National Academy of Sciences of the United States of America* **96**, 12766-12771 (1999). https://doi.org:10.1073/pnas.96.22.12766
199 Barth, H., Schafer, C., Adah, M. I., Zhang, F., Linhardt, R. J., Toyoda, H., Kinoshita-Toyoda, A., Toida, T., Van Kuppevelt, T. H., Depla, E., Von Weizsacker, F., Blum, H. E. & Baumert, T. F. Cellular binding of hepatitis C virus envelope glycoprotein E2 requires cell surface heparan sulfate. *J Biol Chem* **278**, 41003-41012 (2003). https://doi.org:10.1074/jbc.M302267200
200 Scarselli, E., Ansuini, H., Cerino, R., Roccasecca, R. M., Acali, S., Filocamo, G., Traboni, C., Nicosia, A., Cortese, R. & Vitelli, A. The human scavenger receptor class B type I is a novel candidate receptor for the hepatitis C virus. *The EMBO journal* **21**, 5017-5025 (2002). https://doi.org:10.1093/emboj/cdf529
201 Sainz, B., Jr., Barretto, N., Martin, D. N., Hiraga, N., Imamura, M., Hussain, S., Marsh, K. A., Yu, X., Chayama, K., Alrefai, W. A. & Uprichard, S. L. Identification of the Niemann-Pick C1-like 1 cholesterol absorption receptor as a new hepatitis C virus entry factor. *Nat Med* **18**, 281-285 (2012). https://doi.org:10.1038/nm.2581
202 Fan, H., Qiao, L., Kang, K. D., Fan, J., Wei, W. & Luo, G. Attachment and Postattachment Receptors Important for Hepatitis C Virus Infection and Cell-to-Cell Transmission. *J Virol* **91** (2017). https://doi.org:10.1128/jvi.00280-17
203 Evans, M. J., von Hahn, T., Tscherne, D. M., Syder, A. J., Panis, M., Wölk, B., Hatziioannou, T., McKeating, J. A., Bieniasz, P. D. & Rice, C. M. Claudin-1 is a hepatitis C virus co-receptor required for a late step in entry. *Nature* **446**, 801-805 (2007). https://doi.org:10.1038/nature05654
204 Liu, S., Yang, W., Shen, L., Turner, J. R., Coyne, C. B. & Wang, T. Tight junction proteins claudin-1 and occludin control hepatitis C virus entry and are downregulated during infection to prevent superinfection. *J Virol* **83**, 2011-2014 (2009). https://doi.org:10.1128/jvi.01888-08
205 Lupberger, J., Zeisel, M. B., Xiao, F., Thumann, C., Fofana, I., Zona, L., Davis, C., Mee, C. J., Turek, M., Gorke, S., Royer, C., Fischer, B., Zahid, M. N., Lavillette, D., Fresquet, J., Cosset, F. L., Rothenberg, S. M., Pietschmann, T., Patel, A. H., Pessaux, P., Doffoël, M., Raffelsberger, W., Poch, O., McKeating, J. A., Brino, L. & Baumert, T. F. EGFR and EphA2 are host factors for hepatitis C virus entry and possible targets for antiviral therapy. *Nat Med* **17**, 589-595 (2011). https://doi.org:10.1038/nm.2341
206 Cao, L., Chen, J., Wang, Y., Yang, Y., Qing, J., Rao, Z., Chen, X. & Lou, Z. Identification of serotonin 2A receptor as a novel HCV entry factor by a chemical biology strategy. *Protein Cell* **10**, 178-195 (2019). https://doi.org:10.1007/s13238-018-0521-z
207 Witteveldt, J., Evans, M. J., Bitzegeio, J., Koutsoudakis, G., Owsianka, A. M., Angus, A. G., Keck, Z. Y., Foung, S. K., Pietschmann, T., Rice, C. M. & Patel, A. H. CD81 is dispensable for hepatitis C virus cell-to-cell transmission in hepatoma cells. *The Journal of general virology* **90**, 48-58 (2009). https://doi.org:10.1099/vir.0.006700-0
208 Pietschmann, T. & Brown, R. J. P. Hepatitis C Virus. *Trends Microbiol* **27**, 379-380 (2019). https://doi.org:10.1016/j.tim.2019.01.001
209 Trotard, M., Lepère-Douard, C., Régeard, M., Piquet-Pellorce, C., Lavillette, D., Cosset, F. L., Gripon, P. & Le Seyec, J. Kinases required in hepatitis C virus entry and

replication highlighted by small interference RNA screening. *FASEB J* **23**, 3780-3789 (2009). https://doi.org:10.1096/fj.09-131920

210 Colpitts, C. C., Tsai, P. L. & Zeisel, M. B. Hepatitis C Virus Entry: An Intriguingly Complex and Highly Regulated Process. *International journal of molecular sciences* **21** (2020). https://doi.org:10.3390/ijms21062091

211 Pérard, J., Leyrat, C., Baudin, F., Drouet, E. & Jamin, M. Structure of the full-length HCV IRES in solution. *Nat Commun* **4**, 1612 (2013). https://doi.org:10.1038/ncomms2611

212 Kieft, J. S., Zhou, K., Jubin, R. & Doudna, J. A. Mechanism of ribosome recruitment by hepatitis C IRES RNA. *Rna* **7**, 194-206 (2001). https://doi.org:10.1017/s1355838201001790

213 Otto, G. A. & Puglisi, J. D. The pathway of HCV IRES-mediated translation initiation. *Cell* **119**, 369-380 (2004). https://doi.org:10.1016/j.cell.2004.09.038

214 Ji, H., Fraser, C. S., Yu, Y., Leary, J. & Doudna, J. A. Coordinated assembly of human translation initiation complexes by the hepatitis C virus internal ribosome entry site RNA. *Proceedings of the National Academy of Sciences of the United States of America* **101**, 16990-16995 (2004). https://doi.org:10.1073/pnas.0407402101

215 Bartenschlager, R., Ahlborn-Laake, L., Mous, J. & Jacobsen, H. Kinetic and structural analyses of hepatitis C virus polyprotein processing. *J Virol* **68**, 5045-5055 (1994). https://doi.org:10.1128/jvi.68.8.5045-5055.1994

216 Dubuisson, J., Penin, F. & Moradpour, D. Interaction of hepatitis C virus proteins with host cell membranes and lipids. *Trends Cell Biol* **12**, 517-523 (2002). https://doi.org:10.1016/s0962-8924(02)02383-8

217 Kapadia, S. B. & Chisari, F. V. Hepatitis C virus RNA replication is regulated by host geranylgeranylation and fatty acids. *Proceedings of the National Academy of Sciences of the United States of America* **102**, 2561-2566 (2005). https://doi.org:10.1073/pnas.0409834102

218 Rouillé, Y., Helle, F., Delgrange, D., Roingeard, P., Voisset, C., Blanchard, E., Belouzard, S., McKeating, J., Patel, A. H., Maertens, G., Wakita, T., Wychowski, C. & Dubuisson, J. Subcellular localization of hepatitis C virus structural proteins in a cell culture system that efficiently replicates the virus. *J Virol* **80**, 2832-2841 (2006). https://doi.org:10.1128/jvi.80.6.2832-2841.2006

219 He, Y., Staschke, K. A. & Tan, S. L. in *Hepatitis C Viruses: Genomes and Molecular Biology* (ed S. L. Tan) (Horizon Bioscience

220 Romero-Brey, I., Merz, A., Chiramel, A., Lee, J. Y., Chlanda, P., Haselman, U., Santarella-Mellwig, R., Habermann, A., Hoppe, S., Kallis, S., Walther, P., Antony, C., Krijnse-Locker, J. & Bartenschlager, R. Three-dimensional architecture and biogenesis of membrane structures associated with hepatitis C virus replication. *PLoS pathogens* **8**, e1003056 (2012). https://doi.org:10.1371/journal.ppat.1003056

221 Neufeldt, C. J., Joyce, M. A., Van Buuren, N., Levin, A., Kirkegaard, K., Gale, M., Jr., Tyrrell, D. L. & Wozniak, R. W. The Hepatitis C Virus-Induced Membranous Web and Associated Nuclear Transport Machinery Limit Access of Pattern Recognition Receptors to Viral Replication Sites. *PLoS pathogens* **12**, e1005428 (2016). https://doi.org:10.1371/journal.ppat.1005428

222 Miyanari, Y., Hijikata, M., Yamaji, M., Hosaka, M., Takahashi, H. & Shimotohno, K. Hepatitis C virus non-structural proteins in the probable membranous compartment function in viral genome replication. *J Biol Chem* **278**, 50301-50308 (2003). https://doi.org:10.1074/jbc.M305684200

223 Gosert, R., Egger, D., Lohmann, V., Bartenschlager, R., Blum, H. E., Bienz, K. & Moradpour, D. Identification of the hepatitis C virus RNA replication complex in Huh-7 cells harboring subgenomic replicons. *J Virol* **77**, 5487-5492 (2003). https://doi.org:10.1128/jvi.77.9.5487-5492.2003

224 Paul, D., Romero-Brey, I., Gouttenoire, J., Stoitsova, S., Krijnse-Locker, J., Moradpour, D. & Bartenschlager, R. NS4B self-interaction through conserved C-terminal elements is required for the establishment of functional hepatitis C virus replication complexes. *J Virol* **85**, 6963-6976 (2011). https://doi.org:10.1128/jvi.00502-11

225 Paul, D., Madan, V. & Bartenschlager, R. Hepatitis C virus RNA replication and assembly: living on the fat of the land. *Cell host & microbe* **16**, 569-579 (2014). https://doi.org:10.1016/j.chom.2014.10.008

226 Kong, L., Fujimoto, A., Nakamura, M., Aoyagi, H., Matsuda, M., Watashi, K., Suzuki, R., Arita, M., Yamagoe, S., Dohmae, N., Suzuki, T., Sakamaki, Y., Ichinose, S., Suzuki, T., Wakita, T. & Aizaki, H. Prolactin Regulatory Element Binding Protein Is Involved in Hepatitis C Virus Replication by Interaction with NS4B. *J Virol* **90**, 3093-3111 (2016). https://doi.org:10.1128/jvi.01540-15

227 Gewaid, H., Aoyagi, H., Arita, M., Watashi, K., Suzuki, R., Sakai, S., Kumagai, K., Yamaji, T., Fukasawa, M., Kato, F., Hishiki, T., Mimata, A., Sakamaki, Y., Ichinose, S., Hanada, K., Muramatsu, M., Wakita, T. & Aizaki, H. Sphingomyelin Is Essential for the Structure and Function of the Double-Membrane Vesicles in Hepatitis C Virus RNA Replication Factories. *J Virol* **94** (2020). https://doi.org:10.1128/jvi.01080-20

228 Wang, H., Perry, J. W., Lauring, A. S., Neddermann, P., De Francesco, R. & Tai, A. W. Oxysterol-binding protein is a phosphatidylinositol 4-kinase effector required for HCV replication membrane integrity and cholesterol trafficking. *Gastroenterology* **146**, 1373-1385.e1371-1311 (2014). https://doi.org:10.1053/j.gastro.2014.02.002

229 Berger, K. L., Kelly, S. M., Jordan, T. X., Tartell, M. A. & Randall, G. Hepatitis C virus stimulates the phosphatidylinositol 4-kinase III alpha-dependent phosphatidylinositol 4-phosphate production that is essential for its replication. *J Virol* **85**, 8870-8883 (2011). https://doi.org:10.1128/jvi.00059-11

230 Amako, Y., Sarkeshik, A., Hotta, H., Yates, J. & Siddiqui, A. Role of Oxysterol Binding Protein in Hepatitis C Virus infection. *J Virol* **83**, 9237-9246 (2009). https://doi.org:10.1128/jvi.00958-09

231 Reiss, S., Rebhan, I., Backes, P., Romero-Brey, I., Erfle, H., Matula, P., Kaderali, L., Poenisch, M., Blankenburg, H., Hiet, M. S., Longerich, T., Diehl, S., Ramirez, F., Balla, T., Rohr, K., Kaul, A., Bühler, S., Pepperkok, R., Lengauer, T., Albrecht, M., Eils, R., Schirmacher, P., Lohmann, V. & Bartenschlager, R. Recruitment and activation of a lipid kinase by hepatitis C virus NS5A is essential for integrity of the membranous replication compartment. *Cell host & microbe* **9**, 32-45 (2011). https://doi.org:10.1016/j.chom.2010.12.002

232 Li, H., Yang, X., Yang, G., Hong, Z., Zhou, L., Yin, P., Xiao, Y., Chen, L., Chung, R. T. & Zhang, L. Hepatitis C virus NS5A hijacks ARFGAP1 to maintain a phosphatidylinositol 4-phosphate-enriched microenvironment. *J Virol* **88**, 5956-5966 (2014). https://doi.org:10.1128/jvi.03738-13

233 Blanchard, E. & Roingeard, P. The Hepatitis C Virus-Induced Membranous Web in Liver Tissue. *Cells* **7** (2018). https://doi.org:10.3390/cells7110191

234 Zhou, T., Ren, X., Adams, R. L. & Pyle, A. M. NS3 from Hepatitis C Virus Strain JFH-1 Is an Unusually Robust Helicase That Is Primed To Bind and Unwind Viral RNA. *J Virol* **92** (2018). https://doi.org:10.1128/jvi.01253-17

235 Luo, G., Hamatake, R. K., Mathis, D. M., Racela, J., Rigat, K. L., Lemm, J. & Colonno, R. J. De novo initiation of RNA synthesis by the RNA-dependent RNA polymerase

(NS5B) of hepatitis C virus. *J Virol* **74**, 851-863 (2000). https://doi.org:10.1128/jvi.74.2.851-863.2000

236 Lohmann, V., Körner, F., Koch, J., Herian, U., Theilmann, L. & Bartenschlager, R. Replication of subgenomic hepatitis C virus RNAs in a hepatoma cell line. *Science* **285**, 110-113 (1999). https://doi.org:10.1126/science.285.5424.110

237 Zhong, W., Ferrari, E., Lesburg, C. A., Maag, D., Ghosh, S. K., Cameron, C. E., Lau, J. Y. & Hong, Z. Template/primer requirements and single nucleotide incorporation by hepatitis C virus nonstructural protein 5B polymerase. *J Virol* **74**, 9134-9143 (2000). https://doi.org:10.1128/jvi.74.19.9134-9143.2000

238 Cai, Z., Liang, T. J. & Luo, G. Effects of mutations of the initiation nucleotides on hepatitis C virus RNA replication in the cell. *J Virol* **78**, 3633-3643 (2004). https://doi.org:10.1128/jvi.78.7.3633-3643.2004

239 Li, Y. P., Gottwein, J. M., Scheel, T. K., Jensen, T. B. & Bukh, J. MicroRNA-122 antagonism against hepatitis C virus genotypes 1-6 and reduced efficacy by host RNA insertion or mutations in the HCV 5' UTR. *Proceedings of the National Academy of Sciences of the United States of America* **108**, 4991-4996 (2011). https://doi.org:10.1073/pnas.1016606108

240 Ramirez, S. & Bukh, J. Current status and future development of infectious cell-culture models for the major genotypes of hepatitis C virus: Essential tools in testing of antivirals and emerging vaccine strategies. *Antiviral research* **158**, 264-287 (2018). https://doi.org:10.1016/j.antiviral.2018.07.014

241 Jopling, C. L., Norman, K. L. & Sarnow, P. Positive and negative modulation of viral and cellular mRNAs by liver-specific microRNA miR-122. *Cold Spring Harb Symp Quant Biol* **71**, 369-376 (2006). https://doi.org:10.1101/sqb.2006.71.022

242 Lanford, R. E., Hildebrandt-Eriksen, E. S., Petri, A., Persson, R., Lindow, M., Munk, M. E., Kauppinen, S. & Ørum, H. Therapeutic silencing of microRNA-122 in primates with chronic hepatitis C virus infection. *Science* **327**, 198-201 (2010). https://doi.org:10.1126/science.1178178

243 Machlin, E. S., Sarnow, P. & Sagan, S. M. Masking the 5' terminal nucleotides of the hepatitis C virus genome by an unconventional microRNA-target RNA complex. *Proceedings of the National Academy of Sciences of the United States of America* **108**, 3193-3198 (2011). https://doi.org:10.1073/pnas.1012464108

244 Chatterji, U., Bobardt, M., Selvarajah, S., Yang, F., Tang, H., Sakamoto, N., Vuagniaux, G., Parkinson, T. & Gallay, P. The isomerase active site of cyclophilin A is critical for hepatitis C virus replication. *J Biol Chem* **284**, 16998-17005 (2009). https://doi.org:10.1074/jbc.M109.007625

245 Kaul, A., Stauffer, S., Berger, C., Pertel, T., Schmitt, J., Kallis, S., Zayas, M., Lohmann, V., Luban, J. & Bartenschlager, R. Essential role of cyclophilin A for hepatitis C virus replication and virus production and possible link to polyprotein cleavage kinetics. *PLoS pathogens* **5**, e1000546 (2009). https://doi.org:10.1371/journal.ppat.1000546

246 Liu, Z., Yang, F., Robotham, J. M. & Tang, H. Critical role of cyclophilin A and its prolyl-peptidyl isomerase activity in the structure and function of the hepatitis C virus replication complex. *J Virol* **83**, 6554-6565 (2009). https://doi.org:10.1128/jvi.02550-08

247 Gao, L., Aizaki, H., He, J. W. & Lai, M. M. Interactions between viral nonstructural proteins and host protein hVAP-33 mediate the formation of hepatitis C virus RNA replication complex on lipid raft. *J Virol* **78**, 3480-3488 (2004). https://doi.org:10.1128/jvi.78.7.3480-3488.2004

248 Barba, G., Harper, F., Harada, T., Kohara, M., Goulinet, S., Matsuura, Y., Eder, G., Schaff, Z., Chapman, M. J., Miyamura, T. & Bréchot, C. Hepatitis C virus core protein

shows a cytoplasmic localization and associates to cellular lipid storage droplets. *Proceedings of the National Academy of Sciences of the United States of America* **94**, 1200-1205 (1997). https://doi.org:10.1073/pnas.94.4.1200

249 Boulant, S., Targett-Adams, P. & McLauchlan, J. Disrupting the association of hepatitis C virus core protein with lipid droplets correlates with a loss in production of infectious virus. *The Journal of general virology* **88**, 2204-2213 (2007). https://doi.org:10.1099/vir.0.82898-0

250 Shavinskaya, A., Boulant, S., Penin, F., McLauchlan, J. & Bartenschlager, R. The lipid droplet binding domain of hepatitis C virus core protein is a major determinant for efficient virus assembly. *J Biol Chem* **282**, 37158-37169 (2007). https://doi.org:10.1074/jbc.M707329200

251 Camus, G., Schweiger, M., Herker, E., Harris, C., Kondratowicz, A. S., Tsou, C. L., Farese, R. V., Jr., Herath, K., Previs, S. F., Roddy, T. P., Pinto, S., Zechner, R. & Ott, M. The hepatitis C virus core protein inhibits adipose triglyceride lipase (ATGL)-mediated lipid mobilization and enhances the ATGL interaction with comparative gene identification 58 (CGI-58) and lipid droplets. *J Biol Chem* **289**, 35770-35780 (2014). https://doi.org:10.1074/jbc.M114.587816

252 Boson, B., Mialon, C., Schichl, K., Denolly, S. & Cosset, F. L. Nup98 Is Subverted from Annulate Lamellae by Hepatitis C Virus Core Protein to Foster Viral Assembly. *mBio* **13**, e0292321 (2022). https://doi.org:10.1128/mbio.02923-21

253 Shi, S. T., Polyak, S. J., Tu, H., Taylor, D. R., Gretch, D. R. & Lai, M. M. Hepatitis C virus NS5A colocalizes with the core protein on lipid droplets and interacts with apolipoproteins. *Virology* **292**, 198-210 (2002). https://doi.org:10.1006/viro.2001.1225

254 Goh, P. Y., Tan, Y. J., Lim, S. P., Lim, S. G., Tan, Y. H. & Hong, W. J. The hepatitis C virus core protein interacts with NS5A and activates its caspase-mediated proteolytic cleavage. *Virology* **290**, 224-236 (2001). https://doi.org:10.1006/viro.2001.1195

255 Herker, E., Harris, C., Hernandez, C., Carpentier, A., Kaehlcke, K., Rosenberg, A. R., Farese, R. V., Jr. & Ott, M. Efficient hepatitis C virus particle formation requires diacylglycerol acyltransferase-1. *Nat Med* **16**, 1295-1298 (2010). https://doi.org:10.1038/nm.2238

256 Camus, G., Herker, E., Modi, A. A., Haas, J. T., Ramage, H. R., Farese, R. V., Jr. & Ott, M. Diacylglycerol acyltransferase-1 localizes hepatitis C virus NS5A protein to lipid droplets and enhances NS5A interaction with the viral capsid core. *J Biol Chem* **288**, 9915-9923 (2013). https://doi.org:10.1074/jbc.M112.434910

257 Zayas, M., Long, G., Madan, V. & Bartenschlager, R. Coordination of Hepatitis C Virus Assembly by Distinct Regulatory Regions in Nonstructural Protein 5A. *PLoS pathogens* **12**, e1005376 (2016). https://doi.org:10.1371/journal.ppat.1005376

258 Boson, B., Granio, O., Bartenschlager, R. & Cosset, F. L. A concerted action of hepatitis C virus p7 and nonstructural protein 2 regulates core localization at the endoplasmic reticulum and virus assembly. *PLoS pathogens* **7**, e1002144 (2011). https://doi.org:10.1371/journal.ppat.1002144

259 Gentzsch, J., Brohm, C., Steinmann, E., Friesland, M., Menzel, N., Vieyres, G., Perin, P. M., Frentzen, A., Kaderali, L. & Pietschmann, T. hepatitis c Virus p7 is critical for capsid assembly and envelopment. *PLoS pathogens* **9**, e1003355 (2013). https://doi.org:10.1371/journal.ppat.1003355

260 Neveu, G., Barouch-Bentov, R., Ziv-Av, A., Gerber, D., Jacob, Y. & Einav, S. Identification and targeting of an interaction between a tyrosine motif within hepatitis C virus core protein and AP2M1 essential for viral assembly. *PLoS pathogens* **8**, e1002845 (2012). https://doi.org:10.1371/journal.ppat.1002845

261 Dubuisson, J., Hsu, H. H., Cheung, R. C., Greenberg, H. B., Russell, D. G. & Rice, C. M. Formation and intracellular localization of hepatitis C virus envelope glycoprotein complexes expressed by recombinant vaccinia and Sindbis viruses. *J Virol* **68**, 6147-6160 (1994). https://doi.org:10.1128/jvi.68.10.6147-6160.1994

262 Blanchard, E., Hourioux, C., Brand, D., Ait-Goughoulte, M., Moreau, A., Trassard, S., Sizaret, P. Y., Dubois, F. & Roingeard, P. Hepatitis C virus-like particle budding: role of the core protein and importance of its Asp111. *J Virol* **77**, 10131-10138 (2003). https://doi.org:10.1128/jvi.77.18.10131-10138.2003

263 Hourioux, C., Ait-Goughoulte, M., Patient, R., Fouquenet, D., Arcanger-Doudet, F., Brand, D., Martin, A. & Roingeard, P. Core protein domains involved in hepatitis C virus-like particle assembly and budding at the endoplasmic reticulum membrane. *Cell Microbiol* **9**, 1014-1027 (2007). https://doi.org:10.1111/j.1462-5822.2006.00848.x

264 Stapleford, K. A. & Lindenbach, B. D. Hepatitis C virus NS2 coordinates virus particle assembly through physical interactions with the E1-E2 glycoprotein and NS3-NS4A enzyme complexes. *J Virol* **85**, 1706-1717 (2011). https://doi.org:10.1128/jvi.02268-10

265 Popescu, C. I., Rouillé, Y. & Dubuisson, J. Hepatitis C virus assembly imaging. *Viruses* **3**, 2238-2254 (2011). https://doi.org:10.3390/v3112238

266 Aizaki, H., Morikawa, K., Fukasawa, M., Hara, H., Inoue, Y., Tani, H., Saito, K., Nishijima, M., Hanada, K., Matsuura, Y., Lai, M. M., Miyamura, T., Wakita, T. & Suzuki, T. Critical role of virion-associated cholesterol and sphingolipid in hepatitis C virus infection. *J Virol* **82**, 5715-5724 (2008). https://doi.org:10.1128/jvi.02530-07

267 Vieyres, G., Reichert, I., Carpentier, A., Vondran, F. W. R. & Pietschmann, T. The ATGL lipase cooperates with ABHD5 to mobilize lipids for hepatitis C virus assembly. *PLoS pathogens* **16**, e1008554 (2020). https://doi.org:10.1371/journal.ppat.1008554

268 Rösch, K., Kwiatkowski, M., Hofmann, S., Schöbel, A., Grüttner, C., Wurlitzer, M., Schlüter, H. & Herker, E. Quantitative Lipid Droplet Proteome Analysis Identifies Annexin A3 as a Cofactor for HCV Particle Production. *Cell Rep* **16**, 3219-3231 (2016). https://doi.org:10.1016/j.celrep.2016.08.052

269 Chang, K. S., Jiang, J., Cai, Z. & Luo, G. Human apolipoprotein e is required for infectivity and production of hepatitis C virus in cell culture. *J Virol* **81**, 13783-13793 (2007). https://doi.org:10.1128/jvi.01091-07

270 Jiang, J. & Luo, G. Apolipoprotein E but not B is required for the formation of infectious hepatitis C virus particles. *J Virol* **83**, 12680-12691 (2009). https://doi.org:10.1128/jvi.01476-09

271 Evans, M. J., Rice, C. M. & Goff, S. P. Phosphorylation of hepatitis C virus nonstructural protein 5A modulates its protein interactions and viral RNA replication. *Proceedings of the National Academy of Sciences of the United States of America* **101**, 13038-13043 (2004). https://doi.org:10.1073/pnas.0405152101

272 Benga, W. J., Krieger, S. E., Dimitrova, M., Zeisel, M. B., Parnot, M., Lupberger, J., Hildt, E., Luo, G., McLauchlan, J., Baumert, T. F. & Schuster, C. Apolipoprotein E interacts with hepatitis C virus nonstructural protein 5A and determines assembly of infectious particles. *Hepatology (Baltimore, Md.)* **51**, 43-53 (2010). https://doi.org:10.1002/hep.23278

273 Weller, R., Hueging, K., Brown, R. J. P., Todt, D., Joecks, S., Vondran, F. W. R. & Pietschmann, T. Hepatitis C Virus Strain-Dependent Usage of Apolipoprotein E Modulates Assembly Efficiency and Specific Infectivity of Secreted Virions. *J Virol* **91** (2017). https://doi.org:10.1128/jvi.00422-17

274 Gastaminza, P., Cheng, G., Wieland, S., Zhong, J., Liao, W. & Chisari, F. V. Cellular determinants of hepatitis C virus assembly, maturation, degradation, and secretion. *J Virol* **82**, 2120-2129 (2008). https://doi.org:10.1128/jvi.02053-07

275 Shimotohno, K. HCV Assembly and Egress via Modifications in Host Lipid Metabolic Systems. *Cold Spring Harbor perspectives in medicine* **11** (2021). https://doi.org:10.1101/cshperspect.a036814
276 Vieyres, G., Thomas, X., Descamps, V., Duverlie, G., Patel, A. H. & Dubuisson, J. Characterization of the envelope glycoproteins associated with infectious hepatitis C virus. *J Virol* **84**, 10159-10168 (2010). https://doi.org:10.1128/jvi.01180-10
277 Syed, G. H., Khan, M., Yang, S. & Siddiqui, A. Hepatitis C Virus Lipoviroparticles Assemble in the Endoplasmic Reticulum (ER) and Bud off from the ER to the Golgi Compartment in COPII Vesicles. *J Virol* **91** (2017). https://doi.org:10.1128/jvi.00499-17
278 Takacs, C. N., Andreo, U., Dao Thi, V. L., Wu, X., Gleason, C. E., Itano, M. S., Spitz-Becker, G. S., Belote, R. L., Hedin, B. R., Scull, M. A., Rice, C. M. & Simon, S. M. Differential Regulation of Lipoprotein and Hepatitis C Virus Secretion by Rab1b. *Cell Rep* **21**, 431-441 (2017). https://doi.org:10.1016/j.celrep.2017.09.053
279 Wozniak, A. L., Griffin, S., Rowlands, D., Harris, M., Yi, M., Lemon, S. M. & Weinman, S. A. Intracellular proton conductance of the hepatitis C virus p7 protein and its contribution to infectious virus production. *PLoS pathogens* **6**, e1001087 (2010). https://doi.org:10.1371/journal.ppat.1001087
280 Mankouri, J., Walter, C., Stewart, H., Bentham, M., Park, W. S., Heo, W. D., Fukuda, M., Griffin, S. & Harris, M. Release of Infectious Hepatitis C Virus from Huh7 Cells Occurs via a trans-Golgi Network-to-Endosome Pathway Independent of Very-Low-Density Lipoprotein Secretion. *J Virol* **90**, 7159-7170 (2016). https://doi.org:10.1128/jvi.00826-16
281 Benedicto, I., Gondar, V., Molina-Jiménez, F., García-Buey, L., López-Cabrera, M., Gastaminza, P. & Majano, P. L. Clathrin mediates infectious hepatitis C virus particle egress. *J Virol* **89**, 4180-4190 (2015). https://doi.org:10.1128/jvi.03620-14
282 Ariumi, Y., Kuroki, M., Maki, M., Ikeda, M., Dansako, H., Wakita, T. & Kato, N. The ESCRT system is required for hepatitis C virus production. *PloS one* **6**, e14517 (2011). https://doi.org:10.1371/journal.pone.0014517
283 Tamai, K., Shiina, M., Tanaka, N., Nakano, T., Yamamoto, A., Kondo, Y., Kakazu, E., Inoue, J., Fukushima, K., Sano, K., Ueno, Y., Shimosegawa, T. & Sugamura, K. Regulation of hepatitis C virus secretion by the Hrs-dependent exosomal pathway. *Virology* **422**, 377-385 (2012). https://doi.org:10.1016/j.virol.2011.11.009
284 Bunz, M., Ritter, M. & Schindler, M. HCV egress - unconventional secretion of assembled viral particles. *Trends Microbiol* **30**, 364-378 (2022). https://doi.org:10.1016/j.tim.2021.08.005
285 Cousineau, S. E., Rheault, M. & Sagan, S. M. Poly(rC)-Binding Protein 1 Limits Hepatitis C Virus Virion Assembly and Secretion. *Viruses* **14** (2022). https://doi.org:10.3390/v14020291
286 Spångberg, K. & Schwartz, S. Poly(C)-binding protein interacts with the hepatitis C virus 5′ untranslated region. *Journal of General Virology* **80**, 1371-1376 (1999). https://doi.org:https://doi.org/10.1099/0022-1317-80-6-1371
287 Micallef, J. M., Kaldor, J. M. & Dore, G. J. Spontaneous viral clearance following acute hepatitis C infection: a systematic review of longitudinal studies. *J Viral Hepat* **13**, 34-41 (2006). https://doi.org:10.1111/j.1365-2893.2005.00651.x
288 Aisyah, D. N., Shallcross, L., Hully, A. J., O'Brien, A. & Hayward, A. Assessing hepatitis C spontaneous clearance and understanding associated factors-A systematic review and meta-analysis. *J Viral Hepat* **25**, 680-698 (2018). https://doi.org:10.1111/jvh.12866

289 Gerlach, J. T., Diepolder, H. M., Jung, M. C., Gruener, N. H., Schraut, W. W., Zachoval, R., Hoffmann, R., Schirren, C. A., Santantonio, T. & Pape, G. R. Recurrence of hepatitis C virus after loss of virus-specific CD4(+) T-cell response in acute hepatitis C. *Gastroenterology* **117**, 933-941 (1999). https://doi.org:10.1016/s0016-5085(99)70353-7

290 Thimme, R., Oldach, D., Chang, K. M., Steiger, C., Ray, S. C. & Chisari, F. V. Determinants of viral clearance and persistence during acute hepatitis C virus infection. *J Exp Med* **194**, 1395-1406 (2001). https://doi.org:10.1084/jem.194.10.1395

291 Adinolfi, L. E., Rinaldi, L., Guerrera, B., Restivo, L., Marrone, A., Giordano, M. & Zampino, R. NAFLD and NASH in HCV Infection: Prevalence and Significance in Hepatic and Extrahepatic Manifestations. *International journal of molecular sciences* **17** (2016). https://doi.org:10.3390/ijms17060803

292 Bravo, A. A., Sheth, S. G. & Chopra, S. Liver biopsy. *N Engl J Med* **344**, 495-500 (2001). https://doi.org:10.1056/nejm200102153440706

293 Sebastiani, G., Gkouvatsos, K. & Pantopoulos, K. Chronic hepatitis C and liver fibrosis. *World journal of gastroenterology* **20**, 11033-11053 (2014). https://doi.org:10.3748/wjg.v20.i32.11033

294 Horowitz, J. M., Venkatesh, S. K., Ehman, R. L., Jhaveri, K., Kamath, P., Ohliger, M. A., Samir, A. E., Silva, A. C., Taouli, B., Torbenson, M. S., Wells, M. L., Yeh, B. & Miller, F. H. Evaluation of hepatic fibrosis: a review from the society of abdominal radiology disease focus panel. *Abdom Radiol (NY)* **42**, 2037-2053 (2017). https://doi.org:10.1007/s00261-017-1211-7

295 Park, J., Lee, J. M., Lee, G., Jeon, S. K. & Joo, I. Quantitative Evaluation of Hepatic Steatosis Using Advanced Imaging Techniques: Focusing on New Quantitative Ultrasound Techniques. *Korean J Radiol* **23**, 13-29 (2022). https://doi.org:10.3348/kjr.2021.0112

296 Liang, W., Menke, A. L., Driessen, A., Koek, G. H., Lindeman, J. H., Stoop, R., Havekes, L. M., Kleemann, R. & van den Hoek, A. M. Establishment of a general NAFLD scoring system for rodent models and comparison to human liver pathology. *PloS one* **9**, e115922 (2014). https://doi.org:10.1371/journal.pone.0115922

297 Lingala, S. & Ghany, M. G. Natural History of Hepatitis C. *Gastroenterol Clin North Am* **44**, 717-734 (2015). https://doi.org:10.1016/j.gtc.2015.07.003

298 Nassir, F., Rector, R. S., Hammoud, G. M. & Ibdah, J. A. Pathogenesis and Prevention of Hepatic Steatosis. *Gastroenterology & hepatology* **11**, 167-175 (2015).

299 Brunt, E. M. Pathology of nonalcoholic fatty liver disease. *Nat Rev Gastroenterol Hepatol* **7**, 195-203 (2010). https://doi.org:10.1038/nrgastro.2010.21

300 Chowdhury, A. B. & Mehta, K. J. Liver biopsy for assessment of chronic liver diseases: a synopsis. *Clin Exp Med* **23**, 273-285 (2023). https://doi.org:10.1007/s10238-022-00799-z

301 Anderson, N. & Borlak, J. Molecular mechanisms and therapeutic targets in steatosis and steatohepatitis. *Pharmacol Rev* **60**, 311-357 (2008). https://doi.org:10.1124/pr.108.00001

302 Mirandola, S., Bowman, D., Hussain, M. M. & Alberti, A. Hepatic steatosis in hepatitis C is a storage disease due to HCV interaction with microsomal triglyceride transfer protein (MTP). *Nutr Metab (Lond)* **7**, 13 (2010). https://doi.org:10.1186/1743-7075-7-13

303 Ress, C. & Kaser, S. Mechanisms of intrahepatic triglyceride accumulation. *World journal of gastroenterology* **22**, 1664-1673 (2016). https://doi.org:10.3748/wjg.v22.i4.1664

304 Stevenson, H. L. & Utay, N. S. Hepatic steatosis in HCV-infected persons in the direct-acting antiviral era. *Trop Dis Travel Med Vaccines* **2**, 21 (2016). https://doi.org:10.1186/s40794-016-0038-5
305 Gluchowski, N. L., Becuwe, M., Walther, T. C. & Farese, R. V., Jr. Lipid droplets and liver disease: from basic biology to clinical implications. *Nat Rev Gastroenterol Hepatol* **14**, 343-355 (2017). https://doi.org:10.1038/nrgastro.2017.32
306 Mylonis, I., Simos, G. & Paraskeva, E. Hypoxia-Inducible Factors and the Regulation of Lipid Metabolism. *Cells* **8** (2019). https://doi.org:10.3390/cells8030214
307 Modaresi Esfeh, J. & Ansari-Gilani, K. Steatosis and hepatitis C. *Gastroenterol Rep (Oxf)* **4**, 24-29 (2016). https://doi.org:10.1093/gastro/gov040
308 Chaudhari, R., Fouda, S., Sainu, A. & Pappachan, J. M. Metabolic complications of hepatitis C virus infection. *World journal of gastroenterology* **27**, 1267-1282 (2021). https://doi.org:10.3748/wjg.v27.i13.1267
309 Hernandez-Gea, V. & Friedman, S. L. Pathogenesis of liver fibrosis. *Annual review of pathology* **6**, 425-456 (2011). https://doi.org:10.1146/annurev-pathol-011110-130246
310 Schulze-Krebs, A., Preimel, D., Popov, Y., Bartenschlager, R., Lohmann, V., Pinzani, M. & Schuppan, D. Hepatitis C virus-replicating hepatocytes induce fibrogenic activation of hepatic stellate cells. *Gastroenterology* **129**, 246-258 (2005). https://doi.org:10.1053/j.gastro.2005.03.089
311 Shahin, K., Hosseini, S. Y., Jamali, H., Karimi, M. H., Azarpira, N. & Zeraatian, M. The enhancing impact of amino termini of hepatitis C virus core protein on activation of hepatic stellate cells. *Gastroenterol Hepatol Bed Bench* **13**, 57-63 (2020).
312 Schuppan, D. & Afdhal, N. H. Liver cirrhosis. *Lancet* **371**, 838-851 (2008). https://doi.org:10.1016/s0140-6736(08)60383-9
313 Garcia-Tsao, G., Friedman, S., Iredale, J. & Pinzani, M. Now there are many (stages) where before there was one: In search of a pathophysiological classification of cirrhosis. *Hepatol.* **51**, 1445-1449 (2010). https://doi.org:10.1002/hep.23478
314 Planas, R., Ballesté, B., Alvarez, M. A., Rivera, M., Montoliu, S., Galeras, J. A., Santos, J., Coll, S., Morillas, R. M. & Solà, R. Natural history of decompensated hepatitis C virus-related cirrhosis. A study of 200 patients. *Journal of hepatology* **40**, 823-830 (2004). https://doi.org:10.1016/j.jhep.2004.01.005
315 Sung, H., Ferlay, J., Siegel, R. L., Laversanne, M., Soerjomataram, I., Jemal, A. & Bray, F. Global Cancer Statistics 2020: GLOBOCAN Estimates of Incidence and Mortality Worldwide for 36 Cancers in 185 Countries. *CA: A Cancer Journal for Clinicians* **71**, 209-249 (2021). https://doi.org:https://doi.org/10.3322/caac.21660
316 Levrero, M. Viral hepatitis and liver cancer: the case of hepatitis C. *Oncogene* **25**, 3834-3847 (2006). https://doi.org:10.1038/sj.onc.1209562
317 Virzì, A., Roca Suarez, A. A., Baumert, T. F. & Lupberger, J. Oncogenic Signaling Induced by HCV Infection. *Viruses* **10** (2018). https://doi.org:10.3390/v10100538
318 Goto, K., Roca Suarez, A. A., Wrensch, F., Baumert, T. F. & Lupberger, J. Hepatitis C Virus and Hepatocellular Carcinoma: When the Host Loses Its Grip. *International journal of molecular sciences* **21** (2020). https://doi.org:10.3390/ijms21093057
319 Farzaneh, Z., Vosough, M., Agarwal, T. & Farzaneh, M. Critical signaling pathways governing hepatocellular carcinoma behavior; small molecule-based approaches. *Cancer Cell Int* **21**, 208 (2021). https://doi.org:10.1186/s12935-021-01924-w
320 Cacoub, P. & Saadoun, D. Extrahepatic Manifestations of Chronic HCV Infection. *N Engl J Med* **384**, 1038-1052 (2021). https://doi.org:10.1056/NEJMra2033539
321 Uysal, K. T., Wiesbrock, S. M., Marino, M. W. & Hotamisligil, G. S. Protection from obesity-induced insulin resistance in mice lacking TNF-alpha function. *Nature* **389**, 610-614 (1997). https://doi.org:10.1038/39335

322 Wang, C. S., Wang, S. T., Yao, W. J., Chang, T. T. & Chou, P. Hepatitis C virus infection and the development of type 2 diabetes in a community-based longitudinal study. *Am J Epidemiol* **166**, 196-203 (2007). https://doi.org:10.1093/aje/kwm061
323 Sanchez, M. J. & Bergasa, N. V. Hepatitis C associated cardiomyopathy: potential pathogenic mechanisms and clinical implications. *Med Sci Monit* **14**, Ra55-63 (2008).
324 Adinolfi, L. E., Restivo, L., Zampino, R., Guerrera, B., Lonardo, A., Ruggiero, L., Riello, F., Loria, P. & Florio, A. Chronic HCV infection is a risk of atherosclerosis. Role of HCV and HCV-related steatosis. *Atherosclerosis* **221**, 496-502 (2012). https://doi.org:10.1016/j.atherosclerosis.2012.01.051
325 Kuna, L., Jakab, J., Smolic, R., Wu, G. Y. & Smolic, M. HCV Extrahepatic Manifestations. *J Clin Transl Hepatol* **7**, 172-182 (2019). https://doi.org:10.14218/jcth.2018.00049
326 Angeletti, A., Cantarelli, C. & Cravedi, P. HCV-Associated Nephropathies in the Era of Direct Acting Antiviral Agents. *Frontiers in Medicine* **6** (2019). https://doi.org:10.3389/fmed.2019.00020
327 Bruno, S., Crosignani, A., Maisonneuve, P., Rossi, S., Silini, E. & Mondelli, M. U. Hepatitis C virus genotype 1b as a major risk factor associated with hepatocellular carcinoma in patients with cirrhosis: A seventeen-year prospective cohort study. *Hepatol.* **46**, 1350-1356 (2007). https://doi.org:https://doi.org/10.1002/hep.21826
328 Raimondi, S., Bruno, S., Mondelli, M. U. & Maisonneuve, P. Hepatitis C virus genotype 1b as a risk factor for hepatocellular carcinoma development: a meta-analysis. *Journal of hepatology* **50**, 1142-1154 (2009). https://doi.org:10.1016/j.jhep.2009.01.019
329 Alkhatib, M., Di Maio, V. C., De Murtas, V., Polilli, E., Milana, M., Teti, E., Fiorentino, G., Calvaruso, V., Barbaliscia, S., Bertoli, A., Scutari, R., Carioti, L., Cento, V., Santoro, M. M., Orro, A., Maida, I., Lenci, I., Sarmati, L., Craxì, A., Pasquazzi, C., Parruti, G., Babudieri, S., Milanesi, L., Andreoni, M., Angelico, M., Perno, C. F., Ceccherini-Silberstein, F., Svicher, V., Salpini, R., On Behalf Of Hirma Hepatocarcinoma Innovative Research, M. & Fondazione Vironet, C. H. V. I. R. Genetic Determinants in a Critical Domain of NS5A Correlate with Hepatocellular Carcinoma in Cirrhotic Patients Infected with HCV Genotype 1b. *Viruses* **13** (2021). https://doi.org:10.3390/v13050743
330 Goossens, N. & Negro, F. Is genotype 3 of the hepatitis C virus the new villain? *Hepatol.* **59**, 2403-2412 (2014). https://doi.org:10.1002/hep.26905
331 Kumar, D., Farrell, G. C., Fung, C. & George, J. Hepatitis C virus genotype 3 is cytopathic to hepatocytes: Reversal of hepatic steatosis after sustained therapeutic response. *Hepatol.* **36**, 1266-1272 (2002). https://doi.org:10.1053/jhep.2002.36370
332 Castéra, L., Hézode, C., Roudot-Thoraval, F., Lonjon, I., Zafrani, E. S., Pawlotsky, J. M. & Dhumeaux, D. Effect of antiviral treatment on evolution of liver steatosis in patients with chronic hepatitis C: indirect evidence of a role of hepatitis C virus genotype 3 in steatosis. *Gut* **53**, 420-424 (2004). https://doi.org:10.1136/gut.2002.009936
333 Hézode, C., Roudot-Thoraval, F., Zafrani, E. S., Dhumeaux, D. & Pawlotsky, J. M. Different mechanisms of steatosis in hepatitis C virus genotypes 1 and 3 infections. *J Viral Hepat* **11**, 455-458 (2004). https://doi.org:10.1111/j.1365-2893.2004.00528.x
334 Kamal, S. M. & Nasser, I. A. Hepatitis C genotype 4: What we know and what we don't yet know. *Hepatol.* **47**, 1371-1383 (2008). https://doi.org:https://doi.org/10.1002/hep.22127
335 Poynard, T., Bedossa, P. & Opolon, P. Natural history of liver fibrosis progression in patients with chronic hepatitis C. The OBSVIRC, METAVIR, CLINIVIR, and

DOSVIRC groups. *Lancet* **349**, 825-832 (1997). https://doi.org:10.1016/s0140-6736(96)07642-8

336 You, M. & Arteel, G. E. Effect of ethanol on lipid metabolism. *Journal of hepatology* **70**, 237-248 (2019). https://doi.org:10.1016/j.jhep.2018.10.037

337 Rinella, M. E., Lazarus, J. V., Ratziu, V., Francque, S. M., Sanyal, A. J., Kanwal, F., Romero, D., Abdelmalek, M. F., Anstee, Q. M., Arab, J. P., Arrese, M., Bataller, R., Beuers, U., Boursier, J., Bugianesi, E., Byrne, C., Castro Narro, G. E., Chowdhury, A., Cortez-Pinto, H., Cryer, D., Cusi, K., El-Kassas, M., Klein, S., Eskridge, W., Fan, J., Gawrieh, S., Guy, C. D., Harrison, S. A., Kim, S. U., Koot, B., Korenjak, M., Kowdley, K., Lacaille, F., Loomba, R., Mitchell-Thain, R., Morgan, T. R., Powell, E., Roden, M., Romero-Gómez, M., Silva, M., Singh, S. P., Sookoian, S. C., Spearman, C. W., Tiniakos, D., Valenti, L., Vos, M. B., Wong, V. W., Xanthakos, S., Yilmaz, Y., Younossi, Z., Hobbs, A., Villota-Rivas, M. & Newsome, P. N. A multi-society Delphi consensus statement on new fatty liver disease nomenclature. *Hepatol.* (2023). https://doi.org:10.1097/hep.0000000000000520

338 Huang, D. Q., El-Serag, H. B. & Loomba, R. Global epidemiology of NAFLD-related HCC: trends, predictions, risk factors and prevention. *Nature Reviews Gastroenterology & Hepatology* **18**, 223-238 (2021). https://doi.org:10.1038/s41575-020-00381-6

339 Brunt, E. M., Wong, V. W., Nobili, V., Day, C. P., Sookoian, S., Maher, J. J., Bugianesi, E., Sirlin, C. B., Neuschwander-Tetri, B. A. & Rinella, M. E. Nonalcoholic fatty liver disease. *Nat Rev Dis Primers* **1**, 15080 (2015). https://doi.org:10.1038/nrdp.2015.80

340 McCullough, A. J. Pathophysiology of nonalcoholic steatohepatitis. *J Clin Gastroenterol* **40 Suppl 1**, S17-29 (2006). https://doi.org:10.1097/01.mcg.0000168645.86658.22

341 Romeo, S., Kozlitina, J., Xing, C., Pertsemlidis, A., Cox, D., Pennacchio, L. A., Boerwinkle, E., Cohen, J. C. & Hobbs, H. H. Genetic variation in PNPLA3 confers susceptibility to nonalcoholic fatty liver disease. *Nat Genet* **40**, 1461-1465 (2008). https://doi.org:10.1038/ng.257

342 Kozlitina, J., Smagris, E., Stender, S., Nordestgaard, B. G., Zhou, H. H., Tybjærg-Hansen, A., Vogt, T. F., Hobbs, H. H. & Cohen, J. C. Exome-wide association study identifies a TM6SF2 variant that confers susceptibility to nonalcoholic fatty liver disease. *Nat Genet* **46**, 352-356 (2014). https://doi.org:10.1038/ng.2901

343 Dixon, J. B., Bhathal, P. S. & O'Brien, P. E. Nonalcoholic fatty liver disease: predictors of nonalcoholic steatohepatitis and liver fibrosis in the severely obese. *Gastroenterology* **121**, 91-100 (2001). https://doi.org:10.1053/gast.2001.25540

344 Zhou, W. C., Zhang, Q. B. & Qiao, L. Pathogenesis of liver cirrhosis. *World journal of gastroenterology* **20**, 7312-7324 (2014). https://doi.org:10.3748/wjg.v20.i23.7312

345 Ginès, P., Krag, A., Abraldes, J. G., Solà, E., Fabrellas, N. & Kamath, P. S. Liver cirrhosis. *The Lancet* **398**, 1359-1376 (2021). https://doi.org:https://doi.org/10.1016/S0140-6736(21)01374-X

346 Kanwal, F., Kramer, J. R., Asch, S. M., Cao, Y., Li, L. & El-Serag, H. B. Long-Term Risk of Hepatocellular Carcinoma in HCV Patients Treated With Direct Acting Antiviral Agents. *Hepatol.* **71**, 44-55 (2020). https://doi.org:10.1002/hep.30823

347 Rinella, M. E. & Sanyal, A. J. Management of NAFLD: a stage-based approach. *Nat Rev Gastroenterol Hepatol* **13**, 196-205 (2016). https://doi.org:10.1038/nrgastro.2016.3

348 Romero-Gómez, M., Zelber-Sagi, S. & Trenell, M. Treatment of NAFLD with diet, physical activity and exercise. *Journal of hepatology* **67**, 829-846 (2017). https://doi.org:10.1016/j.jhep.2017.05.016

349 Carmona, M., Álvarez, M., Marco, J., Mahíllo, B., Domínguez-Gil, B., Núñez, J. R. & Matesanz, R. Global Organ Transplant Activities in 2015. Data from the Global Observatory on Donation and Transplantation (GODT). *Transplantation* **101**, S29 (2017). https://doi.org:10.1097/01.tp.0000525015.43613.75

350 Bodzin, A. S. & Baker, T. B. Liver Transplantation Today: Where We Are Now and Where We Are Going. *Liver Transplantation* **24**, 1470-1475 (2018). https://doi.org:10.1002/lt.25320

351 Roger, S., Ducancelle, A., Le Guillou-Guillemette, H., Gaudy, C. & Lunel, F. HCV virology and diagnosis. *Clinics and research in hepatology and gastroenterology* **45**, 101626 (2021). https://doi.org:10.1016/j.clinre.2021.101626

352 Larrat, S., Bourdon, C., Baccard, M., Garnaud, C., Mathieu, S., Quesada, J. L., Signori-Schmuck, A., Germi, R., Blanc, M., Leclercq, P., Hilleret, M. N., Leroy, V., Zarski, J. P. & Morand, P. Performance of an antigen-antibody combined assay for hepatitis C virus testing without venipuncture. *J Clin Virol* **55**, 220-225 (2012). https://doi.org:10.1016/j.jcv.2012.07.016

353 Marwaha, N. & Sachdev, S. Current testing strategies for hepatitis C virus infection in blood donors and the way forward. *World journal of gastroenterology* **20**, 2948-2954 (2014). https://doi.org:10.3748/wjg.v20.i11.2948

354 Colin, C., Lanoir, D., Touzet, S., Meyaud-Kraemer, L., Bailly, F. & Trepo, C. Sensitivity and specificity of third-generation hepatitis C virus antibody detection assays: an analysis of the literature. *J Viral Hepat* **8**, 87-95 (2001). https://doi.org:10.1046/j.1365-2893.2001.00280.x

355 Pawlotsky, J. M., Bouvier-Alias, M., Hezode, C., Darthuy, F., Remire, J. & Dhumeaux, D. Standardization of hepatitis C virus RNA quantification. *Hepatol.* **32**, 654-659 (2000). https://doi.org:10.1053/jhep.2000.16603

356 Ghany, M. G., Strader, D. B., Thomas, D. L. & Seeff, L. B. Diagnosis, management, and treatment of hepatitis C: an update. *Hepatol.* **49**, 1335-1374 (2009). https://doi.org:10.1002/hep.22759

357 Lunel, F. & Veillon, P. [Antigen and viral load]. *Transfus Clin Biol* **10**, 74-77 (2003). https://doi.org:10.1016/s1246-7820(03)00028-4

358 Chevaliez, S. & Pawlotsky, J. M. New virological tools for screening, diagnosis and monitoring of hepatitis B and C in resource-limited settings. *Journal of hepatology* **69**, 916-926 (2018). https://doi.org:10.1016/j.jhep.2018.05.017

359 Chen, J., Florian, J., Carter, W., Fleischer, R. D., Hammerstrom, T. S., Jadhav, P. R., Zeng, W., Murray, J. & Birnkrant, D. Earlier sustained virologic response end points for regulatory approval and dose selection of hepatitis C therapies. *Gastroenterology* **144**, 1450-1455.e1452 (2013). https://doi.org:10.1053/j.gastro.2013.02.039

360 Nguyen, V. H., Huang, D. Q., Le, M. H., Jin, M., Lee, E. Y., Henry, L., Nerurkar, S. N., Ogawa, E., Thin, K. N., Teng, M. L. P., Goh, K. S., Kai, J. C. Y., Wong, C., Tan, D. J. H., Thuy, L. T. T., Hai, H., Enomoto, M., Cheung, R. & Nguyen, M. H. Global treatment rate and barriers to direct-acting antiviral therapy: A systematic review and meta-analysis of 146 studies and 1 760 352 hepatitis C virus patients. *Liver international : official journal of the International Association for the Study of the Liver* **43**, 1195-1203 (2023). https://doi.org:10.1111/liv.15550

361 McHutchison, J. G., Gordon, S. C., Schiff, E. R., Shiffman, M. L., Lee, W. M., Rustgi, V. K., Goodman, Z. D., Ling, M. H., Cort, S. & Albrecht, J. K. Interferon alfa-2b alone or in combination with ribavirin as initial treatment for chronic hepatitis C. Hepatitis Interventional Therapy Group. *N Engl J Med* **339**, 1485-1492 (1998). https://doi.org:10.1056/nejm199811193392101

362 Feld, J. J. & Hoofnagle, J. H. Mechanism of action of interferon and ribavirin in treatment of hepatitis C. *Nature* **436**, 967-972 (2005). https://doi.org:10.1038/nature04082
363 Manns, M. P., Cornberg, M. & Wedemeyer, H. Current and future treatment of hepatitis C. *Indian J Gastroenterol* **20 Suppl 1**, C47-51 (2001).
364 Fried, M. W., Shiffman, M. L., Reddy, K. R., Smith, C., Marinos, G., Gonçales, F. L., Jr., Häussinger, D., Diago, M., Carosi, G., Dhumeaux, D., Craxi, A., Lin, A., Hoffman, J. & Yu, J. Peginterferon alfa-2a plus ribavirin for chronic hepatitis C virus infection. *N Engl J Med* **347**, 975-982 (2002). https://doi.org:10.1056/NEJMoa020047
365 Feeney, E. R. & Chung, R. T. Antiviral treatment of hepatitis C. *Bmj* **348**, g3308 (2014). https://doi.org:10.1136/bmj.g3308
366 Hayes, C. N., Imamura, M., Aikata, H. & Chayama, K. Genetics of IL28B and HCV--response to infection and treatment. *Nat Rev Gastroenterol Hepatol* **9**, 406-417 (2012). https://doi.org:10.1038/nrgastro.2012.101
367 Wu, Q., Wang, C., Chen, E. Q., Tang, H., Li, Z. Z. & Lei, X. Z. Interferon Lambda 4 Polymorphism Predicts Sustained Viral Response in Hepatitis C Virus Patients Irrespective of Hepatitis C Virus Genotypes, Ethnicity or Treatment Regimen: Results From a Meta-Analysis. *Hepat Mon* **15**, e32707 (2015). https://doi.org:10.5812/hepatmon.32707
368 EASL recommendations on treatment of hepatitis C: Final update of the series(☆). *Journal of hepatology* **73**, 1170-1218 (2020). https://doi.org:10.1016/j.jhep.2020.08.018
369 Feld, J. J., Jacobson, I. M., Hézode, C., Asselah, T., Ruane, P. J., Gruener, N., Abergel, A., Mangia, A., Lai, C.-L., Chan, H. L. Y., Mazzotta, F., Moreno, C., Yoshida, E., Shafran, S. D., Towner, W. J., Tran, T. T., McNally, J., Osinusi, A., Svarovskaia, E., Zhu, Y., Brainard, D. M., McHutchison, J. G., Agarwal, K. & Zeuzem, S. Sofosbuvir and Velpatasvir for HCV Genotype 1, 2, 4, 5, and 6 Infection. *New England Journal of Medicine* **373**, 2599-2607 (2015). https://doi.org:10.1056/NEJMoa1512610
370 El-Marakby, M. G., Solayman, M. H. & Sabri, N. A. Evaluation of the Safety Profile of Direct-Acting Antivirals on Patients with Hepatitis C Virus: A Pharmacovigilance Study. *Ther Innov Regul Sci* **57**, 997-1007 (2023). https://doi.org:10.1007/s43441-023-00537-x
371 Aleman, S. The hurdle with remaining risk for hepatocellular carcinoma in cirrhotic patients after a hepatitis C cure. *Hepatol Med Policy* **1**, 11 (2016). https://doi.org:10.1186/s41124-016-0019-3
372 Barnes, E., Cooke, G. S., Lauer, G. M. & Chung, R. T. Implementation of a controlled human infection model for evaluation of HCV vaccine candidates. *Hepatol.* **77**, 1757-1772 (2023). https://doi.org:10.1002/hep.32632
373 Yanagi, M., Purcell, R. H., Emerson, S. U. & Bukh, J. Transcripts from a single full-length cDNA clone of hepatitis C virus are infectious when directly transfected into the liver of a chimpanzee. *Proceedings of the National Academy of Sciences* **94**, 8738-8743 (1997). https://doi.org:10.1073/pnas.94.16.8738
374 Lohmann, V. Hepatitis C virus cell culture models: an encomium on basic research paving the road to therapy development. *Medical microbiology and immunology* **208**, 3-24 (2019). https://doi.org:10.1007/s00430-018-0566-x
375 Burm, R., Collignon, L., Mesalam, A. A. & Meuleman, P. Animal Models to Study Hepatitis C Virus Infection. *Front Immunol* **9**, 1032 (2018). https://doi.org:10.3389/fimmu.2018.01032

376 Bartenschlager, R., Frese, M. & Pietschmann, T. Novel insights into hepatitis C virus replication and persistence. *Adv Virus Res* **63**, 71-180 (2004). https://doi.org:10.1016/s0065-3527(04)63002-8
377 Uprichard, S. L., Chung, J., Chisari, F. V. & Wakita, T. Replication of a hepatitis C virus replicon clone in mouse cells. *Virology journal* **3**, 89 (2006). https://doi.org:10.1186/1743-422X-3-89
378 Blight, K. J., Kolykhalov, A. A. & Rice, C. M. Efficient initiation of HCV RNA replication in cell culture. *Science* **290**, 1972-1974 (2000). https://doi.org:10.1126/science.290.5498.1972
379 Ikeda, M., Yi, M., Li, K. & Lemon, S. M. Selectable subgenomic and genome-length dicistronic RNAs derived from an infectious molecular clone of the HCV-N strain of hepatitis C virus replicate efficiently in cultured Huh7 cells. *J Virol* **76**, 2997-3006 (2002). https://doi.org:10.1128/jvi.76.6.2997-3006.2002
380 Grobler, J. A., Markel, E. J., Fay, J. F., Graham, D. J., Simcoe, A. L., Ludmerer, S. W., Murray, E. M., Migliaccio, G. & Flores, O. A. Identification of a key determinant of hepatitis C virus cell culture adaptation in domain II of NS3 helicase. *J Biol Chem* **278**, 16741-16746 (2003). https://doi.org:10.1074/jbc.M212602200
381 Kato, N., Sugiyama, K., Namba, K., Dansako, H., Nakamura, T., Takami, M., Naka, K., Nozaki, A. & Shimotohno, K. Establishment of a hepatitis C virus subgenomic replicon derived from human hepatocytes infected in vitro. *Biochemical and biophysical research communications* **306**, 756-766 (2003). https://doi.org:10.1016/s0006-291x(03)01047-7
382 Maekawa, S., Enomoto, N., Sakamoto, N., Kurosaki, M., Ueda, E., Kohashi, T., Watanabe, H., Chen, C. H., Yamashiro, T., Tanabe, Y., Kanazawa, N., Nakagawa, M., Sato, C. & Watanabe, M. Introduction of NS5A mutations enables subgenomic HCV replicon derived from chimpanzee-infectious HC-J4 isolate to replicate efficiently in Huh-7 cells. *J Viral Hepat* **11**, 394-403 (2004). https://doi.org:10.1111/j.1365-2893.2004.00525.x
383 Ikeda, M., Abe, K., Dansako, H., Nakamura, T., Naka, K. & Kato, N. Efficient replication of a full-length hepatitis C virus genome, strain O, in cell culture, and development of a luciferase reporter system. *Biochemical and biophysical research communications* **329**, 1350-1359 (2005). https://doi.org:10.1016/j.bbrc.2005.02.138
384 Mori, K., Abe, K., Dansako, H., Ariumi, Y., Ikeda, M. & Kato, N. New efficient replication system with hepatitis C virus genome derived from a patient with acute hepatitis C. *Biochemical and biophysical research communications* **371**, 104-109 (2008). https://doi.org:10.1016/j.bbrc.2008.04.005
385 Saeed, M., Scheel, T. K., Gottwein, J. M., Marukian, S., Dustin, L. B., Bukh, J. & Rice, C. M. Efficient replication of genotype 3a and 4a hepatitis C virus replicons in human hepatoma cells. *Antimicrobial agents and chemotherapy* **56**, 5365-5373 (2012). https://doi.org:10.1128/aac.01256-12
386 Saeed, M., Gondeau, C., Hmwe, S., Yokokawa, H., Date, T., Suzuki, T., Kato, T., Maurel, P. & Wakita, T. Replication of hepatitis C virus genotype 3a in cultured cells. *Gastroenterology* **144**, 56-58.e57 (2013). https://doi.org:10.1053/j.gastro.2012.09.017
387 Yu, M., Peng, B., Chan, K., Gong, R., Yang, H., Delaney, W. t. & Cheng, G. Robust and persistent replication of the genotype 6a hepatitis C virus replicon in cell culture. *Antimicrobial agents and chemotherapy* **58**, 2638-2646 (2014). https://doi.org:10.1128/aac.01780-13
388 Wose Kinge, C. N., Espiritu, C., Prabdial-Sing, N., Sithebe, N. P., Saeed, M. & Rice, C. M. Hepatitis C virus genotype 5a subgenomic replicons for evaluation of direct-

acting antiviral agents. *Antimicrobial agents and chemotherapy* **58**, 5386-5394 (2014). https://doi.org:10.1128/aac.03534-14

389 Camus, G., Xu, S., Han, B., Lu, J., Dvory-Sobol, H., Yu, M., Cheng, G., Miller, M. D., Doehle, B. P. & Mo, H. Establishment of robust HCV genotype 4d, 5a, and 6a replicon systems. *Virology* **514**, 134-141 (2018). https://doi.org:10.1016/j.virol.2017.11.003

390 Lohmann, V., Körner, F., Dobierzewska, A. & Bartenschlager, R. Mutations in hepatitis C virus RNAs conferring cell culture adaptation. *J Virol* **75**, 1437-1449 (2001). https://doi.org:10.1128/jvi.75.3.1437-1449.2001

391 Krieger, N., Lohmann, V. & Bartenschlager, R. Enhancement of hepatitis C virus RNA replication by cell culture-adaptive mutations. *J Virol* **75**, 4614-4624 (2001). https://doi.org:10.1128/jvi.75.10.4614-4624.2001

392 Guo, J. T., Bichko, V. V. & Seeger, C. Effect of alpha interferon on the hepatitis C virus replicon. *J Virol* **75**, 8516-8523 (2001). https://doi.org:10.1128/jvi.75.18.8516-8523.2001

393 Bartenschlager, R. & Lohmann, V. Novel cell culture systems for the hepatitis C virus. *Antiviral research* **52**, 1-17 (2001). https://doi.org:10.1016/s0166-3542(01)00164-4

394 Saeed, M., Andreo, U., Chung, H. Y., Espiritu, C., Branch, A. D., Silva, J. M. & Rice, C. M. SEC14L2 enables pan-genotype HCV replication in cell culture. *Nature* **524**, 471-475 (2015). https://doi.org:10.1038/nature14899

395 Blight, K. J., McKeating, J. A. & Rice, C. M. Highly permissive cell lines for subgenomic and genomic hepatitis C virus RNA replication. *J Virol* **76**, 13001-13014 (2002). https://doi.org:10.1128/jvi.76.24.13001-13014.2002

396 Sumpter, R., Jr., Loo, Y. M., Foy, E., Li, K., Yoneyama, M., Fujita, T., Lemon, S. M. & Gale, M., Jr. Regulating intracellular antiviral defense and permissiveness to hepatitis C virus RNA replication through a cellular RNA helicase, RIG-I. *J Virol* **79**, 2689-2699 (2005). https://doi.org:10.1128/jvi.79.5.2689-2699.2005

397 Bartenschlager, R. Hepatitis C virus replicons: potential role for drug development. *Nat Rev Drug Discov* **1**, 911-916 (2002). https://doi.org:10.1038/nrd942

398 Bartosch, B., Dubuisson, J. & Cosset, F. L. Infectious hepatitis C virus pseudo-particles containing functional E1-E2 envelope protein complexes. *J Exp Med* **197**, 633-642 (2003). https://doi.org:10.1084/jem.20021756

399 Hsu, M., Zhang, J., Flint, M., Logvinoff, C., Cheng-Mayer, C., Rice, C. M. & McKeating, J. A. Hepatitis C virus glycoproteins mediate pH-dependent cell entry of pseudotyped retroviral particles. *Proceedings of the National Academy of Sciences of the United States of America* **100**, 7271-7276 (2003). https://doi.org:10.1073/pnas.0832180100

400 Meunier, J. C., Engle, R. E., Faulk, K., Zhao, M., Bartosch, B., Alter, H., Emerson, S. U., Cosset, F. L., Purcell, R. H. & Bukh, J. Evidence for cross-genotype neutralization of hepatitis C virus pseudo-particles and enhancement of infectivity by apolipoprotein C1. *Proceedings of the National Academy of Sciences of the United States of America* **102**, 4560-4565 (2005). https://doi.org:10.1073/pnas.0501275102

401 Pestka, J. M., Zeisel, M. B., Bläser, E., Schürmann, P., Bartosch, B., Cosset, F. L., Patel, A. H., Meisel, H., Baumert, J., Viazov, S., Rispeter, K., Blum, H. E., Roggendorf, M. & Baumert, T. F. Rapid induction of virus-neutralizing antibodies and viral clearance in a single-source outbreak of hepatitis C. *Proceedings of the National Academy of Sciences of the United States of America* **104**, 6025-6030 (2007). https://doi.org:10.1073/pnas.0607026104

402 Owsianka, A., Tarr, A. W., Juttla, V. S., Lavillette, D., Bartosch, B., Cosset, F. L., Ball, J. K. & Patel, A. H. Monoclonal antibody AP33 defines a broadly neutralizing epitope

on the hepatitis C virus E2 envelope glycoprotein. *J Virol* **79**, 11095-11104 (2005). https://doi.org:10.1128/jvi.79.17.11095-11104.2005

403 Tarr, A. W., Owsianka, A. M., Timms, J. M., McClure, C. P., Brown, R. J., Hickling, T. P., Pietschmann, T., Bartenschlager, R., Patel, A. H. & Ball, J. K. Characterization of the hepatitis C virus E2 epitope defined by the broadly neutralizing monoclonal antibody AP33. *Hepatol.* **43**, 592-601 (2006). https://doi.org:10.1002/hep.21088

404 Qian, X. J., Zhu, Y. Z., Zhao, P. & Qi, Z. T. Entry inhibitors: New advances in HCV treatment. *Emerg Microbes Infect* **5**, e3 (2016). https://doi.org:10.1038/emi.2016.3

405 Catanese, M. T. & Dorner, M. Advances in experimental systems to study hepatitis C virus in vitro and in vivo. *Virology* **479-480**, 221-233 (2015). https://doi.org:https://doi.org/10.1016/j.virol.2015.03.014

406 Keck, Z. Y., Li, T. K., Xia, J., Bartosch, B., Cosset, F. L., Dubuisson, J. & Foung, S. K. Analysis of a highly flexible conformational immunogenic domain a in hepatitis C virus E2. *J Virol* **79**, 13199-13208 (2005). https://doi.org:10.1128/jvi.79.21.13199-13208.2005

407 Popescu, C.-I. & Dubuisson, J. Role of lipid metabolism in hepatitis C virus assembly and entry. *Biology of the Cell* **102**, 63-74 (2010). https://doi.org:https://doi.org/10.1042/BC20090125

408 Keck, Z. Y., Xia, J., Cai, Z., Li, T. K., Owsianka, A. M., Patel, A. H., Luo, G. & Foung, S. K. Immunogenic and functional organization of hepatitis C virus (HCV) glycoprotein E2 on infectious HCV virions. *J Virol* **81**, 1043-1047 (2007). https://doi.org:10.1128/jvi.01710-06

409 Oliveira, C., Fournier, C., Descamps, V., Morel, V., Scipione, C. A., Romagnuolo, R., Koschinsky, M. L., Boullier, A., Marcelo, P., Domon, J. M., Brochot, E., Duverlie, G., Francois, C., Castelain, S. & Helle, F. Apolipoprotein(a) inhibits hepatitis C virus entry through interaction with infectious particles. *Hepatol.* **65**, 1851-1864 (2017). https://doi.org:10.1002/hep.29096

410 Kato, T., Miyamoto, M., Furusaka, A., Date, T., Yasui, K., Kato, J., Matsushima, S., Komatsu, T. & Wakita, T. Processing of hepatitis C virus core protein is regulated by its C-terminal sequence. *J Med Virol* **69**, 357-366 (2003). https://doi.org:10.1002/jmv.10297

411 Wakita, T., Pietschmann, T., Kato, T., Date, T., Miyamoto, M., Zhao, Z., Murthy, K., Habermann, A., Kräusslich, H. G., Mizokami, M., Bartenschlager, R. & Liang, T. J. Production of infectious hepatitis C virus in tissue culture from a cloned viral genome. *Nat Med* **11**, 791-796 (2005). https://doi.org:10.1038/nm1268

412 Lindenbach, B. D., Meuleman, P., Ploss, A., Vanwolleghem, T., Syder, A. J., McKeating, J. A., Lanford, R. E., Feinstone, S. M., Major, M. E., Leroux-Roels, G. & Rice, C. M. Cell culture-grown hepatitis C virus is infectious in vivo and can be recultured in vitro. *Proceedings of the National Academy of Sciences of the United States of America* **103**, 3805-3809 (2006). https://doi.org:10.1073/pnas.0511218103

413 Kaul, A., Woerz, I., Meuleman, P., Leroux-Roels, G. & Bartenschlager, R. Cell culture adaptation of hepatitis C virus and in vivo viability of an adapted variant. *J Virol* **81**, 13168-13179 (2007). https://doi.org:10.1128/jvi.01362-07

414 Lindenbach, B. D., Evans, M. J., Syder, A. J., Wölk, B., Tellinghuisen, T. L., Liu, C. C., Maruyama, T., Hynes, R. O., Burton, D. R., McKeating, J. A. & Rice, C. M. Complete replication of hepatitis C virus in cell culture. *Science* **309**, 623-626 (2005). https://doi.org:10.1126/science.1114016

415 Bartenschlager, R. & Pietschmann, T. Efficient hepatitis C virus cell culture system: what a difference the host cell makes. *Proceedings of the National Academy of Sciences*

of the United States of America **102**, 9739-9740 (2005). https://doi.org:10.1073/pnas.0504296102

416 Elaut, G., Henkens, T., Papeleu, P., Snykers, S., Vinken, M., Vanhaecke, T. & Rogiers, V. Molecular mechanisms underlying the dedifferentiation process of isolated hepatocytes and their cultures. *Curr Drug Metab* **7**, 629-660 (2006). https://doi.org:10.2174/138920006778017759

417 Podevin, P., Carpentier, A., Pène, V., Aoudjehane, L., Carrière, M., Zaïdi, S., Hernandez, C., Calle, V., Méritet, J. F., Scatton, O., Dreux, M., Cosset, F. L., Wakita, T., Bartenschlager, R., Demignot, S., Conti, F., Rosenberg, A. R. & Calmus, Y. Production of infectious hepatitis C virus in primary cultures of human adult hepatocytes. *Gastroenterology* **139**, 1355-1364 (2010). https://doi.org:10.1053/j.gastro.2010.06.058

418 Carpentier, A., Sheldon, J., Vondran, F. W. R., Brown, R. J. & Pietschmann, T. Efficient acute and chronic infection of stem cell-derived hepatocytes by hepatitis C virus. *Gut* **69**, 1659-1666 (2020). https://doi.org:10.1136/gutjnl-2019-319354

419 Akbari, S., Arslan, N., Senturk, S. & Erdal, E. Next-Generation Liver Medicine Using Organoid Models. *Frontiers in cell and developmental biology* **7**, 345 (2019). https://doi.org:10.3389/fcell.2019.00345

420 Vercauteren, K., de Jong, Y. P. & Meuleman, P. Animal models for the study of HCV. *Curr Opin Virol* **13**, 67-74 (2015). https://doi.org:10.1016/j.coviro.2015.04.009

421 Yong, K. S. M., Her, Z. & Chen, Q. Humanized Mouse Models for the Study of Hepatitis C and Host Interactions. *Cells* **8** (2019). https://doi.org:10.3390/cells8060604

422 Altevogt, B. M., Pankevich, D. E., Pope, A. M. & Kahn, J. P. Research agenda. Guiding limited use of chimpanzees in research. *Science* **335**, 41-42 (2012). https://doi.org:10.1126/science.1217521

423 Xie, Z. C., Riezu-Boj, J. I., Lasarte, J. J., Guillen, J., Su, J. H., Civeira, M. P. & Prieto, J. Transmission of hepatitis C virus infection to tree shrews. *Virology* **244**, 513-520 (1998). https://doi.org:10.1006/viro.1998.9127

424 Amako, Y., Tsukiyama-Kohara, K., Katsume, A., Hirata, Y., Sekiguchi, S., Tobita, Y., Hayashi, Y., Hishima, T., Funata, N., Yonekawa, H. & Kohara, M. Pathogenesis of hepatitis C virus infection in Tupaia belangeri. *J Virol* **84**, 303-311 (2010). https://doi.org:10.1128/jvi.01448-09

425 Kayesh, M. E. H., Ezzikouri, S., Sanada, T., Chi, H., Hayashi, Y., Rebbani, K., Kitab, B., Matsuu, A., Miyoshi, N., Hishima, T., Kohara, M. & Tsukiyama-Kohara, K. Oxidative Stress and Immune Responses During Hepatitis C Virus Infection in Tupaia belangeri. *Sci Rep* **7**, 9848 (2017). https://doi.org:10.1038/s41598-017-10329-7

426 Liang, T. J., Feld, J. J., Cox, A. L. & Rice, C. M. Controlled Human Infection Model - Fast Track to HCV Vaccine? *N Engl J Med* **385**, 1235-1240 (2021). https://doi.org:10.1056/NEJMsb2109093

427 Choy, R. K. M., Bourgeois, A. L., Ockenhouse, C. F., Walker, R. I., Sheets, R. L. & Flores, J. Controlled Human Infection Models To Accelerate Vaccine Development. *Clin Microbiol Rev* **35**, e0000821 (2022). https://doi.org:10.1128/cmr.00008-21

428 Morrison, H., Jackson, S. & McShane, H. Controlled human infection models in COVID-19 and tuberculosis: current progress and future challenges. *Front Immunol* **14**, 1211388 (2023). https://doi.org:10.3389/fimmu.2023.1211388

429 Feld, J. J., Bruneau, J., Dore, G. J., Ghany, M. G., Hansen, B., Sulkowski, M. & Thomas, D. L. Controlled Human Infection Model for Hepatitis C Virus Vaccine Development: Trial Design Considerations. *Clin Infect Dis* **77**, S262-s269 (2023). https://doi.org:10.1093/cid/ciad362

430 Perez, S., Kaspi, A., Domovitz, T., Davidovich, A., Lavi-Itzkovitz, A., Meirson, T., Alison Holmes, J., Dai, C. Y., Huang, C. F., Chung, R. T., Nimer, A., El-Osta, A., Yaari, G., Stemmer, S. M., Yu, M. L., Haviv, I. & Gal-Tanamy, M. Hepatitis C virus leaves an epigenetic signature post cure of infection by direct-acting antivirals. *PLoS Genet* **15**, e1008181 (2019). https://doi.org:10.1371/journal.pgen.1008181

431 Sandmann, L. & Ploss, A. Barriers of hepatitis C virus interspecies transmission. *Virology* **435**, 70-80 (2013). https://doi.org:10.1016/j.virol.2012.09.044

432 Brown, R. J. P., Tegtmeyer, B., Sheldon, J., Khera, T., Anggakusuma, Todt, D., Vieyres, G., Weller, R., Joecks, S., Zhang, Y., Sake, S., Bankwitz, D., Welsch, K., Ginkel, C., Engelmann, M., Gerold, G., Steinmann, E., Yuan, Q., Ott, M., Vondran, F. W. R., Krey, T., Ströh, L. J., Miskey, C., Ivics, Z., Herder, V., Baumgärtner, W., Lauber, C., Seifert, M., Tarr, A. W., McClure, C. P., Randall, G., Baktash, Y., Ploss, A., Thi, V. L. D., Michailidis, E., Saeed, M., Verhoye, L., Meuleman, P., Goedecke, N., Wirth, D., Rice, C. M. & Pietschmann, T. Liver-expressed Cd302 and Cr1l limit hepatitis C virus cross-species transmission to mice. *Sci Adv* **6** (2020). https://doi.org:10.1126/sciadv.abd3233

433 Barth, H., Robinet, E., Liang, T. J. & Baumert, T. F. Mouse models for the study of HCV infection and virus-host interactions. *Journal of hepatology* **49**, 134-142 (2008). https://doi.org:10.1016/j.jhep.2008.03.012

434 Moriya, K., Nakagawa, K., Santa, T., Shintani, Y., Fujie, H., Miyoshi, H., Tsutsumi, T., Miyazawa, T., Ishibashi, K., Horie, T., Imai, K., Todoroki, T., Kimura, S. & Koike, K. Oxidative stress in the absence of inflammation in a mouse model for hepatitis C virus-associated hepatocarcinogenesis. *Cancer Res* **61**, 4365-4370 (2001).

435 Perlemuter, G., Sabile, A., Letteron, P., Vona, G., Topilco, A., Chrétien, Y., Koike, K., Pessayre, D., Chapman, J., Barba, G. & Bréchot, C. Hepatitis C virus core protein inhibits microsomal triglyceride transfer protein activity and very low density lipoprotein secretion: a model of viral-related steatosis. *FASEB J* **16**, 185-194 (2002). https://doi.org:10.1096/fj.01-0396com

436 Liang, T. J. & Heller, T. Pathogenesis of hepatitis C-associated hepatocellular carcinoma. *Gastroenterology* **127**, S62-71 (2004). https://doi.org:10.1053/j.gastro.2004.09.017

437 Lerat, H., Honda, M., Beard, M. R., Loesch, K., Sun, J., Yang, Y., Okuda, M., Gosert, R., Xiao, S. Y., Weinman, S. A. & Lemon, S. M. Steatosis and liver cancer in transgenic mice expressing the structural and nonstructural proteins of hepatitis C virus. *Gastroenterology* **122**, 352-365 (2002). https://doi.org:10.1053/gast.2002.31001

438 Pasquinelli, C., Shoenberger, J. M., Chung, J., Chang, K. M., Guidotti, L. G., Selby, M., Berger, K., Lesniewski, R., Houghton, M. & Chisari, F. V. Hepatitis C virus core and E2 protein expression in transgenic mice. *Hepatol.* **25**, 719-727 (1997). https://doi.org:10.1002/hep.510250338

439 Kawamura, T., Furusaka, A., Koziel, M. J., Chung, R. T., Wang, T. C., Schmidt, E. V. & Liang, T. J. Transgenic expression of hepatitis C virus structural proteins in the mouse. *Hepatol.* **25**, 1014-1021 (1997). https://doi.org:10.1002/hep.510250437

440 Ploss, A. & Rice, C. M. Towards a small animal model for hepatitis C. *EMBO Rep* **10**, 1220-1227 (2009). https://doi.org:10.1038/embor.2009.223

441 Dorner, M., Horwitz, J. A., Robbins, J. B., Barry, W. T., Feng, Q., Mu, K., Jones, C. T., Schoggins, J. W., Catanese, M. T., Burton, D. R., Law, M., Rice, C. M. & Ploss, A. A genetically humanized mouse model for hepatitis C virus infection. *Nature* **474**, 208-211 (2011). https://doi.org:10.1038/nature10168

442 Dorner, M., Horwitz, J. A., Donovan, B. M., Labitt, R. N., Budell, W. C., Friling, T., Vogt, A., Catanese, M. T., Satoh, T., Kawai, T., Akira, S., Law, M., Rice, C. M. & Ploss,

A. Completion of the entire hepatitis C virus life cycle in genetically humanized mice. *Nature* **501**, 237-241 (2013). https://doi.org:10.1038/nature12427

443 Kneteman, N. M., Howe, A. Y., Gao, T., Lewis, J., Pevear, D., Lund, G., Douglas, D., Mercer, D. F., Tyrrell, D. L., Immermann, F., Chaudhary, I., Speth, J., Villano, S. A., O'Connell, J. & Collett, M. HCV796: A selective nonstructural protein 5B polymerase inhibitor with potent anti-hepatitis C virus activity in vitro, in mice with chimeric human livers, and in humans infected with hepatitis C virus. *Hepatol.* **49**, 745-752 (2009). https://doi.org:10.1002/hep.22717

444 Kamiya, N., Iwao, E., Hiraga, N., Tsuge, M., Imamura, M., Takahashi, S., Miyoshi, S., Tateno, C., Yoshizato, K. & Chayama, K. Practical evaluation of a mouse with chimeric human liver model for hepatitis C virus infection using an NS3-4A protease inhibitor. *The Journal of general virology* **91**, 1668-1677 (2010). https://doi.org:10.1099/vir.0.019315-0

445 Ohara, E., Hiraga, N., Imamura, M., Iwao, E., Kamiya, N., Yamada, I., Kono, T., Onishi, M., Hirata, D., Mitsui, F., Kawaoka, T., Tsuge, M., Takahashi, S., Abe, H., Hayes, C. N., Ochi, H., Tateno, C., Yoshizato, K., Tanaka, S. & Chayama, K. Elimination of hepatitis C virus by short term NS3-4A and NS5B inhibitor combination therapy in human hepatocyte chimeric mice. *Journal of hepatology* **54**, 872-878 (2011). https://doi.org:10.1016/j.jhep.2010.08.033

446 Vanwolleghem, T., Bukh, J., Meuleman, P., Desombere, I., Meunier, J. C., Alter, H., Purcell, R. H. & Leroux-Roels, G. Polyclonal immunoglobulins from a chronic hepatitis C virus patient protect human liver-chimeric mice from infection with a homologous hepatitis C virus strain. *Hepatol.* **47**, 1846-1855 (2008). https://doi.org:10.1002/hep.22244

447 Meuleman, P., Catanese, M. T., Verhoye, L., Desombere, I., Farhoudi, A., Jones, C. T., Sheahan, T., Grzyb, K., Cortese, R., Rice, C. M., Leroux-Roels, G. & Nicosia, A. A human monoclonal antibody targeting scavenger receptor class B type I precludes hepatitis C virus infection and viral spread in vitro and in vivo. *Hepatol.* **55**, 364-372 (2012). https://doi.org:10.1002/hep.24692

448 Lacek, K., Vercauteren, K., Grzyb, K., Naddeo, M., Verhoye, L., Słowikowski, M. P., Fafi-Kremer, S., Patel, A. H., Baumert, T. F., Folgori, A., Leroux-Roels, G., Cortese, R., Meuleman, P. & Nicosia, A. Novel human SR-BI antibodies prevent infection and dissemination of HCV in vitro and in humanized mice. *Journal of hepatology* **57**, 17-23 (2012). https://doi.org:10.1016/j.jhep.2012.02.018

449 Chen, J., Zhao, Y., Zhang, C., Chen, H., Feng, J., Chi, X., Pan, Y., Du, J., Guo, M., Cao, H., Chen, H., Wang, Z., Pei, R., Wang, Q., Pan, L., Niu, J., Chen, X. & Tang, H. Persistent hepatitis C virus infections and hepatopathological manifestations in immune-competent humanized mice. *Cell Res* **24**, 1050-1066 (2014). https://doi.org:10.1038/cr.2014.116

450 Mercer, D. F., Schiller, D. E., Elliott, J. F., Douglas, D. N., Hao, C., Rinfret, A., Addison, W. R., Fischer, K. P., Churchill, T. A., Lakey, J. R., Tyrrell, D. L. & Kneteman, N. M. Hepatitis C virus replication in mice with chimeric human livers. *Nat Med* **7**, 927-933 (2001). https://doi.org:10.1038/90968

451 Strick-Marchand, H., Dusséaux, M., Darche, S., Huntington, N. D., Legrand, N., Masse-Ranson, G., Corcuff, E., Ahodantin, J., Weijer, K., Spits, H., Kremsdorf, D. & Di Santo, J. P. A novel mouse model for stable engraftment of a human immune system and human hepatocytes. *PloS one* **10**, e0119820 (2015). https://doi.org:10.1371/journal.pone.0119820

452 Douam, F. & Ploss, A. The use of humanized mice for studies of viral pathogenesis and immunity. *Curr Opin Virol* **29**, 62-71 (2018). https://doi.org:10.1016/j.coviro.2018.03.003
453 Martin, A., Bodola, F., Sangar, D. V., Goettge, K., Popov, V., Rijnbrand, R., Lanford, R. E. & Lemon, S. M. Chronic hepatitis associated with GB virus B persistence in a tamarin after intrahepatic inoculation of synthetic viral RNA. *Proceedings of the National Academy of Sciences of the United States of America* **100**, 9962-9967 (2003). https://doi.org:10.1073/pnas.1731505100
454 Bukh, J., Engle, R. E., Govindarajan, S. & Purcell, R. H. Immunity against the GBV-B hepatitis virus in tamarins can prevent productive infection following rechallenge and is long-lived. *J Med Virol* **80**, 87-94 (2008). https://doi.org:10.1002/jmv.21013
455 Woollard, D. J., Haqshenas, G., Dong, X., Pratt, B. F., Kent, S. J. & Gowans, E. J. Virus-specific T-cell immunity correlates with control of GB virus B infection in marmosets. *J Virol* **82**, 3054-3060 (2008). https://doi.org:10.1128/jvi.01153-07
456 Kapoor, A., Simmonds, P., Gerold, G., Qaisar, N., Jain, K., Henriquez, J. A., Firth, C., Hirschberg, D. L., Rice, C. M., Shields, S. & Lipkin, W. I. Characterization of a canine homolog of hepatitis C virus. *Proceedings of the National Academy of Sciences of the United States of America* **108**, 11608-11613 (2011). https://doi.org:10.1073/pnas.1101794108
457 Scheel, T. K., Simmonds, P. & Kapoor, A. Surveying the global virome: identification and characterization of HCV-related animal hepaciviruses. *Antiviral research* **115**, 83-93 (2015). https://doi.org:10.1016/j.antiviral.2014.12.014
458 Bukh, J., Forns, X., Emerson, S. U. & Purcell, R. H. Studies of hepatitis C virus in chimpanzees and their importance for vaccine development. *Intervirology* **44**, 132-142 (2001). https://doi.org:10.1159/000050040
459 Lanford, R. E., Bigger, C., Bassett, S. & Klimpel, G. The chimpanzee model of hepatitis C virus infections. *Ilar j* **42**, 117-126 (2001). https://doi.org:10.1093/ilar.42.2.117
460 Feng, Y., Feng, Y. M., Lu, C., Han, Y., Liu, L., Sun, X., Dai, J. & Xia, X. Tree shrew, a potential animal model for hepatitis C, supports the infection and replication of HCV in vitro and in vivo. *The Journal of general virology* **98**, 2069-2078 (2017). https://doi.org:10.1099/jgv.0.000869
461 Meuleman, P. & Leroux-Roels, G. The human liver-uPA-SCID mouse: a model for the evaluation of antiviral compounds against HBV and HCV. *Antiviral research* **80**, 231-238 (2008). https://doi.org:10.1016/j.antiviral.2008.07.006
462 Bukh, J., Meuleman, P., Tellier, R., Engle, R. E., Feinstone, S. M., Eder, G., Satterfield, W. C., Govindarajan, S., Krawczynski, K., Miller, R. H., Leroux-Roels, G. & Purcell, R. H. Challenge pools of hepatitis C virus genotypes 1-6 prototype strains: replication fitness and pathogenicity in chimpanzees and human liver-chimeric mouse models. *J Infect Dis* **201**, 1381-1389 (2010). https://doi.org:10.1086/651579
463 Burchill, M. A., Roby, J. A., Crochet, N., Wind-Rotolo, M., Stone, A. E., Edwards, M. G., Dran, R. J., Kriss, M. S., Gale, M., Jr. & Rosen, H. R. Rapid reversal of innate immune dysregulation in blood of patients and livers of humanized mice with HCV following DAA therapy. *PloS one* **12**, e0186213 (2017). https://doi.org:10.1371/journal.pone.0186213
464 Andreo, U., de Jong, Y. P., Scull, M. A., Xiao, J. W., Vercauteren, K., Quirk, C., Mommersteeg, M. C., Bergaya, S., Menon, A., Fisher, E. A. & Rice, C. M. Analysis of Hepatitis C Virus Particle Heterogeneity in Immunodeficient Human Liver Chimeric fah-/- Mice. *Cell Mol Gastroenterol Hepatol* **4**, 405-417 (2017). https://doi.org:10.1016/j.jcmgh.2017.07.002

465 Washburn, M. L., Bility, M. T., Zhang, L., Kovalev, G. I., Buntzman, A., Frelinger, J. A., Barry, W., Ploss, A., Rice, C. M. & Su, L. A humanized mouse model to study hepatitis C virus infection, immune response, and liver disease. *Gastroenterology* **140**, 1334-1344 (2011). https://doi.org:10.1053/j.gastro.2011.01.001

466 Keng, C. T., Sze, C. W., Zheng, D., Zheng, Z., Yong, K. S., Tan, S. Q., Ong, J. J., Tan, S. Y., Loh, E., Upadya, M. H., Kuick, C. H., Hotta, H., Lim, S. G., Tan, T. C., Chang, K. T., Hong, W., Chen, J., Tan, Y. J. & Chen, Q. Characterisation of liver pathogenesis, human immune responses and drug testing in a humanised mouse model of HCV infection. *Gut* **65**, 1744-1753 (2016). https://doi.org:10.1136/gutjnl-2014-307856

467 Zheng, Z., Sze, C. W., Keng, C. T., Al-Haddawi, M., Liu, M., Tan, S. Y., Kwek, H. L., Her, Z., Chan, X. Y., Barnwal, B., Loh, E., Chang, K. T. E., Tan, T. C., Tan, Y. J. & Chen, Q. Hepatitis C virus mediated chronic inflammation and tumorigenesis in the humanised immune system and liver mouse model. *PloS one* **12**, e0184127 (2017). https://doi.org:10.1371/journal.pone.0184127

468 Trivedi, S., Murthy, S., Sharma, H., Hartlage, A. S., Kumar, A., Gadi, S. V., Simmonds, P., Chauhan, L. V., Scheel, T. K. H., Billerbeck, E., Burbelo, P. D., Rice, C. M., Lipkin, W. I., Vandegrift, K., Cullen, J. M. & Kapoor, A. Viral persistence, liver disease, and host response in a hepatitis C-like virus rat model. *Hepatol.* **68**, 435-448 (2018). https://doi.org:10.1002/hep.29494

469 Billerbeck, E., Wolfisberg, R., Fahnøe, U., Xiao, J. W., Quirk, C., Luna, J. M., Cullen, J. M., Hartlage, A. S., Chiriboga, L., Ghoshal, K., Lipkin, W. I., Bukh, J., Scheel, T. K. H., Kapoor, A. & Rice, C. M. Mouse models of acute and chronic hepacivirus infection. *Science* **357**, 204-208 (2017). https://doi.org:10.1126/science.aal1962

470 Brown, A. J., Won, J. J., Wolfisberg, R., Fahnøe, U., Catanzaro, N., West, A., Moreira, F. R., Nogueira Batista, M., Ferris, M. T., Linnertz, C. L., Leist, S. R., Nguyen, C., De la Cruz, G., Midkiff, B. R., Xia, Y., Evangelista, M. D., Montgomery, S. A., Billerbeck, E., Bukh, J., Scheel, T. K. H., Rice, C. M. & Sheahan, T. P. Host genetic variation guides hepacivirus clearance, chronicity, and liver fibrosis in mice. *Hepatol.* (2023). https://doi.org:10.1097/hep.0000000000000547

471 Bandiera, S., Billie Bian, C., Hoshida, Y., Baumert, T. F. & Zeisel, M. B. Chronic hepatitis C virus infection and pathogenesis of hepatocellular carcinoma. *Curr Opin Virol* **20**, 99-105 (2016). https://doi.org:10.1016/j.coviro.2016.09.010

472 Mesri, E. A., Feitelson, M. A. & Munger, K. Human viral oncogenesis: a cancer hallmarks analysis. *Cell host & microbe* **15**, 266-282 (2014). https://doi.org:10.1016/j.chom.2014.02.011

473 Gremion, C. & Cerny, A. Hepatitis C virus and the immune system: a concise review. *Rev Med Virol* **15**, 235-268 (2005). https://doi.org:10.1002/rmv.466

474 Ahmad, A. & Alvarez, F. Role of NK and NKT cells in the immunopathogenesis of HCV-induced hepatitis. *J Leukoc Biol* **76**, 743-759 (2004). https://doi.org:10.1189/jlb.0304197

475 Ryan, E. J. & O'Farrelly, C. The affect of chronic hepatitis C infection on dendritic cell function: a summary of the experimental evidence. *J Viral Hepat* **18**, 601-607 (2011). https://doi.org:10.1111/j.1365-2893.2011.01453.x

476 Giugliano, S., Kriss, M., Golden-Mason, L., Dobrinskikh, E., Stone, A. E., Soto-Gutierrez, A., Mitchell, A., Khetani, S. R., Yamane, D., Stoddard, M., Li, H., Shaw, G. M., Edwards, M. G., Lemon, S. M., Gale, M., Jr., Shah, V. H. & Rosen, H. R. Hepatitis C virus infection induces autocrine interferon signaling by human liver endothelial cells and release of exosomes, which inhibits viral replication. *Gastroenterology* **148**, 392-402.e313 (2015). https://doi.org:10.1053/j.gastro.2014.10.040

477 Schulz, S., Landi, A., Garg, R., Wilson, J. A. & van Drunen Littel-van den Hurk, S. Indolamine 2,3-dioxygenase expression by monocytes and dendritic cell populations in hepatitis C patients. *Clin Exp Immunol* **180**, 484-498 (2015). https://doi.org:10.1111/cei.12586

478 Leone, P., Di Tacchio, M., Berardi, S., Santantonio, T., Fasano, M., Ferrone, S., Vacca, A., Dammacco, F. & Racanelli, V. Dendritic cell maturation in HCV infection: altered regulation of MHC class I antigen processing-presenting machinery. *Journal of hepatology* **61**, 242-251 (2014). https://doi.org:10.1016/j.jhep.2014.04.007

479 Gerosa, F., Gobbi, A., Zorzi, P., Burg, S., Briere, F., Carra, G. & Trinchieri, G. The reciprocal interaction of NK cells with plasmacytoid or myeloid dendritic cells profoundly affects innate resistance functions. *J Immunol* **174**, 727-734 (2005). https://doi.org:10.4049/jimmunol.174.2.727

480 Miyazaki, M., Kanto, T., Inoue, M., Itose, I., Miyatake, H., Sakakibara, M., Yakushijin, T., Kakita, N., Hiramatsu, N., Takehara, T., Kasahara, A. & Hayashi, N. Impaired cytokine response in myeloid dendritic cells in chronic hepatitis C virus infection regardless of enhanced expression of Toll-like receptors and retinoic acid inducible gene-I. *J Med Virol* **80**, 980-988 (2008). https://doi.org:10.1002/jmv.21174

481 Strunz, B., Hengst, J., Deterding, K., Manns, M. P., Cornberg, M., Ljunggren, H. G., Wedemeyer, H. & Björkström, N. K. Chronic hepatitis C virus infection irreversibly impacts human natural killer cell repertoire diversity. *Nat Commun* **9**, 2275 (2018). https://doi.org:10.1038/s41467-018-04685-9

482 Njiomegnie, G. F., Read, S. A., Fewings, N., George, J., McKay, F. & Ahlenstiel, G. Immunomodulation of the Natural Killer Cell Phenotype and Response during HCV Infection. *J Clin Med* **9** (2020). https://doi.org:10.3390/jcm9041030

483 Gale, M., Jr. & Foy, E. M. Evasion of intracellular host defence by hepatitis C virus. *Nature* **436**, 939-945 (2005). https://doi.org:10.1038/nature04078

484 Wong, M.-T. & Chen, S. S. L. Emerging roles of interferon-stimulated genes in the innate immune response to hepatitis C virus infection. *Cellular & Molecular Immunology* **13**, 11-35 (2016). https://doi.org:10.1038/cmi.2014.127

485 Meylan, E., Curran, J., Hofmann, K., Moradpour, D., Binder, M., Bartenschlager, R. & Tschopp, J. Cardif is an adaptor protein in the RIG-I antiviral pathway and is targeted by hepatitis C virus. *Nature* **437**, 1167-1172 (2005). https://doi.org:10.1038/nature04193

486 Heim, M. H. Innate immunity and HCV. *Journal of hepatology* **58**, 564-574 (2013). https://doi.org:10.1016/j.jhep.2012.10.005

487 Otsuka, M., Kato, N., Moriyama, M., Taniguchi, H., Wang, Y., Dharel, N., Kawabe, T. & Omata, M. Interaction between the HCV NS3 protein and the host TBK1 protein leads to inhibition of cellular antiviral responses. *Hepatol.* **41**, 1004-1012 (2005). https://doi.org:10.1002/hep.20666

488 Ding, Q., Cao, X., Lu, J., Huang, B., Liu, Y. J., Kato, N., Shu, H. B. & Zhong, J. Hepatitis C virus NS4B blocks the interaction of STING and TBK1 to evade host innate immunity. *Journal of hepatology* **59**, 52-58 (2013). https://doi.org:10.1016/j.jhep.2013.03.019

489 Anjum, S., Afzal, M. S., Ahmad, T., Aslam, B., Waheed, Y., Shafi, T. & Qadri, I. Mutations in the STAT1-interacting domain of the hepatitis C virus core protein modulate the response to antiviral therapy. *Mol Med Rep* **8**, 487-492 (2013). https://doi.org:10.3892/mmr.2013.1541

490 Kawaguchi, T., Yoshida, T., Harada, M., Hisamoto, T., Nagao, Y., Ide, T., Taniguchi, E., Kumemura, H., Hanada, S., Maeyama, M., Baba, S., Koga, H., Kumashiro, R., Ueno, T., Ogata, H., Yoshimura, A. & Sata, M. Hepatitis C virus down-regulates insulin

receptor substrates 1 and 2 through up-regulation of suppressor of cytokine signaling 3. *The American journal of pathology* **165**, 1499-1508 (2004). https://doi.org:10.1016/s0002-9440(10)63408-6

491 Miyoshi, H., Fujie, H., Shintani, Y., Tsutsumi, T., Shinzawa, S., Makuuchi, M., Kokudo, N., Matsuura, Y., Suzuki, T., Miyamura, T., Moriya, K. & Koike, K. Hepatitis C virus core protein exerts an inhibitory effect on suppressor of cytokine signaling (SOCS)-1 gene expression. *Journal of hepatology* **43**, 757-763 (2005). https://doi.org:10.1016/j.jhep.2005.03.028

492 Lin, W., Kim, S. S., Yeung, E., Kamegaya, Y., Blackard, J. T., Kim, K. A., Holtzman, M. J. & Chung, R. T. Hepatitis C virus core protein blocks interferon signaling by interaction with the STAT1 SH2 domain. *J Virol* **80**, 9226-9235 (2006). https://doi.org:10.1128/jvi.00459-06

493 Zhang, Q., Wang, Y., Zhai, N., Song, H., Li, H., Yang, Y., Li, T., Guo, X., Chi, B., Niu, J., Crispe, I. N., Su, L. & Tu, Z. HCV core protein inhibits polarization and activity of both M1 and M2 macrophages through the TLR2 signaling pathway. *Sci Rep* **6**, 36160 (2016). https://doi.org:10.1038/srep36160

494 Zhao, S., Si, M., Deng, X., Wang, D., Kong, L. & Zhang, Q. HCV inhibits M2a, M2b and M2c macrophage polarization via HCV core protein engagement with Toll-like receptor 2. *Exp Ther Med* **24**, 522 (2022). https://doi.org:10.3892/etm.2022.11448

495 Taylor, D. R., Shi, S. T., Romano, P. R., Barber, G. N. & Lai, M. M. Inhibition of the interferon-inducible protein kinase PKR by HCV E2 protein. *Science* **285**, 107-110 (1999). https://doi.org:10.1126/science.285.5424.107

496 Tsutsumi, T., Okushin, K., Enooku, K., Fujinaga, H., Moriya, K., Yotsuyanagi, H., Aizaki, H., Suzuki, T., Matsuura, Y. & Koike, K. Nonstructural 5A Protein of Hepatitis C Virus Interferes with Toll-Like Receptor Signaling and Suppresses the Interferon Response in Mouse Liver. *PloS one* **12**, e0170461 (2017). https://doi.org:10.1371/journal.pone.0170461

497 Han, J. Q. & Barton, D. J. Activation and evasion of the antiviral 2'-5' oligoadenylate synthetase/ribonuclease L pathway by hepatitis C virus mRNA. *Rna* **8**, 512-525 (2002). https://doi.org:10.1017/s1355838202020617

498 Polyak, S. J., Khabar, K. S., Paschal, D. M., Ezelle, H. J., Duverlie, G., Barber, G. N., Levy, D. E., Mukaida, N. & Gretch, D. R. Hepatitis C virus nonstructural 5A protein induces interleukin-8, leading to partial inhibition of the interferon-induced antiviral response. *J Virol* **75**, 6095-6106 (2001). https://doi.org:10.1128/jvi.75.13.6095-6106.2001

499 Sène, D., Levasseur, F., Abel, M., Lambert, M., Camous, X., Hernandez, C., Pène, V., Rosenberg, A. R., Jouvin-Marche, E., Marche, P. N., Cacoub, P. & Caillat-Zucman, S. Hepatitis C virus (HCV) evades NKG2D-dependent NK cell responses through NS5A-mediated imbalance of inflammatory cytokines. *PLoS pathogens* **6**, e1001184 (2010). https://doi.org:10.1371/journal.ppat.1001184

500 Loo, Y. M., Owen, D. M., Li, K., Erickson, A. K., Johnson, C. L., Fish, P. M., Carney, D. S., Wang, T., Ishida, H., Yoneyama, M., Fujita, T., Saito, T., Lee, W. M., Hagedorn, C. H., Lau, D. T., Weinman, S. A., Lemon, S. M. & Gale, M., Jr. Viral and therapeutic control of IFN-beta promoter stimulator 1 during hepatitis C virus infection. *Proceedings of the National Academy of Sciences of the United States of America* **103**, 6001-6006 (2006). https://doi.org:10.1073/pnas.0601523103

501 Roux, K. J., Kim, D. I., Burke, B. & May, D. G. BioID: A Screen for Protein-Protein Interactions. *Curr Protoc Protein Sci* **91**, 19.23.11-19.23.15 (2018). https://doi.org:10.1002/cpps.51

502 Rao, V. S., Srinivas, K., Sujini, G. N. & Kumar, G. N. Protein-protein interaction detection: methods and analysis. *Int J Proteomics* **2014**, 147648 (2014). https://doi.org:10.1155/2014/147648

503 Kwofie, S. K., Schaefer, U., Sundararajan, V. S., Bajic, V. B. & Christoffels, A. HCVpro: Hepatitis C virus protein interaction database. *Infection, Genetics and Evolution* **11**, 1971-1977 (2011). https://doi.org:https://doi.org/10.1016/j.meegid.2011.09.001

504 Chatr-aryamontri, A., Ceol, A., Peluso, D., Nardozza, A., Panni, S., Sacco, F., Tinti, M., Smolyar, A., Castagnoli, L., Vidal, M., Cusick, M. E. & Cesareni, G. VirusMINT: a viral protein interaction database. *Nucleic Acids Res* **37**, D669-673 (2009). https://doi.org:10.1093/nar/gkn739

505 Mukhopadhyay, A. & Maulik, U. Network-based study reveals potential infection pathways of hepatitis-C leading to various diseases. *PloS one* **9**, e94029 (2014). https://doi.org:10.1371/journal.pone.0094029

506 Saik, O. V., Ivanisenko, T. V., Demenkov, P. S. & Ivanisenko, V. A. Interactome of the hepatitis C virus: Literature mining with ANDSystem. *Virus research* **218**, 40-48 (2016). https://doi.org:10.1016/j.virusres.2015.12.003

507 Farooq, Q. U. & Khan, F. F. Construction and analysis of a comprehensive protein interaction network of HCV with its host Homo sapiens. *Bmc Infect Dis* **19** (2019). https://doi.org:10.1186/s12879-019-4000-9

508 de Chassey, B., Navratil, V., Tafforeau, L., Hiet, M. S., Aublin-Gex, A., Agaugué, S., Meiffren, G., Pradezynski, F., Faria, B. F., Chantier, T., Le Breton, M., Pellet, J., Davoust, N., Mangeot, P. E., Chaboud, A., Penin, F., Jacob, Y., Vidalain, P. O., Vidal, M., André, P., Rabourdin-Combe, C. & Lotteau, V. Hepatitis C virus infection protein network. *Mol Syst Biol* **4**, 230 (2008). https://doi.org:10.1038/msb.2008.66

509 Tripathi, L. P., Kambara, H., Chen, Y. A., Nishimura, Y., Moriishi, K., Okamoto, T., Morita, E., Abe, T., Mori, Y., Matsuura, Y. & Mizuguchi, K. Understanding the biological context of NS5A-host interactions in HCV infection: a network-based approach. *Journal of proteome research* **12**, 2537-2551 (2013). https://doi.org:10.1021/pr3011217

510 Dolan, P. T., Zhang, C., Khadka, S., Arumugaswami, V., Vangeloff, A. D., Heaton, N. S., Sahasrabudhe, S., Randall, G., Sun, R. & LaCount, D. J. Identification and comparative analysis of hepatitis C virus-host cell protein interactions. *Molecular bioSystems* **9**, 3199-3209 (2013). https://doi.org:10.1039/c3mb70343f

511 Germain, M. A., Chatel-Chaix, L., Gagné, B., Bonneil, É., Thibault, P., Pradezynski, F., de Chassey, B., Meyniel-Schicklin, L., Lotteau, V., Baril, M. & Lamarre, D. Elucidating novel hepatitis C virus-host interactions using combined mass spectrometry and functional genomics approaches. *Molecular & cellular proteomics : MCP* **13**, 184-203 (2014). https://doi.org:10.1074/mcp.M113.030155

512 Ramage, H. R., Kumar, G. R., Verschueren, E., Johnson, J. R., Von Dollen, J., Johnson, T., Newton, B., Shah, P., Horner, J., Krogan, N. J. & Ott, M. A combined proteomics/genomics approach links hepatitis C virus infection with nonsense-mediated mRNA decay. *Mol Cell* **57**, 329-340 (2015). https://doi.org:10.1016/j.molcel.2014.12.028

513 Roohvand, F., Maillard, P., Lavergne, J. P., Boulant, S., Walic, M., Andréo, U., Goueslain, L., Helle, F., Mallet, A., McLauchlan, J. & Budkowska, A. Initiation of hepatitis C virus infection requires the dynamic microtubule network: role of the viral nucleocapsid protein. *J Biol Chem* **284**, 13778-13791 (2009). https://doi.org:10.1074/jbc.M807873200

514 Tripathi, L. P., Kataoka, C., Taguwa, S., Moriishi, K., Mori, Y., Matsuura, Y. & Mizuguchi, K. Network based analysis of hepatitis C virus core and NS4B protein interactions. *Molecular bioSystems* **6**, 2539-2553 (2010). https://doi.org:10.1039/c0mb00103a

515 Dolan, P. T., Roth, A. P., Xue, B., Sun, R., Dunker, A. K., Uversky, V. N. & LaCount, D. J. Intrinsic disorder mediates hepatitis C virus core-host cell protein interactions. *Protein Sci* **24**, 221-235 (2015). https://doi.org:10.1002/pro.2608

516 Meistermann, H., Gao, J., Golling, S., Lamerz, J., Le Pogam, S., Tzouros, M., Sankabathula, S., Gruenbaum, L., Nájera, I., Langen, H., Klumpp, K. & Augustin, A. A novel immuno-competitive capture mass spectrometry strategy for protein-protein interaction profiling reveals that LATS kinases regulate HCV replication through NS5A phosphorylation. *Molecular & cellular proteomics : MCP* **13**, 3040-3048 (2014). https://doi.org:10.1074/mcp.M113.028977

517 Eberle, C. A., Zayas, M., Stukalov, A., Pichlmair, A., Alvisi, G., Müller, A. C., Bennett, K. L., Bartenschlager, R. & Superti-Furga, G. The lysine methyltransferase SMYD3 interacts with hepatitis C virus NS5A and is a negative regulator of viral particle production. *Virology* **462-463**, 34-41 (2014). https://doi.org:10.1016/j.virol.2014.05.016

518 Moradpour, D., Evans, M. J., Gosert, R., Yuan, Z., Blum, H. E., Goff, S. P., Lindenbach, B. D. & Rice, C. M. Insertion of green fluorescent protein into nonstructural protein 5A allows direct visualization of functional hepatitis C virus replication complexes. *J Virol* **78**, 7400-7409 (2004). https://doi.org:10.1128/jvi.78.14.7400-7409.2004

519 Gottwein, J. M., Jensen, T. B., Mathiesen, C. K., Meuleman, P., Serre, S. B. N., Lademann, J. B., Ghanem, L., Scheel, T. K. H., Leroux-Roels, G. & Bukh, J. Development and application of hepatitis C reporter viruses with genotype 1 to 7 core-nonstructural protein 2 (NS2) expressing fluorescent proteins or luciferase in modified JFH1 NS5A. *J Virol* **85**, 8913-8928 (2011). https://doi.org:10.1128/jvi.00049-11

520 Vlaicu, O., Selescu, T., Pastrama, F., Munteanu, C., Riva, L., Dubuisson, J., Rouille, Y. & Popescu, C. I. Novel replicons and trans-encapsidation systems for Hepatitis C Virus proteins live imaging and virus-host interaction proteomics. *J Virol Methods* **246**, 42-50 (2017). https://doi.org:10.1016/j.jviromet.2017.04.009

521 Kao, C. C., Yi, G. & Huang, H. C. The core of hepatitis C virus pathogenesis. *Curr Opin Virol* **17**, 66-73 (2016). https://doi.org:10.1016/j.coviro.2016.01.009

522 Masumi, A., Aizaki, H., Suzuki, T., DuHadaway, J. B., Prendergast, G. C., Komuro, K. & Fukazawa, H. Reduction of hepatitis C virus NS5A phosphorylation through its interaction with amphiphysin II. *Biochemical and biophysical research communications* **336**, 572-578 (2005). https://doi.org:10.1016/j.bbrc.2005.08.142

523 Zech, B., Kurtenbach, A., Krieger, N., Strand, D., Blencke, S., Morbitzer, M., Salassidis, K., Cotten, M., Wissing, J., Obert, S., Bartenschlager, R., Herget, T. & Daub, H. Identification and characterization of amphiphysin II as a novel cellular interaction partner of the hepatitis C virus NS5A protein. *Journal of General Virology* **84**, 555-560 (2003). https://doi.org:https://doi.org/10.1099/vir.0.18801-0

524 Backes, P., Quinkert, D., Reiss, S., Binder, M., Zayas, M., Rescher, U., Gerke, V., Bartenschlager, R. & Lohmann, V. Role of Annexin A2 in the Production of Infectious Hepatitis C Virus Particles. *J Virol* **84**, 5775-5789 (2010). https://doi.org:doi:10.1128/jvi.02343-09

525 Saxena, V., Lai, C.-K., Chao, T.-C., Jeng, K.-S. & Lai, M. M. C. Annexin A2 Is Involved in the Formation of Hepatitis C Virus Replication Complex on the Lipid Raft. *J Virol* **86**, 4139-4150 (2012). https://doi.org:doi:10.1128/jvi.06327-11

526 Chen, Y.-J., Chen, Y.-H., Chow, L.-P., Tsai, Y.-H., Chen, P.-H., Huang, C.-Y. F., Chen, W.-T. & Hwang, L.-H. Heat Shock Protein 72 Is Associated with the Hepatitis C Virus Replicase Complex and Enhances Viral RNA Replication. *Journal of Biological Chemistry* **285**, 28183-28190 (2010). https://doi.org:10.1074/jbc.M110.118323

527 Lim, Y. S., Shin, K. S., Oh, S. H., Kang, S. M., Won, S. J. & Hwang, S. B. Nonstructural 5A protein of hepatitis C virus regulates heat shock protein 72 for its own propagation. *J Viral Hepat* **19**, 353-363 (2012). https://doi.org:10.1111/j.1365-2893.2011.01556.x

528 MacQuillan, G. C., Mamotte, C., Reed, W. D., Jeffrey, G. P. & Allan, J. E. Upregulation of endogenous intrahepatic interferon stimulated genes during chronic hepatitis C virus infection. *Journal of Medical Virology* **70**, 219-227 (2003). https://doi.org:10.1002/jmv.10381

529 Ahmad, W., Ijaz, B. & Hassan, S. Gene expression profiling of HCV genotype 3a initial liver fibrosis and cirrhosis patients using microarray. *J Transl Med* **10**, 41 (2012). https://doi.org:10.1186/1479-5876-10-41

530 Lupberger, J., Croonenborghs, T., Roca Suarez, A. A., Van Renne, N., Jühling, F., Oudot, M. A., Virzì, A., Bandiera, S., Jamey, C., Meszaros, G., Brumaru, D., Mukherji, A., Durand, S. C., Heydmann, L., Verrier, E. R., El Saghire, H., Hamdane, N., Bartenschlager, R., Fereshetian, S., Ramberger, E., Sinha, R., Nabian, M., Everaert, C., Jovanovic, M., Mertins, P., Carr, S. A., Chayama, K., Dali-Youcef, N., Ricci, R., Bardeesy, N. M., Fujiwara, N., Gevaert, O., Zeisel, M. B., Hoshida, Y., Pochet, N. & Baumert, T. F. Combined Analysis of Metabolomes, Proteomes, and Transcriptomes of Hepatitis C Virus-Infected Cells and Liver to Identify Pathways Associated With Disease Development. *Gastroenterology* **157**, 537-551.e539 (2019). https://doi.org:10.1053/j.gastro.2019.04.003

531 Wang, Y., Nakajima, T., Gonzalez, F. J. & Tanaka, N. PPARs as Metabolic Regulators in the Liver: Lessons from Liver-Specific PPAR-Null Mice. *International journal of molecular sciences* **21**, 2061 (2020).

532 Taniguchi, H., Kato, N., Otsuka, M., Goto, T., Yoshida, H., Shiratori, Y. & Omata, M. Hepatitis C virus core protein upregulates transforming growth factor-beta 1 transcription. *J Med Virol* **72**, 52-59 (2004). https://doi.org:10.1002/jmv.10545

533 Bedossa, P., Poynard, T., Mathurin, P., Lemaigre, G. & Chaput, J. C. Transforming growth factor beta 1: in situ expression in the liver of patients with chronic hepatitis C treated with alpha interferon. *Gut* **34**, S146-147 (1993). https://doi.org:10.1136/gut.34.2_suppl.s146

534 Patra, T., Sasaki, R., Meyer, K., Ray, R. B. & Ray, R. Transforming Growth Factor β Acts as a Regulatory Molecule for Lipogenic Pathways among Hepatitis C Virus Genotype-Specific Infections. *J Virol* **93** (2019). https://doi.org:10.1128/jvi.00811-19

535 Kim, K. H., Hong, S. P., Kim, K., Park, M. J., Kim, K. J. & Cheong, J. HCV core protein induces hepatic lipid accumulation by activating SREBP1 and PPARgamma. *Biochemical and biophysical research communications* **355**, 883-888 (2007). https://doi.org:10.1016/j.bbrc.2007.02.044

536 Okuda, M., Li, K., Beard, M. R., Showalter, L. A., Scholle, F., Lemon, S. M. & Weinman, S. A. Mitochondrial injury, oxidative stress, and antioxidant gene expression are induced by hepatitis C virus core protein. *Gastroenterology* **122**, 366-375 (2002). https://doi.org:10.1053/gast.2002.30983

537 Jahan, S., Ashfaq, U. A., Khaliq, S., Samreen, B. & Afzal, N. Dual behavior of HCV Core gene in regulation of apoptosis is important in progression of HCC. *Infection, genetics and evolution : journal of molecular epidemiology and evolutionary genetics in infectious diseases* **12**, 236-239 (2012). https://doi.org:10.1016/j.meegid.2012.01.006

538 Macdonald, A. & Harris, M. Hepatitis C virus NS5A: tales of a promiscuous protein. *Journal of General Virology* **85**, 2485-2502 (2004). https://doi.org:https://doi.org/10.1099/vir.0.80204-0
539 Meng, Z., Liu, Q., Sun, F. & Qiao, L. Hepatitis C virus nonstructural protein 5A perturbs lipid metabolism by modulating AMPK/SREBP-1c signaling. *Lipids Health Dis* **18**, 191 (2019). https://doi.org:10.1186/s12944-019-1136-y
540 Firth, C., Bhat, M., Firth, M. A., Williams, S. H., Frye, M. J., Simmonds, P., Conte, J. M., Ng, J., Garcia, J., Bhuva, N. P., Lee, B., Che, X., Quan, P. L. & Lipkin, W. I. Detection of zoonotic pathogens and characterization of novel viruses carried by commensal Rattus norvegicus in New York City. *mBio* **5**, e01933-01914 (2014). https://doi.org:10.1128/mBio.01933-14
541 Drexler, J. F., Corman, V. M., Müller, M. A., Lukashev, A. N., Gmyl, A., Coutard, B., Adam, A., Ritz, D., Leijten, L. M., van Riel, D., Kallies, R., Klose, S. M., Gloza-Rausch, F., Binger, T., Annan, A., Adu-Sarkodie, Y., Oppong, S., Bourgarel, M., Rupp, D., Hoffmann, B., Schlegel, M., Kümmerer, B. M., Krüger, D. H., Schmidt-Chanasit, J., Setién, A. A., Cottontail, V. M., Hemachudha, T., Wacharapluesadee, S., Osterrieder, K., Bartenschlager, R., Matthee, S., Beer, M., Kuiken, T., Reusken, C., Leroy, E. M., Ulrich, R. G. & Drosten, C. Evidence for novel hepaciviruses in rodents. *PLoS pathogens* **9**, e1003438 (2013). https://doi.org:10.1371/journal.ppat.1003438
542 Thézé, J., Lowes, S., Parker, J. & Pybus, O. G. Evolutionary and Phylogenetic Analysis of the Hepaciviruses and Pegiviruses. *Genome Biol Evol* **7**, 2996-3008 (2015). https://doi.org:10.1093/gbe/evv202
543 Wolfisberg, R., Thorselius, C. E., Salinas, E., Elrod, E., Trivedi, S., Nielsen, L., Fahnøe, U., Kapoor, A., Grakoui, A., Rice, C. M., Bukh, J., Holmbeck, K. & Scheel, T. K. H. Neutralization and receptor use of infectious culture-derived rat hepacivirus as a model for HCV. *Hepatol.* **76**, 1506-1519 (2022). https://doi.org:10.1002/hep.32535
544 Kruepunga, N., Hakvoort, T. B. M., Hikspoors, J., Köhler, S. E. & Lamers, W. H. Anatomy of rodent and human livers: What are the differences? *Biochim Biophys Acta Mol Basis Dis* **1865**, 869-878 (2019). https://doi.org:10.1016/j.bbadis.2018.05.019
545 Van Herck, M. A., Vonghia, L. & Francque, S. M. Animal Models of Nonalcoholic Fatty Liver Disease-A Starter's Guide. *Nutrients* **9** (2017). https://doi.org:10.3390/nu9101072
546 Wolfisberg, R., Holmbeck, K., Nielsen, L., Kapoor, A., Rice, C. M., Bukh, J. & Scheel, T. K. H. Replicons of a Rodent Hepatitis C Model Virus Permit Selection of Highly Permissive Cells. *J Virol* **93** (2019). https://doi.org:10.1128/jvi.00733-19
547 Hartlage, A. S., Murthy, S., Kumar, A., Trivedi, S., Dravid, P., Sharma, H., Walker, C. M. & Kapoor, A. Vaccination to prevent T cell subversion can protect against persistent hepacivirus infection. *Nat Commun* **10**, 1113 (2019). https://doi.org:10.1038/s41467-019-09105-0
548 Hartlage, A. S., Dravid, P., Walker, C. M. & Kapoor, A. Adenovirus-vectored T cell vaccine for hepacivirus shows reduced effectiveness against a CD8 T cell escape variant in rats. *PLoS Pathog* **17**, e1009391 (2021). https://doi.org:10.1371/journal.ppat.1009391
549 Gondeau, C., Briolotti, P., Razafy, F., Duret, C., Rubbo, P. A., Helle, F., Rème, T., Ripault, M. P., Ducos, J., Fabre, J. M., Ramos, J., Pécheur, E. I., Larrey, D., Maurel, P. & Daujat-Chavanieu, M. In vitro infection of primary human hepatocytes by HCV-positive sera: insights on a highly relevant model. *Gut* **63**, 1490-1500 (2014). https://doi.org:10.1136/gutjnl-2013-304623
550 Aicher, S., Kakkanas, A., Cohen, L., Blumen, B., Oprisan, G., Njouom, R., Meurs, E. F., Mavromara, P. & Martin, A. Differential regulation of the Wnt/β-catenin pathway

by hepatitis C virus recombinants expressing core from various genotypes. *Sci Rep* **8**, 11185 (2018). https://doi.org:10.1038/s41598-018-29078-2

551 Reed, L. J. & Muench, H. A simple method of estimating fifty per cent endpoints. *American journal of epidemiology* **27**, 493-497 (1938). https://doi.org:10.1093/oxfordjournals.aje.a118408

552 Rappsilber, J., Mann, M. & Ishihama, Y. Protocol for micro-purification, enrichment, pre-fractionation and storage of peptides for proteomics using StageTips. *Nature Protocols* **2**, 1896-1906 (2007). https://doi.org:10.1038/nprot.2007.261

553 Tyanova, S., Temu, T. & Cox, J. The MaxQuant computational platform for mass spectrometry-based shotgun proteomics. *Nature Protocols* **11**, 2301-2319 (2016). https://doi.org:10.1038/nprot.2016.136

554 Cox, J., Neuhauser, N., Michalski, A., Scheltema, R. A., Olsen, J. V. & Mann, M. Andromeda: a peptide search engine integrated into the MaxQuant environment. *Journal of proteome research* **10**, 1794-1805 (2011). https://doi.org:10.1021/pr101065j

555 Cokelaer, T., Desvillechabrol, D., Legendre, R. & Cardon, M. 'Sequana': a Set of Snakemake NGS pipelines. *Journal of Open Source Software* **2**, 352 (2017). https://doi.org:10.21105/joss.00352

556 Desvillechabrol, D., Bouchier, C., Kennedy, S. & Cokelaer, T. Sequana coverage: detection and characterization of genomic variations using running median and mixture models. *Gigascience* **7** (2018). https://doi.org:10.1093/gigascience/giy110

557 Barik, S., Das, S. & Vikalo, H. QSdpR: Viral quasispecies reconstruction via correlation clustering. *Genomics* **110**, 375-381 (2018). https://doi.org:10.1016/j.ygeno.2017.12.007

558 Osawa, M., Uchida, T., Imamura, M., Teraoka, Y., Fujino, H., Nakahara, T., Ono, A., Murakami, E., Kawaoka, T., Miki, D., Tsuge, M., Hiramatsu, A., Abe-Chayama, H., Hayes, C. N., Makokha, G. N., Aikata, H., Ishida, Y., Tateno, C., Miyayama, Y., Hijikata, M. & Chayama, K. Efficacy of glecaprevir and pibrentasvir treatment for genotype 1b hepatitis C virus drug resistance-associated variants in humanized mice. *Journal of General Virology* **100**, 1123-1131 (2019). https://doi.org:https://doi.org/10.1099/jgv.0.001268

559 Giai Gianetto, Q. Statistical Analysis of Post-Translational Modifications Quantified by Label-Free Proteomics Across Multiple Biological Conditions with R: Illustration from SARS-CoV-2 Infected Cells. *Methods in molecular biology (Clifton, N.J.)* **2426**, 267-302 (2023). https://doi.org:10.1007/978-1-0716-1967-4_12

560 Ritchie, M. E., Phipson, B., Wu, D., Hu, Y., Law, C. W., Shi, W. & Smyth, G. K. limma powers differential expression analyses for RNA-sequencing and microarray studies. *Nucleic Acids Res* **43**, e47 (2015). https://doi.org:10.1093/nar/gkv007

561 Giai Gianetto, Q., Combes, F., Ramus, C., Bruley, C., Couté, Y. & Burger, T. Calibration plot for proteomics: A graphical tool to visually check the assumptions underlying FDR control in quantitative experiments. *Proteomics* **16**, 29-32 (2016). https://doi.org:10.1002/pmic.201500189

562 Pounds, S. & Cheng, C. Robust estimation of the false discovery rate. *Bioinformatics* **22**, 1979-1987 (2006). https://doi.org:10.1093/bioinformatics/btl328

563 Teo, G., Liu, G., Zhang, J., Nesvizhskii, A. I., Gingras, A. C. & Choi, H. SAINTexpress: improvements and additional features in Significance Analysis of INTeractome software. *J Proteomics* **100**, 37-43 (2014). https://doi.org:10.1016/j.jprot.2013.10.023

564 Jäger, S., Cimermancic, P., Gulbahce, N., Johnson, J. R., McGovern, K. E., Clarke, S. C., Shales, M., Mercenne, G., Pache, L., Li, K., Hernandez, H., Jang, G. M., Roth, S. L., Akiva, E., Marlett, J., Stephens, M., D'Orso, I., Fernandes, J., Fahey, M., Mahon, C., O'Donoghue, A. J., Todorovic, A., Morris, J. H., Maltby, D. A., Alber, T., Cagney,

G., Bushman, F. D., Young, J. A., Chanda, S. K., Sundquist, W. I., Kortemme, T., Hernandez, R. D., Craik, C. S., Burlingame, A., Sali, A., Frankel, A. D. & Krogan, N. J. Global landscape of HIV-human protein complexes. *Nature* **481**, 365-370 (2011). https://doi.org:10.1038/nature10719

565 Verschueren, E., Von Dollen, J., Cimermancic, P., Gulbahce, N., Sali, A. & Krogan, N. J. Scoring Large-Scale Affinity Purification Mass Spectrometry Datasets with MiST. *Curr Protoc Bioinformatics* **49**, 8.19.11-18.19.16 (2015). https://doi.org:10.1002/0471250953.bi0819s49

566 Kanehisa, M. & Goto, S. KEGG: kyoto encyclopedia of genes and genomes. *Nucleic Acids Res* **28**, 27-30 (2000). https://doi.org:10.1093/nar/28.1.27

567 Liberzon, A., Birger, C., Thorvaldsdóttir, H., Ghandi, M., Mesirov, J. P. & Tamayo, P. The Molecular Signatures Database (MSigDB) hallmark gene set collection. *Cell Syst* **1**, 417-425 (2015). https://doi.org:10.1016/j.cels.2015.12.004

568 Griss, J., Viteri, G., Sidiropoulos, K., Nguyen, V., Fabregat, A. & Hermjakob, H. ReactomeGSA - Efficient Multi-Omics Comparative Pathway Analysis. *Molecular & cellular proteomics : MCP* **19**, 2115-2125 (2020). https://doi.org:10.1074/mcp.TIR120.002155

569 Gillespie, M., Jassal, B., Stephan, R., Milacic, M., Rothfels, K., Senff-Ribeiro, A., Griss, J., Sevilla, C., Matthews, L., Gong, C., Deng, C., Varusai, T., Ragueneau, E., Haider, Y., May, B., Shamovsky, V., Weiser, J., Brunson, T., Sanati, N., Beckman, L., Shao, X., Fabregat, A., Sidiropoulos, K., Murillo, J., Viteri, G., Cook, J., Shorser, S., Bader, G., Demir, E., Sander, C., Haw, R., Wu, G., Stein, L., Hermjakob, H. & D'Eustachio, P. The reactome pathway knowledgebase 2022. *Nucleic Acids Res* **50**, D687-d692 (2022). https://doi.org:10.1093/nar/gkab1028

570 Pico, A. R., Kelder, T., van Iersel, M. P., Hanspers, K., Conklin, B. R. & Evelo, C. WikiPathways: pathway editing for the people. *PLoS Biol* **6**, e184 (2008). https://doi.org:10.1371/journal.pbio.0060184

571 Martens, M., Ammar, A., Riutta, A., Waagmeester, A., Slenter, D. N., Hanspers, K., R, A. M., Digles, D., Lopes, E. N., Ehrhart, F., Dupuis, L. J., Winckers, L. A., Coort, S. L., Willighagen, E. L., Evelo, C. T., Pico, A. R. & Kutmon, M. WikiPathways: connecting communities. *Nucleic Acids Res* **49**, D613-d621 (2021). https://doi.org:10.1093/nar/gkaa1024

572 Shannon, P., Markiel, A., Ozier, O., Baliga, N. S., Wang, J. T., Ramage, D., Amin, N., Schwikowski, B. & Ideker, T. Cytoscape: a software environment for integrated models of biomolecular interaction networks. *Genome Res* **13**, 2498-2504 (2003). https://doi.org:10.1101/gr.1239303

573 Reimand, J., Isserlin, R., Voisin, V., Kucera, M., Tannus-Lopes, C., Rostamianfar, A., Wadi, L., Meyer, M., Wong, J., Xu, C., Merico, D. & Bader, G. D. Pathway enrichment analysis and visualization of omics data using g:Profiler, GSEA, Cytoscape and EnrichmentMap. *Nat Protoc* **14**, 482-517 (2019). https://doi.org:10.1038/s41596-018-0103-9

574 Szklarczyk, D., Kirsch, R., Koutrouli, M., Nastou, K., Mehryary, F., Hachilif, R., Gable, A. L., Fang, T., Doncheva, N. T., Pyysalo, S., Bork, P., Jensen, L. J. & von Mering, C. The STRING database in 2023: protein-protein association networks and functional enrichment analyses for any sequenced genome of interest. *Nucleic Acids Res* **51**, D638-d646 (2023). https://doi.org:10.1093/nar/gkac1000

575 Ashburner, M., Ball, C. A., Blake, J. A., Botstein, D., Butler, H., Cherry, J. M., Davis, A. P., Dolinski, K., Dwight, S. S., Eppig, J. T., Harris, M. A., Hill, D. P., Issel-Tarver, L., Kasarskis, A., Lewis, S., Matese, J. C., Richardson, J. E., Ringwald, M., Rubin, G.

M. & Sherlock, G. Gene ontology: tool for the unification of biology. The Gene Ontology Consortium. *Nat Genet* **25**, 25-29 (2000). https://doi.org:10.1038/75556

576 The Gene Ontology resource: enriching a GOld mine. *Nucleic Acids Res* **49**, D325-d334 (2021). https://doi.org:10.1093/nar/gkaa1113

577 Schriml, L. M., Mitraka, E., Munro, J., Tauber, B., Schor, M., Nickle, L., Felix, V., Jeng, L., Bearer, C., Lichenstein, R., Bisordi, K., Campion, N., Hyman, B., Kurland, D., Oates, C. P., Kibbey, S., Sreekumar, P., Le, C., Giglio, M. & Greene, C. Human Disease Ontology 2018 update: classification, content and workflow expansion. *Nucleic Acids Res* **47**, D955-d962 (2019). https://doi.org:10.1093/nar/gky1032

578 Wang, Y. Z., Wang, W. B., Cao, M. M., Wang, W., Zhao, L. J., Xu, G., Ren, H. & Qi, Z. T. Function of nonstructural 5A protein of genotype 2a in replication and infection of HCV with gene substitution. *World journal of gastroenterology* **17**, 3398-3406 (2011). https://doi.org:10.3748/wjg.v17.i29.3398

579 Okamoto, Y., Masaki, T., Murayama, A., Munakata, T., Nomoto, A., Nakamoto, S., Yokosuka, O., Watanabe, H., Wakita, T. & Kato, T. Development of recombinant hepatitis C virus with NS5A from strains of genotypes 1 and 2. *Biochemical and biophysical research communications* **410**, 404-409 (2011). https://doi.org:10.1016/j.bbrc.2011.05.144

580 Katsarou, K., Serti, E., Tsitoura, P., Lavdas, A. A., Varaklioti, A., Pickl-Herk, A.-M., Blaas, D., Oz-Arslan, D., Zhu, R., Hinterdorfer, P., Mavromara, P. & Georgopoulou, U. Green fluorescent protein – Tagged HCV non-enveloped capsid like particles: Development of a new tool for tracking HCV core uptake. *Biochimie* **91**, 903-915 (2009). https://doi.org:https://doi.org/10.1016/j.biochi.2009.04.016

581 Kim, C. S., Jung, J. H., Wakita, T., Yoon, S. K. & Jang, S. K. Monitoring the Antiviral Effect of Alpha Interferon on Individual Cells. *J Virol* **81**, 8814-8820 (2007). https://doi.org:doi:10.1128/jvi.02824-06

582 Counihan, N. A., Rawlinson, S. M. & Lindenbach, B. D. Trafficking of hepatitis C virus core protein during virus particle assembly. *PLoS pathogens* **7**, e1002302 (2011). https://doi.org:10.1371/journal.ppat.1002302

583 Coller, K. E., Heaton, N. S., Berger, K. L., Cooper, J. D., Saunders, J. L. & Randall, G. Molecular determinants and dynamics of hepatitis C virus secretion. *PLoS pathogens* **8**, e1002466 (2012). https://doi.org:10.1371/journal.ppat.1002466

584 Remenyi, R., Qi, H., Su, S. Y., Chen, Z., Wu, N. C., Arumugaswami, V., Truong, S., Chu, V., Stokelman, T., Lo, H. H., Olson, C. A., Wu, T. T., Chen, S. H., Lin, C. Y. & Sun, R. A comprehensive functional map of the hepatitis C virus genome provides a resource for probing viral proteins. *mBio* **5**, e01469-01414 (2014). https://doi.org:10.1128/mBio.01469-14

585 Combet, C., Garnier, N., Charavay, C., Grando, D., Crisan, D., Lopez, J., Dehne-Garcia, A., Geourjon, C., Bettler, E., Hulo, C., Le Mercier, P., Bartenschlager, R., Diepolder, H., Moradpour, D., Pawlotsky, J. M., Rice, C. M., Trépo, C., Penin, F. & Deléage, G. euHCVdb: the European hepatitis C virus database. *Nucleic Acids Res* **35**, D363-366 (2007). https://doi.org:10.1093/nar/gkl970

586 Verdegem, D., Badillo, A., Wieruszeski, J. M., Landrieu, I., Leroy, A., Bartenschlager, R., Penin, F., Lippens, G. & Hanoulle, X. Domain 3 of NS5A protein from the hepatitis C virus has intrinsic alpha-helical propensity and is a substrate of cyclophilin A. *J Biol Chem* **286**, 20441-20454 (2011). https://doi.org:10.1074/jbc.M110.182436

587 Galli, A., Scheel, T. K. H., Prentoe, J. C., Mikkelsen, L. S., Gottwein, J. M. & Bukh, J. Analysis of hepatitis C virus core/NS5A protein co-localization using novel cell culture systems expressing core–NS2 and NS5A of genotypes 1–7. *Journal of General Virology* **94**, 2221-2235 (2013). https://doi.org:https://doi.org/10.1099/vir.0.053868-0

588 Cordek, D. G., Croom-Perez, T. J., Hwang, J., Hargittai, M. R., Subba-Reddy, C. V., Han, Q., Lodeiro, M. F., Ning, G., McCrory, T. S., Arnold, J. J., Koc, H., Lindenbach, B. D., Showalter, S. A. & Cameron, C. E. Expanding the proteome of an RNA virus by phosphorylation of an intrinsically disordered viral protein. *J Biol Chem* **289**, 24397-24416 (2014). https://doi.org:10.1074/jbc.M114.589911

589 Fridell, R. A., Valera, L., Qiu, D., Kirk, M. J., Wang, C. & Gao, M. Intragenic complementation of hepatitis C virus NS5A RNA replication-defective alleles. *J Virol* **87**, 2320-2329 (2013). https://doi.org:10.1128/jvi.02861-12

590 Çevik, R. E., Cesarec, M., Da Silva Filipe, A., Licastro, D., McLauchlan, J. & Marcello, A. Hepatitis C Virus NS5A Targets Nucleosome Assembly Protein NAP1L1 To Control the Innate Cellular Response. *J Virol* **91** (2017). https://doi.org:10.1128/jvi.00880-17

591 Bennati, A. M., Castelli, M., Della Fazia, M. A., Beccari, T., Caruso, D., Servillo, G. & Roberti, R. Sterol dependent regulation of human TM7SF2 gene expression: role of the encoded 3beta-hydroxysterol Delta14-reductase in human cholesterol biosynthesis. *Biochimica et biophysica acta* **1761**, 677-685 (2006). https://doi.org:10.1016/j.bbalip.2006.05.004

592 Ng, C. L., Oresic, K. & Tortorella, D. TRAM1 is involved in disposal of ER membrane degradation substrates. *Experimental cell research* **316**, 2113-2122 (2010). https://doi.org:10.1016/j.yexcr.2010.04.010

593 Vassilaki, N., Kalliampakou, K. I., Kotta-Loizou, I., Befani, C., Liakos, P., Simos, G., Mentis, A. F., Kalliaropoulos, A., Doumba, P. P., Smirlis, D., Foka, P., Bauhofer, O., Poenisch, M., Windisch, M. P., Lee, M. E., Koskinas, J., Bartenschlager, R. & Mavromara, P. Low oxygen tension enhances hepatitis C virus replication. *J Virol* **87**, 2935-2948 (2013). https://doi.org:10.1128/jvi.02534-12

594 Nasimuzzaman, M., Waris, G., Mikolon, D., Stupack, D. G. & Siddiqui, A. Hepatitis C Virus Stabilizes Hypoxia-Inducible Factor 1α and Stimulates the Synthesis of Vascular Endothelial Growth Factor. *J Virol* **81**, 10249-10257 (2007). https://doi.org:doi:10.1128/jvi.00763-07

595 Bose, S. K., Meyer, K., Di Bisceglie, A. M., Ray, R. B. & Ray, R. Hepatitis C virus induces epithelial-mesenchymal transition in primary human hepatocytes. *J Virol* **86**, 13621-13628 (2012). https://doi.org:10.1128/jvi.02016-12

596 Li, Q., Brass, A. L., Ng, A., Hu, Z., Xavier, R. J., Liang, T. J. & Elledge, S. J. A genome-wide genetic screen for host factors required for hepatitis C virus propagation. *Proceedings of the National Academy of Sciences* **106**, 16410-16415 (2009). https://doi.org:doi:10.1073/pnas.0907439106

597 Diamond, D. L., Syder, A. J., Jacobs, J. M., Sorensen, C. M., Walters, K. A., Proll, S. C., McDermott, J. E., Gritsenko, M. A., Zhang, Q., Zhao, R., Metz, T. O., Camp, D. G., 2nd, Waters, K. M., Smith, R. D., Rice, C. M. & Katze, M. G. Temporal proteome and lipidome profiles reveal hepatitis C virus-associated reprogramming of hepatocellular metabolism and bioenergetics. *PLoS pathogens* **6**, e1000719 (2010). https://doi.org:10.1371/journal.ppat.1000719

598 Khan, M., Jahan, S., Khaliq, S., Ijaz, B., Ahmad, W., Samreen, B. & Hassan, S. Interaction of the hepatitis C virus (HCV) core with cellular genes in the development of HCV-induced steatosis. *Arch Virol* **155**, 1735-1753 (2010). https://doi.org:10.1007/s00705-010-0797-7

599 Wanders, R. J. A. & Tager, J. M. Lipid metabolism in peroxisomes in relation to human disease. *Molecular Aspects of Medicine* **19**, i-154 (1998). https://doi.org:https://doi.org/10.1016/S0098-2997(98)00003-X

600 Mirandola, S., Realdon, S., Iqbal, J., Gerotto, M., Dal Pero, F., Bortoletto, G., Marcolongo, M., Vario, A., Datz, C., Hussain, M. M. & Alberti, A. Liver microsomal

triglyceride transfer protein is involved in hepatitis C liver steatosis. *Gastroenterology* **130**, 1661-1669 (2006). https://doi.org:10.1053/j.gastro.2006.02.035

601 Dharancy, S., Malapel, M., Perlemuter, G., Roskams, T., Cheng, Y., Dubuquoy, L., Podevin, P., Conti, F., Canva, V., Philippe, D., Gambiez, L., Mathurin, P., Paris, J. C., Schoonjans, K., Calmus, Y., Pol, S., Auwerx, J. & Desreumaux, P. Impaired expression of the peroxisome proliferator-activated receptor alpha during hepatitis C virus infection. *Gastroenterology* **128**, 334-342 (2005). https://doi.org:10.1053/j.gastro.2004.11.016

602 Cheng, Y., Dharancy, S., Malapel, M. & Desreumaux, P. Hepatitis C virus infection down-regulates the expression of peroxisome proliferator-activated receptor alpha and carnitine palmitoyl acyl-CoA transferase 1A. *World journal of gastroenterology* **11**, 7591-7596 (2005). https://doi.org:10.3748/wjg.v11.i48.7591

603 Peyrou, M., Bourgoin, L. & Foti, M. PTEN in liver diseases and cancer. *World journal of gastroenterology* **16**, 4627-4633 (2010). https://doi.org:10.3748/wjg.v16.i37.4627

604 Song, M. J. & Malhi, H. The unfolded protein response and hepatic lipid metabolism in non alcoholic fatty liver disease. *Pharmacol Ther* **203**, 107401 (2019). https://doi.org:10.1016/j.pharmthera.2019.107401

605 Jumper, J., Evans, R., Pritzel, A., Green, T., Figurnov, M., Ronneberger, O., Tunyasuvunakool, K., Bates, R., Žídek, A., Potapenko, A., Bridgland, A., Meyer, C., Kohl, S. A. A., Ballard, A. J., Cowie, A., Romera-Paredes, B., Nikolov, S., Jain, R., Adler, J., Back, T., Petersen, S., Reiman, D., Clancy, E., Zielinski, M., Steinegger, M., Pacholska, M., Berghammer, T., Bodenstein, S., Silver, D., Vinyals, O., Senior, A. W., Kavukcuoglu, K., Kohli, P. & Hassabis, D. Highly accurate protein structure prediction with AlphaFold. *Nature* **596**, 583-589 (2021). https://doi.org:10.1038/s41586-021-03819-2

606 Hofmann, S., Krajewski, M., Scherer, C., Scholz, V., Mordhorst, V., Truschow, P., Schöbel, A., Reimer, R., Schwudke, D. & Herker, E. Complex lipid metabolic remodeling is required for efficient hepatitis C virus replication. *Biochimica et biophysica acta. Molecular and cell biology of lipids* **1863**, 1041-1056 (2018). https://doi.org:10.1016/j.bbalip.2018.06.002

607 Hamdane, N., Jühling, F., Crouchet, E., El Saghire, H., Thumann, C., Oudot, M. A., Bandiera, S., Saviano, A., Ponsolles, C., Roca Suarez, A. A., Li, S., Fujiwara, N., Ono, A., Davidson, I., Bardeesy, N., Schmidl, C., Bock, C., Schuster, C., Lupberger, J., Habersetzer, F., Doffoël, M., Piardi, T., Sommacale, D., Imamura, M., Uchida, T., Ohdan, H., Aikata, H., Chayama, K., Boldanova, T., Pessaux, P., Fuchs, B. C., Hoshida, Y., Zeisel, M. B., Duong, F. H. T. & Baumert, T. F. HCV-Induced Epigenetic Changes Associated With Liver Cancer Risk Persist After Sustained Virologic Response. *Gastroenterology* **156**, 2313-2329.e2317 (2019). https://doi.org:10.1053/j.gastro.2019.02.038

608 Sagnelli, E., Sagnelli, C., Russo, A., Pisaturo, M., Camaioni, C., Astorri, R. & Coppola, N. Impact of DAA-Based Regimens on HCV-Related Extra-Hepatic Damage: A Narrative Review. *Advances in experimental medicine and biology* **1323**, 115-147 (2021). https://doi.org:10.1007/5584_2020_604

609 Oe, N., Takeda, H., Eso, Y., Takai, A. & Marusawa, H. Clinical and Molecular Basis of Hepatocellular Carcinoma after Hepatitis C Virus Eradication. *Pathogens* **11** (2022). https://doi.org:10.3390/pathogens11040430

610 Rubbia-Brandt, L., Quadri, R., Abid, K., Giostra, E., Malé, P. J., Mentha, G., Spahr, L., Zarski, J. P., Borisch, B., Hadengue, A. & Negro, F. Hepatocyte steatosis is a cytopathic effect of hepatitis C virus genotype 3. *Journal of hepatology* **33**, 106-115 (2000). https://doi.org:10.1016/s0168-8278(00)80166-x

611 Roingeard, P. Hepatitis C virus diversity and hepatic steatosis. *J Viral Hepat* **20**, 77-84 (2013). https://doi.org:10.1111/jvh.12035
612 Piccininni, S., Varaklioti, A., Nardelli, M., Dave, B., Raney, K. D. & McCarthy, J. E. Modulation of the hepatitis C virus RNA-dependent RNA polymerase activity by the non-structural (NS) 3 helicase and the NS4B membrane protein. *J Biol Chem* **277**, 45670-45679 (2002). https://doi.org:10.1074/jbc.M204124200
613 Dimitrova, M., Imbert, I., Kieny, M. P. & Schuster, C. Protein-protein interactions between hepatitis C virus nonstructural proteins. *J Virol* **77**, 5401-5414 (2003). https://doi.org:10.1128/jvi.77.9.5401-5414.2003
614 Hagen, N., Bayer, K., Rösch, K. & Schindler, M. The intraviral protein interaction network of hepatitis C virus. *Molecular & cellular proteomics : MCP* **13**, 1676-1689 (2014). https://doi.org:10.1074/mcp.M113.036301
615 Yi, M., Villanueva, R. A., Thomas, D. L., Wakita, T. & Lemon, S. M. Production of infectious genotype 1a hepatitis C virus (Hutchinson strain) in cultured human hepatoma cells. *Proceedings of the National Academy of Sciences of the United States of America* **103**, 2310-2315 (2006). https://doi.org:10.1073/pnas.0510727103
616 Li, Y. P., Ramirez, S., Jensen, S. B., Purcell, R. H., Gottwein, J. M. & Bukh, J. Highly efficient full-length hepatitis C virus genotype 1 (strain TN) infectious culture system. *Proceedings of the National Academy of Sciences of the United States of America* **109**, 19757-19762 (2012). https://doi.org:10.1073/pnas.1218260109
617 Li, Y. P., Ramirez, S., Mikkelsen, L. & Bukh, J. Efficient infectious cell culture systems of the hepatitis C virus (HCV) prototype strains HCV-1 and H77. *J Virol* **89**, 811-823 (2015). https://doi.org:10.1128/jvi.02877-14
618 Li, Y. P., Ramirez, S., Gottwein, J. M., Scheel, T. K., Mikkelsen, L., Purcell, R. H. & Bukh, J. Robust full-length hepatitis C virus genotype 2a and 2b infectious cultures using mutations identified by a systematic approach applicable to patient strains. *Proceedings of the National Academy of Sciences of the United States of America* **109**, E1101-1110 (2012). https://doi.org:10.1073/pnas.1203829109
619 Ramirez, S., Li, Y. P., Jensen, S. B., Pedersen, J., Gottwein, J. M. & Bukh, J. Highly efficient infectious cell culture of three hepatitis C virus genotype 2b strains and sensitivity to lead protease, nonstructural protein 5A, and polymerase inhibitors. *Hepatol.* **59**, 395-407 (2014). https://doi.org:10.1002/hep.26660
620 Ramirez, S., Fernandez-Antunez, C., Mikkelsen, L. S., Pedersen, J., Li, Y. P. & Bukh, J. Cell Culture Studies of the Efficacy and Barrier to Resistance of Sofosbuvir-Velpatasvir and Glecaprevir-Pibrentasvir against Hepatitis C Virus Genotypes 2a, 2b, and 2c. *Antimicrobial agents and chemotherapy* **64** (2020). https://doi.org:10.1128/aac.01888-19
621 Kim, S., Date, T., Yokokawa, H., Kono, T., Aizaki, H., Maurel, P., Gondeau, C. & Wakita, T. Development of hepatitis C virus genotype 3a cell culture system. *Hepatol.* **60**, 1838-1850 (2014). https://doi.org:10.1002/hep.27197
622 Ramirez, S., Mikkelsen, L. S., Gottwein, J. M. & Bukh, J. Robust HCV Genotype 3a Infectious Cell Culture System Permits Identification of Escape Variants With Resistance to Sofosbuvir. *Gastroenterology* **151**, 973-985.e972 (2016). https://doi.org:10.1053/j.gastro.2016.07.013
623 Galli, A., Ramirez, S. & Bukh, J. Lipid Droplets Accumulation during Hepatitis C Virus Infection in Cell-Culture Varies among Genotype 1-3 Strains and Does Not Correlate with Virus Replication. *Viruses* **13** (2021). https://doi.org:10.3390/v13030389
624 Lee, J.-Y., Acosta, E. G., Stoeck, I. K., Long, G., Hiet, M.-S., Mueller, B., Fackler, O. T., Kallis, S. & Bartenschlager, R. Apolipoprotein E Likely Contributes to a Maturation Step of Infectious Hepatitis C Virus Particles and Interacts with Viral Envelope

Glycoproteins. *J Virol* **88**, 12422-12437 (2014). https://doi.org:doi:10.1128/jvi.01660-14

625 Pham, M. T., Lee, J. Y., Ritter, C., Thielemann, R., Meyer, J., Haselmann, U., Funaya, C., Laketa, V., Rohr, K. & Bartenschlager, R. Endosomal egress and intercellular transmission of hepatic ApoE-containing lipoproteins and its exploitation by the hepatitis C virus. *PLoS pathogens* **19**, e1011052 (2023). https://doi.org:10.1371/journal.ppat.1011052

626 Lee, C., Ma, H., Hang, J. Q., Leveque, V., Sklan, E. H., Elazar, M., Klumpp, K. & Glenn, J. S. The hepatitis C virus NS5A inhibitor (BMS-790052) alters the subcellular localization of the NS5A non-structural viral protein. *Virology* **414**, 10-18 (2011). https://doi.org:10.1016/j.virol.2011.03.026

627 Riva, L., Spriet, C., Barois, N., Popescu, C. I., Dubuisson, J. & Rouillé, Y. Comparative Analysis of Hepatitis C Virus NS5A Dynamics and Localization in Assembly-Deficient Mutants. *Pathogens* **10** (2021). https://doi.org:10.3390/pathogens10020172

628 Eyre, N. S., Fiches, G. N., Aloia, A. L., Helbig, K. J., McCartney, E. M., McErlean, C. S., Li, K., Aggarwal, A., Turville, S. G. & Beard, M. R. Dynamic imaging of the hepatitis C virus NS5A protein during a productive infection. *J Virol* **88**, 3636-3652 (2014). https://doi.org:10.1128/jvi.02490-13

629 Quintavalle, M., Sambucini, S., Summa, V., Orsatti, L., Talamo, F., De Francesco, R. & Neddermann, P. Hepatitis C virus NS5A is a direct substrate of casein kinase I-alpha, a cellular kinase identified by inhibitor affinity chromatography using specific NS5A hyperphosphorylation inhibitors. *J Biol Chem* **282**, 5536-5544 (2007). https://doi.org:10.1074/jbc.M610486200

630 Arima, N., Kao, C. Y., Licht, T., Padmanabhan, R., Sasaguri, Y. & Padmanabhan, R. Modulation of cell growth by the hepatitis C virus nonstructural protein NS5A. *J Biol Chem* **276**, 12675-12684 (2001). https://doi.org:10.1074/jbc.M008329200

631 Ide, Y., Tanimoto, A., Sasaguri, Y. & Padmanabhan, R. Hepatitis C virus NS5A protein is phosphorylated in vitro by a stably bound protein kinase from HeLa cells and by cAMP-dependent protein kinase A-α catalytic subunit. *Gene* **201**, 151-158 (1997). https://doi.org:https://doi.org/10.1016/S0378-1119(97)00440-X

632 Matsui, R., Ferran, B., Oh, A., Croteau, D., Shao, D., Han, J., Pimentel, D. R. & Bachschmid, M. M. Redox Regulation via Glutaredoxin-1 and Protein S-Glutathionylation. *Antioxid Redox Signal* **32**, 677-700 (2020). https://doi.org:10.1089/ars.2019.7963

633 Saheki, Y. & De Camilli, P. The Extended-Synaptotagmins. *Biochim Biophys Acta Mol Cell Res* **1864**, 1490-1493 (2017). https://doi.org:10.1016/j.bbamcr.2017.03.013

634 Cho, N. E., Bang, B.-R., Gurung, P., Li, M., Clemens, D. L., Underhill, T. M., James, L. P., Chase, J. R. & Saito, T. Retinoid regulation of antiviral innate immunity in hepatocytes. *Hepatol.* **63**, 1783-1795 (2016). https://doi.org:https://doi.org/10.1002/hep.28380

635 Saeed, A., Bartuzi, P., Heegsma, J., Dekker, D., Kloosterhuis, N., de Bruin, A., Jonker, J. W., van de Sluis, B. & Faber, K. N. Impaired Hepatic Vitamin A Metabolism in NAFLD Mice Leading to Vitamin A Accumulation in Hepatocytes. *Cellular and Molecular Gastroenterology and Hepatology* **11**, 309-325.e303 (2021). https://doi.org:https://doi.org/10.1016/j.jcmgh.2020.07.006

636 Bergelson, J. M., St John, N., Kawaguchi, S., Chan, M., Stubdal, H., Modlin, J. & Finberg, R. W. Infection by echoviruses 1 and 8 depends on the alpha 2 subunit of human VLA-2. *J Virol* **67**, 6847-6852 (1993). https://doi.org:10.1128/jvi.67.11.6847-6852.1993

637 Xiao, J., Palefsky, J. M., Herrera, R., Berline, J. & Tugizov, S. M. The Epstein-Barr virus BMRF-2 protein facilitates virus attachment to oral epithelial cells. *Virology* **370**, 430-442 (2008). https://doi.org:10.1016/j.virol.2007.09.012

638 Feire, A. L., Roy, R. M., Manley, K. & Compton, T. The glycoprotein B disintegrin-like domain binds beta 1 integrin to mediate cytomegalovirus entry. *J Virol* **84**, 10026-10037 (2010). https://doi.org:10.1128/jvi.00710-10

639 Weigel-Kelley, K. A., Yoder, M. C. & Srivastava, A. Alpha5beta1 integrin as a cellular coreceptor for human parvovirus B19: requirement of functional activation of beta1 integrin for viral entry. *Blood* **102**, 3927-3933 (2003). https://doi.org:10.1182/blood-2003-05-1522

640 Graham, K. L., Halasz, P., Tan, Y., Hewish, M. J., Takada, Y., Mackow, E. R., Robinson, M. K. & Coulson, B. S. Integrin-using rotaviruses bind alpha2beta1 integrin alpha2 I domain via VP4 DGE sequence and recognize alphaXbeta2 and alphaVbeta3 by using VP7 during cell entry. *J Virol* **77**, 9969-9978 (2003). https://doi.org:10.1128/jvi.77.18.9969-9978.2003

641 Maginnis, M. S., Forrest, J. C., Kopecky-Bromberg, S. A., Dickeson, S. K., Santoro, S. A., Zutter, M. M., Nemerow, G. R., Bergelson, J. M. & Dermody, T. S. Beta1 integrin mediates internalization of mammalian reovirus. *J Virol* **80**, 2760-2770 (2006). https://doi.org:10.1128/jvi.80.6.2760-2770.2006

642 Barillari, G., Sgadari, C., Fiorelli, V., Samaniego, F., Colombini, S., Manzari, V., Modesti, A., Nair, B. C., Cafaro, A., Stürzl, M. & Ensoli, B. The Tat protein of human immunodeficiency virus type-1 promotes vascular cell growth and locomotion by engaging the alpha5beta1 and alphavbeta3 integrins and by mobilizing sequestered basic fibroblast growth factor. *Blood* **94**, 663-672 (1999).

643 Speicher, T., Siegenthaler, B., Bogorad, R. L., Ruppert, R., Petzold, T., Padrissa-Altes, S., Bachofner, M., Anderson, D. G., Koteliansky, V., Fässler, R. & Werner, S. Knockdown and knockout of β1-integrin in hepatocytes impairs liver regeneration through inhibition of growth factor signalling. *Nature Communications* **5**, 3862 (2014). https://doi.org:10.1038/ncomms4862

644 Kuwashiro, T., Iwane, S., Jinghe, X., Matsuhashi, S., Eguchi, Y., Anzai, K., Fujimoto, K., Mizuta, T., Sakamoto, N., Ikeda, M., Kato, N. & Ozaki, I. Regulation of interferon signaling and HCV-RNA replication by extracellular matrix. *Int J Mol Med* **42**, 957-965 (2018). https://doi.org:10.3892/ijmm.2018.3693

645 Martin de Fourchambault, E., Callens, N., Saliou, J. M., Fourcot, M., Delos, O., Barois, N., Thorel, Q., Ramirez, S., Bukh, J., Cocquerel, L., Bertrand-Michel, J., Marot, G., Sebti, Y., Dubuisson, J. & Rouillé, Y. Hepatitis C virus alters the morphology and function of peroxisomes. *Front Microbiol* **14**, 1254728 (2023). https://doi.org:10.3389/fmicb.2023.1254728

646 Yao, H. & Ye, J. Long chain acyl-CoA synthetase 3-mediated phosphatidylcholine synthesis is required for assembly of very low density lipoproteins in human hepatoma Huh7 cells. *J Biol Chem* **283**, 849-854 (2008). https://doi.org:10.1074/jbc.M706160200

647 Scheller, N., Mina, L. B., Galão, R. P., Chari, A., Giménez-Barcons, M., Noueiry, A., Fischer, U., Meyerhans, A. & Díez, J. Translation and replication of hepatitis C virus genomic RNA depends on ancient cellular proteins that control mRNA fates. *Proceedings of the National Academy of Sciences of the United States of America* **106**, 13517-13522 (2009). https://doi.org:10.1073/pnas.0906413106

648 Capurro, M., Martin, T., Shi, W. & Filmus, J. Glypican-3 binds to Frizzled and plays a direct role in the stimulation of canonical Wnt signaling. *J Cell Sci* **127**, 1565-1575 (2014). https://doi.org:10.1242/jcs.140871

649 Xue, Y., Mars, W. M., Bowen, W., Singhi, A. D., Stoops, J. & Michalopoulos, G. K. Hepatitis C Virus Mimics Effects of Glypican-3 on CD81 and Promotes Development of Hepatocellular Carcinomas via Activation of Hippo Pathway in Hepatocytes. *The American journal of pathology* **188**, 1469-1477 (2018). https://doi.org:10.1016/j.ajpath.2018.02.013

650 Kolluri, A. & Ho, M. The Role of Glypican-3 in Regulating Wnt, YAP, and Hedgehog in Liver Cancer. *Front Oncol* **9**, 708 (2019). https://doi.org:10.3389/fonc.2019.00708

651 Read, S. A., Parnell, G., Booth, D., Douglas, M. W., George, J. & Ahlenstiel, G. The antiviral role of zinc and metallothioneins in hepatitis C infection. *J Viral Hepat* **25**, 491-501 (2018). https://doi.org:10.1111/jvh.12845

652 Dou, J., Liu, P. & Zhang, X. Cellular response to gene expression profiles of different hepatitis C virus core proteins in the Huh-7 cell line with microarray analysis. *J Nanosci Nanotechnol* **5**, 1230-1235 (2005). https://doi.org:10.1166/jnn.2005.209

653 Pazienza, V., Clément, S., Pugnale, P., Conzelmann, S., Pascarella, S., Mangia, A. & Negro, F. Gene expression profile of Huh-7 cells expressing hepatitis C virus genotype 1b or 3a core proteins. *Liver international : official journal of the International Association for the Study of the Liver* **29**, 661-669 (2009). https://doi.org:10.1111/j.1478-3231.2008.01866.x

654 Clément, S., Peyrou, M., Sanchez-Pareja, A., Bourgoin, L., Ramadori, P., Suter, D., Vinciguerra, M., Guilloux, K., Pascarella, S., Rubbia-Brandt, L., Negro, F. & Foti, M. Down-regulation of phosphatase and tensin homolog by hepatitis C virus core 3a in hepatocytes triggers the formation of large lipid droplets. *Hepatol.* **54**, 38-49 (2011). https://doi.org:https://doi.org/10.1002/hep.24340

655 Bridge, S. H., Sheridan, D. A., Felmlee, D. J., Crossey, M. M., Fenwick, F. I., Lanyon, C. V., Dubuc, G., Seidah, N. G., Davignon, J., Thomas, H. C., Taylor-Robinson, S. D., Toms, G. L., Neely, R. D. & Bassendine, M. F. PCSK9, apolipoprotein E and lipoviral particles in chronic hepatitis C genotype 3: evidence for genotype-specific regulation of lipoprotein metabolism. *Journal of hepatology* **62**, 763-770 (2015). https://doi.org:10.1016/j.jhep.2014.11.016

656 Robinson, M. W., Aranday-Cortes, E., Gatherer, D., Swann, R., Liefhebber, J. M., Filipe Ada, S., Sigruener, A., Barclay, S. T., Mills, P. R., Patel, A. H. & McLauchlan, J. Viral genotype correlates with distinct liver gene transcription signatures in chronic hepatitis C virus infection. *Liver international : official journal of the International Association for the Study of the Liver* **35**, 2256-2264 (2015). https://doi.org:10.1111/liv.12830

657 Gerresheim, G. K., Roeb, E., Michel, A. M. & Niepmann, M. Hepatitis C Virus Downregulates Core Subunits of Oxidative Phosphorylation, Reminiscent of the Warburg Effect in Cancer Cells. *Cells* **8**, 1410 (2019).

658 Chang, M. L. Metabolic alterations and hepatitis C: From bench to bedside. *World journal of gastroenterology* **22**, 1461-1476 (2016). https://doi.org:10.3748/wjg.v22.i4.1461

659 Roduit, R., Morin, J., Massé, F., Segall, L., Roche, E., Newgard, C. B., Assimacopoulos-Jeannet, F. & Prentki, M. Glucose down-regulates the expression of the peroxisome proliferator-activated receptor-alpha gene in the pancreatic beta -cell. *J Biol Chem* **275**, 35799-35806 (2000). https://doi.org:10.1074/jbc.M006001200

660 Ali, R. O., Quinn, G. M., Umarova, R., Haddad, J. A., Zhang, G. Y., Townsend, E. C., Scheuing, L., Hill, K. L., Gewirtz, M., Rampertaap, S., Rosenzweig, S. D., Remaley, A. T., Han, J. M., Periwal, V., Cai, H., Walter, P. J., Koh, C., Levy, E. B., Kleiner, D. E., Etzion, O. & Heller, T. Longitudinal multi-omics analyses of the gut-liver axis reveals metabolic dysregulation in hepatitis C infection and cirrhosis. *Nature microbiology* **8**, 12-27 (2023). https://doi.org:10.1038/s41564-022-01273-y

661 Kalousek, F., Darigo, M. D. & Rosenberg, L. E. Isolation and characterization of propionyl-CoA carboxylase from normal human liver. Evidence for a protomeric tetramer of nonidentical subunits. *J Biol Chem* **255**, 60-65 (1980).

662 Paton, C. M. & Ntambi, J. M. Biochemical and physiological function of stearoyl-CoA desaturase. *Am J Physiol Endocrinol Metab* **297**, E28-37 (2009). https://doi.org:10.1152/ajpendo.90897.2008

663 Tsai, P. L., Zhao, C., Turner, E. & Schlieker, C. The Lamin B receptor is essential for cholesterol synthesis and perturbed by disease-causing mutations. *Elife* **5** (2016). https://doi.org:10.7554/eLife.16011

664 Cochard, J., Bull-Maurer, A., Tauber, C., Burlaud-Gaillard, J., Mazurier, F., Meunier, J. C., Roingeard, P. & Chouteau, P. Differentiated Cells in Prolonged Hypoxia Produce Highly Infectious Native-Like Hepatitis C Virus Particles. *Hepatol.* **74**, 627-640 (2021). https://doi.org:10.1002/hep.31788

VII. Annex

Supplementary Table 1: List of previously reported Core interacting partners combined to our list of retrieved Jad Core PPIs.

Summary of reported HCV Core interacting partners			Database		Literature mining		Y2H					Review	AP LC-MS/MS	SELDI-TOF MS	AP-MS	OUR Jad Core data
			HCV pro		Saik et al., 2016		de Chassey et al., 2008	de Chassey et al., 2008	Dolan et al., 2013	Dolan et al., 2014	Tripathi et al., 2010	Kao et al., 2016	Germain et al., 2014	Roohvand et al., 2009	Ramage et al., 2015	
Uniprot ID	Gene Names	Protein Name	Uniprot ID of prey	Validation method	Uniprot ID of prey	Virus Protein	Uniprot ID of prey	Uniprot ID of prey	Uniprot ID of prey	Uniprot ID of prey	Uniprot ID of prey	Uniprot ID of prey	Uniprot ID of prey	Uniprot ID of prey	Uniprot ID of prey	Uniprot ID of prey
A6NHR9	SMCHD1 KIAA0650	Structural maintenance of chromosomes flexible hinge domain-containing protein 1	-	-	-	-	-	-	-	-	-	-	-	-	-	A6NHR9
O00165	HAX1 HS1BP1	HCLS1-associated protein X-1	-	-	O00165	capsid protein	-	-	-	-	-	-	-	-	-	-
O00206	TLR4	Toll-like receptor 4	-	-	O00206	capsid protein	-	-	-	-	-	-	-	-	-	-
O00410	IPO5 KPNB3 RANBP5	Importin-5	-	-	O00410	capsid protein	-	-	-	-	-	-	-	-	-	-
O00463	TRAF5 RNF84	TNF receptor-associated factor 5	-	-	O00463	capsid protein	-	-	-	-	-	-	-	-	-	-
O00468	AGRN AGRIN	Agrin	O00468	Two Hybrid Test (MI:0018)	O00468	capsid protein	-	O00468	-	-	-	O00468	-	-	-	-
O00488	ZNF593 ZT86	Zinc finger protein 593	-	-	-	-	-	-	-	-	-	-	-	-	-	O00488
O00571	DDX3X DBX DDX3	ATP-dependent RNA helicase DDX3X	O00571	Two Hybrid Test (MI:0018); GST pull-down (MI:0059); Affinity Chromatography (MI:0004); Coimmunoprecipitation (MI:0019); Immunostaining (MI:0022)	O00571	capsid protein	O00571	O00571	O00571	O00571	-	O00571	O00571	-	-	-
O00767	SCD FADS5 SCD1 SCDOS	Stearoyl-CoA desaturase	-	-	-	-	-	-	-	-	-	-	-	-	-	O00767
O14543	SOCS3 CIS3 SSI3	Suppressor of cytokine signaling 3	-	-	O14543	capsid protein	-	-	-	-	-	-	-	-	-	-
O14681	EI24 PIG8	Etoposide-induced protein 2.4 homolog	-	-	-	-	-	-	-	-	-	-	O14681	-	-	-
O14818	PSMA7 HSPC	Proteasome subunit alpha type-7	-	-	O14818	capsid protein	-	-	-	-	O14818	-	-	-	-	-
O14980	XPO1 CRM1	Exportin-1	-	-	O14980	capsid protein	-	-	-	-	-	-	-	-	-	-
O15160	POLR1C POLR1E	DNA-directed RNA polymerases I and III subunit RPAC1	-	-	-	-	-	-	-	-	-	-	-	-	-	O15160
O15162	PLSCR1	Phospholipid scramblase 1	O15162	Two Hybrid Test (MI:0018)	O15162	capsid protein	-	O15162	-	-	-	O15162	-	-	-	-
O15350	TP73 P73	Tumor protein p73	O15350	Coimmunoprecipitation (MI:0019); Mutational analysis (MI:0074); Immunostaining (MI:0022)	O15350	capsid protein	O15350	-	-	-	-	O15350	-	-	-	-
O15357	INPPL1 SHIP2	Phosphatidylinositol 3,4,5-trisphosphate 5-phosphatase 2	-	-	O15357	capsid protein	-	-	-	-	-	-	-	-	-	-
O15371	EIF3D EIF3S7	Eukaryotic translation initiation factor 3 subunit D	-	-	O15371	capsid protein	-	-	-	-	-	-	-	-	-	-
O15392	BIRC5 API4 IAP4	Baculoviral IAP repeat-containing protein 5	-	-	-	-	-	-	-	-	-	-	-	-	-	O15392
O15397	IPO8 RANBP8	Importin-8	-	-	-	-	-	-	-	-	-	-	-	-	-	O15397
O15431	SLC31A1 COPT1 CTR1	High affinity copper uptake protein 1	-	-	-	-	-	-	-	-	-	O15431	-	-	-	-
O15432	SLC31A2 COPT2 CTR2	Protein SLC31A2	O15432	Two Hybrid Test (MI:0018)	O15432	capsid protein	-	O15432	-	-	-	-	-	-	-	-
O15523	DDX3Y DBY	ATP-dependent RNA helicase DDX3Y	O15523	Two Hybrid Test (MI:0018)	-	-	-	O15523	-	-	-	O15523	-	-	-	-
O43159	RRP8 KIAA0409 NML hucep-1	Ribosomal RNA-processing protein 8	-	-	-	-	-	-	-	-	-	-	-	-	-	O43159
O43818	RRP9 RNU3IP2 U355K	U3 small nucleolar RNA-interacting protein 2	-	-	-	-	-	-	-	-	-	-	-	-	-	O43818
O43889	CREB3 LZIP	Cyclic AMP-responsive element-binding protein 3	O43889	Two Hybrid Test (MI:0018); Coimmunoprecipitation (MI:0019); GST pull-down (MI:0059)	O43889	capsid protein	-	-	-	-	-	O43889	-	-	-	-
O60508	CDC40 EHB3 PRP17 PRPF17	Pre-mRNA-processing factor 17	-	-	-	-	-	-	-	-	-	-	-	-	-	O60508
O60603	TLR2 TIL4	Toll-like receptor 2	O60603	Enzyme-linked immunosorbent assay (MI:0411); Electrophoretic mobility shift assay (MI:0413); Western blot (MI:0113); Kinase assay (MI:0424) (MI:0424); Confocal microscopy (MI:0663); Flow cytometry (MI:0054); Colocalization (MI:0403)	O60603	capsid protein	-	-	-	-	-	O60603	-	-	-	-
O60674	JAK2	Tyrosine-protein kinase JAK2	O60674	Coimmunoprecipitation (MI:0019); Western blot (MI:0113)	O60674	capsid protein	O60674	-	-	-	-	O60674	-	-	-	-
O60711	LPXN LDLP	Leupaxin	O60711	Two Hybrid Test (MI:0018)	O60711	capsid protein	-	O60711	-	-	-	O60711	-	-	-	-
O60783	MRPS14	Small ribosomal subunit protein uS14m	-	-	-	-	-	-	-	-	-	-	-	-	-	O60783
O60934	NBN NBS NBS1 P95	Nibrin	-	-	O60934	capsid protein	-	-	-	-	-	-	-	-	-	-
O75095	MEGF6 EGFL3 KIAA0815	Multiple epidermal growth factor-like domains protein 6	O75095	Two Hybrid Test (MI:0018)	O75095	capsid protein	-	O75095	-	-	-	O75095	-	-	-	-
O75127	PTCD1 KIAA0632	Pentatricopeptide repeat-containing protein 1, mitochondrial	-	-	-	-	-	-	-	-	-	-	O75127	-	-	-
O75306	NDUFS2	NADH dehydrogenase	-	-	O75306	capsid protein	-	-	-	-	O75306	-	-	-	-	-
O75530	EED	Polycomb protein EED	-	-	-	-	-	-	-	-	-	-	-	-	-	O75530
O75907	DGAT1 AGRP1 DGAT	Diacylglycerol O-acyltransferase 1	-	-	O75907	capsid protein	-	-	-	-	-	-	-	-	-	-
O76003	GLRX3 PICOT TXNL2 HUSSY-22	Glutaredoxin-3	O76003	2-DE (MI:0982); Mass spectrometry (MI:0943); Immunoblotting (MI:0113); Immunofluorescence (MI:0022)	O76003	capsid protein	O76003	-	-	-	-	O76003	-	-	-	-
O94776	MTA2 MTA1L1 PID	Metastasis-associated protein MTA2	-	-	-	-	-	-	-	-	-	-	-	-	-	O94776
O94880	PHF14 KIAA0783	PHD finger protein 14	-	-	-	-	-	-	-	-	-	-	-	-	-	O94880
O95104	SCAF4 KIAA1172 SFRS15	SR-related and CTD-associated factor 4	-	-	-	-	-	-	-	-	-	-	-	-	-	O95104
O95206	PCDH8	Protocadherin-8	-	-	-	-	-	-	-	-	-	-	-	-	-	O95206
O95786	RIGI DDX58	Antiviral innate immune response receptor RIG-I	-	-	O95786	capsid protein	-	-	-	-	-	-	-	-	-	-
O95801	TTC4 My044	Tetratricopeptide repeat protein 4	-	-	O95801	capsid protein	-	-	-	-	-	-	-	-	-	-

O95992	CH25H	Cholesterol 25-hydroxylase	-	-	O95992	capsid protein	-	-	-	-	-	-	-	-	-	-
O96013	PAK4 KIAA1142	Serine/threonine-protein kinase PAK 4	O96013	Two Hybrid Test (MI:0018)	O96013	capsid protein	-	O96013	-	-	-	O96013	-	-	-	-
O96019	ACTL6A BAF53 BAF53A INO80K	Actin-like protein 6A	-	-	-	-	-	-	-	-	-	-	-	-	-	O96019
P01009	SERPINA1 AAT PI PRO0684 PRO2209	Alpha-1-antitrypsin	-	-	P01009	capsid protein	-	-	-	-	P01009	-	-	-	-	-
P01137	TGFB1 TGFB	Transforming growth factor beta-1 proprotein	-	-	P01137	capsid protein	-	-	-	-	-	-	-	-	-	-
P01308	INS	Insulin	-	-	P01308	capsid protein	-	-	-	-	-	-	-	-	-	-
P01375	TNF TNFA TNFSF2	Tumor necrosis factor	P01375	Western blot (MI:0113); GST pull-down (MI:0059); Coimmunoprecipitation (MI:0019)	P01375	capsid protein	-	-	-	-	-	P01375	-	-	-	-
P01579	IFNG	Interferon gamma	-	-	P01579	capsid protein	-	-	-	-	-	-	-	-	-	-
P02647	APOA1	Apolipoprotein A-I	-	-	P02647	capsid protein	-	-	-	-	-	-	-	-	-	-
P02649	APOE	Apolipoprotein E	-	-	P02649	capsid protein	-	-	-	-	-	-	-	-	-	-
P02652	APOA2	Apolipoprotein A-II	P02652	Two Hybrid Test (MI:0018); Confocal microscopy (MI:0663); surface plasmon resonance (MI:0107); Colocalization (MI:0403)	P02652	capsid protein	P02652	-	-	-	-	P02652	-	-	-	-
P02675	FGB	Fibrinogen beta chain	-	-	P02675	capsid protein	-	-	-	-	-	-	-	-	-	-
P02792	FTL	Ferritin light chain	-	-	P02792	capsid protein	-	-	-	-	P02792	-	-	-	-	-
P04049	RAF1 RAF	RAF proto-oncogene serine/threonine-protein kinase	-	-	P04049	capsid protein	-	-	-	-	-	-	-	-	-	-
P04114	APOB	Apolipoprotein B-100	-	-	-	-	-	-	P04114	-	-	-	-	-	-	-
P04275	VWF F8VWF	von Willebrand factor	P04275	Two Hybrid Test (MI:0018)	-	-	-	P04275	-	-	-	P04275	-	-	-	-
P04406	GAPDH GAPD CDABP0047 OK/SW-cl.12	Glyceraldehyde-3-phosphate dehydrogenase	P04406	Two Hybrid Test (MI:0018)	P04406	capsid protein	-	P04406	-	-	-	P04406	-	-	-	-
P04439	HLA-A HLAA	HLA class I histocompatibility antigen, A alpha chain	P04439	Fluorescence-activated cell sorting (MI:0054); Immunostaining (MI:0022)	-	-	P04439	-	-	-	-	P04439	-	-	-	-
P04637	TP53 P53	Cellular tumor antigen p53	P04637	Coimmunoprecipitation (MI:0019); GST pull-down (MI:0059); Far-Western blot (MI:0047); Mutational analysis (MI:0074); Affinity Chromatography (MI:0004); Colocalization (MI:0403); Western blot (MI:0113)	P04637	capsid protein	P04637	-	-	-	-	P04637	-	-	-	-
P05112	IL4	Interleukin-4	-	-	P05112	capsid protein	-	-	-	-	-	-	-	-	-	-
P05141	SLC25A5 AAC2 ANT2	ADP/ATP translocase 2	-	-	P05141	capsid protein	-	-	-	-	P05141	-	-	-	-	-
P05166	PCCB	Propionyl-CoA carboxylase beta chain, mitochondrial	-	-	-	-	-	-	-	-	-	-	-	-	-	P05166
P05209		Tubulin alpha	-	-	-	-	-	-	-	-	-	-	-	P05209	-	-
P05217	TUBB4B TUBB2C	Tubulin beta-4B chain	-	-	-	-	-	-	-	-	-	-	-	P05217	-	-
P05218	TUBB TUBB5 OK/SW-cl.56	Tubulin beta chain	-	-	-	-	-	-	-	-	-	-	-	P05218	-	-
P05231	IL6 IFNB2	Interleukin-6	-	-	P05231	capsid protein	-	-	-	-	-	-	-	-	-	-
P05455	SSB	Lupus La protein	-	-	P05455	capsid protein	-	-	-	-	-	-	-	-	-	-
P05783	KRT18 CYK18 PIG46	Keratin, type I cytoskeletal 18	P05783	2-DE (MI:0982); Mass spectrometry (MI:0943); Immunoblotting (MI:0113); Immunofluorescence (MI:0022)	P05783	capsid protein	P05783	-	-	-	-	P05783	-	-	-	-
P05787	KRT8 CYK8	Keratin, type II cytoskeletal 8	P05787	2-DE (MI:0982); Mass spectrometry (MI:0943); Immunoblotting (MI:0113); Immunofluorescence (MI:0022)	P05787	capsid protein	P05787	-	-	-	-	P05787	-	-	-	-
P06239	LCK	Tyrosine-protein kinase Lck	-	-	P06239	capsid protein	-	-	-	-	-	-	-	-	-	-
P06241	FYN	Tyrosine-protein kinase Fyn	-	-	P06241	capsid protein	-	-	-	-	-	-	-	-	-	-
P06400	RB1	Retinoblastoma-associated protein	-	-	P06400	capsid protein	-	-	-	-	-	-	-	-	-	-
P06733	ENO1 ENO1L1 MBPB1 MPB1	Alpha-enolase	-	-	P06733	capsid protein	-	-	-	-	P06733	-	-	-	-	-
P06748	NPM1 NPM	Nucleophosmin	P06748	Coimmunoprecipitation (MI:0019); GST pull-down (MI:0059)	P06748	capsid protein	P06748	-	P06748	P06748	-	P06748	-	-	-	-
P07355	ANXA2 ANX2 ANX2L4 CAL1H LPC2D	Annexin A2	-	-	P07355	capsid protein	-	-	-	-	-	-	-	-	-	-
P07437	TUBB TUBB5 OK/SW-cl.56	Tubulin beta chain	-	-	-	-	-	-	-	-	-	-	-	P07437	-	-
P07900	HSP90AA1 HSP90A HSPC1 HSPCA	Heat shock protein HSP 90-alpha	-	-	P07900	capsid protein	-	-	-	-	-	-	-	-	-	-
P07910	HNRNPC HNRPC	Heterogeneous nuclear ribonucleoproteins C1/C2	-	-	P07910	capsid protein	-	-	-	-	-	-	-	-	-	-
P07948	LYN JTK8	Tyrosine-protein kinase Lyn	-	-	P07948	capsid protein	-	-	-	-	-	-	-	-	-	-
P08572	COL4A2	Collagen alpha-2	P08572	Two Hybrid Test (MI:0018)	P08572	capsid protein	-	P08572	-	-	-	P08572	-	-	-	-
P08574	CYC1	Cytochrome c1, heme protein, mitochondrial	-	-	-	-	-	-	-	-	-	-	P08574	-	-	-
P08631	HCK	Tyrosine-protein kinase HCK	-	-	P08631	capsid protein	-	-	-	-	-	-	-	-	-	-
P08670	VIM	Vimentin	P08670	2-DE (MI:0982); Mass spectrometry (MI:0943); Immunoblotting (MI:0113); Immunofluorescence (MI:0022)	P08670	capsid protein	P08670	-	-	-	-	P08670	-	-	-	-
P08727	KRT19	Keratin, type I cytoskeletal 19	P08727	2-DE (MI:0982); Mass spectrometry (MI:0943); Immunoblotting (MI:0113); Immunofluorescence (MI:0022)	P08727	capsid protein	P08727	-	-	-	-	P08727	-	-	-	-
P10145	CXCL8 IL8	Interleukin-8	-	-	P10145	capsid protein	-	-	-	-	-	-	-	-	-	-
P10253	GAA	Lysosomal alpha-glucosidase	-	-	-	-	-	-	-	-	-	-	-	-	-	P10253
P10809	HSPD1 HSP60	60 kDa heat shock protein, mitochondrial	P10809	2-DE (MI:0982); Mass spectrometry (MI:0943); Immunoblotting (MI:0113); Immunofluorescence (MI:0022)	P10809	capsid protein	P10809	-	-	-	-	P10809	-	-	-	-
P10909	CLU APOJ CLI KUB1 AAG4	Clusterin	-	-	P10909	capsid protein	-	-	-	-	-	-	-	-	-	-

P11021	HSPA5 GRP78	Endoplasmic reticulum chaperone BiP	-	-	P11021	capsid protein	-	-	-	-	-	-	-	-	-	-
P12814	ACTN1	Alpha-actinin-1	-	-	P12814	capsid protein	-	-	-	-	-	-	-	-	-	-
P12830	CDH1 CDHE UVO	Cadherin-1	-	-	P12830	capsid protein	-	-	-	-	-	-	-	-	-	-
P13378	HOXD8 HOX4E	Homeobox protein Hox-D8	P13378	Two Hybrid Test (MI:0018)	-	-	-	P13378	-	-	-	P13378	-	-	-	-
P13747	HLA-E HLA-6.2 HLAE	HLA class I histocompatibility antigen, alpha chain E	P13747	Fluorescence-activated cell sorting (MI:0054); Immunostaining (MI:0022)	-	-	P13747	-	-	-	-	P13747	-	-	-	-
P15812	CD1E	T-cell surface glycoprotein CD1e, membrane-associated	-	-	P15812	capsid protein	-	-	-	-	-	-	-	-	-	-
P15813	CD1D	Antigen-presenting glycoprotein CD1d	-	-	P15813	capsid protein	-	-	-	-	-	-	-	-	-	-
P16070	CD44 LHR MDU2 MDU3 MIC4	CD44 antigen	-	-	P16070	capsid protein	-	-	-	-	-	-	-	-	-	-
P16220	CREB1	Cyclic AMP-responsive element-binding protein 1	-	-	-	-	-	-	-	-	-	-	-	-	-	P16220
P17096	HMGA1 HMGIY	High mobility group protein HMG-I/HMG-Y	-	-	-	-	-	-	-	-	-	-	-	-	-	P17096
P17676	CEBPB TCF5 PP9092	CCAAT/enhancer-binding protein beta	-	-	-	-	-	-	-	-	-	-	-	-	-	P17676
P17844	DDX5 G17P1 HELR HLR1	Probable ATP-dependent RNA helicase DDX5	P17844	2-DE (MI:0982); Mass spectrometry (MI:0943)	P17844	capsid protein	P17844	-	-	-	-	P17844	-	-	-	-
P18754	RCC1 CHC1	Regulator of chromosome condensation	-	-	-	-	-	-	-	-	-	-	-	-	-	P18754
P19438	TNFRSF1A TNFAR TNFR1	Tumor necrosis factor receptor superfamily member 1A	P19438	GST pull-down (MI:0059); Kinase assay (MI:0424) (MI:0424); Affinity Chromatography (MI:0004)	P19438	capsid protein	P19438	-	-	-	-	P19438	-	-	-	-
P19525	EIF2AK2 PKR PRKR	Interferon-induced, double-stranded RNA-activated protein kinase	P19525	Two Hybrid Test (MI:0018); Colocalization (MI:0403); Coimmunoprecipitation (MI:0019)	P19525	capsid protein	-	-	-	-	-	P19525	-	-	-	-
P19793	RXRA NR2B1	Retinoic acid receptor RXR-alpha	P19793	GST pull-down (MI:0059); Coimmunoprecipitation (MI:0019)	P19793	capsid protein	P19793	-	-	-	-	P19793	-	-	-	-
P19838	NFKB1	Nuclear factor NF-kappa-B p105 subunit	-	-	P19838	capsid protein	-	-	-	-	-	-	-	-	-	-
P20020	ATP2B1 PMCA1	Plasma membrane calcium-transporting ATPase 1	-	-	-	-	-	-	-	-	-	-	-	-	-	P20020
P20226	TBP GTF2D1 TF2D TFIID	TATA-box-binding protein	P20226	Affinity Chromatography (MI:0004)	-	-	P20226	-	-	-	-	P20226	-	-	-	-
P20591	MX1	Interferon-induced GTP-binding protein Mx1	-	-	P20591	capsid protein	-	-	-	-	-	-	-	-	-	-
P21583	KITLG MGF SCF	Kit ligand	-	-	P21583	capsid protein	-	-	-	-	-	-	-	-	-	-
P22301	IL10	Interleukin-10	-	-	P22301	capsid protein	-	-	-	-	-	-	-	-	-	-
P22736	NR4A1 GFRP1 HMR NAK1	Nuclear receptor subfamily 4immunitygroup A member 1	P22736	Two Hybrid Test (MI:0018)	-	-	-	P22736	-	-	-	P22736	-	-	-	-
P23109	AMPD1	AMP deaminase 1	-	-	P23109	capsid protein	-	-	-	-	-	-	-	-	-	-
P23458	JAK1 JAK1A JAK1B	Tyrosine-protein kinase JAK1	P23458	Coimmunoprecipitation (MI:0019); Western blot (MI:0113)	P23458	capsid protein	P23458	-	-	-	-	P23458	-	-	-	-
P23528	CFL1 CFL	Cofilin-1	P23528	2-DE (MI:0982); Mass spectrometry (MI:0943); Immunoblotting (MI:0113); Immunofluorescence (MI:0022)	P23528	capsid protein	P23528	-	-	-	-	P23528	-	-	-	-
P24666	ACP1	Low molecular weight phosphotyrosine protein phosphatase	P24666	2-DE (MI:0982); Mass spectrometry (MI:0943); Immunoblotting (MI:0113); Immunofluorescence (MI:0022)	P24666	capsid protein	P24666	-	-	-	-	P24666	-	-	-	-
P25445	FAS APT1 FAS1 TNFRSF6	Tumor necrosis factor receptor superfamily member 6	P25445	Immunoblotting (MI:0113); Coimmunoprecipitation (MI:0019)	P25445	capsid protein	P25445	-	-	-	-	P25445	-	-	-	-
P25490	YY1 INO80S	Transcriptional repressor protein YY1	P25490	Coimmunoprecipitation (MI:0019); GST pull-down (MI:0059)	P25490	capsid protein	P25490	-	-	-	-	P25490	-	-	-	-
P25788	PSMA3 HC8 PSC8	Proteasome subunit alpha type-3	-	-	P25788	capsid protein	-	-	-	-	-	-	-	-	-	-
P26196	DDX6 HLR2 RCK	Probable ATP-dependent RNA helicase DDX6	-	-	P26196	capsid protein	-	-	-	-	-	-	-	-	-	-
P26641	EEF1G EF1G PRO1608	Elongation factor 1-gamma	-	-	P26641	capsid protein	-	-	-	-	P26641	-	-	-	-	-
P27348	YWHAQ	14-3-3 protein theta	-	-	P27348	capsid protein	-	-	-	-	-	-	-	-	-	-
P28288	ABCD3 PMP70 PXMP1	ATP-binding cassette sub-family D member 3	-	-	-	-	-	-	-	-	-	-	P28288	-	-	-
P28482	MAPK1 ERK2 PRKM1 PRKM2	Mitogen-activated protein kinase 1	-	-	P28482	capsid protein	-	-	-	-	-	-	-	-	-	-
P28799	GRN	Progranulin	P28799	Two Hybrid Test (MI:0018)	P28799	capsid protein	-	P28799	-	-	-	P28799	-	-	-	-
P29590	PML MYL PP8675 RNF71 TRIM19	Protein PML	P29590	Western blot (MI:0113); Coimmunoprecipitation (MI:0019); Colocalization (MI:0403)	P29590	capsid protein	P29590	-	-	-	-	P29590	-	-	-	-
P29965	CD40LG CD40L TNFSF5 TRAP	CD40 ligand	-	-	P29965	capsid protein	-	-	-	-	-	-	-	-	-	-
P30613	PKLR PK1 PKL	Pyruvate kinase PKLR	-	-	P30613	capsid protein	-	-	-	-	-	-	-	-	-	-
P31629	HIVEP2	Transcription factor HIVEP2	P31629	Two Hybrid Test (MI:0018)	-	-	-	P31629	-	-	-	P31629	-	-	-	-
P31749	AKT1 PKB RAC	RAC-alpha serine/threonine-protein kinase	-	-	P31749	capsid protein	-	-	-	-	-	-	-	-	-	-
P31946	YWHAB	14-3-3 protein beta/alpha	P31946	Two Hybrid Test (MI:0018); Colocalization (MI:0403); Coimmunoprecipitation (MI:0019); Affinity Chromatography (MI:0004)	P31946	capsid protein	P31946	-	-	-	-	P31946	-	-	-	-
P34810	CD68	Macrosialin	P34810	Two Hybrid Test (MI:0018)	P34810	capsid protein	-	P34810	-	-	-	P34810	-	-	-	-
P34932	HSPA4 APG2	Heat shock 70 kDa protein 4	-	-	P34932	capsid protein	-	-	-	-	-	-	-	-	-	-
P35659	DEK	Protein DEK	-	-	-	-	-	-	-	-	-	-	-	-	-	P35659
P36897	TGFBR1 ALK5 SKR4	TGF-beta receptor type-1	-	-	P36897	capsid protein	-	-	-	-	-	-	-	-	-	-
P36941	LTBR D12S370 TNFCR TNFR3 TNFRSF3	Tumor necrosis factor receptor superfamily member 3	P36941	Two Hybrid Test (MI:0018); Far-Western blot (MI:0047); Affinity Chromatography (MI:0004); Coimmunoprecipitation (MI:0019)	P36941	capsid protein	P36941	-	-	-	-	P36941	-	-	-	-

P38117	ETFB FP585	Electron transfer flavoprotein subunit beta	-	-	P38117	capsid protein	-	-	-	-	P38117	-	-	-	-	-
P38432	COIL CLN80	Coilin	-	-	-	-	-	-	-	-	-	-	-	-	-	P38432
P38484	IFNGR2 IFNGT1	Interferon gamma receptor 2	-	-	P38484	capsid protein	-	-	-	-	-	-	-	-	-	-
P38936	CDKN1A CAP20 CDKN1 CIP1 MDA6 PIC1 SDI1 WAF1	Cyclin-dependent kinase inhibitor 1	P38936	GST pull-down (MI:0059); Mutational analysis (MI:0074); Affinity Chromatography (MI:0004)	P38936	capsid protein	P38936	-	-	-	-	P38936	-	-	-	-
P39060	COL18A1	Collagen alpha-1	-	-	-	-	-	-	-	-	-	-	-	-	-	P39060
P40763	STAT3 APRF	Signal transducer and activator of transcription 3	P40763	Coimmunoprecipitation (MI:0019); Western blot (MI:0113); GST pull-down (MI:0059)	P40763	capsid protein	P40763	-	-	-	-	P40763	-	-	-	-
P41208	CETN2 CALT CEN2	Centrin-2	-	-	-	-	-	-	-	-	-	-	-	-	-	P41208
P42224	STAT1	Signal transducer and activator of transcription 1-alpha/beta	P42224	Coimmunoprecipitation (MI:0019); Western blot (MI:0113)	P42224	capsid protein	P42224	-	-	-	-	P42224	-	-	-	-
P42338	PIK3CB PIK3C1	Phosphatidylinositol 4,5-bisphosphate 3-kinase catalytic subunit beta isoform	-	-	P42338	capsid protein	-	-	-	-	-	-	-	-	-	-
P43694	GATA4	Transcription factor GATA-4	-	-	-	-	-	-	-	-	-	-	-	-	-	P43694
P45973	CBX5 HP1A	Chromobox protein homolog 5	-	-	-	-	-	-	-	-	-	-	-	-	-	P45973
P45983	MAPK8 JNK1 PRKM8 SAPK1 SAPK1C	Mitogen-activated protein kinase 8	-	-	P45983	capsid protein	-	-	-	-	-	-	-	-	-	-
P47712	PLA2G4A CPLA2 PLA2G4	Cytosolic phospholipase A2	-	-	P47712	capsid protein	-	-	-	-	-	-	-	-	-	-
P47813	EIF1AX EIF1A EIF4C	Eukaryotic translation initiation factor 1A, X-chromosomal	-	-	P47813	capsid protein	-	-	-	-	P47813	-	-	-	-	-
P49023	PXN	Paxillin	-	-	P49023	capsid protein	-	-	-	-	-	-	-	-	-	-
P49327	FASN FAS	Fatty acid synthase	-	-	P49327	capsid protein	-	-	-	-	-	-	-	-	-	-
P50579	METAP2 MNPEP P67EIF2	Methionine aminopeptidase 2	-	-	-	-	-	-	-	-	-	-	-	-	-	P50579
P50591	TNFSF10 APO2L TRAIL	Tumor necrosis factor ligand superfamily member 10	-	-	P50591	capsid protein	-	-	-	-	-	-	-	-	-	-
P50613	CDK7 CAK CAK1 CDKN7 MO15 STK1	Cyclin-dependent kinase 7	-	-	P50613	HCV CORE PROTEIN	-	-	-	-	-	-	-	-	-	-
P51654	GPC3 OCI5	Glypican-3	-	-	-	-	-	-	-	-	-	-	-	-	-	P51654
P51946	CCNH	Cyclin-H	P51946	Immunofluorescence (MI:0022); Confocal microscopy (MI:0663); GST pull-down (MI:0059); Immunoblotting (MI:0113); Coimmunoprecipitation (MI:0019); Western blot (MI:0113); Immunostaining (MI:0022)	P51946	capsid protein	P51946	-	-	-	-	P51946	-	-	-	-
P52294	KPNA1 RCH2	Importin subunit alpha-5	P52294	GST pull-down (MI:0059)	P52294	capsid protein	-	-	-	-	-	P52294	-	-	-	-
P52756	RBM5 H37 LUCA15	RNA-binding protein 5	-	-	-	-	-	-	-	-	-	-	-	-	-	P52756
P53582	METAP1 KIAA0094	Methionine aminopeptidase 1	-	-	-	-	-	-	-	-	-	-	-	-	-	P53582
P53675	CLTCL1 CLH22 CLTCL CLTD	Clathrin heavy chain 2	-	-	-	-	-	-	-	-	-	-	-	-	-	P53675
P53814	SMTN SMSMO	Smoothelin	-	-	-	-	-	-	-	-	-	-	-	-	-	P53814
P53985	SLC16A1 MCT1	Monocarboxylate transporter 1	-	-	-	-	-	-	-	-	-	-	P53985	-	-	-
P54296	MYOM2	Myomesin-2	-	-	P54296	capsid protein	-	-	-	-	-	-	-	-	-	-
P55157	MTTP MTP	Microsomal triglyceride transfer protein large subunit	-	-	P55157	capsid protein	-	-	-	-	-	-	-	-	-	-
P55209	NAP1L1 NRP	Nucleosome assembly protein 1-like 1	-	-	-	-	-	-	-	-	-	-	P55209	-	P55209	P55209
P56182	RRP1 D21S2056E NNP1 NOP52 RRP1A	Ribosomal RNA processing protein 1 homolog A	-	-	-	-	-	-	-	-	-	-	-	-	-	P56182
P56524	HDAC4 KIAA0288	Histone deacetylase 4	-	-	-	-	-	-	-	-	-	-	-	-	-	P56524
P56945	BCAR1 CAS CASS1 CRKAS	Breast cancer anti-estrogen resistance protein 1	P56945	Two Hybrid Test (MI:0018)	P56945	capsid protein	-	P56945	-	-	-	P56945	-	-	-	-
P57088	TMEM33 DB83	Transmembrane protein 33	-	-	-	-	-	-	-	-	-	-	P57088	-	-	-
P57740	NUP107	Nuclear pore complex protein Nup107	-	-	-	-	-	-	-	-	-	-	-	-	-	P57740
P60033	CD81 TAPA1 TSPAN28	CD81 antigen	-	-	P60033	capsid protein	-	-	-	-	-	-	-	-	-	-
P60468	SEC61B	Protein transport protein Sec61 subunit beta	-	-	-	-	-	-	-	-	-	-	P60468	-	-	-
P60484	PTEN MMAC1 TEP1	Phosphatidylinositol 3,4,5-trisphosphate 3-phosphatase and dual-specificity protein phosphatase PTEN	-	-	P60484	capsid protein	-	-	-	-	-	-	-	-	-	-
P60568	IL2	Interleukin-2	-	-	P60568	capsid protein	-	-	-	-	-	-	-	-	-	-
P61289	PSME3	Proteasome activator complex subunit 3	P61289	Western blot (MI:0113)	P61289	capsid protein	P61289	-	-	-	-	P61289	-	-	-	-
P61978	HNRNPK HNRPK	Heterogeneous nuclear ribonucleoprotein K	P61978	Two Hybrid Test (MI:0018); GST pull-down (MI:0059); Far-Western blot (MI:0047); Coimmunoprecipitation (MI:0019); Affinity Chromatography (MI:0004)	P61978	capsid protein	P61978	P61978	-	-	-	P61978	-	-	-	-
P62258	YWHAE	14-3-3 protein epsilon	P62258	Affinity Chromatography (MI:0004); Coimmunoprecipitation (MI:0019); Two Hybrid Test (MI:0018)	P62258	capsid protein	P62258	-	-	-	-	P62258	-	-	-	-
P62937	PPIA CYPA	Peptidyl-prolyl cis-trans isomerase A	-	-	P62937	capsid protein	-	-	-	-	-	-	-	-	-	-

P63104	YWHAZ	14-3-3 protein zeta/delta	P63104	Two Hybrid Test (MI:0018); GST pull-down (MI:0059); Coimmunoprecipitation (MI:0019); Western blot (MI:0113); Affinity Chromatography (MI:0004)	P63104	capsid protein	P63104	-	-	-	-	P63104	-	-	-	-
P67870	CSNK2B CK2N G5A	Casein kinase II subunit beta	-	-	-	-	-	-	-	-	-	-	-	-	P67870	-
P68363	TUBA1B	Tubulin alpha-1B chain	-	-	-	-	-	-	-	-	-	-	-	P68363	-	-
P68371	TUBB4B TUBB2C	Tubulin beta-4B chain	-	-	-	-	-	-	-	-	-	-	-	P68371	-	-
P68400	CSNK2A1 CK2A1	Casein kinase II subunit alpha	-	-	-	-	-	-	-	-	-	-	-	-	P68400	-
P82930	MRPS34	Small ribosomal subunit protein mS34	-	-	-	-	-	-	-	-	-	-	-	-	-	P82930
P84022	SMAD3 MADH3	Mothers against decapentaplegic homolog 3	P84022	Coimmunoprecipitation (MI:0019); GST pull-down (MI:0059); Affinity Chromatography (MI:0004)	P84022	capsid protein	P84022	-	-	-	-	P84022	-	-	-	-
P98095	FBLN2	Fibulin-2	P98095	Two Hybrid Test (MI:0018)	-	-	-	P98095	-	-	-	P98095	-	-	-	-
Q01780	EXOSC10 PMSCL PMSCL2 RRP6	Exosome component 10	-	-	-	-	-	-	-	-	-	-	-	-	-	Q01780
Q05048	CSTF1	Cleavage stimulation factor subunit 1	-	-	-	-	-	-	-	-	-	-	-	-	-	Q05048
Q05086	UBE3A E6AP EPVE6AP HPVE6A	Ubiquitin-protein ligase E3A	-	-	Q05086	capsid protein	-	-	-	-	-	-	-	-	-	-
Q05195	MXD1 MAD	Max dimerization protein 1	-	-	Q05195	capsid protein	-	-	-	-	-	-	-	-	-	-
Q07021	C1QBP GC1QBP HABP1 SF2P32	Complement component 1 Q subcomponent-binding protein, mitochondrial	Q07021	Two Hybrid Test (MI:0018); GST pull-down (MI:0059)	Q07021	capsid protein	Q07021	-	-	-	-	Q07021	Q07021	-	-	Q07021
Q07065	CKAP4	Cytoskeleton-associated protein 4	-	-	-	-	-	-	-	-	-	-	-	-	-	Q07065
Q07812	BAX BCL2L4	Apoptosis regulator BAX	-	-	Q07812	capsid protein	-	-	-	-	-	-	-	-	-	-
Q07820	MCL1 BCL2L3	Induced myeloid leukemia cell differentiation protein Mcl-1	Q07820	Coimmunoprecipitation (MI:0019); Western blot (MI:0113)	Q07820	capsid protein	-	-	-	-	-	Q07820	-	-	-	-
Q07869	PPARA NR1C1 PPAR	Peroxisome proliferator-activated receptor alpha	Q07869	Immunoblotting (MI:0113); Affinity Chromatography (MI:0004)	Q07869	capsid protein	-	-	-	-	-	Q07869	-	-	-	-
Q08170	SRSF4 SFRS4 SRP75	Serine/arginine-rich splicing factor 4	-	-	-	-	-	-	-	-	-	-	-	-	-	Q08170
Q09472	EP300 P300	Histone acetyltransferase p300	Q09472	Coimmunoprecipitation (MI:0019); GST pull-down (MI:0059); Western blot (MI:0113); Affinity Chromatography (MI:0004)	Q09472	capsid protein	Q09472	-	-	-	-	Q09472	-	-	-	-
Q0VDF9	HSPA14 HSP60 HSP70L1	Heat shock 70 kDa protein 14	-	-	Q0VDF9	capsid protein	-	-	-	-	-	-	-	-	-	-
Q12824	SMARCB1 BAF47 INI1 SNF5L1	SWI/SNF-related matrix-associated actin-dependent regulator of chromatin subfamily B member 1	-	-	-	-	-	-	-	-	-	-	-	-	-	Q12824
Q12905	ILF2 NF45 PRO3063	Interleukin enhancer-binding factor 2	-	-	Q12905	capsid protein	-	-	-	-	-	-	-	-	-	-
Q12933	TRAF2 TRAP3	TNF receptor-associated factor 2	Q12933	Western blot (MI:0113); GST pull-down (MI:0059); Coimmunoprecipitation (MI:0019)	Q12933	capsid protein	-	-	-	-	-	Q12933	-	-	-	-
Q12988	HSPB3 HSP27 HSPL27	Heat shock protein beta-3	-	-	Q12988	capsid protein	-	-	-	-	-	-	-	-	-	-
Q12996	CSTF3	Cleavage stimulation factor subunit 3	-	-	-	-	-	-	-	-	-	-	-	-	-	Q12996
Q13099	IFT88 TG737 TTC10	Intraflagellar transport protein 88 homolog	-	-	-	-	-	-	-	-	-	-	-	-	Q13099	-
Q13111	CHAF1A CAF CAF1P150	Chromatin assembly factor 1 subunit A	-	-	-	-	-	-	-	-	-	-	-	-	-	Q13111
Q13136	PPFIA1 LIP1	Liprin-alpha-1	-	-	-	-	-	-	-	-	-	-	-	-	-	Q13136
Q13158	FADD MORT1 GIG3	FAS-associated death domain protein	Q13158	Coimmunoprecipitation (MI:0019); GST pull-down (MI:0059)	Q13158	capsid protein	Q13158	-	-	-	-	Q13158	-	-	-	-
Q13405	MRPL49 C11orf4 NOF1 OK/SW-cl.67	Large ribosomal subunit protein mL49	-	-	-	-	-	-	-	-	-	-	-	-	Q13405	-
Q13625	TP53BP2 ASPP2 BBP	Apoptosis-stimulating of p53 protein 2	Q13625	Two Hybrid Test (MI:0018); Affinity Chromatography (MI:0004); Coimmunoprecipitation (MI:0019); Immunostaining (MI:0022)	Q13625	capsid protein	Q13625	-	-	-	-	Q13625	-	-	-	-
Q13724	MOGS GCS1	Mannosyl-oligosaccharide glucosidase	-	-	-	-	-	-	-	-	-	-	-	-	Q13724	Q13724
Q14008	CKAP5 KIAA0097	Cytoskeleton-associated protein 5	-	-	-	-	-	-	-	-	-	-	-	-	-	Q14008
Q14108	SCARB2 CD36L2 LIMP2 LIMPII	Lysosome membrane protein 2	-	-	Q14108	capsid protein	-	-	-	-	-	-	-	-	-	-
Q14240	EIF4A2 DDX2B EIF4F	Eukaryotic initiation factor 4A-II	-	-	Q14240	capsid protein	-	-	-	-	-	-	-	-	-	-
Q14591		Zinc finger protein 271	Q14591	Two Hybrid Test (MI:0018)	Q14591	capsid protein	-	Q14591	-	-	-	-	-	-	-	-
Q14692	BMS1 BMS1L KIAA0187	Ribosome biogenesis protein BMS1 homolog	-	-	-	-	-	-	-	-	-	-	-	-	-	Q14692
Q14739	LBR	Delta(14)-sterol reductase LBR	-	-	-	-	-	-	-	-	-	-	Q14739	-	-	Q14739
Q14807	KIF22 KID KNSL4	Kinesin-like protein KIF22	-	-	-	-	-	-	-	-	-	-	-	-	-	Q14807
Q15020	SART3 KIAA0156 TIP110	Squamous cell carcinoma antigen recognized by T-cells 3	-	-	-	-	-	-	-	-	-	-	-	-	Q15020	-
Q15116	PDCD1 PD1	Programmed cell death protein 1	-	-	Q15116	capsid protein	-	-	-	-	-	-	-	-	-	-
Q15388	TOMM20 KIAA0016	Mitochondrial import receptor subunit TOM20 homolog	-	-	Q15388	capsid protein	-	-	-	-	Q15388	-	-	-	-	-
Q15543	TAF13 TAF2K TAFII18	Transcription initiation factor TFIID subunit 13	-	-	-	-	-	-	-	-	-	-	-	-	-	Q15543
Q15544	TAF11 TAF2I PRO2134	Transcription initiation factor TFIID subunit 11	Q15544	GST pull-down (MI:0059)	Q15544	capsid protein	Q15544	-	-	-	-	Q15544	-	-	-	-
Q15545	TAF7 TAF2F TAFII55	Transcription initiation factor TFIID subunit 7	-	-	-	-	-	-	-	-	-	-	-	-	-	Q15545

Q15554	TERF2 TRBF2 TRF2	Telomeric repeat-binding factor 2	-	-	-	-	-	-	-	-	-	-	-	-	-	Q15554
Q15628	TRADD	Tumor necrosis factor receptor type 1-associated DEATH domain protein	Q15628	Western blot (MI:0113); GST pull-down (MI:0059); Coimmunoprecipitation (MI:0019)	Q15628	capsid protein	-	-	-	-	-	Q15628	-	-	-	-
Q15629	TRAM1 TRAM	Translocating chain-associated membrane protein 1	-	-	-	-	-	-	-	-	-	-	Q15629	-	-	Q15629
Q15631	TSN	Translin	Q15631	Two Hybrid Test (MI:0018); Coimmunoprecipitation (MI:0019)	Q15631	capsid protein	Q15631	-	-	-	-	Q15631	-	-	-	-
Q15643	TRIP11 CEV14	Thyroid receptor-interacting protein 11	-	-	-	-	-	-	Q15643	Q15643	-	-	-	-	-	-
Q15672	TWIST1 BHLHA38 TWIST	Twist-related protein 1	-	-	-	-	-	-	-	-	-	-	-	-	Q15672	-
Q16540	MRPL23 L23MRP RPL23L	Large ribosomal subunit protein uL23m	-	-	-	-	-	-	-	-	-	-	-	-	-	Q16540
Q16552	IL17A CTLA8 IL17	Interleukin-17A	-	-	Q16552	capsid protein	-	-	-	-	-	-	-	-	-	-
Q16611	BAK1 BAK BCL2L7 CDN1	Bcl-2 homologous antagonist/killer	-	-	Q16611	capsid protein	-	-	-	-	-	-	-	-	-	-
Q16644	MAPKAPK3	MAP kinase-activated protein kinase 3	-	-	Q16644	capsid protein	-	-	-	-	-	-	-	-	-	-
Q16778	H2BC21 H2BFQ HIST2H2BE	Histone H2B type 2-E	-	-	Q16778	capsid protein	-	-	-	-	-	-	-	-	-	-
Q16880	UGT8 CGT UGT4	2-hydroxyacylsphingosine 1-beta-galactosyltransferase	-	-	-	-	-	-	-	-	-	-	Q16880	-	-	-
Q2KHT3	CLEC16A KIAA0350	Protein CLEC16A	-	-	-	-	-	-	-	-	-	-	-	-	Q2KHT3	-
Q2TBE0	CWF19L2	CWF19-like protein 2	-	-	-	-	-	-	-	-	-	-	-	-	Q2TBE0	-
Q3KQU3	MAP7D1 KIAA1187 PARCC1 RPRC1 PP2464	MAP7 domain-containing protein 1	-	-	-	-	-	-	-	-	-	-	-	-	-	Q3KQU3
Q49A26	GLYR1 HIBDL NDF NP60 NPAC	Cytokine-like nuclear factor N-PAC	-	-	-	-	-	-	-	-	-	-	-	-	-	Q49A26
Q53GQ0	HSD17B12 SDR12C1	Very-long-chain 3-oxoacyl-CoA reductase	-	-	-	-	-	-	-	-	-	-	Q53GQ0	-	-	-
Q53HL2	CDCA8 PESCRG3	Borealin	-	-	-	-	-	-	-	-	-	-	-	-	-	Q53HL2
Q5SY16	NOL9	Polynucleotide 5'-hydroxyl-kinase NOL9	-	-	-	-	-	-	-	-	-	-	-	-	-	Q5SY16
Q6I9Y2	THOC7 NIF3L1BP1	THO complex subunit 7 homolog	-	-	-	-	-	-	-	-	-	-	-	-	-	Q6I9Y2
Q6P1J9	CDC73 C1orf28 HRPT2	Parafibromin	-	-	-	-	-	-	-	-	-	-	-	-	-	Q6P1J9
Q6P1L8	MRPL14 MRPL32 RPML32	Large ribosomal subunit protein uL14m	-	-	-	-	-	-	-	-	-	-	-	-	-	Q6P1L8
Q6P1N9	TATDN1 CDA11	Deoxyribonuclease TATDN1	Q6P1N9	2-DE (MI:0982); Mass spectrometry (MI:0943); Immunoblotting (MI:0113); Immunofluorescence (MI:0022)	Q6P1N9	capsid protein	Q6P1N9	-	-	-	-	Q6P1N9	-	-	-	-
Q6P4A8	PLBD1	Phospholipase B-like 1	-	-	-	-	-	-	-	-	-	-	-	-	-	Q6P4A8
Q6P6C2	ALKBH5 ABH5 OFOXD1	RNA demethylase ALKBH5	-	-	-	-	-	-	-	-	-	-	-	-	-	Q6P6C2
Q6PK04	CCDC137 cPERP-B	Coiled-coil domain-containing protein 137	-	-	-	-	-	-	-	-	-	-	-	-	-	Q6PK04
Q6ZUT1	NKAPD1 C11orf57	Uncharacterized protein NKAPD1	-	-	-	-	-	-	-	-	-	-	-	-	-	Q6ZUT1
Q70UQ0	IKBIP IKIP	Inhibitor of nuclear factor kappa-B kinase-interacting protein	-	-	-	-	-	-	-	-	-	-	Q70UQ0	-	-	-
Q71U36	TUBA1A TUBA3	Tubulin alpha-1A chain	-	-	-	-	-	-	-	-	-	-	-	Q71U36	-	-
Q76FK4	NOL8 C9orf34 NOP132	Nucleolar protein 8	-	-	-	-	-	-	-	-	-	-	-	-	-	Q76FK4
Q7KZ85	SUPT6H KIAA0162 SPT6H	Transcription elongation factor SPT6	-	-	-	-	-	-	-	-	-	-	-	-	-	Q7KZ85
Q7Z434	MAVS IPS1 KIAA1271 VISA	Mitochondrial antiviral-signaling protein	-	-	Q7Z434	capsid protein	-	-	-	-	-	-	-	-	-	-
Q7Z6I8	C5orf24	UPF0461 protein C5orf24	-	-	-	-	-	-	-	-	-	-	-	-	-	Q7Z6I8
Q86SX6	GLRX5 C14orf87	Glutaredoxin-related protein 5, mitochondrial	-	-	-	-	-	-	Q86SX6	Q86SX6	-	-	-	-	-	-
Q86T03	PIP4P1 C14orf9 TMEM55B	Type 1 phosphatidylinositol 4,5-bisphosphate 4-phosphatase	-	-	-	-	-	-	-	-	-	-	-	-	-	Q86T03
Q86TB9	PATL1 OK/KNS-cl.5	Protein PAT1 homolog 1	-	-	-	-	-	-	-	-	-	-	-	-	-	Q86TB9
Q86U42	PABPN1 PAB2 PABP2	Polyadenylate-binding protein 2	Q86U42	Two Hybrid Test (MI:0018)	-	-	-	Q86U42	-	-	-	Q86U42	-	-	-	-
Q86UC2	RSPH3 RSHL2 RSP3	Radial spoke head protein 3 homolog	-	-	-	-	-	-	-	-	-	-	-	-	-	Q86UC2
Q86UE6	LRRTM1 UNQ675/PRO1309	Leucine-rich repeat transmembrane neuronal protein 1	Q86UE6	Two Hybrid Test (MI:0018)	Q86UE6	capsid protein	-	Q86UE6	-	-	-	Q86UE6	-	-	-	-
Q86W42	THOC6 WDR58 PSEC0006	THO complex subunit 6 homolog	-	-	-	-	-	-	-	-	-	-	-	-	-	Q86W42
Q86Y07	VRK2	Serine/threonine-protein kinase VRK2	-	-	-	-	-	-	-	-	-	-	-	-	-	Q86Y07
Q8IVW6	ARID3B BDP DRIL2	AT-rich interactive domain-containing protein 3B	-	-	-	-	-	-	-	-	-	-	-	-	-	Q8IVW6
Q8IWX8	CHERP DAN26 SCAF6	Calcium homeostasis endoplasmic reticulum protein	-	-	-	-	-	-	-	-	-	-	-	-	-	Q8IWX8

Q8IZI9	IFNL3 IL28B IL28C ZCYTO22	Interferon lambda-3	-	-	Q8IZI9	capsid protein	-	-	-	-	-	-	-	-	-	-
Q8N1G2	CMTR1 FTSJD2 KIAA0082	Cap-specific mRNA	-	-	-	-	-	-	-	-	-	-	-	-	-	Q8N1G2
Q8N1G4	MTR1 LRRC47 KIAA1185	Leucine-rich repeat-containing protein 47	-	-	-	-	-	-	-	-	-	-	-	-	-	Q8N1G4
Q8N2S1	LTBP4	Latent-transforming growth factor beta-binding protein 4	Q8N2S1	Two Hybrid Test (MI:0018)	-	-	-	Q8N2S1	-	-	-	-	-	-	-	-
Q8N3V2	DKFZp451G125	Nuclear receptor subfamily 4 group A member 1	-	-	Q8N3V2	capsid protein	-	-	-	-	-	-	-	-	-	-
Q8NBJ4	GOLM1 C9orf155 GOLPH2 PSEC0242 UNQ686/PRO1326	Golgi membrane protein 1	-	-	Q8NBJ4	' CORE PROTEIN, N	-	-	-	-	-	-	-	-	-	-
Q8NE86	MCU C10orf42 CCDC109A	Calcium uniporter protein, mitochondrial	-	-	Q8NE86	CORE PROTEIN	-	-	-	-	-	-	-	-	-	-
Q8NEB9	PIK3C3 VPS34	Phosphatidylinositol 3-kinase catalytic subunit type 3	-	-	Q8NEB9	capsid protein	-	-	-	-	-	-	-	-	-	-
Q8NEF9	SRFBP1	Serum response factor-binding protein 1	-	-	-	-	-	-	-	-	-	-	-	-	-	Q8NEF9
Q8NET6	CHST13	Carbohydrate sulfotransferase 13	-	-	-	-	-	-	-	-	-	-	-	-	-	Q8NET6
Q8NG48	LINS LINS1 WINS1	Protein Lines homolog 1	-	-	-	-	-	-	-	-	-	-	-	-	Q8NG48	-
Q8TCT9	HM13 H13 IMP1 PSL3 SPP MSTP086	Minor histocompatibility antigen H13	-	-	Q8TCT9	capsid protein	-	-	-	-	Q8TCT9	-	-	-	-	-
Q8WUD4	CCDC12	Coiled-coil domain-containing protein 12	-	-	-	-	-	-	-	-	-	-	-	-	-	Q8WUD4
Q92499	DDX1	ATP-dependent RNA helicase DDX1	-	-	-	-	-	-	-	-	-	-	Q92499	-	-	-
Q92576	PHF3 KIAA0244	PHD finger protein 3	-	-	-	-	-	-	-	-	-	-	-	-	-	Q92576
Q92793	CREBBP CBP	CREB-binding protein	Q92793	GST pull-down (MI:0059); Western blot (MI:0113); Affinity Chromatography (MI:0004)	Q92793	capsid protein	Q92793	-	-	-	-	Q92793	-	-	-	-
Q92878	RAD50	DNA repair protein RAD50	-	-	-	-	-	-	-	-	-	-	-	-	-	Q92878
Q92925	SMARCD2 BAF60B PRO2451	SWI/SNF-related matrix-associated actin-dependent regulator of chromatin subfamily D member 2	-	-	-	-	-	-	-	-	-	-	-	-	-	Q92925
Q93045	STMN2 SCG10 SCGN10	Stathmin-2	-	-	-	-	-	-	-	-	-	-	-	-	-	Q93045
Q969G3	SMARCE1 BAF57	SWI/SNF-related matrix-associated actin-dependent regulator of chromatin subfamily E member 1	-	-	-	-	-	-	-	-	-	-	-	-	-	Q969G3
Q969X0	RILPL2 RLP2	RILP-like protein 2	-	-	-	-	-	-	Q969X0	Q969X0	-	-	-	-	-	-
Q96AG4	LRRC59 PRO1855	Leucine-rich repeat-containing protein 59	-	-	-	-	-	-	-	-	-	-	-	-	-	Q96AG4
Q96CW1	AP2M1 CLAPM1 KIAA0109	AP-2 complex subunit mu	-	-	Q96CW1	capsid protein	-	-	-	-	-	-	-	-	-	-
Q96DH6	MSI2	RNA-binding protein Musashi homolog 2	-	-	-	-	-	-	-	-	-	-	-	-	Q96DH6	-
Q96DI7	SNRNP40 PRP8BP SFP38 WDR57	U5 small nuclear ribonucleoprotein 40 kDa protein	-	-	-	-	-	-	-	-	-	-	-	-	-	Q96DI7
Q96DV4	MRPL38 HSPC262	Large ribosomal subunit protein mL38	-	-	-	-	-	-	-	-	-	-	-	-	Q96DV4	-
Q96EP0	RNF31 ZIBRA	E3 ubiquitin-protein ligase RNF31	Q96EP0	Two Hybrid Test (MI:0018)	-	-	-	Q96EP0	-	-	-	Q96EP0	-	-	-	-
Q96EU6	RRP36 C6orf153 HSPC253	Ribosomal RNA processing protein 36 homolog	-	-	-	-	-	-	-	-	-	-	-	-	-	Q96EU6
Q96FX7	TRMT61A C14orf172 TRM61	tRNA (adenine(58)-N(1))-methyltransferase catalytic subunit TRMT61A	-	-	-	-	-	-	-	-	-	-	-	-	-	Q96FX7
Q96HD9	ACY3 ASPA2	N-acyl-aromatic-L-amino acid amidohydrolase	Q96HD9	Two Hybrid Test (MI:0018)	Q96HD9	capsid protein	-	-	-	-	-	Q96HD9	-	-	-	-
Q96JN0	LCOR C10orf12 KIAA1795 MLR2	Ligand-dependent corepressor	-	-	-	-	-	-	-	-	-	-	-	-	-	Q96JN0
Q96L58	B3GALT6	Beta-1,3-galactosyltransferase 6	-	-	-	-	-	-	-	-	-	-	-	-	-	Q96L58
Q96RQ3	MCCC1 MCCA	Methylcrotonoyl-CoA carboxylase subunit alpha, mitochondrial	-	-	-	-	-	-	-	-	-	-	-	-	-	Q96RQ3
Q96T23	RSF1 HBXAP XAP8	Remodeling and spacing factor 1	Q96T23	GST pull-down (MI:0059)	Q96T23	capsid protein	Q96T23	-	-	-	-	Q96T23	-	-	-	-
Q96TC7	RMDN3 FAM82A2 FAM82C PTPIP51 hucep-10 UNQ3122/PRO10274	Regulator of microtubule dynamics protein 3	-	-	-	-	-	-	-	-	-	-	-	-	-	Q96TC7
Q99075	HBEGF DTR DTS HEGFL	Proheparin-binding EGF-like growth factor	-	-	Q99075	capsid protein	-	-	-	-	-	-	-	-	-	-
Q99496	RNF2 BAP1 DING HIPI3 RING1B	E3 ubiquitin-protein ligase RING2	-	-	-	-	-	-	-	-	-	-	-	-	-	Q99496
Q99733	NAP1L4 NAP2	Nucleosome assembly protein 1-like 4	-	-	-	-	-	-	-	-	-	-	Q99733	-	Q99733	Q99733
Q99848	EBNA1BP2 EBP2	Probable rRNA-processing protein EBP2	-	-	-	-	-	-	-	-	-	-	-	-	-	Q99848
Q99941	ATF6B CREBL1 G13	Cyclic AMP-dependent transcription factor ATF-6 beta	-	-	Q99941	capsid protein	-	-	-	-	-	-	-	-	-	-

Q99996	AKAP9 AKAP350 AKAP450	A-kinase anchor protein 9	-	-	-	-	-	-	-	-	-	-	-	-	-	Q99996
Q9BRP8	KIAA0803 WIBG PYM	Partner of Y14 and mago	-	-	-	-	-	-	-	-	-	-	-	-	Q9BRP8	-
Q9BRR8	GPATCH1 ECGP GPATC1	G patch domain-containing protein 1	-	-	-	-	-	-	-	-	-	-	-	-	-	Q9BRR8
Q9BSC4	NOL10	Nucleolar protein 10	-	-	-	-	-	-	-	-	-	-	-	-	-	Q9BSC4
Q9BT25	HAUS8 HICE1	HAUS augmin-like complex subunit 8	-	-	-	-	-	-	-	-	-	-	-	-	-	Q9BT25
Q9BVC6	TMEM109	Transmembrane protein 109	-	-	-	-	-	-	-	-	-	-	Q9BVC6	-	-	-
Q9BW19	KIFC1 HSET KNSL2	Kinesin-like protein KIFC1	-	-	-	-	-	-	-	-	-	-	-	-	-	Q9BW19
Q9BWF3	RBM4 RBM4A	RNA-binding protein 4	-	-	-	-	-	-	-	-	-	-	-	-	-	Q9BWF3
Q9BWH2	FUNDC2 HCBP6 DC44 HCC3 PD03104	FUN14 domain-containing protein 2	Q9BWH2	Two Hybrid Test (MI:0018)	Q9BWH2	capsid protein	Q9BWH2	-	-	-	-	Q9BWH2	-	-	-	-
Q9BXK1	KLF16 BTEB4 NSLP2	Krueppel-like factor 16	-	-	-	-	-	-	-	-	-	-	-	-	-	Q9BXK1
Q9BYN8	MRPS26 C20orf193 RPMS13	Small ribosomal subunit protein mS26	-	-	-	-	-	-	-	-	-	-	-	-	-	Q9BYN8
Q9BYW2	SETD2 HIF1 HYPB KIAA1732 KMT3A SET2 HSPC069	Histone-lysine N-methyltransferase SETD2	Q9BYW2	Two Hybrid Test (MI:0018)	-	-	-	Q9BYW2	-	-	-	Q9BYW2	-	-	-	-
Q9BZ29	DOCK9 KIAA1058	Dedicator of cytokinesis protein 9	-	-	-	-	-	-	-	-	-	-	-	-	Q9BZ29	-
Q9BZZ5	API5 MIG8	Apoptosis inhibitor 5	-	-	-	-	-	-	-	-	-	-	-	-	-	Q9BZZ5
Q9C0C9	UBE2O KIAA1734	(E3-independent) E2 ubiquitin-conjugating enzyme	-	-	-	-	-	-	-	-	-	-	-	-	Q9C0C9	Q9C0C9
Q9GZR7	DDX24	ATP-dependent RNA helicase DDX24	-	-	-	-	-	-	-	-	-	-	-	-	-	Q9GZR7
Q9H147	DNTTIP1 C20orf167 TDIF1	Deoxynucleotidyltransferase terminal-interacting protein 1	-	-	-	-	-	-	-	-	-	-	-	-	-	Q9H147
Q9H2P0	ADNP ADNP1 KIAA0784	Activity-dependent neuroprotector homeobox protein	-	-	-	-	-	-	-	-	-	-	-	-	-	Q9H2P0
Q9H444	CHMP4B C20orf178 SHAX1	Charged multivesicular body protein 4b	-	-	Q9H444	capsid protein	-	-	-	-	-	-	-	-	-	-
Q9H5V9	STEEP1 CXorf56	STING ER exit protein	-	-	-	-	-	-	-	-	-	-	-	-	-	Q9H5V9
Q9H814	PHAX RNUXA	Phosphorylated adapter RNA export protein	-	-	-	-	-	-	-	-	-	-	-	-	-	Q9H814
Q9H8L6	MMRN2 EMILIN3	Multimerin-2	Q9H8L6	Two Hybrid Test (MI:0018)	Q9H8L6	capsid protein	-	Q9H8L6	-	-	-	Q9H8L6	-	-	-	-
Q9HB58	SP110	Sp110 nuclear body protein	Q9HB58	Two Hybrid Test (MI:0018); Coimmunoprecipitation (MI:0019); GST pull-down (MI:0059)	Q9HB58	capsid protein	-	-	-	-	-	Q9HB58	-	-	-	-
Q9HD23	MRS2 HPT MRS2L	Magnesium transporter MRS2 homolog, mitochondrial	-	-	-	-	-	-	-	-	-	-	-	-	Q9HD23	-
Q9NPA8	ENY2 DC6	Transcription and mRNA export factor ENY2	-	-	-	-	-	-	-	-	-	-	-	-	-	Q9NPA8
Q9NPH2	ISYNA1 INO1	Inositol-3-phosphate synthase 1	-	-	Q9NPH2	capsid protein	-	-	-	-	-	-	-	-	-	-
Q9NQ55	PPAN BXDC3 SSF1	Suppressor of SWI4 1 homolog	-	-	-	-	-	-	-	-	-	-	-	-	-	Q9NQ55
Q9NQT5	EXOSC3 RRP40 CGI-102	Exosome complex component RRP40	-	-	-	-	-	-	-	-	-	-	-	-	-	Q9NQT5
Q9NSE2	CISH G18	Cytokine-inducible SH2-containing protein	-	-	Q9NSE2	capsid protein	-	-	-	-	-	-	-	-	-	-
Q9NWU5	MRPL22 MRPL25 RPML25 HSPC158	Large ribosomal subunit protein uL22m	-	-	-	-	-	-	-	-	-	-	-	-	Q9NWU5	-
Q9NX02	NLRP2 NALP2 NBS1 PAN1 PYPAF2	NACHT, LRR and PYD domains-containing protein 2	-	-	Q9NX02	capsid protein	-	-	-	-	-	-	-	-	-	-
Q9NXX6	NSMCE4A C10orf86 PP4762	Non-structural maintenance of chromosomes element 4 homolog A	-	-	-	-	-	-	-	-	-	-	-	-	-	Q9NXX6
Q9NZN9	AIPL1 AIPL2	Aryl-hydrocarbon-interacting protein-like 1	-	-	-	-	-	-	-	-	-	-	-	-	-	Q9NZN9
Q9P015	MRPL15 HSPC145	Large ribosomal subunit protein uL15m	-	-	-	-	-	-	-	-	-	-	-	-	Q9P015	-
Q9P035	HACD3 BIND1 PTPLAD1	Very-long-chain	-	-	-	-	-	-	-	-	-	-	Q9P035	-	-	-
Q9P0L0	VAPA VAP33	Vesicle-associated membrane protein-associated protein A	-	-	Q9P0L0	capsid protein	-	-	-	-	-	-	-	-	-	-
Q9UBX5	FBLN5 DANCE UNQ184/PRO210	Fibulin-5	Q9UBX5	Two Hybrid Test (MI:0018)	-	-	-	Q9UBX5	-	-	-	Q9UBX5	-	-	-	-
Q9UGP8	SEC63 SEC63L	Translocation protein SEC63 homolog	-	-	-	-	-	-	-	-	-	-	Q9UGP8	-	-	-
Q9UGR2	ZC3H7B KIAA1031	Zinc finger CCCH domain-containing protein 7B	-	-	-	-	-	-	-	-	-	-	-	-	-	Q9UGR2
Q9UGY1	NOL12	Nucleolar protein 12	-	-	-	-	-	-	-	-	-	-	-	-	-	Q9UGY1
Q9UHF1	EGFL7 MEGF7 UNQ187/PRO1449	Epidermal growth factor-like protein 7	Q9UHF1	Two Hybrid Test (MI:0018)	-	-	-	Q9UHF1	-	-	-	Q9UHF1	-	-	-	-
Q9UJM8	HAO1 GOX1	2-Hydroxyacid oxidase 1	-	-	Q9UJM8	capsid protein	-	-	-	-	-	-	-	-	-	-

Q9ULW0	TPX2 C20orf1 C20orf2 DIL2 HCA519	Targeting protein for Xklp2	-	-	-	-	-	-	-	-	-	-	-	-	-	Q9ULW0
Q9ULW3	ABT1	Activator of basal transcription 1	-	-	-	-	-	-	-	-	-	-	-	-	-	Q9ULW3
Q9ULX9	MAFF	Transcription factor MafF	-	-	-	-	-	-	-	-	-	-	-	-	-	Q9ULX9
Q9UNL2	SSR3 TRAPG	Translocon-associated protein subunit gamma	-	-	-	-	-	-	-	-	-	-	Q9UNL2	-	-	-
Q9UPY3	DICER1 DICER HERNA KIAA0928	Endoribonuclease Dicer	Q9UPY3	Western blot (MI:0113); Coimmunoprecipitation (MI:0019); Immunofluorescence (MI:0022); Immunostaining (MI:0022); Mutational analysis (MI:0074); Confocal microscopy (MI:0663)	Q9UPY3	capsid protein	Q9UPY3	-	-	-	-	Q9UPY3	-	-	-	-
Q9Y224	RTRAF C14orf166 CGI-99	RNA transcription, translation and transport factor protein	-	-	Q9Y224	capsid protein	-	-	-	-	-	-	Q9Y224	-	-	-
Q9Y262	EIF3L EIF3EIP EIF3S6IP HSPC021 HSPC025 MSTP005	Eukaryotic translation initiation factor 3 subunit L	-	-	-	-	-	-	Q9Y262	Q9Y262	-	-	-	-	-	-
Q9Y291	MRPS33 CGI-139 PTD003	Small ribosomal subunit protein mS33	-	-	-	-	-	-	-	-	-	-	-	-	-	Q9Y291
Q9Y3B4	SF3B6 SAP14 SF3B14 SF3B14A CGI-110 HSPC175 HT006	Splicing factor 3B subunit 6	-	-	-	-	-	-	-	-	-	-	-	-	-	Q9Y3B4
Q9Y3D3	MRPS16 RPMS16 CGI-132	Small ribosomal subunit protein bS16m	-	-	-	-	-	-	-	-	-	-	-	-	Q9Y3D3	Q9Y3D3
Q9Y3D5	MRPS18C CGI-134	Small ribosomal subunit protein bS18m	-	-	-	-	-	-	-	-	-	-	-	-	Q9Y3D5	-
Q9Y3I0	RTCB C22orf28 HSPC117	RNA-splicing ligase RtcB homolog	-	-	-	-	-	-	-	-	-	-	Q9Y3I0	-	-	-
Q9Y5C1	ANGPTL3 ANGPT5 UNQ153/PRO 179	Angiopoietin-related protein 3	-	-	Q9Y5C1	capsid protein	-	-	-	-	-	-	-	-	-	-
Q9Y5V0	ZNF706 HSPC038 PNAS-113	Zinc finger protein 706	-	-	-	-	-	-	-	-	-	-	-	-	-	Q9Y5V0
Q9Y5V3	MAGED1 NRAGE PP2250 PRO2292	Melanoma-associated antigen D1	Q9Y5V3	Two Hybrid Test (MI:0018)	-	-	-	Q9Y5V3	-	-	-	Q9Y5V3	-	-	-	-
Q9Y616	IRAK3	Interleukin-1 receptor-associated kinase 3	-	-	Q9Y616	capsid protein	-	-	-	-	-	-	-	-	-	-
Q9Y676	MRPS18B C6orf14 HSPC183 PTD017	Small ribosomal subunit protein mS40	-	-	-	-	-	-	-	-	-	-	-	-	-	Q9Y676
Q9Y680	FKBP7 FKBP23 UNQ670/PRO 1304	Peptidyl-prolyl cis-trans isomerase FKBP7	Q9Y680	2-DE (MI:0982); Mass spectrometry (MI:0943); Immunoblotting (MI:0113); Immunofluorescence (MI:0022)	Q9Y680	capsid protein	Q9Y680	-	-	-	-	Q9Y680	-	-	-	-
Q9Y694	SLC22A7 NLT OAT2	Solute carrier family 22 member 7	Q9Y694	2-DE (MI:0982); Mass spectrometry (MI:0943); Immunoblotting (MI:0113); Immunofluorescence (MI:0022)	Q9Y694	capsid protein	Q9Y694	-	-	-	-	Q9Y694	-	-	-	-
Q9Y6H1	CHCHD2 C7orf17 AAG10	Coiled-coil-helix-coiled-coil-helix domain-containing protein 2	-	-	-	-	-	-	-	-	-	-	-	-	Q9Y6H1	-

Supplementary Table 2: List of previously reported NS5A interacting partners combined to our list of retrieved NS5A PPIs.

Summary of reported HCV NS5A interacting partners				Database		Literature mining				Y2H			Review	AP-MS		ICC-MS	AP LC-MS/MS	TAP-MS		Our Data	
				HCV pro		Tripathi et al., 2013	Saik et al., 2016		de Chassey et al., 2008	de Chassey et al., 2008	Dolan et al., 2013	Tripathi et al., 2013	Ross-Thriepland & Harris, 2015	Vlaicu et al., 2017	Ramage et al., 2015	Meistermann et al., 2014	Germain et al., 2014	Eberle et al., 2014	Pan et al., 2019	Jad NS5A	NS5A chimeras
Uniprot ID	Gene Name	Gene Names	Protein Name	Uniprot ID of prey	Validation method	Uniprot ID of prey	Uniprot ID of prey	Virus protein	Uniprot ID of prey	Uniprot ID of prey	Uniprot ID of prey	Uniprot ID of prey	Uniprot ID of prey	Uniprot ID of prey	Uniprot ID of prey	Uniprot ID of prey	Uniprot ID of prey	Uniprot ID of prey	Uniprot ID of prey	Uniprot ID of prey	Uniprot ID of prey
A0JLT2	A0JLT2	MED19 LCMR1	Mediator of RNA polymerase II transcription subunit 19	-	-	-	-	-	-	-	-	-	-	-	-	-	-	-	-	-	A0JLT2
A0PJW6	A0PJW6	TMEM223	Transmembrane protein 223	-	-	-	-	-	-	-	-	-	-	-	-	-	-	-	-	A0PJW6	-
A1L4H1	SSC5D	SSC5D	Soluble scavenger receptor cysteine-rich domain-containing protein SSC5D	-	-	A1L4H1	-	-	-	-	-	-	-	-	-	-	-	-	-	-	-
A6NJ78	A6NJ78	METTL15 METT5D1	12S rRNA N4-methylcytidine	-	-	-	-	-	-	-	-	-	-	-	-	-	-	-	-	A6NJ78	-
O00116	O00116	AGPS AAG5	Alkyldihydroxyacetonephosphate synthase, peroxisomal	-	-	-	-	-	-	-	-	-	-	-	-	-	-	-	-	O00116	O00116
O00139	O00139	KIF2A KIF2 KNS2	Kinesin-like protein KIF2A	-	-	-	-	-	-	-	-	-	-	-	-	-	-	-	-	O00139	-
O00148	O00148	DDX39A DDX39	ATP-dependent RNA helicase DDX39A	-	-	-	-	-	-	-	-	-	-	-	-	-	-	-	-	O00148	-
O00165	HAX1	HAX1 HS1BP1	HCLS1-associated protein X-1	-	-	-	-	-	-	-	-	-	-	O00165	-	-	-	-	-	-	-
O00206	TLR4	TLR4	Toll-like receptor 4	-	-	-	O00206	hcv non-structural protein 5a	-	-	-	-	-	-	-	-	-	-	-	-	-
O00231	O00231	PSMD11	26S proteasome non-ATPase regulatory subunit 11	-	-	-	-	-	-	-	-	-	-	-	-	-	-	-	-	O00231	O00231
O00264	O00264	PGRMC1 HPR6.6 PGRMC	Membrane-associated progesterone receptor component 1	-	-	-	-	-	-	-	-	-	-	-	-	-	-	-	-	O00264	O00264
O00410	IPO5	IPO5 KPNB3 RANBP5	Importin-5	O00410	Two Hybrid Test (MI:0018); Coimmunoprecipitation (MI:0019); Affinity Chromatography (MI:0004)	O00410	O00410	hcv non-structural protein 5a	O00410	-	-	-	-	-	-	-	-	-	-	O00410	O00410
O00425	IGF2BP3	IGF2BP3 IMP3 KOC1 VICKZ3	Insulin-like growth factor 2 mRNA-binding protein 3	-	-	-	-	-	-	-	-	-	-	-	-	-	-	-	O00425	O00425	O00425
O00479	O00479	HMGN4 HMG17L3 NHC	High mobility group nucleosome-binding domain-containing protein 4	-	-	-	-	-	-	-	-	-	-	-	-	-	-	-	-	-	O00479
O00483	O00483	NDUFA4	Cytochrome c oxidase subunit NDUFA4	-	-	-	-	-	-	-	-	-	-	-	-	-	-	-	-	O00483	-
O00487	O00487	PSMD14 POH1	26S proteasome non-ATPase regulatory subunit 14	-	-	-	-	-	-	-	-	-	-	-	-	-	-	-	-	-	O00487
O00488	ZNF593	ZNF593 ZT86	Zinc finger protein 593	-	-	-	-	-	-	-	-	-	-	O00488	-	-	-	-	-	-	-
O00499	BIN1	BIN1 AMPHL	Myc box-dependent-interacting protein 1	O00499	Mass spectrometry (MI:0943); Mutational analysis (MI:0074); Coimmunoprecipitation (MI:0019); Colocalization (MI:0403); Affinity Chromatography (MI:0004); Immunostaining (MI:0022); Two Hybrid Test (MI:0018); Confocal microscopy (MI:0663)	O00499	O00499	hcv non-structural protein 5a	O00499	O00499	-	O00499	O00499	O00499	O00499	-	O00499	O00499	-	O00499	O00499
O00505	KPNA3	KPNA3 QIP2	Importin subunit alpha-4	-	-	-	-	-	-	-	-	-	O00505	-	-	-	-	-	-	-	-
O00560	SDCBP	SDCBP MDA9 SYCL	Syntenin-1	-	-	-	-	-	-	-	-	-	-	O00560	-	-	-	-	-	-	-
O00571	O00571	DDX3X DBX DDX3	ATP-dependent RNA helicase DDX3X	-	-	-	-	-	-	-	-	-	-	-	-	-	-	-	-	-	O00571
O00767	O00767	SCD FADS5 SCD1 SCDOS	Stearoyl-CoA desaturase	-	-	-	-	-	-	-	-	-	-	-	-	-	-	-	-	-	O00767
O14556	O14556	GAPDHS GAPD2 GAPDH2 GAPDS HSD-35 HSD35	Glyceraldehyde-3-phosphate dehydrogenase, testis-specific	-	-	-	-	-	-	-	-	-	-	-	-	-	-	-	-	O14556	-
O14579	COPE	COPE	Coatomer subunit epsilon	-	-	-	-	-	-	-	-	-	-	O14579	-	-	-	-	-	-	-
O14646	CHD1	CHD1	Chromodomain-helicase-DNA-binding protein 1	-	-	-	-	-	-	-	-	-	-	O14646	-	-	-	-	-	-	-
O14732	IMPA2	IMPA2 IMP.18P	Inositol monophosphatase 2	-	-	-	-	-	-	-	-	-	-	O14732	-	-	-	-	-	-	-
O14734	O14734	ACOT8 ACTEIII PTE1	Acyl-coenzyme A thioesterase 8	-	-	-	-	-	-	-	-	-	-	-	-	-	-	-	-	O14734	-

O14737	PDCD5	PDCD5 TFAR19	Programmed cell death protein 5	-	-	-	-	-	-	-	-	-	-	-	-	-	-	O14737	-	-	-
O14745	O14745	NHERF1 NHERF SLC9A3R1	Na	-	-	-	-	-	-	-	-	-	-	-	-	-	-	-	-	O14745	-
O14757	O14757	CHEK1 CHK1	Serine/threonine-protein kinase Chk1	-	-	-	-	-	-	-	-	-	-	-	-	-	-	-	-	O14757	-
O14763	TNFRSF10B	TNFRSF10B DR5 KILLER TRAILR2 TRICK2 ZTNFR9 UNQ160/PRO186	Tumor necrosis factor receptor superfamily member 10B	-	-	-	-	-	-	-	-	-	-	O14763	-	-	-	-	-	-	-
O14773	O14773	TPP1 CLN2 GIG1 UNQ267/PRO304	Tripeptidyl-peptidase 1	-	-	-	-	-	-	-	-	-	-	-	-	-	-	-	-	O14773	-
O14776	O14776	TCERG1 CA150 TAF2S	Transcription elongation regulator 1	-	-	-	-	-	-	-	-	-	-	-	-	-	-	-	-	-	O14776
O14802	POLR3A	POLR3A	DNA-directed RNA polymerase III subunit RPC1	-	-	-	-	-	-	-	-	-	-	O14802	-	-	-	-	-	-	-
O14818	O14818	PSMA7 HSPC	Proteasome subunit alpha type-7	-	-	-	-	-	-	-	-	-	-	-	-	-	-	-	-	-	O14818
O14828	O14828	SCAMP3 C1orf3 PROPIN1	Secretory carrier-associated membrane protein 3	-	-	-	-	-	-	-	-	-	-	-	-	-	-	-	-	O14828	O14828
O14832	O14832	PHYH PAHX	Phytanoyl-CoA dioxygenase, peroxisomal	-	-	-	-	-	-	-	-	-	-	-	-	-	-	-	-	-	O14832
O14880	MGST3	MGST3	Glutathione S-transferase 3, mitochondrial	-	-	-	-	-	-	-	-	-	-	O14880	-	-	-	-	-	-	-
O14920	IKBKB	IKBKB IKKB	Inhibitor of nuclear factor kappa-B kinase subunit beta	-	-	-	O14920	hcv ns 5	-	-	-	-	-	-	-	-	-	-	-	-	-
O14925	TIMM23	TIMM23 TIM23	Mitochondrial import inner membrane translocase subunit Tim23	-	-	-	-	-	-	-	-	-	-	O14925	-	-	-	-	-	-	O14925
O14949	O14949	UQCRQ	Cytochrome b-c1 complex subunit 8	-	-	-	-	-	-	-	-	-	-	-	-	-	-	-	-	O14949	-
O14980	XPO1	XPO1 CRM1	Exportin-1	-	-	-	-	-	-	-	-	-	-	O14980	-	-	-	-	-	O14980	O14980
O15015	ZNF646	ZNF646 KIAA0296	Zinc finger protein 646	O15015	Two Hybrid Test (MI:0018)	O15015	-	-	-	O15015	-	-	-	-	-	-	-	-	-	-	-
O15018	PDZD2	PDZD2 AIPC KIAA0300 PDZK3	PDZ domain-containing protein 2	-	-	-	O15018	hcv non-structural protein 5a	-	-	-	-	-	-	-	-	-	-	-	-	-
O15027	SEC16A	SEC16A KIAA0310 SEC16 SEC16L	Protein transport protein Sec16A	-	-	-	-	-	-	-	-	-	-	O15027	-	-	-	-	-	-	-
O15042	O15042	U2SURP KIAA0332 SR140	U2 snRNP-associated SURP motif-containing protein	-	-	-	-	-	-	-	-	-	-	-	-	-	-	-	-	-	O15042
O15127	O15127	SCAMP2	Secretory carrier-associated membrane protein 2	-	-	-	-	-	-	-	-	-	-	-	-	-	-	-	-	O15127	-
O15169	AXIN1	AXIN1 AXIN	Axin-1	O15169	Two Hybrid Test (MI:0018)	O15169	-	-	-	O15169	-	-	-	-	-	-	-	-	-	-	-
O15173	PGRMC2	PGRMC2 DG6 PMBP	Membrane-associated progesterone receptor component 2	-	-	-	-	-	-	-	-	-	-	-	-	-	-	O15173	-	-	O15173
O15197	EPHB6	EPHB6	Ephrin type-B receptor 6	-	-	-	-	-	-	-	-	O15197	-	-	-	-	-	-	-	-	-
O15228	O15228	GNPAT DAPAT DHAPAT	Dihydroxyacetone phosphate acyltransferase	-	-	-	-	-	-	-	-	-	-	-	-	-	-	-	-	O15228	-
O15260	O15260	SURF4 SURF-4	Surfeit locus protein 4	-	-	-	-	-	-	-	-	-	-	-	-	-	-	-	-	-	O15260
O15269	SPTLC1	SPTLC1 LCB1	Serine palmitoyltransferase 1	-	-	-	-	-	-	-	-	-	-	O15269	-	-	-	-	-	-	O15269
O15270	SPTLC2	SPTLC2 KIAA0526 LCB2	Serine palmitoyltransferase 2	-	-	-	-	-	-	-	-	-	-	-	-	-	-	O15270	-	-	-
O15400	O15400	STX7	Syntaxin-7	-	-	-	-	-	-	-	-	-	-	-	-	-	-	-	-	O15400	O15400
O15479	O15479	MAGEB2	Melanoma-associated antigen B2	-	-	-	-	-	-	-	-	-	-	-	-	-	-	-	-	-	O15479
O15530	PDPK1	PDPK1 PDK1	3-phosphoinositide-dependent protein kinase 1	O15530	GST pull-down (MI:0059); Kinase assay (MI:0424) (MI:0424)	O15530	O15530	hcv non-structural protein 5a	O15530	-	-	-	-	-	-	-	-	-	-	-	-
O43143	DHX15	DHX15 DBP1 DDX15	ATP-dependent RNA helicase DHX15	-	-	-	-	-	-	-	-	-	-	-	-	-	-	-	O43143	-	-

O43169	O43169	CYB5B CYB5M OMB5	Cytochrome b5 type B	-	-	-	-	-	-	-	-	-	-	-	-	-	-	-	-	-	O43169
O43175	PHGDH	PHGDH PGDH3	D-3-phosphoglycerate dehydrogenase	-	-	-	-	-	-	-	-	-	-	-	-	-	-	O43175	-	O43175	O43175
O43242	O43242	PSMD3	26S proteasome non-ATPase regulatory subunit 3	-	-	-	-	-	-	-	-	-	-	-	-	-	-	-	-	-	O43242
O43290	O43290	SART1	U4/U6.U5 tri-snRNP-associated protein 1	-	-	-	-	-	-	-	-	-	-	-	-	-	-	-	-	-	O43290
O43324	EEF1E1	EEF1E1 AIMP3 P18	Eukaryotic translation elongation factor 1 epsilon-1	-	-	-	-	-	-	-	-	-	-	O43324	-	-	-	-	-	-	O43324
O43390	HNRNPR	HNRNPR HNRPR	Heterogeneous nuclear ribonucleoprotein R	-	-	-	-	-	-	-	-	-	-	-	-	-	-	-	O43390	-	-
O43396	TXNL1	TXNL1 TRP32 TXL TXNL	Thioredoxin-like protein 1	-	-	-	-	-	-	-	-	-	-	O43396	-	-	-	-	-	-	-
O43399	TPD52L2	TPD52L2	Tumor protein D54	-	-	-	-	-	-	-	-	-	-	-	-	-	-	O43399	-	O43399	-
O43505	O43505	B4GAT1 B3GNT1 B3GNT6	Beta-1,4-glucuronyltransferase 1	-	-	-	-	-	-	-	-	-	-	-	-	-	-	-	-	O43505	O43505
O43592	XPOT	XPOT	Exportin-T	-	-	-	-	-	-	-	-	-	-	O43592	-	-	-	-	-	-	-
O43734	O43734	TRAF3IP2 C6orf2 C6orf4 C6orf5 C6orf6	E3 ubiquitin ligase TRAF3IP2	-	-	-	-	-	-	-	-	-	-	-	-	-	-	-	-	-	O43734
O43772	O43772	SLC25A20 CAC CACT	Mitochondrial carnitine/acylcarnitine carrier protein	-	-	-	-	-	-	-	-	-	-	-	-	-	-	-	-	O43772	O43772
O43809	NUDT21	NUDT21 CFIM25 CPSF25 CPSF5	Cleavage and polyadenylation specificity factor subunit 5	-	-	-	-	-	-	-	-	-	-	-	-	-	-	-	O43809	O43809	-
O60264	O60264	SMARCA5 SNF2H WCRF135	SWI/SNF-related matrix-associated actin-dependent regulator of chromatin subfamily A member 5	-	-	-	-	-	-	-	-	-	-	-	-	-	-	-	-	O60264	-
O60427	O60427	FADS1 FADSD5	Acyl-CoA	-	-	-	-	-	-	-	-	-	-	-	-	-	-	-	-	O60427	-
O60488	O60488	ACSL4 ACS4 FACL4 LACS4	Long-chain-fatty-acid--CoA ligase 4	-	-	-	-	-	-	-	-	-	-	-	-	-	-	-	-	O60488	O60488
O60493	SNX3	SNX3	Sorting nexin-3	-	-	-	-	-	-	-	-	-	-	O60493	-	-	-	-	-	-	-
O60504	SORBS3	SORBS3 SCAM1	Vinexin	O60504	Two Hybrid Test (MI:0018)	O60504	-	-	-	O60504	-	-	-	O60504	-	-	-	-	-	-	-
O60506	SYNCRIP	SYNCRIP HNRPQ NSAP1	Heterogeneous nuclear ribonucleoprotein Q	-	-	-	-	-	-	-	-	-	-	-	-	-	-	-	O60506	-	O60506
O60603	TLR2	TLR2 TIL4	Toll-like receptor 2	-	-	-	O60603	hcv non-structural protein 5a	-	-	-	-	-	-	-	-	-	-	-	-	-
O60610	DIAPH1	DIAPH1 DIAP1	Protein diaphanous homolog 1	-	-	-	-	-	-	-	-	-	-	O60610	-	-	-	-	-	-	-
O60664	PLIN3	PLIN3 M6PRBP1 TIP47	Perilipin-3	-	-	-	O60664	hcv non-structural protein 5a	-	-	-	-	O60664	-	-	-	-	-	-	-	-
O60669	O60669	SLC16A7 MCT2	Monocarboxylate transporter 2	-	-	-	-	-	-	-	-	-	-	-	-	-	-	-	-	O60669	-
O60701	O60701	UGDH	UDP-glucose 6-dehydrogenase	-	-	-	-	-	-	-	-	-	-	-	-	-	-	-	-	O60701	O60701
O60716	O60716	CTNND1 KIAA0384	Catenin delta-1	-	-	-	-	-	-	-	-	-	-	-	-	-	-	-	-	O60716	-
O60828	PQBP1	PQBP1 NPW38 JM26	Polyglutamine-binding protein 1	-	-	-	-	-	-	-	-	-	-	O60828	-	-	-	-	-	-	-
O60884	O60884	DNAJA2 CPR3 HIRIP4	DnaJ homolog subfamily A member 2	-	-	-	-	-	-	-	-	-	-	-	-	-	-	-	-	O60884	O60884
O75116	ROCK2	ROCK2 KIAA0619	Rho-associated protein kinase 2	-	-	-	-	-	-	-	-	-	-	O75116	-	-	-	-	-	-	-
O75170	PPP6R2	PPP6R2 KIAA0685 PP6R2 SAPS2	Serine/threonine-protein phosphatase 6 regulatory subunit 2	-	-	-	-	-	-	-	-	-	-	O75170	-	-	-	-	-	-	-
O75190	DNAJB6	DNAJB6 HSJ2 MRJ MSJ1	DnaJ homolog subfamily B member 6	-	-	-	-	-	-	-	-	-	-	O75190	-	-	-	-	-	-	-

O75306	O75306	NDUFS2	NADH dehydrogenase [ubiquinone] iron-sulfur protein 2, mitochondrial	-	-	-	-	-	-	-	-	-	-	-	-	-	-	-	-	O75306	-
O75340	O75340	PDCD6 ALG2	Programmed cell death protein 6	-	-	-	-	-	-	-	-	-	-	-	-	-	-	-	-	O75340	-
O75347	TBCA	TBCA	Tubulin-specific chaperone A	-	-	-	-	-	-	-	-	-	-	-	-	-	-	-	O75347	-	-
O75367	MACROH2A1	MACROH2A1 H2AFY	Core histone macro-H2A.1	-	-	-	O75367	hcv non-structural protein 5a	-	-	-	-	-	-	-	-	-	-	-	-	-
O75380	O75380	NDUFS6	NADH dehydrogenase [ubiquinone] iron-sulfur protein 6, mitochondrial	-	-	-	-	-	-	-	-	-	-	-	-	-	-	-	-	O75380	-
O75396	SEC22B	SEC22B SEC22L1	Vesicle-trafficking protein SEC22b	-	-	-	-	-	-	-	-	-	-	O75396	-	-	-	-	-	O75396	O75396
O75400	PRPF40A	PRPF40A FBP11 FLAF1 FNBP3 HIP10 HYPA HSPC225	Pre-mRNA-processing factor 40 homolog A	-	-	-	-	-	-	-	-	-	-	-	-	-	-	-	O75400	-	-
O75431	O75431	MTX2	Metaxin-2	-	-	-	-	-	-	-	-	-	-	-	-	-	-	-	-	-	O75431
O75477	ERLIN1	ERLIN1 C10orf69 KE04 KEO4 SPFH1	Erlin-1	-	-	-	O75477	hcv ns 5	-	-	-	-	-	O75477	-	-	-	-	-	-	O75477
O75489	O75489	NDUFS3	NADH dehydrogenase [ubiquinone] iron-sulfur protein 3, mitochondrial	-	-	-	-	-	-	-	-	-	-	-	-	-	-	-	-	O75489	O75489
O75521	O75521	ECI2 DRS1 HCA88 PECI	Enoyl-CoA delta isomerase 2	-	-	-	-	-	-	-	-	-	-	-	-	-	-	-	-	O75521	-
O75533	O75533	SF3B1 SAP155	Splicing factor 3B subunit 1	-	-	-	-	-	-	-	-	-	-	-	-	-	-	-	-	-	O75533
O75600	O75600	GCAT KBL	2-amino-3-ketobutyrate coenzyme A ligase, mitochondrial	-	-	-	-	-	-	-	-	-	-	-	-	-	-	-	-	-	O75600
O75607	NPM3	NPM3	Nucleoplasmin-3	-	-	-	-	-	-	-	-	-	-	O75607	-	-	-	-	-	-	-
O75643	SNRNP200	SNRNP200 ASCC3L1 BRR2 HELIC2 KIAA0788	U5 small nuclear ribonucleoprotein 200 kDa helicase	-	-	-	-	-	-	-	-	-	-	-	-	-	-	-	O75643	-	-
O75663	TIPRL	TIPRL	TIP41-like protein	-	-	-	-	-	-	-	-	-	-	O75663	-	-	-	-	-	-	-
O75694	NUP155	NUP155 KIAA0791	Nuclear pore complex protein Nup155	-	-	-	-	-	-	-	-	-	-	O75694	-	-	-	-	-	-	-
O75844	O75844	ZMPSTE24 FACE1 STE24	CAAX prenyl protease 1 homolog	-	-	-	-	-	-	-	-	-	-	-	-	-	-	-	-	O75844	O75844
O75874	O75874	IDH1 PICD	Isocitrate dehydrogenase [NADP] cytoplasmic	-	-	-	-	-	-	-	-	-	-	-	-	-	-	-	-	-	O75874
O75907	DGAT1	DGAT1 AGRP1 DGAT	Diacylglycerol O-acyltransferase 1	-	-	-	O75907	hcv non-structural protein 5a	-	-	-	-	O75907	-	-	-	-	-	-	-	-
O75947	O75947	ATP5PD ATP5H My032	ATP synthase subunit d, mitochondrial	-	-	-	-	-	-	-	-	-	-	-	-	-	-	-	-	O75947	O75947
O75964	O75964	ATP5MG ATP5L	ATP synthase subunit g, mitochondrial	-	-	-	-	-	-	-	-	-	-	-	-	-	-	-	-	O75964	O75964
O76024	O76024	WFS1	Wolframin	-	-	-	-	-	-	-	-	-	-	-	-	-	-	-	-	O76024	-
O76031	O76031	CLPX	ATP-dependent Clp protease ATP-binding subunit clpX-like, mitochondrial	-	-	-	-	-	-	-	-	-	-	-	-	-	-	-	-	O76031	O76031
O94766	O94766	B3GAT3	Galactosylgalactosylxylosylprotein 3-beta-glucuronosyltransferase 3	-	-	-	-	-	-	-	-	-	-	-	-	-	-	-	-	O94766	-
O94782	O94782	USP1	Ubiquitin carboxyl-terminal hydrolase 1	-	-	-	-	-	-	-	-	-	-	-	-	-	-	-	-	-	O94782
O94822	LTN1	LTN1 C21orf10 C21orf98 KIAA0714 RNF160 ZNF294 HSPC087	E3 ubiquitin-protein ligase listerin	-	-	-	-	-	-	-	-	-	-	O94822	-	-	-	-	-	-	-
O94826	O94826	TOMM70 KIAA0719 TOM70 TOMM70A	Mitochondrial import receptor subunit TOM70	-	-	-	-	-	-	-	-	-	-	-	-	-	-	-	-	O94826	O94826

O94855	SEC24D	SEC24D KIAA0755	Protein transport protein Sec24D	-	-	-	-	-	-	-	-	-	-	O94855	-	-	-	-	-	-	-
O94875	SORBS2	SORBS2 ARGBP2 KIAA0777	Sorbin and SH3 domain-containing protein 2	O94875	Two Hybrid Test (MI:0018); Co-affinity purification (MI:0025)	O94875	O94875	hcv non-structural protein 5a	-	O94875	-	-	-	-	-	-	-	-	-	-	-
O94905	ERLIN2	ERLIN2 C8orf2 SPFH2 UNQ2441/PRO5003/PRO9924	Erlin-2	-	-	-	-	-	-	-	-	-	-	O94905	-	-	-	-	-	O94905	-
O94966	USP19	USP19 KIAA0891 ZMYND9	Ubiquitin carboxyl-terminal hydrolase 19	O94966	Two Hybrid Test (MI:0018)	O94966	O94966	hcv non-structural protein 5a	-	O94966	-	-	-	O94966	O94966	O94966	O94966	O94966	-	O94966	-
O95070	O95070	YIF1A 54TM HYIF1P YIF1	Protein YIF1A	-	-	-	-	-	-	-	-	-	-	-	-	-	-	-	-	O95070	-
O95071	UBR5	UBR5 EDD EDD1 HYD KIAA0896	E3 ubiquitin-protein ligase UBR5	-	-	-	-	-	-	-	-	-	-	O95071	-	-	-	-	-	-	-
O95168	O95168	NDUFB4	NADH dehydrogenase [ubiquinone] 1 beta subcomplex subunit 4	-	-	-	-	-	-	-	-	-	-	-	-	-	-	-	-	O95168	O95168
O95178	O95178	NDUFB2	NADH dehydrogenase [ubiquinone] 1 beta subcomplex subunit 2, mitochondrial	-	-	-	-	-	-	-	-	-	-	-	-	-	-	-	-	O95178	-
O95182	O95182	NDUFA7	NADH dehydrogenase [ubiquinone] 1 alpha subcomplex subunit 7	-	-	-	-	-	-	-	-	-	-	-	-	-	-	-	-	O95182	-
O95197	RTN3	RTN3 ASYIP NSPL2	Reticulon-3	-	-	-	-	-	-	-	O95197	-	-	-	-	-	-	-	-	-	-
O95202	O95202	LETM1	Mitochondrial proton/calcium exchanger protein	-	-	-	-	-	-	-	-	-	-	-	-	-	-	-	-	O95202	-
O95232	LUC7L3	LUC7L3 CREAP1 CROP O48	Luc7-like protein 3	-	-	-	-	-	-	-	-	-	-	-	-	-	-	-	O95232	-	-
O95249	O95249	GOSR1 GS28	Golgi SNAP receptor complex member 1	-	-	-	-	-	-	-	-	-	-	-	-	-	-	-	-	O95249	O95249
O95292	VAPB	VAPB UNQ484/PRO983	Vesicle-associated membrane protein-associated protein B/C	O95292	Coimmunoprecipitation (MI:0019); Mutational analysis (MI:0074)	O95292	O95292	hcv non-structural protein 5a	O95292	-	-	O95292	O95292	-	-	-	O95292	O95292	-	O95292	O95292
O95299	O95299	NDUFA10	NADH dehydrogenase [ubiquinone] 1 alpha subcomplex subunit 10, mitochondrial	-	-	-	-	-	-	-	-	-	-	-	-	-	-	-	-	O95299	O95299
O95340	PAPSS2	PAPSS2 ATPSK2	Bifunctional 3'-phosphoadenosine 5'-phosphosulfate synthase 2	-	-	-	-	-	-	-	-	-	-	O95340	-	-	-	-	-	-	-
O95373	O95373	IPO7 RANBP7	Importin-7	-	-	-	-	-	-	-	-	-	-	-	-	-	-	-	-	O95373	-
O95427	O95427	PIGN MCD4	GPI ethanolamine phosphate transferase 1	-	-	-	-	-	-	-	-	-	-	-	-	-	-	-	-	-	O95427
O95433	AHSA1	AHSA1 C14orf3 HSPC322	Activator of 90 kDa heat shock protein ATPase homolog 1	O95433	Two Hybrid Test (MI:0018)	O95433	O95433	hcv non-structural protein 5a	-	-	-	-	-	-	-	-	-	-	-	-	-
O95470	O95470	SGPL1 KIAA1252	Sphingosine-1-phosphate lyase 1	-	-	-	-	-	-	-	-	-	-	-	-	-	-	-	-	O95470	-
O95563	O95563	MPC2 BRP44	Mitochondrial pyruvate carrier 2	-	-	-	-	-	-	-	-	-	-	-	-	-	-	-	-	O95563	-
O95573	O95573	ACSL3 ACS3 FACL3 LACS3	Fatty acid CoA ligase Acsl3	-	-	-	-	-	-	-	-	-	-	-	-	-	-	-	-	O95573	O95573
O95613	O95613	PCNT KIAA0402 PCNT2	Pericentrin	-	-	-	-	-	-	-	-	-	-	-	-	-	-	-	-	O95613	-
O95716	O95716	RAB3D GOV RAB16	Ras-related protein Rab-3D	-	-	-	-	-	-	-	-	-	-	-	-	-	-	-	-	O95716	-
O95747	OXSR1	OXSR1 KIAA1101 OSR1	Serine/threonine-protein kinase OSR1	-	-	-	-	-	-	-	-	-	-	O95747	-	-	-	-	-	-	-
O95757	HSPA4L	HSPA4L APG1 OSP94	Heat shock 70 kDa protein 4L	-	-	-	-	-	-	-	-	-	-	-	-	-	-	O95757	-	-	-
O95786	RIGI	RIGI DDX58	Antiviral innate immune response receptor RIG-I	-	-	-	O95786	hcv ns 5	-	-	-	-	-	-	-	-	-	-	-	-	-
O95816	O95816	BAG2	BAG family molecular chaperone regulator 2	-	-	-	-	-	-	-	-	-	-	-	-	-	-	-	-	O95816	-

O95819	MAP4K4	MAP4K4 HGK KIAA0687 NIK	Mitogen-activated protein kinase kinase kinase kinase 4	-	-	-	-	-	-	-	-	O95819	-	-	-	-	-	-	-	-	-
O95835	LATS1	LATS1 WARTS	Serine/threonine-protein kinase LATS1	-	-	-	-	-	-	-	-	-	O95835	-	-	O95835	-	O95835	-	-	O95835
O95861	BPNT1	BPNT1	3'(2'),5'-bisphosphate nucleotidase 1	-	-	-	-	-	-	-	-	-	-	O95861	-	-	-	-	-	-	-
O95864	FADS2	FADS2	Acyl-CoA 6-desaturase	-	-	-	-	-	-	-	-	-	-	O95864	-	-	-	-	-	O95864	O95864
O95926	O95926	SYF2 CBPIN GCIPIP	Pre-mRNA-splicing factor SYF2	-	-	-	-	-	-	-	-	-	-	-	-	-	-	-	-	O95926	-
O95983	MBD3	MBD3	Methyl-CpG-binding domain protein 3	-	-	-	-	-	-	-	-	-	-	O95983	-	-	-	-	-	-	-
O95992	CH25H	CH25H	Cholesterol 25-hydroxylase	-	-	-	O95992	hcv non-structural protein 5a	-	-	-	-	O95992	-	-	-	-	-	-	-	-
O96000	O96000	NDUFB10	NADH dehydrogenase [ubiquinone] 1 beta subcomplex subunit 10	-	-	-	-	-	-	-	-	-	-	-	-	-	-	-	-	O96000	O96000
O96005	O96005	CLPTM1	Putative lipid scramblase CLPTM1	-	-	-	-	-	-	-	-	-	-	-	-	-	-	-	-	O96005	-
O96008	O96008	TOMM40 C19orf1 PEREC1 TOM40	Mitochondrial import receptor subunit TOM40 homolog	-	-	-	-	-	-	-	-	-	-	-	-	-	-	-	-	O96008	O96008
O96013	O96013	PAK4 KIAA1142	Serine/threonine-protein kinase PAK 4	-	-	-	-	-	-	-	-	-	-	-	-	-	-	-	-	-	O96013
O96017	CHEK2	CHEK2 CDS1 CHK2 RAD53	Serine/threonine-protein kinase Chk2	-	-	-	O96017	hcv ns 5	-	-	-	-	-	-	-	-	-	-	-	-	-
P00167	P00167	CYB5A CYB5	Cytochrome b5	-	-	-	-	-	-	-	-	-	-	-	-	-	-	-	-	P00167	-
P00338	P00338	LDHA PIG19	L-lactate dehydrogenase A chain	-	-	-	-	-	-	-	-	-	-	-	-	-	-	-	-	-	P00338
P00352	P00352	ALDH1A1 ALDC ALDH1 PUMB1	Aldehyde dehydrogenase 1A1	-	-	-	-	-	-	-	-	-	-	-	-	-	-	-	-	-	P00352
P00367	P00367	GLUD1 GLUD	Glutamate dehydrogenase 1, mitochondrial	-	-	-	-	-	-	-	-	-	-	-	-	-	-	-	-	-	P00367
P00374	DHFR	DHFR	Dihydrofolate reductase	-	-	-	-	-	-	-	-	-	-	P00374	-	-	-	-	-	-	-
P00387	P00387	CYB5R3 DIA1	NADH-cytochrome b5 reductase 3	-	-	-	-	-	-	-	-	-	-	-	-	-	-	-	-	P00387	P00387
P00403	P00403	MT-CO2 COII COX2 COXII MTCO2	Cytochrome c oxidase subunit 2	-	-	-	-	-	-	-	-	-	-	-	-	-	-	-	-	P00403	P00403
P00439	P00439	PAH	Phenylalanine-4-hydroxylase	-	-	-	-	-	-	-	-	-	-	-	-	-	-	-	-	P00439	P00439
P00441	SOD1	SOD1	Superoxide dismutase	-	-	-	-	-	-	-	-	-	-	-	-	-	-	P00441	-	-	-
P00491	PNP	PNP NP	Purine nucleoside phosphorylase	-	-	-	-	-	-	-	-	-	-	P00491	-	-	-	-	-	-	-
P00505	GOT2	GOT2 KYAT4	Aspartate aminotransferase, mitochondrial	-	-	-	-	-	-	-	-	-	-	P00505	-	-	-	-	-	-	-
P00533	EGFR	EGFR ERBB ERBB1 HER1	Epidermal growth factor receptor	-	-	-	P00533	NS5A	-	-	-	-	-	P00533	-	-	-	-	-	-	-
P00558	P00558	PGK1 PGKA MIG10 OK/SW-cl.110	Phosphoglycerate kinase 1	-	-	-	-	-	-	-	-	-	-	-	-	-	-	-	-	-	P00558
P00846	MT-ATP6	MT-ATP6 ATP6 ATPASE6 MTATP6	ATP synthase subunit a	-	-	-	-	-	-	-	-	P00846	-	-	-	-	-	-	-	P00846	P00846
P00918	CA2	CA2	Carbonic anhydrase 2	-	-	-	-	-	-	-	-	-	-	P00918	-	-	-	-	-	-	-
P00973	OAS1	OAS1 OIAS	2'-5'-oligoadenylate synthase 1	P00973	GST pull-down (MI:0059); Immunoblotting (MI:0113); Coimmunoprecipitation (MI:0019); Immunofluorescence (MI:0022)	P00973	P00973	hcv non-structural protein 5a	P00973	-	-	-	-	-	-	-	-	-	-	-	-
P01024	C3	C3 CPAMD1	Complement C3	-	-	-	-	-	-	-	-	-	-	P01024	-	-	-	-	-	-	-
P01100	FOS	FOS G0S7	Protein c-Fos	-	-	-	P01100	hcv non-structural protein 5a	-	-	-	-	-	-	-	-	-	-	-	-	-
P01106	MYC	MYC BHLHE39	Myc proto-oncogene protein	-	-	-	P01106	hcv non-structural protein 5a	-	-	-	-	-	-	-	-	-	-	-	-	-
P01112	HRAS	HRAS HRAS1	GTPase HRas	-	-	-	-	-	-	-	-	-	-	P01112	-	-	-	-	-	-	-
P01116	KRAS	KRAS KRAS2 RASK2	GTPase KRas	-	-	-	-	-	-	-	-	-	-	P01116	-	-	-	-	-	-	-
P01344	P01344	IGF2 PP1446	Insulin-like growth factor II	-	-	-	-	-	-	-	-	-	-	-	-	-	-	-	-	-	P01344

P01375	TNF	TNF TNFA TNFSF2	Tumor necrosis factor	-	-	-	P01375	hcv non-structural protein 5a	-	-	-	-	-	-	-	-	-	-	-	-	-
P01562	IFNA1	IFNA1; IFNA13	Interferon alpha-1/13	-	-	-	P01562	hcv non-structural protein 5a	-	-	-	-	-	-	-	-	-	-	-	-	-
P02647	APOA1	APOA1	Apolipoprotein A-I	P02647	Immunofluorescence (MI:0022); Confocal microscopy (MI:0663); Coimmunoprecipitation (MI:0019); Affinity Chromatography (MI:0004); Immunostaining (MI:0022)	P02647	P02647	hcv non-structural protein 5a	P02647	-	-	-	-	-	-	-	-	-	-	-	-	-
P02649	APOE	APOE	Apolipoprotein E	P02649	Two Hybrid Test (MI:0018)	P02649	P02649	hcv non-structural protein 5a	P02649	-	P02649	-	P02649	-	-	-	-	-	-	P02649	P02649
P02652	P02652	APOA2	Apolipoprotein A-II	-	-	-	-	-	-	-	-	-	-	-	-	-	-	-	-	P02652	-
P02675	FGB	FGB	Fibrinogen beta chain	-	-	-	-	-	-	-	P02675	-	-	-	-	-	-	-	-	-	-
P02686	MBP	MBP	Myelin basic protein	-	-	P02686	P02686	hcv non-structural protein 5a	P02686	-	-	-	-	-	-	-	-	-	-	-	-
P02751	FN1	FN1 FN	Fibronectin	-	-	-	-	-	-	-	P02751	-	-	-	-	-	-	-	-	-	-
P02771	AFP	AFP HPAFP	Alpha-fetoprotein	-	-	-	P02771	hcv non-structural protein 5a	-	-	-	-	-	-	-	-	-	-	-	-	P02771
P02786	TFRC	TFRC	Transferrin receptor protein 1	-	-	-	-	-	-	-	-	-	-	P02786	-	-	-	-	-	P02786	P02786
P02794	FTH1	FTH1 FTH FTHL6 OK/SW-cl.84 PIG15	Ferritin heavy chain	P02794	Two Hybrid Test (MI:0018)	P02794	P02794	hcv non-structural protein 5a	P02794	-	-	-	-	-	-	-	-	-	-	-	-
P03372	ESR1	ESR1 ESR NR3A1	Estrogen receptor	-	-	-	P03372	hcv ns 5	-	-	-	-	-	-	-	-	-	-	-	-	-
P03928	P03928	MT-ATP8 ATP8 ATPASE8 MTATP8	ATP synthase protein 8	-	-	-	-	-	-	-	-	-	-	-	-	-	-	-	-	P03928	-
P04035	HMGCR	HMGCR	3-hydroxy-3-methylglutaryl-coenzyme A reductase	-	-	-	-	-	-	-	P04035	-	-	-	-	-	-	-	-	-	-
P04049	RAF1	RAF1 RAF	RAF proto-oncogene serine/threonine-protein kinase	P04049	Affinity Chromatography (MI:0004); Coimmunoprecipitation (MI:0019); Immunofluorescence (MI:0022); Western blot (MI:0113)	P04049	P04049	hcv non-structural protein 5a	P04049	-	-	-	P04049	-	-	-	-	-	-	P04049	-
P04075	ALDOA	ALDOA ALDA	Fructose-bisphosphate aldolase A	-	-	-	-	-	-	-	-	-	-	P04075	-	-	-	-	-	-	P04075
P04083	ANXA1	ANXA1 ANX1 LPC1	Annexin A1	-	-	-	-	-	-	-	-	-	-	P04083	-	-	-	-	-	-	-
P04114	APOB	APOB	Apolipoprotein B-100	P04114	Coimmunoprecipitation (MI:0019)	-	P04114	hcv non-structural protein 5a	-	-	-	-	-	P04114	-	-	-	-	-	-	-
P04196	HRG	HRG	Histidine-rich glycoprotein	-	-	-	-	-	-	-	-	-	-	-	-	-	-	-	P04196	-	-
P04350	P04350	TUBB4A TUBB4 TUBB5	Tubulin beta-4A chain	-	-	-	-	-	-	-	-	-	-	-	-	-	-	-	-	P04350	P04350
P04406	GAPDH	GAPDH GAPD CDABP0047 OK/SW-cl.12	Glyceraldehyde-3-phosphate dehydrogenase	-	-	-	-	-	-	-	-	-	-	-	-	-	-	-	P04406	-	-
P04626	ERBB2	ERBB2 HER2 MLN19 NEU NGL	Receptor tyrosine-protein kinase erbB-2	-	-	-	-	-	-	-	-	-	-	P04626	-	-	-	-	-	-	-
P04637	TP53	TP53 P53	Cellular tumor antigen p53	P04637	Pull-down (MI:0096); Coimmunoprecipitation (MI:0019); Two Hybrid Test (MI:0018); Confocal microscopy (MI:0663); Colocalization (MI:0403); Affinity Chromatography (MI:0004); Immunostaining (MI:0022)	P04637	P04637	hcv non-structural protein 5a	P04637	-	-	-	P04637	P04637	-	-	-	-	-	-	-	-
P04792	HSPB1	HSPB1 HSP27 HSP28	Heat shock protein beta-1	-	-	P04792	P04792	hcv non-structural protein 5a	-	-	-	-	-	-	-	-	-	-	-	-	P04792
P04818	TYMS	TYMS TS OK/SW-cl.29	Thymidylate synthase	-	-	-	-	-	-	-	-	-	-	P04818	-	-	-	-	-	-	-
P04843	P04843	RPN1	Dolichyl-diphosphooligosaccharide--protein glycosyltransferase subunit 1	-	-	-	-	-	-	-	-	-	-	-	-	-	-	-	-	P04843	P04843

P04844	P04844	RPN2	Dolichyl-diphosphooligosaccharide--protein glycosyltransferase subunit 2	-	-	-	-	-	-	-	-	-	-	-	-	-	-	-	-	P04844	P04844
P05023	ATP1A1	ATP1A1	Sodium/potassium-transporting ATPase subunit alpha-1	-	-	-	-	-	-	-	-	-	-	P05023	-	-	-	-	-	P05023	P05023
P05026	ATP1B1	ATP1B1 ATP1B	Sodium/potassium-transporting ATPase subunit beta-1	-	-	-	-	-	-	-	-	-	-	P05026	-	-	-	-	-	-	P05026
P05091	ALDH2	ALDH2 ALDM	Aldehyde dehydrogenase, mitochondrial	-	-	-	-	-	-	-	-	-	-	P05091	-	-	-	-	-	-	-
P05109	P05109	S100A8 CAGA CFAG MRP8	Protein S100-A8	-	-	-	-	-	-	-	-	-	-	-	-	-	-	-	-	P05109	-
P05198	P05198	EIF2S1 EIF2A	Eukaryotic translation initiation factor 2 subunit 1	-	-	-	-	-	-	-	-	-	-	-	-	-	-	-	-	P05198	P05198
P05386	P05386	RPLP1 RRP1	Large ribosomal subunit protein P1	-	-	-	-	-	-	-	-	-	-	-	-	-	-	-	-	-	P05386
P05387	RPLP2	RPLP2 D11S2243E RPP2	Large ribosomal subunit protein P2	-	-	-	-	-	-	-	-	-	-	P05387	-	-	-	-	-	P05387	P05387
P05412	JUN	JUN	Transcription factor Jun	-	-	-	P05412	hcv non-structural protein 5a	-	-	-	-	-	-	-	-	-	-	-	-	-
P05455	SSB	SSB	Lupus La protein	P05455	Coimmunoprecipitation (MI:0019); Affinity Chromatography (MI:0004)	P05455	P05455	hcv non-structural protein 5a	P05455	-	-	-	-	-	-	-	-	P05455	-	-	-
P05556	P05556	ITGB1 FNRB MDF2 MSK12	Integrin beta-1	-	-	-	-	-	-	-	-	-	-	-	-	-	-	-	-	P05556	P05556
P05976	MYL1	MYL1	Myosin light chain 1/3, skeletal muscle isoform	-	-	-	-	-	-	-	-	-	-	P05976	-	-	-	-	-	-	-
P06239	LCK	LCK	Tyrosine-protein kinase Lck	P06239	Coimmunoprecipitation (MI:0019); Affinity Chromatography (MI:0004)	P06239	P06239	hcv non-structural protein 5a	P06239	-	-	-	P06239	-	-	-	-	-	-	-	-
P06241	FYN	FYN	Tyrosine-protein kinase Fyn	P06241	Coimmunoprecipitation (MI:0019); Affinity Chromatography (MI:0004)	P06241	P06241	hcv non-structural protein 5a	P06241	-	-	-	P06241	-	-	-	-	-	-	-	-
P06400	RB1	RB1	Retinoblastoma-associated protein	-	-	-	P06400	hcv ns 5	-	-	-	-	-	-	-	-	-	-	-	-	-
P06454	PTMA	PTMA TMSA	Prothymosin alpha	P06454	Two Hybrid Test (MI:0018)	P06454	P06454	hcv non-structural protein 5a	P06454	-	-	-	-	-	-	-	-	P06454	-	-	-
P06493	CDK1	CDK1 CDC2 CDC28A CDKN1 P34CDC2	Cyclin-dependent kinase 1	P06493	Western blot (MI:0113); Coimmunoprecipitation (MI:0019)	P06493	P06493	hcv non-structural protein 5a	P06493	-	-	-	P06493	-	-	-	-	-	-	-	P06493
P06576	P06576	ATP5F1B ATP5B ATPMB ATPSB	ATP synthase subunit beta, mitochondrial	-	-	-	-	-	-	-	-	-	-	-	-	-	-	-	-	P06576	P06576
P06702	P06702	S100A9 CAGB CFAG MRP14	Protein S100-A9	-	-	-	-	-	-	-	-	-	-	-	-	-	-	-	-	P06702	-
P06730	EIF4E	EIF4E EIF4EL1 EIF4F	Eukaryotic translation initiation factor 4E	-	-	-	P06730	hcv non-structural protein 5a	-	-	-	-	P06730	-	-	-	-	-	-	-	-
P06733	ENO1	ENO1 ENO1L1 MBPB1 MPB1	Alpha-enolase	-	-	-	-	-	-	-	-	-	-	-	-	-	-	P06733	P06733	-	P06733
P06744	P06744	GPI	Glucose-6-phosphate isomerase	-	-	-	-	-	-	-	-	-	-	-	-	-	-	-	-	-	P06744
P06748	NPM1	NPM1 NPM	Nucleophosmin	-	-	-	-	-	-	-	-	-	-	-	-	-	-	-	P06748	-	-
P07099	EPHX1	EPHX1 EPHX EPOX	Epoxide hydrolase 1	-	-	-	-	-	-	-	-	-	-	P07099	-	-	-	-	-	-	-
P07195	LDHB	LDHB	L-lactate dehydrogenase B chain	-	-	-	-	-	-	-	-	-	-	-	-	-	-	P07195	-	-	-
P07237	P07237	P4HB ERBA2L PDI PDIA1 PO4DB	Protein disulfide-isomerase	-	-	-	-	-	-	-	-	-	-	-	-	-	-	-	-	P07237	P07237
P07306	P07306	ASGR1 CLEC4H1	Asialoglycoprotein receptor 1	-	-	-	-	-	-	-	-	-	-	-	-	-	-	-	-	-	P07306
P07339	P07339	CTSD CPSD	Cathepsin D	-	-	-	-	-	-	-	-	-	-	-	-	-	-	-	-	P07339	-
P07355	ANXA2	ANXA2 ANX2 ANX2L4 CAL1H LPC2D	Annexin A2	-	-	P07355	P07355	hcv non-structural protein 5a	-	-	-	-	P07355	-	-	-	-	-	-	-	-

P07437	TUBB	TUBB TUBB5 OK/SW-cl.56	Tubulin beta chain	-	-	-	-	-	-	-	-	-	-	-	-	-	-	P07437	P07437	P07437
P07602	PSAP	PSAP GLBA SAP1	Prosaposin	-	-	-	-	-	-	-	-	-	-	-	-	-	P07602	-	-	-
P07737	P07737	PFN1	Profilin-1	-	-	-	-	-	-	-	-	-	-	-	-	-	-	-	-	P07737
P07814	EPRS1	EPRS1 EPRS GLNS PARS QARS QPRS PIG32	Bifunctional glutamate/proline--tRNA ligase	-	-	-	-	-	-	-	-	-	P07814	-	-	-	-	-	P07814	P07814
P07900	HSP90AA1	HSP90AA1 HSP90A HSPC1 HSPCA	Heat shock protein HSP 90-alpha	P07900	Coimmunoprecipitation (MI:0019)	P07900	P07900	hcv non-structural protein 5a	P07900	-	-	-	-	-	-	-	-	-	P07900	P07900
P07910	HNRNPC	HNRNPC HNRPC	Heterogeneous nuclear ribonucleoproteins C1/C2	-	-	-	-	-	-	-	-	-	P07910	-	-	-	-	-	-	-
P07947	YES1	YES1 YES	Tyrosine-protein kinase Yes	-	-	-	-	-	-	-	-	-	P07947	-	-	-	-	-	-	-
P07948	LYN	LYN JTK8	Tyrosine-protein kinase Lyn	P07948	Coimmunoprecipitation (MI:0019); Affinity Chromatography (MI:0004)	P07948	P07948	hcv non-structural protein 5a	P07948	-	-	P07948	-	-	-	-	-	-	-	-
P07996	THBS1	THBS1 TSP TSP1	Thrombospondin-1	P07996	Two Hybrid Test (MI:0018)	P07996	-	-	-	P07996	-	-	-	-	-	-	-	-	-	-
P08107	SPA1A; HSPA1B		Heat shock 70 kDa protein	-	-	-	P08107	hcv ns 5	-	-	-	-	P08107	-	-	-	-	-	-	-
P08118	MSMB	MSMB PRSP	Beta-microseminoprotein	-	-	-	P08118	hcv non-structural protein 5a	-	-	-	-	-	-	-	-	-	-	-	-
P08134	P08134	RHOC ARH9 ARHC	Rho-related GTP-binding protein RhoC	-	-	-	-	-	-	-	-	-	-	-	-	-	-	-	P08134	P08134
P08183	ABCB1	ABCB1 MDR1 PGY1	ATP-dependent translocase ABCB1	-	-	-	-	-	-	-	-	-	P08183	-	-	-	-	-	-	-
P08195	SLC3A2	SLC3A2 MDU1	Amino acid transporter heavy chain SLC3A2	-	-	-	-	-	-	-	-	-	P08195	-	-	-	-	-	P08195	P08195
P08237	P08237	PFKM PFKX	ATP-dependent 6-phosphofructokinase, muscle type	-	-	-	-	-	-	-	-	-	-	-	-	-	-	-	P08237	-
P08238	P08238	HSP90AB1 HSP90B HSPC2 HSPCB	Heat shock protein HSP 90-beta	-	-	-	-	-	-	-	-	-	-	-	-	-	-	-	P08238	P08238
P08240	P08240	SRPRA SRPR	Signal recognition particle receptor subunit alpha	-	-	-	-	-	-	-	-	-	-	-	-	-	-	-	P08240	P08240
P08493	MGP	MGP MGLAP GIG36	Matrix Gla protein	P08493	Two Hybrid Test (MI:0018)	P08493	P08493	hcv non-structural protein 5a	-	-	-	-	-	-	-	-	-	-	-	-
P08574	P08574	CYC1	Cytochrome c1, heme protein, mitochondrial	-	-	-	-	-	-	-	-	-	-	-	-	-	-	-	P08574	P08574
P08579	SNRPB2	SNRPB2	U2 small nuclear ribonucleoprotein B''	-	-	-	-	-	-	-	-	-	-	-	-	-	-	P08579	-	-
P08590	MYL3	MYL3	Myosin light chain 3	-	-	-	-	-	-	-	-	-	P08590	-	-	-	-	-	-	-
P08631	HCK	HCK	Tyrosine-protein kinase HCK	P08631	Coimmunoprecipitation (MI:0019); Affinity Chromatography (MI:0004)	P08631	P08631	hcv non-structural protein 5a	P08631	-	-	P08631	-	-	-	-	-	-	-	-
P08670	VIM	VIM	Vimentin	-	-	-	P08670	hcv non-structural protein 5a	-	-	-	-	-	-	-	-	P08670	-	-	-
P08708	RPS17	RPS17 RPS17L	Small ribosomal subunit protein eS17	-	-	-	-	-	-	-	-	-	P08708	-	-	-	-	-	-	-
P08754	GNAI3	GNAI3	Guanine nucleotide-binding protein G	-	-	-	-	-	-	-	-	-	-	-	-	P08754	-	-	P08754	-
P09110	P09110	ACAA1 ACAA PTHIO	3-ketoacyl-CoA thiolase, peroxisomal	-	-	-	-	-	-	-	-	-	-	-	-	-	-	-	-	P09110
P09467	FBP1	FBP1 FBP	Fructose-1,6-bisphosphatase 1	-	-	-	-	-	-	-	-	P09467	-	-	-	-	-	-	-	-
P09497	CLTB	CLTB	Clathrin light chain B	-	-	-	-	-	-	-	-	-	P09497	-	-	-	-	-	-	-
P09543	P09543	CNP	2',3'-cyclic-nucleotide 3'-phosphodiesterase	-	-	-	-	-	-	-	-	-	-	-	-	-	-	-	-	P09543
P09622	P09622	DLD GCSL LAD PHE3	Dihydrolipoyl dehydrogenase, mitochondrial	-	-	-	-	-	-	-	-	-	-	-	-	-	-	-	P09622	-
P09651	HNRNPA1	HNRNPA1 HNRPA1	Heterogeneous nuclear ribonucleoprotein A1	-	-	-	P09651	hcv ns 5	-	-	-	-	-	-	-	-	-	P09651	-	P09651
P09661	SNRPA1	SNRPA1	U2 small nuclear ribonucleoprotein A'	-	-	-	-	-	-	-	-	-	-	-	-	-	-	P09661	-	-
P09669	P09669	COX6C	Cytochrome c oxidase subunit 6C	-	-	-	-	-	-	-	-	-	-	-	-	-	-	-	P09669	-
P09758	TACSTD2	TACSTD2 GA733-1 M1S1 TROP2	Tumor-associated calcium signal transducer 2	P09758	Two Hybrid Test (MI:0018)	P09758	P09758	hcv non-structural protein 5a	P09758	-	-	-	-	-	-	-	-	-	-	-

P09874	P09874	PARP1 ADPRT PPOL	Poly [ADP-ribose] polymerase 1	-	-	-	-	-	-	-	-	-	-	-	-	-	-	-	-	P09874
P09884	POLA1	POLA1 POLA	DNA polymerase alpha catalytic subunit	-	-	-	-	-	-	-	-	-	-	P09884	-	-	-	-	-	-	-
P0C0L4	C4A	C4A CO4 CPAMD2	Complement C4-A	-	-	-	-	-	-	-	-	-	-	-	-	-	-	-	P0C0L4	-	-
P0C7P0	P0C7P0	CISD3	CDGSH iron-sulfur domain-containing protein 3, mitochondrial	-	-	-	-	-	-	-	-	-	-	-	-	-	-	-	-	P0C7P0	-
P0CG08	P0CG08	GPR89B GPHRB GPR89C HSPC201	Golgi pH regulator B	-	-	-	-	-	-	-	-	-	-	-	-	-	-	-	-	P0CG08	-
P0CG47	UBB	UBB	Polyubiquitin-B	-	-	-	-	-	-	-	-	-	-	P0CG47	-	-	-	-	-	-	-
P0CG48	UBC	UBC	Polyubiquitin-C	-	-	-	-	-	-	-	-	-	-	P0CG48	-	-	-	-	-	-	-
P0CW22	RPS17	RPS17 RPS17L	Small ribosomal subunit protein eS17	-	-	-	-	-	-	-	-	-	-	P0CW22	-	-	-	-	-	-	-
P0DI83	P0DI83	RAB34 NARR	Ras-related protein Rab-34, isoform NARR	-	-	-	-	-	-	-	-	-	-	-	-	-	-	-	-	P0DI83	-
P0DMV8	HSPA1A	HSPA1A HSP72 HSPA1 HSX70	Heat shock 70 kDa protein 1A	-	-	P0DMV8	-	-	-	-	-	-	P0DMV8	-	-	-	-	-	-	-	-
P0DMV9	HSPA1B	HSPA1B HSP72	Heat shock 70 kDa protein 1B	-	-	P0DMV9	-	-	-	-	-	-	P0DMV9	-	-	-	-	-	-	P0DMV9	P0DMV9
P0DN76	P0DN76	U2AF2	U2 auxiliary factor 2	-	-	-	-	-	-	-	-	-	-	-	-	-	-	-	-	-	P0DN76
P0DP25	P0DP25	CALM3 CALML2 CAM3 CAMC CAMIII	Calmodulin-3	-	-	-	-	-	-	-	-	-	-	-	-	-	-	-	-	P0DP25	-
P10145	CXCL8	CXCL8 IL8	Interleukin-8	-	-	-	P10145	hcv non-structural protein 5a	-	-	-	-	-	-	-	-	-	-	-	-	-
P10586	PTPRF	PTPRF LAR	Receptor-type tyrosine-protein phosphatase F	-	-	-	-	-	-	-	-	-	-	P10586	-	-	-	-	-	-	-
P10599	P10599	TXN TRDX TRX TRX1	Thioredoxin	-	-	-	-	-	-	-	-	-	-	-	-	-	-	-	-	-	P10599
P10606	P10606	COX5B	Cytochrome c oxidase subunit 5B, mitochondrial	-	-	-	-	-	-	-	-	-	-	-	-	-	-	-	-	P10606	P10606
P10620	P10620	MGST1 GST12 MGST	Microsomal glutathione S-transferase 1	-	-	-	-	-	-	-	-	-	-	-	-	-	-	-	-	P10620	P10620
P10768	ESD	ESD	S-formylglutathione hydrolase	-	-	-	-	-	-	-	-	-	-	P10768	-	-	-	-	-	-	-
P10809	HSPD1	HSPD1 HSP60	60 kDa heat shock protein, mitochondrial	-	-	-	-	-	-	-	-	-	-	P10809	-	-	-	P10809	P10809	P10809	P10809
P10909	CLU	CLU APOJ CLI KUB1 AAG4	Clusterin	-	-	-	P10909	hcv non-structural protein 5a	-	-	-	-	P10909	-	-	-	-	-	-	-	-
P11021	HSPA5	HSPA5 GRP78	Endoplasmic reticulum chaperone BiP	-	-	-	P11021	hcv non-structural protein 5a	-	-	-	-	-	-	-	-	P11021	-	-	-	P11021
P11142	P11142	HSPA8 HSC70 HSP73 HSPA10	Heat shock cognate 71 kDa protein	-	-	-	-	-	-	-	-	-	-	-	-	-	-	-	-	-	P11142
P11177	PDHB	PDHB PHE1B	Pyruvate dehydrogenase E1 component subunit beta, mitochondrial	-	-	-	-	-	-	-	-	-	-	P11177	-	-	-	-	-	-	-
P11216	PYGB	PYGB	Glycogen phosphorylase, brain form	-	-	-	-	-	-	-	-	-	-	P11216	-	-	-	-	-	-	-
P11226	MBL2	MBL2 COLEC1 MBL	Mannose-binding protein C	-	-	-	P11226	hcv non-structural protein 5a	-	-	-	-	-	-	-	-	-	-	-	-	-
P11233	P11233	RALA RAL	Ras-related protein Ral-A	-	-	-	-	-	-	-	-	-	-	-	-	-	-	-	-	P11233	P11233
P11274	BCR	BCR BCR1 D22S11	Breakpoint cluster region protein	-	-	-	P11274	hcv non-structural protein 5a	-	-	-	-	-	-	-	-	-	-	-	-	-
P11279	P11279	LAMP1	Lysosome-associated membrane glycoprotein 1	-	-	-	-	-	-	-	-	-	-	-	-	-	-	-	-	P11279	-
P11498	PC	PC	Pyruvate carboxylase, mitochondrial	-	-	-	P11498	hcv non-structural protein 5a	-	-	-	-	P11498	-	-	-	-	-	-	-	P11498
P11940	P11940	PABPC1 PAB1 PABP PABP1 PABPC2	Polyadenylate-binding protein 1	-	-	-	-	-	-	-	-	-	-	-	-	-	-	-	-	P11940	P11940
P12074	P12074	COX6A1 COX6AL	Cytochrome c oxidase subunit 6A1, mitochondrial	-	-	-	-	-	-	-	-	-	-	-	-	-	-	-	-	P12074	-

P12259	F5	F5	Coagulation factor V	-	-	-	-	-	-	-	-	-	-	-	P12259	-	-	-	-	-	-
P12277	CKB	CKB CKBB	Creatine kinase B-type	-	-	-	-	-	-	-	-	-	-	-	-	-	-	P12277	-	-	-
P12931	SRC	SRC SRC1	Proto-oncogene tyrosine-protein kinase Src	P12931	Affinity Chromatography (MI:0004); Mass spectrometry (MI:0943); GST pull-down (MI:0059)	P12931	P12931	hcv non-structural protein 5a	P12931	-	-	-	P12931	-	-	-	-	-	-	-	-
P12955	PEPD	PEPD PRD	Xaa-Pro dipeptidase	-	-	-	-	-	-	-	-	-	-	P12955	-	-	-	-	-	-	-
P13010	P13010	XRCC5 G22P2	X-ray repair cross-complementing protein 5	-	-	-	-	-	-	-	-	-	-	-	-	-	-	-	-	-	P13010
P13073	P13073	COX4I1 COX4	Cytochrome c oxidase subunit 4 isoform 1, mitochondrial	-	-	-	-	-	-	-	-	-	-	-	-	-	-	-	-	P13073	P13073
P13378	HOXD8	HOXD8 HOX4E	Homeobox protein Hox-D8	-	-	-	P13378	hcv ns 5	-	-	-	-	-	-	-	-	-	-	-	-	-
P13639	P13639	EEF2 EF2	Elongation factor 2	-	-	-	-	-	-	-	-	-	-	-	-	-	-	-	-	-	P13639
P13727	PRG2	PRG2 MBP	Bone marrow proteoglycan	-	-	-	P13727	hcv non-structural protein 5a	-	-	-	-	-	-	-	-	-	-	-	-	-
P13798	APEH	APEH D3F15S2 D3S48E DNF15S2	Acylamino-acid-releasing enzyme	-	-	-	-	-	-	-	-	-	-	P13798	-	-	-	-	-	-	-
P13804	P13804	ETFA	Electron transfer flavoprotein subunit alpha, mitochondrial	-	-	-	-	-	-	-	-	-	-	-	-	-	-	-	-	P13804	P13804
P14174	P14174	MIF GLIF MMIF	Macrophage migration inhibitory factor	-	-	-	-	-	-	-	-	-	-	-	-	-	-	-	-	P14174	P14174
P14324	FDPS	FDPS FPS KIAA1293	Farnesyl pyrophosphate synthase	-	-	-	-	-	-	-	-	-	-	P14324	-	-	-	-	-	P14324	-
P14406	P14406	COX7A2 COX7AL	Cytochrome c oxidase subunit 7A2, mitochondrial	-	-	-	-	-	-	-	-	-	-	-	-	-	-	-	-	P14406	-
P14616	INSRR	INSRR IRR	Insulin receptor-related protein	-	-	-	-	-	-	-	-	-	-	P14616	-	-	-	-	-	-	-
P14618	PKM	PKM OIP3 PK2 PK3 PKM2	Pyruvate kinase PKM	-	-	-	P14618	hcv ns 5	-	-	-	-	-	-	-	-	-	P14618	-	-	P14618
P14625	P14625	HSP90B1 GRP94 TRA1	Endoplasmin	-	-	-	-	-	-	-	-	-	-	-	-	-	-	-	-	P14625	P14625
P14678	SNRPB	SNRPB COD SNRPB1	Small nuclear ribonucleoprotein-associated proteins B and B'	-	-	-	-	-	-	-	-	-	-	P14678	-	-	-	-	-	-	-
P14735	IDE	IDE	Insulin-degrading enzyme	-	-	-	-	-	-	-	-	-	-	P14735	-	-	-	-	-	-	-
P14854	P14854	COX6B1 COX6B	Cytochrome c oxidase subunit 6B1	-	-	-	-	-	-	-	-	-	-	-	-	-	-	-	-	-	P14854
P14866	P14866	HNRNPL HNRPL P/OKcl.14	Heterogeneous nuclear ribonucleoprotein L	-	-	-	-	-	-	-	-	-	-	-	-	-	-	-	-	-	P14866
P14923	P14923	JUP CTNNG DP3	Junction plakoglobin	-	-	-	-	-	-	-	-	-	-	-	-	-	-	-	-	P14923	-
P15374	UCHL3	UCHL3	Ubiquitin carboxyl-terminal hydrolase isozyme L3	-	-	-	-	-	-	-	-	-	-	P15374	-	-	-	-	-	-	-
P15814	IGLL1	IGLL1 IGL1	Immunoglobulin lambda-like polypeptide 1	P15814	Two Hybrid Test (MI:0018)	-	-	-	-	P15814	-	-	-	-	-	-	-	-	-	-	-
P15880	P15880	RPS2 RPS4	Small ribosomal subunit protein uS5	-	-	-	-	-	-	-	-	-	-	-	-	-	-	-	-	-	P15880
P15924	P15924	DSP	Desmoplakin	-	-	-	-	-	-	-	-	-	-	-	-	-	-	-	-	P15924	-
P15927	P15927	RPA2 REPA2 RPA32 RPA34	Replication protein A 32 kDa subunit	-	-	-	-	-	-	-	-	-	-	-	-	-	-	-	-	P15927	-
P15954	P15954	COX7C	Cytochrome c oxidase subunit 7C, mitochondrial	-	-	-	-	-	-	-	-	-	-	-	-	-	-	-	-	P15954	-
P16220	P16220	CREB1	Cyclic AMP-responsive element-binding protein 1	-	-	-	-	-	-	-	-	-	-	-	-	-	-	-	-	-	P16220
P16401	H1-5	H1-5 H1F5 HIST1H1B	Histone H1.5	-	-	-	-	-	-	-	-	-	-	-	-	-	-	-	P16401	-	-
P16402	H1-3	H1-3 H1F3 HIST1H1D	Histone H1.3	-	-	-	-	-	-	-	-	-	-	P16402	-	-	-	-	-	-	-
P16435	POR	POR CYPOR	NADPH--cytochrome P450 reductase	-	-	-	-	-	-	-	-	-	-	P16435	-	-	-	-	-	P16435	P16435
P16615	ATP2A2	ATP2A2 ATP2B	Sarcoplasmic/endoplasmic reticulum calcium ATPase 2	-	-	-	-	-	-	-	-	-	-	P16615	-	-	-	-	-	P16615	P16615
P16949	STMN1	STMN1 C1orf215 LAP18 OP18	Stathmin	-	-	-	-	-	-	-	-	-	-	-	-	-	-	P16949	-	-	P16949
P17066	P17066	HSPA6 HSP70B'	Heat shock 70 kDa protein 6	-	-	-	-	-	-	-	-	-	-	-	-	-	-	-	-	-	P17066
P17302	GJA1	GJA1 GJAL	Gap junction alpha-1 protein	-	-	-	-	-	-	-	-	-	-	P17302	-	-	-	-	-	-	-
P17480	P17480	UBTF UBF UBF1	Nucleolar transcription factor 1	-	-	-	-	-	-	-	-	-	-	-	-	-	-	-	-	-	P17480

P17612	PRKACA	PRKACA PKACA	cAMP-dependent protein kinase catalytic subunit alpha	-	-	-	-	-	-	-	-	-	P17612	-	-	-	-	-	-	-	-
P17812	P17812	CTPS1 CTPS	CTP synthase 1	-	-	-	-	-	-	-	-	-	-	-	-	-	-	-	-	P17812	P17812
P17844	DDX5	DDX5 G17P1 HELR HLR1	Probable ATP-dependent RNA helicase DDX5	-	-	-	P17844	hcv ns 5	-	-	P17844	-	-	-	-	-	-	-	-	P17844	-	-
P17931	LGALS3	LGALS3 MAC2	Galectin-3	-	-	-	P17931	hcv non-structural protein 5a	-	-	-	-	-	-	-	-	-	-	-	-	-	-
P17980	P17980	PSMC3 TBP1	26S proteasome regulatory subunit 6A	-	-	-	-	-	-	-	-	-	-	-	-	-	-	-	-	-	P17980
P17987	TCP1	TCP1 CCT1 CCTA	T-complex protein 1 subunit alpha	-	-	-	P17987	hcv ns 5	-	-	-	-	-	-	-	-	-	-	-	P17987	P17987
P18031	P18031	PTPN1 PTP1B	Tyrosine-protein phosphatase non-receptor type 1	-	-	-	-	-	-	-	-	-	-	-	-	-	-	-	-	P18031	-
P18085	P18085	ARF4 ARF2	ADP-ribosylation factor 4	-	-	-	-	-	-	-	-	-	-	-	-	-	-	-	-	-	P18085
P18621	P18621	RPL17	Large ribosomal subunit protein uL22	-	-	-	-	-	-	-	-	-	-	-	-	-	-	-	-	-	P18621
P18859	P18859	ATP5PF ATP5A ATP5J ATPM	ATP synthase-coupling factor 6, mitochondrial	-	-	-	-	-	-	-	-	-	-	-	-	-	-	-	-	P18859	P18859
P19174	PLCG1	PLCG1 PLC1	1-phosphatidylinositol 4,5-bisphosphate phosphodiesterase gamma-1	-	-	-	-	-	-	-	-	-	-	P19174	-	-	-	-	-	-	-
P19338	NCL	NCL	Nucleolin	-	-	-	P19338	hcv ns 5	-	-	-	-	-	-	-	-	-	-	P19338	-	-
P19404	P19404	NDUFV2	NADH dehydrogenase [ubiquinone] flavoprotein 2, mitochondrial	-	-	-	-	-	-	-	-	-	-	-	-	-	-	-	-	-	P19404
P19447	P19447	ERCC3 XPB XPBC	General transcription and DNA repair factor IIH helicase subunit XPB	-	-	-	-	-	-	-	-	-	-	-	-	-	-	-	-	-	P19447
P19525	EIF2AK2	EIF2AK2 PKR PRKR	Interferon-induced, double-stranded RNA-activated protein kinase	P19525	Two Hybrid Test (MI:0018)	P19525	P19525	hcv non-structural protein 5a	P19525	-	-	-	P19525	-	-	-	-	-	-	-	-
P19623	SRM	SRM SPS1 SRML1	Spermidine synthase	-	-	-	-	-	-	-	-	-	-	P19623	-	-	-	-	-	-	-
P19838	NFKB1	NFKB1	Nuclear factor NF-kappa-B p105 subunit	-	-	-	P19838	hcv ns 5	-	-	-	-	-	-	-	-	-	-	-	-	-
P20020	ATP2B1	ATP2B1 PMCA1	Plasma membrane calcium-transporting ATPase 1	-	-	-	-	-	-	-	-	-	-	P20020	-	-	-	-	-	P20020	P20020
P20226	TBP	TBP GTF2D1 TF2D TFIID	TATA-box-binding protein	P20226	Coimmunoprecipitation (MI:0019); Pull-down (MI:0096); Affinity Chromatography (MI:0004)	P20226	P20226	hcv non-structural protein 5a	P20226	-	-	-	P20226	-	-	-	-	-	-	-	-
P20337	RAB3B	RAB3B	Ras-related protein Rab-3B	-	-	-	-	-	-	-	-	-	-	P20337	-	-	-	-	-	-	-
P20338	P20338	RAB4A RAB4	Ras-related protein Rab-4A	-	-	-	-	-	-	-	-	-	-	-	-	-	-	-	-	-	P20338
P20339	P20339	RAB5A RAB5	Ras-related protein Rab-5A	-	-	-	-	-	-	-	-	-	-	-	-	-	-	-	-	-	P20339
P20340	P20340	RAB6A RAB6	Ras-related protein Rab-6A	-	-	-	-	-	-	-	-	-	-	-	-	-	-	-	-	P20340	P20340
P20591	MX1	MX1	Interferon-induced GTP-binding protein Mx1	-	-	-	P20591	hcv non-structural protein 5a	-	-	-	-	-	-	-	-	-	-	-	-	-
P20674	P20674	COX5A	Cytochrome c oxidase subunit 5A, mitochondrial	-	-	-	-	-	-	-	-	-	-	-	-	-	-	-	-	P20674	P20674
P20700	P20700	LMNB1 LMN2 LMNB	Lamin-B1	-	-	-	-	-	-	-	-	-	-	-	-	-	-	-	-	-	P20700
P20701	ITGAL	ITGAL CD11A	Integrin alpha-L	P20701	Two Hybrid Test (MI:0018); Co-affinity purification (MI:0025)	P20701	P20701	hcv non-structural protein 5a	-	P20701	-	-	-	-	-	-	-	-	-	-	-
P20823	HNF1A	HNF1A TCF1	Hepatocyte nuclear factor 1-alpha	-	-	-	P20823	hcv non-structural protein 5a	-	-	-	-	-	-	-	-	-	-	-	-	-
P21108	P21108	PRPS1L1 PRPS3 PRPSL	Ribose-phosphate pyrophosphokinase 3	-	-	-	-	-	-	-	-	-	-	-	-	-	-	-	-	P21108	-
P21281	ATP6V1B2	ATP6V1B2 ATP6B2 VPP3	V-type proton ATPase subunit B, brain isoform	-	-	-	-	-	-	-	-	-	-	P21281	-	-	-	-	-	-	-
P21333	FLNA	FLNA FLN FLN1	Filamin-A	-	-	P21333	-	-	-	-	-	-	-	-	-	-	-	-	-	-	-
P21796	VDAC1	VDAC1 VDAC	Voltage-dependent anion-selective channel protein 1	-	-	-	-	-	-	-	-	-	-	-	-	-	-	P21796	-	P21796	P21796
P21964	P21964	COMT	Catechol O-methyltransferase	-	-	-	-	-	-	-	-	-	-	-	-	-	-	-	-	-	P21964
P22059	OSBP	OSBP OSBP1	Oxysterol-binding protein 1	-	-	P22059	P22059	hcv non-structural protein 5a	-	-	-	-	P22059	P22059	-	-	-	-	-	-	-
P22102	P22102	GART PGFT PRGS	Trifunctional purine biosynthetic protein adenosine-3 [Includes: Phosphoribosylamine--glycine ligase	-	-	-	-	-	-	-	-	-	-	-	-	-	-	-	-	-	P22102

P22234	P22234	PAICS ADE2 AIRC PAIS	Bifunctional phosphoribosylaminoimidazole carboxylase/phosphoribosylaminoimidazole succinocarboxamide synthetase	-	-	-	-	-	-	-	-	-	-	-	-	-	-	-	-	-	P22234
P22307	P22307	SCP2	Sterol carrier protein 2	-	-	-	-	-	-	-	-	-	-	-	-	-	-	-	-	-	P22307
P22455	FGFR4	FGFR4 JTK2 TKF	Fibroblast growth factor receptor 4	-	-	-	-	-	-	-	-	-	-	-	P22455	-	-	-	-	-	-
P22626	HNRNPA2B1	HNRNPA2B1 HNRPA2B1	Heterogeneous nuclear ribonucleoproteins A2/B1	-	-	-	-	-	-	-	-	-	-	-	-	-	-	P22626	P22626	-	-
P22695	P22695	UQCRC2	Cytochrome b-c1 complex subunit 2, mitochondrial	-	-	-	-	-	-	-	-	-	-	-	-	-	-	-	-	P22695	P22695
P22736	NR4A1	NR4A1 GFRP1 HMR NAK1	Nuclear receptor subfamily 4immunitygroup A member 1	-	-	-	P22736	hcv ns 5	-	-	-	-	-	-	-	-	-	-	-	-	-
P23246	SFPQ	SFPQ PSF	Splicing factor, proline- and glutamine-rich	-	-	-	-	-	-	-	-	-	-	P23246	-	-	-	-	-	-	P23246
P23284	PPIB	PPIB CYPB	Peptidyl-prolyl cis-trans isomerase B	-	-	-	P23284	hcv non-structural protein 5a	-	-	-	-	P23284	-	-	-	-	-	-	-	-
P23368	ME2	ME2	NAD-dependent malic enzyme, mitochondrial	-	-	-	-	-	-	-	-	-	-	P23368	-	-	-	-	-	-	-
P23443	RPS6KB1	RPS6KB1 STK14A	Ribosomal protein S6 kinase beta-1	-	-	-	P23443	hcv non-structural protein 5a	-	-	-	-	-	-	-	-	-	-	-	-	-
P23458	JAK1	JAK1 JAK1A JAK1B	Tyrosine-protein kinase JAK1	P23458	Coimmunoprecipitation (MI:0019)	P23458	-	-	P23458	-	-	-	-	-	-	-	-	-	-	-	-
P23528	CFL1	CFL1 CFL	Cofilin-1	-	-	-	-	-	-	-	-	-	-	-	-	-	-	P23528	-	-	-
P23919	P23919	DTYMK CDC8 TMPK TYMK	Thymidylate kinase	-	-	-	-	-	-	-	-	-	-	-	-	-	-	-	-	P23919	-
P24539	P24539	ATP5PB ATP5F1	ATP synthase F	-	-	-	-	-	-	-	-	-	-	-	-	-	-	-	-	P24539	P24539
P24941	CDK2	CDK2 CDKN2	Cyclin-dependent kinase 2	P24941	Western blot (MI:0113); Coimmunoprecipitation (MI:0019)	-	-	-	-	-	-	-	-	-	-	-	-	-	-	-	-
P25398	P25398	RPS12	Small ribosomal subunit protein eS12	-	-	-	-	-	-	-	-	-	-	-	-	-	-	-	-	-	P25398
P25685	DNAJB1	DNAJB1 DNAJ1 HDJ1 HSPF1	DnaJ homolog subfamily B member 1	-	-	-	P25685	hcv non-structural protein 5a	-	-	-	-	P25685	P25685	-	-	-	-	-	P25685	-
P25686	DNAJB2	DNAJB2 HSJ1 HSPF3	DnaJ homolog subfamily B member 2	-	-	-	-	-	-	-	-	-	-	P25686	-	-	-	-	-	-	-
P25705	P25705	ATP5F1A ATP5A ATP5A1 ATP5AL2 ATPM	ATP synthase subunit alpha, mitochondrial	-	-	-	-	-	-	-	-	-	-	-	-	-	-	-	-	P25705	P25705
P25815	P25815	S100P S100E	Protein S100-P	-	-	-	-	-	-	-	-	-	-	-	-	-	-	-	-	-	P25815
P26196	P26196	DDX6 HLR2 RCK	Probable ATP-dependent RNA helicase DDX6	-	-	-	-	-	-	-	-	-	-	-	-	-	-	-	-	-	P26196
P26572	P26572	MGAT1 GGNT1 GLCT1 GLYT1 MGAT	Alpha-1,3-mannosyl-glycoprotein 2-beta-N-acetylglucosaminyltransferase	-	-	-	-	-	-	-	-	-	-	-	-	-	-	-	-	P26572	-
P26599	PTBP1	PTBP1 PTB	Polypyrimidine tract-binding protein 1	-	-	-	P26599	hcv non-structural protein 5a	-	-	-	-	-	-	-	-	-	-	P26599	-	P26599
P26641	P26641	EEF1G EF1G PRO1608	Elongation factor 1-gamma	-	-	-	-	-	-	-	-	-	-	-	-	-	-	-	-	P26641	-
P26927	MST1	MST1 D3F15S2 DNF15S2 HGFL	Hepatocyte growth factor-like protein	-	-	-	P26927	hcv non-structural protein 5a	-	-	-	-	-	-	-	-	-	-	-	-	-
P27105	STOM	STOM BND7 EPB72	Stomatin	-	-	-	P27105	hcv ns 5	-	-	-	-	-	-	-	-	-	-	P27105	P27105	-
P27144	P27144	AK4 AK3 AK3L1	Adenylate kinase 4, mitochondrial	-	-	-	-	-	-	-	-	-	-	-	-	-	-	-	-	-	P27144
P27338	P27338	MAOB	Amine oxidase [flavin-containing] B	-	-	-	-	-	-	-	-	-	-	-	-	-	-	-	-	P27338	P27338
P27348	P27348	YWHAQ	14-3-3 protein theta	-	-	-	-	-	-	-	-	-	-	-	-	-	-	-	-	P27348	-
P27695	APEX1	APEX1 APE APE1 APEX APX HAP1 REF1	DNA-(apurinic or apyrimidinic site) endonuclease	-	-	-	-	-	-	-	-	-	-	P27695	-	-	-	-	-	-	-
P27797	CALR	CALR CRTC	Calreticulin	-	-	-	-	-	-	-	-	-	-	-	-	-	-	P27797	-	-	-

P27824	P27824	CANX	Calnexin	-	-	-	-	-	-	-	-	-	-	-	-	-	-	-	-	P27824	P27824
P27986	PIK3R1	PIK3R1 GRB1	Phosphatidylinositol 3-kinase regulatory subunit alpha	P27986	Coimmunoprecipitation (MI:0019); GST pull-down (MI:0059)	P27986	P27986	hcv non-structural protein 5a	-	-	P27986	-	P27986	-	-	-	-	-	-	-	-
P28065	PSMB9	PSMB9 LMP2 PSMB6i RING12	Proteasome subunit beta type-9	P28065	Two Hybrid Test (MI:0018); Co-affinity purification (MI:0025)	P28065	P28065	hcv non-structural protein 5a	-	P28065	-	-	-	-	-	-	-	-	-	-	-
P28070	PSMB4	PSMB4 PROS26	Proteasome subunit beta type-4	-	-	-	P28070	hcv ns 5	-	-	-	-	-	-	-	-	-	-	-	P28070	
P28288	P28288	ABCD3 PMP70 PXMP1	ATP-binding cassette sub-family D member 3	-	-	-	-	-	-	-	-	-	-	-	-	-	-	-	-	P28288	P28288
P28331	P28331	NDUFS1	NADH-ubiquinone oxidoreductase 75 kDa subunit, mitochondrial	-	-	-	-	-	-	-	-	-	-	-	-	-	-	-	-	P28331	P28331
P28482	P28482	MAPK1 ERK2 PRKM1 PRKM2	Mitogen-activated protein kinase 1	-	-	-	-	-	-	-	-	-	-	-	-	-	-	-	-	P28482	-
P29084	P29084	GTF2E2 TF2E2	Transcription initiation factor IIE subunit beta	-	-	-	-	-	-	-	-	-	-	-	-	-	-	-	-	-	P29084
P29317	EPHA2	EPHA2 ECK	Ephrin type-A receptor 2	-	-	-	-	-	-	-	-	-	-	P29317	-	-	-	-	-	P29317	-
P29353	SHC1	SHC1 SHC SHCA	SHC-transforming protein 1	-	-	-	-	-	-	-	-	-	-	P29353	-	-	-	-	-	-	-
P29372	P29372	MPG AAG ANPG MID1	DNA-3-methyladenine glycosylase	-	-	-	-	-	-	-	-	-	-	-	-	-	-	-	-	-	P29372
P29590	P29590	PML MYL PP8675 RNF71 TRIM19	Protein PML	-	-	-	-	-	-	-	-	-	-	-	-	-	-	-	-	-	P29590
P29692	P29692	EEF1D EF1D	Elongation factor 1-delta	-	-	-	-	-	-	-	-	-	-	-	-	-	-	-	-	P29692	P29692
P29762	CRABP1	CRABP1 RBP5	Cellular retinoic acid-binding protein 1	P29762	Two Hybrid Test (MI:0018); GST pull-down (MI:0059)	P29762	P29762	hcv non-structural protein 5a	P29762	-	-	-	-	-	-	-	-	-	-	-	-
P29965	CD40LG	CD40LG CD40L TNFSF5 TRAP	CD40 ligand	-	-	-	P29965	hcv non-structural protein 5a	-	-	-	-	-	-	-	-	-	-	-	-	-
P29966	MARCKS	MARCKS MACS PRKCSL	Myristoylated alanine-rich C-kinase substrate	-	-	-	-	-	-	-	-	-	-	-	-	-	-	P29966	-	P29966	-
P30041	P30041	PRDX6 AOP2 KIAA0106	Peroxiredoxin-6	-	-	-	-	-	-	-	-	-	-	-	-	-	-	-	-	-	P30041
P30044	PRDX5	PRDX5 ACR1 SBBI10	Peroxiredoxin-5, mitochondrial	-	-	-	-	-	-	-	-	-	-	-	-	-	-	P30044	-	-	-
P30048	PRDX3	PRDX3 AOP1	Thioredoxin-dependent peroxide reductase, mitochondrial	-	-	-	-	-	-	-	-	-	-	-	-	-	-	P30048	-	-	P30048
P30049	ATP5F1D	ATP5F1D ATP5D	ATP synthase subunit delta, mitochondrial	-	-	-	-	-	-	-	-	-	-	-	-	-	-	P30049	-	P30049	P30049
P30085	P30085	CMPK1 CMK CMPK UCK UMK UMPK	UMP-CMP kinase	-	-	-	-	-	-	-	-	-	-	-	-	-	-	-	-	P30085	-
P30086	PEBP1	PEBP1 PBP PEBP	Phosphatidylethanolamine-binding protein 1	-	-	-	-	-	-	-	-	-	-	P30086	-	-	-	-	-	-	P30086
P30101	P30101	PDIA3 ERP57 ERP60 GRP58	Protein disulfide-isomerase A3	-	-	-	-	-	-	-	-	-	-	-	-	-	-	-	-	-	P30101
P30153	PPP2R1A	PPP2R1A	Serine/threonine-protein phosphatase 2A 65 kDa regulatory subunit A alpha isoform	-	-	P30153	-	-	-	-	-	-	-	P30153	-	-	-	-	-	P30153	P30153
P30519	P30519	HMOX2 HO2	Heme oxygenase 2	-	-	-	-	-	-	-	-	-	-	-	-	-	-	-	-	P30519	-
P30613	PKLR	PKLR PK1 PKL	Pyruvate kinase PKLR	-	-	-	P30613	hcv non-structural protein 5a	-	-	-	-	-	-	-	-	-	-	-	-	-
P31040	P31040	SDHA SDH2 SDHF	Succinate dehydrogenase [ubiquinone] flavoprotein subunit, mitochondrial	-	-	-	-	-	-	-	-	-	-	-	-	-	-	-	-	P31040	P31040
P31153	P31153	MAT2A AMS2 MATA2	S-adenosylmethionine synthase isoform type-2	-	-	-	-	-	-	-	-	-	-	-	-	-	-	-	-	-	P31153
P31689	P31689	DNAJA1 DNAJ2 HDJ2 HSJ2 HSPF4	DnaJ homolog subfamily A member 1	-	-	-	-	-	-	-	-	-	-	-	-	-	-	-	-	P31689	P31689

P31749	AKT1	AKT1 PKB RAC	RAC-alpha serine/threonine-protein kinase	P31749	GST pull-down (MI:0059); Kinase assay (MI:0424) (MI:0424)	P31749	P31749	hcv non-structural protein 5a	P31749	-	-	-	-	-	-	-	-	-	-	-	-
P31930	P31930	UQCRC1	Cytochrome b-c1 complex subunit 1, mitochondrial	-	-	-	-	-	-	-	-	-	-	-	-	-	-	-	-	P31930	P31930
P31942	HNRNPH3	HNRNPH3 HNRPH3	Heterogeneous nuclear ribonucleoprotein H3	-	-	-	-	-	-	-	-	-	-	P31942	-	-	-	P31942	-	-	-
P31943	P31943	HNRNPH1 HNRPH HNRPH1	Heterogeneous nuclear ribonucleoprotein H	-	-	-	-	-	-	-	-	-	-	-	-	-	-	-	-	-	P31943
P31946	YWHAB	YWHAB	14-3-3 protein beta/alpha	-	-	-	-	-	-	-	-	-	-	-	-	-	-	P31946	-	-	-
P32119	PRDX2	PRDX2 NKEFB TDPX1	Peroxiredoxin-2	-	-	-	P32119	hcv non-structural protein 5a	-	-	-	-	-	-	-	-	-	P32119	-	-	-
P32121	P32121	ARRB2 ARB2 ARR2	Beta-arrestin-2	-	-	-	-	-	-	-	-	-	-	-	-	-	-	-	-	-	P32121
P32455	GBP1	GBP1	Guanylate-binding protein 1	-	-	-	P32455	hcv ns 5	-	-	-	-	-	-	-	-	-	-	-	-	-
P32780	P32780	GTF2H1 BTF2	General transcription factor IIH subunit 1	-	-	-	-	-	-	-	-	-	-	-	-	-	-	-	-	-	P32780
P33121	P33121	ACSL1 FACL1 FACL2 LACS LACS1 LACS2	Long-chain-fatty-acid--CoA ligase 1	-	-	-	-	-	-	-	-	-	-	-	-	-	-	-	-	P33121	P33121
P33908	P33908	MAN1A1	Mannosyl-oligosaccharide 1,2-alpha-mannosidase IA	-	-	-	-	-	-	-	-	-	-	-	-	-	-	-	-	P33908	-
P33993	P33993	MCM7 CDC47 MCM2	DNA replication licensing factor MCM7	-	-	-	-	-	-	-	-	-	-	-	-	-	-	-	-	-	P33993
P34931	P34931	HSPA1L	Heat shock 70 kDa protein 1-like	-	-	-	-	-	-	-	-	-	-	-	-	-	-	-	-	P34931	P34931
P34932	HSPA4	HSPA4 APG2	Heat shock 70 kDa protein 4	-	-	-	P34932	hcv non-structural protein 5a	-	-	-	-	-	-	-	-	-	P34932	-	-	-
P35030	P35030	PRSS3 PRSS4 TRY3 TRY4	Trypsin-3	-	-	-	-	-	-	-	-	-	-	-	-	-	-	-	-	-	P35030
P35222	CTNNB1	CTNNB1 CTNNB OK/SW-cl.35 PRO2286	Catenin beta-1	-	-	P35222	P35222	hcv non-structural protein 5a	-	-	-	-	-	-	-	-	-	-	-	-	-
P35232	P35232	PHB1 PHB	Prohibitin 1	-	-	-	-	-	-	-	-	-	-	-	-	-	-	-	-	P35232	P35232
P35249	RFC4	RFC4	Replication factor C subunit 4	-	-	-	-	-	-	-	-	-	-	P35249	-	-	-	-	-	-	-
P35579	MYH9	MYH9	Myosin-9	-	-	-	-	-	-	-	-	-	-	-	-	-	-	-	P35579	-	-
P35580	MYH10	MYH10	Myosin-10	-	-	-	-	-	-	-	-	-	-	-	-	-	-	-	P35580	-	-
P35606	COPB2	COPB2	Coatomer subunit beta'	-	-	-	-	-	-	-	-	-	-	P35606	-	-	-	-	-	P35606	-
P35610	P35610	SOAT1 ACACT ACACT1 ACAT ACAT1 SOAT STAT	Sterol O-acyltransferase 1	-	-	-	-	-	-	-	-	-	-	-	-	-	-	-	-	P35610	P35610
P35613	P35613	BSG UNQ6505/PRO21383	Basigin	-	-	-	-	-	-	-	-	-	-	-	-	-	-	-	-	P35613	P35613
P35637	FUS	FUS TLS	RNA-binding protein FUS	-	-	-	-	-	-	-	-	-	-	-	-	-	-	P35637	-	-	P35637
P35659	DEK	DEK	Protein DEK	-	-	-	-	-	-	-	-	-	-	P35659	-	-	-	-	-	-	-
P35754	P35754	GLRX GRX	Glutaredoxin-1	-	-	-	-	-	-	-	-	-	-	-	-	-	-	-	-	-	P35754
P35790	CHKA	CHKA CHK CKI	Choline kinase alpha	-	-	-	P35790	HCV NONSTRUCTURAL PROTEIN 5A	-	-	-	-	-	-	-	-	-	-	-	-	-
P35998	P35998	PSMC2 MSS1	26S proteasome regulatory subunit 7	-	-	-	-	-	-	-	-	-	-	-	-	-	-	-	-	P35998	P35998
P36542	P36542	ATP5F1C ATP5C ATP5C1 ATP5CL1	ATP synthase subunit gamma, mitochondrial	-	-	-	-	-	-	-	-	-	-	-	-	-	-	-	-	-	P36542
P36551	CPOX	CPOX CPO CPX	Oxygen-dependent coproporphyrinogen-III oxidase, mitochondrial	-	-	-	-	-	-	-	-	-	-	P36551	-	-	-	-	-	-	-
P36897	TGFBR1	TGFBR1 ALK5 SKR4	TGF-beta receptor type-1	P36897	GST pull-down (MI:0059); Coimmunoprecipitation (MI:0019)	P36897	-	-	P36897	-	-	-	-	-	-	-	-	-	-	-	-	-
P36941	LTBR	LTBR D12S370 TNFCR TNFR3 TNFRSF3	Tumor necrosis factor receptor superfamily member 3	-	-	-	P36941	hcv non-structural protein 5a	-	-	-	-	-	-	-	-	-	-	-	-	-

P37059	P37059	HSD17B2 EDH17B2 SDR9C2	17-beta-hydroxysteroid dehydrogenase type 2	-	-	-	-	-	-	-	-	-	-	-	-	-	-	-	-	P37059	-
P37173	TGFBR2	TGFBR2	TGF-beta receptor type-2	-	-	-	-	-	-	-	-	-	-	P37173	-	-	-	-	-	-	-
P37268	P37268	FDFT1	Squalene synthase	-	-	-	-	-	-	-	-	-	-	-	-	-	-	-	-	P37268	P37268
P37802	TAGLN2	TAGLN2 KIAA0120 CDABP0035	Transgelin-2	-	-	-	-	-	-	-	-	-	-	-	-	-	-	P37802	-	-	-
P38117	P38117	ETFB FP585	Electron transfer flavoprotein subunit beta	-	-	-	-	-	-	-	-	-	-	-	-	-	-	-	-	P38117	P38117
P38159	RBMX	RBMX HNRPG RBMXP1	RNA-binding motif protein, X chromosome	-	-	-	-	-	-	-	-	-	-	-	-	-	-	-	P38159	-	-
P38435	P38435	GGCX GC	Vitamin K-dependent gamma-carboxylase	-	-	-	-	-	-	-	-	-	-	-	-	-	-	-	-	P38435	-
P38646	HSPA9	HSPA9 GRP75 HSPA9B mt-HSP70	Stress-70 protein, mitochondrial	-	-	-	-	-	-	-	-	-	-	-	-	P38646	-	P38646	-	P38646	
P38936	CDKN1A	CDKN1A CAP20 CDKN1 CIP1 MDA6 PIC1 SDI1 WAF1	Cyclin-dependent kinase inhibitor 1	-	-	-	P38936	hcv non-structural protein 5a	-	-	-	-	-	-	-	-	-	-	-	-	-
P39656	P39656	DDOST KIAA0115 OST48 OK/SW-cl.45	Dolichyl-diphosphooligosaccharide--protein glycosyltransferase 48 kDa subunit	-	-	-	-	-	-	-	-	-	-	-	-	-	-	-	-	P39656	P39656
P40227	P40227	CCT6A CCT6 CCTZ	T-complex protein 1 subunit zeta	-	-	-	-	-	-	-	-	-	-	-	-	-	-	-	-	P40227	P40227
P40429	RPL13A	RPL13A	Large ribosomal subunit protein uL13	-	-	-	-	-	-	-	-	-	-	-	-	-	-	-	P40429	P40429	-
P40926	MDH2	MDH2	Malate dehydrogenase, mitochondrial	-	-	-	-	-	-	-	-	-	-	-	-	-	-	P40926	-	-	P40926
P40939	P40939	HADHA HADH	Trifunctional enzyme subunit alpha, mitochondrial	-	-	-	-	-	-	-	-	-	-	-	-	-	-	-	-	P40939	P40939
P41240	CSK	CSK	Tyrosine-protein kinase CSK	P41240	Affinity Chromatography (MI:0004); Mass spectrometry (MI:0943); GST pull-down (MI:0059)	P41240	P41240	hcv non-structural protein 5a	P41240	-	-	-	-	-	-	-	-	-	-	-	-
P41250	GARS1	GARS1 GARS	Glycine--tRNA ligase	-	-	-	-	-	-	-	-	-	-	P41250	-	-	-	-	-	-	-
P41252	P41252	IARS1 IARS	Isoleucine--tRNA ligase, cytoplasmic	-	-	-	-	-	-	-	-	-	-	-	-	-	-	-	-	P41252	P41252
P42126	ECI1	ECI1 DCI	Enoyl-CoA delta isomerase 1, mitochondrial	-	-	-	-	-	-	-	-	-	-	P42126	-	-	-	-	-	-	-
P42166	P42166	TMPO LAP2	Lamina-associated polypeptide 2, isoform alpha	-	-	-	-	-	-	-	-	-	-	-	-	-	-	-	-	P42166	P42166
P42167	P42167	TMPO LAP2	Lamina-associated polypeptide 2, isoforms beta/gamma	-	-	-	-	-	-	-	-	-	-	-	-	-	-	-	-	P42167	P42167
P42224	STAT1	STAT1	Signal transducer and activator of transcription 1-alpha/beta	P42224	Coimmunoprecipitation (MI:0019); Confocal microscopy (MI:0663)	P42224	P42224	hcv non-structural protein 5a	-	-	-	-	-	P42224	-	-	-	-	-	-	-
P42338	PIK3CB	PIK3CB PIK3C1	Phosphatidylinositol 4,5-bisphosphate 3-kinase catalytic subunit beta isoform	P42338	Coimmunoprecipitation (MI:0019); GST pull-down (MI:0059)	P42338	P42338	hcv non-structural protein 5a	P42338	-	-	-	-	-	-	-	-	-	-	-	-
P42345	MTOR	MTOR FRAP FRAP1 FRAP2 RAFT1 RAPT1	Serine/threonine-protein kinase mTOR	-	-	-	P42345	hcv non-structural protein 5a	-	-	-	-	-	-	-	-	-	-	-	-	-
P42356	PI4KA	PI4KA PIK4 PIK4CA	Phosphatidylinositol 4-kinase alpha	P42356	Two Hybrid Test (MI:0018); GST pull-down (MI:0059)	P42356	P42356	hcv non-structural protein 5a	P42356	-	-	-	P42356	P42356	-	P42356	-	-	-	P42356	P42356
P42685	FRK	FRK PTK5 RAK	Tyrosine-protein kinase FRK	-	-	-	-	-	-	-	-	-	-	P42685	-	-	-	-	-	-	-
P42695	NCAPD3	NCAPD3 CAPD3 KIAA0056	Condensin-2 complex subunit D3	-	-	-	-	-	-	-	-	-	-	P42695	-	-	-	-	-	-	-
P42704	P42704	LRPPRC LRP130	Leucine-rich PPR motif-containing protein, mitochondrial	-	-	-	-	-	-	-	-	-	-	-	-	-	-	-	-	P42704	P42704
P42858	HTT	HTT HD IT15	Huntingtin	-	-	-	-	-	-	-	-	-	-	P42858	-	-	-	-	-	-	-
P43243	MATR3	MATR3 KIAA0723	Matrin-3	-	-	-	P43243	hcv non-structural protein 5a	-	-	-	-	-	-	-	-	-	-	-	-	-
P43304	P43304	GPD2	Glycerol-3-phosphate dehydrogenase, mitochondrial	-	-	-	-	-	-	-	-	-	-	-	-	-	-	-	-	P43304	P43304

P43405	SYK	SYK	Tyrosine-protein kinase SYK	-	-	P43405	P43405	hcv non-structural protein 5a	-	-	-	-	P43405	-	-	-	-	-	-	-	-
P43487	P43487	RANBP1	Ran-specific GTPase-activating protein	-	-	-	-	-	-	-	-	-	-	-	-	-	-	-	-	P43487	-
P43686	P43686	PSMC4 MIP224 TBP7	26S proteasome regulatory subunit 6B	-	-	-	-	-	-	-	-	-	-	-	-	-	-	-	-	P43686	-
P43694	P43694	GATA4	Transcription factor GATA-4	-	-	-	-	-	-	-	-	-	-	-	-	-	-	-	-	P43694	-
P45880	VDAC2	VDAC2	Voltage-dependent anion-selective channel protein 2	-	-	-	-	-	-	-	-	-	-	-	-	-	-	P45880	-	P45880	P45880
P45973	CBX5	CBX5 HP1A	Chromobox protein homolog 5	-	-	-	-	-	-	-	P45973	-	-	-	-	-	-	-	-	-	P45973
P46060	P46060	RANGAP1 KIAA1835 SD	Ran GTPase-activating protein 1	-	-	-	-	-	-	-	-	-	-	-	-	-	-	-	-	-	P46060
P46087	NOP2	NOP2 NOL1 NSUN1	Probable 28S rRNA	-	-	-	-	-	-	-	-	-	-	-	-	-	-	-	P46087	-	-
P46459	P46459	NSF	Vesicle-fusing ATPase	-	-	-	-	-	-	-	-	-	-	-	-	-	-	-	-	P46459	P46459
P46734	MAP2K3	MAP2K3 MEK3 MKK3 PRKMK3 SKK2	Dual specificity mitogen-activated protein kinase kinase 3	-	-	-	-	-	-	-	-	-	P46734	-	-	-	-	-	-	-	-
P46776	P46776	RPL27A	Large ribosomal subunit protein uL15	-	-	-	-	-	-	-	-	-	-	-	-	-	-	-	-	-	P46776
P46778	RPL21	RPL21	Large ribosomal subunit protein eL21	-	-	-	-	-	-	-	-	-	-	-	-	-	-	-	P46778	-	-
P46781	P46781	RPS9	Small ribosomal subunit protein uS4	-	-	-	-	-	-	-	-	-	-	-	-	-	-	-	-	-	P46781
P46939	UTRN	UTRN DMDL DRP1	Utrophin	-	-	-	-	-	-	-	-	-	P46939	-	-	-	-	-	-	-	-
P46977	P46977	STT3A ITM1 TMC	Dolichyl-diphosphooligosaccharide--protein glycosyltransferase subunit STT3A	-	-	-	-	-	-	-	-	-	-	-	-	-	-	-	-	P46977	P46977
P47897	P47897	QARS1 QARS	Glutamine--tRNA ligase	-	-	-	-	-	-	-	-	-	-	-	-	-	-	-	-	-	P47897
P47985	P47985	UQCRFS1	Cytochrome b-c1 complex subunit Rieske, mitochondrial	-	-	-	-	-	-	-	-	-	-	-	-	-	-	-	-	-	P47985
P48047	P48047	ATP5PO ATP5O ATPO	ATP synthase subunit O, mitochondrial	-	-	-	-	-	-	-	-	-	-	-	-	-	-	-	-	-	P48047
P48147	PREP	PREP PEP	Prolyl endopeptidase	-	-	-	-	-	-	-	-	-	P48147	-	-	-	-	-	-	-	-
P48444	ARCN1	ARCN1 COPD	Coatomer subunit delta	-	-	-	-	-	-	-	-	-	P48444	-	-	-	-	-	-	-	-
P48449	LSS	LSS OSC	Lanosterol synthase	-	-	-	-	-	-	-	-	-	P48449	-	-	-	-	-	-	P48449	P48449
P48507	P48507	GCLM GLCLR	Glutamate--cysteine ligase regulatory subunit	-	-	-	-	-	-	-	-	-	-	-	-	-	-	-	-	-	P48507
P48643	CCT5	CCT5 CCTE KIAA0098	T-complex protein 1 subunit epsilon	-	-	-	P48643	hcv ns 5	-	-	-	-	-	-	-	-	-	-	-	P48643	P48643
P48729	CSNK1A1	CSNK1A1	Casein kinase I isoform alpha	-	-	P48729	-	-	-	-	-	P48729	-	-	-	-	-	-	-	-	-
P48735	P48735	IDH2	Isocitrate dehydrogenase [NADP], mitochondrial	-	-	-	-	-	-	-	-	-	-	-	-	-	-	-	-	P48735	P48735
P48739	P48739	PITPNB	Phosphatidylinositol transfer protein beta isoform	-	-	-	-	-	-	-	-	-	-	-	-	-	-	-	-	P48739	-
P49257	P49257	LMAN1 ERGIC53 F5F8D	Protein ERGIC-53	-	-	-	-	-	-	-	-	-	-	-	-	-	-	-	-	P49257	P49257
P49327	FASN	FASN FAS	Fatty acid synthase	-	-	-	P49327	hcv non-structural protein 5a	-	-	-	-	-	-	-	-	-	-	-	P49327	P49327
P49368	P49368	CCT3 CCTG TRIC5	T-complex protein 1 subunit gamma	-	-	-	-	-	-	-	-	-	-	-	-	-	-	-	-	P49368	-
P49411	P49411	TUFM	Elongation factor Tu, mitochondrial	-	-	-	-	-	-	-	-	-	-	-	-	-	-	-	-	P49411	P49411
P49589	CARS1	CARS1 CARS	Cysteine--tRNA ligase, cytoplasmic	-	-	-	-	-	-	-	-	-	P49589	-	-	-	-	-	-	-	-
P49715	P49715	CEBPA CEBP	CCAAT/enhancer-binding protein alpha	-	-	-	-	-	-	-	-	-	-	-	-	-	-	-	-	-	P49715
P49748	P49748	ACADVL VLCAD	Very long-chain specific acyl-CoA dehydrogenase, mitochondrial	-	-	-	-	-	-	-	-	-	-	-	-	-	-	-	-	P49748	P49748
P49755	P49755	TMED10 TMP21	Transmembrane emp24 domain-containing protein 10	-	-	-	-	-	-	-	-	-	-	-	-	-	-	-	-	P49755	P49755
P49756	RBM25	RBM25 RNPC7	RNA-binding protein 25	-	-	-	-	-	-	-	-	-	-	-	-	-	-	-	P49756	-	P49756
P49761	P49761	CLK3	Dual specificity protein kinase CLK3	-	-	-	-	-	-	-	-	-	-	-	-	-	-	-	-	-	P49761

P49821	P49821	NDUFV1 UQOR1	NADH dehydrogenase [ubiquinone] flavoprotein 1, mitochondrial	-	-	-	-	-	-	-	-	-	-	-	-	-	-	-	-	P49821	-
P49840	GSK3A	GSK3A	Glycogen synthase kinase-3 alpha	P49840	GST pull-down (MI:0059); Kinase assay (MI:0424) (MI:0424)	P49840	P49840	hcv non-structural protein 5a	P49840	-	-	-	-	-	-	-	-	-	-	-	-
P49841	GSK3B	GSK3B	Glycogen synthase kinase-3 beta	P49841	GST pull-down (MI:0059); Kinase assay (MI:0424) (MI:0424)	P49841	P49841	hcv non-structural protein 5a	P49841	-	-	-	-	-	-	-	-	-	-	-	-
P50120	RBP2	RBP2 CRBP2	Retinol-binding protein 2	-	-	-	-	-	-	-	-	-	-	P50120	-	-	-	-	-	-	-
P50224	SULT1A3	SULT1A3 STM	Sulfotransferase 1A3	-	-	-	-	-	-	-	-	-	-	P50224	-	-	-	-	-	-	-
P50225	SULT1A1	SULT1A1 STP STP1 OK/SW-cl.88	Sulfotransferase 1A1	-	-	-	-	-	-	-	-	-	-	P50225	-	-	-	-	-	-	-
P50226	SULT1A2	SULT1A2 STP2	Sulfotransferase 1A2	-	-	-	-	-	-	-	-	-	-	P50226	-	-	-	-	-	-	-
P50402	EMD	EMD EDMD STA	Emerin	-	-	-	-	-	-	-	-	-	-	P50402	-	-	-	-	-	P50402	P50402
P50502	ST13	ST13 AAG2 FAM10A1 HIP SNC6	Hsc70-interacting protein	-	-	-	-	-	-	-	-	-	-	-	-	-	-	P50502	-	-	-
P50748	KNTC1	KNTC1 KIAA0166	Kinetochore-associated protein 1	-	-	-	-	-	-	-	-	-	-	P50748	-	-	-	-	-	-	-
P50895	P50895	BCAM LU MSK19	Basal cell adhesion molecule	-	-	-	-	-	-	-	-	-	-	-	-	-	-	-	-	P50895	P50895
P50897	P50897	PPT1 CLN1 PPT	Palmitoyl-protein thioesterase 1	-	-	-	-	-	-	-	-	-	-	-	-	-	-	-	-	P50897	-
P50990	P50990	CCT8 C21orf112 CCTQ KIAA0002	T-complex protein 1 subunit theta	-	-	-	-	-	-	-	-	-	-	-	-	-	-	-	-	P50990	P50990
P50991	P50991	CCT4 CCTD SRB	T-complex protein 1 subunit delta	-	-	-	-	-	-	-	-	-	-	-	-	-	-	-	-	-	P50991
P51114	P51114	FXR1	RNA-binding protein FXR1	-	-	-	-	-	-	-	-	-	-	-	-	-	-	-	-	P51114	P51114
P51116	P51116	FXR2 FMR1L2	RNA-binding protein FXR2	-	-	-	-	-	-	-	-	-	-	-	-	-	-	-	-	-	P51116
P51148	RAB5C	RAB5C RABL	Ras-related protein Rab-5C	-	-	-	-	-	-	-	-	-	-	P51148	-	-	-	-	-	P51148	P51148
P51149	RAB7A	RAB7A RAB7	Ras-related protein Rab-7a	-	-	-	-	-	-	-	-	-	-	-	-	-	-	P51149	-	P51149	P51149
P51397	P51397	DAP DAP1	Death-associated protein 1	-	-	-	-	-	-	-	-	-	-	-	-	-	-	-	-	-	P51397
P51452	DUSP3	DUSP3 VHR	Dual specificity protein phosphatase 3	-	-	-	-	-	-	-	-	-	-	P51452	-	-	-	-	-	-	-
P51570	P51570	GALK1 GALK	Galactokinase	-	-	-	-	-	-	-	-	-	-	-	-	-	-	-	-	P51570	P51570
P51571	SSR4	SSR4 TRAPD	Translocon-associated protein subunit delta	-	-	-	-	-	-	-	-	-	-	P51571	-	-	-	-	-	P51571	P51571
P51572	BCAP31	BCAP31 BAP31 DXS1357E	B-cell receptor-associated protein 31	-	-	-	-	-	-	-	-	-	-	-	-	-	-	P51572	-	P51572	P51572
P51648	P51648	ALDH3A2 ALDH10 FALDH	Aldehyde dehydrogenase family 3 member A2	-	-	-	-	-	-	-	-	-	-	-	-	-	-	-	-	P51648	P51648
P51659	HSD17B4	HSD17B4 EDH17B4	Peroxisomal multifunctional enzyme type 2	-	-	-	-	-	-	-	-	-	-	-	P51659	-	-	-	-	-	P51659
P51665	P51665	PSMD7 MOV34L	26S proteasome non-ATPase regulatory subunit 7	-	-	-	-	-	-	-	-	-	-	-	-	-	-	-	-	P51665	P51665
P51970	P51970	NDUFA8	NADH dehydrogenase [ubiquinone] 1 alpha subcomplex subunit 8	-	-	-	-	-	-	-	-	-	-	-	-	-	-	-	-	P51970	P51970
P51991	HNRNPA3	HNRNPA3 HNRPA3	Heterogeneous nuclear ribonucleoprotein A3	-	-	-	-	-	-	-	-	-	-	-	-	-	-	-	P51991	-	P51991
P52209	PGD	PGD PGDH	6-phosphogluconate dehydrogenase, decarboxylating	-	-	-	-	-	-	-	-	-	-	P52209	-	-	-	-	-	-	P52209
P52272	P52272	HNRNPM HNRPM NAGR1	Heterogeneous nuclear ribonucleoprotein M	-	-	-	-	-	-	-	-	-	-	-	-	-	-	-	-	-	P52272
P52292	P52292	KPNA2 RCH1 SRP1	Importin subunit alpha-1	-	-	-	-	-	-	-	-	-	-	-	-	-	-	-	-	P52292	P52292
P52294	KPNA1	KPNA1 RCH2	Importin subunit alpha-5	-	-	-	P52294	hcv non-structural protein 5a	-	-	-	-	-	-	-	-	-	-	-	-	-
P52594	AGFG1	AGFG1 HRB RAB RIP	Arf-GAP domain and FG repeat-containing protein 1	-	-	-	P52594	hcv non-structural protein 5a	-	-	-	-	-	-	-	-	-	-	-	-	-
P52597	HNRNPF	HNRNPF HNRPF	Heterogeneous nuclear ribonucleoprotein F	-	-	-	P52597	NS3, NS5	-	-	-	-	-	-	-	-	-	-	-	-	-

P52789	HK2	HK2	Hexokinase-2	-	-	-	P52789	HCV NS5A, HCV NS5A PROTEIN	-	-	-	-	P52789	-	-	-	-	-	-	-	-
P52815	P52815	MRPL12 MRPL7 RPML12	Large ribosomal subunit protein bL12m	-	-	-	-	-	-	-	-	-	-	-	-	-	-	-	-	-	P52815
P52907	CAPZA1	CAPZA1	F-actin-capping protein subunit alpha-1	-	-	-	-	-	-	-	-	-	-	-	-	-	P52907	-	-	-	-
P53007	SLC25A1	SLC25A1 SLC20A3	Tricarboxylate transport protein, mitochondrial	-	-	-	-	-	-	-	-	-	-	-	-	-	-	P53007	-	-	-
P53350	PLK1	PLK1 PLK	Serine/threonine-protein kinase PLK1	-	-	P53350	-	-	-	-	-	-	P53350	-	-	-	-	-	-	-	-
P53367	ARFIP1	ARFIP1	Arfaptin-1	P53367	Two Hybrid Test (MI:0018)	P53367	-	-	-	P53367	-	-	-	-	-	-	-	-	-	-	-
P53396	ACLY	ACLY	ATP-citrate synthase	P53396	Two Hybrid Test (MI:0018)	P53396	-	-	-	P53396	-	-	-	-	-	-	-	-	-	-	-
P53618	COPB1	COPB1 COPB MSTP026	Coatomer subunit beta	-	-	-	-	-	-	-	-	-	-	P53618	-	-	-	-	-	-	-
P53621	P53621	COPA	Coatomer subunit alpha	-	-	-	-	-	-	-	-	-	-	-	-	-	-	-	-	P53621	P53621
P53634	CTSC	CTSC CPPI	Dipeptidyl peptidase 1	-	-	-	-	-	-	-	-	-	-	P53634	-	-	-	-	-	-	-
P53778	MAPK12	MAPK12 ERK6 SAPK3	Mitogen-activated protein kinase 12	P53778	Kinase assay (MI:0424) (MI:0424); GST pull-down (MI:0059)	P53778	P53778	hcv non-structural protein 5a	P53778	-	-	-	-	-	-	-	-	-	-	-	-
P53985	P53985	SLC16A1 MCT1	Monocarboxylate transporter 1	-	-	-	-	-	-	-	-	-	-	-	-	-	-	-	-	P53985	P53985
P54132	P54132	BLM RECQ2 RECQL3	RecQ-like DNA helicase BLM	-	-	-	-	-	-	-	-	-	-	-	-	-	-	-	-	-	P54132
P54136	P54136	RARS1 RARS	Arginine--tRNA ligase, cytoplasmic	-	-	-	-	-	-	-	-	-	-	-	-	-	-	-	-	P54136	-
P54577	P54577	YARS1 YARS	Tyrosine--tRNA ligase, cytoplasmic	-	-	-	-	-	-	-	-	-	-	-	-	-	-	-	-	P54577	P54577
P54652	P54652	HSPA2	Heat shock-related 70 kDa protein 2	-	-	-	-	-	-	-	-	-	-	-	-	-	-	-	-	P54652	P54652
P54709	P54709	ATP1B3	Sodium/potassium-transporting ATPase subunit beta-3	-	-	-	-	-	-	-	-	-	-	-	-	-	-	-	-	P54709	P54709
P54819	P54819	AK2 ADK2	Adenylate kinase 2, mitochondrial	-	-	-	-	-	-	-	-	-	-	-	-	-	-	-	-	-	P54819
P54886	ALDH18A1	ALDH18A1 GSAS P5CS PYCS	Delta-1-pyrroline-5-carboxylate synthase	-	-	-	-	-	-	-	-	-	-	-	-	-	-	-	P54886	-	-
P54920	P54920	NAPA SNAPA	Alpha-soluble NSF attachment protein	-	-	-	-	-	-	-	-	-	-	-	-	-	-	-	-	P54920	P54920
P55010	P55010	EIF5	Eukaryotic translation initiation factor 5	-	-	-	-	-	-	-	-	-	-	-	-	-	-	-	-	P55010	-
P55060	P55060	CSE1L CAS XPO2	Exportin-2	-	-	-	-	-	-	-	-	-	-	-	-	-	-	-	-	P55060	-
P55072	VCP	VCP HEL-220 HEL-S-70	Transitional endoplasmic reticulum ATPase	-	-	-	-	-	-	-	-	-	-	-	-	-	-	P55072	-	P55072	-
P55084	P55084	HADHB MSTP029	Trifunctional enzyme subunit beta, mitochondrial	-	-	-	-	-	-	-	-	-	-	-	-	-	-	-	-	-	P55084
P55157	P55157	MTTP MTP	Microsomal triglyceride transfer protein large subunit	-	-	-	-	-	-	-	-	-	-	-	-	-	-	-	-	-	P55157
P55209	NAP1L1	NAP1L1 NRP	Nucleosome assembly protein 1-like 1	P55209	Two Hybrid Test (MI:0018)	P55209	P55209	hcv non-structural protein 5a	-	P55209	-	-	-	-	-	P55209	-	P55209	-	P55209	P55209
P55317	P55317	FOXA1 HNF3A TCF3A	Hepatocyte nuclear factor 3-alpha	-	-	-	-	-	-	-	-	-	-	-	-	-	-	-	-	P55317	-
P55327	P55327	TPD52	Tumor protein D52	-	-	-	-	-	-	-	-	-	-	-	-	-	-	-	-	P55327	P55327
P56134	P56134	ATP5MF ATP5J2 ATP5JL	ATP synthase subunit f, mitochondrial	-	-	-	-	-	-	-	-	-	-	-	-	-	-	-	-	P56134	P56134
P56192	P56192	MARS1 MARS	Methionine--tRNA ligase, cytoplasmic	-	-	-	-	-	-	-	-	-	-	-	-	-	-	-	-	-	P56192
P56385	P56385	ATP5ME ATP5I ATP5K	ATP synthase subunit e, mitochondrial	-	-	-	-	-	-	-	-	-	-	-	-	-	-	-	-	-	P56385
P56556	P56556	NDUFA6 LYRM6 NADHB14	NADH dehydrogenase [ubiquinone] 1 alpha subcomplex subunit 6	-	-	-	-	-	-	-	-	-	-	-	-	-	-	-	-	P56556	P56556
P57053	P57053	H2BC12L H2BFS H2BS1	Histone H2B type F-S	-	-	-	-	-	-	-	-	-	-	-	-	-	-	-	-	-	P57053
P57075	UBASH3A	UBASH3A STS2	Ubiquitin-associated and SH3 domain-containing protein A	P57075	Two Hybrid Test (MI:0018)	P57075	-	-	-	P57075	-	-	-	-	-	-	-	-	-	-	-
P57088	P57088	TMEM33 DB83	Transmembrane protein 33	-	-	-	-	-	-	-	-	-	-	-	-	-	-	-	-	P57088	P57088
P57678	GEMIN4	GEMIN4	Gem-associated protein 4	-	-	-	-	-	-	-	-	-	-	-	-	-	-	-	P57678	-	-
P59998	P59998	ARPC4 ARC20	Actin-related protein 2/3 complex subunit 4	-	-	-	-	-	-	-	-	-	-	-	-	-	-	-	-	-	P59998

P60174	TPI1	TPI1 TPI	Triosephosphate isomerase	-	-	-	-	-	-	-	-	-	-	P60174	-	-	-	P60174	-	P60174	-
P60468	SEC61B	SEC61B	Protein transport protein Sec61 subunit beta	-	-	-	-	-	-	-	-	-	-	P60468	-	-	-	-	-	P60468	P60468
P60520	GABARAPL2	GABARAPL2 FLC3A GEF2	Gamma-aminobutyric acid receptor-associated protein-like 2	-	-	-	-	-	-	-	-	P60520	-	-	-	-	-	-	-	-	-
P60602	P60602	ROMO1 C20orf52	Reactive oxygen species modulator 1	-	-	-	-	-	-	-	-	-	-	-	-	-	-	-	-	P60602	P60602
P60660	MYL6	MYL6	Myosin light polypeptide 6	-	-	-	-	-	-	-	-	-	-	-	-	-	-	-	P60660	-	-
P60709	ACTB	ACTB	Actin, cytoplasmic 1	-	-	P60709	-	-	-	-	-	-	-	-	-	-	-	-	-	-	-
P60903	P60903	S100A10 ANX2LG CAL1L CLP11	Protein S100-A10	-	-	-	-	-	-	-	-	-	-	-	-	-	-	-	-	P60903	P60903
P60953	P60953	CDC42	Cell division control protein 42 homolog	-	-	-	-	-	-	-	-	-	-	-	-	-	-	-	-	P60953	P60953
P61006	RAB8A	RAB8A MEL RAB8	Ras-related protein Rab-8A	-	-	-	-	-	-	-	-	-	-	P61006	-	-	-	-	-	P61006	P61006
P61009	P61009	SPCS3 SPC22 UNQ1841/PRO3567	Signal peptidase complex subunit 3	-	-	-	-	-	-	-	-	-	-	-	-	-	-	-	-	-	P61009
P61019	P61019	RAB2A RAB2	Ras-related protein Rab-2A	-	-	-	-	-	-	-	-	-	-	-	-	-	-	-	-	P61019	P61019
P61020	P61020	RAB5B	Ras-related protein Rab-5B	-	-	-	-	-	-	-	-	-	-	-	-	-	-	-	-	P61020	P61020
P61026	P61026	RAB10	Ras-related protein Rab-10	-	-	-	-	-	-	-	-	-	-	-	-	-	-	-	-	P61026	P61026
P61081	UBE2M	UBE2M UBC12	NEDD8-conjugating enzyme Ubc12	-	-	-	-	-	-	-	-	-	-	P61081	-	-	-	-	-	-	-
P61086	UBE2K	UBE2K HIP2 LIG	Ubiquitin-conjugating enzyme E2 K	-	-	-	-	-	-	-	-	-	-	P61086	-	-	-	-	-	-	-
P61106	P61106	RAB14	Ras-related protein Rab-14	-	-	-	-	-	-	-	-	-	-	-	-	-	-	-	-	P61106	P61106
P61163	P61163	ACTR1A CTRN1	Alpha-centractin	-	-	-	-	-	-	-	-	-	-	-	-	-	-	-	-	-	P61163
P61221	P61221	ABCE1 RLI RNASEL1 RNASELI RNS4I OK/SW-cl.40	ATP-binding cassette sub-family E member 1	-	-	-	-	-	-	-	-	-	-	-	-	-	-	-	-	-	P61221
P61224	P61224	RAP1B OK/SW-cl.11	Ras-related protein Rap-1b	-	-	-	-	-	-	-	-	-	-	-	-	-	-	-	-	-	P61224
P61247	RPS3A	RPS3A FTE1 MFTL	Small ribosomal subunit protein eS1	-	-	-	-	-	-	-	-	-	-	-	-	-	-	-	P61247	-	-
P61289	P61289	PSME3	Proteasome activator complex subunit 3	-	-	-	-	-	-	-	-	-	-	-	-	-	-	-	-	P61289	P61289
P61586	RHOA	RHOA ARH12 ARHA RHO12	Transforming protein RhoA	-	-	-	-	-	-	-	-	-	-	-	-	-	-	P61586	-	P61586	-
P61604	HSPE1	HSPE1	10 kDa heat shock protein, mitochondrial	-	-	-	-	-	-	-	-	-	-	-	-	-	-	P61604	-	-	P61604
P61619	P61619	SEC61A1 SEC61A	Protein transport protein Sec61 subunit alpha isoform 1	-	-	-	-	-	-	-	-	-	-	-	-	-	-	-	-	P61619	P61619
P61803	P61803	DAD1	Dolichyl-diphosphooligosaccharide--protein glycosyltransferase subunit DAD1	-	-	-	-	-	-	-	-	-	-	-	-	-	-	-	-	-	P61803
P61923	P61923	COPZ1 COPZ CGI-120 HSPC181	Coatomer subunit zeta-1	-	-	-	-	-	-	-	-	-	-	-	-	-	-	-	-	-	P61923
P61927	RPL37	RPL37	Large ribosomal subunit protein eL37	-	-	-	-	-	-	-	-	P61927	-	-	-	-	-	-	-	-	-
P61978	HNRNPK	HNRNPK HNRPK	Heterogeneous nuclear ribonucleoprotein K	-	-	-	-	-	-	-	-	-	-	-	-	-	-	-	P61978	-	P61978
P62136	P62136	PPP1CA PPP1A	Serine/threonine-protein phosphatase PP1-alpha catalytic subunit	-	-	-	-	-	-	-	-	-	-	-	-	-	-	-	-	P62136	-
P62191	P62191	PSMC1	26S proteasome regulatory subunit 4	-	-	-	-	-	-	-	-	-	-	-	-	-	-	-	-	P62191	-
P62195	P62195	PSMC5 SUG1	26S proteasome regulatory subunit 8	-	-	-	-	-	-	-	-	-	-	-	-	-	-	-	-	-	P62195
P62244	P62244	RPS15A OK/SW-cl.82	Small ribosomal subunit protein uS8	-	-	-	-	-	-	-	-	-	-	-	-	-	-	-	-	-	P62244
P62258	YWHAE	YWHAE	14-3-3 protein epsilon	-	-	-	-	-	-	-	-	-	-	-	-	-	-	P62258	-	-	-
P62280	RPS11	RPS11	Small ribosomal subunit protein uS17	-	-	-	-	-	-	-	-	-	-	-	-	-	-	-	P62280	-	-
P62304	SNRPE	SNRPE	Small nuclear ribonucleoprotein E	-	-	-	-	-	-	-	-	-	-	-	-	-	-	P62304	P62304	-	-

P62314	SNRPD1	SNRPD1	Small nuclear ribonucleoprotein Sm D1	-	-	-	-	-	-	-	-	-	-	-	-	-	-	P62314	-	-
P62316	SNRPD2	SNRPD2 SNRPD1	Small nuclear ribonucleoprotein Sm D2	-	-	-	-	-	-	-	-	-	-	-	-	-	-	P62316	-	P62316
P62318	SNRPD3	SNRPD3	Small nuclear ribonucleoprotein Sm D3	-	-	-	-	-	-	-	-	-	-	-	-	-	-	P62318	-	-
P62333	P62333	PSMC6 SUG2	26S proteasome regulatory subunit 10B	-	-	-	-	-	-	-	-	-	-	-	-	-	-	-	-	P62333
P62491	RAB11A	RAB11A RAB11	Ras-related protein Rab-11A	-	-	-	-	-	-	-	-	-	-	P62491	-	-	-	-	P62491	-
P62714	PPP2CB	PPP2CB	Serine/threonine-protein phosphatase 2A catalytic subunit beta isoform	-	-	-	-	-	-	-	-	-	-	P62714	-	-	-	-	-	-
P62745	RHOB	RHOB ARH6 ARHB	Rho-related GTP-binding protein RhoB	-	-	-	-	-	-	-	-	-	-	-	-	-	-	P62745	-	-
P62820	P62820	RAB1A RAB1	Ras-related protein Rab-1A	-	-	-	-	-	-	-	-	-	-	-	-	-	-	-	P62820	P62820
P62826	RAN	RAN ARA24 OK/SW-cl.81	GTP-binding nuclear protein Ran	-	-	-	-	-	-	-	-	-	-	P62826	-	-	-	P62826	-	-
P62841	RPS15	RPS15 RIG	Small ribosomal subunit protein uS19	-	-	-	-	-	-	-	-	-	-	P62841	-	-	-	-	-	-
P62873	GNB1	GNB1	Guanine nucleotide-binding protein G	-	-	-	-	-	-	-	-	-	-	P62873	-	-	-	-	P62873	P62873
P62879	GNB2	GNB2	Guanine nucleotide-binding protein G	-	-	-	-	-	-	-	-	-	-	P62879	-	-	-	-	P62879	P62879
P62899	P62899	RPL31	Large ribosomal subunit protein eL31	-	-	-	-	-	-	-	-	-	-	-	-	-	-	-	-	P62899
P62937	PPIA	PPIA CYPA	Peptidyl-prolyl cis-trans isomerase A	-	-	P62937	P62937	hcv non-structural protein 5a	-	-	-	-	P62937	-	-	-	-	P62937	-	-	-
P62942	P62942	FKBP1A FKBP1 FKBP12	Peptidyl-prolyl cis-trans isomerase FKBP1A	-	-	-	-	-	-	-	-	-	-	-	-	-	-	-	-	P62942
P62979	RPS27A	RPS27A UBA80 UBCEP1	Ubiquitin-ribosomal protein eS31 fusion protein	-	-	-	-	-	-	-	-	-	-	P62979	-	-	-	-	-	-	-
P62987	UBA52	UBA52 UBCEP2	Ubiquitin-ribosomal protein eL40 fusion protein	-	-	-	-	-	-	-	-	-	-	P62987	-	-	-	-	-	-	-
P62993	GRB2	GRB2 ASH	Growth factor receptor-bound protein 2	P62993	Immunoblotting (MI:0113); Affinity Chromatography (MI:0004); Two Hybrid Test (MI:0018); Coimmunoprecipitation (MI:0019)	P62993	P62993	hcv non-structural protein 5a	P62993	-	-	-	P62993	-	-	-	-	-	-	-	-
P62995	TRA2B	TRA2B SFRS10	Transformer-2 protein homolog beta	-	-	-	-	-	-	-	-	-	-	-	-	-	-	-	P62995	-	-
P63000	P63000	RAC1 TC25 MIG5	Ras-related C3 botulinum toxin substrate 1	-	-	-	-	-	-	-	-	-	-	-	-	-	-	-	-	P63000	-
P63104	YWHAZ	YWHAZ	14-3-3 protein zeta/delta	-	-	-	-	-	-	-	-	-	-	-	-	-	-	P63104	-	-	P63104
P63162	SNRPN	SNRPN HCERN3 SMN	Small nuclear ribonucleoprotein-associated protein N	-	-	-	-	-	-	-	-	-	-	P63162	-	-	-	-	P63162	-	-
P63167	P63167	DYNLL1 DLC1 DNCL1 DNCLC1 HDLC1	Dynein light chain 1, cytoplasmic	-	-	-	-	-	-	-	-	-	-	-	-	-	-	-	-	P63167	-
P63244	RACK1	RACK1 GNB2L1 HLC7 PIG21	Small ribosomal subunit protein RACK1	-	-	-	-	-	-	-	-	-	-	-	-	-	-	P63244	-	-	-
P63261	ACTG1	ACTG1 ACTG	Actin, cytoplasmic 2	-	-	-	-	-	-	-	-	-	-	-	-	-	-	-	P63261	-	-
P67775	PPP2CA	PPP2CA	Serine/threonine-protein phosphatase 2A catalytic subunit alpha isoform	-	-	P67775	-	-	-	-	-	-	P67775	-	-	-	-	-	-	-	-
P67809	P67809	YBX1 NSEP1 YB1	Y-box-binding protein 1	-	-	-	-	-	-	-	-	-	-	-	-	-	-	-	-	P67809	P67809
P68366	P68366	TUBA4A TUBA1	Tubulin alpha-4A chain	-	-	-	-	-	-	-	-	-	-	-	-	-	-	-	-	P68366	P68366
P68371	TUBB4B	TUBB4B TUBB2C	Tubulin beta-4B chain	-	-	-	P68371	hcv ns 5	-	-	-	-	-	-	-	-	-	P68371	-	-	P68371
P68400	CSNK2A1	CSNK2A1 CK2A1	Casein kinase II subunit alpha	P68400	GST pull-down (MI:0059); Affinity Chromatography (MI:0004); Kinase assay (MI:0424) (MI:0424); Mutational analysis (MI:0074)	P68400	-	-	-	-	-	-	-	-	-	-	-	-	P68400	-	-
P78316	NOP14	NOP14 C4orf9 NOL14 RES4-25	Nucleolar protein 14	-	-	-	-	-	-	-	-	-	-	P78316	-	-	-	-	-	-	-

P78337	PITX1	PITX1 BFT PTX1	Pituitary homeobox 1	P78337	Two Hybrid Test (MI:0018); Coimmunoprecipitation (MI:0019)	P78337	P78337	hcv non-structural protein 5a	P78337	-	-	-	P78337	-	-	-	-	-	-	-	-
P78344	EIF4G2	EIF4G2 DAP5 OK/SW-cl.75	Eukaryotic translation initiation factor 4 gamma 2	-	-	-	-	-	-	-	P78344	-	-	-	-	-	-	-	-	P78344	-
P78347	P78347	GTF2I BAP135 WBSCR6	General transcription factor II-I	-	-	-	-	-	-	-	-	-	-	-	-	-	-	-	-	-	P78347
P78362	SRPK2	SRPK2	SRSF protein kinase 2	-	-	-	-	-	-	-	-	-	-	-	-	-	-	-	P78362	-	-
P78371	P78371	CCT2 99D8.1 CCTB	T-complex protein 1 subunit beta	-	-	-	-	-	-	-	-	-	-	-	-	-	-	-	-	P78371	P78371
P78527	PRKDC	PRKDC HYRC HYRC1	DNA-dependent protein kinase catalytic subunit	-	-	-	-	-	-	-	-	-	-	P78527	-	-	-	P78527	P78527	P78527	P78527
P80723	BASP1	BASP1 NAP22	Brain acid soluble protein 1	-	-	-	-	-	-	-	-	-	-	-	-	-	-	P80723	-	-	-
P82094	TMF1	TMF1 ARA160	TATA element modulatory factor	P82094	Two Hybrid Test (MI:0018)	P82094	-	-	-	P82094	-	-	-	-	-	-	-	-	-	-	-
P82912	MRPS11	MRPS11 RPMS11 HCC2	Small ribosomal subunit protein uS11m	-	-	-	-	-	-	-	-	-	-	P82912	-	-	-	-	-	-	-
P83111	P83111	LACTB MRPL56 UNQ843/PRO1781	Serine beta-lactamase-like protein LACTB, mitochondrial	-	-	-	-	-	-	-	-	-	-	-	-	-	-	-	-	P83111	P83111
P83731	P83731	RPL24	Large ribosomal subunit protein eL24	-	-	-	-	-	-	-	-	-	-	-	-	-	-	-	-	-	P83731
P84085	P84085	ARF5	ADP-ribosylation factor 5	-	-	-	-	-	-	-	-	-	-	-	-	-	-	-	-	P84085	-
P84090	P84090	ERH	Enhancer of rudimentary homolog	-	-	-	-	-	-	-	-	-	-	-	-	-	-	-	-	-	P84090
P84098	P84098	RPL19	Large ribosomal subunit protein eL19	-	-	-	-	-	-	-	-	-	-	-	-	-	-	-	-	-	P84098
P84103	SRSF3	SRSF3 SFRS3 SRP20	Serine/arginine-rich splicing factor 3	-	-	-	-	-	-	-	-	-	-	-	-	-	-	-	P84103	-	-
P85037	FOXK1	FOXK1 MNF	Forkhead box protein K1	-	-	-	-	-	-	-	-	-	-	-	-	-	-	P85037	-	-	P85037
P98175	RBM10	RBM10 DXS8237E GPATC9 GPATCH9 KIAA0122	RNA-binding protein 10	-	-	-	-	-	-	-	P98175	-	-	-	-	-	-	-	-	-	-
P98179	RBM3	RBM3 RNPL	RNA-binding protein 3	-	-	-	-	-	-	-	-	-	-	P98179	-	-	-	-	-	-	-
P98194	P98194	ATP2C1 KIAA1347 PMR1L HUSSY-28	Calcium-transporting ATPase type 2C member 1	-	-	-	-	-	-	-	-	-	-	-	-	-	-	-	-	P98194	P98194
Q00325	Q00325	SLC25A3 PHC OK/SW-cl.48	Solute carrier family 25 member 3	-	-	-	-	-	-	-	-	-	-	-	-	-	-	-	-	Q00325	-
Q00534	CDK6	CDK6 CDKN6	Cyclin-dependent kinase 6	Q00534	Kinase assay (MI:0424) (MI:0424); GST pull-down (MI:0059)	Q00534	Q00534	hcv non-structural protein 5a	Q00534	-	-	-	-	-	-	-	-	-	-	-	-
Q00610	CLTC	CLTC CLH17 CLTCL2 KIAA0034	Clathrin heavy chain 1	-	-	-	-	-	-	-	-	-	-	-	-	-	-	-	Q00610	Q00610	Q00610
Q00796	SORD	SORD	Sorbitol dehydrogenase	-	-	-	-	-	-	-	-	-	-	Q00796	-	-	-	-	-	-	Q00796
Q00839	Q00839	HNRNPU C1orf199 HNRPU SAFA U21.1	Heterogeneous nuclear ribonucleoprotein U	-	-	-	-	-	-	-	-	-	-	-	-	-	-	-	-	Q00839	Q00839
Q01105	SET	SET	Protein SET	-	-	-	-	-	-	-	-	-	-	-	-	-	-	Q01105	-	-	Q01105
Q01167	Q01167	FOXK2 ILF ILF1	Forkhead box protein K2	-	-	-	-	-	-	-	-	-	-	-	-	-	-	-	-	-	Q01167
Q01433	AMPD2	AMPD2	AMP deaminase 2	-	-	-	-	-	-	-	-	-	-	Q01433	-	-	-	-	-	-	-
Q01469	Q01469	FABP5	Fatty acid-binding protein 5	-	-	-	-	-	-	-	-	-	-	-	-	-	-	-	-	-	Q01469
Q01581	Q01581	HMGCS1 HMGCS	Hydroxymethylglutaryl-CoA synthase, cytoplasmic	-	-	-	-	-	-	-	-	-	-	-	-	-	-	-	-	-	Q01581
Q01650	Q01650	SLC7A5 CD98LC LAT1 MPE16	Large neutral amino acids transporter small subunit 1	-	-	-	-	-	-	-	-	-	-	-	-	-	-	-	-	Q01650	Q01650
Q01780	Q01780	EXOSC10 PMSCL PMSCL2 RRP6	Exosome component 10	-	-	-	-	-	-	-	-	-	-	-	-	-	-	-	-	Q01780	-
Q01844	EWSR1	EWSR1 EWS	RNA-binding protein EWS	-	-	-	-	-	-	-	-	-	-	-	-	-	-	Q01844	-	-	-
Q02543	RPL18A	RPL18A	Large ribosomal subunit protein eL20	Q02543	Two Hybrid Test (MI:0018)	Q02543	-	-	-	Q02543	-	-	-	-	-	-	-	-	-	-	Q02543

Q02818	NUCB1	NUCB1 NUC	Nucleobindin-1	Q02818	Two Hybrid Test (MI:0018)	Q02818	-	-	-	Q02818	-	-	-	-	-	-	-	-	-	-	-
Q02978	Q02978	SLC25A11 SLC20A4	Mitochondrial 2-oxoglutarate/malate carrier protein	-	-	-	-	-	-	-	-	-	-	-	-	-	-	-	-	-	Q02978
Q03154	ACY1	ACY1	Aminoacylase-1	-	-	-	-	-	-	-	-	-	-	Q03154	-	-	-	-	-	-	-
Q03188	CENPC	CENPC CENPC1 ICEN7	Centromere protein C	Q03188	Two Hybrid Test (MI:0018)	Q03188	-	-	-	Q03188	-	-	-	-	-	-	-	-	-	-	-
Q04637	Q04637	EIF4G1 EIF4F EIF4G EIF4GI	Eukaryotic translation initiation factor 4 gamma 1	-	-	-	-	-	-	-	-	-	-	-	-	-	-	-	-	-	Q04637
Q04837	SSBP1	SSBP1 SSBP	Single-stranded DNA-binding protein, mitochondrial	-	-	-	-	-	-	-	-	-	-	-	Q04837	-	-	-	-	-	-
Q05086	UBE3A	UBE3A E6AP EPVE6AP HPVE6A	Ubiquitin-protein ligase E3A	-	-	-	Q05086	hcv ns 5	-	-	-	-	-	-	-	-	-	-	-	-	-
Q05519	SRSF11	SRSF11 SFRS11	Serine/arginine-rich splicing factor 11	-	-	-	-	-	-	-	-	-	-	-	-	-	-	-	Q05519	-	-
Q05682	Q05682	CALD1 CAD CDM	Caldesmon	-	-	-	-	-	-	-	-	-	-	-	-	-	-	-	-	Q05682	-
Q06323	Q06323	PSME1 IFI5111	Proteasome activator complex subunit 1	-	-	-	-	-	-	-	-	-	-	-	-	-	-	-	-	Q06323	-
Q06830	PRDX1	PRDX1 PAGA PAGB TDPX2	Peroxiredoxin-1	-	-	-	-	-	-	-	-	-	-	Q06830	-	-	-	Q06830	-	-	Q06830
Q07021	Q07021	C1QBP GC1QBP HABP1 SF2P32	Complement component 1 Q subcomponent-binding protein, mitochondrial	-	-	-	-	-	-	-	-	-	-	-	-	-	-	-	-	-	Q07021
Q07065	Q07065	CKAP4	Cytoskeleton-associated protein 4	-	-	-	-	-	-	-	-	-	-	-	-	-	-	-	-	Q07065	Q07065
Q07666	Q07666	KHDRBS1 SAM68	KH domain-containing, RNA-binding, signal transduction-associated protein 1	-	-	-	-	-	-	-	-	-	-	-	-	-	-	-	-	Q07666	-
Q07812	BAX	BAX BCL2L4	Apoptosis regulator BAX	Q07812	Immunofluorescence (MI:0022); Coimmunoprecipitation (MI:0019)	Q07812	Q07812	hcv non-structural protein 5a	Q07812	-	-	-	Q07812	-	-	-	-	-	-	Q07812	Q07812
Q07954	LRP1	LRP1 A2MR APR	Prolow-density lipoprotein receptor-related protein 1	-	-	-	-	-	-	-	-	-	-	Q07954	-	-	-	-	-	-	-
Q07955	SRSF1	SRSF1 ASF SF2 SF2P33 SFRS1 OK/SW-cl.3	Serine/arginine-rich splicing factor 1	-	-	-	-	-	-	-	-	-	-	-	-	-	-	-	Q07955	-	-
Q08211	DHX9	DHX9 DDX9 LKP NDH2	ATP-dependent RNA helicase A	-	-	-	-	-	-	-	-	-	-	-	-	-	-	-	Q08211	-	-
Q08379	GOLGA2	GOLGA2	Golgin subfamily A member 2	Q08379	Two Hybrid Test (MI:0018); Co-affinity purification (MI:0025)	Q08379	Q08379	hcv non-structural protein 5a	-	Q08379	Q08379	-	-	-	-	-	-	-	-	-	-
Q08752	Q08752	PPID CYP40 CYPD	Peptidyl-prolyl cis-trans isomerase D	-	-	-	-	-	-	-	-	-	-	-	-	-	-	-	-	Q08752	Q08752
Q09472	EP300	EP300 P300	Histone acetyltransferase p300	-	-	-	-	-	-	-	-	-	-	Q09472	-	-	-	-	-	-	-
Q09666	AHNAK	AHNAK PM227	Neuroblast differentiation-associated protein AHNAK	Q09666	Two Hybrid Test (MI:0018); GST pull-down (MI:0059)	Q09666	Q09666	hcv non-structural protein 5a	Q09666	-	-	-	-	-	-	-	-	-	-	-	-
Q10471	Q10471	GALNT2	Polypeptide N-acetylgalactosaminyltransferase 2	-	-	-	-	-	-	-	-	-	-	-	-	-	-	-	-	Q10471	Q10471
Q10570	CPSF1	CPSF1 CPSF160	Cleavage and polyadenylation specificity factor subunit 1	-	-	-	-	-	-	-	-	-	-	Q10570	-	-	-	-	-	-	-
Q12797	Q12797	ASPH BAH	Aspartyl/asparaginyl beta-hydroxylase	-	-	-	-	-	-	-	-	-	-	-	-	-	-	-	-	Q12797	Q12797
Q12805	EFEMP1	EFEMP1 FBLN3 FBNL	EGF-containing fibulin-like extracellular matrix protein 1	Q12805	Two Hybrid Test (MI:0018); Co-affinity purification (MI:0025)	Q12805	Q12805	hcv non-structural protein 5a	-	Q12805	-	-	-	-	-	-	-	-	-	-	-
Q12899	TRIM26	TRIM26 RNF95 ZNF173	Tripartite motif-containing protein 26	-	-	-	Q12899	hcv non-structural protein 5a	-	-	-	-	-	-	-	-	-	-	-	-	-
Q12905	ILF2	ILF2 NF45 PRO3063	Interleukin enhancer-binding factor 2	-	-	-	-	-	-	-	-	-	-	-	-	-	-	-	Q12905	-	Q12905
Q12907	Q12907	LMAN2 C5orf8	Vesicular integral-membrane protein VIP36	-	-	-	-	-	-	-	-	-	-	-	-	-	-	-	-	Q12907	Q12907
Q12931	Q12931	TRAP1 HSP75	Heat shock protein 75 kDa, mitochondrial	-	-	-	-	-	-	-	-	-	-	-	-	-	-	-	-	-	Q12931
Q12933	TRAF2	TRAF2 TRAP3	TNF receptor-associated factor 2	Q12933	Coimmunoprecipitation (MI:0019); Colocalization (MI:0403); Immunostaining (MI:0022); Affinity Chromatography (MI:0004)	Q12933	Q12933	hcv non-structural protein 5a	Q12933	-	-	-	Q12933	-	-	-	-	-	-	-	-

Q12955	Q12955	ANK3	Ankyrin-3	-	-	-	-	-	-	-	-	-	-	-	-	-	-	-	-	Q12955
Q12988	HSPB3	HSPB3 HSP27 HSPL27	Heat shock protein beta-3	-	-	-	Q12988	hcv non-structural protein 5a	-	-	-	-	-	-	-	-	-	-	-	-
Q13011	Q13011	ECH1	Delta	-	-	-	-	-	-	-	-	-	-	-	-	-	-	-	Q13011	-
Q13099	IFT88	IFT88 TG737 TTC10	Intraflagellar transport protein 88 homolog	-	-	-	-	-	-	-	Q13099	-	-	-	-	-	-	-	-	-
Q13148	Q13148	TARDBP TDP43	TAR DNA-binding protein 43	-	-	-	-	-	-	-	-	-	-	-	-	-	-	-	Q13148	Q13148
Q13151	Q13151	HNRNPA0 HNRPA0	Heterogeneous nuclear ribonucleoprotein A0	-	-	-	-	-	-	-	-	-	-	-	-	-	-	-	-	Q13151
Q13155	AIMP2	AIMP2 JTV1 PRO0992	Aminoacyl tRNA synthase complex-interacting multifunctional protein 2	-	-	-	-	-	-	-	-	-	Q13155	-	-	-	-	-	-	-
Q13200	Q13200	PSMD2 TRAP2	26S proteasome non-ATPase regulatory subunit 2	-	-	-	-	-	-	-	-	-	-	-	-	-	-	-	-	Q13200
Q13217	Q13217	DNAJC3 P58IPK PRKRI	DnaJ homolog subfamily C member 3	-	-	-	-	-	-	-	-	-	-	-	-	-	-	-	Q13217	-
Q13227	GPS2	GPS2	G protein pathway suppressor 2	Q13227	Two Hybrid Test (MI:0018); Co-affinity purification (MI:0025)	Q13227	Q13227	hcv non-structural protein 5a	-	Q13227	-	-	Q13227	-	-	-	-	-	-	-	-
Q13263	TRIM28	TRIM28 KAP1 RNF96 TIF1B	Transcription intermediary factor 1-beta	-	-	-	-	-	-	-	-	-	-	-	-	-	-	-	Q13263	-	Q13263
Q13283	G3BP1	G3BP1 G3BP	Ras GTPase-activating protein-binding protein 1	-	-	-	-	-	-	-	-	-	-	-	-	-	-	-	Q13283	-	Q13283
Q13310	Q13310	PABPC4 APP1 PABP4	Polyadenylate-binding protein 4	-	-	-	-	-	-	-	-	-	-	-	-	-	-	-	Q13310	Q13310
Q13315	ATM	ATM	Serine-protein kinase ATM	-	-	-	Q13315	hcv ns 5	-	-	-	-	-	-	-	-	-	-	-	-
Q13325	IFIT5	IFIT5 ISG58 RI58	Interferon-induced protein with tetratricopeptide repeats 5	-	-	-	-	-	-	-	-	-	-	-	-	-	Q13325	-	-	-
Q13347	Q13347	EIF3I EIF3S2 TRIP1	Eukaryotic translation initiation factor 3 subunit I	-	-	-	-	-	-	-	-	-	-	-	-	-	-	-	Q13347	-
Q13405	MRPL49	MRPL49 C11orf4 NOF1 OK/SW-cl.67	Large ribosomal subunit protein mL49	-	-	-	-	-	-	-	-	-	Q13405	-	-	-	-	-	-	-
Q13423	Q13423	NNT	NAD	-	-	-	-	-	-	-	-	-	-	-	-	-	-	-	Q13423	Q13423
Q13427	PPIG	PPIG	Peptidyl-prolyl cis-trans isomerase G	-	-	-	Q13427	hcv non-structural protein 5a	-	-	-	-	-	-	-	-	-	-	-	-
Q13428	TCOF1	TCOF1	Treacle protein	-	-	-	-	-	-	-	-	-	Q13428	-	-	-	-	-	-	Q13428
Q13435	Q13435	SF3B2 SAP145	Splicing factor 3B subunit 2	-	-	-	-	-	-	-	-	-	-	-	-	-	-	-	-	Q13435
Q13451	FKBP5	FKBP5 AIG6 FKBP51	Peptidyl-prolyl cis-trans isomerase FKBP5	-	-	-	Q13451	hcv non-structural protein 5a	-	-	-	-	-	-	-	-	-	-	-	-
Q13459	MYO9B	MYO9B MYR5	Unconventional myosin-IXb	-	-	-	-	-	-	-	-	-	Q13459	-	-	-	-	-	-	-
Q13480	GAB1	GAB1	GRB2-associated-binding protein 1	Q13480	Coimmunoprecipitation (MI:0019)	-	Q13480	hcv non-structural protein 5a	-	-	-	-	-	-	-	-	-	-	-	-
Q13492	Q13492	PICALM CALM	Phosphatidylinositol-binding clathrin assembly protein	-	-	-	-	-	-	-	-	-	-	-	-	-	-	-	Q13492	-
Q13501	Q13501	SQSTM1 ORCA OSIL	Sequestosome-1	-	-	-	-	-	-	-	-	-	-	-	-	-	-	-	-	Q13501
Q13523	PRPF4B	PRPF4B KIAA0536 PRP4 PRP4H PRP4K	Serine/threonine-protein kinase PRP4 homolog	-	-	-	-	-	-	-	-	-	-	-	-	-	-	Q13523	Q13523	-
Q13526	PIN1	PIN1	Peptidyl-prolyl cis-trans isomerase NIMA-interacting 1	-	-	Q13526	Q13526	hcv non-structural protein 5a	-	-	-	-	Q13526	-	-	-	-	-	-	-	-
Q13573	SNW1	SNW1 SKIIP SKIP	SNW domain-containing protein 1	-	-	-	-	-	-	-	-	-	Q13573	-	-	-	-	-	-	-
Q13617	CUL2	CUL2	Cullin-2	-	-	-	-	-	-	-	-	-	Q13617	-	-	-	-	-	-	-
Q13620	CUL4B	CUL4B KIAA0695	Cullin-4B	-	-	-	-	-	-	-	-	-	Q13620	-	-	-	-	-	-	-
Q13625	TP53BP2	TP53BP2 ASPP2 BBP	Apoptosis-stimulating of p53 protein 2	Q13625	Two Hybrid Test (MI:0018)	Q13625	Q13625	hcv ns 5	-	Q13625	-	-	-	-	-	-	-	-	-	-
Q13637	Q13637	RAB32	Ras-related protein Rab-32	-	-	-	-	-	-	-	-	-	-	-	-	-	-	-	-	Q13637
Q13724	Q13724	MOGS GCS1	Mannosyl-oligosaccharide glucosidase	-	-	-	-	-	-	-	-	-	-	-	-	-	-	-	Q13724	Q13724
Q13813	SPTAN1	SPTAN1 NEAS SPTA2	Spectrin alpha chain, non-erythrocytic 1	-	-	-	-	-	-	-	Q13813	-	-	-	-	-	-	-	-	-

Q13885	Q13885	TUBB2A TUBB2	Tubulin beta-2A chain	-	-	-	-	-	-	-	-	-	-	-	-	-	-	-	-	-	Q13885
Q13907	IDI1	IDI1	Isopentenyl-diphosphate Delta-isomerase 1	-	-	-	-	-	-	-	-	-	-	Q13907	-	-	-	-	-	-	Q13907
Q14011	CIRBP	CIRBP A18HNRNP CIRP	Cold-inducible RNA-binding protein	-	-	-	-	-	-	-	-	-	-	Q14011	-	-	-	-	-	-	-
Q14141	SEPTIN6	SEPTIN6 KIAA0128 SEP2 SEPT6	Septin-6	-	-	-	Q14141	hcv ns 5	-	-	-	-	-	-	-	-	-	-	-	-	-
Q14152	Q14152	EIF3A EIF3S10 KIAA0139	Eukaryotic translation initiation factor 3 subunit A	-	-	-	-	-	-	-	-	-	-	-	-	-	-	-	-	Q14152	-
Q14165	Q14165	MLEC KIAA0152	Malectin	-	-	-	-	-	-	-	-	-	-	-	-	-	-	-	-	Q14165	Q14165
Q14192	FHL2	FHL2 DRAL SLIM3	Four and a half LIM domains protein 2	Q14192	Two Hybrid Test (MI:0018)	Q14192	-	-	-	Q14192	-	-	-	-	-	-	-	-	-	-	-
Q14204	DYNC1H1	DYNC1H1 DHC1 DNCH1 DNCL DNECL DYHC KIAA0325	Cytoplasmic dynein 1 heavy chain 1	-	-	-	-	-	-	-	-	-	-	Q14204	-	-	-	-	-	Q14204	Q14204
Q14240	EIF4A2	EIF4A2 DDX2B EIF4F	Eukaryotic initiation factor 4A-II	-	-	-	Q14240	hcv non-structural protein 5a	-	-	-	-	-	-	-	-	-	-	-	-	-
Q14247	Q14247	CTTN EMS1	Src substrate cortactin	-	-	-	-	-	-	-	-	-	-	-	-	-	-	-	-	Q14247	-
Q14257	Q14257	RCN2 ERC55	Reticulocalbin-2	-	-	-	-	-	-	-	-	-	-	-	-	-	-	-	-	-	Q14257
Q14318	FKBP8	FKBP8 FKBP38	Peptidyl-prolyl cis-trans isomerase FKBP8	Q14318	Two Hybrid Test (MI:0018); Coimmunoprecipitation (MI:0019)	Q14318	Q14318	hcv non-structural protein 5a	-	-	-	Q14318	Q14318	-	-	-	Q14318	Q14318	-	Q14318	-
Q14344	GNA13	GNA13	Guanine nucleotide-binding protein subunit alpha-13	-	-	-	-	-	-	-	-	-	-	Q14344	-	-	-	-	-	-	-
Q14376	GALE	GALE	UDP-glucose 4-epimerase	-	-	-	-	-	-	-	-	-	-	Q14376	-	-	-	-	-	-	-
Q14444	CAPRIN1	CAPRIN1 GPIAP1 GPIP137 M11S1 RNG105	Caprin-1	-	-	-	-	-	-	-	-	-	-	-	-	-	-	-	Q14444	Q14444	Q14444
Q14498	RBM39	RBM39 HCC1 RNPC2	RNA-binding protein 39	-	-	-	-	-	-	-	-	-	-	-	-	-	-	-	Q14498	-	-
Q14527	Q14527	HLTF HIP116A RNF80 SMARCA3 SNF2L3 ZBU1	Helicase-like transcription factor	-	-	-	-	-	-	-	-	-	-	-	-	-	-	-	-	Q14527	-
Q14534	Q14534	SQLE ERG1	Squalene monooxygenase	-	-	-	-	-	-	-	-	-	-	-	-	-	-	-	-	Q14534	Q14534
Q14542	Q14542	SLC29A2 DER12 ENT2 HNP36	Equilibrative nucleoside transporter 2	-	-	-	-	-	-	-	-	-	-	-	-	-	-	-	-	Q14542	-
Q14558	Q14558	PRPSAP1	Phosphoribosyl pyrophosphate synthase-associated protein 1	-	-	-	-	-	-	-	-	-	-	-	-	-	-	-	-	Q14558	-
Q14653	IRF3	IRF3	Interferon regulatory factor 3	-	-	-	Q14653	hcv non-structural protein 5a	-	-	-	-	-	-	-	-	-	-	-	-	-
Q14677	Q14677	CLINT1 ENTH EPN4 EPNR KIAA0171	Clathrin interactor 1	-	-	-	-	-	-	-	-	-	-	-	-	-	-	-	-	Q14677	Q14677
Q14697	Q14697	GANAB G2AN KIAA0088	Neutral alpha-glucosidase AB	-	-	-	-	-	-	-	-	-	-	-	-	-	-	-	-	Q14697	Q14697
Q14739	Q14739	LBR	Delta	-	-	-	-	-	-	-	-	-	-	-	-	-	-	-	-	Q14739	Q14739
Q14847	LASP1	LASP1 MLN50	LIM and SH3 domain protein 1	-	-	-	-	-	-	-	-	-	-	Q14847	-	-	-	-	-	-	-
Q14914	PTGR1	PTGR1 LTB4DH	Prostaglandin reductase 1	-	-	-	-	-	-	-	-	-	-	Q14914	-	-	-	-	-	-	-
Q14964	Q14964	RAB39A RAB39	Ras-related protein Rab-39A	-	-	-	-	-	-	-	-	-	-	-	-	-	-	-	-	Q14964	Q14964
Q14974	Q14974	KPNB1 NTF97	Importin subunit beta-1	-	-	-	-	-	-	-	-	-	-	-	-	-	-	-	-	Q14974	Q14974
Q14978	NOLC1	NOLC1 KIAA0035 NS5ATP13	Nucleolar and coiled-body phosphoprotein 1	-	-	-	-	-	-	-	-	-	-	Q14978	-	-	-	-	-	-	-

Q15004	PCLAF	PCLAF KIAA0101 NS5ATP9 PAF L5	PCNA-associated factor	-	-	-	Q15004	hcv non-structural protein 5a	-	-	-	-	-	-	-	-	-	-	-	Q15004	-
Q15005	Q15005	SPCS2 KIAA0102 SPC25	Signal peptidase complex subunit 2	-	-	-	-	-	-	-	-	-	-	-	-	-	-	-	-	Q15005	Q15005
Q15014	MORF4L2	MORF4L2 KIAA0026 MRGX	Mortality factor 4-like protein 2	-	-	-	-	-	-	-	-	-	-	Q15014	-	-	-	-	-	-	-
Q15020	SART3	SART3 KIAA0156 TIP110	Squamous cell carcinoma antigen recognized by T-cells 3	-	-	-	-	-	-	-	-	-	-	-	-	-	-	-	Q15020	-	-
Q15029	EFTUD2	EFTUD2 KIAA0031 SNRP116	116 kDa U5 small nuclear ribonucleoprotein component	-	-	-	-	-	-	-	-	-	-	-	-	-	-	-	Q15029	Q15029	-
Q15041	ARL6IP1	ARL6IP1 ARL6IP ARMER KIAA0069	ADP-ribosylation factor-like protein 6-interacting protein 1	-	-	-	-	-	-	-	-	Q15041	-	-	-	-	-	-	-	Q15041	-
Q15043	Q15043	SLC39A14 KIAA0062 ZIP14	Metal cation symporter ZIP14	-	-	-	-	-	-	-	-	-	-	-	-	-	-	-	-	Q15043	Q15043
Q15046	KARS1	KARS1 KARS KIAA0070	Lysine--tRNA ligase	-	-	-	Q15046	hcv non-structural protein 5a	-	-	-	-	-	-	-	-	-	-	-	Q15046	Q15046
Q15050	Q15050	RRS1 KIAA0112 RRR	Ribosome biogenesis regulatory protein homolog	-	-	-	-	-	-	-	-	-	-	-	-	-	-	-	-	-	Q15050
Q15067	ACOX1	ACOX1 ACOX	Peroxisomal acyl-coenzyme A oxidase 1	-	-	-	-	-	-	-	-	-	-	Q15067	-	-	-	-	-	-	-
Q15125	Q15125	EBP	3-beta-hydroxysteroid-Delta	-	-	-	-	-	-	-	-	-	-	-	-	-	-	-	-	Q15125	Q15125
Q15126	PMVK	PMVK PMKI	Phosphomevalonate kinase	Q15126	Two Hybrid Test (MI:0018)	Q15126	-	-	-	Q15126	-	-	-	-	-	-	-	-	-	-	-
Q15154	PCM1	PCM1	Pericentriolar material 1 protein	-	-	-	-	-	-	-	Q15154	-	-	-	-	-	-	-	-	-	-
Q15155	Q15155	NOMO1 PM5	BOS complex subunit NOMO1	-	-	-	-	-	-	-	-	-	-	-	-	-	-	-	-	Q15155	-
Q15165	Q15165	PON2	Serum paraoxonase/arylesterase 2	-	-	-	-	-	-	-	-	-	-	-	-	-	-	-	-	Q15165	Q15165
Q15233	Q15233	NONO NRB54	Non-POU domain-containing octamer-binding protein	-	-	-	-	-	-	-	-	-	-	-	-	-	-	-	-	-	Q15233
Q15257	PTPA	PTPA PPP2R4	Serine/threonine-protein phosphatase 2A activator	Q15257	GST pull-down (MI:0059); His pull-down (MI:0061); Immunofluorescence (MI:0022); Coimmunoprecipitation (MI:0019); Immunoblotting (MI:0113)	-	Q15257	hcv non-structural protein 5a	-	-	-	-	-	-	-	-	-	-	-	-	-
Q15303	ERBB4	ERBB4 HER4	Receptor tyrosine-protein kinase erbB-4	-	-	-	-	-	-	-	-	-	-	Q15303	-	-	-	-	-	-	-
Q15369	ELOC	ELOC TCEB1	Elongin-C	-	-	-	-	-	-	-	-	-	-	Q15369	-	-	-	-	-	Q15369	-
Q15382	RHEB	RHEB RHEB2	GTP-binding protein Rheb	-	-	-	-	-	-	-	-	-	-	Q15382	-	-	-	-	-	-	-
Q15392	Q15392	DHCR24 KIAA0018	Delta	-	-	-	-	-	-	-	-	-	-	-	-	-	-	-	-	Q15392	Q15392
Q15393	Q15393	SF3B3 KIAA0017 SAP130	Splicing factor 3B subunit 3	-	-	-	-	-	-	-	-	-	-	-	-	-	-	-	-	-	Q15393
Q15424	Q15424	SAFB HAP HET SAFB1	Scaffold attachment factor B1	-	-	-	-	-	-	-	-	-	-	-	-	-	-	-	-	Q15424	Q15424
Q15459	SF3A1	SF3A1 SAP114	Splicing factor 3A subunit 1	-	-	-	-	-	-	-	-	-	-	Q15459	-	-	-	-	-	-	Q15459
Q15477	SKIC2	SKIC2 DDX13 SKI2W SKIV2 SKIV2L W	Superkiller complex protein 2	-	-	-	Q15477	hcv ns 5	-	-	-	-	-	-	-	-	-	-	-	-	-
Q15628	TRADD	TRADD	Tumor necrosis factor receptor type 1-associated DEATH domain protein	Q15628	Pull-down (MI:0096); Coimmunoprecipitation (MI:0019); Colocalization (MI:0403)	-	Q15628	hcv non-structural protein 5a	-	-	-	-	Q15628	-	-	-	-	-	-	-	-
Q15629	Q15629	TRAM1 TRAM	Translocating chain-associated membrane protein 1	-	-	-	-	-	-	-	-	-	-	-	-	-	-	-	-	Q15629	Q15629
Q15691	Q15691	MAPRE1	Microtubule-associated protein RP/EB family member 1	-	-	-	-	-	-	-	-	-	-	-	-	-	-	-	-	Q15691	-
Q15717	ELAVL1	ELAVL1 HUR	ELAV-like protein 1	-	-	-	-	-	-	-	Q15717	-	-	-	-	-	-	Q15717	-	Q15717	Q15717
Q15738	NSDHL	NSDHL H105E3	Sterol-4-alpha-carboxylate 3-dehydrogenase, decarboxylating	-	-	-	-	-	-	-	-	-	-	Q15738	-	-	-	-	-	-	Q15738

Q15758	SLC1A5	SLC1A5 ASCT2 M7V1 RDR RDRC	Neutral amino acid transporter B	-	-	-	-	-	-	-	-	-	-	Q15758	-	-	-	-	-	Q15758	Q15758
Q15773	MLF2	MLF2	Myeloid leukemia factor 2	-	-	-	-	-	-	-	-	-	-	Q15773	-	-	-	-	-	Q15773	-
Q15800	Q15800	MSMO1 DESP4 ERG25 SC4MOL	Methylsterol monooxygenase 1	-	-	-	-	-	-	-	-	-	-	-	-	-	-	-	-	Q15800	Q15800
Q15811	ITSN1	ITSN1 ITSN SH3D1A	Intersectin-1	-	-	-	-	-	-	-	-	Q15811	-	-	-	-	-	-	-	-	-
Q15836	Q15836	VAMP3 SYB3	Vesicle-associated membrane protein 3	-	-	-	-	-	-	-	-	-	-	-	-	-	-	-	-	Q15836	Q15836
Q15843	NEDD8	NEDD8	NEDD8	-	-	-	-	-	-	-	-	-	-	-	-	-	-	Q15843	-	-	-
Q15907	RAB11B	RAB11B YPT3	Ras-related protein Rab-11B	-	-	-	-	-	-	-	-	-	-	Q15907	-	-	-	-	-	Q15907	Q15907
Q15942	Q15942	ZYX	Zyxin	-	-	-	-	-	-	-	-	-	-	-	-	-	-	-	-	Q15942	-
Q16082	HSPB2	HSPB2	Heat shock protein beta-2	-	-	-	Q16082	hcv non-structural protein 5a	-	-	-	-	-	-	-	-	-	-	-	-	-
Q16186	Q16186	ADRM1 GP110	Proteasomal ubiquitin receptor ADRM1	-	-	-	-	-	-	-	-	-	-	-	-	-	-	-	-	Q16186	-
Q16401	Q16401	PSMD5 KIAA0072	26S proteasome non-ATPase regulatory subunit 5	-	-	-	-	-	-	-	-	-	-	-	-	-	-	-	-	Q16401	Q16401
Q16513	PKN2	PKN2 PRK2 PRKCL2	Serine/threonine-protein kinase N2	-	-	-	Q16513	hcv ns 5	-	-	-	-	-	-	-	-	-	-	-	-	-
Q16527	Q16527	CSRP2 LMO5 SMLIM	Cysteine and glycine-rich protein 2	-	-	-	-	-	-	-	-	-	-	-	-	-	-	-	-	-	Q16527
Q16531	Q16531	DDB1 XAP1	DNA damage-binding protein 1	-	-	-	-	-	-	-	-	-	-	-	-	-	-	-	-	-	Q16531
Q16584	MAP3K11	MAP3K11 MLK3 PTK1 SPRK	Mitogen-activated protein kinase kinase kinase 11	-	-	-	Q16584	hcv non-structural protein 5a	-	-	-	-	Q16584	-	-	-	-	-	-	-	-
Q16594	TAF9	TAF9 TAF2G TAFII31	Transcription initiation factor TFIID subunit 9	Q16594	Coimmunoprecipitation (MI:0019); Immunofluorescence (MI:0022)	Q16594	Q16594	hcv non-structural protein 5a	Q16594	-	-	-	-	-	-	-	-	-	-	-	-
Q16621	NFE2	NFE2	Transcription factor NF-E2 45 kDa subunit	Q16621	Two Hybrid Test (MI:0018)	Q16621	-	-	-	Q16621	-	-	-	-	-	-	-	-	-	-	-
Q16629	SRSF7	SRSF7 SFRS7	Serine/arginine-rich splicing factor 7	-	-	-	-	-	-	-	-	-	-	-	-	-	-	-	Q16629	-	-
Q16718	Q16718	NDUFA5	NADH dehydrogenase [ubiquinone] 1 alpha subcomplex subunit 5	-	-	-	-	-	-	-	-	-	-	-	-	-	-	-	-	Q16718	Q16718
Q16762	TST	TST	Thiosulfate sulfurtransferase	-	-	-	-	-	-	-	-	-	-	Q16762	-	-	-	-	-	-	Q16762
Q16763	Q16763	UBE2S E2EPF OK/SW-cl.73	Ubiquitin-conjugating enzyme E2 S	-	-	-	-	-	-	-	-	-	-	-	-	-	-	-	-	Q16763	Q16763
Q16795	Q16795	NDUFA9 NDUFS2L	NADH dehydrogenase [ubiquinone] 1 alpha subcomplex subunit 9, mitochondrial	-	-	-	-	-	-	-	-	-	-	-	-	-	-	-	-	Q16795	Q16795
Q16799	RTN1	RTN1 NSP	Reticulon-1	-	-	-	-	-	-	-	-	Q16799	-	-	-	-	-	-	-	-	-
Q16850	CYP51A1	CYP51A1 CYP51	Lanosterol 14-alpha demethylase	-	-	-	-	-	-	-	-	-	-	Q16850	-	-	-	-	-	Q16850	Q16850
Q16891	Q16891	IMMT HMP MIC60 MINOS2 PIG4 PIG52	MICOS complex subunit MIC60	-	-	-	-	-	-	-	-	-	-	-	-	-	-	-	-	Q16891	Q16891
Q1KMD3	Q1KMD3	HNRNPUL2 HNRPUL2	Heterogeneous nuclear ribonucleoprotein U-like protein 2	-	-	-	-	-	-	-	-	-	-	-	-	-	-	-	-	-	Q1KMD3
Q2TAY7	Q2TAY7	SMU1	WD40 repeat-containing protein SMU1	-	-	-	-	-	-	-	-	-	-	-	-	-	-	-	-	Q2TAY7	-
Q2TBE0	Q2TBE0	CWF19L2	CWF19-like protein 2	-	-	-	-	-	-	-	-	-	-	-	-	-	-	-	-	-	Q2TBE0
Q3L8U1	Q3L8U1	CHD9 KIAA0308 KISH2 PRIC320 AD-013 x0008	Chromodomain-helicase-DNA-binding protein 9	-	-	-	-	-	-	-	-	-	-	-	-	-	-	-	-	-	Q3L8U1
Q3MHD2	Q3MHD2	LSM12	Protein LSM12	-	-	-	-	-	-	-	-	-	-	-	-	-	-	-	-	-	Q3MHD2
Q3V6T2	CCDC88A	CCDC88A APE GRDN KIAA1212	Girdin	-	-	-	-	-	-	-	-	-	-	-	-	-	Q3V6T2	-	-	-	-
Q3ZCM7	TUBB8	TUBB8	Tubulin beta-8 chain	-	-	-	-	-	-	-	-	-	-	Q3ZCM7	-	-	-	-	-	-	Q3ZCM7
Q3ZCQ8	TIMM50	TIMM50 TIM50 PRO1512	Mitochondrial import inner membrane translocase subunit TIM50	-	-	-	-	-	-	-	-	-	-	-	-	-	-	Q3ZCQ8	-	Q3ZCQ8	Q3ZCQ8

Q4KMP7	TBC1D10B	TBC1D10B FP2461	TBC1 domain family member 10B	-	-	-	-	-	-	-	-	-	-	Q4KMP7	-	-	-	-	-	-	Q4KMP7
Q53EP0	FNDC3B	FNDC3B FAD104 NS5ABP37 UNQ2421/PRO4979/PRO34274	Fibronectin type III domain-containing protein 3B	-	-	-	-	-	-	-	-	-	-	Q53EP0	-	-	-	-	-	-	-
Q53F19	NCBP3	NCBP3 C17orf85	Nuclear cap-binding protein subunit 3	-	-	-	-	-	-	-	-	-	-	Q53F19	-	-	-	-	-	-	-
Q53GQ0	Q53GQ0	HSD17B12 SDR12C1	Very-long-chain 3-oxoacyl-CoA reductase	-	-	-	-	-	-	-	-	-	-	-	-	-	-	-	-	Q53GQ0	Q53GQ0
Q53H76	PLA1A	PLA1A NMD PSPLA1	Phospholipase A1 member A	-	-	-	-	-	-	-	-	-	Q53H76	-	-	-	-	-	-	-	-
Q53R41	Q53R41	FASTKD1 KIAA1800	FAST kinase domain-containing protein 1, mitochondrial	-	-	-	-	-	-	-	-	-	-	-	-	-	-	-	-	-	Q53R41
Q562E7	WDR81	WDR81	WD repeat-containing protein 81	-	-	-	-	-	-	-	-	-	-	Q562E7	-	-	-	-	-	-	-
Q58FF8	HSP90AB2P	HSP90AB2P HSP90BB	Putative heat shock protein HSP 90-beta 2	-	-	-	-	-	-	-	-	-	-	Q58FF8	-	-	-	-	-	Q58FF8	Q58FF8
Q59GN2	Q59GN2	RPL39P5	Putative ribosomal protein eL39-like 5	-	-	-	-	-	-	-	-	-	-	-	-	-	-	-	-	-	Q59GN2
Q5BJD5	Q5BJD5	TMEM41B KIAA0033	Transmembrane protein 41B	-	-	-	-	-	-	-	-	-	-	-	-	-	-	-	-	Q5BJD5	-
Q5BKY9	Q5BKY9	FAM133B	Protein FAM133B	-	-	-	-	-	-	-	-	-	-	-	-	-	-	-	-	Q5BKY9	-
Q5F1R6	Q5F1R6	DNAJC21 DNAJA5	DnaJ homolog subfamily C member 21	-	-	-	-	-	-	-	-	-	-	-	-	-	-	-	-	-	Q5F1R6
Q5H9U9	Q5H9U9	DDX60L	Probable ATP-dependent RNA helicase DDX60-like	-	-	-	-	-	-	-	-	-	-	-	-	-	-	-	-	-	Q5H9U9
Q5HYI8	Q5HYI8	RABL3	Rab-like protein 3	-	-	-	-	-	-	-	-	-	-	-	-	-	-	-	-	Q5HYI8	-
Q5HYW2	Q5HYW2	NHSL2	NHS-like protein 2	-	-	-	-	-	-	-	-	-	-	-	-	-	-	-	-	-	Q5HYW2
Q5JRX3	PITRM1	PITRM1 KIAA1104 MP1 PREP	Presequence protease, mitochondrial	-	-	-	-	-	-	-	-	-	-	Q5JRX3	-	-	-	-	-	-	-
Q5JTC6	AMER1	AMER1 FAM123B WTX	APC membrane recruitment protein 1	-	-	-	-	-	-	-	Q5JTC6	-	-	-	-	-	-	-	-	-	-
Q5JTH9	Q5JTH9	RRP12 KIAA0690	RRP12-like protein	-	-	-	-	-	-	-	-	-	-	-	-	-	-	-	-	-	Q5JTH9
Q5JTV8	Q5JTV8	TOR1AIP1 LAP1	Torsin-1A-interacting protein 1	-	-	-	-	-	-	-	-	-	-	-	-	-	-	-	-	Q5JTV8	Q5JTV8
Q5JTW2	Q5JTW2	CEP78 C9orf81	Centrosomal protein of 78 kDa	-	-	-	-	-	-	-	-	-	-	-	-	-	-	-	-	-	Q5JTW2
Q5RI15	Q5RI15	COX20 FAM36A	Cytochrome c oxidase assembly protein COX20, mitochondrial	-	-	-	-	-	-	-	-	-	-	-	-	-	-	-	-	Q5RI15	-
Q5SRD1	TIMM23B	TIMM23B	Mitochondrial import inner membrane translocase subunit Tim23B	-	-	-	-	-	-	-	-	-	-	Q5SRD1	-	-	-	-	-	-	-
Q5T280	SPOUT1	SPOUT1 C9orf114	Putative methyltransferase C9orf114	-	-	-	-	-	-	-	-	-	-	Q5T280	-	-	-	-	-	-	-
Q5T3I0	Q5T3I0	GPATCH4 GPATC4	G patch domain-containing protein 4	-	-	-	-	-	-	-	-	-	-	-	-	-	-	-	-	Q5T3I0	-
Q5T4S7	Q5T4S7	UBR4 KIAA0462 KIAA1307 RBAF600 ZUBR1	E3 ubiquitin-protein ligase UBR4	-	-	-	-	-	-	-	-	-	-	-	-	-	-	-	-	-	Q5T4S7
Q5T749	Q5T749	KPRP C1orf45	Keratinocyte proline-rich protein	-	-	-	-	-	-	-	-	-	-	-	-	-	-	-	-	-	Q5T749
Q5T9A4	Q5T9A4	ATAD3B KIAA1273 TOB3	ATPase family AAA domain-containing protein 3B	-	-	-	-	-	-	-	-	-	-	-	-	-	-	-	-	Q5T9A4	Q5T9A4
Q5VT66	Q5VT66	MTARC1 MARC1 MOSC1	Mitochondrial amidoxime-reducing component 1	-	-	-	-	-	-	-	-	-	-	-	-	-	-	-	-	-	Q5VT66
Q5VTB9	Q5VTB9	RNF220 C1orf164	E3 ubiquitin-protein ligase RNF220	-	-	-	-	-	-	-	-	-	-	-	-	-	-	-	-	-	Q5VTB9
Q5VTL8	Q5VTL8	PRPF38B	Pre-mRNA-splicing factor 38B	-	-	-	-	-	-	-	-	-	-	-	-	-	-	-	-	-	Q5VTL8
Q5VU43	Q5VU43	PDE4DIP CMYA2 KIAA0454 KIAA0477 MMGL	Myomegalin	-	-	-	-	-	-	-	-	-	-	-	-	-	-	-	-	Q5VU43	-
Q5VV42	CDKAL1	CDKAL1	Threonylcarbamoyladenosine tRNA methylthiotransferase	-	-	-	-	-	-	-	-	-	-	-	-	-	-	-	Q5VV42	-	-	-

Q5VWZ2	LYPLAL1	LYPLAL1	Lysophospholipase-like protein 1	-	-	-	-	-	-	-	-	-	-	Q5VWZ2	-	-	-	-	-	-	-
Q66PJ3	Q66PJ3	ARL6IP4	ADP-ribosylation factor-like protein 6-interacting protein 4	-	-	-	-	-	-	-	-	-	-	-	-	-	-	-	-	-	Q66PJ3
Q68CQ1	MROH7	MROH7 C1orf175 HEATR8	Maestro heat-like repeat-containing protein family member 7	-	-	-	Q68CQ1	hcv ns 5	-	-	-	-	-	-	-	-	-	-	-	-	-
Q68EM7	ARHGAP17	ARHGAP17 RICH1 MSTP066 MSTP110	Rho GTPase-activating protein 17	-	-	-	-	-	-	-	-	-	-	-	-	-	-	-	Q68EM7	-	-
Q6DD87	Q6DD87	ZNF787	Zinc finger protein 787	-	-	-	-	-	-	-	-	-	-	-	-	-	-	-	-	Q6DD87	-
Q6DD88	ATL3	ATL3	Atlastin-3	-	-	-	-	-	-	-	-	-	-	Q6DD88	-	-	-	-	-	Q6DD88	Q6DD88
Q6FHJ7	SFRP4	SFRP4 FRPHE	Secreted frizzled-related protein 4	Q6FHJ7	Two Hybrid Test (MI:0018)	Q6FHJ7	Q6FHJ7	hcv non-structural protein 5a	Q6FHJ7	-	-	-	-	-	-	-	-	-	-	-	-
Q6IAN0	DHRS7B	DHRS7B SDR32C1 CGI-93 UNQ212/PRO238	Dehydrogenase/reductase SDR family member 7B	-	-	-	-	-	-	-	-	-	-	Q6IAN0	-	-	-	-	-	-	-
Q6IN84	MRM1	MRM1	rRNA methyltransferase 1, mitochondrial	-	-	-	-	-	-	-	-	-	-	Q6IN84	-	-	-	-	-	-	-
Q6KC79	NIPBL	NIPBL IDN3 SCC2	Nipped-B-like protein	-	-	-	-	-	-	-	-	-	-	Q6KC79	-	-	-	-	-	-	-
Q6NUK1	Q6NUK1	SLC25A24 APC1 MCSC1 SCAMC1	Mitochondrial adenyl nucleotide antiporter SLC25A24	-	-	-	-	-	-	-	-	-	-	-	-	-	-	-	-	Q6NUK1	Q6NUK1
Q6NUQ4	Q6NUQ4	TMEM214 PP446	Transmembrane protein 214	-	-	-	-	-	-	-	-	-	-	-	-	-	-	-	-	-	Q6NUQ4
Q6P1J9	CDC73	CDC73 C1orf28 HRPT2	Parafibromin	-	-	-	-	-	-	-	-	-	-	-	-	-	-	-	Q6P1J9	-	-
Q6P1K8	Q6P1K8	GTF2H2C; GTF2H2C_2 GTF2H2D	General transcription factor IIH subunit 2-like protein	-	-	-	-	-	-	-	-	-	-	-	-	-	-	-	-	-	Q6P1K8
Q6P1X5	Q6P1X5	TAF2 CIF150 TAF2B	Transcription initiation factor TFIID subunit 2	-	-	-	-	-	-	-	-	-	-	-	-	-	-	-	-	-	Q6P1X5
Q6P2Q9	PRPF8	PRPF8 PRPC8	Pre-mRNA-processing-splicing factor 8	-	-	-	-	-	-	-	-	-	-	-	-	-	-	-	Q6P2Q9	-	-
Q6P5R6	Q6P5R6	RPL22L1	Ribosomal protein eL22-like	-	-	-	-	-	-	-	-	-	-	-	-	-	-	-	-	-	Q6P5R6
Q6PCD5	Q6PCD5	RFWD3 RNF201	E3 ubiquitin-protein ligase RFWD3	-	-	-	-	-	-	-	-	-	-	-	-	-	-	-	-	Q6PCD5	-
Q6PD62	CTR9	CTR9 KIAA0155 SH2BP1	RNA polymerase-associated protein CTR9 homolog	-	-	-	-	-	-	-	-	-	-	-	-	-	-	-	Q6PD62	-	-
Q6PID8	Q6PID8	KLHDC10 KIAA0265	Kelch domain-containing protein 10	-	-	-	-	-	-	-	-	-	-	-	-	-	-	-	-	Q6PID8	-
Q6PKC3	TXNDC11	TXNDC11 EFP1	Thioredoxin domain-containing protein 11	Q6PKC3	Two Hybrid Test (MI:0018); Co-affinity purification (MI:0025)	Q6PKC3	Q6PKC3	hcv non-structural protein 5a	-	Q6PKC3	-	-	-	-	-	-	-	-	-	-	-
Q6UW68	Q6UW68	TMEM205 UNQ501/PRO1018	Transmembrane protein 205	-	-	-	-	-	-	-	-	-	-	-	-	-	-	-	-	Q6UW68	-
Q6Y1H2	Q6Y1H2	HACD2 PTPLB	Very-long-chain	-	-	-	-	-	-	-	-	-	-	-	-	-	-	-	-	Q6Y1H2	-
Q6Y7W6	Q6Y7W6	GIGYF2 KIAA0642 PERQ2 TNRC15	GRB10-interacting GYF protein 2	-	-	-	-	-	-	-	-	-	-	-	-	-	-	-	-	Q6Y7W6	Q6Y7W6
Q6YN16	Q6YN16	HSDL2 C9orf99 SDR13C1	Hydroxysteroid dehydrogenase-like protein 2	-	-	-	-	-	-	-	-	-	-	-	-	-	-	-	-	Q6YN16	Q6YN16
Q6ZMI0	PPP1R21	PPP1R21 CCDC128 KLRAQ1	Protein phosphatase 1 regulatory subunit 21	-	-	-	-	-	-	-	-	-	-	-	-	-	-	-	Q6ZMI0	-	-
Q6ZRS2	SRCAP	SRCAP KIAA0309	Helicase SRCAP	Q6ZRS2	Two Hybrid Test (MI:0018); Coimmunoprecipitation (MI:0019); Affinity Chromatography (MI:0004); Immunostaining (MI:0022); Pull-down (MI:0096)	Q6ZRS2	Q6ZRS2	hcv non-structural protein 5a	Q6ZRS2	-	-	-	Q6ZRS2	-	-	-	-	-	-	-	-
Q6ZUT1	Q6ZUT1	NKAPD1 C11orf57	Uncharacterized protein NKAPD1	-	-	-	-	-	-	-	-	-	-	-	-	-	-	-	-	-	Q6ZUT1
Q70UQ0	Q70UQ0	IKBIP IKIP	Inhibitor of nuclear factor kappa-B kinase-interacting protein	-	-	-	-	-	-	-	-	-	-	-	-	-	-	-	-	Q70UQ0	-

Q71RC2	LARP4	LARP4 PP13296	La-related protein 4	-	-	-	-	-	-	-	-	-	-	Q71RC2	-	-	-	-	-	-	-
Q76N32	CEP68	CEP68 KIAA0582	Centrosomal protein of 68 kDa	-	-	-	Q76N32	hcv ns 5	-	-	-	-	-	-	-	-	-	-	-	-	-
Q7KZ85	SUPT6H	SUPT6H KIAA0162 SPT6H	Transcription elongation factor SPT6	-	-	-	-	-	-	-	-	-	-	Q7KZ85	-	-	-	-	-	-	-
Q7KZI7	MARK2	MARK2 EMK1	Serine/threonine-protein kinase MARK2	-	-	-	-	-	-	-	-	-	-	Q7KZI7	-	-	-	-	-	-	-
Q7L0Q8	RHOU	RHOU ARHU CDC42L1 G28K WRCH1 SB128	Rho-related GTP-binding protein RhoU	-	-	-	-	-	-	-	-	-	-	Q7L0Q8	-	-	-	-	-	-	-
Q7L4I2	Q7L4I2	RSRC2	Arginine/serine-rich coiled-coil protein 2	-	-	-	-	-	-	-	-	-	-	-	-	-	-	-	-	Q7L4I2	-
Q7L5N1	COPS6	COPS6 CSN6 HVIP	COP9 signalosome complex subunit 6	-	-	-	-	-	-	-	-	-	-	Q7L5N1	-	-	-	-	-	-	-
Q7L9L4	MOB1B	MOB1B MOB4A MOBKL1A	MOB kinase activator 1B	-	-	-	-	-	-	-	-	-	-	-	-	-	-	Q7L9L4	-	-	-
Q7LGA3	Q7LGA3	HS2ST1 HS2ST KIAA0448	Heparan sulfate 2-O-sulfotransferase 1	-	-	-	-	-	-	-	-	-	-	-	-	-	-	-	-	-	Q7LGA3
Q7RTV0	PHF5A	PHF5A	PHD finger-like domain-containing protein 5A	-	-	-	-	-	-	-	-	-	-	-	Q7RTV0	-	-	-	-	-	Q7RTV0
Q7Z417	Q7Z417	NUFIP2 KIAA1321 PIG1	FMR1-interacting protein NUFIP2	-	-	-	-	-	-	-	-	-	-	-	-	-	-	-	-	-	Q7Z417
Q7Z4I7	LIMS2	LIMS2 PINCH2	LIM and senescent cell antigen-like-containing domain protein 2	Q7Z4I7	Two Hybrid Test (MI:0018)	Q7Z4I7	-	-	-	Q7Z4I7	-	-	-	-	-	-	-	-	-	-	-
Q7Z4R8	C6orf120	C6orf120	UPF0669 protein C6orf120	-	-	-	-	-	-	-	-	-	-	Q7Z4R8	-	-	-	-	-	-	-
Q7Z4S6	KIF21A	KIF21A KIAA1708 KIF2	Kinesin-like protein KIF21A	-	-	-	-	-	-	-	-	-	-	Q7Z4S6	-	-	-	-	-	-	-
Q7Z589	Q7Z589	EMSY C11orf30 GL002	BRCA2-interacting transcriptional repressor EMSY	-	-	-	-	-	-	-	-	-	-	-	-	-	-	-	-	-	Q7Z589
Q7Z5L9	Q7Z5L9	IRF2BP2	Interferon regulatory factor 2-binding protein 2	-	-	-	-	-	-	-	-	-	-	-	-	-	-	-	-	-	Q7Z5L9
Q7Z6Z7	HUWE1	HUWE1 KIAA0312 KIAA1578 UREB1 HSPC272	E3 ubiquitin-protein ligase HUWE1	-	-	-	-	-	-	-	-	-	-	-	-	-	-	Q7Z6Z7	-	-	-
Q7Z739	Q7Z739	YTHDF3	YTH domain-containing family protein 3	-	-	-	-	-	-	-	-	-	-	-	-	-	-	-	-	-	Q7Z739
Q7Z7F7	Q7Z7F7	MRPL55 UNQ5835/PRO19675	Large ribosomal subunit protein mL55	-	-	-	-	-	-	-	-	-	-	-	-	-	-	-	-	Q7Z7F7	-
Q7Z7N9	TMEM179B	TMEM179B	Transmembrane protein 179B	-	-	Q7Z7N9	-	-	-	Q7Z7N9	-	-	-	-	-	-	-	-	-	-	-
Q86TB9	Q86TB9	PATL1 OK/KNS-cl.5	Protein PAT1 homolog 1	-	-	-	-	-	-	-	-	-	-	-	-	-	-	-	-	Q86TB9	-
Q86TG7	Q86TG7	PEG10 EDR KIAA1051e MAR2 MART2 MEF3L1 RGAG3	Retrotransposon-derived protein PEG10	-	-	-	-	-	-	-	-	-	-	-	-	-	-	-	-	-	Q86TG7
Q86U42	Q86U42	PABPN1 PAB2 PABP2	Polyadenylate-binding protein 2	-	-	-	-	-	-	-	-	-	-	-	-	-	-	-	-	-	Q86U42
Q86UE4	Q86UE4	MTDH AEG1 LYRIC	Protein LYRIC	-	-	-	-	-	-	-	-	-	-	-	-	-	-	-	-	Q86UE4	-
Q86UP2	Q86UP2	KTN1 CG1 KIAA0004	Kinectin	-	-	-	-	-	-	-	-	-	-	-	-	-	-	-	-	Q86UP2	-
Q86UW7	CADPS2	CADPS2 CAPS2 KIAA1591	Calcium-dependent secretion activator 2	Q86UW7	Two Hybrid Test (MI:0018)	Q86UW7	-	-	-	Q86UW7	-	-	-	-	-	-	-	-	-	-	-
Q86V81	Q86V81	ALYREF ALY BEF THOC4	THO complex subunit 4	-	-	-	-	-	-	-	-	-	-	-	-	-	-	-	-	-	Q86V81
Q86VD1	Q86VD1	MORC1 MORC	MORC family CW-type zinc finger protein 1	-	-	-	-	-	-	-	-	-	-	-	-	-	-	-	-	-	Q86VD1

Q86VP6	Q86VP6	CAND1 KIAA0829 TIP120 TIP120A	Cullin-associated NEDD8-dissociated protein 1	-	-	-	-	-	-	-	-	-	-	-	-	-	-	-	-	Q86VP6	Q86VP6
Q86W42	THOC6	THOC6 WDR58 PSEC0006	THO complex subunit 6 homolog	-	-	-	-	-	-	-	-	-	-	-	-	-	-	-	Q86W42	-	-
Q86WA6	Q86WA6	BPHL MCNAA	Valacyclovir hydrolase	-	-	-	-	-	-	-	-	-	-	-	-	-	-	-	-	-	Q86WA6
Q86WW8	Q86WW8	COA5 C2orf64	Cytochrome c oxidase assembly factor 5	-	-	-	-	-	-	-	-	-	-	-	-	-	-	-	-	-	Q86WW8
Q86WX3	Q86WX3	RPS19BP1 AROS	Active regulator of SIRT1	-	-	-	-	-	-	-	-	-	-	-	-	-	-	-	-	-	Q86WX3
Q86X95	Q86X95	CIR1 CIR	Corepressor interacting with RBPJ 1	-	-	-	-	-	-	-	-	-	-	-	-	-	-	-	-	-	Q86X95
Q86XR8	CEP57	CEP57 KIAA0092 TSP57	Centrosomal protein of 57 kDa	Q86XR8	Two Hybrid Test (MI:0018)	Q86XR8	Q86XR8	hcv non-structural protein 5a	Q86XR8	-	-	-	-	-	-	-	-	-	-	-	-
Q86YS6	RAB43	RAB43 RAB41	Ras-related protein Rab-43	-	-	-	-	-	-	-	-	-	-	Q86YS6	-	-	-	-	-	-	-
Q8IUD2	ERC1	ERC1 ELKS KIAA1081 RAB6IP2	ELKS/Rab6-interacting/CAST family member 1	-	-	-	Q8IUD2	hcv non-structural protein 5a	-	-	-	-	-	-	-	-	-	-	-	-	Q8IUD2
Q8IVW6	Q8IVW6	ARID3B BDP DRIL2	AT-rich interactive domain-containing protein 3B	-	-	-	-	-	-	-	-	-	-	-	-	-	-	-	-	-	Q8IVW6
Q8IWB7	WDFY1	WDFY1 FENS1 KIAA1435 WDF1 ZFYVE17	WD repeat and FYVE domain-containing protein 1	-	-	-	-	-	-	-	-	-	-	Q8IWB7	-	-	-	-	-	-	-
Q8IWV8	UBR2	UBR2 C6orf133 KIAA0349	E3 ubiquitin-protein ligase UBR2	-	-	-	-	-	-	-	-	-	-	Q8IWV8	-	-	-	-	-	-	-
Q8IWX8	Q8IWX8	CHERP DAN26 SCAF6	Calcium homeostasis endoplasmic reticulum protein	-	-	-	-	-	-	-	-	-	-	-	-	-	-	-	-	-	Q8IWX8
Q8IY17	Q8IY17	PNPLA6 NTE	Patatin-like phospholipase domain-containing protein 6	-	-	-	-	-	-	-	-	-	-	-	-	-	-	-	-	-	Q8IY17
Q8IY67	Q8IY67	RAVER1 KIAA1978	Ribonucleoprotein PTB-binding 1	-	-	-	-	-	-	-	-	-	-	-	-	-	-	-	-	-	Q8IY67
Q8IY81	Q8IY81	FTSJ3 SB92	pre-rRNA 2'-O-ribose RNA methyltransferase FTSJ3	-	-	-	-	-	-	-	-	-	-	-	-	-	-	-	-	-	Q8IY81
Q8IYB8	SUPV3L1	SUPV3L1 SUV3	ATP-dependent RNA helicase SUPV3L1, mitochondrial	-	-	-	-	-	-	-	-	-	-	Q8IYB8	-	-	-	-	-	-	-
Q8IYS2	Q8IYS2	KIAA2013	Uncharacterized protein KIAA2013	-	-	-	-	-	-	-	-	-	-	-	-	-	-	-	-	Q8IYS2	-
Q8IZ81	Q8IZ81	ELMOD2	ELMO domain-containing protein 2	-	-	-	-	-	-	-	-	-	-	-	-	-	-	-	-	Q8IZ81	-
Q8IZI9	IFNL3	IFNL3 IL28B IL28C ZCYTO22	Interferon lambda-3	-	-	-	Q8IZI9	hcv non-structural protein 5a	-	-	-	-	-	-	-	-	-	-	-	-	-
Q8IZL8	PELP1	PELP1 HMX3 MNAR	Proline-, glutamic acid- and leucine-rich protein 1	-	-	-	-	-	-	-	-	-	-	Q8IZL8	-	-	-	-	-	-	-
Q8IZP2	Q8IZP2	ST13P4 FAM10A4	Putative protein FAM10A4	-	-	-	-	-	-	-	-	-	-	-	-	-	-	-	-	Q8IZP2	Q8IZP2
Q8N0Y2	Q8N0Y2	ZNF444 EZF2 ZSCAN17	Zinc finger protein 444	-	-	-	-	-	-	-	-	-	-	-	-	-	-	-	-	-	Q8N0Y2
Q8N183	Q8N183	NDUFAF2 NDUFA12L	NADH dehydrogenase [ubiquinone] 1 alpha subcomplex assembly factor 2	-	-	-	-	-	-	-	-	-	-	-	-	-	-	-	-	Q8N183	-
Q8N1B4	VPS52	VPS52 SACM2L	Vacuolar protein sorting-associated protein 52 homolog	Q8N1B4	Two Hybrid Test (MI:0018); Co-affinity purification (MI:0025)	Q8N1B4	Q8N1B4	hcv non-structural protein 5a	-	Q8N1B4	-	-	-	-	-	-	-	-	-	-	-
Q8N1F7	NUP93	NUP93 KIAA0095	Nuclear pore complex protein Nup93	-	-	-	-	-	-	-	-	-	-	Q8N1F7	-	-	-	-	-	-	Q8N1F7
Q8N2K0	Q8N2K0	ABHD12 C20orf22	Lysophosphatidylserine lipase ABHD12	-	-	-	-	-	-	-	-	-	-	-	-	-	-	-	-	Q8N2K0	Q8N2K0
Q8N357	Q8N357	SLC35F6 C2orf18 UNQ3047/PRO9863	Solute carrier family 35 member F6	-	-	-	-	-	-	-	-	-	-	-	-	-	-	-	-	Q8N357	-
Q8N3V2	NKFZp451G12	DKFZp451G125	Nuclear receptor subfamily 4 group A member 1	-	-	-	Q8N3V2	hcv ns 5	-	-	-	-	-	-	-	-	-	-	-	-	-

Q8N4V1	Q8N4V1	MMGT1 EMC5 TMEM32	ER membrane protein complex subunit 5	-	-	-	-	-	-	-	-	-	-	-	-	-	-	-	-	Q8N4V1	Q8N4V1
Q8N5G0	Q8N5G0	SMIM20 C4orf52 MITRAC7	Small integral membrane protein 20	-	-	-	-	-	-	-	-	-	-	-	-	-	-	-	-	Q8N5G0	Q8N5G0
Q8N5K1	Q8N5K1	CISD2 CDGSH2 ERIS ZCD2	CDGSH iron-sulfur domain-containing protein 2	-	-	-	-	-	-	-	-	-	-	-	-	-	-	-	-	-	Q8N5K1
Q8N5M4	Q8N5M4	TTC9C	Tetratricopeptide repeat protein 9C	-	-	-	-	-	-	-	-	-	-	-	-	-	-	-	-	Q8N5M4	-
Q8N5M9	Q8N5M9	JAGN1	Protein jagunal homolog 1	-	-	-	-	-	-	-	-	-	-	-	-	-	-	-	-	Q8N5M9	-
Q8N684	Q8N684	CPSF7	Cleavage and polyadenylation specificity factor subunit 7	-	-	-	-	-	-	-	-	-	-	-	-	-	-	-	-	Q8N684	-
Q8N6T3	ARFGAP1	ARFGAP1 ARF1GAP	ADP-ribosylation factor GTPase-activating protein 1	-	-	-	Q8N6T3	hcv non-structural protein 5a	-	-	-	-	Q8N6T3	Q8N6T3	-	-	-	-	-	Q8N6T3	-
Q8N729	Q8N729	NPW PPL8 PPNPW	Neuropeptide W	-	-	-	-	-	-	-	-	-	-	-	-	-	-	-	-	-	Q8N729
Q8N766	Q8N766	EMC1 KIAA0090 PSEC0263	ER membrane protein complex subunit 1	-	-	-	-	-	-	-	-	-	-	-	-	-	-	-	-	-	Q8N766
Q8N7H5	PAF1	PAF1 PD2	RNA polymerase II-associated factor 1 homolog	-	-	-	-	-	-	-	-	-	-	-	-	-	-	-	Q8N7H5	-	-
Q8N7W2	BEND7	BEND7 C10orf30	BEN domain-containing protein 7	Q8N7W2	Two Hybrid Test (MI:0018)	Q8N7W2	-	-	-	Q8N7W2	-	-	-	-	-	-	-	-	-	-	-
Q8N960	CEP120	CEP120 CCDC100	Centrosomal protein of 120 kDa	Q8N960	Two Hybrid Test (MI:0018)	Q8N960	-	-	-	Q8N960	-	-	-	-	-	-	-	-	-	-	-
Q8N983	MRPL43	MRPL43	Large ribosomal subunit protein mL43	-	-	-	-	-	-	-	-	-	-	Q8N983	-	-	-	-	-	-	-
Q8N9Q2	Q8N9Q2	SREK1IP1 P18SRP SFRS12IP1	Protein SREK1IP1	-	-	-	-	-	-	-	-	-	-	-	-	-	-	-	-	-	Q8N9Q2
Q8NAT1	Q8NAT1	POMGNT2 AGO61 C3orf39 EOGTL GTDC2	Protein O-linked-mannose beta-1,4-N-acetylglucosaminyltransferase 2	-	-	-	-	-	-	-	-	-	-	-	-	-	-	-	-	Q8NAT1	Q8NAT1
Q8NAV1	Q8NAV1	PRPF38A	Pre-mRNA-splicing factor 38A	-	-	-	-	-	-	-	-	-	-	-	-	-	-	-	-	Q8NAV1	-
Q8NB25	FAM184A	FAM184A C6orf60	Protein FAM184A	-	-	-	Q8NB25	NS3, NS5	-	-	-	-	-	-	-	-	-	-	-	-	-
Q8NBJ4	GOLM1	GOLM1 C9orf155 GOLPH2 PSEC0242 UNQ686/PRO1326	Golgi membrane protein 1	-	-	-	Q8NBJ4	hcv non-structural protein 5a	-	-	-	-	-	-	-	-	-	-	-	Q8NBJ4	-
Q8NBP7	Q8NBP7	PCSK9 NARC1 PSEC0052	Proprotein convertase subtilisin/kexin type 9	-	-	-	-	-	-	-	-	-	-	-	-	-	-	-	-	Q8NBP7	-
Q8NBQ5	Q8NBQ5	HSD17B11 DHRS8 PAN1B SDR16C2 PSEC0029 UNQ207/PRO233	Estradiol 17-beta-dehydrogenase 11	-	-	-	-	-	-	-	-	-	-	-	-	-	-	-	-	Q8NBQ5	Q8NBQ5
Q8NBS9	TXNDC5	TXNDC5 TLP46 UNQ364/PRO700	Thioredoxin domain-containing protein 5	-	-	-	-	-	-	-	-	-	-	-	Q8NBS9	-	-	-	-	-	-
Q8NBX0	Q8NBX0	SCCPDH CGI-49	Saccharopine dehydrogenase-like oxidoreductase	-	-	-	-	-	-	-	-	-	-	-	-	-	-	-	-	Q8NBX0	Q8NBX0
Q8NC51	SERBP1	SERBP1 PAIRBP1 CGI-55	SERPINE1 mRNA-binding protein 1	-	-	-	-	-	-	-	-	-	-	-	-	-	-	Q8NC51	-	-	Q8NC51
Q8NCN5	PDPR	PDPR KIAA1990	Pyruvate dehydrogenase phosphatase regulatory subunit, mitochondrial	-	-	-	-	-	-	-	-	-	-	Q8NCN5	-	-	-	-	-	-	-
Q8NDD1	Q8NDD1	C1orf131 cPERP-A	Uncharacterized protein C1orf131	-	-	-	-	-	-	-	-	-	-	-	-	-	-	-	-	-	Q8NDD1
Q8NDH3	Q8NDH3	NPEPL1 KIAA1974	Probable aminopeptidase NPEPL1	-	-	-	-	-	-	-	-	-	-	-	-	-	-	-	-	Q8NDH3	Q8NDH3
Q8NDX6	Q8NDX6	ZNF740 TB7	Zinc finger protein 740	-	-	-	-	-	-	-	-	-	-	-	-	-	-	-	-	-	Q8NDX6

Q8NEF9	SRFBP1	SRFBP1	Serum response factor-binding protein 1	-	-	-	-	-	-	-	Q8NEF9	-	-	-	-	-	-	-	-	-	-
Q8NHH9	Q8NHH9	ATL2 ARL6IP2	Atlastin-2	-	-	-	-	-	-	-	-	-	-	-	-	-	-	-	-	Q8NHH9	-
Q8NHS0	DNAJB8	DNAJB8	DnaJ homolog subfamily B member 8	-	-	-	-	-	-	-	-	-	-	Q8NHS0	-	-	-	-	-	-	-
Q8NHW5	Q8NHW5	RPLP0P6	Putative ribosomal protein uL10-like	-	-	-	-	-	-	-	-	-	-	-	-	-	-	-	-	Q8NHW5	-
Q8NHY6	ZFP28	ZFP28 KIAA1431	Zinc finger protein 28 homolog	-	-	-	-	-	-	-	-	Q8NHY6	-	-	-	-	-	-	-	-	-
Q8TA86	Q8TA86	RP9	Retinitis pigmentosa 9 protein	-	-	-	-	-	-	-	-	-	-	-	-	-	-	-	-	-	Q8TA86
Q8TAP9	Q8TAP9	MPLKIP C7orf11 TTDN1	M-phase-specific PLK1-interacting protein	-	-	-	-	-	-	-	-	-	-	-	-	-	-	-	-	-	Q8TAP9
Q8TB37	NUBPL	NUBPL C14orf127	Iron-sulfur protein NUBPL	-	-	-	-	-	-	-	-	-	-	-	-	-	-	-	Q8TB37	-	-
Q8TC12	RDH11	RDH11 ARSDR1 PSDR1 SDR7C1 CGI-82	Retinol dehydrogenase 11	-	-	-	-	-	-	-	-	-	-	Q8TC12	-	-	-	-	-	Q8TC12	Q8TC12
Q8TCC3	MRPL30	MRPL30 MRPL28 RPML28 HSPC249	Large ribosomal subunit protein uL30m	-	-	-	-	-	-	-	-	-	-	Q8TCC3	-	-	-	-	-	-	-
Q8TCJ2	Q8TCJ2	STT3B SIMP	Dolichyl-diphosphooligosaccharide--protein glycosyltransferase subunit STT3B	-	-	-	-	-	-	-	-	-	-	-	-	-	-	-	-	Q8TCJ2	Q8TCJ2
Q8TCT9	Q8TCT9	HM13 H13 IMP1 PSL3 SPP MSTP086	Minor histocompatibility antigen H13	-	-	-	-	-	-	-	-	-	-	-	-	-	-	-	-	-	Q8TCT9
Q8TEW0	Q8TEW0	PARD3 PAR3 PAR3A	Partitioning defective 3 homolog	-	-	-	-	-	-	-	-	-	-	-	-	-	-	-	-	-	Q8TEW0
Q8TEX9	IPO4	IPO4 IMP4B RANBP4	Importin-4	Q8TEX9	Two Hybrid Test (MI:0018)	Q8TEX9	Q8TEX9	hcv non-structural protein 5a	Q8TEX9	-	-	-	-	-	-	-	-	-	-	-	Q8TEX9
Q8WUF5	PPP1R13L	PPP1R13L IASPP NKIP1 PPP1R13BL RAI	RelA-associated inhibitor	Q8WUF5	Two Hybrid Test (MI:0018); Co-affinity purification (MI:0025)	Q8WUF5	Q8WUF5	hcv non-structural protein 5a	-	Q8WUF5	-	-	-	-	-	-	-	-	-	Q8WUF5	-
Q8WUH6	Q8WUH6	TMEM263 C12orf23	Transmembrane protein 263	-	-	-	-	-	-	-	-	-	-	-	-	-	-	-	-	-	Q8WUH6
Q8WVM0	Q8WVM0	TFB1M CGI-75	Dimethyladenosine transferase 1, mitochondrial	-	-	-	-	-	-	-	-	-	-	-	-	-	-	-	-	-	Q8WVM0
Q8WVM8	Q8WVM8	SCFD1 C14orf163 KIAA0917 STXBP1L2 FKSG23	Sec1 family domain-containing protein 1	-	-	-	-	-	-	-	-	-	-	-	-	-	-	-	-	Q8WVM8	Q8WVM8
Q8WVP5	Q8WVP5	TNFAIP8L1	Tumor necrosis factor alpha-induced protein 8-like protein 1	-	-	-	-	-	-	-	-	-	-	-	-	-	-	-	-	-	Q8WVP5
Q8WWC4	Q8WWC4	MAIP1 C2orf47	m-AAA protease-interacting protein 1, mitochondrial	-	-	-	-	-	-	-	-	-	-	-	-	-	-	-	-	-	Q8WWC4
Q8WWI1	Q8WWI1	LMO7 FBX20 FBXO20 KIAA0858	LIM domain only protein 7	-	-	-	-	-	-	-	-	-	-	-	-	-	-	-	-	-	Q8WWI1
Q8WWK9	Q8WWK9	CKAP2 LB1 TMAP	Cytoskeleton-associated protein 2	-	-	-	-	-	-	-	-	-	-	-	-	-	-	-	-	Q8WWK9	-
Q8WWM7	Q8WWM7	ATXN2L A2D A2LG A2LP A2RP	Ataxin-2-like protein	-	-	-	-	-	-	-	-	-	-	-	-	-	-	-	-	Q8WWM7	Q8WWM7
Q8WWQ0	Q8WWQ0	PHIP DCAF14 WDR11	PH-interacting protein	-	-	-	-	-	-	-	-	-	-	-	-	-	-	-	-	-	Q8WWQ0
Q8WXF1	PSPC1	PSPC1 PSP1	Paraspeckle component 1	-	-	-	-	-	-	-	-	-	-	Q8WXF1	-	-	-	-	-	-	-
Q8WXG1	RSAD2	RSAD2 CIG5	S-adenosylmethionine-dependent nucleotide dehydratase RSAD2	-	-	Q8WXG1	Q8WXG1	hcv non-structural protein 5a	-	-	-	-	-	-	-	-	-	-	-	-	-
Q8WZ42	TTN	TTN	Titin	-	-	-	-	-	-	-	-	-	-	Q8WZ42	-	-	-	-	-	-	-
Q92499	DDX1	DDX1	ATP-dependent RNA helicase DDX1	-	-	-	-	-	-	-	-	-	-	-	-	-	-	-	Q92499	-	-
Q92504	SLC39A7	SLC39A7 HKE4 RING5	Zinc transporter SLC39A7	-	-	-	-	-	-	-	-	-	-	Q92504	-	-	-	-	-	Q92504	-

Q92538	GBF1	GBF1 KIAA0248	Golgi-specific brefeldin A-resistance guanine nucleotide exchange factor 1	-	-	-	-	-	-	-	-	-	-	Q92538	-	-	-	-	-	Q92538	-
Q92544	Q92544	TM9SF4 KIAA0255 TUCAP1	Transmembrane 9 superfamily member 4	-	-	-	-	-	-	-	-	-	-	-	-	-	-	-	-	Q92544	Q92544
Q92552	MRPS27	MRPS27 KIAA0264	Small ribosomal subunit protein mS27	-	-	-	-	-	-	-	-	-	-	-	-	-	-	-	Q92552	-	-
Q92575	Q92575	UBXN4 KIAA0242 UBXD2 UBXDC1	UBX domain-containing protein 4	-	-	-	-	-	-	-	-	-	-	-	-	-	-	-	-	Q92575	-
Q92576	Q92576	PHF3 KIAA0244	PHD finger protein 3	-	-	-	-	-	-	-	-	-	-	-	-	-	-	-	-	-	Q92576
Q92597	NDRG1	NDRG1 CAP43 DRG1 RTP	Protein NDRG1	Q92597	Two Hybrid Test (MI:0018)	Q92597	Q92597	hcv non-structural protein 5a	Q92597	-	-	-	-	-	-	-	-	-	-	-	-
Q92598	HSPH1	HSPH1 HSP105 HSP110 KIAA0201	Heat shock protein 105 kDa	-	-	-	-	-	-	-	-	-	-	-	-	-	-	Q92598	-	-	-
Q92604	Q92604	LPGAT1 FAM34A KIAA0205	Acyl-CoA:lysophosphatidylglycerol acyltransferase 1	-	-	-	-	-	-	-	-	-	-	-	-	-	-	-	-	Q92604	Q92604
Q92614	MYO18A	MYO18A CD245 KIAA0216 MYSPDZ TIAF1	Unconventional myosin-XVIIIa	-	-	-	-	-	-	-	-	-	-	-	-	-	-	-	Q92614	-	-
Q92616	GCN1	GCN1 GCN1L1 KIAA0219	Stalled ribosome sensor GCN1	-	-	-	-	-	-	-	-	-	-	Q92616	-	-	-	-	-	Q92616	Q92616
Q92621	NUP205	NUP205 C7orf14 KIAA0225	Nuclear pore complex protein Nup205	-	-	-	-	-	-	-	-	-	-	Q92621	-	-	-	-	-	Q92621	-
Q92643	Q92643	PIGK GPI8	GPI-anchor transamidase	-	-	-	-	-	-	-	-	-	-	-	-	-	-	-	-	Q92643	-
Q92667	Q92667	AKAP1 AKAP149 PRKA1	A-kinase anchor protein 1, mitochondrial	-	-	-	-	-	-	-	-	-	-	-	-	-	-	-	-	Q92667	-
Q92759	Q92759	GTF2H4	General transcription factor IIH subunit 4	-	-	-	-	-	-	-	-	-	-	-	-	-	-	-	-	-	Q92759
Q92793	CREBBP	CREBBP CBP	CREB-binding protein	-	-	-	-	-	-	-	-	-	-	Q92793	-	-	-	-	-	-	-
Q92820	GGH	GGH	Gamma-glutamyl hydrolase	-	-	-	-	-	-	-	-	-	-	Q92820	-	-	-	-	-	-	-
Q92879	Q92879	CELF1 BRUNOL2 CUGBP CUGBP1 NAB50	CUGBP Elav-like family member 1	-	-	-	-	-	-	-	-	-	-	-	-	-	-	-	-	Q92879	-
Q92896	Q92896	GLG1 CFR1 ESL1 MG160	Golgi apparatus protein 1	-	-	-	-	-	-	-	-	-	-	-	-	-	-	-	-	Q92896	-
Q92900	Q92900	UPF1 KIAA0221 RENT1	Regulator of nonsense transcripts 1	-	-	-	-	-	-	-	-	-	-	-	-	-	-	-	-	Q92900	Q92900
Q92922	SMARCC1	SMARCC1 BAF155	SWI/SNF complex subunit SMARCC1	-	-	-	-	-	-	-	-	-	-	-	-	-	-	-	Q92922	-	-
Q92930	Q92930	RAB8B	Ras-related protein Rab-8B	-	-	-	-	-	-	-	-	-	-	-	-	-	-	-	-	Q92930	Q92930
Q92945	Q92945	KHSRP FUBP2	Far upstream element-binding protein 2	-	-	-	-	-	-	-	-	-	-	-	-	-	-	-	-	Q92945	Q92945
Q92973	TNPO1	TNPO1 KPNB2 MIP1 TRN	Transportin-1	-	-	-	-	-	-	-	-	-	-	Q92973	-	-	-	-	-	Q92973	Q92973
Q92979	Q92979	EMG1 C2F	Ribosomal RNA small subunit methyltransferase NEP1	-	-	-	-	-	-	-	-	-	-	-	-	-	-	-	-	-	Q92979
Q92985	IRF7	IRF7	Interferon regulatory factor 7	-	-	-	Q92985	hcv non-structural protein 5a	-	-	-	-	-	-	-	-	-	-	-	-	-
Q969M3	Q969M3	YIPF5 FINGER5 YIP1A PP12723 SB140 UNQ3123/PRO10275	Protein YIPF5	-	-	-	-	-	-	-	-	-	-	-	-	-	-	-	-	Q969M3	-

Q969R2	OSBP2	OSBP2 KIAA1664 ORP4 OSBPL4	Oxysterol-binding protein 2	-	-	-	Q969R2	hcv ns 5	-	-	-	-	-	-	-	-	-	-	-	-	-
Q969U7	Q969U7	PSMG2 HCCA3 PAC2 TNFSF5IP1	Proteasome assembly chaperone 2	-	-	-	-	-	-	-	-	-	-	-	-	-	-	-	-	Q969U7	-
Q969X5	Q969X5	ERGIC1 ERGIC32 KIAA1181 HT034	Endoplasmic reticulum-Golgi intermediate compartment protein 1	-	-	-	-	-	-	-	-	-	-	-	-	-	-	-	-	Q969X5	-
Q96A26	Q96A26	FAM162A C3orf28 E2IG5 DC16 FWP001	Protein FAM162A	-	-	-	-	-	-	-	-	-	-	-	-	-	-	-	-	Q96A26	-
Q96A33	CCDC47	CCDC47 GK001 MSTP041 PSEC0077	PAT complex subunit CCDC47	-	-	-	-	-	-	-	-	-	Q96A33	-	-	-	-	-	-	Q96A33	Q96A33
Q96AE4	FUBP1	FUBP1	Far upstream element-binding protein 1	-	-	Q96AE4	Q96AE4	HCV NS5A	-	-	-	-	-	-	-	-	-	-	-	-	-
Q96AG4	Q96AG4	LRRC59 PRO1855	Leucine-rich repeat-containing protein 59	-	-	-	-	-	-	-	-	-	-	-	-	-	-	-	-	-	Q96AG4
Q96B49	Q96B49	TOMM6 OBTP TOM6	Mitochondrial import receptor subunit TOM6 homolog	-	-	-	-	-	-	-	-	-	-	-	-	-	-	-	-	-	Q96B49
Q96BW9	Q96BW9	TAMM41 C3orf31	Phosphatidate cytidylyltransferase, mitochondrial	-	-	-	-	-	-	-	-	-	-	-	-	-	-	-	-	Q96BW9	-
Q96BZ9	TBC1D20	TBC1D20 C20orf140	TBC1 domain family member 20	Q96BZ9	Two Hybrid Test (MI:0018)	-	Q96BZ9	hcv non-structural protein 5a	-	-	-	-	Q96BZ9	-	-	-	-	-	-	-	-
Q96C57	Q96C57	CUSTOS C12orf43	Protein CUSTOS	-	-	-	-	-	-	-	-	-	-	-	-	-	-	-	-	Q96C57	-
Q96CB9	Q96CB9	NSUN4	5-methylcytosine rRNA methyltransferase NSUN4	-	-	-	-	-	-	-	-	-	-	-	-	-	-	-	-	Q96CB9	Q96CB9
Q96CS3	Q96CS3	FAF2 ETEA KIAA0887 UBXD8 UBXN3B	FAS-associated factor 2	-	-	-	-	-	-	-	-	-	-	-	-	-	-	-	-	Q96CS3	Q96CS3
Q96CW5	TUBGCP3	TUBGCP3 GCP3	Gamma-tubulin complex component 3	-	-	-	-	-	-	-	-	-	Q96CW5	-	-	-	-	-	-	-	-
Q96DA0	ZG16B	ZG16B UNQ773/PRO1567	Zymogen granule protein 16 homolog B	-	-	-	-	-	-	-	-	-	Q96DA0	-	-	-	-	-	-	-	-
Q96DA6	Q96DA6	DNAJC19 TIM14 TIMM14	Mitochondrial import inner membrane translocase subunit TIM14	-	-	-	-	-	-	-	-	-	-	-	-	-	-	-	-	Q96DA6	-
Q96EP5	Q96EP5	DAZAP1	DAZ-associated protein 1	-	-	-	-	-	-	-	-	-	-	-	-	-	-	-	-	-	Q96EP5
Q96EU6	Q96EU6	RRP36 C6orf153 HSPC253	Ribosomal RNA processing protein 36 homolog	-	-	-	-	-	-	-	-	-	-	-	-	-	-	-	-	Q96EU6	-
Q96EY1	DNAJA3	DNAJA3 HCA57 TID1	DnaJ homolog subfamily A member 3, mitochondrial	Q96EY1	Two Hybrid Test (MI:0018)	Q96EY1	-	-	-	Q96EY1	-	-	-	-	-	-	-	-	-	Q96EY1	Q96EY1
Q96EY4	TMA16	TMA16 C4orf43	Translation machinery-associated protein 16	-	-	-	-	-	-	-	-	-	Q96EY4	-	-	-	-	-	-	-	-
Q96FJ2	Q96FJ2	DYNLL2 DLC2	Dynein light chain 2, cytoplasmic	-	-	-	-	-	-	-	-	-	-	-	-	-	-	-	-	-	Q96FJ2
Q96FW1	OTUB1	OTUB1 OTB1 OTU1 HSPC263	Ubiquitin thioesterase OTUB1	-	-	-	-	-	-	-	-	-	Q96FW1	-	-	-	-	-	-	-	-
Q96G23	Q96G23	CERS2 LASS2 TMSG1	Ceramide synthase 2	-	-	-	-	-	-	-	-	-	-	-	-	-	-	-	-	Q96G23	-
Q96GQ7	Q96GQ7	DDX27 cPERP-F RHLP HSPC259 PP3241	Probable ATP-dependent RNA helicase DDX27	-	-	-	-	-	-	-	-	-	-	-	-	-	-	-	-	-	Q96GQ7
Q96HR9	Q96HR9	REEP6 C19orf32 DP1L1	Receptor expression-enhancing protein 6	-	-	-	-	-	-	-	-	-	-	-	-	-	-	-	-	Q96HR9	-
Q96HS1	PGAM5	PGAM5	Serine/threonine-protein phosphatase PGAM5, mitochondrial	-	-	-	-	-	-	-	-	-	-	-	Q96HS1	-	-	-	-	-	-

Q96HY6	Q96HY6	DDRGK1 C20orf116 UFBP1	DDRGK domain-containing protein 1	-	-	-	-	-	-	-	-	-	-	-	-	-	-	-	-	Q96HY6	Q96HY6
Q96I24	FUBP3	FUBP3 FBP3	Far upstream element-binding protein 3	-	-	-	-	-	-	-	-	-	-	Q96I24	-	-	-	-	-	-	Q96I24
Q96I25	Q96I25	RBM17 SPF45	Splicing factor 45	-	-	-	-	-	-	-	-	-	-	-	-	-	-	-	-	-	Q96I25
Q96IG2	FBXL20	FBXL20 FBL2	F-box/LRR-repeat protein 20	Q96IG2	Coimmunoprecipitation (MI:0019)	-	Q96IG2	hcv non-structural protein 5a	-	-	-	-	-	-	-	-	-	-	-	-	-
Q96II8	LRCH3	LRCH3	DISP complex protein LRCH3	-	-	-	-	-	-	-	-	-	-	Q96II8	-	-	-	-	-	-	-
Q96IJ6	Q96IJ6	GMPPA	Mannose-1-phosphate guanyltransferase alpha	-	-	-	-	-	-	-	-	-	-	-	-	-	-	-	-	Q96IJ6	-
Q96IZ7	Q96IZ7	RSRC1 SRRP53 BM-011	Serine/Arginine-related protein 53	-	-	-	-	-	-	-	-	-	-	-	-	-	-	-	-	-	Q96IZ7
Q96JN8	NEURL4	NEURL4 KIAA1787	Neuralized-like protein 4	-	-	-	Q96JN8	hcv non-structural protein 5a	-	-	-	-	-	-	-	-	-	-	-	-	-
Q96JP5	ZFP91	ZFP91 ZNF757 FKSG11	E3 ubiquitin-protein ligase ZFP91	-	-	-	-	-	-	-	-	-	-	Q96JP5	-	-	-	-	-	-	-
Q96KG9	SCYL1	SCYL1 CVAK90 GKLP NTKL TAPK TEIF TRAP HT019	N-terminal kinase-like protein	-	-	-	-	-	-	-	-	-	-	Q96KG9	-	-	-	-	-	-	-
Q96KQ4	PPP1R13B	PPP1R13B ASPP1 KIAA0771	Apoptosis-stimulating of p53 protein 1	-	-	-	Q96KQ4	hcv non-structural protein 5a	-	-	-	-	-	-	-	-	-	-	-	-	-
Q96KQ7	EHMT2	EHMT2 BAT8 C6orf30 G9A KMT1C NG36	Histone-lysine N-methyltransferase EHMT2	-	-	-	-	-	-	-	Q96KQ7	-	-	-	-	-	-	-	-	-	-
Q96L58	Q96L58	B3GALT6	Beta-1,3-galactosyltransferase 6	-	-	-	-	-	-	-	-	-	-	-	-	-	-	-	-	Q96L58	-
Q96MC5	BMERB1	BMERB1 C16orf45	bMERB domain-containing protein 1	-	-	-	-	-	-	-	-	Q96MC5	-	-	-	-	-	-	-	-	-
Q96MT8	CEP63	CEP63	Centrosomal protein of 63 kDa	Q96MT8	Two Hybrid Test (MI:0018)	Q96MT8	-	-	-	Q96MT8	Q96MT8	-	-	-	-	-	-	-	-	-	-
Q96N38	Q96N38	ZNF714	Zinc finger protein 714	-	-	-	-	-	-	-	-	-	-	-	-	-	-	-	-	Q96N38	-
Q96NC0	Q96NC0	ZMAT2	Zinc finger matrin-type protein 2	-	-	-	-	-	-	-	-	-	-	-	-	-	-	-	-	-	Q96NC0
Q96P11	Q96P11	NSUN5 NSUN5A WBSCR20 WBSCR20A	28S rRNA	-	-	-	-	-	-	-	-	-	-	-	-	-	-	-	-	Q96P11	Q96P11
Q96P48	ARAP1	ARAP1 CENTD2 KIAA0782	Arf-GAP with Rho-GAP domain, ANK repeat and PH domain-containing protein 1	Q96P48	Two Hybrid Test (MI:0018); GST pull-down (MI:0059)	Q96P48	Q96P48	hcv non-structural protein 5a	Q96P48	-	-	-	-	-	-	-	-	-	-	-	-
Q96P70	Q96P70	IPO9 IMP9 KIAA1192 RANBP9 HSPC273	Importin-9	-	-	-	-	-	-	-	-	-	-	-	-	-	-	-	-	Q96P70	Q96P70
Q96PK6	RBM14	RBM14 SIP	RNA-binding protein 14	-	-	-	-	-	-	-	-	-	-	-	-	-	-	-	-	Q96PK6	-	Q96PK6
Q96PY5	FMNL2	FMNL2 FHOD2 KIAA1902	Formin-like protein 2	-	-	-	-	-	-	-	-	-	-	Q96PY5	-	-	-	-	-	-	-
Q96QK1	VPS35	VPS35 MEM3 TCCCTA00141	Vacuolar protein sorting-associated protein 35	Q96QK1	Two Hybrid Test (MI:0018)	Q96QK1	Q96QK1	hcv non-structural protein 5a	Q96QK1	-	-	-	-	-	-	-	-	-	-	-	-
Q96T37	Q96T37	RBM15 OTT OTT1	RNA-binding protein 15	-	-	-	-	-	-	-	-	-	-	-	-	-	-	-	-	-	Q96T37
Q96T76	MMS19	MMS19 MMS19L	MMS19 nucleotide excision repair protein homolog	-	-	-	-	-	-	-	-	-	-	Q96T76	-	-	-	-	-	Q96T76	-
Q99439	Q99439	CNN2	Calponin-2	-	-	-	-	-	-	-	-	-	-	-	-	-	-	-	-	-	Q99439
Q99442	Q99442	SEC62 TLOC1	Translocation protein SEC62	-	-	-	-	-	-	-	-	-	-	-	-	-	-	-	-	Q99442	-
Q99459	CDC5L	CDC5L KIAA0432 PCDC5RP	Cell division cycle 5-like protein	-	-	-	-	-	-	-	-	-	-	-	-	-	-	-	Q99459	Q99459	-
Q99460	PSMD1	PSMD1	26S proteasome non-ATPase regulatory subunit 1	-	-	-	-	-	-	-	-	-	-	Q99460	-	-	-	-	-	Q99460	-
Q99470	SDF2	SDF2	Stromal cell-derived factor 2	-	-	-	-	-	-	-	-	-	-	Q99470	-	-	-	-	-	-	-
Q99497	PARK7	PARK7	Parkinson disease protein 7	-	-	-	-	-	-	-	-	-	-	-	-	-	-	Q99497	-	-	Q99497

Q99536	VAT1	VAT1	Synaptic vesicle membrane protein VAT-1 homolog	-	-	-	-	-	-	-	-	Q99536	-	-	-	-	-	-	Q99536	Q99536
Q99541	PLIN2	PLIN2 ADFP	Perilipin-2	-	-	-	-	-	-	-	-	-	-	Q99541	-	-	-	-	-	-	Q99541
Q99543	Q99543	DNAJC2 MPHOSPH11 MPP11 ZRF1	DnaJ homolog subfamily C member 2	-	-	-	-	-	-	-	-	-	-	-	-	-	-	-	-	-	Q99543
Q99550	MPHOSPH9	MPHOSPH9 MPP9	M-phase phosphoprotein 9	-	-	-	-	-	-	-	Q99550	-	-	-	-	-	-	-	-	-	-
Q99614	Q99614	TTC1 TPR1	Tetratricopeptide repeat protein 1	-	-	-	-	-	-	-	-	-	-	-	-	-	-	-	-	-	Q99614
Q99615	Q99615	DNAJC7 TPR2 TTC2	DnaJ homolog subfamily C member 7	-	-	-	-	-	-	-	-	-	-	-	-	-	-	-	-	-	Q99615
Q99623	Q99623	PHB2 BAP REA	Prohibitin-2	-	-	-	-	-	-	-	-	-	-	-	-	-	-	-	-	Q99623	Q99623
Q99653	Q99653	CHP1 CHP	Calcineurin B homologous protein 1	-	-	-	-	-	-	-	-	-	-	-	-	-	-	-	-	-	Q99653
Q99661	Q99661	KIF2C KNSL6	Kinesin-like protein KIF2C	-	-	-	-	-	-	-	-	-	-	-	-	-	-	-	-	Q99661	-
Q99729	HNRNPAB	HNRNPAB ABBP1 HNRPAB	Heterogeneous nuclear ribonucleoprotein A/B	-	-	-	-	-	-	-	-	-	-	-	-	-	-	Q99729	Q99729	-	-
Q99733	NAP1L4	NAP1L4 NAP2	Nucleosome assembly protein 1-like 4	-	-	-	-	-	-	-	-	-	-	-	-	Q99733	-	Q99733	-	Q99733	Q99733
Q99735	Q99735	MGST2 GST2	Microsomal glutathione S-transferase 2	-	-	-	-	-	-	-	-	-	-	-	-	-	-	-	-	Q99735	Q99735
Q99798	ACO2	ACO2	Aconitate hydratase, mitochondrial	-	-	-	-	-	-	-	-	-	-	Q99798	-	-	-	-	-	-	-
Q99805	Q99805	TM9SF2	Transmembrane 9 superfamily member 2	-	-	-	-	-	-	-	-	-	-	-	-	-	-	-	-	Q99805	-
Q99816	TSG101	TSG101	Tumor susceptibility gene 101 protein	-	-	-	-	-	-	-	Q99816	-	-	-	-	-	-	-	-	-	-
Q99832	Q99832	CCT7 CCTH NIP7-1	T-complex protein 1 subunit eta	-	-	-	-	-	-	-	-	-	-	-	-	-	-	-	-	Q99832	Q99832
Q99836	MYD88	MYD88	Myeloid differentiation primary response protein MyD88	Q99836	Coimmunoprecipitation (MI:0019)	-	Q99836	hcv non-structural protein 5a	-	-	-	-	Q99836	-	-	-	-	-	-	-	-
Q99856	Q99856	ARID3A DRIL1 DRIL3 DRX E2FBP1	AT-rich interactive domain-containing protein 3A	-	-	-	-	-	-	-	-	-	-	-	-	-	-	-	-	-	Q99856
Q99942	Q99942	RNF5 G16 NG2 RMA1	E3 ubiquitin-protein ligase RNF5	-	-	-	-	-	-	-	-	-	-	-	-	-	-	-	-	Q99942	-
Q99956	Q99956	DUSP9 MKP4	Dual specificity protein phosphatase 9	-	-	-	-	-	-	-	-	-	-	-	-	-	-	-	-	Q99956	Q99956
Q99959	Q99959	PKP2	Plakophilin-2	-	-	-	-	-	-	-	-	-	-	-	-	-	-	-	-	-	Q99959
Q99IB8	CV polyprote		Genome polyprotein	-	-	-	-	-	-	-	-	-	-	-	-	-	-	-	Q99IB8	-	-
Q9BPW8	Q9BPW8	NIPSNAP1	Protein NipSnap homolog 1	-	-	-	-	-	-	-	-	-	-	-	-	-	-	-	-	Q9BPW8	Q9BPW8
Q9BPX3	NCAPG	NCAPG CAPG NYMEL3	Condensin complex subunit 3	-	-	-	-	-	-	-	-	-	-	Q9BPX3	-	-	-	-	-	-	-
Q9BQ52	ELAC2	ELAC2 HPC2	Zinc phosphodiesterase ELAC protein 2	-	-	-	-	-	-	-	-	-	-	Q9BQ52	-	-	-	-	-	-	-
Q9BQ69	Q9BQ69	MACROD1 LRP16	ADP-ribose glycohydrolase MACROD1	-	-	-	-	-	-	-	-	-	-	-	-	-	-	-	-	Q9BQ69	-
Q9BQB6	Q9BQB6	VKORC1 VKOR MSTP134 MSTP576 UNQ308/PRO351	Vitamin K epoxide reductase complex subunit 1	-	-	-	-	-	-	-	-	-	-	-	-	-	-	-	-	Q9BQB6	Q9BQB6
Q9BQE3	Q9BQE3	TUBA1C TUBA6	Tubulin alpha-1C chain	-	-	-	-	-	-	-	-	-	-	-	-	-	-	-	-	-	Q9BQE3
Q9BQG0	Q9BQG0	MYBBP1A P160	Myb-binding protein 1A	-	-	-	-	-	-	-	-	-	-	-	-	-	-	-	-	-	Q9BQG0
Q9BQP7	MGME1	MGME1 C20orf72 DDK1	Mitochondrial genome maintenance exonuclease 1	-	-	-	-	-	-	-	-	-	-	Q9BQP7	-	-	-	-	-	-	-
Q9BRK5	Q9BRK5	SDF4 CAB45 PSEC0034	45 kDa calcium-binding protein	-	-	-	-	-	-	-	-	-	-	-	-	-	-	-	-	-	Q9BRK5
Q9BRX2	Q9BRX2	PELO CGI-17	Protein pelota homolog	-	-	-	-	-	-	-	-	-	-	-	-	-	-	-	-	Q9BRX2	Q9BRX2
Q9BSD7	Q9BSD7	NTPCR C1orf57	Cancer-related nucleoside-triphosphatase	-	-	-	-	-	-	-	-	-	-	-	-	-	-	-	-	-	Q9BSD7
Q9BSJ8	ESYT1	ESYT1 FAM62A KIAA0747 MBC2	Extended synaptotagmin-1	-	-	-	-	-	-	-	-	-	-	Q9BSJ8	-	-	-	-	-	Q9BSJ8	Q9BSJ8

Q9BT67	NDFIP1	NDFIP1 N4WBP5 PSEC0192 PSEC0223	NEDD4 family-interacting protein 1	-	-	-	-	-	-	-	-	-	-	Q9BT67	-	-	-	-	-	-	-
Q9BTC0	DIDO1	DIDO1 C20orf158 DATF1 KIAA0333	Death-inducer obliterator 1	-	-	-	-	-	-	-	-	-	-	Q9BTC0	-	-	-	-	-	-	-
Q9BTV4	Q9BTV4	TMEM43 UNQ2564/PRO6244	Transmembrane protein 43	-	-	-	-	-	-	-	-	-	-	-	-	-	-	-	-	Q9BTV4	-
Q9BU76	MMTAG2	MMTAG2 C1orf35	Multiple myeloma tumor-associated protein 2	-	-	-	-	-	-	-	-	-	-	Q9BU76	-	-	-	-	-	-	Q9BU76
Q9BUF5	Q9BUF5	TUBB6	Tubulin beta-6 chain	-	-	-	-	-	-	-	-	-	-	-	-	-	-	-	-	Q9BUF5	Q9BUF5
Q9BUJ2	Q9BUJ2	HNRNPUL1 E1BAP5 HNRPUL1	Heterogeneous nuclear ribonucleoprotein U-like protein 1	-	-	-	-	-	-	-	-	-	-	-	-	-	-	-	-	-	Q9BUJ2
Q9BUN8	Q9BUN8	DERL1 DER1 UNQ243/PRO276	Derlin-1	-	-	-	-	-	-	-	-	-	-	-	-	-	-	-	-	-	Q9BUN8
Q9BUP3	Q9BUP3	HTATIP2 CC3 TIP30	Oxidoreductase HTATIP2	-	-	-	-	-	-	-	-	-	-	-	-	-	-	-	-	Q9BUP3	Q9BUP3
Q9BUV8	Q9BUV8	RAB5IF C20orf24 OPTI RCAF1 PNAS-11	GEL complex subunit OPTI	-	-	-	-	-	-	-	-	-	-	-	-	-	-	-	-	Q9BUV8	-
Q9BV40	Q9BV40	VAMP8	Vesicle-associated membrane protein 8	-	-	-	-	-	-	-	-	-	-	-	-	-	-	-	-	Q9BV40	-
Q9BV73	CEP250	CEP250 CEP2 CNAP1	Centrosome-associated protein CEP250	Q9BV73	Two Hybrid Test (MI:0018)	Q9BV73	-	-	-	Q9BV73	-	-	-	-	-	-	-	-	-	-	-
Q9BVA1	Q9BVA1	TUBB2B	Tubulin beta-2B chain	-	-	-	-	-	-	-	-	-	-	-	-	-	-	-	-	-	Q9BVA1
Q9BVC6	Q9BVC6	TMEM109	Transmembrane protein 109	-	-	-	-	-	-	-	-	-	-	-	-	-	-	-	-	Q9BVC6	Q9BVC6
Q9BVJ6	Q9BVJ6	UTP14A SDCCAG16	U3 small nucleolar RNA-associated protein 14 homolog A	-	-	-	-	-	-	-	-	-	-	-	-	-	-	-	-	-	Q9BVJ6
Q9BVK6	Q9BVK6	TMED9 GP25L2	Transmembrane emp24 domain-containing protein 9	-	-	-	-	-	-	-	-	-	-	-	-	-	-	-	-	Q9BVK6	Q9BVK6
Q9BW66	CINP	CINP	Cyclin-dependent kinase 2-interacting protein	-	-	-	Q9BW66	hcv ns 5	-	-	-	-	-	-	-	-	-	-	-	-	-
Q9BW72	Q9BW72	HIGD2A	HIG1 domain family member 2A, mitochondrial	-	-	-	-	-	-	-	-	-	-	-	-	-	-	-	-	-	Q9BW72
Q9BWD1	Q9BWD1	ACAT2 ACTL	Acetyl-CoA acetyltransferase, cytosolic	-	-	-	-	-	-	-	-	-	-	-	-	-	-	-	-	-	Q9BWD1
Q9BWS9	Q9BWS9	CHID1 GL008 PSEC0104 SB139	Chitinase domain-containing protein 1	-	-	-	-	-	-	-	-	-	-	-	-	-	-	-	-	-	Q9BWS9
Q9BX93	Q9BX93	PLA2G12B PLA2G13 FKSG71	Group XIIB secretory phospholipase A2-like protein	-	-	-	-	-	-	-	-	-	-	-	-	-	-	-	-	Q9BX93	-
Q9BXB4	OSBPL11	OSBPL11 ORP11 OSBP12	Oxysterol-binding protein-related protein 11	-	-	-	-	-	-	-	-	-	-	Q9BXB4	-	-	-	-	-	-	-
Q9BXB5	OSBPL10	OSBPL10 ORP10 OSBP9	Oxysterol-binding protein-related protein 10	-	-	-	-	-	-	-	-	-	-	Q9BXB5	-	-	-	-	-	-	-
Q9BY42	RTF2	RTF2 C20orf43 RTFDC1 AD-007 CDA05 HSPC164 HSPC169	Replication termination factor 2	-	-	-	-	-	-	-	-	-	-	Q9BY42	-	-	-	-	-	-	-
Q9BYC8	Q9BYC8	MRPL32 HSPC283	Large ribosomal subunit protein bL32m	-	-	-	-	-	-	-	-	-	-	-	-	-	-	-	-	-	Q9BYC8
Q9BYC9	MRPL20	MRPL20	Large ribosomal subunit protein bL20m	-	-	-	-	-	-	-	-	-	-	Q9BYC9	-	-	-	-	-	-	-
Q9BYD6	Q9BYD6	MRPL1 BM-022	Large ribosomal subunit protein uL1m	-	-	-	-	-	-	-	-	-	-	-	-	-	-	-	-	-	Q9BYD6
Q9BYW2	SETD2	SETD2 HIF1 HYPB KIAA1732 KMT3A SET2 HSPC069	Histone-lysine N-methyltransferase SETD2	-	-	-	Q9BYW2	hcv ns 5	-	-	-	-	-	-	-	-	-	-	-	-	-
Q9BZL1	Q9BZL1	UBL5	Ubiquitin-like protein 5	-	-	-	-	-	-	-	-	-	-	-	-	-	-	-	-	-	Q9BZL1
Q9BZV2	Q9BZV2	SLC19A3	Thiamine transporter 2	-	-	-	-	-	-	-	-	-	-	-	-	-	-	-	-	Q9BZV2	Q9BZV2

Q9C0C2	TNKS1BP1	TNKS1BP1 KIAA1741 TAB182	182 kDa tankyrase-1-binding protein	-	-	-	-	-	-	-	-	-	-	Q9C0C2	-	-	-	-	-	-	-
Q9C0E8	Q9C0E8	LNPK KIAA1715 LNP	Endoplasmic reticulum junction formation protein lunapark	-	-	-	-	-	-	-	-	-	-	-	-	-	-	-	-	Q9C0E8	Q9C0E8
Q9GZT3	Q9GZT3	SLIRP C14orf156 DC23 DC50 PD04872	SRA stem-loop-interacting RNA-binding protein, mitochondrial	-	-	-	-	-	-	-	-	-	-	-	-	-	-	-	-	Q9GZT3	Q9GZT3
Q9GZT9	EGLN1	EGLN1 C1orf12 PNAS-118 PNAS-137	Egl nine homolog 1	-	-	-	-	-	-	-	-	-	-	-	-	-	Q9GZT9	Q9GZT9	-	-	-
Q9GZY8	Q9GZY8	MFF C2orf33 AD030 AD033 GL004	Mitochondrial fission factor	-	-	-	-	-	-	-	-	-	-	-	-	-	-	-	-	-	Q9GZY8
Q9GZZ1	NAA50	NAA50 MAK3 NAT13 NAT5	N-alpha-acetyltransferase 50	-	-	-	-	-	-	-	-	-	-	Q9GZZ1	-	-	-	-	-	-	-
Q9H0A0	Q9H0A0	NAT10 ALP KIAA1709	RNA cytidine acetyltransferase	-	-	-	-	-	-	-	-	-	-	-	-	-	-	-	-	Q9H0A0	-
Q9H0F6	SHARPIN	SHARPIN SIPL1 PSEC0216	Sharpin	Q9H0F6	Two Hybrid Test (MI:0018)	Q9H0F6	-	-	-	Q9H0F6	-	-	-	-	-	-	-	-	-	-	-
Q9H0G5	Q9H0G5	NSRP1 CCDC55 NSRP70	Nuclear speckle splicing regulatory protein 1	-	-	-	-	-	-	-	-	-	-	-	-	-	-	-	-	-	Q9H0G5
Q9H0U3	Q9H0U3	MAGT1 IAG2 PSEC0084 UNQ628/PRO1244	Magnesium transporter protein 1	-	-	-	-	-	-	-	-	-	-	-	-	-	-	-	-	Q9H0U3	-
Q9H0U4	Q9H0U4	RAB1B	Ras-related protein Rab-1B	-	-	-	-	-	-	-	-	-	-	-	-	-	-	-	-	Q9H0U4	Q9H0U4
Q9H0U6	MRPL18	MRPL18 HSPC071	Large ribosomal subunit protein uL18m	-	-	-	-	-	-	-	-	-	-	Q9H0U6	-	-	-	-	-	-	-
Q9H1Y0	ATG5	ATG5 APG5L ASP	Autophagy protein 5	-	-	-	Q9H1Y0	hcv ns 5	-	-	-	-	-	-	-	-	-	-	-	-	-
Q9H270	VPS11	VPS11 RNF108 PP3476	Vacuolar protein sorting-associated protein 11 homolog	-	-	-	Q9H270	NS5	-	-	-	-	-	-	-	-	-	-	-	-	-
Q9H2D6	TRIOBP	TRIOBP KIAA1662 TARA HRIHFB2122	TRIO and F-actin-binding protein	Q9H2D6	Two Hybrid Test (MI:0018)	Q9H2D6	-	-	-	Q9H2D6	-	-	-	-	-	-	-	-	-	-	-
Q9H2K8	Q9H2K8	TAOK3 DPK JIK KDS MAP3K18	Serine/threonine-protein kinase TAO3	-	-	-	-	-	-	-	-	-	-	-	-	-	-	-	-	Q9H2K8	-
Q9H2M9	RAB3GAP2	RAB3GAP2 KIAA0839	Rab3 GTPase-activating protein non-catalytic subunit	-	-	-	-	-	-	-	-	-	-	Q9H2M9	-	-	-	-	-	-	-
Q9H307	PNN	PNN DRS MEMA	Pinin	-	-	-	-	-	-	-	-	-	-	-	-	-	-	-	Q9H307	-	-
Q9H330	Q9H330	TMEM245 C9orf5	Transmembrane protein 245	-	-	-	-	-	-	-	-	-	-	-	-	-	-	-	-	Q9H330	-
Q9H3N1	Q9H3N1	TMX1 TMX TXNDC TXNDC1 PSEC0085 UNQ235/PRO268	Thioredoxin-related transmembrane protein 1	-	-	-	-	-	-	-	-	-	-	-	-	-	-	-	-	Q9H3N1	Q9H3N1
Q9H3P7	ACBD3	ACBD3 GCP60 GOCAP1 GOLPH1	Golgi resident protein GCP60	-	-	-	Q9H3P7	NS5A	-	-	-	-	-	Q9H3P7	-	-	-	-	-	-	-
Q9H444	CHMP4B	CHMP4B C20orf178 SHAX1	Charged multivesicular body protein 4b	-	-	-	Q9H444	hcv non-structural protein 5a	-	-	-	-	-	-	-	-	-	-	-	-	-
Q9H4L4	SENP3	SENP3 SSP3 SUSP3	Sentrin-specific protease 3	-	-	-	-	-	-	-	-	-	-	Q9H4L4	-	-	-	-	-	-	-
Q9H5Z1	Q9H5Z1	DHX35 C20orf15 DDX35	Probable ATP-dependent RNA helicase DHX35	-	-	-	-	-	-	-	-	-	-	-	-	-	-	-	-	-	Q9H5Z1

Q9H6F5	CCDC86	CCDC86 CYCLON	Coiled-coil domain-containing protein 86	Q9H6F5	Two Hybrid Test (MI:0018); GST pull-down (MI:0059)	Q9H6F5	Q9H6F5	hcv non-structural protein 5a	Q9H6F5	-	-	-	-	-	-	-	-	-	-	-	-
Q9H7B4	SMYD3	SMYD3 ZMYND1 ZNFN3A1	Histone-lysine N-methyltransferase SMYD3	Q9H7B4	Two Hybrid Test (MI:0018)	Q9H7B4	Q9H7B4	hcv non-structural protein 5a	-	Q9H7B4	-	-	Q9H7B4	-	-	-	Q9H7B4	Q9H7B4	-	Q9H7B4	-
Q9H7P9	PLEKHG2	PLEKHG2	Pleckstrin homology domain-containing family G member 2	-	-	-	-	-	-	-	-	-	-	-	-	Q9H7P9	-	-	-	-	-
Q9H845	Q9H845	ACAD9	Complex I assembly factor ACAD9, mitochondrial	-	-	-	-	-	-	-	-	-	-	-	-	-	-	-	-	Q9H845	Q9H845
Q9H8H3	Q9H8H3	TMT1A METTL7A PRO0066 UNQ1902/PRO4348	N6-adenosine-methyltransferase TMT1A	-	-	-	-	-	-	-	-	-	-	-	-	-	-	-	-	Q9H8H3	Q9H8H3
Q9H8S9	MOB1A	MOB1A C2orf6 MOB4B MOBK1B MOBKL1B	MOB kinase activator 1A	Q9H8S9	Two Hybrid Test (MI:0018); Co-affinity purification (MI:0025)	Q9H8S9	Q9H8S9	hcv non-structural protein 5a	-	Q9H8S9	-	-	Q9H8S9	-	-	-	Q9H8S9	-	-	-	Q9H8S9
Q9H8Y8	GORASP2	GORASP2 GOLPH6	Golgi reassembly-stacking protein 2	-	-	-	-	-	-	-	Q9H8Y8	-	-	-	-	-	-	-	-	-	-
Q9H910	JPT2	JPT2 C16orf34 HN1L L11	Jupiter microtubule associated homolog 2	-	-	-	-	-	-	-	-	-	-	-	-	-	-	Q9H910	-	-	-
Q9H9B4	Q9H9B4	SFXN1	Sideroflexin-1	-	-	-	-	-	-	-	-	-	-	-	-	-	-	-	-	Q9H9B4	Q9H9B4
Q9HAV0	GNB4	GNB4	Guanine nucleotide-binding protein subunit beta-4	-	-	-	-	-	-	-	-	-	-	Q9HAV0	-	-	-	-	-	-	-
Q9HBI0	PARVG	PARVG	Gamma-parvin	Q9HBI0	Two Hybrid Test (MI:0018)	Q9HBI0	-	-	-	Q9HBI0	-	-	-	-	-	-	-	-	-	-	-
Q9HC07	Q9HC07	TMEM165 TPARL	Transmembrane protein 165	-	-	-	-	-	-	-	-	-	-	-	-	-	-	-	-	Q9HC07	Q9HC07
Q9HC38	GLOD4	GLOD4 C17orf25 CGI-150 My027	Glyoxalase domain-containing protein 4	-	-	-	-	-	-	-	-	-	-	Q9HC38	-	-	-	-	-	-	-
Q9HCE1	Q9HCE1	MOV10 KIAA1631	Helicase MOV-10	-	-	-	-	-	-	-	-	-	-	-	-	-	-	-	-	Q9HCE1	Q9HCE1
Q9HCL2	GPAM	GPAM GPAT1 KIAA1560	Glycerol-3-phosphate acyltransferase 1, mitochondrial	-	-	-	-	-	-	-	-	-	-	Q9HCL2	-	-	-	-	-	-	-
Q9HCM4	Q9HCM4	EPB41L5 KIAA1548	Band 4.1-like protein 5	-	-	-	-	-	-	-	-	-	-	-	-	-	-	-	-	-	Q9HCM4
Q9HCU5	PREB	PREB SEC12	Prolactin regulatory element-binding protein	-	-	-	-	-	-	-	-	-	-	Q9HCU5	-	-	-	-	-	Q9HCU5	-
Q9HD20	Q9HD20	ATP13A1 ATP13A KIAA1825 CGI-152	Endoplasmic reticulum transmembrane helix translocase	-	-	-	-	-	-	-	-	-	-	-	-	-	-	-	-	Q9HD20	Q9HD20
Q9HD45	Q9HD45	TM9SF3 SMBP UNQ245/PRO282	Transmembrane 9 superfamily member 3	-	-	-	-	-	-	-	-	-	-	-	-	-	-	-	-	Q9HD45	Q9HD45
Q9HDC9	APMAP	APMAP C20orf3 UNQ1869/PRO4305	Adipocyte plasma membrane-associated protein	-	-	-	-	-	-	-	-	-	-	Q9HDC9	-	-	-	-	-	Q9HDC9	Q9HDC9
Q9NNW5	WDR6	WDR6	tRNA	-	-	-	-	-	-	-	-	-	-	-	-	-	-	Q9NNW5	-	-	Q9NNW5
Q9NP61	ARFGAP3	ARFGAP3 ARFGAP1	ADP-ribosylation factor GTPase-activating protein 3	-	-	-	Q9NP61	hcv non-structural protein 5a	-	-	-	-	-	Q9NP61	-	-	-	-	-	-	-
Q9NP64	Q9NP64	ZCCHC17 PS1D HSPC243 HSPC251 LDC4	Zinc finger CCHC domain-containing protein 17	-	-	-	-	-	-	-	-	-	-	-	-	-	-	-	-	-	Q9NP64
Q9NP72	RAB18	RAB18	Ras-related protein Rab-18	-	-	-	Q9NP72	hcv non-structural protein 5a	-	-	-	-	Q9NP72	-	-	-	-	-	-	Q9NP72	Q9NP72
Q9NPA0	Q9NPA0	EMC7 C11orf3 C15orf24 HT022 UNQ905/PRO1926	ER membrane protein complex subunit 7	-	-	-	-	-	-	-	-	-	-	-	-	-	-	-	-	Q9NPA0	Q9NPA0
Q9NPA8	Q9NPA8	ENY2 DC6	Transcription and mRNA export factor ENY2	-	-	-	-	-	-	-	-	-	-	-	-	-	-	-	-	-	Q9NPA8

Q9NPI7	Q9NPI7	KRCC1 CHBP2 BM-003 BM-044	Lysine-rich coiled-coil protein 1	-	-	-	-	-	-	-	-	-	-	-	-	-	-	-	-	-	Q9NPI7
Q9NQ29	LUC7L	LUC7L LUC7L1	Putative RNA-binding protein Luc7-like 1	-	-	-	-	-	-	-	-	-	-	-	-	-	-	-	Q9NQ29	-	-
Q9NQ94	Q9NQ94	A1CF ACF ASP	APOBEC1 complementation factor	-	-	-	-	-	-	-	-	-	-	-	-	-	-	-	-	-	Q9NQ94
Q9NQC3	Q9NQC3	RTN4 KIAA0886 NOGO My043 SP1507	Reticulon-4	-	-	-	-	-	-	-	-	-	-	-	-	-	-	-	-	Q9NQC3	Q9NQC3
Q9NQH7	XPNPEP3	XPNPEP3	Xaa-Pro aminopeptidase 3	-	-	-	-	-	-	-	-	-	-	Q9NQH7	-	-	-	-	-	-	-
Q9NQT8	KIF13B	KIF13B GAKIN KIAA0639	Kinesin-like protein KIF13B	-	-	-	-	-	-	-	-	-	-	Q9NQT8	-	-	-	-	-	-	-
Q9NQZ6	Q9NQZ6	ZC4H2 HCA127 KIAA1166	Zinc finger C4H2 domain-containing protein	-	-	-	-	-	-	-	-	-	-	-	-	-	-	-	-	-	Q9NQZ6
Q9NR31	Q9NR31	SAR1A SAR1 SARA SARA1	GTP-binding protein SAR1a	-	-	-	-	-	-	-	-	-	-	-	-	-	-	-	-	-	Q9NR31
Q9NR45	Q9NR45	NANS SAS	Sialic acid synthase	-	-	-	-	-	-	-	-	-	-	-	-	-	-	-	-	-	Q9NR45
Q9NRG9	Q9NRG9	AAAS ADRACALA GL003	Aladin	-	-	-	-	-	-	-	-	-	-	-	-	-	-	-	-	Q9NRG9	-
Q9NRM7	LATS2	LATS2 KPM	Serine/threonine-protein kinase LATS2	-	-	-	-	-	-	-	-	-	Q9NRM7	-	-	Q9NRM7	-	-	-	-	-
Q9NRP0	Q9NRP0	OSTC DC2 HDCMD45P HSPC307	Oligosaccharyltransferase complex subunit OSTC	-	-	-	-	-	-	-	-	-	-	-	-	-	-	-	-	Q9NRP0	Q9NRP0
Q9NRZ9	Q9NRZ9	HELLS PASG SMARCA6 Nbla10143	Lymphoid-specific helicase	-	-	-	-	-	-	-	-	-	-	-	-	-	-	-	-	Q9NRZ9	-
Q9NS69	TOMM22	TOMM22 TOM22	Mitochondrial import receptor subunit TOM22 homolog	-	-	-	-	-	-	-	-	-	-	Q9NS69	-	-	-	-	-	-	Q9NS69
Q9NSA3	CTNNBIP1	CTNNBIP1 ICAT	Beta-catenin-interacting protein 1	-	-	-	-	-	-	-	-	-	Q9NSA3	-	-	-	-	-	-	-	-
Q9NSD9	FARSB	FARSB FARSLB FRSB HSPC173	Phenylalanine--tRNA ligase beta subunit	-	-	-	-	-	-	-	-	-	-	Q9NSD9	-	-	-	-	-	-	-
Q9NSE2	CISH	CISH G18	Cytokine-inducible SH2-containing protein	-	-	-	Q9NSE2	hcv ns 5	-	-	-	-	-	-	-	-	-	-	-	-	-
Q9NTI5	PDS5B	PDS5B APRIN AS3 KIAA0979	Sister chromatid cohesion protein PDS5 homolog B	-	-	-	-	-	-	-	-	-	-	Q9NTI5	-	-	-	-	-	-	-
Q9NTJ3	Q9NTJ3	SMC4 CAPC SMC4L1	Structural maintenance of chromosomes protein 4	-	-	-	-	-	-	-	-	-	-	-	-	-	-	-	-	Q9NTJ3	-
Q9NTJ5	Q9NTJ5	SACM1L KIAA0851 SAC1	Phosphatidylinositol-3-phosphatase SAC1	-	-	-	-	-	-	-	-	-	-	-	-	-	-	-	-	Q9NTJ5	Q9NTJ5
Q9NUD5	Q9NUD5	ZCCHC3 C20orf99	Zinc finger CCHC domain-containing protein 3	-	-	-	-	-	-	-	-	-	-	-	-	-	-	-	-	-	Q9NUD5
Q9NUI1	Q9NUI1	DECR2 PDCR SDR17C1	Peroxisomal 2,4-dienoyl-CoA reductase [	-	-	-	-	-	-	-	-	-	-	-	-	-	-	-	-	-	Q9NUI1
Q9NUQ2	Q9NUQ2	AGPAT5	1-acyl-sn-glycerol-3-phosphate acyltransferase epsilon	-	-	-	-	-	-	-	-	-	-	-	-	-	-	-	-	-	Q9NUQ2
Q9NUQ6	Q9NUQ6	SPATS2L DNAPTP6 SP1224	SPATS2-like protein	-	-	-	-	-	-	-	-	-	-	-	-	-	-	-	-	-	Q9NUQ6
Q9NVH1	Q9NVH1	DNAJC11	DnaJ homolog subfamily C member 11	-	-	-	-	-	-	-	-	-	-	-	-	-	-	-	-	-	Q9NVH1
Q9NVI7	ATAD3A	ATAD3A	ATPase family AAA domain-containing protein 3A	-	-	-	-	-	-	-	-	-	-	-	-	-	-	Q9NVI7	-	Q9NVI7	Q9NVI7
Q9NVJ2	Q9NVJ2	ARL8B ARL10C GIE1	ADP-ribosylation factor-like protein 8B	-	-	-	-	-	-	-	-	-	-	-	-	-	-	-	-	-	Q9NVJ2
Q9NVM6	Q9NVM6	DNAJC17	DnaJ homolog subfamily C member 17	-	-	-	-	-	-	-	-	-	-	-	-	-	-	-	-	-	Q9NVM6
Q9NVP1	Q9NVP1	DDX18 cPERP-D	ATP-dependent RNA helicase DDX18	-	-	-	-	-	-	-	-	-	-	-	-	-	-	-	-	Q9NVP1	-
Q9NVV0	Q9NVV0	TMEM38B C9orf87	Trimeric intracellular cation channel type B	-	-	-	-	-	-	-	-	-	-	-	-	-	-	-	-	Q9NVV0	-
Q9NWB6	Q9NWB6	ARGLU1	Arginine and glutamate-rich protein 1	-	-	-	-	-	-	-	-	-	-	-	-	-	-	-	-	-	Q9NWB6
Q9NWS0	PIH1D1	PIH1D1 NOP17	PIH1 domain-containing protein 1	-	-	-	-	-	-	-	-	-	-	Q9NWS0	-	-	-	-	-	-	-

Q9NX14	NDUFB11	NDUFB11 UNQ111/PRO1064	NADH dehydrogenase	-	-	-	-	-	-	-	-	-	-	Q9NX14	-	-	-	-	-	-	-
Q9NX24	Q9NX24	NHP2 NOLA2 HSPC286	H/ACA ribonucleoprotein complex subunit 2	-	-	-	-	-	-	-	-	-	-	-	-	-	-	-	-	-	Q9NX24
Q9NX38	ABITRAM	ABITRAM C9orf6 FAM206A	Protein Abitram	Q9NX38	Two Hybrid Test (MI:0018)	Q9NX38	Q9NX38	hcv non-structural protein 5a	Q9NX38	-	-	-	-	-	-	-	-	-	-	-	-
Q9NX58	Q9NX58	LYAR PNAS-5	Cell growth-regulating nucleolar protein	-	-	-	-	-	-	-	-	-	-	-	-	-	-	-	-	-	Q9NX58
Q9NX63	CHCHD3	CHCHD3 MIC19 MINOS3	MICOS complex subunit MIC19	-	-	-	-	-	-	-	-	-	-	Q9NX63	-	-	-	-	-	Q9NX63	Q9NX63
Q9NXE8	Q9NXE8	CWC25 CCDC49	Pre-mRNA-splicing factor CWC25 homolog	-	-	-	-	-	-	-	-	-	-	-	-	-	-	-	-	-	Q9NXE8
Q9NXP7	GIN1	GIN1 TGIN1 ZH2C2	Gypsy retrotransposon integrase-like protein 1	Q9NXP7	Two Hybrid Test (MI:0018)	Q9NXP7	-	-	-	Q9NXP7	-	-	-	-	-	-	-	-	-	-	-
Q9NXS2	Q9NXS2	QPCTL	Glutaminyl-peptide cyclotransferase-like protein	-	-	-	-	-	-	-	-	-	-	-	-	-	-	-	-	-	Q9NXS2
Q9NXV6	Q9NXV6	CDKN2AIP CARF	CDKN2A-interacting protein	-	-	-	-	-	-	-	-	-	-	-	-	-	-	-	-	Q9NXV6	-
Q9NYF8	BCLAF1	BCLAF1 BTF KIAA0164	Bcl-2-associated transcription factor 1	-	-	-	-	-	-	-	-	-	-	-	-	-	-	-	Q9NYF8	-	Q9NYF8
Q9NYL4	Q9NYL4	FKBP11 FKBP19 UNQ336/PRO535	Peptidyl-prolyl cis-trans isomerase FKBP11	-	-	-	-	-	-	-	-	-	-	-	-	-	-	-	-	Q9NYL4	Q9NYL4
Q9NYU2	UGGT1	UGGT1 GT UGCGL1 UGGT UGT1 UGTR	UDP-glucose:glycoprotein glucosyltransferase 1	-	-	-	-	-	-	-	-	-	-	Q9NYU2	-	-	-	-	-	-	-
Q9NZ01	Q9NZ01	TECR GPSN2 SC2	Very-long-chain enoyl-CoA reductase	-	-	-	-	-	-	-	-	-	-	-	-	-	-	-	-	-	Q9NZ01
Q9NZ08	ERAP1	ERAP1 APPILS ARTS1 KIAA0525 UNQ584/PRO1154	Endoplasmic reticulum aminopeptidase 1	-	-	-	-	-	-	-	-	-	-	Q9NZ08	-	-	-	-	-	-	-
Q9NZ45	Q9NZ45	CISD1 C10orf70 ZCD1 MDS029	CDGSH iron-sulfur domain-containing protein 1	-	-	-	-	-	-	-	-	-	-	-	-	-	-	-	-	Q9NZ45	-
Q9NZB2	Q9NZB2	FAM120A C9orf10 KIAA0183 OSSA	Constitutive coactivator of PPAR-gamma-like protein 1	-	-	-	-	-	-	-	-	-	-	-	-	-	-	-	-	-	Q9NZB2
Q9NZI8	IGF2BP1	IGF2BP1 CRDBP VICKZ1 ZBP1	Insulin-like growth factor 2 mRNA-binding protein 1	-	-	-	-	-	-	-	-	-	-	-	-	-	-	-	Q9NZI8	Q9NZI8	Q9NZI8
Q9P032	Q9P032	NDUFAF4 C6orf66 HRPAP20 HSPC125 My013	NADH dehydrogenase [ubiquinone] 1 alpha subcomplex assembly factor 4	-	-	-	-	-	-	-	-	-	-	-	-	-	-	-	-	-	Q9P032
Q9P035	HACD3	HACD3 BIND1 PTPLAD1	Very-long-chain	Q9P035	Two Hybrid Test (MI:0018)	-	Q9P035	hcv non-structural protein 5a	-	-	-	-	Q9P035	-	-	-	-	Q9P035	-	Q9P035	Q9P035
Q9P0J0	Q9P0J0	NDUFA13 GRIM19 CDA016 CGI-39	NADH dehydrogenase [ubiquinone] 1 alpha subcomplex subunit 13	-	-	-	-	-	-	-	-	-	-	-	-	-	-	-	-	Q9P0J0	Q9P0J0
Q9P0L0	VAPA	VAPA VAP33	Vesicle-associated membrane protein-associated protein A	Q9P0L0	Coimmunoprecipitation (MI:0019); Immunofluorescence (MI:0022); Immunostaining (MI:0022); Affinity Chromatography (MI:0004)	Q9P0L0	Q9P0L0	hcv non-structural protein 5a	Q9P0L0	-	-	-	Q9P0L0	Q9P0L0	-	Q9P0L0	Q9P0L0	Q9P0L0	-	Q9P0L0	Q9P0L0
Q9P0L1	Q9P0L1	ZKSCAN7 ZNF167 ZNF448 ZNF64	Zinc finger protein with KRAB and SCAN domains 7	-	-	-	-	-	-	-	-	-	-	-	-	-	-	-	-	Q9P0L1	-
Q9P0M9	MRPL27	MRPL27 HSPC250	Large ribosomal subunit protein bL27m	-	-	-	-	-	-	-	-	-	-	Q9P0M9	-	-	-	-	-	-	-

Q9P219	CCDC88C	CCDC88C DAPLE KIAA1509	Protein Daple	-	-	-	-	-	-	-	-	-	-	-	-	-	Q9P219	-	-	-	-
Q9P253	VPS18	VPS18 KIAA1475	Vacuolar protein sorting-associated protein 18 homolog	-	-	-	-	-	-	-	-	-	-	Q9P253	-	-	-	-	-	-	-
Q9P2E9	RRBP1	RRBP1 KIAA1398	Ribosome-binding protein 1	Q9P2E9	Two Hybrid Test (MI:0018)	Q9P2E9	-	-	-	Q9P2E9	-	-	-	-	-	-	-	-	Q9P2E9	-	Q9P2E9
Q9P2N5	RBM27	RBM27 KIAA1311	RNA-binding protein 27	-	-	-	-	-	-	-	-	-	-	Q9P2N5	-	-	-	-	-	-	-
Q9P2X0	Q9P2X0	DPM3	Dolichol-phosphate mannosyltransferase subunit 3	-	-	-	-	-	-	-	-	-	-	-	-	-	-	-	-	-	Q9P2X0
Q9UBB4	Q9UBB4	ATXN10 SCA10	Ataxin-10	-	-	-	-	-	-	-	-	-	-	-	-	-	-	-	-	Q9UBB4	Q9UBB4
Q9UBF8	PI4KB	PI4KB PIK4CB	Phosphatidylinositol 4-kinase beta	-	-	-	Q9UBF8	hcv non-structural protein 5a	-	-	-	-	Q9UBF8	-	-	-	-	-	-	-	-
Q9UBM7	DHCR7	DHCR7 D7SR	7-dehydrocholesterol reductase	-	-	-	-	-	-	-	-	-	-	Q9UBM7	-	-	-	-	-	Q9UBM7	Q9UBM7
Q9UBN7	HDAC6	HDAC6 KIAA0901 JM21	Histone deacetylase 6	-	-	-	-	-	-	-	-	-	-	Q9UBN7	-	-	-	-	-	-	-
Q9UBQ7	GRHPR	GRHPR GLXR MSTP035	Glyoxylate reductase/hydroxypyruvate reductase	-	-	-	-	-	-	-	-	-	-	Q9UBQ7	-	-	-	-	-	Q9UBQ7	-
Q9UBT2	UBA2	UBA2 SAE2 UBLE1B HRIHFB2115	SUMO-activating enzyme subunit 2	-	-	-	-	-	-	-	-	-	-	Q9UBT2	-	-	-	-	-	-	-
Q9UBU8	MORF4L1	MORF4L1 MRG15 FWP006 HSPC008 HSPC061 PP368	Mortality factor 4-like protein 1	-	-	-	-	-	-	-	-	-	-	Q9UBU8	-	-	-	-	-	-	-
Q9UBX3	Q9UBX3	SLC25A10 DIC	Mitochondrial dicarboxylate carrier	-	-	-	-	-	-	-	-	-	-	-	-	-	-	-	-	Q9UBX3	Q9UBX3
Q9UDY4	DNAJB4	DNAJB4 DNAJW HLJ1	DnaJ homolog subfamily B member 4	-	-	-	-	-	-	-	-	-	-	Q9UDY4	-	-	-	-	-	-	-
Q9UET6	Q9UET6	FTSJ1 JM23	tRNA	-	-	-	-	-	-	-	-	-	-	-	-	-	-	-	-	-	Q9UET6
Q9UFW8	Q9UFW8	CGGBP1 CGGBP	CGG triplet repeat-binding protein 1	-	-	-	-	-	-	-	-	-	-	-	-	-	-	-	-	-	Q9UFW8
Q9UGP8	SEC63	SEC63 SEC63L	Translocation protein SEC63 homolog	-	-	-	-	-	-	-	-	-	-	Q9UGP8	-	-	-	-	-	Q9UGP8	Q9UGP8
Q9UH99	SUN2	SUN2 FRIGG KIAA0668 RAB5IP UNC84B	SUN domain-containing protein 2	-	-	-	-	-	-	-	-	Q9UH99	-	-	-	-	-	-	-	-	-
Q9UHD1	CHORDC1	CHORDC1 CHP1	Cysteine and histidine-rich domain-containing protein 1	-	-	-	-	-	-	-	-	-	-	Q9UHD1	-	-	-	-	-	-	-
Q9UHD8	Q9UHD8	SEPTIN9 KIAA0991 MSF SEPT9	Septin-9	-	-	-	-	-	-	-	-	-	-	-	-	-	-	-	-	Q9UHD8	-
Q9UHG3	Q9UHG3	PCYOX1 KIAA0908 PCL1 UNQ597/PRO1183	Prenylcysteine oxidase 1	-	-	-	-	-	-	-	-	-	-	-	-	-	-	-	-	Q9UHG3	-
Q9UHI6	DDX20	DDX20 DP103 GEMIN3	Probable ATP-dependent RNA helicase DDX20	-	-	-	-	-	-	-	-	-	-	-	-	-	Q9UHI6	-	Q9UHI6	-	-
Q9UHQ9	Q9UHQ9	CYB5R1 NQO3A2 UNQ3049/PRO9865	NADH-cytochrome b5 reductase 1	-	-	-	-	-	-	-	-	-	-	-	-	-	-	-	-	Q9UHQ9	-
Q9UHV9	Q9UHV9	PFDN2 PFD2 HSPC231	Prefoldin subunit 2	-	-	-	-	-	-	-	-	-	-	-	-	-	-	-	-	Q9UHV9	-
Q9UHX1	PUF60	PUF60 FIR ROBPI SIAHBP1	Poly(U)-binding-splicing factor PUF60	-	-	-	-	-	-	-	-	-	-	-	-	-	-	-	Q9UHX1	-	-
Q9UI09	Q9UI09	NDUFA12 DAP13	NADH dehydrogenase [ubiquinone] 1 alpha subcomplex subunit 12	-	-	-	-	-	-	-	-	-	-	-	-	-	-	-	-	Q9UI09	Q9UI09
Q9UJA5	Q9UJA5	TRMT6 KIAA1153 TRM6 CGI-09	tRNA	-	-	-	-	-	-	-	-	-	-	-	-	-	-	-	-	Q9UJA5	-

Q9UJS0	Q9UJS0	SLC25A13	Electrogenic aspartate/glutamate antiporter SLC25A13, mitochondrial	-	-	-	-	-	-	-	-	-	-	-	-	-	-	-	-	-	Q9UJS0
Q9UJV9	Q9UJV9	DDX41 ABS	Probable ATP-dependent RNA helicase DDX41	-	-	-	-	-	-	-	-	-	-	-	-	-	-	-	-	-	Q9UJV9
Q9UJZ1	Q9UJZ1	STOML2 SLP2 HSPC108	Stomatin-like protein 2, mitochondrial	-	-	-	-	-	-	-	-	-	-	-	-	-	-	-	Q9UJZ1	Q9UJZ1	
Q9UKA9	PTBP2	PTBP2 NPTB PTB PTBLP	Polypyrimidine tract-binding protein 2	-	-	-	Q9UKA9	hcv non-structural protein 5a	-	-	-	-	-	-	-	-	-	-	-	-	-
Q9UKB1	FBXW11	FBXW11 BTRCP2 FBW1B FBXW1B KIAA0696	F-box/WD repeat-containing protein 11	-	-	-	-	-	-	-	-	-	-	-	-	Q9UKB1	-	-	-	-	-
Q9UKC9	FBXL2	FBXL2 FBL2 FBL3	F-box/LRR-repeat protein 2	Q9UKC9	[(3)H]mevalonate labeling (MI:2131); Coimmunoprecipitation (MI:0019)	Q9UKC9	Q9UKC9	hcv non-structural protein 5a	Q9UKC9	-	-	-	-	-	-	-	-	-	-	-	-
Q9UKR5	Q9UKR5	ERG28 C14orf1 AD-011 HSPC288 x0006	Ergosterol biosynthetic protein 28 homolog	-	-	-	-	-	-	-	-	-	-	-	-	-	-	-	Q9UKR5	-	
Q9UKV3	Q9UKV3	ACIN1 ACINUS KIAA0670	Apoptotic chromatin condensation inducer in the nucleus	-	-	-	-	-	-	-	-	-	-	-	-	-	-	-	-	Q9UKV3	
Q9UL25	RAB21	RAB21 KIAA0118	Ras-related protein Rab-21	-	-	-	-	-	-	-	-	-	-	Q9UL25	-	-	-	-	-	Q9UL25	Q9UL25
Q9UL46	Q9UL46	PSME2	Proteasome activator complex subunit 2	-	-	-	-	-	-	-	-	-	-	-	-	-	-	-	-	Q9UL46	-
Q9ULJ7	ANKRD50	ANKRD50 KIAA1223	Ankyrin repeat domain-containing protein 50	-	-	-	-	-	-	-	Q9ULJ7	-	-	-	-	-	-	-	-	-	-
Q9ULU8	CADPS	CADPS CAPS CAPS1 KIAA1121	Calcium-dependent secretion activator 1	Q9ULU8	Two Hybrid Test (MI:0018)	Q9ULU8	-	-	-	Q9ULU8	-	-	-	-	-	-	-	-	-	-	-
Q9ULW6	NAP1L2	NAP1L2 BPX	Nucleosome assembly protein 1-like 2	Q9ULW6	Two Hybrid Test (MI:0018); Co-affinity purification (MI:0025)	Q9ULW6	Q9ULW6	hcv non-structural protein 5a	-	Q9ULW6	-	-	-	-	-	-	-	-	-	-	-
Q9ULX6	Q9ULX6	AKAP8L NAKAP NAKAP95 HRIHFB2018	A-kinase anchor protein 8-like	-	-	-	-	-	-	-	-	-	-	-	-	-	-	-	-	Q9ULX6	
Q9UM00	Q9UM00	TMCO1 TMCC4 PNAS-10 PNAS-136 UNQ151/PRO177	Calcium load-activated calcium channel	-	-	-	-	-	-	-	-	-	-	-	-	-	-	-	Q9UM00	Q9UM00	
Q9UMS4	Q9UMS4	PRPF19 NMP200 PRP19 SNEV	Pre-mRNA-processing factor 19	-	-	-	-	-	-	-	-	-	-	-	-	-	-	-	Q9UMS4	Q9UMS4	
Q9UMX0	UBQLN1	UBQLN1 DA41 PLIC1	Ubiquilin-1	-	-	-	Q9UMX0	hcv ns 5	-	-	-	-	-	-	-	-	-	-	-	-	Q9UMX0
Q9UN81	Q9UN81	L1RE1 LRE1	LINE-1 retrotransposable element ORF1 protein	-	-	-	-	-	-	-	-	-	-	-	-	-	-	-	Q9UN81	Q9UN81	
Q9UN86	G3BP2	G3BP2 KIAA0660	Ras GTPase-activating protein-binding protein 2	-	-	-	-	-	-	-	-	-	-	-	-	-	-	Q9UN86	Q9UN86	Q9UN86	
Q9UNF1	MAGED2	MAGED2 BCG1	Melanoma-associated antigen D2	-	-	-	-	-	-	-	-	-	-	-	-	-	Q9UNF1	Q9UNF1	-	Q9UNF1	Q9UNF1
Q9UNL2	Q9UNL2	SSR3 TRAPG	Translocon-associated protein subunit gamma	-	-	-	-	-	-	-	-	-	-	-	-	-	-	-	-	Q9UNL2	-
Q9UNM6	Q9UNM6	PSMD13	26S proteasome non-ATPase regulatory subunit 13	-	-	-	-	-	-	-	-	-	-	-	-	-	-	-	-	Q9UNM6	-
Q9UNS2	COPS3	COPS3 CSN3	COP9 signalosome complex subunit 3	-	-	-	-	-	-	-	Q9UNS2	-	-	-	-	-	-	-	-	-	-
Q9UPN3	Q9UPN3	MACF1 ABP620 ACF7 KIAA0465 KIAA0754 KIAA1251	Microtubule-actin cross-linking factor 1, isoforms 1/2/3/4/5	-	-	-	-	-	-	-	-	-	-	-	-	-	-	-	-	Q9UPN3	-
Q9UPU5	USP24	USP24 KIAA1057	Ubiquitin carboxyl-terminal hydrolase 24	-	-	-	-	-	-	-	-	-	-	Q9UPU5	-	-	-	-	-	-	-

Q9UPW5	Q9UPW5	AGTPBP1 CCP1 KIAA1035 NNA1	Cytosolic carboxypeptidase 1	-	-	-	-	-	-	-	-	-	-	-	-	-	-	-	-	Q9UPW5	-
Q9UPY3	DICER1	DICER1 DICER HERNA KIAA0928	Endoribonuclease Dicer	-	-	-	Q9UPY3	hcv ns 5	-	-	-	-	-	-	-	-	-	-	-	-	-
Q9UQ13	Q9UQ13	SHOC2 KIAA0862	Leucine-rich repeat protein SHOC-2	-	-	-	-	-	-	-	-	-	-	-	-	-	-	-	-	-	Q9UQ13
Q9UQ35	SRRM2	SRRM2 KIAA0324 SRL300 SRM300 HSPC075	Serine/arginine repetitive matrix protein 2	-	-	-	-	-	-	-	-	-	-	-	-	-	-	-	Q9UQ35	-	Q9UQ35
Q9UQ90	SPG7	SPG7 CAR CMAR PGN	Paraplegin	-	-	-	-	-	-	-	Q9UQ90	-	-	-	-	-	-	-	-	-	-
Q9Y224	Q9Y224	RTRAF C14orf166 CGI-99	RNA transcription, translation and transport factor protein	-	-	-	-	-	-	-	-	-	-	-	-	-	-	-	-	-	Q9Y224
Q9Y230	RUVBL2	RUVBL2 INO80J TIP48 TIP49B CGI-46	RuvB-like 2	-	-	-	-	-	-	-	-	-	-	-	-	-	-	Q9Y230	-	Q9Y230	Q9Y230
Q9Y241	Q9Y241	HIGD1A HIG1 HSPC010	HIG1 domain family member 1A, mitochondrial	-	-	-	-	-	-	-	-	-	-	-	-	-	-	-	-	-	Q9Y241
Q9Y261	Q9Y261	FOXA2 HNF3B TCF3B	Hepatocyte nuclear factor 3-beta	-	-	-	-	-	-	-	-	-	-	-	-	-	-	-	-	Q9Y261	-
Q9Y262	EIF3L	EIF3L EIF3EIP EIF3S6IP HSPC021 HSPC025 MSTP005	Eukaryotic translation initiation factor 3 subunit L	-	-	-	Q9Y262	hcv non-structural protein 5a	-	-	-	-	-	-	-	-	-	-	-	-	-
Q9Y265	Q9Y265	RUVBL1 INO80H NMP238 TIP49 TIP49A	RuvB-like 1	-	-	-	-	-	-	-	-	-	-	-	-	-	-	-	-	Q9Y265	Q9Y265
Q9Y266	NUDC	NUDC	Nuclear migration protein nudC	-	-	-	-	-	-	-	-	-	-	-	-	-	-	Q9Y266	-	-	-
Q9Y277	VDAC3	VDAC3	Voltage-dependent anion-selective channel protein 3	-	-	-	-	-	-	-	-	-	Q9Y277	-	-	-	-	Q9Y277	-	Q9Y277	Q9Y277
Q9Y285	Q9Y285	FARSA FARS FARSL FARSLA	Phenylalanine--tRNA ligase alpha subunit	-	-	-	-	-	-	-	-	-	-	-	-	-	-	-	-	Q9Y285	Q9Y285
Q9Y287	ITM2B	ITM2B BRI BRI2	Integral membrane protein 2B	-	-	-	-	-	-	-	-	-	Q9Y287	-	-	-	-	-	-	-	-
Q9Y2B0	CNPY2	CNPY2 MSAP TMEM4 ZSIG9 UNQ1943/PRO4426	Protein canopy homolog 2	-	-	-	-	-	-	-	-	-	-	-	-	-	-	Q9Y2B0	-	-	-
Q9Y2G8	DNAJC16	DNAJC16 ERDJ8 KIAA0962	DnaJ homolog subfamily C member 16	-	-	-	-	-	-	-	-	-	Q9Y2G8	-	-	-	-	-	-	-	Q9Y2G8
Q9Y2I1	NISCH	NISCH IRAS KIAA0975	Nischarin	-	-	-	-	-	-	-	-	Q9Y2I1	-	-	-	-	-	-	-	-	-
Q9Y2R0	Q9Y2R0	COA3 CCDC56 MITRAC12 HSPC009	Cytochrome c oxidase assembly factor 3 homolog, mitochondrial	-	-	-	-	-	-	-	-	-	-	-	-	-	-	-	-	-	Q9Y2R0
Q9Y2R9	Q9Y2R9	MRPS7	Small ribosomal subunit protein uS7m	-	-	-	-	-	-	-	-	-	-	-	-	-	-	-	-	-	Q9Y2R9
Q9Y2S7	POLDIP2	POLDIP2 PDIP38 POLD4 HSPC017	Polymerase delta-interacting protein 2	-	-	-	-	-	-	-	-	-	Q9Y2S7	-	-	-	-	-	-	-	-
Q9Y2U8	Q9Y2U8	LEMD3 MAN1	Inner nuclear membrane protein Man1	-	-	-	-	-	-	-	-	-	-	-	-	-	-	-	-	Q9Y2U8	Q9Y2U8

Q9Y2W1	THRAP3	THRAP3 BCLAF2 TRAP150	Thyroid hormone receptor-associated protein 3	-	-	-	-	-	-	-	-	-	-	-	-	-	-	-	Q9Y2W1	-	Q9Y2W1
Q9Y2X8	Q9Y2X8	UBE2D4 UBCH5D	Ubiquitin-conjugating enzyme E2 D4	-	-	-	-	-	-	-	-	-	-	-	-	-	-	-	-	-	Q9Y2X8
Q9Y2Z0	Q9Y2Z0	SUGT1	Protein SGT1 homolog	-	-	-	-	-	-	-	-	-	-	-	-	-	-	-	-	Q9Y2Z0	Q9Y2Z0
Q9Y320	TMX2	TMX2 TXNDC14 CGI-31 My009 PIG26 PSEC0045 UNQ237/PRO270	Thioredoxin-related transmembrane protein 2	-	-	-	-	-	-	-	-	-	-	Q9Y320	-	-	-	-	-	Q9Y320	Q9Y320
Q9Y383	LUC7L2	LUC7L2 CGI-59 CGI-74	Putative RNA-binding protein Luc7-like 2	-	-	-	-	-	-	-	-	-	-	-	-	-	-	-	Q9Y383	-	-
Q9Y388	RBMX2	RBMX2 CGI-79	RNA-binding motif protein, X-linked 2	-	-	-	-	-	-	-	-	-	-	Q9Y388	-	-	-	-	-	-	-
Q9Y394	Q9Y394	DHRS7 DHRS7A RETSDR4 SDR34C1 CGI-86 UNQ285/PRO3448	Dehydrogenase/reductase SDR family member 7	-	-	-	-	-	-	-	-	-	-	-	-	-	-	-	-	Q9Y394	Q9Y394
Q9Y3B3	Q9Y3B3	TMED7 CGI-109	Transmembrane emp24 domain-containing protein 7	-	-	-	-	-	-	-	-	-	-	-	-	-	-	-	-	Q9Y3B3	-
Q9Y3B8	REXO2	REXO2 SFN SMFN CGI-114	Oligoribonuclease, mitochondrial	-	-	-	-	-	-	-	-	-	-	Q9Y3B8	-	-	-	-	-	-	-
Q9Y3B9	RRP15	RRP15 KIAA0507 CGI-115	RRP15-like protein	-	-	-	-	-	-	-	-	-	-	Q9Y3B9	-	-	-	-	-	-	-
Q9Y3C1	Q9Y3C1	NOP16 CGI-117 HSPC111	Nucleolar protein 16	-	-	-	-	-	-	-	-	-	-	-	-	-	-	-	-	-	Q9Y3C1
Q9Y3D7	Q9Y3D7	PAM16 MAGMAS TIM16 TIMM16 CGI-136	Mitochondrial import inner membrane translocase subunit TIM16	-	-	-	-	-	-	-	-	-	-	-	-	-	-	-	-	Q9Y3D7	-
Q9Y3E0	Q9Y3E0	GOLT1B GCT2 GOT1A CGI-141 HDCMA39P UNQ432/PRO793	Vesicle transport protein GOT1B	-	-	-	-	-	-	-	-	-	-	-	-	-	-	-	-	-	Q9Y3E0
Q9Y3E5	Q9Y3E5	PTRH2 BIT1 PTH2 CGI-147	Peptidyl-tRNA hydrolase 2, mitochondrial	-	-	-	-	-	-	-	-	-	-	-	-	-	-	-	-	Q9Y3E5	Q9Y3E5
Q9Y3I0	RTCB	RTCB C22orf28 HSPC117	RNA-splicing ligase RtcB homolog	-	-	-	-	-	-	-	-	-	-	-	-	-	-	-	Q9Y3I0	-	-
Q9Y4B5	Q9Y4B5	MTCL1 CCDC165 KIAA0802 SOGA2	Microtubule cross-linking factor 1	-	-	-	-	-	-	-	-	-	-	-	-	-	-	-	-	-	Q9Y4B5
Q9Y4C2	Q9Y4C2	TCAF1 FAM115A KIAA0738	TRPM8 channel-associated factor 1	-	-	-	-	-	-	-	-	-	-	-	-	-	-	-	-	-	Q9Y4C2
Q9Y4P3	Q9Y4P3	TBL2 WBSCR13 UNQ563/PRO1125	Transducin beta-like protein 2	-	-	-	-	-	-	-	-	-	-	-	-	-	-	-	-	Q9Y4P3	Q9Y4P3
Q9Y4W6	Q9Y4W6	AFG3L2	AFG3-like protein 2	-	-	-	-	-	-	-	-	-	-	-	-	-	-	-	-	-	Q9Y4W6
Q9Y512	Q9Y512	SAMM50 SAM50 CGI-51 TRG3	Sorting and assembly machinery component 50 homolog	-	-	-	-	-	-	-	-	-	-	-	-	-	-	-	-	Q9Y512	Q9Y512
Q9Y520	PRRC2C	PRRC2C BAT2D1 BAT2L2 KIAA1096 XTP2	Protein PRRC2C	-	-	-	-	-	-	-	-	-	-	Q9Y520	-	-	-	-	Q9Y520	-	Q9Y520

Q9Y5A9	Q9Y5A9	YTHDF2 HGRG8	YTH domain-containing family protein 2	-	-	-	-	-	-	-	-	-	-	-	-	-	-	-	-	Q9Y5A9	-
Q9Y5L4	Q9Y5L4	TIMM13 TIM13B TIMM13A TIMM13B	Mitochondrial import inner membrane translocase subunit Tim13	-	-	-	-	-	-	-	-	-	-	-	-	-	-	-	-	-	Q9Y5L4
Q9Y5M8	Q9Y5M8	SRPRB PSEC0230	Signal recognition particle receptor subunit beta	-	-	-	-	-	-	-	-	-	-	-	-	-	-	-	-	Q9Y5M8	Q9Y5M8
Q9Y678	COPG1	COPG1 COPG	Coatomer subunit gamma-1	-	-	-	-	-	-	-	-	-	-	Q9Y678	-	-	-	-	-	Q9Y678	-
Q9Y6C9	Q9Y6C9	MTCH2 MIMP HSPC032	Mitochondrial carrier homolog 2	-	-	-	-	-	-	-	-	-	-	-	-	-	-	-	-	Q9Y6C9	Q9Y6C9
Q9Y6D5	ARFGEF2	ARFGEF2 ARFGEP2 BIG2	Brefeldin A-inhibited guanine nucleotide-exchange protein 2	-	-	-	-	-	-	-	-	-	-	Q9Y6D5	-	-	-	-	-	-	-
Q9Y6E2	Q9Y6E2	BZW2 5MP1 HSPC028 MSTP017	eIF5-mimic protein 1	-	-	-	-	-	-	-	-	-	-	-	-	-	-	-	-	Q9Y6E2	Q9Y6E2
Q9Y6K0	Q9Y6K0	CEPT1 PRO1101	Choline/ethanolaminephosphotransferase 1	-	-	-	-	-	-	-	-	-	-	-	-	-	-	-	-	Q9Y6K0	Q9Y6K0
Q9Y6M1	Q9Y6M1	IGF2BP2 IMP2 VICKZ2	Insulin-like growth factor 2 mRNA-binding protein 2	-	-	-	-	-	-	-	-	-	-	-	-	-	-	-	-	-	Q9Y6M1
Q9Y6M7	SLC4A7	SLC4A7 BT NBC2 NBC2B NBC3 NBCn1 SBC2 SLC4A6	Sodium bicarbonate cotransporter 3	-	-	-	-	-	-	-	-	-	-	Q9Y6M7	-	-	-	-	-	-	-
Q9Y6M9	Q9Y6M9	NDUFB9 LYRM3 UQOR22	NADH dehydrogenase [ubiquinone] 1 beta subcomplex subunit 9	-	-	-	-	-	-	-	-	-	-	-	-	-	-	-	-	-	Q9Y6M9
Q9Y6Y8	SEC23IP	SEC23IP MSTP053	SEC23-interacting protein	-	-	-	-	-	-	-	-	-	-	Q9Y6Y8	-	-	-	-	-	-	-

Supplementary Table 3: List of Jad NS5A retrieved PPIs.

			Statistical Score		MiST Score		SAINT Score				
Leading protein Uniprot ID	Uniprot Entry Name	Gene Names	418	449	418	449	418	449	SUM OF SCORES (+0.5 if the problem is SAINT)	NS5A Bait	Final Score
A0PJW6	TM223	TMEM223	0	1	0	1	0	0	2,00	449	4
A6NJ78	MET15	METTL15 METT5D1	1	0	0	0	0	0	1,00	418	2
		E2	0	1	0	1	0	0	2,00	449	4
		NS3	1	1	0	0	1	1	4,00	BOTH	4
		NS4B	1	0	1	1	1	1	5,00	BOTH	5
		NS5A	1	1	1	1	1	1	6,00	BOTH	6
		NS5B	1	0	1	1	1	1	5,00	BOTH	5
O00116	ADAS	AGPS AAG5	1	1	0	0	1	1	4,00	BOTH	4
O00139	KIF2A	KIF2A KIF2 KNS2	0	1	0	1	0	0	2,00	449	4
O00148	DX39A	DDX39A DDX39	1	1	0	0	1	0	3,00	BOTH	3
O00231	PSD11	PSMD11	1	1	1	0	0	1	4,00	BOTH	4
O00264	PGRC1	PGRMC1 HPR6.6 PGRMC	1	1	0	0	1	1	4,00	BOTH	4
O00410	IPO5	IPO5 KPNB3 RANBP5	1	1	1	0	0	0	3,00	BOTH	3
O00425	IF2B3	IGF2BP3 IMP3 KOC1 VICKZ3	1	1	0	0	0	1	3,00	BOTH	3
O00483	NDUA4	NDUFA4	0	1	0	0	0	0	1,00	449	2
O00499	BIN1	BIN1 AMPHL	1	1	1	1	1	1	6,00	BOTH	6
O14556	G3PT	GAPDHS GAPD2 GAPDH2 GAPDS HSD-35 HSD35	0	1	0	1	0	1	3,00	449	6
O14734	ACOT8	ACOT8 ACTEIII PTE1	1	0	1	0	0	0	2,00	418	4
O14745	NHRF1	NHERF1 NHERF SLC9A3R1	0	1	0	0	0	0	1,00	449	2
O14757	CHK1	CHEK1 CHK1	1	0	1	0	0	0	2,00	418	4
O14773	TPP1	TPP1 CLN2 GIG1 UNQ267/PRO304	1	0	1	1	0	0	3,00	BOTH	3
O14828	SCAM3	SCAMP3 C1orf3 PROPIN1	1	1	1	1	0	0	4,50	BOTH	4,5
O14949	QCR8	UQCRQ	0	1	0	1	0	0	2,00	449	4
O14980	XPO1	XPO1 CRM1	1	1	1	0	0	1	4,00	BOTH	4
O15127	SCAM2	SCAMP2	1	1	1	1	0	1	5,50	BOTH	5,5
O15228	GNPAT	GNPAT DAPAT DHAPAT	1	0	1	0	0	0	2,00	418	4
O15400	STX7	STX7	1	1	0	0	1	1	4,00	BOTH	4
O43175	SERA	PHGDH PGDH3	1	1	0	0	0	0	2,00	BOTH	2
O43399	TPD54	TPD52L2	1	1	1	1	0	0	4,50	BOTH	4,5
O43505	B4GA1	B4GAT1 B3GNT1 B3GNT6	1	1	0	0	1	1	4,00	BOTH	4
O43772	MCAT	SLC25A20 CAC CACT	0	1	0	0	0	0	1,00	449	2
O43809	CPSF5	NUDT21 CFIM25 CPSF25 CPSF5	1	0	0	0	0	0	1,00	418	2
O60264	SMCA5	SMARCA5 SNF2H WCRF135	0	1	0	0	0	0	1,00	449	2
O60427	FADS1	FADS1 FADSD5	1	1	1	1	0	1	5,50	BOTH	5,5
O60488	ACSL4	ACSL4 ACS4 FACL4 LACS4	1	1	1	0	1	1	5,00	BOTH	5
O60669	MOT2	SLC16A7 MCT2	0	1	0	0	0	0	1,00	449	2
O60701	UGDH	UGDH	1	1	0	0	1	1	4,00	BOTH	4
O60716	CTND1	CTNND1 KIAA0384	1	0	0	0	0	0	1,00	418	2
O60884	DNJA2	DNAJA2 CPR3 HIRIP4	1	0	0	0	0	0	1,00	418	2
O75306	NDUS2	NDUFS2	0	1	0	1	0	0	2,00	449	4
O75340	PDCD6	PDCD6 ALG2	1	1	1	1	0	0	4,50	BOTH	4,5
O75380	NDUS6	NDUFS6	0	1	0	1	0	0	2,00	449	4
O75396	SC22B	SEC22B SEC22L1	1	1	0	0	1	0	3,00	BOTH	3
O75489	NDUS3	NDUFS3	1	1	1	1	0	1	5,50	BOTH	5,5
O75521	ECI2	ECI2 DRS1 HCA88 PECI	1	1	1	1	0	0	4,50	BOTH	4,5
O75844	FACE1	ZMPSTE24 FACE1 STE24	1	1	0	1	0	0	3,00	BOTH	3
O75947	ATP5H	ATP5PD ATP5H My032	1	1	0	0	0	0	2,00	BOTH	2
O75964	ATP5L	ATP5MG ATP5L	1	1	0	0	1	0	3,00	BOTH	3
O76024	WFS1	WFS1	0	1	0	1	0	0	2,00	449	4
O76031	CLPX	CLPX	1	1	0	0	0	0	2,00	BOTH	2
O94766	B3GA3	B3GAT3	0	1	0	1	0	0	2,00	449	4
O94826	TOM70	TOMM70 KIAA0719 TOM70 TOMM70A	1	1	1	1	1	0	5,50	BOTH	5,5
O94905	ERLN2	ERLIN2 C8orf2 SPFH2 UNQ2441/PRO5003/PRO9924	1	1	1	1	0	0	4,50	BOTH	4,5
O94966	UBP19	USP19 KIAA0891 ZMYND9	0	1	0	1	0	1	3,00	449	6
O95070	YIF1A	YIF1A 54TM HYIF1P YIF1	1	1	1	1	0	0	4,50	BOTH	4,5
O95168	NDUB4	NDUFB4	1	1	0	0	0	0	2,00	BOTH	2
O95178	NDUB2	NDUFB2	0	1	0	1	0	0	2,00	449	4
O95182	NDUA7	NDUFA7	1	0	1	0	0	0	2,00	418	4
O95202	LETM1	LETM1	1	1	1	1	0	0	4,50	BOTH	4,5
O95249	GOSR1	GOSR1 GS28	1	1	1	1	0	0	4,50	BOTH	4,5
O95292	VAPB	VAPB UNQ484/PRO983	1	1	0	0	1	1	4,00	BOTH	4
O95299	NDUAA	NDUFA10	1	1	0	0	1	0	3,00	BOTH	3
O95373	IPO7	IPO7 RANBP7	1	1	1	0	0	1	4,00	BOTH	4
O95470	SGPL1	SGPL1 KIAA1252	1	1	0	0	0	0	2,00	BOTH	2

O95563	MPC2	MPC2 BRP44	1	1	1	1	0	0	4,50	BOTH	4,5
O95573	ACSL3	ACSL3 ACS3 FACL3 LACS3	1	1	0	0	1	1	4,00	BOTH	4
O95613	PCNT	PCNT KIAA0402 PCNT2	1	0	1	0	1	0	3,00	418	6
O95716	RAB3D	RAB3D GOV RAB16	1	1	1	1	0	0	4,50	BOTH	4,5
O95816	BAG2	BAG2	0	1	0	0	0	1	2,00	449	4
O95864	FADS2	FADS2	1	1	0	0	0	0	2,00	BOTH	2
O95926	SYF2	SYF2 CBPIN GCIPIP	1	0	0	0	0	0	1,00	418	2
O96000	NDUBA	NDUFB10	1	1	1	1	0	0	4,50	BOTH	4,5
O96005	CLPT1	CLPTM1	1	1	1	0	0	0	3,00	BOTH	3
O96008	TOM40	TOMM40 C19orf1 PEREC1 TOM40	1	1	1	1	1	1	6,00	BOTH	6
P00167	CYB5	CYB5A CYB5	1	1	1	1	0	0	4,50	BOTH	4,5
P00387	NB5R3	CYB5R3 DIA1	1	1	0	0	1	1	4,00	BOTH	4
P00403	COX2	MT-CO2 COII COX2 COXII MTCO2	1	1	0	0	0	1	3,00	BOTH	3
P00439	PH4H	PAH	1	1	1	0	0	0	3,00	BOTH	3
P00846	ATP6	MT-ATP6 ATP6 ATPASE6 MTATP6	1	0	1	0	0	0	2,00	418	4
P02649	APOE	APOE	1	1	1	1	1	0	5,50	BOTH	5,5
P02652	APOA2	APOA2	0	1	0	1	0	0	2,00	449	4
P02786	TFR1	TFRC	1	1	1	0	1	1	5,00	BOTH	5
P03928	ATP8	MT-ATP8 ATP8 ATPASE8 MTATP8	0	1	0	0	0	0	1,00	449	2
P04049	RAF1	RAF1 RAF	1	0	1	0	0	0	2,00	418	4
P04350	TBB4A	TUBB4A TUBB4 TUBB5	1	0	1	0	0	0	2,00	418	4
P04843	RPN1	RPN1	1	1	0	0	0	0	2,00	BOTH	2
P04844	RPN2	RPN2	1	1	0	0	0	0	2,00	BOTH	2
P05023	AT1A1	ATP1A1	1	1	0	0	0	0	2,00	BOTH	2
P05109	S10A8	S100A8 CAGA CFAG MRP8	1	0	1	0	0	0	2,00	418	4
P05198	IF2A	EIF2S1 EIF2A	1	0	1	0	0	0	2,00	418	4
P05387	RLA2	RPLP2 D11S2243E RPP2	1	0	1	0	1	0	3,00	418	6
P05556	ITB1	ITGB1 FNRB MDF2 MSK12	1	1	1	1	1	1	6,00	BOTH	6
P06576	ATPB	ATP5F1B ATP5B ATPMB ATPSB	0	1	0	0	0	0	1,00	449	2
P06702	S10A9	S100A9 CAGB CFAG MRP14	1	1	0	1	0	1	4,00	BOTH	4
P07237	PDIA1	P4HB ERBA2L PDI PDIA1 PO4DB	1	0	1	0	0	0	2,00	418	4
P07339	CATD	CTSD CPSD	0	1	0	1	0	0	2,00	449	4
P07437	TBB5	TUBB TUBB5 OK/SW-cl.56	1	0	0	0	0	0	1,00	418	2
P07814	SYEP	EPRS1 EPRS GLNS PARS QARS QPRS PIG32	1	1	0	0	0	0	2,00	BOTH	2
P07900	HS90A	HSP90AA1 HSP90A HSPC1 HSPCA	1	1	0	0	0	0	2,00	BOTH	2
P08134	RHOC	RHOC ARH9 ARHC	0	1	0	0	0	1	2,00	449	4
P08195	4F2	SLC3A2 MDU1	1	1	0	0	1	1	4,00	BOTH	4
P08237	PFKAM	PFKM PFKX	1	1	0	0	1	0	3,00	BOTH	3
P08238	HS90B	HSP90AB1 HSP90B HSPC2 HSPCB	1	1	0	0	0	0	2,00	BOTH	2
P08240	SRPRA	SRPRA SRPR	1	1	0	1	1	0	4,00	BOTH	4
P08574	CY1	CYC1	1	1	1	0	0	1	4,00	BOTH	4
P08754	GNAI3	GNAI3	0	1	0	1	0	0	2,00	449	4
P09622	DLDH	DLD GCSL LAD PHE3	1	0	0	0	0	0	1,00	418	2
P09669	COX6C	COX6C	0	1	0	0	0	1	2,00	449	4
P0C7P0	CISD3	CISD3	1	0	0	0	0	0	1,00	418	2
P0CG08	GPHRB	GPR89B GPHRB GPR89C HSPC201	0	1	0	1	0	0	2,00	449	4
P0DI83	NARR	RAB34 NARR	0	1	0	1	0	0	2,00	449	4
P0DMV9	HS71B	HSPA1B HSP72	1	1	0	0	0	0	2,00	BOTH	2
P0DP25	CALM3	CALM3 CALML2 CAM3 CAMC CAMIII	1	1	1	1	0	1	5,50	BOTH	5,5
P10606	COX5B	COX5B	1	1	1	0	0	1	4,00	BOTH	4
P10620	MGST1	MGST1 GST12 MGST	1	1	0	0	0	1	3,00	BOTH	3
P10809	CH60	HSPD1 HSP60	1	1	0	0	0	0	2,00	BOTH	2
P11233	RALA	RALA RAL	0	1	0	1	0	0	2,00	449	4
P11279	LAMP1	LAMP1	0	1	0	1	0	0	2,00	449	4
P11940	PABP1	PABPC1 PAB1 PABP PABP1 PABPC2	1	1	0	0	0	0	2,00	BOTH	2
P12074	CX6A1	COX6A1 COX6AL	0	1	1	1	0	1	4,00	BOTH	4
P13073	COX41	COX4I1 COX4	1	1	0	0	1	1	4,00	BOTH	4
P13804	ETFA	ETFA	1	1	0	0	0	0	2,00	BOTH	2
P14174	MIF	MIF GLIF MMIF	1	0	1	0	1	0	3,00	418	6
P14324	FPPS	FDPS FPS KIAA1293	1	1	1	1	0	0	4,50	BOTH	4,5
P14406	CX7A2	COX7A2 COX7AL	1	1	1	1	0	0	4,50	BOTH	4,5
P14625	ENPL	HSP90B1 GRP94 TRA1	1	1	1	0	1	1	5,00	BOTH	5
P14923	PLAK	JUP CTNNG DP3	1	1	1	0	0	0	3,00	BOTH	3
P15924	DESP	DSP	0	1	0	0	0	1	2,00	449	4

P15927	RFA2	RPA2 REPA2 RPA32 RPA34	1	0	0	0	0	0	1,00	418	2
P15954	COX7C	COX7C	0	1	0	1	0	0	2,00	449	4
P16435	NCPR	POR CYPOR	1	1	0	0	1	1	4,00	BOTH	4
P16615	AT2A2	ATP2A2 ATP2B	1	1	0	0	0	0	2,00	BOTH	2
P17812	PYRG1	CTPS1 CTPS	0	1	0	0	0	0	1,00	449	2
P17987	TCPA	TCP1 CCT1 CCTA	1	1	0	0	0	0	2,00	BOTH	2
P18031	PTN1	PTPN1 PTP1B	0	1	0	1	0	0	2,00	449	4
P18859	ATP5J	ATP5PF ATP5A ATP5J ATPM	0	1	0	0	0	0	1,00	449	2
P20020	AT2B1	ATP2B1 PMCA1	1	1	0	0	0	1	3,00	BOTH	3
P20340	RAB6A	RAB6A RAB6	0	1	0	0	0	0	1,00	449	2
P20674	COX5A	COX5A	1	1	0	1	1	1	5,00	BOTH	5
P21108	PRPS3	PRPS1L1 PRPS3 PRPSL	1	1	0	0	0	0	2,00	BOTH	2
P21796	VDAC1	VDAC1 VDAC	1	1	0	0	1	1	4,00	BOTH	4
P22695	QCR2	UQCRC2	1	1	1	0	1	1	5,00	BOTH	5
P23919	KTHY	DTYMK CDC8 TMPK TYMK	1	0	0	0	0	0	1,00	418	2
P24539	AT5F1	ATP5PB ATP5F1	1	1	0	0	0	0	2,00	BOTH	2
P25685	DNJB1	DNAJB1 DNAJ1 HDJ1 HSPF1	1	0	0	0	0	0	1,00	418	2
P25705	ATPA	ATP5F1A ATP5A ATP5A1 ATP5AL2 ATPM	0	1	0	0	0	0	1,00	449	2
P26572	MGAT1	MGAT1 GGNT1 GLCT1 GLYT1 MGAT	0	1	1	1	0	0	3,00	BOTH	3
P26641	EF1G	EEF1G EF1G PRO1608	1	1	0	0	0	0	2,00	BOTH	2
P27105	STOM	STOM BND7 EPB72	1	1	1	1	0	0	4,50	BOTH	4,5
P27338	AOFB	MAOB	0	1	1	1	0	0	3,00	BOTH	3
P27348	1433T	YWHAQ	0	1	0	0	0	0	1,00	449	2
P27824	CALX	CANX	1	1	0	0	1	1	4,00	BOTH	4
P28288	ABCD3	ABCD3 PMP70 PXMP1	1	1	0	0	0	1	3,00	BOTH	3
P28331	NDUS1	NDUFS1	1	1	1	1	0	1	5,50	BOTH	5,5
P28482	MK01	MAPK1 ERK2 PRKM1 PRKM2	0	1	0	0	0	0	1,00	449	2
P29317	EPHA2	EPHA2 ECK	0	1	0	1	0	0	2,00	449	4
P29692	EF1D	EEF1D EF1D	1	1	0	0	0	0	2,00	BOTH	2
P29966	MARCS	MARCKS MACS PRKCSL	1	1	0	0	0	0	2,00	BOTH	2
P30049	ATPD	ATP5F1D ATP5D	1	1	0	0	0	0	2,00	BOTH	2
P30085	KCY	CMPK1 CMK CMPK UCK UMK UMPK	0	1	0	1	0	0	2,00	449	4
P30153	2AAA	PPP2R1A	0	1	0	1	0	0	2,00	449	4
P30519	HMOX2	HMOX2 HO2	1	1	1	1	0	0	4,50	BOTH	4,5
P31040	SDHA	SDHA SDH2 SDHF	0	1	0	1	0	0	2,00	449	4
P31689	DNJA1	DNAJA1 DNAJ2 HDJ2 HSJ2 HSPF4	1	1	0	0	1	0	3,00	BOTH	3
P31930	QCR1	UQCRC1	1	1	0	0	1	1	4,00	BOTH	4
P33121	ACSL1	ACSL1 FACL1 FACL2 LACS LACS1 LACS2	1	1	1	1	0	0	4,50	BOTH	4,5
P33908	MA1A1	MAN1A1	1	1	1	1	0	0	4,50	BOTH	4,5
P34931	HS71L	HSPA1L	0	1	0	1	0	0	2,00	449	4
P35232	PHB1	PHB1 PHB	1	1	0	0	1	1	4,00	BOTH	4
P35606	COPB2	COPB2	1	0	1	0	0	0	2,00	418	4
P35610	SOAT1	SOAT1 ACACT ACACT1 ACAT ACAT1 SOAT STAT BSG	1	1	1	1	0	0	4,50	BOTH	4,5
P35613	BASI	UNQ6505/PRO21383	0	1	1	0	0	0	2,00	BOTH	2
P35998	PRS7	PSMC2 MSS1	0	1	0	0	0	1	2,00	449	4
P37059	DHB2	HSD17B2 EDH17B2 SDR9C2	0	1	0	1	0	0	2,00	449	4
P37268	FDFT	FDFT1	1	1	0	0	0	1	3,00	BOTH	3
P38117	ETFB	ETFB FP585	1	0	0	0	1	0	2,00	418	4
P38435	VKGC	GGCX GC	0	1	0	0	0	0	1,00	449	2
P39656	OST48	DDOST KIAA0115 OST48 OK/SW-cl.45	1	1	0	0	0	1	3,00	BOTH	3
P40227	TCPZ	CCT6A CCT6 CCTZ	1	1	0	0	0	0	2,00	BOTH	2
P40429	RL13A	RPL13A	0	1	0	1	0	0	2,00	449	4
P40939	ECHA	HADHA HADH	0	1	0	0	0	0	1,00	449	2
P41252	SYIC	IARS1 IARS	1	1	0	0	0	0	2,00	BOTH	2
P42166	LAP2A	TMPO LAP2	1	0	0	0	0	0	1,00	418	2
P42167	LAP2B	TMPO LAP2	1	1	0	0	0	0	2,00	BOTH	2
P42356	PI4KA	PI4KA PIK4 PIK4CA	1	1	1	1	1	1	6,00	BOTH	6
P42704	LPPRC	LRPPRC LRP130	1	1	0	0	1	1	4,00	BOTH	4
P43304	GPDM	GPD2	1	1	1	1	0	0	4,50	BOTH	4,5
P43487	RANG	RANBP1	1	0	1	1	0	0	3,00	BOTH	3
P43686	PRS6B	PSMC4 MIP224 TBP7	0	1	0	1	0	0	2,00	449	4
P43694	GATA4	GATA4	1	1	1	1	0	0	4,50	BOTH	4,5
P45880	VDAC2	VDAC2	1	1	0	0	1	1	4,00	BOTH	4
P46459	NSF	NSF	1	1	0	0	0	0	2,00	BOTH	2
P46977	STT3A	STT3A ITM1 TMC	1	1	1	0	1	0	4,00	BOTH	4
P48449	LSS	LSS OSC	1	1	1	1	0	1	5,50	BOTH	5,5
P48643	TCPE	CCT5 CCTE KIAA0098	1	1	0	0	0	0	2,00	BOTH	2
P48735	IDHP	IDH2	1	0	0	0	0	0	1,00	418	2
P48739	PIPNB	PITPNB	1	1	1	1	0	0	4,50	BOTH	4,5

P49257	LMAN1	LMAN1 ERGIC53 F5F8D	1	1	0	0	1	1	4,00	BOTH	4
P49327	FAS	FASN FAS	1	0	0	0	0	0	1,00	418	2
P49368	TCPG	CCT3 CCTG TRIC5	0	1	0	0	0	1	2,00	449	4
P49411	EFTU	TUFM	1	0	0	0	0	0	1,00	418	2
P49748	ACADV	ACADVL VLCAD	1	1	1	1	0	0	4,50	BOTH	4,5
P49755	TMEDA	TMED10 TMP21	1	1	0	0	1	0	3,00	BOTH	3
P49821	NDUV1	NDUFV1 UQOR1	0	1	0	1	0	0	2,00	449	4
P50402	EMD	EMD EDMD STA	0	1	1	1	0	0	3,00	BOTH	3
P50895	BCAM	BCAM LU MSK19	1	1	1	0	1	1	5,00	BOTH	5
P50897	PPT1	PPT1 CLN1 PPT	1	0	1	1	0	0	3,00	BOTH	3
P50990	TCPQ	CCT8 C21orf112 CCTQ KIAA0002	1	1	0	0	0	0	2,00	BOTH	2
P51114	FXR1	FXR1	0	1	0	0	0	1	2,00	449	4
P51148	RAB5C	RAB5C RABL	1	1	0	0	1	1	4,00	BOTH	4
P51149	RAB7A	RAB7A RAB7	1	1	0	0	1	1	4,00	BOTH	4
P51570	GALK1	GALK1 GALK	0	1	0	0	0	0	1,00	449	2
P51571	SSRD	SSR4 TRAPD	1	0	0	0	0	0	1,00	418	2
P51572	BAP31	BCAP31 BAP31 DXS1357E	1	1	0	0	1	1	4,00	BOTH	4
P51648	AL3A2	ALDH3A2 ALDH10 FALDH	1	1	1	1	0	0	4,50	BOTH	4,5
P51665	PSMD7	PSMD7 MOV34L	1	1	1	1	0	0	4,50	BOTH	4,5
P51970	NDUA8	NDUFA8	1	0	0	0	0	0	1,00	418	2
P52292	IMA1	KPNA2 RCH1 SRP1	1	1	0	0	0	0	2,00	BOTH	2
P53621	COPA	COPA	1	1	0	0	0	1	3,00	BOTH	3
P53985	MOT1	SLC16A1 MCT1	0	1	0	0	0	0	1,00	449	2
P54136	SYRC	RARS1 RARS	1	1	0	1	0	0	3,00	BOTH	3
P54577	SYYC	YARS1 YARS	0	1	1	1	0	0	3,00	BOTH	3
P54652	HSP72	HSPA2	1	0	1	0	0	0	2,00	418	4
P54709	AT1B3	ATP1B3	1	1	1	1	1	1	6,00	BOTH	6
P54920	SNAA	NAPA SNAPA	0	1	0	1	0	0	2,00	449	4
P55010	IF5	EIF5	1	0	0	0	0	0	1,00	418	2
P55060	XPO2	CSE1L CAS XPO2	1	1	0	0	1	1	4,00	BOTH	4
P55072	TERA	VCP HEL-220 HEL-S-70	0	1	0	1	0	0	2,00	449	4
P55209	NP1L1	NAP1L1 NRP	1	0	1	0	1	0	3,00	418	6
P55317	FOXA1	FOXA1 HNF3A TCF3A	0	1	0	0	0	0	1,00	449	2
P55327	TPD52	TPD52	0	1	0	1	0	0	2,00	449	4
P56134	ATPK	ATP5MF ATP5J2 ATP5JL	0	1	0	0	0	0	1,00	449	2
P56556	NDUA6	NDUFA6 LYRM6 NADHB14	0	1	0	1	0	0	2,00	449	4
P57088	TMM33	TMEM33 DB83	0	1	0	0	0	0	1,00	449	2
P60174	TPIS	TPI1 TPI	0	1	0	0	0	0	1,00	449	2
P60468	SC61B	SEC61B	1	1	0	0	0	0	2,00	BOTH	2
P60602	ROMO1	ROMO1 C20orf52	1	1	1	0	0	0	3,00	BOTH	3
P60903	S10AA	S100A10 ANX2LG CAL1L CLP11	1	0	0	0	0	0	1,00	418	2
P60953	CDC42	CDC42	1	1	1	0	1	1	5,00	BOTH	5
P61006	RAB8A	RAB8A MEL RAB8	1	1	0	0	0	1	3,00	BOTH	3
P61019	RAB2A	RAB2A RAB2	1	1	0	0	1	1	4,00	BOTH	4
P61020	RAB5B	RAB5B	1	0	1	0	0	0	2,00	418	4
P61026	RAB10	RAB10	1	1	1	0	0	1	4,00	BOTH	4
P61106	RAB14	RAB14	1	1	0	0	0	1	3,00	BOTH	3
P61289	PSME3	PSME3	1	1	1	1	0	0	4,50	BOTH	4,5
P61586	RHOA	RHOA ARH12 ARHA RHO12	1	0	0	0	0	0	1,00	418	2
P61619	S61A1	SEC61A1 SEC61A	1	1	0	0	0	0	2,00	BOTH	2
P62136	PP1A	PPP1CA PPP1A	1	0	1	0	0	0	2,00	418	4
P62191	PRS4	PSMC1	1	0	0	0	0	0	1,00	418	2
P62491	RB11A	RAB11A RAB11	1	0	0	0	1	0	2,00	418	4
P62820	RAB1A	RAB1A RAB1	1	1	1	0	1	1	5,00	BOTH	5
P62873	GBB1	GNB1	1	1	0	0	1	1	4,00	BOTH	4
P62879	GBB2	GNB2	1	1	1	1	0	1	5,50	BOTH	5,5
P63000	RAC1	RAC1 TC25 MIG5	1	1	1	1	0	0	4,50	BOTH	4,5
P63167	DYL1	DYNLL1 DLC1 DNCL1 DNCLC1 HDLC1	1	0	0	0	0	0	1,00	418	2
P67809	YBOX1	YBX1 NSEP1 YB1	0	1	0	0	0	0	1,00	449	2
P68366	TBA4A	TUBA4A TUBA1	0	1	0	0	0	0	1,00	449	2
P78344	IF4G2	EIF4G2 DAP5 OK/SW-cl.75	1	1	1	0	0	0	3,00	BOTH	3
P78371	TCPB	CCT2 99D8.1 CCTB	1	1	0	0	0	0	2,00	BOTH	2
P78527	PRKDC	PRKDC HYRC HYRC1	0	1	0	0	0	0	1,00	449	2
P83111	LACTB	LACTB MRPL56 UNQ843/PRO1781	1	0	0	0	1	0	2,00	418	4
P84085	ARF5	ARF5	1	0	0	0	0	0	1,00	418	2
P98194	AT2C1	ATP2C1 KIAA1347 PMR1L HUSSY-28	1	1	1	1	0	0	4,50	BOTH	4,5
Q00325	S25A3	SLC25A3 PHC OK/SW-cl.48	1	0	0	0	0	0	1,00	418	2
Q00610	CLH1	CLTC CLH17 CLTCL2 KIAA0034	0	1	0	1	0	0	2,00	449	4
Q00839	HNRPU	HNRNPU C1orf199 HNRPU SAFA U21.1	0	1	0	0	0	0	1,00	449	2
Q01650	LAT1	SLC7A5 CD98LC LAT1 MPE16	1	1	0	0	1	0	3,00	BOTH	3
Q01780	EXOSX	EXOSC10 PMSCL PMSCL2 RRP6	1	0	1	0	0	0	2,00	418	4
Q05682	CALD1	CALD1 CAD CDM	1	0	1	0	0	0	2,00	418	4
Q06323	PSME1	PSME1 IFI5111	0	1	0	1	0	0	2,00	449	4
Q07065	CKAP4	CKAP4	0	1	0	0	0	0	1,00	449	2

Q07666	KHDR1	KHDRBS1 SAM68	0	1	0	0	0	0	1,00	449	2
Q07812	BAX	BAX BCL2L4	0	1	0	1	0	0	2,00	449	4
Q08752	PPID	PPID CYP40 CYPD	1	1	0	0	0	0	2,00	BOTH	2
Q10471	GALT2	GALNT2	0	1	0	1	0	0	2,00	449	4
Q12797	ASPH	ASPH BAH	0	1	0	0	0	0	1,00	449	2
Q12907	LMAN2	LMAN2 C5orf8	1	1	0	1	1	0	4,00	BOTH	4
Q13011	ECH1	ECH1	0	1	0	1	0	0	2,00	449	4
Q13148	TADBP	TARDBP TDP43	1	1	0	0	1	0	3,00	BOTH	3
Q13217	DNJC3	DNAJC3 P58IPK PRKRI	1	0	0	0	0	0	1,00	418	2
Q13310	PABP4	PABPC4 APP1 PABP4	1	1	0	0	0	0	2,00	BOTH	2
Q13347	EIF3I	EIF3I EIF3S2 TRIP1	1	1	1	1	0	0	4,50	BOTH	4,5
Q13423	NNTM	NNT	0	1	1	1	0	0	3,00	BOTH	3
Q13492	PICAL	PICALM CALM	1	0	1	0	0	0	2,00	418	4
Q13523	PRP4B	PRPF4B KIAA0536 PRP4 PRP4H PRP4K	0	1	0	1	0	0	2,00	449	4
Q13724	MOGS	MOGS GCS1	1	1	1	1	0	0	4,50	BOTH	4,5
Q14152	EIF3A	EIF3A EIF3S10 KIAA0139	0	1	0	0	0	1	2,00	449	4
Q14165	MLEC	MLEC KIAA0152	1	1	0	1	1	1	5,00	BOTH	5
Q14204	DYHC1	DYNC1H1 DHC1 DNCH1 DNCL DNECL DYHC KIAA0325	0	1	0	0	0	0	1,00	449	2
Q14247	SRC8	CTTN EMS1	1	1	1	0	0	1	4,00	BOTH	4
Q14318	FKBP8	FKBP8 FKBP38	1	1	1	1	0	0	4,50	BOTH	4,5
Q14444	CAPR1	CAPRIN1 GPIAP1 GPIP137 M11S1 RNG105	0	1	0	1	0	0	2,00	449	4
Q14527	HLTF	HLTF HIP116A RNF80 SMARCA3 SNF2L3 ZBU1	1	0	1	0	0	0	2,00	418	4
Q14534	ERG1	SQLE ERG1	1	0	1	0	0	0	2,00	418	4
Q14542	S29A2	SLC29A2 DER12 ENT2 HNP36	1	1	1	0	0	0	3,00	BOTH	3
Q14558	KPRA	PRPSAP1	0	1	0	1	0	0	2,00	449	4
Q14677	EPN4	CLINT1 ENTH EPN4 EPNR KIAA0171	1	0	0	0	0	0	1,00	418	2
Q14697	GANAB	GANAB G2AN KIAA0088	1	1	0	0	1	1	4,00	BOTH	4
Q14739	LBR	LBR	1	1	0	0	0	0	2,00	BOTH	2
Q14964	RB39A	RAB39A RAB39	1	1	1	1	0	0	4,50	BOTH	4,5
Q14974	IMB1	KPNB1 NTF97	1	1	0	0	1	1	4,00	BOTH	4
Q15004	PAF15	PCLAF KIAA0101 NS5ATP9 PAF L5	1	0	0	0	0	0	1,00	418	2
Q15005	SPCS2	SPCS2 KIAA0102 SPC25	1	1	1	1	1	1	6,00	BOTH	6
Q15029	U5S1	EFTUD2 KIAA0031 SNRP116	0	1	0	1	0	0	2,00	449	4
Q15041	AR6P1	ARL6IP1 ARL6IP ARMER KIAA0069	1	1	1	1	0	0	4,50	BOTH	4,5
Q15043	S39AE	SLC39A14 KIAA0062 ZIP14	1	1	0	0	1	1	4,00	BOTH	4
Q15046	SYK	KARS1 KARS KIAA0070	0	1	0	0	0	0	1,00	449	2
Q15125	EBP	EBP	1	1	0	0	0	0	2,00	BOTH	2
Q15155	NOMO1	NOMO1 PM5	0	1	1	1	0	0	3,00	BOTH	3
Q15165	PON2	PON2	0	1	0	0	0	0	1,00	449	2
Q15369	ELOC	ELOC TCEB1	1	0	1	0	0	0	2,00	418	4
Q15392	DHC24	DHCR24 KIAA0018	1	1	0	0	1	0	3,00	BOTH	3
Q15424	SAFB1	SAFB HAP HET SAFB1	0	1	0	0	0	0	1,00	449	2
Q15629	TRAM1	TRAM1 TRAM	0	1	0	1	0	0	2,00	449	4
Q15691	MARE1	MAPRE1	0	1	0	0	0	0	1,00	449	2
Q15717	ELAV1	ELAVL1 HUR	1	1	0	0	1	1	4,00	BOTH	4
Q15758	AAAT	SLC1A5 ASCT2 M7V1 RDR RDRC	1	1	0	0	0	1	3,00	BOTH	3
Q15773	MLF2	MLF2	0	1	0	1	0	0	2,00	449	4
Q15800	MSMO1	MSMO1 DESP4 ERG25 SC4MOL	1	1	1	1	0	0	4,50	BOTH	4,5
Q15836	VAMP3	VAMP3 SYB3	1	1	1	1	0	1	5,50	BOTH	5,5
Q15907	RB11B	RAB11B YPT3	0	1	0	0	0	1	2,00	449	4
Q15942	ZYX	ZYX	1	0	1	0	0	0	2,00	418	4
Q16186	ADRM1	ADRM1 GP110	1	1	1	1	0	0	4,50	BOTH	4,5
Q16401	PSMD5	PSMD5 KIAA0072	1	1	1	0	0	0	3,00	BOTH	3
Q16718	NDUA5	NDUFA5	1	1	1	1	1	1	6,00	BOTH	6
Q16763	UBE2S	UBE2S E2EPF OK/SW-cl.73	1	0	1	0	0	0	2,00	418	4
Q16795	NDUA9	NDUFA9 NDUFS2L	1	1	1	1	0	0	4,50	BOTH	4,5
Q16850	CP51A	CYP51A1 CYP51	1	1	1	1	0	0	4,50	BOTH	4,5
Q16891	MIC60	IMMT HMP MIC60 MINOS2 PIG4 PIG52	1	1	0	0	1	1	4,00	BOTH	4
Q2TAY7	SMU1	SMU1	0	1	0	1	0	0	2,00	449	4
Q3ZCQ8	TIM50	TIMM50 TIM50 PRO1512	0	1	0	0	0	0	1,00	449	2
Q53GQ0	DHB12	HSD17B12 SDR12C1	1	1	1	0	0	1	4,00	BOTH	4
Q58FF8	H90B2	HSP90AB2P HSP90BB	1	0	1	0	0	0	2,00	418	4
Q5BJD5	TM41B	TMEM41B KIAA0033	0	1	1	0	0	0	2,00	BOTH	2

Q5BKY9	F133B	FAM133B	0	1	0	0	0	0	1,00	449	2
Q5HYI8	RABL3	RABL3	1	0	1	1	0	0	3,00	BOTH	3
Q5JTV8	TOIP1	TOR1AIP1 LAP1	0	1	0	1	0	0	2,00	449	4
Q5RI15	COX20	COX20 FAM36A	0	1	0	1	0	0	2,00	449	4
Q5T3I0	GPTC4	GPATCH4 GPATC4	1	0	1	0	0	0	2,00	418	4
Q5T9A4	ATD3B	ATAD3B KIAA1273 TOB3	1	0	0	1	0	0	2,00	BOTH	2
Q5VU43	MYOME	PDE4DIP CMYA2 KIAA0454 KIAA0477 MMGL	1	0	1	0	0	0	2,00	418	4
Q6DD87	ZN787	ZNF787	1	0	0	0	0	0	1,00	418	2
Q6DD88	ATLA3	ATL3	1	1	0	0	0	1	3,00	BOTH	3
Q6NUK1	SCMC1	SLC25A24 APC1 MCSC1 SCAMC1	1	0	1	0	0	0	2,00	418	4
Q6PCD5	RFWD3	RFWD3 RNF201	1	1	1	1	0	0	4,50	BOTH	4,5
Q6PID8	KLD10	KLHDC10 KIAA0265	1	0	1	0	0	0	2,00	418	4
Q6UW68	TM205	TMEM205 UNQ501/PRO1018	0	1	0	0	0	1	2,00	449	4
Q6Y1H2	HACD2	HACD2 PTPLB	1	1	0	0	0	0	2,00	BOTH	2
Q6Y7W6	GGYF2	GIGYF2 KIAA0642 PERQ2 TNRC15	1	0	1	0	0	0	2,00	418	4
Q6YN16	HSDL2	HSDL2 C9orf99 SDR13C1	1	0	0	0	0	0	1,00	418	2
Q70UQ0	IKIP	IKBIP IKIP	0	1	0	1	0	0	2,00	449	4
Q7L4I2	RSRC2	RSRC2	1	0	0	0	0	0	1,00	418	2
Q7Z7F7	RM55	MRPL55 UNQ5835/PRO19675	1	0	1	0	0	0	2,00	418	4
Q86TB9	PATL1	PATL1 OK/KNS-cl.5	1	0	1	0	0	0	2,00	418	4
Q86UE4	LYRIC	MTDH AEG1 LYRIC	0	1	0	0	0	0	1,00	449	2
Q86UP2	KTN1	KTN1 CG1 KIAA0004	1	0	0	0	0	0	1,00	418	2
Q86VP6	CAND1	CAND1 KIAA0829 TIP120 TIP120A	1	1	1	0	1	0	4,00	BOTH	4
Q8IYS2	K2013	KIAA2013	0	1	0	1	0	0	2,00	449	4
Q8IZ81	ELMD2	ELMOD2	1	1	1	1	0	0	4,50	BOTH	4,5
Q8IZP2	ST134	ST13P4 FAM10A4	1	0	1	0	0	0	2,00	418	4
Q8N183	NDUF2	NDUFAF2 NDUFA12L	0	1	1	1	0	0	3,00	BOTH	3
Q8N2K0	ABD12	ABHD12 C20orf22	1	1	0	0	0	0	2,00	BOTH	2
Q8N357	S35F6	SLC35F6 C2orf18 UNQ3047/PRO9863	0	1	0	1	0	0	2,00	449	4
Q8N4V1	EMC5	MMGT1 EMC5 TMEM32	1	1	1	1	0	0	4,50	BOTH	4,5
Q8N5G0	SIM20	SMIM20 C4orf52 MITRAC7	1	1	0	1	0	1	4,00	BOTH	4
Q8N5M4	TTC9C	TTC9C	1	0	1	0	0	0	2,00	418	4
Q8N5M9	JAGN1	JAGN1	1	1	0	0	0	0	2,00	BOTH	2
Q8N684	CPSF7	CPSF7	1	0	0	0	0	0	1,00	418	2
Q8N6T3	ARFG1	ARFGAP1 ARF1GAP	1	1	1	1	0	0	4,50	BOTH	4,5
Q8NAT1	PMGT2	POMGNT2 AGO61 C3orf39 EOGTL GTDC2	1	1	1	1	0	0	4,50	BOTH	4,5
Q8NAV1	PR38A	PRPF38A	1	0	0	0	0	0	1,00	418	2
Q8NBJ4	GOLM1	GOLM1 C9orf155 GOLPH2 PSEC0242 UNQ686/PRO1326	0	1	1	1	0	0	3,00	BOTH	3
Q8NBP7	PCSK9	PCSK9 NARC1 PSEC0052	1	0	0	0	0	0	1,00	418	2
Q8NBQ5	DHB11	HSD17B11 DHRS8 PAN1B SDR16C2 PSEC0029 UNQ207/PRO233	1	1	1	1	0	0	4,50	BOTH	4,5
Q8NBX0	SCPDL	SCCPDH CGI-49	1	1	0	0	0	0	2,00	BOTH	2
Q8NDH3	PEPL1	NPEPL1 KIAA1974	1	0	1	0	1	0	3,00	418	6
Q8NHH9	ATLA2	ATL2 ARL6IP2	1	1	1	1	0	0	4,50	BOTH	4,5
Q8NHW5	RLA0L	RPLP0P6	1	0	0	0	0	0	1,00	418	2
Q8TC12	RDH11	RDH11 ARSDR1 PSDR1 SDR7C1 CGI-82	1	1	1	1	1	1	6,00	BOTH	6
Q8TCJ2	STT3B	STT3B SIMP	1	1	0	0	0	0	2,00	BOTH	2
Q8WUF5	IASPP	PPP1R13L IASPP NKIP1 PPP1R13BL RAI	0	1	0	1	0	0	2,00	449	4
Q8WVM8	SCFD1	SCFD1 C14orf163 KIAA0917	0	1	0	0	0	1	2,00	449	4
Q8WWK9	CKAP2	STXBP1L2 FKSG23 CKAP2 LB1 TMAP	0	1	0	1	0	1	3,00	449	6
Q8WWM7	ATX2L	ATXN2L A2D A2LG A2LP A2RP	0	1	0	0	0	0	1,00	449	2
Q92504	S39A7	SLC39A7 HKE4 RING5	1	1	0	0	0	0	2,00	BOTH	2
Q92538	GBF1	GBF1 KIAA0248	0	1	0	0	0	1	2,00	449	4
Q92544	TM9S4	TM9SF4 KIAA0255 TUCAP1	1	1	0	0	0	1	3,00	BOTH	3
Q92575	UBXN4	UBXN4 KIAA0242 UBXD2 UBXDC1	0	1	0	1	0	0	2,00	449	4
Q92604	LGAT1	LPGAT1 FAM34A KIAA0205	1	1	1	0	0	0	3,00	BOTH	3
Q92616	GCN1	GCN1 GCN1L1 KIAA0219	1	1	0	1	1	1	5,00	BOTH	5

Q92621	NU205	NUP205 C7orf14 KIAA0225	1	1	1	0	0	0	3,00	BOTH	3
Q92643	GPI8	PIGK GPI8	0	1	0	0	0	0	1,00	449	2
Q92667	AKAP1	AKAP1 AKAP149 PRKA1	0	1	1	1	0	0	3,00	BOTH	3
Q92879	CELF1	CELF1 BRUNOL2 CUGBP CUGBP1 NAB50	0	1	0	1	0	0	2,00	449	4
Q92896	GSLG1	GLG1 CFR1 ESL1 MG160	1	1	1	1	0	1	5,50	BOTH	5,5
Q92900	RENT1	UPF1 KIAA0221 RENT1	0	1	0	1	0	0	2,00	449	4
Q92930	RAB8B	RAB8B	1	1	0	0	1	1	4,00	BOTH	4
Q92945	FUBP2	KHSRP FUBP2	1	0	0	0	0	0	1,00	418	2
Q92973	TNPO1	TNPO1 KPNB2 MIP1 TRN	1	1	1	1	0	0	4,50	BOTH	4,5
Q969M3	YIPF5	YIPF5 FINGER5 YIP1A PP12723 SB140 UNQ3123/PRO10275	1	0	1	0	0	0	2,00	418	4
Q969U7	PSMG2	PSMG2 HCCA3 PAC2 TNFSF5IP1	1	1	1	1	0	0	4,50	BOTH	4,5
Q969X5	ERGI1	ERGIC1 ERGIC32 KIAA1181 HT034	0	1	0	0	0	0	1,00	449	2
Q96A26	F162A	FAM162A C3orf28 E2IG5 DC16 FWP001	1	1	1	1	0	0	4,50	BOTH	4,5
Q96A33	CCD47	CCDC47 GK001 MSTP041 PSEC0077	0	1	1	1	0	0	3,00	BOTH	3
Q96BW9	TAM41	TAMM41 C3orf31	0	1	0	1	0	0	2,00	449	4
Q96C57	CSTOS	CUSTOS C12orf43	1	0	0	1	0	0	2,00	BOTH	2
Q96CB9	NSUN4	NSUN4	0	1	0	0	0	0	1,00	449	2
Q96CS3	FAF2	FAF2 ETEA KIAA0887 UBXD8 UBXN3B	1	1	0	0	1	1	4,00	BOTH	4
Q96DA6	TIM14	DNAJC19 TIM14 TIMM14	0	1	0	0	0	0	1,00	449	2
Q96EU6	RRP36	RRP36 C6orf153 HSPC253	1	0	0	0	0	0	1,00	418	2
Q96EY1	DNJA3	DNAJA3 HCA57 TID1	1	0	0	0	0	0	1,00	418	2
Q96G23	CERS2	CERS2 LASS2 TMSG1	1	1	0	0	0	1	3,00	BOTH	3
Q96HR9	REEP6	REEP6 C19orf32 DP1L1	1	1	1	1	0	0	4,50	BOTH	4,5
Q96HY6	DDRGK	DDRGK1 C20orf116 UFBP1	1	1	1	1	0	0	4,50	BOTH	4,5
Q96IJ6	GMPPA	GMPPA	1	0	1	0	0	0	2,00	418	4
Q96L58	B3GT6	B3GALT6	1	0	1	0	0	0	2,00	418	4
Q96N38	ZN714	ZNF714	0	1	0	0	0	0	1,00	449	2
Q96P11	NSUN5	NSUN5 NSUN5A WBSCR20 WBSCR20A	1	0	0	0	1	0	2,00	418	4
Q96P70	IPO9	IPO9 IMP9 KIAA1192 RANBP9 HSPC273	0	1	0	1	0	0	2,00	449	4
Q96T76	MMS19	MMS19 MMS19L	1	1	1	1	0	0	4,50	BOTH	4,5
Q99442	SEC62	SEC62 TLOC1	1	0	1	0	0	0	2,00	418	4
Q99459	CDC5L	CDC5L KIAA0432 PCDC5RP	0	1	0	1	0	0	2,00	449	4
Q99460	PSMD1	PSMD1	0	1	0	1	0	0	2,00	449	4
Q99536	VAT1	VAT1	0	1	1	1	0	1	4,00	BOTH	4
Q99623	PHB2	PHB2 BAP REA	1	1	0	0	0	1	3,00	BOTH	3
Q99661	KIF2C	KIF2C KNSL6	0	1	0	1	0	0	2,00	449	4
Q99733	NP1L4	NAP1L4 NAP2	1	1	1	1	1	0	5,50	BOTH	5,5
Q99735	MGST2	MGST2 GST2	1	1	0	0	1	1	4,00	BOTH	4
Q99805	TM9S2	TM9SF2	1	1	1	0	0	0	3,00	BOTH	3
Q99832	TCPH	CCT7 CCTH NIP7-1	1	1	0	0	0	1	3,00	BOTH	3
Q99942	RNF5	RNF5 G16 NG2 RMA1	0	1	0	1	0	0	2,00	449	4
Q99956	DUS9	DUSP9 MKP4	1	1	1	0	0	0	3,00	BOTH	3
Q9BPW8	NIPS1	NIPSNAP1	1	1	0	1	1	1	5,00	BOTH	5
Q9BQ69	MACD1	MACROD1 LRP16	1	0	0	0	0	0	1,00	418	2
Q9BQB6	VKOR1	VKORC1 VKOR MSTP134 MSTP576	0	1	0	0	0	0	1,00	449	2
Q9BRX2	PELO	UNQ308/PRO351 PELO CGI-17	1	0	0	0	0	0	1,00	418	2
Q9BSJ8	ESYT1	ESYT1 FAM62A KIAA0747 MBC2	1	1	1	1	1	1	6,00	BOTH	6
Q9BTV4	TMM43	TMEM43 UNQ2564/PRO6244	0	1	1	1	0	0	3,00	BOTH	3
Q9BUF5	TBB6	TUBB6	1	1	0	0	0	1	3,00	BOTH	3
Q9BUP3	HTAI2	HTATIP2 CC3 TIP30	1	1	1	1	1	1	6,00	BOTH	6
Q9BUV8	RCAF1	RAB5IF C20orf24 OPTI RCAF1 PNAS-11	1	1	0	0	0	0	2,00	BOTH	2
Q9BV40	VAMP8	VAMP8	0	1	0	1	0	0	2,00	449	4
Q9BVC6	TM109	TMEM109	1	1	1	1	1	1	6,00	BOTH	6
Q9BVK6	TMED9	TMED9 GP25L2	1	1	0	0	1	1	4,00	BOTH	4
Q9BX93	PG12B	PLA2G12B PLA2G13 FKSG71	0	1	0	1	0	0	2,00	449	4
Q9BZV2	S19A3	SLC19A3	0	1	0	1	0	0	2,00	449	4

Q9C0E8	LNP	LNPK KIAA1715 LNP	0	1	1	1	0	0	3,00	BOTH	3
Q9GZT3	SLIRP	SLIRP C14orf156 DC23 DC50 PD04872	1	1	0	1	0	0	3,00	BOTH	3
Q9H0A0	NAT10	NAT10 ALP KIAA1709	1	0	0	0	1	0	2,00	418	4
Q9H0U3	MAGT1	MAGT1 IAG2 PSEC0084 UNQ628/PRO1244	1	1	1	1	0	0	4,50	BOTH	4,5
Q9H0U4	RAB1B	RAB1B	1	1	0	0	1	1	4,00	BOTH	4
Q9H2K8	TAOK3	TAOK3 DPK JIK KDS MAP3K18	1	0	1	0	0	0	2,00	418	4
Q9H330	TM245	TMEM245 C9orf5	0	1	0	1	0	0	2,00	449	4
Q9H3N1	TMX1	TMX1 TMX TXNDC TXNDC1 PSEC0085 UNQ235/PRO268	1	1	1	1	0	1	5,50	BOTH	5,5
Q9H7B4	SMYD3	SMYD3 ZMYND1 ZNFN3A1	0	1	0	1	0	1	3,00	449	6
Q9H845	ACAD9	ACAD9	0	1	0	1	0	0	2,00	449	4
Q9H8H3	TMT1A	TMT1A METTL7A PRO0066 UNQ1902/PRO4348	1	1	1	1	0	0	4,50	BOTH	4,5
Q9H9B4	SFXN1	SFXN1	1	1	0	0	1	1	4,00	BOTH	4
Q9HC07	TM165	TMEM165 TPARL	1	1	0	1	0	0	3,00	BOTH	3
Q9HCE1	MOV10	MOV10 KIAA1631	1	1	1	1	0	0	4,50	BOTH	4,5
Q9HCU5	PREB	PREB SEC12	1	1	1	1	0	0	4,50	BOTH	4,5
Q9HD20	AT131	ATP13A1 ATP13A KIAA1825 CGI-152	1	1	1	1	0	1	5,50	BOTH	5,5
Q9HD45	TM9S3	TM9SF3 SMBP UNQ245/PRO282	1	1	0	0	1	1	4,00	BOTH	4
Q9HDC9	APMAP	APMAP C20orf3 UNQ1869/PRO4305	1	1	0	0	1	1	4,00	BOTH	4
Q9NP72	RAB18	RAB18	1	1	1	1	0	1	5,50	BOTH	5,5
Q9NPA0	EMC7	EMC7 C11orf3 C15orf24 HT022 UNQ905/PRO1926	0	1	0	1	0	0	2,00	449	4
Q9NQC3	RTN4	RTN4 KIAA0886 NOGO My043 SP1507	1	0	1	1	0	0	3,00	BOTH	3
Q9NRG9	AAAS	AAAS ADRACALA GL003	1	1	1	1	0	0	4,50	BOTH	4,5
Q9NRP0	OSTC	OSTC DC2 HDCMD45P HSPC307	1	1	0	0	0	0	2,00	BOTH	2
Q9NRZ9	HELLS	HELLS PASG SMARCA6 Nbla10143	1	0	0	0	0	0	1,00	418	2
Q9NTJ3	SMC4	SMC4 CAPC SMC4L1	0	1	0	1	0	0	2,00	449	4
Q9NTJ5	SAC1	SACM1L KIAA0851 SAC1	1	1	1	1	0	1	5,50	BOTH	5,5
Q9NVI7	ATD3A	ATAD3A	1	1	0	0	0	0	2,00	BOTH	2
Q9NVP1	DDX18	DDX18 cPERP-D	0	1	0	1	0	0	2,00	449	4
Q9NVV0	TM38B	TMEM38B C9orf87	1	1	1	1	0	0	4,50	BOTH	4,5
Q9NX63	MIC19	CHCHD3 MIC19 MINOS3	1	1	1	1	1	1	6,00	BOTH	6
Q9NXV6	CARF	CDKN2AIP CARF	0	1	0	0	0	0	1,00	449	2
Q9NYL4	FKB11	FKBP11 FKBP19 UNQ336/PRO535	0	1	0	0	0	0	1,00	449	2
Q9NZ45	CISD1	CISD1 C10orf70 ZCD1 MDS029	0	1	0	1	0	0	2,00	449	4
Q9NZI8	IF2B1	IGF2BP1 CRDBP VICKZ1 ZBP1	1	1	0	0	0	1	3,00	BOTH	3
Q9P035	HACD3	HACD3 BIND1 PTPLAD1	1	1	1	1	1	1	6,00	BOTH	6
Q9P0J0	NDUAD	NDUFA13 GRIM19 CDA016 CGI-39	1	1	1	0	0	0	3,00	BOTH	3
Q9P0L0	VAPA	VAPA VAP33	1	1	0	0	1	1	4,00	BOTH	4
Q9P0L1	ZKSC7	ZKSCAN7 ZNF167 ZNF448 ZNF64	0	1	0	0	0	0	1,00	449	2
Q9UBB4	ATX10	ATXN10 SCA10	1	0	1	1	0	0	3,00	BOTH	3
Q9UBM7	DHCR7	DHCR7 D7SR	0	1	0	0	0	0	1,00	449	2
Q9UBQ7	GRHPR	GRHPR GLXR MSTP035	1	0	1	0	0	0	2,00	418	4
Q9UBX3	DIC	SLC25A10 DIC	1	1	0	0	1	1	4,00	BOTH	4
Q9UGP8	SEC63	SEC63 SEC63L	1	1	0	1	0	0	3,00	BOTH	3
Q9UHD8	Sep-09	SEPTIN9 KIAA0991 MSF SEPT9	1	0	0	0	0	0	1,00	418	2
Q9UHG3	PCYOX	PCYOX1 KIAA0908 PCL1 UNQ597/PRO1183	0	1	0	1	0	0	2,00	449	4
Q9UHQ9	NB5R1	CYB5R1 NQO3A2 UNQ3049/PRO9865	0	1	0	1	0	0	2,00	449	4
Q9UHV9	PFD2	PFDN2 PFD2 HSPC231	1	1	1	1	0	0	4,50	BOTH	4,5
Q9UI09	NDUAC	NDUFA12 DAP13	1	0	1	0	0	0	2,00	418	4
Q9UJA5	TRM6	TRMT6 KIAA1153 TRM6 CGI-09	1	0	1	0	0	0	2,00	418	4

Q9UJZ1	STML2	STOML2 SLP2 HSPC108	1	1	1	1	0	1	5,50	BOTH	5,5
Q9UKR5	ERG28	ERG28 C14orf1 AD-011 HSPC288 x0006	1	0	1	0	0	0	2,00	418	4
Q9UL25	RAB21	RAB21 KIAA0118	1	1	1	0	1	1	5,00	BOTH	5
Q9UL46	PSME2	PSME2	1	1	1	1	0	0	4,50	BOTH	4,5
Q9UM00	TMCO1	TMCO1 TMCC4 PNAS-10 PNAS-136 UNQ151/PRO177	0	1	0	0	0	0	1,00	449	2
Q9UMS4	PRP19	PRPF19 NMP200 PRP19 SNEV	0	1	0	0	0	1	2,00	449	4
Q9UN81	LORF1	L1RE1 LRE1	1	1	1	1	0	0	4,50	BOTH	4,5
Q9UN86	G3BP2	G3BP2 KIAA0660	1	0	1	0	0	0	2,00	418	4
Q9UNF1	MAGD2	MAGED2 BCG1	1	0	1	0	0	0	2,00	418	4
Q9UNL2	SSRG	SSR3 TRAPG	1	1	0	0	1	0	3,00	BOTH	3
Q9UNM6	PSD13	PSMD13	1	0	1	0	0	0	2,00	418	4
Q9UPN3	MACF1	MACF1 ABP620 ACF7 KIAA0465 KIAA0754 KIAA1251	0	1	0	0	0	1	2,00	449	4
Q9UPW5	CBPC1	AGTPBP1 CCP1 KIAA1035 NNA1	1	0	1	0	0	0	2,00	418	4
Q9Y230	RUVB2	RUVBL2 INO80J TIP48 TIP49B CGI-46	1	1	0	0	0	0	2,00	BOTH	2
Q9Y261	FOXA2	FOXA2 HNF3B TCF3B	0	1	0	1	0	0	2,00	449	4
Q9Y265	RUVB1	RUVBL1 INO80H NMP238 TIP49 TIP49A	1	1	0	0	1	1	4,00	BOTH	4
Q9Y277	VDAC3	VDAC3	1	1	0	0	1	1	4,00	BOTH	4
Q9Y285	SYFA	FARSA FARS FARSL FARSLA	1	1	0	1	1	1	5,00	BOTH	5
Q9Y2U8	MAN1	LEMD3 MAN1	1	1	1	1	0	0	4,50	BOTH	4,5
Q9Y2Z0	SGT1	SUGT1	1	1	0	0	0	0	2,00	BOTH	2
Q9Y320	TMX2	TMX2 TXNDC14 CGI-31 My009 PIG26 PSEC0045 UNQ237/PRO270	1	1	0	0	1	1	4,00	BOTH	4
Q9Y394	DHRS7	DHRS7 DHRS7A RETSDR4 SDR34C1 CGI-86 UNQ285/PRO3448	1	1	1	1	0	1	5,50	BOTH	5,5
Q9Y3B3	TMED7	TMED7 CGI-109	0	1	0	0	0	1	2,00	449	4
Q9Y3D7	TIM16	PAM16 MAGMAS TIM16 TIMM16 CGI-136	1	1	0	0	0	0	2,00	BOTH	2
Q9Y3E5	PTH2	PTRH2 BIT1 PTH2 CGI-147	1	1	0	1	1	1	5,00	BOTH	5
Q9Y4P3	TBL2	TBL2 WBSCR13 UNQ563/PRO1125	1	1	0	0	1	1	4,00	BOTH	4
Q9Y512	SAM50	SAMM50 SAM50 CGI-51 TRG3	0	1	0	1	0	0	2,00	449	4
Q9Y5A9	YTHD2	YTHDF2 HGRG8	0	1	1	0	0	1	3,00	BOTH	3
Q9Y5M8	SRPRB	SRPRB PSEC0230	1	1	0	0	1	1	4,00	BOTH	4
Q9Y678	COPG1	COPG1 COPG	1	1	1	1	0	0	4,50	BOTH	4,5
Q9Y6C9	MTCH2	MTCH2 MIMP HSPC032	1	1	0	1	1	1	5,00	BOTH	5
Q9Y6E2	5MP1	BZW2 5MP1 HSPC028 MSTP017	0	1	0	1	0	0	2,00	449	4
Q9Y6K0	CEPT1	CEPT1 PRO1101	0	1	0	1	0	0	2,00	449	4

Supplementary Table 4: String enriched pathways in our Jad NS5A interactomic network.

Category	term name	description	FDR	#genes	#background genes
GO Biological Process	GO:0006810	Transport	5,89E-35	253	4353
GO Biological Process	GO:0051234	Establishment of localization	3,84E-34	255	4479
GO Biological Process	GO:0051641	Cellular localization	4,33E-32	197	2967
Reactome Pathways	HSA-1428517	The citric acid (TCA) cycle and respiratory electron transport	6,40E-31	52	176
GO Biological Process	GO:0051179	Localization	2,12E-30	282	5591
GO Biological Process	GO:0051649	Establishment of localization in cell	2,59E-30	170	2375
Reactome Pathways	HSA-163200	Respiratory electron transport, ATP synthesis by chemiosmotic coupling, and heat production by uncoupling proteins.	9,04E-30	45	125
KEGG Pathways	hsa05012	Parkinson disease	9,68E-30	56	240
KEGG Pathways	hsa05020	Prion disease	9,68E-30	58	265
Reactome Pathways	HSA-1430728	Metabolism	4,48E-28	153	2089
WikiPathways	GO:0006119	Oxidative phosphorylation	3,46E-27	42	118
KEGG Pathways	hsa05014	Amyotrophic lateral sclerosis	5,47E-26	60	352
GO Biological Process	GO:0046034	ATP metabolic process	1,50E-25	49	204
Reactome Pathways	HSA-392499	Metabolism of proteins	2,00E-25	143	1977
WikiPathways	WP111	Electron transport chain: OXPHOS system in mitochondria	2,43E-25	38	103
KEGG Pathways	hsa00190	Oxidative phosphorylation	3,43E-25	40	130
KEGG Pathways	hsa05010	Alzheimer disease	3,43E-25	59	355
KEGG Pathways	hsa05016	Huntington disease	1,12E-24	54	298
GO Biological Process	GO:0046907	Intracellular transport	3,02E-24	122	1520
Reactome Pathways	HSA-611105	Respiratory electron transport	1,19E-22	35	101
KEGG Pathways	hsa04714	Thermogenesis	1,39E-22	46	229
KEGG Pathways	hsa01100	Metabolic pathways	3,05E-22	112	1447
GO Biological Process	GO:0006091	Generation of precursor metabolites and energy	5,00E-22	60	405
GO Biological Process	GO:0055114	Oxidation-reduction process	8,69E-22	90	939
KEGG Pathways	hsa04141	Protein processing in endoplasmic reticulum	2,42E-21	39	165
GO Biological Process	GO:0006996	Organelle organization	3,77E-21	190	3450
GO Biological Process	GO:0009987	Cellular process	7,04E-21	484	15024
GO Molecular Function	GO:0016491	Oxidoreductase activity	7,19E-21	78	726
GO Molecular Function	GO:0000166	Nucleotide binding	7,19E-21	141	2119
GO Biological Process	GO:0022904	Respiratory electron transport chain	1,35E-20	34	107
GO Biological Process	GO:0022900	Electron transport chain	3,96E-20	40	174
GO Biological Process	GO:0033036	Macromolecule localization	3,96E-20	152	2473
GO Biological Process	GO:0008152	Metabolic process	7,59E-20	332	8298
GO Biological Process	GO:0042775	Mitochondrial atp synthesis coupled electron transport	6,46E-19	30	87
GO Biological Process	GO:0045333	Cellular respiration	7,97E-19	37	158
GO Molecular Function	GO:0003824	Catalytic activity	1,22E-18	249	5486
GO Molecular Function	GO:0036094	Small molecule binding	1,22E-18	150	2516
GO Biological Process	GO:0070727	Cellular macromolecule localization	1,95E-18	114	1616
GO Biological Process	GO:0061024	Membrane organization	3,86E-18	76	796
GO Biological Process	GO:0034613	Cellular protein localization	3,90E-18	113	1610
GO Biological Process	GO:0007005	Mitochondrion organization	3,90E-18	57	452
Reactome Pathways	GO:0008104	Protein localization	4,71E-18	134	2139
GO Biological Process	GO:0044237	Cellular metabolic process	6,20E-18	305	7513
GO Biological Process	GO:0071702	Organic substance transport	6,20E-18	135	2173
GO Biological Process	GO:0071705	Nitrogen compound transport	7,23E-18	121	1823
GO Biological Process	GO:0065003	Protein-containing complex assembly	1,58E-17	98	1293
KEGG Pathways	hsa04932	Non-alcoholic fatty liver disease	2,23E-17	33	148
GO Biological Process	GO:0045184	Establishment of protein localization	2,97E-17	109	1564
GO Biological Process	GO:0015980	Energy derivation by oxidation of organic compounds	4,75E-17	40	223
GO Biological Process	GO:0015031	Protein transport	6,17E-17	105	1486
GO Biological Process	GO:0015833	Peptide transport	8,68E-17	106	1518
GO Biological Process	GO:0006886	Intracellular protein transport	9,85E-17	83	999

WikiPathways	WP4396	Nonalcoholic fatty liver disease	1,02E-16	34	155
Reactome Pathways	HSA-597592	Post-translational protein modification	1,50E-16	100	1390
GO Biological Process	WP623	Oxidative phosphorylation	1,53E-16	24	60
GO Molecular Function	GO:0017111	Nucleoside-triphosphatase activity	2,31E-16	71	760
GO Biological Process	GO:0006457	Protein folding	4,06E-16	38	213
GO Molecular Function	GO:0003723	RNA binding	4,43E-16	110	1649
GO Molecular Function	GO:0032553	Ribonucleotide binding	4,93E-16	119	1880
GO Biological Process	GO:0022607	Cellular component assembly	5,74E-16	137	2359
GO Biological Process	GO:0071840	Cellular component organization or biogenesis	1,08E-15	244	5633
GO Molecular Function	GO:0017076	Purine nucleotide binding	1,10E-15	118	1878
GO Molecular Function	GO:0032555	Purine ribonucleotide binding	1,54E-15	117	1864
GO Biological Process	GO:0044085	Cellular component biogenesis	1,66E-15	144	2583
Reactome Pathways	GO:0016192	Vesicle-mediated transport	3,04E-15	114	1805
GO Biological Process	GO:0016043	Cellular component organization	3,04E-15	237	5447
GO Biological Process	GO:0043933	Protein-containing complex subunit organization	4,06E-15	103	1539
GO Biological Process	GO:0055085	Transmembrane transport	2,23E-14	92	1314
GO Molecular Function	GO:0035639	Purine ribonucleoside triphosphate binding	3,23E-14	111	1799
GO Biological Process	GO:0044403	Symbiotic process	7,52E-14	71	865
GO Molecular Function	GO:0043168	Anion binding	7,64E-14	147	2805
GO Biological Process	GO:0048193	Golgi vesicle transport	1,79E-13	44	359
GO Biological Process	GO:0009058	Biosynthetic process	3,27E-13	145	2788
GO Biological Process	GO:0140352	Export from cell	3,57E-13	77	1028
GO Biological Process	GO:0006887	Exocytosis	3,75E-13	66	789
GO Molecular Function	GO:0009055	Electron transfer activity	4,71E-13	25	103
GO Biological Process	GO:0002446	Neutrophil mediated immunity	4,72E-13	51	495
GO Biological Process	GO:0016032	Viral process	5,70E-13	65	776
GO Biological Process	GO:0036230	Granulocyte activation	7,59E-13	51	502
Reactome Pathways	GO:0043312	Neutrophil degranulation	7,76E-13	50	484
GO Biological Process	GO:0032940	Secretion by cell	7,88E-13	74	979
GO Biological Process	GO:0046903	Secretion	9,43E-13	79	1097
GO Biological Process	GO:0044281	Small molecule metabolic process	9,47E-13	103	1684
GO Molecular Function	GO:0045296	Cadherin binding	1,12E-12	41	334
GO Molecular Function	GO:0097367	Carbohydrate derivative binding	1,12E-12	123	2226
GO Biological Process	GO:1901576	Organic substance biosynthetic process	1,50E-12	141	2734
Reactome Pathways	HSA-446203	Asparagine N-linked glycosylation	1,63E-12	39	300
GO Biological Process	GO:0002275	Myeloid cell activation involved in immune response	2,68E-12	51	522
GO Biological Process	GO:1902600	Proton transmembrane transport	3,37E-12	28	150
GO Molecular Function	GO:0008137	NADH dehydrogenase (ubiquinone) activity	3,90E-12	18	46
GO Biological Process	GO:0034622	Cellular protein-containing complex assembly	4,09E-12	65	816
GO Biological Process	HSA-6798695	Neutrophil degranulation	5,74E-12	48	473
GO Biological Process	GO:0045055	Regulated exocytosis	6,47E-12	59	697
GO Biological Process	GO:1990542	Mitochondrial transmembrane transport	6,51E-12	23	95
GO Biological Process	GO:0006839	Mitochondrial transport	6,64E-12	33	225
GO Molecular Function	GO:0051082	Unfolded protein binding	6,69E-12	24	108
GO Molecular Function	GO:0097159	Organic cyclic compound binding	6,77E-12	239	5916
GO Molecular Function	GO:1901363	Heterocyclic compound binding	9,11E-12	236	5831
GO Biological Process	GO:0006120	Mitochondrial electron transport, nadh to ubiquinone	1,08E-11	18	49
GO Molecular Function	GO:0003924	GTPase activity	1,70E-11	38	318
GO Biological Process	GO:0006986	Response to unfolded protein	2,83E-11	28	166
Reactome Pathways	HSA-382551	Transport of small molecules	2,97E-11	59	721
GO Biological Process	HSA-5653656	Vesicle-mediated transport	3,00E-11	56	660
GO Molecular Function	GO:0016651	Oxidoreductase activity, acting on nad(p)h	3,52E-11	23	107
WikiPathways	WP4718	Cholesterol metabolism with Bloch and Kandutsch-Russell pathways	4,38E-11	17	46

GO Biological Process	GO:0006890	Retrograde vesicle-mediated transport, golgi to endoplasmic reticulum	4,74E-11	21	84
Reactome Pathways	HSA-6799198	Complex I biogenesis	5,57E-11	18	55
GO Biological Process	GO:0010608	Posttranscriptional regulation of gene expression	6,84E-11	51	574
GO Biological Process	GO:0035966	Response to topologically incorrect protein	7,38E-11	29	188
Reactome Pathways	HSA-199991	Membrane Trafficking	1,02E-10	53	622
GO Biological Process	GO:0006793	Phosphorus metabolic process	1,24E-10	114	2134
GO Biological Process	GO:0032482	Rab protein signal transduction	1,43E-10	19	69
GO Biological Process	GO:0002263	Cell activation involved in immune response	1,55E-10	53	630
GO Biological Process	GO:0072594	Establishment of protein localization to organelle	1,72E-10	43	433
GO Biological Process	GO:0042776	Mitochondrial atp synthesis coupled proton transport	1,84E-10	13	21
GO Biological Process	GO:0071704	Organic substance metabolic process	1,98E-10	286	7755
GO Molecular Function	GO:0005525	GTP binding	2,59E-10	39	370
GO Biological Process	GO:0006796	Phosphate-containing compound metabolic process	2,60E-10	112	2107
GO Biological Process	GO:1901566	Organonitrogen compound biosynthetic process	3,40E-10	83	1346
GO Biological Process	GO:0002366	Leukocyte activation involved in immune response	3,73E-10	52	626
GO Biological Process	GO:0044238	Primary metabolic process	4,31E-10	273	7332
GO Molecular Function	GO:0015078	Proton transmembrane transporter activity	4,79E-10	23	125
WikiPathways	WP4324	Mitochondrial complex I assembly model OXPHOS system	4,82E-10	17	56
GO Biological Process	GO:0032981	Mitochondrial respiratory chain complex i assembly	5,88E-10	18	66
Reactome Pathways	GO:0042407	Cristae formation	5,88E-10	14	31
GO Biological Process	GO:0033365	Protein localization to organelle	5,88E-10	57	743
GO Biological Process	GO:0034976	Response to endoplasmic reticulum stress	6,02E-10	32	256
GO Biological Process	GO:0006629	Lipid metabolic process	6,22E-10	76	1190
GO Biological Process	GO:0006888	Endoplasmic reticulum to golgi vesicle-mediated transport	6,95E-10	28	195
GO Biological Process	GO:0007007	Inner mitochondrial membrane organization	6,95E-10	16	48
Reactome Pathways	HSA-1852241	Organelle biogenesis and maintenance	7,14E-10	34	290
GO Biological Process	GO:0002443	Leukocyte mediated immunity	7,59E-10	52	641
GO Biological Process	GO:0046390	Ribose phosphate biosynthetic process	8,68E-10	26	168
GO Biological Process	GO:0033108	Mitochondrial respiratory chain complex assembly	8,68E-10	21	102
GO Biological Process	GO:0043488	Regulation of mrna stability	8,97E-10	27	183
Reactome Pathways	HSA-8856688	Golgi-to-ER retrograde transport	1,49E-09	23	130
GO Biological Process	GO:0045321	Leukocyte activation	1,76E-09	64	929
GO Biological Process	GO:0009165	Nucleotide biosynthetic process	1,76E-09	30	236
Reactome Pathways	HSA-8873719	RAB geranylgeranylation	3,09E-09	17	64
GO Biological Process	GO:0044249	Cellular biosynthetic process	3,30E-09	126	2611
Reactome Pathways	HSA-199977	ER to Golgi Anterograde Transport	3,85E-09	24	152
Reactome Pathways	HSA-948021	Transport to the Golgi and subsequent modification	3,98E-09	26	182
Reactome Pathways	HSA-6811442	Intra-Golgi and retrograde Golgi-to-ER traffic	4,06E-09	27	198
GO Biological Process	GO:0007029	Endoplasmic reticulum organization	4,10E-09	17	66
GO Biological Process	HSA-8949613	Cristae formation	5,50E-09	13	31
Reactome Pathways	HSA-68886	M Phase	5,64E-09	37	376
KEGG Pathways	GO:0019882	Antigen processing and presentation	7,14E-09	28	219
GO Biological Process	GO:0006164	Purine nucleotide biosynthetic process	7,25E-09	24	158
GO Biological Process	GO:0009894	Regulation of catabolic process	7,48E-09	67	1038
GO Biological Process	GO:1901137	Carbohydrate derivative biosynthetic process	7,83E-09	48	602
GO Biological Process	GO:0009260	Ribonucleotide biosynthetic process	8,80E-09	24	160
GO Biological Process	GO:0009117	Nucleotide metabolic process	1,02E-08	39	422
GO Molecular Function	GO:0005215	Transporter activity	1,10E-08	72	1181
GO Molecular Function	GO:0019899	Enzyme binding	1,10E-08	111	2239
GO Biological Process	GO:0016310	Phosphorylation	1,11E-08	76	1275
GO Biological Process	GO:0019693	Ribose phosphate metabolic process	1,14E-08	34	329
GO Biological Process	GO:0031647	Regulation of protein stability	1,14E-08	32	293
Reactome Pathways	HSA-68882	Mitotic Anaphase	1,24E-08	28	227

Reactome Pathways	HSA-6811434	COPI-dependent Golgi-to-ER retrograde traffic	1,30E-08	19	97
GO Biological Process	GO:0007006	Mitochondrial membrane organization	1,63E-08	22	137
Reactome Pathways	HSA-8852276	The role of GTSE1 in G2/M progression after G2 checkpoint	1,63E-08	17	75
GO Molecular Function	GO:0050839	Cell adhesion molecule binding	1,69E-08	44	538
GO Biological Process	GO:0007265	Ras protein signal transduction	1,78E-08	28	230
Reactome Pathways	HSA-6807878	COPI-mediated anterograde transport	1,86E-08	19	100
GO Biological Process	GO:0006811	Ion transport	1,88E-08	78	1344
GO Biological Process	GO:0009142	Nucleoside triphosphate biosynthetic process	1,97E-08	16	64
GO Biological Process	GO:1903311	Regulation of mrna metabolic process	2,06E-08	34	338
GO Biological Process	GO:0001775	Cell activation	2,64E-08	67	1075
GO Biological Process	GO:0065008	Regulation of biological quality	2,67E-08	169	4042
GO Biological Process	GO:0034620	Cellular response to unfolded protein	3,17E-08	21	129
GO Biological Process	GO:0009199	Ribonucleoside triphosphate metabolic process	3,35E-08	16	67
GO Biological Process	GO:0009141	Nucleoside triphosphate metabolic process	3,76E-08	18	91
GO Biological Process	GO:0006163	Purine nucleotide metabolic process	3,87E-08	33	329
GO Biological Process	GO:0055086	Nucleobase-containing small molecule metabolic process	3,94E-08	42	508
GO Biological Process	GO:0019637	Organophosphate metabolic process	4,34E-08	58	870
GO Biological Process	GO:0009152	Purine ribonucleotide biosynthetic process	4,76E-08	22	147
WikiPathways	WP3888	VEGFA-VEGFR2 signaling pathway	4,91E-08	38	428
GO Biological Process	GO:0031329	Regulation of cellular catabolic process	5,23E-08	58	875
GO Biological Process	GO:0035967	Cellular response to topologically incorrect protein	5,25E-08	22	148
KEGG Pathways	hsa04723	Retrograde endocannabinoid signaling	6,12E-08	21	145
KEGG Pathways	hsa00100	Steroid biosynthesis	6,32E-08	10	20
GO Biological Process	GO:0009259	Ribonucleotide metabolic process	6,37E-08	32	318
GO Biological Process	GO:0090407	Organophosphate biosynthetic process	6,39E-08	43	539
GO Biological Process	GO:0060341	Regulation of cellular localization	6,39E-08	64	1027
GO Biological Process	GO:0034248	Regulation of cellular amide metabolic process	6,59E-08	39	456
GO Biological Process	GO:0008610	Lipid biosynthetic process	7,22E-08	45	585
GO Biological Process	GO:0009205	Purine ribonucleoside triphosphate metabolic process	7,68E-08	15	61
GO Biological Process	GO:0072521	Purine-containing compound metabolic process	8,07E-08	34	360
Reactome Pathways	HSA-450531	Regulation of mRNA stability by proteins that bind AU-rich elements	8,08E-08	17	85
Reactome Pathways	HSA-163210	Formation of ATP by chemiosmotic coupling	8,31E-08	10	18
GO Biological Process	GO:1904872	Regulation of telomerase rna localization to cajal body	9,62E-08	10	18
GO Biological Process	GO:0009201	Ribonucleoside triphosphate biosynthetic process	1,01E-07	14	52
Reactome Pathways	HSA-5687128	MAPK6/MAPK4 signaling	1,02E-07	17	87
Reactome Pathways	HSA-5663205	Infectious disease	1,02E-07	55	826
GO Biological Process	GO:0050821	Protein stabilization	1,05E-07	24	186
GO Biological Process	GO:0051640	Organelle localization	1,31E-07	45	598
Reactome Pathways	HSA-389957	Prefoldin mediated transfer of substrate to CCT/TriC	1,40E-07	11	27
GO Biological Process	HSA-9609507	Protein localization	1,40E-07	22	160
Reactome Pathways	HSA-69275	G2/M Transition	1,52E-07	24	193
GO Biological Process	GO:0033554	Cellular response to stress	1,92E-07	89	1725
GO Biological Process	GO:0007264	Small gtpase mediated signal transduction	1,92E-07	31	316
GO Biological Process	GO:0034220	Ion transmembrane transport	1,93E-07	62	1010
GO Biological Process	GO:1901135	Carbohydrate derivative metabolic process	2,06E-07	61	987
KEGG Pathways	hsa04260	Cardiac muscle contraction	2,24E-07	16	87
Reactome Pathways	HSA-1236974	ER-Phagosome pathway	2,25E-07	16	81
GO Biological Process	GO:0006417	Regulation of translation	2,38E-07	35	398
WikiPathways	WP2359	Parkin-ubiquitin proteasomal system pathway	2,40E-07	15	67
Reactome Pathways	HSA-5678895	Defective CFTR causes cystic fibrosis	2,75E-07	14	59
GO Biological Process	GO:0009150	Purine ribonucleotide metabolic process	2,76E-07	30	303
GO Biological Process	GO:0010389	Regulation of g2/m transition of mitotic cell cycle	2,99E-07	24	198
GO Biological Process	GO:0010033	Response to organic substance	2,99E-07	132	3011

Reactome Pathways	HSA-1640170	Cell Cycle	3,00E-07	46	647
GO Biological Process	GO:1902749	Regulation of cell cycle g2/m phase transition	3,02E-07	25	215
GO Biological Process	GO:1904874	Positive regulation of telomerase rna localization to cajal body	3,64E-07	9	15
GO Biological Process	GO:0006812	Cation transport	3,66E-07	56	881
Reactome Pathways	HSA-69278	Cell Cycle, Mitotic	3,68E-07	40	518
Reactome Pathways	HSA-168249	Innate Immune System	4,93E-07	61	1025
Reactome Pathways	HSA-389960	Formation of tubulin folding intermediates by CCT/TriC	4,93E-07	10	24
GO Biological Process	GO:0016126	Sterol biosynthetic process	5,11E-07	13	50
GO Molecular Function	GO:0016675	Oxidoreductase activity, acting on a heme group of donors	5,39E-07	10	23
GO Biological Process	GO:0002252	Immune effector process	5,98E-07	59	969
Reactome Pathways	HSA-450408	AUF1 (hnRNP D0) binds and destabilizes mRNA	5,98E-07	13	53
Reactome Pathways	HSA-191273	Cholesterol biosynthesis	6,35E-07	10	25
GO Biological Process	GO:0002478	Antigen processing and presentation of exogenous peptide antigen	6,47E-07	22	174
GO Biological Process	GO:0048002	Antigen processing and presentation of peptide antigen	6,78E-07	23	191
Reactome Pathways	HSA-3371497	HSP90 chaperone cycle for steroid hormone receptors (SHR)	6,91E-07	13	54
Reactome Pathways	HSA-72766	Translation	8,13E-07	28	289
GO Molecular Function	GO:0030554	Adenyl nucleotide binding	8,37E-07	80	1534
GO Biological Process	GO:0043687	Post-translational protein modification	8,42E-07	32	360
Reactome Pathways	HSA-2467813	Separation of Sister Chromatids	9,61E-07	22	184
GO Biological Process	GO:0010256	Endomembrane system organization	9,77E-07	35	424
GO Biological Process	GO:0022406	Membrane docking	1,01E-06	22	179
GO Molecular Function	GO:0032559	Adenyl ribonucleotide binding	1,25E-06	79	1522
GO Biological Process	GO:0098662	Inorganic cation transmembrane transport	1,29E-06	44	628
GO Biological Process	GO:0016050	Vesicle organization	1,29E-06	29	308
GO Biological Process	GO:0009060	Aerobic respiration	1,34E-06	15	79
GO Biological Process	GO:0098655	Cation transmembrane transport	1,44E-06	48	725
WikiPathways	WP4922	Mitochondrial complex IV assembly	1,51E-06	11	35
GO Molecular Function	GO:0022857	Transmembrane transporter activity	1,57E-06	61	1050
GO Biological Process	GO:0044419	Interspecies interaction between organisms	1,59E-06	92	1899
GO Biological Process	GO:0070585	Protein localization to mitochondrion	1,77E-06	15	81
GO Biological Process	GO:0140056	Organelle localization by membrane tethering	1,90E-06	21	170
GO Biological Process	GO:1901360	Organic cyclic compound metabolic process	2,10E-06	132	3118
Reactome Pathways	HSA-162909	Host Interactions of HIV factors	2,20E-06	18	129
GO Biological Process	GO:0002474	Antigen processing and presentation of peptide antigen via mhc class i	2,21E-06	16	96
GO Biological Process	GO:0032880	Regulation of protein localization	2,23E-06	56	934
GO Biological Process	GO:0015672	Monovalent inorganic cation transport	2,26E-06	35	441
Reactome Pathways	HSA-69601	Ubiquitin Mediated Degradation of Phosphorylated Cdc25A	2,31E-06	12	50
Reactome Pathways	HSA-382556	ABC-family proteins mediated transport	2,37E-06	16	101
GO Biological Process	GO:0002376	Immune system process	2,46E-06	111	2481
Reactome Pathways	hsa01212	Fatty acid metabolism	2,54E-06	12	54
GO Biological Process	GO:0044255	Cellular lipid metabolic process	2,60E-06	56	939
Reactome Pathways	HSA-5358346	Hedgehog ligand biogenesis	2,73E-06	13	63
Reactome Pathways	HSA-180585	Vif-mediated degradation of APOBEC3G	2,98E-06	12	52
WikiPathways	WP183	Proteasome degradation	3,04E-06	13	60
GO Biological Process	GO:0044248	Cellular catabolic process	3,17E-06	86	1758
GO Biological Process	GO:0017038	Protein import	3,27E-06	19	144
GO Biological Process	GO:0032787	Monocarboxylic acid metabolic process	3,34E-06	38	515
GO Biological Process	GO:1901362	Organic cyclic compound biosynthetic process	3,68E-06	66	1211
GO Biological Process	GO:0072657	Protein localization to membrane	3,68E-06	37	495
GO Biological Process	GO:0035567	Non-canonical wnt signaling pathway	3,74E-06	18	130
GO Molecular Function	GO:0019003	GDP binding	4,08E-06	14	74
GO Biological Process	GO:0019752	Carboxylic acid metabolic process	4,15E-06	52	853
Reactome Pathways	HSA-5362768	Hh mutants are degraded by ERAD	4,18E-06	12	54

GO Molecular Function	GO:0004129	Cytochrome-c oxidase activity	4,22E-06	9	22
GO Biological Process	GO:0002479	Antigen processing and presentation of exogenous peptide antigen via mhc class i, tap-dependent	4,38E-06	14	75
Reactome Pathways	HSA-390450	Folding of actin by CCT/TriC	4,40E-06	7	10
Reactome Pathways	HSA-1592230	Mitochondrial biogenesis	4,48E-06	15	93
GO Biological Process	GO:1903827	Regulation of cellular protein localization	4,61E-06	40	568
GO Biological Process	GO:0006695	Cholesterol biosynthetic process	4,85E-06	11	41
GO Biological Process	GO:0006900	Vesicle budding from membrane	4,88E-06	16	103
Reactome Pathways	HSA-390466	Chaperonin-mediated protein folding	4,98E-06	15	94
GO Biological Process	GO:0070201	Regulation of establishment of protein localization	5,42E-06	43	642
GO Biological Process	GO:0098660	Inorganic ion transmembrane transport	5,47E-06	46	714
GO Biological Process	GO:0032879	Regulation of localization	5,59E-06	118	2740
GO Biological Process	GO:0019058	Viral life cycle	6,06E-06	22	202
GO Biological Process	GO:0006605	Protein targeting	6,07E-06	30	356
GO Molecular Function	GO:0015075	Ion transmembrane transporter activity	6,18E-06	52	865
Reactome Pathways	HSA-3858494	Beta-catenin independent WNT signaling	6,38E-06	18	142
Reactome Pathways	HSA-2262752	Cellular responses to stress	6,38E-06	38	544
GO Biological Process	GO:0048194	Golgi vesicle budding	6,43E-06	14	78
GO Biological Process	GO:0016125	Sterol metabolic process	6,50E-06	18	136
GO Biological Process	GO:0030968	Endoplasmic reticulum unfolded protein response	6,67E-06	16	106
GO Biological Process	GO:0045540	Regulation of cholesterol biosynthetic process	6,96E-06	11	43
GO Biological Process	GO:1904851	Positive regulation of establishment of protein localization to telomere	7,35E-06	7	10
GO Molecular Function	GO:0016787	Hydrolase activity	7,53E-06	107	2419
GO Biological Process	GO:1903829	Positive regulation of cellular protein localization	8,43E-06	29	342
GO Biological Process	GO:0071786	Endoplasmic reticulum tubular network organization	8,67E-06	8	17
Reactome Pathways	HSA-1236978	Cross-presentation of soluble exogenous antigens (endosomes)	9,55E-06	11	48
Reactome Pathways	HSA-211733	Regulation of activated PAK-2p34 by proteasome mediated degradation	9,55E-06	11	48
Reactome Pathways	HSA-9694548	Maturation of spike protein	1,03E-05	9	28
Reactome Pathways	HSA-174084	Autodegradation of Cdh1 by Cdh1:APC/C	1,07E-05	12	61
Reactome Pathways	HSA-350562	Regulation of ornithine decarboxylase (ODC)	1,07E-05	11	49
GO Biological Process	GO:0060071	Wnt signaling pathway, planar cell polarity pathway	1,08E-05	15	96
GO Biological Process	GO:0090150	Establishment of protein localization to membrane	1,11E-05	25	267
GO Biological Process	GO:1904871	Positive regulation of protein localization to cajal body	1,13E-05	7	11
GO Biological Process	GO:0010564	Regulation of cell cycle process	1,13E-05	47	760
GO Biological Process	GO:0009628	Response to abiotic stimulus	1,13E-05	62	1147
Reactome Pathways	HSA-8953854	Metabolism of RNA	1,24E-05	42	659
Reactome Pathways	HSA-556833	Metabolism of lipids	1,24E-05	45	733
Reactome Pathways	HSA-349425	Autodegradation of the E3 ubiquitin ligase COP1	1,24E-05	11	50
Reactome Pathways	HSA-75815	Ubiquitin-dependent degradation of Cyclin D	1,24E-05	11	50
Reactome Pathways	HSA-180534	Vpu mediated degradation of CD4	1,24E-05	11	50
GO Biological Process	GO:0006950	Response to stress	1,25E-05	140	3485
GO Biological Process	GO:0090181	Regulation of cholesterol metabolic process	1,27E-05	12	58
GO Molecular Function	GO:0015318	Inorganic molecular entity transmembrane transporter activity	1,33E-05	49	813
Reactome Pathways	HSA-4086400	PCP/CE pathway	1,34E-05	14	90
Reactome Pathways	HSA-1234176	Oxygen-dependent proline hydroxylation of Hypoxia-inducible Factor Alpha	1,34E-05	12	63
GO Biological Process	GO:0043436	Oxoacid metabolic process	1,37E-05	54	944
GO Biological Process	GO:0006631	Fatty acid metabolic process	1,40E-05	27	311
GO Molecular Function	GO:0016887	ATPase activity	1,40E-05	31	393
Reactome Pathways	HSA-1268020	Mitochondrial protein import	1,49E-05	12	64
Reactome Pathways	HSA-9604323	Negative regulation of NOTCH4 signaling	1,54E-05	11	52
Reactome Pathways	HSA-8941858	Regulation of RUNX3 expression and activity	1,54E-05	11	52
GO Biological Process	GO:0051049	Regulation of transport	1,55E-05	84	1776
GO Biological Process	GO:0006694	Steroid biosynthetic process	1,55E-05	17	130
GO Biological Process	GO:0010952	Positive regulation of peptidase activity	1,57E-05	21	198

GO Biological Process	GO:0009056	Catabolic process	1,60E-05	93	2042
Reactome Pathways	HSA-174154	APC/C:Cdc20 mediated degradation of Securin	1,66E-05	12	65
GO Biological Process	GO:0071806	Protein transmembrane transport	1,69E-05	12	60
GO Molecular Function	GO:0005524	ATP binding	1,72E-05	73	1464
Reactome Pathways	HSA-5619115	Disorders of transmembrane transporters	1,73E-05	19	174
Reactome Pathways	HSA-4641257	Degradation of AXIN	1,73E-05	11	53
Reactome Pathways	HSA-8854050	FBXL7 down-regulates AURKA during mitotic entry and in early mitosis	1,73E-05	11	53
Reactome Pathways	HSA-174113	SCF-beta-TrCP mediated degradation of Emi1	1,73E-05	11	53
GO Biological Process	GO:1901564	Organonitrogen compound metabolic process	1,79E-05	192	5244
KEGG Pathways	hsa04145	Phagosome	1,79E-05	17	142
Reactome Pathways	HSA-6814122	Cooperation of PDCL (PhLP1) and TRiC/CCT in G-protein beta folding	1,80E-05	10	42
KEGG Pathways	hsa03050	Proteasome	1,81E-05	10	43
GO Biological Process	GO:1901532	Regulation of hematopoietic progenitor cell differentiation	1,84E-05	14	87
GO Biological Process	GO:1902652	Secondary alcohol metabolic process	1,84E-05	17	132
GO Biological Process	GO:0072655	Establishment of protein localization to mitochondrion	1,99E-05	13	74
GO Biological Process	GO:1902036	Regulation of hematopoietic stem cell differentiation	1,99E-05	13	74
GO Biological Process	GO:0032386	Regulation of intracellular transport	2,04E-05	29	360
GO Biological Process	GO:0006123	Mitochondrial electron transport, cytochrome c to oxygen	2,08E-05	8	20
Reactome Pathways	HSA-8949215	Mitochondrial calcium ion transport	2,14E-05	8	23
Reactome Pathways	HSA-4641258	Degradation of DVL	2,20E-05	11	55
GO Biological Process	GO:0062012	Regulation of small molecule metabolic process	2,23E-05	33	449
GO Biological Process	GO:2000736	Regulation of stem cell differentiation	2,34E-05	16	119
GO Biological Process	GO:1901987	Regulation of cell cycle phase transition	2,52E-05	33	452
GO Biological Process	GO:0008203	Cholesterol metabolic process	2,54E-05	16	120
GO Biological Process	GO:0065002	Intracellular protein transmembrane transport	2,57E-05	11	51
GO Biological Process	GO:0018279	Protein n-linked glycosylation via asparagine	2,74E-05	9	30
GO Molecular Function	GO:0031072	Heat shock protein binding	2,87E-05	16	120
Reactome Pathways	HSA-5676590	NIK-->noncanonical NF-kB signaling	2,96E-05	11	57
Reactome Pathways	HSA-174184	Cdc20:Phospho-APC/C mediated degradation of Cyclin A	2,96E-05	12	70
Reactome Pathways	HSA-69017	CDK-mediated phosphorylation and removal of Cdc6	2,96E-05	12	70
Reactome Pathways	HSA-68827	CDT1 association with the CDC6:ORC:origin complex	2,96E-05	11	57
Reactome Pathways	HSA-5607761	Dectin-1 mediated noncanonical NF-kB signaling	3,20E-05	11	58
Reactome Pathways	HSA-174178	APC/C:Cdh1 mediated degradation of Cdc20 and other APC/C:Cdh1 targeted proteins in late mitosis/early G1	3,20E-05	12	71
Reactome Pathways	HSA-5610780	Degradation of GLI1 by the proteasome	3,20E-05	11	58
Reactome Pathways	HSA-5610783	Degradation of GLI2 by the proteasome	3,20E-05	11	58
Reactome Pathways	HSA-5610785	GLI3 is processed to GLI3R by the proteasome	3,20E-05	11	58
Reactome Pathways	HSA-187577	SCF(Skp2)-mediated degradation of p27/p21	3,20E-05	11	58
Reactome Pathways	HSA-5689880	Ub-specific processing proteases	3,20E-05	20	203
Reactome Pathways	HSA-5357801	Programmed Cell Death	3,21E-05	19	185
GO Biological Process	GO:1901990	Regulation of mitotic cell cycle phase transition	3,68E-05	31	416
GO Biological Process	GO:0051128	Regulation of cellular component organization	4,61E-05	103	2402
GO Biological Process	GO:0036498	IRE1-mediated unfolded protein response	4,82E-05	11	55
GO Biological Process	GO:0032210	Regulation of telomere maintenance via telomerase	4,82E-05	11	55
GO Molecular Function	GO:0008324	Cation transmembrane transporter activity	4,87E-05	40	629
GO Molecular Function	GO:0044389	Ubiquitin-like protein ligase binding	4,87E-05	26	312
Reactome Pathways	HSA-109581	Apoptosis	4,91E-05	18	173
GO Biological Process	GO:0006901	Vesicle coating	4,94E-05	12	68
Reactome Pathways	HSA-4608870	Asymmetric localization of PCP proteins	5,10E-05	11	62
GO Biological Process	GO:1900182	Positive regulation of protein localization to nucleus	5,13E-05	13	82
GO Biological Process	GO:0006626	Protein targeting to mitochondrion	5,52E-05	11	56
GO Biological Process	GO:0008202	Steroid metabolic process	5,55E-05	23	256
WikiPathways	WP197	Cholesterol biosynthesis pathway	6,02E-05	7	15
GO Molecular Function	GO:0051287	NAD binding	6,12E-05	11	56

GO Molecular Function	GO:0031625	Ubiquitin protein ligase binding	6,12E-05	25	296
GO Biological Process	GO:0090114	COPII-coated vesicle budding	6,38E-05	12	70
Reactome Pathways	HSA-176408	Regulation of APC/C activators between G1/S and early anaphase	6,58E-05	12	78
Reactome Pathways	HSA-5617833	Cilium Assembly	6,90E-05	19	197
Reactome Pathways	HSA-1643685	Disease	7,19E-05	72	1548
Reactome Pathways	HSA-1168372	Downstream signaling events of B Cell Receptor (BCR)	7,21E-05	12	79
Reactome Pathways	HSA-1169091	Activation of NF-kappaB in B cells	7,21E-05	11	65
Reactome Pathways	HSA-5689603	UCH proteinases	7,21E-05	13	94
GO Biological Process	GO:0048199	Vesicle targeting, to, from or within golgi	7,26E-05	12	71
Reactome Pathways	HSA-5610787	Hedgehog off state	7,29E-05	14	110
WikiPathways	WP143	Fatty acid beta-oxidation	7,50E-05	9	34
GO Biological Process	GO:0051345	Positive regulation of hydrolase activity	7,87E-05	45	772
Reactome Pathways	HSA-5658442	Regulation of RAS by GAPs	7,99E-05	11	66
Reactome Pathways	HSA-9679506	SARS-CoV Infections	7,99E-05	16	145
GO Biological Process	GO:1904951	Positive regulation of establishment of protein localization	8,34E-05	28	368
Reactome Pathways	HSA-195253	Degradation of beta-catenin by the destruction complex	8,56E-05	12	81
Reactome Pathways	HSA-5358351	Signaling by Hedgehog	8,56E-05	16	146
GO Molecular Function	GO:0005515	Protein binding	8,65E-05	239	7026
Reactome Pathways	HSA-8948751	Regulation of PTEN stability and activity	8,72E-05	11	67
GO Biological Process	GO:0048284	Organelle fusion	9,02E-05	14	102
GO Biological Process	GO:0007346	Regulation of mitotic cell cycle	9,16E-05	41	676
GO Biological Process	GO:0043618	Regulation of transcription from rna polymerase ii promoter in response to stress	9,17E-05	15	118
GO Molecular Function	GO:0031489	Myosin v binding	9,62E-05	7	17
Reactome Pathways	HSA-3371568	Attenuation phase	1,00E-04	6	13
Reactome Pathways	HSA-69002	DNA Replication Pre-Initiation	1,00E-04	12	83
GO Molecular Function	GO:0044183	Protein folding chaperone	1,00E-04	8	26
Reactome Pathways	HSA-8957322	Metabolism of steroids	1,10E-04	16	150
GO Biological Process	GO:1902750	Negative regulation of cell cycle g2/m phase transition	1,10E-04	14	104
GO Biological Process	GO:0034249	Negative regulation of cellular amide metabolic process	1,10E-04	17	154
Reactome Pathways	HSA-68949	Orc1 removal from chromatin	1,10E-04	11	69
Reactome Pathways	HSA-69620	Cell Cycle Checkpoints	1,20E-04	22	269
WikiPathways	WP4352	Ciliary landscape	1,20E-04	20	209
Reactome Pathways	HSA-1445148	Translocation of SLC2A4 (GLUT4) to the plasma membrane	1,20E-04	11	70
Reactome Pathways	HSA-8939902	Regulation of RUNX2 expression and activity	1,30E-04	11	71
GO Biological Process	GO:0019725	Cellular homeostasis	1,40E-04	49	895
Reactome Pathways	HSA-5663220	RHO GTPases Activate Formins	1,40E-04	15	136
Reactome Pathways	HSA-5628897	TP53 Regulates Metabolic Genes	1,50E-04	12	87
GO Biological Process	GO:0010972	Negative regulation of g2/m transition of mitotic cell cycle	1,50E-04	13	92
GO Biological Process	GO:0010950	Positive regulation of endopeptidase activity	1,50E-04	18	176
GO Biological Process	GO:0006521	Regulation of cellular amino acid metabolic process	1,60E-04	11	64
Reactome Pathways	HSA-168256	Immune System	1,60E-04	84	1956
KEGG Pathways	HSA-8978868	Fatty acid metabolism	1,60E-04	17	175
Reactome Pathways	HSA-8876198	RAB GEFs exchange GTP for GDP on RABs	1,60E-04	12	88
Reactome Pathways	HSA-9007101	Rab regulation of trafficking	1,60E-04	14	120
GO Biological Process	GO:0061418	Regulation of transcription from rna polymerase ii promoter in response to hypoxia	1,60E-04	12	78
GO Biological Process	GO:0051246	Regulation of protein metabolic process	1,70E-04	114	2828
Reactome Pathways	HSA-3371556	Cellular response to heat stress	1,70E-04	12	89
KEGG Pathways	hsa03060	Protein export	1,80E-04	7	23
GO Biological Process	GO:0044271	Cellular nitrogen compound biosynthetic process	1,90E-04	71	1522
Reactome Pathways	HSA-5688426	Deubiquitination	2,00E-04	22	280
Reactome Pathways	HSA-381038	XBP1(S) activates chaperone genes	2,10E-04	9	48
Reactome Pathways	HSA-75105	Fatty acyl-CoA biosynthesis	2,20E-04	8	36
Reactome Pathways	HSA-381119	Unfolded Protein Response (UPR)	2,30E-04	12	92

GO Molecular Function	GO:0005488	Binding	2,40E-04	380	12516
GO Biological Process	GO:0033238	Regulation of cellular amine metabolic process	2,60E-04	12	82
Reactome Pathways	HSA-1799339	SRP-dependent cotranslational protein targeting to membrane	2,60E-04	13	110
GO Biological Process	GO:0006807	Nitrogen compound metabolic process	2,80E-04	231	6852
GO Biological Process	GO:0043604	Amide biosynthetic process	2,80E-04	33	512
GO Molecular Function	GO:0050660	Flavin adenine dinucleotide binding	2,80E-04	12	82
GO Molecular Function	GO:0022890	Inorganic cation transmembrane transporter activity	2,90E-04	36	584
GO Biological Process	GO:0031145	Anaphase-promoting complex-dependent catabolic process	2,90E-04	12	83
GO Biological Process	GO:0032204	Regulation of telomere maintenance	2,90E-04	12	83
GO Biological Process	GO:0034641	Cellular nitrogen compound metabolic process	3,00E-04	127	3282
Reactome Pathways	HSA-2454202	Fc epsilon receptor (FCERI) signaling	3,00E-04	14	129
GO Biological Process	GO:0038095	Fc-epsilon receptor signaling pathway	3,00E-04	14	115
Reactome Pathways	HSA-195258	RHO GTPase Effectors	3,10E-04	22	289
Reactome Pathways	HSA-2871837	FCERI mediated NF-kB activation	3,20E-04	11	80
Reactome Pathways	HSA-5607764	CLEC7A (Dectin-1) signaling	3,20E-04	12	96
Reactome Pathways	HSA-9663891	Selective autophagy	3,20E-04	11	80
GO Biological Process	GO:0051701	Interaction with host	3,30E-04	16	151
GO Biological Process	GO:0045862	Positive regulation of proteolysis	3,30E-04	27	377
Reactome Pathways	HSA-390471	Association of TriC/CCT with target proteins during biosynthesis	3,40E-04	8	39
KEGG Pathways	hsa00510	N-Glycan biosynthesis	3,50E-04	9	50
GO Biological Process	GO:0071456	Cellular response to hypoxia	3,50E-04	18	189
GO Molecular Function	GO:0043167	Ion binding	3,50E-04	212	6188
Reactome Pathways	HSA-9694516	SARS-CoV-2 Infection	3,50E-04	10	66
Reactome Pathways	HSA-204005	COPII-mediated vesicle transport	3,90E-04	10	67
WikiPathways	WP4724	Omega-9 fatty acid synthesis	4,00E-04	6	14
WikiPathways	WP4804	Cholesterol biosynthesis with skeletal dysplasias	4,00E-04	5	7
Reactome Pathways	HSA-5632684	Hedgehog on state	4,10E-04	11	83
Reactome Pathways	HSA-5683057	MAPK family signaling cascades	4,10E-04	23	319
GO Biological Process	GO:0017148	Negative regulation of translation	4,10E-04	15	136
Reactome Pathways	HSA-69239	Synthesis of DNA	4,10E-04	13	116
GO Biological Process	GO:0071616	acyl-CoA biosynthetic process	4,20E-04	9	45
GO Biological Process	GO:0032781	Positive regulation of atpase activity	4,20E-04	10	58
GO Biological Process	GO:0021762	Substantia nigra development	4,20E-04	9	45
GO Molecular Function	GO:0015077	Monovalent inorganic cation transmembrane transporter activity	4,30E-04	27	381
GO Molecular Function	GO:0017022	Myosin binding	4,50E-04	11	72
Reactome Pathways	HSA-376176	Signaling by ROBO receptors	4,50E-04	18	213
GO Biological Process	GO:0032212	Positive regulation of telomere maintenance via telomerase	4,60E-04	8	34
GO Molecular Function	GO:0044877	Protein-containing complex binding	4,60E-04	59	1216
Reactome Pathways	HSA-8878166	Transcriptional regulation by RUNX2	4,70E-04	13	118
GO Biological Process	GO:0030433	Ubiquitin-dependent erad pathway	4,70E-04	11	73
GO Biological Process	GO:0019218	Regulation of steroid metabolic process	4,80E-04	14	121
WikiPathways	WP5124	Alzheimers disease	4,90E-04	21	255
GO Biological Process	GO:1901575	Organic substance catabolic process	5,10E-04	77	1750
Reactome Pathways	HSA-9646399	Aggrephagy	5,10E-04	8	42
GO Biological Process	GO:1901988	Negative regulation of cell cycle phase transition	5,10E-04	20	235
GO Biological Process	GO:0050810	Regulation of steroid biosynthetic process	5,10E-04	12	89
GO Biological Process	GO:0001666	Response to hypoxia	5,10E-04	25	342
GO Biological Process	GO:0038093	Fc receptor signaling pathway	5,40E-04	17	177
GO Biological Process	GO:0009057	Macromolecule catabolic process	5,40E-04	53	1058
WikiPathways	WP2059	Alzheimers disease and miRNA effects	5,40E-04	21	258
WikiPathways	hsa04216	Ferroptosis	5,80E-04	8	41
GO Biological Process	GO:0051726	Regulation of cell cycle	5,80E-04	59	1230
GO Biological Process	GO:0006139	Nucleobase-containing compound metabolic process	6,10E-04	106	2659

GO Biological Process	GO:0006725	Cellular aromatic compound metabolic process	6,10E-04	113	2882
KEGG Pathways	hsa05134	Legionellosis	6,20E-04	9	55
GO Biological Process	GO:1901991	Negative regulation of mitotic cell cycle phase transition	6,30E-04	19	219
GO Biological Process	GO:0009896	Positive regulation of catabolic process	6,50E-04	30	465
Reactome Pathways	HSA-9683686	Maturation of spike protein	6,50E-04	4	5
Reactome Pathways	HSA-8854214	TBC/RABGAPs	6,70E-04	8	44
Reactome Pathways	HSA-2995410	Nuclear Envelope (NE) Reassembly	7,00E-04	10	73
GO Biological Process	GO:0006487	Protein n-linked glycosylation	7,00E-04	11	77
GO Biological Process	GO:0050896	Response to stimulus	7,10E-04	261	8046
GO Biological Process	GO:0030163	Protein catabolic process	7,40E-04	39	694
GO Biological Process	GO:0007339	Binding of sperm to zona pellucida	7,40E-04	8	37
GO Biological Process	GO:0006906	Vesicle fusion	7,60E-04	11	78
WikiPathways	WP368	Mitochondrial long chain fatty acid beta-oxidation	7,90E-04	6	17
Reactome Pathways	HSA-202424	Downstream TCR signaling	8,30E-04	11	91
GO Biological Process	GO:0048208	COPII vesicle coating	8,30E-04	10	64
GO Biological Process	GO:0033043	Regulation of organelle organization	8,30E-04	61	1306
GO Biological Process	GO:0055082	Cellular chemical homeostasis	8,70E-04	41	753
GO Biological Process	GO:0090087	Regulation of peptide transport	8,80E-04	37	649
GO Biological Process	GO:0070482	Response to oxygen levels	8,80E-04	26	379
GO Biological Process	GO:0044265	Cellular macromolecule catabolic process	9,30E-04	47	917
GO Biological Process	GO:0060627	Regulation of vesicle-mediated transport	9,40E-04	33	550
Reactome Pathways	HSA-71291	Metabolism of amino acids and derivatives	1,00E-03	24	365
GO Biological Process	GO:2000278	Regulation of dna biosynthetic process	1,00E-03	13	114
GO Biological Process	GO:0038061	NIK/NF-kappaB signaling	1,00E-03	11	81
Reactome Pathways	HSA-195721	Signaling by WNT	1,00E-03	21	296
GO Molecular Function	GO:0070325	Lipoprotein particle receptor binding	1,00E-03	7	27
GO Biological Process	GO:0006892	post-Golgi vesicle-mediated transport	1,00E-03	12	97
Reactome Pathways	HSA-69206	G1/S Transition	1,00E-03	13	129
Reactome Pathways	HSA-9010553	Regulation of expression of SLITs and ROBOs	1,00E-03	15	167
GO Biological Process	GO:0043462	Regulation of atpase activity	1,10E-03	11	82
Reactome Pathways	HSA-532668	N-glycan trimming in the ER and Calnexin/Calreticulin cycle	1,10E-03	7	35
GO Biological Process	GO:0006873	Cellular ion homeostasis	1,10E-03	37	657
GO Biological Process	GO:0051656	Establishment of organelle localization	1,10E-03	26	385
KEGG Pathways	WP4313	Ferroptosis	1,10E-03	8	40
Reactome Pathways	HSA-69481	G2/M Checkpoints	1,10E-03	14	149
GO Biological Process	GO:0042026	Protein refolding	1,10E-03	6	18
GO Biological Process	GO:0009266	Response to temperature stimulus	1,10E-03	16	170
GO Molecular Function	GO:0045182	Translation regulator activity	1,10E-03	14	131
GO Molecular Function	GO:1901567	Fatty acid derivative binding	1,20E-03	7	28
Reactome Pathways	HSA-75876	Synthesis of very long-chain fatty acyl-CoAs	1,20E-03	6	24
Reactome Pathways	HSA-379716	Cytosolic tRNA aminoacylation	1,20E-03	6	24
WikiPathways	WP2272	Pathogenic Escherichia coli infection	1,20E-03	9	54
GO Biological Process	GO:0042221	Response to chemical	1,20E-03	155	4333
GO Biological Process	GO:1901998	Toxin transport	1,30E-03	8	41
Reactome Pathways	HSA-5620912	Anchoring of the basal body to the plasma membrane	1,30E-03	11	97
Reactome Pathways	HSA-8939236	RUNX1 regulates transcription of genes involved in differentiation of HSCs	1,30E-03	11	97
GO Biological Process	GO:0010498	Proteasomal protein catabolic process	1,40E-03	24	345
GO Biological Process	GO:0043161	Proteasome-mediated ubiquitin-dependent protein catabolic process	1,40E-03	23	323
GO Biological Process	hsa04612	Antigen processing and presentation	1,40E-03	9	63
KEGG Pathways	hsa04979	Cholesterol metabolism	1,40E-03	8	48
Reactome Pathways	HSA-210991	Basigin interactions	1,40E-03	6	25
Reactome Pathways	HSA-5620920	Cargo trafficking to the periciliary membrane	1,40E-03	8	50
GO Biological Process	GO:0061025	Membrane fusion	1,40E-03	14	136

KEGG Pathways	hsa04146	Peroxisome	1,40E-03	10	79
GO Biological Process	GO:0009408	Response to heat	1,40E-03	12	101
GO Biological Process	GO:0032268	Regulation of cellular protein metabolic process	1,50E-03	105	2693
GO Biological Process	GO:2000573	Positive regulation of dna biosynthetic process	1,50E-03	10	70
Reactome Pathways	HSA-9020702	Interleukin-1 signaling	1,50E-03	11	99
GO Biological Process	GO:0051223	Regulation of protein transport	1,50E-03	35	617
GO Biological Process	GO:0006066	Alcohol metabolic process	1,50E-03	23	324
Reactome Pathways	HSA-5621481	C-type lectin receptors (CLRs)	1,50E-03	13	136
Reactome Pathways	HSA-109582	Hemostasis	1,50E-03	33	605
GO Molecular Function	GO:0008536	Ran GTPase binding	1,50E-03	8	41
Reactome Pathways	HSA-6807070	PTEN Regulation	1,60E-03	13	137
GO Biological Process	GO:0030003	Cellular cation homeostasis	1,60E-03	36	644
GO Biological Process	GO:0043085	Positive regulation of catalytic activity	1,60E-03	66	1489
GO Molecular Function	GO:0140142	Nucleocytoplasmic carrier activity	1,70E-03	7	30
GO Biological Process	GO:0048522	Positive regulation of cellular process	1,70E-03	190	5579
KEGG Pathways	hsa05017	Spinocerebellar ataxia	1,70E-03	13	135
GO Biological Process	GO:0044283	Small molecule biosynthetic process	1,80E-03	33	572
GO Molecular Function	GO:0003730	mRNA 3-UTR binding	1,80E-03	11	86
GO Biological Process	GO:0070972	Protein localization to endoplasmic reticulum	1,80E-03	14	140
GO Biological Process	GO:0046483	Heterocycle metabolic process	1,90E-03	109	2840
GO Biological Process	GO:0051650	Establishment of vesicle localization	1,90E-03	17	200
KEGG Pathways	hsa00513	Various types of N-glycan biosynthesis	1,90E-03	7	38
Reactome Pathways	HSA-380259	Loss of Nlp from mitotic centrosomes	2,00E-03	9	69
Reactome Pathways	HSA-3371453	Regulation of HSF1-mediated heat shock response	2,00E-03	9	69
GO Biological Process	GO:1905330	Regulation of morphogenesis of an epithelium	2,00E-03	16	180
GO Biological Process	GO:0046949	fatty-acyl-CoA biosynthetic process	2,10E-03	7	32
GO Biological Process	GO:0032388	Positive regulation of intracellular transport	2,20E-03	18	223
GO Molecular Function	GO:0015288	Porin activity	2,20E-03	4	5
Reactome Pathways	HSA-71406	Pyruvate metabolism and Citric Acid (TCA) cycle	2,30E-03	8	55
GO Biological Process	GO:0090090	Negative regulation of canonical wnt signaling pathway	2,30E-03	16	183
Reactome Pathways	HSA-1655829	Regulation of cholesterol biosynthesis by SREBP (SREBF)	2,30E-03	8	55
KEGG Pathways	hsa03013	RNA transport	2,30E-03	14	160
Reactome Pathways	HSA-2565942	Regulation of PLK1 Activity at G2/M Transition	2,30E-03	10	87
GO Biological Process	GO:0006891	intra-Golgi vesicle-mediated transport	2,40E-03	7	33
Reactome Pathways	HSA-432722	Golgi Associated Vesicle Biogenesis	2,50E-03	8	56
Reactome Pathways	HSA-8854518	AURKA Activation by TPX2	2,60E-03	9	72
Reactome Pathways	HSA-199992	trans-Golgi Network Vesicle Budding	2,60E-03	9	72
GO Biological Process	GO:0044267	Cellular protein metabolic process	2,70E-03	134	3696
Reactome Pathways	HSA-2426168	Activation of gene expression by SREBF (SREBP)	2,70E-03	7	42
GO Biological Process	GO:0034654	Nucleobase-containing compound biosynthetic process	2,80E-03	48	995
Reactome Pathways	HSA-2995383	Initiation of Nuclear Envelope (NE) Reformation	2,80E-03	5	18
GO Biological Process	GO:0031146	SCF-dependent proteasomal ubiquitin-dependent protein catabolic process	2,80E-03	11	93
GO Molecular Function	GO:0050750	Low-density lipoprotein particle receptor binding	2,90E-03	6	22
GO Biological Process	GO:0051336	Regulation of hydrolase activity	2,90E-03	58	1284
GO Molecular Function	GO:0019905	Syntaxin binding	2,90E-03	10	75
GO Biological Process	GO:0090263	Positive regulation of canonical wnt signaling pathway	3,00E-03	14	148
KEGG Pathways	hsa00071	Fatty acid degradation	3,00E-03	7	42
GO Biological Process	GO:1903371	Regulation of endoplasmic reticulum tubular network organization	3,00E-03	4	6
GO Biological Process	GO:0002223	Stimulatory c-type lectin receptor signaling pathway	3,00E-03	12	111
GO Biological Process	GO:0098771	Inorganic ion homeostasis	3,10E-03	38	723
Reactome Pathways	HSA-5626467	RHO GTPases activate IQGAPs	3,10E-03	6	30
KEGG Pathways	hsa05132	Salmonella infection	3,10E-03	16	209
WikiPathways	WP4723	Omega-3 / omega-6 fatty acid synthesis	3,30E-03	5	14

GO Biological Process	GO:1901615	Organic hydroxy compound metabolic process	3,40E-03	28	467
GO Biological Process	GO:0043248	Proteasome assembly	3,50E-03	5	14
Reactome Pathways	HSA-380320	Recruitment of NuMA to mitotic centrosomes	3,50E-03	10	93
GO Biological Process	GO:1900034	Regulation of cellular response to heat	3,50E-03	10	79
GO Biological Process	GO:0070498	interleukin-1-mediated signaling pathway	3,60E-03	11	96
GO Molecular Function	GO:0016614	Oxidoreductase activity, acting on ch-oh group of donors	3,70E-03	13	130
KEGG Pathways	hsa04962	Vasopressin-regulated water reabsorption	3,70E-03	7	44
GO Biological Process	GO:0019395	Fatty acid oxidation	3,80E-03	10	80
GO Biological Process	GO:2000027	Regulation of animal organ morphogenesis	3,80E-03	19	257
GO Biological Process	GO:0031331	Positive regulation of cellular catabolic process	3,90E-03	25	397
GO Molecular Function	GO:0033218	Amide binding	4,00E-03	24	369
GO Biological Process	GO:0019438	Aromatic compound biosynthetic process	4,00E-03	50	1070
GO Biological Process	GO:0016055	Wnt signaling pathway	4,10E-03	23	351
GO Biological Process	GO:0032469	Endoplasmic reticulum calcium ion homeostasis	4,20E-03	6	25
GO Biological Process	GO:0090151	Establishment of protein localization to mitochondrial membrane	4,20E-03	6	25
GO Biological Process	GO:0010948	Negative regulation of cell cycle process	4,20E-03	22	328
Reactome Pathways	HSA-168255	Influenza Infection	4,30E-03	13	154
GO Biological Process	GO:0031204	Posttranslational protein targeting to membrane, translocation	4,30E-03	4	7
GO Biological Process	GO:0055080	Cation homeostasis	4,50E-03	37	712
GO Biological Process	GO:0044257	Cellular protein catabolic process	4,60E-03	34	633
GO Biological Process	GO:0030178	Negative regulation of wnt signaling pathway	4,60E-03	17	218
KEGG Pathways	hsa04144	Endocytosis	4,60E-03	17	241
GO Biological Process	GO:0010638	Positive regulation of organelle organization	4,60E-03	34	633
GO Biological Process	GO:0006984	ER-nucleus signaling pathway	4,70E-03	7	38
GO Biological Process	GO:0042592	Homeostatic process	4,70E-03	70	1676
GO Biological Process	GO:0045930	Negative regulation of mitotic cell cycle	4,70E-03	21	308
GO Biological Process	GO:0070887	Cellular response to chemical stimulus	4,80E-03	109	2919
GO Molecular Function	GO:0001671	ATPase activator activity	5,00E-03	6	25
Reactome Pathways	HSA-380270	Recruitment of mitotic centrosome proteins and complexes	5,00E-03	9	80
GO Biological Process	GO:0080134	Regulation of response to stress	5,00E-03	62	1437
Reactome Pathways	HSA-5625970	RHO GTPases activate KTN1	5,00E-03	4	11
GO Biological Process	GO:0035556	Intracellular signal transduction	5,10E-03	71	1712
Reactome Pathways	HSA-157118	Signaling by NOTCH	5,50E-03	15	202
GO Biological Process	GO:0051052	Regulation of dna metabolic process	5,60E-03	23	360
GO Biological Process	GO:0000278	Mitotic cell cycle	5,60E-03	36	695
GO Biological Process	GO:2001233	Regulation of apoptotic signaling pathway	5,60E-03	25	409
Reactome Pathways	HSA-1280218	Adaptive Immune System	5,70E-03	36	743
Reactome Pathways	HSA-6807047	Cholesterol biosynthesis via desmosterol	5,70E-03	3	4
Reactome Pathways	HSA-6807062	Cholesterol biosynthesis via lathosterol	5,70E-03	3	4
Reactome Pathways	HSA-5620922	BBSome-mediated cargo-targeting to cilium	5,70E-03	5	22
GO Biological Process	GO:0018130	Heterocycle biosynthetic process	5,80E-03	49	1061
GO Biological Process	GO:0006090	Pyruvate metabolic process	5,80E-03	9	69
GO Biological Process	GO:0060828	Regulation of canonical wnt signaling pathway	5,90E-03	20	291
GO Biological Process	GO:0044260	Cellular macromolecule metabolic process	5,90E-03	169	4976
Reactome Pathways	HSA-2132295	MHC class II antigen presentation	6,00E-03	11	120
GO Biological Process	GO:0030177	Positive regulation of wnt signaling pathway	6,20E-03	15	182
WikiPathways	WP4932	7q11.23 copy number variation syndrome	6,20E-03	11	104
Reactome Pathways	HSA-3371511	HSF1 activation	6,20E-03	4	12
GO Biological Process	GO:0048518	Positive regulation of biological process	6,20E-03	201	6112
GO Molecular Function	GO:0090079	Translation regulator activity, nucleic acid binding	6,20E-03	11	101
GO Biological Process	GO:0034250	Positive regulation of cellular amide metabolic process	6,30E-03	14	162
GO Biological Process	GO:0002218	Activation of innate immune response	6,30E-03	13	142
Reactome Pathways	HSA-6811436	COPI-independent Golgi-to-ER retrograde traffic	6,30E-03	7	50

GO Biological Process	GO:0051050	Positive regulation of transport	6,30E-03	44	923
GO Biological Process	GO:0048878	Chemical homeostasis	6,30E-03	51	1124
GO Molecular Function	GO:0003729	mRNA binding	6,70E-03	20	289
GO Biological Process	GO:0090316	Positive regulation of intracellular protein transport	6,80E-03	15	184
KEGG Pathways	hsa04022	cGMP-PKG signaling pathway	6,90E-03	13	162
GO Biological Process	GO:0030901	Midbrain development	7,00E-03	10	88
GO Biological Process	GO:0033209	Tumor necrosis factor-mediated signaling pathway	7,30E-03	12	125
GO Biological Process	GO:0006635	Fatty acid beta-oxidation	7,30E-03	8	56
GO Molecular Function	GO:0061133	Endopeptidase activator activity	7,30E-03	4	8
GO Molecular Function	GO:0060590	ATPase regulator activity	7,40E-03	7	40
Reactome Pathways	HSA-194315	Signaling by Rho GTPases	7,50E-03	24	429
GO Biological Process	GO:0030111	Regulation of wnt signaling pathway	7,70E-03	23	370
GO Biological Process	GO:0007049	Cell cycle	7,70E-03	57	1313
GO Biological Process	GO:0006955	Immune response	7,90E-03	66	1588
Reactome Pathways	HSA-2046106	Alpha-linolenic acid (ala) metabolism	7,90E-03	4	13
GO Biological Process	GO:1901617	Organic hydroxy compound biosynthetic process	7,90E-03	15	187
GO Biological Process	GO:0052126	Movement in host environment	8,10E-03	11	108
GO Biological Process	GO:0050852	T cell receptor signaling pathway	8,20E-03	14	167
GO Biological Process	GO:1901570	Fatty acid derivative biosynthetic process	8,70E-03	10	91
GO Biological Process	GO:0052547	Regulation of peptidase activity	8,70E-03	26	449
GO Biological Process	GO:0019216	Regulation of lipid metabolic process	8,80E-03	25	424
Reactome Pathways	HSA-8957275	Post-translational protein phosphorylation	8,90E-03	10	107
Reactome Pathways	HSA-9612973	Autophagy	9,10E-03	12	148
GO Biological Process	GO:0043603	Cellular amide metabolic process	9,40E-03	38	773
Reactome Pathways	HSA-9675108	Nervous system development	9,60E-03	29	572
Reactome Pathways	HSA-162658	Golgi Cisternae Pericentriolar Stack Reorganization	9,70E-03	4	14
KEGG Pathways	hsa00062	Fatty acid elongation	9,80E-03	5	25
GO Biological Process	GO:0035338	Long-chain fatty-acyl-coa biosynthetic process	9,80E-03	5	19
GO Biological Process	GO:0030150	Protein import into mitochondrial matrix	9,80E-03	5	19
Reactome Pathways	HSA-68875	Mitotic Prophase	9,90E-03	10	109
Reactome Pathways	HSA-936837	Ion transport by P-type ATPases	1,01E-02	7	55
GO Molecular Function	GO:0005384	Manganese ion transmembrane transporter activity	1,01E-02	4	9
Reactome Pathways	HSA-422475	Axon guidance	1,01E-02	28	547
GO Biological Process	GO:0065005	Protein-lipid complex assembly	1,03E-02	6	31
GO Biological Process	GO:0045727	Positive regulation of translation	1,04E-02	12	131
GO Biological Process	GO:0072659	Protein localization to plasma membrane	1,05E-02	15	193
Reactome Pathways	HSA-9006931	Signaling by Nuclear Receptors	1,05E-02	17	265
GO Biological Process	GO:0034605	Cellular response to heat	1,07E-02	8	60
GO Biological Process	GO:0051248	Negative regulation of protein metabolic process	1,09E-02	49	1096
Reactome Pathways	HSA-447115	Interleukin-12 family signaling	1,09E-02	7	56
GO Molecular Function	GO:0042625	ATPase-coupled ion transmembrane transporter activity	1,10E-02	8	58
GO Biological Process	GO:0006997	Nucleus organization	1,10E-02	12	132
GO Biological Process	GO:0043281	Regulation of cysteine-type endopeptidase activity involved in apoptotic process	1,10E-02	16	216
KEGG Pathways	hsa01040	Biosynthesis of unsaturated fatty acids	1,11E-02	5	26
Reactome Pathways	HSA-5663202	Diseases of signal transduction by growth factor receptors and second messengers	1,12E-02	22	392
GO Biological Process	GO:1903047	Mitotic cell cycle process	1,12E-02	32	616
GO Biological Process	GO:2001056	Positive regulation of cysteine-type endopeptidase activity	1,15E-02	13	153
GO Biological Process	GO:0019538	Protein metabolic process	1,16E-02	146	4251
GO Biological Process	GO:0006637	acyl-CoA metabolic process	1,16E-02	10	95
GO Biological Process	GO:0097711	Ciliary basal body-plasma membrane docking	1,16E-02	10	95
GO Biological Process	GO:0061157	mRNA destabilization	1,16E-02	6	32
GO Biological Process	GO:0006486	Protein glycosylation	1,16E-02	17	240
GO Biological Process	GO:2000116	Regulation of cysteine-type endopeptidase activity	1,16E-02	17	240

GO Biological Process	GO:0072599	Establishment of protein localization to endoplasmic reticulum	1,17E-02	11	114
GO Biological Process	GO:0032269	Negative regulation of cellular protein metabolic process	1,18E-02	47	1043
Reactome Pathways	HSA-433692	Proton-coupled monocarboxylate transport	1,19E-02	3	6
GO Biological Process	GO:0002429	Immune response-activating cell surface receptor signaling pathway	1,19E-02	20	311
Reactome Pathways	HSA-5218920	VEGFR2 mediated vascular permeability	1,19E-02	5	27
GO Molecular Function	GO:0003725	Double-stranded rna binding	1,19E-02	9	75
GO Biological Process	GO:0055117	Regulation of cardiac muscle contraction	1,19E-02	9	78
GO Molecular Function	GO:0036402	Proteasome-activating atpase activity	1,21E-02	3	3
Reactome Pathways	HSA-201681	TCF dependent signaling in response to WNT	1,22E-02	14	199
GO Biological Process	GO:0046890	Regulation of lipid biosynthetic process	1,22E-02	15	197
Reactome Pathways	HSA-9648025	EML4 and NUDC in mitotic spindle formation	1,22E-02	10	113
Reactome Pathways	HSA-68877	Mitotic Prometaphase	1,22E-02	14	199
GO Biological Process	GO:0035821	Modulation of process of other organism	1,23E-02	11	115
WikiPathways	WP4535	Envelope proteins and their potential roles in EDMD physiopathology	1,24E-02	7	46
GO Biological Process	GO:1903902	Positive regulation of viral life cycle	1,25E-02	8	62
KEGG Pathways	hsa03015	mRNA surveillance pathway	1,28E-02	9	93
GO Biological Process	GO:0051817	Modulation of process of other organism involved in symbiotic interaction	1,29E-02	10	97
GO Biological Process	GO:0044093	Positive regulation of molecular function	1,29E-02	73	1842
GO Molecular Function	GO:0000149	SNARE binding	1,29E-02	11	112
GO Molecular Function	GO:0048156	Tau protein binding	1,31E-02	7	45
GO Biological Process	GO:0050851	Antigen receptor-mediated signaling pathway	1,33E-02	15	199
GO Biological Process	GO:0043280	Positive regulation of cysteine-type endopeptidase activity involved in apoptotic process	1,34E-02	12	136
GO Biological Process	GO:0043043	Peptide biosynthetic process	1,35E-02	23	389
GO Biological Process	GO:0051131	Chaperone-mediated protein complex assembly	1,35E-02	5	21
GO Biological Process	GO:0051204	Protein insertion into mitochondrial membrane	1,35E-02	5	21
GO Biological Process	GO:0042176	Regulation of protein catabolic process	1,38E-02	24	415
GO Biological Process	GO:0033157	Regulation of intracellular protein transport	1,38E-02	18	268
GO Biological Process	GO:0009895	Negative regulation of catabolic process	1,39E-02	20	316
Reactome Pathways	HSA-5673001	RAF/MAP kinase cascade	1,40E-02	17	274
GO Molecular Function	GO:0042288	MHC class I protein binding	1,41E-02	5	20
GO Molecular Function	GO:0061608	Nuclear import signal receptor activity	1,41E-02	5	20
GO Biological Process	GO:0009409	Response to cold	1,43E-02	7	48
GO Biological Process	GO:0044272	Sulfur compound biosynthetic process	1,43E-02	14	179
GO Biological Process	GO:0006412	Translation	1,43E-02	22	366
GO Biological Process	GO:1902369	Negative regulation of rna catabolic process	1,46E-02	8	64
GO Biological Process	GO:1903313	Positive regulation of mrna metabolic process	1,46E-02	9	81
GO Biological Process	GO:0051170	Import into nucleus	1,46E-02	11	118
GO Biological Process	GO:0048278	Vesicle docking	1,46E-02	8	64
GO Biological Process	GO:0010941	Regulation of cell death	1,47E-02	68	1696
GO Biological Process	GO:0071310	Cellular response to organic substance	1,52E-02	89	2369
GO Biological Process	GO:0033489	Cholesterol biosynthetic process via desmosterol	1,53E-02	3	4
GO Biological Process	GO:0033490	Cholesterol biosynthetic process via lathosterol	1,53E-02	3	4
GO Biological Process	GO:0006613	Cotranslational protein targeting to membrane	1,53E-02	10	100
GO Biological Process	GO:1990809	Endoplasmic reticulum tubular network membrane organization	1,53E-02	3	4
GO Biological Process	GO:1900208	Regulation of cardiolipin metabolic process	1,53E-02	3	4
GO Biological Process	GO:0051130	Positive regulation of cellular component organization	1,54E-02	52	1209
GO Molecular Function	GO:0016874	Ligase activity	1,62E-02	13	156
GO Biological Process	GO:0002768	Immune response-regulating cell surface receptor signaling pathway	1,63E-02	21	346
GO Biological Process	GO:0044743	Protein transmembrane import into intracellular organelle	1,63E-02	6	35
GO Molecular Function	GO:0000062	fatty-acyl-CoA binding	1,65E-02	5	21
WikiPathways	WP357	Fatty acid biosynthesis	1,67E-02	5	22
KEGG Pathways	hsa00970	Aminoacyl-tRNA biosynthesis	1,67E-02	6	44
WikiPathways	WP107	Translation factors	1,67E-02	7	49

KEGG Pathways	hsa00061	Fatty acid biosynthesis	1,68E-02	4	17
KEGG Pathways	hsa04972	Pancreatic secretion	1,68E-02	9	98
GO Biological Process	GO:0030162	Regulation of proteolysis	1,68E-02	36	747
GO Biological Process	GO:0061014	Positive regulation of mrna catabolic process	1,71E-02	7	50
GO Biological Process	GO:0061951	Establishment of protein localization to plasma membrane	1,71E-02	7	50
GO Molecular Function	GO:0097718	Disordered domain specific binding	1,81E-02	6	34
GO Biological Process	GO:0061136	Regulation of proteasomal protein catabolic process	1,83E-02	15	207
GO Biological Process	GO:0045088	Regulation of innate immune response	1,86E-02	19	301
GO Biological Process	GO:2001242	Regulation of intrinsic apoptotic signaling pathway	1,88E-02	13	164
GO Molecular Function	GO:0016434	rRNA (cytosine) methyltransferase activity	1,90E-02	3	4
Reactome Pathways	HSA-9020591	Interleukin-12 signaling	1,91E-02	6	46
GO Molecular Function	GO:0017025	TBP-class protein binding	1,92E-02	5	22
GO Molecular Function	GO:0008135	Translation factor activity, rna binding	1,92E-02	9	82
GO Molecular Function	GO:0019904	Protein domain specific binding	1,93E-02	35	716
Reactome Pathways	HSA-70268	Pyruvate metabolism	1,95E-02	5	31
KEGG Pathways	hsa05164	Influenza A	1,95E-02	12	165
GO Biological Process	GO:0051222	Positive regulation of protein transport	1,97E-02	21	352
GO Molecular Function	GO:0043531	ADP binding	1,97E-02	6	35
GO Biological Process	GO:0070838	Divalent metal ion transport	1,99E-02	19	303
GO Biological Process	GO:2001234	Negative regulation of apoptotic signaling pathway	2,00E-02	16	232
Reactome Pathways	HSA-2500257	Resolution of Sister Chromatid Cohesion	2,00E-02	10	122
GO Biological Process	GO:0045070	Positive regulation of viral genome replication	2,05E-02	6	37
GO Biological Process	GO:0086004	Regulation of cardiac muscle cell contraction	2,05E-02	6	37
GO Biological Process	GO:0006403	RNA localization	2,06E-02	15	210
GO Molecular Function	GO:0016860	Intramolecular oxidoreductase activity	2,07E-02	7	50
Reactome Pathways	HSA-8939211	ESR-mediated signaling	2,07E-02	13	189
GO Biological Process	GO:0007051	Spindle organization	2,08E-02	12	145
GO Biological Process	GO:0036109	Alpha-linolenic acid metabolic process	2,09E-02	4	13
GO Biological Process	GO:0006851	Mitochondrial calcium ion transmembrane transport	2,09E-02	5	24
Reactome Pathways	HSA-2046105	Linoleic acid (LA) metabolism	2,13E-02	3	8
KEGG Pathways	hsa04130	SNARE interactions in vesicular transport	2,13E-02	5	32
GO Biological Process	GO:0002831	Regulation of response to biotic stimulus	2,15E-02	23	406
GO Biological Process	GO:0006875	Cellular metal ion homeostasis	2,16E-02	29	565
GO Biological Process	GO:0031330	Negative regulation of cellular catabolic process	2,18E-02	17	258
Reactome Pathways	HSA-381426	Regulation of Insulin-like Growth Factor (IGF) transport and uptake by Insulin-like Growth Factor Binding Proteins (IGFBPs)	2,21E-02	10	124
GO Biological Process	GO:0070934	CRD-mediated mRNA stabilization	2,25E-02	3	5
GO Biological Process	GO:0010565	Regulation of cellular ketone metabolic process	2,26E-02	14	190
GO Biological Process	GO:0006458	De novo protein folding	2,27E-02	6	38
Reactome Pathways	HSA-983169	Class I MHC mediated antigen processing & presentation	2,29E-02	20	366
Reactome Pathways	HSA-5694530	Cargo concentration in the ER	2,43E-02	5	33
GO Biological Process	GO:0045786	Negative regulation of cell cycle	2,48E-02	29	571
GO Biological Process	GO:0048524	Positive regulation of viral process	2,48E-02	10	108
GO Molecular Function	GO:0046915	Transition metal ion transmembrane transporter activity	2,51E-02	6	37
GO Biological Process	GO:0080135	Regulation of cellular response to stress	2,51E-02	35	739
GO Molecular Function	GO:0051087	Chaperone binding	2,54E-02	10	105
GO Biological Process	GO:0006122	Mitochondrial electron transport, ubiquinol to cytochrome c	2,55E-02	4	14
GO Biological Process	GO:0051603	Proteolysis involved in cellular protein catabolic process	2,55E-02	30	600
GO Biological Process	GO:0042981	Regulation of apoptotic process	2,55E-02	62	1550
GO Biological Process	GO:0007030	Golgi organization	2,61E-02	11	129
GO Biological Process	GO:0022402	Cell cycle process	2,75E-02	43	976
GO Biological Process	GO:0032527	Protein exit from endoplasmic reticulum	2,76E-02	5	26
GO Biological Process	GO:0045047	Protein targeting to er	2,77E-02	10	110
GO Biological Process	GO:0051247	Positive regulation of protein metabolic process	2,82E-02	67	1715

GO Biological Process	GO:0044242	Cellular lipid catabolic process	2,89E-02	14	196
GO Biological Process	GO:0034645	Cellular macromolecule biosynthetic process	2,94E-02	63	1592
GO Biological Process	GO:0052548	Regulation of endopeptidase activity	2,97E-02	23	418
GO Biological Process	GO:0050778	Positive regulation of immune response	2,98E-02	30	607
GO Biological Process	GO:0043632	Modification-dependent macromolecule catabolic process	2,98E-02	28	552
GO Molecular Function	GO:0050661	NADP binding	3,00E-02	7	54
GO Molecular Function	GO:0019829	ATPase-coupled cation transmembrane transporter activity	3,00E-02	7	54
GO Biological Process	GO:0034097	Response to cytokine	3,00E-02	47	1101
WikiPathways	WP4949	16p11.2 proximal deletion syndrome	3,03E-02	8	73
WikiPathways	WP2526	PDGF pathway	3,03E-02	6	40
GO Biological Process	GO:0042159	Lipoprotein catabolic process	3,09E-02	4	15
GO Molecular Function	GO:0016863	Intramolecular oxidoreductase activity, transposing c=c bonds	3,09E-02	4	14
GO Biological Process	GO:0001845	Phagolysosome assembly	3,09E-02	4	15
GO Biological Process	GO:0044794	Positive regulation by host of viral process	3,09E-02	4	15
GO Biological Process	GO:0034377	Plasma lipoprotein particle assembly	3,11E-02	5	27
GO Biological Process	GO:0048205	COPI coating of Golgi vesicle	3,13E-02	3	6
Reactome Pathways	HSA-9609523	Insertion of tail-anchored proteins into the endoplasmic reticulum membrane	3,13E-02	4	21
GO Biological Process	GO:0030223	Neutrophil differentiation	3,13E-02	3	6
GO Biological Process	GO:0071763	Nuclear membrane organization	3,13E-02	3	6
Reactome Pathways	HSA-5627123	RHO GTPases activate PAKs	3,13E-02	4	21
GO Biological Process	GO:0009062	Fatty acid catabolic process	3,14E-02	9	93
GO Biological Process	GO:0051702	Interaction with symbiont	3,14E-02	9	93
GO Biological Process	GO:0016042	Lipid catabolic process	3,18E-02	18	294
GO Biological Process	GO:0006914	Autophagy	3,22E-02	17	270
GO Biological Process	GO:0006446	Regulation of translational initiation	3,22E-02	8	75
GO Biological Process	GO:0010243	Response to organonitrogen compound	3,22E-02	43	987
GO Biological Process	GO:0042326	Negative regulation of phosphorylation	3,25E-02	24	449
GO Biological Process	GO:0000086	G2/M transition of mitotic cell cycle	3,26E-02	11	134
GO Biological Process	GO:0051054	Positive regulation of dna metabolic process	3,28E-02	14	200
Reactome Pathways	HSA-5619070	Defective SLC16A1 causes symptomatic deficiency in lactate transport (SDLT)	3,31E-02	2	2
GO Biological Process	GO:0023057	Negative regulation of signaling	3,31E-02	56	1385
Reactome Pathways	HSA-111885	Opioid Signalling	3,31E-02	8	90
GO Biological Process	GO:0002833	Positive regulation of response to biotic stimulus	3,31E-02	16	247
Reactome Pathways	HSA-192905	vRNP Assembly	3,31E-02	2	2
KEGG Pathways	hsa04915	Estrogen signaling pathway	3,37E-02	10	133
WikiPathways	WP2034	Leptin signaling pathway	3,38E-02	8	75
GO Biological Process	GO:0006643	Membrane lipid metabolic process	3,41E-02	14	201
GO Biological Process	GO:0043254	Regulation of protein-containing complex assembly	3,41E-02	24	451
Reactome Pathways	HSA-8963888	Chylomicron assembly	3,43E-02	3	10
GO Biological Process	GO:0023056	Positive regulation of signaling	3,51E-02	70	1831
Reactome Pathways	HSA-71403	Citric acid cycle (TCA cycle)	3,53E-02	4	22
GO Biological Process	GO:0030004	Cellular monovalent inorganic cation homeostasis	3,53E-02	10	115
GO Biological Process	GO:0031334	Positive regulation of protein-containing complex assembly	3,54E-02	16	249
Reactome Pathways	HSA-9006925	Intracellular signaling by second messengers	3,60E-02	17	304
GO Biological Process	GO:0050790	Regulation of catalytic activity	3,60E-02	87	2386
Reactome Pathways	HSA-8950505	Gene and protein expression by JAK-STAT signaling after Interleukin-12 stimulation	3,65E-02	5	37
Reactome Pathways	HSA-177243	Interactions of Rev with host cellular proteins	3,65E-02	5	37
GO Biological Process	GO:0006904	Vesicle docking involved in exocytosis	3,65E-02	6	43
Reactome Pathways	HSA-5578775	Ion homeostasis	3,68E-02	6	54
WikiPathways	WP4921	Mitochondrial complex III assembly	3,69E-02	4	16
GO Biological Process	GO:1903362	Regulation of cellular protein catabolic process	3,75E-02	17	275
Reactome Pathways	HSA-449147	Signaling by Interleukins	3,77E-02	22	440
GO Molecular Function	GO:0034190	Apolipoprotein receptor binding	3,82E-02	3	6

GO Molecular Function	GO:0140296	General transcription initiation factor binding	3,82E-02	6	41
GO Molecular Function	GO:0060090	Molecular adaptor activity	3,82E-02	18	293
GO Molecular Function	GO:0030235	Nitric-oxide synthase regulator activity	3,82E-02	3	6
GO Molecular Function	GO:0016504	Peptidase activator activity	3,82E-02	6	41
GO Molecular Function	GO:0070717	Poly-purine tract binding	3,82E-02	5	27
GO Molecular Function	GO:0008187	Poly-pyrimidine tract binding	3,82E-02	5	27
GO Biological Process	GO:0032369	Negative regulation of lipid transport	3,91E-02	5	29
GO Biological Process	GO:0009101	Glycoprotein biosynthetic process	3,91E-02	18	301
GO Biological Process	GO:0044788	Modulation by host of viral process	3,91E-02	5	29
GO Biological Process	GO:0006606	Protein import into nucleus	3,91E-02	9	97
WikiPathways	WP430	Statin inhibition of cholesterol production	3,92E-02	5	29
WikiPathways	WP3932	Focal adhesion: PI3K-Akt-mTOR-signaling pathway	3,94E-02	18	302
GO Biological Process	GO:0044087	Regulation of cellular component biogenesis	3,99E-02	42	971
GO Molecular Function	GO:0004812	aminoacyl-tRNA ligase activity	4,01E-02	6	42
WikiPathways	WP5027	nsp1 from SARS-CoV-2 inhibits translation initiation in the host cell	4,04E-02	4	17
Reactome Pathways	HSA-9009391	Extra-nuclear estrogen signaling	4,06E-02	7	74
GO Biological Process	GO:2000646	Positive regulation of receptor catabolic process	4,12E-02	3	7
GO Biological Process	GO:0019941	Modification-dependent protein catabolic process	4,17E-02	27	541
GO Biological Process	GO:0051851	Modulation by host of symbiont process	4,18E-02	7	61
KEGG Pathways	hsa04071	Sphingolipid signaling pathway	4,21E-02	9	116
GO Biological Process	GO:0061158	3-UTR-mediated mRNA destabilization	4,24E-02	4	17
GO Biological Process	GO:0044827	Modulation by host of viral genome replication	4,24E-02	4	17
GO Biological Process	GO:0090083	Regulation of inclusion body assembly	4,24E-02	4	17
GO Biological Process	GO:0070588	Calcium ion transmembrane transport	4,26E-02	14	207
GO Biological Process	GO:0006790	Sulfur compound metabolic process	4,26E-02	20	355
GO Molecular Function	GO:0016627	Oxidoreductase activity, acting on the ch-ch group of donors	4,29E-02	7	59
GO Biological Process	GO:0006937	Regulation of muscle contraction	4,35E-02	12	162
GO Biological Process	GO:0048255	mRNA stabilization	4,37E-02	6	45
GO Biological Process	GO:0045089	Positive regulation of innate immune response	4,41E-02	14	208
Reactome Pathways	HSA-76002	Platelet activation, signaling and aggregation	4,46E-02	15	260
GO Biological Process	GO:0042493	Response to drug	4,51E-02	17	281
Reactome Pathways	HSA-5668599	RHO GTPases Activate NADPH Oxidases	4,51E-02	4	24
GO Biological Process	GO:0055065	Metal ion homeostasis	4,52E-02	30	629
KEGG Pathways	hsa05130	Pathogenic Escherichia coli infection	4,53E-02	12	187
GO Biological Process	GO:0051046	Regulation of secretion	4,53E-02	32	686
GO Molecular Function	GO:0098631	Cell adhesion mediator activity	4,61E-02	7	60
GO Molecular Function	GO:0016853	Isomerase activity	4,61E-02	12	159
WikiPathways	WP4301	Inhibition of exosome biogenesis and secretion by Manumycin A in CRPC cells	4,69E-02	4	18
GO Biological Process	GO:0002253	Activation of immune response	4,73E-02	21	385
GO Biological Process	GO:0015718	Monocarboxylic acid transport	4,73E-02	11	142
GO Biological Process	GO:0007052	Mitotic spindle organization	4,73E-02	8	81
GO Biological Process	GO:0043066	Negative regulation of apoptotic process	4,76E-02	39	893
GO Biological Process	GO:0006418	tRNA aminoacylation for protein translation	4,76E-02	6	46
GO Biological Process	GO:0007040	Lysosome organization	4,80E-02	7	63
GO Biological Process	GO:0010648	Negative regulation of cell communication	4,80E-02	55	1382
GO Biological Process	GO:0043001	Golgi to plasma membrane protein transport	4,84E-02	5	31
GO Biological Process	GO:0034504	Protein localization to nucleus	4,88E-02	12	165
GO Biological Process	GO:0030970	Retrograde protein transport, er to cytosol	4,89E-02	4	18
GO Molecular Function	GO:0004128	cytochrome-b5 reductase activity, acting on NAD(P)H	4,90E-02	3	7
KEGG Pathways	hsa04152	AMPK signaling pathway	4,92E-02	9	120
GO Molecular Function	GO:0019901	Protein kinase binding	4,94E-02	31	653
GO Biological Process	GO:0000041	Transition metal ion transport	4,96E-02	10	122
GO Molecular Function	GO:0008308	Voltage-gated anion channel activity	4,98E-02	4	17

Supplementary Table 5: List of Jad Core retrieved PPIs.

Uniprot accession	Uniprot Entry name	Gene names	Statistics 3values	Statistics 2values	MiST	SAINT	Final Score	BAIT
A6NHR9	SMHD1	SMCHD1 KIAA0650	1	0	1	0	2	Core
		E2	1	1	0	1	3,5	Core
		NS2	1	1	0	1	3,5	Core
		NS3	1	1	0	0	2,5	Core
O00488	ZN593	ZNF593 ZT86	1	1	0	0	2,5	Core
O00767	ACOD	SCD FADS5 SCD1 SCDOS	1	1	0	0	2,5	Core
O15160	RPAC1	POLR1C POLR1E	1	1	0	0	2,5	Core
O15392	BIRC5	BIRC5 API4 IAP4	1	0	0	0	1	Core
O15397	IPO8	IPO8 RANBP8	1	0	0	0	1	Core
O43159	RRP8	RRP8 KIAA0409 NML hucep-1	1	0	1	0	2	Core
O43818	U3IP2	RRP9 RNU3IP2 U355K	1	1	0	0	2,5	Core
O60508	PRP17	CDC40 EHB3 PRP17 PRPF17	1	0	0	0	1	Core
O60783	RT14	MRPS14	1	1	0	0	2,5	Core
O75530	EED	EED	1	0	0	0	1	Core
O94776	MTA2	MTA2 MTA1L1 PID	1	1	0	1	3,5	Core
O94880	PHF14	PHF14 KIAA0783	1	0	1	0	2	Core
O95104	SCAF4	SCAF4 KIAA1172 SFRS15	1	1	0	1	3,5	Core
O95206	PCDH8	PCDH8	1	1	0	0	2,5	Core
O96019	ACL6A	ACTL6A BAF53 BAF53A INO80K	1	1	0	0	2,5	Core
P05166	PCCB	PCCB	1	1	0	0	2,5	Core
P10253	LYAG	GAA	1	0	0	0	1	Core
P16220	CREB1	CREB1	1	1	0	0	2,5	Core
P17096	HMGA1	HMGA1 HMGIY	1	1	0	0	2,5	Core
P17676	CEBPB	CEBPB TCF5 PP9092	1	1	0	0	2,5	Core
P18754	RCC1	RCC1 CHC1	1	0	0	0	1	Core
P20020	AT2B1	ATP2B1 PMCA1	1	0	1	0	2	Core
P35659	DEK	DEK	1	1	0	0	2,5	Core
P38432	COIL	COIL CLN80	1	1	0	0	2,5	Core
P39060	COIA1	COL18A1	1	1	0	0	2,5	Core
P41208	CETN2	CETN2 CALT CEN2	1	0	1	0	2	Core
P43694	GATA4	GATA4	1	1	0	1	3,5	Core
P45973	CBX5	CBX5 HP1A	1	1	0	0	2,5	Core
P50579	MAP2	METAP2 MNPEP P67EIF2	1	0	0	0	1	Core
P51654	GPC3	GPC3 OCI5	1	1	0	0	2,5	Core
P52756	RBM5	RBM5 H37 LUCA15	1	0	1	0	2	Core
P53582	MAP11	METAP1 KIAA0094	1	0	0	0	1	Core
P53675	CLH2	CLTCL1 CLH22 CLTCL CLTD	1	1	0	0	2,5	Core
P53814	SMTN	SMTN SMSMO	1	0	0	0	1	Core
P55209	NP1L1	NAP1L1 NRP	1	1	0	0	2,5	Core
P56182	RRP1	RRP1 D21S2056E NNP1 NOP52 RRP1A	1	1	0	1	3,5	Core
P56524	HDAC4	HDAC4 KIAA0288	1	0	0	0	1	Core
P57740	NU107	NUP107	1	1	0	0	2,5	Core
P82930	RT34	MRPS34	1	1	0	1	3,5	Core
Q01780	EXOSX	EXOSC10 PMSCL PMSCL2 RRP6	1	1	0	0	2,5	Core
Q05048	CSTF1	CSTF1	1	0	0	0	1	Core
Q07021	C1QBP	C1QBP GC1QBP HABP1 SF2P32	1	1	0	1	3,5	Core
Q07065	CKAP4	CKAP4	1	1	0	0	2,5	Core
Q08170	SRSF4	SRSF4 SFRS4 SRP75	1	1	0	0	2,5	Core
Q12824	SNF5	SMARCB1 BAF47 INI1 SNF5L1	1	1	0	0	2,5	Core
Q12996	CSTF3	CSTF3	1	1	0	0	2,5	Core
Q13111	CAF1A	CHAF1A CAF CAF1P150	1	0	0	0	1	Core
Q13136	LIPA1	PPFIA1 LIP1	1	1	0	0	2,5	Core

Q13724	MOGS	MOGS GCS1	1	1	0	1	3,5	Core
Q14008	CKAP5	CKAP5 KIAA0097	1	1	0	0	2,5	Core
Q14692	BMS1	BMS1 BMS1L KIAA0187	1	1	0	0	2,5	Core
Q14739	LBR	LBR	1	1	0	0	2,5	Core
Q14807	KIF22	KIF22 KID KNSL4	1	1	0	0	2,5	Core
Q15543	TAF13	TAF13 TAF2K TAFII18	1	0	0	0	1	Core
Q15545	TAF7	TAF7 TAF2F TAFII55	1	1	0	0	2,5	Core
Q15554	TERF2	TERF2 TRBF2 TRF2	1	0	0	0	1	Core
Q15629	TRAM1	TRAM1 TRAM	1	1	0	0	2,5	Core
Q16540	RM23	MRPL23 L23MRP RPL23L	1	0	0	0	1	Core
Q3KQU3	MA7D1	MAP7D1 KIAA1187 PARCC1 RPRC1 PP2464	1	1	0	0	2,5	Core
Q49A26	GLYR1	GLYR1 HIBDL NDF NP60 NPAC	1	1	0	0	2,5	Core
Q53HL2	BOREA	CDCA8 PESCRG3	1	1	0	0	2,5	Core
Q5SY16	NOL9	NOL9	1	0	0	0	1	Core
Q6I9Y2	THOC7	THOC7 NIF3L1BP1	1	1	0	0	2,5	Core
Q6P1J9	CDC73	CDC73 C1orf28 HRPT2	1	1	0	0	2,5	Core
Q6P1L8	RM14	MRPL14 MRPL32 RPML32	1	1	0	0	2,5	Core
Q6P4A8	PLBL1	PLBD1	1	1	0	0	2,5	Core
Q6P6C2	ALKB5	ALKBH5 ABH5 OFOXD1	1	0	0	0	1	Core
Q6PK04	CC137	CCDC137 cPERP-B	1	1	0	0	2,5	Core
Q6ZUT1	NKAP1	NKAPD1 C11orf57	1	0	1	0	2	Core
Q76FK4	NOL8	NOL8 C9orf34 NOP132	1	0	1	0	2	Core
Q7KZ85	SPT6H	SUPT6H KIAA0162 SPT6H	1	1	0	0	2,5	Core
Q7Z6I8	CE024	C5orf24	1	1	0	0	2,5	Core
Q86T03	PP4P1	PIP4P1 C14orf9 TMEM55B	1	0	0	0	1	Core
Q86TB9	PATL1	PATL1 OK/KNS-cl.5	1	1	0	1	3,5	Core
Q86UC2	RSPH3	RSPH3 RSHL2 RSP3	1	1	0	0	2,5	Core
Q86W42	THOC6	THOC6 WDR58 PSEC0006	1	1	0	0	2,5	Core
Q86Y07	VRK2	VRK2	1	1	0	0	2,5	Core
Q8IVW6	ARI3B	ARID3B BDP DRIL2	1	1	0	0	2,5	Core
Q8IWX8	CHERP	CHERP DAN26 SCAF6	1	1	0	0	2,5	Core
Q8N1G2	CMTR1	CMTR1 FTSJD2 KIAA0082 MTR1	1	1	0	0	2,5	Core
Q8N1G4	LRC47	LRRC47 KIAA1185	1	1	0	0	2,5	Core
Q8NEF9	SRFB1	SRFBP1	1	1	0	0	2,5	Core
Q8NET6	CHSTD	CHST13	1	1	0	0	2,5	Core
Q8WUD4	CCD12	CCDC12	1	1	0	0	2,5	Core
Q92576	PHF3	PHF3 KIAA0244	1	1	0	0	2,5	Core
Q92878	RAD50	RAD50	1	1	0	0	2,5	Core
Q92925	SMRD2	SMARCD2 BAF60B PRO2451	1	1	0	0	2,5	Core
Q93045	STMN2	STMN2 SCG10 SCGN10	1	1	0	0	2,5	Core
Q969G3	SMCE1	SMARCE1 BAF57	1	1	0	0	2,5	Core
Q96AG4	LRC59	LRRC59 PRO1855	1	1	0	0	2,5	Core
Q96DI7	SNR40	SNRNP40 PRP8BP SFP38 WDR57	1	1	0	1	3,5	Core
Q96EU6	RRP36	RRP36 C6orf153 HSPC253	1	0	0	0	1	Core
Q96FX7	TRM61	TRMT61A C14orf172 TRM61	1	1	1	0	3,5	Core

Q96JN0	LCOR	LCOR C10orf12 KIAA1795 MLR2	1	1	0	0	2,5	Core
Q96L58	B3GT6	B3GALT6	1	0	0	0	1	Core
Q96RQ3	MCCA	MCCC1 MCCA	1	1	0	0	2,5	Core
Q96TC7	RMD3	RMDN3 FAM82A2 FAM82C PTPIP51 hucep-10 UNQ3122/PRO10274	1	0	0	0	1	Core
Q99496	RING2	RNF2 BAP1 DING HIPI3 RING1B	1	0	0	0	1	Core
Q99733	NP1L4	NAP1L4 NAP2	1	1	0	1	3,5	Core
Q99848	EBP2	EBNA1BP2 EBP2	1	1	0	0	2,5	Core
Q99996	AKAP9	AKAP9 AKAP350 AKAP450 KIAA0803	1	1	0	0	2,5	Core
Q9BRR8	GPTC1	GPATCH1 ECGP GPATC1	1	0	1	0	2	Core
Q9BSC4	NOL10	NOL10	1	1	0	0	2,5	Core
Q9BT25	HAUS8	HAUS8 HICE1	1	0	0	0	1	Core
Q9BW19	KIFC1	KIFC1 HSET KNSL2	1	0	0	0	1	Core
Q9BWF3	RBM4	RBM4 RBM4A	1	1	0	0	2,5	Core
Q9BXK1	KLF16	KLF16 BTEB4 NSLP2	1	1	0	1	3,5	Core
Q9BYN8	RT26	MRPS26 C20orf193 RPMS13	1	0	0	0	1	Core
Q9BZZ5	API5	API5 MIG8	1	0	0	0	1	Core
Q9C0C9	UBE2O	UBE2O KIAA1734	1	1	0	1	3,5	Core
Q9GZR7	DDX24	DDX24	1	1	0	0	2,5	Core
Q9H147	TDIF1	DNTTIP1 C20orf167 TDIF1	1	1	0	0	2,5	Core
Q9H2P0	ADNP	ADNP ADNP1 KIAA0784	1	0	1	0	2	Core
Q9H5V9	CX056	STEEP1 CXorf56	1	1	0	0	2,5	Core
Q9H814	PHAX	PHAX RNUXA	1	0	0	0	1	Core
Q9NPA8	ENY2	ENY2 DC6	1	1	0	0	2,5	Core
Q9NQ55	SSF1	PPAN BXDC3 SSF1	1	0	1	0	2	Core
Q9NQT5	EXOS3	EXOSC3 RRP40 CGI-102	1	1	0	1	3,5	Core
Q9NXX6	NSE4A	NSMCE4A C10orf86 PP4762	1	0	0	0	1	Core
Q9NZN9	AIPL1	AIPL1 AIPL2	1	0	0	0	1	Core
Q9UGR2	Z3H7B	ZC3H7B KIAA1031	1	0	0	0	1	Core
Q9UGY1	NOL12	NOL12	1	1	0	0	2,5	Core
Q9ULW0	TPX2	TPX2 C20orf1 C20orf2 DIL2 HCA519	1	1	0	0	2,5	Core
Q9ULW3	ABT1	ABT1	1	1	0	0	2,5	Core
Q9ULX9	MAFF	MAFF	1	1	0	0	2,5	Core
Q9Y291	RT33	MRPS33 CGI-139 PTD003	1	1	0	0	2,5	Core
Q9Y3B4	SF3B6	SF3B6 SAP14 SF3B14 SF3B14A CGI-110 HSPC175 HT006	1	1	0	1	3,5	Core
Q9Y3D3	RT16	MRPS16 RPMS16 CGI-132	1	1	0	0	2,5	Core
Q9Y5V0	ZN706	ZNF706 HSPC038 PNAS-113	1	1	0	0	2,5	Core
Q9Y676	RT18B	MRPS18B C6orf14 HSPC183 PTD017	1	1	0	0	2,5	Core

Supplementary Table 6: String enriched pathways in our Jad Core interactomic network.

category	term name	description	FDR value	# genes	# background genes	genes
GO Molecular Function	GO:0003676	Nucleic acid binding	4.02E-19	78	3947	KIF22|GPATCH1|CSTF1|C1QBP|LRRC59|RRP9|SF3B6|COIL|RRP36|KLF16|PPAN|RRP8|TERF2|SMARCB1|EED|SNRNP40|HDAC4|ABT1|MTA2|C10orf12|SCAF4|THOC7|PHAX|PATL1|CEBPB|TAF7|CSTF3|SUPT6H|GLYR1|EXOSC3|UBE2O|SMARCE1|METAP2|THOC6|SMCHD1|CCDC137|GATA4|LBR|SRFBP1|RBM5|ARID3B|MAFF|ZC3H7B|AKAP9|NOL12|TAF13|CDC40|MRPL14|POLR1C|DNTTIP1|CMTR1|SRSF4|RCC1|ZNF593|BMS1|EXOSC10|NOL9|CKAP4|LRRC47|RAD50|MRPS26|NAP1L4|NOL10|ADNP|DEK|RPL23L|ALKBH5|RBM4|CREB1|HMGA1|EBNA1BP2|RRP1|MRPS14|API5|CHERP|NOL8|NAP1L1|DDX24
GO Molecular Function	GO:0003723	RNA binding	5.05E-19	52	1649	GPATCH1|CSTF1|C1QBP|LRRC59|RRP9|SF3B6|COIL|RRP36|PPAN|RRP8|SNRNP40|ABT1|SCAF4|THOC7|PHAX|PATL1|CSTF3|SUPT6H|EXOSC3|UBE2O|SMARCE1|METAP2|THOC6|CCDC137|LBR|SRFBP1|RBM5|ZC3H7B|NOL12|CDC40|MRPL14|SRSF4|BMS1|EXOSC10|NOL9|CKAP4|LRRC47|MRPS26|NAP1L4|NOL10|DEK|RPL23L|ALKBH5|RBM4|EBNA1BP2|RRP1|MRPS14|API5|CHERP|NOL8|NAP1L1|DDX24
GO Biological Process	GO:0010467	Gene expression	2.85E-16	55	2056	GPATCH1|MRPS34|CSTF1|C1QBP|NUP107|RRP9|SF3B6|COIL|RRP36|RRP8|MRPS18B|PHF3|SMARCB1|SNRNP40|ABT1|SCAF4|THOC7|PHAX|TAF7|CSTF3|SUPT6H|EXOSC3|METAP2|THOC6|SRFBP1|RBM5|MAFF|ZC3H7B|TAF13|CDC73|RNF2|CDC40|MRPL14|POLR1C|MRPS16|CMTR1|SRSF4|BMS1|EXOSC10|NOL9|MRPS26|NOL10|TRMT61A|MRPS33|DEK|RPL23L|ALKBH5|RBM4|CREB1|EBNA1BP2|RRP1|MRPS14|ENY2|CHERP|NOL8
GO Biological Process	GO:0034641	Cellular nitrogen compound metabolic process	3.35E-16	68	3282	KIF22|GPATCH1|MRPS34|CSTF1|C1QBP|RRP9|SF3B6|COIL|RRP36|RRP8|TERF2|MRPS18B|PHF3|SMARCB1|EED|SNRNP40|MCCC1|ABT1|MTA2|SCAF4|THOC7|PHAX|PATL1|CHAF1A|TAF7|CSTF3|SUPT6H|EXOSC3|THOC6|SMCHD1|SRFBP1|RBM5|MAFF|ZC3H7B|TAF13|CDC73|CDC40|NSMCE4A|CETN2|SCD|MRPL14|POLR1C|MRPS16|CMTR1|SRSF4|BMS1|EXOSC10|NOL9|RAD50|MRPS26|NOL10|TRMT61A|MRPS33|DEK|RPL23L|ALKBH5|RBM4|CREB1|ACTL6A|HMGA1|EBNA1BP2|RRP1|PCCB|MRPS14|ENY2|CHERP|NOL8|DDX24
GO Biological Process	GO:0090304	Nucleic acid metabolic process	3.35E-16	56	2178	KIF22|GPATCH1|CSTF1|C1QBP|RRP9|SF3B6|COIL|RRP36|RRP8|TERF2|PHF3|SMARCB1|SNRNP40|ABT1|MTA2|SCAF4|THOC7|PHAX|PATL1|CHAF1A|TAF7|CSTF3|SUPT6H|EXOSC3|THOC6|SMCHD1|SRFBP1|RBM5|MAFF|ZC3H7B|TAF13|CDC73|CDC40|NSMCE4A|CETN2|POLR1C|CMTR1|SRSF4|BMS1|EXOSC10|NOL9|RAD50|NOL10|TRMT61A|DEK|ALKBH5|RBM4|CREB1|ACTL6A|HMGA1|EBNA1BP2|RRP1|ENY2|CHERP|NOL8|DDX24
GO Biological Process	GO:0016070	RNA metabolic process	1.49E-14	46	1584	GPATCH1|CSTF1|C1QBP|RRP9|SF3B6|COIL|RRP36|RRP8|PHF3|SMARCB1|SNRNP40|ABT1|SCAF4|THOC7|PHAX|PATL1|TAF7|CSTF3|SUPT6H|EXOSC3|THOC6|SRFBP1|RBM5|MAFF|ZC3H7B|TAF13|CDC73|CDC40|POLR1C|CMTR1|SRSF4|BMS1|EXOSC10|NOL9|NOL10|TRMT61A|DEK|ALKBH5|RBM4|CREB1|EBNA1BP2|RRP1|ENY2|CHERP|NOL8|DDX24
GO Biological Process	GO:0006139	Nucleobase-containing compound metabolic process	4.06E-14	58	2659	KIF22|GPATCH1|CSTF1|C1QBP|RRP9|SF3B6|COIL|RRP36|RRP8|TERF2|PHF3|SMARCB1|EED|SNRNP40|ABT1|MTA2|SCAF4|THOC7|PHAX|PATL1|CHAF1A|TAF7|CSTF3|SUPT6H|EXOSC3|THOC6|SMCHD1|SRFBP1|RBM5|MAFF|ZC3H7B|TAF13|CDC73|CDC40|NSMCE4A|CETN2|SCD|POLR1C|CMTR1|SRSF4|BMS1|EXOSC10|NOL9|RAD50|NOL10|TRMT61A|DEK|ALKBH5|RBM4|CREB1|ACTL6A|HMGA1|EBNA1BP2|RRP1|ENY2|CHERP|NOL8|DDX24
GO Biological Process	GO:0046483	Heterocycle metabolic process	4.06E-14	60	2840	KIF22|GPATCH1|CSTF1|C1QBP|RRP9|SF3B6|COIL|RRP36|RRP8|TERF2|PHF3|SMARCB1|EED|SNRNP40|MCCC1|ABT1|MTA2|SCAF4|THOC7|PHAX|PATL1|CHAF1A|TAF7|CSTF3|SUPT6H|EXOSC3|THOC6|SMCHD1|SRFBP1|RBM5|MAFF|ZC3H7B|TAF13|CDC73|CDC40|NSMCE4A|CETN2|SCD|POLR1C|CMTR1|SRSF4|BMS1|EXOSC10|NOL9|RAD50|NOL10|TRMT61A|DEK|ALKBH5|RBM4|CREB1|ACTL6A|HMGA1|EBNA1BP2|RRP1|PCCB|ENY2|CHERP|NOL8|DDX24
GO Biological Process	GO:0006396	RNA processing	7.81E-14	34	854	GPATCH1|CSTF1|C1QBP|RRP9|SF3B6|COIL|RRP36|RRP8|SNRNP40|ABT1|SCAF4|THOC7|CSTF3|SUPT6H|EXOSC3|THOC6|SRFBP1|RBM5|ZC3H7B|CDC73|CDC40|CMTR1|SRSF4|BMS1|EXOSC10|NOL9|NOL10|TRMT61A|ALKBH5|RBM4|EBNA1BP2|RRP1|CHERP|NOL8
GO Biological Process	GO:1901360	Organic cyclic compound metabolic process	9.78E-14	62	3118	CAF4|THOC7|PHAX|PATL1|CHAF1A|TAF7|CSTF3|SUPT6H|EXOSC3|THOC6|SMCHD1|LBR|SRFBP1|RBM5|MAFF|ZC3H7B|TAF13|CDC73|CDC40|NSMCE4A|CETN2|SCD|POLR1C|CMTR1|SRSF4|BMS1|EXOSC10|NOL9|RAD50|NOL10|TRMT61A|DEK|TMEM55B|ALKBH5|RBM4|CREB1|ACTL6A|HMGA1|EBNA1BP2|RRP1|PCCB|ENY2|CHERP|NOL8|DDX24
GO Molecular Function	GO:1901363	Heterocyclic compound binding	3.02E-12	83	5831	KIF22|GPATCH1|CSTF1|C1QBP|LRRC59|RRP9|SF3B6|COIL|RRP36|KLF16|PPAN|RRP8|TERF2|SMARCB1|EED|SNRNP40|HDAC4|MCCC1|ABT1|MTA2|C10orf12|SCAF4|THOC7|PHAX|PATL1|CEBPB|TAF7|CSTF3|SUPT6H|GLYR1|EXOSC3|UBE2O|SMARCE1|METAP2|THOC6|SMCHD1|CCDC137|GATA4|LBR|SRFBP1|RBM5|ARID3B|MAFF|ZC3H7B|AKAP9|NOL12|TAF13|CDC40|MRPL14|POLR1C|DNTTIP1|CMTR1|SRSF4|RCC1|ZNF593|BMS1|EXOSC10|NOL9|CKAP4|LRRC47|RAD50|MRPS26|NAP1L4|NOL10|ADNP|DEK|RPL23L|ALKBH5|RBM4|CREB1|ATP2B1|KIFC1|HMGA1|EBNA1BP2|VRK2|RRP1|PCCB|MRPS14|API5|CHERP|NOL8|NAP1L1|DDX24
GO Molecular Function	GO:0097159	Organic cyclic compound binding	5.58E-12	83	5916	KIF22|GPATCH1|CSTF1|C1QBP|LRRC59|RRP9|SF3B6|COIL|RRP36|KLF16|PPAN|RRP8|TERF2|SMARCB1|EED|SNRNP40|HDAC4|MCCC1|ABT1|MTA2|C10orf12|SCAF4|THOC7|PHAX|PATL1|CEBPB|TAF7|CSTF3|SUPT6H|GLYR1|EXOSC3|UBE2O|SMARCE1|METAP2|THOC6|SMCHD1|CCDC137|GATA4|LBR|SRFBP1|RBM5|ARID3B|MAFF|ZC3H7B|AKAP9|NOL12|TAF13|CDC40|MRPL14|POLR1C|DNTTIP1|CMTR1|SRSF4|RCC1|ZNF593|BMS1|EXOSC10|NOL9|CKAP4|LRRC47|RAD50|MRPS26|NAP1L4|NOL10|ADNP|DEK|RPL23L|ALKBH5|RBM4|CREB1|ATP2B1|KIFC1|HMGA1|EBNA1BP2|VRK2|RRP1|PCCB|MRPS14|API5|CHERP|NOL8|NAP1L1|DDX24
GO Biological Process	GO:0043170	Macromolecule metabolic process	1.13E-9	81	6137	KIF22|GPATCH1|MRPS34|CSTF1|C1QBP|NUP107|RRP9|SF3B6|MOGS|COIL|RRP36|RRP8|TERF2|MRPS18B|PHF3|SMARCB1|EED|SNRNP40|HDAC4|ABT1|MTA2|SCAF4|THOC7|METAP1|PHAX|PATL1|CHAF1A|BIRC5|GAA|TAF7|CSTF3|CHST13|SUPT6H|EXOSC3|UBE2O|METAP2|THOC6|SMCHD1|SRFBP1|RBM5|MAFF|ZC3H7B|TAF13|CDC73|RNF2|CDC40|NSMCE4A|CETN2|MRPL14|POLR1C|MRPS16|CMTR1|SRSF4|BMS1|EXOSC10|NOL9|CKAP4|RAD50|B3GALT6|MRPS26|AIPL1|NOL10|TRMT61A|MRPS33|GPC3|DEK|RPL23L|ALKBH5|RBM4|CREB1|ACTL6A|HMGA1|EBNA1BP2|VRK2|RRP1|MRPS14|ENY2|CHERP|NOL8|NAP1L1|DDX24

GO Biological Process	GO:0006403	RNA localization	3.19E-8	15	210	NUP107|TERF2|THOC7|PHAX|SUPT6H|EXOSC3|THOC6|CDC40|CETN2|SRSF4|ZNF593|EXOSC10|ALKBH5|ENY2|CKAP5
GO Biological Process	GO:0006807	Nitrogen compound metabolic process	4.84E-8	83	6852	KIF22|GPATCH1|MRPS34|CSTF1|C1QBP|NUP107|RRP9|SF3B6|MOGS|COIL|PLBD1|RRP36|RRP8|TERF2|MRPS18B|PHF3|SMA RCB1|EED|SNRNP40|HDAC4|MCCC1|ABT1|MTA2|SCAF4|THOC7|METAP1|PHAX|PATL1|CHAF1A|BIRC5|TAF7|CSTF3|CHST13|S UPT6H|EXOSC3|UBE2O|METAP2|THOC6|SMCHD1|SRFBP1|RBM5|MAFF|ZC3H7B|TAF13|CDC73|RNF2|CDC40|NSMCE4A|CETN 2|SCD|MRPL14|POLR1C|MRPS16|CMTR1|SRSF4|BMS1|EXOSC10|NOL9|CKAP4|RAD50|B3GALT6|MRPS26|AIPL1|NOL10|TRMT 61A|MRPS33|GPC3|DEK|RPL23L|ALKBH5|RBM4|CREB1|ACTL6A|HMGA1|EBNA1BP2|VRK2|RRP1|PCCB|MRPS14|ENY2|CHERP |NOL8|DDX24
GO Biological Process	GO:0044238	Primary metabolic process	7.05E-8	86	7332	KIF22|GPATCH1|MRPS34|CSTF1|C1QBP|NUP107|RRP9|SF3B6|MOGS|COIL|PLBD1|RRP36|RRP8|TERF2|MRPS18B|PHF3|SMA RCB1|EED|SNRNP40|HDAC4|MCCC1|ABT1|MTA2|SCAF4|THOC7|METAP1|PHAX|PATL1|CHAF1A|BIRC5|GAA|TAF7|CSTF3|CHS T13|SUPT6H|EXOSC3|UBE2O|METAP2|THOC6|SMCHD1|LBR|SRFBP1|RBM5|MAFF|ZC3H7B|TAF13|CDC73|RNF2|CDC40|NSM CE4A|CETN2|SCD|MRPL14|POLR1C|MRPS16|CMTR1|SRSF4|BMS1|EXOSC10|NOL9|CKAP4|RAD50|B3GALT6|MRPS26|AIPL1|N OL10|TRMT61A|MRPS33|GPC3|DEK|RPL23L|TMEM55B|ALKBH5|RBM4|CREB1|ACTL6A|HMGA1|EBNA1BP2|VRK2|RRP1|PCCB |MRPS14|ENY2|CHERP|NOL8|DDX24
GO Biological Process	GO:0022613	Ribonucleoprotein complex biogenesis	1.02E-7	19	423	C1QBP|RRP9|COIL|RRP36|PPAN|RRP8|ABT1|EXOSC3|SRFBP1|RBM5|CDC73|ZNF593|BMS1|EXOSC10|NOL9|NOL10|EBNA1BP 2|RRP1|NOL8
GO Biological Process	GO:0016071	mRNA metabolic process	1.9E-7	23	678	GPATCH1|CSTF1|C1QBP|SF3B6|COIL|SNRNP40|SCAF4|THOC7|PATL1|CSTF3|SUPT6H|EXOSC3|THOC6|RBM5|CDC73|CDC40|C MTR1|SRSF4|EXOSC10|TRMT61A|ALKBH5|RBM4|CHERP
GO Biological Process	GO:0042254	Ribosome biogenesis	1.91E-7	16	292	C1QBP|RRP9|RRP36|PPAN|RRP8|ABT1|EXOSC3|SRFBP1|ZNF593|BMS1|EXOSC10|NOL9|NOL10|EBNA1BP2|RRP1|NOL8
GO Biological Process	GO:0044237	Cellular metabolic process	2.26E-7	86	7513	KIF22|GPATCH1|MRPS34|CSTF1|C1QBP|NUP107|RRP9|SF3B6|MOGS|COIL|PLBD1|RRP36|RRP8|TERF2|MRPS18B|PHF3|SMA RCB1|EED|SNRNP40|HDAC4|MCCC1|ABT1|MTA2|SCAF4|THOC7|METAP1|PHAX|PATL1|CHAF1A|BIRC5|GAA|TAF7|CSTF3|CHS T13|SUPT6H|EXOSC3|UBE2O|METAP2|THOC6|SMCHD1|SRFBP1|RBM5|MAFF|ZC3H7B|TAF13|CDC73|RNF2|CDC40|NSMCE4A |CETN2|SCD|MRPL14|POLR1C|MRPS16|CMTR1|SRSF4|BMS1|EXOSC10|NOL9|CKAP4|RAD50|B3GALT6|MRPS26|AIPL1|NOL10 |TRMT61A|MRPS33|GPC3|DEK|RPL23L|TMEM55B|ALKBH5|RBM4|CREB1|ACTL6A|HMGA1|EBNA1BP2|VRK2|RRP1|PCCB|MRP S14|ENY2|CHERP|NOL8|NAP1L1|DDX24
Reactome Pathways	HSA-8953854	Metabolism of RNA	2.82E-7	23	659	CSTF1|NUP107|RRP9|SF3B6|RRP36|SNRNP40|THOC7|PHAX|PATL1|CSTF3|EXOSC3|THOC6|RBM5|NOL12|CDC40|SRSF4|BMS 1|EXOSC10|NOL9|TRMT61A|EBNA1BP2|RRP1|CHERP
GO Biological Process	GO:0006397	mRNA processing	4.07E-7	19	468	GPATCH1|CSTF1|C1QBP|SF3B6|COIL|SNRNP40|SCAF4|THOC7|CSTF3|SUPT6H|THOC6|RBM5|CDC73|CDC40|CMTR1|SRSF4|AL KBH5|RBM4|CHERP
GO Biological Process	GO:0071704	Organic substance metabolic process	4.22E-7	87	7755	KIF22|GPATCH1|MRPS34|CSTF1|C1QBP|NUP107|RRP9|SF3B6|MOGS|COIL|PLBD1|RRP36|RRP8|TERF2|MRPS18B|PHF3|SMA RCB1|EED|SNRNP40|HDAC4|MCCC1|ABT1|MTA2|SCAF4|THOC7|METAP1|PHAX|PATL1|CHAF1A|BIRC5|GAA|TAF7|CSTF3|CHS T13|SUPT6H|EXOSC3|UBE2O|METAP2|THOC6|SMCHD1|LBR|SRFBP1|RBM5|MAFF|ZC3H7B|TAF13|CDC73|RNF2|CDC40|NSM CE4A|CETN2|SCD|MRPL14|POLR1C|MRPS16|CMTR1|SRSF4|BMS1|EXOSC10|NOL9|CKAP4|RAD50|B3GALT6|MRPS26|AIPL1|N OL10|TRMT61A|MRPS33|GPC3|DEK|RPL23L|TMEM55B|ALKBH5|RBM4|CREB1|ACTL6A|HMGA1|EBNA1BP2|VRK2|RRP1|PCCB |MRPS14|ENY2|CHERP|NOL8|NAP1L1|DDX24
Reactome Pathways	HSA-74160	Gene expression (Transcription)	5.25E-7	33	1455	CBX5|CSTF1|NUP107|RRP8|IPO8|SMARCB1|EED|HDAC4|MTA2|THOC7|PHAX|TPX2|CEBPB|TAF7|CSTF3|SUPT6H|SMARCE1|T HOC6|GATA4|LBR|TAF13|CDC73|RNF2|CDC40|POLR1C|SRSF4|RAD50|DEK|TMEM55B|CREB1|SMARCD2|ACTL6A|ZNF706
GO Biological Process	GO:0032984	Protein-containing complex disassembly	5.69E-7	14	229	MRPS34|MRPS18B|SMARCB1|SMARCE1|MRPL14|MRPS16|MRPS26|MRPS33|RPL23L|SMARCD2|HMGA1|MRPS14|STMN2|CKA P5
GO Biological Process	GO:0050658	RNA transport	5.8E-7	13	189	NUP107|TERF2|THOC7|PHAX|SUPT6H|THOC6|CDC40|CETN2|SRSF4|ZNF593|ALKBH5|ENY2|CKAP5
GO Biological Process	GO:0006364	rRNA processing	1.89E-6	13	212	RRP9|RRP36|RRP8|ABT1|EXOSC3|SRFBP1|BMS1|EXOSC10|NOL9|NOL10|EBNA1BP2|RRP1|NOL8
GO Biological Process	GO:0009059	Macromolecule biosynthetic process	4.75E-6	33	1643	MRPS34|CSTF1|MOGS|TERF2|MRPS18B|PHF3|SMARCB1|ABT1|PHAX|CHAF1A|TAF7|CSTF3|CHST13|SUPT6H|MAFF|TAF13|C DC73|MRPL14|POLR1C|MRPS16|RAD50|B3GALT6|MRPS26|MRPS33|GPC3|DEK|RPL23L|RBM4|CREB1|HMGA1|MRPS14|ENY2 |NAP1L1
GO Biological Process	GO:0008152	Metabolic process	5.06E-6	88	8298	KIF22|GPATCH1|MRPS34|CSTF1|C1QBP|NUP107|RRP9|SF3B6|MOGS|COIL|PLBD1|RRP36|RRP8|TERF2|MRPS18B|PHF3|SMA RCB1|EED|SNRNP40|HDAC4|MCCC1|ABT1|MTA2|SCAF4|THOC7|METAP1|PHAX|PATL1|CHAF1A|BIRC5|GAA|TAF7|CSTF3|CHS T13|SUPT6H|GLYR1|EXOSC3|UBE2O|METAP2|THOC6|SMCHD1|LBR|SRFBP1|RBM5|MAFF|ZC3H7B|TAF13|CDC73|RNF2|CDC4 0|NSMCE4A|CETN2|SCD|MRPL14|POLR1C|MRPS16|CMTR1|SRSF4|BMS1|EXOSC10|NOL9|CKAP4|RAD50|B3GALT6|MRPS26|A IPL1|NOL10|TRMT61A|MRPS33|GPC3|DEK|RPL23L|TMEM55B|ALKBH5|RBM4|CREB1|ACTL6A|HMGA1|EBNA1BP2|VRK2|RRP1 |PCCB|MRPS14|ENY2|CHERP|NOL8|NAP1L1|DDX24
GO Biological Process	GO:0034645	Cellular macromolecule biosynthetic process	7.72E-6	32	1592	MRPS34|CSTF1|MOGS|TERF2|MRPS18B|PHF3|SMARCB1|ABT1|PHAX|CHAF1A|TAF7|CSTF3|CHST13|SUPT6H|MAFF|TAF13|C DC73|MRPL14|POLR1C|MRPS16|RAD50|B3GALT6|MRPS26|MRPS33|DEK|RPL23L|RBM4|CREB1|HMGA1|MRPS14|ENY2|NAP1 L1
Reactome Pathways	HSA-73857	RNA Polymerase II Transcription	9.75E-6	29	1318	CBX5|CSTF1|SMARCB1|EED|HDAC4|MTA2|THOC7|PHAX|TPX2|CEBPB|TAF7|CSTF3|SUPT6H|SMARCE1|THOC6|GATA4|LBR|TA F13|CDC73|RNF2|CDC40|SRSF4|RAD50|DEK|TMEM55B|CREB1|SMARCD2|ACTL6A|ZNF706

GO Biological Process	GO:0071840	Cellular component organization or biogenesis	1.13E-5	68	5633	KIF22|MRPS34|C1QBP|NUP107|RRP9|COIL|RRP36|PPAN|HAUS8|PPFIA1|RRP8|TERF2|MRPS18B|SMARCB1|EED|HDAC4|ABT1|MTA2|PATL1|TPX2|CHAF1A|BIRC5|GAA|TAF7|SUPT6H|EXOSC3|SMARCE1|SMCHD1|SRFBP1|RBM5|COL18A1|AKAP9|CDC73|RNF2|CETN2|MRPL14|MRPS16|CDCA8|MAP7D1|RCC1|ZNF593|BMS1|EXOSC10|NOL9|RAD50|MRPS26|NAP1L4|NOL10|MRPS33|ADNP|DEK|RPL23L|TMEM55B|CREB1|SMARCD2|KIFC1|ACTL6A|HMGA1|EBNA1BP2|RRP1|MRPS14|STMN2|ENY2|CKAP5|NOL8|CLTCL1|NAP1L1|SMTN
GO Biological Process	GO:0051276	Chromosome organization	2.04E-5	25	1066	KIF22|NUP107|RRP8|TERF2|SMARCB1|EED|HDAC4|MTA2|CHAF1A|SUPT6H|SMARCE1|SMCHD1|CDC73|RNF2|CETN2|CDCA8|RAD50|NAP1L4|DEK|SMARCD2|KIFC1|ACTL6A|HMGA1|ENY2|NAP1L1
GO Biological Process	GO:0000469	Cleavage involved in rrna processing	2.44E-5	6	26	RRP36|ABT1|EXOSC3|BMS1|EXOSC10|NOL9
GO Biological Process	GO:0043624	Cellular protein complex disassembly	2.48E-5	10	140	MRPS34|MRPS18B|MRPL14|MRPS16|MRPS26|MRPS33|RPL23L|MRPS14|STMN2|CKAP5
GO Biological Process	GO:0008380	RNA splicing	3.82E-5	15	396	GPATCH1|CSTF1|C1QBP|SF3B6|COIL|SNRNP40|THOC7|CSTF3|SUPT6H|THOC6|RBM5|CDC40|SRSF4|RBM4|CHERP
GO Molecular Function	GO:0003682	Chromatin binding	4.58E-5	18	570	CBX5|EED|HDAC4|MTA2|CHAF1A|CEBPB|SUPT6H|GLYR1|SMARCE1|RNF2|DNTTIP1|RCC1|NAP1L4|ADNP|ACTL6A|HMGA1|ENY2|NAP1L1
GO Biological Process	GO:0070125	Mitochondrial translational elongation	1.1E-4	8	90	MRPS34|MRPS18B|MRPL14|MRPS16|MRPS26|MRPS33|RPL23L|MRPS14
GO Biological Process	GO:0070126	Mitochondrial translational termination	1.1E-4	8	91	MRPS34|MRPS18B|MRPL14|MRPS16|MRPS26|MRPS33|RPL23L|MRPS14
GO Biological Process	GO:0043933	Protein-containing complex subunit organization	1.2E-4	29	1539	MRPS34|NUP107|COIL|PPAN|MRPS18B|SMARCB1|ABT1|TPX2|CHAF1A|TAF7|SUPT6H|SMARCE1|RBM5|AKAP9|CDC73|CETN2|MRPL14|MRPS16|MRPS26|NAP1L4|MRPS33|RPL23L|TMEM55B|SMARCD2|HMGA1|MRPS14|STMN2|CKAP5|NAP1L1
GO Biological Process	GO:0006405	RNA export from nucleus	1.3E-4	9	131	NUP107|THOC7|PHAX|THOC6|CDC40|SRSF4|ZNF593|ALKBH5|ENY2
GO Biological Process	GO:0034470	ncRNA processing	1.3E-4	14	381	RRP9|RRP36|RRP8|ABT1|EXOSC3|SRFBP1|BMS1|EXOSC10|NOL9|NOL10|TRMT61A|EBNA1BP2|RRP1|NOL8
Reactome Pathways	HSA-5368286	Mitochondrial translation initiation	1.4E-4	8	88	MRPS34|MRPS18B|MRPL14|MRPS16|MRPS26|MRPS33|RPL23L|MRPS14
Reactome Pathways	HSA-5389840	Mitochondrial translation elongation	1.4E-4	8	88	MRPS34|MRPS18B|MRPL14|MRPS16|MRPS26|MRPS33|RPL23L|MRPS14
Reactome Pathways	HSA-5419276	Mitochondrial translation termination	1.4E-4	8	88	MRPS34|MRPS18B|MRPL14|MRPS16|MRPS26|MRPS33|RPL23L|MRPS14
GO Biological Process	GO:0031123	RNA 3-end processing	1.7E-4	9	135	CSTF1|THOC7|CSTF3|EXOSC3|THOC6|CDC73|CDC40|SRSF4|EXOSC10
Reactome Pathways	HSA-72203	Processing of Capped Intron-Containing Pre-mRNA	2.4E-4	11	238	CSTF1|NUP107|SF3B6|SNRNP40|THOC7|CSTF3|THOC6|RBM5|CDC40|SRSF4|CHERP
GO Biological Process	GO:0006333	Chromatin assembly or disassembly	3.2E-4	10	193	RRP8|SMARCB1|MTA2|CHAF1A|SMARCE1|SMCHD1|NAP1L4|SMARCD2|HMGA1|NAP1L1
GO Biological Process	GO:0051028	mRNA transport	3.2E-4	9	148	NUP107|THOC7|SUPT6H|THOC6|CDC40|CETN2|SRSF4|ALKBH5|ENY2
GO Biological Process	GO:0006325	Chromatin organization	4.7E-4	18	713	RRP8|SMARCB1|EED|HDAC4|MTA2|CHAF1A|SUPT6H|SMARCE1|SMCHD1|CDC73|RNF2|NAP1L4|DEK|SMARCD2|ACTL6A|HMGA1|ENY2|NAP1L1
GO Biological Process	GO:0006338	Chromatin remodeling	5.1E-4	10	206	RRP8|SMARCB1|HDAC4|MTA2|SUPT6H|SMARCE1|SMCHD1|SMARCD2|ACTL6A|HMGA1
GO Biological Process	GO:0031124	mRNA 3-end processing	5.9E-4	7	83	CSTF1|THOC7|CSTF3|THOC6|CDC73|CDC40|SRSF4
GO Biological Process	GO:0051169	Nuclear transport	6.3E-4	11	266	NUP107|IPO8|THOC7|PHAX|THOC6|CDC40|SRSF4|ZNF593|ALKBH5|HMGA1|ENY2
GO Biological Process	GO:0044271	Cellular nitrogen compound biosynthetic process	7.4E-4	27	1522	MRPS34|CSTF1|TERF2|MRPS18B|PHF3|SMARCB1|ABT1|PHAX|TAF7|CSTF3|SUPT6H|MAFF|TAF13|CDC73|SCD|MRPL14|POLR1C|MRPS16|RAD50|MRPS26|MRPS33|DEK|RPL23L|RBM4|CREB1|MRPS14|ENY2
GO Biological Process	GO:0071426	Ribonucleoprotein complex export from nucleus	7.4E-4	8	125	NUP107|THOC7|THOC6|CDC40|SRSF4|ZNF593|ALKBH5|ENY2
Reactome Pathways	HSA-72187	mRNA 3-end processing	8.4E-4	6	56	CSTF1|THOC7|CSTF3|THOC6|CDC40|SRSF4
GO Biological Process	GO:0044085	Cellular component biogenesis	0.0011	37	2583	C1QBP|NUP107|RRP9|COIL|RRP36|PPAN|HAUS8|RRP8|SMARCB1|ABT1|PATL1|TPX2|CHAF1A|BIRC5|TAF7|EXOSC3|SMCHD1|SRFBP1|RBM5|AKAP9|CDC73|CETN2|RCC1|ZNF593|BMS1|EXOSC10|NOL9|NAP1L4|NOL10|TMEM55B|KIFC1|HMGA1|EBNA1BP2|RRP1|CKAP5|NOL8|NAP1L1
Reactome Pathways	HSA-6791226	or pathway of rRNA processing in the nucleolus and cyto	0.0011	9	180	RRP9|RRP36|EXOSC3|NOL12|BMS1|EXOSC10|NOL9|EBNA1BP2|RRP1
GO Biological Process	GO:0044260	Cellular macromolecule metabolic process	0.0013	57	4976	KIF22|MRPS34|CSTF1|NUP107|MOGS|TERF2|MRPS18B|PHF3|SMARCB1|EED|HDAC4|ABT1|MTA2|METAP1|PHAX|PATL1|CHAF1A|BIRC5|GAA|TAF7|CSTF3|CHST13|SUPT6H|EXOSC3|UBE2O|METAP2|SMCHD1|MAFF|TAF13|CDC73|RNF2|NSMCE4A|CETN2|MRPL14|POLR1C|MRPS16|CMTR1|EXOSC10|CKAP4|RAD50|B3GALT6|MRPS26|AIPL1|TRMT61A|MRPS33|GPC3|DEK|RPL23L|ALKBH5|RBM4|CREB1|ACTL6A|HMGA1|VRK2|MRPS14|ENY2|NAP1L1
GO Biological Process	GO:2001251	Negative regulation of chromosome organization	0.0013	8	137	TERF2|SMARCB1|BIRC5|TAF7|SUPT6H|EXOSC10|RAD50|HMGA1
GO Biological Process	GO:0000398	mRNA splicing, via spliceosome	0.0014	11	294	GPATCH1|CSTF1|SF3B6|COIL|SNRNP40|CSTF3|RBM5|CDC40|SRSF4|RBM4|CHERP
Reactome Pathways	HSA-73856	RNA Polymerase II Transcription Termination	0.0015	6	65	CSTF1|THOC7|CSTF3|THOC6|CDC40|SRSF4
Reactome Pathways	HSA-8939243	ts with co-factors whose precise effect on RUNX1 target	0.0015	5	36	SMARCB1|SMARCE1|RNF2|SMARCD2|ACTL6A
GO Biological Process	GO:0006351	Transcription, dna-templated	0.0016	15	567	CSTF1|PHF3|SMARCB1|ABT1|PHAX|TAF7|CSTF3|SUPT6H|MAFF|TAF13|CDC73|POLR1C|DEK|CREB1|ENY2
GO Biological Process	GO:0071824	protein-DNA complex subunit organization	0.0022	10	255	SMARCB1|CHAF1A|TAF7|SUPT6H|SMARCE1|CETN2|NAP1L4|SMARCD2|HMGA1|NAP1L1
GO Biological Process	GO:0006406	mRNA export from nucleus	0.0023	7	109	NUP107|THOC7|THOC6|CDC40|SRSF4|ALKBH5|ENY2
GO Biological Process	GO:0031503	Protein-containing complex localization	0.0023	10	257	NUP107|TERF2|THOC7|BIRC5|THOC6|CDC40|SRSF4|ZNF593|ALKBH5|ENY2
WikiPathways	WP4204	Tumor suppressor activity of SMARCB1	0.0023	5	30	SMARCB1|EED|SMARCE1|SMARCD2|ACTL6A
GO Biological Process	GO:0006337	Nucleosome disassembly	0.0027	4	19	SMARCB1|SMARCE1|SMARCD2|HMGA1
GO Biological Process	GO:0006913	Nucleocytoplasmic transport	0.0027	10	263	NUP107|IPO8|THOC7|PHAX|THOC6|CDC40|SRSF4|ZNF593|ALKBH5|ENY2
GO Biological Process	GO:0006366	Transcription by rna polymerase ii	0.004	12	406	CSTF1|ABT1|PHAX|TAF7|CSTF3|SUPT6H|MAFF|TAF13|CDC73|DEK|CREB1|ENY2

GO Molecular Function	GO:0005488	Binding	0.0041	107	12516	KIF22|GPATCH1|CBX5|CSTF1|C1QBP|LRRC59|RRP9|SF3B6|COIL|RRP36|KLF16|PPAN|HAUS8|RRP8|TERF2|IPO8|PHF3|SMARCB1|EED|SNRNP40|HDAC4|MCCC1|ABT1|MTA2|C10orf12|SCAF4|THOC7|METAP1|PHAX|PATL1|TPX2|CHAF1A|BIRC5|CEBPB|GAA|TAF7|CSTF3|SUPT6H|GLYR1|EXOSC3|UBE2O|SMARCE1|METAP2|THOC6|SMCHD1|CCDC137|GATA4|LBR|SRFBP1|RBM5|ARID3B|MAFF|ZC3H7B|COL18A1|AKAP9|NOL12|TAF13|CDC73|RNF2|CDC40|CETN2|SCD|MRPL14|POLR1C|DNTTIP1|CMTR1|SRSF4|RCC1|ZNF593|BMS1|EXOSC10|NOL9|PCDH8|CKAP4|LRRC47|RAD50|MRPS26|NAP1L4|AIPL1|NOL10|ADNP|DEK|RPL23L|ALKBH5|PHF14|RBM4|CREB1|ATP2B1|KIFC1|ACTL6A|HMGA1|EBNA1BP2|VRK2|RRP1|PCCB|MRPS14|STMN2|ENY2|ZNF706|API5|CKAP5|CHERP|NOL8|CLTCL1|NAP1L1|DDX24|SMTN
GO Biological Process	GO:0000466	5.8s rrna from tricistronic rrna transcript (ssu-rrna, 5.8s	0.0049	4	23	ABT1|EXOSC3|EXOSC10|NOL9
GO Biological Process	GO:0030490	Maturation of ssu-rrna	0.0049	5	49	RRP36|ABT1|SRFBP1|BMS1|NOL10
Reactome Pathways	HSA-72163	mRNA Splicing - Major Pathway	0.0051	8	178	CSTF1|SF3B6|SNRNP40|CSTF3|RBM5|CDC40|SRSF4|CHERP
GO Biological Process	GO:0034728	Nucleosome organization	0.0053	8	176	SMARCB1|CHAF1A|SUPT6H|SMARCE1|NAP1L4|SMARCD2|HMGA1|NAP1L1
GO Molecular Function	GO:0031491	Nucleosome binding	0.0113	5	47	SUPT6H|GLYR1|DNTTIP1|RCC1|NAP1L4
GO Biological Process	GO:0010639	Negative regulation of organelle organization	0.0141	11	395	PPFIA1|TERF2|SMARCB1|TPX2|BIRC5|TAF7|SUPT6H|EXOSC10|RAD50|HMGA1|STMN2
GO Molecular Function	GO:0003712	Transcription coregulator activity	0.0145	14	571	C1QBP|SMARCB1|HDAC4|ABT1|MTA2|TAF7|SMARCE1|GATA4|TAF13|CREB1|SMARCD2|ACTL6A|HMGA1|ENY2
GO Biological Process	GO:0006357	Regulation of transcription by rna polymerase ii	0.0153	30	2172	CBX5|C1QBP|KLF16|SMARCB1|EED|HDAC4|ABT1|MTA2|C10orf12|SCAF4|CEBPB|TAF7|SUPT6H|GLYR1|SMARCE1|GATA4|ARID3B|MAFF|TAF13|CDC73|RNF2|ZNF593|ADNP|DEK|PHF14|CREB1|SMARCD2|ACTL6A|HMGA1|ENY2
GO Biological Process	GO:1901576	Organic substance biosynthetic process	0.0156	35	2734	MRPS34|CSTF1|MOGS|TERF2|MRPS18B|PHF3|SMARCB1|ABT1|PHAX|CHAF1A|TAF7|CSTF3|CHST13|SUPT6H|LBR|MAFF|TAF13|CDC73|SCD|MRPL14|POLR1C|MRPS16|RAD50|B3GALT6|MRPS26|MRPS33|GPC3|DEK|RPL23L|RBM4|CREB1|HMGA1|MRPS14|ENY2|NAP1L1
GO Biological Process	GO:0090501	RNA phosphodiester bond hydrolysis	0.0191	7	159	RRP36|ABT1|CSTF3|EXOSC3|BMS1|EXOSC10|NOL9
GO Biological Process	GO:0000462	ssu-rrna from tricistronic rrna transcript (ssu-rrna, 5.8s	0.0196	4	35	RRP36|ABT1|BMS1|NOL10
GO Biological Process	GO:0034622	Cellular protein-containing complex assembly	0.0198	16	816	NUP107|COIL|PPAN|SMARCB1|ABT1|TPX2|CHAF1A|TAF7|RBM5|AKAP9|CDC73|CETN2|NAP1L4|TMEM55B|CKAP5|NAP1L1
GO Biological Process	GO:0034654	Nucleobase-containing compound biosynthetic process	0.0198	18	995	CSTF1|TERF2|PHF3|SMARCB1|ABT1|PHAX|TAF7|CSTF3|SUPT6H|MAFF|TAF13|CDC73|SCD|POLR1C|RAD50|DEK|CREB1|ENY2
Reactome Pathways	HSA-159236	rt of Mature mRNA derived from an Intron-Containing Tr	0.0199	5	73	NUP107|THOC7|THOC6|CDC40|SRSF4
Reactome Pathways	HSA-212436	Generic Transcription Pathway	0.0199	20	1197	CBX5|SMARCB1|EED|HDAC4|MTA2|TPX2|CEBPB|TAF7|SMARCE1|GATA4|LBR|TAF13|RNF2|RAD50|DEK|TMEM55B|CREB1|SMARCD2|ACTL6A|ZNF706
Reactome Pathways	HSA-3108232	SUMO E3 ligases SUMOylate target proteins	0.0199	7	166	CBX5|NUP107|HDAC4|RNF2|NSMCE4A|CETN2|CDCA8
Reactome Pathways	HSA-72766	Translation	0.0199	9	289	MRPS34|MRPS18B|TRAM1|MRPL14|MRPS16|MRPS26|MRPS33|RPL23L|MRPS14
Reactome Pathways	HSA-8854518	AURKA Activation by TPX2	0.0199	5	72	HAUS8|TPX2|AKAP9|CETN2|CKAP5
GO Biological Process	GO:0010629	Negative regulation of gene expression	0.0223	28	2014	CBX5|C1QBP|KLF16|RRP8|TERF2|EED|HDAC4|MTA2|SCAF4|PATL1|BIRC5|CEBPB|TAF7|EXOSC3|SMARCE1|SMCHD1|ZC3H7B|CDC73|RNF2|SRSF4|EXOSC10|ADNP|PHF14|RBM4|CREB1|ATP2B1|HMGA1|ZNF706
GO Molecular Function	GO:0003713	Transcription coactivator activity	0.0238	10	316	SMARCB1|ABT1|MTA2|TAF7|SMARCE1|GATA4|SMARCD2|ACTL6A|HMGA1|ENY2
GO Biological Process	GO:0033044	Regulation of chromosome organization	0.0261	10	359	TERF2|SMARCB1|EED|BIRC5|TAF7|SUPT6H|GLYR1|EXOSC10|RAD50|HMGA1
GO Biological Process	GO:0016043	Cellular component organization	0.0265	56	5447	KIF22|MRPS34|C1QBP|NUP107|COIL|PPAN|HAUS8|PPFIA1|RRP8|TERF2|MRPS18B|SMARCB1|EED|HDAC4|ABT1|MTA2|PATL1|TPX2|CHAF1A|BIRC5|GAA|TAF7|SUPT6H|SMARCE1|SMCHD1|RBM5|COL18A1|AKAP9|CDC73|RNF2|CETN2|MRPL14|MRPS16|CDCA8|MAP7D1|RCC1|RAD50|MRPS26|NAP1L4|MRPS33|ADNP|DEK|RPL23L|TMEM55B|CREB1|SMARCD2|KIFC1|ACTL6A|HMGA1|MRPS14|STMN2|ENY2|CKAP5|CLTCL1|NAP1L1|SMTN
GO Biological Process	GO:0044249	Cellular biosynthetic process	0.0295	33	2611	MRPS34|CSTF1|MOGS|TERF2|MRPS18B|PHF3|SMARCB1|ABT1|PHAX|CHAF1A|TAF7|CSTF3|CHST13|SUPT6H|MAFF|TAF13|CDC73|SCD|MRPL14|POLR1C|MRPS16|RAD50|B3GALT6|MRPS26|MRPS33|DEK|RPL23L|RBM4|CREB1|HMGA1|MRPS14|ENY2|NAP1L1
GO Biological Process	GO:0000479	ic cleavage of tricistronic rrna transcript (ssu-rrna, 5.8s	0.0301	3	15	ABT1|BMS1|NOL9
GO Biological Process	GO:0045934	regulation of nucleobase-containing compound metabol	0.0301	23	1528	CBX5|C1QBP|KLF16|RRP8|TERF2|EED|HDAC4|MTA2|SCAF4|BIRC5|CEBPB|TAF7|SMARCE1|SMCHD1|CDC73|RNF2|SRSF4|EXOSC10|RAD50|PHF14|CREB1|HMGA1|ZNF706
GO Biological Process	GO:0006996	Organelle organization	0.031	40	3450	KIF22|C1QBP|NUP107|PPAN|HAUS8|RRP8|TERF2|SMARCB1|EED|HDAC4|ABT1|MTA2|PATL1|TPX2|CHAF1A|BIRC5|GAA|SUPT6H|SMARCE1|SMCHD1|AKAP9|CDC73|RNF2|CETN2|CDCA8|MAP7D1|RCC1|RAD50|NAP1L4|DEK|CREB1|SMARCD2|KIFC1|ACTL6A|HMGA1|STMN2|ENY2|CKAP5|NAP1L1|SMTN
GO Biological Process	GO:0044403	Symbiotic process	0.0333	16	865	CBX5|C1QBP|NUP107|TRAM1|SMARCB1|EED|THOC7|SUPT6H|THOC6|ZC3H7B|RCC1|RAD50|DEK|CREB1|HMGA1|VRK2
GO Biological Process	GO:0007052	Mitotic spindle organization	0.0358	5	81	TPX2|BIRC5|RCC1|KIFC1|CKAP5
GO Biological Process	GO:0019219	lation of nucleobase-containing compound metabolic pr	0.0376	44	3982	CBX5|C1QBP|NUP107|KLF16|RRP8|TERF2|SMARCB1|EED|HDAC4|ABT1|MTA2|C10orf12|SCAF4|BIRC5|CEBPB|TAF7|SUPT6H|GLYR1|EXOSC3|SMARCE1|SMCHD1|GATA4|RBM5|ARID3B|MAFF|TAF13|CDC73|RNF2|SRSF4|ZNF593|EXOSC10|RAD50|ADNP|DEK|ALKBH5|PHF14|RBM4|CREB1|SMARCD2|ACTL6A|HMGA1|ENY2|ZNF706|NOL8
Reactome Pathways	HSA-3214858	RMTs methylate histone arginines	0.0385	4	49	SMARCB1|SMARCE1|SMARCD2|ACTL6A
GO Molecular Function	GO:0003735	Structural constituent of ribosome	0.04	7	159	MRPS34|MRPS18B|MRPL14|MRPS16|MRPS33|RPL23L|MRPS14
GO Biological Process	GO:2000113	tive regulation of cellular macromolecule biosynthetic pr	0.0416	22	1470	CBX5|C1QBP|KLF16|RRP8|TERF2|EED|HDAC4|MTA2|SCAF4|BIRC5|CEBPB|TAF7|SMARCE1|SMCHD1|CDC73|RNF2|EXOSC10|PHF14|RBM4|CREB1|HMGA1|ZNF706
GO Molecular Function	GO:0042393	Histone binding	0.0441	8	221	CBX5|RRP8|SUPT6H|GLYR1|RCC1|NAP1L4|DEK|NAP1L1
GO Biological Process	GO:0051225	Spindle assembly	0.0489	5	88	HAUS8|TPX2|BIRC5|RCC1|KIFC1

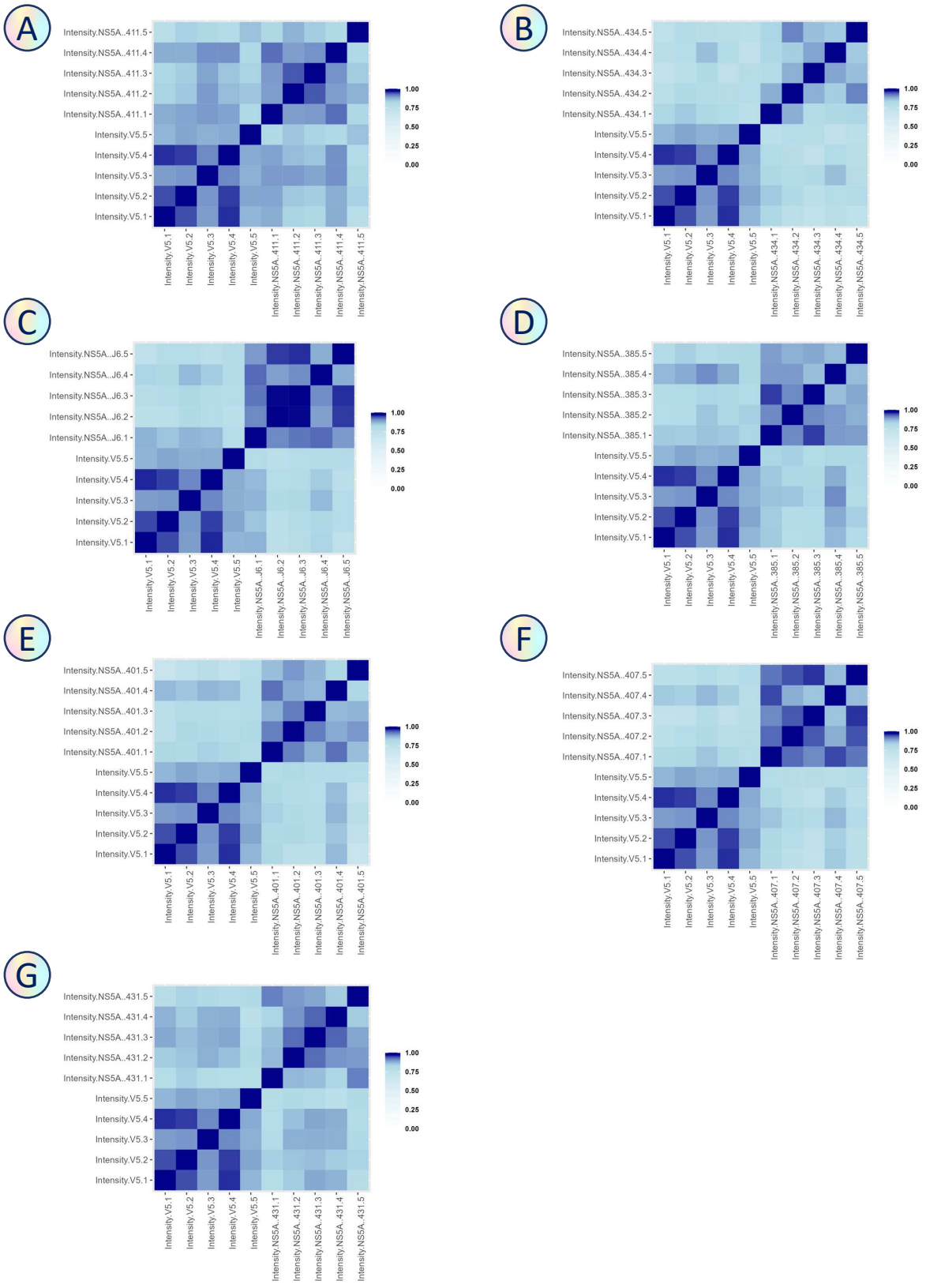

Supplementary Figure 1: Pearson correlation of different tagged NS5A isoforms replicate samples and differential analysis of retrieved proteins.

Quality control correlation matrix based on Pearson correlation coefficient among ST replicate samples and V5 replicate samples, with the tag insertion downstream of amino acid 418.

Supplementary Table 7: List of PPIs retrieved using tagged NS5A proteins of diverse genotypic origins as baits.

	statistical Score							MiST Score							SAINT Score							Final Score									Jad NSSA comparison	
Gene name	411	434	J6	385	401	407	431	411	434	j6	385	401	407	431	411	434	j6	385	401	407	431	411	434	j6	385	401	407	431	Sum of scores	Number of NS5A baits	Final Score	Jad Bait	Final Score Jad
MED19	0	0	1	1	1	1	0	0	0	0	0	0	0	0	0	0	0	0	0	0	0			1	1	1	1		4	4	1,00	0	0
Core	1,5	1,5	1,5	0	1,5	1,5	1,5	1	1	1	0	1	1	1	1	1	1	0	1	1	1	3,5	3,5	3,5		3,5	3,5	3,5	21	6	3,50	0	0
E2	0	1,5	1,5	0	0	0	0	1	1	1	0	0	0	1	0	0	0	0	0	0	0		2,5	2,5					5	2	2,50	449	4
NS2	1	1	1	0	1	1	1	0	0	0	0	0	0	0	1	1	1	0	1	1	1	2	2	2		2	2	2	12	6	2,00	0	0
NS3	1	1	1	0	0	0	1	0	0	0	0	0	0	0	1	1	1	0	0	0	1	2	2	2				2	8	4	2,00	BOTH	4
NS3_3a_385_401_407	0	0	0	1,5	1,5	1,5	0	0	0	0	1	1	1	0	0	0	0	1	1	1	0				3,5	3,5	3,5		10,5	3	3,50	0	0
NS4B_385_401_431;NS4B	1,5	1,5	1,5	0	1,5	0	1,5	1	1	1	1	1	1	1	1	1	1	0	1	0	1	3,5	3,5	3,5		3,5		3,5	17,5	5	3,50	0	0
NS4B_407	0	0	0	0	0	1,5	0	0	0	0	0	0	1	0	0	0	0	0	0	0	0						2,5		2,5	1	2,50	0	0
NS5A_Jad/NS5A(TEV)-ST-418-385	0	0	0	1	0	0	0	0	0	0	1	0	0	0	0	0	0	1	0	0	0				3				3	1	3,00	0	0
NS5A_Jad/NS5A(TEV)-ST-418-401	0	0	0	0	1,5	1,5	0	0	0	0	1	1	1	0	0	0	0	0	1	1	0					3,5	3,5		7	2	3,50	0	0
NS5A_Jad/NS5A(TEV)-ST-418-407	0	0	0	1	1	1	0	0	0	0	1	1	1	0	0	0	0	1	1	1	0				3	3	3		9	3	3,00	0	0
NS5A_Jad/NS5A(TEV)-ST-418-431	0	0	0	0	0	0	1,5	0	0	0	0	0	0	1	0	0	0	0	0	0	1							3,5	3,5	1	3,50	0	0
NS5A_Jad/NS5A(TEV)-ST-418-434	1	1	0	0	0	0	1	1	1	0	0	0	1	1	1	1	0	0	0	0	1	3	3					3	9	3	3,00	0	0
NS5A_Jad/NS5A(TEV)-ST-418-J6	0	0	1,5	0	0	0	0	0	0	1	0	0	0	0	0	0	1	0	0	0	0			3,5					3,5	1	3,50	0	0
NS5A_Jad/NS5A(TEV)-V5-418-411;NS5A_Jad/NS5A(TEV)-ST-418-411	1,5	0	0	0	0	0	0	1	0	0	0	0	0	0	1	0	0	0	0	0	0	3,5							3,5	1	3,50	0	0
NS5B	1	1	1	1	1	1	1	0	0	0	0	0	0	0	1	1	1	1	1	1	1	2	2	2	2	2	2	2	14	7	2,00	BOTH	5
AGPS	0	1,5	1,5	0	1,5	1,5	0	0	1	1	1	1	1	1	0	0	0	0	0	0	0		2,5	2,5		2,5	2,5		10	4	2,50	BOTH	4
PSMD11	1,5	1,5	1,5	0	1,5	1,5	1,5	1	1	1	1	1	1	1	0	0	0	0	0	0	0	2,5	2,5	2,5		2,5	2,5	2,5	15	6	2,50	BOTH	4
PGRMC1	0	1,5	1,5	1,5	1,5	1,5	1,5	0	1	1	1	1	1	1	0	0	0	0	0	0	0		2,5	2,5	2,5	2,5	2,5	2,5	15	6	2,50	BOTH	4
IPO5	1,5	0	0	0	1,5	1,5	1,5	1	1	1	1	1	1	1	0	0	0	0	0	0	0	2,5				2,5	2,5	2,5	10	4	2,50	BOTH	3
IGF2BP3	1,5	1,5	1,5	1,5	1,5	1,5	1,5	1	1	1	1	1	1	1	0	1	1	1	1	1	1	2,5	3,5	3,5	3,5	3,5	3,5	3,5	23,5	7	3,36	BOTH	3
HMGN4	0	0	0	0	0	0	1	0	0	0	0	0	0	0	0	0	0	0	0	0	0							1	1	1	1,00	0	0
PSMD14	0	0	1,5	1,5	0	0	0	1	1	1	1	1	1	1	0	0	0	0	0	0	0			2,5	2,5				5	2	2,50	0	0
BIN1	1,5	1,5	1,5	1,5	1,5	1,5	1,5	1	1	1	1	1	1	1	1	1	1	1	1	1	1	3,5	3,5	3,5	3,5	3,5	3,5	3,5	24,5	7	3,50	BOTH	6
DDX3X;DDX3Y	0	0	0	1	1	0	1	0	0	0	0	0	0	0	0	0	0	0	0	0	0					1	1	1	3	3	1,00	0	0
SCD	0	1	1	0	1	1	1	0	0	0	0	0	0	0	0	0	0	0	0	0	0		1	1		1	1	1	5	5	1,00	0	0
TCERG1	0	0	1	0	0	0	0	0	0	0	0	0	0	0	0	0	0	0	0	0	0			1					1	1	1,00	0	0
PSMA7;PSMA8	0	0	0	0	0	1,5	0	0	1	1	0	1	1	0	0	0	0	0	0	0	0						2,5		2,5	1	2,50	0	0
SCAMP3	1,5	1,5	1,5	0	1,5	1,5	0	1	1	1	1	1	1	1	0	0	0	0	0	0	0	2,5	2,5	2,5		2,5	2,5		12,5	5	2,50	BOTH	4,5
PHYH	1,5	1,5	1,5	0	1,5	1,5	0	1	1	1	1	1	1	0	0	0	0	0	0	0	0	2,5	2,5	2,5		2,5	2,5		12,5	5	2,50	0	0
TIMM23;TIMM23B	0	0	0	0	1,5	0	0	0	0	1	1	1	1	1	0	0	0	0	0	0	0					2,5			2,5	1	2,50	0	0
XPO1	0	1,5	1,5	0	1,5	1,5	1,5	1	1	1	1	1	1	1	0	0	0	0	0	0	0		2,5	2,5		2,5	2,5	2,5	12,5	5	2,50	BOTH	4
U2SURP	1	1	1	1	1	1	0	0	0	0	0	0	0	0	0	1	0	0	0	0	0	1	2	1	1	1	1		7	6	1,17	0	0
PGRMC2	0	1,5	1,5	0	0	0	0	0	1	1	0	1	1	0	0	0	0	0	0	0	0		2,5	2,5					5	2	2,50	0	0
SURF4	0	0	1,5	0	1,5	0	0	0	0	1	1	1	0	0	0	0	0	0	0	0	0			2,5		2,5			5	2	2,50	0	0
SPTLC1	0	0	0	0	1,5	0	0	1	0	0	0	1	1	1	0	0	0	0	0	0	0					2,5			2,5	1	2,50	0	0
STX7	1,5	1,5	1,5	1,5	1,5	1,5	1,5	1	1	1	1	1	1	1	0	0	0	0	0	0	0	2,5	2,5	2,5	2,5	2,5	2,5	2,5	17,5	7	2,50	BOTH	4
MAGEB2	0	0	1,5	0	1,5	0	0	1	0	1	1	1	1	1	0	0	0	0	0	0	0			2,5		2,5			5	2	2,50	0	0
CYB5B	0	0	1,5	0	1,5	1,5	1,5	1	1	1	1	1	1	1	0	0	1	0	0	1	1			3,5		2,5	3,5	3,5	13	4	3,25	0	0
PHGDH	1	1	1	1	1	1	1	0	0	0	0	0	0	0	0	1	1	0	1	1	1	1	2	2	1	2	2	2	12	7	1,71	BOTH	2
PSMD3	0	0	0	0	0	1,5	0	0	0	1	0	1	1	1	0	0	0	0	0	0	0						2,5		2,5	1	2,50	0	0
SART1	0	0	0	0	0	0	1	0	0	0	0	0	0	0	0	0	0	0	0	0	0							1	1	1	1,00	0	0
EEF1E1	0	1,5	1,5	1,5	0	1,5	1,5	0	1	1	1	1	1	1	0	0	0	0	0	0	0		2,5	2,5	2,5		2,5	2,5	12,5	5	2,50	0	0
B4GAT1	0	0	1,5	1,5	1,5	1,5	0	0	1	1	1	1	1	1	0	0	0	0	0	0	0			2,5	2,5	2,5	2,5		10	4	2,50	BOTH	4
TRAF3IP2	1,5	0	0	1,5	0	0	0	1	0	0	1	1	0	0	0	0	0	0	0	0	0	2,5			2,5				5	2	2,50	0	0
SLC25A20	0	0	1,5	0	1,5	0	0	0	1	1	1	1	1	1	0	0	0	0	0	0	0			2,5		2,5			5	2	2,50	449	2
ACSL4	1,5	1,5	1,5	1,5	1,5	1,5	1,5	1	1	1	1	1	1	1	0	1	1	1	1	1	1	2,5	3,5	3,5	3,5	3,5	3,5	3,5	23,5	7	3,36	BOTH	5
SYNCRIP	0	1	0	0	1	0	0	0	0	0	0	0	0	0	0	0	0	0	0	0	0		1			1			2	2	1,00	0	0
UGDH	1	1	1	1	1	1	1	0	0	0	0	0	0	0	1	1	1	0	1	1	1	2	2	2	1	2	2	2	13	7	1,86	BOTH	4
DNAJA2	0	0	1	0	1	0	1	0	0	1	0	0	1	1	0	0	1	0	0	0	0			3		1		2	6	3	2,00	418	2
SEC22B	0	1,5	1,5	1,5	1,5	1,5	1,5	0	1	1	1	1	1	1	0	0	0	0	0	0	0		2,5	2,5	2,5	2,5	2,5	2,5	15	6	2,50	BOTH	3

MTX2	0	1,5	1,5	0	1,5	0	0	0	1	1	0	1	1	0	0	0	0	0	0	0	0		2,5	2,5		2,5			7,5	3	2,50	0	0
ERLIN1;ERLIN2	0	0	0	1,5	0	0	0	1	0	1	1	1	1	1	0	0	0	0	0	0	0				2,5				2,5	1	2,50	0	0
NDUFS3	0	1	1	0	1	1	1	0	1	1	0	0	1	1	0	1	1	0	1	1	1		3	3		2	3	3	14	5	2,80	BOTH	5,5
SF3B1	1	1	0	0	1	1	0	0	0	0	0	0	0	0	0	1	0	0	1	1	0	1	2			2	2		7	4	1,75	0	0
GCAT	0	0	0	0	0	1,5	0	0	0	0	0	1	1	0	0	0	0	0	0	0	0						2,5		2,5	1	2,50	0	0
ZMPSTE24	0	1,5	0	0	1,5	1,5	1,5	0	1	1	1	1	1	1	0	0	0	0	0	0	0		2,5			2,5	2,5	2,5	10	4	2,50	BOTH	3
IDH1	0	1	0	1	1	1	0	0	1	0	1	1	1	1	0	1	0	0	0	1	0		3		2	2	3		10	4	2,50	0	0
ATP5H	0	1,5	1,5	0	1,5	1,5	1,5	1	1	1	0	1	1	1	0	0	0	0	0	0	0		2,5	2,5		2,5	2,5	2,5	12,5	5	2,50	BOTH	2
ATP5L	1,5	1,5	1,5	1,5	1,5	1,5	1,5	1	1	1	1	1	1	1	0	0	0	0	1	1	0	2,5	2,5	2,5	2,5	3,5	3,5	2,5	19,5	7	2,79	BOTH	3
CLPX	0	0	0	0	0	0	1	0	0	0	0	0	0	0	0	0	0	0	0	0	0							1	1	1	1,00	BOTH	2
USP1	0	0	1,5	0	0	0	0	0	0	1	0	0	0	0	0	0	0	0	0	0	0				2,5				2,5	1	2,50	0	0
TOMM70A	0	1,5	1,5	1,5	1,5	1,5	1,5	1	1	1	1	1	1	1	0	0	1	0	1	1	0		2,5	3,5	2,5	3,5	3,5	2,5	18	6	3,00	BOTH	5,5
NDUFB4	0	1	0	1	0	1	0	0	0	0	0	0	0	0	0	0	0	0	0	0	0		1		1		1		3	3	1,00	BOTH	2
GOSR1	0	0	1,5	0	0	0	0	0	1	1	0	0	1	0	0	0	0	0	0	0	0			2,5					2,5	1	2,50	BOTH	4,5
VAPB	1,5	1,5	1,5	1,5	1,5	1,5	1,5	1	1	1	1	1	1	1	0	1	1	0	1	1	1	2,5	3,5	3,5	2,5	3,5	3,5	3,5	22,5	7	3,21	BOTH	4
NDUFA10	0	0	0	0	1,5	0	1,5	0	1	0	0	1	1	1	0	0	0	0	0	0	0					2,5		2,5	5	2	2,50	BOTH	3
PIGN	1,5	0	0	1,5	0	0	1,5	1	0	1	1	1	1	1	0	0	0	0	0	0	0	2,5			2,5			2,5	7,5	3	2,50	0	0
ACSL3	1	1	1	1	1	1	1	0	0	0	0	0	0	0	1	1	1	0	1	1	1	2	2	2	1	2	2	2	13	7	1,86	BOTH	4
LATS1	0	1,5	0	0	1,5	0	0	0	1	0	0	1	0	0	0	0	0	0	0	0	0		2,5			2,5			5	2	2,50	0	0
FADS2	1	1	1	1	1	1	1	0	0	0	0	0	0	0	1	1	1	0	1	1	1	2	2	2	1	2	2	2	13	7	1,86	BOTH	2
NDUFB10	0	0	1	0	0	1	1	0	0	0	0	0	0	0	0	0	0	0	0	0	0				1		1	1	3	3	1,00	BOTH	4,5
TOMM40	0	1,5	1,5	0	1,5	0	1,5	1	1	1	1	1	1	1	0	0	0	0	0	0	0		2,5	2,5		2,5		2,5	10	4	2,50	BOTH	6
PAK4	0	1,5	0	1,5	0	0	0	0	1	0	1	0	1	0	0	0	0	0	0	0	0		2,5		2,5				5	2	2,50	0	0
LDHA	0	0	0	0	1	1	1	0	0	0	0	0	0	0	0	0	0	0	0	0	0					1	1	1	3	3	1,00	0	0
ALDH1A1	0	0	0	1	0	1	0	0	0	0	0	0	0	0	0	0	0	0	0	0	0				1		1		2	2	1,00	0	0
GLUD1;GLUD2	1	1	1	0	1	0	0	0	0	0	0	0	0	0	0	1	0	0	0	0	0	1	2	1		1			5	4	1,25	0	0
CYB5R3	1	1	1	1	1	1	1	0	0	0	0	0	0	0	1	1	1	1	1	1	1	2	2	2	2	2	2	2	14	7	2,00	BOTH	4
MT-CO2	1	1	1	1	1	1	1	1	1	1	1	1	1	1	0	1	1	1	0	1	1	2	3	3	3	2	3	3	19	7	2,71	BOTH	3
PAH	0	1,5	0	0	1,5	0	1,5	0	1	0	0	1	1	1	0	0	0	0	0	0	0		2,5			2,5		2,5	7,5	3	2,50	BOTH	3
PGK1	1	0	0	1	1	1	0	0	0	0	0	0	0	0	0	0	0	1	1	1	0	1			2	2	2		7	4	1,75	0	0
MT-ATP6	0	1,5	1,5	0	1,5	1,5	0	0	1	1	1	1	1	1	0	0	0	0	0	0	0		2,5	2,5		2,5	2,5		10	4	2,50	418	4
IGF2	0	0	0	0	1	0	0	0	0	1	0	1	1	1	0	0	0	0	0	0	0					2			2	1	2,00	0	0
APOE	0	0	1,5	0	1,5	0	0	0	1	1	0	1	1	0	0	0	1	0	0	0	0			3,5		2,5			6	2	3,00	BOTH	5,5
AFP	0	0	0	0	1,5	0	0	0	0	0	0	1	1	1	0	0	0	0	0	0	0					2,5			2,5	1	2,50	0	0
TFRC	1,5	1,5	1,5	1,5	1,5	1,5	1,5	1	1	1	1	1	1	1	0	1	1	0	1	1	0	2,5	3,5	3,5	2,5	3,5	3,5	2,5	21,5	7	3,07	BOTH	5
ALDOA	0	0	0	1,5	1,5	0	0	1	0	1	1	1	1	0	0	0	0	0	0	0	0				2,5	2,5			5	2	2,50	0	0
TUBB4A	0	0	1,5	1,5	1,5	1,5	0	0	0	0	0	0	0	0	0	0	0	0	0	0	0				1,5	1,5	1,5	1,5	6	4	1,50	418	4
HSPB1	0	1	1	0	1	1	1	0	0	0	0	0	0	0	0	0	0	0	0	0	0		1	1		1	1	1	5	5	1,00	0	0
RPN1	1	1	1	1	1	1	1	0	0	0	0	0	0	0	1	1	1	1	1	1	1	2	2	2	2	2	2	2	14	7	2,00	BOTH	2
RPN2	1	1	1	1	1	1	1	0	0	0	0	0	0	0	1	1	1	1	1	1	1	2	2	2	2	2	2	2	14	7	2,00	BOTH	2
ATP1A1	1	1	1	1	1	1	1	0	0	0	0	0	0	0	1	1	1	1	1	1	1	2	2	2	2	2	2	2	14	7	2,00	BOTH	2
ATP1B1	0	0	1,5	0	0	1,5	1,5	1	1	1	1	1	1	1	0	0	0	0	0	0	0				2,5			2,5	7,5	3	2,50	0	0
EIF2S1	0	0	1	0	0	0	1	0	0	1	0	0	0	0	0	0	0	0	0	0	1				2			2	4	2	2,00	418	4
RPLP1	0	1	1	0	0	1	1	1	1	1	1	0	0	1	0	0	0	0	0	0	1		2	2			1	3	8	4	2,00	0	0
RPLP2	0	0	0	0	0	0	1	1	1	0	0	1	1	1	0	0	0	0	0	0	0							2	2	1	2,00	418	6
ITGB1	0	0	1,5	0	1,5	1,5	1,5	0	1	1	0	1	1	1	0	0	0	0	0	0	0			2,5		2,5	2,5	2,5	10	4	2,50	BOTH	6
CDK1	1	0	1	0	1	1	1	0	0	0	0	0	0	0	1	0	1	0	1	1	0	2		2		2	2	1	9	5	1,80	0	0
ATP5B	1	1	1	1	1	1	1	0	0	0	0	0	0	0	0	1	1	1	1	1	1	1	2	2	2	2	2	2	13	7	1,86	449	2
ENO1	0	0	0	1	1	1	0	0	0	0	0	0	0	0	0	0	0	0	0	0	0					1	1	1	3	3	1,00	0	0
GPI	0	0	0	0	1,5	0	0	0	0	0	0	0	1	0	0	0	0	0	0	0	0					2,5			2,5	1	2,50	0	0
P4HB	0	0	1,5	0	0	0	1,5	1	1	1	0	1	0	1	0	0	0	0	0	0	0			2,5				2,5	5	2	2,50	418	4
ASGR1	0	0	0	0	1,5	0	0	0	0	0	0	0	1	1	0	0	0	0	0	0	0					2,5			2,5	1	2,50	0	0
TUBB	1	1	1	1	1	1	1	0	0	0	0	0	0	0	0	0	0	0	0	1	0	1	1	1	1	1	2	1	8	7	1,14	418	2
PFN1	0	0	0	1	0	0	0	0	0	0	0	0	0	0	0	0	0	0	0	0	0					1			1	1	1,00	0	0
EPRS	0	1,5	0	0	1,5	1,5	1,5	0	1	0	0	1	1	1	0	0	0	0	0	0	0		2,5			2,5	2,5	2,5	10	4	2,50	BOTH	2
HSP90AA1	1,5	1,5	1,5	0	1,5	1,5	1,5	1	1	1	1	1	1	1	0	0	0	0	0	0	0	2,5	2,5	2,5		2,5	2,5	2,5	15	6	2,50	BOTH	2
RHOC;RHOA	1,5	1,5	1,5	0	1,5	1,5	1,5	1	1	1	1	1	1	1	0	1	0	0	0	0	0	2,5	3,5	2,5		2,5	2,5	2,5	16	6	2,67	0	0
SLC3A2	1	1	1	1	1	1	1	0	0	0	0	0	0	0	1	1	1	1	1	1	1	2	2	2	2	2	2	2	14	7	2,00	BOTH	4
HSP90AB1	1	1	1	1	1	1	1	0	0	0	0	0	0	0	1	1	1	1	1	1	1	2	2	2	2	2	2	2	14	7	2,00	BOTH	2
SRPR	0	0	1	0	1	1	1	0	1	1	0	0	1	1	0	0	0	0	0	1	0				2		1	3	8	4	2,00	BOTH	4
CYC1	1,5	1,5	1,5	0	1,5	1,5	0	1	1	1	1	1	1	1	0	0	0	0	0	0	0	2,5	2,5	2,5		2,5	2,5		12,5	5	2,50	BOTH	4
ACAA1	1,5	0	0	0	1,5	1,5	1,5	1	1	1	1	1	1	1	0	0	0	0	0	0	0	2,5				2,5	2,5	2,5	10	4	2,50	0	0

CNP	0	0	0	0	0	0	1,5	1	1	1	0	1	1	1	0	0	0	0	0	0	0							2,5	2,5	1	2,50	0	0
HNRNPA1	0	1	0	0	0	0	0	0	0	0	0	0	0	0	0	0	0	0	0	0	0		1							1	1	1,00	0	0
PARP1	0	1	0	0	0	0	0	0	0	0	0	0	0	0	0	0	0	0	0	0	0		1							1	1	1,00	0	0
HSPA1B;HSPA1A	1	1	1	1	1	1	1	0	0	0	0	0	0	0	1	1	1	1	1	1	1	2	2	2	2	2	2	2	14	7	2,00	BOTH	2
U2AF1	0	0	0	0	0	0	1	0	0	0	0	0	0	0	0	0	0	0	0	0	0							1	1	1	1,00	0	0
TXN	0	0	0	0	1	0	0	0	0	0	0	0	0	0	0	0	0	0	0	0	0					1				1	1	1,00	0	0
COX5B	0	1,5	1,5	0	1,5	1,5	1,5	1	1	1	1	1	1	1	0	0	0	0	0	0	0		2,5	2,5		2,5	2,5	2,5	12,5	5	2,50	BOTH	4
MGST1	1,5	1,5	1,5	1,5	1,5	1,5	1,5	1	1	1	1	1	1	1	0	1	1	0	1	1	1	2,5	3,5	3,5	2,5	3,5	3,5	3,5	22,5	7	3,21	BOTH	3
HSPD1	1	1	1	1	1	1	1	0	0	0	0	0	0	0	0	1	1	1	1	1	1	1	2	2	2	2	2	2	13	7	1,86	BOTH	2
HSPA5	1	1	1	1	1	1	1	0	0	0	0	0	0	0	0	1	0	0	0	0	0	1	2	1	1	1	1	1	8	7	1,14	0	0
HSPA8	1	1	1	0	0	0	1	0	0	0	0	0	0	0	0	0	0	0	0	0	0	1	1	1				1	4	4	1,00	0	0
RALA	0	1,5	1,5	0	1,5	0	1,5	1	1	1	0	1	1	1	0	0	0	0	0	0	0		2,5	2,5		2,5		2,5	10	4	2,50	0	0
PC	0	0	0	0	0	1	0	0	0	0	0	0	0	0	0	0	0	0	0	0	0						1		1	1	1,00	0	0
PABPC1	1	1	1	1	1	1	1	0	0	0	0	0	0	0	1	1	1	1	1	1	1	2	2	2	2	2	2	2	14	7	2,00	BOTH	2
XRCC5	1,5	1,5	0	0	0	0	0	1	1	1	0	0	0	1	0	0	0	0	0	0	0	2,5	2,5						5	2	2,50	0	0
COX4I1	1,5	1,5	1,5	1,5	1,5	1,5	1,5	1	1	1	1	1	1	1	0	1	1	0	1	0	0	2,5	3,5	3,5	2,5	3,5	2,5	2,5	20,5	7	2,93	BOTH	4
EEF2	0	1	0	1	1	1	0	0	0	0	0	0	0	0	0	0	0	0	0	0	0		1		1	1	1		4	4	1,00	0	0
ETFA	1	1	1	1	1	1	1	0	0	0	0	0	0	0	0	1	0	1	0	0	0	1	2	1	2	1	1	1	9	7	1,29	BOTH	2
MIF	0	0	0	0	0	1	0	0	0	0	0	0	0	0	0	0	0	0	0	0	0						1		1	1	1,00	418	6
PKM	1	1	1	0	1	1	0	0	0	0	0	0	0	0	0	0	0	0	0	0	0	1	1	1		1	1		5	5	1,00	0	0
HSP90B1	1,5	1,5	1,5	0	1,5	1,5	1,5	1	1	1	1	1	1	1	0	0	0	0	0	0	0	2,5	2,5	2,5		2,5	2,5	2,5	15	6	2,50	BOTH	5
COX6B1	0	0	0	0	1	0	0	1	1	1	1	1	1	1	0	0	0	0	0	0	0					2			2	1	2,00	0	0
HNRNPL	0	0	0	1	1	0	0	0	0	0	0	0	0	0	0	0	0	1	1	0	0					2	2		4	2	2,00	0	0
RPS2	0	1	1	1	1	1	1	0	0	0	0	0	0	0	0	0	0	0	0	0	0		1	1	1	1	1	1	6	6	1,00	0	0
CREB1;ATF1	0	0	0	0	1,5	1,5	0	1	1	0	0	1	1	1	0	0	0	0	0	0	0						2,5	2,5	5	2	2,50	0	0
POR	1,5	1,5	1,5	1,5	1,5	1,5	1,5	1	1	1	1	1	1	1	0	1	1	0	1	1	0	2,5	3,5	3,5	2,5	3,5	3,5	2,5	21,5	7	3,07	BOTH	4
ATP2A2	1	1	1	1	1	1	1	0	0	0	0	0	0	0	1	1	1	1	1	1	1	2	2	2	2	2	2	2	14	7	2,00	BOTH	2
STMN1	0	0	1,5	1,5	0	1,5	0	0	1	1	1	0	1	0	0	0	0	0	0	0	0				2,5	2,5		2,5		7,5	3	2,50	0	0
HSPA6;HSPA7	0	1	1	0	1	0	1	0	0	0	0	0	0	0	0	0	0	0	0	0	0		1	1		1		1	4	4	1,00	0	0
UBTF	0	1,5	0	0	0	0	1,5	1	1	1	0	1	1	1	0	0	0	0	0	0	0		2,5					2,5	5	2	2,50	0	0
CTPS1	0	1	0	0	0	1	0	0	1	0	0	0	0	0	0	1	0	0	0	0	0		3				1		4	2	2,00	0	0
PSMC3	1,5	1,5	1,5	1,5	1,5	1,5	1,5	1	1	1	1	1	1	1	0	0	0	0	0	0	0	2,5	2,5	2,5	2,5	2,5	2,5	2,5	17,5	7	2,50	0	0
TCP1	1	1	0	1	1	1	1	0	0	0	0	0	0	0	0	1	0	0	1	0	0	1	2		1	2	1	1	8	6	1,33	BOTH	2
ARF4;ARF1;ARF3	0	1,5	1,5	1,5	0	0	1,5	0	0	0	0	0	0	0	0	0	0	0	0	0	0		1,5	1,5	1,5			1,5	6	4	1,50	0	0
RPL17	0	1	0	0	0	0	0	0	0	0	0	0	0	0	0	0	0	0	0	0	0		1						1	1	1,00	0	0
ATP5J	0	0	0	1,5	1,5	1,5	0	0	1	0	1	1	1	0	0	0	0	0	0	0	0				2,5	2,5	2,5		7,5	3	2,50	449	2
NDUFV2	0	1,5	1,5	0	1,5	1,5	1,5	0	1	1	1	1	1	1	0	0	0	0	0	0	0		2,5	2,5		2,5	2,5	2,5	12,5	5	2,50	0	0
ERCC3	1,5	1,5	0	0	1,5	0	0	1	1	0	0	1	1	0	0	1	0	0	0	0	0	2,5	3,5			2,5			8,5	3	2,83	0	0
ATP2B1	0	0	1,5	0	1,5	1,5	0	1	1	1	1	1	1	1	0	0	0	0	0	0	0			2,5		2,5	2,5		7,5	3	2,50	BOTH	3
RAB4A;RAB4B	1,5	1,5	0	0	0	0	1,5	1	1	0	1	0	1	1	0	0	0	0	0	0	0	2,5	2,5					2,5	7,5	3	2,50	0	0
RAB5A	0	1,5	1,5	0	1,5	1,5	1,5	1	1	1	1	1	1	1	0	0	0	0	0	0	0		2,5	2,5		2,5	2,5	2,5	12,5	5	2,50	0	0
RAB6A;RAB6B	0	1,5	1,5	0	0	1,5	1,5	0	0	0	0	0	0	0	0	1	1	0	0	1	1		2,5	2,5			2,5	2,5	10	4	2,50	449	2
COX5A	0	0	1,5	0	1,5	1,5	1,5	0	1	1	0	1	1	1	0	0	0	0	1	0	0			2,5		3,5	2,5	2,5	11	4	2,75	BOTH	5
LMNB1	1	0	0	0	0	0	0	0	0	0	0	0	0	0	0	0	0	0	0	0	0	1							1	1	1,00	0	0
VDAC1	1	1	1	1	1	1	1	0	0	0	0	0	0	0	1	1	1	1	1	1	1	2	2	2	2	2	2	2	14	7	2,00	BOTH	4
COMT	0	0	0	0	1,5	1,5	0	0	0	0	1	1	1	0	0	0	0	0	0	0	0					2,5	2,5		5	2	2,50	0	0
GART	0	0	0	0	0	0	1,5	0	1	0	0	0	0	1	0	0	0	0	0	0	0							2,5	2,5	1	2,50	0	0
PAICS	0	0	1,5	1,5	1,5	1,5	0	1	1	1	1	1	1	0	0	0	0	0	0	0	0			2,5	2,5	2,5	2,5		10	4	2,50	0	0
SCP2	0	0	0	0	0	1	0	0	0	0	0	0	0	0	0	0	0	0	0	0	0						1		1	1	1,00	0	0
UQCRC2	0	1	1	1	1	1	1	0	1	1	1	1	1	1	0	1	1	0	1	1	1		3	3	2	3	3	3	17	6	2,83	BOTH	5
SFPQ	0	1	1	1	1	1	0	0	0	0	0	0	0	0	0	1	0	0	0	0	0		2	1	1	1	1		6	5	1,20	0	0
ATP5F1	0	1	0	0	0	0	1	0	0	0	0	0	0	0	0	1	0	0	0	0	1		2					2	4	2	2,00	BOTH	2
RPS12	1	1	1	1	1	1	1	0	0	0	0	0	0	0	0	1	0	0	1	0	0	1	2	1	1	2	1	1	9	7	1,29	0	0
ATP5A1	1	1	1	1	1	1	1	0	0	0	0	0	0	0	1	1	1	1	1	1	1	2	2	2	2	2	2	2	14	7	2,00	449	2
S100P	0	0	0	0	0	0	1,5	0	0	0	0	1	1	1	0	0	0	0	0	0	0							2,5	2,5	1	2,50	0	0
DDX6	0	0	0	0	0	1	0	0	0	0	0	0	0	0	0	0	0	0	0	0	0						1		1	1	1,00	0	0
PTBP1	0	1	0	0	0	0	1	0	0	0	0	0	0	0	0	0	0	0	0	0	0		1					1	2	2	1,00	0	0
AK4	0	0	1,5	0	0	0	0	0	0	1	0	0	1	1	0	0	0	0	0	0	0			2,5					2,5	1	2,50	0	0
MAOB	0	1,5	1,5	0	1,5	1,5	1,5	1	1	1	1	1	1	1	0	0	0	0	0	0	0		2,5	2,5		2,5	2,5	2,5	12,5	5	2,50	0	0
CANX	1	1	1	1	1	1	1	0	0	0	0	0	0	0	0	1	1	1	1	1	1	1	2	2	2	2	2	2	13	7	1,86	BOTH	4
PSMB4	0	0	1	1	0	0	0	0	0	0	0	0	0	0	0	0	0	0	0	0	0				1	1			2	2	1,00	0	0
ABCD3	1	1	1	1	1	1	1	0	1	1	1	1	1	1	0	1	1	0	1	1	0	1	3	3	2	3	3	2	17	7	2,43	BOTH	3

NDUFS1	0	1,5	0	0	1,5	1,5	0	0	1	1	0	1	1	0	0	0	0	0	0	0	0	[redacted]	2,5	[redacted]	2,5	2,5	[redacted]	7,5	3	2,50	BOTH	5,5
GTF2E2	0	0	0	0	0	1,5	0	0	1	1	0	1	1	0	0	0	0	0	0	0	0	[redacted]	[redacted]	[redacted]	[redacted]	2,5	[redacted]	2,5	1	2,50	0	0
MPG	0	0	1	1	0	1	0	0	0	0	0	0	0	0	0	0	0	1	0	0	0	[redacted]	[redacted]	1	2	[redacted]	1	[redacted]	4	3	1,33	0	0
PML	1	0	1	1	1	1	0	0	0	0	0	0	0	0	0	0	0	0	0	0	0	1	[redacted]	1	1	1	1	[redacted]	5	5	1,00	0	0
EEF1D	1,5	1,5	1,5	0	1,5	1,5	0	1	1	1	1	1	1	1	0	0	0	0	0	0	0	2,5	2,5	2,5	[redacted]	2,5	2,5	[redacted]	12,5	5	2,50	BOTH	2
PRDX6	1	1	1	1	1	1	1	0	0	0	0	0	0	0	0	0	0	0	0	0	0	1	1	1	1	1	1	1	7	7	1,00	0	0
PRDX3	0	0	0	1	1	0	0	0	0	0	0	0	0	0	0	0	0	0	0	0	0	[redacted]	[redacted]	[redacted]	[redacted]	1	1	[redacted]	2	2	1,00	0	0
ATP5D	1	1	1	1	1	1	1	0	0	0	0	0	0	0	0	1	1	1	1	1	0	1	2	2	2	2	2	1	12	7	1,71	BOTH	2
PEBP1	0	0	1	1	0	1	0	0	1	1	1	1	1	0	0	0	0	0	0	1	0	[redacted]	[redacted]	2	2	[redacted]	3	[redacted]	7	3	2,33	0	0
PDIA3	0	0	0	1	1	1	0	0	0	0	0	0	0	0	0	0	0	0	0	0	0	[redacted]	[redacted]	[redacted]	1	1	1	[redacted]	3	3	1,00	0	0
PPP2R1A;PPP2R1B	0	0	0	1,5	1,5	1,5	1,5	1	0	0	1	1	1	1	0	0	0	0	0	0	0	[redacted]	[redacted]	[redacted]	2,5	2,5	2,5	2,5	10	4	2,50	0	0
SDHA	0	1,5	1,5	0	1,5	1,5	1,5	0	1	1	1	1	1	1	0	0	0	0	0	0	0	[redacted]	2,5	2,5	[redacted]	2,5	2,5	2,5	12,5	5	2,50	449	4
MAT2A	1	0	1	0	0	0	0	0	0	0	0	0	0	0	0	0	0	0	0	0	0	1	[redacted]	1	[redacted]	[redacted]	[redacted]	[redacted]	2	2	1,00	0	0
DNAJA1	1	1	1	1	1	1	1	0	0	0	0	0	0	0	0	1	1	0	1	0	1	1	2	2	1	2	1	2	11	7	1,57	BOTH	3
UQCRC1	0	1,5	1,5	1,5	1,5	1,5	1,5	0	1	1	1	1	1	1	0	0	0	0	0	0	0	[redacted]	2,5	2,5	2,5	2,5	2,5	2,5	15	6	2,50	BOTH	4
HNRNPH1	0	1	0	0	0	0	0	0	0	0	0	0	0	0	0	0	0	0	0	0	0	[redacted]	1	[redacted]	[redacted]	[redacted]	[redacted]	[redacted]	1	1	1,00	0	0
ARRB2	0	1	1	0	1	1	0	0	0	0	0	0	0	0	0	0	0	0	0	0	0	[redacted]	1	1	[redacted]	1	1	[redacted]	4	4	1,00	0	0
GTF2H1	1,5	1,5	0	0	0	0	0	1	1	0	0	0	1	0	0	0	0	0	0	0	0	2,5	2,5	[redacted]	[redacted]	[redacted]	[redacted]	[redacted]	5	2	2,50	0	0
ACSL1	0	0	1,5	0	1,5	0	1,5	0	1	1	1	1	1	1	0	0	0	0	0	0	0	[redacted]	[redacted]	2,5	[redacted]	2,5	[redacted]	2,5	7,5	3	2,50	BOTH	4,5
MCM7	0	0	0	0	0	0	1	0	0	0	0	0	0	0	0	0	0	0	0	0	0	[redacted]	[redacted]	[redacted]	[redacted]	[redacted]	[redacted]	1	1	1	1,00	0	0
HSPA1L	1,5	1,5	1,5	0	1,5	1,5	1,5	1	1	1	1	1	1	1	0	0	0	0	0	0	0	2,5	2,5	2,5	[redacted]	2,5	2,5	2,5	15	6	2,50	0	0
PRSS3	1,5	0	1,5	0	1,5	0	0	1	1	1	1	1	1	1	0	0	0	0	0	0	0	2,5	[redacted]	2,5	[redacted]	2,5	[redacted]	[redacted]	7,5	3	2,50	0	0
PHB	1	1	1	1	1	1	1	0	0	0	0	0	0	0	0	1	1	1	1	1	1	2	2	2	2	2	2	2	14	7	2,00	BOTH	4
SOAT1	0	1,5	1,5	0	0	1,5	0	0	1	1	0	1	1	1	0	0	0	0	0	0	0	[redacted]	2,5	2,5	[redacted]	[redacted]	2,5	[redacted]	7,5	3	2,50	BOTH	4,5
BSG	0	0	1,5	0	0	0	0	1	0	1	0	1	1	1	0	0	0	0	0	0	0	[redacted]	[redacted]	2,5	[redacted]	[redacted]	[redacted]	[redacted]	2,5	1	2,50	BOTH	2
FUS	1	1	0	0	0	0	0	0	0	0	0	0	0	0	0	0	0	0	0	0	0	1	1	[redacted]	[redacted]	[redacted]	[redacted]	[redacted]	2	2	1,00	0	0
GLRX	0	0	0	1	0	1	0	0	0	0	0	0	0	0	0	0	0	0	0	0	0	[redacted]	[redacted]	[redacted]	[redacted]	1	[redacted]	1	2	2	1,00	0	0
PSMC2	0	1,5	1,5	0	0	1,5	1,5	1	1	1	1	1	1	1	0	0	0	0	0	0	0	[redacted]	2,5	2,5	[redacted]	2,5	2,5	10	4	2,50	449	4
ATP5C1	1	1	1	0	1	1	1	0	0	0	0	0	0	0	0	0	0	0	0	0	0	1	1	1	[redacted]	1	1	1	6	6	1,00	0	0
FDFT1	0	1,5	1,5	1,5	1,5	1,5	1,5	1	1	1	1	1	1	1	0	0	0	0	0	0	0	[redacted]	2,5	2,5	2,5	2,5	2,5	2,5	15	6	2,50	BOTH	3
ETFB	0	1	0	0	1	1	0	0	0	0	0	0	0	0	0	0	0	0	0	0	0	[redacted]	1	[redacted]	[redacted]	[redacted]	1	1	3	3	1,00	418	4
HSPA9	0	1	0	0	0	0	0	0	0	0	0	0	0	0	0	0	0	0	0	0	0	[redacted]	1	[redacted]	[redacted]	[redacted]	[redacted]	[redacted]	1	1	1,00	0	0
DDOST	1	1	1	1	1	1	1	0	0	0	0	0	0	0	0	1	1	1	1	1	1	1	2	2	2	2	2	2	13	7	1,86	BOTH	3
CCT6A	1	1	1	0	1	1	1	0	0	0	0	0	0	0	0	1	0	0	0	1	0	1	2	1	[redacted]	1	2	1	8	6	1,33	BOTH	2
MDH2	0	0	0	1,5	0	0	1,5	0	1	0	1	1	0	1	0	0	0	0	0	0	0	[redacted]	[redacted]	[redacted]	[redacted]	2,5	[redacted]	2,5	5	2	2,50	0	0
HADHA	0	1,5	1,5	1,5	1,5	1,5	1,5	1	1	1	1	1	1	1	0	0	0	0	0	0	0	[redacted]	2,5	2,5	2,5	2,5	2,5	2,5	15	6	2,50	449	2
IARS	0	0	0	1,5	0	0	0	1	1	1	1	0	1	0	0	0	0	0	0	0	0	[redacted]	[redacted]	[redacted]	[redacted]	2,5	[redacted]	[redacted]	2,5	1	2,50	BOTH	2
TMPO	0	1	1	1	1	0	1	0	0	0	0	0	0	0	0	1	0	0	0	0	0	[redacted]	2	1	1	1	[redacted]	1	6	5	1,20	418	2
TMPO	1	1	1	1	1	1	1	0	0	0	0	0	0	0	0	1	1	0	1	0	0	1	2	2	1	2	1	1	10	7	1,43	BOTH	2
PI4KA	1,5	1,5	1,5	1,5	1,5	1,5	1,5	1	1	1	1	1	1	1	0	1	1	0	1	1	1	2,5	3,5	3,5	2,5	3,5	3,5	3,5	22,5	7	3,21	BOTH	6
LRPPRC	0	1	1	0	1	1	0	1	1	1	1	1	1	1	0	1	0	0	1	1	0	[redacted]	3	2	[redacted]	3	3	[redacted]	11	4	2,75	BOTH	4
GPD2	0	0	1,5	1,5	1,5	1,5	1,5	1	0	1	1	1	1	1	0	0	0	0	0	0	0	[redacted]	[redacted]	2,5	2,5	2,5	2,5	2,5	12,5	5	2,50	BOTH	4,5
VDAC2	1	1	1	1	1	1	1	0	0	0	0	0	0	0	1	1	1	1	1	1	1	2	2	2	2	2	2	2	14	7	2,00	BOTH	4
CBX5	1	1	1	1	1	1	1	0	0	0	0	0	0	0	0	0	1	0	0	0	0	1	1	2	1	1	1	1	8	7	1,14	0	0
RANGAP1	0	1,5	0	0	0	1,5	1,5	0	1	0	0	1	1	1	0	0	0	0	0	0	0	[redacted]	2,5	[redacted]	[redacted]	[redacted]	[redacted]	2,5	7,5	3	2,50	0	0
NSF	0	0	0	0	0	1,5	0	0	1	0	0	1	1	1	0	0	0	0	0	0	0	[redacted]	[redacted]	[redacted]	[redacted]	[redacted]	2,5	[redacted]	2,5	1	2,50	BOTH	2
RPL27A	1	0	0	0	0	0	0	0	0	0	0	0	0	0	0	0	0	0	0	0	0	1	[redacted]	[redacted]	[redacted]	[redacted]	[redacted]	[redacted]	1	1	1,00	0	0
RPS9	0	0	0	0	0	1	0	0	0	0	0	0	0	0	0	0	0	0	0	0	0	[redacted]	[redacted]	[redacted]	[redacted]	[redacted]	1	[redacted]	1	1	1,00	0	0
STT3A	0	1,5	1,5	0	1,5	1,5	1,5	0	1	1	1	1	1	1	0	0	0	0	0	0	0	[redacted]	2,5	2,5	[redacted]	2,5	2,5	2,5	12,5	5	2,50	BOTH	4
QARS	0	0	1,5	0	1,5	1,5	0	0	0	1	0	1	1	1	0	0	0	0	0	0	0	[redacted]	[redacted]	2,5	[redacted]	2,5	2,5	[redacted]	7,5	3	2,50	0	0
UQCRFS1;UQCRFS1P1	0	1,5	0	0	0	0	0	0	1	0	0	1	0	0	0	0	0	0	0	0	0	[redacted]	2,5	[redacted]	[redacted]	[redacted]	[redacted]	[redacted]	2,5	1	2,50	0	0
ATP5O	1	1	1	1	1	1	1	0	0	0	0	0	0	0	0	0	0	0	1	0	0	1	1	1	1	2	1	1	8	7	1,14	0	0
LSS	0	1,5	1,5	0	1,5	1,5	1,5	0	1	1	1	1	1	1	0	0	0	0	0	0	0	[redacted]	2,5	2,5	[redacted]	2,5	2,5	2,5	12,5	5	2,50	BOTH	5,5
GCLM	0	0	0	1,5	0	0	0	1	1	1	1	0	1	1	0	0	0	0	0	0	0	[redacted]	[redacted]	[redacted]	[redacted]	2,5	[redacted]	[redacted]	2,5	1	2,50	0	0
CCT5	0	0	0	0	1,5	0	0	1	1	0	1	1	1	1	0	0	0	0	0	0	0	[redacted]	[redacted]	[redacted]	[redacted]	[redacted]	2,5	[redacted]	2,5	1	2,50	BOTH	2
IDH2	1	1	0	1	1	1	0	0	0	0	0	0	0	0	0	0	0	0	0	0	0	1	1	[redacted]	[redacted]	1	1	1	5	5	1,00	418	2
LMAN1	0	1,5	0	0	0	0	0	0	1	1	1	1	1	0	0	0	0	0	0	0	0	[redacted]	2,5	[redacted]	[redacted]	[redacted]	[redacted]	[redacted]	2,5	1	2,50	BOTH	4
FASN	1	1	1	1	1	1	1	0	0	0	0	0	0	0	0	1	1	1	1	1	1	1	2	2	2	2	2	2	13	7	1,86	418	2
TUFM	1	1	1	1	1	1	1	0	0	0	0	0	0	0	0	0	0	0	0	0	0	1	1	1	1	1	1	1	7	7	1,00	418	2
CEBPA	0	1	0	0	0	0	0	0	0	0	0	0	0	0	0	0	0	0	0	0	0	[redacted]	1	[redacted]	[redacted]	[redacted]	[redacted]	[redacted]	1	1	1,00	0	0
ACADVL	0	0	1,5	1,5	1,5	1,5	0	1	1	1	1	1	1	0	0	0	0	0	0	0	0	[redacted]	[redacted]	2,5	2,5	2,5	2,5	[redacted]	10	4	2,50	BOTH	4,5
TMED10	1,5	0	1,5	1,5	1,5	1,5	1,5	1	1	1	1	1	1	1	0	0	0	0	1	0	0	2,5	[redacted]	2,5	2,5	3,5	2,5	2,5	16	6	2,67	BOTH	3

RBM25	1,5	1,5	1,5	0	1,5	1,5	1,5	1	1	1	1	1	1	1	0	0	0	0	0	0	0	2,5	2,5	2,5		2,5	2,5	2,5	15	6	2,50	0	0
CLK3	0	0	1,5	0	0	0	0	1	1	1	0	0	1	1	0	0	0	0	0	0	0			2,5					2,5	1	2,50	0	0
EMD	0	0	1,5	0	1,5	0	0	0	1	1	1	1	1	0	0	0	0	0	0	0	0			2,5		2,5			5	2	2,50	0	0
BCAM	0	1,5	1,5	1,5	1,5	1,5	1,5	1	1	1	1	1	1	1	0	0	0	0	0	0	0		2,5	2,5	2,5	2,5	2,5	2,5	15	6	2,50	BOTH	5
CCT8	1,5	1,5	1,5	1,5	1,5	1,5	1,5	1	1	1	1	1	1	1	0	0	0	0	0	0	0	2,5	2,5	2,5	2,5	2,5	2,5	2,5	17,5	7	2,50	BOTH	2
CCT4	1	1	1	1	1	1	1	0	0	0	0	0	0	0	0	1	0	0	1	1	0	1	2	1	1	2	2	1	10	7	1,43	0	0
FXR1	1,5	1,5	1,5	0	1,5	1,5	1,5	1	1	1	1	1	1	1	0	0	0	0	0	0	0	2,5	2,5	2,5		2,5	2,5	2,5	15	6	2,50	449	4
FXR2	0	0	1,5	0	0	0	0	1	1	1	0	1	1	0	0	0	0	0	0	0	0			2,5					2,5	1	2,50	0	0
RAB5C	0	1	1	1	1	1	0	1	1	1	1	1	1	1	0	1	1	1	1	1	0		3	3	3	3	3		15	5	3,00	BOTH	4
RAB7A	1	1	1	1	1	1	1	0	0	0	0	0	0	0	1	1	1	1	1	1	1	2	2	2	2	2	2	2	14	7	2,00	BOTH	4
DAP	0	0	1,5	0	1,5	1,5	0	0	1	1	0	1	1	0	0	0	0	0	0	0	0			2,5		2,5	2,5		7,5	3	2,50	0	0
GALK1	1,5	1,5	1,5	1,5	1,5	1,5	1,5	1	1	1	1	1	1	1	0	0	0	0	0	0	0	2,5	2,5	2,5	2,5	2,5	2,5	2,5	17,5	7	2,50	449	2
SSR4	0	1	1	0	1	1	0	0	0	0	0	0	0	0	0	0	0	0	1	1	0		1	1		2	2		6	4	1,50	418	2
BCAP31	0	1,5	1,5	1,5	1,5	1,5	1,5	1	1	1	1	1	1	1	0	0	0	0	0	0	0		2,5	2,5	2,5	2,5	2,5	2,5	15	6	2,50	BOTH	4
ALDH3A2	0	0	1,5	0	0	0	0	0	0	1	1	1	0	0	0	0	0	0	0	0	0			2,5					2,5	1	2,50	BOTH	4,5
HSD17B4	1	1	1	1	1	1	1	0	0	0	0	0	0	0	0	1	1	0	0	1	0	1	2	2	1	1	2	1	10	7	1,43	0	0
PSMD7	1,5	1,5	0	0	0	0	0	1	1	1	0	0	0	0	0	0	0	0	0	0	0	2,5	2,5						5	2	2,50	BOTH	4,5
NDUFA8	0	1,5	1,5	1,5	1,5	1,5	1,5	1	1	1	1	1	1	1	0	0	0	0	0	0	0		2,5	2,5	2,5	2,5	2,5	2,5	15	6	2,50	418	2
HNRNPA3	0	1	0	0	0	0	0	0	0	0	0	0	0	0	0	0	0	0	0	0	0		1						1	1	1,00	0	0
PGD	0	0	1,5	0	0	0	0	1	0	1	1	1	0	0	0	0	0	0	0	0	0			2,5					2,5	1	2,50	0	0
HNRNPM	0	1	0	0	0	0	1	0	0	0	0	0	0	0	0	0	0	0	0	0	0		1					1	2	2	1,00	0	0
KPNA2	1	1	1	0	1	0	1	0	0	0	0	0	0	0	0	1	0	0	1	0	1	1	2	1		2		2	8	5	1,60	BOTH	2
MRPL12	0	1,5	0	0	0	0	0	1	1	0	1	1	1	0	0	0	0	0	0	0	0		2,5						2,5	1	2,50	0	0
COPA	0	0	0	0	1,5	1,5	1,5	0	0	1	0	1	1	1	0	0	0	0	0	0	0					2,5	2,5	2,5	7,5	3	2,50	BOTH	3
SLC16A1	0	1,5	1,5	0	1,5	0	0	1	1	1	1	1	1	1	0	0	0	0	0	0	0		2,5	2,5		2,5			7,5	3	2,50	449	2
BLM	0	1,5	0	0	0	0	1,5	1	1	0	0	0	0	1	0	0	0	0	0	0	0		2,5					2,5	5	2	2,50	0	0
YARS	0	1	1	0	0	0	1	0	0	0	0	0	0	0	0	0	0	0	0	0	0		1	1				1	3	3	1,00	BOTH	3
HSPA2	0	1,5	1,5	0	0	0	0	1	1	1	0	0	0	1	0	0	0	0	0	0	0		2,5	2,5					5	2	2,50	418	4
ATP1B3	1,5	1,5	1,5	1,5	1,5	1,5	1,5	1	1	1	1	1	1	1	0	0	0	0	0	0	0	2,5	2,5	2,5	2,5	2,5	2,5	2,5	17,5	7	2,50	BOTH	6
AK2	1,5	1,5	1,5	1,5	1,5	0	1,5	1	1	1	1	1	1	1	0	0	0	0	0	0	0	2,5	2,5	2,5	2,5	2,5		2,5	15	6	2,50	0	0
NAPA	0	0	1,5	0	0	0	1,5	0	1	1	0	1	1	1	0	0	0	0	0	0	0			2,5				2,5	5	2	2,50	0	0
HADHB	0	0	0	0	1,5	1,5	1,5	1	1	0	0	1	1	1	0	0	0	0	0	0	0					2,5	2,5	2,5	7,5	3	2,50	0	0
MTTP	0	1,5	0	0	0	0	0	0	1	0	0	0	0	1	0	0	0	0	0	0	0		2,5						2,5	1	2,50	0	0
NAP1L1	1,5	1,5	1,5	1,5	1,5	1,5	1,5	1	1	1	1	1	1	1	1	1	1	1	1	1	1	3,5	3,5	3,5	3,5	3,5	3,5	3,5	24,5	7	3,50	418	6
TPD52	0	0	0	0	1,5	1,5	0	0	0	0	0	1	1	0	0	0	0	0	0	0	0					2,5	2,5		5	2	2,50	0	0
ATP5J2	0	1	1	1	1	1	0	0	0	0	0	0	0	0	0	0	0	0	0	0	0		1	1	1	1	1		5	5	1,00	449	2
MARS	1,5	1,5	1,5	1,5	1,5	1,5	1,5	1	1	1	1	1	1	1	0	0	0	0	0	0	0	2,5	2,5	2,5	2,5	2,5	2,5	2,5	17,5	7	2,50	NONE	2
ATP5I	0	0	1	0	0	0	0	1	0	1	1	1	1	0	0	0	0	0	0	0	0			2					2	1	2,00	0	0
NDUFA6	1,5	0	0	0	0	0	0	1	1	0	1	1	0	0	0	0	0	0	0	0	0	2,5							2,5	1	2,50	0	0
H2BFS	1,5	1,5	0	0	0	0	1,5	0	0	0	0	0	0	0	1	1	0	0	0	0	1	2,5	2,5					2,5	7,5	3	2,50	0	0
TMEM33	0	1	0	0	1	0	0	0	0	0	0	0	0	0	0	0	0	0	0	0	0		1			1			2	2	1,00	449	2
ARPC4	0	0	1,5	0	0	1,5	0	0	0	1	1	1	1	1	0	0	0	0	0	0	0			2,5			2,5		5	2	2,50	0	0
SEC61B	0	1	1	1	1	1	1	1	1	1	1	1	1	1	0	0	0	0	0	0	0		2	2	2	2	2	2	12	6	2,00	BOTH	2
ROMO1	0	1,5	1,5	1,5	1,5	1,5	1,5	1	1	1	1	1	1	1	0	0	0	0	0	0	0		2,5	2,5	2,5	2,5	2,5	2,5	15	6	2,50	BOTH	3
S100A10	0	1	0	1	1	0	0	0	0	0	0	0	0	0	0	0	0	0	1	0	0		1		1	2			4	3	1,33	418	2
CDC42	0	1,5	1,5	0	1,5	0	1,5	1	1	1	0	1	0	1	0	0	0	0	0	0	0		2,5	2,5		2,5		2,5	10	4	2,50	BOTH	5
RAB8A	1,5	1,5	1,5	1,5	1,5	1,5	1,5	1	1	1	1	1	1	1	0	0	0	0	0	0	0	2,5	2,5	2,5	2,5	2,5	2,5	2,5	17,5	7	2,50	BOTH	3
SPCS3	0	0	0	0	1,5	1,5	0	0	1	0	1	1	1	1	0	0	0	0	0	0	0					2,5	2,5		5	2	2,50	0	0
RAB2A;RAB2B	1,5	1,5	1,5	1,5	1,5	1,5	1,5	1	1	1	1	1	1	1	0	1	1	0	1	1	0	2,5	3,5	3,5	2,5	3,5	3,5	2,5	21,5	7	3,07	BOTH	4
RAB5B	0	1,5	0	0	0	0	1,5	0	1	1	1	1	1	1	0	0	0	0	0	0	0		2,5					2,5	5	2	2,50	418	4
RAB10	0	1	1	1	1	1	1	0	1	1	1	0	1	1	0	1	1	1	1	1	1		3	3	3	2	3	3	17	6	2,83	BOTH	4
RAB14	0	1	1	1	1	1	1	0	1	1	0	1	1	1	0	1	1	1	1	1	1		3	3	2	3	3	3	17	6	2,83	BOTH	3
ACTR1A;ACTR1B	0	0	0	0	1,5	1,5	1,5	0	0	0	0	1	1	1	0	0	0	0	0	0	0					2,5	2,5	2,5	7,5	3	2,50	0	0
ABCE1	0	1	1	1	1	1	1	0	0	0	0	0	0	0	0	1	0	0	1	1	0		2	1	1	2	2	1	9	6	1,50	0	0
RAP1B;RAP1A	1,5	1,5	1,5	1,5	1,5	1,5	1,5	1	1	1	1	1	1	1	0	0	0	0	1	0	0	2,5	2,5	2,5	2,5	3,5	2,5	2,5	18,5	7	2,64	0	0
PSME3	1,5	0	1,5	0	1,5	1,5	0	1	1	1	1	1	1	1	0	0	0	0	0	0	0	2,5		2,5		2,5	2,5		10	4	2,50	BOTH	4,5
HSPE1	0	0	0	0	1	0	0	0	0	0	0	0	0	0	0	0	0	0	0	0	0					1			1	1	1,00	0	0
SEC61A1;SEC61A2	0	1,5	1,5	1,5	1,5	1,5	1,5	1	1	1	1	1	1	1	0	0	0	0	0	0	0		2,5	2,5	2,5	2,5	2,5	2,5	15	6	2,50	BOTH	2
DAD1	0	0	1,5	0	0	0	1,5	0	0	1	1	0	0	1	0	0	0	0	0	0	0			2,5				2,5	5	2	2,50	NONE	4
COPZ1	0	0	1,5	0	1,5	1,5	1,5	1	1	1	1	1	1	1	0	0	0	0	0	0	0			2,5		2,5	2,5	2,5	10	4	2,50	0	0
HNRNPK	0	0	0	1	1	0	0	0	0	0	0	0	0	0	0	0	0	0	0	0	0				1	1			2	2	1,00	0	0
PSMC5	0	0	1	0	1	0	1	0	0	0	0	0	0	1	0	0	1	0	1	0	0			2		2		2	6	3	2,00	0	0

RPS15A	0	1	0	0	0	1	1	0	0	0	0	0	0	0	0	0	0	0	0	0	0		1				1	1	3	3	1,00	0	0
SNRPD2	1	0	0	1	1	1	0	0	0	0	0	0	0	0	0	0	0	0	0	0	0	1			1	1	1		4	4	1,00	0	0
PSMC6	1,5	0	1,5	0	0	1,5	1,5	1	0	1	0	0	1	1	0	0	0	0	0	0	0	2,5		2,5			2,5	2,5	10	4	2,50	0	0
RAB1A	0	1,5	1,5	1,5	1,5	1,5	1,5	1	1	1	1	1	1	1	0	1	0	0	1	1	0		3,5	2,5	2,5	3,5	3,5	2,5	18	6	3,00	BOTH	5
GNB1	0	0	1	1	1	0	1	0	0	0	0	0	0	0	0	0	0	0	0	0	0			1	1	1		1	4	4	1,00	BOTH	4
GNB2;GNB4	0	0	0	0	1,5	0	0	0	1	1	1	1	1	1	0	0	0	0	0	0	0					2,5			2,5	1	2,50	BOTH	5,5
RPL31	0	1	1	1	0	0	0	0	0	0	0	0	0	0	0	0	0	0	0	0	0		1	1	1				3	3	1,00	0	0
FKBP1A	0	0	0	1	0	0	0	0	0	0	0	0	0	0	0	0	0	0	0	0	0				1				1	1	1,00	0	0
YWHAZ	0	0	1,5	0	0	0	0	0	0	1	1	1	1	1	0	0	0	0	0	0	0			2,5					2,5	1	2,50	0	0
YBX1	1	1	1	1	1	1	1	0	0	0	0	0	0	0	0	1	0	0	0	0	0	1	2	1	1	1	1	1	8	7	1,14	449	2
TUBA4A	0	0	0	0	0	0	1,5	0	0	0	0	0	0	0	0	0	0	0	0	0	1							2,5	2,5	1	2,50	0	0
TUBB4B	0	1	1	1	1	1	1	0	0	0	0	0	0	0	0	0	0	0	0	1	0		1	1	1	1	2	1	7	6	1,17	0	0
GTF2I	1	1	0	0	0	0	0	0	0	0	0	0	0	0	0	0	0	0	0	0	0	1	1						2	2	1,00	0	0
CCT2	1	0	1	1	1	1	1	0	0	0	0	0	0	0	0	0	1	0	1	1	1	1		2	1	2	2	2	10	6	1,67	BOTH	2
PRKDC	1	1	1	1	1	1	1	0	0	0	0	0	0	0	1	1	1	1	1	1	1	2	2	2	2	2	2	2	14	7	2,00	449	2
LACTB	0	0	1,5	0	1,5	1,5	0	0	0	1	0	1	1	0	0	0	0	0	0	0	0			2,5		2,5	2,5		7,5	3	2,50	418	4
RPL24	0	1	1	0	1	1	1	0	0	0	0	0	0	0	0	1	1	0	1	1	0		2	2		2	2	1	9	5	1,80	0	0
ERH	0	0	0	1	1	1	0	0	0	0	0	0	0	0	0	0	0	0	0	0	0				1	1	1		3	3	1,00	0	0
RPL19	0	1	0	0	0	0	0	0	0	0	0	0	0	0	0	0	0	0	0	0	0		1						1	1	1,00	0	0
FOXK1	0	0	0	0	1,5	0	1,5	0	1	0	0	1	0	1	0	0	0	0	0	0	0					2,5		2,5	5	2	2,50	0	0
ATP2C1	0	0	1,5	0	1,5	1,5	0	0	1	1	0	1	1	0	0	0	0	0	0	0	0			2,5		2,5	2,5		7,5	3	2,50	BOTH	4,5
CLTC	1	1	1	1	1	1	1	0	0	0	0	0	0	0	0	1	0	0	0	1	0	1	2	1	1	1	2	1	9	7	1,29	0	0
SORD	0	0	0	0	0	0	1,5	0	1	0	0	1	1	1	0	0	0	0	0	0	0							2,5	2,5	1	2,50	0	0
HNRNPU	0	1	0	0	0	0	0	0	0	0	0	0	0	0	0	0	0	0	0	0	0		1						1	1	1,00	449	2
SET;SETSIP	1	1	1	1	1	1	1	0	0	0	0	0	0	0	0	0	0	0	1	1	0	1	1	1	1	2	2	1	9	7	1,29	0	0
FOXK2	0	1,5	0	1,5	1,5	1,5	1,5	0	1	0	1	1	1	1	0	0	0	0	1	0	1		2,5		2,5	3,5	2,5	3,5	14,5	5	2,90	0	0
FABP5	0	0	0	1	0	0	0	0	0	0	0	0	0	0	0	0	0	0	0	0	0				1				1	1	1,00	0	0
HMGCS1	0	0	0	1	0	0	0	0	0	0	0	0	0	0	0	0	0	0	0	0	0				1				1	1	1,00	0	0
SLC7A5	1	1	1	0	1	1	1	1	0	1	0	1	1	0	0	1	1	0	1	1	1	2	2	3		3	3	2	15	6	2,50	BOTH	3
RPL18A	0	0	0	0	0	0	1,5	0	1	0	0	0	0	1	0	0	0	0	0	0	0							2,5	2,5	1	2,50	0	0
SLC25A11	0	1	0	0	0	0	0	0	0	0	0	0	0	0	0	0	0	0	0	0	0		1						1	1	1,00	0	0
EIF4G1	0	0	0	0	1,5	0	0	0	0	1	1	1	1	0	0	0	0	0	0	0	0					2,5			2,5	1	2,50	0	0
PRDX1	0	1	0	1	0	0	0	0	0	0	0	0	0	0	0	0	0	0	0	0	0		1		1				2	2	1,00	0	0
C1QBP	0	1,5	1,5	1,5	1,5	0	1,5	0	1	1	1	1	1	1	0	0	0	0	0	0	0		2,5	2,5	2,5	2,5		2,5	12,5	5	2,50	0	0
CKAP4	1	1	1	1	1	1	1	0	0	0	0	0	0	0	1	1	1	1	1	1	1	2	2	2	2	2	2	2	14	7	2,00	449	2
BAX	0	0	1,5	0	1,5	1,5	0	0	1	1	0	1	1	1	0	0	0	0	0	0	0			2,5		2,5	2,5		7,5	3	2,50	0	0
PPID	0	0	1,5	0	1,5	1,5	1,5	0	0	1	1	1	1	1	0	0	0	0	0	0	0			2,5		2,5	2,5	2,5	10	4	2,50	BOTH	2
GALNT2	0	0	1,5	0	0	1,5	0	0	1	1	1	0	1	1	0	0	0	0	0	0	0			2,5			2,5		5	2	2,50	0	0
ASPH	0	0	0	0	0	1,5	0	0	0	1	0	1	1	0	0	0	0	0	0	0	0						2,5		2,5	1	2,50	0	0
ILF2	1	1	1	0	1	1	1	0	0	0	0	0	0	0	1	1	0	0	0	0	1	2	2	1		1	1	2	9	6	1,50	0	0
LMAN2	0	0	1,5	0	0	0	0	1	1	1	1	0	0	0	0	0	0	0	0	0	0			2,5					2,5	1	2,50	BOTH	4
TRAP1	0	0	1,5	0	0	1,5	0	0	0	1	0	1	1	1	0	0	0	0	0	0	0			2,5			2,5		5	2	2,50	0	0
ANK3	0	0	0	0	1,5	0	0	0	1	0	0	1	0	0	0	0	0	0	1	0	0					3,5			3,5	1	3,50	0	0
TARDBP	0	1	1	0	1	1	1	0	0	0	0	0	0	0	0	1	0	0	1	0	1		2	1		2	1	2	8	5	1,60	BOTH	3
HNRNPA0	0	1	0	1	0	0	0	0	0	0	0	0	0	0	0	0	0	0	0	0	0		1		1				2	2	1,00	0	0
PSMD2	0	1,5	1,5	1,5	0	0	1,5	0	1	1	1	1	1	1	0	0	0	0	0	0	0		2,5	2,5	2,5			2,5	10	4	2,50	0	0
TRIM28	0	0	0	0	0	0	1	1	0	0	0	1	0	0	0	0	0	0	0	0	0							1	1	1	1,00	0	0
G3BP1	0	1,5	0	1,5	1,5	1,5	0	1	1	1	1	1	1	0	0	0	0	0	0	0	0		2,5		2,5	2,5	2,5		10	4	2,50	0	0
PABPC4	0	1,5	1,5	1,5	1,5	1,5	0	1	1	1	1	1	1	1	0	0	0	0	0	0	0		2,5	2,5	2,5	2,5	2,5		12,5	5	2,50	BOTH	2
NNT	0	0	0	0	1,5	1,5	0	0	1	1	0	1	1	1	0	0	0	0	0	0	0					2,5	2,5		5	2	2,50	0	0
TCOF1	0	0	0	0	0	0	1,5	1	1	0	1	1	1	1	0	0	0	0	0	0	0							2,5	2,5	1	2,50	0	0
SF3B2	1	0	0	0	1	1	0	0	0	0	0	0	0	0	0	0	0	0	0	0	0	1				1	1		3	3	1,00	0	0
SQSTM1	0	1	0	0	0	0	0	0	0	0	0	0	0	0	0	0	0	0	0	0	0		1						1	1	1,00	0	0
RAB32	0	0	0	0	0	0	1,5	0	0	0	0	0	0	1	0	0	0	0	0	0	0							2,5	2,5	1	2,50	0	0
MOGS	0	1	0	0	0	0	0	1	1	1	0	1	1	1	0	1	0	0	0	0	0		3						3	1	3,00	BOTH	4,5
TUBB2A	1	1	0	1	0	1	1	0	0	0	0	0	0	0	0	0	0	0	0	0	0	1	1		1		1	1	5	5	1,00	0	0
IDI1	0	0	0	1	0	0	0	0	0	0	0	0	0	0	0	0	0	0	0	0	0				1				1	1	1,00	0	0
MLEC	1,5	1,5	1,5	1,5	1,5	1,5	0	1	1	1	1	1	1	1	0	0	0	0	0	0	0	2,5	2,5	2,5	2,5	2,5	2,5		15	6	2,50	BOTH	5
DYNC1H1	1,5	1,5	1,5	1,5	0	1,5	1,5	1	1	1	1	1	1	1	0	0	0	0	0	0	0	2,5	2,5	2,5	2,5		2,5	2,5	15	6	2,50	449	2
RCN2	1	1	1	1	1	1	1	0	0	0	0	0	0	0	0	0	0	0	0	1	0	1	1	1	1	1	2	1	8	7	1,14	0	0
CAPRIN1	0	0	1	1	0	1	0	0	0	1	1	1	1	1	0	0	0	1	1	0	0			2	3		2		7	3	2,33	0	0
SQLE	0	1,5	1,5	0	1,5	1,5	1,5	0	1	1	1	1	1	1	0	0	0	0	0	0	0		2,5	2,5		2,5	2,5	2,5	12,5	5	2,50	418	4

CLINT1	0	1	0	1	0	0	0	1	1	1	1	1	1	1	1	1	0	0	0	1	0		3		2					5	2	2,50	418	2
GANAB	0	1,5	1,5	1,5	1,5	1,5	1,5	1	1	1	1	1	1	1	0	0	0	0	0	0	0		2,5	2,5	2,5	2,5	2,5	2,5	15	6	2,50	BOTH	4
LBR	1	1	1	1	1	1	1	0	0	0	0	0	0	0	0	1	1	0	1	1	0	1	2	2	1	2	2	1	11	7	1,57	BOTH	2
RAB39A	0	1,5	1,5	0	0	0	0	0	1	1	1	1	1	0	0	0	0	0	0	0	0		2,5	2,5						5	2	2,50	BOTH	4,5
KPNB1	1	1	1	1	1	1	1	1	1	1	1	1	1	1	0	1	1	0	1	1	1	2	3	3	2	3	3	3	19	7	2,71	BOTH	4
SPCS2	0	1,5	1,5	0	1,5	0	1,5	0	1	1	0	1	1	1	0	0	0	0	0	0	0		2,5	2,5		2,5		2,5	10	4	2,50	BOTH	6
SLC39A14	0	0	0	1,5	0	0	0	0	1	1	1	1	1	0	1	0	0	0	0	0	0	0				2,5				2,5	1	2,50	BOTH	4
KARS	0	0	0	0	1	1	0	1	0	0	0	1	1	1	0	0	0	0	0	0	0						2	2		4	2	2,00	0	0
RRS1	0	0	0	0	0	0	1,5	1	0	0	0	0	0	1	0	0	0	0	0	0	0							2,5	2,5	1	2,50	0	0
EBP	1	1	0	1	1	1	1	0	0	0	0	0	0	0	0	1	0	0	1	0	0	1	2		1	2	1	1	8	6	1,33	BOTH	2
PON2	1	1	1	1	1	1	1	0	0	0	0	0	0	0	0	1	0	1	0	1	0	1	2	1	2	1	2	1	10	7	1,43	449	2
NONO	0	1	1	0	1	1	1	0	0	0	0	0	0	0	0	1	1	0	1	1	0		2	2		2	2	1	9	5	1,80	0	0
DHCR24	1	1	1	1	1	1	0	1	1	1	1	1	1	1	1	1	1	1	1	1	0	3	3	3	3	3	3		18	6	3,00	BOTH	3
SF3B3	0	1	0	1	0	0	0	0	0	0	0	0	0	0	0	0	0	0	0	0	0		1		1				2	2	1,00	0	0
SAFB	0	0	0	0	0	0	1	0	0	0	0	0	0	0	0	0	0	0	0	0	0							1	1	1	1,00	449	2
SF3A1	1	0	0	1	0	0	0	0	0	0	0	0	0	0	0	0	0	0	0	0	0	1			1				2	2	1,00	0	0
TRAM1	0	0	1,5	0	1,5	1,5	1,5	0	1	1	1	1	1	1	0	0	0	0	0	0	0			2,5		2,5	2,5	2,5	10	4	2,50	449	4
ELAVL1	1	1	1	1	1	1	1	0	0	0	0	0	0	0	1	1	1	1	1	1	1	2	2	2	2	2	2	2	14	7	2,00	BOTH	4
NSDHL	0	0	0	0	1,5	0	0	1	0	0	0	0	1	1	0	0	0	0	0	0	0					2,5			2,5	1	2,50	0	0
SLC1A5	0	1	1	0	1	1	0	1	1	1	1	1	1	1	0	1	0	0	1	0	0		3	2		3	2		10	4	2,50	BOTH	3
MSMO1	1,5	1,5	1,5	1,5	1,5	0	1,5	1	1	1	1	1	1	1	0	0	0	0	0	0	0	2,5	2,5	2,5	2,5	2,5		2,5	15	6	2,50	BOTH	4,5
VAMP3;VAMP2	0	1,5	1,5	0	1,5	0	0	1	1	1	1	1	1	1	0	0	0	0	0	0	0		2,5	2,5		2,5			7,5	3	2,50	BOTH	5,5
RAB11B;RAB11A	1	1	1	1	1	1	1	0	0	0	0	0	0	0	1	1	1	1	1	1	1	2	2	2	2	2	2	2	14	7	2,00	0	0
PSMD5	1,5	0	0	0	1,5	1,5	0	1	1	0	1	1	1	1	0	0	0	0	0	0	0	2,5				2,5	2,5		7,5	3	2,50	BOTH	3
CSRP2	1	0	0	1	1	1	0	0	0	0	0	0	0	0	0	0	0	0	0	0	0	1				1	1	1	4	4	1,00	0	0
DDB1	0	0	0	1	1	1	0	1	0	1	1	1	1	1	0	0	0	1	1	1	0					3	3	3	9	3	3,00	0	0
NDUFA5	0	0	0	1,5	1,5	1,5	0	1	0	1	1	1	1	1	0	0	0	0	0	0	0					2,5	2,5	2,5	7,5	3	2,50	BOTH	6
TST	0	0	0	0	0	0	1,5	0	0	1	0	1	1	1	0	0	0	0	0	0	0							2,5	2,5	1	2,50	0	0
UBE2S	0	0	1	0	0	0	0	0	0	0	0	0	0	0	0	0	0	0	0	0	0			1					1	1	1,00	418	4
NDUFA9	0	0	1,5	0	0	0	0	0	0	1	0	0	0	0	0	0	0	0	0	0	0			2,5					2,5	1	2,50	BOTH	4,5
CYP51A1	0	1,5	1,5	1,5	1,5	1,5	1,5	1	1	1	1	1	1	1	0	1	1	0	1	1	0		3,5	3,5	2,5	3,5	3,5	2,5	19	6	3,17	BOTH	4,5
IMMT	1,5	1,5	1,5	1,5	1,5	1,5	1,5	1	1	1	1	1	1	1	0	1	1	0	1	1	1	2,5	3,5	3,5	2,5	3,5	3,5	3,5	22,5	7	3,21	BOTH	4
HNRNPUL2	0	1	0	0	1	0	0	0	0	0	0	0	0	0	0	1	0	0	0	0	0		2			1			3	2	1,50	0	0
CWF19L2	1	0	0	1	0	1	0	0	0	0	0	0	0	0	0	0	0	0	0	0	0	1			1		1		3	3	1,00	0	0
CHD9	0	0	1,5	0	1,5	1,5	0	0	0	1	0	1	1	1	0	0	1	0	0	0	0			3,5		2,5	2,5		8,5	3	2,83	0	0
LSM12	1,5	1,5	1,5	1,5	1,5	1,5	1,5	1	1	1	1	1	1	1	0	0	0	0	0	0	0	2,5	2,5	2,5	2,5	2,5	2,5	2,5	17,5	7	2,50	0	0
TUBB8	0	0	1	0	0	1	0	0	0	0	0	0	0	0	0	0	0	0	0	0	0				1			1	2	2	1,00	0	0
TIMM50	1	1	1	1	1	1	1	1	1	1	1	1	1	1	0	1	1	0	1	1	1	2	3	3	2	3	3	3	19	7	2,71	449	2
TBC1D10B	1,5	0	0	0	0	0	0	1	0	0	1	0	0	0	0	0	0	0	0	0	0	2,5							2,5	1	2,50	0	0
HSD17B12	0	1	1	0	1	1	1	1	1	1	0	1	1	1	0	1	1	0	1	1	1		3	3		3	3	3	15	5	3,00	BOTH	4
FASTKD1	0	0	0	0	0	1,5	0	0	0	0	0	0	1	0	0	0	0	0	0	0	0						2,5		2,5	1	2,50	0	0
HSP90AB2P	0	0	1,5	0	0	1,5	1,5	0	1	1	1	1	1	1	0	0	0	0	0	0	0			2,5			2,5	2,5	7,5	3	2,50	418	4
RPL39P5;RPL39	1	1	0	0	0	0	0	0	0	0	0	0	0	0	0	0	0	0	0	0	0	1	1						2	2	1,00	0	0
DNAJC21	0	0	0	0	1,5	1,5	1,5	0	0	0	0	1	1	1	0	0	0	0	0	0	0					2,5	2,5	2,5	7,5	3	2,50	0	0
DDX60L	0	1	0	0	0	0	0	0	0	0	0	0	0	0	0	1	0	0	0	0	0		2						2	1	2,00	0	0
NHSL2	1,5	0	0	0	1,5	0	0	1	1	0	1	1	1	0	0	0	0	0	0	0	0	2,5				2,5			5	2	2,50	0	0
RRP12	0	0	1,5	0	0	0	1,5	0	1	1	0	1	0	1	0	0	0	0	0	0	0			2,5				2,5	5	2	2,50	0	0
TOR1AIP1	1,5	1,5	1,5	0	1,5	1,5	1,5	1	1	1	1	1	1	1	0	0	0	0	0	0	0	2,5	2,5	2,5		2,5	2,5	2,5	15	6	2,50	0	0
CEP78	0	1,5	1,5	1,5	1,5	1,5	0	0	1	1	1	1	1	0	0	0	0	0	1	1	0		2,5	2,5	2,5	3,5	3,5		14,5	5	2,90	0	0
UBR4	1	1	1	1	1	1	0	0	0	0	0	0	0	0	0	0	0	1	1	1	0	1	1	1	2	2	2		9	6	1,50	0	0
KPRP	0	0	1	0	0	0	0	0	0	0	0	0	0	0	0	0	0	0	0	0	0				1				1	1	1,00	0	0
ATAD3B	0	0	1,5	0	0	0	0	1	1	1	1	0	0	0	0	0	0	0	0	0	0			2,5					2,5	1	2,50	BOTH	2
MARC1	0	0	1,5	0	0	0	0	0	0	1	0	0	0	0	0	0	0	0	0	0	0			2,5					2,5	1	2,50	0	0
RNF220	1	1	0	1	1	1	0	0	0	0	0	0	0	0	0	0	0	0	1	0	0	1	1		1	2	1		6	5	1,20	0	0
PRPF38B	1	1	0	0	0	0	1	0	0	0	0	0	0	0	0	0	0	0	0	0	0	1	1					1	3	3	1,00	0	0
ARL6IP4	1	1	1	1	1	1	0	0	0	0	0	0	0	0	0	0	0	1	0	0	0	1	1	1	2	1	1		7	6	1,17	0	0
ATL3	0	1,5	0	0	1,5	0	0	0	1	0	0	1	1	0	0	0	0	0	0	0	0		2,5			2,5			5	2	2,50	BOTH	3
SLC25A24	0	1,5	1,5	1,5	1,5	0	0	0	1	1	1	1	1	1	0	0	0	0	0	0	0		2,5	2,5	2,5	2,5			10	4	2,50	418	4
TMEM214	0	0	1,5	0	0	0	0	0	1	1	0	1	0	0	0	0	0	0	0	0	0			2,5					2,5	1	2,50	0	0
GTF2H2C;GTF2H2	0	1,5	1,5	0	0	1,5	0	1	1	1	0	0	1	0	0	0	0	0	0	0	0		2,5	2,5			2,5		7,5	3	2,50	0	0
TAF2	0	1,5	1,5	0	0	0	0	0	1	1	1	0	1	1	0	0	0	0	0	0	0		2,5	2,5					5	2	2,50	0	0
RPL22L1	0	1	0	0	0	0	0	0	0	0	0	0	0	0	0	0	0	0	0	0	0		1						1	1	1,00	0	0

GIGYF2	1	1	1	1	1	1	1	0	0	0	0	0	0	0	0	1	0	1	1	1	0	1	2	1	2	2	2	1	11	7	1,57	418	4
HSDL2	0	1	1	1	1	0	1	0	0	0	0	0	0	0	0	0	0	0	0	0	0		1	1	1	1		1	5	5	1,00	418	2
C11orf57	0	0	1	0	0	1	0	0	0	0	0	0	0	0	0	0	0	0	0	0	0			1			1		2	2	1,00	0	0
HS2ST1	0	0	0	0	1,5	0	0	0	0	0	1	1	1	1	0	0	0	0	0	0	0					2,5			2,5	1	2,50	0	0
PHF5A	0	0	1,5	0	1,5	0	1,5	1	1	1	1	1	1	1	0	0	0	0	0	0	0			2,5		2,5		2,5	7,5	3	2,50	0	0
NUFIP2	0	1	0	1	1	1	0	1	0	0	1	1	1	0	0	0	0	0	1	1	0		1		3	3	3		10	4	2,50	0	0
EMSY	0	1,5	1,5	0	1,5	1,5	0	0	1	1	0	1	1	0	0	1	0	0	1	0	0		3,5	2,5		3,5	2,5		12	4	3,00	0	0
IRF2BP2	1	0	0	0	0	0	0	0	0	0	0	0	0	0	0	0	0	0	0	0	0	1							1	1	1,00	0	0
YTHDF3;YTHDF1	0	0	0	0	0	1,5	0	1	0	0	1	0	1	0	0	0	0	0	0	0	0						2,5		2,5	1	2,50	0	0
PEG10	0	1,5	0	0	1,5	0	0	0	1	0	1	1	1	1	0	0	0	0	0	0	0		2,5			2,5			5	2	2,50	0	0
PABPN1	0	1	0	0	0	0	0	0	0	0	0	0	0	0	0	0	0	0	0	0	0		1						1	1	1,00	0	0
ALYREF	0	0	1	1	0	1	0	0	0	0	0	0	0	0	0	0	0	0	0	0	0			1	1		1		3	3	1,00	0	0
MORC1	0	0	1,5	0	0	0	0	0	0	1	0	0	0	1	0	0	0	0	0	0	0			2,5					2,5	1	2,50	0	0
CAND1	0	0	1	0	1	1	0	0	1	1	1	1	1	0	0	0	0	0	1	1	0			2		3	3		8	3	2,67	BOTH	4
BPHL	0	0	1,5	0	0	0	0	0	0	1	0	0	0	0	0	0	0	0	0	0	0			2,5					2,5	1	2,50	0	0
COA5	0	1	0	0	0	0	0	0	1	0	0	0	0	0	0	0	0	0	0	0	0		2						2	1	2,00	0	0
RPS19BP1	0	0	1	1	1	1	0	0	0	0	0	0	0	0	0	0	0	0	0	1	0			1	1	1	2		5	4	1,25	0	0
CIR1	1,5	0	0	1,5	1,5	1,5	0	1	1	0	1	1	1	0	0	0	0	0	1	0	0	2,5			2,5	3,5	2,5		11	4	2,75	0	0
ERC1	0	0	1,5	0	0	0	1,5	0	1	1	0	1	1	1	0	0	1	0	0	0	0			3,5				2,5	6	2	3,00	0	0
ARID3B	0	0	0	1	1	1	0	0	0	0	0	0	0	0	0	0	0	0	0	0	0				1	1	1		3	3	1,00	0	0
CHERP	1	1	0	1	1	1	0	0	0	0	0	0	0	0	0	0	0	0	0	0	0	1	1		1	1	1		5	5	1,00	0	0
PNPLA6	0	0	1,5	0	0	0	0	0	0	1	0	0	0	0	0	0	0	0	0	0	0			2,5					2,5	1	2,50	0	0
RAVER1	1	1	0	1	1	1	0	0	0	0	0	0	0	0	0	0	0	0	0	0	0	1	1		1	1	1		5	5	1,00	0	0
FTSJ3	0	1,5	0	0	0	0	0	0	1	0	0	0	0	1	0	0	0	0	0	0	0		2,5						2,5	1	2,50	0	0
ST13P4;ST13;ST13P5	0	1,5	1,5	0	0	0	1,5	0	1	1	1	1	1	1	0	0	0	0	0	0	0		2,5	2,5				2,5	7,5	3	2,50	418	4
ZNF444	0	1	0	0	0	0	0	0	0	0	0	0	0	0	0	0	0	0	0	0	0		1						1	1	1,00	0	0
NUP93	0	0	0	1,5	1,5	1,5	1,5	1	1	1	1	1	1	1	0	0	0	0	0	0	0				2,5	2,5	2,5	2,5	10	4	2,50	NONE	4
ABHD12	0	1,5	1,5	1,5	0	1,5	0	1	1	1	1	1	1	1	0	0	0	0	0	0	0		2,5	2,5	2,5		2,5		10	4	2,50	BOTH	2
MMGT1	0	0	1,5	0	0	0	0	1	1	1	0	1	1	1	0	0	0	0	0	0	0			2,5					2,5	1	2,50	BOTH	4,5
SMIM20	0	0	1,5	0	1,5	1,5	1,5	1	1	1	1	1	1	1	0	0	0	0	0	0	0			2,5		2,5	2,5	2,5	10	4	2,50	BOTH	4
CISD2	0	0	1,5	0	0	0	0	0	1	1	1	0	1	1	0	0	0	0	0	0	0			2,5					2,5	1	2,50	0	0
NPW	0	0	0	1,5	0	0	0	0	0	0	1	0	1	0	0	0	0	0	0	0	0				2,5				2,5	1	2,50	0	0
EMC1	0	1,5	1,5	0	0	0	0	0	1	1	0	0	1	0	0	0	0	0	0	0	0		2,5	2,5					5	2	2,50	0	0
SREK1IP1	1	1	1	1	1	1	0	0	0	0	0	0	0	0	0	1	1	1	1	1	0	1	2	2	2	2	2		11	6	1,83	0	0
POMGNT2	0	1,5	0	0	0	0	0	0	1	0	0	0	0	0	0	1	0	0	0	0	0		3,5						3,5	1	3,50	BOTH	4,5
HSD17B11	1,5	1,5	1,5	0	1,5	1,5	1,5	1	1	1	1	1	1	1	0	0	0	0	0	0	0	2,5	2,5	2,5		2,5	2,5	2,5	15	6	2,50	BOTH	4,5
SCCPDH	0	1,5	1,5	0	1,5	0	0	1	1	1	0	1	0	0	0	0	0	0	0	0	0		2,5	2,5		2,5			7,5	3	2,50	BOTH	2
SERBP1	0	0	0	0	0	1	1	0	0	0	0	0	0	0	0	0	0	0	0	0	0						1	1	2	2	1,00	0	0
C1orf131	0	1	0	0	1	1	1	0	0	0	0	0	0	0	0	0	0	0	0	0	0		1			1	1	1	4	4	1,00	0	0
NPEPL1	0	1,5	1,5	0	1,5	0	1,5	1	1	1	1	1	1	1	0	0	0	0	0	0	0		2,5	2,5		2,5		2,5	10	4	2,50	418	6
ZNF740	1,5	0	0	0	1,5	1,5	0	1	1	0	0	1	1	0	0	0	0	0	0	0	0	2,5				2,5	2,5		7,5	3	2,50	0	0
RP9	1	1	1	1	1	1	0	0	0	0	0	0	0	0	0	0	0	1	1	1	0	1	1	1	2	2	2		9	6	1,50	0	0
MPLKIP	0	0	1,5	0	0	0	0	1	1	1	0	1	0	1	0	0	0	0	0	0	0			2,5					2,5	1	2,50	0	0
RDH11	0	0	1,5	0	1,5	0	1,5	0	1	1	1	1	1	1	0	0	0	0	0	0	0			2,5		2,5		2,5	7,5	3	2,50	BOTH	6
STT3B	0	1,5	1,5	0	1,5	1,5	1,5	1	1	1	0	1	1	1	0	0	0	1	0	0	1	0	2,5	3,5		2,5	3,5	2,5	14,5	5	2,90	BOTH	2
HM13	0	0	1,5	0	0	1,5	0	0	0	1	0	1	1	0	0	0	0	0	0	0	0			2,5			2,5		5	2	2,50	0	0
PARD3	0	0	0	0	0	1,5	0	0	0	0	0	0	1	0	0	0	0	0	0	0	0						2,5		2,5	1	2,50	0	0
IPO4	0	0	0	0	1,5	0	0	0	1	0	0	1	0	1	0	0	0	0	0	0	0					2,5			2,5	1	2,50	0	0
TMEM263	0	0	1,5	1,5	1,5	1,5	1,5	1	0	1	1	1	1	1	0	0	0	0	0	1	0			2,5	2,5	2,5	3,5	2,5	13,5	5	2,70	0	0
TFB1M	0	0	0	1	0	0	0	0	0	0	0	0	0	0	0	0	0	0	0	0	0				1				1	1	1,00	0	0
SCFD1	0	0	0	0	1,5	0	0	1	1	1	1	1	1	1	0	0	0	0	0	0	0					2,5			2,5	1	2,50	449	4
TNFAIP8L1	1	0	0	1	0	1	0	0	0	0	0	0	0	0	0	0	0	0	0	0	0	1			1		1		3	3	1,00	0	0
C2orf47	0	0	1,5	0	0	0	0	0	0	1	0	1	0	0	0	0	0	0	0	0	0			2,5					2,5	1	2,50	0	0
LMO7	0	0	1,5	0	0	0	0	0	0	1	0	0	0	0	0	0	0	0	0	0	0			2,5					2,5	1	2,50	0	0
ATXN2L	1,5	1,5	1,5	0	1,5	1,5	0	1	1	1	1	1	1	1	0	0	0	0	0	1	0	2,5	2,5	2,5		3,5	2,5		13,5	5	2,70	449	2
PHIP	0	0	0	0	0	0	1,5	0	0	0	0	0	0	1	0	0	0	0	0	0	0							2,5	2,5	1	2,50	0	0
TM9SF4	0	1,5	1,5	0	1,5	1,5	1,5	0	1	1	1	1	1	1	0	0	0	0	0	0	0		2,5	2,5		2,5	2,5	2,5	12,5	5	2,50	BOTH	3
PHF3	0	0	0	0	1,5	0	1,5	0	1	1	0	1	0	1	0	0	0	0	0	0	0					2,5		2,5	5	2	2,50	0	0
LPGAT1	0	0	1	0	0	0	0	0	0	1	0	1	0	0	0	0	0	0	0	0	0			2					2	1	2,00	BOTH	3
GCN1L1	0	0	0	0	1,5	0	0	1	1	0	1	1	1	0	0	0	0	0	0	0	0					2,5			2,5	1	2,50	BOTH	5
GTF2H4	1,5	1,5	0	0	1,5	0	0	1	1	0	0	1	1	0	0	1	0	0	0	0	0	2,5	3,5			2,5			8,5	3	2,83	0	0
UPF1	1,5	1,5	0	0	1,5	1,5	0	1	1	0	1	1	1	1	0	0	0	0	0	0	0	2,5	2,5			2,5	2,5		10	4	2,50	0	0

RAB8B	0	1,5	1,5	1,5	1,5	1,5	1,5	0	1	1	1	1	1	1	0	0	0	0	0	0	0		2,5	2,5	2,5	2,5	2,5	2,5	15	6	2,50	BOTH	4
KHSRP	1	1	1	1	1	1	1	1	1	1	1	1	1	1	1	1	1	1	1	1	1	3	3	3	3	3	3	3	21	7	3,00	418	2
TNPO1	0	1,5	0	0	0	0	0	0	1	0	1	0	1	1	0	0	0	0	0	0	0		2,5						2,5	1	2,50	BOTH	4,5
EMG1	0	0	0	0	0	0	1	0	0	0	0	0	0	0	0	0	0	0	0	0	0							1	1	1	1,00	0	0
CCDC47	0	1,5	1,5	1,5	1,5	0	1,5	1	1	1	1	1	1	1	0	0	0	0	0	0	0		2,5	2,5	2,5	2,5		2,5	12,5	5	2,50	BOTH	3
LRRC59	0	1	1	0	0	1	0	0	0	0	0	0	0	0	0	0	0	0	0	0	0		1	1			1		3	3	1,00	0	0
TOMM6	0	0	1,5	0	0	0	0	0	0	1	0	0	1	1	0	0	0	0	0	0	0			2,5					2,5	1	2,50	0	0
NSUN4	0	1	0	0	0	0	0	0	0	0	0	0	0	0	0	0	0	0	0	0	0		1						1	1	1,00	449	2
FAF2	1,5	1,5	1,5	0	1,5	1,5	1,5	1	1	1	1	1	1	1	0	0	0	0	0	0	0	2,5	2,5	2,5		2,5	2,5	2,5	15	6	2,50	BOTH	4
DAZAP1	0	0	0	0	0	0	1,5	0	1	0	0	1	0	1	0	0	0	0	0	0	0							2,5	2,5	1	2,50	0	0
DNAJA3	0	0	0	0	1	0	0	0	0	0	0	0	0	0	0	0	0	0	0	0	0					1			1	1	1,00	418	2
DYNLL2;DYNLL1	1,5	1,5	1,5	1,5	1,5	1,5	1,5	1	1	1	1	1	1	1	0	0	0	0	0	0	0	2,5	2,5	2,5	2,5	2,5	2,5	2,5	17,5	7	2,50	0	0
DDX27	0	0	0	0	0	0	1,5	0	1	0	0	0	0	1	0	0	0	0	0	0	0							2,5	2,5	1	2,50	0	0
DDRGK1	0	0	0	0	1,5	0	0	0	1	0	0	1	0	1	0	0	0	0	0	0	0					2,5			2,5	1	2,50	BOTH	4,5
FUBP3	1	1	1	1	1	1	1	0	0	0	0	0	0	0	0	0	0	0	0	0	0	1	1	1	1	1	1	1	7	7	1,00	0	0
RBM17	1,5	1,5	1,5	1,5	1,5	1,5	1,5	1	1	1	1	1	1	1	0	0	0	1	0	0	0	2,5	2,5	2,5	3,5	2,5	2,5	2,5	18,5	7	2,64	0	0
RSRC1	0	0	0	1,5	0	0	0	1	1	0	1	1	0	0	0	0	0	0	0	0	0				2,5				2,5	1	2,50	0	0
ZMAT2	1	0	0	0	1	0	0	0	0	0	0	0	0	0	0	0	0	0	0	0	0	1				1			2	2	1,00	0	0
NSUN5;NSUN5P2	0	0	1	0	0	0	0	0	0	0	0	0	0	0	0	0	0	0	0	0	0			1					1	1	1,00	418	4
IPO9	0	0	0	1,5	1,5	0	0	0	0	0	1	1	1	1	0	0	0	0	0	0	0				2,5	2,5			5	2	2,50	0	0
RBM14	1	1	1	1	1	0	1	0	0	0	0	0	0	0	0	1	0	0	1	0	0	1	2	1	1	2		1	8	6	1,33	0	0
RBM15	0	0	0	0	0	0	1	0	0	0	0	0	0	0	0	0	0	0	0	0	0							1	1	1	1,00	0	0
CNN2	0	0	1	0	0	0	0	0	0	0	0	0	0	0	0	0	0	0	0	0	0			1					1	1	1,00	0	0
PARK7	0	0	0	0	1	0	0	0	0	0	0	0	0	0	0	0	0	0	0	0	0					1			1	1	1,00	0	0
VAT1	0	0	1	0	1	1	1	0	1	1	0	1	1	1	0	1	0	0	1	1	1			2		3	3	3	11	4	2,75	0	0
PLIN2	1,5	1,5	1,5	0	1,5	1,5	1,5	1	1	1	1	1	1	1	0	0	0	0	0	0	0	2,5	2,5	2,5		2,5	2,5	2,5	15	6	2,50	0	0
DNAJC2	0	0	0	0	0	0	1,5	0	1	1	0	1	0	1	0	0	0	0	0	0	0							2,5	2,5	1	2,50	0	0
TTC1	0	0	0	0	1,5	1,5	0	0	0	0	1	1	1	0	0	0	0	0	0	0	0					2,5	2,5		5	2	2,50	0	0
DNAJC7	0	0	0	0	0	1,5	0	0	0	0	0	1	1	0	0	0	0	0	0	0	0						2,5		2,5	1	2,50	0	0
PHB2	1	1	1	1	1	1	1	0	0	0	0	0	0	0	1	1	1	1	1	1	1	2	2	2	2	2	2	2	14	7	2,00	BOTH	3
CHP1	0	0	0	0	1,5	0	0	0	1	0	0	1	0	0	0	0	0	0	0	0	0					2,5			2,5	1	2,50	0	0
NAP1L4	1,5	1,5	1,5	1,5	1,5	1,5	1,5	1	1	1	1	1	1	1	1	1	1	1	1	1	1	3,5	3,5	3,5	3,5	3,5	3,5	3,5	24,5	7	3,50	BOTH	5,5
MGST2	0	1	1	1	1	1	0	0	1	1	1	1	1	0	0	1	0	0	1	1	0		3	2	2	3	3		13	5	2,60	BOTH	4
CCT7	0	1,5	0	0	1,5	1,5	0	1	1	1	0	1	1	1	0	0	0	0	0	0	0		2,5			2,5	2,5		7,5	3	2,50	BOTH	3
ARID3A	1	1	1	1	1	1	1	0	0	0	0	0	0	0	0	0	0	1	1	1	0	1	1	1	2	2	2	1	10	7	1,43	0	0
DUSP9	0	0	1,5	0	0	1,5	0	0	0	1	1	1	1	0	0	0	0	0	0	0	0			2,5			2,5		5	2	2,50	BOTH	3
PKP2	1	1	1	1	0	1	0	0	0	0	0	0	0	0	0	0	0	0	0	0	0	1	1	1	1		1		5	5	1,00	0	0
NIPSNAP1	0	0	0	0	1,5	1,5	1,5	0	1	1	1	1	1	1	0	0	0	0	0	0	0					2,5	2,5	2,5	7,5	3	2,50	BOTH	5
VKORC1	0	0	0	0	0	1	0	0	1	1	1	1	1	1	0	0	0	0	0	0	0						2		2	1	2,00	449	2
TUBA1C	0	0	1	0	1	1	0	0	0	0	0	0	0	0	0	0	0	0	0	0	0			1		1	1		3	3	1,00	0	0
MYBBP1A	0	0	1	0	0	0	0	0	1	1	0	0	0	1	0	0	0	0	0	0	0			2					2	1	2,00	0	0
SDF4	0	0	0	0	1,5	0	0	0	0	0	0	1	0	0	0	0	0	0	0	0	0					2,5			2,5	1	2,50	0	0
PELO	0	0	0	0	1,5	0	1,5	1	1	1	1	1	1	1	0	0	0	0	0	0	0					2,5		2,5	5	2	2,50	418	2
NTPCR	1	0	0	0	1	1	0	0	0	0	0	0	0	0	0	0	0	0	0	0	0	1				1	1		3	3	1,00	0	0
ESYT1	1,5	1,5	1,5	1,5	1,5	1,5	1,5	1	1	1	1	1	1	1	0	0	1	0	1	0	0	2,5	2,5	3,5	2,5	3,5	2,5	2,5	19,5	7	2,79	BOTH	6
MMTAG2	1	1	1	1	0	1	0	0	0	0	0	0	0	0	0	0	0	0	0	0	0	1	1	1	1		1		5	5	1,00	0	0
TUBB6	0	0	0	1	1	0	1	0	0	0	0	0	0	0	0	0	0	0	0	0	0				1	1		1	3	3	1,00	BOTH	3
HNRNPUL1	0	1	1	1	1	1	1	1	0	0	0	1	1	1	0	1	0	1	1	1	1		2	1	2	3	3	3	14	6	2,33	0	0
DERL1	0	0	0	0	0	1,5	1,5	1	1	0	1	1	1	1	0	0	0	0	0	0	0						2,5	2,5	5	2	2,50	0	0
HTATIP2	0	0	1,5	0	1,5	1,5	1,5	1	1	1	1	1	1	1	0	0	0	0	0	0	0			2,5		2,5	2,5	2,5	10	4	2,50	BOTH	6
TUBB2B	0	1	1	1	1	1	1	0	0	0	0	0	0	0	0	0	0	0	0	0	0		1	1	1	1	1	1	6	6	1,00	0	0
TMEM109	0	0	1,5	0	0	1,5	0	0	1	1	1	1	1	0	0	0	0	0	0	0	0			2,5			2,5		5	2	2,50	BOTH	6
UTP14A	0	0	0	0	0	0	1,5	1	1	0	1	0	0	1	0	0	0	0	0	0	0							2,5	2,5	1	2,50	0	0
TMED9	1	1	1	1	1	1	1	0	0	0	0	0	0	0	1	1	1	0	1	1	1	2	2	2	1	2	2	2	13	7	1,86	BOTH	4
HIGD2A	0	0	1,5	0	0	1,5	0	1	1	1	0	1	1	0	0	0	0	0	0	0	0			2,5			2,5		5	2	2,50	0	0
ACAT2	0	0	0	0	0	1	0	0	0	0	1	1	1	0	0	0	0	0	0	0	0						2		2	1	2,00	0	0
CHID1	0	1	0	0	0	1	0	0	0	0	0	0	0	0	0	1	0	0	0	0	0		2				1		3	2	1,50	0	0
MRPL32	0	1	0	0	0	0	0	0	0	0	0	0	0	0	0	0	0	0	0	0	0		1						1	1	1,00	0	0
MRPL1	0	1	0	0	0	0	0	0	0	0	0	0	0	0	0	1	0	0	0	0	0		2						2	1	2,00	0	0
UBL5	0	0	0	1	0	0	0	0	0	0	0	1	0	0	0	0	0	0	0	0	0				1				1	1	1,00	0	0
SLC19A3	0	1,5	0	0	1,5	0	1,5	1	1	1	0	1	1	1	0	0	0	0	0	0	0		2,5			2,5		2,5	7,5	3	2,50	0	0
LNP	0	0	1,5	0	0	0	0	0	1	1	0	1	1	1	0	0	0	0	0	0	0			2,5					2,5	1	2,50	0	0

SLIRP	0	0	1,5	0	0	0	1,5	1	1	1	1	1	1	1	0	0	0	0	0	0	0			2,5				2,5	5	2	2,50	BOTH	3
MFF	0	1,5	1,5	0	1,5	1,5	1,5	0	1	1	1	1	1	1	0	0	0	0	0	0	0		2,5	2,5			2,5	2,5	12,5	5	2,50	0	0
NSRP1	1	1	1	0	1	1	0	0	0	0	0	0	0	0	0	0	0	0	0	0	0	1	1	1			1	1	5	5	1,00	0	0
RAB1B	1	1	1	1	1	1	1	0	0	0	0	0	0	0	1	1	1	1	1	1	1	2	2	2	2	2	2	2	14	7	2,00	BOTH	4
TMX1	0	0	1,5	0	1,5	1,5	0	1	1	1	1	1	1	1	0	0	0	0	0	0	0			2,5		2,5	2,5		7,5	3	2,50	BOTH	5,5
DHX35	0	0	1,5	0	0	1,5	0	0	1	1	0	1	1	1	0	0	0	0	0	0	0			2,5			2,5		5	2	2,50	0	0
ACAD9	0	0	0	0	1,5	0	0	1	1	0	1	1	1	0	0	0	0	0	0	0	0					2,5			2,5	1	2,50	0	0
METTL7A	0	1,5	1,5	1,5	1,5	1,5	1,5	0	1	1	1	1	1	1	0	0	0	0	0	0	0		2,5	2,5	2,5	2,5	2,5	2,5	15	6	2,50	BOTH	4,5
MOB1A;MOB1B	0	1,5	0	1,5	1,5	1,5	0	0	1	0	1	1	1	1	0	1	0	0	1	0	0		3,5		2,5	3,5	2,5		12	4	3,00	0	0
SFXN1	0	1	1	0	1	0	0	0	1	1	1	1	1	0	0	1	1	0	1	0	0		3	3		3			9	3	3,00	BOTH	4
TMEM165	0	0	0	0	1,5	1,5	0	1	1	0	1	1	1	1	0	0	0	0	0	0	0					2,5	2,5		5	2	2,50	BOTH	3
MOV10	0	0	0	0	1,5	1,5	1,5	0	1	0	0	1	1	1	0	0	0	0	0	0	0					2,5	2,5	2,5	7,5	3	2,50	BOTH	4,5
EPB41L5	1,5	1,5	0	1,5	1,5	0	0	1	1	1	1	1	1	1	0	0	0	0	0	0	0	2,5	2,5		2,5	2,5			10	4	2,50	0	0
ATP13A1	0	1,5	1,5	0	1,5	1,5	0	0	1	1	1	1	1	1	0	0	0	0	0	0	0		2,5	2,5		2,5	2,5		10	4	2,50	BOTH	5,5
TM9SF3	0	0	1,5	0	0	0	0	0	1	1	0	1	1	0	0	0	0	0	0	0	0			2,5					2,5	1	2,50	BOTH	4
APMAP	1,5	1,5	1,5	0	1,5	1,5	1,5	1	1	1	1	1	1	1	0	0	0	0	0	0	0	2,5	2,5	2,5		2,5	2,5	2,5	15	6	2,50	BOTH	4
WDR6	0	0	0	0	1,5	0	0	0	0	0	0	1	1	0	0	0	0	0	1	0	0					3,5			3,5	1	3,50	0	0
ZCCHC17	1	1	1	1	1	1	0	0	0	0	0	0	0	0	0	0	0	0	0	1	0	1	1	1	1	1	2		7	6	1,17	0	0
RAB18	0	1,5	1,5	1,5	1,5	1,5	1,5	0	1	1	1	1	1	1	0	0	0	0	0	0	0		2,5	2,5	2,5	2,5	2,5	2,5	15	6	2,50	BOTH	5,5
EMC7	0	1,5	1,5	0	0	0	1,5	0	1	1	0	1	1	1	0	0	0	0	0	0	0		2,5	2,5				2,5	7,5	3	2,50	0	0
ENY2	0	0	0	0	0	1,5	0	0	0	1	0	0	1	0	0	0	0	0	0	0	0						2,5		2,5	1	2,50	0	0
KRCC1	0	0	0	1	1	0	0	0	0	0	0	0	0	0	0	0	0	0	0	0	0				1	1			2	2	1,00	0	0
A1CF	0	0	0	0	1,5	1,5	0	1	1	1	0	1	1	1	0	0	0	0	0	0	0					2,5	2,5		5	2	2,50	0	0
RTN4	0	0	0	0	1,5	0	1,5	1	1	0	1	1	0	1	0	0	0	0	0	0	0					2,5		2,5	5	2	2,50	BOTH	3
ZC4H2	1	0	1	1	1	1	0	0	0	0	0	0	0	0	0	0	0	0	0	0	0	1		1	1	1	1		5	5	1,00	0	0
SAR1A	0	0	0	0	1,5	0	1,5	0	0	1	0	1	1	1	0	0	0	0	0	0	0					2,5		2,5	5	2	2,50	0	0
NANS	0	0	0	1,5	0	0	0	0	0	0	1	1	0	0	0	0	0	0	0	0	0				2,5				2,5	1	2,50	0	0
OSTC	1	1	1	1	1	1	1	0	0	0	0	0	0	0	0	1	1	0	1	1	0	1	2	2	1	2	2	1	11	7	1,57	BOTH	2
TOMM22	0	1,5	1,5	0	1,5	1,5	0	0	1	1	1	1	1	1	0	0	0	0	0	0	0		2,5	2,5		2,5	2,5		10	4	2,50	0	0
SACM1L	0	1,5	0	0	0	0	1,5	0	1	0	1	1	1	1	0	0	0	0	0	0	0		2,5					2,5	5	2	2,50	BOTH	5,5
ZCCHC3	0	1,5	0	0	0	0	0	0	1	0	0	0	0	0	0	0	0	0	0	0	0		2,5						2,5	1	2,50	0	0
DECR2	0	0	0	1	1	0	1	0	0	0	0	0	0	0	0	0	0	0	1	0	0				1	2		1	4	3	1,33	0	0
AGPAT5	0	0	0	0	1,5	0	0	0	0	0	0	1	0	1	0	0	0	0	0	0	0					2,5			2,5	1	2,50	0	0
SPATS2L	0	0	0	0	0	0	1	1	0	0	0	0	0	1	0	0	0	0	0	0	0							2	2	1	2,00	0	0
DNAJC11	0	1,5	1,5	0	0	1,5	1,5	0	1	1	0	0	1	1	0	0	0	0	0	0	0		2,5	2,5			2,5	2,5	10	4	2,50	0	0
ATAD3A	0	1	1	1	1	1	1	0	0	0	0	0	0	0	0	1	1	0	1	1	0		2	2	1	2	2	1	10	6	1,67	BOTH	2
ARL8B	0	1,5	1,5	0	1,5	0	1,5	0	1	1	0	1	0	1	0	0	0	0	0	0	0		2,5	2,5		2,5		2,5	10	4	2,50	0	0
DNAJC17	0	0	1,5	0	0	0	0	1	1	1	0	1	1	0	0	0	0	0	0	0	0			2,5					2,5	1	2,50	0	0
ARGLU1	0	0	0	0	1	1	0	0	0	0	0	0	0	0	0	0	0	0	0	0	0					1	1		2	2	1,00	0	0
NHP2	0	0	0	1	1	1	0	0	0	0	0	0	0	0	0	0	0	0	0	0	0				1	1	1		3	3	1,00	0	0
LYAR	0	0	0	0	0	0	1	0	0	0	0	0	0	1	1	0	0	0	0	0	0							2	2	1	2,00	0	0
CHCHD3	0	1,5	1,5	0	1,5	1,5	1,5	1	1	1	1	1	1	1	0	1	0	0	0	0	0		3,5	2,5		2,5	2,5	2,5	13,5	5	2,70	BOTH	6
CWC25	0	1	0	1	0	0	0	0	0	0	0	0	0	0	0	0	0	0	0	0	0		1		1				2	2	1,00	0	0
QPCTL	0	0	1,5	0	0	0	0	1	1	1	0	0	0	0	0	0	0	0	0	0	0			2,5					2,5	1	2,50	0	0
BCLAF1	0	1	1	1	1	1	0	0	0	0	0	0	0	0	0	1	0	1	1	1	0		2	1	2	2	2		9	5	1,80	0	0
FKBP11	0	1	1	0	1	0	0	0	0	0	0	0	0	0	0	0	0	0	0	0	0		1	1		1			3	3	1,00	449	2
TECR	0	0	1	0	1	1	0	0	0	0	0	0	0	0	0	1	0	0	0	0	0			1		1	1		3	3	1,00	0	0
FAM120A	0	0	0	0	1,5	0	0	0	1	0	1	1	1	0	0	0	0	0	0	0	0					2,5			2,5	1	2,50	0	0
IGF2BP1	1	1	1	1	1	1	1	0	0	0	0	0	0	0	0	1	1	1	1	1	1	1	2	2	2	2	2	2	13	7	1,86	BOTH	3
NDUFAF4	0	0	0	0	1,5	1,5	1,5	0	0	0	0	1	1	1	0	0	0	0	0	0	0					2,5	2,5	2,5	7,5	3	2,50	0	0
HACD3	0	1,5	0	0	1,5	0	0	0	1	1	1	1	1	1	0	0	0	0	0	0	0		2,5			2,5			5	2	2,50	BOTH	6
NDUFA13	1	1	1	1	1	1	1	0	0	0	0	0	0	0	0	0	0	1	1	1	0	1	1	1	2	2	2	1	10	7	1,43	BOTH	3
VAPA	1,5	1,5	1,5	1,5	1,5	1,5	1,5	1	1	1	1	1	1	1	1	1	1	1	1	1	1	3,5	3,5	3,5	3,5	3,5	3,5	3,5	24,5	7	3,50	BOTH	4
RRBP1	0	0	1	0	0	0	1	0	0	0	0	0	0	0	0	0	0	0	0	0	0				1			1	2	2	1,00	0	0
DPM3	0	1,5	1,5	0	0	1,5	1,5	0	1	1	0	1	1	1	0	0	0	0	0	0	0		2,5	2,5			2,5	2,5	10	4	2,50	0	0
ATXN10	0	0	0	0	1,5	0	0	1	0	0	0	1	0	0	0	0	0	0	0	0	0					2,5			2,5	1	2,50	BOTH	3
DHCR7	1	1	1	1	1	1	1	0	0	0	0	0	0	0	1	1	1	0	1	1	1	2	2	2	1	2	2	2	13	7	1,86	449	2
SLC25A10	0	0	0	0	0	0	1	0	1	1	0	0	1	1	0	0	0	0	0	0	1							3	3	1	3,00	BOTH	4
FTSJ1	0	0	0	0	1,5	1,5	1,5	0	1	0	0	1	1	1	0	0	0	0	0	0	0					2,5	2,5	2,5	7,5	3	2,50	0	0
CGGBP1	0	1	0	0	0	0	0	0	0	0	0	0	0	0	0	0	0	0	0	0	0		1						1	1	1,00	0	0
SEC63	0	1,5	0	0	1,5	0	1,5	0	1	1	1	1	1	1	0	0	0	0	0	0	0		2,5			2,5		2,5	7,5	3	2,50	BOTH	3
NDUFA12	0	0	1,5	0	0	0	0	0	0	1	0	1	1	0	0	0	0	0	0	0	0			2,5					2,5	1	2,50	418	4

SLC25A13	0	0	0	0	1	1	1	0	0	0	0	0	0	0	0	0	0	0	0	0	0					1	1	1	3	3	1,00	0	0
DDX41	0	1,5	1,5	1,5	0	0	0	1	1	1	1	1	1	1	0	0	0	0	0	0	0		2,5	2,5	2,5				7,5	3	2,50	0	0
STOML2	1,5	1,5	1,5	1,5	1,5	1,5	1,5	1	1	1	1	1	1	1	0	0	1	0	0	1	0	2,5	2,5	3,5	2,5	2,5	3,5	2,5	19,5	7	2,79	BOTH	5,5
ACIN1	0	0	0	0	0	0	1,5	0	1	1	1	0	0	1	0	0	0	0	0	0	0							2,5	2,5	1	2,50	0	0
RAB21	1,5	1,5	1,5	1,5	1,5	1,5	1,5	1	1	1	1	1	1	1	0	0	0	0	0	0	0	2,5	2,5	2,5	2,5	2,5	2,5	2,5	17,5	7	2,50	BOTH	5
AKAP8L	0	0	0	0	0	1,5	0	0	0	0	0	0	1	0	0	0	0	0	0	0	0						2,5		2,5	1	2,50	0	0
TMCO1	0	0	1	0	0	0	0	0	0	0	0	0	0	0	0	0	0	0	0	0	0			1					1	1	1,00	449	2
PRPF19	1	0	0	1	0	1	1	0	0	0	0	0	0	0	0	0	0	0	0	0	0	1			1		1	1	4	4	1,00	449	4
UBQLN1;UBQLN4	0	1,5	1,5	0	0	0	1,5	0	1	1	1	1	1	1	0	0	0	0	0	0	0		2,5	2,5				2,5	7,5	3	2,50	0	0
L1RE1	0	1,5	0	0	0	0	0	0	1	0	1	1	1	1	0	0	0	0	0	0	0		2,5						2,5	1	2,50	BOTH	4,5
G3BP2	0	1	1	1	1	1	0	0	0	0	0	0	0	0	0	1	0	1	1	1	0		2	1	2	2	2		9	5	1,80	418	4
MAGED2	1,5	1,5	1,5	1,5	1,5	1,5	1,5	1	1	1	1	1	1	1	0	0	1	0	0	0	0	2,5	2,5	3,5	2,5	2,5	2,5	2,5	18,5	7	2,64	418	4
SHOC2	0	0	0	0	0	0	1,5	0	0	0	0	0	1	1	0	0	0	0	0	0	0							2,5	2,5	1	2,50	0	0
SRRM2	0	0	0	1	0	1	0	0	0	0	0	0	0	0	0	0	0	0	0	0	0				1		1		2	2	1,00	0	0
C14orf166	0	0	0	1	1	0	0	0	0	0	0	0	0	0	0	0	0	0	0	0	0				1	1			2	2	1,00	0	0
RUVBL2	1,5	1,5	1,5	1,5	1,5	1,5	1,5	1	1	1	1	1	1	1	0	1	1	0	0	0	1	2,5	3,5	3,5	2,5	2,5	2,5	3,5	20,5	7	2,93	BOTH	2
HIGD1A	0	1	0	0	1	1	1	0	0	0	0	0	0	0	0	0	0	0	0	0	0		1			1	1	1	4	4	1,00	0	0
RUVBL1	1	1	1	1	1	1	1	0	0	0	0	0	0	0	1	1	1	0	1	1	1	2	2	2	1	2	2	2	13	7	1,86	BOTH	4
VDAC3	1	1	1	1	1	1	1	0	0	0	0	0	0	0	1	1	1	1	1	1	1	2	2	2	2	2	2	2	14	7	2,00	BOTH	4
FARSA	0	0	1	1	0	0	1	0	0	0	0	0	0	0	0	0	0	0	0	0	0			1	1			1	3	3	1,00	BOTH	5
DNAJC16	0	0	0	0	1,5	0	0	0	0	0	0	1	0	0	0	0	0	0	1	0	0					3,5			3,5	1	3,50	0	0
COA3	0	1,5	1,5	0	0	1,5	0	0	1	1	0	1	1	1	0	0	0	0	0	0	0		2,5	2,5			2,5		7,5	3	2,50	0	0
MRPS7	0	1,5	0	0	0	0	0	0	1	0	0	1	0	0	0	0	0	0	0	0	0		2,5						2,5	1	2,50	0	0
LEMD3	0	0	1,5	0	0	0	0	0	1	1	0	1	1	0	0	0	0	0	0	0	0			2,5					2,5	1	2,50	BOTH	4,5
THRAP3	1	1	0	1	1	1	0	0	0	0	0	0	0	0	0	0	0	0	1	0	0	1	1		1	2	1		6	5	1,20	0	0
UBE2D4;UBE2D2;UBE2D3;UBE2D1	0	0	1,5	0	0	0	0	1	0	1	0	0	1	0	0	0	0	0	0	0	0			2,5					2,5	1	2,50	0	0
SUGT1	0	0	1,5	0	0	0	0	0	0	1	0	0	0	0	0	0	0	0	0	0	0			2,5					2,5	1	2,50	BOTH	2
TMX2	1	1	1	1	1	1	1	0	0	0	0	0	0	0	1	1	1	1	1	1	1	2	2	2	2	2	2	2	14	7	2,00	BOTH	4
DHRS7	0	1,5	1,5	1,5	1,5	1,5	1,5	0	1	1	1	1	1	1	0	0	0	0	0	0	0		2,5	2,5	2,5	2,5	2,5	2,5	15	6	2,50	BOTH	5,5
NOP16	0	1,5	0	0	0	0	0	0	1	0	0	0	0	1	0	0	0	0	0	0	0		2,5						2,5	1	2,50	0	0
GOLT1B	0	0	1,5	0	0	0	0	0	0	1	0	0	1	0	0	0	0	0	0	0	0			2,5					2,5	1	2,50	0	0
PTRH2	1,5	1,5	1,5	1,5	1,5	1,5	1,5	1	1	1	1	1	1	1	1	1	1	0	1	1	1	3,5	3,5	3,5	2,5	3,5	3,5	3,5	23,5	7	3,36	BOTH	5
MTCL1	0	0	0	0	1,5	0	0	0	1	0	0	1	0	0	0	0	0	0	1	0	0					3,5			3,5	1	3,50	0	0
TCAF1	0	0	0	0	1,5	0	0	1	1	0	0	1	0	1	0	0	0	0	0	0	0					2,5			2,5	1	2,50	0	0
TBL2	0	0	1	0	0	1	0	0	1	1	0	1	1	1	0	0	0	0	0	0	0			2			2		4	2	2,00	BOTH	4
AFG3L2	0	0	1	0	0	0	0	0	0	1	0	1	1	1	0	0	0	0	0	0	0			2					2	1	2,00	0	0
SAMM50	0	1,5	1,5	0	1,5	0	1,5	0	1	1	1	1	1	1	0	1	0	0	0	0	0		3,5	2,5		2,5		2,5	11	4	2,75	0	0
PRRC2C	0	0	0	0	0	1,5	0	0	1	0	0	0	1	0	0	0	0	0	0	0	0						2,5		2,5	1	2,50	0	0
TIMM13	0	1,5	1,5	1,5	0	1,5	1,5	0	1	1	1	1	1	1	0	0	0	0	0	0	0		2,5	2,5	2,5		2,5	2,5	12,5	5	2,50	0	0
SRPRB	0	1	1	0	1	1	0	0	1	1	1	1	1	1	0	1	1	0	1	0	0		3	3		3	2		11	4	2,75	BOTH	4
MTCH2	0	1	1	1	1	1	1	0	0	0	0	0	0	0	0	1	1	1	1	1	1		2	2	2	2	2	2	12	6	2,00	BOTH	5
BZW2	0	0	1,5	0	0	0	0	0	1	1	1	0	1	0	0	0	0	0	0	0	0			2,5					2,5	1	2,50	0	0
CEPT1	0	1,5	1,5	0	0	1,5	1,5	0	1	1	0	1	1	1	0	0	0	0	0	0	0		2,5	2,5			2,5	2,5	10	4	2,50	0	0
IGF2BP2	0	1,5	1,5	1,5	1,5	1,5	1,5	1	1	1	1	1	1	1	0	0	0	0	0	0	0		2,5	2,5	2,5	2,5	2,5	2,5	15	6	2,50	0	0
NDUFB9	0	0	1,5	0	0	1,5	0	0	0	1	1	0	1	1	0	0	0	0	0	0	0			2,5			2,5		5	2	2,50	0	0

Supplementary Table 8: String enriched pathways in our interactomic network of NS5A proteins of diverse genotypic origins.

Category	term name	description	FDR	#genes	#background genes
GO Molecular Function	GO:0003723	RNA binding	1,42E-57	203	1649
GO Molecular Function	GO:1901363	Heterocyclic compound binding	2,40E-37	353	5831
GO Molecular Function	GO:0097159	Organic cyclic compound binding	5,16E-37	355	5916
Reactome Pathways	HSA-1430728	Metabolism	7,46E-35	189	2089
GO Biological Process	GO:0008152	Metabolic process	1,48E-33	431	8298
GO Biological Process	GO:0044237	Cellular metabolic process	8,33E-33	403	7513
GO Biological Process	GO:0051649	Establishment of localization in cell	2,06E-31	197	2375
KEGG Pathways	hsa05014	Amyotrophic lateral sclerosis	1,00E-30	73	352
KEGG Pathways	hsa05012	Parkinson disease	1,13E-30	62	240
KEGG Pathways	hsa05020	Prion disease	1,95E-30	64	265
GO Biological Process	GO:0006810	Transport	1,65E-29	279	4353
GO Biological Process	GO:0051641	Cellular localization	1,75E-29	220	2967
GO Biological Process	GO:0051234	Establishment of localization	5,35E-28	280	4479
GO Biological Process	GO:0046907	Intracellular transport	5,40E-28	146	1520
GO Biological Process	GO:0046034	ATP metabolic process	3,94E-25	53	204
GO Biological Process	GO:1901360	Organic cyclic compound metabolic process	4,64E-25	216	3118
GO Biological Process	GO:0009987	Cellular process	9,45E-25	590	15024
KEGG Pathways	hsa05016	Huntington disease	3,77E-24	59	298
Reactome Pathways	HSA-1428517	The citric acid (TCA) cycle and respiratory electron transport	1,67E-23	48	176
Reactome Pathways	HSA-392499	Metabolism of proteins	7,20E-23	158	1977
GO Biological Process	GO:0071704	Organic substance metabolic process	8,90E-23	384	7755
Reactome Pathways	HSA-163200	Respiratory electron transport, ATP synthesis by chemiosmotic coupling, and heat production by uncoupling proteins.	1,23E-22	41	125
GO Molecular Function	GO:0000166	Nucleotide binding	1,87E-22	164	2119
GO Biological Process	GO:0051179	Localization	2,25E-22	307	5591
GO Biological Process	GO:0006139	Nucleobase-containing compound metabolic process	2,25E-22	189	2659
GO Biological Process	GO:0055114	Oxidation-reduction process	2,83E-22	102	939
GO Biological Process	GO:0044238	Primary metabolic process	2,86E-22	368	7332
Reactome Pathways	HSA-8953854	Metabolism of RNA	2,88E-22	84	659
GO Biological Process	GO:0007005	Mitochondrion organization	2,96E-22	70	452
GO Biological Process	GO:0006725	Cellular aromatic compound metabolic process	3,68E-22	198	2882
GO Biological Process	GO:0006886	Intracellular protein transport	1,46E-21	104	999
KEGG Pathways	hsa05010	Alzheimer disease	1,52E-21	60	355
GO Biological Process	GO:0016032	Viral process	3,24E-21	90	776
GO Biological Process	GO:0046483	Heterocycle metabolic process	5,81E-21	193	2840
GO Biological Process	GO:0071705	Nitrogen compound transport	6,38E-21	146	1823
GO Molecular Function	GO:0016491	Oxidoreductase activity	8,27E-21	86	726
GO Molecular Function	GO:0036094	Small molecule binding	8,27E-21	178	2516
GO Biological Process	GO:0006091	Generation of precursor metabolites and energy	1,04E-20	64	405
GO Biological Process	GO:0034641	Cellular nitrogen compound metabolic process	1,19E-20	211	3282
GO Biological Process	GO:0044403	Symbiotic process	1,57E-20	94	865
GO Biological Process	GO:1903311	Regulation of mRNA metabolic process	3,38E-20	58	338
KEGG Pathways	hsa01100	Metabolic pathways	4,69E-20	123	1447
GO Biological Process	GO:0009058	Biosynthetic process	1,30E-19	187	2788
GO Biological Process	GO:0033036	Macromolecule localization	1,33E-19	173	2473
GO Biological Process	GO:0015031	Protein transport	1,33E-19	126	1486
GO Biological Process	GO:1901576	Organic substance biosynthetic process	2,07E-19	184	2734

GO Molecular Function	GO:0003676	Nucleic acid binding	3,18E-19	234	3947
GO Molecular Function	GO:0005488	Binding	3,66E-19	516	12516
GO Biological Process	GO:0043488	Regulation of mRNA stability	4,22E-19	43	183
GO Biological Process	GO:0006996	Organelle organization	6,28E-19	213	3450
GO Biological Process	GO:0006119	Oxidative phosphorylation	6,28E-19	36	118
GO Biological Process	GO:0071702	Organic substance transport	9,47E-19	157	2173
GO Molecular Function	GO:0017111	Nucleoside-triphosphatase activity	1,01E-18	84	760
GO Biological Process	GO:0034613	Cellular protein localization	1,07E-18	130	1610
GO Biological Process	GO:0045184	Establishment of protein localization	2,04E-18	127	1564
KEGG Pathways	hsa00190	Oxidative phosphorylation	7,87E-18	35	130
GO Biological Process	GO:0016071	mRNA metabolic process	1,27E-17	77	678
WikiPathways	WP111	Electron transport chain: OXPHOS system in mitochondria	1,45E-17	33	103
GO Molecular Function	GO:0017076	Purine nucleotide binding	1,56E-17	140	1878
GO Molecular Function	GO:0032553	Ribonucleotide binding	1,56E-17	140	1880
GO Molecular Function	GO:0032555	Purine ribonucleotide binding	1,82E-17	139	1864
KEGG Pathways	hsa04141	Protein processing in endoplasmic reticulum	1,83E-17	38	165
GO Biological Process	GO:0008104	Protein localization	1,84E-17	152	2139
Reactome Pathways	HSA-5663205	Infectious disease	4,06E-17	85	826
KEGG Pathways	hsa04714	Thermogenesis	5,94E-17	43	229
GO Molecular Function	GO:0035639	Purine ribonucleoside triphosphate binding	2,17E-16	133	1799
GO Biological Process	GO:0006457	Protein folding	2,52E-16	42	213
GO Biological Process	GO:0016070	RNA metabolic process	2,52E-16	123	1584
GO Biological Process	GO:0010467	Gene expression	3,09E-16	145	2056
GO Biological Process	GO:0008380	RNA splicing	3,27E-16	56	396
GO Molecular Function	GO:0045296	Cadherin binding	4,47E-16	51	334
GO Molecular Function	GO:0051082	Unfolded protein binding	7,31E-16	31	108
GO Biological Process	GO:0044281	Small molecule metabolic process	1,32E-15	126	1684
GO Molecular Function	GO:0003824	Catalytic activity	1,65E-15	280	5486
WikiPathways	WP2359	Parkin-ubiquitin proteasomal system pathway	1,77E-15	26	67
Reactome Pathways	HSA-1852241	Organelle biogenesis and maintenance	2,18E-15	47	290
GO Biological Process	GO:0072594	Establishment of protein localization to organelle	2,91E-15	57	433
GO Biological Process	GO:0007007	Inner mitochondrial membrane organization	2,94E-15	23	48
Reactome Pathways	HSA-2262752	Cellular responses to stress	4,21E-15	64	544
Reactome Pathways	HSA-611105	Respiratory electron transport	1,16E-14	29	101
GO Biological Process	GO:0010608	Posttranscriptional regulation of gene expression	1,23E-14	65	574
GO Biological Process	GO:0033365	Protein localization to organelle	1,33E-14	75	743
GO Biological Process	GO:0061024	Membrane organization	1,35E-14	78	796
GO Biological Process	GO:0006839	Mitochondrial transport	3,27E-14	40	225
GO Biological Process	GO:0006807	Nitrogen compound metabolic process	4,68E-14	324	6852
GO Biological Process	GO:0006397	mRNA processing	5,94E-14	57	468
DISEASES	DOID:655	Inherited metabolic disorder	7,21E-14	75	726
GO Molecular Function	GO:0097367	Carbohydrate derivative binding	1,12E-13	145	2226
GO Biological Process	GO:0044249	Cellular biosynthetic process	1,25E-13	162	2611
GO Biological Process	GO:0090304	Nucleic acid metabolic process	1,49E-13	143	2178
Reactome Pathways	HSA-597592	Post-translational protein modification	2,22E-13	106	1390
GO Biological Process	GO:0045333	Cellular respiration	2,54E-13	33	158
GO Biological Process	GO:0022904	Respiratory electron transport chain	2,91E-13	28	107

GO Molecular Function	GO:0003729	mRNA binding	4,15E-13	43	289
GO Biological Process	GO:0006396	RNA processing	4,19E-13	78	854
GO Biological Process	GO:0022900	Electron transport chain	4,98E-13	34	174
GO Biological Process	GO:1901566	Organonitrogen compound biosynthetic process	5,19E-13	103	1346
Reactome Pathways	HSA-8949613	Cristae formation	5,66E-13	18	31
Reactome Pathways	HSA-8852276	The role of GTSE1 in G2/M progression after G2 checkpoint	5,86E-13	24	75
KEGG Pathways	hsa03040	Spliceosome	6,89E-13	29	132
GO Biological Process	GO:0043312	Neutrophil degranulation	7,18E-13	56	484
GO Biological Process	GO:0036230	Granulocyte activation	8,29E-13	57	502
GO Biological Process	GO:1990542	Mitochondrial transmembrane transport	1,10E-12	26	95
WikiPathways	WP623	Oxidative phosphorylation	1,13E-12	22	60
Reactome Pathways	HSA-72766	Translation	1,92E-12	42	289
Reactome Pathways	HSA-6798695	Neutrophil degranulation	2,69E-12	54	473
GO Biological Process	GO:0006754	ATP biosynthetic process	2,90E-12	18	35
GO Biological Process	GO:0002275	Myeloid cell activation involved in immune response	3,50E-12	57	522
GO Molecular Function	GO:0043168	Anion binding	3,63E-12	165	2805
GO Biological Process	GO:0065003	Protein-containing complex assembly	4,18E-12	98	1293
GO Biological Process	GO:0045055	Regulated exocytosis	4,35E-12	67	697
GO Biological Process	GO:0006887	Exocytosis	4,77E-12	72	789
Reactome Pathways	HSA-450531	Regulation of mRNA stability by proteins that bind AU-rich elements	4,83E-12	24	85
GO Biological Process	GO:0006605	Protein targeting	5,50E-12	46	356
GO Biological Process	GO:0042407	Cristae formation	6,37E-12	17	31
GO Biological Process	GO:0007006	Mitochondrial membrane organization	7,72E-12	29	137
Reactome Pathways	HSA-1643685	Disease	8,13E-12	109	1548
GO Biological Process	GO:0044419	Interspecies interaction between organisms	1,02E-11	125	1899
WikiPathways	WP3888	VEGFA-VEGFR2 signaling pathway	1,11E-11	50	428
WikiPathways	WP4718	Cholesterol metabolism with Bloch and Kandutsch-Russell pathways	1,11E-11	19	46
GO Biological Process	GO:0042776	Mitochondrial ATP synthesis coupled proton transport	1,14E-11	15	21
GO Biological Process	GO:0071840	Cellular component organization or biogenesis	1,71E-11	271	5633
GO Biological Process	GO:0000375	RNA splicing, via transesterification reactions	1,87E-11	41	297
GO Biological Process	GO:0009894	Regulation of catabolic process	3,34E-11	83	1038
GO Biological Process	GO:0009152	Purine ribonucleotide biosynthetic process	3,41E-11	29	147
GO Biological Process	GO:0009260	Ribonucleotide biosynthetic process	4,11E-11	30	160
GO Biological Process	GO:0140352	Export from cell	5,17E-11	82	1028
GO Biological Process	GO:0000398	mRNA splicing, via spliceosome	5,38E-11	40	294
Reactome Pathways	HSA-68882	Mitotic Anaphase	5,54E-11	35	227
GO Biological Process	GO:0009201	Ribonucleoside triphosphate biosynthetic process	5,57E-11	19	52
GO Biological Process	GO:0044085	Cellular component biogenesis	5,58E-11	152	2583
GO Biological Process	GO:0042775	Mitochondrial ATP synthesis coupled electron transport	5,58E-11	23	87
GO Biological Process	GO:0031329	Regulation of cellular catabolic process	5,61E-11	74	875
Reactome Pathways	HSA-446203	Asparagine N-linked glycosylation	7,07E-11	40	300
Reactome Pathways	HSA-3371497	HSP90 chaperone cycle for steroid hormone receptors (SHR)	7,07E-11	19	54
GO Molecular Function	GO:0003924	GTPase activity	1,20E-10	41	318
Reactome Pathways	HSA-1592230	Mitochondrial biogenesis	1,26E-10	23	93
GO Biological Process	GO:0009142	Nucleoside triphosphate biosynthetic process	1,33E-10	20	64
GO Biological Process	GO:0043933	Protein-containing complex subunit organization	1,63E-10	105	1539
GO Biological Process	GO:0015980	Energy derivation by oxidation of organic compounds	1,66E-10	34	223

GO Biological Process	GO:0016043	Cellular component organization	1,72E-10	260	5447
GO Biological Process	GO:0032940	Secretion by cell	1,81E-10	78	979
KEGG Pathways	hsa04932	Non-alcoholic fatty liver disease	2,28E-10	27	148
Reactome Pathways	HSA-68886	M Phase	2,40E-10	44	376
GO Biological Process	GO:0009199	Ribonucleoside triphosphate metabolic process	2,51E-10	20	67
GO Molecular Function	GO:0050839	Cell adhesion molecule binding	2,65E-10	54	538
Reactome Pathways	HSA-389960	Formation of tubulin folding intermediates by CCT/TriC	3,34E-10	14	24
Reactome Pathways	HSA-69275	G2/M Transition	3,44E-10	31	193
Reactome Pathways	HSA-1799339	SRP-dependent cotranslational protein targeting to membrane	3,49E-10	24	110
Reactome Pathways	HSA-450408	AUF1 (hnRNP D0) binds and destabilizes mRNA	3,56E-10	18	53
GO Biological Process	GO:0044271	Cellular nitrogen compound biosynthetic process	4,17E-10	103	1522
GO Biological Process	GO:0009205	Purine ribonucleoside triphosphate metabolic process	4,72E-10	19	61
Reactome Pathways	HSA-9609507	Protein localization	5,49E-10	28	160
GO Biological Process	GO:0002443	Leukocyte mediated immunity	5,94E-10	59	641
GO Biological Process	GO:0016192	Vesicle-mediated transport	6,93E-10	115	1805
GO Biological Process	GO:0002366	Leukocyte activation involved in immune response	7,00E-10	58	626
GO Biological Process	GO:0006793	Phosphorus metabolic process	8,22E-10	129	2134
Reactome Pathways	HSA-389957	Prefoldin mediated transfer of substrate to CCT/TriC	8,93E-10	14	27
GO Biological Process	GO:0046903	Secretion	8,99E-10	82	1097
Reactome Pathways	HSA-72163	mRNA Splicing - Major Pathway	1,02E-09	29	178
Reactome Pathways	HSA-9010553	Regulation of expression of SLITs and ROBOs	1,22E-09	28	167
GO Biological Process	GO:0009150	Purine ribonucleotide metabolic process	1,43E-09	38	303
GO Biological Process	GO:0009259	Ribonucleotide metabolic process	1,43E-09	39	318
GO Biological Process	GO:0006796	Phosphate-containing compound metabolic process	1,45E-09	127	2107
Reactome Pathways	HSA-6807878	COPI-mediated anterograde transport	1,88E-09	22	100
Reactome Pathways	HSA-9663891	Selective autophagy	2,04E-09	20	80
WikiPathways	WP4396	Nonalcoholic fatty liver disease	2,16E-09	27	155
Reactome Pathways	HSA-376176	Signaling by ROBO receptors	2,32E-09	31	213
Reactome Pathways	HSA-163210	Formation of ATP by chemiosmotic coupling	2,45E-09	12	18
GO Molecular Function	GO:0005525	GTP binding	2,45E-09	42	370
Reactome Pathways	HSA-5653656	Vesicle-mediated transport	2,45E-09	58	660
Reactome Pathways	HSA-71291	Metabolism of amino acids and derivatives	2,57E-09	41	365
GO Biological Process	GO:0090150	Establishment of protein localization to membrane	3,04E-09	35	267
GO Molecular Function	GO:0030554	Adenyl nucleotide binding	3,15E-09	101	1534
Reactome Pathways	HSA-191273	Cholesterol biosynthesis	3,41E-09	13	25
Reactome Pathways	HSA-199977	ER to Golgi Anterograde Transport	3,41E-09	26	152
GO Biological Process	GO:0043604	Amide biosynthetic process	3,64E-09	50	512
GO Molecular Function	GO:0032559	Adenyl ribonucleotide binding	4,06E-09	100	1522
GO Biological Process	GO:0022607	Cellular component assembly	4,21E-09	136	2359
Reactome Pathways	HSA-8856688	Golgi-to-ER retrograde transport	4,47E-09	24	130
GO Biological Process	GO:0019752	Carboxylic acid metabolic process	4,69E-09	68	853
GO Biological Process	GO:0044248	Cellular catabolic process	5,54E-09	110	1758
Reactome Pathways	HSA-199991	Membrane Trafficking	5,58E-09	55	622
GO Biological Process	GO:0009056	Catabolic process	6,56E-09	122	2042
DISEASES	DOID:0014667	Disease of metabolism	7,55E-09	78	997
GO Biological Process	GO:0033554	Cellular response to stress	8,21E-09	108	1725
GO Biological Process	GO:0009165	Nucleotide biosynthetic process	9,38E-09	32	236

KEGG Pathways	hsa01212	Fatty acid metabolism	1,03E-08	16	54
GO Biological Process	GO:1901362	Organic cyclic compound biosynthetic process	1,48E-08	84	1211
GO Biological Process	GO:0032482	Rab protein signal transduction	1,67E-08	18	69
GO Biological Process	GO:0010033	Response to organic substance	1,79E-08	160	3011
Reactome Pathways	HSA-2995410	Nuclear Envelope (NE) Reassembly	1,81E-08	18	73
Reactome Pathways	HSA-1268020	Mitochondrial protein import	2,06E-08	17	64
Reactome Pathways	HSA-8873719	RAB geranylgeranylation	2,06E-08	17	64
GO Biological Process	GO:0045321	Leukocyte activation	2,22E-08	70	929
GO Biological Process	GO:0019637	Organophosphate metabolic process	2,36E-08	67	870
GO Biological Process	GO:0009117	Nucleotide metabolic process	2,43E-08	43	422
GO Molecular Function	GO:0009055	Electron transfer activity	2,53E-08	21	103
Reactome Pathways	HSA-2467813	Separation of Sister Chromatids	2,67E-08	27	184
GO Biological Process	GO:0034622	Cellular protein-containing complex assembly	3,06E-08	64	816
Reactome Pathways	HSA-5687128	MAPK6/MAPK4 signaling	3,17E-08	19	87
GO Molecular Function	GO:0016887	ATPase activity	3,23E-08	41	393
KEGG Pathways	hsa00100	Steroid biosynthesis	3,25E-08	11	20
GO Biological Process	GO:0043436	Oxoacid metabolic process	4,06E-08	70	944
GO Molecular Function	GO:0005524	ATP binding	4,41E-08	94	1464
GO Biological Process	GO:0042026	Protein refolding	4,96E-08	11	18
DISEASES	DOID:700	Mitochondrial metabolism disease	5,46E-08	28	173
GO Biological Process	GO:0055085	Transmembrane transport	5,47E-08	87	1314
Reactome Pathways	HSA-69278	Cell Cycle, Mitotic	5,51E-08	47	518
GO Biological Process	GO:0055086	Nucleobase-containing small molecule metabolic process	6,36E-08	47	508
Reactome Pathways	HSA-1236974	ER-Phagosome pathway	6,72E-08	18	81
Reactome Pathways	HSA-72203	Processing of Capped Intron-Containing Pre-mRNA	7,22E-08	30	238
GO Biological Process	GO:0007265	Ras protein signal transduction	7,45E-08	30	230
Reactome Pathways	HSA-168255	Influenza Infection	7,57E-08	24	154
GO Biological Process	GO:0043043	Peptide biosynthetic process	7,71E-08	40	389
GO Biological Process	GO:0006695	Cholesterol biosynthetic process	8,94E-08	14	41
Reactome Pathways	HSA-422475	Axon guidance	9,09E-08	48	547
Reactome Pathways	HSA-6811442	Intra-Golgi and retrograde Golgi-to-ER traffic	9,62E-08	27	198
GO Biological Process	GO:0044283	Small molecule biosynthetic process	1,02E-07	50	572
GO Biological Process	GO:0019882	Antigen processing and presentation	1,02E-07	29	219
GO Biological Process	GO:0002252	Immune effector process	1,06E-07	70	969
GO Biological Process	GO:0001775	Cell activation	1,09E-07	75	1075
Reactome Pathways	HSA-1640170	Cell Cycle	1,16E-07	53	647
GO Biological Process	GO:0072599	Establishment of protein localization to endoplasmic reticulum	1,16E-07	21	114
Reactome Pathways	HSA-9675108	Nervous system development	1,21E-07	49	572
GO Biological Process	GO:0090407	Organophosphate biosynthetic process	1,23E-07	48	539
Reactome Pathways	HSA-6799198	Complex I biogenesis	1,26E-07	15	55
Reactome Pathways	HSA-6811434	COPI-dependent Golgi-to-ER retrograde traffic	1,26E-07	19	97
GO Biological Process	GO:0016310	Phosphorylation	1,29E-07	84	1275
GO Biological Process	GO:0006986	Response to unfolded protein	1,31E-07	25	166
GO Biological Process	GO:0070972	Protein localization to endoplasmic reticulum	1,34E-07	23	140
GO Biological Process	GO:0006629	Lipid metabolic process	1,38E-07	80	1190
Reactome Pathways	HSA-5610787	Hedgehog off state	1,47E-07	20	110
GO Biological Process	GO:1904874	Positive regulation of telomerase RNA localization to Cajal body	1,47E-07	10	15

GO Biological Process	GO:0006412	Translation	1,47E-07	38	366
GO Biological Process	GO:1901137	Carbohydrate derivative biosynthetic process	1,72E-07	51	602
GO Biological Process	GO:0034976	Response to endoplasmic reticulum stress	1,75E-07	31	256
GO Biological Process	GO:0065008	Regulation of biological quality	1,87E-07	195	4042
GO Biological Process	GO:1901135	Carbohydrate derivative metabolic process	2,00E-07	70	987
GO Biological Process	GO:0072657	Protein localization to membrane	2,11E-07	45	495
GO Biological Process	GO:1901575	Organic substance catabolic process	2,28E-07	104	1750
GO Biological Process	GO:0032787	Monocarboxylic acid metabolic process	2,31E-07	46	515
KEGG Pathways	hsa04145	Phagosome	2,31E-07	22	142
GO Biological Process	GO:0031647	Regulation of protein stability	2,66E-07	33	293
Reactome Pathways	HSA-5678895	Defective CFTR causes cystic fibrosis	2,70E-07	15	59
GO Biological Process	GO:0006458	De novo protein folding	3,00E-07	13	38
GO Biological Process	GO:0045047	Protein targeting to ER	3,11E-07	20	110
GO Biological Process	GO:0043603	Cellular amide metabolic process	3,22E-07	59	773
GO Biological Process	GO:0006518	Peptide metabolic process	3,22E-07	45	503
GO Biological Process	GO:0062012	Regulation of small molecule metabolic process	3,23E-07	42	449
GO Biological Process	GO:1902600	Proton transmembrane transport	3,89E-07	23	150
Reactome Pathways	HSA-9604323	Negative regulation of NOTCH4 signaling	4,53E-07	14	52
GO Biological Process	GO:0002376	Immune system process	4,67E-07	133	2481
Reactome Pathways	HSA-5358351	Signaling by Hedgehog	5,12E-07	22	146
GO Biological Process	GO:0033108	Mitochondrial respiratory chain complex assembly	5,16E-07	19	102
WikiPathways	WP411	mRNA processing	5,71E-07	21	125
GO Molecular Function	GO:0019899	Enzyme binding	6,19E-07	123	2239
GO Biological Process	GO:0070585	Protein localization to mitochondrion	6,75E-07	17	81
Reactome Pathways	HSA-168249	Innate Immune System	7,88E-07	69	1025
GO Biological Process	GO:1903829	Positive regulation of cellular protein localization	7,95E-07	35	342
Reactome Pathways	HSA-556833	Metabolism of lipids	8,34E-07	55	733
WikiPathways	WP4290	Metabolic reprogramming in colon cancer	9,12E-07	13	42
GO Biological Process	GO:0045540	Regulation of cholesterol biosynthetic process	9,61E-07	13	43
GO Biological Process	GO:0006417	Regulation of translation	1,03E-06	38	398
GO Biological Process	GO:1901564	Organonitrogen compound metabolic process	1,07E-06	235	5244
GO Biological Process	GO:0002474	Antigen processing and presentation of peptide antigen via MHC class I	1,12E-06	18	96
Reactome Pathways	HSA-2408522	Selenoamino acid metabolism	1,12E-06	19	114
GO Molecular Function	GO:0031072	Heat shock protein binding	1,18E-06	20	120
GO Molecular Function	GO:0016651	Oxidoreductase activity, acting on NAD(P)H	1,18E-06	19	107
GO Molecular Function	GO:0044389	Ubiquitin-like protein ligase binding	1,18E-06	33	312
GO Molecular Function	GO:0031625	Ubiquitin protein ligase binding	1,18E-06	32	296
GO Biological Process	GO:0043170	Macromolecule metabolic process	1,27E-06	266	6137
GO Biological Process	GO:0034248	Regulation of cellular amide metabolic process	1,28E-06	41	456
GO Biological Process	GO:0007264	Small GTPase mediated signal transduction	1,28E-06	33	316
Reactome Pathways	HSA-1236978	Cross-presentation of soluble exogenous antigens (endosomes)	1,29E-06	13	48
Reactome Pathways	HSA-211733	Regulation of activated PAK-2p34 by proteasome mediated degradation	1,29E-06	13	48
GO Biological Process	GO:0006521	Regulation of cellular amino acid metabolic process	1,33E-06	15	64
GO Molecular Function	GO:0019003	GDP binding	1,35E-06	16	74
GO Biological Process	GO:0006950	Response to stress	1,35E-06	170	3485
GO Biological Process	GO:0002479	Antigen processing and presentation of exogenous peptide antigen via MHC class I, TAP-dependent	1,40E-06	16	75
GO Molecular Function	GO:0003730	mRNA 3-UTR binding	1,51E-06	17	86

Reactome Pathways	HSA-350562	Regulation of ornithine decarboxylase (ODC)	1,54E-06	13	49
GO Biological Process	GO:0061077	Chaperone-mediated protein folding	1,59E-06	14	55
Reactome Pathways	HSA-174184	Cdc20:Phospho-APC/C mediated degradation of Cyclin A	1,67E-06	15	70
WikiPathways	WP197	Cholesterol biosynthesis pathway	1,78E-06	9	15
Reactome Pathways	HSA-349425	Autodegradation of the E3 ubiquitin ligase COP1	1,84E-06	13	50
Reactome Pathways	HSA-6811436	COPI-independent Golgi-to-ER retrograde traffic	1,84E-06	13	50
Reactome Pathways	HSA-75815	Ubiquitin-dependent degradation of Cyclin D	1,84E-06	13	50
Reactome Pathways	HSA-69601	Ubiquitin Mediated Degradation of Phosphorylated Cdc25A	1,84E-06	13	50
Reactome Pathways	HSA-180534	Vpu mediated degradation of CD4	1,84E-06	13	50
GO Biological Process	GO:0032981	Mitochondrial respiratory chain complex I assembly	1,85E-06	15	66
GO Molecular Function	GO:0008137	NADH dehydrogenase (ubiquinone) activity	1,92E-06	13	46
Reactome Pathways	HSA-174084	Autodegradation of Cdh1 by Cdh1:APC/C	1,94E-06	14	61
WikiPathways	WP4324	Mitochondrial complex I assembly model OXPHOS system	1,98E-06	14	56
Reactome Pathways	HSA-9612973	Autophagy	2,08E-06	21	148
Reactome Pathways	HSA-9646399	Aggrephagy	2,13E-06	12	42
Reactome Pathways	HSA-8941858	Regulation of RUNX3 expression and activity	2,28E-06	13	52
Reactome Pathways	HSA-180585	Vif-mediated degradation of APOBEC3G	2,28E-06	13	52
KEGG Pathways	hsa03050	Proteasome	2,32E-06	12	43
Reactome Pathways	HSA-8957322	Metabolism of steroids	2,41E-06	21	150
GO Biological Process	GO:0010389	Regulation of G2/M transition of mitotic cell cycle	2,49E-06	25	198
Reactome Pathways	HSA-5358346	Hedgehog ligand biogenesis	2,51E-06	14	63
Reactome Pathways	HSA-4641257	Degradation of AXIN	2,61E-06	13	53
Reactome Pathways	HSA-8854050	FBXL7 down-regulates AURKA during mitotic entry and in early mitosis	2,61E-06	13	53
Reactome Pathways	HSA-174113	SCF-beta-TrCP mediated degradation of Emi1	2,61E-06	13	53
GO Biological Process	GO:0008610	Lipid biosynthetic process	2,76E-06	47	585
GO Biological Process	GO:0090181	Regulation of cholesterol metabolic process	2,76E-06	14	58
Reactome Pathways	HSA-5617833	Cilium Assembly	2,96E-06	24	197
Reactome Pathways	HSA-5362768	Hh mutants are degraded by ERAD	2,98E-06	13	54
GO Biological Process	GO:0050821	Protein stabilization	3,16E-06	24	186
Reactome Pathways	HSA-174154	APC/C:Cdc20 mediated degradation of Securin	3,18E-06	14	65
DISEASES	DOID:3146	Lipid metabolism disorder	3,18E-06	17	74
GO Biological Process	GO:0006120	Mitochondrial electron transport, NADH to ubiquinone	3,20E-06	13	49
Reactome Pathways	HSA-382556	ABC-family proteins mediated transport	3,48E-06	17	101
Reactome Pathways	HSA-4641258	Degradation of DVL	3,48E-06	13	55
Reactome Pathways	HSA-68867	Assembly of the pre-replicative complex	3,64E-06	14	66
WikiPathways	WP183	Proteasome degradation	3,79E-06	14	60
GO Biological Process	GO:0033238	Regulation of cellular amine metabolic process	3,96E-06	16	82
GO Biological Process	GO:1902652	Secondary alcohol metabolic process	3,96E-06	20	132
Reactome Pathways	HSA-176408	Regulation of APC/C activators between G1/S and early anaphase	4,02E-06	15	78
Reactome Pathways	HSA-4086400	PCP/CE pathway	4,03E-06	16	90
Reactome Pathways	HSA-5676590	NIK-->noncanonical NF-kB signaling	4,73E-06	13	57
Reactome Pathways	HSA-68827	CDT1 association with the CDC6:ORC:origin complex	4,73E-06	13	57
GO Biological Process	GO:0060071	Wnt signaling pathway, planar cell polarity pathway	5,30E-06	17	96
GO Biological Process	GO:0006614	SRP-dependent cotranslational protein targeting to membrane	5,30E-06	17	96
Reactome Pathways	HSA-5607761	Dectin-1 mediated noncanonical NF-kB signaling	5,42E-06	13	58
Reactome Pathways	HSA-5610780	Degradation of GLI1 by the proteasome	5,42E-06	13	58
Reactome Pathways	HSA-5610783	Degradation of GLI2 by the proteasome	5,42E-06	13	58

Reactome Pathways	HSA-5610785	GLI3 is processed to GLI3R by the proteasome	5,42E-06	13	58
Reactome Pathways	HSA-975956	Nonsense Mediated Decay (NMD) independent of the Exon Junction Complex (EJC)	5,42E-06	16	93
Reactome Pathways	HSA-68949	Orc1 removal from chromatin	5,42E-06	14	69
Reactome Pathways	HSA-187577	SCF(Skp2)-mediated degradation of p27/p21	5,42E-06	13	58
Reactome Pathways	HSA-69017	CDK-mediated phosphorylation and removal of Cdc6	6,00E-06	14	70
Reactome Pathways	HSA-390466	Chaperonin-mediated protein folding	6,00E-06	16	94
Reactome Pathways	HSA-1445148	Translocation of SLC2A4 (GLUT4) to the plasma membrane	6,00E-06	14	70
Reactome Pathways	HSA-5689603	UCH proteinases	6,00E-06	16	94
GO Biological Process	GO:0034645	Cellular macromolecule biosynthetic process	6,04E-06	92	1592
Reactome Pathways	HSA-168256	Immune System	6,22E-06	105	1956
GO Biological Process	GO:0048024	Regulation of mRNA splicing, via spliceosome	6,31E-06	18	110
GO Biological Process	GO:0072655	Establishment of protein localization to mitochondrion	6,43E-06	15	74
GO Biological Process	GO:1902036	Regulation of hematopoietic stem cell differentiation	6,43E-06	15	74
Reactome Pathways	HSA-174178	APC/C:Cdh1 mediated degradation of Cdc20 and other APC/C:Cdh1 targeted proteins in late mitosis/early G1	6,69E-06	14	71
GO Molecular Function	GO:0044183	Protein folding chaperone	6,99E-06	10	26
GO Biological Process	GO:0048518	Positive regulation of biological process	7,09E-06	261	6112
GO Biological Process	GO:1903827	Regulation of cellular protein localization	7,32E-06	45	568
GO Biological Process	GO:0043484	Regulation of RNA splicing	7,32E-06	21	152
WikiPathways	WP2272	Pathogenic Escherichia coli infection	7,53E-06	13	54
Reactome Pathways	HSA-390450	Folding of actin by CCT/TriC	7,56E-06	7	10
GO Biological Process	GO:1904816	Positive regulation of protein localization to chromosome, telomeric region	7,58E-06	8	13
Reactome Pathways	HSA-1234174	Cellular response to hypoxia	7,64E-06	14	72
GO Molecular Function	GO:0015078	Proton transmembrane transporter activity	8,44E-06	19	125
Reactome Pathways	HSA-4608870	Asymmetric localization of PCP proteins	9,11E-06	13	62
GO Biological Process	GO:0009628	Response to abiotic stimulus	9,38E-06	72	1147
GO Biological Process	GO:0046364	Monosaccharide biosynthetic process	9,48E-06	13	55
GO Biological Process	GO:0034654	Nucleobase-containing compound biosynthetic process	1,04E-05	65	995
Reactome Pathways	HSA-1234176	Oxygen-dependent proline hydroxylation of Hypoxia-inducible Factor Alpha	1,06E-05	13	63
Reactome Pathways	HSA-5357801	Programmed Cell Death	1,06E-05	22	185
Reactome Pathways	HSA-975957	Nonsense Mediated Decay (NMD) enhanced by the Exon Junction Complex (EJC)	1,10E-05	17	113
GO Biological Process	GO:0006626	Protein targeting to mitochondrion	1,12E-05	13	56
Reactome Pathways	HSA-3858494	Beta-catenin independent WNT signaling	1,21E-05	19	142
Reactome Pathways	HSA-69052	Switching of origins to a post-replicative state	1,21E-05	15	88
GO Biological Process	GO:0035567	Non-canonical Wnt signaling pathway	1,28E-05	19	130
GO Biological Process	GO:0017038	Protein import	1,29E-05	20	144
GO Biological Process	GO:0070201	Regulation of establishment of protein localization	1,31E-05	48	642
Reactome Pathways	HSA-109581	Apoptosis	1,33E-05	21	173
Reactome Pathways	HSA-1169091	Activation of NF-kappaB in B cells	1,34E-05	13	65
Reactome Pathways	HSA-190840	Microtubule-dependent trafficking of connexons from Golgi to the plasma membrane	1,34E-05	8	18
GO Biological Process	GO:0002478	Antigen processing and presentation of exogenous peptide antigen	1,40E-05	22	174
GO Molecular Function	GO:0016614	Oxidoreductase activity, acting on CH-OH group of donors	1,43E-05	19	130
WikiPathways	WP5124	Alzheimers disease	1,51E-05	27	255
Reactome Pathways	HSA-5658442	Regulation of RAS by GAPs	1,52E-05	13	66
Reactome Pathways	HSA-382551	Transport of small molecules	1,58E-05	50	721
GO Biological Process	GO:0048002	Antigen processing and presentation of peptide antigen	1,64E-05	23	191
Reactome Pathways	HSA-156842	Eukaryotic Translation Elongation	1,66E-05	15	91
Reactome Pathways	HSA-8948751	Regulation of PTEN stability and activity	1,73E-05	13	67

WikiPathways	WP2059	Alzheimers disease and miRNA effects	1,74E-05	27	258
Reactome Pathways	HSA-1168372	Downstream signaling events of B Cell Receptor (BCR)	1,74E-05	14	79
GO Biological Process	GO:0018279	Protein N-linked glycosylation via asparagine	1,75E-05	10	30
GO Biological Process	GO:0001666	Response to hypoxia	1,75E-05	32	342
GO Biological Process	GO:0008203	Cholesterol metabolic process	1,83E-05	18	120
GO Biological Process	GO:1900182	Positive regulation of protein localization to nucleus	1,88E-05	15	82
GO Biological Process	GO:0019319	Hexose biosynthetic process	1,92E-05	12	49
GO Biological Process	GO:0050684	Regulation of mRNA processing	2,02E-05	20	149
Reactome Pathways	HSA-380320	Recruitment of NuMA to mitotic centrosomes	2,05E-05	15	93
Reactome Pathways	HSA-9007101	Rab regulation of trafficking	2,06E-05	17	120
GO Biological Process	GO:0071806	Protein transmembrane transport	2,09E-05	13	60
GO Biological Process	GO:0031145	Anaphase-promoting complex-dependent catabolic process	2,11E-05	15	83
GO Biological Process	GO:0006888	Endoplasmic reticulum to Golgi vesicle-mediated transport	2,17E-05	23	195
Reactome Pathways	HSA-195253	Degradation of beta-catenin by the destruction complex	2,19E-05	14	81
GO Biological Process	GO:1904851	Positive regulation of establishment of protein localization to telomere	2,29E-05	7	10
GO Biological Process	GO:0032880	Regulation of protein localization	2,35E-05	61	934
Reactome Pathways	HSA-156827	L13a-mediated translational silencing of Ceruloplasmin expression	2,45E-05	16	108
GO Biological Process	GO:0019438	Aromatic compound biosynthetic process	2,57E-05	67	1070
GO Biological Process	GO:1903312	Negative regulation of mRNA metabolic process	2,68E-05	15	85
GO Biological Process	GO:0048522	Positive regulation of cellular process	2,68E-05	239	5579
GO Biological Process	GO:0044265	Cellular macromolecule catabolic process	2,72E-05	60	917
Reactome Pathways	HSA-5632684	Hedgehog on state	2,79E-05	14	83
GO Molecular Function	GO:0005515	Protein binding	2,85E-05	289	7026
Reactome Pathways	HSA-8939902	Regulation of RUNX2 expression and activity	2,86E-05	13	71
GO Biological Process	GO:0034249	Negative regulation of cellular amide metabolic process	3,05E-05	20	154
DISEASES	DOID:4	Disease	3,18E-05	257	5921
KEGG Pathways	hsa05017	Spinocerebellar ataxia	3,19E-05	18	135
GO Biological Process	GO:1904871	Positive regulation of protein localization to Cajal body	3,49E-05	7	11
Reactome Pathways	HSA-5626467	RHO GTPases activate IQGAPs	3,55E-05	9	30
GO Biological Process	GO:0018130	Heterocycle biosynthetic process	3,73E-05	66	1061
GO Biological Process	GO:0002218	Activation of innate immune response	3,77E-05	19	142
GO Biological Process	GO:0046165	Alcohol biosynthetic process	3,77E-05	17	114
Reactome Pathways	HSA-9633012	Response of EIF2AK4 (GCN2) to amino acid deficiency	3,88E-05	15	99
GO Biological Process	GO:0051084	De novo posttranslational protein folding	4,06E-05	10	34
GO Biological Process	GO:0034620	Cellular response to unfolded protein	4,22E-05	18	129
GO Molecular Function	GO:0016874	Ligase activity	4,29E-05	20	156
GO Biological Process	GO:0071456	Cellular response to hypoxia	4,37E-05	22	189
GO Biological Process	GO:1901990	Regulation of mitotic cell cycle phase transition	4,41E-05	35	416
Reactome Pathways	HSA-156902	Peptide chain elongation	4,42E-05	14	87
GO Biological Process	GO:0070482	Response to oxygen levels	4,49E-05	33	379
GO Biological Process	GO:0006006	Glucose metabolic process	4,55E-05	17	116
GO Biological Process	GO:0006694	Steroid biosynthetic process	4,58E-05	18	130
Reactome Pathways	HSA-162909	Host Interactions of HIV factors	4,71E-05	17	129
Reactome Pathways	HSA-8978868	Fatty acid metabolism	4,83E-05	20	175
Reactome Pathways	HSA-8876198	RAB GEFs exchange GTP for GDP on RABs	4,88E-05	14	88
GO Biological Process	GO:0061418	Regulation of transcription from RNA polymerase II promoter in response to hypoxia	4,96E-05	14	78
Reactome Pathways	HSA-8949215	Mitochondrial calcium ion transport	5,03E-05	8	23

Reactome Pathways	HSA-9609690	HCMV Early Events	5,19E-05	15	102
Reactome Pathways	HSA-72737	Cap-dependent Translation Initiation	5,21E-05	16	116
GO Biological Process	GO:0021762	Substantia nigra development	5,28E-05	11	45
Reactome Pathways	HSA-2426168	Activation of gene expression by SREBF (SREBP)	5,43E-05	10	42
WikiPathways	WP4804	Cholesterol biosynthesis with skeletal dysplasias	5,95E-05	6	7
GO Biological Process	GO:0010972	Negative regulation of G2/M transition of mitotic cell cycle	5,95E-05	15	92
Reactome Pathways	HSA-8878166	Transcriptional regulation by RUNX2	6,23E-05	16	118
GO Biological Process	GO:0006403	RNA localization	6,24E-05	23	210
KEGG Pathways	hsa04260	Cardiac muscle contraction	6,28E-05	14	87
Reactome Pathways	HSA-379716	Cytosolic tRNA aminoacylation	6,29E-05	8	24
GO Biological Process	GO:0006094	Gluconeogenesis	6,29E-05	11	46
GO Biological Process	GO:0019395	Fatty acid oxidation	6,33E-05	14	80
GO Biological Process	GO:0009057	Macromolecule catabolic process	6,37E-05	65	1058
GO Biological Process	GO:1904951	Positive regulation of establishment of protein localization	6,47E-05	32	368
KEGG Pathways	hsa04612	Antigen processing and presentation	6,49E-05	12	63
GO Biological Process	GO:0022406	Membrane docking	6,52E-05	21	179
KEGG Pathways	hsa03060	Protein export	6,56E-05	8	23
KEGG Pathways	hsa03010	Ribosome	6,56E-05	17	130
Reactome Pathways	HSA-69481	G2/M Checkpoints	6,95E-05	18	149
Reactome Pathways	HSA-168273	Influenza Viral RNA Transcription and Replication	6,97E-05	17	134
GO Molecular Function	GO:0051287	NAD binding	7,09E-05	12	56
GO Biological Process	GO:0006090	Pyruvate metabolic process	7,19E-05	13	69
GO Biological Process	GO:0006612	Protein targeting to membrane	7,30E-05	20	165
GO Biological Process	GO:0034063	Stress granule assembly	7,45E-05	8	20
GO Biological Process	GO:0042221	Response to chemical	7,52E-05	192	4333
Reactome Pathways	HSA-1655829	Regulation of cholesterol biosynthesis by SREBP (SREBF)	7,54E-05	11	55
Reactome Pathways	HSA-8854214	TBC/RABGAPs	7,54E-05	10	44
Reactome Pathways	HSA-70263	Gluconeogenesis	7,59E-05	9	34
Reactome Pathways	HSA-162906	HIV Infection	7,59E-05	23	232
GO Biological Process	GO:0032781	Positive regulation of ATPase activity	7,60E-05	12	58
GO Biological Process	GO:0017148	Negative regulation of translation	7,74E-05	18	136
Reactome Pathways	HSA-2871837	FCERI mediated NF-kB activation	8,09E-05	13	80
Reactome Pathways	HSA-5663220	RHO GTPases Activate Formins	8,09E-05	17	136
GO Biological Process	GO:0010564	Regulation of cell cycle process	8,97E-05	51	760
GO Biological Process	GO:0051085	Chaperone cofactor-dependent protein refolding	9,10E-05	9	29
KEGG Pathways	hsa04146	Peroxisome	9,16E-05	13	79
GO Biological Process	GO:1901987	Regulation of cell cycle phase transition	9,21E-05	36	452
GO Biological Process	GO:0043620	Regulation of DNA-templated transcription in response to stress	9,53E-05	17	124
Reactome Pathways	HSA-157118	Signaling by NOTCH	9,58E-05	21	202
GO Biological Process	GO:0051204	Protein insertion into mitochondrial membrane	9,65E-05	8	21
Reactome Pathways	HSA-72706	GTP hydrolysis and joining of the 60S ribosomal subunit	9,75E-05	15	109
GO Biological Process	GO:0044255	Cellular lipid metabolic process	9,88E-05	59	939
GO Biological Process	GO:0006890	Retrograde vesicle-mediated transport, Golgi to endoplasmic reticulum	9,89E-05	14	84
GO Biological Process	GO:0046031	ADP metabolic process	9,94E-05	11	49
GO Biological Process	GO:0048193	Golgi vesicle transport	1,00E-04	31	359
Reactome Pathways	HSA-2995383	Initiation of Nuclear Envelope (NE) Reformation	1,00E-04	7	18
GO Biological Process	GO:0006066	Alcohol metabolic process	1,10E-04	29	324

GO Biological Process	GO:0010941	Regulation of cell death	1,10E-04	91	1696
KEGG Pathways	hsa01040	Biosynthesis of unsaturated fatty acids	1,20E-04	8	26
Reactome Pathways	HSA-9619483	Activation of AMPK downstream of NMDARs	1,20E-04	8	27
Reactome Pathways	HSA-9609646	HCMV Infection	1,20E-04	16	126
GO Molecular Function	GO:0016787	Hydrolase activity	1,20E-04	120	2419
Reactome Pathways	HSA-8939236	RUNX1 regulates transcription of genes involved in differentiation of HSCs	1,20E-04	14	97
Reactome Pathways	HSA-5619115	Disorders of transmembrane transporters	1,30E-04	19	174
GO Biological Process	GO:0019318	Hexose metabolic process	1,30E-04	19	157
GO Biological Process	GO:0008202	Steroid metabolic process	1,30E-04	25	256
Reactome Pathways	HSA-9020702	Interleukin-1 signaling	1,40E-04	14	99
GO Biological Process	GO:0050896	Response to stimulus	1,40E-04	318	8046
Reactome Pathways	HSA-69206	G1/S Transition	1,50E-04	16	129
Reactome Pathways	HSA-9694548	Maturation of spike protein	1,50E-04	8	28
GO Biological Process	GO:1901998	Toxin transport	1,50E-04	10	41
GO Biological Process	GO:0070887	Cellular response to chemical stimulus	1,60E-04	138	2919
Reactome Pathways	HSA-9679506	SARS-CoV Infections	1,60E-04	17	145
GO Biological Process	GO:1902369	Negative regulation of RNA catabolic process	1,70E-04	12	64
GO Biological Process	GO:0050810	Regulation of steroid biosynthetic process	1,70E-04	14	89
GO Biological Process	GO:1904356	Regulation of telomere maintenance via telomere lengthening	1,70E-04	12	64
Reactome Pathways	HSA-192823	Viral mRNA Translation	1,70E-04	13	87
Reactome Pathways	HSA-3371568	Attenuation phase	2,00E-04	6	13
Reactome Pathways	HSA-3371556	Cellular response to heat stress	2,00E-04	13	89
GO Biological Process	GO:0043618	Regulation of transcription from RNA polymerase II promoter in response to stress	2,00E-04	16	118
Reactome Pathways	HSA-9668328	Sealing of the nuclear envelope (NE) by ESCRT-III	2,10E-04	8	30
Reactome Pathways	HSA-69620	Cell Cycle Checkpoints	2,20E-04	24	269
GO Biological Process	GO:0007029	Endoplasmic reticulum organization	2,20E-04	12	66
GO Biological Process	GO:0000184	Nuclear-transcribed mRNA catabolic process, nonsense-mediated decay	2,20E-04	16	119
Reactome Pathways	HSA-389977	Post-chaperonin tubulin folding pathway	2,20E-04	7	21
GO Biological Process	GO:2001242	Regulation of intrinsic apoptotic signaling pathway	2,20E-04	19	164
GO Biological Process	GO:2000736	Regulation of stem cell differentiation	2,20E-04	16	119
Reactome Pathways	HSA-9033500	TYSND1 cleaves peroxisomal proteins	2,20E-04	5	7
GO Biological Process	GO:0009060	Aerobic respiration	2,40E-04	13	79
GO Biological Process	GO:0006812	Cation transport	2,40E-04	55	881
GO Biological Process	GO:0005996	Monosaccharide metabolic process	2,40E-04	21	198
GO Biological Process	GO:0045899	Positive regulation of RNA polymerase II transcription preinitiation complex assembly	2,40E-04	6	10
GO Biological Process	GO:0032210	Regulation of telomere maintenance via telomerase	2,40E-04	11	55
KEGG Pathways	hsa01200	Carbon metabolism	2,50E-04	15	117
Reactome Pathways	HSA-202424	Downstream TCR signaling	2,50E-04	13	91
Reactome Pathways	HSA-72764	Eukaryotic Translation Termination	2,50E-04	13	91
GO Molecular Function	GO:0042802	Identical protein binding	2,50E-04	98	1896
GO Biological Process	GO:0032212	Positive regulation of telomere maintenance via telomerase	2,50E-04	9	34
GO Molecular Function	GO:0044877	Protein-containing complex binding	2,50E-04	70	1216
Reactome Pathways	HSA-2408557	Selenocysteine synthesis	2,50E-04	13	91
GO Biological Process	GO:0019218	Regulation of steroid metabolic process	2,60E-04	16	121
WikiPathways	WP368	Mitochondrial long chain fatty acid beta-oxidation	2,60E-04	7	17
GO Biological Process	GO:0033157	Regulation of intracellular protein transport	2,60E-04	25	268
GO Biological Process	GO:0032386	Regulation of intracellular transport	2,60E-04	30	360

GO Biological Process	GO:0006635	Fatty acid beta-oxidation	2,70E-04	11	56
GO Biological Process	GO:0043067	Regulation of programmed cell death	2,70E-04	84	1569
Reactome Pathways	HSA-6814122	Cooperation of PDCL (PhLP1) and TRiC/CCT in G-protein beta folding	2,80E-04	9	42
GO Biological Process	GO:0048255	mRNA stabilization	2,80E-04	10	45
GO Molecular Function	GO:0043021	Ribonucleoprotein complex binding	2,80E-04	17	133
Reactome Pathways	HSA-5689880	Ub-specific processing proteases	2,80E-04	20	203
GO Biological Process	GO:0038061	NIK/NF-kappaB signaling	2,90E-04	13	81
GO Biological Process	GO:0042981	Regulation of apoptotic process	3,00E-04	83	1550
GO Biological Process	GO:0019222	Regulation of metabolic process	3,00E-04	279	6948
KEGG Pathways	hsa04216	Ferroptosis	3,10E-04	9	41
GO Biological Process	GO:0010498	Proteasomal protein catabolic process	3,10E-04	29	345
GO Biological Process	GO:0060341	Regulation of cellular localization	3,10E-04	61	1027
GO Biological Process	GO:0019058	Viral life cycle	3,10E-04	21	202
GO Biological Process	GO:0140056	Organelle localization by membrane tethering	3,20E-04	19	170
GO Biological Process	GO:0022613	Ribonucleoprotein complex biogenesis	3,20E-04	33	423
GO Biological Process	GO:0010256	Endomembrane system organization	3,30E-04	33	424
GO Biological Process	GO:0070498	interleukin-1-mediated signaling pathway	3,40E-04	14	96
KEGG Pathways	hsa00071	Fatty acid degradation	3,50E-04	9	42
GO Biological Process	GO:2000573	Positive regulation of DNA biosynthetic process	3,50E-04	12	70
GO Biological Process	GO:0006631	Fatty acid metabolic process	3,60E-04	27	311
DISEASES	DOID:0060536	Mitochondrial complex I deficiency	3,60E-04	11	41
GO Biological Process	GO:0032204	Regulation of telomere maintenance	3,60E-04	13	83
GO Biological Process	GO:1901615	Organic hydroxy compound metabolic process	3,70E-04	35	467
GO Molecular Function	GO:0016616	Oxidoreductase activity, acting on the CH-OH group of donors, NAD or NADP as acceptor	3,80E-04	16	122
GO Biological Process	GO:0032388	Positive regulation of intracellular transport	3,80E-04	22	223
GO Biological Process	GO:1902175	Regulation of oxidative stress-induced intrinsic apoptotic signaling pathway	3,80E-04	8	27
GO Biological Process	GO:0050658	RNA transport	3,80E-04	20	189
GO Biological Process	GO:0006413	Translational initiation	3,80E-04	17	141
Reactome Pathways	HSA-5683057	MAPK family signaling cascades	3,90E-04	26	319
Reactome Pathways	HSA-447115	Interleukin-12 family signaling	3,90E-04	10	56
GO Biological Process	GO:0006811	Ion transport	3,90E-04	74	1344
GO Biological Process	GO:0007339	Binding of sperm to zona pellucida	4,00E-04	9	37
KEGG Pathways	hsa04144	Endocytosis	4,00E-04	22	241
KEGG Pathways	hsa05134	Legionellosis	4,00E-04	10	55
GO Biological Process	GO:0006734	NADH metabolic process	4,00E-04	9	37
Reactome Pathways	HSA-3371453	Regulation of HSF1-mediated heat shock response	4,10E-04	11	69
GO Molecular Function	GO:0051787	Misfolded protein binding	4,20E-04	8	26
GO Biological Process	GO:0061620	Glycolytic process through glucose-6-phosphate	4,60E-04	8	28
GO Biological Process	GO:2000278	Regulation of DNA biosynthetic process	4,80E-04	15	114
Reactome Pathways	HSA-9020591	Interleukin-12 signaling	5,00E-04	9	46
WikiPathways	WP4629	Aerobic glycolysis	5,00E-04	6	12
Reactome Pathways	HSA-210991	Basigin interactions	5,00E-04	7	25
GO Biological Process	GO:0006913	Nucleocytoplasmic transport	5,00E-04	24	263
GO Biological Process	GO:0042493	Response to drug	5,00E-04	25	281
Reactome Pathways	HSA-72689	Formation of a pool of free 40S subunits	5,10E-04	13	99
Reactome Pathways	HSA-190828	Gap junction trafficking	5,70E-04	9	47
Reactome Pathways	HSA-437239	Recycling pathway of L1	5,70E-04	9	47

GO Biological Process	GO:1900180	Regulation of protein localization to nucleus	5,70E-04	16	131
GO Biological Process	GO:1903902	Positive regulation of viral life cycle	5,80E-04	11	62
Reactome Pathways	HSA-75105	Fatty acyl-CoA biosynthesis	5,90E-04	8	36
GO Biological Process	GO:0048284	Organelle fusion	5,90E-04	14	102
GO Biological Process	GO:0043687	Post-translational protein modification	5,90E-04	29	360
GO Biological Process	GO:0031334	Positive regulation of protein-containing complex assembly	6,10E-04	23	249
GO Biological Process	GO:0046890	Regulation of lipid biosynthetic process	6,20E-04	20	197
GO Biological Process	GO:0006402	mRNA catabolic process	6,20E-04	21	214
GO Biological Process	GO:0043161	Proteasome-mediated ubiquitin-dependent protein catabolic process	6,20E-04	27	323
GO Biological Process	GO:0065002	Intracellular protein transmembrane transport	6,40E-04	10	51
GO Biological Process	GO:0032206	Positive regulation of telomere maintenance	6,40E-04	10	51
Reactome Pathways	HSA-72312	rRNA processing	6,40E-04	19	200
GO Biological Process	GO:0006096	Glycolytic process	6,50E-04	9	40
GO Biological Process	GO:0072329	Monocarboxylic acid catabolic process	6,60E-04	15	118
WikiPathways	WP4313	Ferroptosis	6,90E-04	9	40
Reactome Pathways	HSA-8950505	Gene and protein expression by JAK-STAT signaling after Interleukin-12 stimulation	6,90E-04	8	37
GO Biological Process	GO:0044282	Small molecule catabolic process	7,20E-04	32	424
GO Biological Process	GO:0006487	Protein N-linked glycosylation	7,40E-04	12	77
Reactome Pathways	HSA-195721	Signaling by WNT	7,70E-04	24	296
GO Biological Process	GO:0002831	Regulation of response to biotic stimulus	7,70E-04	31	406
GO Molecular Function	GO:0016408	C-acyltransferase activity	7,80E-04	7	20
GO Biological Process	GO:0090316	Positive regulation of intracellular protein transport	7,80E-04	19	184
Reactome Pathways	HSA-1280218	Adaptive Immune System	8,10E-04	45	743
Reactome Pathways	HSA-2132295	MHC class II antigen presentation	8,10E-04	14	120
GO Biological Process	GO:0048194	Golgi vesicle budding	8,20E-04	12	78
GO Biological Process	GO:0042254	Ribosome biogenesis	8,40E-04	25	292
GO Biological Process	GO:2001233	Regulation of apoptotic signaling pathway	8,60E-04	31	409
Reactome Pathways	HSA-6807070	PTEN Regulation	8,70E-04	15	137
WikiPathways	WP4724	Omega-9 fatty acid synthesis	8,80E-04	6	14
Reactome Pathways	HSA-449147	Signaling by Interleukins	8,80E-04	31	440
Reactome Pathways	HSA-5688426	Deubiquitination	8,90E-04	23	280
GO Biological Process	GO:0009062	Fatty acid catabolic process	9,20E-04	13	93
GO Biological Process	GO:0051640	Organelle localization	9,20E-04	40	598
GO Biological Process	GO:0043254	Regulation of protein-containing complex assembly	9,20E-04	33	451
GO Biological Process	GO:0031146	SCF-dependent proteasomal ubiquitin-dependent protein catabolic process	9,20E-04	13	93
Reactome Pathways	HSA-5620924	Intraflagellar transport	9,30E-04	9	51
Reactome Pathways	HSA-2500257	Resolution of Sister Chromatid Cohesion	9,30E-04	14	122
GO Biological Process	GO:1901617	Organic hydroxy compound biosynthetic process	9,40E-04	19	187
GO Biological Process	GO:0031330	Negative regulation of cellular catabolic process	9,60E-04	23	258
Reactome Pathways	HSA-70326	Glucose metabolism	9,60E-04	12	92
KEGG Pathways	hsa00510	N-Glycan biosynthesis	0,001	9	50
GO Molecular Function	GO:0003988	acetyl-CoA C-acyltransferase activity	0,001	5	7
GO Biological Process	GO:0009895	Negative regulation of catabolic process	0,0011	26	316
GO Biological Process	GO:0010565	Regulation of cellular ketone metabolic process	0,0011	19	190
GO Biological Process	GO:0016051	Carbohydrate biosynthetic process	0,0011	15	125
GO Biological Process	GO:0044260	Cellular macromolecule metabolic process	0,0011	207	4976
GO Biological Process	GO:1903313	Positive regulation of mRNA metabolic process	0,0011	12	81

GO Biological Process	GO:0098662	Inorganic cation transmembrane transport	0,0012	41	628
GO Molecular Function	GO:0043167	Ion binding	0,0012	250	6188
GO Biological Process	GO:0045088	Regulation of innate immune response	0,0013	25	301
WikiPathways	WP143	Fatty acid beta-oxidation	0,0013	8	34
GO Biological Process	GO:0051817	Modulation of process of other organism involved in symbiotic interaction	0,0013	13	97
GO Biological Process	GO:0019674	NAD metabolic process	0,0013	9	45
GO Biological Process	GO:0001649	Osteoblast differentiation	0,0013	15	127
GO Biological Process	GO:0031328	Positive regulation of cellular biosynthetic process	0,0013	98	2005
GO Biological Process	GO:0051052	Regulation of DNA metabolic process	0,0013	28	360
GO Biological Process	GO:0007346	Regulation of mitotic cell cycle	0,0013	43	676
WikiPathways	WP1982	Sterol regulatory element-binding proteins (SREBP) signaling	0,0013	11	69
Reactome Pathways	HSA-9609736	Assembly and cell surface presentation of NMDA receptors	0,0014	8	42
GO Biological Process	GO:0090114	COPII-coated vesicle budding	0,0014	11	70
GO Biological Process	GO:0000956	Nuclear-transcribed mRNA catabolic process	0,0014	19	194
GO Biological Process	GO:0006401	RNA catabolic process	0,0014	22	247
GO Biological Process	GO:0098655	Cation transmembrane transport	0,0015	45	725
WikiPathways	WP4922	Mitochondrial complex IV assembly	0,0015	8	35
GO Biological Process	GO:0015931	Nucleobase-containing compound transport	0,0015	22	249
GO Biological Process	GO:0006165	Nucleoside diphosphate phosphorylation	0,0015	10	58
Reactome Pathways	HSA-201681	TCF dependent signaling in response to WNT	0,0016	18	199
GO Biological Process	GO:0006955	Immune response	0,0016	81	1588
Reactome Pathways	HSA-2046106	Alpha-linolenic acid (ALA) metabolism	0,0016	5	13
GO Biological Process	GO:0005975	Carbohydrate metabolic process	0,0016	33	467
Reactome Pathways	HSA-8955332	Carboxyterminal post-translational modifications of tubulin	0,0016	8	43
Reactome Pathways	HSA-9648025	EML4 and NUDC in mitotic spindle formation	0,0016	13	113
Reactome Pathways	HSA-380259	Loss of Nlp from mitotic centrosomes	0,0016	10	69
Reactome Pathways	HSA-68877	Mitotic Prometaphase	0,0016	18	199
WikiPathways	WP477	Cytoplasmic ribosomal proteins	0,0017	12	86
Reactome Pathways	HSA-5205685	PINK1-PRKN Mediated Mitophagy	0,0017	6	22
GO Biological Process	GO:1905330	Regulation of morphogenesis of an epithelium	0,0017	18	180
GO Biological Process	GO:0051223	Regulation of protein transport	0,0017	40	617
GO Biological Process	GO:0016050	Vesicle organization	0,0017	25	308
GO Biological Process	GO:0035722	interleukin-12-mediated signaling pathway	0,0018	9	47
GO Biological Process	GO:0045727	Positive regulation of translation	0,0018	15	131
KEGG Pathways	hsa04723	Retrograde endocannabinoid signaling	0,0018	15	145
GO Biological Process	GO:0090263	Positive regulation of canonical Wnt signaling pathway	0,0019	16	148
GO Biological Process	GO:0071310	Cellular response to organic substance	0,0019	111	2369
GO Biological Process	GO:0034504	Protein localization to nucleus	0,0019	17	165
GO Biological Process	GO:0000381	Regulation of alternative mRNA splicing, via spliceosome	0,0019	11	73
GO Molecular Function	GO:0005215	Transporter activity	0,0019	65	1181
GO Biological Process	GO:0019080	Viral gene expression	0,0019	15	132
GO Biological Process	GO:0090090	Negative regulation of canonical Wnt signaling pathway	0,002	18	183
GO Biological Process	GO:0051054	Positive regulation of DNA metabolic process	0,002	19	200
GO Molecular Function	GO:0003735	Structural constituent of ribosome	0,002	17	159
Reactome Pathways	HSA-8854518	AURKA Activation by TPX2	0,0021	10	72
GO Biological Process	GO:0051170	Import into nucleus	0,0021	14	118
GO Biological Process	GO:0046365	Monosaccharide catabolic process	0,0021	10	61

GO Biological Process	GO:1901991	Negative regulation of mitotic cell cycle phase transition	0,0021	20	219
GO Biological Process	GO:0045070	Positive regulation of viral genome replication	0,0021	8	37
GO Biological Process	GO:0009889	Regulation of biosynthetic process	0,0021	178	4210
Reactome Pathways	HSA-9637690	Response of Mtb to phagocytosis	0,0021	6	23
GO Molecular Function	GO:0043022	Ribosome binding	0,0021	10	57
KEGG Pathways	hsa04962	Vasopressin-regulated water reabsorption	0,0021	8	44
GO Biological Process	GO:0006900	Vesicle budding from membrane	0,0021	13	103
KEGG Pathways	hsa05203	Viral carcinogenesis	0,0021	17	182
Reactome Pathways	HSA-5628897	TP53 Regulates Metabolic Genes	0,0022	11	87
WikiPathways	WP4932	7q11.23 copy number variation syndrome	0,0022	13	104
GO Biological Process	GO:0061621	Canonical glycolysis	0,0022	7	27
GO Biological Process	GO:0051130	Positive regulation of cellular component organization	0,0022	65	1209
GO Biological Process	GO:2000027	Regulation of animal organ morphogenesis	0,0022	22	257
GO Biological Process	GO:0090087	Regulation of peptide transport	0,0022	41	649
Reactome Pathways	HSA-2565942	Regulation of PLK1 Activity at G2/M Transition	0,0022	11	87
GO Molecular Function	GO:0043531	ADP binding	0,0024	8	35
GO Molecular Function	GO:0001671	ATPase activator activity	0,0024	7	25
GO Biological Process	GO:0080090	Regulation of primary metabolic process	0,0024	241	6032
Reactome Pathways	HSA-983169	Class I MHC mediated antigen processing & presentation	0,0025	26	366
Reactome Pathways	HSA-75876	Synthesis of very long-chain fatty acyl-CoAs	0,0025	6	24
WikiPathways	WP3925	Amino acid metabolism	0,0025	12	91
GO Molecular Function	GO:0004386	Helicase activity	0,0026	16	147
Reactome Pathways	HSA-109582	Hemostasis	0,0026	37	605
GO Molecular Function	GO:0016627	Oxidoreductase activity, acting on the CH-CH group of donors	0,0026	10	59
Reactome Pathways	HSA-8868773	rRNA processing in the nucleus and cytosol	0,0026	17	190
GO Biological Process	GO:0032508	DNA duplex unwinding	0,0027	13	106
GO Molecular Function	GO:0031489	Myosin V binding	0,0027	6	17
KEGG Pathways	hsa01230	Biosynthesis of amino acids	0,0028	10	73
WikiPathways	WP4352	Ciliary landscape	0,0029	19	209
GO Biological Process	GO:0019320	catabolic process	0,0029	9	51
GO Biological Process	GO:2000142	Regulation of DNA-templated transcription, initiation	0,0029	9	51
GO Biological Process	GO:0034097	Response to cytokine	0,0029	60	1101
GO Biological Process	GO:0070934	CRD-mediated mRNA stabilization	0,0031	4	5
GO Biological Process	GO:0044788	Modulation by host of viral process	0,0031	7	29
GO Biological Process	GO:0010557	Positive regulation of macromolecule biosynthetic process	0,0031	92	1906
GO Biological Process	GO:0051702	Interaction with symbiont	0,0032	12	93
GO Biological Process	GO:0048524	Positive regulation of viral process	0,0032	13	108
KEGG Pathways	hsa03320	PPAR signaling pathway	0,0033	10	75
GO Biological Process	GO:0071345	Cellular response to cytokine stimulus	0,0034	56	1013
GO Molecular Function	GO:0003725	Double-stranded RNA binding	0,0034	11	75
GO Biological Process	GO:0002833	Positive regulation of response to biotic stimulus	0,0034	21	247
Reactome Pathways	HSA-8949664	Processing of SMDT1	0,0034	5	16
GO Biological Process	GO:0033209	Tumor necrosis factor-mediated signaling pathway	0,0035	14	125
GO Biological Process	GO:0044267	Cellular protein metabolic process	0,0036	158	3696
GO Biological Process	GO:0031667	Response to nutrient levels	0,0036	31	449
GO Biological Process	GO:0035337	fatty-acyl-CoA metabolic process	0,0037	8	41
GO Biological Process	GO:0038093	Fc receptor signaling pathway	0,0039	17	177

Reactome Pathways	HSA-6791226	Major pathway of rRNA processing in the nucleolus and cytosol	0,004	16	180
Reactome Pathways	HSA-438064	Post NMDA receptor activation events	0,004	10	79
GO Biological Process	GO:0002223	Stimulatory C-type lectin receptor signaling pathway	0,004	13	111
GO Biological Process	GO:0044242	Cellular lipid catabolic process	0,0041	18	196
KEGG Pathways	hsa03015	mRNA surveillance pathway	0,0041	11	93
KEGG Pathways	hsa03013	RNA transport	0,0041	15	160
GO Biological Process	GO:2000144	Positive regulation of DNA-templated transcription, initiation	0,0042	8	42
GO Molecular Function	GO:0008320	Protein transmembrane transporter activity	0,0043	6	19
GO Molecular Function	GO:0046933	Proton-transporting ATP synthase activity, rotational mechanism	0,0043	5	11
Reactome Pathways	HSA-380270	Recruitment of mitotic centrosome proteins and complexes	0,0043	10	80
GO Biological Process	GO:0034250	Positive regulation of cellular amide metabolic process	0,0044	16	162
Reactome Pathways	HSA-390471	Association of TriC/CCT with target proteins during biosynthesis	0,0045	7	39
GO Molecular Function	GO:0015288	Porin activity	0,0045	4	5
GO Molecular Function	GO:0060590	ATPase regulator activity	0,0047	8	40
Reactome Pathways	HSA-77305	Beta oxidation of palmitoyl-CoA to myristoyl-CoA	0,0047	3	3
Reactome Pathways	HSA-428359	Insulin-like Growth Factor-2 mRNA Binding Proteins (IGF2BPs/IMPs/VICKZs) bind RNA	0,0047	3	3
Reactome Pathways	HSA-5684996	MAPK1/MAPK3 signaling	0,0047	21	280
GO Biological Process	GO:0031325	Positive regulation of cellular metabolic process	0,0047	147	3413
Reactome Pathways	HSA-5620912	Anchoring of the basal body to the plasma membrane	0,0048	11	97
Reactome Pathways	HSA-390918	Peroxisomal lipid metabolism	0,0048	6	28
WikiPathways	WP357	Fatty acid biosynthesis	0,0049	6	22
Reactome Pathways	HSA-204005	COPII-mediated vesicle transport	0,0049	9	67
GO Biological Process	GO:0010638	Positive regulation of organelle organization	0,0049	39	633
GO Biological Process	GO:0036109	Alpha-linolenic acid metabolic process	0,005	5	13
GO Biological Process	GO:0046949	fatty-acyl-CoA biosynthetic process	0,0051	7	32
Reactome Pathways	HSA-1266738	Developmental Biology	0,0051	56	1087
GO Biological Process	GO:0009893	Positive regulation of metabolic process	0,0051	164	3893
GO Molecular Function	GO:0042288	MHC class I protein binding	0,0052	6	20
GO Molecular Function	GO:0061608	Nuclear import signal receptor activity	0,0052	6	20
GO Biological Process	GO:0016052	Carbohydrate catabolic process	0,0053	13	115
GO Biological Process	GO:0038095	Fc-epsilon receptor signaling pathway	0,0053	13	115
GO Biological Process	GO:0034220	Ion transmembrane transport	0,0053	55	1010
GO Molecular Function	GO:0140142	Nucleocytoplasmic carrier activity	0,0053	7	30
GO Biological Process	GO:0019083	Viral transcription	0,0053	13	115
GO Biological Process	GO:0009991	Response to extracellular stimulus	0,0054	32	483
WikiPathways	WP534	Glycolysis and gluconeogenesis	0,0055	8	45
GO Biological Process	GO:0006997	Nucleus organization	0,0055	14	132
GO Biological Process	GO:0015672	Monovalent inorganic cation transport	0,0056	30	441
GO Biological Process	GO:0051173	Positive regulation of nitrogen compound metabolic process	0,0059	140	3239
Reactome Pathways	HSA-71406	Pyruvate metabolism and Citric Acid (TCA) cycle	0,0061	8	55
GO Biological Process	GO:0080134	Regulation of response to stress	0,0061	72	1437
GO Molecular Function	GO:0003727	Single-stranded RNA binding	0,0062	11	82
GO Biological Process	GO:0051701	Interaction with host	0,0064	15	151
GO Biological Process	GO:0019216	Regulation of lipid metabolic process	0,0065	29	424
GO Biological Process	GO:0044087	Regulation of cellular component biogenesis	0,0065	53	971
GO Biological Process	GO:0098660	Inorganic ion transmembrane transport	0,0068	42	714
Reactome Pathways	HSA-373760	L1CAM interactions	0,0069	12	119

GO Biological Process	GO:0006418	tRNA aminoacylation for protein translation	0,0069	8	46
GO Biological Process	GO:0060548	Negative regulation of cell death	0,007	54	999
GO Biological Process	GO:0031204	Posttranslational protein targeting to membrane, translocation	0,007	4	7
GO Biological Process	GO:0030433	Ubiquitin-dependent ERAD pathway	0,007	10	73
GO Biological Process	GO:0036503	ERAD pathway	0,0072	11	88
GO Biological Process	GO:0019219	Regulation of nucleobase-containing compound metabolic process	0,0072	166	3982
GO Biological Process	GO:0030163	Protein catabolic process	0,0073	41	694
GO Molecular Function	GO:0045182	Translation regulator activity	0,0074	14	131
GO Biological Process	GO:0006851	Mitochondrial calcium ion transmembrane transport	0,0075	6	24
GO Biological Process	GO:0045454	Cell redox homeostasis	0,0076	9	60
GO Biological Process	GO:0010942	Positive regulation of cell death	0,0076	42	719
Reactome Pathways	HSA-6807047	Cholesterol biosynthesis via desmosterol	0,0078	3	4
Reactome Pathways	HSA-6807062	Cholesterol biosynthesis via lathosterol	0,0078	3	4
GO Biological Process	GO:0043069	Negative regulation of programmed cell death	0,0078	50	908
GO Biological Process	GO:0008053	Mitochondrial fusion	0,0081	5	15
GO Biological Process	GO:0044794	Positive regulation by host of viral process	0,0081	5	15
Reactome Pathways	HSA-5673001	RAF/MAP kinase cascade	0,0082	20	274
GO Biological Process	GO:0051851	Modulation by host of symbiont process	0,0084	9	61
GO Biological Process	GO:0010948	Negative regulation of cell cycle process	0,0085	24	328
GO Biological Process	GO:0051726	Regulation of cell cycle	0,0085	63	1230
KEGG Pathways	hsa04540	Gap junction	0,0086	10	87
GO Biological Process	GO:0032469	Endoplasmic reticulum calcium ion homeostasis	0,0089	6	25
Reactome Pathways	HSA-983189	Kinesins	0,009	8	59
GO Biological Process	GO:0051128	Regulation of cellular component organization	0,009	108	2402
KEGG Pathways	hsa00970	Aminoacyl-tRNA biosynthesis	0,0091	7	44
KEGG Pathways	hsa03022	Basal transcription factors	0,0091	7	44
GO Molecular Function	GO:0016675	Oxidoreductase activity, acting on a heme group of donors	0,0091	6	23
GO Biological Process	GO:0043066	Negative regulation of apoptotic process	0,0094	49	893
GO Biological Process	GO:0006979	Response to oxidative stress	0,0094	27	393
GO Biological Process	GO:2001234	Negative regulation of apoptotic signaling pathway	0,0096	19	232
GO Biological Process	GO:0051222	Positive regulation of protein transport	0,0096	25	352
GO Biological Process	GO:0019439	Aromatic compound catabolic process	0,0097	29	437
GO Biological Process	GO:0019725	Cellular homeostasis	0,0098	49	895
GO Molecular Function	GO:0051920	Peroxiredoxin activity	0,0101	4	7
GO Biological Process	GO:0050792	Regulation of viral process	0,0105	18	215
Reactome Pathways	HSA-5620922	BBSome-mediated cargo-targeting to cilium	0,0107	5	22
Reactome Pathways	HSA-9613829	Chaperone Mediated Autophagy	0,0107	5	22
Reactome Pathways	HSA-68875	Mitotic Prophase	0,0108	11	109
GO Biological Process	GO:0006984	ER-nucleus signaling pathway	0,0116	7	38
GO Biological Process	GO:0007031	Peroxisome organization	0,0117	10	79
Reactome Pathways	HSA-9683686	Maturation of spike protein	0,0118	3	5
GO Biological Process	GO:0080135	Regulation of cellular response to stress	0,0124	42	739
GO Biological Process	GO:0071786	Endoplasmic reticulum tubular network organization	0,0125	5	17
Reactome Pathways	HSA-8878171	Transcriptional regulation by RUNX1	0,0125	16	204
Reactome Pathways	HSA-532668	N-glycan trimming in the ER and Calnexin/Calreticulin cycle	0,0126	6	35
Reactome Pathways	HSA-4419969	Depolymerisation of the Nuclear Lamina	0,0126	4	13
GO Biological Process	GO:0035556	Intracellular signal transduction	0,0127	81	1712

GO Biological Process	GO:0006998	Nuclear envelope organization	0,0134	8	52
GO Biological Process	GO:0033043	Regulation of organelle organization	0,0136	65	1306
GO Biological Process	GO:0046395	Carboxylic acid catabolic process	0,0139	20	260
Reactome Pathways	HSA-195258	RHO GTPase Effectors	0,0143	20	289
GO Biological Process	GO:0002253	Activation of immune response	0,0146	26	385
GO Biological Process	GO:1901361	Organic cyclic compound catabolic process	0,0147	30	472
GO Biological Process	GO:1903201	Regulation of oxidative stress-induced cell death	0,0148	9	67
Reactome Pathways	HSA-5620920	Cargo trafficking to the periciliary membrane	0,0149	7	50
GO Molecular Function	GO:0003678	DNA helicase activity	0,015	9	63
GO Molecular Function	GO:0023026	MHC class II protein complex binding	0,015	5	16
GO Biological Process	GO:0051049	Regulation of transport	0,0151	83	1776
GO Biological Process	GO:0030970	Retrograde protein transport, ER to cytosol	0,0152	5	18
GO Molecular Function	GO:0048027	mRNA 5-UTR binding	0,0154	6	26
GO Molecular Function	GO:0016628	Oxidoreductase activity, acting on the CH-CH group of donors, NAD or NADP as acceptor	0,0154	6	26
Reactome Pathways	HSA-9679191	Potential therapeutics for SARS	0,0155	9	81
Reactome Pathways	HSA-162658	Golgi Cisternae Pericentriolar Stack Reorganization	0,0156	4	14
KEGG Pathways	hsa05130	Pathogenic Escherichia coli infection	0,0157	15	187
GO Biological Process	GO:0044257	Cellular protein catabolic process	0,0159	37	633
GO Biological Process	GO:0046822	Regulation of nucleocytoplasmic transport	0,0159	12	115
GO Biological Process	GO:0044089	Positive regulation of cellular component biogenesis	0,016	33	542
GO Biological Process	GO:0051246	Regulation of protein metabolic process	0,016	122	2828
GO Biological Process	GO:0006901	Vesicle coating	0,016	9	68
GO Biological Process	GO:2001243	Negative regulation of intrinsic apoptotic signaling pathway	0,0162	11	99
Reactome Pathways	HSA-1280215	Cytokine Signaling in Immune system	0,0167	37	681
Reactome Pathways	HSA-5336415	Uptake and function of diphtheria toxin	0,0167	3	6
KEGG Pathways	hsa05132	Salmonella infection	0,0171	16	209
GO Biological Process	GO:0031326	Regulation of cellular biosynthetic process	0,0177	168	4125
GO Biological Process	GO:0034975	Protein folding in endoplasmic reticulum	0,0178	4	10
GO Molecular Function	GO:0070717	Poly-purine tract binding	0,0179	6	27
GO Molecular Function	GO:0008187	Poly-pyrimidine tract binding	0,0179	6	27
GO Biological Process	GO:0009266	Response to temperature stimulus	0,0179	15	170
KEGG Pathways	hsa00062	Fatty acid elongation	0,0181	5	25
GO Biological Process	GO:0035338	Long-chain fatty-acyl-CoA biosynthetic process	0,0184	5	19
GO Biological Process	GO:0044093	Positive regulation of molecular function	0,0184	85	1842
GO Biological Process	GO:0009408	Response to heat	0,0187	11	101
KEGG Pathways	hsa00620	Pyruvate metabolism	0,019	6	38
GO Biological Process	GO:0043574	Peroxisomal transport	0,019	9	70
GO Biological Process	GO:1903900	Regulation of viral life cycle	0,019	14	153
KEGG Pathways	hsa00513	Various types of N-glycan biosynthesis	0,019	6	38
GO Molecular Function	GO:0005384	Manganese ion transmembrane transporter activity	0,0192	4	9
GO Biological Process	GO:0070925	Organelle assembly	0,0192	41	735
GO Biological Process	GO:0044839	Cell cycle G2/M phase transition	0,0198	13	136
GO Biological Process	GO:0045935	Positive regulation of nucleobase-containing compound metabolic process	0,0198	88	1927
GO Biological Process	GO:0019538	Protein metabolic process	0,0198	172	4251
GO Molecular Function	GO:0050633	acetyl-CoA C-myristoyltransferase activity	0,0199	3	3
GO Biological Process	GO:0010604	Positive regulation of macromolecule metabolic process	0,02	149	3600
WikiPathways	WP4657	22q11.2 copy number variation syndrome	0,0201	12	119

KEGG Pathways	hsa00480	Glutathione metabolism	0,0201	7	53
GO Biological Process	GO:0006914	Autophagy	0,0204	20	270
GO Biological Process	GO:0048199	Vesicle targeting, to, from or within Golgi	0,0205	9	71
GO Biological Process	GO:0060828	Regulation of canonical Wnt signaling pathway	0,0208	21	291
KEGG Pathways	hsa04152	AMPK signaling pathway	0,0208	11	120
GO Biological Process	GO:0010970	Transport along microtubule	0,0209	14	155
GO Molecular Function	GO:0050660	Flavin adenine dinucleotide binding	0,021	10	82
GO Biological Process	GO:0071347	Cellular response to interleukin-1	0,0216	15	174
GO Biological Process	GO:0006123	Mitochondrial electron transport, cytochrome c to oxygen	0,0216	5	20
GO Biological Process	GO:0065005	Protein-lipid complex assembly	0,0216	6	31
GO Biological Process	GO:0051603	Proteolysis involved in cellular protein catabolic process	0,0216	35	600
GO Biological Process	GO:0031396	Regulation of protein ubiquitination	0,0216	17	212
GO Biological Process	GO:0000038	Very long-chain fatty acid metabolic process	0,0216	6	31
GO Biological Process	GO:0002181	Cytoplasmic translation	0,022	9	72
WikiPathways	WP5049	Glycolysis in senescence	0,022	4	11
WikiPathways	WP1941	Peroxisomal beta-oxidation of tetracosanoyl-CoA	0,022	3	4
GO Biological Process	GO:0033489	Cholesterol biosynthetic process via desmosterol	0,0222	3	4
GO Biological Process	GO:0033490	Cholesterol biosynthetic process via lathosterol	0,0222	3	4
GO Biological Process	GO:0045040	Protein insertion into mitochondrial outer membrane	0,0222	3	4
WikiPathways	WP4949	16p11.2 proximal deletion syndrome	0,0223	9	73
WikiPathways	WP2882	Nuclear receptors meta-pathway	0,0223	22	316
GO Biological Process	GO:0051099	Positive regulation of binding	0,0224	15	175
GO Molecular Function	GO:0019829	ATPase-coupled cation transmembrane transporter activity	0,0228	8	54
GO Biological Process	GO:0016042	Lipid catabolic process	0,0229	21	294
GO Molecular Function	GO:0015036	Disulfide oxidoreductase activity	0,0231	7	41
GO Molecular Function	GO:0140296	General transcription initiation factor binding	0,0231	7	41
GO Molecular Function	GO:0008536	Ran GTPase binding	0,0231	7	41
GO Biological Process	GO:0010332	Response to gamma radiation	0,0233	8	58
GO Biological Process	GO:0030705	Cytoskeleton-dependent intracellular transport	0,0235	16	195
Reactome Pathways	HSA-936837	Ion transport by P-type ATPases	0,0237	7	55
Reactome Pathways	HSA-72649	Translation initiation complex formation	0,0237	7	55
Reactome Pathways	HSA-5663202	Diseases of signal transduction by growth factor receptors and second messengers	0,0238	24	392
GO Biological Process	GO:0061157	mRNA destabilization	0,0244	6	32
GO Biological Process	GO:1902186	Regulation of viral release from host cell	0,0244	6	32
GO Biological Process	GO:0006293	Nucleotide-excision repair, preincision complex stabilization	0,0253	5	21
GO Biological Process	GO:1902307	Positive regulation of sodium ion transmembrane transport	0,0253	5	21
GO Molecular Function	GO:0004812	aminoacyl-tRNA ligase activity	0,0254	7	42
GO Molecular Function	GO:0030544	Hsp70 protein binding	0,0254	7	42
Reactome Pathways	HSA-432722	Golgi Associated Vesicle Biogenesis	0,0257	7	56
GO Biological Process	GO:0007584	Response to nutrient	0,0267	14	160
KEGG Pathways	hsa00061	Fatty acid biosynthesis	0,0273	4	17
Reactome Pathways	HSA-8876725	Protein methylation	0,0274	4	17
GO Biological Process	GO:0019941	Modification-dependent protein catabolic process	0,0275	32	541
GO Biological Process	GO:0032879	Regulation of localization	0,0276	117	2740
GO Biological Process	GO:0006891	intra-Golgi vesicle-mediated transport	0,0277	6	33
KEGG Pathways	hsa00020	Citrate cycle (TCA cycle)	0,0279	5	29
GO Biological Process	GO:0051235	Maintenance of location	0,028	14	161

GO Biological Process	GO:0034379	Very-low-density lipoprotein particle assembly	0,0284	4	12
Reactome Pathways	HSA-499943	Interconversion of nucleotide di- and triphosphates	0,0285	5	29
KEGG Pathways	hsa04918	Thyroid hormone synthesis	0,029	8	74
WikiPathways	WP4016	DNA IR-damage and cellular response via ATR	0,0295	9	77
GO Biological Process	GO:0030258	Lipid modification	0,0299	17	220
GO Biological Process	GO:0000717	Nucleotide-excision repair, DNA duplex unwinding	0,0299	5	22
GO Biological Process	GO:0006295	Nucleotide-excision repair, DNA incision, 3-to lesion	0,0299	5	22
GO Biological Process	GO:0048026	Positive regulation of mRNA splicing, via spliceosome	0,0299	5	22
GO Biological Process	GO:0016579	Protein deubiquitination	0,0301	20	281
GO Biological Process	GO:0042255	Ribosome assembly	0,0302	8	61
Reactome Pathways	HSA-450520	HuR (ELAVL1) binds and stabilizes mRNA	0,0305	3	8
GO Molecular Function	GO:0005200	Structural constituent of cytoskeleton	0,0308	11	104
GO Biological Process	GO:0031349	Positive regulation of defense response	0,0312	24	367
GO Biological Process	GO:0010765	Positive regulation of sodium ion transport	0,0312	6	34
WikiPathways	WP4190	Mevalonate arm of cholesterol biosynthesis pathway	0,0318	4	13
Reactome Pathways	HSA-71387	Metabolism of carbohydrates	0,0328	19	292
GO Biological Process	GO:2000112	Regulation of cellular macromolecule biosynthetic process	0,0328	157	3878
GO Biological Process	GO:0044791	Positive regulation by host of viral release from host cell	0,033	3	5
GO Biological Process	GO:0090666	scaRNA localization to Cajal body	0,033	3	5
GO Biological Process	GO:0042592	Homeostatic process	0,0332	77	1676
GO Biological Process	GO:0043068	Positive regulation of programmed cell death	0,0332	37	666
GO Biological Process	GO:0016072	rRNA metabolic process	0,0334	17	223
GO Biological Process	GO:2001252	Positive regulation of chromosome organization	0,0336	15	184
GO Biological Process	GO:0031323	Regulation of cellular metabolic process	0,0336	238	6239
Reactome Pathways	HSA-8951664	Neddylation	0,034	16	229
DISEASES	DOID:3652	Leigh disease	0,0341	11	72
GO Biological Process	GO:0051457	Maintenance of protein location in nucleus	0,0342	5	23
GO Biological Process	GO:0048025	Negative regulation of mRNA splicing, via spliceosome	0,0342	5	23
GO Biological Process	GO:0000154	rRNA modification	0,0347	6	35
GO Biological Process	GO:0009892	Negative regulation of metabolic process	0,0348	130	3124
GO Molecular Function	GO:0000062	fatty-acyl-CoA binding	0,0349	5	21
GO Molecular Function	GO:0016667	Oxidoreductase activity, acting on a sulfur group of donors	0,0349	8	59
GO Molecular Function	GO:0008143	poly(A) binding	0,0349	5	21
GO Molecular Function	GO:0003724	RNA helicase activity	0,0349	9	74
GO Biological Process	GO:0097711	Ciliary basal body-plasma membrane docking	0,0358	10	95
GO Biological Process	GO:0051028	mRNA transport	0,0361	13	148
GO Biological Process	GO:0050852	T cell receptor signaling pathway	0,0366	14	167
GO Biological Process	GO:0034655	Nucleobase-containing compound catabolic process	0,0368	24	373
GO Biological Process	GO:0010468	Regulation of gene expression	0,0368	189	4813
GO Biological Process	GO:0051252	Regulation of RNA metabolic process	0,0368	151	3722
GO Molecular Function	GO:0015662	Ion transmembrane transporter activity, phosphorylative mechanism	0,0371	6	33
GO Molecular Function	GO:0019905	Syntaxin binding	0,0371	9	75
GO Biological Process	GO:0048208	COPII vesicle coating	0,038	8	64
KEGG Pathways	hsa00280	Valine, leucine and isoleucine degradation	0,038	6	46
Reactome Pathways	HSA-9033241	Peroxisomal protein import	0,0384	7	61
GO Molecular Function	GO:0022857	Transmembrane transporter activity	0,0384	53	1050
GO Molecular Function	GO:0004129	Cytochrome-c oxidase activity	0,0385	5	22

GO Molecular Function	GO:0008649	rRNA methyltransferase activity	0,0385	5	22
GO Molecular Function	GO:0017025	TBP-class protein binding	0,0385	5	22
GO Biological Process	GO:0070588	Calcium ion transmembrane transport	0,0386	16	207
GO Biological Process	GO:0051973	Positive regulation of telomerase activity	0,0386	6	36
WikiPathways	WP4723	Omega-3 / omega-6 fatty acid synthesis	0,0388	4	14
GO Biological Process	GO:0046394	Carboxylic acid biosynthetic process	0,0403	20	290
GO Biological Process	GO:0061014	Positive regulation of mRNA catabolic process	0,0403	7	50
GO Biological Process	GO:0006606	Protein import into nucleus	0,0404	10	97
Reactome Pathways	HSA-5619070	Defective SLC16A1 causes symptomatic deficiency in lactate transport (SDLT)	0,0406	2	2
Reactome Pathways	HSA-9636667	Manipulation of host energy metabolism	0,0406	2	2
Reactome Pathways	HSA-192905	vRNP Assembly	0,0406	2	2
GO Biological Process	GO:0006511	Ubiquitin-dependent protein catabolic process	0,0409	31	535
GO Molecular Function	GO:0033218	Amide binding	0,0411	24	369
GO Molecular Function	GO:0016453	C-acetyltransferase activity	0,0411	3	5
GO Biological Process	GO:0006790	Sulfur compound metabolic process	0,0411	23	355
GO Biological Process	GO:0010629	Negative regulation of gene expression	0,0415	89	2014
GO Biological Process	GO:0044270	Cellular nitrogen compound catabolic process	0,0416	26	422
GO Biological Process	GO:0034660	ncRNA metabolic process	0,0416	28	467
DISEASES	DOID:2978	Carbohydrate metabolic disorder	0,0418	15	135
GO Biological Process	GO:0010248	Establishment or maintenance of transmembrane electrochemical gradient	0,042	4	14
GO Biological Process	GO:0006122	Mitochondrial electron transport, ubiquinol to cytochrome c	0,042	4	14
Reactome Pathways	HSA-211859	Biological oxidations	0,0421	15	214
GO Biological Process	GO:0050778	Positive regulation of immune response	0,0423	34	607
GO Molecular Function	GO:0015037	Peptide disulfide oxidoreductase activity	0,0432	4	13
WikiPathways	WP3942	PPAR signaling pathway	0,0434	8	67
GO Biological Process	GO:0051972	Regulation of telomerase activity	0,0438	7	51
GO Biological Process	GO:0000086	G2/M transition of mitotic cell cycle	0,0444	12	134
KEGG Pathways	hsa04979	Cholesterol metabolism	0,0448	6	48
GO Biological Process	GO:0042256	Mature ribosome assembly	0,0451	3	6
GO Biological Process	GO:0046826	Negative regulation of protein export from nucleus	0,0451	3	6
GO Biological Process	GO:1903371	Regulation of endoplasmic reticulum tubular network organization	0,0451	3	6
GO Biological Process	GO:0045069	Regulation of viral genome replication	0,0451	10	99
DISEASES	DOID:1289	Neurodegenerative disease	0,0458	32	462
GO Biological Process	GO:0006364	rRNA processing	0,0464	16	212
GO Biological Process	GO:0071466	Cellular response to xenobiotic stimulus	0,0465	11	117
GO Biological Process	GO:0043065	Positive regulation of apoptotic process	0,0475	36	660
KEGG Pathways	hsa00270	Cysteine and methionine metabolism	0,0479	6	49
KEGG Pathways	hsa00010	Glycolysis / Gluconeogenesis	0,0479	7	65
GO Biological Process	GO:0060255	Regulation of macromolecule metabolic process	0,0481	242	6407
GO Biological Process	GO:0061025	Membrane fusion	0,0488	12	136
GO Biological Process	GO:0007338	Single fertilization	0,0488	12	136
WikiPathways	WP4018	Clear cell renal cell carcinoma pathways	0,049	9	85
Reactome Pathways	HSA-8963888	Chylomicron assembly	0,0492	3	10

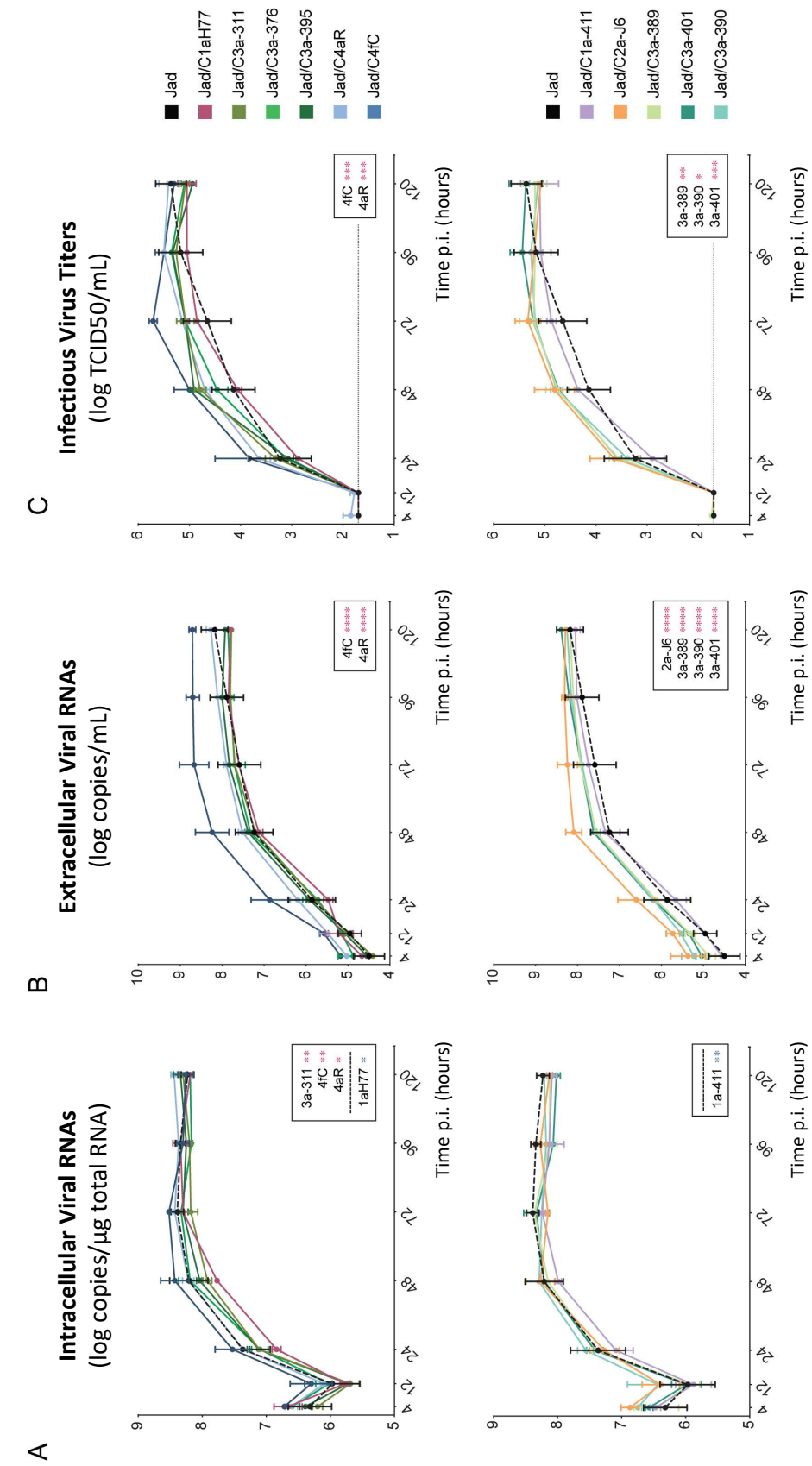

Supplementary Figure 2: Core intergenotypic recombinant characterization by Emeline Simon (unpublished data).

Figure translated and reproduced from Emeline Simon's PhD thesis manuscript with permission.

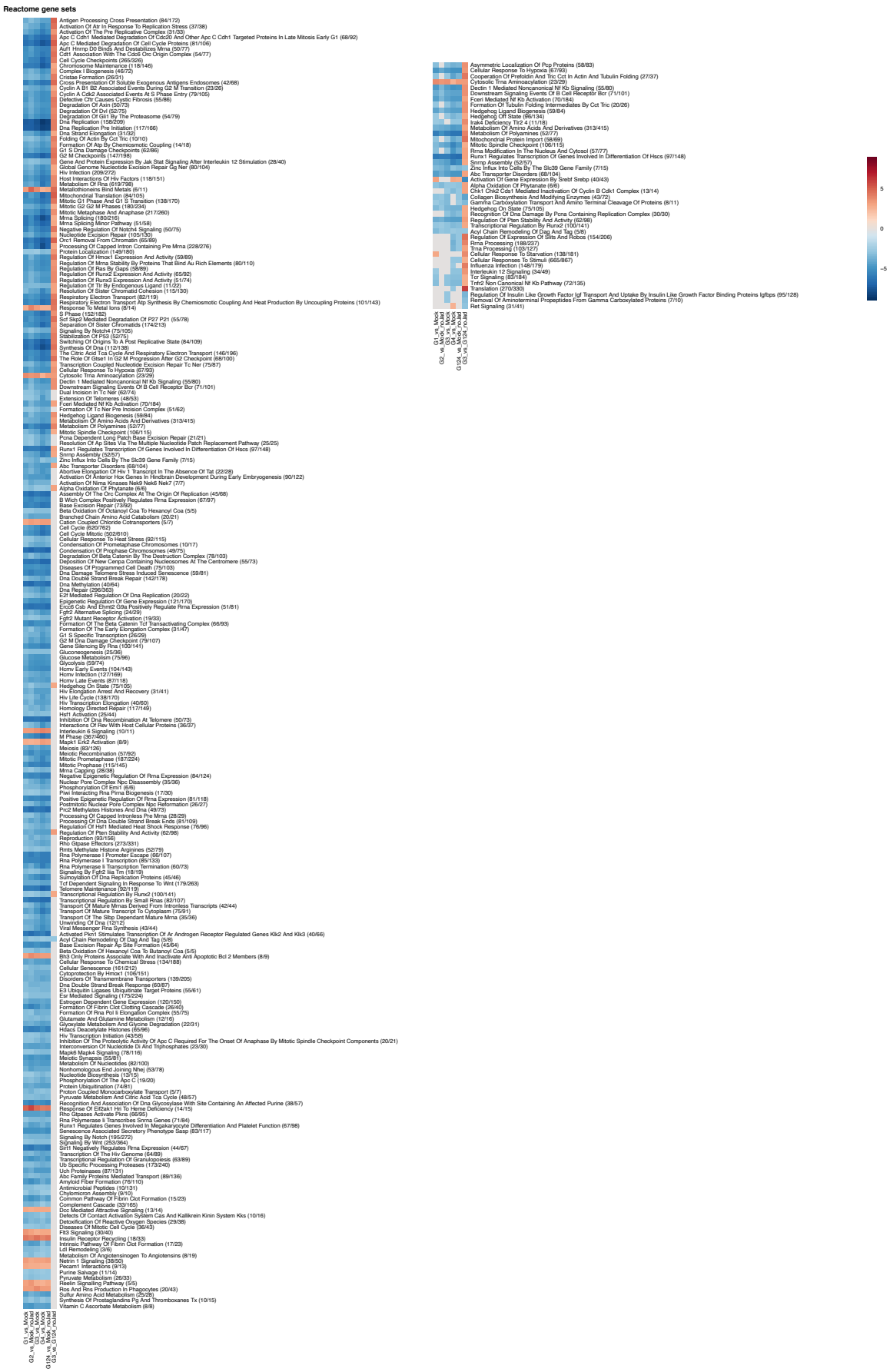
Reactome gene sets
Antigen Processing Cross Presentation (84/172)
Activation Of Atr In Response To Replication Stress (37/38)
Activation Of The Pre Replicative Complex (31/33)
Apc C Cdh1 Mediated Degradation Of Cdc20 And Other Apc C Cdh1 Targeted Proteins In Late Mitosis Early G1 (68/92)
Apc C Mediated Degradation Of Cell Cycle Proteins (81/106)
Auf1 Hnrnp D0 Binds And Destabilizes Mrna (50/77)
Cdh1 Association With The Cdc6 Orc Origin Complex (54/77)
Cell Cycle Checkpoints (265/326)
Chromosome Maintenance (118/146)
Complex I Biogenesis (46/72)
Cristae Formation (26/31)
Cross Presentation Of Soluble Exogenous Antigens Endosomes (42/68)
Cyclin A B1 B2 Associated Events During G2 M Transition (23/26)
Cyclin A Cdk2 Associated Events At S Phase Entry (79/105)
Defective Cftr Causes Cystic Fibrosis (55/86)
Degradation Of Axin (50/75)
Degradation Of Dvl (52/75)
Degradation Of Gli1 By The Proteasome (54/79)
Dna Replication (158/209)
Dna Replication Pre Initiation (117/166)
Dna Strand Elongation (31/32)
Folding Of Actin By Cct Tric (10/10)
Formation Of Atp By Chemiosmotic Coupling (14/18)
G1 S Dna Damage Checkpoints (62/86)
G2 M Checkpoints (147/198)
Gene And Protein Expression By Jak Stat Signaling After Interleukin 12 Stimulation (28/40)
Global Genome Nucleotide Excision Repair Gg Ner (80/104)
Hiv Infection (209/272)
Host Interactions Of Hiv Factors (118/151)
Metabolism Of Rna (619/798)
Metallothioneins Bind Metals (6/11)
Mitochondrial Translation (84/105)
Mitotic G1 Phase And G1 S Transition (138/170)
Mitotic G2 G2 M Phases (180/234)
Mitotic Metaphase And Anaphase (217/260)
Mrna Splicing (180/216)
Mrna Splicing Minor Pathway (51/58)
Negative Regulation Of Notch4 Signaling (50/75)
Nucleotide Excision Repair (105/130)
Orc1 Removal From Chromatin (80/89)
Processing Of Capped Intron Containing Pre Mrna (228/276)
Protein Localization (149/180)
Regulation Of Hmox1 Expression And Activity (59/89)
Regulation Of Mrna Stability By Proteins That Bind Au Rich Elements (80/110)
Regulation Of Ras By Gaps (58/89)
Regulation Of Runx2 Expression And Activity (65/92)
Regulation Of Runx3 Expression And Activity (51/74)
Regulation Of Tp By Endogenous Ligand (11/22)
Resolution Of Sister Chromatid Cohesion (115/130)
Respiratory Electron Transport (82/119)
Respiratory Electron Transport Atp Synthesis By Chemiosmotic Coupling And Heat Production By Uncoupling Proteins (101/143)
Response To Metal Ions (9/14)
S Phase (152/182)
Scf Skp2 Mediated Degradation Of P27 P21 (55/78)
Separation Of Sister Chromatids (174/213)
Signaling By Notch4 (75/105)
Stabilization Of P53 (52/75)
Switching Of Origins To A Post Replicative State (84/109)
Synthesis Of Dna (112/138)
The Citric Acid Tca Cycle And Respiratory Electron Transport (146/196)
The Role Of Gtse1 In G2 M Progression After G2 Checkpoint (68/100)
Transcription Coupled Nucleotide Excision Repair Tc Ner (75/87)
Cellular Response To Hypoxia (67/93)
Cytosolic Trna Aminoacylation (23/29)
Dectin 1 Mediated Noncanonical Nf Kb Signaling (55/80)
Downstream Signaling Events Of B Cell Receptor Bcr (71/101)
Dual Incision In Tc Ner (62/74)
Extension Of Telomeres (48/53)
Foxm Mediated Nf Kb Activation (70/184)
Formation Of Tc Ner Pre Incision Complex (51/62)
Hedgehog Ligand Biogenesis (59/84)
Metabolism Of Amino Acids And Derivatives (313/415)
Metabolism Of Polyamines (52/77)
Mitotic Spindle Checkpoint (106/115)
Pcna Dependent Long Patch Base Excision Repair (21/21)
Resolution Of Ap Sites Via The Multiple Nucleotide Patch Replacement Pathway (25/25)
Runx1 Regulates Transcription Of Genes Involved In Differentiation Of Hscs (97/148)
Snrnp Assembly (52/67)
Zinc Influx Into Cells By The Slc39 Gene Family (7/15)
Abc Transporter Disorders (68/104)
Abortive Elongation Of Hiv 1 Transcript In The Absence Of Tat (22/28)
Activation Of Anterior Hox Genes In Hindbrain Development During Early Embryogenesis (90/122)
Activation Of Nima Kinases Nek9 Nek6 Nek7 (7/7)
Alpha Oxidation Of Phytanate (6/6)
Assembly Of The Orc Complex At The Origin Of Replication (45/68)
B Wich Complex Positively Regulates Rrna Expression (67/97)
Base Excision Repair (73/92)
Beta Oxidation Of Octanoyl Coa To Hexanoyl Coa (5/5)
Branched Chain Amino Acid Catabolism (20/21)
Cation Coupled Chloride Cotransporters (5/7)
Cell Cycle (620/762)
Cell Cycle Mitotic (502/610)
Cellular Response To Heat Stress (92/115)
Condensation Of Prometaphase Chromosomes (10/17)
Condensation Of Prophase Chromosomes (49/75)
Degradation Of Beta Catenin By The Destruction Complex (78/103)
Deposition Of New Cenpa Containing Nucleosomes At The Centromere (55/73)
Diseases Of Programmed Cell Death (75/103)
Dna Damage Telomere Stress Induced Senescence (59/81)
Dna Double Strand Break Repair (142/178)
Dna Methylation (40/64)
Dna Repair (296/363)
E2f Mediated Regulation Of Dna Replication (20/22)
Epigenetic Regulation Of Gene Expression (121/170)
Ercc6 Csb And Ehmt2 G9a Positively Regulate Rrna Expression (51/81)
Fgfr2 Alternative Splicing (24/29)
Fgfr2 Mutant Receptor Activation (19/33)
Formation Of The Beta Catenin Tcf Transactivating Complex (66/93)
Formation Of The Early Elongation Complex (81/47)
G1 S Specific Transcription (26/29)
G2 M Dna Damage Checkpoint (79/107)
Gene Silencing By Rna (100/141)
Gluconeogenesis (25/36)
Glucose Metabolism (75/96)
Glycolysis (59/74)
Hcmv Early Events (104/143)
Hcmv Infection (127/169)
Hcmv Late Events (87/118)
Hedgehog On State (75/105)
Hiv Elongation Arrest And Recovery (31/41)
Hiv Life Cycle (138/170)
Hiv Transcription Elongation (40/60)
Homology Directed Repair (117/149)
Hsf1 Activation (25/44)
Inhibition Of Dna Recombination At Telomere (50/73)
Interactions Of Rev With Host Cellular Proteins (36/37)
Interleukin 6 Signaling (10/11)
M Phase (367/460)
Mapk1 Erk2 Activation (8/9)
Meiosis (83/126)
Meiotic Recombination (57/92)
Mitotic Prometaphase (187/224)
Mitotic Prophase (115/145)
Mrna Capping (28/38)
Negative Epigenetic Regulation Of Rrna Expression (84/124)
Nuclear Pore Complex Npc Disassembly (35/36)
Phosphorylation Of Emi1 (6/8)
Pkmyt1 Interacting Rna Pirna Biogenesis (17/30)
Positive Epigenetic Regulation Of Rrna Expression (81/118)
Postmitotic Nuclear Pore Complex Npc Reformation (26/27)
Prc2 Methylates Histones And Dna (49/73)
Processing Of Capped Intronless Pre Mrna (28/29)
Processing Of Dna Double Strand Break Ends (81/109)
Regulation Of Hsf1 Mediated Heat Shock Response (76/96)
Regulation Of Pten Stability And Activity (62/98)
Reproduction (93/156)
Rho Gtpase Effectors (273/331)
Rmts Methylate Histone Arginines (52/79)
Rna Polymerase I Promoter Escape (66/107)
Rna Polymerase I Transcription (85/133)
Rna Polymerase Ii Transcription Termination (60/73)
Signaling By Fgfr2 Iiia Tm (18/19)
Sumoylation Of Dna Replication Proteins (45/46)
Tcf Dependent Signaling In Response To Wnt (179/263)
Telomere Maintenance (92/119)
Transcriptional Regulation By Runx2 (100/141)
Transcriptional Regulation By Small Rnas (82/107)
Transport Of Mature Mrnas Derived From Intronless Transcripts (42/44)
Transport Of Mature Transcript To Cytoplasm (75/91)
Transport Of The Slbp Dependant Mature Mrna (35/36)
Unwinding Of Dna (12/12)
Viral Messenger Rna Synthesis (43/44)
Activated Pkn1 Stimulates Transcription Of Ar Androgen Receptor Regulated Genes Klk2 And Klk3 (40/66)
Acyl Chain Remodeling Of Dag And Tag (9/9)
Base Excision Repair Ap Site Formation (45/64)
Beta Oxidation Of Hexanoyl Coa To Butanoyl Coa (5/5)
Bh3 Only Proteins Associate With And Inactivate Anti Apoptotic Bcl 2 Members (8/9)
Cellular Response To Chemical Stress (134/188)
Cellular Senescence (161/212)
Cytoprotection By Hmox1 (106/151)
Disorders Of Transmembrane Transporters (139/205)
Dna Double Strand Break Response (60/87)
E3 Ubiquitin Ligases Ubiquitinate Target Proteins (55/61)
Er Mediated Signaling (175/224)
Estrogen Dependent Gene Expression (120/150)
Formation Of Fibrin Clot Clotting Cascade (26/40)
Formation Of Rna Pol Ii Elongation Complex (55/75)
Glutamate And Glutamine Metabolism (12/16)
Glyoxylate Metabolism And Glycine Degradation (22/31)
Hdacs Deacetylate Histones (65/96)
Hiv Transcription Initiation (43/58)
Inhibition Of The Proteolytic Activity Of Apc C Required For The Onset Of Anaphase By Mitotic Spindle Checkpoint Components (20/21)
Interconversion Of Nucleotide Di And Triphosphates (23/30)
Mapk6 Mapk4 Signaling (78/116)
Meiotic Synapsis (55/81)
Metabolism Of Nucleotides (82/100)
Nonhomologous End Joining Nhej (53/78)
Nucleotide Biosynthesis (13/15)
Phosphorylation Of The Apc C (19/20)
Protein Ubiquitination (74/81)
Proton Coupled Monocarboxylate Transport (5/7)
Pyruvate Metabolism And Citric Acid Tca Cycle (48/57)
Recognition And Association Of Dna Glycosylase With Site Containing An Affected Purine (38/57)
Response Of Eif2ak1 Hri To Heme Deficiency (14/15)
Rho Gtpases Activate Pkns (66/95)
Rna Polymerase Ii Transcribes Snrna Genes (71/84)
Runx1 Regulates Genes Involved In Megakaryocyte Differentiation And Platelet Function (67/98)
Senescence Associated Secretory Phenotype Sasp (83/117)
Signaling By Notch (195/272)
Signaling By Wnt (253/364)
Sirt1 Negatively Regulates Rrna Expression (44/67)
Transcription Of The Hiv Genome (64/89)
Transcriptional Regulation Of Granulopoiesis (63/89)
Ub Specific Processing Proteases (173/240)
Uch Proteinases (87/131)
Abc Family Proteins Mediated Transport (89/136)
Amyloid Fiber Formation (76/110)
Antimicrobial Peptides (10/131)
Chylomicron Assembly (9/10)
Common Pathway Of Fibrin Clot Formation (15/23)
Complement Cascade (33/165)
Dcc Mediated Attractive Signaling (13/14)
Defects Of Contact Activation System Cas And Kallikrein Kinin System Kks (10/16)
Detoxification Of Reactive Oxygen Species (29/38)
Diseases Of Mitotic Cell Cycle (36/43)
Fli3 Signaling (30/40)
Insulin Receptor Recycling (18/33)
Intrinsic Pathway Of Fibrin Clot Formation (17/23)
Ldl Remodeling (3/6)
Metabolism Of Angiotensinogen To Angiotensins (8/19)
Netrin 1 Signaling (38/50)
Pecam1 Interactions (9/13)
Purine Salvage (11/14)
Pyruvate Metabolism (26/33)
Reelin Signalling Pathway (5/5)
Ros And Rns Production In Phagocytes (20/43)
Sulfur Amino Acid Metabolism (25/28)
Synthesis Of Prostaglandins Pg And Thromboxanes Tx (10/15)
Vitamin C Ascorbate Metabolism (8/8)
G1_vs_Mock
G2_vs_Mock
G3_vs_Mock
G24_vs_Mock
G48_vs_Mock
G1_vs_noJad
G2_vs_noJad
G3_vs_noJad
G24_vs_noJad
G48_vs_noJad
Asymmetric Localization Of Pcp Proteins (58/83)
Cellular Response To Hypoxia (67/93)
Cooperation Of Prefoldin And Tric Cct In Actin And Tubulin Folding (27/37)
Cytosolic Trna Aminoacylation (23/29)
Dectin 1 Mediated Noncanonical Nf Kb Signaling (55/80)
Downstream Signaling Events Of B Cell Receptor Bcr (71/101)
Foxm Mediated Nf Kb Activation (70/184)
Formation Of Tubulin Folding Intermediates By Cct Tric (20/26)
Hedgehog Ligand Biogenesis (59/84)
Hedgehog Off State (96/134)
Irak4 Deficiency Tlr2 4 (11/18)
Metabolism Of Amino Acids And Derivatives (313/415)
Metabolism Of Polyamines (52/77)
Mitochondrial Protein Import (58/69)
Mitotic Spindle Checkpoint (106/115)
Rrna Modification In The Nucleus And Cytosol (57/77)
Runx1 Regulates Transcription Of Genes Involved In Differentiation Of Hscs (97/148)
Snrnp Assembly (52/57)
Zinc Influx Into Cells By The Slc39 Gene Family (7/15)
Abc Transporter Disorders (68/104)
Activation Of Gene Expression By Srebf Srebp (40/43)
Alpha Oxidation Of Phytanate (6/6)
Cdk1 Cks2 Cdc1 Mediated Inactivation Of Cyclin B Cdk1 Complex (13/14)
Collagen Biosynthesis And Modifying Enzymes (43/72)
Gamma Carboxylation Transport And Amino Terminal Cleavage Of Proteins (8/11)
Hedgehog On State (75/105)
Recognition Of Dna Damage By Pcna Containing Replication Complex (30/30)
Regulation Of Pten Stability And Activity (62/98)
Transcriptional Regulation By Runx2 (100/141)
Acyl Chain Remodeling Of Dag And Tag (5/8)
Regulation Of Expression Of Slits And Robos (154/206)
Rrna Processing (188/237)
Trna Processing (103/127)
Cellular Response To Starvation (138/181)
Cellular Responses To Stimuli (665/867)
Influenza Infection (148/179)
Interleukin 12 Signaling (34/49)
Tcr Signaling (85/184)
Tnfr2 Non Canonical Nf Kb Pathway (72/135)
Translation (270/330)
Regulation Of Insulin Like Growth Factor Igf Transport And Uptake By Insulin Like Growth Factor Binding Proteins Igfbps (95/128)
Removal Of Aminoterminal Propeptides From Gamma Carboxylated Proteins (7/10)
Ret Signaling (31/41)
5
0
−5

Supplementary Figure 3: Pathways and gene sets deregulated between groups of genotype 3 Vs nongenotype 3 Core intergenotypic Jad strains enriched within the reactome database.
Enrichment score computed by CAMERA was used as a proxy of the regulation direction of significant genes sets (p-adjusted < 5%) and the scale for each gene set database illustrated are added on the right. Positive enrichment score (in red) suggests higher expressions of the respective gene set in group A rather in group B for each A Vs B comparison. Similarly for negative enrichment score (in blue) and lower expressions. Comparisons among HCV genotypes and Mock infected cells are shown in the first five columns, while genotype 3 versus nongenotype 3 (excluding the parent Jad) comparisons are shown in the last column.